

Jihočeská univerzita v Českých Budějovicích
Přírodovědecká fakulta

**INHIBITORY REPLIKAČNÍHO CYKLU MEDICÍNSKY
VÝZNAMNÝCH VIROVÝCH PATOGENŮ**

HABILITAČNÍ PRÁCE

RNDr. Luděk Eyer, Ph.D.

2022

ANOTACE

Emergentní virové nákazy představují významné zdravotní riziko pro člověka. To platí zejména v dnešní době, kdy dochází k výrazným změnám klimatu a kdy intenzivní pohyb lidí napříč kontinenty usnadňuje a urychluje přenos medicínsky významných patogenů a šíření jejich vektorů a zvířecích rezervoárů. Ačkoli proti řadě virových infekcí existuje účinné očkování, efektivní antivirová terapie je úspěšně zavedena pouze pro velmi omezený počet virových onemocnění. Studie, které jsou součástí této habilitační práce, se zaměřují na hledání nových antivirových aktivních proti důležitým virovým patogenům z čeledi *Flaviviridae*, zejména proti viru klíšťové encefalitidy, který působí závažné infekce centrálního nervového systému a který je rozšířen na evropském a asijském kontinentu. Pozornost je věnována také některým flavivirům přenášeným komáry, zejména viru Zika a viru horečky Západního Nilu. Okrajově jsou studovány rovněž viry čeledí *Coronaviridae*, *Phenuiviridae*, *Rhabdoviridae* a *Herpesviridae*. Hlavní studovanou skupinou inhibitorů výše uvedených virů jsou nukleosidové analogy. Z rozsáhlých studií, které řeší vztah mezi strukturou a antivirovou aktivitou látek, vyplývá, že nejvyšší aktivitu proti flavivirům a současně nejnižší cytotoxicitu vykazují nukleosidy modifikované methylovou skupinou v pozici 2' C nebo 4' C a dále galidesivir, který byl nedávno zařazen do klinických testů pro léčbu infekcí virem Ebola a žluté zimnice. Kromě nukleosidových analogů byly dále studovány inhibitory fúze virionu s hostitelskou buňkou, blokátory vakuolárních ATPáz, nenukleosidové inhibitory virových polymeráz, ligandy interagující s některými sekundárními strukturami virové RNA a řada dalších. Studie se zaměřují nejen na prostý popis antivirové aktivity látek, ale zabývají se též studiem mechanismu účinku pomocí specializovaných metod využívajících rekombinantní virové polymerázy nebo spektroskopické techniky pro studium vazby ligandů na cílové virové makromolekuly. Práce klade značný důraz také studium aktivity inhibitorů ve zvířecích modelech, což poskytuje cenné informace pro navazující (pre)klinické testy. V neposlední řadě je pozornost věnována studiu rezistence na inhibitory virové replikace, analýzu mutací zodpovědných za rezistenci a ověřování biologických vlastností rezistentních virových mutant jak v buněčné kultuře (in vitro), tak v experimentálním zvířeti (in vivo).

PODĚKOVÁNÍ

Rád bych na tomto místě poděkoval zejména Prof. Danielu Růžkovi za cenné rady a připomínky při sepisování tohoto habilitačního spisu, dále za inspirativní dialogy a diskuze během méj vědecké kariéry, vstřícnou podporu při realizaci mých vědeckých projektů a zájmů a v neposlední řadě také za vytvoření tvůrčího a velmi přátelského prostředí v rámci našeho výzkumného týmu.

Můj velký dík patří dále Prof. Janu Kopeckému a Dr. Jindřichu Chmelařovi za to, že mi vyšli vstříc a umožnili mi realizovat výuku na Přírodovědecké fakultě Jihočeské univerzity v Českých Budějovicích. Děkuji také všem, kteří mi umožnili moji pedagogickou činnost na jiných univerzitách, zejména na Masarykově univerzitě v Brně, Mendelově Univerzitě v Brně a Univerzitě Palackého v Olomouci.

Dále děkuji Mgr. Zuzaně Beránkové za ochotu, obětavost a profesionální asistenci při realizaci laboratorního cvičení z Metod mikrobiální diagnostiky na Přírodovědecké fakultě Jihočeské univerzity v Českých Budějovicích. Velký dík patří rovněž všem členům našeho výzkumného týmu a mým bakalářským, magisterským a doktorským studentům, zejména Ing. Michalu Štefánikovi a Mgr. Jiřímu Holoubkovi, za perfektní spolupráci a nadšení, které je tolik nezbytné pro vědeckou práci.

A na závěr děkuji také méj rodině a přítelkyni Janě za podporu, trpělivost a pochopení pro moji fascinaci vědou a vědeckou prací vůbec.

OBSAH

Seznam příložených prací.....	5
1. Úvod	10
2. Charakteristika vybraných medicínsky významných virových patogenů	12
2.1. Čeleď <i>Flaviviridae</i>	12
2.1.1. Flaviviry přenášené klíšťaty	12
2.1.2. Flaviviry přenášené komáry	13
2.2. Čeleď <i>Coronaviridae</i>	15
2.3. Další medicínsky významné viry studované v této habilitační práci	16
3. Přehledové články a knižní kapitoly prezentované v habilitačním spisu	18
Příloha 1.....	20
4. Nukleosidové analogy jako terapeutika závažných virových infekcí	133
Příloha 2.....	141
5. Antivirotika strukturně odlišná od nukleosidů	281
5.1. Inhibitory fúze virionu s hostitelskou buňkou.....	281
5.2. Inhibitory acidifikace buněčných endozomů	282
5.3. Nenukleosidové inhibitory virových polymeráz.....	282
5.4. Ligandy stabilizující guaninové kvadruplexy	283
5.5. Ostatní studované inhibitory virových patogenů.....	284
Příloha 3.....	286
6. Shrnutí	390
7. Použitá literatura.....	391

SEZNAM PŘILOŽENÝCH PRACÍ

1. Ruzek D, Avšič Županc T, Borde J, Chrdle A, **Eyer L**, Karganova G, Kholodilov I, Knap N, Kozlovskaya L, Matveev A, Miller AD, Osolodkin DI, Överby AK, Tikunova N, Tkachev S, Zajkowska J. Tick-borne encephalitis in Europe and Russia: Review of pathogenesis, clinical features, therapy, and vaccines. *Antiviral Res.* 2019 Apr;164:23-51.
Na předloženém review jsem se podílel přípravou kapitoly o inhibitech viru klíšťové encefalitidy a korekcí finálního textu.
2. **Eyer L**, Nencka R, de Clercq E, Seley-Radtke K, Růžek D. Nucleoside analogs as a rich source of antiviral agents active against arthropod-borne flaviviruses. *Antivir Chem Chemother.* 2018 Jan-Dec;26:2040206618761299.
Můj podíl spočíval v navržení konceptu a struktury tohoto review, vyhledání relevantní literatury, sepsání manuskriptu a přípravě obrázků. Jsem korespondenční autor.
3. Thames JE, **Eyer L**, Seley-Radtke K. Small molecule-based inhibitors for treatment of tick-borne encephalitis virus infection: nucleoside analogues and non-nucleoside antivirals. 2022. In: *Medicinal Chemistry of Tick borne encephalitis.* Accepted for publishing.
Moje role v předložené práci spočívala v sepsání manuscriptu, výstavbě struktury článku, vyhledání literatury a přípravy některých obrázků. Dále jsem se podílel na korekci a úpravách finálního textu.
4. **Eyer, L.**, Hruska, K. Antiviral agents targeting the influenza virus: A review and publication analysis. 2013. *Vet Med*, 58: 113-185.
Můj podíl spočíval v navržení konceptu tohoto přehledového článku, sepsání manuskriptu, vyhledání relevantní literatury, provedení analýzy publikací a přípravě obrázků. Jsem korespondenční autor.
5. **Eyer L**, Valdés JJ, Gil VA, Nencka R, Hřebabecký H, Šála M, Salát J, Černý J, Palus M, De Clercq E, Růžek D. Nucleoside inhibitors of tick-borne encephalitis virus. *Antimicrob Agents Chemother.* 2015 Sep;59(9):5483-93.
Na tomto článku jsem se podílel navržením konceptu práce, provedením in vitro experimentů (ověření cytotoxicity a antivirové aktivity inhibitorů), zpracováním dat a sepsáním a korekcí manuscriptu.
6. **Eyer L**, Šmídková M, Nencka R, Neča J, Kastl T, Palus M, De Clercq E, Růžek D. Structure-activity relationships of nucleoside analogues for inhibition of tick-borne encephalitis virus. *Antiviral Res.* 2016 Sep;133:119-29.
Kromě návrhu koncepce práce jsem se na článku podílel provedením většiny in vitro experimentů, zpracováním dat a sepsáním a korekcí manuscriptu.
7. **Eyer L**, Nencka R, Huvarová I, Palus M, Joao Alves M, Gould EA, De Clercq E, Růžek D. Nucleoside Inhibitors of Zika Virus. *J Infect Dis.* 2016 Sep 1;214(5):707-11.
Provedl jsem veškeré experimenty, které jsou součástí práce, zpracoval data a sepsal manuscript.

8. **Eyer L**, Fojtíková M, Nencka R, Rudolf I, Hubálek Z, Ruzek D. Viral RNA-Dependent RNA Polymerase Inhibitor 7-Deaza-2'-C-Methyladenosine Prevents Death in a Mouse Model of West Nile Virus Infection. *Antimicrob Agents Chemother.* 2019 Feb 26;63(3):e02093-18.
Můj podíl na tomto článku spočíval v návrhu konceptu studie, provedení některých experimentů (zejména in vivo studie), vedení mladších kolegů v rámci mentorování, zpracování dat a sepsání a korekci manuscriptu.
9. **Eyer L**, Kondo H, Zouharova D, Hirano M, Valdés JJ, Muto M, Kastl T, Kobayashi S, Haviernik J, Igarashi M, Kariwa H, Vaculovicova M, Cerny J, Kizek R, Kröger A, Lienenklaus S, Dejmek M, Nencka R, Palus M, Salat J, De Clercq E, Yoshii K, Ruzek D. Escape of Tick-Borne Flavivirus from 2'-C-Methylated Nucleoside Antivirals Is Mediated by a Single Conservative Mutation in NS5 That Has a Dramatic Effect on Viral Fitness. *J Virol.* 2017 Oct 13;91(21):e01028-17.
Moje role spočívala v návrhu konceptu práce, provedení většiny klíčových experimentů (zejména selekce rezistentních mutant, analýza genotypu a fenotypu mutant, in vivo studie na myším modelu), zpracování mnou získaných dat a sepsání a korekci manuscriptu.
10. **Eyer L**, Zouharová D, Širmarová J, Fojtíková M, Štefánik M, Haviernik J, Nencka R, de Clercq E, Růžek D. Antiviral activity of the adenosine analogue BCX4430 against West Nile virus and tick-borne flaviviruses. *Antiviral Res.* 2017 Jun;142:63-67.
Kromě návrhu konceptu práce spočívala moje role v mentorování mladších kolegů a studentů (v rámci in vitro antivirových studií), zpracování dat a sepsání a korekci manuscriptu.
11. **Eyer L**, Nougairède A, Uhlířová M, Driouich JS, Zouharová D, Valdés JJ, Haviernik J, Gould EA, De Clercq E, de Lamballerie X, Ruzek D. An E460D Substitution in the NS5 Protein of Tick-Borne Encephalitis Virus Confers Resistance to the Inhibitor Galidesivir (BCX4430) and Also Attenuates the Virus for Mice. *J Virol.* 2019 Jul 30;93(16):e00367-19.
Moje role spočívala v návrhu konceptu práce, mentorování studentů (zejména v rámci detailní analýzy antivirové aktivity látky a jejího mechanismu účinku), provedení některých experimentů (zejména selekce rezistentních mutant, analýza genotypu a fenotypu mutant, in vivo studie na myším modelu), zpracování dat a sepsání a korekci manuscriptu. V rámci této studie jsem se také zúčastnil pracovní stáže na Faculte de medecine, Emergence des pathologies virales, Marseille, kde jsem byl vyškolen v technologii přípravy a využití reverzně-genetického systému pro studium rezistence virů k antivirotikům.
12. Krol E, Wandzik I, Brzuska G, **Eyer L**, Růžek D, Szewczyk B. Antiviral Activity of Uridine Derivatives of 2-Deoxy Sugars against Tick-Borne Encephalitis Virus. *Molecules.* 2019 Mar 21;24(6):1129.
Podílel jsem se na mentoringu zahraničních kolegů v naší laboratoři při provádění experimentů a na sepsání a korekci manuscriptu.

13. **Eyer L**, Svoboda P, Balvan J, Vičar T, Raudenská M, Štefánik M, Haviernik J, Huvarová I, Straková P, Rudolf I, Hubálek Z, Seley-Radtke K, de Clercq E, Růžek D. Broad-Spectrum Antiviral Activity of 3'-Deoxy-3'-Fluoroadenosine against Emerging Flaviviruses. *Antimicrob Agents Chemother*. 2021 Jan 20;65(2):e01522-20.
Kromě návrhu konceptu práce spočívala moje role v mentorování mladších kolegů a studentů (zejména v rámci biologických testů pro ověření antivirové aktivity a toxicity studovaných nukleosidů), provedení náročnějších experimentů (zejména in vivo studie na myším modelu), komunikaci se spolupracujícími pracovišti, zpracování dat a sepsání a korekci manuscriptu.
14. Milisavljevic N, Konkolová E, Kozák J, Hodek J, Veselovská L, Sýkorová V, Čížek K, Pohl R, **Eyer L**, Svoboda P, Růžek D, Weber J, Nencka R, Bouřa E, Hocek M. Antiviral Activity of 7-Substituted 7-Deazapurine Ribonucleosides, Monophosphate Prodrugs, and Triphosphates against Emerging RNA Viruses. *ACS Infect Dis*. 2021 Feb 12;7(2):471-478.
Moje role spočívala v provedení in vitro testování látek na viru klíšťové encefalitidy, viru Zika a viru západonilské horečky, zpracování mnou získaných dat a sepsání relevantní části manuscriptu.
15. Haviernik J, **Eyer L**, Yoshii K, Kobayashi S, Cerny J, Nougairède A, Driouich JS, Volf J, Palus M, de Lamballerie X, Gould EA, Ruzek D. Development and characterization of recombinant tick-borne encephalitis virus expressing mCherry reporter protein: A new tool for high-throughput screening of antiviral compounds, and neutralizing antibody assays. *Antiviral Res*. 2021 Jan;185:104968.
Na této práci jsem se podílel provedením některých in vitro experimentů, mentorování mladších kolegů (práce s reverzně-genetickými a reportérovými systémy) a sepsáním a korekcí manuscriptu. V rámci této studie jsem se zúčastnil pracovní stáže na Graduate School of Veterinary Medicine, Laboratory of public health, Sapporo, kde jsem byl vyškolen v technologii přípravy a využití reportérových virových systémů.
16. Zouharova D, Lipenska I, Fojtikova M, Kulich P, Neca J, Slany M, Kovarcik K, Turanek-Knotigova P, Hubatka F, Celechovska H, Masek J, Koudelka S, Prochazka L, **Eyer L**, Plockova J, Bartheldyova E, Miller AD, Ruzek D, Raska M, Janeba Z, Turanek J. Antiviral activities of 2,6-diaminopurine-based acyclic nucleoside phosphonates against herpesviruses: In vitro study results with pseudorabies virus (PrV, SuHV-1). *Vet Microbiol*. 2016 Feb 29;184:84-93.
Můj podíl na této studii spočíval v provedení některých in vitro experimentů (zavedení metodiky pro testování látek na PrV), mentorování mladších kolegů a studentů a sepsání a korekci manuscriptu.
17. Haviernik J, Štefánik M, Fojtíková M, Kali S, Tordo N, Rudolf I, Hubálek Z, **Eyer L**, Ruzek D. Arbidol (Umifenovir): A Broad-Spectrum Antiviral Drug That Inhibits Medically Important Arthropod-Borne Flaviviruses. *Viruses*. 2018 Apr 10;10(4):184.
Moje role spočívala v návrhu konceptu celé studie, provedení některých in vivo experimentů, mentorování mladších kolegů (zejména v rámci zavedení a využití testů pro studium biologické aktivity látek, imunofluorescenčního barvení atd.), zpracování získaných dat a sepsání a korekci manuscriptu. Jsem sdíleným korespondenčním autorem.

18. Stefanik M, Strakova P, Haviernik J, Miller AD, Ruzek D, **Eyer L**. Antiviral Activity of Vacuolar ATPase Blocker Diphyllin against SARS-CoV-2. *Microorganisms*. 2021 Feb 25;9(3):471.
Na této studii jsem se podílel návrhem celkového konceptu práce a struktury experimentů, mentorování mladších kolegů a studentů, zpracováním získaných dat a přípravou a korekcí manuscriptu. Jsem korespondenční autor.
19. Štefánik M, Bhosale DS, Haviernik J, Straková P, Fojtíková M, Dufková L, Huvarová I, Salát J, Bartáček J, Svoboda J, Sedlák M, Růžek D, Miller AD, **Eyer L**. Diphyllin Shows a Broad-Spectrum Antiviral Activity against Multiple Medically Important Enveloped RNA and DNA Viruses. *Viruses*. 2022 Feb 9;14(2):354.
Můj podíl na této studii spočíval v návrhu celkového konceptu práce a struktury experimentů, mentorování mladších kolegů a studentů (zejména v rámci in vitro studií a specializovaných testů pro analýzu mechanismu účinku antivirových látek), zpracováním získaných dat a přípravou a korekcí manuscriptu. Jsem korespondenční autor.
20. Konkolova E, Krejčová K, **Eyer L**, Hodek J, Zgarbová M, Fořtová A, Jirasek M, Teply F, Reyes-Gutierrez PE, Růžek D, Weber J, Boura E. A Helquat-like Compound as a Potent Inhibitor of Flaviviral and Coronaviral Polymerases. *Molecules*. 2022 Mar 15;27(6):1894.
Na této práci jsem se podílel provedením některých klíčových experimentů (zejména testováním látky s využitím viru klíšťové encefalitidy in vitro a také in vivo na myším modelu), dále analýzou mnou získaných dat a sepsáním relevantní části manuscriptu. Dále jsem se podílel na korekci manuscriptu po revizi.
21. Dejmek M, Konkol'ová E, **Eyer L**, Straková P, Svoboda P, Šála M, Krejčová K, Růžek D, Boura E, Nencka R. Non-Nucleotide RNA-Dependent RNA Polymerase Inhibitor That Blocks SARS-CoV-2 Replication. *Viruses*. 2021 Aug 11;13(8):1585.
Moje role spočívala v provedení klíčových experimentů s infekčním virem, mentorování mladších kolegů a studentů (zejména v rámci využití in vitro technik pro analýzu antivirové aktivity látek), zpracování dat a sepsání a korekci manuscriptu.
22. Holoubek J, Bednářová K, Haviernik J, Huvarová I, Dvořáková Z, Černý J, Outlák M, Salát J, Konkol'ová E, Boura E, Růžek D, Vorlíčková M, **Eyer L**, Renčuk D. Guanine quadruplexes in the RNA genome of the tick-borne encephalitis virus: their role as a new antiviral target and in virus biology. *Nucleic Acids Res*. 2022 May 6;50(8):4574-4600.
Na této rozsáhlé studii jsem se podílel návrhem konceptu práce, zejména jeho virologické části, provedením některých klíčových in vitro experimentů (zejména testování antivirové aktivity a cytotoxicity G4 ligandů), mentorování mladších kolegů a studentů (zejména v rámci přípravy virových mutant s pozměněnými sekvencemi genomu, které mají schopnost tvořit G4), analýzou a zpracováním biologických dat, přípravou a korekcí virologické části manuscriptu. Jsem sdílený korespondenční autor.

23. Stefanik M, Valdes JJ, Ezebuo FC, Haviernik J, Uzochukwu IC, Fojtikova M, Salat J, **Eyer L**, Ruzek D. FDA-Approved Drugs Efavirenz, Tipranavir, and Dasabuvir Inhibit Replication of Multiple Flaviviruses in Vero Cells. *Microorganisms*. 2020 Apr 20;8(4):599.

Moje role spočívala v návrhu konceptu práce, mentorování mladších kolegů (zejména v rámci testování látek proti flavivirům in vitro), zpracování získaných dat a sepsání a korekci manuscriptu.

1. Úvod

Infekční onemocnění provázejí lidstvo odnepaměti. Ze starověkých spisů se dovídáme o dávných epidemiích, které udeřily nečekaně jako morové rány a zanechávaly za sebou smrt. Stopy po těžkých infekčních chorobách nalézají archeologové a antropologové na kosterních pozůstatcích i mumifikovaných tělesných ostatcích starých tisíce let. Dnes víme, že epidemie ve starověku a středověku souvisely kromě jiného s pohybem lidských mas, zejména vojsk během válečných událostí a civilního obyvatelstva při cestách za obchodem, dále při osídlování nových území a v neposlední řadě byly šířeny kočovnými barbarskými kmeny. V novověku měly infekční choroby šířené evropskými objeviteli a kolonizátory za následek téměř úplné vyhlazení některých etnik na americkém kontinentu i v jiných nově objevených zemích. I když zlepšení hygienických podmínek v rozrůstajících se městech výrazným způsobem omezilo šíření infekčních chorob, četným epidemiím a pandemiím čelilo lidstvo i nadále. Ve 20. století, během let 1918 – 1920, proběhla pandemie tzv. španělské chřipky, která si vyžádala 20 milionů lidských životů, tedy více než celkový počet obětí během 1. světové války. Epidemie chřipky přicházely během 20. století opakovaně, jako tzv. asijská, hong-kongská nebo ruská chřipka. V 80. letech 20. století pronikl do lidské populace virus HIV a koncem 20. století se stává HIV infekce infekcí pandemickou. Značné ztráty na životech si vyžádaly rovněž nákazy vyvolané viry žloutenky typu B a C a komárem přenášenými flaviviry, jako je virus žluté zimnice a virus Dengue (Doherty, 2013).

V posledních 2 dekadách jsme byli svědky několika rozsáhlých epidemií nebo pandemií, jejichž původci jsou koronavirus těžkého akutního respiračního syndromu (SARS-CoV) v r. 2002, virus prasečí chřipky v r. 2009, koronavirus respiračního syndromu z Blízkého východu (MERS-CoV) v r. 2012, virus Ebola v r. 2013 a virus Zika v r. 2015. V r. 2019 propukla pandemie onemocnění COVID-19, jejímž původcem je SARS-CoV-2 a která si dosud vyžádala více než 6 milionů životů (Nihala et al., 2021). V dnešním světě připisujeme šíření emergentních a re-emergentních infekcí globalizačním vlivům, převážně rozvoji letecké dopravy a s ní souvisejícímu masivnímu a extrémně rychlému pohybu lidí napříč kontinenty, rychlým a výrazným klimatickým změnám, které mají za následek šíření vektorů na nová území, ústup přirozených biotopů a výskyt divokých druhů a jejich patogenů, původně izolovaných od lidí, v blízkosti lidských sídel (Takane et al., 2022).

Vakcinace a antivirová terapie jsou v současnosti dva dostupné přístupy, jak bojovat se závažnými virovými (a samozřejmě i bakteriálními) infekcemi a předcházet tak ztrátám na životech i ztrátám ekonomickým. Zatímco vakcinace je preventivní (profylaktické) opatření, bránící vzniku a rozvoji onemocnění, antivirová terapie si klade za cíl eliminovat již manifestovanou infekci, případně zmírnit či zcela eliminovat její klinické symptomy. Klasické očkovací látky (vakcíny), využívající usmrcené nebo živé (avšak oslabené, atenuované) viry, případně jejich rekombinantní proteiny jsou dnes k dispozici proti celé řadě virových onemocnění, jako je klíšťová encefalitida, vzteklina, dětská obrna, žloutenka typu B a mnoho dalších (Monto, 2006). Setkáváme se však i s modernějšími typy vakcín, např. s mRNA vakcínami nebo vakcínami využívající adenovirové vektory, které našly svoje uplatnění zejména v boji s pandemií SARS-CoV-2 (Kis et al., 2022).

První terapeutikum s antivirovým účinkem, idoxuridin, bylo legislativně schváleno pro klinické použití na počátku 60. let 20. století (De Clercq et Guangdi, 2016). Od té doby úspěšně

prošlo klinickými zkouškami přes 90 antivirových terapeutik, které jsou dnes využívány pro léčbu závažných virových onemocnění člověka, jako jsou infekce virem HIV, virem hepatitidy B, virem hepatitidy C, herpetickými viry, viry chřipky, lidským cytomegalovirem a virem varicella-zoster. Dále existují schválená antivirotika proti infekci respiračním syncytiálním virem a proti povrchovým anogenitálním bradavicím způsobených lidským papillomavirem. Dostupná antivirotika lze dle jejich mechanismu účinku rozdělit do 13 funkčních skupin, pro představu uveďme alespoň některé hlavní skupiny: nukleosidové analogy, nenukleosidové inhibitory reverzní transkriptázy, inhibitory virových proteáz, inhibitory integrázy HIV, inhibitory polymerázy HCV, inhibitory viru chřipky nebo různé imunostimulátory, interferony a oligonukleotidová antivirotika (De Clercq et Guangdi, 2016). Proti současným emergentním virovým nákazám, jako jsou infekce způsobené flaviviry, filoviry nebo koronaviry, však nejsou k dispozici žádná legislativně schválená antivirová terapeutika, nebo jich existuje pouze velmi omezený počet. Některá antivirotika jsou dnes dosud ve fázi klinických testů, např. galidesivir pro léčbu infekce virem Ebola nebo virem žluté zimnice (Warren et al., 2014; Taylor et al., 2016). Pro léčbu onemocnění COVID-19 je jediným lékem schváleným agenturou Food and Drug Administration (FDA) remdesivir. Další preparáty jako Paxlovid (kombinace ritonaviru a nirmatrelviru), molnupiravir a některé monoklonální protilátky obdržely povolení pouze k nouzovému použití pro léčbu COVID-19 (<https://www.covid19treatmentguidelines.nih.gov>). Proto patří vývoj nových, specifických a účinných inhibitorů s antivirovou aktivitou mezi významné priority medicínského výzkumu.

Předložený habilitační spis se zabývá studiem antivirové aktivity nově objevených inhibitorů medicínsky významných virových patogenů, zejména zástupců rodu *Flavivirus*, čeledi *Flaviviridae*. Následující kapitola je proto primárně věnována charakteristice flavivirů přenášených členovci. Největší pozornost se soustřeďuje na virus klíšťové encefalitidy (VKE), který představuje hlavní výzkumný objekt této práce a kterým se podrobně zabývají prezentované autorské publikace. Dále jsou stručně popsány také virus Zika a virus horečky západního Nilu, neboť byly v příložených pracích rovněž studovány. Ostatní uvedení zástupci čeledi *Flaviviridae* (tj. virus Dengue, virus žluté zimnice a virus japonské encefalitidy) jsou pouze krátce zmíněni, protože se jejich výzkumem tato habilitační práce nezabývá, ale bez jejich charakteristiky by nebyl výčet medicínsky významných flavivirů kompletní. Protože některé studie prezentované v tomto habilitačním spisu byly prováděny také s využitím významných zástupců čeledi *Coronaviridae*, je věnována pozornost i těmto virům, zejména pak viru SARS-CoV-2. Na závěr jsou zmíněni a stručně popsáni také zástupci jiných virových čeledí, které byly rovněž okrajově studovány, např. virus horečky údolí Rift (*Phenuiviridae*), virus vztekliny (*Rhabdoviridae*) a některé viry z čeledi *Herpesviridae*, jako virus herpes simplex typu 1 (HSV-1) a virus Aujezskyho choroby.

2. CHARAKTERISTIKA VYBRANÝCH MEDICÍNSKY VÝZNAMNÝCH VIROVÝCH PATOGENŮ

2.1. ČELEĎ FLAVIVIRIDAE

Rod Flavivirus patří do čeledi *Flaviviridae* a zahrnuje více než 70 druhů virů, které jsou řazeny mezi arboviry, tedy mezi viry, které jsou přenášeny krev sajícími členovci. Zástupci čeledi *Flaviviridae* vyvolávají závažná onemocnění u člověka, která se projevují širokým spektrem klinických příznaků od relativně mírných (teplota, bolest kloubů) až po vážné viscerotropní symptomy (např. horečka Dengue a žlutá zimnice), hemoragické horečky (např. horečka kyassanurského lesa, omská hemoragická horečka), encefalitidy/myelitidy (např. klíšťová encefalitida, západonilská horečka, japonská encefalitida) a neuropatické nebo teratogenní změny (infekce virem Zika) (Baier, 2011). Přestože je ročně v celosvětovém měřítku hlášeno více než 200 milionů klinických případů flavivirových infekcí, které jsou v mnoha případech smrtelné, nejsou v současné době pro léčbu flavivirových infekcí k dispozici žádná schválená antivirová terapeutika (Deval et al., 2014). Zástupce čeledi *Flaviviridae* lze rozdělit do tří skupin dle způsobu přenosu na viry přenášené klíšťaty, viry přenášené komáry a viry bez známého vektoru (Baier, 2011).

2.1.1. FLAVIVIRY PŘENÁŠENÉ KLÍŠŤATY

Na eurasijském kontinentu představuje hlavní medicínský problém zejména klíšťová encefalitida s více než 13 000 případy ročně (Heinz a Mandel, 1993). V České Republice se incidence této závažné neuroinfekce pohybuje kolem 450 až 750 případů za rok, což je nevyšší incidence v rámci střední Evropy (Mickiene a kol. 2002). Původcem tohoto onemocnění je VKE, který byl poprvé popsán v r. 1937 ruskými vědci (Zilber, 1939). Na území naší republiky byly případy klíšťové encefalitidy poprvé dokumentovány v r. 1948 (Růžek et al., 2019).

Viriony viru klíšťové encefalitidy (VKE) jsou kulovitěho tvaru o průměru cca 50 nm (Füzik et al., 2018). Obsahují jednu lineární molekulu +ssRNA o velikosti cca 11 kb, která je opatřena na 3' konci čepičkou (m7G) a na 5' konci není polyadenylována. Na 3'a 5' koncích genomu jsou přítomny nepřekládané oblasti („untranslated regions“, UTR), které mají regulační funkce. Genom viru klíšťové encefalitidy je tvořen jediným otevřeným čtecím rámcem (ORF) kódujícím jeden polyprotein, který je ko- a post-translačně štěpen pomocí virových a hostitelských proteáz na 7 nestrukturních (NS1, NS2A, NS2B, NS3, NS4A, NS4B, and NS5) a 3 strukturní (C, prM, and E) proteiny (Chambers et al., 1990).

Infekce VKE je zahájena adsorpcí virionu k buněčným receptorům, dále následuje receptorem zprostředkovaná endocytóza a fúze virového obalu s membránou endozomu. Fúze je závislá na sníženém pH v lumenu endozomu a je zprostředkována fúzogenními proteiny E na povrchu virionů. Po uvolnění virové genomové RNA do cytosolu se virový genom replikuje, přičemž se syntetizuje negativní řetězec RNA (anti-sense RNA, -ssRNA), který slouží jako templát pro produkci genomové +ssRNA. Replikace virové genomové RNA, sestavení infekčních virionů a maturace virionu nastávají v přímém kontaktu s endoplazmatickým retikulem a Golgiho komplexem. Proces maturace je spojen s proteolytickým štěpením a restrukturalizací povrchových proteinů prM a E za vzniku aktivního fúzogenního komplexu. Nakonec jsou zralé virové částice transportovány v cytoplazmatických váčcích z Golgiho komplexu, a jsou uvolněny z hostitelské buňky exocytózou (Růžek et al., 2019).

Na základě rozdílů v sekvenci genu pro protein E rozlišujeme tři subtypy VKE - evropský, sibiřský a dálnovýchodní subtyp. Infekce VKE se přenáší dvěma různými cestami: (i) sáním klíštěte infikovaného VKE (*Ixodes ricinus* v Evropě a *Ixodes persulcatus* v Rusku), nebo (ii) alimentární cestou konzumací nepasterizovaného mléka a mléčných výrobků od virem infikovaných přežvýkavců (koz, krav a ovcí) (Růžek et al., 2019; Kríz et al., 2009; Gritsun et al., 2003b). V Evropě má infekce evropským subtypem VKE obvykle za následek úmrtnost < 2 %. Celková úmrtnost na klíšťovou encefalitidu v Rusku je asi 2 %, a to navzdory skutečnosti, že sibiřský a dálnovýchodní subtypy VKE jsou popisovány jako původci výrazně závažnější formy infekce než VKE evropského subtypu (Růžek et al., 2019). Inkubační doba VKE se pohybuje od sedmi do čtrnácti dnů; ve vzácných případech byl nástup příznaků pozorován během tří až čtyř dnů (Růžek et al., 2019; Gritsun et al., 2003a; Yoshii et al., 2019).

Klíšťová encefalitida u lidí je známa jako dvoufázové onemocnění s primárními příznaky podobnými chřipce (horečka, únava, nevolnost, bolest hlavy a bolest celého těla) (Auksé et al., 2002). Ve druhé fázi se onemocnění může rozvinout v meningitidu nebo meningoencefalitidu. Nejzávažnější formou onemocnění je encefalomyelitida, která může být spojena s poškozením centrálního nervového systému. Taková poškození mohou vyústit v trvalé neurologické potíže, paralýzu nebo smrt pacienta (Lindquist et al., 2008; Gritsun et al., 2003a). Postencefalitický syndrom se rozvíjí u 40–50 % pacientů s VKE, který se projevuje dlouho přetrvávajícími následky, které významně ovlivňují kvalitu života. V současné době jsou k dispozici vakcíny pro prevenci klíšťové encefalitidy, nicméně neexistuje účinná schválená terapie (Majerus, et al., 2009; Haglund et al., 2003; Bogovič et al., 2018).

K dalším zástupcům klíšťaty přenášených flavivirů patří virus vrtivky (skotské encefalitidy) s výskytem převážně na Britských ostrovech. Vektorem tohoto viru je klíště *I. ricinus*. Virus je původcem horečnatých onemocnění některých ptáků a savců, zejména ovcí a skotu, a někdy mívá podobu fatální encefalitidy. K infekci člověka dochází vzácně a ve většině případů je infekce zcela benigní (Jeffries et al., 2014). Virus Langat, izolovaný v Jihovýchodní Asii, nevyvolává u člověka závažná onemocnění a vzhledem k antigenní podobnosti s VKE byl testován jako živá vakcína proti VKE. Virus Powassan je endemický v Severní Americe a Rusku. Na americkém kontinentu je přenášen klíšťay *I. cookei* a *I. scapularis*. V Rusku pak zejména klíšťaty *I. persulcatus* a některými zástupci rodů *Haemophysalis* a *Dermacentor*. Pravděpodobnost nákazy člověka je nízká, v některých případech se však může vyvinout v život ohrožující encefalitidu s vysokou úmrtností (Ebel, 2010). Mezi ostatní flaviviry přenášené klíšťaty dále náleží virus horečky kyassanurského lesa (Holbrook, 2012), virus Alkhurma (Flint et al., 2014) a virus omské hemoragické horečky (Růžek et al., 2010). Všechny tři uvedené viry se vyskytují na asijském kontinentu, jsou patogenní pro člověka a způsobují závažná horečnatá onemocnění, provázená bolestmi hlavy a hemoragickými projevy.

2.1.2. FLAVIVIRY PŘENÁŠENÉ KOMÁRY

Infekce virem Zika jsou v Africe a Asii známé již od 40. let 20. století. Po dlouhá desetiletí byl tento virus opomíjeným flavivirem přenášeným komáry *Aedes aegypti* nebo *Aedes albopictus*. Virus byl spojován s benigními infekcemi u lidí s běžnými příznaky, které zahrnují horečku, vyrážku, bolesti kloubů a konjunktivitidu. Onemocnění bylo obvykle mírné, trvající pouze několik dní. Situace se však výrazně změnila, když během let 2015 a 2016 virus způsobil

propuknutí epidemie v Oceánii a následně se rozšířil do Brazílie. Během několika následujících měsíců byly ve většině zemí Latinské Ameriky a Karibiku monitorovány četné případy lokálního přenosu viru (Lazear et al., 2016; Mlakar et al., 2016; Broutet et al., 2016). Dnes existují přímé důkazy, že virus Zika může způsobovat velmi závažné vrozené vady mozku (mikrocefalii) (Mlakar et al., 2016) a neurologické poruchy u dospělých, včetně tzv. Guillain-Barrého syndromu, meningoencefalitidy a myelitidy (Carteaux et al., 2016; Mécharles et al., 2016; Roth et al., 2014). Dne 1. února 2016 proto vyhlásila Světová zdravotnická organizace (WHO) krizovou situaci mezinárodního významu v oblasti veřejného zdraví týkající se zvýšené incidence výskytu vrozených neurologických poruch spojených s rychlým šířením viru Zika v Oceánii a Americe. V současnosti neexistuje ani očkování, ani specifická antivirová terapie proti infekci způsobené tímto virem (Lazear et al., 2016).

Virus horečky západního Nilu patří mezi další medicínsky významné emergentní flaviviry přenášené komáry. V přírodě virus cirkuluje v rámci enzootického přenosového cyklu mezi ptáky jako rezervoáry a komáry rodu *Culex*, kteří jsou hlavními vektory viru (Hubálek et al., 2000). Poprvé byl virus horečky Západního Nilu izolován v Africe v roce 1937 (Smithburn et al., 1940). Později působil ohniska infekcí v Evropě, na Středním východě a v některých částech Asie a Austrálie. Po té, co se virus v roce 1999 poprvé objevil v USA, došlo k jeho rychlému rozšíření po Severní Americe. Následně virus pronikl do Mexika, Jižní Ameriky a Karibiku (Komar et al., 2006; Mostashari et al., 1999). Infekce virem horečky Západního Nilu je často bezpříznaková, ale u 20 % až 40 % infikovaných jedinců se může rozvinout onemocnění, které se projevuje horečnatými stavy a které může přejít v letální encefalitidu. V takovém případě se mohou vyvinout charakteristické příznaky jako kognitivní dysfunkce a akutní paralýzy (Lim et al., 2011; Chowers et al., 2001). V roce 2017 bylo celkově v USA hlášeno 2 002 případů onemocnění infekcí virem Západního Nilu, z nichž 67 % bylo klasifikováno jako neuroinvasivní meningitida nebo encefalitida a 33 % jako infekce bez neuroinvasivních příznaků ([https://www.cdc.gov/západní Nile](https://www.cdc.gov/západní%20Nile)). Podobně jako v případě viru Zika, ani proti viru horečky Západního Nilu neexistuje vakcína ani terapeutikum.

Dalším významným komáry přenášeným flavivirem je virus Dengue. V současné době je tento virus endemický ve 112 zemí, a to zejména v tropických oblastech amerického, afrického, asijského a australského kontinentu. Ročně se vyskytne přibližně 100 milionů případů horečky Dengue, přičemž půl milionu případů je doprovázeno hemoragickými projevy. V asijských zemích je průměrná úmrtnost na toto onemocnění 0,5–3,5 %. Virus Dengue zahrnuje 4 sérotypy, vzhledem k čemuž je vývoj univerzální vakcíny značně problematický a očkování proti tomuto onemocnění není stále k dispozici (Malavice et al., 2004).

Kromě horečky Dengue je jednou z nejzávažnějších flavivirových infekcí žlutá zimnice, onemocnění s ohnisky výskytu hlavně v Africe a Jižní Americe a s každoroční incidencí přibližně 80 000 - 200 000 případů, přičemž cca 60 000 případů ročně je smrtelných. Předpokládá se, že virus žluté zimnice pochází z Afriky, avšak před 400 lety se rozšířil do Severní a Jižní Ameriky díky obchodu s otroky a způsobil řadu závažných epidemií v mnoha amerických městech. Proti žluté zimnici existuje účinná vakcinace, nicméně celosvětová proočkovanost zůstává stále nízká (Gardner and Ryman, 2010).

Jako dalšího důležitého zástupce komáry přenášených flavivirů uvedme virus japonské encefalitidy. Toto závažné onemocnění se vyskytuje zejména v Asii, a to převážně v zemích

západního Pacifiku a v severní Austrálii, kde je ročně hlášeno přibližně 70 000 případů, s úmrtností 20 až 30 %. Neurologické nebo psychiatrické následky byly pozorovány u 30 až 50 % přeživších. Vakcíny proti viru japonské encefalitidy jsou založené na živém atenuovaném nebo formaldehydem inaktivovaném viru (Kumar et al., 2022).

Jako posledního komáry přenášeného zástupce čeledi Flaviviridae zmiňujeme virus Usutu, který byl poprvé izolován v Jižní Africe v roce 1959. Virus cirkuluje v prostředí prostřednictvím typického enzootického cyklu zahrnujícího komáry (nejčastěji rodu *Culex*, vzácněji také *Aedes*, *Anopheles* nebo *Mansonia*) a ptáky. Během minulých dvou dekád se virus rozšířil po evropském kontinentu, což vedlo k významnému úhynu ptáků a ke zvýšené četnosti ptačích infekcí zaznamenaných v celé Evropě během několika posledních let. Infekce virem Usutu u lidí jsou většinou asymptomatické nebo vyvolávají pouze mírné klinické příznaky. Bylo však evidováno několik případů neurologických komplikací (encefalitida nebo meningoencefalitida) (Clé et al., 2019).

Závěrem dodejme, že ke globálnímu rozšíření komáry přenášených flavivirů přispívá nekontrolovatelný růst lidské populace, neplánovaná a nekontrolovaná urbanizace a nedostatečné nakládání s odpadními vodami, což vede ke zvýšenému výskytu a hustotě komářích vektorů.

2.2. ČELEĎ CORONAVIRIDAE

Zástupci čeledi *Coronaviridae* jsou obalené viry s genomem tvořeným +ssRNA o velikosti přibližně 30 kb, které běžně způsobují mírné, ale občas i závažné komunitní akutní respirační infekce u lidí. Působí také rozmanité onemocnění u zvířat a je známo, že některé koronaviry pronikly do lidské populace ze zvířecích rezervoárů (Cui et al., 2019). Koronaviry jsou klasifikovány do čtyř rodů: Alpha-, Beta, Gamma- a Deltacoronavirus. Zatímco gamakoronaviry a deltakoronaviry jsou schopny infikovat pouze zvířecí hostitele (většinou ptáky), alfakoronaviry a betakoronaviry zahrnují četné savčí a lidské patogeny (Monchatre-Leroy et al., 2017; Chen et al., 2020). Medicínsky významnými alfakoronaviry jsou lidské koronaviry (HCoV) 229E a NL63, kočičí koronavirus (FIPV, původce infekční peritonitidy koček) a prasečí koronavirus (PEDV, původce průjmových onemocnění u prasat). Naproti tomu betakoronaviry zahrnují původce infekcí u člověka, jako např. HCoV-OC43, HCoV-HKU1, dále SARS-CoV a SARS-CoV-2, MERS-CoV a řadu zvířecích patogenů. Zatímco koronaviry, které přetrvávají v lidské populaci po dlouhou dobu (např. HCoV-229E, HCoV-NL63, HCoV-OC43 a HCoVHKU1), způsobují mírnější onemocnění horních cest dýchacích, emergentní koronaviry SARS-CoV, SARS-CoV-2 a MERS-CoV jsou vysoce patogenní viry způsobující závažná onemocnění dolních dýchacích cest, které může progradovat do život ohrožující pneumonie s vysokou úmrtností (De Wit et al., 2016; Zumla et al., 2016). SARS-CoV je zodpovědný za pandemii v letech 2002 – 2004. Virus má původ v Číně, avšak rozšířil se do 30 zemí, kde působil závažné pneumonické stavy s úmrtností až 11%. MERS-CoV se poprvé objevil v Saúdské Arábii v roce 2012 a od té doby je na celosvětové úrovni považován za významný lidský respirační patogen. Rezervoárem MERS-CoV je velbloud. Z celkového počtu 2 519 nakažených zemřelo 34.3% (Nihala et al., 2021).

SARS-CoV-2 je původcem onemocnění COVID-19. Virus byl poprvé izolován z respiračního traktu pacientů s pneumonií v čínském Wu-chanu koncem prosince 2019, poté

se virus během několika měsíců rozšířil do mnoha dalších zemí po celém světě (Tu et al., 2020) V důsledku toho 11. března 2020 WHO deklarovala COVID-19 jako nové pandemické onemocnění. K 15. červenci 2022 bylo celosvětově potvrzeno více než 535 milionů případů COVID-19, včetně více než šest milionů úmrtí (<https://covid19.who.int/>). SARS-CoV-2 je respirační virus, který se obvykle přenáší z člověka na člověka prostřednictvím respiračních kapének, i když přenos kontaminovaným povrchem je také vysoce pravděpodobný (Huang et al., 2019). Klinický průběh COVID-19 může být velmi rozmanitý. Infekce může být asymptomatická nebo relativně mírná, jindy je doprovázená horečkou, kašlem, dušností a bolestmi svalů. V některých případech však, zejména u starších pacientů a u pacientů se srdečními a respiračními poruchami, může infekce SARS-CoV-2 progradovat v závažný a život ohrožující syndrom akutní respirační tísně (ARDS) nebo pneumonii vedoucí až k sepsi, dysfunkci orgánů a smrti (Paraskevis et al., 2020).

2.3. DALŠÍ MEDICÍNSKY VÝZNAMNÉ VIRY STUDOVANÉ V TÉTO HABILITAČNÍ PRÁCI

K dalším zástupcům RNA virů, které jsou v této práci studovány v souvislosti s citlivostí na antivirotika je virus horečky údolí Rift. Je to obalený virus, zástupce čeledi *Phenuiviridae*, jehož genomem jsou tři segmenty -ssRNA, která kóduje 7 proteinů. Virus je původcem onemocnění, které se nejčastěji vyskytuje u domestikovaných zvířat v subsaharské Africe (u skotu, buvolů, ovcí, koz a velbloudů). Lidé se mohou nakazit kontaktem s krví, tělesnými tekutinami nebo tkáněmi infikovaných zvířat nebo kousnutím infikovanými komáry. Šíření z člověka na člověka nebylo prokázáno. Ačkoli tento virus často způsobuje závažné onemocnění u zvířat, většina infikovaných lidí buď nevykazuje žádné příznaky, nebo se u nich projeví mírné onemocnění s horečkou, slabostí, bolestmi zad a závratí. U 8–10 % infikovaných se však rozvinou mnohem závažnější příznaky, včetně očních onemocnění, krvácení a encefalitidy (Boshra et al., 2011).

Virus vztekliny je zástupcem čeledi *Rhabdoviridae*. Je to obalený virus, jehož genomem je nesegmentovaná negativní -ssRNA, která kóduje 5 proteinů. Vzteklyna je onemocnění, které se nejčastěji přenáší kousnutím nakaženým zvířetem. Ve střední a východní Evropě bylo za posledních 35 let evidováno 200 případů u lidí a více než 200 000 případů u volně žijících a domácích zvířat (zdroj: <http://www.who-rabies-bulletin.org>). Česká republika je považována za zemi prostou vzteklyny, ale případy infekce byly hlášeny po kontaktu s infikovanými netopýry (Helesic et al., 2007); navíc je infekce stále přítomna v řadě východoevropských zemí. Virus vztekliny infikuje centrální nervový systém savců, v konečném důsledku způsobuje těžké onemocnění mozku a smrt. (Albertini et al., 2012). Proti viru vztekliny existuje očkování, avšak bylo popsáno pouze velmi málo aktivních látek, které inhibují replikační cyklus viru v hostitelské buňce (Appolinário and Jackson, 2015).

Herpes simplex virus typu 1 (HSV-1, čeleď *Herpesviridae*) je obalený virus, jehož genomem je lineární dsDNA. Běžně se přenáší orálním kontaktem a způsobuje infekci v ústech nebo kolem úst (orální herpes). Může však také způsobit genitální herpes. Proinfikovanost lidské populace je značná. HSV-1 je také neurotropní virus. Může se reaktivovat z neuronů v trigeminálních gangliích, kde perzistuje jako latentní infekce, a dostat se do kůže nebo do centrálního nervového systému prostřednictvím anterográdního transportu. HSV-1 je primárně citlivý na acyklovir a příbuzné nukleosidové analogy, nicméně v současné době již existuje řada acyklovir-rezistentních kmenů (Sehrawat et al., 2018).

Do čeledi *Herpesviridae* patří také virus Aujeszkyho choroby. Jedná se o letální onemocnění pro většinu savců s výjimkou vyšších primátů a člověka. Toto onemocnění způsobuje vážné ekonomické ztráty zejména v chovech prasat, vyskytuje se však také u volně žijící zvěře, zejména divokých prasat. Onemocnění představuje vysokou hrozbu hlavně pro lovecké psy, kteří se mohou dostat do těsného kontaktu s nakaženými kanci. Vakcíny, které jsou nyní k dispozici pro prasata, nejsou pro psy vhodné. Neexistuje ani účinná terapie schválená pro veterinární použití (Zouharová et al., 2016).

3. PŘEHLEDOVÉ ČLÁNKY A KNIŽNÍ KAPITOLY PREZENTOVANÉ V HABILITAČNÍM SPISU

V této části habilitačního spisu jsou prezentovány 3 přehledové články a 1 knižní kapitola shrnující dosavadní poznatky o vývoji antivirových léčiv proti medicínsky významným virům. Tři práce se věnují antivirovým léčivům aktivním proti flavivirům a zejména proti VKE, jedna práce pojednává o dosud popsaných inhibitech viru chřipky. Vzhledem jejich rozsahu a zaměření doplňují a zčásti nahrazují tyto práce teoretický úvod habilitačního spisu.

První práce **„Tick-borne encephalitis in Europe and Russia: Review of pathogenesis, clinical features, therapy, and vaccines“** (Růžek et al., 2019) shrnuje dostupné informace o struktuře a patogenezí VKE a dále pojednává o epidemiologii, klinických projevech a imunologii klíšťové encefalidity jako závažné virové neuroinfekce. V neposlední řadě práce podává aktuální informace o současných možnostech terapie tohoto onemocnění a je doplněna podrobným přehledem experimentálních léčiv, vykazujících silný antivirový účinek proti VKE jak *in vitro*, tak na zvířecím modelu. Práce popisuje také složení a mechanismus účinku legislativně schválených vakcín dostupných v Západní Evropě i na území Ruské federace, které v současné době tvoří hlavní profylaktický přístup v boji proti klíšťové encefalitidě. Na sepsání práce se podílel rozsáhlý autorský kolektiv složený z předních českých i zahraničních odborníků zabývajících se problematikou klíšťové encefalidity.

Práce **„Nucleoside analogs as a rich source of antiviral agents active against arthropod-borne flaviviruses“** (Eyer et al., 2018) sumarizuje současné poznatky o nukleosidech s antivirovou aktivitou působících zejména proti komáry a klíšťaty přenášeným flavivirům (zejména viru Zika, viru horečky Západního Nilu, viru Dengue, VKE a dalších). Pojednává o jednotlivých chemických modifikacích antivirových nukleosidů a doslova prochází molekulou nukleosidu atom po atomu s cílem popsat jednotlivé funkční skupiny a substituenty introdukované do nukleosidového skeletu tak, aby bylo dosaženo maximálního antivirového účinku s minimální cytotoxickou aktivitou. Dále řeší současné problémy a výzvy při použití nukleosidů jako antivirových léčiv, zabývá se otázkou využití profarmak odvozených z nukleosidových analogů, zavedením vhodných zvířecích modelů při ověřování účinku látek, rezistencí k antivirovým léčivům atd. Práce vznikla ve spolupráci s Ústavem organické chemie a biochemie AVČR v Praze a dále s pracovišti Rega Institute for Medical Research, KU Leuven (Lovaň, Belgie) a Department of Chemistry and Biochemistry, University of Maryland (Baltimore, USA).

Další přehledová práce **„Small molecule-based inhibitors as prospective candidates for treatment of tick-borne encephalitis virus infection“** (Thames et al., přijato k publikování) je kapitolou v knižní sérii Annual Reports in Medicinal Chemistry, Elsevier Inc. Kapitola se zabývá výhradně popsanými inhibitory aktivními proti VKE a je rozdělena do dvou částí. První popisuje nukleosidové inhibitory VKE, druhá pojednává o inhibitech strukturně odlišných od nukleosidů (nukleosidových antivirových léčiv), jako jsou látky interagující s proteinem E, inhibitory fúze virionu s endozomy hostitelské buňky interkalující do virové membrány, či ligandy vázající se na virovou RNA a stabilizující guaninové kvadruplexy. Pozornost je věnována také některým inhibitorům hostitelských biochemických procesů esenciálních pro virovou replikaci; takovými jsou např. blokátory acidifikace buněčných endozomů. Práce popisuje také obecné metodologické přístupy a techniky používané při testování knihoven inhibitorů i specializované techniky pro podrobnou charakterizaci jejich mechanismu účinku. Práce vznikla

ve spolupráci s Department of Chemistry and Biochemistry, University of Maryland (Baltimore, USA).

Poslední prezentovaný přehledový článek „***Antiviral agents targeting the influenza virus: a review and publication analysis***“ (Eyer and Hruška, 2013) shrnuje poznatky o inhibitech viru chřipky jako reakce na proběhlé epidemie/pandemie, jejichž původci byly vysoce patogenní chřipkové kmeny. Zaměřuje se na popis designu, syntézy a evaluace nových antivirových látek aktivních proti chřipkovým virům a pojednává o hlavních třídách léčiv v současné době používaných na léčbu chřipky nebo o experimentálních antivirových látkách. Dále diskutuje možnosti kombinační terapie při léčbě chřipky a problémy spojené se vznikem rezistence. Práce zahrnuje také analýzu publikační aktivity na toto téma do roku 2013 (zdroj Web of Science); nevýznamnější publikace jsou prezentovány v tabulkách, které následují za krátkým souhrnným textem. Netradiční formát tohoto přehledového článku umožňuje čtenáři získat komplexní informaci o známých inhibitech chřipkových virů, usnadnit a urychlit orientaci v početných publikacích na toto téma a efektivně získat potřebná data. Vzhledem k rozsahu práce (celkem 73 stran) není její tabulková část prezentována v tomto habilitačním spisu. Kompletní práci může čtenář nalézt na <https://doi.org/10.17221/6746-VETMED>.

PŘÍLOHA 1

1. Ruzek D, Avšič Županc T, Borde J, Chrdle A, **Eyer L**, Karganova G, Kholodilov I, Knap N, Kozlovskaya L, Matveev A, Miller AD, Osolodkin DI, Överby AK, Tikunova N, Tkachev S, Zajkowska J. Tick-borne encephalitis in Europe and Russia: Review of pathogenesis, clinical features, therapy, and vaccines. *Antiviral Res.* 2019 Apr;164:23-51.
2. **Eyer L**, Nencka R, de Clercq E, Seley-Radtke K, Růžek D. Nucleoside analogs as a rich source of antiviral agents active against arthropod-borne flaviviruses. *Antivir Chem Chemother.* 2018 Jan-Dec;26:2040206618761299.
3. Thames JE, **Eyer L**, Seley-Radtke K. Small molecule-based inhibitors for treatment of tick-borne encephalitis virus infection: nucleoside analogues and non-nucleoside antivirals. Přijato k publikování. ANNUAL REPORTS IN MEDICINAL CHEMISTRY. Medicinal Chemistry of Tick-Borne Encephalitis. Elsevier Inc. In press.
4. **Eyer, L.**, Hruska, K. Antiviral agents targeting the influenza virus: A review and publication analysis. 2013. *Vet Med*, 58: 113-185.



Tick-borne encephalitis in Europe and Russia: Review of pathogenesis, clinical features, therapy, and vaccines



Daniel Ruzek^{a,b,*}, Tatjana Avšič Županc^c, Johannes Borde^{d,e}, Ales Chrdle^{f,g}, Ludek Eyer^{a,b}, Galina Karganova^{h,i}, Ivan Kholodilov^h, Nataša Knap^c, Liubov Kozlovskaya^{h,i}, Andrey Matveev^j, Andrew D. Miller^{a,k}, Dmitry I. Osolodkin^{h,i}, Anna K. Överby^l, Nina Tikunova^j, Sergey Tkachev^j, Joanna Zajkowska^m

^a Veterinary Research Institute, Hudcova 70, CZ-62100, Brno, Czech Republic

^b Institute of Parasitology, Biology Centre of the Czech Academy of Sciences, Branisovska 31, CZ-37005, Ceske Budejovice, Czech Republic

^c Institute of Microbiology and Immunology, Faculty of Medicine, University of Ljubljana, Zaloška 4, Ljubljana, Slovenia

^d Department of Medicine II, Division of Infectious Diseases, Medical Center – University of Freiburg, Faculty of Medicine, University of Freiburg, 79106, Freiburg, Germany

^e Gesundheitszentrum Oberkirch, Am Marktplatz 8, 77704, Oberkirch, Germany

^f Department of Infectious Diseases, Ceske Budejovice Hospital, České Budejovice, Czech Republic

^g Tropical and Infectious Disease Unit, Royal Liverpool University Hospital, Liverpool, UK

^h FSBSI "Chumakov FSC R&D IBP RAS", Moscow, 108819, Russia

ⁱ Sechenov First Moscow State Medical University, Moscow, 119991, Russia

^j Institute of Chemical Biology and Fundamental Medicine, Siberian Branch of Russian Academy of Science, Novosibirsk, Russia

^k KP Therapeutics Ltd, 86 Deansgate, Manchester, M3 2ER, UK

^l Department of Clinical Microbiology, Virology, Umeå University and Laboratory for Molecular Infection Sweden (MIMS), Umeå University, Umeå, Sweden

^m Department of Infectious Diseases and Neuroinfections, Medical University of Białystok, Białystok, Poland

ARTICLE INFO

Keywords:

Tick-borne encephalitis
Tick-borne encephalitis virus
Clinical course
Antiviral therapy
Vaccines
Pathogenesis

ABSTRACT

Tick-borne encephalitis (TBE) is an illness caused by tick-borne encephalitis virus (TBEV) infection which is often limited to a febrile illness, but may lead to very aggressive downstream neurological manifestations. The disease is prevalent in forested areas of Europe and northeastern Asia, and is typically caused by infection involving one of three TBEV subtypes, namely the European (TBEV-Eu), the Siberian (TBEV-Sib), or the Far Eastern (TBEV-FE) subtypes. In addition to the three main TBEV subtypes, two other subtypes; i.e., the Baikalian (TBEV-Bkl) and the Himalayan subtype (TBEV-Him), have been described recently. In Europe, TBEV-Eu infection usually results in only mild TBE associated with a mortality rate of < 2%. TBEV-Sib infection also results in a generally mild TBE associated with a non-paralytic febrile form of encephalitis, although there is a tendency towards persistent TBE caused by chronic viral infection. TBE-FE infection is considered to induce the most severe forms of TBE. Importantly though, viral subtype is not the sole determinant of TBE severity; both mild and severe cases of TBE are in fact associated with infection by any of the subtypes. In keeping with this observation, the overall TBE mortality rate in Russia is ~2%, in spite of the fact that TBEV-Sib and TBEV-FE subtypes appear to be inducers of more severe TBE than TBEV-Eu. On the other hand, TBEV-Sib and TBEV-FE subtype infections in Russia are associated with essentially unique forms of TBE rarely seen elsewhere if at all, such as the hemorrhagic and chronic (progressive) forms of the disease. For post-exposure prophylaxis and TBE treatment in Russia and Kazakhstan, a specific anti-TBEV immunoglobulin is currently used with well-documented efficacy, but the use of specific TBEV immunoglobulins has been discontinued in Europe due to concerns regarding antibody-enhanced disease in naïve individuals. Therefore, new treatments are essential. This review summarizes available data on the pathogenesis and clinical features of TBE, plus different vaccine preparations available in Europe and Russia. In addition, new treatment possibilities, including small molecule drugs and experimental immunotherapies are reviewed. The authors caution that their descriptions of approved or experimental therapies should not be considered to be recommendations for patient care.

* Corresponding author. Veterinary Research Institute, Hudcova 70, CZ-62100, Brno, Czech Republic.

E-mail address: ruzekd@paru.cas.cz (D. Ruzek).

<https://doi.org/10.1016/j.antiviral.2019.01.014>

Received 23 July 2018; Received in revised form 10 December 2018; Accepted 22 January 2019

Available online 31 January 2019

0166-3542/ © 2019 Elsevier B.V. All rights reserved.

1. Introduction

Tick-borne encephalitis (TBE) is the most important arboviral disease affecting the human central nervous system (CNS) in Europe and northeastern Asia. TBE is preventable by vaccination. Different vaccines are available in Europe and Russia, and one vaccine is also produced in China. Currently, there is no general, specific treatment available for TBE, but there are several ways to positively influence the disease severity in both acute and convalescent periods (as discussed further in this review). Here, we provide a comprehensive compilation and discussion of the data available on the pathogenesis and clinical presentation of TBE, as well as on the treatments and vaccines in use or in development in Europe and Russia. The data compiled in this review were obtained from searching PubMed, Web of Science and eLibrary, using keywords corresponding to the individual sections. We also include data from references that are not recorded in these databases, the majority of which are reports published in Russian-language journals and monographs. The authors caution that their descriptions of approved or experimental therapies should not be considered to be recommendations for patient care.

2. Background

2.1. Causative agent and routes of transmission

TBE is caused by tick-borne encephalitis virus (TBEV), a positive-sense, single-stranded RNA (+ssRNA) virus with a spherical enveloped virion approximately 50 nm in diameter (Füzik et al., 2018) (Fig. 1). TBEV is a member of the *Flaviviridae* family, genus *Flavivirus*. The viral genome is approximately 11 kb in length, and comprises a 5'-cap plus a single large open reading frame (ORF), that is flanked by 5' and 3' untranslated regions. The ORF codes for a single polyprotein that is co- and post-translationally cleaved by viral and cellular proteases into three structural (C, prM and E) and seven non-structural proteins (NS1, NS2A, NS2B, NS3, NS4A, NS4B and NS5) (Fig. 1). Replication of the virus occurs through the synthesis of negative (anti-sense) mRNA, which serves as the template for genomic + ssRNA production. Replication complexes are found localized in membrane structures within the endoplasmic reticulum (ER). Accordingly, assembled nucleocapsids acquire their lipid envelopes by budding into the ER lumen. Immature particles so formed pass through the Golgi complex and undergo maturation on passage through to the *trans*-Golgi. Maturation involves

transformation from spiky immature into mature smooth viral particles. This process involves cleavage of prM and the reorganization of E proteins to form fusion-competent homodimers. Mature viral particles are then exported from the Golgi complex in cytoplasmic vesicles for their release from host cells by exocytosis (Fig. 2).

TBEV is typically able to infect humans starting from the bite of a TBEV-infected tick, primarily *Ixodes ricinus* in Europe and *Ixodes persulcatus* in Russia. In addition, approximately 1% of all TBE cases are thought to be caused by foodborne TBEV, although the numbers can differ greatly in different regions. In this case, patients are infected by consuming unpasteurized dairy (goat, sheep, and cow) milk and milk products containing TBEV (Kriz et al., 2009). This mode of transmission has been reported mostly in Eastern Europe and the Balkans; however, small outbreaks of foodborne TBE have also been reported in Central and Western Europe and Russia (Kohl et al., 1996; Gresikova et al., 1975; Holzmann et al., 2009; Caini et al., 2012; Hudopisk et al., 2013). Furthermore, a cluster of TBEV infections related to solid organ transplantation has recently been described in Poland (Lipowski et al., 2017).

TBE became notifiable at the EU level in 2012 and is now under the surveillance of the European Centre for Disease Prevention and Control (ECDC). Today, the disease is endemic in 27 European and in at least four Asian countries (Steffen, 2016). [Note: in this paper, “European” refers to countries to the west of the Russian Federation.] An increase in TBE morbidity has been observed in Europe, whereas a decrease in TBE incidence was noted in Russia compared to the late 1990s and the incidence is now at a constant level (Süss, 2008; Erber et al., 2018). However, we do note that there is a reporting problem with TBE cases, given that some countries report only clinical illness, while others (such as some Baltic countries) also report asymptomatic sero-converters.

2.2. Viral diversity and virulence variation in humans

Phylogenetic analysis has revealed three main subtypes of TBEV: European (TBEV-Eu), Siberian (TBEV-Sib), and Far Eastern (TBEV-FE) (Ecker et al., 1999). Two additional subtype lineages (“178–79” and “886–84 group”) have also been proposed as TBEV subtypes (Demina et al., 2010), although the strain 178-79 represents a single finding. On the other hand, the “886-84 group” (also named Baikalian TBEV subtype [TBEV-Bkl]) actually comprises 13 strains with the “886-84 group” as prototype. These strains were found in East Siberia near Lake Baikal and in Northern Mongolia (Kozlova et al., 2018). Finally, another new

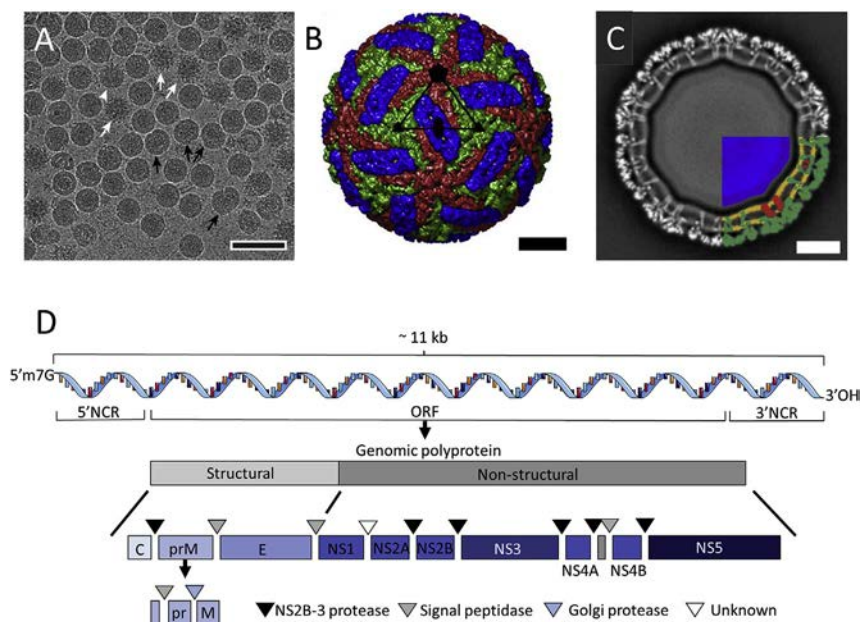
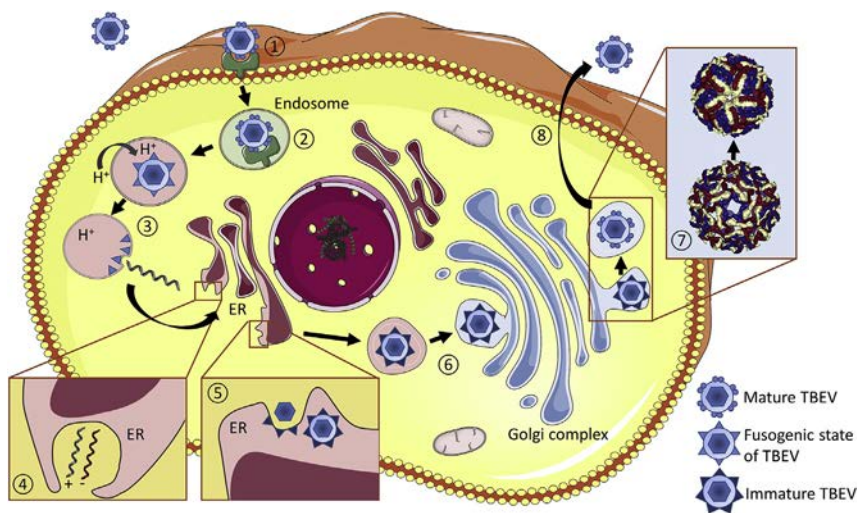


Fig. 1. Structure of a mature TBEV virion. (A) Cryo-electron microscopy image of TBEV virions. The sample contains mature, immature (white arrows), half-mature (white arrowheads), and damaged (black arrows) particles. Scale bar 100 nm. (B) Molecular surface of TBEV virion. The three E-protein subunits within each icosahedral asymmetric unit are shown in red, green, and blue. Scale bars 10 nm. (C) Central slice of TBEV electron-density map, perpendicular to the virus 5-fold axis. The virus membrane is deformed by the transmembrane helices of E-proteins and M-proteins. The lower right quadrant of the slice is color-coded as follows: nucleocapsid—blue; inner and outer membrane leaflets—orange; M-proteins—red; E-proteins—green. Scale bars 10 nm. (A–C) are reproduced from Füzik et al. (2018), under Creative Commons Attribution 4.0 International License, <http://creativecommons.org/licenses/by/4.0/>. (D) Schematic representation of TBEV genome organization and polyprotein-processing events. Figure created using Servier Medical Art available on www.servier.com.



flavivirus (West Nile virus) particles are shown. (8) Mature particles are transported in cytoplasmic vesicles and released into the extracellular space by exocytosis. Figure created using Servier Medical Art available on www.servier.com.

potential TBEV subtype (Himalayan [TBEV-Him]) was identified recently in wild rodent *Marmota himalayana* in the Qinghai-Tibet Plateau in China (Dai et al., 2018). The TBEV-Eu subtype is prevalent across Europe, including the European part of Russia, whereas the TBEV-Sib and TBEV-FE subtypes are present mainly in Asia. In some areas, two or all three main subtypes coexist (e.g., Baltic States, Siberia, Ukraine).

In Europe, TBEV-Eu infection usually results in a rather mild form of TBE with a mortality rate of < 2%. TBEV-Sib infection also results in a generally mild illness associated with a non-paralytic febrile form of encephalitis (Gritsun et al., 2003a), although there is a tendency towards persistent TBE caused by chronic viral infection. In contrast, TBEV-FE infection is thought to instigate the most severe forms of TBE and is associated with high fatality rates (Gritsun et al., 2003b). Indeed, in Russia, hemorrhagic forms of TBE have been reported that are not typically seen in Europe (Ternovoi et al., 2003). In addition, chronic (or progressive) forms of TBE have also been seen in Russia that are rarely seen if at all in Europe (Gritsun et al., 2003a, 2003b; Mickienė et al., 2002). Importantly though, viral subtype is not the sole determinant of TBE severity; both mild and severe cases of TBE are in fact associated with infection by any of the subtypes. So viral genotype or the apparent virulence of a particular TBEV subtype are not the sole determinants of disease severity. Other factors that are possibly involved include the infectious viral dose, the age, genotype, immune and nutritional state of an infected individual, plus his/her overall health status (Mickienė et al., 2014; Barkhash et al., 2010, 2012, 2013, 2016, 2018; Kaiser, 2012; Zajkowska et al., 2011).

3. Pathogenesis of TBE

For TBEV to cause disease after the tick bite, it must overcome a series of barriers that a vertebrate host employs in protection (Fig. 2). The first main barrier is the skin. However, since TBEV is transmitted by ticks, this barrier is immediately breached by injection of virus particles via the saliva during feeding. Tick saliva contains pharmacologically active molecules that modulate host defenses, such as pain and itch reflexes, hemostasis, inflammation, innate and adaptive immunity, plus wound healing, as reviewed in (Wikel, 2013). Accordingly, tick saliva components synergize with TBEV transmission between tick bites (Labuda et al., 1996) and so enhance TBEV infection and dissemination (Labuda et al., 1993). After such inoculation, the virus replicates locally in Langerhans cells and neutrophils of the skin. Migratory monocytes/macrophages produce infectious virus (Labuda et al., 1996), and these cells are likely to serve as vectors to transport virus particles to draining

lymph nodes.

The second main barrier that the virus encounters is the immune response triggered by the virus infection itself. If the virus overcomes this second main barrier, it may spread and cause viremia. Infection is often cleared in this stage and seroconversion takes place without any obvious clinical signs (Prokopowicz et al., 1995). The third barrier that TBEV needs to cross is the blood brain barrier (BBB), which protects the CNS from toxic substances and pathogens. The BBB is composed of endothelial cells connected by tight junctions, astrocyte foot processes, and pericytes, all designed to prevent unrestricted entry of blood dispersed molecules into the brain. There are several different ways that virus particles could cross the BBB (Fig. 3):

- induction of BBB opening directly;
- infection of microvascular endothelial cells that make up the BBB frontline;
- direct axonal retrograde transport from infected peripheral neurons, spreading via neuromuscular junctions (NMJs) from muscles into somatic motor neurons in the spinal cord; and
- infection of olfactory neurons and spreading to the olfactory bulb.

There is also a so-called “Trojan horse” mechanism in which the virus is transported by infected immune cells that traffic to the CNS (Palus et al., 2017; Ruzek et al., 2013a, b).

Exactly how TBEV crosses the BBB is not clear, and it would seem most likely to be a combination of mechanisms. TBEV, Langat virus (LGTV), West Nile virus (WNV), and Japanese encephalitis virus (JEV) enter the CNS without disrupting the BBB (Li et al., 2015; Ruzek et al., 2011; Roe et al., 2012; Weber et al., 2014), since the permeability of the BBB is a consequence of cytokine release in response to viral replication within the brain (Roe et al., 2012). Therefore, TBEV neuroinvasion by direct infection of the microvascular endothelial cells seems rather probable. Although less than 5% of cells are infected in an *in vitro* BBB model, the infection is persistent thereby enabling the virus to cross the BBB, in high viral yield (Palus et al., 2017). LGTV infection probably makes use of the olfactory route of infection. After peripheral infection of mice, this virus was detected successfully first in the olfactory bulb before spreading to other brain regions (Kurahde et al., 2016). However, whether or not TBEV enters the brain via olfactory neurons or by another way is still not completely clear. It should be noted that most studies of this topic have been performed with *in vitro* or *in vivo* animal models, which may be rather poor models of the human situation.

Once the virus has crossed the BBB in humans, it replicates in the

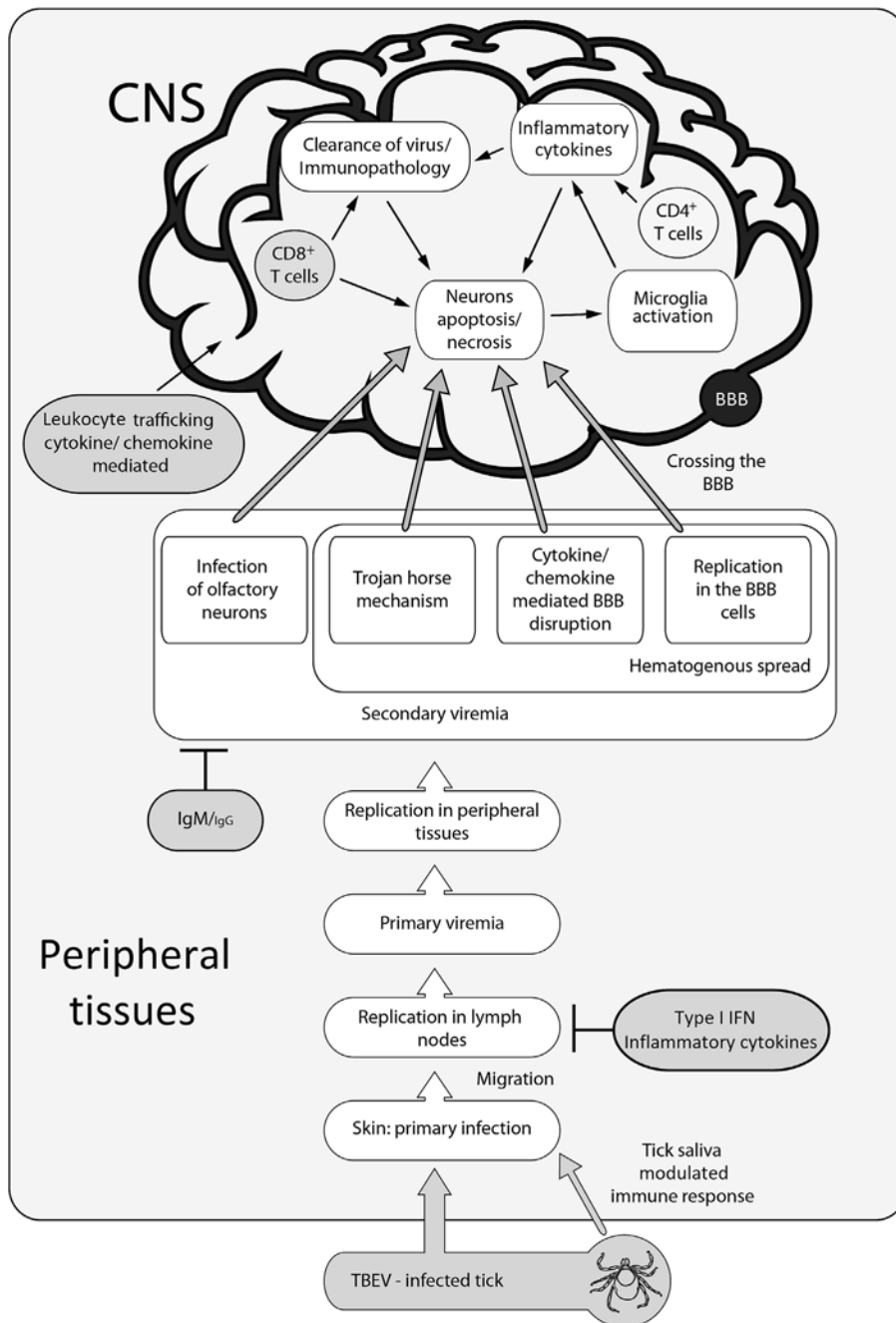


Fig. 3. Schematic of TBEV infection of the mammalian host. After a tick bite, TBEV replicates in subcutaneous tissues, and Langerhans cells transport virus particles to the draining lymph nodes. Viral replication in the nodes leads to spread into the bloodstream and induction of viremia. During primary viremia, the virus infects various peripheral organs and tissues; infection of these cells results in secondary viremia. At this time, the virus crosses the blood-brain barrier (several mechanisms have been proposed for viral transit – see text) and initiates infection in the brain. The biphasic nature of TBE reflects an initial spread of virus in peripheral tissues, eliciting a cytokine response, followed in some cases by viral penetration into the CNS and the establishment of a second neurological phase of the disease. BBB, blood-brain barrier; CNS, central nervous system. (Graphics by Patrik Kilian, adapted from Ruzek et al., 2013b).

large neurons of the anterior horns, medulla oblongata, pons, dentate nucleus, Purkinje cells, and striatum. Lymphocytic meningeal and perivascular infiltrates, plus microglial nodules, and neuronophagia are the predominant histological inflammatory reactions observed following TBEV infection of the brain (Fig. 4) (Gelpi et al., 2005, 2006).

3.1. Innate and adaptive immune responses against TBEV

The innate immune response is the first line of defense against any viral infection. This can be divided into an intrinsic intracellular response (e.g., mediated by type I interferon [IFN] responses) elicited by virus infection, and an innate extracellular response mediated by specialized immune cells (e.g., natural killer cells and antigen-presenting cells). Such an innate immune response is not specific to any one pathogen, but is rapid and necessary for downstream activation of pathogen-specific adaptive immune responses. Such adaptive immune

responses combine antibody-associated humoral responses with cell-mediated responses involving T cells, and provide for long-term immune memory. Together these responses can clear TBEV infection.

3.2. Innate immune responses

3.2.1. Interferon responses

All nucleated cells can mount an innate immune response upon infection. This response is initiated by the recognition of pathogen-associated molecular patterns (PAMPs), which are conserved proteins or molecules specific to pathogens (Pichlmair and Reis e Sousa, 2007). These PAMPs include double-stranded RNA (dsRNA), which is a replication intermediate of RNA and DNA viruses (Weber et al., 2006), or 5'-triphosphate RNA which is a hallmark of most negative (anti-sense) ssRNA viruses (Habjan et al., 2008). The PAMPs are recognized in the cell by pattern recognition receptors (PRRs), which are classified

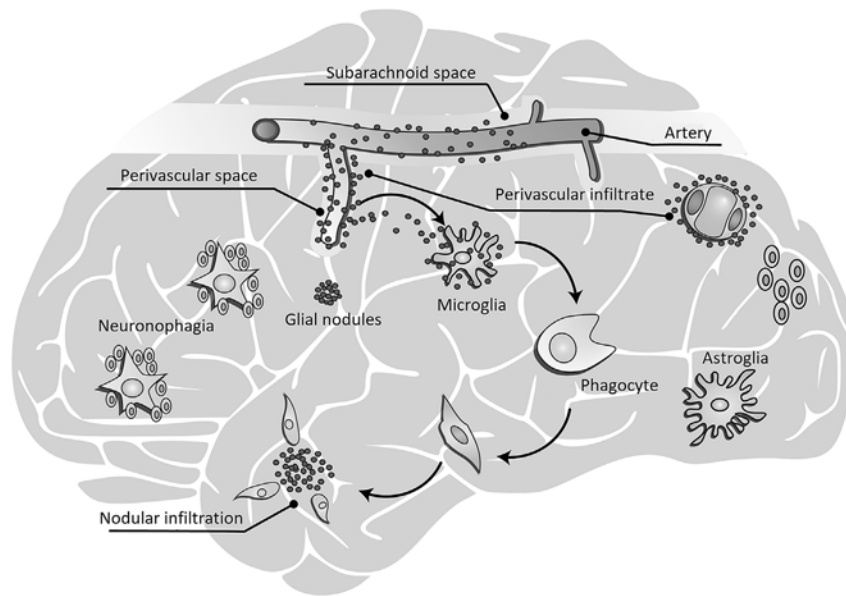


Fig. 4. Inflammatory histopathological changes in the TBEV-infected brain. Lymphocytic meningeal and perivascular infiltrates, microglial nodules, and neuronophagia are the predominant histological inflammatory reactions. (Graphics by Patrik Kilian, used with permission).

according to their intracellular localization, ligand specificity, and function. The most prominent PRRs that recognize RNA viruses are Toll-like receptors (TLRs) located in endosomes and the plasma membrane or the cytoplasmic retinoic-acid-inducible gene I (RIG-I)-like receptors (RLRs; RIG-I and melanoma differentiation-associated gene 5 [MDA5]) (Pichlmair and Reis e Sousa, 2007). Activated PRRs initiate a downstream signaling cascade that results in the activation of interferon regulatory factor 3 (IRF3) and the production of IFN.

IFN Type I (IFN α and β) and IFN type II (IFN γ) are the most well-studied interferons. Type I IFNs are expressed by most cells following viral infection, after which secreted IFN α and β bind to the IFN α receptor (IFNAR), a heterodimer of IFNAR1 and 2. IFN binding activates tyrosine kinases Jak1 and Tyk2, which then phosphorylate signal transducer and activator of transcription (STAT)-1 and STAT2 proteins, resulting in activation and translocation of the Interferon-stimulated gene factor 3 (ISGF3) into the nucleus. This results in the transcriptional activation of hundreds of IFN-stimulated genes (ISGs) encoding proteins that can either amplify IFN responses (e.g., PRRs and IRFs), modulate IFN responses (e.g., suppressor of cytokine signaling [SOCS]), or target the invading pathogen (e.g., antiviral effector proteins) (Schneider et al., 2014).

For TBEV, it is not clear which PRRs are dominant. For the RLRs, RIG-I is important (Miorin et al., 2012), but the involvement of MDA5 cannot be ruled out, as it has been shown to be important for other flaviviruses (Fredericksen et al., 2008; Loo et al., 2008). Upon RNA ligand binding to MDA5/RIG-I, a conformational change occurs that facilitates the association between PRRs and adaptor proteins such as IFN β promoter stimulator 1 (IPS-1, also known as MAVS, VISA, or CARDIF). This interaction activates the transcription factors IFN regulatory factor 3 (IRF3), IFN regulatory factor 7 (IRF7), and NF- κ B. IRF3 and IRF7 become phosphorylated and form homodimers and heterodimers, which translocate into the nucleus to activate the transcription of IFN. After TBEV infection, IPS1 is crucial for IFN β upregulation both *in vitro* and *in vivo* (Kurhade et al., 2016; Overby et al., 2010). As mouse embryonic fibroblasts (MEFs) lacking IPS1 are more susceptible to TBEV and are unable to induce IFN β transcription (Overby et al., 2010), mice deficient in IPS1 succumb to LGTV and TBEV infection earlier, with lower systemic IFN α levels and higher viral loads (Kurhade et al., 2016) resulting in earlier neuroinvasion. In the CNS, IPS1 expression appears important for controlling viral spread and replication (Kurhade et al., 2016; Zegenhagen et al., 2016a, 2016b), indicating a very

important role for RLRs in the type I IFN response in TBEV infection. Upregulation of IFN β after TBEV infection has also been shown to be highly dependent on IRF3 expression (Overby et al., 2010). IRF3 dimerizes and translocates into the nucleus upon TBEV infection, but this occurs quite late in infection, resulting in late IFN β production (Overby et al., 2010; Miorin et al., 2012). The reason for this is that the TBEV replication complexes and dsRNA produced by the virus during replication are hidden away from cellular PRRs in vesicular structures, making them inaccessible early in infection (Overby et al., 2010; Overby and Weber, 2011).

Very little is known about the importance of TLRs in TBEV infection. TLR3 is present in different types of glial cells in the CNS, and its expression is upregulated during inflammation. Several studies of TLR3 polymorphisms have concluded that functional TLR3 is a risk factor for severe TBE (Mickiene et al., 2014; Kindberg et al., 2011); however, the underlying mechanism behind is not clear. Since TBE is at least partly immunologically driven, it is possible that an impaired TLR3 response attenuates immunopathological responses and thus a more severe disease (Kindberg et al., 2011). Only TLR7 has been investigated in the context of LGTV infection in a mouse model. TLR7-deficient mice have higher viral loads in the CNS and lower levels of pro-inflammatory cytokines after LGTV infection. Although primary neurons have not been found to exhibit different infection rates, the TLR7-deficient neurons had higher levels of IFN β (Baker et al., 2013), indicating that TLR7 may be important for regulating neuroinflammation.

After secretion, IFN binds to the IFNAR, a key receptor molecule in the IFN type I responses. In its absence, cells are unable to upregulate ISGs. For many viruses, mice deficient in the IFNAR have been shown to be highly sensitive to viral infections (Muller et al., 1994). For instance, Weber et al. have shown that LGTV and TBEV replicate uncontrollably and that mice lacking the IFNAR die very quickly (Weber et al., 2014). The IFNAR is important in controlling and limiting LGTV replication in all cell types, including hematopoietic, stroma, and neuroectodermal cells, plus cells in the periphery. Astrocytes within the brain are resistant to TBEV replication due to their ability to mount a fast IFN type I response. IFNs secreted from astrocytes can prevent infection of neurons and astrocytes already 3 and 6 h post infection, respectively (Lindqvist et al., 2016). On the other hand, IFNAR-deficient astrocytes are sensitive to infection. As this response is so strong and important, natural selection has favored the evolution of viruses that are able to block IFN signaling. LGTV and TBEV do this by expressing the NS5

protein, which interferes with the phosphorylation of Jak1 and Tyk2 and subsequent STAT1/2 phosphorylation (Best et al., 2005; Werme et al., 2008). In addition, NS5 has been shown to block the transportation and maturation of the IFNAR1 subunit to the plasma membrane (Lubick et al., 2015), ensuring a reduced antiviral response within infected cells.

The antiviral effector proteins responsible for the strong antiviral effect of IFNs are the ISGs, that can target most steps of the viral life cycle, therefore there is some functional redundancy between the different proteins (Schneider et al., 2014; Schoggins and Rice, 2011). For TBEV, two critical antiviral proteins have been identified thus far: the murine tripartite motif 79 α (TRIM79 α) protein and the virus inhibitory protein, endoplasmic reticulum-associated, interferon-inducible (viperin) protein (Taylor et al., 2011; Upadhyay et al., 2014; Vonderstein et al., 2017). TRIM79 α directly targets viral NS5 for lysosomal degradation and seems to be specific for TBEV and LGTV, since mosquito-borne flaviviruses are not affected (Taylor et al., 2011). On the other hand, viperin appears to be a broad-spectrum antiviral protein that inhibits many different viruses from different families, including DNA viruses (Chin and Cresswell, 2001), negative (anti-sense) ssRNA viruses (Wang et al., 2007), retroviruses (Nasr et al., 2012), and positive (sense) ssRNA viruses (Helbig et al., 2011; Szretter et al., 2011; Teng et al., 2012; Upadhyay et al., 2014). Viperin seems to target TBEV in two different ways. First, it inhibits positive-sense ssRNA replication by interacting with and degrading the viral NS3 protein via the proteasome (Upadhyay et al., 2014; Panayiotou et al., 2018). Second, it targets viral assembly by interacting with the cellular protein Golgi Brefeldin A resistant guanine nucleotide exchange factor 1 (GBF1), a key protein in the cellular secretory pathway. The interaction of GBF1 with viperin induces capsid particle release from cells (Vonderstein et al., 2017).

3.2.2. NK and antigen-presenting cells

Another branch of the innate immune system includes natural killer (NK) and antigen-presenting cells. NK cells are large granular cells that limit viral infection by killing infected cells during early stages of infection. The direct killing of infected cells is primarily mediated by perforin and granzyme release, as well as the production of several pro-inflammatory cytokines, including IFN γ and tumour necrosis factor α (TNF α) (Jost and Altfeld, 2013). The role of NK cells in TBEV infection is largely unknown. One study demonstrated a decrease in perforin and granzyme B expression in activated NK cells from TBE patients, indicating that cytotoxic granules are released early in NK cell activation, possibly contributing to the pathogenesis of infection (Blom et al., 2016). Furthermore, low pathogenic TBEV strains were shown to activate NK cells post *ex vivo* infection of whole blood cells, whereas highly pathogenic TBEVs were shown to inhibit NK activation, which may be one way that the virus suppresses the innate immune system (Krylova et al., 2015). Tick saliva may also contribute to suppressing NK cell activity, since salivary gland extracts from ticks have been shown to decrease NK cell activity *in vitro* (Kubes et al., 1994).

NK cells do not seem to be the only cells affected by tick saliva, since saliva from *I. ricinus* inhibits dendritic cell (DC) maturation. Treatment of TBEV-infected DCs with tick saliva was found to increase the proportion of virus-infected cells and decrease the virus-induced expression of TNF α and Interleukin-6 (IL-6) (Fialova et al., 2010). Immature DCs are among the first cells to recognize infection and may be among the first infected after a tick bite. Immature DCs migrate to the lymphoid tissue and undergo maturation and antigen presentation to activate naïve T cells in order to shape the adaptive immune response. DCs bridge the innate and adaptive immune responses, partly by the production of IFN type I, inducing co-stimulatory molecules CD40, CD80, and CD86, MHC class I and MHC II, and cytokine Interleukin-12 (IL-12) in addition to ISG effector proteins (Steinman and Hemmi, 2006). One study has shown that the infection of DCs with LGTV and TBEV *in vitro* inhibits DC maturation and selective inhibition of IL-12

secretion, reducing T cell proliferation (Robertson et al., 2014). These findings indicate that the interplay between TBEV and the immune system is a balancing act, and successful establishment of viral infection requires reduced and altered activation on many levels. Notably, TBEV strains differ regarding the characteristics of their interactions with DCs in terms of the replication in these cells, virus dose triggering IFN α production, and the impact on DC maturation (Shevtsova et al., 2017).

3.3. Adaptive immune response

3.3.1. Humoral immunity

Immunity elicited by natural infection with TBEV is known to confer lifelong protection against TBE due to the long-lasting presence of virus-neutralizing antibodies (Holzmann, 2003; Remoli et al., 2015). In TBE patients, TBEV-specific IgM and IgG can be found in serum and cerebrospinal fluid (CSF). However, the intensity and duration of antibody production in serum and CSF do not correlate with disease severity (Günther et al., 1997). At the time of the first CNS symptoms, TBEV-specific IgM, and often IgG, is present in serum; CSF TBEV-specific IgM starts to increase between day 0 and day 6, reaching peak concentration approximately 14 days after the onset of CNS symptoms (Holzmann, 2003). However, large variations in the kinetics of the antibody response are seen in individual patients (Günther et al., 1997). TBEV-specific IgM persists for 6–7 weeks post-infection. In some rare cases IgMs can be detected for several months, or even years, even if there are no persisting neurological symptoms (Krylova et al., 2015). IgG levels increase only moderately during the CNS phase of the infection, peaking in both serum and CSF approximately 6 weeks after the onset of the first neurological symptoms (Holzmann, 2003; Günther et al., 1997; Dörrbecker et al., 2010); however, their presence in serum is long-lasting, or even lifelong, conferring immunological protection to the host.

The antibody response to TBE is targeted primarily against the E and NS1 proteins of TBEV and is critically important in controlling and clearing the infection. Both TBEV-neutralizing antibodies (mainly against E) and in part non-neutralizing antibodies (against NS1 or prM) can prevent development of disease post viral infection (Gould et al., 1986; Schlesinger et al., 1985; Iacono-Connors et al., 1996; Kreil et al., 1998a). Passive administration of human or mouse monoclonal or polyclonal TBEV-specific antibodies (against E protein) can protect mice against an otherwise highly lethal challenge with TBEV (Kreil and Eibl, 1997; Elsterova et al., 2017). However, although TBEV-neutralizing antibodies provide protection against the disease, they do not prevent localized infections in the host (Kreil et al., 1998b), even though rapidly cleared. Interestingly, infectious TBEV can be recovered from infected mice, which were passively protected by TBEV-specific antibodies, indicating that short-term, low-level virus replication occurs in passively protected mice. These challenged animals develop an antibody response, which is predominantly specific for NS1, which is a sign of active virus replication (Kreil et al., 1998a). Similarly, an anti-NS1 antibody response is observed in mice vaccinated with whole-killed TBEV vaccine and challenged with a lethal dose of TBEV (Kreil et al., 1998b). In this regard, TBEV-specific antibodies are not necessarily associated with sterilizing immunity (i.e., extensive neutralization of the virus inoculum), but antiviral defense mechanisms other than antibodies are also involved (Kreil et al., 1998a,b; Chambers and Diamond, 2003). However, it should also be noted that some E-specific monoclonal neutralizing antibodies do protect *in vivo* when administered passively whilst others do not necessarily provide any protection. Different strains of the virus may react differently in these tests. Thus a single monoclonal antibody might (i) neutralize the virus *in vitro* and provide protection *in vivo*, or (ii) neutralize the virus *in vitro* but fail to protect against the disease/death *in vivo*, or (iii) provide protection *in vivo* but fail to neutralize the virus *in vitro* depending on the particular flavivirus or strain of flavivirus concerned (Iacono-Connors et al., 1996; Gould and Buckley, 1989; Gould et al., 1986).

Most neutralizing antibodies recognize the viral E protein, and a subset of neutralizing epitopes are also found on the prM protein (Chambers and Diamond, 2003). There are several possible mechanisms by which antibodies can neutralize the virus, such as direct neutralization of receptor binding, post-binding/pre-fusion neutralization inside endosomes, and Fc receptor-mediated clearance by cells of the reticuloendothelial system (Chambers and Diamond, 2003; Marasco and Sui, 2007). A recent study investigated the molecular mechanisms underlying TBEV neutralization by IgG monoclonal antibody 19/1786. The antibody blocked the low-pH-triggered structural changes in E protein, and reorganization of this protein from dimer to trimer as required for the fusion between viral and endosomal membranes during virus entry. This resulted in a delay or actual prevention of viral nucleocapsid penetration of target-cell cytoplasm (Füzik et al., 2018).

Non-neutralizing, yet protective, antibodies that target the NS1 protein are also known (Timofeev et al., 1998; Kreil et al., 1998a). Such anti-NS1 antibodies are thought to mediate the lysis of TBEV-infected cells via the presentation of NS1 on cell surfaces leading to cell death by complement or antibody-dependent cell-mediated cytotoxicity (Chambers and Diamond, 2003; Kurane et al., 1984). Otherwise, antibodies bound to TBEV particles can mediate the attachment and endocytosis of these complexes by Fc γ receptor-bearing cells, such as monocytes, macrophages or DCs, causing subsequent antibody-dependent enhancement (ADE) of infection (Haslwanter et al., 2017; Philippotts et al., 1985; Kopecký et al., 1991). However, the same antibodies that enhance TBEV replication in mouse peritoneal macrophages *in vitro* were found protective against lethal TBEV infection in mice (Kreil and Eibl, 1997). Neither sublethal TBEV challenge nor suboptimal dilutions of the immunoglobulins, even if applied together, have provided any indication of antibody-enhanced disease occurring *in vivo* (Kreil and Eibl, 1997). Therefore, the antibody-mediated enhancement of infectivity during TBE lacks clear *in vivo* proof. However, the situation does remain somewhat controversial since *in vivo* studies on Langat virus, louping ill virus as well as yellow fever virus and JEV all demonstrate antibody-enhanced disease (Webb et al., 1968; Gould and Buckley, 1989).

3.3.2. Cellular immunity

Research on animal models as well as in human patients indicates that both humoral and cellular immunity are usually required to clear TBEV infection from a vertebrate host. Infection in the CNS leads to the recruitment of T cells, therefore infected neurons are potential targets for cytotoxic T cells. Studies in mice have revealed that the number and activation level of T cells in the brain has no impact on the outcome of infection, but differences were found between recovering and dying mice in terms of the accumulation of specific T cell clones in brain tissue (Fujii et al., 2011). By contrast, only a poor topographic correlation was reported between inflammatory changes in post-mortem human brains (consisting primarily of T cells and macrophages/microglia) and the distribution of viral antigen (Gelpi et al., 2005, 2006). As early as the 1970's and 1980's under certain conditions, immune responses were found activated in parallel with virus-mediated damage of host tissue (reviewed in Ruzek et al., 2010). Consistent with these observations, pharmacological immunosuppression was shown to prolong the mean survival time of infected mice for 5 days (Semenov et al., 1981; Vince and Grcevic, 1981). Furthermore, adoptive transfer of sensitized splenocytes to immunosuppressed mice significantly decreased the mean survival time of infected animals (Semenov et al., 1981). However, this immunopathological effect was only observed when splenocytes were introduced to mice at later time points post-infection. If the splenocytes were adoptively transferred on the day of infection, the mean survival time increased, suggesting a protective role of immune responses early stage peripheral infection, even though immunopathology is still generated post CNS infection (Semenov et al., 1981). There again, immunosuppression of mice with sublethal X-ray irradiation appears to reduce the development of cellular immune

infiltrations to the CNS following TBEV inoculation thereby significantly delaying the onset of disease symptoms compared to the situation with non-irradiated TBEV-infected mice (Vince et al., 1972). Similarly, recent data indicate that SCID or CD8 knockout mice infected with TBEV have longer mean survival times compared to TBEV-infected immunocompetent controls, though infection is ultimately fatal in all groups (Ruzek et al., 2009).

Mechanistically speaking, adoptive transfer of CD8⁺ T-cells into TBEV-infected SCID mice was found to decrease the mean survival time, suggesting that CD8⁺ T cells contribute to immunopathological reactions in the infected brain. However, if the mice were infected with a low-pathogenic strain, CD8⁺ T cells appeared instead to contribute to increased survival (Ruzek et al., 2009). These data support the notion that T cells have both protective and immunopathological roles, although the division between these two roles is unclear. The virulence/pathogenicity of a particular strain, the infectious dose, the immunological status of the host, and even the host genotype may influence the pathogenesis of the disease and determine whether or not T cell responses are protective or pathological during TBE. Nevertheless, in mild TBE cases, the immune response appears substantially protective. Indeed, CD8⁺ T cell-mediated cross-protection has been demonstrated between different flaviviruses (Wen et al., 2017). Therefore, T-cell mediated cross-immunity might also arise amongst strains of TBEV and such interactions might have relevance to vaccine performance against different strains (for instance comparing European versus Russian viruses and vaccines, and also vaccination efficacy in those parts of Europe where the Asian and European TBEV strains overlap geographically).

Little is known about the role of CD4⁺ T cells during TBE, though experimental models indicate a requirement for such cells in protection against acute flavivirus infections (Chambers and Diamond, 2003). CD4⁺ T cells are thought to control viral infections through several mechanisms, such as the priming of neutralizing antibody production and sustaining CD8⁺ T cell responses (Aberle et al., 2015), the production of inflammatory and antiviral cytokines, direct cytotoxic effects on infected cells through Fas-Fas ligand or perforin-dependent pathways, and in promoting immune memory responses (Sitati and Diamond, 2006). Adoptive transfer of CD4⁺ T cells into TBEV-infected SCID mice prevents the development of lethal TBE, though the mechanism is not yet clear; it is probably based on CD4⁺-mediated secretion of IFN- γ and other pro-inflammatory cytokines and/or the stimulation of macrophage-like cells (Ruzek et al., 2009).

4. TBE in humans

Clinical case definitions and criteria for diagnosis of TBE in Europe are presented in Table 1. Details of methods used in TBE diagnosis are outside the scope of this article, but are reviewed by Ergunay et al. (2016). The incubation period of TBE post-infection ranges from 2 to 28 days, most commonly between 7 and 14 days. Shorter lead time of 3–4 days to clinical symptoms is seen in the case of foodborne infections (Zajkowska and Czupryna, 2013; Kaiser, 2012; Hudopisk et al., 2013). TBEV infections and resulting TBE are categorized with a first viremic phase, which can progress to a second (neurological) phase (Smorodintsev and Dubov, 1986). The virus spreads systemically during the first phase, producing fever and other symptoms, such as headache, fatigue, myalgia, anorexia, nausea, and/or vomiting. In some patients, there is no virus invasion of the CNS and the disease terminates after the first phase (monophasic disease). In others, virus does penetrate the CNS, and there is a second phase of illness, with neurologic signs and symptoms (biphasic TBE). In the first phase, TBEV can be detected in blood samples by RT-PCR (Saksida et al., 2018), while patients during the neurological phase are diagnosed serologically (Table 1, Ergunay et al., 2016).

TBE is typically an acute disease and progression may even terminate after the first phase and go no further. This clinical pattern is

Table 1

Clinical case definitions of TBE/criteria for the diagnosis of TBE in Europe (Tabá et al., 2017). The table combines diagnostic criteria for confirmed and probable cases based on EU decisions. A case is defined by the presence of clinical signs, epidemiological links, pleocytosis ($> 5 \times 10^6$ cells/l), and recent TBEV infection, as demonstrated by the presence of specific serum IgM and IgG. Probable cases are defined as patients (i) meeting the clinical criteria, having pleocytosis and detectable TBEV-specific IgM in a single serum sample, or (ii) meeting the clinical criteria, with an epidemiological link, and having pleocytosis. CNS, central nervous system; CSF, cerebrospinal fluid; Ig, immunoglobulin.

	Confirmed TBE	Probable TBE	
Clinical criteria	Symptoms of CNS inflammation: meningitis, meningoencephalitis, or encephalomyelitis	Symptoms of CNS inflammation: meningitis, meningoencephalitis, or encephalomyelitis	Symptoms of CNS inflammation: meningitis, meningoencephalitis, or encephalomyelitis
Epidemiological link	Yes	Yes	No
CSF findings	Pleocytosis $> 5 \times 10^6$ cells/l	Pleocytosis $> 5 \times 10^6$ cells/l	Pleocytosis $> 5 \times 10^6$ cells/l
Microbiological/serological criteria	TBE-specific IgM and IgG antibodies ^a in serum; or TBE-specific IgM antibodies in CSF; or seroconversion or 4-fold increase in TBE-specific IgG antibodies in paired serum samples; or detection of TBE viral nucleic acid in a clinical specimen	No	TBE-specific IgM antibodies in a single serum sample

^a The antibodies used in the ELISA methods are cross-reactive with other flaviviruses. In patients immunized against TBE, intrathecal synthesis of TBEV-specific antibodies in the CSF should be shown.

termed ‘abortive’. This abortive form of TBE may be asymptomatic or manifest in a mild febrile illness including headache, fever, fatigue, myalgia, anorexia, nausea, and vomiting. There is no progression to any form of encephalitis (Bogovic et al., 2010). The term monophasic is used to describe TBE which terminates after the first phase but manifests itself in a mild febrile illness during disease progression.

At least one-third of TBE patients develop full second phase neurological symptoms. TBE cases with neurological symptoms are reported mandatorily in the majority of endemic countries (ECDC technical report 2012). Second (neurological) phase TBE can be further classified into meningeal and focal forms (i.e., TBE with brain damage leading to paresis and/or paralysis). These focal forms may be differentiated as meningoencephalitis, meningoencephalomyelitis, and encephaloradiculitis based on the leading, most functionally significant syndrome observed (Smorodintsev and Dubov, 1986; Ammosov, 2006; Lobzin et al., 2015). In some TBE patients, TBEV can persist active in the CNS for an extended time, and the infectious process continues unabated. In this case, TBE becomes a chronic (progressive) disease (Pogodina et al., 1986; Smorodintsev and Dubov, 1986; Lobzin et al., 2015).

Epidemiological studies and epidemiological benchmarking data have certain limitations with TBE. The frequency of asymptomatic TBEV infections has been estimated as between 70 and 98% of total infections on the basis of published data (Bogovic and Strle, 2015). In one highly endemic region of Sweden, 88 of 745 subjects had TBE antibodies, and of those 88 seroconvertants, only 23 (26%) had a substantive history consistent with TBE-induced CNS disease (Gustafson et al., 1993). However, overall the fatality rate in Europe is certainly $< 2\%$ (Kaiser, 2012; Lindquist and Vapalahti, 2008; Borde and Zajkowska, 2017). Indeed, the annual TBE epidemiological report for 2015 published in 2018 by the ECDC indicated a fatality rate of only about 0.2% (five deaths among 1908 confirmed TBE cases). These probably represent the most reliable current data on fatality rates and epidemiology, despite variations in TBE definitions in different European countries. The number of asymptomatic TBEV-Sib and TBEV-FE infections has similarly been estimated as between 70 and 95% of total infections (Gritsun et al., 2003b), although up to 50% of infections in the Far East resulted in some kind of monophasic TBE (Leonova et al., 2013).

4.1. Asymptomatic infection, febrile form of TBE

Seroprevalence studies from highly-endemic regions indicate that a significant proportion of TBEV infections remain asymptomatic (Gustafson et al., 1992; Gustafson et al., 1993; Bogovic and Strle, 2015; Leonova et al., 1996). As noted above, the number of asymptomatic TBEV infections has been estimated as between 70 and 98% of total

infections (Kaiser, 2008; Gustafson et al., 1992; Bogovic and Strle, 2015). However, a serological survey conducted in the Czech Republic, in a highly endemic TBEV focus, revealed a ratio of 6.07:9.64 manifest TBE cases to asymptomatic seroconvertants, i.e. suggesting that approx. 40 % of TBEV infections resulted in some form of illness (Lunácková et al., 2003).

The first phase lasts for 2–4 days (range 1–8 days) and manifests as a mild febrile illness including headache, fever, fatigue, myalgia, anorexia, nausea, and vomiting. In this case, a patient’s body temperature quickly reaches 38–39 °C and fever lasts from a few hours to several days. (Bogovic and Strle, 2015). The first phase is followed by clinical amelioration or an interval without any symptoms for up to 1 week (range 1–21 days). Up to 46% of patients with the first clinical phase of TBE may go on to experience a second phase of TBE and develop long-term sequelae (Bogovic and Strle, 2015).

4.2. Neurological forms of TBE

The asymptomatic period between the first and second (neurological) phase lasts for an average of 8 (range 1–20) days. The second (neurological) phase of TBE begins with increased body temperature, 1–2 °C higher than peak temperatures in the first phase, frequently exceeding 40 °C (i.e., fever resolves after the first phase, but then returns at the beginning of the second phase of the disease). The clinical course of acute, second-phase TBE can be classified as mild, moderate, or severe. The disease involves the CNS, with meningitis or focal forms: meningoencephalitis, meningoencephalomyelitis or encephaloradiculitis, characterized by lesions in the CNS. Specific areas of the brain can be affected by virus replication and/or neuroinflammation, resulting in movement disorders (Zajkowska et al., 2013; Lenhard et al., 2016). In Russia, data on the relative frequency of different forms of TBE differ significantly between regions. In all regions, except the Far East, meningoencephalitis is registered less frequently than the meningeal form. Apparently, these data are very dependent on the level of registration of mild forms of the disease, which in turn is a function of available diagnostics, access to medical care (when patients live far from medical centres) and the general health of the population.

4.2.1. Meningitis

Meningitis is associated with headache, nausea, vomiting, vertigo, eye pain, photophobia and nuchal rigidity. Approximately 10% of patients without meningeal signs show pleocytosis in the CSF. Patients feel weak and sluggish, have stiff neck muscles and Kernig and Brudzinsky signs are observed. A moderate increase in lymphocyte count and increased protein concentrations in the CSF are detected. Intracranial pressure is increased. CSF changes that occur during the acute period of the disease may persist long-term, even during recovery.

Fever typically lasts 7–14 days. In pediatric TBE patients, fever without neurological symptoms is the chief complaint (Kaiser, 2012; Zajkowska and Czupryna, 2013; Bogovic and Strle, 2015).

4.2.2. Meningoencephalitis

Meningoencephalitis is observed in about 50% of adult TBEV-infected individuals with neurological symptoms. This form of TBE is severe and more often lethal compared to meningitis. Patients feel weak, sluggish, and sleepy, and complain of severe headache, nausea, and vomiting. Stiff neck muscles and Kernig and Brudzinsky signs are observed. Patients may have delusions, hallucinations, psychomotor agitation with loss of orientation in place and time, and epileptic seizures. The altered mental state can range from somnolence to coma. Disorientation, excitation, seizures and confusion may also be observed, as well as hyperkinesia of the limbs and facial muscles. Cranial nerve involvement with paresis of the facial and ocular nerves, cerebellar ataxia, and autonomic disturbances are frequently diagnosed. Spinal nerve paralysis has been documented in about 4% of neurologic TBE patients. Severe myalgia of the extremities sometimes precedes paresis. Involvement of the cranial nerve nuclei and spinal cord motor neurons results in flaccid paralysis of the neck and upper extremity muscles (Mickienė et al., 2002).

With *diffuse meningoencephalitis*, cerebral disorders, such as consciousness disorders and epileptic seizures, are typical. Scattered focal lesions in the brain manifest as pseudobulbar disorders and cardiovascular system dysfunction. Fibrillation (twitching) of facial limb muscles, hand tremor, suppression of deep reflexes, and decreased muscle tone are also observed. In the case of a favorable outcome, consciousness becomes clear in 2 weeks (Lenhard et al., 2016; Lobzin et al., 2015). With *focal meningoencephalitis*, clinical presentation is determined by the location of damage to the brain. Using MRI, one of the two cerebral hemispheres shows damage with spasmodic paresis of the right or left extremities, and paresis of the facial and IX cranial nerve (glossopharyngeal nerve) may develop on the same side. When the process is localized in the left hemisphere, speech problems occur. If white matter is damaged in the brain stem, so-called alternating syndrome develops, which manifests as cranial nerve paresis on the side of the inflammatory focus and limb paresis on the opposite side of the body. Among the affected cranial nerves are the III, IV, V, and VI pairs, and somewhat more often cranial nerve VII, IX, X, XI, and XII pairs, resulting in paresis of the soft palate, slurred speech, aphonia, inability to swallow, tachycardia, and dyspnea. CSF tests performed in the acute period reveal lymphocytosis and increased protein content. Therefore, when it comes to the severe encephalitic form of the disease, the focal CNS lesions are revealed in addition to cerebral and toxic syndrome manifestations (Lobzin et al., 2015).

4.2.3. Meningoencephalomyelitis

Patients with meningoencephalomyelitis (polio-like) may experience paresis of the arms, back, and legs, symmetrically affecting the musculature of the neck, shoulder girdle, upper limbs, and sometimes the intercostal muscles and diaphragm. The upper extremities are affected more often than the lower extremities. A characteristic of such patients is “floppy head” or “dropped head” syndrome, in which the patient cannot hold their head in a vertical position, so their head hangs passively (Panov, 1956). Involvement of the medulla oblongata and central parts of the brainstem indicate a poor prognosis. Cranial nerve involvement is associated mainly with ocular, facial, and pharyngeal motor dysfunctions. Occasionally, TBE can be linked to autonomic dysfunction, including reduced heart rate variability and tachycardia. Flaccid paralysis with mono-, para-, or tetraparesis develops in 5–10% of second (neurological) phase TBE patients. Furthermore, respiratory muscle paralysis may develop, resulting in respiratory failure, making respiratory support essential; a risk of sudden respiratory and circulatory failure is sometimes present (Kaiser, 2012; Lindquist and Vapalahti, 2008). Motor disorders gradually develop in patients over

the course of 7–12 days, and atrophy of the affected muscles develops by the end of week 2–3 of the disease.

4.2.4. Encephaloradiculitis or the polyradiculoneuritic form

The polyradiculoneuritic form of TBE is relatively rare (up to 3% of clinical TBE reported in Russia; however, not all physicians classify polyradiculoneuritis as a separate form of TBE). In addition to general transient febrile and meningeal symptoms, patients develop signs of damage to the roots and peripheral nerves, which manifests as paresthesia in the form of the “crawling ants” sensation, tingling in various areas of the skin, pain along the nerve trunks, Lasègue's sign (the straight leg raise), Wasserman symptoms (a condition caused by irritation of the femoral nerve, which runs along the upper-outer thigh), and polyneurial type sensitivity disorders (“gloves” and “socks” type) in distal segments of the extremities. Flaccid paralysis usually begins with the legs and spreads to the musculature of the trunk and hands. The process may begin with the muscles of the shoulder girdle, affecting neck muscles.

4.2.5. Chronic (progressive) disease

Many patients with neurologic forms of TBE resolve their acute illness, but are left with chronic sequelae of infection. In contrast, some patients show evidence of a continuing disease, which is described as chronic (progressive) TBE. The chronic form is reported in Russia, where it represents 1–3% of cases, but virtually no cases of this form have been seen in Europe. Russian clinicians divide chronic TBE into persistent, relapsing, and progressive forms of the disease. In patients with chronic infection, focal CNS lesions are observed during later periods of the disease, weeks or even months after the body temperature drops to normal levels during a period of convalescence (Pogodina et al., 1986; Smorodintsev and Dubov, 1986; Lobzin et al., 2015). Chronic infection can occur in a latent form and manifest after several months or years under certain circumstances (hypothermia, physical or psychological trauma, overwhelming physical labor, alcohol intoxication, abortion, labour or even physiotherapy) or may manifest as a continuously progressive form with an increase in focal CNS lesions, leading to patient death (Shapoval, 1976). An early sign of the disease is headache, which increases in intensity as the disease progresses. CSF tests continue to show signs of inflammation, and blood tests reveal moderate increases in the erythrocyte sedimentation rates (ESR) and mild leukocytosis, usually with a shift towards absolute or relative lymphocytosis. The duration of the disease course ranges from 1 to 20 years or more. In 17% of cases, chronic forms result in death between 9 and 20 years post infection (Umansky, 1977).

Our understanding of chronic TBE is based on long-term persistence of TBEV in patients who showed clear symptoms of disease for several years, decades, or their entire life. This includes patients with a clinical diagnosis of hyperkinetic syndrome, Kozhevnikov epilepsy, amyotrophic lateral sclerosis, epidemic encephalitis, arachnoencephalitis, syringomyelia, and progressive polyencephalomyelitis, among others (Umansky, 1977; Ammosov, 2006; Lobzin et al., 2015). In some chronic and focal forms of TBE, a form of epilepsy develops, known as Kozhevnikov epilepsy, which was first described by A. Kozhevnikov in 1894, half a century before the discovery of TBEV (Lobzin et al., 2015). Kozhevnikov epilepsy typically begins with local convulsive twitching of the muscles of the paretic limbs, usually the hand muscles. Occasionally, the local muscle twitching can be multi-focal, affecting the muscles of the hand, face, and feet. Seizures are characterized by asynchrony and irregularity. The second sign of Kozhevnikov epilepsy is generalized convulsive seizures, which, as a rule, are rare. After a seizure episode, the patient's paresis may worsen. On the other hand, hyperkinesia may decrease (Shapoval, 1976). After the discovery of TBEV, researchers suggested that patients with Kozhevnikov epilepsy syndrome have long-term persistence of TBEV in the CNS (Chumakov et al., 1944). This assumption was later confirmed in experiments using fluorescent antibodies and isolating the virus from lesions in laboratory

animals (Frolova et al., 1982). It is also interesting to note that the postmortal brain sample of Professor M. P. Chumakov, who underwent a severe form of TBE in 1937 and died in 1993, was positive for TBEV RNA (Pogodina, 2009).

Chronic forms of TBE are described following infection by TBEV-FE and -Sib, although it is believed that the Sib subtype produces chronic disease more often (Pogodina, 2005). There is a whole set of strains isolated from the blood or CSF of patients with chronic TBE, for example, strains Aina and Zausaev. Comparison of these strains with those isolated from patients with acute TBE did not show unambiguous differences (Gritsun et al., 2003a; Pogodina et al., 2004a,b; Sobolev et al., 2010).

4.2.6. Hemorrhagic form

In the last few years, sporadic cases of hemorrhagic TBE have been reported in the Asian part of Russia. A hemorrhagic syndrome during TBE was documented for the first time in the Novosibirsk Oblast of Siberia in 1999, when eight fatal cases were observed (Ternovoi et al., 2003). The latent period was 5–26 days (average 12.8 days). Disease onset included typical clinical symptoms of TBE, such as fever, myalgia, and malaise, then was followed by severe viral encephalitis accompanied by loss of consciousness, paresis, and paralysis. Hemorrhagic signs developed as massive gastrointestinal bleeding and local hemorrhages on the mucosa and skin. The first sign of the hemorrhagic syndrome was the presence of erythrocytes in the urine on day 7 of the infection, which is not usual from TBEV infection. Common CNS manifestations occurred 3 days later. Despite intensive treatment, patients died 2–3 days after the massive hemorrhagic syndrome developed. The average time of death was 16 days after disease onset. Importantly, the presence of TBEV was confirmed by sequencing in six brain samples from the patients.

4.3. Post-encephalitic syndrome

TBE may cause persistent sequelae with significant consequences for daily activities and the quality of life. Studies suggest that 40–50% patients with TBE develop a post-encephalitic syndrome (Misić Majerus et al., 2009; Haglund and Günther, 2003; Bogovič et al., 2018). The most frequently reported signs are neuropsychiatric disorders, such as apathy, irritability, memory and concentration dysfunction, and altered sleep patterns. Sensory disturbances and persistent flaccid paresis or paralysis have been documented (Fig. 5), but which clinical details, if any at all, of the post-encephalitic syndrome are TBE-specific is still matter of debate (Schmolck et al., 2005). It should also be noted that risk factors for severe forms of the disease may not be identical with risk factors for the development of post-encephalitic syndrome.

4.4. Predisposition and risk factors

All age groups are at risk of infection with TBEV from an epidemiological perspective. Age, neurological signs at onset, and a low early IgM response in the CSF are risk factors for severe forms of TBE. A disease that progresses from a febrile syndrome to CNS manifestations without an intervening asymptomatic period, or a biphasic course with a prompt febrile onset and a short asymptomatic interval (rapid progression to the second neurological phase) have been associated with severe forms of TBE. Comorbidities and immunomodulating therapies are associated with severe clinical forms of TBE. Fatal outcomes after TBEV infection are reported in solid organ transplant recipients (kidney) and in patients with longstanding immunosuppressive therapy in the context of rheumatoid arthritis (Zajkowska et al., 2011; Lipowski et al., 2017). The potential role of genetic background in TBE is currently being studied. Most of the analyzed factors are part of the innate immune response to TBEV of the mammalian host. Select genetic predispositions to TBE or severe forms of TBE are polymorphisms in genes encoding C–C chemokine receptor type 5 (CCR5), TLR3, 2'-5'-

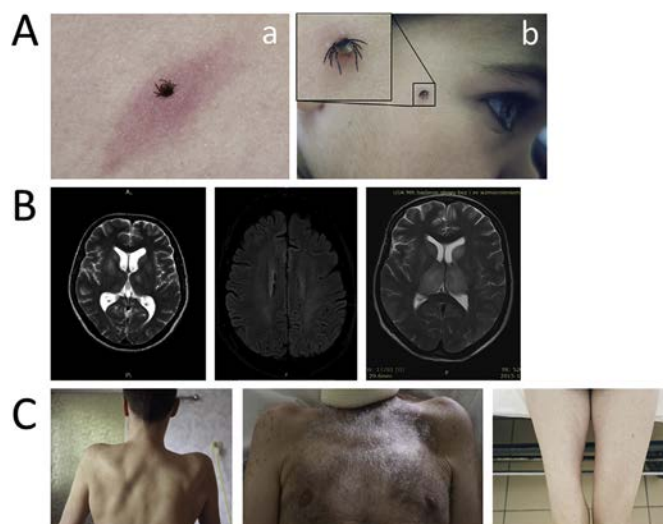


Fig. 5. TBE in humans. (A) Tick attachment. In most cases, TBEV is transmitted to humans via the bite of a TBEV-infected tick, mainly *Ixodes ricinus* in Europe and *Ixodes persulcatus* in Russia. (a) Tick bite with nonspecific skin reaction. Nonspecific reactions around the site of tick bite are common and usually disappear quickly, without any clinical significance. (b) Tick bite without any skin reaction. (B) The brain is the main target for TBEV in humans. MRI findings are usually normal in TBE patients, but MRI signal abnormalities can be seen in severe TBE cases. Examples of MRI lesions are shown. (C) Inflammation can affect the spinal cord and nerve roots. Examples of muscle atrophy as sequelae of radiculomyelitis are shown. All photographs belong to the authors.

oligoadenylate synthetase 2 (OAS2), 2'-5'-oligoadenylate synthetase 3 (OAS3), interleukin-28 (IL-28), interleukin-10 (IL-10), matrix metalloproteinase-9 (MMP-9), and CD209 (DC-SIGN) (Mickienė et al., 2014; Barkhash et al., 2010, 2012, 2013, 2016, 2018). Also, virological factors, such as dose and virulence of particular TBEV strain, may be important for the severity and long-term sequelae in TBE (Ruzek et al., 2008).

4.5. Laboratory and clinical analyses

Leukocyte counts are low in the CSF of TBE patients with neurologic disease (median 60/μl, range 5–1200/μl) compared to other forms of viral or aseptic meningitis. This laboratory syndrome is very similar to the white blood cell findings in other flaviviral infections such as West Nile virus (WNV) or dengue virus (DENV) infection. Initially, there is a predominance of polymorphonuclear cells (granulocytes) in the CSF, but the immune response switches within a few days towards an increased lymphocytic cell count. Albumin is moderately increased in the CSF, and patients with TBE exhibit only moderate markers of inflammation in serum samples. At the time of hospital admission, TBE-specific IgM and IgG antibodies are usually present in serum and in CSF samples. Prior to the development of neurological signs and symptoms when serology is negative, RT-PCR can be used to detect viral RNA in blood/serum. RT-PCR can be, therefore, used as complementary method in TBE diagnostics (Veje et al., 2018; Saksida et al., 2005, 2018). However, during the first, febrile stage of the illness, specific tests are rarely performed.

4.5.1. Neuroimaging

Cranial and spinal magnetic resonance imaging (MRI) is the imaging standard for the evaluation of patients with any type of encephalitis, including TBE. However, only about 18% of neurologic TBE patients presenting with meningitis and encephalomyelitis have abnormalities in cranial MRI scans. These radiological findings are mainly located in the thalamus, cerebellum, brainstem, and nucleus caudatus

(Lenhard et al., 2016); (Bender et al., 2005) (Fig. 5). Cranial computed tomography (CCT) is usually negative and not recommended for the diagnosis of encephalitic brain lesions (Tabá et al., 2017).

4.5.2. EEG

In acute CNS inflammation, the EEG shows pathological patterns. EEG may be of prognostic value regarding long-term sequelae or fatal outcomes when there is a persistence of pathological patterns or new irregularities (Juhász and Szirmai, 1993).

4.6. Prognosis and long-term sequelae

The fatality rate from infection with TBEV-Eu is < 2%. TBEV-FE strains are believed to cause a more severe form of the disease with high fatality rates (up to 20%). In lethal cases, death occurs within 5–10 days from the onset of neurological symptoms in the context of diffuse brain oedema and bulbar involvement (Kaiser, 2011). Up to 46% of patients experiencing the second (neurological) phase of TBE develop long-term sequelae (Bogovic and Strle, 2015) resulting in a high burden of disability. Recovery from acute TBE depends on the form of infection, as well as its severity. For febrile and meningeal forms, the outcome is mostly favorable, whereas adverse outcomes are recorded more often in polio-like and polyradiculoneuritis forms. The recovery period after the focal form of acute TBE is long, up to 2 years. Atrophic paralysis of the muscles is often partially restored, whereas sequelae related to the CNS damage persist for 1–2 years, and sometimes for life (Ammosov, 2006; Lobzin et al., 2015).

4.7. Pediatric aspects of TBE

Pediatric TBE cases account for an estimated 6–20% of all ECDC reported cases in European countries (ECDC, 2012). In Europe, the incidence of TBE in the age group < 4 years is about ~0.2 cases/100,000 population and in the age group 5–14 years about 0.3 cases/100,000 population (ECDC, 2012). Children typically present non-specific symptoms such as elevated temperature, headache, fatigue, and exhaustion. Toddlers are not able to fully verbalize symptoms, which may delay times to diagnosis. Fully 5–30% of TBEV-infected children develop a second phase of the disease after exhibiting non-specific febrile syndrome (Sundin, 2017). The disease reappears with febrile temperatures and clinical signs suggestive of meningitis or meningoencephalitis. Impaired consciousness (from mild apathy and drowsiness to coma), convulsions, ataxia, tremors, cranial nerve palsies, or hemiparesis are rare in pediatric patients. Clinical signs of white matter and brainstem involvement is also extremely rare in children (Zuccoli et al., 2015). The course of the encephalitic form of TBE in children, though less frequent than in adults, is more severe and often requires specialized intensive care.

Overall, the course of the disease is usually milder in children than in adults. However, even a mild course of the disease may result in long-term sequelae. It is hypothesized that a developing CNS is more susceptible to long-term deficits than an adult CNS. Neuropsychiatric disorders, such as attention and concentration deficits, are persistent in 2% of pediatric TBE patients (Krbkova et al., 2015; Steffen, 2019).

5. Management of TBE

Given that there is no specific treatment, supportive and symptomatic therapy are the mainstay of TBE management. The clinical course of the disease (neurological phase) has three partially overlapping domains that require specific approaches: the early stages of the neurological phase of the disease, in which management is focused on differential diagnosis and empirical treatment of other conditions/co-infections; the in-hospital phase focused on symptom relief, supportive management and managing co-morbidities, preferably in neurointensive care for more severe manifestations of the disease; and the post-

acute phase in which recovery and neurorehabilitation are facilitated after the hospital stay and discharge.

5.1. Management while determining diagnosis

During the initial diagnostic work-up of a patient with febrile headache and neurological symptoms of varying severity (usually seen in patients who are awaiting the results of TBE blood serology and tests of CSF), other etiologies with available effective treatment regimes must be actively investigated and treated empirically until disease origins are otherwise proven. This includes the administration of acyclovir, especially in cases of patients with hemiparesis, aphasia, and confusion, where brain imaging suggests the possibility of herpetic encephalitis (Solomon et al., 2012). Bacterial infections with non-purulent inflammation in the CSF also need to be considered, including Lyme neuroborreliosis, leptospirosis, listeriosis, syphilis, and tuberculosis (Studahl et al., 2013). However, a thorough discussion of the non-infective causes of aseptic meningitis/encephalitis is beyond the scope of this review.

In non-endemic regions of TBE, this diagnostically uncertain phase may be prolonged, since the medical teams concerned may not fully appreciate the importance of prior travel to endemic areas, and/or serological testing for TBEV is not readily available. After a TBE diagnosis is confirmed, potential co-infections must be considered, especially of *Borrelia* spp., but also other tick-borne zoonotic agents, including *Babesia* and *Anaplasma phagocytophylum* (Moniuszko et al., 2014; Moutailler et al., 2016; Lotric-Furlan et al., 2005). There have been rare individual cases of other coinfections that clinicians need to be more fully aware of, including *Rickettsiae* (TIBO-LA), *Francisella tularensis*, and *Coxiella burnetii* (Suess et al., 2004). In addition, a fatal case of TBE and *Listeria monocytogenes* coinfection has also been reported (Zajkowska et al., 2008, 2011).

In Russia, there is a defined course of action after a tick bite (Sanitary rules SP 3.1.3.2352–08). The following scheme is used: (1) the potential patient brings ticks/ticks to a laboratory of the Russian Federal Service for Surveillance on Consumer Rights Protection and Human Well-being (Rospotrebnadzor); (2) the ticks are examined by PCR for the presence of up to four potential infectious agents (TBEV, *Borrelia burgdorferi* sensu lato [except for *B. myamotoi*], *Ehrlichia* and *Anaplasma phagocytophylum*); (3) if the tick is positive for TBEV RNA, a specific immunoglobulin is administered (no later than 96 h after removal of the tick). To patients from any territory of Russia, if bacteria are found in the tick, then appropriate antibiotics are administered, whereas if the tick is not available for PCR, then antibiotics are administered plus immunoglobulin if the potential patient was in a TBE-endemic area; (4) the patient is hospitalized if first clinical symptoms of TBE emerge after the tick bite. In some regions of Russia, patients use jodantipyrin for emergency prevention after a tick bite (see section 6.3.1 for details).

5.2. In-hospital management

5.2.1. Acute neurologic phase

There are several leading and specific manifestations that need to be controlled during the acute neurological phase of TBE (Kaiser, 1999; Chmelík et al., 1999), including headache, electrolyte disturbance, cognitive impairment/delirium, signs of intracranial hypertension, and palsies of the cranial nerves and limbs. Signs of the most severe form of TBE include bulbar syndrome with difficulty in swallowing and impaired clearance of airway secretions. Concurrent and preceding health conditions must also be managed, especially those with poorer outcomes, such as cardiovascular and cerebrovascular impairment associated with older age, and diabetes mellitus (Lenhard et al., 2016).

5.2.2. Management of pain and fever

Paracetamol and non-steroidal anti-inflammatory drugs, including

metamizol, are the mainstay of pain and fever management in viral meningoencephalitis. Other physical measures, such as cooling blankets or the infusion of cooled intravenous fluids, can be employed to reduce body temperature effectively. Opioid analgesia should be avoided if possible, as it may increase intracranial pressure, deepen the loss of consciousness, and decompensate for subclinical respiratory depression.

5.2.3. Nausea and vomiting

Nausea and vomiting are mainly a manifestation of meningitis or meningoencephalitis. These symptoms may be moderated by 5-HT₃ receptor antagonists (setrons). Another useful group is that of dopamine receptor antagonists, such as domperidone, olanzapine, haloperidol, chlorpromazine, and prochlorperazine (keeping in mind the risk of extrapyramidal side effects and over-sedation). Metoclopramide should not be used for longer than 5 days. Another option in refractory nausea is the administration of mirtazapine or corticosteroids.

5.2.4. Ataxia and risk of falls

Ataxia and poor balance are common signs and symptoms of TBE. There is an increased risk of falls, especially in elderly patients with TBE. This needs to be considered during nursing care.

5.2.5. Electrolyte balance

Electrolyte imbalance is seen uniformly in patients with severe TBE, but even patients with milder disease should be monitored closely. Ongoing fever with perspiration, vomiting, and/or nausea, loss of appetite, and possible low hypoactive delirium or cognitive impairment and/or confusion may exacerbate dehydration and electrolyte disturbances. On the other hand, excessive hydration may deteriorate brain oedema. Furthermore, thalamic lesions may cause the development of the syndrome of inappropriate antidiuretic hormone secretion (SIADH) (Czupryna et al., 2014).

5.2.6. Neurointensive specialized unit

In severe cases, patients should be managed in an intensive care unit or, preferably a neurointensive unit under the care of a multidisciplinary team with experience in the management of CNS infections (Suarez et al., 2004). Timely and proactive symptom management not only improves patient experience, but prevents loss of muscle mass and strength, plus the development of healthcare-associated complications, including aspiration pneumonia, urinary tract infection, or delirium (Kelesidis et al., 2014; Sarpong et al., 2017).

5.2.7. Intracranial hypertension

TBEV causes both direct neuronal damage and an inflammatory response resulting in brain oedema. Intracranial pressure (ICP) and/or cerebral perfusion pressure monitoring should help in decision-making regarding the means of lowering ICP, including mechanical ventilation, deepened analgo-sedation, and therapeutic hypothermia (Venkatesan and Geocadin, 2014; Taba et al., 2017). Continuous osmotherapy with mannitol or hypertonic saline should not be employed, as it increases fatality rates; however, hyperosmotic boluses may be considered for a short period of 1–2 days at most (Taba et al., 2017). Decompressive craniotomy has been reported for the treatment of other flaviviral diseases, but not for TBE, though it might be considered if other measures fail (Kofler et al., 2016).

5.2.8. Brain stem involvement

The main signs of damage to the brainstem and surrounding structures include singultus (hiccups), dysarthria, weak swallowing, and respiratory depression. Persistent singultus should be closely monitored for the risk of developing of respiratory insufficiency. Drugs used to moderate singultus include older antipsychotics, such as haloperidol, and metoclopramide or dexamethasone.

5.2.9. Difficulty swallowing

When the brain stem is affected in TBE, bulbar palsy may develop as a result of the impairment of cranial nerves IX, X, XI and XII lower motor neurons. This may lead to a swallowing dysfunction, in some cases with normal findings on brainstem MRI. Checking the ability to swallow must be a daily routine in the nursing and medical care of patients with encephalitic forms of TBE, and warning signs of poor swallowing and/or dysarthria must be actively sought. Adequate measures for managing bulbar syndrome range from thickened fluids or nasogastric tube feeding and nil by mouth to insertion of a balloon-cuffed tracheostomy (Lenhard et al., 2016).

5.2.10. Respiratory insufficiency and difficulty coughing

Brain stem damage may also be associated with respiratory depression and an inability to maintain airway patency due to poor cough and mucus build-up. Deterioration may develop very rapidly after a prolonged period of borderline respiratory compensation, especially in previously fit and well people. Poor clearance of respiratory secretions and/or repeated micro-aspirations may contribute to this problem and result in hospital-acquired/aspiration pneumonia. Early intubation and/or cuffed tracheostomy may prevent the development of more extensive lung damage (Gaeski et al., 2017). In Russia before the 1980s, pneumonia was the cause of about 50% of fatal outcomes in TBE patients.

5.2.11. Seizures

Unlike TBEV-Sib and TBEV-FE, TBEV-Eu infection is rarely associated with seizures. Thus, a different etiology should be investigated (Kaiser, 2012). In the case of seizures, treatment usually begins with intravenous benzodiazepines, followed by phenytoin, valproate, levetiracetam, ketamine to deepen anesthesia in refractory cases, and propofol or barbiturates if intracranial pressure monitoring is in place (Michael and Solomon, 2012). In cases of prolonged unresponsiveness, EEG monitoring is advisable to identify non-convulsive status epilepticus (Brophy et al., 2012; Claassen et al., 2013). Primary prophylaxis of seizures in TBE is not recommended (Pandey et al., 2014).

5.2.12. Use of corticosteroids

The role of corticosteroids in the management of TBE is disputed. Their anti-oedematous effect on CNS infection has been known for a long time (Cantu and Ojemann, 1967). An anti-oedematous dosage (i.v. hydrocortisone 5–10 mg/kg/day) resulted in faster resolution of fever and the moderation of headache, nausea, and other symptoms (Duniewicz et al., 1974). However, later studies have suggested that continued dexamethasone administration can lead to poorer long-term outcomes, although these were observational studies in which there is a tendency for patients to be administered steroids more readily in cases of severe disease (Mickiene et al., 2002). Therefore, corticosteroids should not be used routinely in anti-oedema treatment, but might be administered by experienced clinicians in selected cases (Wengse et al., 2017). Treatment is most likely to be beneficial for patients in the early stages of developing neurological deficits, increasing somnolence or sopor, severe headache, intense vomiting and singultus (Panciewicz et al., 2015). However, in patients with acute encephalitis due to JEV infection, no statistically significant benefit on the outcome of the disease was observed following high-dose dexamethasone administration (Hoke et al., 1992).

5.3. Post-acute phase and neurorehabilitation

More than 90% of lost disability-adjusted life years for TBE are due to long-term disability in survivors. Moderate long-term neurological disability contributes the most to the disease burden in endemic countries (Šmit and Postma, 2015). Neurorehabilitation is a key element in returning patients to normal life. Historical studies have suggested that a neurological deficit lasting one year will not greatly

improve afterwards (Duniewicz et al., 1975). Apart from permanent palsies in approximately 5% of patients, roughly one-third to one-half report postencephalitic syndrome as a subtle consequence of TBE. This may disturb the quality of life for months to years, including tremor, persistent headache (especially during stress), poor concentration/memory loss, hypersensitivity to light and noise, depressive moods and increased anxiety, pseudoneurasthenia, and social role dysfunction (Haglund et al., 1996; Chmelík et al., 2004). The time from hospital discharge to a full return to work or school may range from 2 to 4 months in mild cases of TBE, up to one year in cases with post-encephalitic syndrome. Adjustments in school or work may be required for those with permanent neurological deficits. Given recent developments in neuroscience, one may expect a more effective and expanded window of opportunity for recovery and return to normal life.

5.3.1. Neurorehabilitation

Patients with acquired brain injury depend on neurorehabilitation to be able to return to activities of daily living. Plasticity of the nerve tissue in the brain is suggested to facilitate such a transition (Kolb and Muhammad, 2014). Interdisciplinary coordination of rehabilitation is more effective for recovery than a spontaneous return to daily living (Formisano et al., 2017), and rehabilitation has also been shown to improve quality of life (Fortune et al., 2015). However, which type of neurorehabilitation is the most beneficial in post-encephalitis acquired brain injury is not known, although the concept of setting performance goals and associated social interactions during a given rehabilitation process may have beneficial effects on quality of life and a return to pre-morbid performance status (Rogan et al., 2013). The universal timing and extent of neurorehabilitation after TBE is not known and should be individualized. The key to successful rehabilitation appears to be the rationing of activity and sufficient rest.

5.3.2. Social and community support

The first weeks after discharge from the hospital require, apart from family involvement in supportive care, a significant input from the community and adequate mental and physical stimulation to help with convalescence. Further phases focus on re-learning the skills of daily activities. In mild cases, a phased return to work with pre-negotiated time-outs may be beneficial. Adjustment to new situations in cases of long-term neurological deficit may last months to years for both the patient and their families.

5.3.3. Psychological and psychiatric support

Facing real life following a convalescence period may be associated with increased anxiety and/or depressive mood (Rogan et al., 2013). Apart from pharmacotherapy, training in coping strategies reduces the level of distress perceived by the patient (Brands et al., 2014). In general, children are thought to have a milder disease course; however, “soft” signs have been reported, including learning difficulties and poor concentration (Rostasy, 2012). Therefore, a coordination between learning processes and adjustments at school are desirable.

6. Current and experimental antiviral therapy

No specific antivirals are approved for the treatment of TBE in Europe (Studahl et al., 2013; Taba et al., 2017), and patient care is mainly symptomatic and supportive, including intensive care interventions in severe cases. Therefore, specific therapeutic agents and strategies are required for the treatment of unvaccinated patients and vaccinated individuals with postvaccine complications and breakthrough TBE. Immunotherapy or use of specific antivirals represent possible approaches.

6.1. Immunotherapy

Specific anti-TBEV immunoglobulins, nonspecific immunoglobulins,

or recombinant anti-TBEV immunoglobulins are used or tested for prophylaxis or treatment. Vaccines can also be used in a therapeutic context as well.

6.1.1. Specific anti-TBEV immunoglobulin

In Russia and Kazakhstan, specific immunoglobulins produced from the plasma of donors are currently used for post-exposure prophylaxis and treatment (Pen'evskaia and Rudakov, 2010). This preparation is able to prevent or decrease the severity of clinical symptoms (Lashkevitch and Karganova, 2007). Analysis of the results of cohort studies has established that a timely single administration of a specific immunoglobulin (0.05 ml/kg body weight) ensures protection in 79% of cases on average. For post-exposure prophylaxis, it is necessary to use immunoglobulins with an anti-hemagglutination titre of at least 1:80. (Pen'evskaia and Rudakov, 2010). However, in Europe, the anti-TBE immunoglobulin Encegam (FSME-Bulin) was previously administered for post-exposure prophylaxis and treatment, but is no longer used. Encegam demonstrated therapeutic effects, but concerns regarding antibody-enhanced disease led to its suspension (Kluger et al., 1995; Arras et al., 1996; Waldvogel et al., 1996). Notably, no clinical cases of aggravated disease have been described after correct and timely administration of anti-TBE immunoglobulins (Bröker and Kollaritsch, 2008). Importantly, antibody-enhanced course of TBE has not been observed in *in vivo* experiments in mice after pre- and post-exposure administration of specific anti-TBEV antibodies (Kreil and Eibl, 1997; Baykov et al., 2014; Huisman et al., 2009). Nevertheless, some researchers speculate that immunoglobulin therapy may be responsible for the relatively high incidence of chronic forms of TBE in Russia, compared to Europe; however, no data are currently available to support this concern. On the other hand, antibody-enhanced disease has been observed in mouse studies with Langkat virus and louping ill virus, close relatives to TBEV. Furthermore, observations of similar effects in mice following administration of JEV does suggest that concerns about antibody-enhanced disease during flavivirus encephalitis are not unfounded (Webb et al., 1968; Gould and Buckley, 1989). More research needs to be done with TBEV to clarify this important issue.

6.1.2. Nonspecific immunoglobulin

One possible immunotherapy approach is the administration of high doses of intravenous immunoglobulin (IVIG). The preparation is approved for clinical use (Rhoades et al., 2000) in patients with various diseases, including flavivirus encephalitides (reviewed in Ruzek et al., 2013a; Elsterova et al., 2017). Its effectiveness is due to the inclusion of a broad repertoire of neutralizing antibodies against various pathogens and its immunomodulatory activity (Boros et al., 2005). The use of IVIG has been reported in the treatment of a patient with severe TBE, who received IVIG for 5 days at a dose of 400 mg/kg body weight/day (Kleiter et al., 2007). After treatment, some symptoms improved, but not the neurological symptoms. However, no data were available on the presence of TBEV-specific antibodies in this batch of IVIG. More recently, only IVIG preparations containing neutralizing anti-TBEV antibodies were shown to prevent infection *in vitro* and TBEV-infected mice (Elsterova et al., 2017).

6.1.3. Recombinant antibodies

The administration of recombinant antibodies, including chimeric and humanized antibodies, could be another possible approach for immunotherapy going forward. Such engineered antibodies have some advantages over immunoglobulin preparations from human blood, including production in blood-free biotechnological conditions and standardization of the ratio of protein concentration to neutralizing activity in each prepared batch. An engineered chimeric anti-TBEV antibody has been demonstrated to be significantly more effective than commercial anti-TBEV serum immunoglobulin in an animal model post-exposure and does not elicit antibody-enhanced disease in a lethal mouse model (Baykov et al., 2014). Further investigations should

confirm the applicability of this antibody for specific therapy, and the prospect that this antibody could enhance the anti-TBEV activity of IVIG preparations that do not contain any directly TBEV-specific antibodies.

6.1.4. Therapeutic vaccination

There have only been a few cases in which inactivated vaccine has been administered for treatment. In one case, the TBEV-Sofjin vaccine was administered to a patient with chronic TBE (Pogodina et al., 1986), who had been infected with TBEV-Sib and developed chronic disease 4 years after the onset of illness. The patient received a complete vaccination course with three consequent doses at the end of the fourth year of the disease, which led to an increase in the anti-hemagglutination titers of specific antibodies. The anti-hemagglutination activity in the patient's serum decreased, and a three-dose course of immunization was repeated a year after the first therapeutic vaccination. After that, the hemagglutination titre in the serum dropped (Pogodina et al., 1986). The reader should note that patients usually have high levels of TBEV-specific antibodies, which can interact with the vaccine antigens, thus the effect of therapeutic vaccination remains unclear. In other cases, inactivated vaccine was used for therapeutic immunization, supplemented with glucocorticoids (Umanskyi et al., 1981), so that the observed improvements in symptoms might have been caused by the hormones and other non-specific therapeutic agents. Importantly, elimination of virus has not been recorded in patients with chronic TBE (Pogodina et al., 1986).

6.2. Small molecule antivirals

As for other flaviviruses, no schemes for the specific treatment with small molecule antivirals have been recognized or introduced widely. For a detailed discussion of flavivirus biology and drug targets see the review (Boldescu et al., 2017). Target-based drug design is also restrained by the limited availability of enzymatic assays for the main non-structural enzymes of TBEV, and the paucity of structural protein binding assays.

6.2.1. Screening small molecules for anti-TBEV activity

Currently, the most accessible strategy for the measurement of potential small molecule activity is that of a primary assay, which at least provides robust experimental data and establishes potential mechanisms of action (MoAs) for hit compounds. The most important technical limitations of such a strategy are the requirement for a BSL3 containment laboratory, and the fact that only low-throughput cellular assays are available, denying opportunities for the mass screening of thousands of compounds in a short time frame. These limitations dictate that compounds for testing should undergo some form of pre-selection, to limit the number in evaluation as potential anti-TBEV agents.

Two main strategies have been used for compound pre-selection. In the first, Osolodkin et al. developed a structure-based virtual screening procedure (Osolodkin et al., 2013), accessing a homology model of the E protein β -n-octyl-D-glucoside binding site, which was further supported by molecular dynamics simulation data (Dueva et al., 2014). In the second, a ligand-based strategy was devised relying on drug or hit repurposing and an exploration of compounds such as nucleoside analogues (Jordheim et al., 2013).

6.2.2. Non-nucleoside compounds

In this and the following sections, numbers in bold refer to molecules in Fig. 6. 1,4-Dihydropyridine and 1,3,5-thiadiazine derivatives **1** and **2** were identified using the structure-based virtual screening procedure described above (Osolodkin et al., 2013), and show activity against the Absettarov strain of TBEV at low micromolar concentrations. The same docking-based approach was also employed in structure-activity relationship studies of tetrahydroquinazoline N-oxides **3** (Sednkova et al., 2015) and several other yet to be disclosed

compound classes. Compounds identified using this approach were studied in 'time-of-addition' assays; the results suggested inhibition of virus reproduction through virion binding. Poliovirus (a non-enveloped virus) was not inhibited, suggesting a MoA involving a specific interaction with the viral envelope (Sednkova et al., 2015). Strain selectivity profiling revealed a wide range of activity of tetrahydroquinazoline N-oxides against various TBEV strains (Dueva, 2016). Several selenorganic compounds also showed TBEV reproduction inhibition at micromolar concentration levels (Orlov et al., 2018).

6.2.3. Nucleoside analogues

Several series of nucleoside analogues have been assessed against TBEV (Eyer et al., 2015, 2016, 2017a, 2017b; Lo et al., 2016; Orlov et al., 2017; Kozlovskaya et al., 2018). Nucleoside analogues form the backbone of therapy for many serious diseases induced by medically important DNA or RNA viruses (De Clercq, 2011), and they have promising potential for the treatment of TBE (Eyer et al., 2015, 2016, 2017a, 2017b). The general MoA for most nucleoside inhibitors is their interaction with the viral polymerase, resulting in premature termination of nucleic acid synthesis (De Clercq and Neyts, 2009); however, other MoAs have been considered, including inhibition of the viral helicase/NTase, inhibition of enzymes responsible for intracellular nucleoside/nucleotide biosynthesis (Leyssen et al., 2005), increased mutagenesis in viral genomes, resulting in "error catastrophe" (Crotty et al., 2001), and immunomodulation (Hultgren et al., 1998).

Well-studied nucleoside-based TBEV inhibitors include the 2'-C-methyl-substituted analogues originally developed as therapeutics for chronic hepatitis C (Carroll et al., 2003, 2011; Eldrup et al., 2004; Migliaccio et al., 2003; Olsen et al., 2004). They suppress TBEV replication (Hypr and Neudorfl strains) in both porcine stable kidney cells (PS) and human neuroblastoma cells (UKF-NB4) at low micromolar concentrations with favorable cytotoxicity profiles (Eyer et al., 2015, 2016). One of these molecules, 7-deaza-2'-C-methyladenosine **4** (7DCMA), substantially improves disease outcomes, with increased survival, and reduces signs of neuroinfection and viral titres in the brains of BALB/c mice infected with a lethal dose of TBEV Hypr (Eyer et al., 2017b). However, *in vitro* treatment of TBEV-infected PS cells with 7DCMA results in the rapid evolution of resistance to 2'-C-methylated nucleoside inhibitors, associated with a signature mutation (S603T) within the active site of the viral RdRp. The biological properties of this resistant variant are manifested as a loss of replication efficacy in cell culture and markedly reduced virulence for mice (Eyer et al., 2017b).

Introduction of the ethynyl moiety to the C2' position of nucleoside **4** provided 7-deaza-2'-C-ethynyladenosine **5** (NITD008), initially synthesized for DENV inhibition (Chen et al., 2010, 2015; Latour et al., 2010; Yin et al., 2009), exhibiting nanomolar or low micromolar anti-TBEV activity in various cell-based screening systems (Lo et al., 2016). Another important family of nucleoside inhibitors are the 4'-azido-substituted analogues of cytidine, particularly 4'-azidocytidine **6** (RO-1479) and its arabino counterpart 4'-azido-aracytidine **7** (RO-9187) (Eyer et al., 2016). The anti-TBEV efficacy of both is cell-type dependent, as they exhibit antiviral activity only in PS cells, not in UKF-NB4 neuroblastoma cells. The ester prodrug of 4'-azidocytidine, balapiravir, is completely inactive against TBEV *in vitro*, probably because of its poor intracellular uptake or insufficient kinase phosphorylation in the tested cell lines (Eyer et al., 2016).

The adenosine analogue BCX4430 **8** also exhibits a low micromolar level of anti-TBEV activity (Eyer et al., 2017a), which is important, given that this compound is representative of the imino-C-nucleosides that have entered Phase I clinical trials for treatment of Ebola virus infection (De Clercq, 2016; Taylor et al., 2016; Warren et al., 2014). Another interesting compound is the 1'-C-cyano-substituted nucleoside prodrug GS-5734, that has micromolar activity against TBEV Hypr strain, but also exhibits pronounced toxicity (reported SI value of 4.8), indicating a limited therapeutic potential in TBEV infection (Lo et al.,

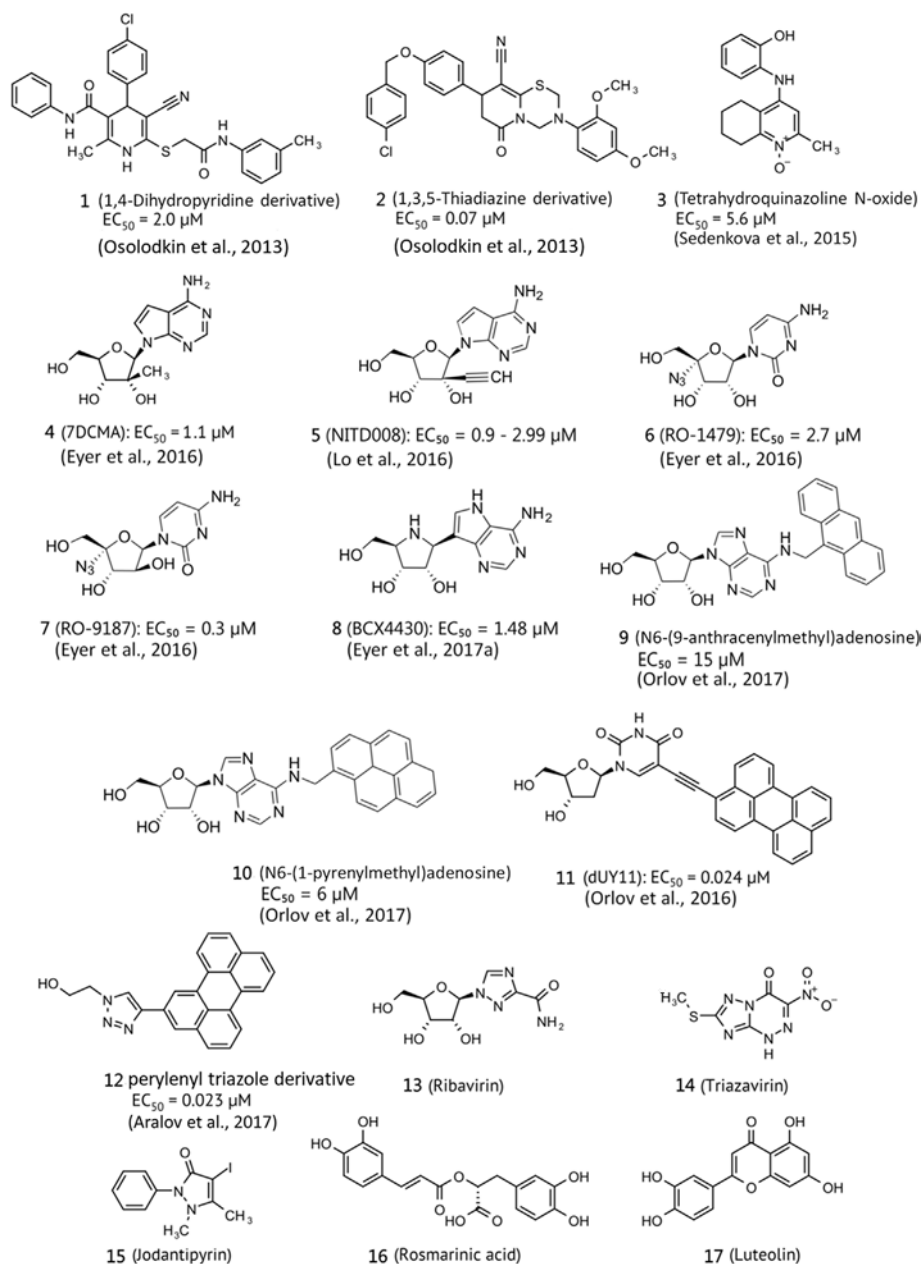


Fig. 6. Examples of small-molecule compounds tested for anti-TBEV activity. No specific drugs are approved for TBE therapy, but several molecules exhibit anti-TBEV activity *in vitro* and/or in animal models. They represent either potential TBEV antivirals or promising lead candidates for further development.

2017). In addition, several *N*⁶-alkyl/aryl-substituted nucleosides, such as *N*⁶-(9-anthracenylmethyl)adenosine **9** and *N*⁶-(1-pyrenylmethyl)adenosine **10** (Orlov et al., 2017), have shown micromolar level inhibition of the TBEV Absettarov strain *in vitro*. Many other nucleoside analogues have been evaluated *in vitro*, but most of the tested ribose/heterobase substitutions resulted in complete abrogation of anti-TBEV effects. Such modifications include methylation of the O2', O3', or C3' positions, as well as deoxy-modification of the C3' position (Eyer et al., 2016; Orlov et al., 2017). Similarly, nucleosides possessing the 2'-α-fluoro-2'-β-C-methyl substitution (PSI-6206, its prodrug sofosbuvir and mercicitabine) have no anti-TBEV activity (Eyer et al., 2016). In contrast, heterobase-modified analogues of 2'-C-methyladenosine (e.g., tubercidin, sangivamycin, and toyocamycin) are highly cytotoxic, so that their antiviral effect could not be assessed (Eyer et al., 2016).

A specific group of nucleoside derivatives, the so-called rigid amphipathic fusion inhibitors (RAFIs) **11** and **12**, were initially described as nucleoside analogues bearing a perylene moiety (Orlov et al., 2016;

Aralov et al., 2017; Proskurin et al., 2018). These compounds inhibit the reproduction of various enveloped viruses in a rather non-specific manner, attributed to mechanical or photochemical impairment of the function of the viral membrane (Colpitts et al., 2013; Vigant et al., 2014; Speerstra et al., 2018; Hakobyan et al., 2018). RAFIs exhibit the highest potency among all compounds tested against TBEV in plaque assays, up to nanomolar levels, but many are poorly soluble. More soluble analogues show higher anti-TBEV potency (Proskurin et al., 2018). The nucleoside moiety seems to be non-essential for antiviral activity (Aralov et al., 2017), whereas the substitution of perylenyl with a long alkyl chain reduces anti-TBEV activity back to micromolar concentrations (Kozlovskaya et al., 2018). Thus, viral titre is reduced by RAFIs with pronounced efficiency, and total virus elimination can be achieved for virus doses up to 10⁵ PFU (Orlov et al., 2016). RAFIs are supposed to have low cytotoxicity, due to the presence of membrane repair machinery in cells.

Ribavirin **13** is a broad-spectrum antiviral commonly used in the

treatment of several viral diseases and is often the first choice in the *in vitro* search for reproduction inhibitors of poorly studied viruses; at least 36 virus species from 17 genera have been tested for sensitivity to ribavirin (Nikitina et al., 2019). Several attempts have been made to study the anti-TBEV efficiency of ribavirin, but mixed results have been obtained. Eyer et al. (2015, 2016) and Rogova et al. (2008) did not observe any sufficient antiviral effect, whereas Krylova and Leonova (2016) and Loginova et al. (2014) found that ribavirin was active, and used it as a positive control in their studies of other antivirals. In the latter studies, however, ribavirin concentrations were as high as 127–2047 and 400 μM , respectively; such high concentrations in *in vitro* studies are a sign of low therapeutic efficiency. Triazavirin 14 was initially suggested as an anti-influenza drug (Karpenko et al., 2010) and was approved for influenza therapy in Russia, based on a small phase III trial (Sologub et al., 2017). It demonstrated anti-TBEV activity comparable to ribavirin *in vitro* (Loginova et al., 2014), and antiviral effect of triazavirin was also observed in TBEV-infected mice, when dose of 400 mg/kg was used (Loginova et al., 2015). The clinical relevance of such high doses is not clear. The mechanism of action of triazavirin has not been clearly established.

Taken together, nucleoside analogues represent promising potential drugs for TBE. In particular, 7-deaza-2'-C-methyladenosine demonstrates high antiviral effects in mice. However, research needs to continue on the development and testing of nucleoside analogue inhibitors active against TBEV (Eyer et al., 2018).

6.3. Interferon and interferon inducers

6.3.1. Interferon inducers

Interferon inducers are compounds developed principally in Russia to increase interferon levels and, thus, non-specifically protect humans against viral infections. Administration of these compounds usually does not cause undesired side effects; however, their therapeutic efficacy remains questionable (Penievskaia, 2010). This class of compounds includes tilorone, cycloferon (meglumine acridonacetate), ridostin (sodium ribonucleate), sodium polyphenylphosphate, and jodantipyridin 15. The latter was initially described as a radiologic imaging agent and is apparently the most studied and widely used; its interferon-inducing properties were described in (Khudoley et al., 2008). However, the significance of jodantipyridin use data in pre-2010 studies of TBE was heavily criticized by Penievskaia (2010), because most publications describing the efficacy of this drug were affiliated with or sponsored by the manufacturer. More recent studies presented by the manufacturer have reported the clinical efficacy of jodantipyridin using a prophylactic scheme of treatment starting a couple of weeks before expected exposure to the virus (Lepekhin et al., 2012; Doroshenko et al., 2013; Lepekhin et al., 2016). *In vitro* TBEV titre reduction by 3 lg TCID₅₀ was observed at a jodantipyridin concentration of 3.2 mM (1000 $\mu\text{g}/\text{ml}$) (Krylova and Leonova, 2016).

6.3.2. Interferon preparations

A recombinant interferon preparation formulated into a liposomal carrier for oral administration, marketed as Reaferon-ES-Lipint, was studied in combination with specific immunoglobulins (Reaferon-ES-Lipint was administered perorally; immunoglobulins intrathecally). Available data from manufacturer-sponsored studies demonstrated an improved clinical outcome in different forms of TBE (Salabay et al., 2012; Vorobeva et al., 2012). The administration of this interferon without immunoglobulins also improved prognosis, but was less effective than the interferon-immunoglobulin combination.

6.4. Natural extracts

Natural extracts have been assessed for anti-TBEV activity. The most studied are luromarin (*Zostera asiatica* extract containing rosmarinic acid (95%) and luteolin (5%)) and tinrostim (peptide extract from

Berryteuthis magister optical ganglia, containing 1–12.5 kDa peptides (84%) and free amino acids (16%, mostly Asp, Glu, and Lys)). Luromarin contains two main components, well-known as anti-flavivirals: rosmarinic acid 16, which has been shown to be effective against JEV in mice (Swarup et al., 2007), and luteolin 17, which inhibits reproduction of JEV in cell culture (Fan et al., 2016). The difference in potency between luromarin and its main components was not statistically significant (Krylova et al., 2009; Krylova et al., 2010, 2011a). Combinations of luromarin with ribavirin or cycloferon were found to effect improved survival rates in mice compared to rates observed with individual preparations (Krylova et al., 2011b). As oxidative stress is observed during TBE (reactive oxygen species contribute to antiviral defence but also cause pathology to the host) (Łuczaj et al., 2016; Kovalskii et al., 2013), the use of antioxidants, such as rosmarinic acid 16 and luteolin 17, may be a viable therapeutic strategy.

Alternatively, the peptide mixture tinrostim inhibits TBEV reproduction and positively modulates ribavirin efficiency (Krylova and Leonova, 2016), although this has not been characterized properly, and a precise MoA cannot be defined. The current hypothesis is that the peptides mediate immune system modulation, and/or may interact non-specifically with viral particles to prevent cell entry and interactions with E-protein trimers (Schmidt et al., 2010; Chew et al., 2017).

Plant-derived carbohydrate mixtures also demonstrate anti-TBEV activity *in vitro* and in mice. Cellular glycosaminoglycans significantly bind TBEV (Mandl et al., 2001; Kroschewski et al., 2003; Kozlovskaya et al., 2010) and play a role as low-affinity binders to receptors. Anionic carbohydrates are considered to be a viable class of anti-flaviviral compounds (Hidari et al., 2013). Fucoidans derived from brown seaweeds are sulphated fucans, typically containing galactose and mannose residues along with fucose, providing protective effects in mice and inhibiting TBEV reproduction *in vitro* (Makarenkova et al., 2009, 2012). A hexose polysaccharide derived from potato (*Solanum tuberosum*) shoots is marketed as a broad-spectrum antiviral drug in Russia under the trade name Panavir (Lepekhin et al., 2007; Litvin et al., 2009). However, the quality of the clinical studies leading to the approval for clinical use of this preparation in Russia was questioned by Penievskaia (2010). The MoA of panavir is claimed to be immunomodulation, with polysaccharide nanoparticles presumably mimicking virions (Stovbun et al., 2012), although non-specific binding with virions cannot be excluded.

6.5. Other treatments

Arbidol, also known as umifenovir, is a broad-spectrum antiviral compound licensed in Russia and China for the prophylaxis and treatment of human influenza A and B infections, plus post-influenza complications (Blaising et al., 2014). It is active against numerous DNA/RNA and enveloped/non-enveloped viruses (Blaising et al., 2014). Recently, it was shown that arbidol possesses micromolar antiviral effects against TBEV and other flaviviruses (Haviernik et al., 2018), but no animal or human studies investigating the efficacy of arbidol against TBEV have been done so far.

Anaferon is another marketed preparation for TBE treatment in Russia (Tarasov et al., 2016; Pavlova et al., 2009; Skripchenko et al., 2015; Skripchenko et al., 2007). It is claimed to contain “ultra-low doses” of polyclonal rabbit antibodies to IFN γ , so this is an essentially homeopathic remedy prepared by sequential dilutions (Don et al., 2017; The PLOS ONE Editors, 2018). Consequently, the anti-TBEV effect of this preparation, if any, is unclear. Clinical data are represented by a single open-label study, in which Anaferon or immunoglobulin were used for treatment of patients after a tick bite (Skripchenko et al., 2007). The quality of the Anaferon studies has been generally criticized (Penievskaia, 2010; Dueva and Panchin, 2017), pointing out a number of issues, including non-transparency of sample preparation, undisclosed conflicts of interests, unacceptable study design, biased cohort assignment, and poor statistical analyses. This criticism led to retraction

Table 2

Characteristics of TBE vaccines licensed in Europe and Russia. All are produced in primary chicken embryonic cells (PCECs), with aluminium hydroxide as an adjuvant.

	Strain	Amount of antigen
FSME-IMMUN [®] (Pfizer)	Neudoerfl (TBEV-Eu)	2.4 µg (adults)/1.2 µg (children)
Encepur [®] (GSK)	K23 (TBEV-Eu)	1.5 µg (adults)/0.75 µg (children)
TBE Moscow (FSBSI "Chumakov FSC R&D IBP RAS")	Sofjin (TBEV-FE)	1.0 ± 0.5 µg/ml (dose 0.5 ml for children from 3 years old and adults)
Tick-E-Vac/Klesch-E-Vac (FSBSI "Chumakov FSC R&D IBP RAS")	Sofjin (TBEV-FE)	1.0 ± 0.5 µg/ml (dose 0.25 ml for children 1–13 years old; 0.5 ml for adults)
EnceVir [®] (Microgen)	205 (TBEV-FE)	2.0–2.5 µg

of a published study claiming the antiviral activity of this preparation (The PLOS ONE Editors, 2018).

7. TBEV vaccines in Europe

European vaccines have been used for more than 30 years and have been highly effective in preventing TBE (Barrett et al., 2003). The first European vaccine, FSME-IMMUN[®] (Pfizer, USA), was first approved for people living and working in highly endemic areas in 1976. The vaccine is prepared from seed virus, the Neudoerfl strain of the European subtype, isolated from ticks (Barrett et al., 2003). The second vaccine, Encepur[®] (GlaxoSmithKline), was registered in 1991 in Germany and is based on the Karlsruhe (K23) strain (Harabacz et al., 1992; Girgsdies and Rosenkranz, 1996). The vaccines can be used interchangeably (Table 2).

Over the last few decades, there have been changes in the manufacturing processes of both vaccines, which consist of formaldehyde-inactivated whole virus purified by ultracentrifugation, with the antigen adsorbed to aluminum hydroxide. The production of FSME-IMMUN[®] was originally based on a master seed virus passaged in mouse brain, with the actual working seeds subsequently propagated in primary chicken embryo fibroblast cells (PCECs). In the late 1990s, the virus master cell bank was modified by passaging the seed virus through chicken embryo cells instead of mouse brain cells. The antigen content in the current version of the vaccine is now specified for a narrower range than the historic vaccine (Zent and Broker, 2005). Encepur[®] is prepared similarly, but the master and working seeds of the K23 strain have always been prepared from PCECs. Sucrose is used as a stabilizer in Encepur[®], whereas FSME-IMMUN[®] uses human serum albumin; neither contains polygeline or thiomersal (Barrett et al., 2003; Zent and Broker, 2005).

Both vaccines have adult and pediatric formulations, namely FSME-IMMUN[®]/Encepur[®] and FSME-IMMUN[®] (Junior)/Encepur-K[®]. The age-specific formulations were initiated due to the frequency and degree of fever, which is age-dependent and most common in preschool-aged children. Therefore, additional dose-finding studies have been performed in children (Girgsdies and Rosenkranz, 1996), and the antigen content of the pediatric vaccines was reduced to half the antigen dose, compared with the adult vaccines. The antigen content per dose of FSME-IMMUN[®] is currently 2.4 µg for adults and 1.2 µg for children aged 1–15 years old; for Encepur[®], it is 1.5 µg for adults and 0.75 µg for children aged 1–11 years old (Barrett et al., 2003; Pavlova et al., 2003a; Zent and Broker, 2005).

Both vaccines are generally considered safe, though mild to moderate adverse effects occur in 16–25% of individuals, compared to 13% in placebo groups. Frequently reported events include mild local transient redness or pain at the site of injection, and fever, headache, muscle and joint pain and fatigue (Loew-Baselli et al., 2006; Demicheli et al., 2009). Such adverse effects were common in children prior to the introduction of pediatric vaccines, but since the reduction in antigen content, they have been reported much less frequently (Girgsdies and Rosenkranz, 1996; Barrett et al., 2003).

7.1. Vaccine immunogenicity

Data from clinical studies and post-marketing surveillance show that FSME-IMMUN[®] and Encepur[®] are safe, efficacious and interchangeable (Zavadska et al., 2013; Zent and Broker, 2005; Demicheli et al., 2009). Both are highly immunogenic, with seroconversion rates reaching 92%–100% after complete vaccination. Several studies have been performed to determine the cross-protection of European TBE vaccines, which were shown to offer protection against TBEV-FE and TBEV-Sib (Hayasaka et al., 2001; Leonova and Pavlenko, 2009; Orlinger et al., 2011; Domnich et al., 2014). Additional studies involving sera from donors following TBEV vaccination or infection and experiments in laboratory animals found a cross-protection against OHFV, Kyasanur virus (KFV) and Alkhumra/Alkuhrma virus, but the neutralization of Powassan virus (POWV) was minimal (Chidumayo et al., 2014; McAuley et al., 2017). However, the strain selected was an isolate from a human in Canada, while all the other viruses were from Europe/Asia. Canadian POWV isolates may provide different results in neutralization and *in vivo* protection experiments, since they have been evolving in very different environments for many years.

The presence of circulating TBEV antibodies is used to assess the immune response to the vaccine and estimate necessary booster intervals. The methods most commonly used to determine the antibody concentration are ELISA, virus neutralization or the hemagglutination-inhibition assay (HI) (Holzmann et al., 1996). Differences in detected antibody levels can be a consequence of different tests used; the commercially available ELISA tests, in particular, can produce significantly different results, due to the strain used for antigen production (Jilkova et al., 2009). Neutralization tests produce the most reliable results and are the best surrogate marker of protection against TBEV (Vene et al., 2007; Stiasny et al., 2009).

Several studies have been published on the immunogenicity of Encepur[®] and FSME-IMMUN[®] following primary immunization (Ehrlich et al., 2003; Zent et al., 2003; Loew-Baselli et al., 2006; Schoendorf et al., 2007; Schondorf et al., 2007; Wittermann et al., 2009b; Heinz et al., 2007). Various schedules have been proposed for both vaccines. Standard and rapid vaccination schemes are available. Rapid schedule is used in summer months to reduce the time interval between first and second application for rapid protection. Both approaches lead to similar protection efficiency in terms of antibody levels after the third dose. However, rapid schedule elicits lower immune response than the conventional schedule after the second dose, and antibodies decline more rapidly after the rapid immunization (Schondorf et al., 2007; Amicizia et al., 2013). The standard schedule recommends the administration of the first two doses 1–3 months apart and the third dose 5–12 month (FSME-IMMUN[®]) or 9–12 months (Encepur[®]) later (Fig. 7). Under the rapid schedule, FSME-IMMUN[®] is given on days 0 and 14, and the third dose after 5–12 months, and for Encepur[®] on days 0, 7, and 21 and a fourth dose 12–18 months later. With both vaccines, the seroconversion rate determined by ELISA, HI, or NT has been found to be 92–100%, and similarly high levels of immunogenicity have also been achieved with the rapid immunization schedule (Heinz et al., 2007; Wittermann et al., 2009a, 2009b; Pöllabauer et al., 2010; Loew-Baselli et al., 2011). Similar results were obtained for both standard and accelerated schemes in children with both FSME-IMMUN[®] (Junior) and Encepur-K[®],

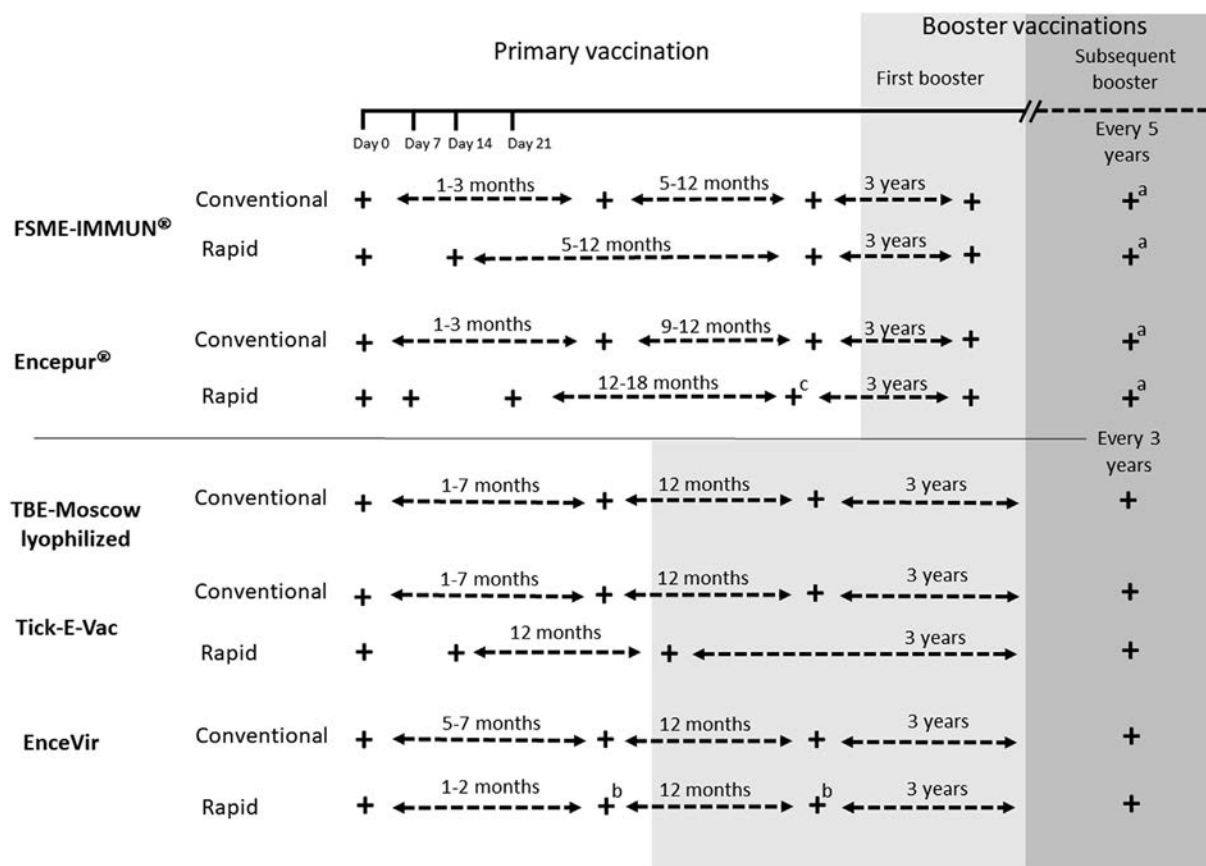


Fig. 7. Conventional (standard) and rapid vaccination schedules. Two vaccines are available in Europe: ^aFSME-IMMUN and ^aEncepur. The standard schedule calls for administration of the first two doses 1–3 months apart and the third dose 5–12 months (FSME-IMMUN) or 9–12 (Encepur). The rapid schedule is recommended for FSME-IMMUN on days 0 and 14, and the third dose after 5–12 months, and for ENCEPUR on days 0, 7, and 21 and a fourth dose 12–18 months later. Conventional schemes of the Russian vaccines TBE-Moscow and Tick-E-Vac are administered 1–7 months apart, first booster after 12 months with subsequent boosters every 3 years. During rapid schedule for Tick-E-Vac two doses are 14 days apart with first booster in 12 months and the following boosters every 3 years. Conventional vaccination scheme with EnceVir consists of second dose administered 5–7 months after the first dose, a first booster after 12 months and the following boosters every 3 years. In the case of the rapid schedule, the second dose is administered 1–2 months after the first dose, the first booster after 12 months and following boosters every 3 years. Vaccinations are marked with +. First booster is indicated with a light grey background, subsequent boosters with dark grey background. a = Booster intervals should be every 3 years for the elderly. b = Double dose of total 1 ml c = Considered as the first booster.

after receiving all three primary doses (Wittermann et al., 2009b; Pöllabauer et al., 2010).

Several studies have shown that the antibody response to vaccination is generally lower in the elderly population than in young adults, and the rate of antibody decline is faster in those over 60 years of age (Hainz et al., 2005; Weinberger et al., 2010; Paulke-Korinek et al., 2013). Data on immunogenicity induced by TBE vaccines in immunosuppressed patients are scarce. A study in Sweden of treated rheumatoid arthritis patients showed that the standard vaccination scheme does not produce a satisfactory antibody response, and the immune response was significantly different from age-matched healthy controls. An additional dose of vaccine is recommended (Hertzell et al., 2016). With both vaccines, the manufacturers recommend a booster 3 years after primary vaccination, followed by boosters every 5 years, or every 3 years in the elderly. Longitudinal studies have shown that geometric mean titres (GMTs) of neutralizing antibodies decline at a slower rate following at least one booster, compared to primary vaccination (Rendi-Wagner et al., 2004, 2006; 2007; Loew-Baselli et al., 2009; Paulke-Korinek et al., 2009; Plentz et al., 2009; Beran et al., 2014; Wittermann et al., 2015). Immunity after at least one booster vaccination lasts more than 5 years. Several studies have reported that, even 10 years after receiving primary vaccination followed by a booster, 77–84% of adult recipients remain seropositive (Paulke-Korinek et al., 2013; Konior et al., 2017).

Studies performed to date have described similar rates of antibody

decline in all age groups. Nevertheless, the antibody decline is greater in those over 60, because they achieve lower antibody titres after booster vaccinations, especially if primary vaccination occurs after the age of 60 (Hainz et al., 2005;; Weinberger et al., 2010; Galgani et al., 2017; Konior et al., 2017). Irregular vaccination schedules may lead to temporarily inadequate protection, but it can be re-established quickly through the administration of a single catch-up dose of either vaccine, regardless of age, number of previous vaccinations or interval since last vaccination (Askling et al., 2012; Schosser et al., 2014; Aerssens et al., 2016).

7.2. Vaccine effectiveness, safety, and coverage in EU countries

The incidence of TBE has decreased substantially in endemic regions of Europe where vaccination programs have been implemented successfully. Prior to vaccination, Austria had the highest recorded morbidity for TBE in Europe, but vaccination coverage has been steadily increasing since the 1970s, when the first vaccine was developed. Almost 88% of the Austrian population has now received at least one dose, and 58% maintain a regular vaccination schedule. Field studies have shown that the overall effectiveness in regularly vaccinated individuals is almost 99% and, according to available data, vaccination prevented approximately 2800 cases in Austria between 2000 and 2006 (Kunz, 2003; Heinz et al., 2007).

Vaccination rates in other TBE-endemic European countries are still

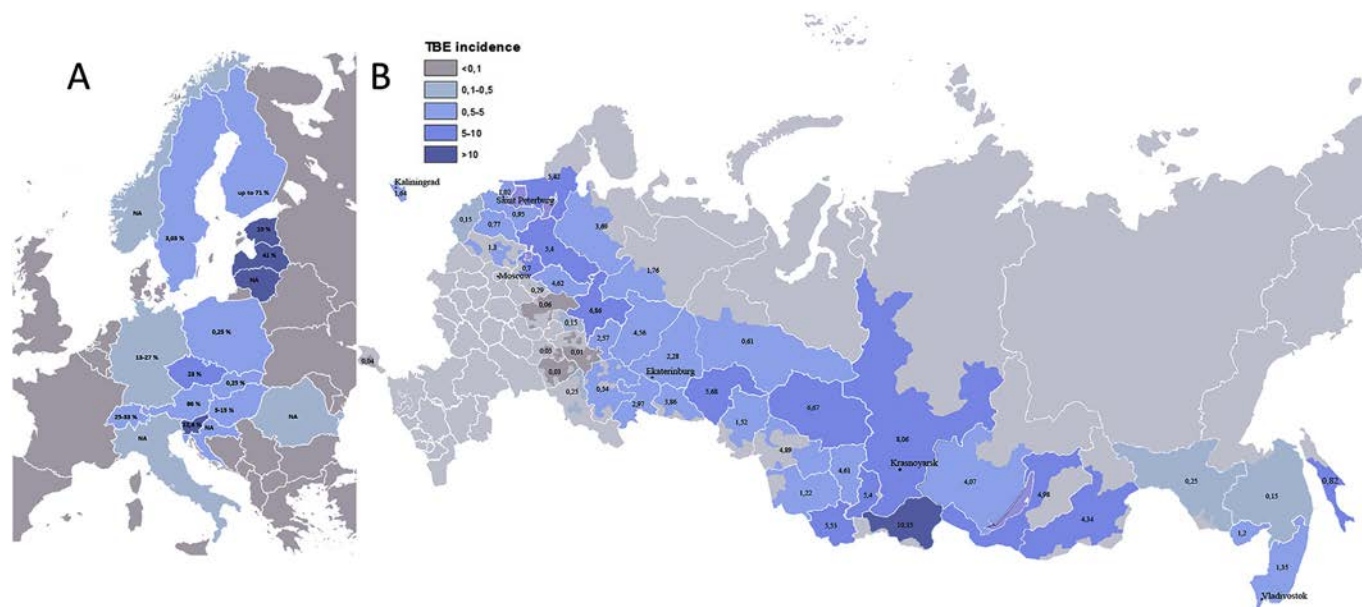


Fig. 8. TBE incidence in endemic countries in Europe (A) and in Russia (B). Endemic areas are wide-spread across the southern part of the non-tropical forest belt of Eurasia, from far eastern Russia to western Europe. The maps were prepared based on data originating from local public health authorities. Black numbers in (A) indicate TBE vaccination rates in Europe. NA, no data available on vaccination rates in (A). Black numbers in (B) indicate TBE incidence rates in Russia.

relatively low, with little or no effect on disease incidence (Fig. 8A). The only country other than Austria in which the vaccination rate exceeds 50% is Latvia, where the rate in children in highly endemic areas is 77%. In this case, TBE has been part of the national vaccination scheme since 2007, and a reduction of 12.5% in cases has occurred in children in highly endemic areas. By 2010, the vaccination rate for the whole population of Latvia was 41% (Zavadska et al., 2013). Åland Island in Finland also has high vaccination coverage (71%). In other endemic European countries, vaccination rates are between 0 and 33% (Czech Republic 23%, Germany 13–27%, Estonia 10%, Hungary 5–15%, Lithuania low, Poland 0.34%, Slovakia 0.25% in adults and 0.4% in children, Slovenia 12.4%, Sweden 11%, and Switzerland 25–33%) (Zavadska et al., 2013; Kunze, 2015). Both vaccines are available in most European countries, apart from Bulgaria, where none is registered, and Romania, where only the German vaccine is available. Apart from Latvia, TBE vaccination is not a part of a national vaccination program in European countries, but it is highly recommended in high-risk areas and advised for high-risk groups such as forestry workers, farmers and military personnel (Zavadska et al., 2013).

Vaccine breakthroughs are rare, but there have been several confirmed cases of TBE which developed despite vaccination. Twenty-five cases of TBE after vaccination were reported in Austria in the years 2002–2008, 27 in Sweden in the years 2000–2008, and 39 in Slovenia in the past 15 years, which is 1.7% of all laboratory-confirmed cases. Of these 91 cases, 54 received complete vaccination and 37 received with only 1–2 doses, or received irregular vaccination (Stiasny et al., 2009; Andersson et al., 2010; Lotric-Furlan et al., 2017). Approximately 70% of these patients are more than 50 years old, and acute illness in patients with breakthrough TBE is more severe than in unvaccinated patients who develop the disease. The mechanism of vaccine breakthrough has not been studied to date, therefore any hypothesis is premature. Generally, diagnosing vaccine failure can be confusing because the development of specific IgM is delayed, and initially undetectable, but there is an increase in TBEV-specific IgG in the serum (Stiasny et al., 2009; Andersson et al., 2010; Grgic-Vitek et al., 2010; Lotric-Furlan et al., 2017).

8. TBE vaccines in Russia

8.1. History of vaccine production

In 1937–1939 three expeditions to the Far East of USSR were organized, where many cases of severe CNS damage were recorded with a high mortality rate, and TBEV was discovered (Silber, 1939). During the first expedition in 1937 M. P. Chumakov, V. D. Solovyov and A. A. Shubladze suffered TBE and remained disabled for life. Following the first expedition, the first vaccine was prepared and it underwent clinical trials in 1938. In that year, Dr. N. V. Kagan and her technician N. Y. Utkina died during vaccine preparation, and in 1939 parasitologist B. I. Pomerantsev died after multiple tick bites.

The vaccine was prepared as a formaldehyde-inactivated 1% mouse brain suspension from the brains of mice intracerebrally infected with the Sofjin strain of TBEV-FE that had been isolated from the brain of a patient in Primorskiy Krai, Russia, in 1937 (Kagan, 1939; Smorodintseff et al., 1941). The first human trials were conducted in 1939. Among 925 volunteers who received two subcutaneous doses of the vaccine, only two suffered from mild forms of TBE after a subsequent tick bite, while in the control group of 1185 individuals, 27 cases were recorded, 7 with a fatal outcome. Beginning in 1958, a vaccine variant of formaldehyde-inactivated 2.5% mouse brain suspension was used in different regions of the USSR. It was effective, but a major problem was the high level of allergic reactions among vaccinated individuals (Smorodintsev and Doubov, 1986).

In the 1960s, studies were begun on the development of inactivated vaccines using virus grown in various cell lines. Since 1962, several versions, based on the Sofjin strain, were developed and released. The first was a formaldehyde-inactivated antigen of the Sofjin strain adsorbed on aluminum hydroxide (Chumakov et al., 1963a, 1963b, 1965a,b). Vaccine was prepared from the culture supernatant of PCECs infected with brain suspensions from TBEV-inoculated suckling mice. After virus inactivation with formaldehyde (200 $\mu\text{g}/\text{ml}$), the preparation was purified by separation, followed by clarification and sterile filtration. Human albumin (1 mg/ml) was used as a preservative. The vaccine was administered subcutaneously at a dose volume of 1 ml for recipients aged 7 years and older and 0.5 ml for those 4–6 years of age. As it had low immunogenicity, the primary course consisted of four

injections, with annual revaccinations for the next 3 years. Several clinical trial campaigns with different vaccine preparations were carried out from 1960 to 1975. These were the first carefully performed field trials to provide evidence of efficacy with this low-concentration vaccine (Lvov et al., 1963). The vaccine was widely used in the 1970s–1980s throughout the USSR, but ultimately required too many injections and did not provide the level of protection needed (Smorodintsev and Doubov, 1986). At the same time, a highly virulent TBEV strain 205 was used for the preparation and use of a non-concentrated, non-purified inactivated vaccine (Chumakov et al., 1990, 1991), but a high rate of post-vaccine adverse reactions led to its discontinuation.

It was concluded that the best solution was to use a concentrated inactivated, purified vaccine, or to make use of a live vaccine. Several attempts were made to prepare a live vaccine from Langat virus (Price et al., 1970; Il'enko et al., 1968, 1989; Mayer et al., 1975; Doubov et al., 1969, 1971), or from louping ill virus, which is closely related to TBEV (Andzhaparidze and Stepanova, 1970), and from various TBEV strains (Erofeev et al., 1976; Mayer and Rajcani, 1967). The most elaborate randomized double-blind clinical trials with the Langat virus involved 649,479 persons (Doubov et al., 1969; 1971). They were performed in comparison with inactivated, purified vaccine in two regions (Perm and Sverdlovsk) involving 10 administrative districts, that included 684 settlements. In total 35 post-vaccination cases were recorded, after which live vaccine development was terminated. Nevertheless, the Doubov vaccination trials demonstrated the efficacy of such a vaccine not only with subcutaneous administration, but also per oral administration, and no cases of chronic infections in vaccinated individuals were reported (Shapoval et al., 1989).

An inactivated TBE vaccine based on the Sofjin strain was developed in the 1980s (El'bert et al., 1980, 1984, 1985) and has been produced as a commercial preparation since 1982. This vaccine was a lyophilized purified concentrated suspension of formaldehyde-inactivated virus obtained by reproduction in PCECs, and was intended for the prophylactic vaccination of adults (> 18 years of age), and also for vaccination of blood donors to obtain specific immunoglobulins. Initially, a combination of two methods was used to purify the preparation: filtration and flow ultracentrifugation in a sucrose gradient. The efficiency of purification was later increased by using ultrafiltration and chromatography. Vaccination was performed with two subcutaneous injections of 0.5 ml of vaccine at 1–7-month intervals. Clinical trials demonstrated a high level of immunogenicity and a low level of reactogenicity (Popov et al., 1985). In 1989, a new technology for vaccine purification with protamine sulfate was introduced (El'bert et al., 1989, 1990). To date, over 25 million doses of this highly effective concentrated vaccine have been used for prophylactic vaccination against TBE in Russia and countries of the former Soviet Union.

8.2. Currently produced Russian vaccines

Three vaccines are produced in the Russian Federation. “TBE vaccine Moscow” and “Tick-E-Vac” (“Klesch-E-Vac”) are both produced by the Chumakov FSC R&D IBP RAS in Moscow. “EnceVir[®]” vaccine is produced by Microgen (a branch of the FSUC “SIC “Microgen” of the MoH of Russia “SIC “Virion”, Tomsk) (Table 2). The vaccines produced in Moscow are based on the Sofjin strain (Vorovitch et al., 2015) and EnceVir[®] on strain 205 (Safronov et al., 1991; Krasilnikov et al., 2004) of the Far Eastern subtype.

“TBE vaccine Moscow” is tissue cultured, purified, concentrated, inactivated, and lyophilized. It has been in use since 1982, and was approved for pediatric use in 2002. This vaccine is intended for the vaccination of children from 3 years of age to adults (dose 0.5 ml). During its development, the optimal containment of antigen was determined ($1 \pm 0.5 \mu\text{g/ml}$ for the Sofjin strain). The vaccine is sold in solution, together with an aluminum hydroxide gel (0.6–1.0 mg/ml in the final suspension).

“Tick-E-Vac” is the second preparation of a cultured, purified,

concentrated, inactivated, adsorbed vaccine based on the Sofjin strain, which was released in 2012. It is available in two versions: a 0.25 ml dose for children from 1 to 16 years of age and a 0.5 ml dose for individuals 16 and older (Vorovitch et al., 2012).

“EnceVir[®]” is a tissue cultured, purified, concentrated, inactivated, adsorbed suspension based on strain 205, which has been produced since 2001 (Krasilnikov et al., 2004). It is also available in two versions: as EnceVir Neo[®] for children from 3 to 17 years of age (dose 0.25 ml; 0.3–1.5 μg TBEV antigen) and as EnceVir[®] for individuals of 18 years and older (dose 0.5 ml).

The vaccination schemes are similar for all three vaccines. The primary course includes two intramuscular injections. Vaccines can be used according to a standard schedule with an interval of 1–7 months, plus an emergency schedule with an interval of just 14 days. The course of two vaccinations provide a full protective effect, and the recipient can visit endemic territories just 2 weeks after a second vaccination. The first revaccination should be done 1 year after the second immunization with subsequent revaccinations every 3 years. Like the European vaccines, the Russian vaccines belong to the third generation of TBE vaccines. Manufacturing technologies are practically identical between the two manufacturers due to the technology transfer from the FSBSI “Chumakov FSC R&D IBP RAS” in Moscow to Microgen in Tomsk. PCECs are used as the cell substrate for amplification. Virus-containing cell supernatant is inactivated by formaldehyde, clarified from cell debris and tissue fragments by filtration, concentrated by centrifugation, then further fractionated by gel filtration to obtain a specific fraction. The final preparation is stabilized with human albumin, sucrose, gelatose (only in the lyophilized TBE vaccine Moscow), protamine sulfate (up to 5 mg per dose), and buffer salts. The manufacturing process was in accordance with the national control regulations. Quality controls include safety testing to prove complete inactivation of the virus, and immunogenicity testing using BALB/c mice for immunization followed by challenge with the Absettarov strain of the European subtype to determine the immunogenicity coefficient in comparison to standard samples and the minimal immunization dose (MID₅₀). Russian vaccines do not contain antibiotics or other preservatives. The protein content (including viral antigen) in TBE vaccine Moscow and EnceVir[®] is $12 \pm 8 \mu\text{g}$ per dose.

8.3. Clinical trials

Each vaccine version from each manufacturer has passed through clinical trials. Trials of the formerly used preparations showed low reactogenicity and immunogenicity (Vorob'eva et al., 1983; Elbert et al., 1989; Pavlova et al., 1999, 2003a; Gorbunov et al., 2002a, 2002b; Vorovitch et al., 2017). Clinical trials of the lyophilized version of the vaccine TBE Moscow were conducted in the 1980–90s. In 2001–2002, blinded controlled trials were conducted with the EnceVir[®] TBE vaccine Moscow (lyophilized) in 400 adults (Gorbunov et al., 2002a, 2002b) and 325 children aged 3–18 (Pavlova et al., 2003b). According to standard and rapid schedules for both vaccines, these studies showed adult seroconversion rates of 100% and of > 96% in children. In 2011, randomized blind comparative trials of Tick-E-Vac and EnceVir[®] vaccines were conducted with adults 17–60 years old (Vorovitch et al., 2017; Maikova et al., 2019). Studies involving children and adolescents age 1–16 were conducted with Tick-E-Vac and FSME-IMMUN[®] (Ankudinova et al., 2014; Maikova et al., 2016). Seroconversion rates after two immunizations in both adults and children were 100% for both vaccines using the standard vaccination scheme, and 95% after rapid vaccination.

8.4. Vaccine safety and coverage

The immunogenicity of Russian vaccines against a wide range of TBEV strains has been shown in *in vitro* studies of sera from immunized mice (Khotlubei et al., 1982; Chernokhaeva et al., 2016), in studies of

protective efficacy in mice (Afonina et al., 2014; Chernokhaeva et al., 2016), and in vaccine recipients (Lvov et al., 1963; Vorob'eva et al., 1996; Surova et al., 2002; Leonova and Pavlenko, 2009, 2010; Morozova et al., 2014; Maikova et al., 2016). The introduction of widespread vaccination has resulted in a significant decrease in the incidence of TBE (Borodina et al., 2004; Loshko et al., 2004). This impact on disease incidence was reported in a region with > 80% vaccination coverage, where the subtype of the vaccine strain differed from the locally circulating strain(s) (Pogodina et al., 2006; Romanenko et al., 2006, 2007).

Overall in Russia, vaccination coverage differs significantly between regions. Vaccination of adolescents (at school) and of high-risk groups is obligatory in the endemic territories as prescribed by the Rospotrebnadzor regulations, funded from the regional budget. The list of endemic territories is updated annually. In some endemic areas, vaccination coverage is high, for example, in the Sverdlovsk region vaccination coverage is 88% (Romanenko et al., 2006, 2007) and in the Altaysky Krai more than 50% (www.rospotrebnadzot.ru), but in other endemic regions, less than 10% of the population is vaccinated. The reason for these differences is that vaccination is carried out in endemic districts, but the level of vaccine coverage is calculated for the entire regions as a whole. In non-endemic areas, vaccination is optional, and, therefore vaccination effects are hard to assess.

9. Cross-protection against other flaviviruses

With a growing abundance of ticks and an increasing area of distribution, the population threatened by tick-borne infections, including flaviviral infections, has increased. Based on high genome conservation (Grard et al., 2007) and significant cross-reactivity among tick-borne flaviviruses (Clarke, 1964; Casals and Webster, 1944; Calisher et al., 1989; Pervikov et al., 1975), attempts have been made to use approved TBE vaccines for prophylaxis against other flaviviral infections. Two million doses of a TBEV-FE inactivated vaccine were administered during a KFD outbreak in India, but without a desired effect when KFD has been reported also in the vaccinated individuals (Aniker and Work, 1962; Shah et al., 1962). Live-attenuated candidate vaccines have demonstrated some protection against OHFV (Smorodintsev and Doubov, 1986) and Kyasanur forest disease virus (KFDV) (Erofeev et al., 1976) in mice and nonhuman primates. Modern concentrated TBE vaccines also demonstrated high protection from OHFV in mice (Chernokhaeva et al., 2016; Chidumayo et al., 2014).

Live, attenuated vaccines may be more likely than inactivated vaccines to cause antibody-enhanced replication during subsequent infection by the virus, because the epitopes are likely to be modified during the inactivation process, as seen for other viruses (Fergusson et al., 1993). In experiments with monkeys challenged with OHFV, it was shown that double immunization with an inactivated TBE vaccine protected animals against the hemorrhagic syndrome, but did not prevent virus invasion of the CNS (Pripuzova et al., 2013). The vaccine could be used for further studies as a surrogate vaccine against other tick-borne infections. Inactivated TBE vaccines have also been studied in mice challenged with POWV. Little protection was observed, but there were no signs of ADE (Chernokhaeva et al., 2016).

10. Recommendations for future TBE research

Future research should focus on the development and application of practical and affordable disease control approaches, including cheaper and more effective vaccines conferring long-lasting protection, together with effective therapies, such as small-molecule antivirals. The possible role of specific immunoglobulins in ADE reactions or the development of chronic forms of TBE requires further investigation. Detailed knowledge of TBEV biology and mechanisms of pathogenesis, including virus-host interactions at the molecular and cellular levels, are prerequisites for successful future research.

Disclaimer regarding Russian-language sources

When available, translations of the article title and journal name/abbreviation are given according to English-language abstracts or PubMed references. Translations made by the authors of this paper are given in square brackets. Author names are used according to the source or PubMed, but converted to the ASCII symbol space. As a result, the names of some authors may appear under different transliterations, depending on the source.

Acknowledgements

We are grateful to all of our colleagues provided insight for this review and/or shared unpublished research with us.

The authors acknowledge financial support from:

- The Russian Scientific Foundation (project #16-14-00083) to NT and AM,
- Ministry of Education and Science of the Russian Federation (project 0309-2016-0002) to NT and ST,
- Ministry of Health of the Czech Republic (grant No. 16-34238A) (to DR and LE), by Project "FIT" (Pharmacology, Immunotherapy, nanoToxicology; CZ.02.1.01/0.0/0.0/15_003/0000495), which was funded by the European Regional Development Fund (to ADM and DR),
- The Laboratory for Molecular Medicine Sweden (MIMS), the Swedish Research Council (VR; 2017-02438), the Swedish Foundation for Strategic Research (SSF; FFL12-0089) to AKÖ,
- The Ministry of Higher Education, Science and Sport of Slovenia (grant no. P3-0083) to TAŽ and NK.

References

- Aberle, J.H., Schwaiger, J., Aberle, S.W., Stiasny, K., Scheinost, O., Kundi, M., Chmelik, V., Heinz, F.X., 2015. Human CD4+ T Helper Cell Responses after Tick-Borne Encephalitis Vaccination and Infection. *PLoS One* 10 (10). <https://doi.org/10.1371/journal.pone.0140545>. e0140545.
- Aerssens, A., Cochez, C., Niedrig, M., Heyman, P., Kuhlmann-Rabens, I., Soentjens, P., 2016. Analysis of delayed TBE-vaccine booster after primary vaccination. *J. Trav. Med.* 23 (2), tav020.
- Afonina, O.S., Terekhina, L.L., Barkhaleva, O.A., Ladyzhenskaya, I.P., Sarkisyan, K.A., Vorob'eva, M.S., Karganova, G.G., Rukavishnikov, A.V., Shevtsov, V.A., Bondarev, V.P., 2014. Experimental studies cross immune response to antigens of the virus strains of tick-borne encephalitis different genotypes in BALB/c mice, immunized with various embodiments of tick-borne encephalitis vaccine. *Epidemiology and Vaccinal prevention* 5 (78), 88–95.
- Amicizia, D., Domnich, A., Panatto, D., Lai, P.L., Cristina, M.L., Avio, U., Gasparini, R., 2013. Epidemiology of tick-borne encephalitis (TBE) in Europe and its prevention by available vaccines. *Hum. Vaccines Immunother.* 9 (5), 1163–1171. <https://doi.org/10.4161/hv.23802>.
- Ammosov, A.D., 2006. Tick-borne Encephalitis. Koltsovo (In Russian).
- Andersson, C., Vene, S., Insulander, M., Lindquist, L., Lundkvist, A., Günther, G., 2010. Vaccine failures after active immunisation against tick-borne encephalitis. *Vaccine* 28 (16), 2827–2831. <https://doi.org/10.1016/j.vaccine.2010.02.001>.
- Andzhaparidze, O.G., Stepanova, L.G., 1970. The variability of tick-borne encephalitis virus. 7. Reactogenic and immunogenic properties of attenuated strain I-40 D upon oral vaccination of volunteers. *Vopr. Virusol.* 15 (4), 428–432.
- Aniker, S.P., Work, T.H., Chandrasekharaiya, T., Murthy, D.P., Rodrigues, F.M., Ahmed, R., Kulkarni, K.G., Rahman, S.H., Mansharamani, H., Prasanna, H.A., 1962. The administration of formalin-inactivated RSSE virus vaccine in the Kyasanur Forest disease area of Shimoga District, Mysore State. *Indian J. Med. Res.* 50, 147–152.
- Ankudinova, A.V., Romanenko, V.V., Vorovich, M.F., Kovtun, O.P., Eshyunina, M.S., Kiktenko, A.V., Kilychina, A.S., Averyanov, O.Yu., 2014. Results of a clinical immunogenicity and safety trial of Tick-E-Vac 0.25 ml vaccine (pediatric dosage). *Vestnik uralskoi meditsinskoi akademicheskoi nauki* 5 (51), 64–69.
- Aralov, A.V., Proskurin, G.V., Orlov, A.A., Kozlovskaya, L.I., Chistov, A.A., Kut'yakov, S.V., Karganova, G.G., Palyulin, V.A., Osolodkin, D.I., Korshun, V.A., 2017. Perylenyltriazoles inhibit reproduction of enveloped viruses. *Eur. J. Med. Chem.* 138, 293–299. <https://doi.org/10.1016/j.ejmech.2017.06.014>.
- Arras, C., Fescherek, R., Gregersen, J., 1996. Do specific hyperimmunoglobulins aggravate clinical course of tick-borne encephalitis? *Lancet* 347 (9011), 1331.
- Askling, H.H., Vene, S., Rombo, L., Lindquist, L., 2012. Immunogenicity of delayed TBE-vaccine booster. *Vaccine* 30 (3), 499–502.
- Baker, D.G., Woods, T.A., Butchi, N.B., Morgan, T.M., Taylor, R.T., Sunyakumthorn, P., Mukherjee, P., Lubick, K.J., Best, S.M., Peterson, K.E., 2013. Toll-like receptor 7 suppresses virus replication in neurons but does not affect viral pathogenesis in a mouse model of Langkat virus infection. *J. Gen. Virol.* 94 (Pt 2), 336–347. <https://doi.org/10.1099/vir.0.043984-0>.

- Barkhash, A.V., Perelygin, A.A., Babenko, V.N., Myasnikova, N.G., Pilipenko, P.I., Romaschenko, A.G., Voevoda, M.I., Brinton, M.A., 2010. Variability in the 2'-5'-oligoadenylate synthetase gene cluster is associated with human predisposition to tick-borne encephalitis virus-induced disease. *J. Infect. Dis.* 202 (12), 1813–1818. <https://doi.org/10.1086/657418>.
- Barkhash, A.V., Perelygin, A.A., Babenko, V.N., Brinton, M.A., Voevoda, M.I., 2012. Single nucleotide polymorphism in the promoter region of the CD209 gene is associated with human predisposition to severe forms of tick-borne encephalitis. *Antivir. Res.* 93 (1), 64–68. <https://doi.org/10.1016/j.antiviral.2011.10.017>.
- Barkhash, A.V., Voevoda, M.I., Romaschenko, A.G., 2013. Association of single nucleotide polymorphism rs3775291 in the coding region of the TLR3 gene with predisposition to tick-borne encephalitis in a Russian population. *Antivir. Res.* 99 (2), 136–138. <https://doi.org/10.1016/j.antiviral.2013.05.008>.
- Barkhash, A.V., Babenko, V.N., Voevoda, M.I., Romaschenko, A.G., 2016. Association of IL28B and IL10 gene polymorphism with predisposition to tick-borne encephalitis in a Russian population. *Ticks Tick Borne Dis* 7 (5), 808–812. <https://doi.org/10.1016/j.ttbdis.2016.03.019>.
- Barkhash, A.V., Yurchenko, A.A., Yudin, N.S., Ignatieva, E.V., Kozlova, I.V., Borishchuk, I.A., Pozdnyakova, L.L., Voevoda, M.I., Romaschenko, A.G., 2018. A matrix metalloproteinase 9 (MMP9) gene single nucleotide polymorphism is associated with predisposition to tick-borne encephalitis virus-induced severe central nervous system disease. *Ticks Tick Borne Dis* 9 (4), 763–767. <https://doi.org/10.1016/j.ttbdis.2018.02.010>. pii: S1877-959X(17)30315-1.
- Barrett, P.N., Schober-Bendixen, S., Ehrlich, H.J., 2003. History of TBE vaccines. *Vaccine* 21 (Suppl. 1), S41–S49.
- Baykov, I.K., Matveev, A.L., Stronin, O.V., Ryzhikov, A.B., Matveev, L.E., Kasakin, M.F., Richter, V.A., Tikunova, N.V., 2014. A protective chimeric antibody to tick-borne encephalitis virus. *Vaccine* 32 (29), 3589–3594. <https://doi.org/10.1016/j.vaccine.2014.05.012>.
- Bender, A., Schulte-Altdorneburg, G., Walther, E.U., Pfister, H.-W., 2005. Severe tick borne encephalitis with simultaneous brain stem, thalamic, and spinal cord involvement documented by MRI. *J. Neurol. Neurosurg. Psychiatry* 76 (1), 135–137.
- Beran, J., Xie, F., Zent, O., 2014. Five year follow-up after a first booster vaccination against tick-borne encephalitis following different primary vaccination schedules demonstrates long-term antibody persistence and safety. *Vaccine* 32 (34), 4275–4280.
- Best, S.M., Morris, K.L., Shannon, J.G., Robertson, S.J., Mitzel, D.N., Park, G.S., Boer, E., Wolfenbarger, J.B., Bloom, M.E., 2005. Inhibition of interferon-stimulated JAK-STAT signaling by a tick-borne flavivirus and identification of NS5 as an interferon antagonist. *J. Virol.* 79 (20), 12828–12839.
- Blaising, J., Polyak, S.J., Pécheur, E.L., 2014. Arbidol as a broad-spectrum antiviral: an update. *Antivir. Res.* 107, 84–94. <https://doi.org/10.1016/j.antiviral.2014.04.006>.
- Blom, K., Braun, M., Pakalniene, J., Lunemann, S., Enqvist, M., Dailidyte, L., Schaffer, M., Lindquist, L., Mickiene, A., Michaëlsson, J., Ljunggren, H.G., Gredmark-Russ, S., 2016. NK cell responses to human tick-borne encephalitis virus infection. *J. Immunol.* 197 (7), 2762–2771. <https://doi.org/10.1049/jimmunol.1600950>.
- Bogovic, P., Strle, F., 2015. Tick-borne encephalitis: a review of epidemiology, clinical characteristics, and management. *World Journal of Clinical Cases: WJCC.* 3 (5), 430–441. <https://doi.org/10.12998/wjcc.v3.i5.430>.
- Bogovic, P., Lotric-Furlan, S., Strle, F., 2010. What tick-borne encephalitis may look like: clinical signs and symptoms. *Trav. Med. Infect. Dis.* 8 (4), 246–250. <https://doi.org/10.1016/j.tmaid.2010.05.011>.
- Bogovič, P., Stupica, D., Rojko, T., Lotrič-Furlan, S., Avšič-Županc, T., Kastrin, A., Lusa, L., Strle, F., 2018. The long-term outcome of tick-borne encephalitis in Central Europe. *Ticks Tick Borne Dis* 9 (2), 369–378. <https://doi.org/10.1016/j.ttbdis.2017.12.001>.
- Boldescu, V., Behnam, M.A.M., Vasiliakis, N., Klein, C.D., 2017. Broad-spectrum agents for flaviviral infections: dengue, Zika and beyond. *Nat. Rev. Drug Discov.* 16, 565–586. <https://doi.org/10.1038/nrd.2017.33>.
- Borde, J.P., Zajkowska, J., 2017. Tick-borne encephalitis in adults. In: *Dobler G.TBE Chapter TBE in Adults*, pp. 1–29.
- Borodina, T.N., Evtushok, G.A., Tevelenok, O.G., Opeykina, N.N., 2004. Epidemiological efficacy of the vaccination against tick-borne encephalitis in the Krasnoyarsky krai. *Biopreparations* 2, 30–31.
- Boros, P., Gondolesi, G., Bromberg, J., 2005. High dose intravenous immunoglobulin treatment: mechanisms of action. *Liver Transplant.* 11 (12), 1469–1480. <https://doi.org/10.1002/lt.20594>.
- Brands, I., Köhler, S., Stapert, S., Wade, D., van Heugten, C., 2014. How flexible is coping after acquired brain injury? A 1-year prospective study investigating coping patterns and influence of self-efficacy, executive functioning and self-awareness. *J. Rehabil. Med.* 46 (9), 869–875. <https://doi.org/10.2340/16501977-1849>.
- Bröker, M., Kollaritsch, H., 2008. After a tick bite in a tick-borne encephalitis virus-endemic area: current positions about post-exposure treatment. *Vaccine* 26 (7), 863–868. <https://doi.org/10.1016/j.vaccine.2007.11.046>.
- Brophy, G.M., Bell, R., Claassen, J., et al., 2012. Guidelines for the evaluation and management of status epilepticus. *Neurocrit Care* 17, 3–23.
- Caini, S., Szomor, K., Ferenczi, E., Szekelyne Gaspar, A., Csohan, A., Krisztalovics, K., Molnar, Z., Horvath, J., 2012. Tick-borne encephalitis transmitted by unpasteurised cow milk in western Hungary, September to October 2011. *Euro Surveill.* 17 (12).
- Calisher, C.H., Karabatsos, N., Dalrymple, J.M., Shope, R.E., Porterfield, J.S., Westaway, E.G., Brandt, W.E., 1989. Antigenic relationships between flaviviruses as determined by cross-neutralization tests with polyclonal antisera. *J. Gen. Virol.* 70 (Pt 1), 37–43.
- Cantu, R.C., Ojemann, R.G., 1967. Corticosteroid in aseptic meningitis. *Lancet* 23, 1360–1361.
- Carroll, S.S., Tomassini, J.E., Bosserman, M., et al., 2003. Inhibition of hepatitis C virus RNA replication by 2'-modified nucleoside analogs. *J. Biol. Chem.* 278, 11979–11984.
- Carroll, S.S., Koeplinger, K., Vavrek, M., et al., 2011. Antiviral efficacy upon administration of a HepDirect prodrug of 2'-C-methylcytidine to hepatitis C virus-infected chimpanzees. *Antimicrob. Agents Chemother.* 55, 3854–3860.
- Casals, S., Webster, T., 1944. Relationship of the virus of Louping ill in sheep and the virus of Russian spring-summer encephalitis in man. *J. Exp. Med.* 79 (1), 45–63.
- Chambers, T.J., Diamond, M.S., 2003. Pathogenesis of flavivirus encephalitis. *Adv. Virus Res.* 60, 273–342.
- Chen, Y.L., Yin, Z., Duraismwamy, J., et al., 2010. Inhibition of dengue virus RNA synthesis by an adenosine nucleoside. *Antimicrob. Agents Chemother.* 54, 2932–2939.
- Chen, Y.L., Yokokawa, F., Shi, P.Y., 2015. The search for nucleoside/nucleotide analog inhibitors of dengue virus. *Antivir. Res.* 122, 12–19.
- Chernokhaeva, L.L., Rogova, Y.V., Vorovitch, M.F., Romanova, L.Iu, Kozlovskaya, L.I., Maikova, G.B., Kholodilov, I.S., Karganova, G.G., 2016. Protective immunity spectrum induced by immunization with a vaccine from the TBEV strain Sofjin. *Vaccine* 34 (20), 2354–2361. <https://doi.org/10.1016/j.vaccine.2016.03.041>.
- Chew, M.-F., Poh, K.-S., Poh, C.-L., 2017. Peptides as therapeutic agents for dengue virus. *Int. J. Med. Sci.* 14 (13), 1342–1359. <https://doi.org/10.7150/ijms.21875>.
- Chidumayo, N.N., Yoshii, K., Kariwa, H., 2014. Evaluation of the European tick-borne encephalitis vaccine against Omsk hemorrhagic fever virus. *Microbiol. Immunol.* 58 (2), 112–118.
- Chin, K.C., Cresswell, P., 2001. Viperin (cig5), an IFN-inducible antiviral protein directly induced by human cytomegalovirus. *Proc. Natl. Acad. Sci. U.S.A.* 98 (26), 15125–15130.
- Chmelik, V., Trnovcová, R., Bouzková, M., Slámová, I., Houserová, L., Chrdle, A., et al., 1999. Clinical picture of TBE; a retrospective study of 493 cases. *Zentbl. Bakteriol.* 289, 583–584.
- Chmelik, V., Bouzková, M., Slámová, I., Houserová, L., Chrdle, A., Petr, P., 2004. In: *Quality of Life after Tick Borne Encephalitis. ECCMID Praha 1 - 4.5.2004 P1418 Abstract in Clinical Microbiology and Infection*, vol. 10. pp. 397.
- Chumakov, M.P., Vorobyeva, N.N., Belyaeva, A.P., 1944. Study of ultraviral encephalitis. *Message 3. Kozhevnikov epilepsy and tick-borne encephalitis. J. of neuropathology and psychiatry* 13 (2), 65–68.
- Chumakov, M.P., Gagarina, A.V., Vilner, L.M., Khanina, M.K., Rodin, I.M., Vasenovich, M.I., Lakina, V.I., Finogenova, E.V., 1963a. Experience in the experimental production and control of tissue culture vaccine against tick encephalitis. *Vopr. Virusol.* 29, 415–420.
- Chumakov, M.P., L'vov, D.K., Sarmanova, E.S., Goldfarb, L.G., Naidich, G.N., Chumak, N.F., Vilner, L.M., Zasukhina, G.D., Isotov, V.K., Zaklinskaia, V.A., Umanski, K.G., 1963b. Comparative study of the epidemiological effectiveness of vaccination with tissue-culture and brain vaccine against tick encephalitis. *Vopr. Virusol.* 22, 307–315.
- Chumakov, M.P., L'vov, D.K., Goldfarb, L.G., Zaklinskaia, V.A., Gagarina, A.V., Mashkov, V.T., Iasin, A.E., Podin, V.I., Vil'ner, L.M., 1965a. Effect of the duration of intervals between vaccinations on the effectiveness of vaccination and revaccination against tick-borne encephalitis. *Vopr. Virusol.* 10 (3), 266–270.
- Chumakov, M.P., L'vov, D.K., Gagarina, A.V., Vil'ner, L.M., Rodin, I.M., Zaklinskaia, V.A., Goldfarb, L.G., Khanina, M.K., 1965b. Studies on factors influencing the effectiveness of immunization against tick-borne encephalitis. I. Effect of immunogenic properties of vaccines on the effectiveness of vaccination and revaccination. *Vopr. Virusol.* 10 (2), 168–172.
- Chumakov, M.P., Rubin, S.G., Semashko, I.V., Matrosovich, M.N., Mironova, L.L., Martyanova, L.I., Kniaginskaya, Y.A., Salnikov, Y.A., Gambaryan, A.S., Karavanov, A.S., Kurennapa, O.V., 1990. New perspective vaccines from tick-borne encephalitis virus propagated in green monkey kidney cell cultures. *Arch. Virol. (Suppl.)* 1, 161–168.
- Chumakov, M.P., Rubin, S.G., Semashko, I.V., Karavanov, A.S., Avdeeva, L.I., Gagarina, A.V., Gambaryan, A.S., Matrosovich, M.N., Mart'yanova, L.I., Mironova, L.L., et al., 1991. A new prospective vaccine against tick-borne encephalitis. *Zh. Mikrobiol. Epidemiol. Immunobiol.* (1), 36–40.
- Claassen, J.I., Taccone, F.S., Horn, P., Holtkamp, M., Stocchetti, N., Oddo, M., 2013. Neurointensive Care Section of the European Society of Intensive Care Medicine. Recommendations on the use of EEG monitoring in critically ill patients: consensus statement from the neurointensive care section of the ESICM. *Intensive Care Med.* 39 (8), 1337–1351. <https://doi.org/10.1007/s00134-013-2938-4>. Epub 2013 May 8.
- Clarke, D.H., 1964. Studies on antigenic relationships among the viruses of the group B tick-borne complex. *Bull. World Health Organ.* 31, 45–56.
- Colpitts, C.C., Ustinov, A.V., Epand, R.F., Epand, R.M., Korshun, V.A., Schang, L.M., 2013. 5-(Perylen-3-yl)ethynyl-arabino-uridine (aUY11), an arabino-based rigid amphipathic fusion inhibitor, targets virus envelope lipids to inhibit fusion of influenza virus, hepatitis C virus, and other enveloped viruses. *J. Virol.* 87 (7), 3640–3654. <https://doi.org/10.1128/JVI.02882-12>.
- Crotty, S., Cameron, C.E., Andino, R., 2001. RNA virus error catastrophe: direct molecular test by using ribavirin. *P Natl Acad Sci USA* 98, 6895–6900.
- Czupryna, P., Moniuszko, A., Garkowski, A., et al., 2014. Evaluation of hyponatraemia in patients with tick-borne encephalitis—a preliminary study. *Ticks Tick Borne Dis* 5 (3), 284–286. <https://doi.org/10.1016/j.ttbdis.2013.11.005>. Epub 2014 Feb 10.
- Dai, X., Shang, G., Lu, S., Yang, J., Xu, J., 2018. A new subtype of eastern tick-borne encephalitis virus discovered in Qinghai-Tibet Plateau, China. *Emerg. Microb. Infect.* 7 (1), 74. <https://doi.org/10.1038/s41426-018-0081-6>.
- De Clercq, E., 2011. A 40-year journey in search of selective antiviral chemotherapy. *Annu. Rev. Pharmacol. Toxicol.* 51, 1–24.
- De Clercq, E., 2016. C-nucleosides to be revisited. *J. Med. Chem.* 59, 2301–2311.
- De Clercq, E., Neyts, J., 2009. Antiviral agents acting as DNA or RNA chain terminators. *Handb. Exp. Pharmacol.* 189, 53–84.
- Demicheli, V., Debalini, M.G., Rivetti, A., 2009. Vaccines for preventing tick-borne encephalitis. *Cochrane Database Syst. Rev.* 1 Cd000977.
- Demina, T.V., Dzhiyev, Y.P., Verkhovina, M.M., Kozlova, I.V., Tkachev, S.E., Plyusnin, A.,

- Doroshchenko, E.K., Lisak, O.V., Zlobin, V.I., 2010. Genotyping and characterization of the geographical distribution of tick-borne encephalitis virus variants with a set of molecular probes. *J. Med. Virol.* 82 (6), 965–976. <https://doi.org/10.1002/jmv.21765>.
- Domnich, A., Panatto, D., Arbuzova, E.K., Signori, A., Avio, U., Gasparini, R., Amicizia, D., 2014. Immunogenicity against Far Eastern and Siberian subtypes of tick-borne encephalitis (TBE) virus elicited by the currently available vaccines based on the European subtype: systematic review and meta-analysis. *Hum. Vaccines Immunother.* 10 (10), 2819–2833.
- Don, E.S., Emelyanova, A.G., Yakovleva, N.N., Petrova, N.V., Nikiforova, M.V., Gorbunov, E.A., Tarasov, S.A., Morozov, S.G., Epstein, O.I., 2017. The phenomenon of released-activity. Reply on comment on Don et al.: dose-dependent antiviral activity of released-active form of antibodies to interferon-gamma against influenza A/California/07/09(H1N1) in murine model. *J. Med. Virol.* 89 (7), 1127–1130. <https://doi.org/10.1002/jmv.24759>.
- Doroshenko, A.S., Pomortseva, E.A., Morozova, K.V., Fokin, V.A., 2013. Meta-analysis of post-registration monitoring of Jodantipyrim® for emergency prevention of tick-borne encephalitis in endemic areas of Russia. *Terra Medica* (1), 27–29.
- Dörbecker, B., Dobler, G., Spiegel, M., Hufert, F.T., 2010. Tick-borne encephalitis virus and the immune response of the mammalian host. *Trav. Med. Infect. Dis.* 8 (4), 213–222. <https://doi.org/10.1016/j.tmaid.2010.05.010>.
- Doubov, A., Gorozhankina, T.S., Smorodintsev, A.A., 1969. Main biological properties of the vaccine strain Elantsev of tick-borne encephalitis virus. Life vaccine against tick-borne encephalitis. *Proceedings of Tyumen SRI of infectious pathology* 3, 16–26.
- Doubov, A., Gorozhankina, T.S., Ivanova, L.M., Molotilov, B.A., Kost'ev, S.G., Gubina, S.V., et al., 1971. Results of life vaccine against tick-borne encephalitis elaborated epidemiological trials. *Proceedings of Tyumen SRI of infectious pathology* 4, 11–17.
- Dueva, E.V., 2016. [Molecular Design of Fusion Inhibitors for Tick-borne Flaviviruses]. PhD thesis. Department of Chemistry, Lomonosov Moscow State University.
- Dueva, E.V., Panchin, A.Y., 2017. Homeopathy in disguise. Comment on Don et al.: dose-dependent antiviral activity of released-active form of antibodies to interferon-gamma against influenza A/California/07/09(H1N1) in murine model. *J. Med. Virol.* 89, 1125–1126. <https://doi.org/10.1002/jmv.24761>.
- Dueva, E.V., Osolodkin, D.I., Kozlovskaya, L.L., Palyulin, V.A., Pentkovski, V.M., Zefirov, N.S., 2014. Interaction of flaviviruses with reproduction inhibitors binding in β -OG pocket: insights from molecular dynamics simulations. *Mol Inf* 33 (10), 695–708. <https://doi.org/10.1002/minf.201300185>.
- Duniewicz, M., et al., 1974. Corticoids in the therapy of TBE and other viral encephalitis. *Cas. Lek. Cesk.* 113 (32), 984–987.
- Duniewicz, M., Mertenová, J., Moravcová, E., Jelinková, E., Holý, M., Kulková, H., Doutlik, S., 1975. [Central European tick-borne encephalitis from 1969 to 1972 in central bohemia (Czech)]. *Infection* 3 (4), 223–228.
- ECDC, 2012. Epidemiological Situation of Tick-borne Encephalitis in the European Union and Europe Free Trade Association Countries. ECDC Technical Report.
- Ecker, M., Allison, S.L., Meixner, T., Heinz, F.X., 1999. Sequence analysis and genetic classification of tick-borne encephalitis viruses from Europe and Asia. *J. Gen. Virol.* 80 (Pt 1), 179–185.
- Ehrlich, H.J., Pavlova, B.G., Fritsch, S., Poellabauer, E.M., Loew-Baselli, A., Obermann-Slupetzky, O., Maritsch, F., Cil, I., Dorner, F., Barrett, P.N., 2003. Randomized, phase II dose-finding studies of a modified tick-borne encephalitis vaccine: evaluation of safety and immunogenicity. *Vaccine* 22 (2), 217–223.
- El'bert, L.B., Gagarina, A.V., Khanina, M.K., Krutiaskaia, G.L., Grachev, V.P., 1980. Concentrated purified vaccine against tick-borne encephalitis prepared by means of zonal ultracentrifugation. Development of the preparation. *Vopr. Virusol.* (3), 341–345.
- El'bert, L.B., Pervikov, Iu.V., Grachev, V.P., Rusanov, V.M., Krokchina, M.A., 1984. Donor immunization with an inactivated concentrated purified vaccine against tick-borne encephalitis to obtain immune blood preparations. *Vopr. Virusol.* 29 (1), 56–69.
- El'bert, L.B., Krasi'nikov, I.V., Drozdov, S.G., Grachev, V.P., Pervikov, Iu.V., 1985. Concentrated and purified vaccine against tick-borne encephalitis prepared by ultracentrifugation and chromatography. *Vopr. Virusol.* 30 (1), 90–93.
- El'bert, L.B., Terletskaia, E.N., Timofeev, A.V., Amosenko, F.A., Khapchayev, Iu.Kh., Mironova, L.L., Svitkin, Iu.V., Vorovich, M.F., Lisitsyna, E.A., 1990. The purification of tick-borne encephalitis virus preparations of cellular DNA. *Vopr. Virusol.* 35 (3), 219–221.
- Elbert, L.B., Terletskaia, E.N., Timofeev, A.V., Mironova, L.L., Khapchayev, U.K., Amosenko, F.A., Svitkin, Y.V., Alpatova, G.A., Krutyanskaya, G.L., 1989. Inactivated vaccine against tick-borne encephalitis (TBE) derived from heteroplod continuous monkey cell line. *Vaccine* 7 (5), 475–477.
- Eldrup, A.B., Allerson, C.R., Bennett, C.F., et al., 2004. Structure-activity relationship of purine ribonucleosides for inhibition of hepatitis C virus RNA-dependent RNA polymerase. *J. Med. Chem.* 47, 2283–2295.
- Elsterova, J., Palus, M., Sirmarova, J., Kopecky, J., Niller, H., Ruzek, D., 2017. Tick-borne encephalitis virus neutralization by high dose intravenous immunoglobulin. *Ticks Tick Borne Dis* 8 (2), 253–258. <https://doi.org/10.1016/j.ttbdis.2016.11.007>.
- Erber, W., Schmitt, H.-J., Vuković Janković, T., 2018. Epidemiology by country. In: *In: Dobler, G., Erber, W., Schmitt, H.-J. (Eds.), Tick-borne Encephalitis (TBE)*, vol. 114. Global Health Press, Singapore, pp. 274 ISBN: 978-981-11-1903-3.
- Ergunay, K., Tkachev, S., Kozlova, I., Růžek, D., 2016. A review of methods for detecting tick-borne encephalitis virus infection in tick, animal, and human specimens. *Vector Borne Zoonotic Dis.* 16 (1), 4–12. <https://doi.org/10.1089/vbz.2015.1896>.
- Erofeev, V.S., Karpov, S.P., Kulikova, N.N., 1976. Immunobiological characteristics of tick-borne encephalitis vaccine, prepared from attenuated virus. In: *Proceeding of Tomsk SRI of Vaccines and Sera and Tomsk Medical University*, vol. 26. pp. 229–235.
- Eyer, L., Valdés, J.J., Gil, V.A., Nencka, R., Hřebáčková, H., Šála, M., Salát, J., Černý, J., Palus, M., De Clercq, E., Růžek, D., 2015. Nucleoside inhibitors of tick-borne encephalitis virus. *Antimicrob. Agents Chemother.* 59 (9), 5483–5493. <https://doi.org/10.1128/AAC.00807-15>.
- Eyer, L., Šmídová, M., Nencka, R., Neča, J., Kastl, T., Palus, M., De Clercq, E., Růžek, D., 2016. Structure-activity relationships of nucleoside analogues for inhibition of tick-borne encephalitis virus. *Antivir. Res.* 133, 119–129. <https://doi.org/10.1016/j.antiviral.2016.07.018>.
- Eyer, L., Zouharová, D., Širmarová, J., Fojtková, M., Štefánik, M., Haviernik, J., Nencka, R., de Clercq, E., Růžek, D., 2017a. Antiviral activity of the adenosine analogue BCX4430 against West Nile virus and tick-borne flaviviruses. *Antivir. Res.* 142, 63–67. <https://doi.org/10.1016/j.antiviral.2017.03.012>.
- Eyer, L., Kondo, H., Zouharova, D., Hirano, M., Valdés, J.J., Muto, M., Kastl, T., Kobayashi, S., Haviernik, J., Igarashi, M., Kariwa, H., Vaculovicova, M., Cerny, J., Kizek, R., Kröger, A., Lienenklaus, S., Dejmeck, M., Nencka, R., Palus, M., Salát, J., De Clercq, E., Yoshii, K., Ruzek, D., 2017b. Escape of tick-borne flavivirus from 2'-C-methylated nucleoside antivirals is mediated by a single conservative mutation in NS5 that has a dramatic effect on viral fitness. *J. Virol.* 91 (21). <https://doi.org/10.1128/JVI.101028-17>. e01028-17.
- Eyer, L., Nencka, R., de Clercq, E., Seley-Radtke, K., Růžek, D., 2018. Nucleoside analogs as a rich source of antiviral agents active against arthropod-borne flaviviruses. *Antivir. Chem. Chemother.* 26 <https://doi.org/10.1177/2040206618761299>. 2040206618761299.
- Fan, W., Qian, S., Qian, P., Li, X., 2016. Antiviral activity of luteolin against Japanese encephalitis virus. *Virus Res.* 220, 112–116. <https://doi.org/10.1016/j.virusres.2016.04.021>.
- Fialová, A., Cimburek, Z., Iezzi, G., Kopecký, J., 2010. Ixodes ricinus tick saliva modulates tick-borne encephalitis virus infection of dendritic cells. *Microb. Infect.* 12 (7), 580–585. <https://doi.org/10.1016/j.micinf.2010.03.015>.
- Formisano, R., Contrada, M., Aloisi, M., et al., 2017. Improvement rate of patients with severe brain injury during post-acute intensive rehabilitation. *Neurol. Sci.* <https://doi.org/10.1007/s10072-017-3203-3>.
- Fortune, D.G., Walsh, R.S., Waldron, B., et al., 2015. Changes in aspects of social functioning depend upon prior changes in neurodisability in people with acquired brain injury undergoing post-acute neurorehabilitation. *Front. Psychol.* 6, 1368. <https://doi.org/10.3389/fpsyg.2015.01368>.
- Fredericksen, B.L., Keller, B.C., Fornik, J., Katze, M.G., Gale Jr., M., 2008. Establishment and maintenance of the innate antiviral response to West Nile Virus involves both RIG-I and MDA5 signaling through IPS-1. *J. Virol.* 82 (2), 609–616.
- Frolova, T.V., Pogodina, V.V., Frolova, M.P., Karmysheva, V.I., 1982. Characteristics of long-term persisting strains of tick-borne encephalitis virus in different forms of the chronic process in animals. *Vopr. Virusol.* 27 (4), 473–479.
- Fujii, Y., Hayasaka, D., Kitaura, K., Takasaki, T., Suzuki, R., Kurane, I., 2011. T-cell clones expressing different T-cell receptors accumulate in the brains of dying and surviving mice after peripheral infection with far eastern strain of tick-borne encephalitis virus. *Viral Immunol.* 24 (4), 291–302. <https://doi.org/10.1089/vim.2011.0017>.
- Füzik, T., Formanová, P., Růžek, D., Yoshii, K., Niedrig, M., Plevka, P., 2018. Structure of tick-borne encephalitis virus and its neutralization by a monoclonal antibody. *Nat. Commun.* 9 (1), 436. <https://doi.org/10.1038/s41467-018-02882-0>.
- Gaieski, D.F., O'Brien, N.F., Hernandez, R., 2017. *Neurocrit Care* 27 (Suppl. 1), 124. <https://doi.org/10.1007/s12028-017-0455-y>.
- Galgani, L., Bunge, E.M., Hendriks, L., Schludermann, C., Marano, C., De Moerloose, L., 2017. Systematic literature review comparing rapid 3-dose administration of the GSK tick-borne encephalitis vaccine with other primary immunization schedules. *Expert Rev. Vaccines* 16 (9), 919–932.
- Gelpi, E., Preusser, M., Garzuly, F., Holzmann, H., Heinz, F.X., Budka, H., 2005. Visualization of Central European tick-borne encephalitis infection in fatal human cases. *J. Neuropathol. Exp. Neurol.* 64 (6), 506–512.
- Gelpi, E., Preusser, M., Lagner, U., Garzuly, F., Holzmann, H., Heinz, F.X., Budka, H., 2006. Inflammatory response in human tick-borne encephalitis: analysis of post-mortem brain tissue. *J. Neurovirol.* 12 (4), 322–327.
- Girgisdies, O.E., Rosenkranz, G., 1996. Tick-borne encephalitis: development of a paediatric vaccine. A controlled, randomized, double-blind and multicentre study. *Vaccine* 14 (15), 1421–1428.
- Gorbunov, M.A., Pavlova, L.L., Vorob'eva, M.S., Rasschepkina, M.N., Stronin, O.V., 2002a. Results of the clinical trials of the vaccine against tick-borne encephalitis EnceVir. *Epidemiology and Vaccinal Prevention* 5 (2), 49.
- Gorbunov, M.A., Pavlova, L.L., Vorob'eva, M.S., Rasschepkina, M.N., 2002b. Report of the results of field clinical trials of a new concentrated inactivated vaccine against tick-borne encephalitis EnceVir. *Epidemiologiia Infektsionnye Bolezni* 5, 57–60.
- Gould, E.A., Buckley, A., 1989. Antibody-dependent enhancement of yellow fever and Japanese encephalitis virus neurovirulence. *J. Gen. Virol.* 70 (Pt 6), 1605–1608.
- Gould, E.A., Buckley, A., Barrett, A.D., Cammack, N., 1986. Neutralizing (54K) and non-neutralizing (54K and 48K) monoclonal antibodies against structural and non-structural yellow fever virus proteins confer immunity in mice. *J. Gen. Virol.* 67 (Pt 3), 591–595.
- Grard, G., Moureau, G., Charrel, R.N., Lemasson, J.J., Gonzalez, J.P., Gallian, P., Gritsun, T.S., Holmes, E.C., Gould, E.A., de Lamballerie, X., 2007. Genetic characterization of tick-borne flaviviruses: new insights into evolution, pathogenic determinants and taxonomy. *Virology* 361 (1), 80–92.
- Gresfková, M., Sekeyová, M., Stupalová, S., Necas, S., 1975. Sheep milk-borne epidemic of tick-borne encephalitis in Slovakia. *Intervirology* 5 (1–2), 57–61.
- Grgic-Vitek, M., Avsic-Zupanc, T., Klavs, I., 2010. Tick-borne encephalitis after vaccination: vaccine failure or misdiagnosis. *Vaccine* 28 (46), 7396–7400.
- Gritsun, T.S., Frolova, T.V., Zhankov, A.I., Armento, M., Turner, S.L., Frolova, M.P., Pogodina, V.V., Lashkevich, V.A., Gould, E.A., 2003a. Characterization of a siberian virus isolated from a patient with progressive chronic tick-borne encephalitis. *J. Virol.* 77 (1), 25–36.

- Grits, T.S., Lashkevich, V.A., Gould, E.A., 2003b. Tick-borne encephalitis. *Antivir. Res.* 57 (1–2), 129–146.
- Günther, G., Haglund, M., Lindquist, L., Sköldenberg, B., Forsgren, M., 1997. Intrathecal IgM, IgA and IgG antibody response in tick-borne encephalitis. Long-term follow-up related to clinical course and outcome. *Clin. Diagn. Virol.* 8 (1), 17–29.
- Gustafson, R., Svenungsson, B., Forsgren, M., Gardulf, A., Granström, M., 1992. Two-year survey of the incidence of Lyme borreliosis and tick-borne encephalitis in a high-risk population in Sweden. *Eur. J. Clin. Microbiol. Infect. Dis.* 11 (10), 894–900.
- Gustafson, R., Forsgren, M., Gardulf, A., Granström, M., Svenungsson, B., 1993. Clinical manifestations and antibody prevalence of Lyme borreliosis and tick-borne encephalitis in Sweden: a study in five endemic areas close to Stockholm. *Scand. J. Infect. Dis.* 25 (5), 595–603.
- Habjan, M., Andersson, I., Klingström, J., Schümann, M., Martin, A., Zimmermann, P., Wagner, V., Pichlmair, A., Schneider, U., Mühlberger, E., Mirazimi, A., Weber, F., 2008. Processing of genome 5' termini as a strategy of negative-strand RNA viruses to avoid RIG-I-dependent interferon induction. *PLoS One* 3 (4). <https://doi.org/10.1371/journal.pone.0002032>. e2032.
- Haglund, M., Günther, G., 2003. Tick-borne encephalitis—pathogenesis, clinical course and long-term follow-up. *Vaccine* 21 (Suppl. 1), S11–S18.
- Haglund, M., Forsgren, M., Lindh, G., Lindquist, L., 1996. A 10-year follow-up study of tick-borne encephalitis in the stockholm area and a review of the literature: need for a vaccination strategy. *Scand. J. Infect. Dis.* 28 (3), 217–224. <https://doi.org/10.3109/00365549609027160>.
- Hainz, U., Jenewein, B., Asch, E., Pfeiffer, K.P., Berger, P., Grubeck-Loebenstien, B., 2005. Insufficient protection for healthy elderly adults by tetanus and TBE vaccines. *Vaccine* 23 (25), 3232–3235.
- Hakobyan, A., Galindo, I., Nañez, A., Arabyan, E., Karalyan, Z., Chistov, A.A., Streshnev, P.P., Korschun, V.A., Alonso, C., Zakaryan, H., 2018. Rigid amphipathic fusion inhibitors demonstrate antiviral activity against African swine fever virus. *J. Gen. Virol.* 99, 148–156. <https://doi.org/10.1099/jgv.0.000991>.
- Harabacz, I., Bock, H., Jungst, C., Klockmann, U., Praus, M., Weber, R., 1992. A randomized phase II study of a new tick-borne encephalitis vaccine using three different doses and two immunization regimens. *Vaccine* 10 (3), 145–150.
- Haslwanter, D., Blaas, D., Heinz, F.X., Stiasny, K., 2017. A novel mechanism of antibody-mediated enhancement of flavivirus infection. *PLoS Pathog.* 13 (9). <https://doi.org/10.1371/journal.ppat.1006643>. e1006643.
- Havirník, J., Štefánik, M., Fojtíková, M., Kali, S., Tordo, N., Rudolf, I., Hubálek, Z., Eyer, L., Ruzek, D., 2018. Arbidol (umifenovir): a broad-spectrum antiviral drug that inhibits medically important arthropod-borne flaviviruses. *Viruses* 10 (4), E184. <https://doi.org/10.3390/v10040184>.
- Hayasaka, D., Goto, A., Yoshii, K., Mizutani, T., Kariwa, H., Takashima, I., 2001. Evaluation of European tick-borne encephalitis virus vaccine against recent Siberian and far-eastern subtype strains. *Vaccine* 19 (32), 4774–4779.
- Heinz, F.X., Holzmann, H., Essl, A., Kundi, M., 2007. Field effectiveness of vaccination against tick-borne encephalitis. *Vaccine* 25 (43), 7559–7567. <https://doi.org/10.1016/j.vaccine.2007.08.024>.
- Helbig, K.J., Eyre, N.S., Yip, E., Narayana, S., Li, K., Fiches, G., McCartney, E.M., Jangra, R.K., Lemon, S.M., Beard, M.R., 2011. The antiviral protein viperin inhibits hepatitis C virus replication via interaction with nonstructural protein 5A. *Hepatology* 54 (5), 1506–1517. <https://doi.org/10.1002/hep.24542>.
- Hertzell, K.B., Pauksens, K., Rombo, L., Knight, A., Vene, S., Askling, H.H., 2016. Tick-borne encephalitis (TBE) vaccine to medically immunosuppressed patients with rheumatoid arthritis: a prospective, open-label, multi-centre study. *Vaccine* 34 (5), 650–655.
- Hidari, K.I.P.J., Abe, T., Suzuki, T., 2013. Carbohydrate-related inhibitors of dengue virus entry. *Viruses* 5 (2), 605–618. <https://doi.org/10.3390/v5020605>.
- Hoke Jr., C.H., Vaughn, D.W., Nisalak, A., Intralawan, P., Poolsupparit, S., Jongasawas, V., Titsyakorn, U., Johnson, R.T., 1992. Effect of high-dose dexamethasone on the outcome of acute encephalitis due to Japanese encephalitis virus. *J. Infect. Dis.* 165 (4), 631–637.
- Holzmann, H., 2003. Diagnosis of tick-borne encephalitis. *Vaccine* 21 (Suppl. 1), S36–S40.
- Holzmann, H., Kundi, M., Stiasny, K., Clement, J., McKenna, P., Kunz, C., Heinz, F.X., 1996. Correlation between ELISA, hemagglutination inhibition, and neutralization tests after vaccination against tick-borne encephalitis. *J. Med. Virol.* 48 (1), 102–107.
- Holzmann, H., Aberle, S.W., Stiasny, K., Werner, P., Mischak, A., Zainer, B., Netzer, M., Koppi, S., Bechter, E., Heinz, F.X., 2009. Tick-borne encephalitis from eating goat cheese in a mountain region of Austria. *Emerg. Infect. Dis.* 15 (10), 1671–1673. <https://doi.org/10.3201/eid1510.090743>.
- Hudopisk, N., Korva, M., Janet, E., Simetinger, M., Grgič-Vitek, M., Gubenšek, J., Natek, V., Kraigher, A., Strle, F., Avšič-Županc, T., 2013. Tick-borne encephalitis associated with consumption of raw goat milk, Slovenia, 2012. *Emerg. Infect. Dis.* 19 (5), 806–808. <https://doi.org/10.3201/eid1905.121442>.
- Huisman, W., Martina, B.E., Rimmelzwaan, G.F., Gruters, R.A., Osterhaus, A.D., 2009. Vaccine-induced enhancement of viral infections. *Vaccine* 27 (4), 505–512. <https://doi.org/10.1016/j.vaccine.2008.10.087>.
- Hultgren, C., Milich, D.R., Weiland, O., et al., 1998. The antiviral compound ribavirin modulates the T helper (Th)1/Th2 subset balance in hepatitis B and C virus-specific immune responses. *J. Gen. Virol.* 79, 2381–2391.
- Iacono-Connors, L.C., Smith, J.F., Ksiazek, T.G., Kelley, C.L., Schmaljohn, C.S., 1996. Characterization of Langat virus antigenic determinants defined by monoclonal antibodies to E, NS1 and preM and identification of a protective, non-neutralizing preM-specific monoclonal antibody. *Virus Res.* 43 (2), 125–136.
- Ilenko, V.I., Smorodincev, A.A., Prozorova, I.N., Platonov, V.G., 1968. Experience in the study of a live vaccine made from the TP-21 strain of Malayan Langat virus. *Bull. World Health Organ.* 39 (3), 425–431 1968.
- Ilenko, V.I., Platonov, V.G., Prozorova, I.N., Smorodintsev, A.A., 1989. The possibility of preparing a live vaccine against tick-borne encephalitis from Malay langat virus TP-21. *Tr. Inst. Im. Pastera* 65, 126–132.
- Jilkova, E., Vejvalkova, P., Stiborova, I., Skorkovskiy, J., Kral, V., 2009. Serological response to tick-borne encephalitis (TBE) vaccination in the elderly—results from an observational study. *Expert Opin. Biol. Ther.* 9 (7), 797–803.
- Jordheim, L.P., Duranet, D., Zoulim, F., Dumontet, C., 2013. Advances in the development of nucleoside and nucleotide analogues for cancer and viral diseases. *Nat. Rev. Drug Discov.* 12, 447–464. <https://doi.org/10.1038/nrd4010>.
- Jost, S., Altfeld, M., 2013. Control of human viral infections by natural killer cells. *Annu. Rev. Immunol.* 31, 163–194. <https://doi.org/10.1146/annurev-immunol-032712-100001>.
- Juhász, C., Szirmai, I., 1993. Spectral EEG parameters in patients with tick-borne encephalitis: a follow-up study. *Clin. Electroencephalogr.* 24 (2), 53–58.
- Kagan, N.V., 1939. Experimental contributions to active immunization of mice against the Spring-Summer (tick-borne) encephalitis by means of preparations of live and killed virus. *Arch. Sci. Biol.* 56 (2), 97–111.
- Kaiser, R., 1999. The clinical and epidemiological profile of tick-borne encephalitis in southern Germany 1994–1998: a prospective study of 656 patients. *Brain* 122, 2067–2078.
- Kaiser, R., 2008. Tick-borne encephalitis. *Infect. Dis. Clin.* 22 (3), 561–575.
- Kaiser, R., 2011. Langzeitprognose bei primär myelitischer Manifestation der FSME. *Nervenarzt* 82 (8), 1020–1025.
- Kaiser, R., 2012. Tick-borne encephalitis: clinical findings and prognosis in adults. *Wien Med. Wochenschr.* 162 (11–12), 239–243.
- Karpenko, I., Deev, S., Kiselev, O., Charushin, V., Rusinov, V., Ulomsky, E., Deeva, E., Yanvarev, D., Ivanov, A., Smirnova, O., Kochetkov, S., Chupakhin, O., Kukhanova, M., 2010. Antiviral properties, metabolism, and pharmacokinetics of a novel azolo-1,2,4-triazine-derived inhibitor of influenza A and B virus replication. *Antimicrob. Agents Chemother.* 54 (5), 2017–2022. <https://doi.org/10.1128/AAC.01186-09>.
- Kelesidis, T., Mastoris, I., Metsini, A., Tsiodras, S., 2014. How to approach and treat viral infections in ICU patients. *BMC Infect. Dis.* 14, 321. <https://doi.org/10.1186/1471-2334-14-321>.
- Khotubei, L.I., Pervikov, IuV., Krutianskaia, G.L., Vil'ner, L.M., Semenov, B.F., 1982. Concentrated purified vaccine against tick-borne encephalitis. An immunological evaluation in experiments on mice. *Vopr. Virusol.* 27 (3), 316–320.
- Khudoley, V.N., Saratkov, A.S., Lepekhin, A.V., Yavorskaya, V.E., Evstropov, A.N., Portnyagina, E.V., Pomogaeva, A.D., Beloborodova, E.I., Vnushinkaia, M.A., Schmidt, E.V., Krilova, N.V., Khunafina, D.K., Mezenzeva, M.V., Ershov, F.I., Raevski, K.K., Vlasova, E.V., Abdulova, G.A., Kropotkina, E.A., 2008. Antiviral activity of jodanti-pyrin: an anti-inflammatory oral therapeutic with interferon-inducing properties. *Anti-Inflammatory Anti-Allergy Agents Med. Chem.* 7, 106–115.
- Kindberg, E., Vene, S., Mickiene, A., Lundkvist, Å., Lindquist, L., Svensson, L., 2011. A functional Toll-like receptor 3 gene (TLR3) may be a risk factor for tick-borne encephalitis virus (TBEV) infection. *J. Infect. Dis.* 203 (4), 523–528. <https://doi.org/10.1093/infdis/jiq082>.
- Kleiter, I., Jilg, W., Bogdahn, U., Steinbrecher, A., 2007. Delayed humoral immunity in a patient with severe tick-borne encephalitis after complete active vaccination. *Infection* 35 (1), 26–29. <https://doi.org/10.1007/s15010-006-6614-2>.
- Kluger, G., Schöttler, A., Waldvogel, K., Nadal, D., Hinrichs, W., Wündisch, G.F., Laub, M.C., 1995. Tickborne encephalitis despite specific immunoglobulin prophylaxis. *Lancet* 346 (8988), 1502.
- Kofler, M., Schiefecker, A., Beer, R., et al., 2016. Neuroglucopenia and metabolic distress in two patients with viral meningoencephalitis: a microdialysis study. *Neurocritical Care* 25 (2), 273–281. <https://doi.org/10.1007/s12028-016-0272-8>.
- Kohl, I., Kozuch, O., Elecková, E., Labuda, M., Zalužko, J., 1996. Family outbreak of alimentary tick-borne encephalitis in Slovakia associated with a natural focus of infection. *Eur. J. Epidemiol.* 12 (4), 373–375.
- Kolb, B., Muhammad, A., 2014. Harnessing the power of neuroplasticity for intervention. *Front. Hum. Neurosci.* 8, 377. <https://doi.org/10.3389/fnhum.2014.00377>.
- Konior, R., Brzostek, J., Poellabauer, E.M., Jiang, Q., Harper, L., Erber, W., 2017. Seropersistence of TBE virus antibodies 10 years after first booster vaccination and response to a second booster vaccination with FSME-IMMUN 0.5mL in adults. *Vaccine* 35 (28), 3607–3613.
- Kopecný, J., Grubhoffer, L., Tomková, E., 1991. Interaction of tick/borne encephalitis virus with mouse peritoneal macrophages. The effect of antiviral antibody and lectin. *Acta Virol.* 35 (3), 218–225.
- Kovalskii, Y.G., Lebed'ko, O.A., Zaharicheva, T.A., Sen'kevich, O.A., Mzhelskaya, T.V., Sapuntsova, S.P., Ryabtseva, E.G., 2013. Selenium concentration and status of antioxidant system in patients with tick-borne encephalitis in the Russian Far East. *Dalnevostochny Zhurnal Infektsionnoy Patologii* (22), 18–22.
- Kozlova, I.V., Demina, T.V., Tkachev, S.E., Doroshchenko, E.K., Lisak, O.V., Verkhovina, M.M., Karan, L.S., Dzhioev, Y.P., Pamonov, A.I., Suntsova, O.V., Savinova, Y.S., Chernovanova, O.O., Ruzek, D., Tikhunova, N.V., Zlobin, V.I., 2018. Characteristics of the Baikal subtype of tick-borne encephalitis virus circulating in Eastern Siberia. *Acta Biomedica Scientifica* 3 (4), 53–60. <https://doi.org/10.29413/ABS.2018.3.4.9>.
- Kozlovskaya, L.I., Osolodkin, D.I., Shevtsova, A.S., Romanova, Llu, Rogova, Y.V., Dzhivanian, T.I., Lyapustin, V.N., Pivanova, G.P., Gmyl, A.P., Palyulin, V.A., Karganova, G.G., 2010. GAG-binding variants of tick-borne encephalitis virus. *Virology* 398 (2), 262–272. <https://doi.org/10.1016/j.viro.2009.12.012>.
- Kozlovskaya, L.I., Golinets, A.D., Eletskaia, A.A., Orlov, A.A., Palyulin, V.A., Kochetkov, S.N., Alexandrova, L.A., Osolodkin, D.I., 2018. Selective inhibition of Enterovirus A species members' reproduction by furano[2,3-d]pyrimidine nucleosides revealed by antiviral activity profiling against (+)ssRNA viruses. *ChemistrySelect* 3 (8), 2321–2325. <https://doi.org/10.1002/slct.201703052>.
- Krasilnikov, I.V., Mischenko, I.A., Sharova, O.I., Bilalova, G.P., Stavitskaya, N.K.,

- Vorob'eva, M.S., Rasshepkina, M.N., Pavlova, L.I., Gorbunov, M.A., Ustinov, O.B., 2004. EnceVir vaccine: development and implementation in practice. *Biopreparations* 2, 21–24.
- Krbkova, L., Štroblová, H., Bednářová, J., 2015. Clinical course and sequelae for tick-borne encephalitis among children in South Moravia (Czech Republic). *Eur. J. Pediatr.* 174 (4), 449–458. <https://doi.org/10.1007/s00431-014-2401-8>.
- Kreil, T.R., Eibl, M.M., 1997. Pre- and postexposure protection by passive immunoglobulin but no enhancement of infection with a flavivirus in a mouse model. *J. Virol.* 71 (4), 2921–2927.
- Kreil, T.R., Maier, E., Fraiss, S., Eibl, M.M., 1998a. Neutralizing antibodies protect against lethal flavivirus challenge but allow for the development of active humoral immunity to a nonstructural virus protein. *J. Virol.* 72 (4), 3076–3081.
- Kreil, T.R., Maier, E., Fraiss, S., Attakpah, E., Burger, I., Mannhalter, J.W., Eibl, M.M., 1998b. Vaccination against tick-borne encephalitis virus, a flavivirus, prevents disease but not infection, although viremia is undetectable. *Vaccine* 16 (11–12), 1083–1086.
- Kriz, B., Benes, C., Daniel, M., 2009. Alimentary transmission of tick-borne encephalitis in the Czech Republic (1997–2008). *Epidemiol. Mikrobiol. Imunol.* 58 (2), 98–103.
- Kroschewski, H., Allison, S.L., Heinz, F.X., Mandl, C.W., 2003. Role of heparan sulfate for attachment of Tick-Borne encephalitis virus. *Virology* 308 (1), 92–100.
- Krylova, N.V., Leonova, G.N., Popov, A.M., Artyukov, A.A., Maistrovskaya, O.S., Kozlovskaya, E.P., 2009. Antiviral activity of combined medication Zoster a asiatica-derived rosmarinic acid against tick-borne encephalitis pathogen. *Pacific Med J* 3, 86–88.
- Krylova, N.V., Leonova, G.N., 2016. Antiviral activity of various drugs with different mechanisms of action in patients with experimental tick-borne encephalitis. *Vopr. Virusol.* 61 (3), 139–144. <https://doi.org/10.18821/0507-4088-2016-61-3-139-144>.
- Krylova, N.V., Leonova, G.N., Maistrovskaya, O.S., Popov, A.M., Artyukov, A.A., Kozlovskaya, E.P., 2010. In vitro activity of luromarin against tick-borne encephalitis virus. *Antibiot. Khimioter.* 55 (7–8), 17–19.
- Krylova, N.V., Popov, A.M., Leonova, G.N., Artyukov, A.A., Maistrovskaya, O.S., 2011a. Comparative study of antiviral activity of luteolin and 7,3'-disulfate luteolin. *Antibiot. Khimioter.* 56 (11–12), 7–10.
- Krylova, N.V., Popov, A.M., Leonova, G.N., Artyukov, A.A., Kozlovskaya, E.P., 2011b. Investigation of luromarin efficacy on mice with experimental tick-borne encephalitis. *Antibiot. Khimioter.* 56 (11–12), 13–15.
- Krylova, N.V., Smolina, T.P., Leonova, G.N., 2015. Molecular mechanisms of interaction between human immune cells and far eastern tick-borne encephalitis virus strains. *Viral Immunol.* 28 (5), 272–281. <https://doi.org/10.1089/vim.2014.0083>.
- Kubes, M., Fuchsberger, N., Labuda, M., Zuffova, E., Nuttall, P.A., 1994. Salivary gland extracts of partially fed Dermacentor reticulatus ticks decrease natural killer cell activity in vitro. *Immunology* 82 (1), 113–116.
- Kunz, C., 2003. TBE vaccination and the Austrian experience. *Vaccine* 21 (Suppl. 1), S50–S55.
- Kunze, U., 2015. Tick-borne encephalitis as a notifiable disease—Status quo and the way forward. Report of the 17th annual meeting of the International Scientific Working Group on Tick-Borne Encephalitis (ISW-TBE). *Ticks Tick Borne Dis* 6 (5), 545–548.
- Kurane, I., Hebblewaite, D., Brandt, W.E., Ennis, F.A., 1984. Lysis of dengue virus-infected cells by natural cell-mediated cytotoxicity and antibody-dependent cell-mediated cytotoxicity. *J. Virol.* 52 (1), 223–230.
- Kurhade, C., Zegenhagen, L., Weber, E., Nair, S., Michaelsen-Preusse, K., Spanier, J., Gekara, N.O., Kröger, A., Överby, A.K., 2016. Type I Interferon response in olfactory bulb, the site of tick-borne flavivirus accumulation, is primarily regulated by IPS-1. *J. Neuroinflammation* 13, 22. <https://doi.org/10.1186/s12974-016-0487-9>.
- Labuda, M., Jones, L.D., Williams, T., Nuttall, P.A., 1993. Enhancement of tick-borne encephalitis virus transmission by tick salivary gland extracts. *Med. Vet. Entomol.* 7 (2), 193–196.
- Labuda, M., Austyn, J.M., Zuffova, E., Kozuch, O., Fuchsberger, N., Lysy, J., Nuttall, P.A., 1996. Importance of localized skin infection in tick-borne encephalitis virus transmission. *Virology* 219 (2), 357–366.
- Lashkevitch, V.A., Karganova, G.G., 2007. Modern aspects of the prevention of tick-borne encephalitis. *Vopr. Virusol.* 52 (5), 31–32 (In Russian).
- Latour, D.R., Jekle, A., Javanbakht, H., et al., 2010. Biochemical characterization of the inhibition of the dengue virus RNA polymerase by beta-D-2'-ethynyl-7-deaza-adenosine triphosphate. *Antivir. Res.* 87, 213–222.
- Lenhard, T., Ott, D., Jakob, N.J., Pham, M., Bäumer, P., Martinez-Torres, F., et al., 2016. Predictors, Neuroimaging Characteristics and Long-Term Outcome of Severe European Tick-Borne Encephalitis: a Prospective Cohort Study. *Klein RS, editor. PLoS One* 11 (4) e0154143.
- Leonova, G.N., Pavlenko, E.V., 2009. Characterization of neutralizing antibodies to Far Eastern of tick-borne encephalitis virus subtype and the antibody avidity for four tick-borne encephalitis vaccines in human. *Vaccine* 27 (21), 2899–2904. <https://doi.org/10.1016/j.vaccine.2009.02.069>. 2009 May 11.
- Leonova, G.N., Pavlenko, E.V., 2010. Functional activity of specific antibodies in patients vaccinated against tick-borne encephalitis in relation to different virus strains. *Vopr. Virusol.* 55 (3), 33–37.
- Leonova, G.N., Maistrovskaya, O.S., Borisevich, V.B., 1996. Antigenemia in people infected with tick-borne encephalitis virus. *Vopr. Virusol.* 41 (6), 260–263.
- Leonova, G.N., Belikov, S.I., Kondratov, I.G., Takashima, I., 2013. Comprehensive assessment of the genetics and virulence of tick-borne encephalitis virus strains isolated from patients with inapparent and clinical forms of the infection in the Russian Far East. *Virology* 443 (1), 89–98. <https://doi.org/10.1016/j.viro.2013.04.029>.
- Lepekhin, A.V., Ratnikova, L.I., Litvin, A.A., Stovbun, S.V., Sergienko, V.I., 2007. An experience of using Panavir in therapy of tick-borne encephalitis. *Infektsionnye Bolezni* 5 (1), 41–46.
- Lepekhin, A.V., Ilyinskikh, E.N., Lukashova, L.V., Doroshenko, A.S., Zamyatina, E.V., 2012. Assessment of effectiveness of iodantipyrene preventive use in treatment of Russian tick-borne encephalitis. *Sibirskiy Meditsinsky Zhurnal* 111 (4), 55–58.
- Lepekhin, A.V., Ilyinskikh, E.N., Lukashova, L.V., Zamyatina, E.V., Portnyagina, E.V., Buzhak, N.S., Puchkova, N.N., 2016. New approaches to emergency prevention and treatment of viral infections by the example of tick-borne encephalitis and influenza. *Meditsinsky Sovet* (4), 82–87. <https://doi.org/10.21518/2079-701X-2016-4-82-87>.
- Leyssen, P., Balzarini, J., De Clercq, E., et al., 2005. The predominant mechanism by which ribavirin exerts its antiviral activity in vitro against flaviviruses and paramyxoviruses is mediated by inhibition of inosine monophosphate dehydrogenase. *J. Virol.* 79, 1943–1947.
- Li, F., Wang, Y., Yu, L., Cao, S., Wang, K., Yuan, J., Wang, C., Wang, K., Cui, M., Fu, Z.F., 2015. Viral infection of the central nervous system and neuroinflammation precede blood-brain barrier disruption during Japanese encephalitis virus infection. *J. Virol.* 89 (10), 5602–5614. <https://doi.org/10.1128/JVI.00143-15>.
- Lindquist, L., Vapalahti, O., 2008. Tick-borne encephalitis. *Lancet* 371 (9627), 1861–1871. [https://doi.org/10.1016/S0140-6736\(08\)60800-4](https://doi.org/10.1016/S0140-6736(08)60800-4).
- Lindqvist, R., Mundt, F., Gilthorpe, J.D., Wölfel, S., Gekara, N.O., Kröger, A., Överby, A.K., 2016. Fast type I interferon response protects astrocytes from flavivirus infection and virus-induced cytopathic effects. *J. Neuroinflammation* 13 (1), 277.
- Lipowski, D., Szablowska, M., Perlejewski, K., Nakamura, S., Bukowska-Oško, I., Rzdakiewicz, E., et al., 2017. A cluster of fatal tick-borne encephalitis virus infection in organ transplant setting. *J. Infect. Dis.* 215 (6), 896–901. <https://doi.org/10.1093/infdis/jix040>.
- Litvin, A.A., Ratnikova, L.I., Deryabin, P.G., 2009. Preclinical and clinical studies of the efficacy of panavir in therapy for tick-borne encephalitis. *Vopr. Virusol.* 54 (3), 26–32.
- Lo, M.K., Shi, P.Y., Chen, Y.L., Flint, M., Spiropoulou, C.F., 2016. In vitro antiviral activity of adenosine analog NITD008 against tick-borne flaviviruses. *Antivir. Res.* 130, 46–49. <https://doi.org/10.1016/j.antiviral.2016.03.013>.
- Lo, M.K., Jordan, R., Arvey, A., et al., 2017. GS-5734 and its parent nucleoside analog inhibit Filo-, Pneumo-, and Paramyxoviruses. *Sci Rep UK* 7, 43395.
- Lobzin, Yu.V., Belozero, E.S., Belyaeva, T.V., Volzhanin, V.M., 2015. Human Viral Diseases. "SpetsLit", Sankt-Petersburg (In Russian).
- Loew-Baselli, A., Konior, R., Pavlova, B.G., Fritsch, S., Poellabauer, E., Maritsch, F., Harmacek, P., Krammer, M., Barrett, P.N., Ehrlich, H.J., 2006. Safety and immunogenicity of the modified adult tick-borne encephalitis vaccine FSME-IMMUN: results of two large phase 3 clinical studies. *Vaccine* 24 (24), 5256–5263.
- Loew-Baselli, A., Poellabauer, E.M., Pavlova, B.G., Fritsch, S., Koska, M., Bobrovsky, R., Konior, R., Ehrlich, H.J., 2009. Seropersistence of tick-borne encephalitis antibodies, safety and booster response to FSME-IMMUN 0.5 ml in adults aged 18–67 years. *Hum Vaccin* 5 (8), 551–556.
- Loew-Baselli, A., Poellabauer, E.M., Pavlova, B.G., Fritsch, S., Firth, C., Petermann, R., Barrett, P.N., Ehrlich, H.J., 2011. Prevention of tick-borne encephalitis by FSME-IMMUN vaccines: review of a clinical development programme. *Vaccine* 29 (43), 7307–7319.
- Loginova, S.Y., Borisevich, S.V., Rusinov, V.L., Ulomsky, U.N., Charushin, V.N., Chupakhin, O.N., 2014. Investigation of Triazavirin antiviral activity against tick-borne encephalitis pathogen in cell culture. *Antibiot. Khimioter.* 59 (1–2), 3–5.
- Loginova, S.Y., Borisevich, S.V., Rusinov, V.L., Ulomsky, U.N., Charushin, V.N., Chupakhin, N., Sorokin, P.V., 2015. Investigation of prophylactic efficacy of triazavirin against experimental forest-spring encephalitis on albino mice. *Antibiot. Khimioter.* 60 (5–6), 8–11.
- Loo, Y.M., Fornek, J., Crochet, N., Bajwa, G., Perwitasari, O., Martinez-Sobrido, L., Akira, S., Gill, M.A., García-Sastre, A., Katze, M.G., Gale Jr., M., 2008. Distinct RIG-I and MDA5 signaling by RNA viruses in innate immunity. *J. Virol.* 82 (1), 335–345.
- Loshko, K.V., Lobzin, Yu.V., Kozlov, S.S., 2004. Experience of tick-borne encephalitis vaccine use in the Leningrad military region. *Biopreparations* 22, 9–30.
- Lotric-Furlan, S., Petrovec, M., Avsic-Zupanc, T., Strle, F., 2005. Concomitant tickborne encephalitis and human granulocytic ehrlichiosis. *Emerg. Infect. Dis.* 11, 485–488.
- Lotric-Furlan, S., Bogovic, P., Avsic-Zupanc, T., Jelovsek, M., Lusa, L., Strle, F., 2017. Tick-borne encephalitis in patients vaccinated against this disease. 282 (2), 142–155.
- Lubick, K.J., Robertson, S.J., McNally, K.L., Freedman, B.A., Rasmussen, A.L., Taylor, R.T., Walts, A.D., Tsuruda, S., Sakai, M., Ishizuka, M., Boer, E.F., Foster, E.C., Chiramel, A.I., Addison, C.B., Green, R., Kastner, D.L., Katze, M.G., Holland, S.M., Forlino, A., Freeman, A.F., Boehm, M., Yoshii, K., Best, S.M., 2015. Flavivirus antagonism of type I interferon signaling reveals prolylase as a regulator of IFNAR1 surface expression. *Cell Host Microbe* 18 (1), 61–74. <https://doi.org/10.1016/j.chom.2015.06.007>.
- Łuczaj, W., Moniuszko, A., Jarocka-Karpowicz, I., Pancewicz, S., Andrisic, L., Zarkovic, N., Skrzydlewska, E., 2016. Tick-borne encephalitis – lipid peroxidation and its consequences. *Scand. J. Clin. Lab. Investig.* 76 (1), 1–9. <https://doi.org/10.3109/00365513.2015.1084040>.
- Lunáček, J., Chmelfík, V., Sípová, I., Zampachová, E., Becvářová, J., 2003. [Epidemiologic monitoring of tick-borne encephalitis in rimov in southern bohemia]. *Epidemiol. Mikrobiol. Imunol.* 52 (2), 51–58 (in Czech).
- Lvov, D.K., ZaklinskaiA, V.A., FokinA, K.V., 1963. Dynamics of serological indices of immunity in animals immunized with vaccines against tick-borne encephalitis. *Vopr. Virusol.* 29, 420–427.
- Maikova, G.B., Chernokhaeva, L.L., Vorovitch, M.F., Rogova, Yu.V., Karganova, G.G., 2016. Vaccines based on the Far-Eastern and European strains induce the neutralizing antibodies against all known tick-borne encephalitis virus subtypes. *Vopr. Virusol.* 61 (3), 135–139.
- Maikova, G.B., Chernokhaeva, L.L., Rogova, Y.V., Kozlovskaya, L.I., Kholodilov, I.S., Romanenko, V.V., Esyunina, M.S., Ankudinova, A.A., Kilyachina, A.S., Vorovitch, M.F., Karganova, G.G., 2019. Ability of inactivated vaccines based on far-eastern tick-borne encephalitis virus strains to induce humoral immune response in originally

- seropositive and seronegative recipients. *J. Med. Virol.* 91 (2), 190–200. <https://doi.org/10.1002/jmv.25316>.
- Makarenkova, I.D., Kryilova, N.V., Leonova, G.N., Besednova, N.N., Zvyagintseva, T.N., Shevchenko, N.M., 2009. Protective effects of fucoidan derived from brown algae *Laminaria japonica* under experimental tick-borne encephalitis. *Pacific Med J* 3, 89–92.
- Makarenkova, I.D., Leonova, G.N., Maistrovskaya, O.S., Zvyagintseva, T.N., Imbs, T.I., Ermakova, S.P., Besednova, N.N., 2012. Antiviral effect of brown algae-derived sulphated polysaccharides in case of experimental tick-borne encephalitis: tying structure and function. *Pacific Med J* 1, 44–46.
- Mandl, C.W., Kroschewski, H., Allison, S.L., Kofler, R., Holzmann, H., Meixner, T., Heinz, F.X., 2001. Adaptation of Tick-Borne encephalitis virus to BHK-21 cells results in the formation of multiple heparan sulfate binding sites in the envelope protein and attenuation in vivo. *J. Virol.* 75 (1), 5627–5637.
- Marasco, W.A., Sui, J., 2007. The growth and potential of human antiviral monoclonal antibody therapeutics. *Nat. Biotechnol.* 25 (12), 1421–1434.
- Mayer, V., Rajčani, J., 1967. Study of the virulence of tick-borne encephalitis virus. VI. Intracerebral infection of monkeys with clones experimentally attenuated virus. *Acta Virol.* 11 (4), 321–333.
- Mayer, V., Pogády, J., Starek, M., Hrbka, J., 1975. A live vaccine against tick-borne encephalitis: integrated studies. III. Response of man to a single dose of the E5 "14" clone (Langat virus). *Acta Virol.* 19 (3), 229–236.
- McAuley, A.J., Sawatsky, B., Książek, T., Torres, M., Korva, M., Lotrič-Furlan, S., Avšič-Županc, T., von Messling, V., Holbrook, M.R., Freiberg, A.N., Beasley, D.W.C., Bente, D.A., 2017. Cross-neutralisation of viruses of the tick-borne encephalitis complex following tick-borne encephalitis vaccination and/or infection. *NPJ Vaccines*. <https://doi.org/10.1038/s41541-017-0009-5>. 2.5.
- Michael, B.D., Solomon, T., 2012. Seizures and encephalitis: clinical features, management, and potential pathophysiological mechanisms. *Epilepsia* 53 (Suppl. 4), 63–71.
- Mickienė, A., Laiškoniš, A., Günther, G., Vene, S., Lundkvist, Å., Lindquist, L., 2002. Tickborne encephalitis in an area of high endemicity in Lithuania: disease severity and long-term prognosis. *Clin. Infect. Dis.* 35 (6), 650–658.
- Mickienė, A., Pakalნიė, J., Nordgren, J., Carlsson, B., Hagbom, M., Svensson, L., Lindquist, L., 2014. Polymorphisms in chemokine receptor 5 and Toll-like receptor 3 genes are risk factors for clinical tick-borne encephalitis in the Lithuanian population. *PLoS One* 9 (9). <https://doi.org/10.1371/journal.pone.0106798>. e106798.
- Migliaccio, G., Tomassini, J.E., Carroll, S.S., et al., 2003. Characterization of resistance to non-obligate chain-terminating ribonucleoside analogs that inhibit hepatitis C virus replication in vitro. *J. Biol. Chem.* 278, 49164–49170.
- Miorin, L., Albornoz, A., Baba, M.M., D'Agaro, P., Marcello, A., 2012. Formation of membrane-defined compartments by tick-borne encephalitis virus contributes to the early delay in interferon signaling. *Virus Res.* 163 (2), 660–666. <https://doi.org/10.1016/j.virusres.2011.11.020>.
- Mišić Majerus, L., Daković Rode, O., Ruzić Sabljčić, E., 2009. [Post-encephalitic syndrome in patients with tick-borne encephalitis]. *Acta Med. Croat.* 63 (4), 269–278.
- Moniuszko, A., Dunaj, J., Święcicka, I., et al., 2014. Co-infections with *Borrelia* species, *Anaplasma phagocytophilum* and *Babesia* spp. in patients with tick-borne encephalitis. *Eur. J. Clin. Microbiol. Infect. Dis.* 33 (10), 1835–1841. <https://doi.org/10.1007/s10096-014-2134-7>.
- Morozova, O.V., Bakhvalova, V.N., Potapova, O.F., Grishechkin, A.E., Isaeva, E.I., Aldarov, K.V., Klinov, D.V., Vorovich, M.F., 2014. Evaluation of immune response and protective effect of four vaccines against the tick-borne encephalitis virus. *Vaccine* 32 (25), 3101–3106. <https://doi.org/10.1016/j.vaccine.2014.02.046>.
- Moutailler, S., Valiente Moro, C., Vaumourin, E., et al., 2016. Co-infection of Ticks: the Rule Rather Than the Exception. *Vinetz, J.M. (Ed.), PLoS Neglected Trop. Dis.* 10 (3). <https://doi.org/10.1371/journal.pntd.0004539>. e0004539.
- Muller, U., Steinhoff, U., Reis, L.F., Hemmi, S., Pavlovic, J., Zinkernagel, R.M., Aguet, M., 1994. Functional role of type I and type II interferons in antiviral defense. *Science* 264 (5167), 1918–1921.
- Nasr, N., Maddocks, S., Turville, S.G., Harman, A.N., Woolger, N., Helbig, K.J., Wilkinson, J., Bye, C.R., Wright, T.K., Rambukwelle, D., Donaghy, H., Beard, M.R., Cunningham, A.L., 2012. HIV-1 infection of human macrophages directly induces viperin which inhibits viral production. *Blood* 120 (4), 778–788. <https://doi.org/10.1182/blood-2012-01-407395>.
- Nikitina, A.A., Orlov, A.A., Kozlovskaya, L.I., Palyulin, V.A., Osolodkin, D.I., 2019. Enhanced taxonomy annotation of antiviral activity data from ChEMBL. Database. <https://doi.org/10.1093/database/bay139>. bay139.
- Olsen, D.B., Eldrup, A.B., Bartholomew, L., et al., 2004. A 7-deaza-adenosine analog is potent and selective inhibitor of hepatitis C virus replication with excellent pharmacokinetic properties. *Antimicrob. Agents Chemother.* 48, 3944–3953.
- Orlinger, K.K., Hofmeister, Y., Fritz, R., Holzer, G.W., Falkner, F.G., Unger, B., Loew-Baselli, A., Poellabauer, E.M., Ehrlich, H.J., Barrett, P.N., Kreil, T.R., 2011. A tick-borne encephalitis virus vaccine based on the European prototype strain induces broadly reactive cross-neutralizing antibodies in humans. *J. Infect. Dis.* 203 (11), 1556–1564.
- Orlov, A.A., Chistov, A.A., Kozlovskaya, L.I., Ustinov, A.V., Korshun, V.A., Karganova, G.G., Osolodkin, D.I., 2016. Rigid amphipathic nucleosides suppress reproduction of the tick-borne encephalitis virus. *Med Chem Commun* 7, 495–499. <https://doi.org/10.1039/c5md00538h>.
- Orlov, A.A., Drenichev, M.S., Oslovsky, V.E., Kurochkin, N.N., Solov, P.N., Kozlovskaya, L.I., Palyulin, V.A., Karganova, G.G., Mikhailov, S.N., Osolodkin, D.I., 2017. New tools in nucleoside toolbox of tick-borne encephalitis virus reproduction inhibitors. *Bioorg. Med. Chem. Lett.* 27 (5), 1267–1273. <https://doi.org/10.1016/j.bmcl.2017.01.040>.
- Orlov, A.A., Eletskaia, A.A., Frolov, K.A., Golinet, A.D., Palyulin, V.A., Krivokolysko, S.G., Kozlovskaya, L.I., Dotsenko, V.V., Osolodkin, D.I., 2018. Probing chemical space of tick-borne encephalitis virus reproduction inhibitors with organoselenium compounds. *Arch. Pharm. (Weinheim)* 351 (6) e1700353.
- Osolodkin, D.I., Kozlovskaya, L.I., Dueva, E.V., Dotsenko, V.V., Rogova, Y.V., Frolov, K.A., Krivokolysko, S.G., Romanova, E.G., Morozov, A.S., Karganova, G.G., Palyulin, V.A., Pentkovski, V.M., Zefirov, N.S., 2013. Inhibitors of tick-borne flavivirus reproduction from structure-based virtual screening. *ACS Med. Chem. Lett.* 4 (9), 869–874. <https://doi.org/10.1021/ml400226s>.
- Overby, A.K., Weber, F., 2011. Hiding from intracellular pattern recognition receptors, a passive strategy of flavivirus immune evasion. *Virulence* 2 (3), 238–240.
- Overby, A.K., Popov, V.L., Niedrig, M., Weber, F., 2010. Tick-borne encephalitis virus delays interferon induction and hides its double-stranded RNA in intracellular membrane vesicles. *J. Virol.* 84 (17), 8470–8483. <https://doi.org/10.1128/JVI.00176-10>.
- Palus, M., Vancova, M., Sirmarova, J., Elsterova, J., Perner, J., Ruzek, D., 2017. Tick-borne encephalitis virus infects human brain microvascular endothelial cells without compromising blood-brain barrier integrity. *Virology* 507, 110–122. <https://doi.org/10.1016/j.virol.2017.04.012>.
- Panayiotou, C., Lindqvist, R., Kurhade, C., Vonderstein, K., Pasto, J., Edlund, K., Upadhyay, A.S., Överby, A.K., 2018. Viperin restricts Zika virus and tick-borne encephalitis virus replication by targeting NS3 for proteasomal degradation. *J. Virol.* <https://doi.org/10.1128/JVI.02054-17>.
- Pancewicz, S.A., Garlicki, A.M., Moniuszko-Malinowska, A., et al., 2015. Diagnosis and treatment of tick-borne diseases recommendations of the polish society of epidemiology and infectious diseases. *Przegl. Epidemiol.* 69 (2), 309–316.
- Pandey, S., Rathore, C., Michael, B.D., 2014. Antiepileptic drugs for the primary and secondary prevention of seizures in viral encephalitis. *Cochrane Database Syst. Rev.* 10 CD010247.
- Panov, A.G., 1956. Tick-borne Encephalitis. Leningrad. pp. 282 (In Russian).
- Paulke-Korinek, M., Rendi-Wagner, P., Kundi, M., Laaber, B., Wiedermann, U., Kollaritsch, H., 2009. Booster vaccinations against tick-borne encephalitis: 6 years follow-up indicates long-term protection. *Vaccine* 27 (50), 7027–7030.
- Paulke-Korinek, M., Kundi, M., Laaber, B., Brodttraeger, N., Seidl-Friedrich, C., Wiedermann, U., Kollaritsch, H., 2013. Factors associated with seroimmunity against tick borne encephalitis virus 10 years after booster vaccination. *Vaccine* 31 (9), 1293–1297.
- Pavlova, L.I., Gorbunov, M.A., Vorob'eva, M.S., Karavanov, A.S., Grachev, V.P., Ladyshenskaia, I.P., Rasshchepkina, M.N., Mel'nikova, L.N., Lebedeva, T.M., Mel'nikov, N.A., Gusmanova, A.G., Deviatkov, M.Iu, Rozanova, E.V., Mukachev, M.A., 1999. A cultured concentrated inactivated vaccine against tick-borne encephalitis studied during the immunization of children and adolescents. *Zh. Mikrobiol. Epidemiol. Immunobiol.* (6), 50–53.
- Pavlova, B.G., Loew-Baselli, A., Fritsch, S., Poellabauer, E.M., Vartian, N., Rinke, I., Ehrlich, H.J., 2003a. Tolerability of modified tick-borne encephalitis vaccine FSME-IMMUN "NEW" in children: results of post-marketing surveillance. *Vaccine* 21 (7–8), 742–745.
- Pavlova, L.I., Stavitskaya, I.V., Gorbunov, M.A., Shkuratova, O.V., Pomagaeva, A.G., Stronin, O.V., et al., 2003b. Characteristics of national inactivated vaccines against TBE for children and adolescents immunization. *BIOPreparation* 1, 24–28.
- Pavlova, A.Y., Kachanova, M.V., Zak, M.S., Sergeeva, S.A., 2009. [Use of Anaferon for treatment and prophylaxis of tick-borne encephalitis]. *Poliklinika* (3), 92–93.
- Pen'evskaia, N.A., Rudakov, N.V., 2010. [Efficiency of use of immunoglobulin preparations for the postexposure prevention of tick-borne encephalitis in Russia (a review of semi-centennial experience)]. *Med Parazitol (Mosk)*. (1), 53–59.
- Penievskaia, N.A., 2010. Etiotropic preparations for post-exposure tick-borne encephalitis prevention: perspective development and problems of epidemiological effectiveness evaluation. *Epidemiologiya i Vaktsinoprofilaktika* (1), 39–45.
- Pervikov, Iu.V., Chumakov, M.P., Voroshilova, M.K., Rubin, S.G., 1975. Use of cross-absorbed sera in neutralization tests with viral titration by the cytopathogenic effect. *Vopr. Virusol.* (3), 309–312.
- Phillipotts, R.J., Stephenson, J.R., Porterfield, J.S., 1985. Antibody-dependent enhancement of tick-borne encephalitis virus infectivity. *J. Gen. Virol.* 66 (Pt 8), 1831–1837.
- Pichlmair, A., Reis e Sousa, C., 2007. Innate recognition of viruses. *Immunity* 27 (3), 370–383.
- Plentz, A., Jilg, W., Schwarz, T.F., Kuhr, H.B., Zent, O., 2009. Long-term persistence of tick-borne encephalitis antibodies in adults 5 years after booster vaccination with Encepur Adults. *Vaccine* 27 (6), 853–856.
- Pogodina, V.V., 2005. [Monitoring of tick-borne encephalitis virus populations and etiological structure of morbidity over 60 years]. *Vopr. Virusol.* 50 (3), 7–13 PMID: 16078427.
- Pogodina, V.V., 2009. Everything started from tick-borne encephalitis. In: Mikhailov, M., Pogodina, V.V. (Eds.), *Reminiscences on M. P. Chumakov*, second ed. pp. 21–31 Moscow.
- Pogodina, V.V., Frolova, M.P., Erman, B.A., 1986. Chronic Tick-borne Encephalitis. "Nauka", Novosibirsk (In Russian).
- Pogodina, V.V., Bochkova, N.G., Karan, L.S., Trukhina, A.G., Levina, L.S., Malenko, G.V., Druzhinina, T.A., Lukashenko, Z.S., Dul'keit OF, Platonov, A.E., 2004a. [The Siberian and Far-Eastern subtypes of tick-borne encephalitis virus registered in Russia's Asian regions: genetic and antigen characteristics of the strains]. *Vopr. Virusol.* 49 (4), 20–25 PMID: 15293507.
- Pogodina, V.V., Bochkova, N.G., Karan, L.S., Frolova, M.P., Trukhina, A.G., Malenko, G.V., Levina, L.S., Platonov, A.E., 2004b. [Comparative analysis of virulence of the Siberian and Far-East subtypes of the tick-borne encephalitis virus]. *Vopr. Virusol.* 49 (6), 24–30 PMID: 15597957.
- Pogodina, V.V., Romanenko, V.V., Karan, L.S., Esunina, M.S., Kiliachina, A.S., Kolyasnikova, N.M., Bulgakova, T.A., Gamova, E.G., Levina, L.S., Malenko, G.V., Bochkova, N.G., Pimenova, T.A., 2006. Structure of tick-borne encephalitis

- populations in the Sverdlovsk region nowadays and vaccine prevention questions. *Medical virology. Proceedings of Chumakov Institute of poliomyelitis and viral encephalitis* 23, 110–115.
- Pöllabauer, E.M., Pavlova, B.G., Löw-Baselli, A., Fritsch, S., Prymula, R., Angermayr, R., Draxler, W., Firth, C., Bosman, J., Valenta, B., Harmacek, P., Maritsch, F., Barrett, P.N., Ehrlich, H.J., 2010. Comparison of immunogenicity and safety between two paediatric TBE vaccines. *Vaccine* 28 (29), 4680–4685.
- Popov, O.V., Sumarokov, A.A., Shkol'nik, R.I., El'bert, L.B., Vorob'eva, M.S., 1985 Jun. Reactogenicity and antigenic activity of a chromatographic cultured purified and concentrated inactivated dried vaccine against tick-borne encephalitis. *Zh. Mikrobiol. Epidemiol. Immunobiol.* (6), 34–39.
- Price, W.H., Thind, I.S., Teasdale, R.D., O'Leary, W., 1970. Vaccination of human volunteers against Russian spring-summer (RSS) virus complex with attenuated Langat E5 virus. *Bull. World Health Organ.* 42 (1), 82–94.
- Pripuzova, N.S., Gmyl, L.V., Romanova, L.L., Tereshkina, N.V., Rogova, Y.V., Terekhina, L.L., Kozlovskaya, L.I., Vorovitch, M.F., Grishina, K.G., Timofeev, A.V., Karganova, G.G., 2013. Exploring of primate models of tick-borne flaviviruses infection for evaluation of vaccines and drugs efficacy. *PLoS One* 8 (4), e61094. <https://doi.org/10.1371/journal.pone.0061094>. 2013 Apr 9.
- Prokopowicz, D., Bobrowska, E., Bobrowski, M., Grzeszczuk, A., 1995. Prevalence of antibodies against tick-borne encephalitis among residents of north-eastern Poland. *Scand. J. Infect. Dis.* 27 (1), 15–16.
- Proskurin, G.V., Orlov, A.A., Brylev, V.A., Kozlovskaya, L.I., Chistov, A.A., Karganova, G.G., Palyulin, V.A., Osolodkin, D.I., Korshun, V.A., Aralov, A.V., 2018. 3'-O-Substituted 5-(perylene-3-ylethynyl)-2'-deoxyuridines as tick-borne encephalitis virus reproduction inhibitors. *Eur. J. Med. Chem.* 155, 77–83.
- Remoli, M.E., Marchi, A., Fortuna, C., Benedetti, E., Minelli, G., Fiorentini, C., Mel, R., Venturi, G., Ciufolini, M.G., 2015. Anti-tick-borne encephalitis (TBE) virus neutralizing antibodies dynamics in natural infections versus vaccination. *Pathog Dis* 73 (2), 1–3. <https://doi.org/10.1093/femspd/ftu002>.
- Rendi-Wagner, P., Kundi, M., Zent, O., Dvorak, G., Jaehnic, P., Holzmann, H., Mikolasek, A., Kollaritsch, H., 2004. Persistence of protective immunity following vaccination against tick-borne encephalitis—longer than expected? *Vaccine* 22 (21–22), 2743–2749.
- Rendi-Wagner, P., Zent, O., Jilg, W., Plentz, A., Beran, J., Kollaritsch, H., 2006. Persistence of antibodies after vaccination against tick-borne encephalitis. *Int J Med Microbiol* 296 (Suppl. 40), 202–207.
- Rendi-Wagner, P., Paulke-Korinek, M., Kundi, M., Wiedermann, U., Laaber, B., Kollaritsch, H., 2007. Antibody persistence following booster vaccination against tick-borne encephalitis: 3-year post-booster follow-up. *Vaccine* 25 (27), 5097–5101.
- Rhoades, C., Williams, M., Kelsey, S., Newland, A., 2000. Monocyte-macrophage system as targets for immunomodulation by intravenous immunoglobulin. *Blood Rev.* 14 (1), 14–30. <https://doi.org/10.1054/blre.1999.0121>.
- Robertson, S.J., Lubick, K.J., Freedman, B.A., Carmody, A.B., Best, S.M., 2014. Tick-borne flaviviruses antagonize both IRF-1 and type I IFN signaling to inhibit dendritic cell function. *Immunol.* 192 (6), 2744–2755. <https://doi.org/10.4049/jimmunol.1302110>.
- Roe, K., Kumar, M., Lum, S., Orillo, B., Nerurkar, V.R., Verma, S., 2012. West Nile virus-induced disruption of the blood-brain barrier in mice is characterized by the degradation of the junctional complex proteins and increase in multiple matrix metalloproteinases. *J. Gen. Virol.* 93 (Pt 6), 1193–1203. <https://doi.org/10.1099/vir.0.040899-0>.
- Rogan, C., Fortune, D.G., Prentice, G., 2013. Post-traumatic growth, illness perceptions and coping in people with acquired brain injury. *Neuropsychol. Rehabil.* 23 (5), 639–657. <https://doi.org/10.1080/09602011.2013.799076>. Epub 2013 May 24.
- Rogova, Y.V., Kozlovskaya, L.I., Shevtsova, A.S., Maldov, D.G., Karganova, G.G., 2008. [Evaluation of virasole efficiency for prevention of tick-borne encephalitis in experiments in laboratory mice]. *Medical virology. In: Proceedings of Chumakov Institute of Poliomyelitis and Viral Encephalitis*, vol. 25. pp. 115–118.
- Romanenko, V.V., Esiunina, M.S., Kiliachina, A.S., Pimenova, T.A., 2006. Massive immunization of the Sverdlovsk region population against tick-borne encephalitis, its epidemiological, clinical and immunological efficacy. *Medical virology. In: Proceedings of Chumakov Institute of Poliomyelitis and Viral Encephalitis*, vol. 23. pp. 116–125.
- Romanenko, V.V., Esiunina, M.S., Kiliachina, A.S., 2007. Experience in implementing the mass immunization program against tick-borne encephalitis in the Sverdlovsk Region. *Vopr. Virusol.* 52 (6), 22–25.
- Rostasy, K., 2012. Tick-borne encephalitis in children. *Wien Med. Wochenschr.* 162 (11–12), 244–247. <https://doi.org/10.1007/s10354-012-0101-4>. Epub 2012 Jun 12.
- Ruzek, D., Dobler, G., Niller, H.H., 2013a. May early intervention with high dose intravenous immunoglobulin pose a potentially successful treatment for severe cases of tick-borne encephalitis? *BMC Infect. Dis.* 13, 306. <https://doi.org/10.1186/1471-2334-13-306>.
- Ruzek, D., Bilski, B., Günther, G., 2013b. Tick-borne encephalitis. In: Singh, S.K., Ruzek, D. (Eds.), *Neuroviral Infections*. CRC Press, Boca Raton, pp. 211–237.
- Ruzek, D., Gritsun, T.S., Forrester, N.L., Gould, E.A., Kopecký, J., Golovchenko, M., Rudenko, N., Grubhoffer, L., 2008. Mutations in the NS2B and NS3 genes affect mouse neuroinvasiveness of a Western European field strain of tick-borne encephalitis virus. *Virology* 374 (2), 249–255. <https://doi.org/10.1016/j.virol.2008.01.010>.
- Ruzek, D., Salát, J., Palus, M., Gritsun, T.S., Gould, E.A., Dyková, I., Skallová, A., Jelínek, J., Kopecký, J., Grubhoffer, L., 2009. CD8+ T-cells mediate immunopathology in tick-borne encephalitis. *Virology* 384 (1), 1–6. <https://doi.org/10.1016/j.virol.2008.11.023>.
- Ruzek, D., Dobler, G., Donoso Mantke, O., 2010. Tick-borne encephalitis: pathogenesis and clinical implications. *Trav. Med. Infect. Dis.* 8 (4), 223–232. <https://doi.org/10.1016/j.tmaid.2010.06.004>.
- Ruzek, D., Salát, J., Singh, S.K., Kopecký, J., 2011. Breakdown of the blood-brain barrier during tick-borne encephalitis in mice is not dependent on CD8+ T-cells. *PLoS One* 6 (5), e20472. <https://doi.org/10.1371/journal.pone.0020472>.
- Safronov, P.F., Netesov, S.V., Mikriukova, T.P., Blinov, V.M., Osipova, E.G., Kiseleva, N.N., Sandakhchiev, L.S., 1991. Nucleotide sequence of genes and complete amino acid sequence of tick-borne encephalitis virus strain 205. *Mol Gen Mikrobiol Virusol* (4), 23–29 1991 Apr.
- Saksida, A., Duh, D., Lotric-Furlan, S., Strle, F., Petrovec, M., Avsic-Zupanc, T., 2005. The importance of tick-borne encephalitis virus RNA detection for early differential diagnosis of tick-borne encephalitis. *J. Clin. Virol.* 33 (4), 331–335.
- Saksida, A., Jakopin, N., Jelovšek, M., Knap, N., Fajs, L., Lusa, L., Lotric-Furlan, S., Bogovič, P., Arnež, M., Strle, F., Avšič-Zupanc, T., 2018. Virus RNA load in patients with tick-borne encephalitis, Slovenia. *Emerg. Infect. Dis.* 24 (7), 1315–1323. <https://doi.org/10.3201/eid2407.180059>.
- Salabay, N.S., Chuiukova, K.I., Usova, S.V., Targonsky, S.N., 2012. Clinical and laboratory parameters when using combined therapy (immunoglobulin and interferon $\alpha 2v$) in patients with feverish and meningeal forms of tick-borne encephalitis. *Zemsky Vrach* (3), 31–36.
- Sarpong, Y., Nattanmai, P., Schelp, G., et al., 2017. Improvement in quality metrics outcomes and patient and family satisfaction in a neurosciences intensive care unit after creation of a dedicated neurocritical care team. *Critical Care Res. Practice* 2017, 6394105. <https://doi.org/10.1155/2017/6394105>.
- Schlesinger, J.J., Brandriss, M.W., Walsh, E.E., 1985. Protection against 17D yellow fever encephalitis in mice by passive transfer of monoclonal antibodies to the nonstructural glycoprotein gp48 and by active immunization with gp48. *J. Immunol.* 135 (4), 2805–2809.
- Schmidt, A.G., Yang, P.L., Harrison, S.C., 2010. Peptide inhibitors of flavivirus entry derived from the E protein stem. *J. Virol.* 84 (24), 12549–12554. <https://doi.org/10.1128/JVI.01440-10>.
- Schmolck, H., Maritz, E., Kletzin, I., Korinthenberg, R., 2005. Neurologic, neuropsychologic, and electroencephalographic findings after European tick-borne encephalitis in children. *J. Child Neurol.* 20 (6), 500–508.
- Schneider, W.M., Chevillotte, M.D., Rice, C.M., 2014. Interferon-stimulated genes: a complex web of host defenses. *Annu. Rev. Immunol.* 32, 513–545. <https://doi.org/10.1146/annurev-immunol-032713-120231>.
- Schoendorf, I., Ternak, G., Oroszlan, G., Nicolay, U., Banzhoff, A., Zent, O., 2007. Tick-borne encephalitis (TBE) vaccination in children: advantage of the rapid immunization schedule (i.e., days 0, 7, 21). *Hum Vaccin* 3 (2), 42–47.
- Schoggins, J.W., Rice, C.M., 2011. Interferon-stimulated genes and their antiviral effector functions. *Curr Opin Virol* 1 (6), 519–525. <https://doi.org/10.1016/j.coviro.2011.10.008>.
- Schondorf, I., Beran, J., Cizkova, D., Lesna, V., Banzhoff, A., Zent, O., 2007. Tick-borne encephalitis (TBE) vaccination: applying the most suitable vaccination schedule. *Vaccine* 25 (8), 1470–1475.
- Schosser, R., Reichert, A., Mansmann, U., Unger, B., Heining, U., Kaiser, R., 2014. Irregular tick-borne encephalitis vaccination schedules: the effect of a single catch-up vaccination with FSME-IMMUN. A prospective non-interventional study. *Vaccine* 32 (20), 2375–2381.
- Sedenkova, K.N., Dueva, E.V., Averina, E.B., Grishin, Y.K., Osolodkin, D.I., Kozlovskaya, L.I., Palyulin, V.A., Savelyev, E.N., Orlinson, B.S., Novakov, I.A., Butov, G.M., Kuznetsova, T.S., Karganova, G.G., Zefirov, N.S., 2015. Synthesis and assessment of 4-aminotetrahydroquinazoline derivatives as tick-borne encephalitis virus reproduction inhibitors. *Org. Biomol. Chem.* 13 (11), 3406–3415. <https://doi.org/10.1039/c4ob02649g>.
- Semenov, B.F., Khozinsky, V.V., Vargin, V.V., 1981. Immunopathology and immunotherapy of tick-borne encephalitis. In: Kunz, Ch. (Ed.), *Tick-borne Encephalitis. International Symposium Baden/Vienna 19th–20th October 1979*. Facultas-Verlag, Vienna, pp. 45–58.
- Shah, K.V., Aniker, S.P., Murthy, D.P., Rodrigues, F.M., Jayadevia, M.S., Prasanna, H.A., 1962. Evaluation of the field experience with formalin-inactivated mouse brain vaccine of Russian spring-summer encephalitis virus against Kyasanur Forest disease. *Indian J. Med. Res.* 50, 162–174.
- Shapoval, A.N., 1976. *Chronic Forms of Tick-borne Encephalitis*. Medicine, Leningrad (In Russian).
- Shapoval, A.N., Kamalov II, J., Denisova, Elu, Sokolova, E.D., Luzin, P.M., Shamarina, A.G., Gusmanova, A.G., Pinaeva, N.I., 1989. Study of the distant consequences of immunizing people with a live vaccine against tick-borne encephalitis. *Tr. Inst. Im. Pastera* 65, 133–135.
- Shevtsova, A.S., Motuzova, O.V., Kuragina, V.M., Akhmatova, N.K., Gmyl, L.V., Kondrat'eva, Y.I., Kozlovskaya, L.I., Rogova, Y.V., Litov, A.G., Romanova, L.I., Karganova, G.G., 2017. Lethal experimental tick-borne encephalitis infection: influence of two strains with similar virulence on the immune response. *Front. Microbiol.* 7, 2172. <https://doi.org/10.3389/fmicb.2016.02172>.
- Silber, L.A., 1939. Vernal (Verno-aestival) endemic tick-borne encephalitis. *Arch. Sci. Biol.* 56 (2), 9–37.
- Sitati, E.M., Diamond, M.S., 2006. CD4+ T-cell responses are required for clearance of West Nile virus from the central nervous system. *J. Virol.* 80 (24), 12060–12069.
- Skripchenko, N.V., Morgatskiy, N.V., Ivanova, G.P., Aksenov, O.A., Ivanova, M.V., Karasev, V.V., Pulman, N.F., Vilnits, A.A., Murina, E.A., Gorelik, E.Y., 2007. Contemporary possibilities of extra nonspecific prophylaxis of tick born encephalitis in children. *Pediatricheskaya Farmakologiya* 7, 23–26.
- Skripchenko, N.V., Ivanova, G.P., Ivanova, M.V., Skripchenko, E.Y., Pulman, N.F., Vilnits, A.A., 2015. P63–2804: chemoprophylaxis of tick-borne encephalitis in children. *Eur. J. Paediatr. Neurol.* 19 (Suppl. 1), S111–S112. [https://doi.org/10.1016/S1090-3798\(15\)30376-7](https://doi.org/10.1016/S1090-3798(15)30376-7).

- Šmit, R., Postma, M.J., 2015. The Burden of Tick-Borne Encephalitis in Disability-Adjusted Life Years (DALYs) for Slovenia. Munderloh, U.G. (Ed.), PLoS One 10 (12). <https://doi.org/10.1371/journal.pone.0144988>. e0144988.
- Smorodintseff, A.A., Kagan, N.V., Levkovich, E.N., 1941. Experimental materials on active immunization against tick-borne (spring-summer) encephalitis. Zh. Mikrobiol. Epidemiol. Immunobiol. 4, 3–12.
- Smorodintsev, A.A., Dubov, A.V., 1986. Tick-borne Encephalitis and Prevention Tick-borne Encephalitis and its Vaccine Prophylaxis. AMS USSR, Leningrad, "Medicine". (In Russian).
- Sobolev, S.G., Frolova, T.V., Pogodina, V.V., 2010. [Morphogenesis of tick-borne encephalitis virus in the brain of mice infected with its persistent strains]. Vopr. Virusol. 55 (6), 31–35 PMID: 21381338.
- Sologub, T.V., Tokin II, , Midikari, A.S., Tsvetkov, V.V., 2017. A comparative efficacy and safety of using antiviral drugs in therapy of patients with influenza. Infectious Diseases 15 (3), 25–32. <https://doi.org/10.20953/1729-9225-2017-3-25-32>.
- Solomon, T., Michael, B.D., Smith, P., et al., National Encephalitis Guidelines Development and Stakeholder Groups, 2012. Management of suspected viral encephalitis in adults – association of British neurologists and British infection association national guidelines. J. Infect. 64, 347–373.
- Speerstra, S., Chistov, A.A., Proskurin, G.V., Aralov, A.V., Ulashchik, E.A., Streshnev, P.P., Shmanai, V.V., Korshun, V.A., Schang, L.M., 2018. Antivirals acting on viral envelopes via biophysical mechanisms of action. Antivir. Res. 149, 164–173.
- Steffen, R., 2016. Epidemiology of tick-borne encephalitis (TBE) in international travellers to Western/Central Europe and conclusions on vaccination recommendations. J. Trav. Med. 23 (4), 1–10.
- Steffen, R., 2019. Tick-borne encephalitis (TBE) in children in Europe: Epidemiology, clinical outcome and comparison of vaccination recommendations. Ticks Tick Borne Dis 10 (1), 100–110. <https://doi.org/10.1016/j.ttbdis.2018.08.003>.
- Steinman, R.M., Hemmi, H., 2006. Dendritic cells: translating innate to adaptive immunity. Curr. Top. Microbiol. Immunol. 311, 17–58.
- Stiasny, K., Holzmann, H., Heinz, F.X., 2009. Characteristics of antibody responses in tick-borne encephalitis vaccination breakthroughs. Vaccine 27 (50), 7021–7026.
- Stovbun, S.V., Berlin, A.A., Mikhailov, A.I., Sergienko, V.I., Govorun, V.M., Demina, I.A., Kalinina, T.S., 2012. Physicochemical properties of high-molecular-weight plant polysaccharide of hexose glycoside class (Panavir) with antiviral activity. Nanotechnologies in Russia 7 (9–10), 539–543. <https://doi.org/10.1134/S1995078012050138>.
- Studahl, M., Lindquist, L., Eriksson, B., Günther, G., Bengner, M., Franzen-Röhl, E., Fohlman, J., Bergström, T., Aurelius, E., 2013. Acute viral infections of the central nervous system in immunocompetent adults: diagnosis and management. Drugs 73 (2), 131–158. <https://doi.org/10.1007/s40265-013-0007-5>.
- Suarez, J.I., Zaidat, O.O., Suri, M.F., Feen, E.S., Lynch, G., Hickman, J., Georgiadis, A., Selman, W.R., 2004. Length of stay and mortality in neurocritically ill patients: impact of a specialized neurocritical care team. Crit. Care Med. 32, 2311–2317.
- Suess, J., et al., 2004. Durch Zecken uebertragene humanpathogene und bisher als apathogen geltende Mikroorganismen in Europa. Teil II: bakterien, Parasiten und Mischinfektion. Bundesgesundheitsbl. Gesundheitsforsch. Gesundheitsschutz. 47, 470–486.
- Sundin, M., 2017. TBE in children. In: Dobler, G., Erber, W., Schmitt, H.-J. (Eds.), TBE - the Book. Global Health Press, Singapore, pp. 85–90.
- Surova, J.I., Stronin, O.V., Solyanik, R.G., Bilalova, G.P., 2002. Dynamics of specific immunity development during vaccination against tick-borne encephalitis. In: Tick-borne Encephalitis (65th Anniversary) Vladivostok. GUL "Primpolygraphcombinat", Russia, pp. 170–179.
- Suss, J., 2008. Tick-borne encephalitis in Europe and beyond—the epidemiological situation as of 2007. Euro Surveill. 13 (26).
- Swarup, V., Ghosh, J., Ghosh, S., Saxena, A., Basu, A., 2007. Antiviral and anti-inflammatory effects of rosmarinic acid in an experimental murine model of Japanese encephalitis. Antimicrob. Agents Chemother. 51 (9), 3367–3370. <https://doi.org/10.1128/AAC.00041-07>.
- Szretter, K.J., Brien, J.D., Thackray, L.B., Virgin, H.W., Cresswell, P., Diamond, M.S., 2011. The interferon-inducible gene viperin restricts West Nile virus pathogenesis. J. Virol. 85 (22), 11557–11566. <https://doi.org/10.1128/JVI.05519-11>.
- Taba, P., Schmutzhard, E., Forsberg, P., Lutsar, I., Ljøstad, U., Mygland, Å., Levchenko, I., Strle, F., Steiner, I., 2017. EAN consensus review on prevention, diagnosis and management of tick-borne encephalitis. Eur. J. Neurol. 24 (10). <https://doi.org/10.1111/ene.13356>. 1214-e61.
- Tarasov, S.A., Kachanova, M.V., Gorbunov, E.A., Zabolotneva, J.A., Ertuzun, I.A., Belopolskaya, M.V., Borodavkina, M.V., Dugina, J.L., Epstein, O.I., 2016. Anaferon, released-active form of antibodies to IFN γ , as an effective medicine for treatment and prophylaxis of a wide spectrum of infections. Clin Res Trials 2 (5), 229–232. <https://doi.org/10.15761/CRT.1000152>.
- Taylor, R.T., Lubick, K.J., Robertson, S.J., Broughton, J.P., Bloom, M.E., Bresnahan, W.A., Best, S.M., 2011. TRIM79alpha, an interferon-stimulated gene product, restricts tick-borne encephalitis virus replication by degrading the viral RNA polymerase. Cell Host Microbe 10 (3), 185–196. <https://doi.org/10.1016/j.chom.2011.08.004>.
- Taylor, R., Kotian, P., Warren, T., et al., 2016. BCX4430-A broad-spectrum antiviral adenosine nucleoside analog under development for the treatment of Ebola virus disease. J Infect Public Heal 9, 220–226.
- Teng, T.S., Foo, S.S., Simamarta, D., Lum, F.M., Teo, T.H., Lulla, A., Yeo, N.K., Koh, E.G., Chow, A., Leo, Y.S., Merits, A., Chin, K.C., Ng, L.F., 2012. Viperin restricts chikungunya virus replication and pathology. J. Clin. Invest. 122 (12), 4447–4460. <https://doi.org/10.1172/JCI63120>.
- Ternovoi, V.A., Kurzhukov, G.P., Sokolov, Y.V., Ivanov, G.Y., Ivanisenko, V.A., Loktev, A.V., Ryder, R.W., Netesov, S.V., Loktev, V.B., 2003. Tick-borne encephalitis with hemorrhagic syndrome, Novosibirsk region, Russia, 1999. Emerg. Infect. Dis. 9 (6), 743–746.
- The PLOS ONE, 2018. Retraction: novel Approach to Activity Evaluation for Release-Active Forms of Anti-Interferon-Gamma Antibodies Based on Enzyme-Linked Immunoassay. PLoS One 13 (5). <https://doi.org/10.1371/journal.pone.0197086>. e0197086.
- Timofeev, A.V., Ozherelkov, S.V., Pronin, A.V., Deeva, A.V., Karganova, G.G., Elbert, L.B., Stephenson, J.R., 1998. Immunological basis for protection in a murine model of tick-borne encephalitis by a recombinant adenovirus carrying the gene encoding the NS1 non-structural protein. J. Gen. Virol. 79 (Pt 4), 689–695.
- Umansky, K.G., 1977. About the pathogenesis of prodromal forms of tick-borne encephalitis. J. Neuropathol. Psychiatry 77 (2), 166–171 (In Russian).
- Umanskiy, K., Shishov, A., Dekonenko, E., 1981. Immunotherapy of some acute and chronic neuroinfections. Zh. Nevropatol. Psikhiatr. Im. S S Korsakova 81 (2), 10–16 (In Russian).
- Upadhyay, A.S., Vonderstein, K., Pichlmair, A., Stehling, O., Bennett, K.L., Dobler, G., Guo, J.T., Superti-Furga, G., Lill, R., Överby, A.K., Weber, F., 2014. Viperin is an iron-sulfur protein that inhibits genome synthesis of tick-borne encephalitis virus via radical SAM domain activity. Cell Microbiol. 16 (6), 834–848. <https://doi.org/10.1111/cmi.12241>.
- Veje, M., Studahl, M., Johansson, M., Johansson, P., Nolskog, P., Bergström, T., 2018. Diagnosing tick-borne encephalitis: a re-evaluation of notified cases. Eur. J. Clin. Microbiol. Infect. Dis. 37 (2), 339–344. <https://doi.org/10.1007/s10096-017-3139-9>.
- Vene, S., Haglund, M., Lundkvist, A., Lindquist, L., Forsgren, M., 2007. Study of the serological response after vaccination against tick-borne encephalitis in Sweden. Vaccine 25 (2), 366–372.
- Venkatesan, A., Geocadin, R.G., 2014. Diagnosis and management of acute encephalitis: a practical approach. Neurology: Clin. Pract. 4 (3), 206–215. <https://doi.org/10.1212/CPJ.0000000000000036>.
- Vigant, F., Hollmann, A., Lee, J., Santos, N.C., Jung, M.E., Lee, B., 2014. The rigid amphipathic fusion inhibitor dUY11 acts through photosensitization of viruses. J. Virol. 88 (3), 1849–1853. <https://doi.org/10.1128/JVI.02907-13>.
- Vince, V., Grčević, N., 1981. Pathogenetic problems arising from experiences in series of experiments with TBE in mice. In: Kunz, Ch. (Ed.), Tick-borne Encephalitis. International Symposium Baden/Vienna 19th–20th October 1979. Facultas-Verlag, Vienna, pp. 76–92.
- Vince, V., Grčević, N., Stanković, V., 1972. Comparative study of CNS lesions induced by tick-borne encephalitis virus in normal and x-irradiated white mice. Pathol. Microbiol. 38 (6), 438–451.
- Vonderstein, K., Nilsson, E., Hubel, P., Nygård Skalmann, L., Upadhyay, A., Pasto, J., Pichlmair, A., Lundmark, R., Överby, A.K., 2017. Viperin targets flavivirus virulence by inducing assembly of non-infectious capsid particles. J. Virol. <https://doi.org/10.1128/JVI.01751-17>.
- Vorob'eva, M.S., El'bert, L.B., Grachev, V.P., Lelikov, V.L., Pervikov, IuV., 1983. Reactogenicity and immunological effectiveness of a concentrated, purified vaccine against tick-borne encephalitis. Vopr. Virusol. 28 (5), 622–626 1983 Sep-Oct.
- Vorob'eva, M.S., Rasshchepkina, M.N., Ladyzhenskaia, I.P., Gorbunov, M.A., Pavlova, L.I., Bektimirov, T.A., 1996. Comparative study of inactivated cultured vaccines against tick-borne encephalitis manufactured in Russia and in Austria by the "Immuno" firm. Vopr. Virusol. 41 (5), 221–224.
- Vorobeva, N.N., Naumova, L.M., Targonsky, S.N., Usova, S.V., 2012. The application of preparation «Reaferon-ES-LIPIN» for the prevention of the Tick-borne encephalitis. Zemsy Vrach (2), 25–29.
- Vorovitch, M.F., Kiktenko, A.V., Khapchaev, Y.K., Grachev, V.P., 2012. New inactivated TBE vaccines. J Infectious Pathology 19 (3), 117.
- Vorovitch, M.F., Kozlovskaya, L.L., Romanova, L.L., Chernokhaeva, L.L., Ishmukhametov, A.A., Karganova, G.G., 2015. Genetic description of a tick-borne encephalitis virus strain Sofjin with the longest history as a vaccine strain. SpringerPlus 4, 761. <https://doi.org/10.1186/s40064-015-1561-y>.
- Vorovitch, M.F., Maikova, G.B., Chernokhaeva, L.L., Romanenko, V.V., Ankudinova, A.V., Khapchaev, Y.K., Karganova, G.G., Ishmukhametov, A.A., Drozdov, S.G., 2017. Immunogenicity and safety of the adult TBE vaccine «Tick-E-Vac». Vopr. Virusol. 62 (2), 73–80.
- Waldvogel, K., Bossart, W., Huisman, T., Boltshauser, E., Nadal, D., 1996. Severe tick-borne encephalitis following passive immunization. Eur. J. Pediatr. 155 (9), 775–779.
- Wang, X., Hinson, E.R., Cresswell, P., 2007. The interferon-inducible protein viperin inhibits influenza virus release by perturbing lipid rafts. Cell Host Microbe 2 (2), 96–105.
- Warren, T.K., Wells, J., Panchal, R.G., et al., 2014. Protection against filovirus diseases by a novel broad-spectrum nucleoside analogue BCX4430. Nature 508, 402–405.
- Webb, H.E., Wight, D.G., Platt, G.S., Smith, C.E., 1968. Langat virus encephalitis in mice. I. The effect of the administration of specific antiserum. J. Hyg. 66 (3), 343–354.
- Weber, F., Wagner, V., Rasmussen, S.B., Hartmann, R., Paludan, S.R., 2006. Double-stranded RNA is produced by positive-strand RNA viruses and DNA viruses but not in detectable amounts by negative-strand RNA viruses. J. Virol. 80 (10), 5059–5064.
- Weber, E., Finsterbusch, K., Lindquist, R., Nair, S., Lienenklaus, S., Gekara, N.O., Janik, D., Weiss, S., Kalinke, U., Överby, A.K., Kröger, A., 2014. Type I interferon protects mice from fatal neurotropic infection with Langat virus by systemic and local antiviral responses. J. Virol. 88 (21), 12202–12212. <https://doi.org/10.1128/JVI.01215-14>.
- Weinberger, B., Keller, M., Fischer, K.H., Stiasny, K., Neuner, C., Heinz, F.X., Grubeck-Loebenstein, B., 2010. Decreased antibody titers and booster responses in tick-borne encephalitis vaccinees aged 50–90 years. Vaccine 28 (20), 3511–3515.
- Wen, J., Elong Ngono, A., Regla-Nava, J.A., Kim, K., Gorman, M.J., Diamond, M.S., Shresta, S., 2017. Dengue virus-reactive CD8+ T cells mediate cross-protection against subsequent Zika virus challenge. Nat. Commun. 8 (1), 1459. <https://doi.org/>

- 10.1038/s41467-017-01669-z.
- Wengse, C., Ericsson, J., Hallberg, S., Ursing, J., 2017. Patient med TBE förbättrades snabbt vid behandling med kortison - evidens saknas dock för värdet av immunmodulerande terapi. [Article in Swedish]. *Lakartidningen* 114(. pii: ELAI).
- Werme, K., Wigerius, M., Johansson, M., 2008. Tick-borne encephalitis virus NS5 associates with membrane protein scribble and impairs interferon-stimulated JAK-STAT signalling. *Cell Microbiol.* 10 (3), 696–712.
- Wikel, S., 2013. Ticks and tick-borne pathogens at the cutaneous interface: host defenses, tick countermeasures, and a suitable environment for pathogen establishment. *Front. Microbiol.* 4, 337. <https://doi.org/10.3389/fmicb.2013.00337>.
- Wittermann, C., Petri, E., Zent, O., 2009a. Long-term persistence of tick-borne encephalitis antibodies in children 5 years after first booster vaccination with Encepur Children. *Vaccine* 27 (10), 1585–1588.
- Wittermann, C., Schondorf, I., Gniel, D., 2009b. Antibody response following administration of two paediatric tick-borne encephalitis vaccines using two different vaccination schedules. *Vaccine* 27 (10), 1661–1666.
- Wittermann, C., Izu, A., Petri, E., Gniel, D., Fracapane, E., 2015. Five year follow-up after primary vaccination against tick-borne encephalitis in children. *Vaccine* 33 (15), 1824–1829.
- Yin, Z., Chen, Y.L., Schul, W., Wang, Q.Y., Gu, F., Duraiswamy, J., Kondreddi, R.R., Niyomrattanakit, P., Lakshminarayana, S.B., Goh, A., Xu, H.Y., Liu, W., Liu, B., Lim, J.Y., Ng, C.Y., Qing, M., Lim, C.C., Yip, A., Wang, G., Chan, W.L., Tan, H.P., Lin, K., Zhang, B., Zou, G., Bernard, K.A., Garrett, C., Beltz, K., Dong, M., Weaver, M., He, H., Pichota, A., Dartois, V., Keller, T.H., Shi, P.Y., 2009. An adenosine nucleoside inhibitor of dengue virus. *Proc. Natl. Acad. Sci. U. S. A.* 106 (48), 20435–20439.
- Zajkowska, J., Czupryna, P., 2013. Tick-borne encephalitis – epidemiology, pathogenesis and clinical course, prophylaxis and treatment. *Forum Zakażeń* 4 (1), 43–51.
- Zajkowska, J., Moniuszko, A., Czupryna, P., Kuśmierczyk, J., Pancewicz, S.A., 2008. [Encephalomeningitis caused by *Listeria monocytogenes* in patient infected by TBE virus—case report]. *Przegl. Epidemiol.* 62 (Suppl. 1), 158–162.
- Zajkowska, J., Czupryna, P., Pancewicz, S., Adamczyk-Przychodze, A., Kondrusik, M., Grygorczuk, S., Moniuszko, A., 2011. Fatal outcome of tick-borne encephalitis – a case series. *Neurol. Neurochir. Pol.* 45 (4), 402–406.
- Zajkowska, J., Moniuszko, A., Czupryna, P., Drozdowski, W., Krupa, W., Guziejko, K., Kondrusik, M., Grygorczuk, S., Pancewicz, S., 2013. Chorea and tick-borne encephalitis, Poland. *Emerg. Infect. Dis.* 19 (9), 1544–1545. <https://doi.org/10.3201/eid1909.130804>.
- Zavadaska, D., Anca, I., Andre, F., Bakir, M., Chlibek, R., Cizman, M., Ivaskeviciene, I., Mangarov, A., Meszner, Z., Pokorn, M., Prymula, R., Richter, D., Salman, N., Simurka, P., Tamm, E., Tesovic, G., Urbancikova, I., Usonis, V., 2013. Recommendations for tick-borne encephalitis vaccination from the central european vaccination awareness group (CEVAG). *Hum. Vaccines Immunother.* 9 (2), 362–374.
- Zegenhagen, L., Kurhade, C., Koniszewski, N., Överby, A.K., Kröger, A., 2016a. Brain heterogeneity leads to differential innate immune responses and modulates pathogenesis of viral infections. *Cytokine Growth Factor Rev.* 30, 95–101. <https://doi.org/10.1016/j.cytogfr.2016.03.006>.
- Zegenhagen, L., Kurhade, C., Kroger, A., Overby, A.K., 2016b. Differences in IPS-1 mediated innate immune responses between neurotrophic flavivirus infection. *J. Neuroinfectious Diseases* 7, 210. <https://doi.org/10.4172/2314-7326.1000210>.
- Zent, O., Broker, M., 2005. Tick-borne encephalitis vaccines: past and present. *Expert Rev. Vaccines* 4 (5), 747–755.
- Zent, O., Banzhoff, A., Hilbert, A.K., Meriste, S., Sluzewski, W., Wittermann, C., 2003. Safety, immunogenicity and tolerability of a new pediatric tick-borne encephalitis (TBE) vaccine, free of protein-derived stabilizer. *Vaccine* 21 (25–26), 3584–3592.
- Zuccoli, G., Yannes, M.P., Nardone, R., Bailey, A., Goldstein, A., 2015. Bilateral symmetrical basal ganglia and thalamic lesions in children: an update (2015). *Neuroradiology* 57 (10), 973–989.

Nucleoside analogs as a rich source of antiviral agents active against arthropod-borne flaviviruses

Antiviral Chemistry and Chemotherapy
2018, Vol. 26: 1–28
! The Author(s) 2018
Reprints and permissions:
sagepub.co.uk/journalsPermissions.nav
DOI: 10.1177/2040206618761299
journals.sagepub.com/home/avc



Luděk Eyer^{1,2}, Radim Nencka³, Erik de Clercq⁴,
Katherine Seley-Radtke⁵ and Daniel Růžek^{1,2}

Abstract

Nucleoside analogs represent the largest class of small molecule-based antivirals, which currently form the backbone of chemotherapy of chronic infections caused by HIV, hepatitis B or C viruses, and herpes viruses. High antiviral potency and favorable pharmacokinetics parameters make some nucleoside analogs suitable also for the treatment of acute infections caused by other medically important RNA and DNA viruses. This review summarizes available information on antiviral research of nucleoside analogs against arthropod-borne members of the genus *Flavivirus* within the family Flaviviridae, being primarily focused on description of nucleoside inhibitors of flaviviral RNA-dependent RNA polymerase, methyltransferase, and helicase/NTPase. Inhibitors of intracellular nucleoside synthesis and newly discovered nucleoside derivatives with high anti-flavivirus potency, whose modes of action are currently not completely understood, have drawn attention. Moreover, this review highlights important challenges and complications in nucleoside analog development and suggests possible strategies to overcome these limitations.

Keywords

Nucleoside analog, antiviral agent, arthropod-borne flavivirus, antiviral therapy, inhibitor

Date received: 24 November 2017; accepted: 30 January 2018

Introduction

The genus *Flavivirus* belongs to the Flaviviridae family and includes more than 70 single-stranded plus-sense RNA viral species. Flaviviruses of human medical importance are tick- or mosquito-transmitted viruses with typical representatives being tick-borne encephalitis virus (TBEV), Omsk hemorrhagic fever virus (OHFV), Kyasanur Forest disease virus (KFDV), Alkhurma hemorrhagic fever virus (AHFV), Powassan virus (POWV), West Nile virus (WNV), dengue virus (DENV), Japanese encephalitis virus (JEV), yellow fever virus (YFV), or Zika virus (ZIKV).^{1,2} The Flaviviridae family also includes some less known or neglected viruses, such as louping ill virus (LIV), Usutu virus, Langat virus, or Wesselsbron virus.^{3–6} The flaviviral genome is a single-stranded, plus-sense RNA of about 11 kb in length that encodes a single polyprotein, which is co- and posttranslationally processed into three structural (capsid, premembrane or membrane, and envelope) and seven nonstructural proteins (NS1, NS2A, NS2B,

NS3, NS4A, NS4B, and NS5).⁷ Both NS3 and NS5 proteins possess enzymatic activities reported to be important targets for antiviral development. Whereas NS3 acts as a serine protease, a 5'-RNA triphosphatase, a nucleoside triphosphatase (NTPase), and a helicase,^{8,9} NS5 consists of a complex containing the RNA-dependent RNA polymerase (RdRp) and the methyltransferase (MTase) activities.^{10,11}

¹Department of Virology, Veterinary Research Institute, Brno, Czech Republic

²Institute of Parasitology, Biology Centre of the Czech Academy of Sciences, České Budějovice, Czech Republic

³Institute of Organic Chemistry and Biochemistry of the Czech Academy of Sciences, Prague, Czech Republic

⁴Rega Institute for Medical Research, KU Leuven, Leuven, Belgium

⁵Department of Chemistry and Biochemistry, University of Maryland, Baltimore, USA

Corresponding author:

Luděk Eyer, Veterinary Research Institute, Hudcova 70, Brno CZ-62100, Czech Republic.

Email: eyer@vri.cz



Flaviviral infections are accompanied by a wide spectrum of distinct clinical manifestations, ranging from relatively mild fevers and arthralgia to severe viscerotropic symptoms (YFV and DENV), hemorrhagic fevers (KFDV and OHFV), encephalitis/myelitis (JEV, WNV, and TBEV), and neuropathic or teratogenic manifestations (ZIKV). More than 200 million clinical cases of flaviviral infections, including numerous deaths, are reported annually worldwide.¹² Currently no specific antiviral therapies are available to treat patients with flaviviral infections, thus the search for safe and effective small-molecule inhibitors that would be active against these viruses represents a high research priority.¹³

Nucleoside analog inhibitors have figured prominently in the search for effective antiviral agents.¹⁴ Nucleoside analogs are synthetic, chemically modified nucleosides that mimic their physiological counterparts (endogenous nucleosides) and block cellular division or viral replication by impairment DNA/RNA synthesis or by inhibition of cellular or viral enzymes involved in nucleoside/tide metabolism (Figure 1).¹⁵ The first antiviral analogs were developed in the late 1960s and currently there are over 25 approved therapeutic nucleosides used for the therapy of viral infections of high medical importance, such as HIV/AIDS (tenofovir),^{16,17} hepatitis B (lamivudine/entecavir),^{18,19} hepatitis C (sofosbuvir),²⁰ or herpes infections (acyclovir).²¹ So far, numerous nucleoside analogs have been described to inhibit arthropod-transmitted flaviviruses. Since these viruses are closely related to the hepatitis C virus (HCV), for which many potent inhibitors are being currently developed, anti-HCV nucleoside analogs represent promising tools to be repurposed against other viruses within the Flaviviridae family.¹²

The aim of this review is to provide an overview of known antiviral agents targeting selected arthropod-borne flaviviruses and to discuss their characteristic properties, modes of action, and advantages or limitations of their therapeutic use. Moreover, the important challenges and complications in antflavivirus nucleoside analog development are highlighted and possible strategies to overcome their shortcomings are suggested.

Major classes of antflavivirus nucleosides

Nucleoside analogs active against arthropod-borne flaviviruses are usually classified according to their targets in the viral life cycle. Such antiviral molecules act as inhibitors of flaviviral RdRp,^{22–26} MTase,^{27,28} and helicase/NTPase.^{29,30} Other nucleoside scaffolds suppress host cell enzymes involved particularly in nucleoside biosynthetic pathways^{31–34} or in some cases, exhibit multiple modes of action.^{32,35} In vitro antiviral effects

and cytotoxicity profiles of the most important antflavivirus nucleoside analogs are summarized in Table 1. An overview of in vivo antflaviviral activities of selected nucleosides as evaluated in different animal models is presented in Table 2.

Inhibitors of flaviviral NS5 RdRp

The flavivirus NS5 protein is approximately 900 amino acids in length and consists of the NH₂-terminal MTase domain required for the 5'-RNA capping process and the COOH-terminal RdRp domain responsible for the replication of the viral RNA genome.^{10,36} Flaviviral RdRp is a right hand-shaped structure with fingers, palm, and thumb domains; the palm domain is the catalytic domain carrying the polymerase active site that coordinates two Mg²⁺ ions essential for catalyzing the polymerization reaction.³⁷ Nucleoside inhibitors of flaviviral RdRp are the most attractive targets for antiviral drug design; as human replication/transcription enzymes lack RdRp activity, such compounds are expected to show fewer deleterious side effects and favorable safety profiles.^{12,15,38,39}

The mode of action for nucleoside RdRp inhibitors is based on the premature termination of viral nucleic acid synthesis.⁴⁰ Following the intracellular phosphorylation, the 5'-triphosphate metabolites are competitively incorporated into the flaviviral RNA nascent chains (Figure 1). This prevents further extension of the incorporated analog by addition of the next nucleoside triphosphate resulting in formation of incomplete (nonfunctional) viral RNA chains.⁴¹ Nucleoside inhibitors of flaviviral RdRp act as “nonobligate chain terminators,” as their 3'-hydroxyl group is conformationally constrained or sterically/electronically hindered, thus decreasing the potency to form a phosphodiester linkage with the incoming nucleoside triphosphate.⁴⁰ The nonobligate terminators differ from “obligate chain terminators,” in which the 3'-hydroxy group is completely missing, as exemplified by numerous nucleoside reverse transcriptase inhibitors for the treatment of HIV infections.⁴² Chemical modifications of the heterobase moiety, different types of glycosidic bonds, and substitutions at different positions of the sugar ring, which are typical modifications for nucleoside inhibitors of flaviviral RdRps, are shown in Table 3.

1'-Cyano substituted nucleosides

GS-441524, a 1'-cyano substituted C-nucleoside derived from 4-aza-7,9-dideazaadenosine,⁴³ was developed by Gilead Sciences, Inc. as a treatment for filovirus infections also showing reasonable antiviral activity against paramyxo- and pneumoviruses.⁴⁴ Within the

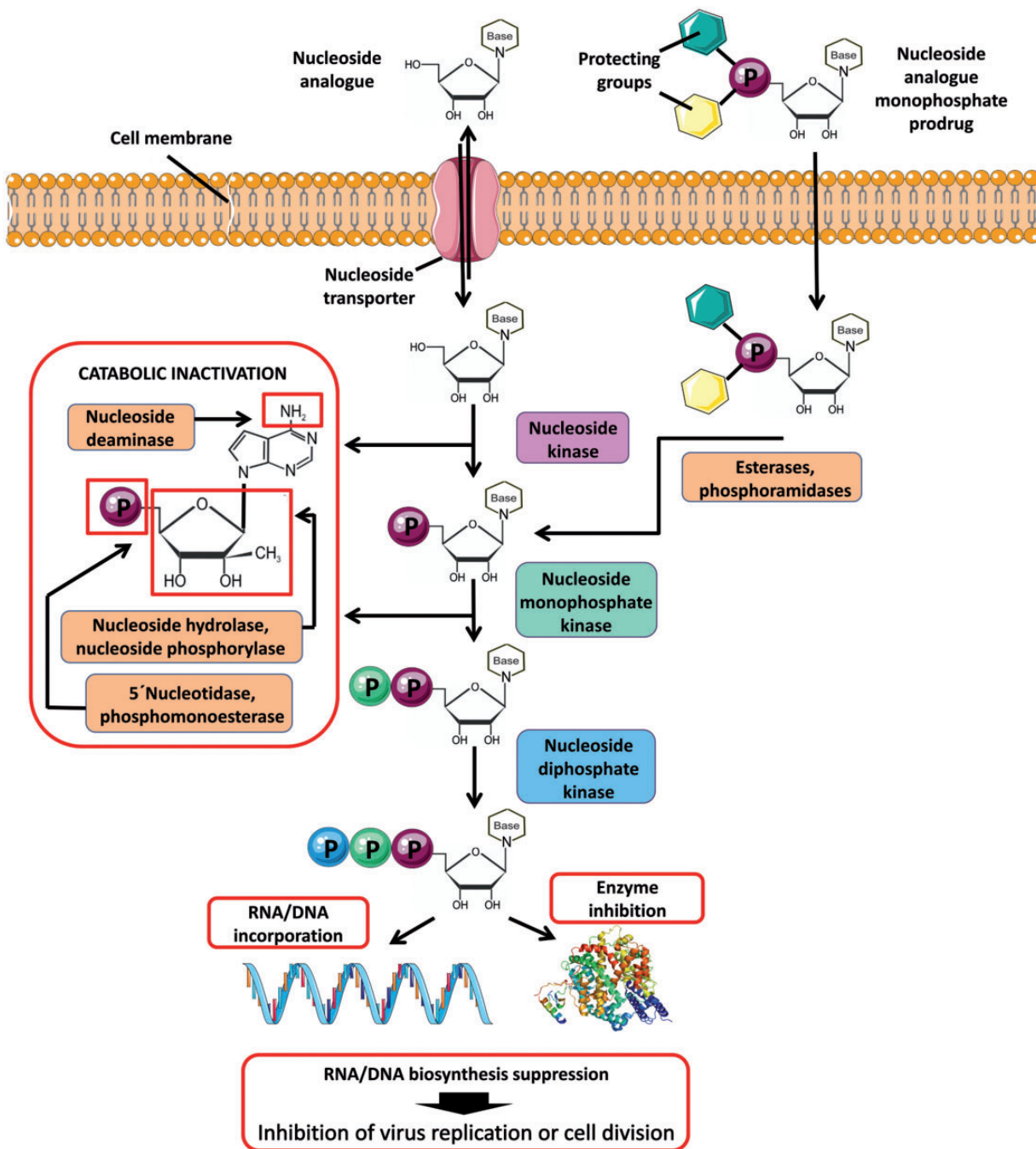
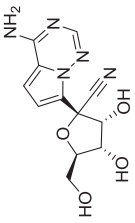
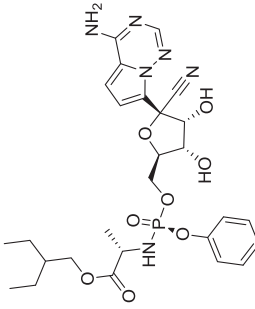
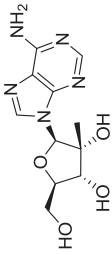
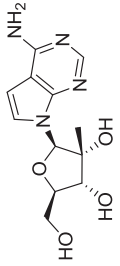


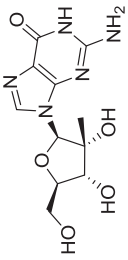
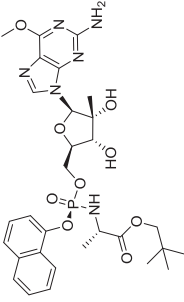
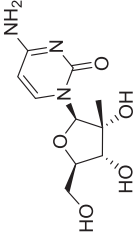
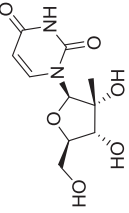
Figure 1. Intracellular uptake and metabolism of nucleoside analogs and nucleoside analog prodrugs. Nucleoside analogs enter cells through specific plasma membrane nucleoside transporters. Inside the cell, the compounds are phosphorylated by cellular nucleoside kinases resulting in formation of nucleoside mono-, di-, and triphosphates. The first kinase phosphorylation is the rate-limiting step of the triphosphate conversion, which can be overcome by the monophosphate prodrug approach based on the introduction of a phosphorylated group into the 5' nucleoside position. The phosphorylated group includes protecting moieties to increase hydrophobicity and facilitate the cellular uptake of the prodrug. Monophosphate prodrugs enter cells independently of membrane transporters and the protecting groups are removed by intracellular esterases or phosphoramidases after cell penetration. The triphosphates of nucleoside species represent the active forms of nucleoside analogs that act by inhibiting cellular or viral enzymes, such as DNA/RNA polymerases. During DNA/RNA replication, nucleoside analogs are incorporated into nascent DNA or RNA chains resulting in termination of nucleic acid synthesis or in accumulation of mutations in viral genomes to suppress viral replication due to error catastrophe. At normal physiological conditions, intracellular nucleoside concentrations are maintained at low levels due to nucleoside/nucleotide catabolic pathways, such as deamination (oxidation) of heterocyclic base, hydrolysis or phosphorolysis of heterocyclic base, and hydrolysis of phosphomonoester bonds. These catabolic reactions also concern most nucleoside analogs containing the natural *N*-glycosidic bond and/or the degradable functional groups of the heterocyclic base. Figure created using Servier Medical Art available on www.servier.com.

Table 1. In vitro antiviral activities and cytotoxicity profiles of selected nucleoside inhibitors of flaviviral replication.

Structure	Virus	Strain	Cell line	Assay	EC ₅₀ (μM)	CC ₅₀ (μM)	References
Inhibitors of flaviviral RdRp GS-441524 	AHFV	200300001	Vero	CPE	49.9	ND	Lo et al. ⁴⁵
	KFDV	P9605	Vero	CPE	46.3	ND	Lo et al. ⁴⁵
	TBEV	Hypr	Vero	CPE	51.2	ND	Lo et al. ⁴⁵
	OHFV	Bogoluvovska	Vero	CPE	50.6	ND	Lo et al. ⁴⁵
	YFV	ND	ND	Cell based	11	>30	Cho et al. ⁴³
GS-5734 	AHFV	200300001	Vero	CPE	4.2	ND	Lo et al. ⁴⁵
	KFDV	P9605	Vero	CPE	1.8	ND	Lo et al. ⁴⁵
	TBEV	Hypr	Vero	CPE	2.1	ND	Lo et al. ⁴⁵
	OHFV	Bogoluvovska	Vero	CPE	1.2	ND	Lo et al. ⁴⁵
	2'-C-methyladenosine 	TBEV	Hypr	PS	VTR	1.4	>50
WNV		New York isol.	Vero	CPE	5.1	25	Migliaccio et al. ⁴⁹
DENV-2		New Guinea C	Vero	CPE	4	18	Migliaccio et al. ⁴⁹
YFV		I7-D	Vero	CPE	3.2	13	Migliaccio et al. ⁴⁹
ZIKV		MR766	Vero	VTR	5.26	>100	Eyer et al. ²³
7-Deaza-2'-C-methyladenosine 	TBEV	Hypr	PS	VTR	1.1	>50	Eyer et al. ⁵⁴
	WNV	New York isol.	Vero	CPE	4.5	250	Olsen et al. ⁵⁰
	DENV-2	New Guinea C	Vero	CPE	15	>320	Olsen et al. ⁵⁰
	YFV	I7-D	Vero	CPE	15	>320	Olsen et al. ⁵⁰
	ZIKV	MR766	Vero	CPE	20	>357	Zmurko et al. ⁶²
ZIKV	MR766	Vero	VYR	9.6	>357	Zmurko et al. ⁶²	
ZIKV	MR766	Vero	PA	1.3	>357	Zmurko et al. ⁶²	
ZIKV	MR766	Vero	IFA	5.7	>357	Zmurko et al. ⁶²	

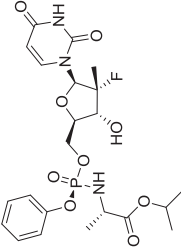
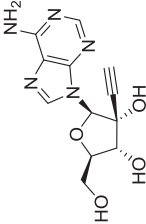
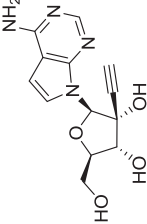
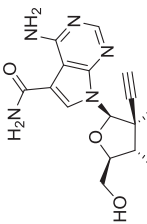
(continued)

Table 1. Continued

Structure	Virus	Strain	Cell line	Assay	EC ₅₀ (μM)	CC ₅₀ (μM)	References
	TBEV WNV DENV-2 YFV ZIKV	Hypr New York isol. New Guinea C 17-D MR766	PS Vero Vero Vero Vero	VTR CPE CPE CPE VTR	1.4 30 13.6 17 22.25	>50 >100 >60 >50 >100	Eyer et al. ⁵⁴ Migliaccio et al. ⁴⁹ Migliaccio et al. ⁴⁹ Migliaccio et al. ⁴⁹ Eyer et al. ²³
	DENV-2	ND	Huh-7	Replicon	0.0142	>1	Yeo et al. ⁵⁸
	TBEV AHFV AHFV KDFV OHFV POWV DENV YFV YFV YFV ZIKV	Hypr 200300001 200300001 P9605 Bogoluvovska Byers ND 17-D 17-D 17-D MR766	PS A549 A549 A549 A549 A549 Huh-7 Vero Vero Vero Vero	VTR qRT-PCR CPE CPE CPE CPE Replicon Visual inspection Neutral red uptake VYR VTR	1.8 2.5 15.3 7.2 3.2 5.5 11.2 2.5 ^a 2.1 ^a 0.7 ^a 10.51	>50	Eyer et al. ⁵⁴ Flint et al. ⁵⁵ Lee et al. ⁵⁶ Julander et al. ⁶³ Julander et al. ⁶³ Julander et al. ⁶³ Eyer et al. ²³
	TBEV ZIKV	Hypr MR776	PS Vero	VTR VTR	11.1 45.45	>50 >100	Eyer et al. ⁵⁴ Eyer et al. ²³

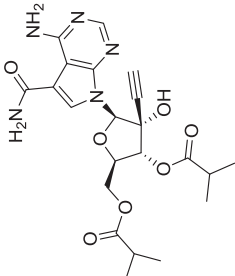
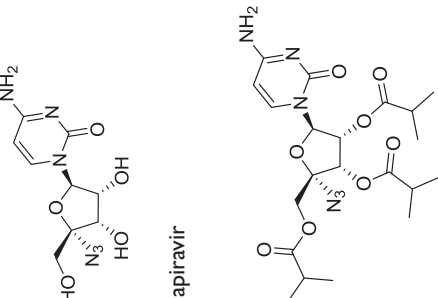
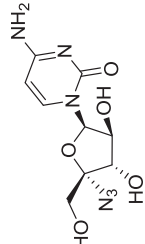
(continued)

Table 1. Continued

Structure	Virus	Strain	Cell line	Assay	EC ₅₀ (μM)	CC ₅₀ (μM)	References
	ZIKV	ND	BHK-21, SH-sy5y, Huh-7	CPE	0.12–1.9	>300	Sacramento et al. ²⁵
	ZIKV	ND	-	RdRp inhibition	0.38	ND	Sacramento et al. ²⁵
	ZIKV	PRVABC59	Huh-7, Jan	PA	1–5	>200	Bullard-Feibelman et al. ⁶⁹
	ZIKV	Paraitba	Huh-7, Jan	qRT-PCR	1–5	>200	
	ZIKV	Dakar 41519	Huh-7, Jan		1–5	>200	
2'-C-ethynyladenosine	DENV-2	ND	A549	CFI	1.41	40	Chen et al. ²²
							
NITD008	DENV-2	New Guinea C	A549	CFI	0.46–2.61	>100	Chen et al. ⁷²
	DENV-2	MY10245	PBMC	CFI	0.58	>100	Chen et al. ⁷²
	DENV-2	MY10340	PBMC	CFI	0.58	>100	Chen et al. ⁷²
	DENV-2	MY22366	PBMC	CFI	0.58	>100	Chen et al. ⁷²
	DENV-2	MY22713	PBMC	CFI	0.58	>100	Chen et al. ⁷²
	ZIKV	GZ01/2016	Vero	VTR	0.241	ND	Deng et al. ⁷⁶
	ZIKV	GZ01/2016	Vero	qRT-PCR	0.137	ND	Deng et al. ⁷⁶
	ZIKV	FSS13025/2010	Vero	VTR	0.950	ND	Deng et al. ⁷⁶
	ZIKV	FSS13025/2010	Vero	qRT-PCR	0.283	ND	Deng et al. ⁷⁶
	TBEV	Hypr	A549	CPE, CFI, VTR	0.9–2.99	>100	Lo et al. ⁷⁷
	AHFV	200300001	A549	CPE, CFI, VTR	1.51–9.29	>100	Lo et al. ⁷⁷
	KDFV	P9605	A549	CPE, CFI, VTR	1.42–4.01	>100	Lo et al. ⁷⁷
	OHFV	Bogoluvovska	A549	CPE, CFI, VTR	0.61–3.04	>100	Lo et al. ⁷⁷
NITD449	DENV (1–4)	New Guinea C	A549	CFI	1.62–6.99	ND	Chen et al. ⁷²
		MY10245	PBMC	CFI	5	ND	Chen et al. ⁷²
		MY10340	PBMC	CFI	5	ND	Chen et al. ⁷²
		MY22366	PBMC	CFI	5	ND	Chen et al. ⁷²
		MY22713	PBMC	CFI	5	ND	Chen et al. ⁷²

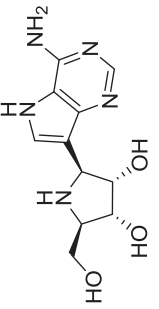
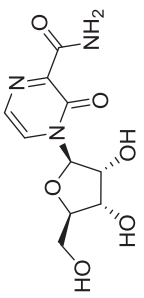
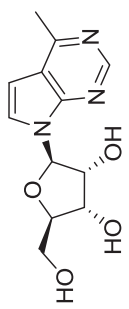
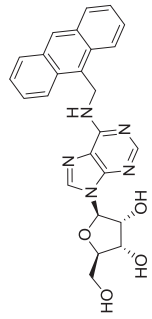
(continued)

Table 1. Continued

Structure	Virus	Strain	Cell line	Assay	EC ₅₀ (μM)	CC ₅₀ (μM)	References		
	DENV (1-4)	New Guinea C MY10245 MY10340 MY22366 MY22713	A549 PBMC PBMC PBMC PBMC	CFI CFI CFI CFI CFI	0.54-0.71 <0.1 <0.1 <0.1 <0.1	ND ND ND ND ND	Chen et al. ⁷² Chen et al. ⁷² Chen et al. ⁷² Chen et al. ⁷² Chen et al. ⁷²		
	4'-C-azidocytidine	TBEV	Hypr	PS	VTR	2.7	>50	Eyer et al. ⁵⁴	
		DENV (1-4)	Various	DC Huh-7 PHM	qRT-PCR qRT-PCR qRT-PCR	5.2-6 1.9-11 1.3-3.2	ND ND ND	Nguyen et al. ⁸³ Nguyen et al. ⁸³ Nguyen et al. ⁸³	
		RO-9187	TBEV	Hypr	PS	VTR	0.3	>50	Eyer et al. ⁵⁴
									

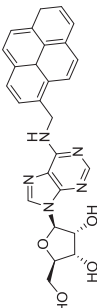
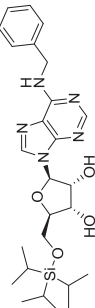
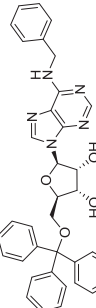
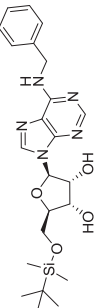
(continued)

Table 1. Continued

Structure	Virus	Strain	Cell line	Assay	EC ₅₀ (μM)	CC ₅₀ (μM)	References
	TBEV	Hypr	PS	VTR	1.48	> 100	Eyer et al. ⁹⁰
	LIV	LI/31	PS	VTR	12.33	> 100	Eyer et al. ⁹⁰
	KFDV	W-377	PS	VTR	11.37	> 100	Eyer et al. ⁹⁰
	WNV	Egl101	PS	VTR	2.33	> 100	Eyer et al. ⁹⁰
	YFV	I7-D	NID	ND	14.1	> 100	Warren et al. ⁸⁹
	JEV	SAI4	NID	ND	43.6	> 100	Warren et al. ⁸⁹
	DENV-2	New Guinea C			32.8	> 296	Warren et al. ⁸⁹
	ZIKV	Various	Vero, Huh-7, RD	CPE	3.8–11.7 ^a	> 100 ^a	Julander et al. ⁹¹
	ZIKV	Various	Vero, Huh-7, RD	VYR	5.4–18.2 ^b	> 100 ^a	Julander et al. ⁹¹
	T-1106	YFV	I7-D	Vero	Neutral red uptake	1800	> 4000
	YFV	I7-D	Vero	CPE	2630	> 4000	Julander et al. ⁹⁴
	YFV	I7-D	Vero	Luciferase based	1080	> 4000	Julander et al. ⁹⁴
	DENV-2	ND	Vero	PA	0.062	NID	Wu et al. ⁹⁶
	DENV-2	ND	Vero	qRT-PCR	0.039	NID	Wu et al. ⁹⁶
	TBEV	Absettarov	PEK	PA	15	> 50 ^c	Orlov et al. ³⁵

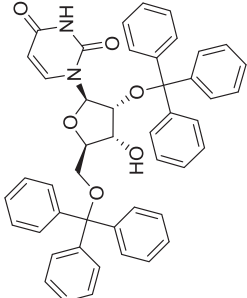
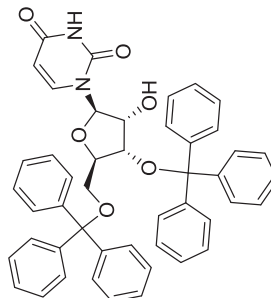
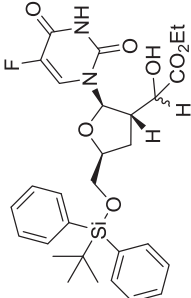
(continued)

Table 1. Continued

Structure	Virus	Strain	Cell line	Assay	EC ₅₀ (μM)	CC ₅₀ (μM)	References
 N6-(1-pyrenylmethyl) adenosine	TBEV	Absettarov	PEK	PA	6	> 50 ^c	
 N6-benzyl-5'-O-triisopropylsilyl adenosine	TBEV	Absettarov	PEK	PA	5	> 50 ^c	
 N6-benzyl-5'-O-trityl adenosine	TBEV	Absettarov	PEK	PA	2	> 50 ^c	
 N6-benzyl-5'-O-tert-butyl(dimethylsilyl) adenosine	TBEV	Absettarov	PEK	PA	20	> 50 ^c	

(continued)

Table 1. Continued

Structure	Virus	Strain	Cell line	Assay	EC ₅₀ (μM)	CC ₅₀ (μM)	References
	DENV-2	New Guinea C	Vero	CPE	30 ^a	> 100 ^a	Saudi et al. ¹⁰⁴
	YFV	I7-D	Vero	CPE	1.2 ^a	> 100 ^a	Saudi et al. ¹⁰⁴
	DENV-2	New Guinea C	Vero	CPE	1.75 ^a	> 10 ^a	
	YFV	I7-D	Vero	CPE	1 ^a	> 85 ^a	
Inhibitors of flaviviral methyltransferase GRL-002 	WNV	NY99	-	N-7 methylation inhibition	33.9 ^d	-	Chen et al. ¹¹¹
	WMV	NY99	-	2'-O-methylation inhibition	5.5 ^d	-	Chen et al. ¹¹¹
	WMV	NY99	A549	VTR		52	48

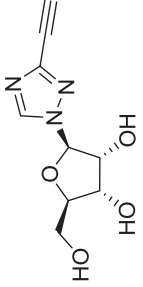
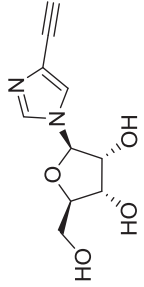
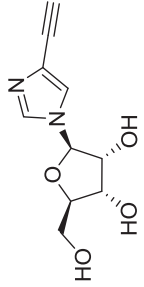
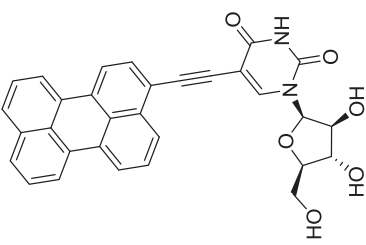
(continued)

Table 1. Continued

Structure	Virus	Strain	Cell line	Assay	EC ₅₀ (μM)	CC ₅₀ (μM)	References
	WMV	NY99	–	N-7 methylation inhibition	17.3 ^d	–	Chen et al. ¹¹¹
	WMV	NY99	–	2'-O-methylation inhibition	19.8 ^d	–	Chen et al. ¹¹¹
	WMV	NY99	A549	VTR	27	236	Chen et al. ¹¹¹
 Flex 1, R=H, Ac, Flex 1-TP, R=triphosphate	DENV-3	ND	–	2'-O-methylation inhibition	22 ^d	–	K. Seley-Radtke, manuscript in preparation
	ZIKV	French Polynesisa (2013/PF KJ776791.2)	–	2'-O-methylation inhibition	22 ^d	–	
 Flex 2	DENV-3	ND	–	2'-O-methylation inhibition	3.2 ^d	–	unpublished results, Smeelaboratory, Utah
 Ribavirin and other nucleoside synthesis inhibitors	DENV (1–4)	Various	Vero	CPE	19.8–41.9 ^a	> 100 ^{a,e}	Crance et al. ³¹
	JEV	Nakayama	Vero	CPE	134.1 ^a	> 100 ^{a,e}	Crance et al. ³¹
	WMV	E101	Vero	CPE	71.2 ^a	> 100 ^{a,e}	Crance et al. ³¹
	USUV	DakArD 19848	Vero	CPE	62.6 ^a	> 100 ^{a,e}	Crance et al. ³¹
	LGTV	ND	Vero	CPE	33.9 ^a	> 100 ^{a,e}	Crance et al. ³¹
	YFV	I7D and FNV	Vero	CPE	42.4; 48.2 ^a	> 100 ^{a,e}	Crance et al. ³¹
	WESSV	ND	Vero	CPE	91.7 ^a	> 100 ^{a,e}	Crance et al. ³¹
	ZIKV	Various	Vero, Huh-7, RD	CPE	3.8–142.9 ^a	> 100 ^{a,e}	Crance et al. ³¹
	ZIKV	Various	Vero, Huh-7, RD	VYR	9.52–281 ^b	> 100 ^{a,e}	Crance et al. ³¹ and Julander et al. ⁹¹

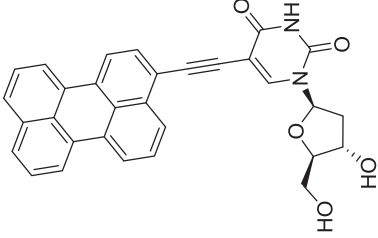
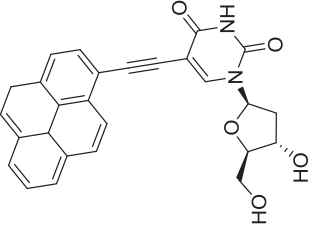
(continued)

Table 1. Continued

Structure	Virus	Strain	Cell line	Assay	EC ₅₀ (μM)	CC ₅₀ (μM)	References
	DENV-2	ND	Vero	ND	9.5	> 1000	McDowell et al. ¹³⁵
IM18	DENV-2	ND	Vero	ND	106.1	ND	McDowell et al. ¹³⁵
	DENV (1-4)	Various	Vero	CPE	0.1–0.5 ^a	> 100 ^{a,e}	Crance et al. ³¹
	JEV	Nakayama	Vero	CPE	0.5 ^a	> 100 ^{a,e}	Crance et al. ³¹
	WNV	E101	Vero	CPE	0.2 ^a	> 100 ^{a,e}	Crance et al. ³¹
	USUV	DakArD 19848	Vero	CPE	0.1 ^a	> 100 ^{a,e}	Crance et al. ³¹
	LGTV	ND	Vero	CPE	0.2 ^a	> 100 ^{a,e}	Crance et al. ³¹
	YFV	I7D and FNV	Vero	CPE	0.2; 0.2 ^a	> 100 ^{a,e}	Crance et al. ³¹
	WESSV	ND	Vero	CPE	1.3 ^a	> 100 ^{a,e}	Crance et al. ³¹
	ZIKV	DakArB 11514	Vero	CPE	1.5 ^a	> 100 ^{a,e}	Crance et al. ³¹
	TBEV	Absettarov	PEK	PA	0.018 ^f	> 50 ^c	Orlov et al. ¹⁰¹

(continued)

Table 1. Continued

Structure	Virus	Strain	Cell line	Assay	EC ₅₀ (μM)	CC ₅₀ (μM)	References
5-(Perylen-3-yl)ethynyl-2'-deoxy-uridine	TBEV	Absettarov	PEK	PA	0.024 ^f	>50 ^c	Orlov et al. ¹⁰¹
	TBEV	Absettarov	PEK	PA	0.98 ^f	>50 ^c	Orlov et al. ¹⁰¹
5-(Pyren-1-yl)ethynyl-2'-deoxy-uridine	TBEV	Absettarov	PEK	PA	0.98 ^f	>50 ^c	Orlov et al. ¹⁰¹
	TBEV	Absettarov	PEK	PA	0.98 ^f	>50 ^c	Orlov et al. ¹⁰¹

AHFV: Alkhurma hemorrhagic fever virus; CFI: cellular flavivirus immunodetection; CPE: cytopathic effect reduction assay; DC: dendritic cells; DENV: dengue virus; JEV: Japanese encephalitis virus; KFDV: Kyasanur Forest disease virus; LGTV: Langkat virus; LIV: louping ill virus; ND: not determined; OHFV: Omsk hemorrhagic fever virus; PA: plaque reduction assay; PBMC: peripheral blood mononuclear cells; PHM: primary human macrophages; POWV: Powassan virus; TBEV: tick-borne encephalitis virus; USUV: Usutu virus; VTR: viral titer reduction assay; YR: viral yield reduction assay; WESSV: Wesselsbron virus; WNV: West Nile virus; YFV: yellow fever virus; ZIKV: Zika virus.

^aEC₅₀ and CC₅₀ values are expressed as μg/ml.

^bEC₉₀ values, expressed as μg/ml.

^cCC₅₀ (24 h): the cell culture was treated for 24 h with the appropriate compound to obtain the cytotoxicity data.

^dIC₅₀ values obtained from enzyme-based inhibition assays.

^eCC₅₀ values for confluent compound-treated cells.

^fEC₅₀ (sim): the cell culture was TBEV infected and simultaneously treated with the appropriate compound.

Table 2. Examples of in vivo ant flaviviral activities of selected nucleoside analogs.

Compound	Animal model	Admin. route	Treatment start	Treatment length	Dose	Virus	Infection route	Survival rate (%)	References
7-Deza-2'-C-methyladenosine	BALB/c mouse	i.p.	0 dpi	17 days	25 mg/kg/2 × day 5–15 mg/kg/2 × day	TBEV	s.c.	60 35–50	Eyer et al. ⁶¹
2'-C-methylcytidine	AG129 mouse	p.o.	–1 h	10 days	50 mg/kg/day	ZIKV	i.p.	25	Zmurko et al. ⁶²
	ICR suckling mouse Syrian golden hamster	i.c. i.p.	1 dpi –4 h	5 days 4–7 days	15 or 30 mg/kg/day 120 mg/kg/day	DENV YFV	i.c. i.p.	60 90	Lee et al. ⁵⁶ Julander et al. ⁶³
Sofosbuvir	C57BL/6j mouse	p.o.	3 dpi	7 days	33 mg/kg/day	ZIKV	s.c.	80	Bullard-Feibelman et al. ⁶⁹
	Suckling Swiss mouse	i.p.	1 dpi –24 h	7 days	20 mg/kg/day	ZIKV	i.p.	50	Ferreira et al. ⁷¹
NITD008	AG129 mouse	p.o.	2 dpi 0 h	ND	25–50 mg/kg/day	DENV	i.v.	25 100	Yin et al. ²⁶
	A129 mouse	p.o.	1 dpi	5 days	25 mg/kg/day	ZIKV	i.p.	70	Deng et al. ⁷⁶
T-1106	Syrian golden hamster	i.p.	ND –4 h	8 days	50 mg/kg/day 100 mg/kg/2 × day	ZIKV YFV	i.p. i.p.	50 100	Julander et al. ⁹³
			3 dpi 5 dpi					100	
BCX4430	Syrian golden hamster	i.p.	–4 h	7 days	12.5–125 mg/kg/day	YFV	i.p.	20	Julander et al. ⁹²
	AG129 mouse	i.m.	4 dpi –4 h	7–8 days	200 mg/kg/day 300 mg/kg/day	ZIKV	s.c.	100 80 90	Julander et al. ⁹¹
			1 dpi 3 dpi					85 10	

DENV: dengue virus; i.c.: intracerebral administration; i.m.: intramuscular administration; i.p.: intraperitoneal administration; i.v.: intravenous administration; ND: not determined; p.o.: per os (oral administration); s.c.: subcutaneous administration; TBEV: tick-borne encephalitis virus; YFV: yellow fever virus; ZIKV: Zika virus.

Table 3. Heterobase substitutions and ribose modifications of selected flaviviral RdRp nucleoside inhibitors.

Heterobase identity/ modification	Type of the glycosidic bond	Ribose substitution	Ribose position	Example
4-Aza-7,9-dideazaadenine	C-glycosidic	-CN (α)	C1'	GS-441524
4-Aza-7,9-dideazaadenine	C-glycosidic	-CN (α)	C1'	GS-5734
Adenine	N-glycosidic	-CH ₃ (β)	C2'	2'-C-methyladenosine
7-Deazaadenine	N-glycosidic	-CH ₃ (β)	C2'	7-Deaza-2'-C-methyladenosine
Guanine	N-glycosidic	-CH ₃ (β)	C2'	2'-C-methylguanosine
Cytosine	N-glycosidic	-CH ₃ (β)	C2'	2'-C-methylcytidine
Uracil	N-glycosidic	-CH ₃ (β)	C2'	2'-C-methyluridine
6-O-methylguanine	N-glycosidic	-CH ₃ (β)	C2'	INX-08189
Uracil	N-glycosidic	-F (α), CH ₃ (β)	C2'	Sofosbuvir
Adenine	N-glycosidic	-ethynyl (β)	C2'	2'-C-ethynyladenosine
7-Deazaadenine	N-glycosidic	-ethynyl (β)	C2'	NITD008
7-Deaza-7-carbamoyladenine	N-glycosidic	-ethynyl (β)	C2'	NITD449
Cytosine	N-glycosidic	-H (α), OH (β) + N ₃ (α)	C2' + C4'	4'-Azido
Cytosine	N-glycosidic	-N ₃ (α)	C4'	4'-Azido-aracytidine
9-Deazaadenine	C-glycosidic	O exchanged for N	–	BCX4430
3-Oxopyrazine-2-carboxamide	N-glycosidic	No substitution	–	T-1106
6-Methyl-7-deazaadenine	N-glycosidic	No substitution	–	6-Methyl-7-deazadenosine
Uracil	N-glycosidic	Trityl	C2' and C5'	2',5'-di-O-trityluridine
Uracil	N-glycosidic	Trityl	C3' and C5'	3',5'-di-O-trityluridine

Flaviviridae family, this compound exerted micromolar inhibitory activity against YFV and DENV-2 (EC₅₀ values of 11 and 9.46 μ M, respectively) in various cell-based screening systems.⁴³ Surprisingly, considerably less favorable in vitro activities (>30–51.2 μ M) were reported for WNV and tick-borne flaviviruses, such as AHFV, KFDV, TBEV, and OHFV.^{43,45}

A phosphoramidate prodrug of GS-441524, referred to as GS-5734, recently entered Phase II clinical trials for treatment of Ebola infections, displayed 10- to 40-fold higher antiviral effect against members of the TBEV serocomplex when compared with its parental analog GS-441524. The increased antiviral potency could be related to an improved conversion of the prodrug to the biologically active form; however, the reported SI values (2.4–8.3) indicate a low therapeutic potential for this nucleoside to treat flaviviral infections.⁴⁵ Further substitutions of GS-441524 molecule at the C1' position with methyl, vinyl, or methyl-ethynyl moieties yielded compounds with considerably reduced potency and a narrower spectrum of antiviral activity.⁴³

2'-C-methyl substituted nucleosides

2'-C-Methyl-nucleoside scaffolds represent the initial major class of therapeutic nucleosides developed by Merck Research Laboratories to demonstrate potent inhibition of HCV replication.^{46–50} Antiviral activity of 2'-C-methylated nucleosides beyond the Flaviviridae family was reported for representatives

of Picornaviridae and Caliciviridae families,^{51–53} indicating the potential for broad-spectrum inhibitory activity for these compounds within the positive single-stranded RNA viruses.

The 2'-C-methyl substituent introduced at the nucleoside β -face appears to be an important structural element for highly selective micromolar inhibition of tick-borne flaviviruses, particularly for TBEV, AHFV, KDFV, OHFV, and POWV, when assayed in porcine stable kidney cells (PS), human neuroblastoma cells UKF-NB4, or adenocarcinomic human alveolar basal epithelial cells A549.^{24,54,55} From mosquito-transmitted flaviviruses, 2'-C-methylated nucleosides inhibited WNV, DENV, and YFV in cell-based or cell-free reporter assay systems, showing low micromolar antiviral activities.^{50,56,57} A phosphoramidate prodrug of 6-O-methyl-2'-C-methylguanosine, denoted as INX-08189, exerted nanomolar inhibitory activity against DENV-2, and the combination of INX-08189 with ribavirin resulted in significant synergistic anti-DENV activity in vitro.⁵⁸ 7-Deaza-2'-C-methyladenosine together with other 2'-C-methylated species was the first described nucleoside-based inhibitors of ZIKV, after its epidemiological outbreaks in Oceania and Latin America.^{23,59} 7-Deaza-2'-C-methyladenosine showed anti-ZIKV potency not only on immortalized cell lines, but also on induced pluripotent stem cell-derived neuronal cell types, such as cortical neurons, motor neurons, and astrocytes.⁶⁰ The triphosphate analogs of 2'-C-methylated nucleosides exhibited strong inhibitory activity in a

polymerase-based in vitro assay using an active recombinant ZIKV RdRp.⁶¹

Strong antinflaviviral activity for several 2'-C-methyl modified nucleosides was also demonstrated using numerous in vivo efficacy models. For example, 7-deaza-2'-C-methyladenosine substantially improved disease outcome, increased survival, and reduced signs of neuroinfection and viral titers in the brains of BALB/c mice infected with a lethal dose of TBEV.⁶² This compound also reduced viremia in AG129 mice infected with the African strain of ZIKV.⁵⁹ Moreover, 2'-C-methylcytidine protected suckling mice challenged with DENV⁵⁶ and hamsters infected with a lethal dose of YFV, even when administered up to three days postinfection.⁶³

2'-Fluoro-2'-C-methyl substituted nucleosides

Similar to the 2'-C-methylated nucleosides, analogs possessing the 2'- α -fluoro-2'- β -C-methyl modification were initially identified as promising inhibitors of HCV polymerase activity.⁶⁴ Sofosbuvir, a phosphoramidate prodrug of 2'-fluoro-2'-C-methyluridine developed by Gilead Sciences, Inc., is one of the most potent and selective inhibitors in this series and was approved by the Food and Drug Administration (FDA) for the treatment of chronic HCV infection.⁶⁵ Sofosbuvir is nontoxic for most human cell lines and is a very poor substrate for human mitochondrial RdRp, resulting in an acceptable safety profile and negligible mitochondrial toxicity.^{66,67}

Sofosbuvir was demonstrated to inhibit the ZIKV RdRp in a recombinant polymerase assay⁶⁸ and to suppress ZIKV replication in different cell-based systems using U87 glioblastoma cells, baby hamster kidney fibroblasts (BHK-21), SH-sy5y neuroblasts, hepatocarcinoma Huh-7 cells, Jar human placental choriocarcinoma cells, neural stem cells, and brain organoids with nanomolar or low micromolar inhibitory activity.^{25,69} Interestingly, no inhibition of ZIKV replication with sofosbuvir even at the 50 μ M level was observed in Vero cells,²³ indicating that the sofosbuvir-mediated anti-ZIKV effect is strongly cell-type dependent.⁷⁰ Sofosbuvir protected inbred C57BL/6J mice, which were previously immunosuppressed with a single dose of anti-Ifnar1 blocking monoclonal antibody, against ZIKV-induced mortality.⁶⁹ Moreover, this compound reduced viral titer in blood plasma, spleen, kidney, and brain in suckling Swiss albino mice and prevented virus-induced neuromotor impairment in ZIKV-infected animals.⁷¹

Surprisingly however, sofosbuvir was inactive against TBEV, when screened on both PS and UKF-NB4 cells.⁵⁴ Another 2'- α -fluoro-2'- β -C-methyl modified nucleoside, PSI-6206, and its 3',5'-diester prodrug

mericitabine, also displayed no activity against TBEV replication. The lack of anti-TBEV activity for the 2'- α -fluoro-2'- β -C-methyl modified nucleosides could be ascribed to their inefficient intracellular conversion to their corresponding triphosphates and, moreover, to extensive deamination/demethylation in the tested cell cultures resulting in their conversion to uridine.^{46,54}

2'-C-ethynyl substituted nucleosides

2'-C-Ethynyl substituted nucleosides have been primarily identified as inhibitors of DENV.^{22,72-75} 2'-C-Ethynyladenosine represents the lead compound in this series, which inhibited DENV-2 replication with an EC₅₀ of 1.41 μ M in cell-based assays and with a CC₅₀ value of 40 μ M.²² The 7-deaza derivative of 2'-C-ethynyladenosine, denoted as NITD008, inhibited DENV of different serotypes at submicromolar or low micromolar concentrations when tested in BHK-21 cells, A549 cells, Huh-7 hepatocarcinoma cells, and human peripheral blood mononuclear cells (PBMCs), showing a significantly improved cytotoxicity profile (CC₅₀ of >100 μ M) compared with that of 2'-C-ethynyladenosine.²⁶ NITD008 was also assayed against WNV, YFV, and ZIKV and exhibited excellent in vitro inhibitory parameters and a protective effect against WNV and ZIKV infections in mouse efficacy models.^{26,76} NITD008 was also reported to effectively inhibit the in vitro replication of TBEV, AHFV, KDFV, OHFV, and POWV, with nanomolar or low micromolar antiviral levels observed in various cell-based screening systems.⁷⁷

Introduction of the C7 carbamoyl moiety to NITD008 molecule provided another 2'-ethynyl modified derivative, referred to as NITD449. Despite its low micromolar anti-DENV efficacy, this nucleoside disappointingly exhibited only low levels in plasma when dosed orally.⁷² To increase the oral bioavailability, the isobutyryl ester prodrug of NITD449, designed as NITD203, was synthesized. NITD203 successfully exhibited both nanomolar anti-DENV activity as well as improved pharmacokinetic parameters.⁷² Although NITD008 and NITD203 showed anti-DENV potency in rodent models, even when the treatment was delayed up to 48 h after infection, both nucleosides failed in preclinical toxicity studies in rats and dogs due to their insufficient safety profiles.^{26,72} NITD008 failed to achieve no-observed-adverse-effect levels (NOAEL) when rats (10 mg/kg/day) and dogs (1 mg/kg/day) were dosed daily for two weeks.²⁶ Similarly, NOAEL was not achieved for NITD203 in the two-week toxicity test when rats were dosed at 30 and 75 mg/kg/day.⁷²

Further substitutions of the C7 position of NITD008 with fluoro or cyano moieties provided compounds with nano- or low micromolar anti-DENV activities and acceptable cytotoxicity profiles. In contrast, 2'-C-ethyl, -vinyl, or -methylethynyl substituted derivatives of 2'-C-ethynyladenosine were completely inactive when tested against DENV. Similarly, the exchange of the adenine base for cytosine or guanine also yielded inactive compounds.^{22,72}

2'-O-substituted nucleosides

2'-O-Methyl substituted adenosine, guanosine, cytidine, and uridine were evaluated for their potential anti-TBEV activity; however, no or negligible antiviral effects were observed when tested in both PS and UKF-NB4 cells.⁵⁴ Such abrogation of the nucleoside inhibitory activity could be related to the elimination of the 2'- α -hydroxy hydrogen bond donor/acceptor properties when the methyl moiety is introduced at the nucleoside O2' position.^{46,54} The ability of flaviviral RdRp to discriminate among nucleosides modified at the 2'-position on the nucleoside α -face is likely related to the need of the polymerase to avoid incorporation of 2'- α -deoxynucleoside monophosphates into the viral nascent RNA chain.⁴⁶

3'-C- and 3'-O-substituted nucleosides

Methylation of the C3' or O3' position to generate the corresponding 3'-C-methyl or 3'-O-methyl modified structures resulted in a complete loss of anti-TBEV activity, regardless of the purine/pyrimidine heterobase identity. These nucleosides exerted no cytotoxic effects and caused no morphological changes in PS or porcine embryo kidney (PEK) cell cultures.^{35,54} Similarly, 3'-deoxynucleosides exhibited no detectable inhibitory effect on TBEV replication.⁵⁴ In contrast, several nucleosides with a trityl group at the C3' position showed micromolar inhibitory activity against DENV and YFV (see below).⁷⁸ The observed inactivity of 3'-O-methylated and 3'-dehydroxylated nucleosides could be related to either a strict requirement of the TBEV RdRp active site for a 3'-hydroxyl group to form the appropriate hydrogen bonding interactions with the nucleoside triphosphate molecule, or, to inefficient cellular uptake and metabolism to convert the nucleoside molecule into the corresponding triphosphate form.^{46,54}

4'-Azido substituted nucleosides

Using high-throughput screening of large nucleoside libraries in combination with a rational drug design approach by investigators at Roche, several cytidine analogs with an azido group at the C4' position were

identified as potent inhibitors of HCV replication in subgenomic replicon assays.⁷⁹⁻⁸¹ It was later shown that these compounds were also highly active against henipaviruses and other paramyxoviruses.⁸² Two 4'-azido modified nucleoside analogs, 4'-azidocytidine (R-1479) and 4'-azido-aracytidine (RO-9187), showed nano- or micromolar in vitro antiviral activity against TBEV.⁵⁴ Moreover, both compounds were found to be active also against WNV (L. Eyer, manuscript in preparation).

The anti-TBEV activity of RO-9187 (the arabino-counterpart of 4'-azidocytidine) was unexpected, as this compound lacks the 2'- α -hydroxy moiety, a determinant which was generally considered to be crucial for specific hydrogen-bonding interactions with RdRps during the RNA replication process.^{54,80} Some additional interactions of the polymerase active site with both the 2'- β -hydroxy substituent and the 4'-azido substituent are thought to compensate for the loss of the 2'- α -hydroxy interaction, resulting in the strong and selective anti-TBEV activity of RO-9187. Interestingly, the anti-TBEV efficacy of both 4'-azido modified nucleosides was cell-type dependent; the compounds were active only in PS cells, but not in UKF-NB4 cells.⁵⁴

An ester prodrug of 4'-azidocytidine, denoted as balapiravir, was completely inactive against TBEV in vitro, probably because of its poor intracellular uptake or insufficient kinase phosphorylation in the tested host cell lines.⁵⁴ In contrast, balapiravir was reported to show strong in vitro antiviral activity against DENV of various serotypes; it was the first direct antiviral agent tested clinically for DENV infection. Unfortunately, this compound failed to achieve antiviral efficacy in DENV patients, which was reflected in a negligible reduction of DENV viremia and persistence of clinical symptoms, even though the plasma concentration of the compound was higher than the 50% effective concentration.⁸³ One of the possible explanations is that DENV infection stimulates PBMCs to produce cytokines, which are responsible for the decreased efficiency of the conversion of balapiravir to its triphosphate form.⁸⁴

Interestingly, nucleoside analogs combining the 4'-azido moiety with the 2'-C-methyl group in one molecule (e.g. 2'-C-methyl-4'-azidocytidine) did not exhibit any antiviral activity when tested against HCV; however, the corresponding 5'-monophosphate prodrugs displayed considerably improved virus inhibitory effects (EC₅₀ values in the micromolar ranges) without apparent cytotoxicity.⁸⁵ Other interesting compounds, 4'-azido-2'-deoxy-2'-C-methylcytidine and its ester prodrugs, were found to show nano- or low micromolar antiviral efficacy in vitro.⁸⁶ Unfortunately, such nucleoside scaffolds have not been evaluated against

arthropod-borne flaviviruses; the reported results originate from HCV replicon-based assays.^{85,86}

Imino-C-nucleoside analog BCX4430

BCX4430, developed by BioCryst Pharmaceuticals Inc., is an adenosine analog with the furanose oxygen on the ribose ring replaced by nitrogen and the heterobase nitrogen 9 replaced by carbon.⁸⁷ This interesting nucleoside is classified as imino-*C*-nucleoside.⁸⁸ BCX4430 was initially described as an inhibitor of filovirus infections, exerting antiviral activity against a broad spectrum of single-stranded RNA viruses, particularly against members of the Bunyaviridae, Arenaviridae, Picornaviridae, Orthomyxoviridae, Paramyxoviridae, Coronaviridae, and Flaviviridae families.⁸⁹ Currently, this compound has entered Phase I clinical trials for Ebola virus disease treatment focused on intramuscular administration of BCX4430 in healthy volunteers and to date has shown promising pharmacokinetics properties and good tolerability.⁸⁷

BCX4430 is active against numerous mosquito-transmitted flaviviruses, such as WNV (EC₅₀ of 2.33 μM)⁹⁰ and representatives of both the African and Asian lineages of ZIKV (3.8–11.7 μg/ml).⁹¹ For YFV, JEV, and DENV-2, micromolar EC₅₀ values were reported.⁸⁹ In vivo efficacy of BCX4430 was also demonstrated in a lethal hamster model of YFV infection and in a mouse model of ZIKV infection.^{91,92} Low micromolar antiviral activity of BCX4430 was also described for some of the medically important tick-borne flaviviruses, such as TBEV, LIV, and KFDV.⁹⁰

Heterocyclic base-modified nucleosides

Heterocyclic base-modified nucleosides with demonstrated antiflaviviral activities include T-1106,^{93–95} 6-methyl-7-deazaadenosine,⁹⁶ and numerous *N6*-alkyl or aryl substituted nucleosides.^{35,97} T-1106 is a ribosylated analog of the pyrazine derivative T-705 (6-fluoro-3-hydroxy-2-pyrazinecarboxamide, favipiravir),⁹⁸ which was described to inhibit the HCV RdRp in enzyme assays.⁹³ Nucleoside inhibitor T-1106 displayed a negligible in vitro activity against YFV in Vero cells, as well as in luciferase-based assays.⁹⁴ In contrast, this compound exerted favorable efficacy, bioavailability, and low toxicity in a hamster model of YFV infection, using a hamster-adapted Jimenez YFV strain. After intraperitoneal application of 100 mg/kg/day, T-1106 improved survival rates, serum parameters, weight gain, and mean day to death when administered up to four days after virus challenge.^{93,94} In this model, the combination of T-

1106 with ribavirin gave superior effects compared to monotherapy (with either T-1106 or ribavirin).⁹⁵

6-Methyl-7-deazaadenosine is a hydrophobic mimic of adenosine showing nanomolar antiviral activity against DENV-2 in a Vero cell-based screening system, as well as in luciferase-driven DENV-2 replicon assay, with no cytotoxic effects noted after 7 h of treatment.⁹⁶ Related compounds such as 6-methyl-1-deazaadenosine and 6-methyl-4-deazaadenosine were completely inactive when tested against DENV-2. Mechanistic studies of the 5'-triphosphate of 6-methyl-7-deazaadenosine revealed that this nucleotide is an efficient substrate for viral RdRp (screened against polio RdRp) and is incorporated into nascent viral RNA strains mimicking both ATP and GTP.⁹⁶

N6-Alkyl or aryl substituted nucleosides, originally identified as inhibitors of Lassa fever virus, Marburg virus, and enterovirus A71, showed interesting bioactivity profiles when tested against TBEV.^{35,99,100} Whereas *N6*-methyladenosine and *N6*-benzyladenosine were completely inactive, nucleosides with bulky substituents, such as *N6*-(9-anthracenylmethyl)adenosine and *N6*-(1-pyrenylmethyl)adenosine, exerted a micromolar anti-TBEV effect. In contrast, *N2*- and *N4*-substituted analogs showed no antiviral activity. Moderate anti-YFV and anti-DENV activities were also observed in *N6*-substituted analogs of 5',3'-*O*- and 5',2'-*O*-*tert*-butyldiphenylsilyl-modified adenosine.⁹⁷ The mechanism of action of these nucleosides is poorly understood; however, they likely interact with the RdRp or MTase domain of the flaviviral NS5 protein, as demonstrated by docking studies.³⁵ Bulky aromatic substituents could also play a role in the interaction with the viral membrane resulting in cell entry inhibition.¹⁰¹

Tritylated nucleosides

In a large-scale cell-based screening campaign of alkylated, silylated, or acylated pyrimidine nucleosides, 2',5'-*di-O*-trityluridine and 3',5'-*di-O*-trityluridine were identified as inhibitors of DENV-2 and YFV replication, showing high antiviral potency and favorable cytotoxicity profiles in Vero cells.^{78,102,103} Substantial antiviral effect against YFV was observed also in 2'-deoxy-3',5'-*di-O*-trityluridine and in several 5-halogenated bis-tritylated pyrimidine nucleosides; however, their anti-DENV activity was proven to be weaker.¹⁰⁴ Thymidine or 2'-deoxyuridine congeners of 2',5'- and 3',5'-tritylated nucleosides led to the loss of antiflavivirus activity or to increased compound cytotoxicity.

The mechanisms of action of tritylated nucleosides are not completely understood. Based on the observed inhibition of DENV replication in subgenomic replicon assays, it is assumed that these compounds may be

acting as inhibitors of intracellular viral replication events rather than suppressing either early or late processes of viral infection, such as entry or assembly.¹⁰³ Although the presence of large, hydrophobic trityl moieties does not make these structures ideal candidates for further drug development, their chemical structures may provide valuable information for advanced mechanistic studies and for further development of related nucleoside scaffolds with improved biological parameters.¹⁰⁴

Nucleoside inhibitors of flaviviral MTase

The NH₂ domain of flaviviral NS5 protein is associated with the virus's MTase activity, which is involved in methylation of the 5'-cap structure of genomic RNA.^{8,105} The flaviviral cap structure is formed by the conserved dinucleotide sequence AG (m⁷GpppAm) and is crucial for mRNA stability and efficient translation.¹⁰⁶ Two topologically distinct methylation reactions are mediated by the flaviviral NS5 MTase: the *N7* of guanine is methylated by the (guanine-*N7*)-MTase and the first nucleotide of RNA transcript is further methylated at the ribose 2'-hydroxyl by (nucleoside-2'-*O*)-MTase. The resulting product of the methyl donation for both methylation reactions by S-adenosyl-L-methionine is the nucleoside analog S-adenosyl-L-homocysteine (SAH).¹⁰⁷

SAH and the nucleoside antibiotic sinefungin are natural nonselective inhibitors of many eukaryotic and viral MTases, including those of DENV^{108,109} or ZIKV.⁶¹ Chemical derivatization of SAH at the *N6* position provided inhibitors with nano- or low micromolar activity against DENV MTase, which did not inhibit the corresponding human enzymes.¹¹⁰ Other rationally designed nucleosides with potent inhibitory activity against MTase contain a thymine base with a hydrophobic methyl *tert*-butyl substituent at the 5' position of the sugar moiety.¹¹¹ Two of these nucleosides, GRL-002 and GRL-003, inhibited the *N7* and 2'-*O* MTase activity of WNV in enzyme-based assays and the observed MTase inhibition was in agreement with the micromolar *in vitro* anti-WNV efficacy.¹¹¹ Another class of promising selective ant Flavivirus compounds is represented by 5'-silylated 3'-1,2,3-triazole-substituted nucleoside scaffolds derived from 3'-azidothymidine. Similar structures were originally developed for HIV-1 inhibition.²⁷ Both the 5'-silyl protecting group and the 3' bulky triazole substituent appeared to be crucial structural elements for low micromolar inhibition of flaviviral MTase in enzyme-based assays, as well as for inhibition of WNV and DENV replication in cell culture. These nucleosides inhibit the methylation reactions through competitive interactions with the

substrate binding site and also with the GTP-binding pocket of the flaviviral NS5 MTase.²⁸

Recently, a novel series of flexible nucleoside analogs known as "fleximers" have exhibited activity against several hard to treat viruses, including filoviruses such as Ebola and Sudan,¹¹² coronaviruses including Severe Acute Respiratory Virus and Middle East Respiratory Virus,¹¹³ as well as most recently, flaviviruses including ZIKV and DENV. The fleximers feature a "split" purine nucleobase that has been shown to impart significant activity to the nucleoside scaffold as well as to allow it to overcome resistance related to point mutations.¹¹⁴⁻¹¹⁶ The most recent series combined the fleximer approach with the acyclic nucleoside acyclovir, an FDA approved drug for herpes virus. While these analogs inhibited the aforementioned viruses, acyclovir shows no activity against any of those viruses, thereby underscoring the importance of the fleximer approach. Since those initial findings, these compounds have also demonstrated potent activity against DENV and ZIKV (K. Seley-Radtke, manuscript in preparation). Preliminary results indicate that these compounds target the DENV and ZIKV NS5 in at least its cap-MTase activity, with negligible effects on the cognate human *N7*-MTase. In that regard, initial screening revealed promising levels of MTase inhibition, particularly for the triphosphate of the compound (Flex 1-TP), with an IC₅₀ of 22 μM for both the DENV and ZIKV 2'-*O*-MTase (K. Seley-Radtke, manuscript in preparation). As a result, Flex 1-TP was further tested against DENV NS5, and while it was not incorporated, it successfully inhibited further incorporations of additional nucleotides, thereby halting replication, however not as a typical chain terminator. In addition, the acetate-protected dimethoxy analog (Flex 2) is a potent DENV inhibitor (3.2 μM, unpublished results, Smee laboratory, Utah); however, more work needs to be done to fully elucidate these novel compounds' mechanism of action. It may well be that these nucleotide analogs target the NS5 protein at both the RdRp and MTase regions, which would make them highly effective viral inhibitors, with low probability of viral resistance developing.

Nucleoside inhibitors of flaviviral NTPase/helicase

Flaviviral NTPase and helicase activities are associated with the COOH-proximal domain of the NS3 protein.¹¹⁷ Flaviviral helicases are capable of unwinding duplex RNA structures during viral replication by disrupting the hydrogen bonds keeping the two strands together.^{118,119} The helicase activity is strictly associated with NTP hydrolysis (NTPase activity); the released

chemical energy is used for the translocation of the enzyme along the double-helix structures, capturing the exposed single strand regions or for a direct disruption of the hydrogen bonds between the two RNA strands.¹²⁰

Specific nucleoside inhibitors of flaviviral NTPase/helicase can interact with dsRNA or DNA resulting in the weakened stability of double-helix structures or by steric hindrance of translocation of the enzyme along the polynucleotide chain. Such a mechanism could modulate the efficacy of the unwinding reaction or NTPase activity of the enzyme and therefore, affect the viral replication process.^{117–121} Weak inhibitory effects on flaviviral NTPase/helicases were described for ribavirin triphosphate,^{124,125} 5'-*O*-fluorosulfonyl-benzoyl esters of purine nucleosides,^{126,127} or halogenated benzotriazole-modified nucleosides.^{30,122} These compounds were primarily evaluated in enzyme-based assays for their putative anti-HCV activity; however, some of them have been found to inhibit also NTPase/helicases of WNV, JEV, or DENV.^{117–127}

Ribavirin and other nucleoside synthesis inhibitors

Ribavirin, a nucleoside analog featuring a [1,2,4]triazole ring for a nucleobase, is a licensed drug against various RNA viruses. The predominant inhibitory mechanism for ribavirin against flaviviral replication is the suppression of de novo biosynthesis of guanine nucleotides through direct inhibition of inosine monophosphate dehydrogenase, an enzyme converting inosine monophosphate to xanthosine monophosphate, a precursor in GTP biosynthesis.³² Speculation over other modes of action for ribavirin includes specific inhibition of the viral RdRp,¹²⁸ accumulation of mutations in viral genomes resulting in error catastrophe,^{129,130} interference with mRNA capping guanylation,¹³¹ and immuno-modulation promoting the Th1 antiviral response.^{32,132,133}

Ribavirin was shown to exert a moderate inhibitory effect for multiple mosquito-borne flaviviruses in various cell cultures,^{31,134,135} often being used as a positive control in many in vitro^{25,59,92} and in vivo antiviral studies.^{91–94} Ribavirin administered to YFV-infected hamsters challenged intraperitoneally, resulted in significant improvement in survival rates, even if the therapy was started two days post-YFV infection.^{93,94} In contrast however, in primates, only a weak prophylactic effect on viremia in rhesus monkeys challenged with DENV was observed.¹³⁶ Several ribavirin derivatives were recently synthesized and showed interesting bioactivity profiles: ETAR (1- β -D-ribofuranosyl-3-ethynyl-[1,2,4]triazole) and IM18 (1- β -D-ribofuranosyl-4-

ethynyl-[1,3]imidazole) inhibited DENV-2 replication in Vero cells by more than 10-fold compared with ribavirin and showed no detectable cytotoxic effects up to 1000 μ M.¹³⁵ Another derivative, EICAR (1- β -D-ribofuranosyl-5-ethynyl-imidazole-4-carboxamide), was reported to possess a similar in vitro spectrum of antiviral activity, but lower selectivity compared with those of ribavirin.¹³⁷

Two nucleosides whose antiviral activity is based on the depletion of the intracellular nucleoside pool are 6-azauridine and 5-aza-7-deazaguanosine. 6-Azauridine and its derivatives are inhibitors of orotidine monophosphate decarboxylase blocking cellular de novo pyrimidine biosynthesis.^{31,33} 6-Azauridine proved to be active against numerous arthropod-borne flaviviruses,⁵⁵ however exhibited slight cytotoxicity with an inhibitory effect on the growth of host cells.²⁴ A triacetate prodrug of 6-azauridine showed low micromolar activity against AHFV and WNV in vitro⁵⁵ and very low toxicity in both animal and human studies.¹³⁸ Another derivative, 2-thio-6-azauridine, exerted a moderate inhibitory effect on WNV.³³ Similar results were achieved using 5-aza-7-deazaguanosine (ZX-2401)¹³⁹; this compound exhibited synergistic in vitro anti-YFV activity in combination with interferon. The mechanism of action for 5-aza-7-deazaguanosine is currently unknown; however, it is conceivable that it likely resembles that of ribavirin.³⁴

Rigid amphipathic nucleosides

Nucleoside derivatives containing bulky aromatic substituents (perylene or pyrene moieties) attached to the heterocyclic base were originally synthesized as fluorescent nucleoside probes^{140–142}; later these structures were identified as inhibitors of herpes simplex virus, type 1 and 2 (HSV-1 and HSV-2), vesicular stomatitis virus, and Sindbis virus replication.¹⁴³ Further studies demonstrated their broad-spectrum antiviral activity against other enveloped viruses, such as influenza virus, murine cytomegalovirus, and HCV.¹⁴⁴ The mechanism of action of these rigid amphipathic nucleosides is based on their incorporation into the viral or cellular membranes, preventing fusion.^{143,144} Alternatively, these nucleosides may also function by photosensitization of lipid membranes, resulting in irreversible damage of enveloped virion particles.¹⁴⁵

5-(Perylen-3-yl)ethynyl-arabinouridine and 5-(perylene-3-yl)ethynyl-2'-deoxyuridine were shown to act as strong inhibitors of TBEV in PEK cell culture.¹⁰¹ The perylene moiety as well as the rigid ethynyl linker appeared as crucial structural elements for nanomolar anti-TBEV activity and low cytotoxicity (>50 μ M). Interestingly, uracil nucleosides bearing the pyrene moiety, such as 5-[(pyren-3-yl)methoxypropyn-1-yl]-

2'-deoxyuridine and 5-(pyren-1-yl)ethynyl-2'-deoxyuridine, showed almost a 10-fold lower anti-TBEV potency compared to their perylene-substituted counterparts. Such compounds, if not used as therapeutic agents, could still contribute to a better understanding of different modes of action of various nucleoside scaffolds.¹⁰¹

Challenges and complications of ant flavivirus nucleoside analog development

Introduction of various chemical substituents into different positions of the nucleoside scaffold can dramatically affect the physicochemical properties of the compound. Such modifications can also significantly influence the compound's biological/pharmacokinetic parameters, such as cellular uptake,^{15,146} the ability of the compound to be activated (phosphorylated) by cellular kinases,¹⁴⁷ degradation by nucleoside catabolic enzymes,¹⁴⁸ or cellular toxicity.^{149,150} Use of nucleoside analogs can also result in the undesirable emergence of drug-resistant virus mutants.^{151–153} This section highlights the most important challenges and complications toward the development of nucleoside inhibitors of arthropod-transmitted flaviviruses and suggests possible strategies to surmount these difficulties.

For most nucleoside analogs, the first kinase phosphorylation is the rate-limiting step for the conversion to the nucleoside triphosphates. This limitation has a major influence on nucleoside analog antiviral activity^{147,154} but can be bypassed by the use of a monophosphate prodrug approach based on the introduction of the phosphorylated group into the 5' nucleoside position. The phosphorylated group includes masking moieties on the charged phosphate leading to a neutral and eventually hydrophobic entity able to deliver the nucleoside 5'-monophosphate into the cells (Figure 1).¹⁵ The monophosphate prodrug approach has been shown to convert some inactive nucleosides into strong inhibitors, or, has improved the kinetics parameters of intracellular nucleoside triphosphate formation.⁸⁵ This strategy, together with enantioselective purification, led to the development of the phosphoramidate prodrug sofosbuvir, which exhibited considerably increased phosphorylation efficacy compared to the parent nucleoside, 2'-C-fluoro-2'-C-methyluridine.^{155,156}

Rapid degradation of nucleoside analogs by nucleoside catabolic pathways (Figure 1) is another undesirable phenomenon, which can adversely affect the antiviral potency of some nucleoside analogs.¹⁴⁸ To address this problem, appropriate structural changes can be introduced into the nucleoside scaffolds to protect the nucleosides from metabolic deactivation.¹⁵⁷

Such a strategy was successful for 2'-C-methyladenosine, which was found to be rapidly deaminated by cellular adenosine deaminase to the inactive inosine derivative and/or degraded by purine nucleoside phosphorylase, resulting in poor bioavailability and rapid clearance of the nucleoside in plasma.^{49,50} Substitution of the adenine N7 nitrogen for a carbon provided metabolically stable 7-deaza-2'-C-methyladenosine, which is a poor substrate for both nucleoside catabolic enzymes. This compound was characterized by excellent bioavailability and half-life in beagle dogs and rhesus monkeys.⁵⁰ Another possible strategy to increase the metabolic stability of therapeutic nucleosides is based on the introduction of a C-glycosidic bond into the nucleoside scaffold to generate C-nucleoside analogs, such as BCX4430⁸⁹ or GS-5734.⁴³ The major advantage of C-nucleosides over the canonical N-nucleosides lies in their resistance to unwanted phosphorylation by intracellular phosphorylases, which otherwise would cleave the N-glycosidic linkage.⁸⁸

Individual host cellular types can display differences in expression levels of nucleoside kinases and other enzymes/proteins involved in nucleoside metabolism and transport. This can then result in cell-type dependent antiviral activity as manifested by different EC₅₀ values for the same inhibitor when assayed on different cell lines.^{158,159} Strong anti-TBEV activity for 2'-C-methylguanosine, 4'-azidocytidine, and 4'-azido-aracytidine in PS cells was associated with rapid and efficient nucleoside conversion to the corresponding triphosphates. On the other hand, no anti-TBEV effect or phosphorylation products were observed when both compounds were tested in UKF-NB4.⁵⁴ Similarly, the loss of anti-ZIKV activity in Vero cells for sofosbuvir is likely related to the increased expression of the multi-drug resistance ABC transporter in this cell line, resulting in the efflux of the compound from the cells.^{23,25} Clearly, cell-type dependent antiviral activity of some nucleosides can considerably affect the results of antiviral screens and therefore, using multiple clinically relevant cell lines for evaluation of compounds for antiviral activity is important.⁷⁰

Another possible complication in nucleoside drug development is an undesirable toxicity profile for the nucleoside inhibitor, which can be related to poor selectivity between viral and human enzymes.^{39,149,150} A typical example of a nonselective nucleoside analog is 7-deazaadenosine (tubercidin), which exhibits high in vitro cytotoxicity. This has been attributed to the incorporation of tubercidin monophosphate into cellular DNA/RNA by human polymerases.⁵⁰ In contrast, two derivatives of tubercidin, 7-deaza-2'-C-methyladenosine and 6-methyl-7-deazaadenosine, are selectively recognized by flaviviral RdRp and are nontoxic in most mammalian cell lines.^{50,96} Some nucleoside analogs

inhibit the mitochondrial DNA or RNA polymerase γ , resulting in mitochondrial toxicity.^{149,160} This has been the primary reason for the failure of several promising nucleosides/prodrugs in clinical trials, as has been shown for some 2'-C-methyl- and 4'-azido modified nucleosides.⁶⁷ Newly developed compounds should also be evaluated for their genotoxicity and mutagenicity, as well as for renal, cardiovascular, or liver toxicity using various biochemical *in vitro* assays.^{161–163} Nevertheless, even if a compound successfully passes through numerous *in vitro* tests, it can still exhibit harmful side effects when tested in animals, as observed with the adenosine analog NITD008.²⁶

In that regard, the availability of suitable animal models is crucial for the successful evaluation of a nucleoside's therapeutic *in vivo* antiviral efficacy. Some flaviviruses, particularly DEVN and ZIKV, do not readily replicate or cause pathology in immunocompetent mice and, therefore, the use of these rodents as animal infection models is substantially limited.^{164–166} To overcome this problem, suckling or young mice,¹⁶⁷ AG129 mice lacking INF- α/β and INF- γ receptors,¹⁶⁸ IFNAR^{-/-} mice lacking only the INF- α/β receptor,¹⁶⁹ or immunosuppressed mice¹⁷⁰ can be used as appropriate models to evaluate nucleosides *in vivo*. However, as these animals are defective in an immune response, this model may also underestimate the real efficacy of the test compounds. Rodent-adapted flavivirus strains, such as the hamster-adapted YFV strain Jimenez,¹⁷¹ mice-adapted DENV strain D2S10,²⁶ or ZIKV African strain Dakar 41519,¹⁷² represent other possible options for *in vivo* antiviral studies; the biological properties of such viruses can be, however, considerably different compared with those of the parent human-adapted strains.¹⁶⁹

Another issue is related to the length of therapeutic treatment. Most tick- and mosquito-borne flaviviruses cause acute infections, in which short-time treatment duration is expected, ranging between several days to weeks.¹⁷³ This is in contrast to chronic diseases, such as HCV, HBV, and HIV infections, which require long-lasting, and sometimes lifelong, treatment regimens.^{72,173} The differences between the acute and chronic diseases should be considered during preclinical development of antflaviviral inhibitors. Thus, some compounds that show insufficient safety profiles when tested for treatment of chronic infections can be still suitable and safe for short-term therapy of acute flaviviral diseases.⁷²

Antiviral therapies based on chemical inhibitors of viral replication can be accompanied with a rapid emergence of drug-resistant mutants which substantially complicates the course of infection treatment, as seen in HIV, HBV, or HCV infections.^{152,153} In flaviviruses, a rapid evolution of resistance to 2'-C-methylated nucleoside inhibitors was observed; this resistance

was associated with a signature mutation S603T (in AHVF and TBEV)^{55,62} or S604T (in ZIKV)⁶⁸ within the active site of the viral RdRp. Interestingly, the biological properties of the TBEV mutant viruses were dramatically affected, which was manifested by resistance-associated loss of viral replication efficacy in cell culture and a highly attenuated virulence phenotype in mice. This resulted in an unusually low mortality rate when mice were infected with the mutant strain.⁶² As TBEV mutants resistant to 2'-C-methylated nucleosides are highly sensitive to 4'-azido substituted nucleosides,⁶² a combination treatment based on two or more inhibitors could be a possible strategy in order to minimize the risks for the emergence of viral drug resistance.^{174–176}

Conclusions

More than 200 million clinical cases caused by arthropod-borne flaviviruses, including numerous deaths, are reported worldwide annually. So many cases of infection indicate the importance for the pursuit of new small molecule-based therapeutics to combat emerging viral pathogens. Among these, inhibitors of flaviviruses represent a critical unmet medical need. In that regard, nucleoside inhibitors of flaviviral RdRps are the most attractive targets for antiviral drug design. Nucleosides with the methyl- or ethynyl- modification at the C2' position and their 2'-fluoro derivatives are the best understood antflavivirus nucleoside analogs, many of which were initially developed for treatment of HCV infections and later reemployed to suppress replication of other non-HCV flaviviruses. Other important antflavivirus nucleosides are represented by inhibitors of nucleoside biosynthesis, whose mode of action is predominantly based on depletion of the intracellular nucleoside pool. Nucleoside inhibitors of flaviviral MTase and NTPase/helicase, as well as some newly discovered flavivirus inhibitors, such as tritylated nucleosides, rigid amphipathic nucleosides, or N6-aryl-substituted adenosine derivatives, whose mechanisms of action are still poorly understood, can be used as initial structures or starting points for further developments of new generations of nucleoside scaffolds with improved biological parameters. Taken together, specific nucleoside analog-based antiviral therapy in combination with effective vaccination strategies could provide potent prophylactic and curative tools to treat human infections caused by flaviviruses.

Declaration of conflicting interests

The author(s) declared no potential conflicts of interest with respect to the research, authorship, and/or publication of this article.

Funding

The author(s) disclosed receipt of the following financial support for the research, authorship, and/or publication of this article: This study was supported by a grant from the Ministry of Health of the Czech Republic (grant no. 16–34238A), Czech Science Foundation (grant no. 16–20054S) (to DR and RN), and by Project “FIT” (Pharmacology, Immunotherapy, nanotoxicology; CZ.02.1.01/0.0/0.0/15_003/0000495), which was funded by the European Regional Development Fund (to DR).

References

- Baier A. Flaviviral infections and potential targets for antiviral therapy. In: Ruzek D (ed) *Flavivirus encephalitis*. 1st ed. Rijeka: InTech, 2011, pp.89–104.
- Lazear HM, Stringer EM and de Silva AM. The emerging zika virus epidemic in the Americas research priorities. *J Am Med Assoc* 2016; 315: 1945–1946.
- Jeffries CL, Mansfield KL, Phipps LP, et al. Louping ill virus: an endemic tick-borne disease of Great Britain. *J Gen Virol* 2014; 95: 1005–1014.
- Ashraf U, Ye J, Ruan XD, et al. Usutu virus: an emerging flavivirus in Europe. *Viruses* 2015; 7: 219–238.
- Rumyantsev AA, Murphy BR and Pletnev AG. A tick-borne Langat virus mutant that is temperature sensitive and host range restricted in neuroblastoma cells and lacks neuroinvasiveness for immunodeficient mice. *J Virol* 2006; 80: 1427–1439.
- Blackburn NK and Swanepoel R. An investigation of flavivirus infections of cattle in Zimbabwe-Rhodesia with particular reference to Wesselsbron virus. *J Hyg* 1980; 85: 1–33.
- Chambers TJ, Hahn CS, Galler R, et al. Flavivirus genome organization, expression, and replication. *Annu Rev Microbiol* 1990; 44: 649–688.
- Koonin EV. Computer-assisted identification of a putative methyltransferase domain in Ns5 protein of flaviviruses and lambda-2 protein of reovirus. *J Gen Virol* 1993; 74: 733–740.
- Zhou YS, Ray D, Zhao YW, et al. Structure and function of flavivirus NS5 methyltransferase. *J Virol* 2007; 81: 3891–3903.
- Wu JQ, Liu WC and Gong P. A structural overview of RNA-dependent RNA polymerases from the Flaviviridae family. *Int J Mol Sci* 2015; 16: 12943–12957.
- Zou G, Chen YL, Dong H, et al. Functional analysis of two cavities in flavivirus NS5 polymerase. *J Biol Chem* 2011; 286: 14362–14372.
- Deval J, Symons JA and Beigelman L. Inhibition of viral RNA polymerases by nucleoside and nucleotide analogs: therapeutic applications against positive-strand RNA viruses beyond hepatitis C virus. *Curr Opin Virol* 2014; 9: 1–7.
- Puig-Basagoiti F, Tilgner M, Forshey BM, et al. Triaryl pyrazoline compound inhibits flavivirus RNA replication. *Antimicrob Agents Chemother* 2006; 50: 1320–1329.
- De Clercq E. A 40-year journey in search of selective antiviral chemotherapy. *Annu Rev Pharmacol Toxicol* 2011; 51: 1–24.
- Jordheim LP, Durantel D, Zoulim F, et al. Advances in the development of nucleoside and nucleotide analogues for cancer and viral diseases. *Nat Rev Drug Discov* 2013; 12: 447–464.
- Benhamou Y, Tubiana R and Thibault V. Tenofovir disoproxil fumarate in patients with HIV and lamivudine-resistant hepatitis B virus. *N Engl J Med* 2003; 348: 177–178.
- Ray AS, Fordyce MW and Hitchcock MJM. Tenofovir alafenamide: a novel prodrug of tenofovir for the treatment of human immunodeficiency virus. *Antiviral Res* 2016; 125: 63–70.
- Huang YS, Chang SY, Sheng WH, et al. Virological response to tenofovir disoproxil fumarate in HIV-positive patients with lamivudine-resistant hepatitis B virus coinfection in an area hyperendemic for hepatitis B virus infection. *PLoS One* 2016; 11: e0169228.
- Lam YF, Seto WK, Wong D, et al. Seven-year treatment outcome of entecavir in a real-world cohort: effects on clinical parameters, HBsAg and HBcrAg levels. *Clin Trans Gastroenterol* 2017; 8: e125.
- Stedman C. Sofosbuvir, a NS5B polymerase inhibitor in the treatment of hepatitis C: a review of its clinical potential. *Ther Adv Gastroenterol* 2014; 7: 131–140.
- De Clercq E and Holý A. Acyclic nucleoside phosphonates: a key class of antiviral drugs. *Nat Rev Drug Discov* 2005; 4: 928–940.
- Chen YL, Yin Z, Duraiswamy J, et al. Inhibition of dengue virus RNA synthesis by an adenosine nucleoside. *Antimicrob Agents Chemother* 2010; 54: 2932–2939.
- Eyer L, Nencka R, Huvarova I, et al. Nucleoside inhibitors of zika virus. *J Infect Dis* 2016; 214: 707–711.
- Eyer L, Valdes JJ, Gil VA, et al. Nucleoside inhibitors of tick-borne encephalitis virus. *Antimicrob Agents Chemother* 2015; 59: 5483–5493.
- Sacramento CQ, de Melo GR, de Freitas CS, et al. The clinically approved antiviral drug sofosbuvir inhibits zika virus replication. *Sci Rep* 2017; 7: 40920.
- Yin Z, Chen YL, Schul W, et al. An adenosine nucleoside inhibitor of dengue virus. *Proc Natl Acad Sci USA* 2009; 106: 20435–20439.
- Vernekar SK, Qiu L and Zacharias J. Synthesis and antiviral evaluation of 4'-(1,2,3-triazol-1-yl)thymidines. *MedChemComm* 2014; 5: 603–608.
- Vernekar SK, Qiu L, Zhang J, et al. 5'-Silylated 3'-1,2,3-triazolyl thymidine analogues as inhibitors of West Nile Virus and Dengue Virus. *J Med Chem* 2015; 58: 4016–4028.
- Borowski P, Lang M, Haag A, et al. Characterization of imidazo[4,5-d]pyridazine nucleosides as modulators of unwinding reaction mediated by West Nile virus nucleoside triphosphatase/helicase: evidence for activity on the level of substrate and/or enzyme. *Antimicrob Agents Chemother* 2002; 46: 1231–1239.
- Borowski P, Deinert J, Schalinski S, et al. Halogenated benzimidazoles and benzotriazoles as inhibitors of the

- NTPase/helicase activities of hepatitis C and related viruses. *Eur J Biochem* 2003; 270: 1645–1653.
31. Crance JM, Scaramozzino N, Jouan A, et al. Interferon, ribavirin, 6-azauridine and glycyrrhizin: antiviral compounds active against pathogenic flaviviruses. *Antiviral Res* 2003; 58: 73–79.
 32. Leyssen P, Balzarini J, De Clercq E, et al. The predominant mechanism by which ribavirin exerts its antiviral activity in vitro against flaviviruses and paramyxoviruses is mediated by inhibition of inosine monophosphate dehydrogenase. *J Virol* 2005; 79: 1943–1947.
 33. Morrey JD, Smee DF, Sidwell RW, et al. Identification of active antiviral compounds against a New York isolate of West Nile virus. *Antiviral Res* 2002; 55: 107–116.
 34. Ojwang JO, Ali S, Smee DF, et al. Broad-spectrum inhibitor of viruses in the Flaviviridae family. *Antiviral Res* 2005; 68: 49–55.
 35. Orlov AA, Drenichev MS, Oslovsky VE, et al. New tools in nucleoside toolbox of tick-borne encephalitis virus reproduction inhibitors. *Bioorg Med Chem Lett* 2017; 27: 1267–1273.
 36. Lescar J and Canard B. RNA-dependent RNA polymerases from flaviviruses and Picornaviridae. *Curr Opin Struct Biol* 2009; 19: 759–767.
 37. Choi KH and Rossmann MG. RNA-dependent RNA polymerases from Flaviviridae. *Curr Opin Struct Biol* 2009; 19: 746–751.
 38. Behnam MAM, Nitsche C, Boldescu V, et al. The medicinal chemistry of Dengue virus. *J Med Chem* 2016; 59: 5622–5649.
 39. Boldescu V, Behnam MAM, Vasilakis N, et al. Broad-spectrum agents for flaviviral infections: Dengue, Zika and beyond. *Nat Rev Drug Discov* 2017; 16: 565–586.
 40. De Clercq E and Neyts J. Antiviral agents acting as DNA or RNA chain terminators. *Handb Exp Pharmacol* 2009; 189: 53–84.
 41. De Clercq E. Antivirals and antiviral strategies. *Nat Rev Microbiol* 2004; 2: 704–720.
 42. Cihlar T and Ray AS. Nucleoside and nucleotide HIV reverse transcriptase inhibitors: 25 years after zidovudine. *Antiviral Res* 2010; 85: 39–58.
 43. Cho A, Saunders OL, Butler T, et al. Synthesis and antiviral activity of a series of 1'-substituted 4-aza-7,9-dideazaadenosine C-nucleosides. *Bioorg Med Chem Lett* 2012; 22: 2705–2707.
 44. Warren TK, Jordan R, Lo MK, et al. Therapeutic efficacy of the small molecule GS-5734 against Ebola virus in rhesus monkeys. *Nature* 2016; 531: 381–385.
 45. Lo MK, Jordan R, Arvey A, et al. GS-5734 and its parent nucleoside analog inhibit filo-, pneumo-, and paramyxoviruses. *Sci Rep* 2017; 7: 43395.
 46. Eldrup AB, Allerson CR, Bennett CF, et al. Structure-activity relationship of purine ribonucleosides for inhibition of hepatitis C virus RNA-dependent RNA polymerase. *J Med Chem* 2004; 47: 2283–2295.
 47. Carroll SS, Tomassini JE, Bosserman M, et al. Inhibition of hepatitis C virus RNA replication by 2'-modified nucleoside analogs. *J Biol Chem* 2003; 278: 11979–11984.
 48. Carroll SS, Koeplinger K, Vavrek M, et al. Antiviral efficacy upon administration of a HepDirect prodrug of 2'-C-methylcytidine to hepatitis C virus-infected chimpanzees. *Antimicrob Agents Chemother* 2011; 55: 3854–3860.
 49. Migliaccio G, Tomassini JE, Carroll SS, et al. Characterization of resistance to non-obligate chain-terminating ribonucleoside analogs that inhibit hepatitis C virus replication in vitro. *J Biol Chem* 2003; 278: 49164–49170.
 50. Olsen DB, Eldrup AB, Bartholomew L, et al. A 7-deaza-adenosine analog is a potent and selective inhibitor of hepatitis C virus replication with excellent pharmacokinetic properties. *Antimicrob Agents Chemother* 2004; 48: 3944–3953.
 51. Lefebvre DJ, De Vleeschauwer AR, Goris N, et al. Proof of concept for the inhibition of foot-and-mouth disease virus replication by the anti-viral drug 2'-C-methylcytidine in severe combined immunodeficient mice. *Transbound Emerg Dis* 2014; 61: E89–E91.
 52. Rocha-Pereira J, Jochmans D, Dallmeier K, et al. Inhibition of norovirus replication by the nucleoside analogue 2'-C-methylcytidine. *Biochem Biophys Res Commun* 2012; 427: 796–800.
 53. Rocha-Pereira J, Jochmans D, Debing Y, et al. The viral polymerase inhibitor 2'-C-methylcytidine inhibits Norwalk virus replication and protects against norovirus-induced diarrhea and mortality in a mouse model. *J Virol* 2013; 87: 11798–11805.
 54. Eyer L, Smidkova M, Nencka R, et al. Structure-activity relationships of nucleoside analogues for inhibition of tick-borne encephalitis virus. *Antiviral Res* 2016; 133: 119–129.
 55. Flint M, McMullan LK, Dodd KA, et al. Inhibitors of the tick-borne, hemorrhagic fever-associated flaviviruses. *Antimicrob Agents Chemother* 2014; 58: 3206–3216.
 56. Lee JC, Tseng CK, Wu YH, et al. Characterization of the activity of 2'-C-methylcytidine against dengue virus replication. *Antiviral Res* 2015; 116: 1–9.
 57. Mateo R, Nagamine CM and Kirkegaard K. Suppression of drug resistance in Dengue virus. *MBio* 2015; 6: e01960–15.
 58. Yeo KL, Chen YL, Xu HY, et al. Synergistic suppression of dengue virus replication using a combination of nucleoside analogs and nucleoside synthesis inhibitors. *Antimicrob Agents Chemother* 2015; 59: 2086–2093.
 59. Lanko K, Eggermont K, Patel A, et al. Replication of the Zika virus in different iPSC-derived neuronal cells and implications to assess efficacy of antivirals. *Antiviral Res* 2017; 145: 82–86.
 60. Hercik K, Brynda J, Nencka R, et al. Structural basis of Zika virus methyltransferase inhibition by sinefungin. *Arch Virol* 2017; 162: 2091–2096.
 61. Eyer L, Kondo H, Zouharova D, et al. Escape of tick-borne flavivirus from 2'-C-methylated nucleoside antivirals is mediated by a single conservative mutation in NS5 that has a dramatic effect on viral fitness. *J Virol* 2017; e01028–17.

62. Zmurko J, Marques RE, Schols D, et al. The viral polymerase inhibitor 7-deaza-2'-C-methyladenosine is a potent inhibitor of in vitro Zika virus replication and delays disease progression in a robust mouse infection model. *PLoS Negl Trop Dis* 2016; 10: e0004695.
63. Julander JG, Jha AK, Choi JA, et al. Efficacy of 2'-C-methylcytidine against yellow fever virus in cell culture and in a hamster model. *Antiviral Res* 2010; 86: 261–267.
64. Sofia MJ, Chang W, Furman PA, et al. Nucleoside, nucleotide, and non-nucleoside inhibitors of hepatitis C virus NS5B RNA-dependent RNA-polymerase. *J Med Chem* 2012; 55: 2481–2531.
65. Keating GM and Vaidya A. Sofosbuvir: first global approval. *Drugs* 2014; 74: 273–282.
66. Arnold JJ, Sharma SD, Feng JY, et al. Sensitivity of mitochondrial transcription and resistance of RNA polymerase II dependent nuclear transcription to antiviral ribonucleosides. *PLoS Pathog* 2012; 8: e1003030.
67. Feng JY, Xu YL, Barauskas O, et al. Role of mitochondrial RNA polymerase in the toxicity of nucleotide inhibitors of hepatitis C virus. *Antimicrob Agents Chemother* 2016; 60: 806–817.
68. Xu HT, Hassounah SA, Colby-Germinario SP, et al. Purification of Zika virus RNA-dependent RNA polymerase and its use to identify small-molecule Zika inhibitors. *J Antimicrob Chemother* 2017; 72: 727–734.
69. Bullard-Feibelman KM, Govero J, Zhu Z, et al. The FDA-approved drug sofosbuvir inhibits Zika virus infection. *Antiviral Res* 2017; 137: 134–140.
70. Mumtaz N, Jimmerson LC, Bushman LR, et al. Cell-line dependent antiviral activity of sofosbuvir against Zika virus. *Antiviral Res* 2017; 146: 161–163.
71. Ferreira AC, Zaverucha-do-Valle C, Reis PA, et al. Sofosbuvir protects Zika virus-infected mice from mortality, preventing short- and long-term sequelae. *Sci Rep* 2017; 7: 9409.
72. Chen YL, Yin Z, Lakshminarayana SB, et al. Inhibition of Dengue Virus by an ester prodrug of an adenosine analog. *Antimicrob Agents Chemother* 2010; 54: 3255–3261.
73. Chen YL, Yokokawa F and Shi PY. The search for nucleoside/nucleotide analog inhibitors of dengue virus. *Antiviral Res* 2015; 122: 12–19.
74. Latour DR, Jekle A, Javanbakht H, et al. Biochemical characterization of the inhibition of the dengue virus RNA polymerase by beta-D-2'-ethynyl-7-deaza-adenosine triphosphate. *Antiviral Res* 2010; 87: 213–222.
75. Yin XQ and Schneller SW1. Deaza-5'-noraisteromycin. *Nucleosides Nucleotides Nucleic Acids* 2004; 23: 67–76.
76. Deng YQ, Zhang NN, Li CF, et al. Adenosine analog NITD008 is a potent inhibitor of Zika virus. *Open Forum Infect Dis* 2016; 3: ofw175.
77. Lo MK, Shi PY, Chen YL, et al. In vitro antiviral activity of adenosine analog NITD008 against tick borne flaviviruses. *Antiviral Res* 2016; 130: 46–49.
78. McGuigan C, Serpi M, Slusarczyk M, et al. Anti-flavivirus activity of different tritylated pyrimidine and purine nucleoside analogues. *Chem Open* 2016; 5: 227–235.
79. Klumpp K, Leveque V, Le Pogam S, et al. The novel nucleoside analog R1479 (4'-azidocytidine) is a potent inhibitor of NS5B-dependent RNA synthesis and hepatitis C virus replication in cell culture. *J Biol Chem* 2006; 281: 3793–3799.
80. Klumpp K, Kalayanov G, Ma H, et al. Deoxy-4'-azido nucleoside analogs are highly potent inhibitors of hepatitis C virus replication despite the lack of 2'-alpha-hydroxyl groups. *J Biol Chem* 2008; 283: 2167–2175.
81. Smith DB, Kalayanov G, Sund C, et al. The design, synthesis, and antiviral activity of 4'-azidocytidine analogues against hepatitis C virus replication: the discovery of 4'-azidoarabincytidine. *J Med Chem* 2009; 52: 219–223.
82. Hotard AL, He B, Nichol ST, et al. 4'-Azidocytidine (R1479) inhibits henipaviruses and other paramyxoviruses with high potency. *Antiviral Res* 2017; 144: 147–152.
83. Nguyen NM, Tran CNB, Phung LK, et al. A randomized, double-blind placebo controlled trial of balapiravir, a polymerase inhibitor, in adult dengue patients. *J Infect Dis* 2013; 207: 1442–1450.
84. Chen YL, Ghafar NA, Karuna R, et al. Activation of peripheral blood mononuclear cells by Dengue virus infection depotentiates balapiravir. *J Virol* 2014; 88: 1740–1747.
85. Rondla R, Coats SJ, McBrayer TR, et al. Anti-hepatitis C virus activity of novel beta-d-2'-C-methyl-4'-azido pyrimidine nucleoside phosphoramidate prodrugs. *Antivir Chem Chemother* 2009; 20: 99–106.
86. Nilsson M, Kalayanov G, Winqvist A, et al. Discovery of 4'-azido-2'-deoxy-2'-C-methyl cytidine and prodrugs thereof: a potent inhibitor of hepatitis C virus replication. *Bioorg Med Chem Lett* 2012; 22: 3265–3268.
87. Taylor R, Kotian P, Warren T, et al. BCX4430-A broad-spectrum antiviral adenosine nucleoside analog under development for the treatment of Ebola virus disease. *J Infect Public Health* 2016; 9: 220–226.
88. De Clercq E. C-nucleosides to be revisited. *J Med Chem* 2016; 59: 2301–2311.
89. Warren TK, Wells J, Panchal RG, et al. Protection against filovirus diseases by a novel broad-spectrum nucleoside analogue BCX4430. *Nature* 2014; 508: 402–405.
90. Eyer L, Zouharova D, Sirmarova J, et al. Antiviral activity of the adenosine analogue BCX4430 against West Nile virus and tick-borne flaviviruses. *Antiviral Res* 2017; 142: 63–67.
91. Julander JG, Siddharthan V, Evans J, et al. Efficacy of the broad-spectrum antiviral compound BCX4430 against Zika virus in cell culture and in a mouse model. *Antiviral Res* 2017; 137: 14–22.
92. Julander JG, Bantia S, Taubenheim BR, et al. BCX4430, a novel nucleoside analog, effectively treats yellow fever in a hamster model. *Antimicrob Agents Chemother* 2014; 58: 6607–6614.
93. Julander JG, Furuta Y, Shafer K, et al. Activity of T-1106 in a hamster model of yellow fever virus infection. *Antimicrob Agents Chemother* 2007; 51: 1962–1966.
94. Julander JG, Shafer K, Smee DF, et al. Activity of T-705 in a hamster model of yellow fever virus infection in

- comparison with that of a chemically related compound, T-1106. *Antimicrob Agents Chemother* 2009; 53: 202–209.
95. Julander J, Shafer K, Smee D, et al. Efficacy of T-1106 or T-705, alone or in combination with ribavirin, in the treatment of hamsters infected with yellow fever virus. *Antiviral Res* 2008; 78: A34.
96. Wu R, Smidansky ED, Oh HS, et al. Synthesis of a 6-methyl-7-deaza analogue of adenosine that potently inhibits replication of polio and Dengue viruses. *J Med Chem* 2010; 53: 7958–7966.
97. Angusti A, Manfredini S, Durini E, et al. Design, synthesis and anti Flaviviridae activity of N-6-, 5',3'-O- and 5',2'-O-substituted adenosine nucleoside analogs. *Chem Pharm Bull* 2008; 56: 423–432.
98. Morrey JD, Taro BS, Siddharthan V, et al. Efficacy of orally administered T-705 pyrazine analog on lethal West Nile virus infection in rodents. *Antiviral Res* 2008; 80: 377–379.
99. Drenichev MS, Oslovsky VE, Sun L, et al. Modification of the length and structure of the linker of N-6-benzyladenosine modulates its selective antiviral activity against enterovirus 71. *Eur J Med Chem* 2016; 111: 84–94.
100. Tararov VI, Tijsma A, Kolyachkina SV, et al. Chemical modification of the plant isoprenoid cytokinin N-6-isopentenyladenosine yields a selective inhibitor of human enterovirus 71 replication. *Eur J Med Chem* 2015; 90: 406–413.
101. Orlov AA, Chistov AA, Kozlovskaya LI, et al. Rigid amphipathic nucleosides suppress reproduction of the tick-borne encephalitis virus. *Med Chem Commun* 2016; 7: 495–499.
102. Chatelain G, Debing Y, De Burghgraeve T, et al. In search of flavivirus inhibitors: evaluation of different tritylated nucleoside analogues. *Eur J Med Chem* 2013; 65: 249–255.
103. De Burghgraeve T, Selisko B, Kaptein S, et al. 3',5' Di-O-trityluridine inhibits in vitro flavivirus replication. *Antiviral Res* 2013; 98: 242–247.
104. Saudi M, Zmurko J, Kaptein S, et al. In search of flavivirus inhibitors part 2: tritylated, diphenylmethylated and other alkylated nucleoside analogues. *Eur J Med Chem* 2014; 76: 98–109.
105. Koonin EV and Dolja VV. Evolution taxonomy of positive-strand RNA viruses – implications of comparative-analysis of amino-acid-sequences. *Crit Rev Biochem Mol Biol* 1993; 28: 375–430.
106. Cleaves GR and Dubin DT. Methylation status of intracellular dengue type-2 40-S RNA. *Virology* 1979; 96: 159–165.
107. Dong H, Fink K, Zuest R, et al. Flavivirus RNA methylation. *J Gen Virol* 2014; 95: 763–778.
108. Chung KY, Dong HP, Chao AT, et al. Higher catalytic efficiency of N-7-methylation is responsible for processive N-7 and 2'-O methyltransferase activity in dengue virus. *Virology* 2010; 402: 52–60.
109. Lim SP, Wen DY, Yap TL, et al. A scintillation proximity assay for dengue virus NS5 2'-O-methyltransferase-kinetic and inhibition analyses. *Antiviral Res* 2008; 80: 360–369.
110. Lim SP, Sonntag LS, Noble C, et al. Small molecule inhibitors that selectively block dengue virus methyltransferase. *J Biol Chem* 2011; 286: 6233–6240.
111. Chen H, Liu L, Jones SA, et al. Selective inhibition of the West Nile virus methyltransferase by nucleoside analogs. *Antiviral Res* 2013; 97: 232–239.
112. Yates MK, Raje MR, Chatterjee P, et al. Flex-nucleoside analogues – novel therapeutics against flaviviruses. *Bioorg Med Chem Lett* 2017; 27: 2800–2802.
113. Peters HL, Jochmans D, de Wilde AH, et al. Design, synthesis and evaluation of a series of acyclic fleximer nucleoside analogues with anti-coronavirus activity. *Bioorg Med Chem Lett* 2015; 25: 2923–2926.
114. Seley KL, Zhang L, Hagos A, et al. “Fleximers”. Design and synthesis of a new class of novel shape-modified nucleosides. *J Org Chem* 2002; 67: 3365–3373.
115. Seley KL, Quirk S, Salim S, et al. Unexpected inhibition of S-adenosyl-L-homocysteine hydrolase by a guanosine nucleoside. *Bioorg Med Chem Lett* 2003; 13: 1985–1988.
116. Quirk S and Seley KL. Substrate discrimination by the human GTP fucose pyrophosphorylase. *Biochemistry* 2005; 44: 10854–10863.
117. Gallinari P, Brennan D, Nardi C, et al. Multiple enzymatic activities associated with recombinant NS3 protein of hepatitis C virus. *J Virol* 1998; 72: 6758–6769.
118. Hodgman TC. A new superfamily of replicative proteins. *Nature* 1988; 333: 22–23.
119. Kim JL, Morgenstern KA, Griffith JP, et al. Hepatitis C virus NS3 RNA helicase domain with a bound oligonucleotide: the crystal structure provides insights into the mode of unwinding. *Structure* 1998; 6: 89–100.
120. Yao NH, Hesson T, Cable M, et al. Structure of the hepatitis C virus RNA helicase domain. *Nat Struct Biol* 1997; 4: 463–467.
121. Tai CL, Chi WK, Chen DS, et al. The helicase activity associated with hepatitis C virus nonstructural protein 3 (NS3). *J Virol* 1996; 70: 8477–8484.
122. Bretner M, Baier A, Kopańska K, et al. Synthesis and biological activity of 1H-benzotriazole and 1H-benzimidazole analogues – inhibitors of the NTPase/helicase of HCV and of some related Flaviviridae. *Antivir Chem Chemother* 2005; 16: 315–326.
123. Borowski P, Kuehl R, Mueller O, et al. Biochemical properties of a minimal functional domain with ATP-binding activity of the NTPase/helicase of hepatitis C virus. *Eur J Biochem* 1999; 266: 715–723.
124. Borowski P, Lang M, Niebuhr A, et al. Inhibition of the helicase activity of HCV NTPase/helicase by 1-beta-D-ribofuranosyl-1,2,4-triazole-3-carboxamide-5'-triphosphate (ribavirin-TP). *Acta Biochim Pol* 2001; 48: 739–744.
125. Borowski P, Mueller O, Niebuhr A, et al. ATP-binding domain of NTPase/helicase as a target for hepatitis C antiviral therapy. *Acta Biochim Pol* 2000; 47: 173–180.
126. Bretner M, Schalinski S, Borowski P, et al. 5'-O-fluoro-sulfonylbenzoyl esters of purine nucleosides as potential

- inhibitors of NTPase/helicase and polymerase of Flaviviridae viruses. *Nucleosides Nucleotides Nucleic Acids* 2003; 22: 1531–1533.
127. Bretner M, Schalinski S, Haag A, et al. Synthesis and evaluation of ATP-binding site directed potential inhibitors of nucleoside triphosphatases/helicases and polymerases of hepatitis C and other selected Flaviviridae viruses. *Antivir Chem Chemother* 2004; 15: 35–42.
 128. Eriksson B, Helgstrand E, Johansson NG, et al. Inhibition of influenza-virus ribonucleic-acid polymerase by ribavirin triphosphate. *Antimicrob Agents Chemother* 1977; 11: 946–951.
 129. Crotty S, Cameron CE and Andino R. RNA virus error catastrophe: direct molecular test by using ribavirin. *Proc Natl Acad Sci USA* 2001; 98: 6895–6900.
 130. Graci JD and Cameron CE. Quasispecies, error catastrophe, and the antiviral activity of ribavirin. *Virology* 2002; 298: 175–180.
 131. Li CQ, Guillen J, Rabah N, et al. mRNA capping by Venezuelan Equine Encephalitis virus nsP1: functional characterization and implications for antiviral research. *J Virol* 2015; 89: 8292–8303.
 132. Graci JD and Cameron CE. Mechanisms of action of ribavirin against distinct viruses. *Rev Med Virol* 2006; 16: 37–48.
 133. Hultgren C, Milich DR, Weiland O, et al. The antiviral compound ribavirin modulates the T helper (Th)1/Th2 subset balance in hepatitis B and C virus-specific immune responses. *J Gen Virol* 1998; 79: 2381–2391.
 134. Jordan I, Briese T, Fischer N, et al. Ribavirin inhibits West Nile virus replication and cytopathic effect in neural cells. *J Infect Dis* 2000; 182: 1214–1217.
 135. McDowell M, Gonzales SR, Kumarapperuma SC, et al. A novel nucleoside analog, 1-beta-D-ribofuranosyl-3-ethynyl-[1,2,4]triazole (ETAR), exhibits efficacy against a broad range of flaviviruses in vitro. *Antiviral Res* 2010; 87: 78–80.
 136. Malinoski FJ, Hasty SE, Ussery MA, et al. Prophylactic ribavirin treatment of dengue type-1 infection in rhesus-monkeys. *Antiviral Res* 1990; 13: 139–150.
 137. Gabrielsen B, Phelan MJ, Barthelrosa L, et al. Synthesis and antiviral evaluation of N-carboxamidine-substituted analogs of 1-beta-D-ribofuranosyl-1,2,4-triazole-3-carboxamidine hydrochloride. *J Med Chem* 1992; 35: 3231–3238.
 138. Crutcher WA and Moschella SL. Double-blind controlled crossover high-dose study of azaribine in psoriasis. *Br J Dermatol* 1975; 92: 199–205.
 139. Dukhan D, Leroy F, Peyronnet J, et al. Synthesis of 5-aza-7-deazaguanine nucleoside derivatives as potential anti-flavivirus agents. *Nucleosides Nucleotides Nucleic Acids* 2005; 24: 671–674.
 140. Korshun VA, Prokhorenko IA, Gontarev SV, et al. New pyrene derivatives for fluorescent labeling of oligonucleotides. *Nucleosides Nucleotides* 1997; 16: 1461–1464.
 141. Korshun VA, Manasova EV, Balakin KV, et al. New fluorescent nucleoside derivatives – 5-alkynylated 2'-deoxyuridines. *Nucleosides Nucleotides* 1998; 17: 1809–1812.
 142. Skorobogatyi MV, Malakhov AD, Pchelintseva AA, et al. Fluorescent 5-alkynyl-2'-deoxyuridines: high emission efficiency of a conjugated perylene nucleoside in a DNA duplex. *Chembiochem* 2006; 7: 810–816.
 143. St Vincent MR, Colpitts CC, Ustinov AV, et al. Rigid amphipathic fusion inhibitors, small molecule antiviral compounds against enveloped viruses. *Proc Natl Acad Sci USA* 2010; 107: 17339–17344.
 144. Colpitts CC, Ustinov AV, Epand RF, et al. 5-(Perylene-3-yl) ethynyl-arabino-uridine (aUY11), an arabino-based rigid amphipathic fusion inhibitor, targets virion envelope lipids to inhibit fusion of influenza virus, hepatitis C virus, and other enveloped viruses. *J Virol* 2013; 87: 3640–3654.
 145. Vigant F, Hollmann A, Lee J, et al. The rigid amphipathic fusion inhibitor dUY11 acts through photosensitization of viruses. *J Virol* 2014; 88: 1849–1853.
 146. Li FJ, Maag H and Alfredson T. Prodrugs of nucleoside analogues for improved oral absorption and tissue targeting. *J Pharm Sci* 2008; 97: 1109–1134.
 147. Hecker SJ and Erion MD. Prodrugs of phosphates and phosphonates. *J Med Chem* 2008; 51: 2328–2345.
 148. Lane AN and Fan TWM. Regulation of mammalian nucleotide metabolism and biosynthesis. *Nucleic Acids Res* 2015; 43: 2466–2485.
 149. Johnson AA, Ray AS, Hanes J, et al. Toxicity of antiviral nucleoside analogs and the human mitochondrial DNA polymerase. *J Biol Chem* 2001; 276: 40847–40857.
 150. Lee H, Hanes J and Johnson KA. Toxicity of nucleoside analogues used to treat AIDS and the selectivity of the mitochondrial DNA polymerase. *Biochemistry* 2003; 42: 14711–14719.
 151. Locarnini S and Warner N. Major causes of antiviral drug resistance and implications for treatment of hepatitis B virus mono-infection and coinfection with HIV. *Antiviral Ther* 2007; 12: H15–H23.
 152. Menendez-Arias L, Alvarez M and Pacheco B. Nucleoside/nucleotide analog inhibitors of hepatitis B virus polymerase: mechanism, of action and resistance. *Curr Opin Virol* 2014; 8: 1–9.
 153. Poveda E, Wyles DL, Mena A, et al. Update on hepatitis C virus resistance to direct-acting antiviral agents. *Antiviral Res* 2014; 108: 181–191.
 154. McGuigan C, Cahard D, Sheeka HM, et al. Aryl phosphoramidate derivatives of d4T have improved anti-HIV efficacy in tissue culture and may act by the generation of a novel intracellular metabolite. *J Med Chem* 1996; 39: 1748–1753.
 155. Lam AM, Espiritu C, Bansal S, et al. Genotype and subtype profiling of PSI-7977 as a nucleotide inhibitor of hepatitis C virus. *Antimicrob Agents Chemother* 2012; 56: 3359–3368.
 156. Ross BS, Reddy PG, Zhang HR, et al. Synthesis of diastereomerically pure nucleotide phosphoramidates. *J Org Chem* 2011; 76: 8311–8319.
 157. Peterson LW and McKenna CE. Prodrug approaches to improving the oral absorption of antiviral nucleotide analogues. *Expert Opin Drug Deliv* 2009; 6: 405–420.

158. Becher F, Landman R, Mboup S, et al. Monitoring of didanosine and stavudine intracellular triphosphorylated anabolite concentrations in HIV-infected patients. *AIDS* 2004; 18: 181–187.
159. Gao WY, Shirasaka T, Johns DG, et al. Differential phosphorylation of azidothymidine, dideoxycytidine, and dideoxyinosine in resting and activated peripheral-blood mononuclear-cells. *J Clin Invest* 1993; 91: 2326–2333.
160. Kohler JJ and Lewis W. A brief overview of mechanisms of mitochondrial toxicity from NRTIs. *Environ Mol Mutagen* 2007; 48: 166–172.
161. Maurer HH. Screening procedures for simultaneous detection of several drug classes used for high throughput toxicological analyses and doping control. A review. *Comb Chem High Throughput Screen* 2000; 3: 467–480.
162. Mckim JM. Building a tiered approach to in vitro predictive toxicity screening: a focus on assays with in vivo relevance. *Comb Chem High Throughput Screen* 2010; 13: 188–206.
163. Szymanski P, Markowicz M and Mikiciuk-Olasik E. Adaptation of high-throughput screening in drug discovery-toxicological screening tests. *Int J Mol Sci* 2012; 13: 427–452.
164. Adachi A and Miura T. Animal model studies on viral infections. *Front Microbiol* 2014; 5: 672.
165. Dowall SD, Graham VA, Rayner E, et al. A susceptible mouse model for Zika virus infection. *PLoS Negl Trop Dis* 2016; 10: e0004658.
166. Zompi S and Harris E. Animal models of Dengue virus infection. *Viruses* 2012; 4: 62–82.
167. Lee YR, Huang KJ, Lei HY, et al. Suckling mice were used to detect infectious dengue-2 viruses by intracerebral injection of the full-length RNA transcript. *Intervirology* 2005; 48: 161–166.
168. Sarathy VV, White M, Li L, et al. A lethal murine infection model for Dengue Virus 3 in AG129 mice deficient in type I and II interferon receptors leads to systemic disease. *J Virol* 2015; 89: 1254–1266.
169. Zellweger RM and Shresta S. Mouse models to study dengue virus immunology and pathogenesis. *Front Immunol* 2014; 5: 151.
170. Chan JFW, Zhang AJ, Chan CCS, et al. Zika virus infection in dexamethasone-immunosuppressed mice demonstrating disseminated infection with multi-organ involvement including orchitis effectively treated by recombinant type I interferons. *EBioMedicine* 2016; 14: 112–122.
171. McArthur MA, Suderman MT, Mutebi JP, et al. Molecular characterization of a hamster viscerotropic strain of yellow fever virus. *J Virol* 2003; 77: 1462–1468.
172. Govero J, Esakky P, Scheaffer SM, et al. Zika virus infection damages the testes in mice. *Nature* 2016; 540: 438–442.
173. Gubler D, Kuno G and Markoff L. Flaviviruses In: Knipe DM and Howley PM (eds) *Fields virology*. 5th ed. Philadelphia, PA: Lippincott Williams & Wilkins, 2007, pp.1153–1253.
174. Carey I and Harrison PM. Monotherapy versus combination therapy for the treatment of chronic hepatitis B. *Expert Opin Investig Drug* 2009; 18: 1655–1666.
175. Wong GLH, Wong VWS and Chan HLY. Combination therapy of interferon and nucleotide/nucleoside analogues for chronic hepatitis B. *J Viral Hepat* 2014; 21: 825–834.
176. Su TH and Liu CJ. Combination therapy for chronic hepatitis B: current updates and perspectives. *Gut Liver* 2017; 11: 590–603.

Small molecule-based inhibitors for treatment of tick-borne encephalitis virus infection: nucleoside analogues and non-nucleoside antivirals

Joy E. Thames¹, Ludek Eyer^{2,3}, and Katherine Seley-Radtke¹

¹Department of Chemistry and Biochemistry, University of Maryland, Baltimore County, Baltimore, MD 21250, USA

²Laboratory of Emerging Viral Diseases, Veterinary Research Institute, CZ-621 00 Brno, Czech Republic

³Institute of Parasitology, Biology Centre of the Czech Academy of Sciences, CZ-370 05 Ceske Budejovice, Czech Republic

Abstract

Tick-borne encephalitis (TBE) is one of the most serious neurological infections in Europe and Northeastern Asia. The causative agent of TBE is the tick-borne encephalitis virus (TBEV). Although several effective vaccines are legislated to prevent TBE, there are currently no approved treatments/anti-TBEV drugs other than supportive measures. Therefore, there is an urgent medical need for the development of novel, specific, and effective antivirals to treat patients with TBEV infection. This report summarizes the available information on antiviral research on small molecule-based inhibitors of TBEV replication. The main focus is on the description of nucleoside analogues, a leading group of antiviral compounds with the highest anti-TBEV potency. Various sugar/nucleobase modifications of the nucleoside scaffold that have been made to maximize the antiviral activity and decrease the cytotoxicity of the compounds are discussed. Emphasis is also placed on elucidating the mechanism of action of the inhibitors studied and their relationship to the development of antiviral resistance. Moreover, a brief overview of non-nucleoside inhibitors, natural compounds, repurposed drugs, and synthetic broad-spectrum antivirals is also part of this chapter. The review shows that specific therapies based on small-molecule inhibitors, in combination with effective vaccination strategies, could be effective prophylactic and curative tools to control TBEV infections in humans.

Keywords

Tick-borne encephalitis, tick-borne encephalitis virus, small molecule-based inhibitor, nucleoside analogue, non-nucleoside inhibitor.

Introduction

Tick-borne encephalitis (TBE) is a neurotropic infection that affects the human nervous system and is endemic in Europe and Northeastern Asia. A causative agent of TBE is the tick-borne encephalitis virus (TBEV), which is a member of the *Flaviviridae* family and the *Flavivirus* genus. Together with other related human and animal pathogenic arboviruses of major medical importance, such as West Nile virus (WNV), Japanese encephalitis virus (JEV), yellow fever virus (YFV), and dengue virus (DENV), TBEV is also of serious concern.^{1,2}

TBEV virions are approximately 50 nm in diameter and are composed of a spherical nucleocapsid surrounded by a host-derived lipid bilayer.³ The TBEV genome is a single-stranded, positive-sense RNA (+ssRNA) about 11 kb in length that comprises of a 5'-cap and a single large open reading frame (ORF) flanked at its 5' and 3' ends by untranslated regions (5'- and 3'-UTRs). The 3'-UTR is not polyadenylated. The ORF encodes a single polyprotein, which is co- and post-translationally processed into three structural (C, prM, and E) and seven non-structural (NS1, NS2A, NS2B, NS3, NS4A, NS4B, and NS5) proteins.⁴ TBEV infection is typically initiated by the virus attachment to the cellular receptors, followed by receptor-mediated endocytosis and low-pH-directed fusion of the viral envelope with the endosome membrane mediated by the fusogenic E proteins. After releasing of the viral genome RNA into cytosol, the viral RNA replicates through the synthesis of negative-sense (anti-sense) RNA, used as a template for production of genomic +ssRNA. Replication of viral genomic RNA, virion assembly, and virus maturation occur in a direct contact with endoplasmic reticulum and Golgi complex. The maturation process is associated with a proteolytic cleavage and restructuralization of prM and E proteins to form a fusion-competent complex. Finally, mature viral particles are transported from the Golgi complex in cytoplasmic vesicles to be released from the host cell to the outside environment by exocytosis pathways.¹

TBE is prevalent in forested areas and is typically caused by infection involving one of three tick-borne encephalitis virus subtypes, namely the European (TBEV-Eu), the Siberian (TBEV-Sib), or the Far Eastern (TBEV-FE) subtypes. TBEV infections are transmitted by two different routes: (i) from the bite of a TBEV-infected tick (*Ixodes ricinus* in Europe and *Ixodes persulcatus* in Russia), or (ii) by consumption of unpasteurized dairy milk and milk products from virus-infected goats, cows, and sheep (foodborne TBEV).^{1,5,6} The virus is considered endemic in almost 30 European and 4 Asian countries, with over 10,000 people a year becoming infected with TBEV, including numerous deaths.^{1,7} This number varies as incidences per year are different in the various geographic regions of Europe and Asia.⁶ In Europe, TBEV-Eu infection usually results in a mortality rate of < 2%. The overall TBE mortality rate in Russia is about 2%, in spite of the fact that TBEV-Sib and TBEV-FE subtypes appear to be inducers of more severe TBE than TBEV-Eu.¹

The incubation period of TBE ranges from seven to fourteen days; in rare cases the onset of symptoms was observed within three to four days.^{1,7} TBE in humans is characterized as a biphasic disease with primary influenza-like symptoms (fever, fatigue, nausea, headache, and whole-body pain). In the second phase, the disease may develop into meningitis or meningoencephalitis.⁸ The most serious form of the disease is encephalomyelitis, which is associated with severe central nervous system damage. In the most serious cases, such damage may result in permanent

neurological problems, paralysis, or death of the patient.^{9, 10} Post-encephalitic syndrome develops in 40–50% patients with TBE, which is manifested by persistent sequelae with significant consequences for daily activities and quality of life.^{11, 12, 13}

Despite the medical importance of TBEV and other flavivirus infections, there is no specific treatment other than supportive measures.¹⁴ Therefore, effective treatment strategies are urgently needed to treat patients with TBEV infections and search for new effective antivirals belongs to the main research priorities in the field of research in European countries and in Russia.

Tick-Borne Encephalitis Prophylaxis and Experimental Treatments

Vaccination is currently the most widespread prophylaxis strategy to prevent TBEV infections in humans. In addition to vaccinations, various types of experimental treatments have been described in scientific literature, including immunotherapies, interferon administrations, and therapies based on chemical TBEV inhibitors.^{1, 14} Vaccination and immunotherapeutic anti-TBE approaches will be briefly discussed in this report. The main attention will be paid to small molecule-based antiviral drugs currently being investigated against TBEV.

I. Vaccines

Currently there are five vaccines on the market to protect against TBEV infections. Two are used in Europe and three are available in Russia.^{1, 15, 16} The two vaccines used in Europe, FSME-IMMUN and Encepur, can be used interchangeably, even though they are based on two different strains of the virus. The European vaccines require boosters after the initial dose, and the first and second doses should be administered one to three months apart, while the third dose should be given anytime from six to twelve months after the second dose. Both manufacturers of the vaccines recommend that more boosters be administered, with a fourth dose given 3 years after the initial set and then every 5 years for healthy, young individuals and every 3 years for the elderly.^{17, 18, 19, 20} Missing a booster may lead to inadequate protection against the virus.²¹

The three vaccines that are produced in Russia, TBE vaccine Moscow, Tick-E-Vac, and Encevir, are all based on cultured and inactivated TBEV.^{1, 16} The vaccine schedule for the Russian vaccines is similar to that of the European vaccines: the first and second doses should be administered within a one to seven-month time period, while the first revaccination (third dose) should be administered one year after the second dose. Thereafter, revaccination should occur every three years.²²

II. Immunotherapies

Immunotherapies involve administration of specific, non-specific, or recombinant antibodies (immunoglobulins) to patients with TBE. Specific immunoglobulins are produced from plasma of donors for post-exposure prophylaxis and treatment.²³ Application of specific immunoglobulins (in combination with recombinant interferon or alone) has been proven to prevent and to decrease the severity of the side effects but has not prevented disease.¹ These are typically given as a single administration.²³ Some of the specific immunoglobulins used in treatments and experimental studies however have also resulted in antibody-enhanced disease.¹ The immunotherapy based on

intravenous injection of non-specific immunoglobulins provides a broad repertoire of neutralizing antibodies against various pathogens and also has immunomodulatory activity. The recombinant antibodies allow for blood-free production of highly specific immunoglobulins or immunoglobulin fragments for therapeutic and/or prophylactic applications.^{1, 24}

III. Small Molecule-based TBEV Inhibitors

Numerous chemical inhibitors have been designed, synthesized, and evaluated for their anti-TBEV activity and cytotoxicity. The focus of this report will be to discuss the different types of antiviral compounds, with the main emphasis on nucleoside analogues, whose anti-TBEV effects have been currently explored, including the elucidation of their molecular mechanism of antiviral action.

For virtual pre-screening of potential anti-TBEV scaffolds, Osolodkin et al. developed a structure-based homology model of the envelope (E) protein β -n-octyl-D-glucoside binding site.²⁵ This model was further improved and supported by molecular dynamics simulation data,²⁶ enabling a more precise pre-screening procedure and/or rational design of anti-TBEV compounds. Another virtual homology model based on flaviviral NS3 protein complexed with NS2B cofactor was developed and used for the screening of TBEV protease inhibitors.²⁷

Cell-based screening of small-molecule inhibitors as candidate treatments of TBE require specialized *in vitro* assay systems, which could be adopted for either low- or high-throughput screening formats. Such specialized antiviral assays enable to evaluate the inhibitory efficacies of the studied compounds, as well as their cytotoxicity effects for various types of primary cells or immortalized cell lines. TBEV is a typical neurotropic virus, but during infection it also replicates in multiple cell types other than neurons. Therefore, cells of neuronal, as well as non-neural origin, are widely used in anti-TBEV cell-based assays. From non-neural cell lines, porcine embryonal kidney cells (PEK),^{25, 28} porcine kidney stable cells (PS),^{29, 30} A549 human lung adenocarcinoma cells,³¹ or Vero cells (African Green Monkey, adult kidney, epithelial)³² are used for TBEV multiplication, passaging, and performing of antiviral screenings and plaque assays. On the other hand, human neuroblastoma cells or primary human brain cortical astrocytes (HBCA) are target cells for TBEV replication, which represent a clinically relevant model to study anti-TBEV activities of small molecule-based inhibitors in cells of neural origin.^{29, 30}

Virus quantification in TBEV-infected and compound-treated cell culture is typically performed using plaque reduction assays or virus titer reduction assays followed by plaque assays,^{30, 33} fluorescent immunostaining³⁴ or using quantitative reverse transcription-PCR (RT-qPCR) for quantitative determination of numbers of TBEV RNA copies in cells.³⁵ General procedures are depicted in Figure 1. Thorough studies of the compound mechanism of action are based on time-of-addition assays to determine the exact stage of viral cycle in which the inhibitory effect of the compound is applied. As these methods are based on the manipulation with an infectious (native) virus, there is a strict requirement for biosafety level 3 (BSL3, in the majority of European Union countries) or BSL4 (in the US) laboratory facilities.¹

Molecular mechanisms of action of small molecule-based antivirals can be studied in detail using a variety of enzyme-based biochemical techniques, such as viral polymerase- or methyltransferase-based assays,³⁶ or biophysical approaches to study virus-small molecule interactions. For the

advanced studies of cellular up-take of the antiviral compounds and their metabolism profiling, or phosphorylation efficacies in host cells, analytical-chemical methods are preferably used, such as high performance liquid chromatography or mass-spectrometry.³⁰ Recently, the TBEV-based reporter system was developed, expressing the mCherry reporter protein for the easy and rapid high-throughput antiviral screenings and performing of virus-neutralization tests.³⁷ The identified hit compounds showing highest anti-TBEV potencies in cell-based assays can be further tested for their antiviral activities in rodent models of TBEV infection, using mice as an appropriate animal model highly sensitive for TBEV infection.^{38, 39, 40}

Nucleoside analogues

Modified nucleosides represent attractive candidates for development of potent antimicrobial and/or anticancer drugs by mimicking the structure of natural nucleosides/nucleotides, which are involved in many crucial biological processes such as DNA/RNA synthesis, methylation, and reparation.¹⁴ The basic structure of the nucleotide molecule involves the following structural units: (i) a sugar scaffold (β -D-ribose or 2'-deoxy- β -D-ribose), (ii) a heterocyclic purine or pyrimidine nucleobase linked via a glycosidic bond to the sugar scaffold, and (iii) a phosphate or phosphate-like group attached to the 5' carbon of the sugar (Figure 2). Numerous modifications can be introduced to various positions of the basic nucleoside molecule with the aim to enhance their antiviral activity and minimalize their cytotoxic site effects.⁴¹

As antivirals, nucleoside analogues operate via numerous modes of action. The inhibition of viral nucleic acid replication is considered as a crucial antiviral mechanism due to the highly specific interactions of nucleoside analogues with viral polymerases resulting in premature DNA/RNA chain termination. As such, two classes of chain terminators are generally distinguished: (i) obligate chain terminators, which lack the 3'-hydroxyl resulting in the inability to form a phosphodiesteric bond with the incoming nucleoside-triphosphate (NTP), and (ii) non-obligate chain terminators, in which the 3'-hydroxyl is still present but is sterically or electronically constrained to interact with a 5'-phosphate group of the incoming NTP.⁴² Other important modes of action for antiviral nucleosides include suppression of the viral methyltransferases, which are responsible for viral RNA methylation and capping,^{43, 44} and inhibition of enzymes that ensure nucleotide/nucleoside metabolism, resulting in depletion of the cellular nucleotide pool.^{45, 46} Alternatively, some antiviral nucleosides, referred to as lethal mutagens, are responsible for the accumulation of multiple point mutations in viral genomes, leading to error catastrophe.^{47, 48}

Currently, there are more than 30 approved drugs based on modified nucleosides on the market used to treat viral diseases of high medical importance, such as HIV, hepatitis B and C (HBV and HCV), and herpes simplex (HSV) infections.^{41, 49} Nucleosides have proven to have potent antiviral activity against numerous viruses in the *Flaviviridae* family⁴² and some of them have been demonstrated to efficiently inhibit TBEV replication.⁵⁰ Various types of nucleoside modifications are discussed below indicating that nucleoside analogues and nucleoside-based prodrugs are prospective targets for TBEV infection treatments.^{1, 29}

1'-Sugar Modifications

One of the less commonly studied modifications on nucleoside analogues against TBEV are those at the 1' position of the sugar moiety. Previously, the compound GS-441524 (Figure 3), which features a 1'-cyano group and is also a C-nucleoside, had shown broad-spectrum antiviral activity against viruses such as HCV, DENV, severe acute respiratory syndrome coronavirus (SARS-CoV), and parainfluenza virus type 3.^{31, 51} The monophosphate prodrug of this compound, GS-5734, better known as remdesivir (Figure 3), has also shown antiviral activity against coronaviruses and filoviruses^{31, 52} and plays an important role in the current epidemiological situation to combat a life-threatening infection caused by SARS-CoV-2.⁵³ Lo et. al. attempted to understand the full spectrum of antiviral activities of the two 1'-cyano nucleosides, testing them against a wide array of viruses including TBEV. Activity against the Hypr strain of TBEV was tested using cytopathic effect (CPE) inhibition assays in A549 cells. For the parent compound GS-441524, there was only weak antiviral activity against TBEV resulting in an EC₅₀ of only 51.2 μM and an EC₉₀ of >150 μM. Remdesivir was more promising, exhibiting an EC₅₀ value of 2.1 μM and an EC₉₀ of 3.5 μM. Unfortunately, remdesivir also has high toxicity as given by the low selectivity index value (4.8).³¹ Furthermore, the ability of remdesivir to inhibit RdRp of various flaviviruses was demonstrated in enzyme-based assay using recombinant flavivirus-specific RdRp expressed in *E. coli* and the active form of remdesivir (chemically synthesized remdesivir triphosphate) had an IC₅₀ value of 1.1 μM for TBEV RdRp.³⁶

2'-Sugar Modifications

Originally, 2'-C-methyl nucleoside analogues were developed to treat chronic HCV infections,^{1, 14, 54, 55} which later showed broad-spectrum activity also against viruses of the *Picornaviridae* and *Caliciviridae* families.^{14, 56, 57, 58} Additionally, 2'-C-methyl nucleosides were the first nucleoside analogues described to inhibit replication of TBEV *in vitro*.²⁹ The early studies were primarily focused on 2'-C-methyladenosine (2'-CMA), 2'-C-methylguanosine (2'-CMG), 7-deaza-2'-C-methyladenosine (7-deaza-2'-CMA), 2'-C-methylcytidine (2'-CMC), and 2'-C-methyluridine (2'-CMU) (Figure 4). The compounds were demonstrated to show strong inhibitory effects against TBEV strains Hypr and Neudoerfl in PS cells and in neuroblastoma (UKF-NB-4) cells. The most potent compound of the tested series was 7-deaza-2'-CMA exerting low-micromolar EC₅₀ value (1.1 ± 0.1 μM). On the other hand, the 2'-C-methyl nucleoside analogues with the lowest anti-TBEV activity was 2'-CMU (EC₅₀ value of 11.1 ± 0.4 μM).^{29, 30} All 2'-C-methyl nucleosides tested were not cytotoxic for both cell lines, with the exception of 2'-CMC displaying moderate cytotoxicity with a CC₅₀ value of ~50 μM. These compounds were also demonstrated to suppress CPE formation in virus-infected PS cells²⁹ and to inhibit the expression of the TBEV-specific surface E protein, as demonstrated by immunofluorescence staining. Interestingly, a structurally related nucleoside tubercidin (7-deazaadenosine), differing from 7-deaza-2'-CMA in lacking a 2'-methyl substituent, was found to be highly cytotoxic (CC₅₀ value of 2.1 ± 0.2 μM) for PS cells. This observation indicates that the 2'-methyl modification of 7-deazaadenosine is needed for highly selective interaction of the nucleoside analogue with TBEV RdRp active site resulting in discrimination of TBEV RdRp over host cell polymerases.³⁰

Anti-TBEV activity of 7-deaza-2'-CMA was further evaluated *in vivo* using a mouse infection model.³⁸ The dose of 25 mg/kg twice daily resulted in a survival rate of 60%, improved clinical

signs of infection, and prolonged the mean survival time of infected and drug-treated mice compared with control animals. No signs of toxicity for the mice were observed over 28 days. Lower doses (i.e. 5 and 15 mg/kg of 7-deaza-2'-CMA once daily) still significantly increased survival rates to 35% and 50%, respectively, and led to better clinical scores compared to controls. The anti-TBEV effect was further demonstrated using a bioluminescent mouse model, based on IFN $\beta^{+\Delta}$ -luc mice. 7-Deaza-2'-CMA, when administered at 25 mg/kg two times a day, significantly reduced the bioluminescence signal intensity in brain, peritoneal cavity, and/or lymph nodes.³⁸ Following these findings, a group in Switzerland took inspiration from the studies conducted by Eyer et. al.^{29, 30, 38} and designed a rat model to test antiviral activities of 2'-CMA, 7-deaza-2'-CMA, and 2'-CMC. The aim was to create an animal model in which a tissue sample from the cerebellum of a rat could be utilized for *in vitro* testing of various compounds.⁵⁹ The compounds were delivered to the tissue sample cells at 50 μ M similar to the Eyer et. al. studies. Similarly to the previous study, 2'-CMA and 7-deaza-2'-CMA decreased the viral titers better than 2'-CMC.⁵⁹ Overall the most promising 2'-methyl modified nucleoside was 7-deaza-2'-CMA, which was investigated further to determine if it could be a potential anti-TBEV treatment.

To better understand the mechanism of action of 7-deaza-2'-CMA, Eyer et. al. selected the drug-resistant TBEV mutant and compared its genotypical and phenotypical properties with the wild-type virus. The sequence analysis of the genome RNA of the obtained mutant revealed a signature mutation S603T located in the active site of the viral NS5 RdRp.³⁸ The S603T mutant showed high resistance not only to 7-deaza-2'-CMA, which was primarily used for the *in vitro* mutant selection, but also to all members of the 2'-C-methylated nucleoside family. Importantly, the S603T mutant showed significantly decreased replication fitness and altered plaque morphology in cell culture. Moreover, it was highly attenuated in a mouse infection model, causing only 40% mortality rate in mice compared with the wild-type virus. Overall, although relatively fast resistance occurred after 7-deaza-2'-CMA treatment in cell culture, the viral fitness and ability to spread in cell culture and develop clinical signs in animal model was highly limited, making 7-deaza-2'-CMA (and other members of the 2'-C-methylated family) suitable for further anti-TBEV optimization and drug development.³⁸

Apart from the 2'-C-methyl analogues discussed above (Figure 4)³⁰, different types of 2'- sugar modification were also tested against TBEV, which included predominantly the 2'-O-methyl substituted nucleosides, such as 2'-O-methyladenosine, 2'-O-methylguanosine, 2'-O-methylcytidine, and 2'-O-methyluridine (Figure 5).^{14, 30} These compounds however had little to no activity against TBEV. While none of these compounds appeared to be toxic to the different types of cells, the antiviral activity was not ideal and therefore these analogues were not studied further.³⁰ 2'-Deoxy-modified nucleosides, such as 2'-deoxyadenosine, 2'-deoxyguanosine, 2'-deoxycytidine, and 2'-deoxyuridine were observed to be completely inactive against TBEV in cell culture, suggesting that 2'-hydroxyl is required for specific recognition of the nucleoside molecule by viral RdRp active site.³⁰ In contrast, some phenoxazine-substituted deoxyribonucleosides (**11a**, **11b**, **12b**, and **12c**, see below) showed a low-micromolar anti-TBEV effects. It is speculative, however, if these nucleosides act as classical inhibitors of viral RNA synthesis or rather disrupt other stages of TBEV life cycle.⁶⁰

The introduction of an ethynyl group to the 2' position of the sugar moiety was another modification on nucleosides that was tested against TBEV, as exemplified by a 7-deaza nucleoside derivative NITD008 (Figure 6). This compound had previously shown antiviral activity against numerous flaviviruses.^{1, 14, 61} Lo et. al. tested antiviral activity of NITD008 against multiple tick-borne viruses, including TBEV, utilizing various cell-based assays, such as CPE-reduction assay in A549 cells or flavivirus detection method based on immunofluorescence staining.⁶² The compound exhibited no toxicity and had a low micromolar EC₅₀, with a high selectivity index. NITD008 previously protected mice against other viruses requiring the drug to cross the blood brain barrier,⁶³ thus future studies for this compound should focus on *in vivo* studies to further evaluate its antiviral activity and its ability to cross the blood brain barrier to treat TBEV infections.⁶⁴

Taken together, the methyl or ethynyl substituent at the 2'-C position of the nucleoside β-face is an important structural element for highly selective TBEV inhibition and reduced cytotoxicity *in vitro*. This nucleoside substitution does not adversely affect the hydrogen bonding of the appropriate nucleotide with TBEV RdRp active site. The binding is probably due to presence of some additional steric space surrounding the 2'-carbon, allowing the RdRp active site to accommodate the 2'-C-methyl/ethynyl substituent. After incorporation into the nascent viral RNA chain, the 2'-C-substituent is likely responsible for efficient stalling of viral RNA chain elongation, working by a non-obligate chain terminator mechanism.⁵⁵

3'-Sugar Modifications

Walking around the nucleoside scaffold, the next type of modification to be discussed is the C3' position. Similar to the 2'-methyl-modified nucleoside analogues, a methyl group can either be added to the C3' or O3' position on the sugar moiety.¹⁴ Four different analogues were inspected for their anti-TBEV potency: 3'-*O*-methyladenosine, 3'-*O*-methylguanosine, 3'-*O*-methylcytidine, and 3'-*O*-methyluridine (Figure 7).³⁰ This modification proved to be unsuccessful in suppressing TBEV replication *in vitro*, as there was negligible or no reduction in TBEV titers in virus-infected compound-treated PS cells. The compounds were not toxic in either PS or UKF-NB-4 cells.³⁰ Later, 3'-*C*-methyl modifications were investigated by Orlov et. al. in an SAR study against TBEV in PEK cells.⁶⁵ Four different 3'-*C*-methyl analogues were studied: 3'-*C*-methyluridine, 3'-*C*-methyl-2'-hydroxythymidine, 3'-*C*-methylcytidine, and 3'-*C*-methylguanosine (Figure 7). Unfortunately, none of these analogues exhibited meaningful antiviral activity (EC₅₀ >50 μM) and thus not pursued further.⁶⁵ Overall, both reports of the 3'-methyl modifications revealed less than satisfactory results, thus damping enthusiasm for their potential use as TBEV treatments.

Eyer et. al also studied the effects of removing the 3'-hydroxyl on the sugar moiety.^{14, 30} 3'-Deoxyadenosine, 3'-deoxyguanosine, and 3'-deoxycytidine (Figure 8) were tested against TBEV in PS cells.³⁰ The 3'-deoxy modification resulted in little to no activity against TBEV. Only 3'-deoxycytidine showed moderate activity (EC₅₀ = 41.2 ± 0.1 μM) in PS cells and an even greater EC₅₀ value of 79.4 ± 2.3 μM in neuroblastoma cells. The other two nucleosides studied had EC₅₀

values $>50 \mu\text{M}$. Moreover, 3'-deoxycytidine also exhibited some cytotoxic effects in PS cells, slightly reducing cell viability. The absence of antiviral activity from the 3'-modified nucleosides could be explained by two speculative hypotheses, the first being that the RdRp of TBEV may require a 3'-hydroxyl for hydrogen-bonding interaction of the nucleoside triphosphate with the RdRp active site. Alternatively, the loss of antiviral activity of 3'-deoxy nucleosides could be due to their poor cellular uptake and/or insufficient conversion to the triphosphate (active) forms by host kinases.^{30, 54}

One of the 3'-deoxy modified nucleosides showing a high anti-TBEV efficacy was 3'-deoxy-3'-fluoroadenosine (Figure 9). This compound is representative of fluoro-substituted nucleosides, which are currently widely used for medical purposes as anticancer or antiviral drugs.⁴¹ 3'-Deoxy-3'-fluoroadenosine was described as a broad-spectrum antiviral agent, exerting strong inhibitory effects against numerous RNA viruses of *Picornaviridae*, *Togaviridae*, *Reoviridae*, and *Arenaviridae* families and even against vaccinia virus among DNA viruses.^{66, 67} Due to the absence of the reactive 3'-hydroxyl, the anti-TBEV effect of 3'-deoxy-3'-fluoroadenosine could be explained by a typical non-obligate chain terminator mechanism. In 2020, Eyer et al. reported this compound to be active against multiple arthropod-borne flaviviruses in both PS and HBCA cells, including TBEV (Hypr and Neudoerfl strains) with EC_{50} values ranging from 1.6 to 4.5 μM . 3'-Deoxy-3'-fluoroadenosine exerted observable cytostatic effects at concentrations $\geq 25 \mu\text{M}$ for PS cells and at $\geq 12.5 \mu\text{M}$ for primary HBCA cells; however, at lower concentrations, the compound was well tolerated by both cell types. It could be speculated that the cytostatic activity could be related to low selectivity of 3'-deoxy-3'-fluoroadenosine 5'-triphosphate for the TBEV RdRp over other types of viral and cellular polymerases. The extremely broad range of viruses sensitive to this nucleoside supports this hypothesis.⁶⁶ In TBEV-infected mice, the antiviral effect of 3'-deoxy-3'-fluoroadenosine (dosage of 25 mg/kg twice daily) resulted in significantly longer survival time and slower progress of development of clinical signs compared with control animals. In mice infected with WNV, 3'-deoxy-3'-fluoroadenosine exerted even higher antiviral efficacy (survival rate of 70%).³⁵

4'-Sugar Modifications

Previously, 4'-azido-substituted nucleosides have shown antiviral activity against HCV, henipaviruses, and paramyxoviruses.^{1, 14, 68, 69} 4'-Azidocytidine (RO-1479, Figure 10) and its arabino counterpart 4'-azido-aracytidine (RO-9187, Figure 10) were also studied for their ability to suppress replication of TBEV in cell culture.^{1, 14, 30} Both azido-analogues of cytosine had dose dependent antiviral responses in PS cells, with both compounds exhibiting low micromolar activity against TBEV. RO-9187 is a compound structurally related to 2'-C-deoxyribonucleosides, particularly due to the absence of the 2'- α -hydroxyl on the ribose ring. Therefore, the anti-TBEV activity of RO-9187 was somewhat surprising, as the 2'- α -hydroxyl was generally considered to be highly important for specific hydrogen-bonding interactions of the nucleoside triphosphate with viral RdRp.⁶⁸ In that regard, 4'-azidocytidine exhibited an EC_{50} of $2.7 \pm 0.1 \mu\text{M}$, while RO-9187 had an even lower EC_{50} of $0.3 \pm 0.01 \mu\text{M}$. Interestingly, in neuroblastoma cells these compounds lost their antiviral activities, indicating the cell line dependent anti-TBEV effects. In

immunofluorescence staining assays, both compounds were able to inhibit expression of the TBEV E protein.³⁰

5'-Sugar Modifications

Numerous prodrugs with modifications at the nucleoside 5'-position derived from various parental nucleosides were tested against TBEV *in vitro*. Sofosbuvir, a McGuigan ProTide of 2'-fluoro-2'-methyluridine, originally developed for treatment of chronic HCV infections, appeared to show no observable anti-TBEV activity when tested against TBEV Hypr in PS cells. This is not surprising, as the parental nucleoside also showed no anti-TBEV activity.³⁰ Another interesting McGuigan prodrug is remdesivir (Figure 3), which was about 25-fold more active against TBEV than the parental nucleoside GS-441524 (Figure 3) but showed a worse cytotoxicity profile (see above- 1' sugar modifications). An ester prodrug of 4'-azidocytidine, denoted as balapiravir (Figure 10), modified at the 2', 3', and 5'-positions was completely inactive against TBEV *in vitro*, probably because of its poor intracellular uptake or insufficient kinase phosphorylation.^{1, 14, 30}

Other interesting examples of 5'-modified nucleosides are uridine derivatives modified with 2-deoxy sugars at the 5'-position (Figure 11) showing antiviral activity against several members of the *Flaviviridae* and *Orthomyxoviridae* families. These compounds were observed to target the late steps of the N-glycosylation process and affected the maturation of viral proteins. They showed (low)micromolar inhibitory effects against Hypr and Neudoerfl TBEV (IC₅₀ of 1.4 to 10.2 μM) and low cytotoxicity in A549 cells. Such glycosylation inhibitors could also represent perspective candidates for future antiviral therapies against TBEV, although they do not act as typical nucleoside-based disruptors of viral RNA synthesis/replication.⁷⁰

Functional Group Nucleobase Modifications

Modifications can also be made at many positions on the heterocyclic nucleobase of the nucleoside scaffold.^{1, 14} An SAR study completed by Orlov et. al. investigated various substituents on the amino groups of different types of nucleobases, as well as other nucleobase modifications, including the N⁶ position on adenosine, the N² position of guanosine, the N⁴ position of cytidine, as well polar substituents on ribose-nucleosides (Figure 12). A total of 21 different N⁶ substituents were evaluated for their anti-TBEV potency (Absettarov strain) and cytotoxicity.⁶⁵ Cytotoxicities for most of the N⁶ analogues were not determined or negligible. However N⁶-(1-pyrenylmethyl)adenosine and N⁶-benzyl-5'-*O*-trityl-adenosine both had CC₅₀ values around 10 μM. The N⁶ series had almost no inhibitory activity against TBEV, likely due to their increased hydrophobicity.⁶⁵

Interestingly, as the size of the substituent increased, some of the analogues did prove to have some low to mid micromolar activities. For example, N⁶-(1-pyrenylmethyl)adenosine and N⁶-benzyl-5'-*O*-trityl-adenosine had some of the lowest EC₅₀ values (6 μM and 2 μM respectively), but due to their high toxicities were not pursued further.^{1, 14, 65} Only two N² analogues were investigated in detail: N²-benzoylguanosine and N²-isobutylguanosine.⁶⁵ Both compounds showed acceptable cytotoxicity profiles but negligible inhibition activity against TBEV. N⁴-Benzoylcytidine and N¹-methyladenosine exhibited the same antiviral/cytotoxicity properties as the N² analogues.⁶⁵ Overall, substituted amino groups on the nucleobase did not exhibit meaningful

antiviral activity. Larger substituents increased the antiviral activity but enhanced the cytotoxicity and therefore were not tested further as potential TBEV therapeutics.

Other nucleobase-modified compounds, N⁴-hydroxycytidine and furano[2,3-*d*]pyrimidine nucleosides (Figure 13), inhibited replication of enteroviruses (enterovirus A71 and coxsackievirus A16) but were inactive against TBEV. In contrast 5-(tetradec-1-yn-1-yl)-uridine (Figure 13) showed selective inhibition effects on tick-borne encephalitis virus only, having no activity against enteroviruses tested.⁷¹

Finally, a series of 7-deazaadenine ribonucleosides (Figure 14) modified with alkyl, alkenyl, alkynyl, aryl, or hetaryl groups at position 7 were synthesized and tested for antiviral activity against selected RNA viruses, including the TBEV Hypr strain.⁷² The corresponding triphosphate forms inhibited the viral RdRps at micromolar levels in enzyme-based assays by stopping further extension of the nascent viral RNA chain (chain terminator mechanism). 7-Deazaadenosine nucleosides with ethynyl or small hetaryl groups at position 7 showed (sub)micromolar antiviral activities but had significant cytotoxicity, whereas the nucleosides bearing bulkier heterocycles were still active but less toxic.⁷²

Other Nucleoside Modifications

Several additional nucleosides that have been pursued have unique modifications, including variations of the heterocyclic atom found in the sugar moiety,^{1, 14} five membered triazole nucleobases,¹ and expanded nucleobase modifications.⁷³

In that regard, galidesivir (referred to as BCX4430) is a typical imino-C-nucleoside (Figure 15) that has the furanose oxygen replaced with a nitrogen and the *N*-glycosidic bond replaced with a *C*-glycosidic bond.¹ This compound is considered a non-obligate chain terminator and has exhibited broad-spectrum antiviral activity against a variety of viral pathogens including filoviruses, coronaviruses, and picornaviruses just to name a few.⁷⁴ Galidesivir also entered Phase I clinical trials for Ebola virus infections in 2014.^{1, 14, 75, 76} Galidesivir and its hydrochloride form were evaluated for their antiviral activity against multiple types of tick-borne viruses, including the Hypr strain of TBEV.³⁴ Both compounds showed low-micromolar EC₅₀ values when used to suppress TBEV replication in virus titer inhibition tests.

In order to determine the mode of action of galidesivir in more details, Eyer et al. selected a drug resistant TBEV mutant by serial passaging of the TBEV Hypr strain through PS cells at increasing concentrations of the compound up to 50 μM. The obtained mutant was characterized by a single amino acid change, E460D, located in the active site of the NS5 RdRp.³⁹ This mutation was responsible for the resistance of TBEV to galidesivir; however, it did not confer resistance to other structurally distinct nucleoside inhibitors of TBEV replication, such as 2'-*C*-methyl modified or 4'-*C*-azido modified nucleosides.³⁹ Similarly to the S603T mutant, the E460D mutated TBEV showed decreased replication fitness in the cell culture, predominantly during the first 35 hours post infection, and exerted a high degree of attenuation and strongly limited infectivity in a mouse model of TBEV infection. Mice infected with E460D mutant showed 100% survival rate in comparison with 0-10% survival rate in control mice infected with wild type.³⁹

Another modification focused on triazole, a five membered nucleobase, found in compounds such as ribavirin (Figure 16). Ribavirin has exhibited broad-spectrum antiviral activity against many virus families.^{1, 77} This compound was described to have multiple modes of action, predominantly acting as a lethal mutagenic nucleoside and/or inhibitor of inosine monophosphate dehydrogenase, an important enzyme in GTP metabolism. Antiviral activity of ribavirin against TBEV has led to conflicting data as some research groups have reported that ribavirin does exhibit anti-TBEV activity, while other investigators decline its anti-TBEV effects.^{1, 29, 30} In a study performed by Eyer et al. in 2015, ribavirin did not suppress TBEV titers and caused no reduction of CPE on PS cells up to 50 μM .²⁹

An additional modification on nucleosides that has been tested against TBEV was an expanded nucleobase such as the phenoxazine analogues tested by Kozlovskaya et. al (Figure 17). Expanded nucleosides have shown antiviral activity against various types of viruses and are attractive targets because of their unique chemical properties.⁷³ Expanded nucleosides that bear a phenoxazine group are readily incorporated into growing strands of DNA and RNA, but their antiviral properties have not been studied completely.^{73, 78} A series of compounds were tested in PEK cells against the Absettarov strain of TBEV.⁷³ Compounds **12a** and **12b** (Figure 17), which featured a 2-aminomethoxy moiety on the nucleobase, had mid-micromolar activity against TBEV ($\text{EC}_{50} = 12 \pm 1 \mu\text{M}$ and $14.1 \pm 1.9 \mu\text{M}$ respectively). After seven days, however, the compounds were observed to have cytotoxic effects on the cells. Compound **7c** (Figure 20) possessing a 2'-*O*-methyl group had a severe decrease in antiviral activity, but no cytotoxicity. Compounds **13a**, **13b**, and **14a** (Figure 17) all exhibited low micromolar activity ($\text{EC}_{50} < 1 \mu\text{M}$), with little to no cytotoxicity. As a result, these could potentially be pursued further *in vivo* and for mechanism of action studies.⁷³ Other phenoxazine nucleoside derivatives (compounds **11a**, **11b**, **12b**, and **12c**) as shown in Figure 18 were active against TBEV and showed also broad-range antiviral potency against multiple RNA and DNA viruses.⁶⁰

Non-nucleoside inhibitors of TBEV

A variety of structurally diverse molecules have been synthesized and evaluated against TBEV. These include non-nucleoside inhibitors targeting TBEV protein E, TBEV-host cell fusion inhibitors with rigid amphipathic perylene-based core or numerous repurposed antivirals and natural compounds, discovered originally as potent blockers of other (unrelated) viruses. This section represents only a brief overview of these molecules, as without them, the list of the compounds with anti-TBEV activity would not be complete. The reader can find a detailed description of some of these inhibitors in other chapters of this publication.

Repurposed non-nucleoside TBEV inhibitors

The first class of repurposed non-nucleoside compounds to be discussed for TBEV treatment are natural extracts.¹ These include compounds/compound mixtures isolated from natural products including various medically-interesting plant and animal species.^{1, 79} One example of a highly studied natural extract is luromarin, which contains two known antiviral compounds: rosmarinic

acid and luteolin (Figure 19). Both rosmarinic acid and luteolin have shown antflaviviral activity against Japanese encephalitis virus (JEV) in mice and cultured cells. As a result, they may prove to be a viable option for TBEV treatment.^{1, 80, 81}

The second class of repurposed compounds that were investigated to inhibit TBEV replication and spreading were interferon inducers, which increase interferon levels in virus-infected cells to enhance natural antiviral defense.⁸² One of the most commonly tested interferon inducers is jodantipyrine¹ (Figure 20), an iodinated derivative of antipyrine (Figure 20). It was observed in mouse studies that jodantipyrine increased interferon levels from 8 to 256 units/mL within a 24-hour period. Even though this drug was shown to affect the humoral immune system with varying effects, the exact mechanism of action has yet to be elucidated.^{83, 84}

In addition, jodantipyrine was shown to exhibit a wide array of antiviral activities against viruses such as influenza, hepatitis viruses, as well as against TBEV.⁸³ When the drug was administered orally to mice challenged with TBEV, a therapeutic effect (those mice whose clinical symptoms improved) of up to 60% was observed. When administered via parenteral (non-oral) injection, a therapeutic effect of 53.4% was observed, but if administered as a prophylactic prior to viral challenge, the therapeutic effect was even less (47%).⁸³ The drug has also been tested in clinical trials for individuals who have been bitten by TBEV-infected ticks. The clinical trials revealed that only three out of 460 individuals developed TBEV infections while taking jodantipyrine, however these results were criticized since the studies were sponsored by the manufacturer of the drug.^{1, 83}

Inhibitors targeting protein E

Virtual pre-screening of a library of various 1,4-dihydropyridines and pyrido[2,1-b][1,3,5]-thiadiazines was undertaken using the homology model of the envelope (E) proteins of tick-borne flaviviruses.²⁵ The most active compounds against TBEV **1m** and **2a** (Figure 21) featured a chlorobenzene, dimethoxy benzene, or *p*-toluidine group and exerted CC₅₀ of > 10 μM and EC₅₀ of 2.0 ± 0.4 μM and 0.07 ± 0.02 μM, respectively.^{1, 25} These results provided the proof of concept that this type of screening could be usable in finding structures that had activity against TBEV and other tick-borne flaviviruses.²⁵ Similarly, Sedenkova et. al. screened 4-fluorosubstituted pyrimidine *N*-oxides as these types of pyrimidines are typically amiable to aromatic nucleophilic substitution and functional group modifications. The most promising compound from the tested series was **3c** (Figure 22) as the tert-butyl group participated in various interactions in the hydrophobic region of the *n*-octyl-β-D-glucoside pocket of the TBEV E protein. The tetramethylene ring was also shown to reside deeply in this pocket, while the fluorine exhibited binding over a very wide region, allowing for a large functionalization at this position.⁸⁵ Other highly active derivatives were compounds **7o** (Figure 22) and **7z** (Figure 22), exhibiting EC₅₀ values of 8 ± 3 μM and 4 ± 1 μM, respectively, when tested against the Absettarov TBEV strain.⁸⁶ Most of the synthesized 4-aminopyrimidine *N*-oxides exhibited activity also against all three TBEV subtypes; thus, such compounds were considered to be broad-spectrum anti-TBEV agents. Later, Vasilenko et. al. synthesized a series of compounds featuring an isoxazole scaffold modified with a lipophilic group at the isoxazole ester moiety, substituted on the adamantane core, modified with linkers to the ester group and/or with various functional groups on the isoxazole core itself.⁸⁷

^{88, 89, 90} For some derivatives, mid-, low- or sub-micromolar anti-TBEV activities were demonstrated in PEK cells, as exemplified by compounds substituted with 1-adamantyl group ($EC_{50} = 11 \pm 4 \mu\text{M}$, Figure 23) or 2-adamantyl groups ($EC_{50} = 11 \pm 2 \mu\text{M}$, Figure 23).⁸⁷⁻⁹⁰ Detailed information on these compounds will be provided in a separate chapter.

Inhibitors of virus-cell fusion

An extremely interesting group of small molecules with broad-range antiviral activity are rigid amphipathic fusion inhibitors (RAFIs). These compounds were initially used as fluorescent labels for oligonucleotide probes,^{91, 92} but later they were demonstrated to show inhibitory effects against enveloped viruses such as influenza and HCV.^{93, 94, 95} Antiviral effects of a large series of RAFIs and their derivatives were evaluated against the TBEV strain Absettarov using plaque reduction assays.^{28, 33, 96} From a structural point of view, RAFIs are synthetic compounds of inverted cone molecular geometry. They are formed by hydrophilic heads of larger diameter than their planar hydrophobic tails represented by an ethynyl-perylene moiety. Incorporation of such structures to the viral envelope results in the inhibition of virion-to-cell fusion of numerous unrelated enveloped viruses.^{95, 97} As viral lipid membranes are evolutionary highly conservative and represent a common structural element for majority of enveloped viruses, RAFIs are typical broad-spectrum antiviral agents, with minimal potential for antiviral resistance development.⁹³ Another described mode of action of these molecules is light-dependent peroxidation of viral lipids via generation of singlet oxygen leading in photodynamic inactivation of enveloped viruses by destruction of viral membranes.⁹⁸ An important factor for the high antiviral activity of RAFIs is good water solubility; some poorly soluble derivatives bearing the large aromatic groups and additional hydrophobic substitutions displayed significantly reduced antiviral activities.⁹⁶ Typical representatives of RAFIs are perylene-modified nucleoside analogues, 5-(perylene-3-ylethynyl)-substituted 2'-deoxyuridine or arabinouridine and their derivatives substituted in O3' position (**4**, **6**, **8a**, and **8b**, Figure 24), or polycyclic perylene-related compounds like perylenyltriazoles, perylenylanilines, perylenylthiophene compounds and aglycosylated/ribose-free non-nucleoside compound (aglycone of RAFI, **5a-d** Figure 25).^{1, 99, 100} Detailed information on RAFIs will be provided in a specialized chapter describing their structure and biological properties.

Another virus-cell/endosome membrane fusion inhibitor is arbidol (umifenovir, Figure 26), which was approved for treatment of influenza A and B in Russia and in China.^{1, 101} Mechanistically, the inhibition of virus-cell fusion is mediated by the intercalation of this compound into lipid membranes and the interaction with viral fusion proteins.¹⁰² In influenza virus, arbidol was observed to interact also with hemagglutinin molecules (HA) and prevent the pH-induced transition of HA into its active fusogenic form.¹⁰³ Crystal structures of arbidol in complex with influenza HA advances the understanding of the molecular arbidol-HA interaction.¹⁰⁴ Alternatively, arbidol may also exhibit immunomodulatory actions, resulting in interferon induction and macrophage activation.¹⁰⁵ Haviernik et. al. tested arbidol against various flaviviruses including TBEV (strains Hypr and Neudoerfl).³² The cytotoxicity of arbidol was determined in multiple immortalized cell lines (i.e. PS cells, Vero cells, human hepatocarcinoma cells (Huh-7), and neuroblasts UKF-NB-4), as well as in primary HBCA cells. The lowest cytotoxicity was observed in Vero cells ($89.72 \pm 0.19 \mu\text{M}$), while all other cell lines experienced varying toxicities.

The observed toxicity could be explained by the unspecific interaction of arbidol with both viral and host cell targets, probably also affecting cellular membranes and cellular metabolic pathways. In HCBA or Vero cells challenged with TBEV, arbidol displayed mild anti-TBEV activity with EC₅₀ of 18.67 ± 0.15 μM based on a viral titer reduction assay.³²

Inhibitors of vacuolar (H⁺)ATPase proton pumps and endosomal acidification

Anti-TBEV activity was recently demonstrated also for diphyllin (Figure 27), a natural arylnaphtalide lignan originally extracted from tropical plants of particular importance in traditional Chinese medicine.^{106, 107, 108, 109} Diphyllin is a potent inhibitor of vacuolar (H⁺)ATPase proton pumps and hence of the endosomal acidification process.^{110, 111} This molecular mechanism is crucial for numerous enveloped viruses entering the host cells via the low-pH-directed membrane fusion followed by receptor-mediated endocytosis.¹¹² Diphyllin showed a broad-range of antiviral activities against variety of enveloped viruses, included those from the *Flaviviridae*, *Coronaviridae*, *Phenuiviridae*, *Rhabdoviridae*, and *Herpesviridae* families.^{113, 114} As a typical host-targeting antiviral agent, diphyllin was considerably cytotoxic for multiple primary and immortalized cells, particularly for UKF-NB-4 and HBCA. This compound showed low-micromolar inhibitory activity against TBEV (strain Hypr) in Vero cells (EC₅₀ around 1 μM). Currently, broad spectrum of structural derivatives of diphyllin are being designed and analyzed in order to optimize their therapeutical properties, to increase water solubility and bioavailability, to reduce cellular toxicity, and to retain/increase antiviral potency.¹¹⁴

Guanine quadruplex-binding ligands

Guanine quadruplexes (G4s) are non-canonical four-stranded secondary structures of nucleic acids. They were identified in genomes of numerous DNA or RNA viruses, including TBEV, serving as important regulators of crucial biological processes during virus infection. Interaction of G4s with small molecule-based ligands resulted in significant inhibition of RdRp-mediated synthesis of TBEV genomic RNA, expression of TBEV structural proteins and decrease of viral titers in TBEV-infected PS cell culture. Most of G4-binding ligands are formed by a large planar aromatic core that stacks on the guanine tetrad of the G4 structure to stabilize G4s, which makes viral RNA genome inaccessible for replication enzymes and host cell ribosomes. Unfortunately, G4 ligands are characterized by a low selectivity and are not able to discriminate among different types of G4s (e.g., viral over cellular). Therefore, many G4-binding ligands are highly cytotoxic and therefore unsuitable as pharmacophores. There are, however, several promising compounds, such as pyridostatin, carboxy pyridostatin, berberine, bisquinolinium derivative PhenDC3, or N-methylmesoporphyrin IX (Figure 28), which displayed good cytotoxicity profiles in vitro and showed strong antiviral effects, when applied on PS cells infected with Hypr or Neudoerfl TBEV¹¹⁵. It should be noted that G4-binding ligands are often associated with multiple mechanisms of action and can recognize and bind numerous molecular targets, other than G4s only. A typical example are porphyrins, which can also be incorporated into viral envelopes and other membranes and block virus-cell fusion processes.

Conclusion

More than 10,000 people a year become infected with TBEV, in which many cases are fatal. Despite the considerable medical importance of TBE, there is currently no approved antiviral treatment available to cure TBEV infections. Therefore, development of highly efficient and safe anti-TBEV drugs is an urgent medical need. Currently, numerous small molecule-based drugs are used to combat long-lasting/chronic viral infections, including those caused by HIV, HBV, HCV or HSV. Many of these antivirals, showing anti-TBEV activities, could be repurposed for the treatment of TBEV infections. However, it should be noted that small molecule-based treatments of acute viral infection, including TBE, could be somewhat challenging, as the serious/life-threatening symptoms of acute infections are very often a consequence of both viral replication in the host cells/tissues and the pro-inflammatory immune response combined with cytokine storms. The solution to this problem could be solved by a combination or sequential therapy based on application of both direct-acting antivirals, as well as anti-inflammatory agents. Together with effective vaccination strategies, specific small molecule-based therapy could provide a potent prophylactic and curative tools to combat human infections caused by TBEV.

Acknowledgments

This study was supported by a grant from the Ministry of Education, Youth, and Sports of the Czech Republic (grant LTAUSA18016) (to L.E). We are greatly indebted to Jiří Holoubek for preparation of Figure 1.

References

- (1) Ruzek, D.; Avšič Županc, T.; Borde, J.; Chrdle, A.; Eyer, L.; Karganova, G.; Kholodilov, I.; Knap, N.; Kozlovskaya, L.; Matveev, A.; et al. Tick-borne encephalitis in Europe and Russia: Review of pathogenesis, clinical features, therapy, and vaccines. *Antivir. Res.* **2019**, *164*, 23-51. DOI: 10.1016/j.antiviral.2019.01.014
- (2) Pierson, T. C.; Diamond, M. S. The continued threat of emerging flaviviruses. *Nat. Microbiol.* **2020**, *5* (6), 796-812. DOI: 10.1038/s41564-020-0714-0
- (3) Füzik, T.; Formanová, P.; Růžek, D.; Yoshii, K.; Niedrig, M.; Plevka, P. Structure of tick-borne encephalitis virus and its neutralization by a monoclonal antibody. *Nat. Commun.* **2018**, *9* (1), 436. DOI: 10.1038/s41467-018-02882-0
- (4) Chambers, T. J.; Hahn, C. S.; Galler, R.; Rice, C. M. Flavivirus genome organization, expression, and replication. *Annu. Rev. Microbiol.* **1990**, *44*, 649-688. DOI: 10.1146/annurev.mi.44.100190.003245
- (5) Kríz, B.; Benes, C.; Daniel, M. Alimentary transmission of tick-borne encephalitis in the Czech Republic (1997-2008). *Epidemiol Mikrobiol Imunol.* **2009**, *58* (2), 98-103.
- (6) Gritsun, T. S.; Lashkevich, V. A.; Gould, E. A. Tick-borne encephalitis. *Antivir. Res.* **2003**, *57* (1), 129-146. DOI: 10.1016/S0166-3542(02)00206-1
- (7) Kentaro, Y. Epidemiology and pathological mechanisms of tick-borne encephalitis. *J. Vet. Med. Sci.* **2019**, *81* (3), 343-347.
- (8) Auksė, M.; Alvydas, L.; Göran, G.; Sirkka, V.; Åke, L.; Lars, L. Tickborne Encephalitis in an Area of High Endemicity in Lithuania: Disease Severity and Long-Term Prognosis. *Clin. Infect. Dis.* **2002**, *35* (6), 650-658.
- (9) Lindquist, L.; Vapalahti, O. Tick-borne encephalitis. *The Lancet* **2008**, *371* (9627), 1861-1871. DOI: 10.1016/S0140-6736(08)60800-4
- (10) Gritsun, T. S.; Nuttall, P. A.; Gould, E. A. Tick-borne Flaviviruses. *Adv Virus Res.* **2003**, *61*, 317-371. DOI: 10.1016/S0065-3527(03)61008-0
- (11) Misić Majerus, L.; Daković Rode, O.; Ruzić Sabljčić, E. [Post-encephalitic syndrome in patients with tick-borne encephalitis]. *Acta Medica Croatica* **2009**, *63* (4), 269-278.
- (12) Haglund, M.; Günther, G. Tick-borne encephalitis—pathogenesis, clinical course and long-term follow-up. *Vaccine* **2003**, *21* (Supplement 1), S11-S18. DOI: 10.1016/S0264-410X(02)00811-3
- (13) Bogovič, P.; Stupica, D.; Rojko, T.; Lotrič-Furlan, S.; Avšič-Županc, T.; Kastrin, A.; Lusa, L.; Strle, F. The long-term outcome of tick-borne encephalitis in Central Europe. *Ticks Tick Borne Dis.* **2018**, *9* (2), 369-378. DOI: 10.1016/j.ttbdis.2017.12.001
- (14) Eyer, L.; Nencka, R.; de Clercq, E.; Seley-Radtke, K.; Růžek, D. Nucleoside analogs as a rich source of antiviral agents active against arthropod-borne flaviviruses. *Antivir. Chem. Chemother.* **2018**, *26*, 2040206618761299. DOI: 10.1177/2040206618761299

- (15) Barrett, P. N.; Schober-Bendixen, S.; Ehrlich, H. J. History of TBE vaccines. *Vaccine* **2003**, *21* (Supplement 1), S41-S49. DOI: 10.1016/S0264-410X(02)00814-9
- (16) Vorovitch, M. F.; Kozlovskaya, L. I.; Romanova, L. I.; Chernokhaeva, L. L.; Ishmukhametov, A. A.; Karganova, G. G. Genetic description of a tick-borne encephalitis virus strain Sofjin with the longest history as a vaccine strain. *SpringerPlus* **2015**, *4*, 761. DOI: 10.1186/s40064-015-1561-y
- (17) Paulke-Korinek, M.; Rendi-Wagner, P.; Kundi, M.; Laaber, B.; Wiedermann, U.; Kollaritsch, H. Booster vaccinations against tick-borne encephalitis: 6 Years follow-up indicates long-term protection. *Vaccine* **2009**, *27* (50), 7027-7030. DOI: 10.1016/j.vaccine.2009.09.068
- (18) Plentz, A.; Jilg, W.; Schwarz, T. F.; Kuhr, H. B.; Zent, O. Long-term persistence of tick-borne encephalitis antibodies in adults 5 years after booster vaccination with Encepur® Adults. *Vaccine* **2009**, *27* (6), 853-856. DOI: 10.1016/j.vaccine.2008.11.082
- (19) Beran, J.; Xie, F.; Zent, O. Five year follow-up after a first booster vaccination against tick-borne encephalitis following different primary vaccination schedules demonstrates long-term antibody persistence and safety. *Vaccine* **2014**, *32* (34), 4275-4280. DOI: 10.1016/j.vaccine.2014.06.028
- (20) Wittermann, C.; Izu, A.; Petri, E.; Gniel, D.; Fragapane, E. Five year follow-up after primary vaccination against tick-borne encephalitis in children. *Vaccine* **2015**, *33* (15), 1824-1829. DOI: 10.1016/j.vaccine.2015.02.038
- (21) Kubinski, M.; Beicht, J.; Gerlach, T.; Volz, A.; Sutter, G.; Rimmelzwaan, G. F. Tick-Borne Encephalitis Virus: A Quest for Better Vaccines against a Virus on the Rise. *Vaccines* **2020**, *8* (3). DOI: 10.3390/vaccines8030451
- (22) Lehrer, A. T.; Holbrook, M. R. Tick-borne Encephalitis Vaccines. *J. Bioterror. Biodef.* **2011**, *2011* (Suppl 1), 3. DOI: 10.4172/2157-2526.S1-003
- (23) Pen'evskaia, N. A.; Rudakov, N. V. [Efficiency of use of immunoglobulin preparations for the postexposure prevention of tick-borne encephalitis in Russia (a review of semi-centennial experience)]. *Med. Parazitol (Mosk)* **2010**, (1), 53-59.
- (24) Baykov, I. K.; Matveev, A. L.; Stronin, O. V.; Ryzhikov, A. B.; Matveev, L. E.; Kasakin, M. F.; Richter, V. A.; Tikunova, N. V. A protective chimeric antibody to tick-borne encephalitis virus. *Vaccine* **2014**, *32* (29), 3589-3594.
- (25) Osolodkin, D. I.; Kozlovskaya, L. I.; Dueva, E. V.; Dotsenko, V. V.; Rogova, Y. V.; Frolov, K. A.; Krivokolysko, S. G.; Romanova, E. G.; Morozov, A. S.; Karganova, G. G.; et al. Inhibitors of tick-borne flavivirus reproduction from structure-based virtual screening. *ACS Med. Chem. Lett.* **2013**, *4* (9), 869-874. DOI: 10.1021/ml400226s
- (26) Dueva, E. V.; Osolodkin, D. I.; Kozlovskaya, L. I.; Palyulin, V. A.; Pentkovski, V. M.; Zefirov, N. S. Interaction of Flaviviruses with Reproduction Inhibitors Binding in β -OG Pocket: Insights from Molecular Dynamics Simulations. *Mol. Inform.* **2014**, *33* (10), 695-708. DOI: 10.1002/minf.201300185

- (27) Akaberi, D.; Båhlström, A.; Chinthakindi, P. K.; Nyman, T.; Sandström, A.; Järhult, J. D.; Palanisamy, N.; Lundkvist, Å.; Lennerstrand, J. Targeting the NS2B-NS3 protease of tick-borne encephalitis virus with pan-flaviviral protease inhibitors. *Antivir. Res.* **2021**, *190*. DOI: 10.1016/j.antiviral.2021.105074
- (28) Sapozhnikova, K. A.; Slesarchuk, N. A.; Orlov, A. A.; Khvatov, E. V.; Radchenko, E. V.; Chistov, A. A.; Ustinov, A. V.; Palyulin, V. A.; Kozlovskaya, L. I.; Osolodkin, D. I.; et al. Ramified derivatives of 5-(perylene-3-ylethynyl)uracil-1-acetic acid and their antiviral properties. *RSC Adv.* **2019**, *9* (45), 26014-26023.
- (29) Eyer, L.; Valdés, J. J.; Gil, V. A.; Nencka, R.; Hřebabecký, H.; Šála, M.; Salát, J.; Černý, J.; Palus, M.; De Clercq, E.; et al. Nucleoside inhibitors of tick-borne encephalitis virus. *Antimicrob. Agents Chemother.* **2015**, *59* (9), 5483-5493. DOI: 10.1128/AAC.00807-15
- (30) Eyer, L.; Šmídková, M.; Nencka, R.; Neča, J.; Kastl, T.; Palus, M.; De Clercq, E.; Růžek, D. Structure-activity relationships of nucleoside analogues for inhibition of tick-borne encephalitis virus. *Antivir. Res.* **2016**, *133*, 119-129. DOI: 10.1016/j.antiviral.2016.07.018
- (31) Lo, M. K.; Jordan, R.; Arvey, A.; Sudhamsu, J.; Shrivastava-Ranjan, P.; Hotard, A. L.; Flint, M.; McMullan, L. K.; Siegel, D.; Clarke, M. O.; et al. GS-5734 and its parent nucleoside analog inhibit Filo-, Pneumo-, and Paramyxoviruses. *Sci. Rep.* **2017**, *7*, 43395. DOI: 10.1038/srep43395
- (32) Haviernik, J.; Štefánik, M.; Fojtíková, M.; Kali, S.; Tordo, N.; Rudolf, I.; Hubálek, Z.; Eyer, L.; Ruzek, D. Arbidol (Umifenovir): A Broad-Spectrum Antiviral Drug That Inhibits Medically Important Arthropod-Borne Flaviviruses. *Viruses* **2018**, *10* (4). DOI: 10.3390/v10040184
- (33) Orlov, A.; Chistov, A.; Kozlovskaya, L.; Ustinov, A.; Korshun, V.; Karganova, G.; Osolodkin, D. Rigid amphipathic nucleosides suppress reproduction of the tick-borne encephalitis virus. *Med. Chem. Comm.* **2016**, *7*(3), 495-499.
- (34) Eyer, L.; Zouharová, D.; Širmarová, J.; Fojtíková, M.; Štefánik, M.; Haviernik, J.; Nencka, R.; de Clercq, E.; Růžek, D. Antiviral activity of the adenosine analogue BCX4430 against West Nile virus and tick-borne flaviviruses. *Antivir. Res.* **2017**, *142*, 63-67. DOI: 10.1016/j.antiviral.2017.03.012
- (35) Gejji, V.; Svoboda, P.; Stefanik, M.; Wang, H.; Salat, J.; Eyer, L.; Ruzek, D.; Fernando, S. An RNA-dependent RNA polymerase inhibitor for tick-borne encephalitis virus. *Virology* **2020**, *546*, 13-19. DOI: 10.1016/j.virol.2020.03.006
- (36) Konkolova, E.; Dejmek, M.; Hřebabecký, H.; Šála, M.; Böserle, J.; Nencka, R.; Boura, E. Remdesivir triphosphate can efficiently inhibit the RNA-dependent RNA polymerase from various flaviviruses. *Antivir. Res.* **2020**, *182*, 104899. DOI: 10.1016/j.antiviral.2020.104899
- (37) Haviernik, J.; Eyer, L.; Yoshii, K.; Kobayashi, S.; Cerny, J.; Nougairède, A.; Driouich, J.-S.; Volf, J.; Palus, M.; de Lamballerie, X.; et al. Development and characterization of recombinant tick-borne encephalitis virus expressing mCherry reporter protein: A new tool for high-throughput screening of antiviral compounds, and neutralizing antibody assays. *Antivir. Res.* **2021**, *185*. DOI: 10.1016/j.antiviral.2020.104968
- (38) Eyer, L.; Kondo, H.; Zouharova, D.; Hirano, M.; Valdés, J. J.; Muto, M.; Kastl, T.; Kobayashi, S.; Haviernik, J.; Igarashi, M.; et al. Escape of Tick-Borne Flavivirus from 2'-C-Methylated Nucleoside

Antivirals Is Mediated by a Single Conservative Mutation in NS5 That Has a Dramatic Effect on Viral Fitness. *J. Virol.* **2017**, *91* (21). DOI: 10.1128/JVI.01028-17

(39) Eyer, L.; Nougairède, A.; Uhlířová, M.; Driouich, J.-S.; Zouharová, D.; Valdés, J. J.; Haviernik, J.; Gould, E. A.; De Clercq, E.; de Lamballerie, X.; et al. An E460D Substitution in the NS5 Protein of Tick-Borne Encephalitis Virus Confers Resistance to the Inhibitor Galidesivir (BCX4430) and Also Attenuates the Virus for Mice. *J. Virol.* **2019**, *93* (16). DOI: 10.1128/JVI.00367-19

(40) Eyer, L.; Svoboda, P.; Balvan, J.; Vičar, T.; Raudenská, M.; Štefánik, M.; Haviernik, J.; Huvarová, I.; Straková, P.; Rudolf, I.; et al. Broad-Spectrum Antiviral Activity of 3'-Deoxy-3'-Fluoroadenosine against Emerging Flaviviruses. *Antimicrob. Agents Chemother.* **2021**, *65* (2). DOI: 10.1128/AAC.01522-20

(41) Seley-Radtke, K. L.; Yates, M. K. The evolution of nucleoside analogue antivirals: A review for chemists and non-chemists. Part 1: Early structural modifications to the nucleoside scaffold. *Antivir. Res.* **2018**, *154*, 66-86. DOI: 10.1016/j.antiviral.2018.04.004

(42) De Clercq, E.; Neyts, J. Antiviral agents acting as DNA or RNA chain terminators. *Handb Exp Pharmacol* **2009**, (189), 53-84. DOI: 10.1007/978-3-540-79086-0_3

(43) Chen, H.; Liu, L.; Jones, S. A.; Banavali, N.; Kass, J.; Li, Z.; Zhang, J.; Kramer, L. D.; Ghosh, A. K.; Li, H. Selective inhibition of the West Nile virus methyltransferase by nucleoside analogs. *Antivir. Res.* **2013**, *97* (3), 232-239. DOI: 10.1016/j.antiviral.2012.12.012

(44) Vernekar, S. K. V.; Qiu, L.; Zhang, J.; Kankanala, J.; Li, H.; Geraghty, R. J.; Wang, Z. 5'-Silylated 3'-1,2,3-triazolyl Thymidine Analogues as Inhibitors of West Nile Virus and Dengue Virus. *J. Med. Chem.* **2015**, *58* (9), 4016-4028. DOI: 10.1021/acs.jmedchem.5b00327

(45) Leyssen, P.; Balzarini, J.; De Clercq, E.; Neyts, J. The Predominant Mechanism by Which Ribavirin Exerts Its Antiviral Activity In Vitro against Flaviviruses and Paramyxoviruses Is Mediated by Inhibition of IMP Dehydrogenase. *J. Virol.* **2005**, *79*(3), 1943-1947.

(46) Lee, K.; Kim, D.-E.; Jang, K.-S.; Kim, S.-J.; Cho, S.; Kim, C. Gemcitabine, a broad-spectrum antiviral drug, suppresses enterovirus infections through innate immunity induced by the inhibition of pyrimidine biosynthesis and nucleotide depletion. *Oncotarget* **2017**, *8* (70), 115315-115325. DOI: 10.18632/oncotarget.23258

(47) Shane, C.; Craig, E. C.; Raul, A. RNA Virus Error Catastrophe: Direct Molecular Test by Using Ribavirin. *PNAS* **2001**, *98* (12), 6895-6900.

(48) Graci, J. D.; Cameron, C. E. Quasispecies, Error Catastrophe, and the Antiviral Activity of Ribavirin. *Virology* **2002**, *298*, 175-180.

(49) Périgaud, C.; Gosselin, G.; Imbach, J. L. Nucleoside Analogues as Chemotherapeutic Agents: A Review. *Nucleosides and Nucleotides* **1992**, *11* (2), 903-945.

(50) Koonin, E. V.; Dolja, V. V. Evolution and taxonomy of positive-strand RNA viruses: implications of comparative analysis of amino acid sequences. *Crit. Rev. Biochem. Mol. Biol.* **1993**, *28* (5), 375-430. DOI: 10.3109/10409239309078440

- (51) Cho, A.; Saunders, O. L.; Butler, T.; Zhang, L.; Xu, J.; Vela, J. E.; Feng, J. Y.; Ray, A. S.; Kim, C. U. Synthesis and antiviral activity of a series of 1'-substituted 4-aza-7,9-dideazaadenosine C-nucleosides. *Bioorganic Med. Chem. Lett.* **2012**, *22* (8), 2705-2707. DOI: 10.1016/j.bmcl.2012.02.105
- (52) Warren, T. K.; Jordan, R.; Lo, M. K.; Ray, A. S.; Mackman, R. L.; Soloveva, V.; Siegel, D.; Perron, M.; Bannister, R.; Hui, H. C. Therapeutic efficacy of the small molecule GS-5734 against Ebola virus in rhesus monkeys. *Nature* **2016**, *531*, 381-385.
- (53) Kokic, G.; Hillen, H. S.; Tegunov, D.; Dienemann, C.; Seitz, F.; Schmitzova, J.; Farnung, L.; Siewert, A.; Höbartner, C.; Cramer, P. Mechanism of SARS-CoV-2 polymerase stalling by remdesivir. *Nat. Commun.* **2021**, *12* (1), 279. DOI: 10.1038/s41467-020-20542-0
- (54) Eldrup, A. B.; Allerson, C. R.; Bennett, C. F.; Bera, S.; Bhat, B.; Bhat, N.; Bosserman, M. R.; Brooks, J.; Burlein, C.; Carroll, S. S. Structure-Activity Relationship of Purine Ribonucleosides for Inhibition of Hepatitis C Virus RNA-Dependent RNA Polymerase. *J. Med. Chem.* **2004**, *47*, 2283-2295.
- (55) Carroll, S. S.; Tomassini, J. E.; Bosserman, M.; Getty, K.; Stahlhut, M. W.; Eldrup, A. B.; Bhat, B.; Hall, D.; Simcoe, A. L.; LaFemina, R. Inhibition of Hepatitis C Virus RNA Replication by 2'-Modified Nucleoside Analogs. *J. Biol. Chem.* **2003**, *278*, 11979-12077.
- (56) Lefebvre, D. J.; De Vleeschauwer, A. R.; Goris, N.; Kollanur, D.; Billiet, A.; Murao, L.; Neyts, J.; De Clercq, K. Proof of concept for the inhibition of foot-and-mouth disease virus replication by the anti-viral drug 2'-C-methylcytidine in severe combined immunodeficient mice. *Transbound. Emerg. Dis.* **2014**, *61* (6), e89-e91. DOI: 10.1111/tbed.12069
- (57) Rocha-Pereira, J.; Jochmans, D.; Dallmeier, K.; Leyssen, P.; Cunha, R.; Costa, I.; Nascimento, M. S. J.; Neyts, J. Inhibition of norovirus replication by the nucleoside analogue 2'-C-methylcytidine. *Biochem. Biophys. Res. Commun.* **2012**, *427* (4), 796-800. DOI: 10.1016/j.bbrc.2012.10.003
- (58) Rocha-Pereira, J.; Jochmans, D.; Debing, Y.; Verbeken, E.; Nascimento, M. S. J.; Neyts, J. The Viral Polymerase Inhibitor 2'-C-Methylcytidine Inhibits Norwalk Virus Replication and Protects against Norovirus-Induced Diarrhea and Mortality in a Mouse Model. *J. Virol.* **2013**, *87*, 11798-11805.
- (59) Lenz, N.; Engler, O.; Grandgirard, D.; Leib, S. L.; Ackermann-Gäumann, R. Evaluation of antivirals against tick-borne encephalitis virus in organotypic brain slices of rat cerebellum. *PLoS one* **2018**, *13* (10), e0205294. DOI: 10.1371/journal.pone.0205294
- (60) Kozlovskaya, L. I.; Volok, V. P.; Shtro, A. A.; Nikolaeva, Y. V.; Chistov, A. A.; Matyugina, E. S.; Belyaev, E. S.; Jegorov, A. V.; Snoeck, R.; Korshun, V. A.; et al. Phenoxazine nucleoside derivatives with a multiple activity against RNA and DNA viruses. *Eur. J. Med. Chem.* **2021**, *220*. DOI: 10.1016/j.ejmech.2021.113467
- (61) Zheng, Y.; Yen-Liang, C.; Wouter, S.; Qing-Yin, W.; Feng, G.; Jeyaraj, D.; Ravinder Reddy, K.; Pornwaratt, N.; Suresh, B. L.; Anne, G.; et al. An Adenosine Nucleoside Inhibitor of Dengue Virus. *PNAS* **2009**, *106* (48), 20435-20439. DOI: 10.1073/pnas.0907010106

- (62) Flint, M.; McMullan, L. K.; Dodd, K. A.; Bird, B. H.; Khristova, M. L.; Nichol, S. T.; Spiropoulou, C. F. Inhibitors of the Tick-Borne, Hemorrhagic Fever-Associated Flaviviruses. *Antimicrob. Agent Chemother.* **2014**, *58*, 3206-3216.
- (63) Nelson, J.; Roe, K.; Orillo, B.; Shi, P. Y.; Verma, S. Combined treatment of adenosine nucleoside inhibitor NITD008 and histone deacetylase inhibitor vorinostat represents an immunotherapy strategy to ameliorate West Nile virus infection. *Antivir. Res.* **2015**, *122*, 39-45. DOI: 10.1016/j.antiviral.2015.07.008
- (64) Lo, M. K.; Shi, P. Y.; Chen, Y. L.; Flint, M.; Spiropoulou, C. F. In vitro antiviral activity of adenosine analog NITD008 against tick-borne flaviviruses. *Antivir. Res.* **2016**, *130*, 46-49. DOI: 10.1016/j.antiviral.2016.03.013
- (65) Orlov, A. A.; Drenichev, M. S.; Oslovsky, V. E.; Kurochkin, N. N.; Solyev, P. N.; Kozlovskaya, L. I.; Palyulin, V. A.; Karganova, G. G.; Mikhailov, S. N.; Osolodkin, D. I. New tools in nucleoside toolbox of tick-borne encephalitis virus reproduction inhibitors. *Biorganic Med. Chem. Lett.* **2017**, *27*, 1267-1273.
- (66) Van Aerschot, A.; Herdewijn, P.; Janssen, G.; Cools, M.; De Clercq, E. Synthesis and antiviral activity evaluation of 3'-fluoro-3'-deoxyribonucleosides: broad-spectrum antiviral activity of 3'-fluoro-3'-deoxyadenosine. *Antivir. Res.* **1989**, *12* (3), 133-150. DOI: 10.1016/0166-3542(89)90047-8
- (67) Smee, D. F.; Morris, J. L.; Barnard, D. L.; Van Aerschot, A. Selective inhibition of arthropod-borne and arenaviruses in vitro by 3'-fluoro-3'-deoxyadenosine. *Antivir. Res.* **1992**, *18* (2), 151-162. DOI: 10.1016/0166-3542(92)90035-4.
- (68) Klumpp, K.; Lévêque, V.; Le Pogam, S.; Ma, H.; Jiang, W.-R.; Kang, H.; Granycome, C.; Singer, M.; Laxton, C.; Hang, J. Q.; et al. The Novel Nucleoside Analog R1479 (4'-Azidocytidine) Is a Potent Inhibitor of NS5B-dependent RNA Synthesis and Hepatitis C Virus Replication in Cell Culture. *JBC* **2006**, *281* (7), 3793-3799. DOI: 10.1074/jbc.M510195200
- (69) Hotard, A. L.; He, B.; Nichol, S. T.; Spiropoulou, C. F.; Lo, M. K. 4'-Azidocytidine (R1479) inhibits henipaviruses and other paramyxoviruses with high potency. *Antivir. Res.* **2017**, *144*, 147-152.
- (70) Krol, E.; Wandzik, I.; Brzuska, G.; Eyer, L.; Růžek, D.; Szewczyk, B. Antiviral Activity of Uridine Derivatives of 2-Deoxy Sugars against Tick-Borne Encephalitis Virus. *Molecules (Basel, Switzerland)* **2019**, *24* (6). DOI: 10.3390/molecules24061129
- (71) Kozlovskaya, L. I.; Golinets, A. D.; Eletskaia, A. A.; Orlov, A. A.; Palyulin, V. A.; Kochetkov, S. N.; Alexandrova, L. A.; Osolodkin, D. I. Selective Inhibition of Enterovirus A Species Members' Reproduction by Furano[2, 3- d]pyrimidine Nucleosides Revealed by Antiviral Activity Profiling against (+)ssRNA Viruses. *ChemistrySelect* **2018**, *3* (8), 2321-2325. DOI: 10.1002/slct.201703052
- (72) Milisavljevic, N.; Konkolová, E.; Kozák, J.; Hodek, J.; Veselovská, L.; Sýkorová, V.; Čížek, K.; Pohl, R.; Eyer, L.; Svoboda, P.; et al. Antiviral Activity of 7-Substituted 7-Deazapurine Ribonucleosides, Monophosphate Prodrugs, and Triphosphates against Emerging RNA Viruses. *ACS Infect. Dis.* **2021**, *7* (2), 471-478.

- (73) Kozlovskaya, L. I.; Andrei, G.; Orlov, A. A.; Khvatov, E. V.; Koruchekov, A. A.; Belyaev, E. S.; Nikolaev, E. N.; Korshun, V. A.; Snoeck, R.; Osolodkin, D. I.; et al. Antiviral activity spectrum of phenoxazine nucleoside derivatives. *Antivir. Res.* **2019**, *163*, 117-124. DOI: 10.1016/j.antiviral.2019.01.010
- (74) Warren, T. K.; Wells, J.; Panchal, R. G.; Stuthman, K. S.; Garza, N. L.; Van Tongeren, S. A.; Dong, L.; Retterer, C. J.; Eaton, B. P.; Pegoraro, G.; et al. Protection against filovirus diseases by a novel broad-spectrum nucleoside analogue BCX4430. *Nature* **2014**, *508* (7496), 402-405. DOI: 10.1038/nature13027.
- (75) Taylor, R.; Kotian, P.; Warren, T.; Panchal, R.; Bavari, S.; Julander, J.; Dobo, S.; Rose, A.; El-Kattan, Y.; Taubenheim, B.; et al. BCX4430 - A broad-spectrum antiviral adenosine nucleoside analog under development for the treatment of Ebola virus disease. *J Infect Public Health* **2016**, *9* (3), 220-226. DOI: 10.1016/j.jiph.2016.04.002
- (76) Julander, J. G.; Demarest, J. F.; Taylor, R.; Gowen, B. B.; Walling, D. M.; Mathis, A.; Babu, Y. S. An update on the progress of galidesivir (BCX4430), a broad-spectrum antiviral. *Antivir. Res.* **2021**, *195*, 105180. DOI: 10.1016/j.antiviral.2021.105180
- (77) Nikitina, A. A.; Orlov, A. A.; Kozlovskaya, L. I.; Palyulin, V. A.; Osolodkin, D. I. Enhanced taxonomy annotation of antiviral activity data from ChEMBL. *J. Biol. Databases Curation* **2019**, *2019*. DOI: 10.1093/database/bay139
- (78) Edwards, T. E.; Cekan, P.; Reginsson, G. W.; Shelke, S. A.; Ferré-D'Amaré, A. R.; Schiemann, O.; Sigurdsson, S. T. Crystal structure of a DNA containing the planar, phenoxazine-derived bi-functional spectroscopic probe C. *Nucleic Acids Res.* **2011**, *39* (10), 4419-4426. DOI: 10.1093/nar/gkr015
- (79) Katiyar, C.; Gupta, A.; Kanjilal, S.; Katiyar, S. Drug discovery from plant sources: An integrated approach. *Ayu* **2012**, *33* (1), 10-19. DOI: 10.4103/0974-8520.100295
- (80) Swarup, V.; Ghosh, J.; Ghosh, S.; Saxena, A.; Basu, A. Antiviral and Anti-Inflammatory Effects of Rosmarinic Acid in an Experimental Murine Model of Japanese Encephalitis. *Antimicrob. Agents Chemother.* **2007**, *51*, 3367-3370.
- (81) Fan, W.; Qian, S.; Qian, P.; Li, X. Antiviral activity of luteolin against Japanese encephalitis virus. *Virus Res.* **2016**, *220*, 112-116. DOI: 10.1016/j.virusres.2016.04.021
- (82) Bagheri, A.; Moezzi, S. M. I.; Mosaddeghi, P.; Nadimi Parashkouhi, S.; Fazel Hoseini, S. M.; Badakhshan, F.; Negahdaripour, M. Interferon-inducer antivirals: Potential candidates to combat COVID-19. *Int. Immunopharmacol.* **2021**, *91*. DOI: 10.1016/j.intimp.2020.107245
- (83) Khudoley, V. N.; Saratikov, A. S.; Lepekhin, A. V.; Yavorskaya, V. E.; Evstropov, A. N.; Portnyagina, E. V.; Pomogaeva, A. D.; Beloborodova, E. I.; Vnushinkaia, M. A.; Schmidt, E. V. Antiviral Activity of Jodantipyrin - An Anti-Inflammatory Oral Therapeutic with Interferon-Inducing Properties. *Antiinflamm. Antiallergy Agents Med. Chem.* **2008**, *7*, 106-115.
- (84) Loeb, L. Beating the Flu: Orthodox and Commercial Responses to Influenza in Britain, 1889–1919. *Soc. Hist. Med.* **2005**, *18*, 203-224.

(85) Sedenkova, K.; Dueva, E.; Averina, E.; Grishin, Y.; Osolodkin, D.; Kozlovskaya, L.; Palyulin, V.; Savelyev, E.; Orlinson, B.; Novakov, I. Synthesis and assessment of 4-aminotetrahydroquinazoline derivatives as tick-borne encephalitis virus reproduction inhibitors. *Org. Biomol. Chem.* **2015**, *13*, 3406-3415.

(86) Dueva, E. V.; Tuchynskaya, K. K.; Kozlovskaya, L. I.; Osolodkin, D. I.; Sedenkova, K. N.; Averina, E. B.; Palyulin, V. A.; Karganova, G. G. Spectrum of antiviral activity of 4-aminopyrimidine N -oxides against a broad panel of tick-borne encephalitis virus strains. *Antivir. Chem. Chemother.* **2020**, *28*, 2040206620943462. DOI: 10.1177/2040206620943462

(87) Averina, E. B.; Samoilichenko, Y. V.; Volkova, Y. A.; Grishin, Y. K.; Rybakov, V. B.; Kutateladze, A. G.; Elyashberg, M. E.; Kuznetsova, T. S.; Zefirov, N. S. Heterocyclization of electrophilic alkenes with tetranitromethane revisited: regiochemistry and the mechanism of nitroisoxazole formation. *Tetrahedron Lett.* **2012**, *53*, 1472-1475.

(88) Averina, E. B.; Vasilenko, D. A.; Samoilichenko, Y. V.; Grishin, Y. K.; Rybakov, V. B.; Kuznetsova, T. S.; Zefirov, N. S. Chemoselective Reduction of Functionalized 5-Nitroisoxazoles: Synthesis of 5-Amino- and 5-[Hydroxy(tetrahydrofuran-2-yl)amino]isoxazoles. *Synthesis* **2014**, *46*, 1107-1113.

(89) Averina, E. B.; Vasilenko, D. A.; Gracheva, Y. A.; Grishin, Y. K.; Radchenko, E. V.; Burmistrov, V. V.; Butov, G. M.; Neganova, M. E.; Serkova, T. P.; Redkozubova, O. M.; et al. Synthesis and biological evaluation of novel 5-hydroxylaminoisoxazole derivatives as lipooxygenase inhibitors and metabolism enhancing agents. *Bioorganic Med. Chem.* **2016**, *24* (4), 712-720. DOI: 10.1016/j.bmc.2015.12.040

(90) Vasilenko, D. A.; Averina, E. B.; Zefirov, N. A.; Wobith, B.; Grishin, Y. K.; Rybakov, V. B.; Zefirova, O. N.; Kuznetsova, T. S.; Kuznetsov, S. A.; Zefirov, N. S. Synthesis and antimetabolic activity of novel 5-aminoisoxazoles bearing alkoxyaryl moieties. *Mendeleev Commun.* **2017**, *27* (3), 228-230. DOI: 10.1016/j.mencom.2017.05.003

(91) Skorobogatyi, M. V.; Malakhov, A. D.; Pchelintseva, A. A.; Turban, A. A.; Bondarev, S. L.; Korshun, V. A. Fluorescent 5-alkynyl-2'-deoxyuridines: high emission efficiency of a conjugated perylene nucleoside in a DNA duplex. *ChemBiochem* **2006**, *7* (5), 810-816. DOI: 10.1002/cbic.200600040

(92) Korshun, V. A.; Prokhorenko, I. A.; Gontarev, S. V.; Skorobogatyi, M. V.; Balakin, K. V.; Manasova, E. V.; Malakhov, A. D.; Berlin, Y. A. New Pyrene Derivatives for Fluorescent Labeling of Oligonucleotides. *Nucleosides and Nucleotides* **1997**, *16*, 1461-1464.

(93) Mireille, R. S. V.; Che, C. C.; Alexey, V. U.; Muhammad, M.; Michael, A. J.; Nicola, L. B.; Raquel, F. E.; Richard, M. E.; Stanislav, A. K.; Olga, A. V.; et al. Rigid amphipathic fusion inhibitors, small molecule antiviral compounds against enveloped viruses. *PNAS* **2010**, *107* (40), 17339-17344.

(94) Colpitts, C. C.; Ustinov, A. V.; Epand, R. F.; Epand, R. M.; Korshun, V. A.; Schang, L. M. 5-(Perylen-3-yl)Ethyne-uridine (aUY11), an Arabino-Based Rigid Amphipathic Fusion Inhibitor, Targets Virion Envelope Lipids To Inhibit Fusion of Influenza Virus, Hepatitis C Virus, and Other Enveloped Viruses. *J. Virol.* **2013**, *87*, 3640-3654.

(95) Speerstra, S.; Chistov, A. A.; Proskurin, G. V.; Aralov, A. V.; Ulashchik, E. A.; Streshnev, P. P.; Shmanai, V. V.; Korshun, V. A.; Schang, L. M. Antivirals acting on viral envelopes via biophysical mechanisms of action. *Antivir. Res.* **2018**, *149*, 164-173. DOI: 10.1016/j.antiviral.2017.11.018

- (96) Proskurin, G. V.; Orlov, A. A.; Brylev, V. A.; Kozlovskaya, L. I.; Chistov, A. A.; Karganova, G. G.; Palyulin, V. A.; Osolodkin, D. I.; Korshun, V. A.; Aralov, A. V. 3'-O-Substituted 5-(perylene-3-ylethynyl)-2'-deoxyuridines as tick-borne encephalitis virus reproduction inhibitors. *Eur. J. Med. Chem.* **2018**, *155*, 77-83. DOI: 10.1016/j.ejmech.2018.05.040
- (97) Vigant, F.; Jung, M.; Lee, B. Positive Reinforcement for Viruses. *Chemistry & Biology* **2010**, *17* (10), 1049-1051, Short Survey. DOI: 10.1016/j.chembiol.2010.10.002
- (98) Vigant, F.; Hollmann, A.; Lee, J.; Santos, N. C.; Jung, M. E.; Lee, B. The Rigid Amphipathic Fusion Inhibitor dUY11 Acts through Photosensitization of Viruses. *J. Virol.* **2014**, *88*, 1849-1853.
- (99) Aralov, A. V.; Proskurin, G. V.; Orlov, A. A.; Kozlovskaya, L. I.; Chistov, A. A.; Kutyaikov, S. V.; Karganova, G. G.; Palyulin, V. A.; Osolodkin, D. I.; Korshun, V. A. Perylenyltriazoles inhibit reproduction of enveloped viruses. *Eur. J. Med. Chem.* **2017**, *138*, 293-299. DOI: 10.1016/j.ejmech.2017.06.014
- (100) Slesarchuk, N. A.; Khvatov, E. V.; Chistov, A. A.; Proskurin, G. V.; Nikitin, T. D.; Lazarevich, A. I.; Ulanovskaya, A. A.; Ulashchik, E. A.; Orlov, A. A.; Jegorov, A. V.; et al. Simplistic perylene-related compounds as inhibitors of tick-borne encephalitis virus reproduction. *Bioorganic Med. Chem. Lett.* **2020**, *30* (10), 127100. DOI: 10.1016/j.bmcl.2020.127100
- (101) Blaising, J.; Polyak, S. J.; Pécheur, E.-I. Arbidol as a broad-spectrum antiviral: An update. *Antivir. Res.* **2014**, *107*, 84-94. DOI: 10.1016/j.antiviral.2014.04.006
- (102) Villalain, J. Membranotropic Effects of Arbidol, a Broad Anti-Viral Molecule, on Phospholipid Model Membranes. *J. Phys. Chem.* **2010**, *114*, 8544-8554.
- (103) Leneva, I. A.; Russell, R. J.; Boriskin, Y. S.; Hay, A. J. Characteristics of arbidol-resistant mutants of influenza virus: Implications for the mechanism of anti-influenza action of arbidol. *Antivir. Res.* **2009**, *81* (2), 132-140. DOI: 10.1016/j.antiviral.2008.10.009
- (104) Kadam, R. U.; Wilson, I. A. Structural basis of influenza virus fusion inhibition by the antiviral drug Arbidol. *PNAS* **2017**, *114* (2), 206-214.
- (105) Liu, Q.; Xiong, H.-r.; Lu, L.; Liu, Y.-y.; Luo, F.; Hou, W.; Yang, Z.-q. Antiviral and anti-inflammatory activity of arbidol hydrochloride in influenza A (H1N1) virus infection. *Acta pharmacologica Sinica* **2013**, *34* (8), 1075-1083. DOI: 10.1038/aps.2013.54
- (106) Jullian-Pawlicki, N.; Lequart-Pillon, M.; Huynh-Cong, L.; Lesur, D.; Cailleu, D.; Mesnard, F.; Laberche, J. C.; Gontier, E.; Boitel-Conti, M. Arylnaphthalene and aryltetralin-type lignans in hairy root cultures of *Linum perenne*, and the stereochemistry of 6-methoxy podophyllotoxin and one diastereoisomer by HPLC-MS and NMR spectroscopy. *Phytochemical analysis : PCA* **2015**, *26* (5), 310-319. DOI: 10.1002/pca.2565
- (107) Cui, Q.; Du, R.; Liu, M.; Rong, L. Lignans and Their Derivatives from Plants as Antivirals. *Molecules (Basel, Switzerland)* **2020**, *25* (1). DOI: 10.3390/molecules25010183 From EBSCOhost MEDLINE.
- (108) Lv, J.-P.; Yang, S.; Dong, J.-X.; Jin, H. New cyclopeptide alkaloids from the whole plant of *Justicia procumbens* L. *Nat. Prod. Res.* **2021**, *35* (21), 4032-4040. DOI: 10.1080/14786419.2020.1758090

- (109) Ramesh, C.; Ravindranath, N.; Ram, T. S.; Das, B. Arylnaphthalide lignans from *Cleistanthus collinus*. *Chem. Pharm. Bull.* **2003**, *51* (11), 1299-1300. DOI: 10.1248/cpb.51.1299
- (110) Sørensen, M. G.; Henriksen, K.; Neutzsky-Wulff, A. V.; Dziegiel, M. H.; Karsdal, M. A. Diphyllin, a Novel and Naturally Potent V-ATPase Inhibitor, Abrogates Acidification of the Osteoclastic Resorption Lacunae and Bone Resorption. *JBMR* **2007**, *22* (10), 1640-1648.
- (111) Shen, W.; Zou, X.; Chen, M.; Liu, P.; Shen, Y.; Huang, S.; Guo, H.; Zhang, L. Effects of diphyllin as a novel V-ATPase inhibitor on gastric adenocarcinoma. *Eur. J. Pharmacol.* **2011**, *667* (1), 330-338. DOI: 10.1016/j.ejphar.2011.05.042
- (112) Martinez-Lopez, A.; Persaud, M.; Chavez, M. P.; Zhang, H.; Rong, L.; Liu, S.; Wang, T. T.; Sarafianos, S. G.; Diaz-Griffero, F. Glycosylated diphyllin as a broad-spectrum antiviral agent against Zika virus. *EBioMedicine* **2019**, *47*, 269-283. DOI: 10.1016/j.ebiom.2019.08.060
- (113) Stefanik, M.; Strakova, P.; Haviernik, J.; Miller, A. D.; Ruzek, D.; Eyer, L. Antiviral Activity of Vacuolar ATPase Blocker Diphyllin against SARS-CoV-2. *Microorganisms* **2021**, *9* (3). DOI: 10.3390/microorganisms9030471
- (114) Eyer, L., *Manuscript in progress*.
- (115) Holoubek, J.; Bednářová, K.; Haviernik, J.; Huvarová, I.; Dvořáková, Z.; Černý, J.; Outláš, M.; Salát, J.; Konkol'ová, E.; Boura, E.; et al. Guanine quadruplexes in the RNA genome of the tick-borne encephalitis virus: their role as a new antiviral target and in virus biology. *Nucleic Acids. Res.* **2022**, *50* (8), 4574-4600. DOI: 10.1093/nar/gkac225.

Figures.

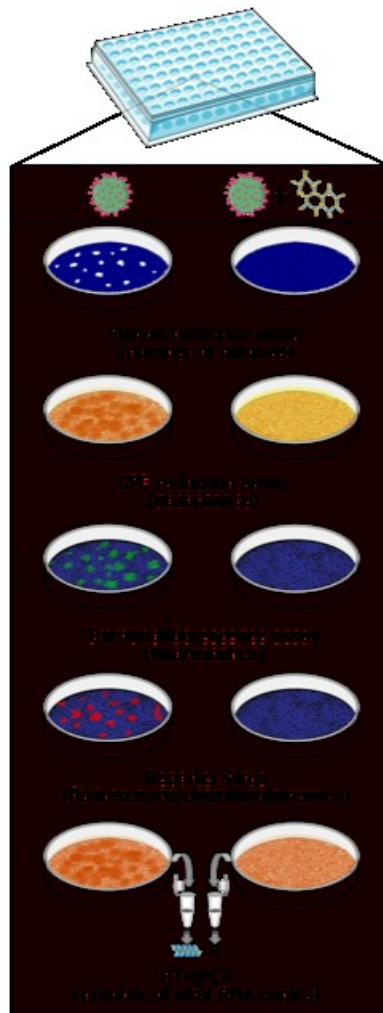


Figure 1. Schematic representation of in vitro methods commonly used to evaluate the antiviral efficacy of small molecule-based viral inhibitors. The left column represents a virus-infected cell culture (control cells), while the right column shows virus-infected cells treated with an antiviral agent.

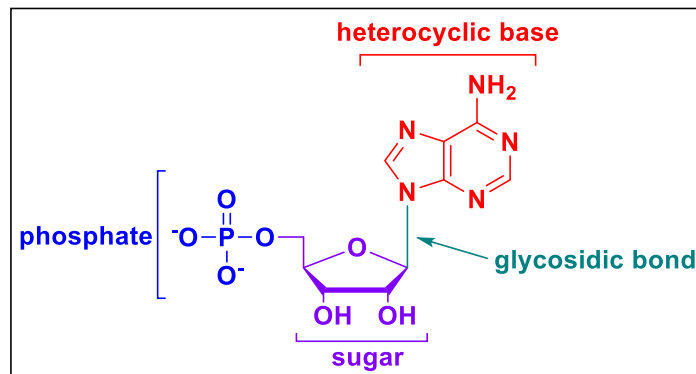


Figure 2. Basic structure of a nucleos(t)ide.

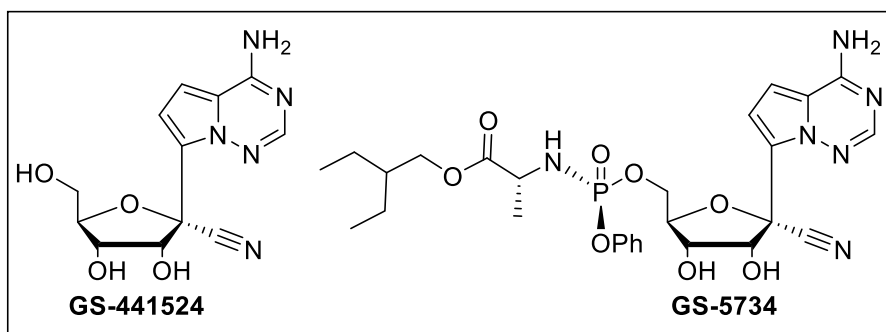


Figure 3. Structures of the 1'-modified, C-nucleoside, GS-441524 and its prodrug GS-5734.

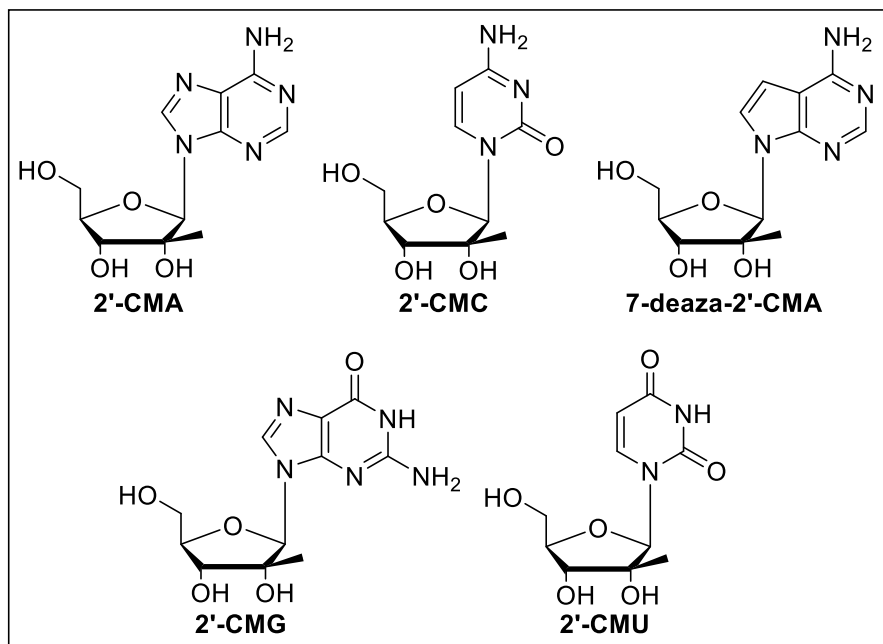


Figure 4. Structures of the 2'-C-methyl modified nucleosides.

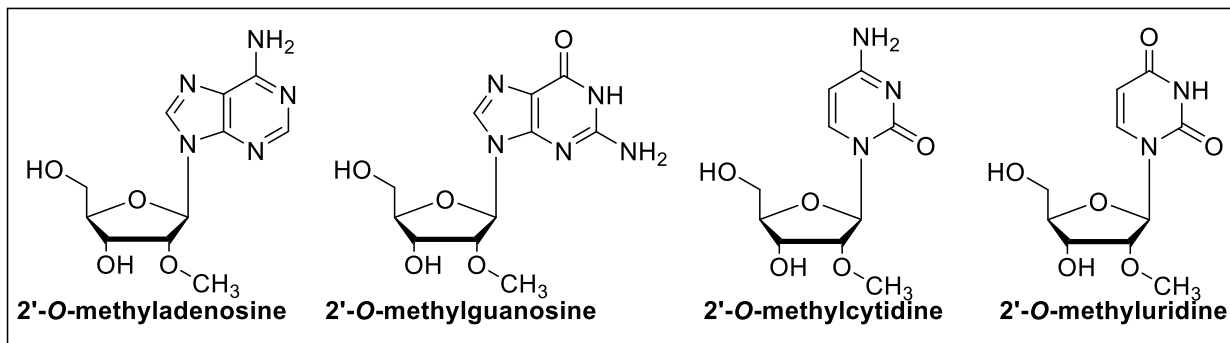


Figure 5. Structures of various 2'-*O*-methyl nucleoside analogues tested for antiviral activity by Eyer et al.

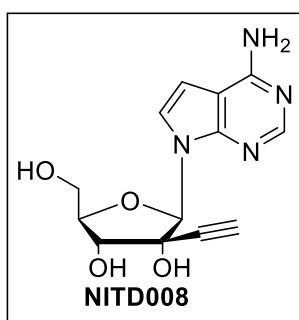


Figure 6. Structure of the 2'-modified nucleoside analogue NITD008.

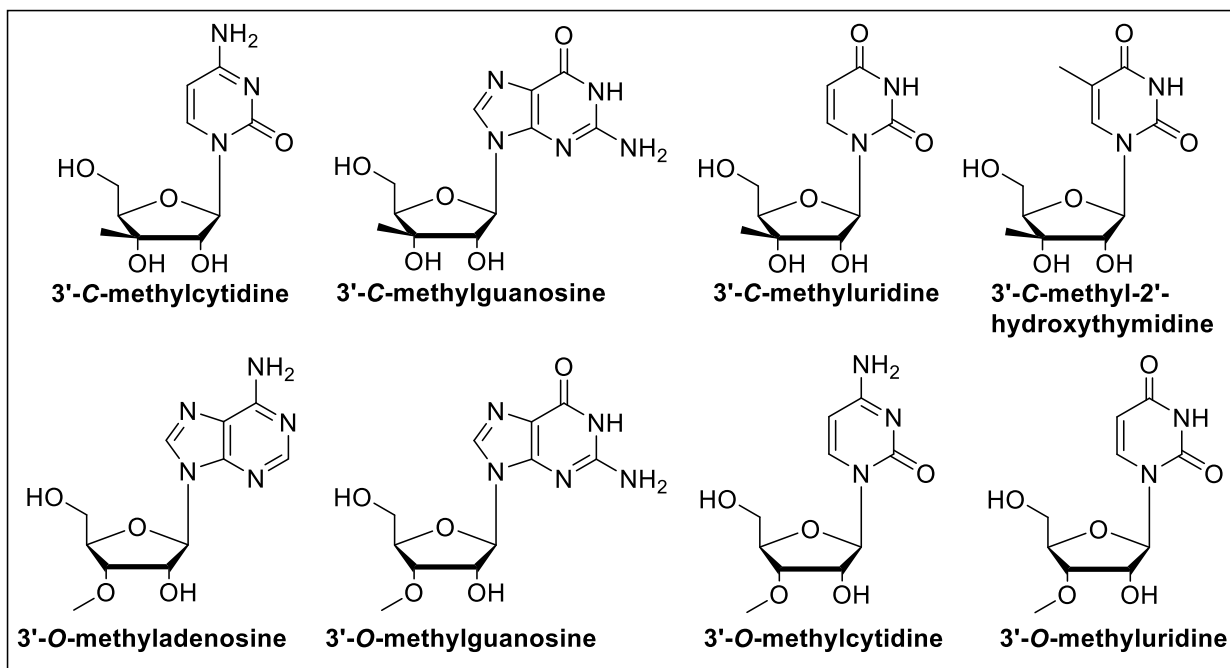


Figure 7. Structures of various C3' and O3' modified nucleoside analogues.

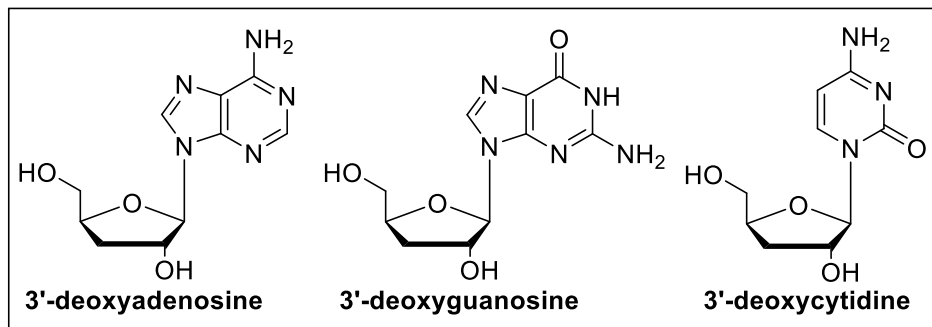


Figure 8. Structures of 3'-deoxy nucleoside analogues tested by Eyer et al for anti-TBEV activity.

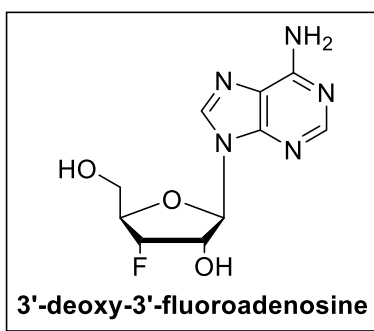


Figure 9. Structure of the 3'- modified nucleoside, 3'-deoxy-3'-fluoroadenosine.

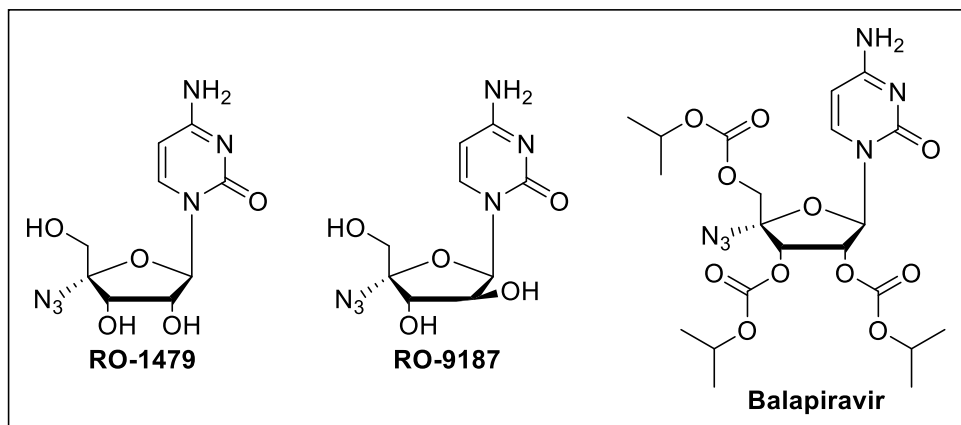


Figure 10. Structures of the 4'-azido nucleoside analogues tested for anti-TBEV activity by Eyer et al.

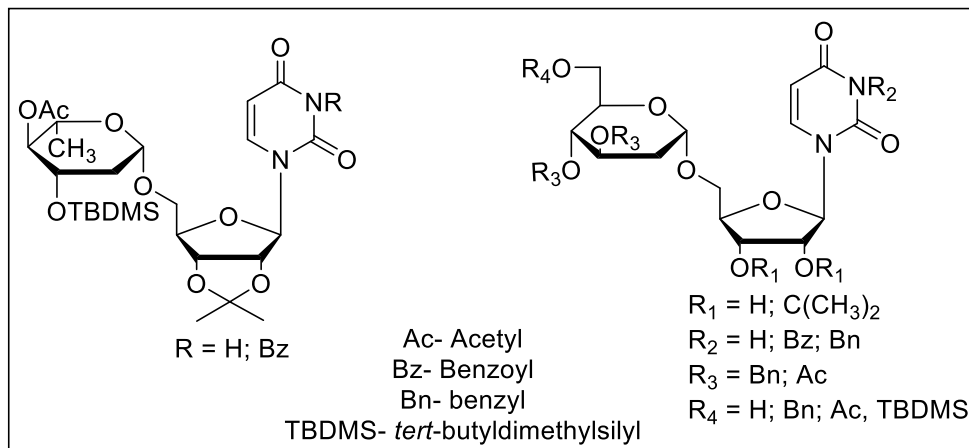


Figure 11. Structures of the 2'-deoxy uridine derivatives tested against TBEV.

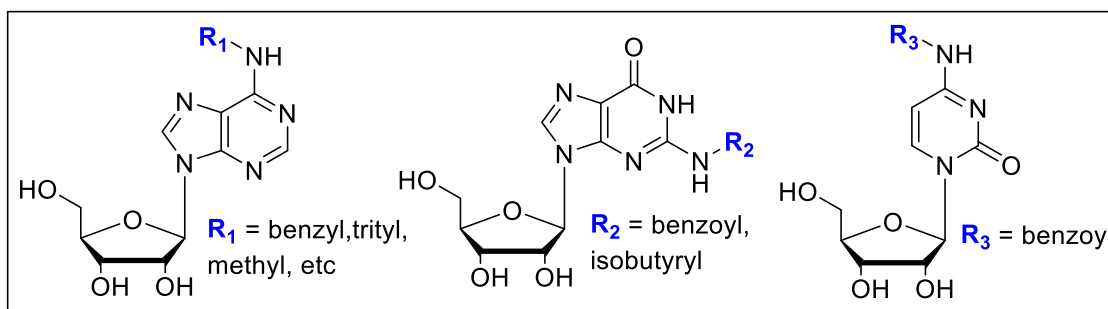


Figure 12. Various locations and types of modifications made on the nucleoside nucleobase in the SAR study conducted by Orlov et al.

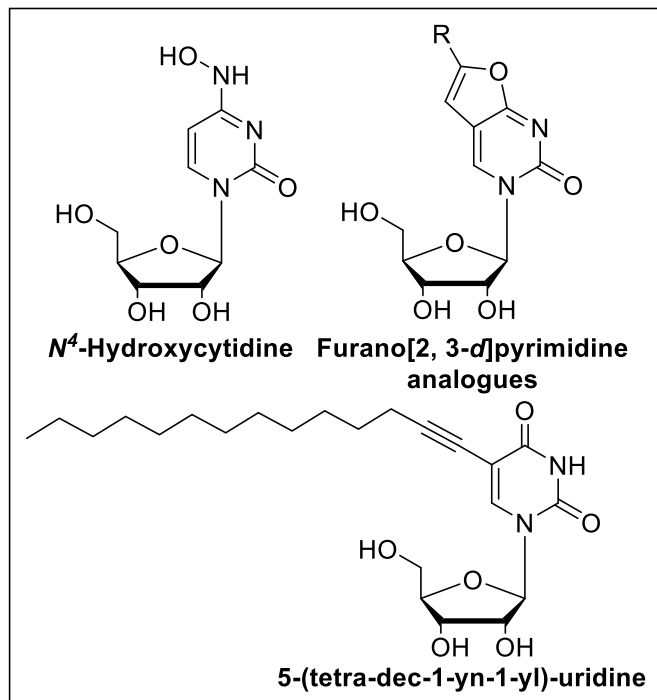


Figure 13. Structure of various nucleoside analogues tested for anti-TBEV activity by Kozlovskaya et. al.

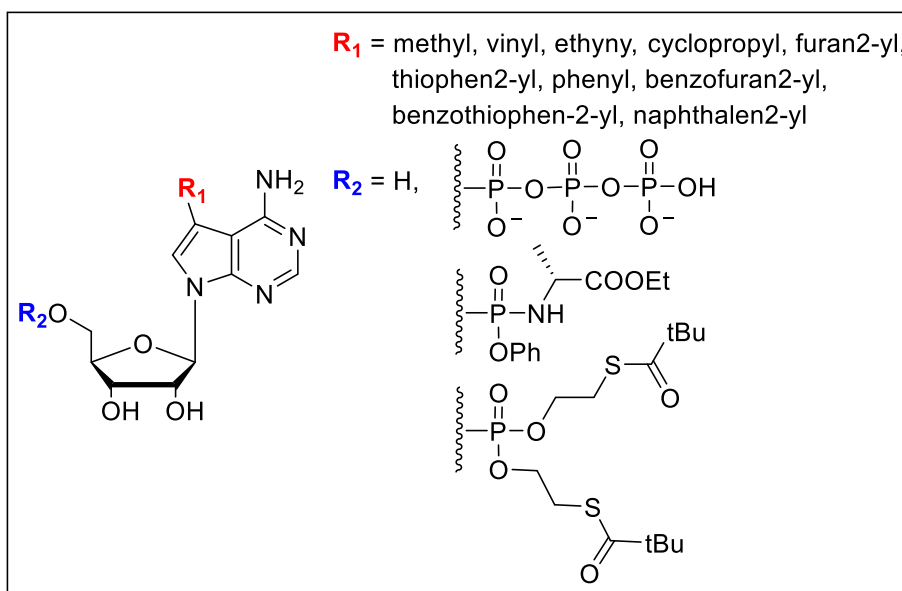


Figure 14. Structure of modified 7-deazaadenine nucleosides synthesized and tested against TBEV by Konkolová et. al.

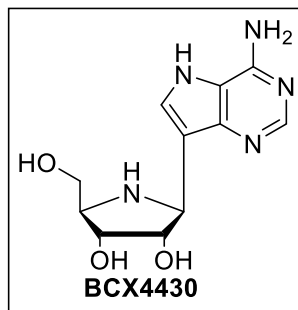


Figure 15. Structure of imino C-nucleoside, BCX4430.

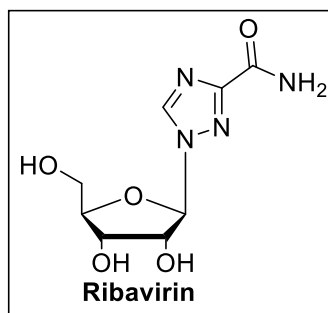


Figure 16. Structure of the triazole nucleoside, Ribavirin.

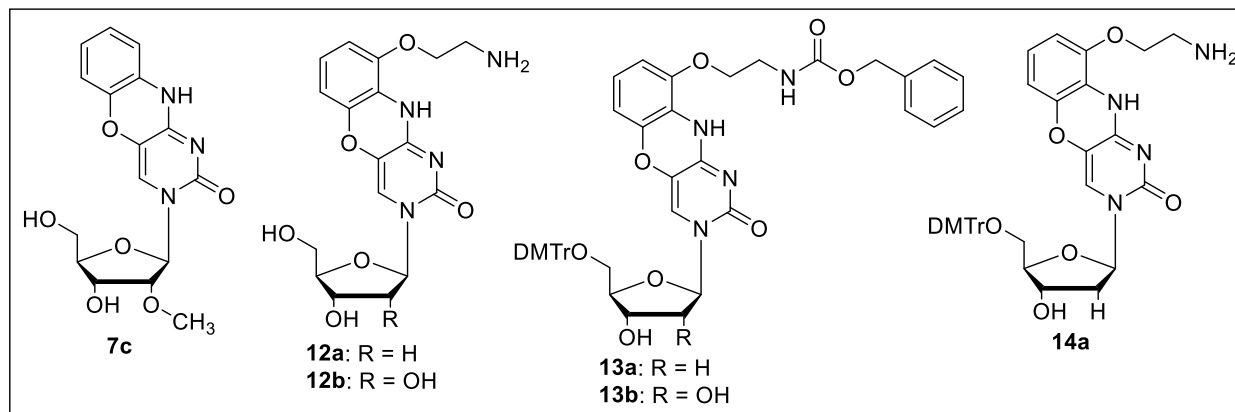


Figure 17. Structures of the various phenoxazine nucleoside derivatives tested against TBEV.

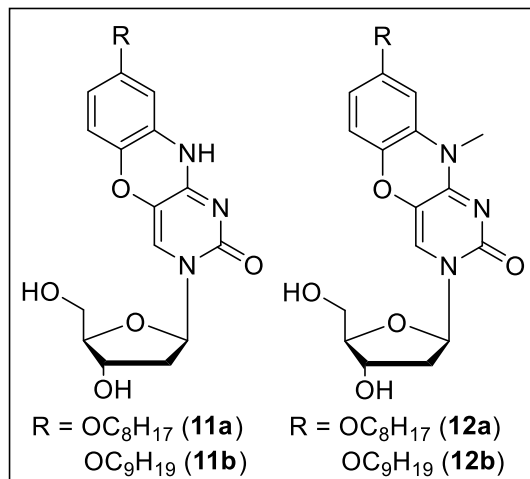


Figure 18. Structures of the other phenoxazine nucleoside derivatives tested against TBEV.

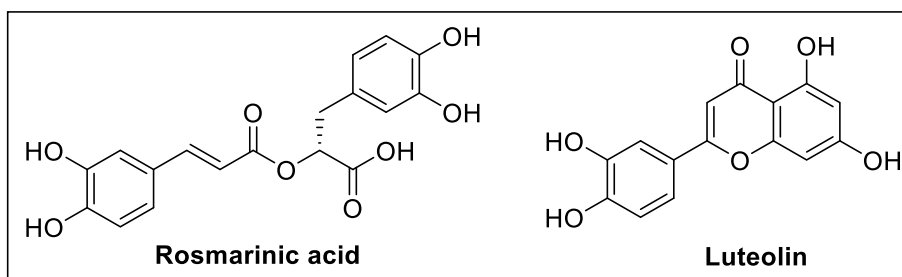


Figure 19. Structures of the antiviral compounds, rosmarinic acid and luteolin, that comprise the natural extract luromarin.

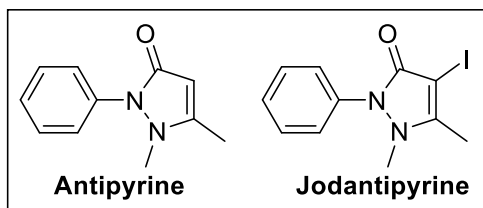


Figure 20. Structures of non-nucleoside small molecule interferon inducers antipyrine and its iodinated counterpart, jodantipyrine.

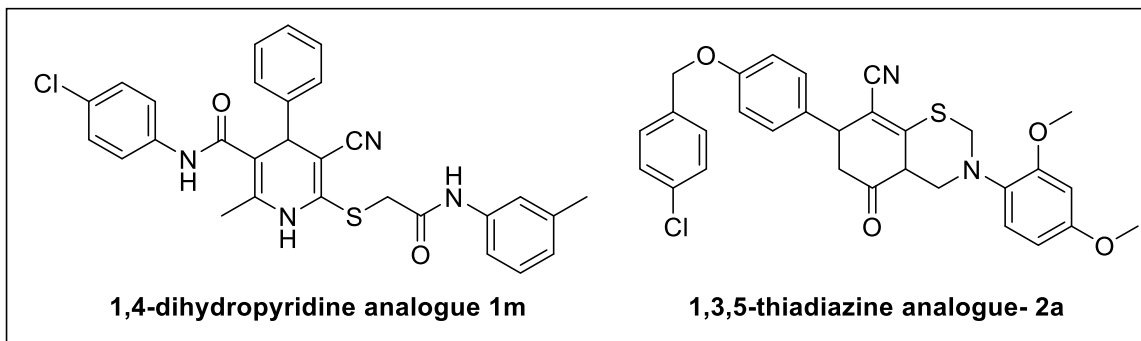


Figure 21. Structures of the most active 1,4-dihydropyridine (**1m**) and pyrido[2,1-b][1,3,5]-thiadiazine (**2a**) in the study conducted by Osolodkin et al.

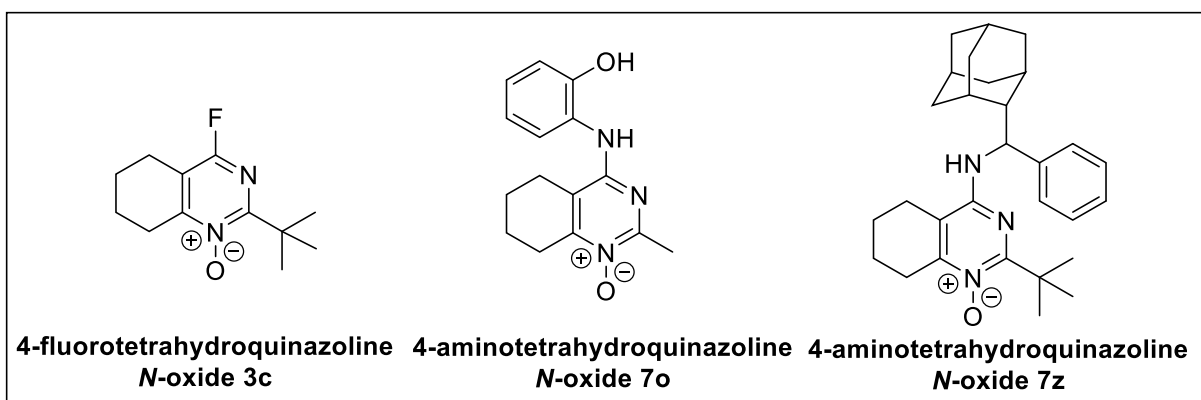


Figure 22. Structure of compound **3c** used to synthesize 4-aminotetrahydroquinazoline derivatives, including the most active compounds **7o** and **7z** synthesized by Sedenkova et al.

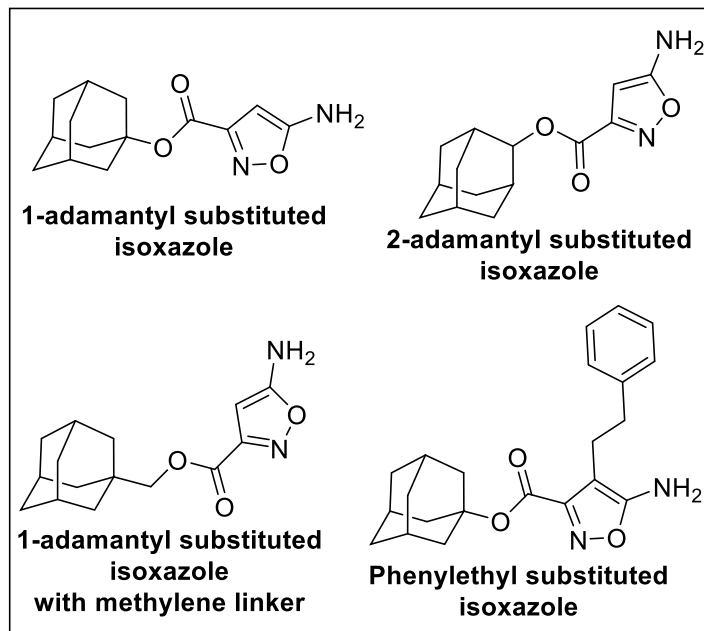


Figure 23. Structures of various substituted isoxazole analogues synthesized by Vasilenko et al.

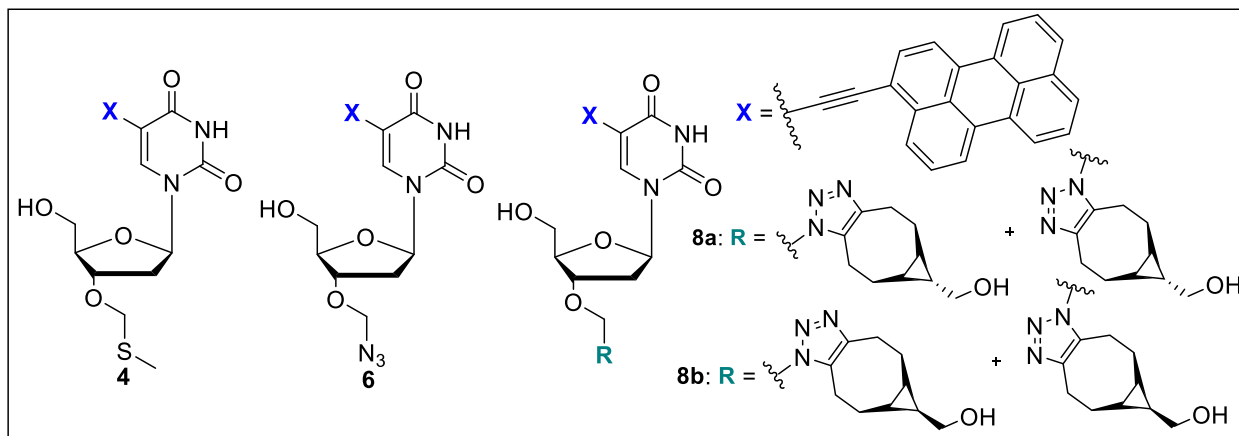


Figure 24. Structures of various substituted dUY11 analogues **4**, **6**, **8a**, **8b** synthesized by Proskurin et al.

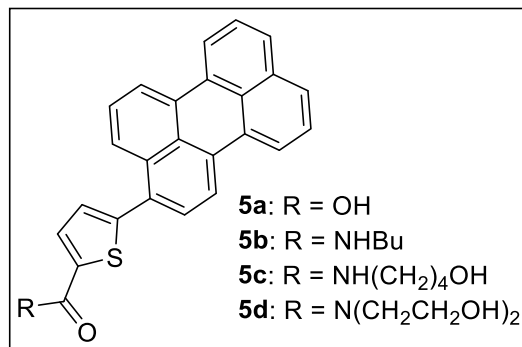


Figure 25. Structure of the polycyclic perylene derivatives synthesized by Slesarchuk et al.

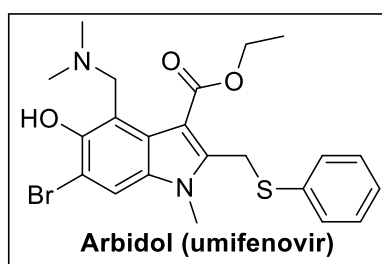


Figure 26. Structure of the antiviral non-nucleoside compound, arbidol.

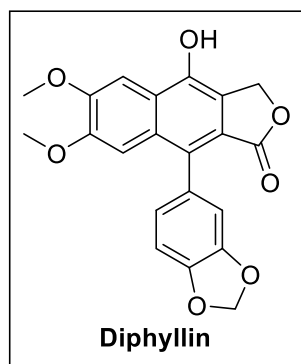


Figure 27. Structure of the broad-spectrum antiviral compound, diphyllin.

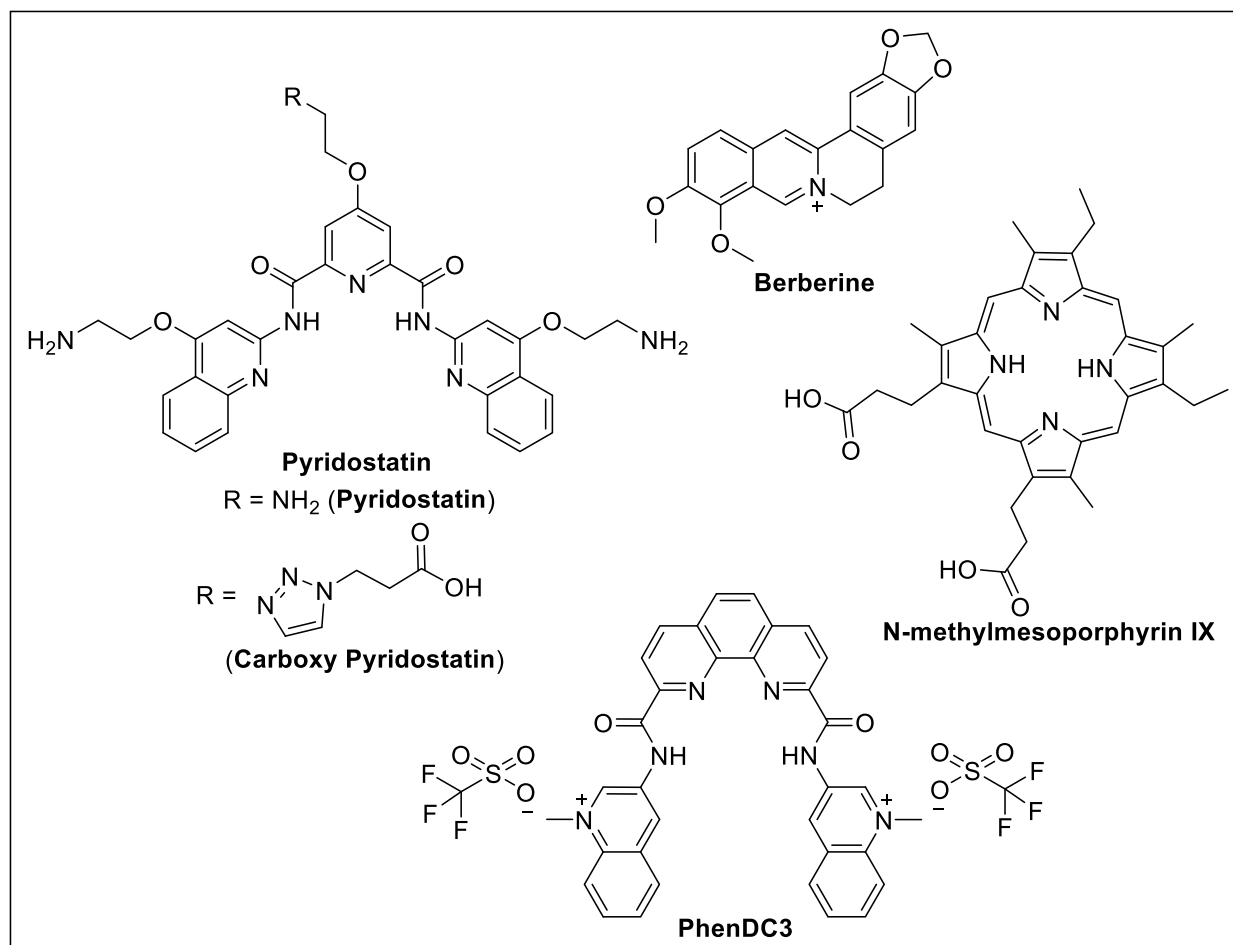


Figure 28. Structure of the G4 quadruplex ligands.

Antiviral agents targeting the influenza virus: a review and publication analysis

L. EYER, K. HRUSKA

Veterinary Research Institute, Brno, Czech Republic

ABSTRACT: Influenza is a serious infectious disease, which is life-threatening especially in children, seniors and immunocompromised patients. In addition to vaccination, the development of new anti-influenza agents represents a crucial defence strategy to combat seasonal and pandemic influenza strains. At present most attention is paid to the development of inhibitors of influenza neuraminidase, which has been established as a key drug target for the prophylaxis and treatment of influenza infections. However, the emergence of drug-resistant influenza variants highlights the need of continuously innovative strategies for the development of new drugs with improved antiviral effects, higher safety and increased tolerability. In this review article, an analysis of publications describing anti-influenza agents indexed in the Web of Science® database has been carried out. The most important publications are presented in tables and are characterised by several key words, abstracts and references. The presented publications have been sorted according to five basic criteria: (i) review articles, (ii) design, synthesis and evaluation of new anti-influenza drugs, (iii) major classes of anti-influenza drugs, (iv) combination therapy of influenza infections and (v) influenza drug resistance. The design of this review article allows us to offer a complex overview of known antiviral agents targeting influenza viruses, facilitates easy and rapid orientation in numerous publications written on this subject, and aids the gathering of required data.

Keywords: influenza; virus; antiviral; agents; drug; resistance; therapy; structure-based drug design

Contents

1. Introduction

1.1. Database used as the source of information

Table 1.1. Analysis of publications: search profiles and numbers of results retrieved

1.2. Basic analysis of publications on antiviral agents targeting the influenza virus

Figure 1. The number of publications on anti-influenza agents during the period from 1990 to 2012

Table 1.2. Analysis of publications: TopTen authors, institutions and countries according to the number of published papers (Web of Science®, publications in total 14 458)

2. Review articles

Table 2. Review articles

3. Design, synthesis and evaluation of new anti-influenza drugs

Table 3. Design, synthesis and evaluation of new anti-influenza drugs

4. Major classes of anti-influenza drugs

Figure 2. Life-cycle of the influenza virus (according to Beigel and Bray 2008)

Figure 3. Structure of the influenza virus (according to Ludwig et al. 2003)

Figure 4. Chemical structures of the most important anti-influenza drugs

4.1. Inhibitors of haemagglutinin

Table 4.1. Inhibitors of haemagglutinin

Supported by the Ministry of Education, Youth and Sports, Czech Republic (AdmireVet; Grant No. CZ 1.05/2.1.00/01.0006-ED 0006/01/01) and the Ministry of Agriculture of the Czech Republic (Grant No. MZe 0002716202).

- 4.2. M2 ion channel blockers
Table 4.2. M2 ion channel blockers
- 4.3. Inhibitors of viral RNA polymerase
Table 4.3. Inhibitors of viral RNA polymerase
- 4.4. Inhibitors of neuraminidase
Table 4.4. Inhibitors of neuraminidase
- 4.5. Host cell factor targeting
Table 4.5. Host cell factor targeting
- 4.6. Other anti-influenza agents
Table 4.6. Other anti-influenza agents
- 5. Combination therapy of influenza infections
Table 5. Combination therapy of influenza infections
- 6. Influenza drug resistance
Table 6. Influenza drug resistance
- 7. Acknowledgement
- 8. References

1. INTRODUCTION

Influenza is considered to be one of the life-threatening infectious diseases. In some countries seasonal influenza affects annually up to 40% of the population and 500 million people die from it worldwide every year. New highly-virulent influenza strains can arise unexpectedly to cause world-wide pandemics with markedly increased morbidity and mortality, such as the “avian flu” in 1997 and “swine flu” in 2009. At present, the development of antiviral drugs represents a crucial strategy in the control and prevention of seasonal and pandemic influenza infections. Antiviral drugs can overcome the limitations of vaccination strategies, such as the time-consuming vaccine design, insufficient protection for immunocompromised patients and the unpredictable antigenic changes in influenza strains which render vaccination ineffective. In general, the anti-influenza agents can be divided into two basic groups, i.e., synthetic analogues of biomolecules required during virus infection and substances derived from natural plant extracts. With regard to the considerable genetic and antigenic variability of the influenza virus, research has been predominantly focused on broad-spectrum antiviral drugs, which are effective against a large variety of influenza strains. The development of antivirals targeting host-cell proteins, which play an important role in viral replication, has also gathered pace recently. Moreover, combination therapy based on the application of two or more different antivirals represents a promising approach to combat influenza infections.

The aim of this review is to offer an overview of known antiviral agents targeting influenza viruses and to discuss their characteristic properties, modes of action and advantages or limitations of their therapeutic use. Publications which contain key information concerning the issues of anti-influenza agents are in this review presented in tables and characterised with descriptive words, full or shortened abstracts and relevant references. The text in the tables contains several format imperfections, which exist in the Web of Science® database and are caused by transmission and copying of data between various information sources. The loss of cursive typeface in Latin names in titles of references and in abstracts is such an example. The presented publications have been classified according to five basic criteria: (i) review articles, (ii) design, synthesis and evaluation of new anti-influenza drugs, (iii) major classes of anti-influenza drugs, (iv) combination therapy of influenza infections and (v) influenza drug resistance. This review article should facilitate orientation in numerous publications dealing with anti-influenza drugs and enable rapid and easy search for specific data, information and protocols. The previous reviews in this format have been well received (Vass et al. 2008; Eyer and Hruska 2012; Hruska and Kaevska 2012; Hruska and Franek 2012).

1.1. Database used as the source of information

The publications were retrieved from the Web of Science® database using the general search profile:

Table 1.1. Analysis of publications: search profiles and numbers of results retrieved

Timespan	All years	2010–2012
General search profile		
Topic=(influenza OR flu) AND (antivir* OR virostatic* OR drug* OR “anti-influenza” OR “anti-flu” OR inhibit*)		
Results	14 458	4 673
Review articles cited in Table 2	17	
Design, synthesis and evaluation of new anti-influenza drugs		
Topic=(influenza OR flu) AND (antivir* OR virostatic* OR drug* OR “anti-influenza” OR “anti-flu” OR inhibit*) AND (design OR synthesis OR evaluation)		
Results	3083	1048
Cited in Table 3	19	
Haemagglutinin inhibitors		
Topic=(influenza OR flu) AND (antivir* OR virostatic* OR drug* OR “anti-influenza” OR “anti-flu” OR inhibit*) AND (hemagglutinin OR haemagglutinin)		
Results	2616	742
Cited in Table 4.1	18	
M2 ion channel blockers		
Topic=(influenza OR flu) AND (antivir* OR virostatic* OR drug* OR “anti-influenza” OR “anti-flu” OR inhibit*) AND (adamantane* OR amantadine OR rimantadine)		
Results	897	249
Cited in Table 4.2	15	
Inhibitors of viral RNA polymerase		
Topic=(influenza OR flu) AND (antivir* OR virostatic* OR drug* OR “anti-influenza” OR “anti-flu” OR inhibit*) AND polymerase*		
Results	824	344
Cited in Table 4.3	22	
Inhibitors of neuraminidase		
Topic=(influenza OR flu) AND (antivir* OR virostatic* OR drug* OR “anti-influenza” OR “anti-flu” OR inhibit*) AND neuraminidase*		
Results	2658	930
Cited in Table 4.4	21	
Host cell factor targeting		
Topic=(influenza OR flu) AND (antivir* OR virostatic* OR drug* OR “anti-influenza” OR “anti-flu” OR inhibit*) AND (“host factor*” OR “host protein”*)		
Results	43	22
Cited in Table 4.5	14	
Other anti-influenza agents		
Topic=(influenza OR flu) AND (antivir* OR virostatic* OR drug* OR “anti-influenza” OR “anti-flu” OR inhibit*) AND (nucleoprotein* OR “non-structural protein” OR siRNA* OR plant* OR herbal* OR antibod*)		
Results	3899	1382
Cited in Table 4.6	16	
Combination therapy of influenza infections		
Topic=(influenza OR flu) AND (antivir* OR virostatic* OR drug* OR “anti-influenza” OR “anti-flu” OR inhibit*) AND “combination therapy”		
Results	102	38
Cited in Table 5	11	
Influenza drug resistance		
Topic=(influenza OR flu) AND (antivir* OR virostatic* OR drug* OR “anti-influenza” OR “anti-flu” OR inhibit*) AND resistance		
Results	1757	700
Cited in Table 6	19	

Topic = (influenza OR flu) AND (antivir* OR virostatic* OR drug* OR “anti-influenza” OR “anti-flu” OR inhibit*), Timespan = all years. A total of 14 458 publications were obtained, demonstrating the huge number of papers on the subject published during the period from 1945 to 2012. To ease orientation through the numerous publications, the results were subsequently refined using more specific search profiles as described in Table 1.1. A selection of the most important publications has been based on reading abstracts and hundreds of available full papers.

1.2. Basic analysis of publications on antiviral agents targeting the influenza virus

The Web of Science® utilities were employed for search result analysis. Regarding the high number of retrieved publications, attention has been predominantly paid to papers published in the period 2010 to 2012; however, some older key papers are also included in the tables. As is evident from Figure 1, publication activity on the topic has continuously increased since the early 1990s. In the last three years, 4673 papers were published, with 1529 papers in 2012. The oldest papers were published in the late 1940s and describe the research on the first influenza haemagglutinin inhibitors in pigs. In 1960s, the antiviral effects of the first ion channel blockers were reported. The latest publications are focused on computer-aided structure-based design of new neuraminidase and viral polymerase inhibitors to combat pandemic influenza strains. Of all the published papers, original research articles prevail (82.7%). Our analysis shows that 2938 institutions from 112 countries are concerned with the

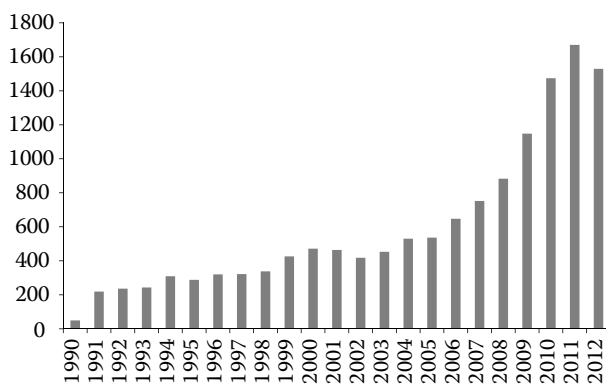


Figure 1. The number of publications on anti-influenza agents during the period from 1990 to 2012

Table 1.2. Analysis of publications: TopTen authors, institutions and countries according to the number of published papers (Web of Science®, publications in total 14 458)

Item	Number of publications
Authors (12 596 in total)	
Garcia-Sastre A	156
Webster RG	112
Suzuki Y	103
Hayden FG	95
Kawaoka Y	85
Gubareva LV	74
Suzuki T	66
Palese P	62
Kochs G	61
Li Y	61
Institutions (2938 in total)	
Centers for Disease Control and Prevention	307
Harvard University	197
Chinese Academy of Sciences	175
Icahn School of Medicine at Mount Sinai, New York	165
National Institute of Allergy and Infectious Diseases	164
University of Virginia	155
University of Wisconsin	150
University of Washington	149
University of Oxford	133
Emory University	125
Countries (112 in total)	
USA	5695
Japan	1344
England	1169
People's Republic of China	1097
Germany	963
Canada	710
France	653
Australia	637
Italy	561
Netherlands	484

subject of antiviral agents targeting the influenza virus. The authors, institutions and countries which show the highest publication activities (TopTen) are listed in Table 1.2.

2. Review articles

Review articles represent 9.2% of all publications retrieved from the Web of Science® database using the above mentioned search profile. In Table 2, seventeen key review articles are presented and characterised with a few descriptive words (left column), abstract (in the middle), and source reference (right column). These papers offer overall reviews on all important topics, especially regarding structure-based drug design techniques (Du et al. 2012), chemical synthesis of antiviral drugs (Gong and Xu 2008; Marra et al. 2008), biochemical and cell-based antiviral screen assays (Tisdale 2000; Atkins et al. 2012), animal models for study of influenza virus inhibitors (Sidwell and Smees 2000), structure, chemical properties and modes of action of the major groups of anti-influenza drugs (Gong et al. 2009; Chintakrindi et al. 2012; Grienke et al. 2012), influenza virus-neutralising antibodies (Martinez et al. 2009), natural products with antiviral activity (Grienke et al. 2012), combination therapy of influenza infections (Kaihatsu and Barnard 2012) and mechanisms of influenza drug resistance (Pizzorno et al. 2011). All the topics are also discussed in detail in the original papers presented in Tables 3 to 6.

3. Design, synthesis and evaluation of new anti-influenza drugs

The first anti-influenza drugs were usually identified using large-scale screening methods or by chance and their chemical structure and modes of action were not completely understood (Davies et al. 1964). In contrast, the current development of new antivirals is based on detailed knowledge of the X-ray crystallography-derived structure of influenza proteins as drug targets. Such an inventive process of finding new drugs, which is termed structure-based drug design, involves the development of organic molecules or macromolecular scaffolds that are complementary in shape and charge to potential ligand-binding pockets of the viral target protein (Kim et al. 1997; Lv et al. 2011).

The designed structures that are predicted to show high affinity to the viral target are then synthesised using various chemical procedures (Shie et al. 2011; Rawat et al. 2012) and their anti-influenza effects are evaluated using standardised *in vitro* screening methods. These methods include biochemical assays (Hung et al. 2012) and cell-based antiviral screens (Schmidtke et al. 2001), such as the plaque reduction assay to monitor viral replication efficiency, dye-uptake assays for measuring virus cytopathic effect, and yield-reduction assays for quantification of specific virus antigens. Through the combination of bioinformatic approaches, applicative robotics and miniaturisation strategies, most of these techniques can be adapted to high-throughput screen formats, which are applicable for testing large drug libraries containing millions of unique chemical structures (Dai et al. 2012). As an alternative to experimental screening methods, virtual (computational) screening can be used to select the desired chemical structure from large molecular databases (Yamada et al. 2012).

Besides *in vitro* tests, potential influenza virus inhibitors are further studied using animal models, such as the ferret, laboratory mouse, and chicken (Yoshimoto et al. 2000; Sauerbrei et al. 2006). Such *in vivo* studies play a crucial role in the preclinical evaluation of new drugs. The final step in the development of new medications is represented by clinical trials, which focus particularly on clinical pharmacokinetic studies and evaluation of antiviral efficacy, safety and tolerability in human volunteers (He et al. 1999; Cao et al. 2012). For key publications describing the design, synthesis and evaluation of anti-influenza drugs see Table 3.

4. Major classes of anti-influenza drugs

The anti-influenza drugs are usually classified according to their target in the viral life-cycle, which is schematically depicted in Figure 2. Such antiviral molecules are particularly used as inhibitors of the following processes: attachment of the virus to host cell receptors, endocytosis and fusion of viral and cell membranes, replication and transcription of the viral genome, synthesis of viral proteins, assembly of the viral progeny and release of the new virions into the outside environment. The following paragraphs are focused on the description of basic classes of influenza virus inhibitors.

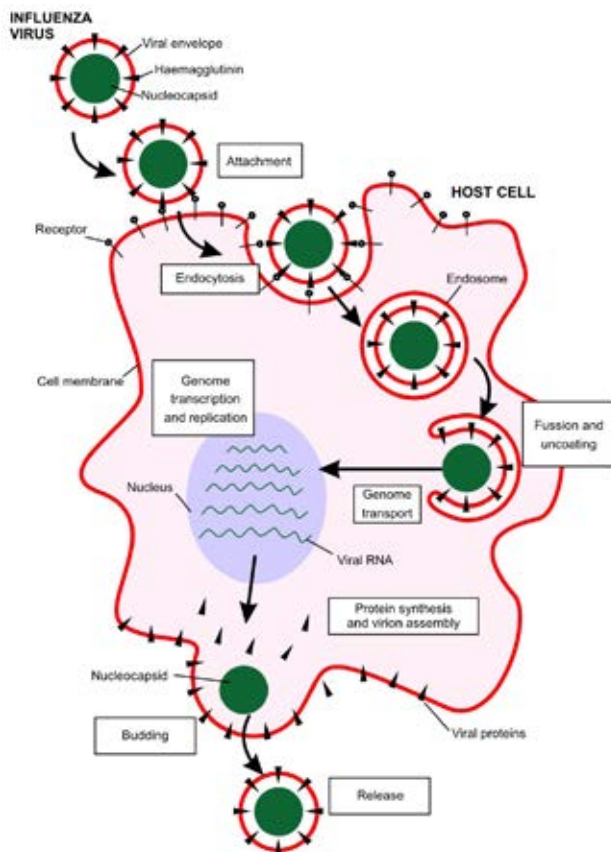


Figure 2. Life-cycle of the influenza virus (according to Beigel and Bray 2008)

4.1. Inhibitors of haemagglutinin

Haemagglutinin is a trimeric rod-shaped glycoprotein located on the surface of influenza virions (Figure 3). During the initial step of infection, haemagglutinin molecules bind specifically to host cell sialic acid receptors and enable entry of the virus into the cell cytoplasm by fusion of viral and cell membranes (Skehel and Wiley 2000). The binding interaction of haemagglutinin with cellular receptors can be efficiently inhibited by synthetic macromolecules composed of multiple sialic acid residues conjugated to glycan, glycopeptide or polyacrylamide backbones (Sigal et al. 1996; Feng et al. 2010; Narla and Sun 2012). Such therapeutic constructs have been observed to exhibit higher antiviral effects than monovalent sialic acid analogues. Haemagglutinin-mediated membrane fusion has been successfully blocked by a large variety of small organic compounds, e.g. quinones (Larson et al. 2012), the antibiotic stachyflin produced by *Stachybotrys* sp. (Yoshimoto et al. 1999) and derivatives of benzamide and podocarpic acid (Luo

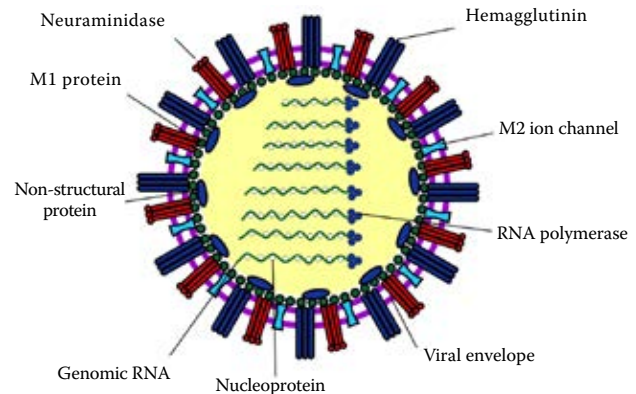


Figure 3. Structure of the influenza virus (according to Ludwig et al. 2003)

et al. 1997; Staschke et al. 1998). Although these structures show significant anti-influenza potency *in vitro*, most of them are characterised by strong strain specificity and apparent cytotoxicity.

The sialidase fusion protein DAS181 is an entirely novel broad-spectrum haemagglutinin inhibitor that enzymatically removes sialic acid receptors from respiratory epithelium cells, preventing virus attachment (Malakhov et al. 2006). This new antiviral is active against both A and B influenza strains at nanomolar concentrations, causing minimal cytopathic effects. This substance is at present being tested in phase II human trials (Moss et al. 2012). Recently, research has also focused on fusion-inhibitory peptides (Lee et al. 2011), and anti-haemagglutinin RNA aptamers (Park et al. 2011). Eighteen key publications concerning influenza haemagglutinin inhibitors are presented in Table 4.1.

4.2. M2 ion channel blockers

M2 ion channel is a transmembrane viral protein (Figure 3) that mediates the selective transport of protons into the interior of the influenza virion. Conductance of protons acidifies the internal space of the viral particle and facilitates the haemagglutinin-mediated membrane fusion which in turn results in the uncoating of the influenza nucleocapsid and import of the viral genome into the nucleus (Schnell and Chou 2008). Adamantanes are potent M2 channel blockers, which are known as the first synthetic anti-influenza drugs described in the mid-1960s (Davies et al. 1964). Two adamantane derivatives, amantadine and rimantadine

(Figure 4), have been licensed for influenza control and are commercially available under the trademarks Symmetrel® and Flumadine®, respectively (Galvao et al. 2012). The adamantanes are relatively cheap, highly stable in storage and show strong anti-influenza activity at micromolar concentrations. At present, the application of adamantanes for prevention and treatment of influenza infections is, however, not recommended because of the rapid emergence of drug-resistant virus variants that retain full virulence and transmissibility (Bright et al. 2005; Barr et al. 2008). Moreover, serious gastrointestinal and neurological side effects were observed in patients undergoing adamantane therapy (Galvao et al. 2012). Another disadvantage of adamantanes is their strong specificity against influenza A strains only (Rosenberg and Casarotto 2010). Selected publications describing the structure, chemical properties and application of adamantanes, adamantane-derivatives and other M2 ion channel blockers are presented in Table 4.2.

4.3. Inhibitors of viral RNA polymerase

Transcription and replication of the influenza virus genome is carried out by the influenza RNA polymerase holoenzyme, which is characterised by two catalytic activities. Polymerase activity is

needed for the elongation of nascent RNA chains, whereas endonuclease activity is essential for cleavage of the 5'-capped primer sequence of the host mRNA. The cap is the terminal 7-methylguanosin bound through a triphosphate group to the host mRNA. This "cap snatching" process is needed for the initiation of viral RNA transcription (Lv et al. 2011). Influenza RNA polymerase is an extremely suitable target for the development of new broad-specific antivirals because of its highly conserved structure among influenza strains. It is thought that the influenza polymerase plays a crucial role in virus adaptation to human-to-human transmission and, consequently, in the formation of pandemic influenza variants (Miotto et al. 2008; Boivin et al. 2010; Aggarwal et al. 2011; Ping et al. 2011).

Two basic classes of RNA polymerase inhibitors have been described based on different mechanisms of action. The first group is represented by nucleoside analogues for the blocking of viral RNA chain elongation (Tisdale et al. 1995). A typical member of this group is favipiravir (T-705, Figure 4), which is an inhibitor of influenza A, B and C strains, including variants resistant to amantadine or oseltamivir. This compound is currently in the stage of clinical testing (Furuta et al. 2005). Other nucleoside analogs with anti-influenza activity include ribavirin (Virazole®)

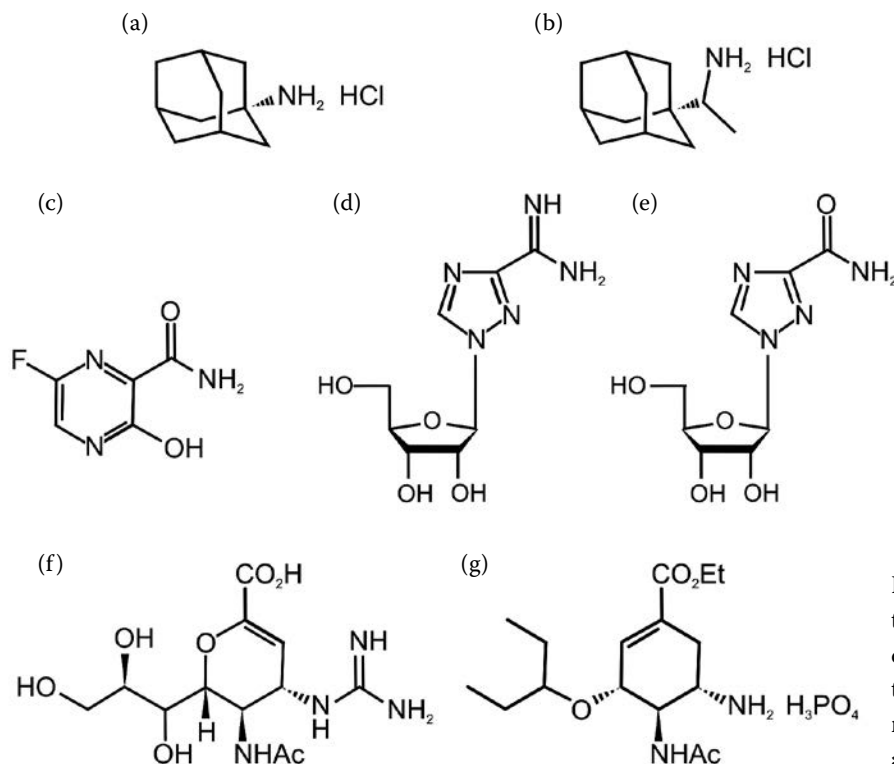


Figure 4. Chemical structures of the most important anti-influenza drugs; (a) amantadine, (b) rimantadine, (c) favipiravir (T-705), (d) ribavirin, (e) viramidine, (f) zanamivir, (g) oseltamivir

and its derivative viramidine, originally licensed for treatment of hepatitis C infections (Figure 4). Their application is, however, sometimes connected with the development of haemolytic anaemia (Sidwell et al. 2005). The second class of antiviral molecules targeting the influenza polymerase is represented by compounds which block the endonuclease and cap-binding domains of the polymerase holoenzyme. These antivirals include cap analogues (Lv et al. 2011), short capped oligonucleotides (Tado et al. 2001), and small organic compounds, such as 4-substitued 2,4-phenylbutanoic acid (Hastings et al. 1996) and flutimide isolated from the fungus *Delitschia confertaspora* (Tomassini et al. 1996). For the representative publications concerning viral RNA polymerase inhibitors, see Table 4.3.

4.4. Inhibitors of neuraminidase

Neuraminidase, also referred to as sialidase, is an antigenic glycoprotein anchored in the surface envelope of the influenza virions, which hydrolytically cleaves the terminal sialic acid from the host cell receptors (Figure 3). Thus, it plays a crucial role in the release of viral progeny from the membranes of infected cells, prevents self-aggregation of virions and facilitates the movement of the infectious viral particles in the mucus of the respiratory epithelia (Matrosovich et al. 2004; Suzuki et al. 2005). Influenza neuraminidase has been established as a key drug target for the prophylaxis and treatment of influenza infections, predominantly for the following reasons: Firstly, the structure of the influenza neuraminidase active site is highly conserved between influenza A and B strains, making neuraminidase an attractive target for the development of broad-spectrum inhibitors (Yen et al. 2006). Secondly, resistance to neuraminidase inhibitors develops less commonly than to other anti-influenza drugs. Nevertheless, the intensive application of neuraminidase inhibitors for influenza treatment results in a permanently increasing number of drug-resistant strains (Garcia et al. 2009). Thirdly, in contrast to adamantanes, neuraminidase inhibitors are mostly well tolerated in patients under therapy (Cao et al. 2012). Finally, neuraminidase protein is a freely accessible target for antiviral molecules with an extracellular mode of action.

The development of neuraminidase inhibitors started in the middle 1970s, when the first

structural analogues of sialic acid were described and denoted as DANA (2-deoxy-2,3-didehydro-N-acetyl neuraminic acid) and its trifluoroacetyl derivative FANA (Schulman and Palese 1975). At present, several licensed anti-influenza medications are available on the market, most notably the inhalant zanamivir with the trademark Releza[®], and the orally administered oseltamivir (Tamiflu[®]) having excellent bioavailability and relatively long half-life *in vivo* (He et al. 1999; Greengard et al. 2000) (Figure 4). In response to the emergence of some oseltamivir-resistant influenza strains, peramivir and laninamivir have been recently developed (Bantia et al. 2006; Kubo et al. 2010). New-generation neuraminidase inhibitors are currently under investigation, e.g., multimeric forms of zanamivir (Watson et al. 2004), dual-targeted bifunctional antivirals (Liu et al. 2012), and several herbal remedies, such as flavonols, alkaloids and saponins (Jeong et al. 2009). The key publications on the structure, synthesis and therapeutic application of neuraminidase inhibitors are presented in Table 4.4.

4.5. Host cell factor targeting

Many human host cell molecules play a crucial role in influenza virus propagation and, therefore, represent promising targets for the design of new generation inhibitors of the virus-cell interaction. Muller et al. (2012) describes in his review 35 cellular factors essential for influenza virus infection for which 57 inhibitors with apparent anti-influenza activity are available. The most intensively studied are the compounds which effectively inhibit intracellular signalling cascades with a resulting negative influence on the establishment of viral infection (Nacken et al. 2012). Studies have also focused on inhibitors of vacuolar proton-ATPase which render the viral M2 ion channels inactive (Guinea and Carrasco 1994), inhibitors of cellular proteases which block the proteolytic activation of haemagglutinin (Zhirnov et al. 2011), and blockers of the cellular ubiquitin-proteasome system (Dudek et al. 2010). Although the development of host factor inhibitors is a promising research strategy to limit the emergence of drug-resistant mutants, their possible toxic side-effects *in vivo* need to be carefully studied. Selected papers on the topic are presented in Table 4.5.

4.6. Other anti-influenza agents

During the last decades, a large variety of chemical compounds with anti-influenza activity have been investigated. Several examples of such novel drugs are the inhibitors of viral nucleoprotein (Hung et al. 2012), blockers of influenza non-structural proteins (Basu et al. 2009) and short interfering oligonucleotides (siRNAs) used for viral RNA silencing (Stewart et al. 2011). Using large-scale screening techniques, new antiviral molecules which show significant anti-influenza effects have been identified; however, their chemical structure and mechanism of action remains unknown. These include, for instance, natural substances isolated from plants in chemical and pharmaceutical studies (He et al. 2012; Jiao et al. 2012). Another important group of prospective therapeutics are monoclonal antibodies and recombinant antibody fragments with high virus-neutralising activities (Hanson et al. 2006; Wei et al. 2011). Sixteen publications describing alternative anti-influenza agents are presented in Table 4.6.

5. Combination therapy of influenza infections

Recent *in vitro* and *in vivo* studies have demonstrated that the simultaneous application of two or more anti-influenza drugs with different modes of action, e.g. oseltamivir and amantadine, results in increased virus inhibition and enhanced therapeutic efficiency (Masihi et al. 2007). Similar findings were made with the combination of influenza virus inhibitors and immunomodulatory agents, especially corticosteroids (Zheng et al. 2008; Quispe-Laime et al. 2010). These observations are in accordance with the hypothesis that the applied drugs exert additive or synergistic anti-influenza effects in the infected cells. Such a combination regimen enables a reduction in the concentration of the individual inhibitory drugs, resulting in decreased drug toxicity and a reduced risk of antiviral resistance emergence in seasonal and pandemic influenza viruses (Govorkova et al. 2004; Smee et al. 2010; Nguyen et al. 2012). The principals of the combination therapy can in the future become a crucial strategy not only in the treatment of influenza infections, but also in the therapy of other serious viral, bacterial and parasitic diseases. Selected publications, which discuss combination antiviral therapy, are presented in Table 5.

6. Influenza drug resistance

As with all antimicrobials, propagation of viruses in the presence of antiviral drugs increases the selection pressure for mutations in the viral target proteins, which results in the induction of virus drug resistance. As an example, adamantane-resistant strains are typically characterised by a single substitution in the transmembrane region of the M2 ion channel (Saito et al. 2003; Shiraishi et al. 2003). On the other hand, resistance to neuraminidase inhibitors can result from mutations in the neuraminidase active cavity, but also from amino acid substitutions on the molecular surface of the neuraminidase protein (Yen et al. 2006; Du et al. 2010). It is noteworthy that resistance to adamantanes is acquired rapidly and by a high number of virus strains (Bright et al. 2005). In contrast to adamantane resistance, neuraminidase inhibitor resistance has developed over a longer time period and occurs with a relatively lower frequency (Garcia et al. 2009). This may be due to the fact that some mutations significantly affect viral infectivity and ability to replicate in the host cell. While amantadine-resistant strains do not show growth or virulence impairment (Sweet et al. 1991), influenza variants resistant to oseltamivir exhibit reduced neuraminidase activity and viral fitness *in vitro* (Yen et al. 2006), and decreased transmissibility in ferret models (Herlocher et al. 2004). The increasing emergence of drug-resistant influenza strains highlights the need to search continuously for innovative strategies for the development of new drugs with improved antiviral effects, higher safety and better tolerability. For key publications describing the mechanisms of viral drug resistance, as well as prevalence and clinical impact of drug resistant influenza strains see Table 6.

7. Acknowledgement

We wish to thank A. Durisova (Veterinary Research Institute, Brno) for her excellent graphical service.

8. REFERENCES

Aggarwal S, Dewhurst S, Takimoto T, Kim B (2011): Biochemical impact of the host adaptation-associated PB2 E627K mutation on the temperature-dependent RNA

- synthesis kinetics of influenza A virus polymerase complex. *Journal of Biological Chemistry* 286, 34504–34513.
- Al-qattan MN, Mordi MN (2010a): Docking of sialic acid analogues against influenza A hemagglutinin: a correlational study between experimentally measured and computationally estimated affinities. *Journal of Molecular Modeling* 16, 1047–1058.
- Al-qattan MN, Mordi MN (2010b): Site-directed fragment-based generation of virtual sialic acid databases against influenza A hemagglutinin. *Journal of Molecular Modeling* 16, 975–991.
- Atkins C, Evans CW, White EL, Noah JW (2012): Screening methods for influenza antiviral drug discovery. *Expert Opinion on Drug Discovery* 7, 429–438.
- Balannik V, Wang J, Ohigashi Y, Jing XH, Magavern E, Lamb RA, DeGrado WF, Pinto LH (2009): Design and pharmacological characterization of inhibitors of amantadine-resistant mutants of the M2 ion channel of influenza A virus. *Biochemistry* 48, 11872–11882.
- Bantia S, Arnold CS, Parker CD, Upshaw R, Chand P (2006): Anti-influenza virus activity of peramivir in mice with single intramuscular injection. *Antiviral Research* 69, 39–45.
- Bantia S, Kellogg D, Parker C, Upshaw R, Ilyushina N, Prichard M, Babu YS (2010): A single intramuscular injection of peramivir demonstrates anti-influenza activity against recently isolated pandemic flu virus H1N1 (A/CA/04/2009). *Antiviral Research* 86, A29–A30.
- Barlow PG, Svoboda P, Mackellar A, Nash AA, York IA, Pohl J, Davidson DJ, Donis RO (2011): Antiviral activity and increased host defense against influenza infection elicited by the human cathelicidin LL-37. *Plos One* 6.
- Barr IG, Deng YM, Iannello P, Hurt AC, Komadina N (2008): Adamantane resistance in influenza A(H1) viruses increased in 2007 in South East Asia but decreased in Australia and some other countries. *Antiviral Research* 80, 200–205.
- Basu D, Walkiewicz MP, Frieman M, Baric RS, Auble DT, Engel DA (2009): Novel influenza virus NS1 antagonists block replication and restore innate immune function. *Journal of Virology* 83, 1881–1891.
- Baughman BM, Slavish PJ, Dubois RM, Boyd VA, White SW, Webb TR (2012): Identification of influenza endonuclease inhibitors using a novel fluorescence polarization assay. *Acs Chemical Biology* 7, 526–534.
- Beigel J, Bray M (2008): Current and future antiviral therapy of severe seasonal and avian influenza. *Antiviral Research* 78, 91–102.
- Boivin S, Cusack S, Ruigrok RWH, Hart DJ (2010): Influenza A virus polymerase: structural insights into replication and host adaptation mechanisms. *Journal of Biological Chemistry* 285, 28411–28417.
- Bright RA, Medina MJ, Xu XY, Perez-Oroz G, Wallis TR, Davis XHM, Povinelli L, Cox NJ, Klimov AI (2005): Incidence of adamantane resistance among influenza A (H3N2) viruses isolated worldwide from 1994 to 2005: a cause for concern. *Lancet* 366, 1175–1181.
- Bright RA, Shay D, Bresee J, Klimov A, Cox N, Ortiz J (2006): High levels of adamantane resistance among influenza A (H3N2) viruses and interim guidelines for use of antiviral agents – United States, 2005–06 influenza season (Reprinted from *MMWR*, vol. 55, pg 44–46, 2006). *Jama-Journal of the American Medical Association* 295, 881–882.
- Cao B, Wang DY, Yu XM, We LQ, Pu ZH, Gao Y, Wang J, Dong JP, Li XL, Xu Q, Hu K, Chen BY, Yu YS, Song SF, Shu YL, Wang C (2012): An uncontrolled open-label, multicenter study to monitor the antiviral activity and safety of inhaled zanamivir (as Rotadisk via Diskhaler device) among Chinese adolescents and adults with influenza-like illness. *Chinese Medical Journal* 125, 3002–3007.
- Carrat F, Duval X, Tubach F, Mosnier A, Van der Werf S, Tibi A, Blanchon T, Lepout C, Flahault A, Mentre F (2012): Effect of oseltamivir, zanamivir or oseltamivir-zanamivir combination treatments on transmission of influenza in households. *Antiviral Therapy* 17, 1085–1090.
- Cheng HM, Wan JT, Lin MI, Liu YX, Lu XY, Liu JS, Xu Y, Chen JX, Tu ZC, Cheng YSE, Ding K (2012): Design, synthesis, and in vitro biological evaluation of 1H-1,2,3-triazole-4-carboxamide derivatives as new anti-influenza A agents targeting virus nucleoprotein. *Journal of Medicinal Chemistry* 55, 2144–2153.
- Chintakrindi A, D'souza C, Kanyalkar M (2012): Rational development of neuraminidase inhibitor as novel anti-flu drug. *Mini-Reviews in Medicinal Chemistry* 12, 1273–1281.
- Cianci C, Colonna RJ, Krystal M (1997): Differential effect of modified capped RNA substrates on influenza virus transcription. *Virus Research* 50, 65–75.
- Dai JP, Wang GF, Li WZ, Zhang L, Yang JC, Zhao XF, Chen XX, Xu YX, Li KS (2012): High-throughput screening for anti-influenza A virus drugs and study of the mechanism of procyanidin on influenza A virus-induced autophagy. *Journal of Biomolecular Screening* 17, 605–617.
- Davies WL, Hoffmann CE, Paulshock M, Wood TR, Haff RE, Grunert RR, Watts JC, Hermann EC, Neumayer EM, MCGAHEN JW (1964): Antiviral activity of 1-adamantanamine (amantadine). *Science* 144, 862–863.
- Deyde VM, Tung N, Bright RA, Balish A, Shu B, Lindstrom S, Klimov AI, Gubareva LV (2009): Detection of molecular markers of antiviral resistance in influ-

- enza A (H5N1) viruses using a pyrosequencing method. *Antimicrobial Agents and Chemotherapy* 53, 1039–1047.
- Droebner K, Pleschka S, Ludwig S, Planz O (2011): Antiviral activity of the MEK-inhibitor U0126 against pandemic H1N1v and highly pathogenic avian influenza virus in vitro and in vivo. *Antiviral Research* 92, 195–203.
- Du QS, Wang SQ, Huang RB, Chou KC (2010): Computational 3D structures of drug-targeting proteins in the 2009-H1N1 influenza A virus. *Chemical Physics Letters* 485, 191–195.
- Du J, Cross TA, Zhou HX (2012): Recent progress in structure-based anti-influenza drug design. *Drug Discovery Today* 17, 1111–1120.
- Dudek SE, Luig C, Pauli EK, Schubert U, Ludwig S (2010): The clinically approved proteasome inhibitor PS-341 efficiently blocks influenza A Virus and vesicular stomatitis virus propagation by establishing an antiviral state. *Journal of Virology* 84, 9439–9451.
- Eleftheratos S, Spearpoint P, Ortore G, Kolocouris A, Martinelli A, Martin S, Hay A (2010): Interaction of aminoadamantane derivatives with the influenza A virus M2 channel-docking using a pore blocking model. *Bioorganic and Medicinal Chemistry Letters* 20, 4182–4187.
- Eyer L, Hruska K (2012): Single-domain antibody fragments derived from heavy-chain antibodies: a review. *Veterinarni Medicina* 57, 439–513.
- Feng F, Miura N, Isoda N, Sakoda Y, Okamatsu M, Kida H, Nishimura SI (2010): Novel trivalent anti-influenza reagent. *Bioorganic and Medicinal Chemistry Letters* 20, 3772–3776.
- Fukuoka M, Minakuchi M, Kawaguchi A, Nagata K, Kamatari YO, Kuwata K (2012): Structure-based discovery of anti-influenza virus A compounds among medicines. *Biochimica et Biophysica Acta-General Subjects* 1820, 90–95.
- Fukushi M, Yamashita M, Miyoshi-Akiyama T, Kubo S, Yamamoto K, Kudo K (2012): Laninamivir octanoate and artificial surfactant combination therapy significantly increases survival of mice infected with lethal influenza H1N1 virus. *Plos One* 7.
- Furuta Y, Takahashi K, Fukuda Y, Kuno M, Kamiyama T, Kozaki K, Nomura N, Egawa H, Minami S, Watanabe Y, Narita H, Shiraki K (2002): In vitro and in vivo activities of anti-influenza virus compound T-705. *Antimicrobial Agents and Chemotherapy* 46, 977–981.
- Furuta Y, Takahashi K, Kuno-Maekawa M, Sangawa H, Uehara S, Kozaki K, Nomura N, Egawa H, Shiraki K (2005): Mechanism of action of T-705 against influenza virus. *Antimicrobial Agents and Chemotherapy* 49, 981–986.
- Galvao MGA, Santos MARC, da Cunha AJLA (2012): Amantadine and rimantadine for influenza A in children and the elderly. *Cochrane Database of Systematic Reviews*, vol. 23.
- Garcia J, Sovero M, Torres AL, Gomez J, Douce R, Barrantes M, Sanchez F, Jimenez M, Comach G, de Rivera I, Agudo R, Kochel T (2009): Antiviral resistance in influenza viruses circulating in Central and South America based on the detection of established genetic markers. *Influenza and Other Respiratory Viruses* 3, 69–74.
- Gauld NJ, Jennings LC, Frampton C, Huang QS (2012): Five years of non-prescription oseltamivir: effects on resistance, immunization and stockpiling. *Journal of Antimicrobial Chemotherapy* 67, 2949–2956.
- Ge H, Wang YF, Xu J, Gu Q, Liu HB, Xiao PG, Zhou JJ, Liu YH, Yang ZR, Su H (2010): Anti-influenza agents from traditional Chinese medicine. *Natural Product Reports* 27, 1758–1780.
- Giannecchini S, Wise HM, Digard P, Clausi V, Del Poggetto E, Vesco L, Puzelli S, Donatelli I, Azzi A (2011): Packaging signals in the 5'-ends of influenza virus PA, PB1, and PB2 genes as potential targets to develop nucleic-acid based antiviral molecules. *Antiviral Research* 92, 64–72.
- Goktas F, Vanderlinden E, Naesens L, Cesur N, Cesur Z (2012): Microwave assisted synthesis and anti-influenza virus activity of 1-adamantyl substituted N-(1-thia-4-azaspiro[4.5]decan-4-yl)carboxamide derivatives. *Bioorganic and Medicinal Chemistry* 20, 7155–7159.
- Gong JZ, Xu WF (2008): Different synthetic strategies of oseltamivir phosphate: a potent influenza neuraminidase inhibitor. *Current Medicinal Chemistry* 15, 3145–3159.
- Gong JZ, Fang H, Li MY, Liu Y, Yang KH, Liu YZ, Xu WF (2009): Potential targets and their relevant inhibitors in anti-influenza fields. *Current Medicinal Chemistry* 16, 3716–3739.
- Govorkova EA, Webster RG (2010): Combination chemotherapy for influenza. *Viruses-Basel* 2, 1510–1529.
- Govorkova EA, Fang HB, Tan M, Webster RG (2004): Neuraminidase inhibitor-rimantadine combinations exert additive and synergistic anti-influenza virus effects in MDCK cells. *Antimicrobial Agents and Chemotherapy* 48, 4855–4863.
- Greengard O, Poltoratskaia N, Leikina E, Zimmerberg J, Moscona A (2000): The anti-influenza virus agent 4-GU-DANA (Zanamivir) inhibits cell fusion mediated by human parainfluenza virus and influenza virus HA. *Journal of Virology* 74, 11108–11114.
- Grienke U, Schmidtke M, von Grafenstein S, Kirchmair J, Liedl KR, Rollinger JM (2012): Influenza neurami-

- nidase: A druggable target for natural products. *Natural Product Reports* 29, 11–36.
- Guinea R, Carrasco L (1994): Concanamycin-A blocks influenza-virus entry into cells under acidic conditions. *Febs Letters* 349, 327–330.
- Haasbach E, Pauli EK, Spranger R, Mitzner D, Schubert U, Kircheis R, Planz O (2011): Antiviral activity of the proteasome inhibitor VL-01 against influenza A viruses. *Antiviral Research* 91, 304–313.
- Hanson BJ, Boon ACM, Lim APC, Webb A, Ooi EE, Webby RJ (2006): Passive immunoprophylaxis and therapy with humanized monoclonal antibody specific for influenza A H5 hemagglutinin in mice. *Respiratory Research* 7, 126.
- Hastings JC, Selnick H, Wolanski B, Tomassini JE (1996): Anti-influenza virus activities of 4-substituted 2,4-dioxobutanoic acid inhibitors. *Antimicrobial Agents and Chemotherapy* 40, 1304–1307.
- He G, Massarella J, Ward P (1999): Clinical pharmacokinetics of the prodrug oseltamivir and its active metabolite Ro 64-0802. *Clinical Pharmacokinetics* 37, 471–484.
- He J, Qi WB, Tian J, Jiao PR, Liu GQ, Zhang CH, Liao M (2012): Amarylidaceae alkaloids exhibit anti-influenza activity in MDCK cells, an investigation of Amarylidaceae alkaloids and MDCK cells insight. *Journal of Animal and Veterinary Advances* 11, 2485–2492.
- Herlocher ML, Truscon R, Elias S, Yen HL, Roberts NA, Ohmit SE, Monto AS (2004): Influenza viruses resistant to the antiviral drug oseltamivir: Transmission studies in ferrets. *Journal of Infectious Diseases* 190, 1627–1630.
- Hoffman LR, Kuntz ID, White JM (1997): Structure-based identification of an inducer of the low-pH conformational change in the influenza virus hemagglutinin: Irreversible inhibition of infectivity. *Journal of Virology* 71, 8808–8820.
- Hosoya M, Matsuyama S, Baba M, Suzuki H, Shigeta S (1992): Effects of protease inhibitors on replication of various myxoviruses. *Antimicrobial Agents and Chemotherapy* 36, 1432–1436.
- Hosoya M, Shigeta S, Ishii T, Suzuki H, Declercq E (1993): Comparative inhibitory effects of various nucleoside and nonnucleoside analogs on replication of influenza-virus type-A and type-B in-vitro and in vivo. *Journal of Infectious Diseases* 168, 641–646.
- Hruska K, Franek M (2012): Sulfonamides in the environment: a review and a case report. *Veterinarni Medicina* 57, 1–35.
- Hruska K, Kaevska M (2012): Mycobacteria in water, soil, plants and air: a review. *Veterinarni Medicina* 57, 623–679.
- Hsieh HP, Hsu JTA (2007): Strategies of development of antiviral agents directed against influenza virus replication. *Current Pharmaceutical Design* 13, 3531–3542.
- Hu YX, Jin Y, Han DP, Zhang GZ, Cao SP, Xie JJ, Xue J, Li Y, Meng D, Fan XX, Sun LQ, Wang M (2012): Mast cell-induced lung injury in mice infected with H5N1 influenza virus. *Journal of Virology* 86, 3347–3356.
- Hung HC, Liu CL, Hsu JTA, Horng JT, Fang MY, Wu SY, Ueng SH, Wang MY, Yaw CW, Hou MH (2012): Development of an anti-influenza drug screening assay targeting nucleoproteins with tryptophan fluorescence quenching. *Analytical Chemistry* 84, 6391–6399.
- Ibanez LI, De Filette M, Hultberg A, Verrips T, Temperon N, Weiss RA, Vandeveld W, Schepens B, Vanlandschoot P, Saelens X (2011): Nanobodies with in vitro neutralizing activity protect mice against H5N1 influenza virus infection. *Journal of Infectious Diseases* 203, 1063–1072.
- Intharathep P, Rungrotmongkol T, Decha P, Nunthaboot N, Kaiyawet N, Kerdcharoen T, Sompornpisut P, Hanongbua S (2011): Evaluating how rimantadines control the proton gating of the influenza A M2-proton port via allosteric binding outside of the M2-channel: MD simulations. *Journal of Enzyme Inhibition and Medicinal Chemistry* 26, 162–168.
- Iwai Y, Murakami K, Gomi Y, Hashimoto T, Asakawa Y, Okuno Y, Ishikawa T, Hatakeyama D, Echigo N, Kuzuhara T (2011): Anti-influenza activity of marchantins, macrocyclic bisbibenzyls contained in liverworts. *Plos One* 6.
- Jeong HJ, Ryu YB, Park SJ, Kim JH, Kwon HJ, Kim JH, Park KH, Rho MC, Lee WS (2009): Neuraminidase inhibitory activities of flavonols isolated from *Rhodiola rosea* roots and their in vitro anti-influenza viral activities. *Bioorganic and Medicinal Chemistry* 17, 6816–6823.
- Jiao GL, Yu GL, Wang W, Zhao XL, Zhang JZ, Ewart SH (2012): Properties of polysaccharides in several seaweeds from Atlantic Canada and their potential anti-influenza viral activities. *Journal of Ocean University of China* 11, 205–212.
- Kaihatsu K, Barnard DL (2012): Recent developments in anti-influenza A virus drugs and use in combination therapies. *Mini-Reviews in Organic Chemistry* 9, 3–10.
- Kido H, Okumura Y, Yamada H, Le TQ, Yano M (2007): Proteases essential for human influenza virus entry into cells and their inhibitors as potential therapeutic agents. *Current Pharmaceutical Design* 13, 405–414.
- Kim CU, Lew W, Williams MA, Liu HT, Zhang LJ, Swaminathan S, Bischofberger N, Chen MS, Mendel DB,

- Tai CY, Laver WG, Stevens RC (1997): Influenza neuraminidase inhibitors possessing a novel hydrophobic interaction in the enzyme active site: Design, synthesis, and structural analysis of carbocyclic sialic acid analogues with potent anti-influenza activity. *Journal of the American Chemical Society* 119, 681–690.
- Kim WY, Suh GY, Huh JW, Kim SH, Kim MJ, Kim YS, Kim HR, Ryu YJ, Han MS, Ko YG, Chon GR, Lee KH, Choi SH, Hong SB (2011): Triple-combination antiviral drug for pandemic H1N1 influenza virus infection in critically ill patients on mechanical ventilation. *Antimicrobial Agents and Chemotherapy* 55, 5703–5709.
- Kinger M, Park YD, Park JH, Hur MG, Jeong HJ, Park SJ, Lee WS, Kim SW, Yang SD (2012): Design, synthesis, and anti-influenza viral activities of 1,3-diarylprop-2-en-1-ones: A novel class of neuraminidase inhibitors. *Archives of Pharmacal Research* 35, 633–638.
- Kongkamnerd J, Milani A, Cattoli G, Terregino C, Capua I, Beneduce L, Gallotta A, Pengo P, Fassina G, Miertus S, De-Eknamkul W (2012): A screening assay for neuraminidase inhibitors using neuraminidases N1 and N3 from a baculovirus expression system. *Journal of Enzyme Inhibition and Medicinal Chemistry* 27, 5–11.
- Konig R, Stertz S, Zhou Y, Inoue A, Hoffmann HH, Bhattacharyya S, Alamares JG, Tscherne DM, Ortigoza MB, Liang YH, Gao QS, Andrews SE, Bandyopadhyay S, De Jesus P, Tu BP, Pache L, Shih C, Orth A, Bonamy G, Miraglia L, Ideker T, Garcia-Sastre A, Young JAT, Palese P, Shaw ML, Chanda SK (2010): Human host factors required for influenza virus replication. *Nature* 463, 813–817.
- Kowalinski E, Zubieta C, Wolkerstorfer A, Szolar OHJ, Ruigrok RWH, Cusack S (2012): Structural analysis of specific metal chelating inhibitor binding to the endonuclease domain of influenza pH1N1 (2009) Polymerase. *Plos Pathogens* 8.
- Kubo S, Tomozawa T, Kakuta M, Tokumitsu A, Yamashita M (2010): Laninamivir prodrug CS-8958, a long-acting neuraminidase inhibitor, shows superior anti-influenza virus activity after a single administration. *Antimicrobial Agents and Chemotherapy* 54, 1256–1264.
- Larson AM, Wang HM, Cao Y, Jiang TJ, Chen JZ, Klivanov A (2012): Conjugating drug candidates to polymeric chains does not necessarily enhance anti-influenza activity. *Journal of Pharmaceutical Sciences* 101, 3896–3905.
- Lee KK, Pessi A, Gui L, Santoprete A, Talekar A, Moscona A, Porotto M (2011): Capturing a fusion intermediate of influenza hemagglutinin with a cholesterol-conjugated peptide, a new antiviral strategy for influenza virus. *Journal of Biological Chemistry* 286, 42141–42149.
- Li Y, Zhang XZ, Wang XY, Li S, Ruan JX, Zhang ZQ (2009): Quantification of peramivir (a novel anti-influenza drug) in human plasma by hydrophilic interaction chromatography/tandem mass spectrometry. *Journal of Chromatography B – Analytical Technologies in the Biomedical and Life Sciences* 877, 933–938.
- Li L, Chang SH, Xiang JF, Li Q, Liang HH, Tang YL, Liu YF (2012a): NMR identification of anti-influenza lead compound targeting at PA(C) subunit of H5N1 polymerase. *Chinese Chemical Letters* 23, 89–92.
- Li L, Chang SH, Xiang JF, Li Q, Liang HH, Tang YL, Liu YF (2012b): Screen anti-influenza lead compounds that target the PA(C) subunit of H5N1 viral RNA polymerase. *Plos One* 7.
- Liu HX, Yao XJ, Wang CQ, Han JA (2010): In silico identification of the potential drug resistance sites over 2009 influenza A (H1N1) virus neuraminidase. *Molecular Pharmaceutics* 7, 894–904.
- Liu KC, Fang JM, Jan JT, Cheng TJR, Wang SY, Yang ST, Cheng YSE, Wong CH (2012): Enhanced anti-influenza agents conjugated with anti-inflammatory activity. *Journal of Medicinal Chemistry* 55, 8493–8501.
- Ludwig S, Planz O, Pleschka S, Wolff T (2003): Influenza-virus-induced signaling cascades: targets for antiviral therapy? *Trends in Molecular Medicine* 9, 46–52.
- Luo GX, Torri A, Harte WE, Danetz S, Cianci C, Tiley L, Day S, Mullaney D, Yu KL, Ouellet C, Dextraze P, Meanwell N, Colonno R, Krystal M (1997): Molecular mechanism underlying the action of a novel fusion inhibitor of influenza A virus. *Journal of Virology* 71, 4062–4070.
- Lv HM, Guo XL, Gu RX, Wei DQ (2011): Free energy calculations and binding analysis of two potential anti-influenza drugs with polymerase basic protein-2 (PB2). *Protein and Peptide Letters* 18, 1002–1009.
- Malakhov MP, Aschenbrenner LM, Smee DF, Wandersee MK, Sidwell RW, Gubareva LV, Mishin VP, Hayden FG, Kim DH, Ing A, Campbell ER, Yu M, Fang F (2006): Sialidase fusion protein as a novel broad-spectrum inhibitor of influenza virus infection. *Antimicrobial Agents and Chemotherapy* 50, 1470–1479.
- Marra A, Moni L, Pazzi D, Corallini A, Bridi D, Dondoni A (2008): Synthesis of sialoclusters appended to calix[4]arene platforms via multiple azide-alkyne cycloaddition. New inhibitors of hemagglutination and cytopathic effect mediated by BK and influenza A viruses. *Organic and Biomolecular Chemistry* 6, 1396–1409.
- Martinez O, Tsibane T, Basler CF (2009): Neutralizing anti-influenza virus monoclonal antibodies: therapeutic

- tics and tools for discovery. *International Reviews of Immunology* 28, 69–92.
- Masihi KN, Schweiger B, Finsterbusch T, Hengel H (2007): Low dose oral combination chemoprophylaxis with oseltamivir and amantadine for influenza A virus infections in mice. *Journal of Chemotherapy* 19, 295–303.
- Massarella JW, He GZ, Dorr A, Nieforth K, Ward P, Brown A (2000): The pharmacokinetics and tolerability of the oral neuraminidase inhibitor oseltamivir (Ro 64-0796/GS4104) in healthy adult and elderly volunteers. *Journal of Clinical Pharmacology* 40, 836–843.
- Masuda T, Yoshida S, Arai M, Kaneko S, Yamashita M, Honda T (2003): Synthesis and anti-influenza evaluation of polyvalent sialidase inhibitors bearing 4-guanidino-Neu5Ac2en derivatives. *Chemical and Pharmaceutical Bulletin* 51, 1386–1398.
- Matrosovich MN, Matrosovich TY, Gray T, Roberts NA, Klenk HD (2004): Neuraminidase is important for the initiation of influenza virus infection in human airway epithelium. *Journal of Virology* 78, 12665–12667.
- Miotto O, Heiny AT, Tan TW, August JT, Brusica V (2008): Identification of human-to-human transmissibility factors in PB2 proteins of influenza A by large-scale mutual information analysis. *Bmc Bioinformatics* 9 (Suppl. 1), S18.
- Moss RB, Hansen C, Sanders RL, Hawley S, Li TJ, Steigbigel RT (2012): A phase II study of DAS181, a novel host directed antiviral for the treatment of influenza infection. *Journal of Infectious Diseases* 206, 1844–1851.
- Muller KH, Kakkola L, Nagaraj AS, Cheltsov AV, Anastasina M, Kainov DE (2012): Emerging cellular targets for influenza antiviral agents. *Trends in Pharmacological Sciences* 33, 89–99.
- Nacken W, Ehrhardt C, Ludwig S (2012): Small molecule inhibitors of the c-Jun N-terminal kinase (JNK) possess antiviral activity against highly pathogenic avian and human pandemic influenza A viruses. *Biological Chemistry* 393, 525–534.
- Nakazawa M, Kadowaki SE, Watanabe I, Kadowaki Y, Takei M, Fukuda H (2008): PA subunit of RNA polymerase as a promising target for anti-influenza virus agents. *Antiviral Research* 78, 194–201.
- Narla SN, Sun XL (2012): Immobilized sialyloligo-macroligand and its protein binding specificity. *Biomacromolecules* 13, 1675–1682.
- Nguyen JT, Smee DF, Barnard DL, Julander JG, Gross M, de Jong MD, Went GT (2012): Efficacy of combined therapy with amantadine, oseltamivir, and ribavirin in vivo against susceptible and amantadine-resistant influenza A Viruses. *Plos One* 7.
- Ochiai H, Sakai S, Hirabayashi T, Shimizu Y, Terasawa K (1995): Inhibitory effect of bafilomycin A1, a specific inhibitor of vacuolar-type proton pump, on the growth of influenza-A and influenza-B viruses in MdcK cells. *Antiviral Research* 27, 425–430.
- Park SY, Kim S, Yoon H, Kim KB, Kalme SS, Oh S, Song CS, Kim DE (2011): Selection of an antiviral RNA aptamer against hemagglutinin of the subtype H5 avian influenza virus. *Nucleic Acid Therapeutics* 21, 395–402.
- Peng JX, Jiao JY, Li J, Wang W, Gu QQ, Zhu TJ, Li DH (2012): Pyronepolyene C-glucosides with NF-kappa B inhibitory and anti-influenza A viral (H1N1) activities from the sponge-associated fungus *Epicoccum* sp. JY40. *Bioorganic and Medicinal Chemistry Letters* 22, 3188–3190.
- Pielak RM, Oxenoid K, Chou JJ (2011): Structural investigation of rimantadine inhibition of the AM2-BM2 chimera channel of influenza viruses. *Structure* 19, 1655–1663.
- Ping JH, Keleta L, Forbes NE, Dankar S, Stecho W, Tyler S, Zhou Y, Babiuk L, Weingartl H, Halpin RA, Boyne A, Bera J, Hostetler J, Fedorova NB, Proudfoot K, Katzel DA, Stockwell TB, Ghedin E, Spiro DJ, Brown EG (2011): Genomic and protein structural maps of adaptive evolution of human influenza A virus to increased virulence in the mouse. *Plos One* 6.
- Pizzorno A, Abed Y, Boivin G (2011): Influenza drug resistance. *Seminars in Respiratory and Critical Care Medicine* 32, 409–422.
- Pontoriero A, Baumeister E, Campos AM, Savy VL (2011): Virological surveillance and antiviral resistance of human influenza virus in Argentina, 2005–2008. *Revista Panamericana de Salud Publica-Pan American Journal of Public Health* 30, 634–640.
- Priyadarzini TRK, Selvin JFA, Gromiha MM, Fukui K, Veluraja K (2012): Theoretical investigation on the binding specificity of sialydisaccharides with hemagglutinins of influenza A virus by molecular dynamics simulations. *Journal of Biological Chemistry* 287, 34547–34557.
- Quispe-Laime AM, Bracco JD, Barberio PA, Campagne CG, Rolfo VE, Umberger R, Meduri GU (2010): H1N1 influenza A virus-associated acute lung injury: response to combination oseltamivir and prolonged corticosteroid treatment. *Intensive Care Medicine* 36, 33–41.
- Rawat V, Dey S, Sudalai A (2012): Synthesis of the anti-influenza agent (–)-oseltamivir free base and (–)-methyl 3-epi-shikimate. *Organic and Biomolecular Chemistry* 10, 3988–3990.
- Rosenberg MR, Casarotto MG (2010): Coexistence of two adamantane binding sites in the influenza A M2 ion channel. *Proceedings of the National Academy of Sciences of the United States of America* 107, 13866–13871.

- Saito R, Sakai T, Sato I, Sano Y, Oshitani H, Sato M, Suzuki H (2003): Frequency of amantadine-resistant influenza A viruses during two seasons featuring co-circulation of H1N1 and H3N2. *Journal of Clinical Microbiology* 41, 2164–2165.
- Sakurai J, Kikuchi T, Takahashi O, Watanabe K, Katoh T (2011): Enantioselective total synthesis of (+)-stachyflin: A potential anti-influenza virus agent isolated from a microorganism. *European Journal of Organic Chemistry* 2948–2957.
- Sauerbrei A, Haertl A, Brandstaedt A, Schmidtke M, Wutzler P (2006): Utilization of the embryonated egg for in vivo evaluation of the anti-influenza virus activity of neuraminidase inhibitors. *Medical Microbiology and Immunology* 195, 65–71.
- Schmidtke M, Schnittler U, Jahn B, Dahse HM, Stelzner A (2001): A rapid assay for evaluation of antiviral activity against coxsackie virus B3, influenza virus A, and herpes simplex virus type 1. *Journal of Virological Methods* 95, 133–143.
- Schnell JR, Chou JJ (2008): Structure and mechanism of the M2 proton channel of influenza A virus. *Nature* 451, 591–595.
- Schulman JL, Palese P (1975): Susceptibility of different strains of influenza A virus to inhibitory effects of 2-deoxy-2,3-dehydro-N-trifluoroacetylneuraminic acid (FANA). *Virology* 63, 98–104.
- Sgarbanti R, Nencioni L, Amatore D, Coluccio P, Fraternali A, Sale P, Mammola CL, Carpino G, Gaudio E, Magnani M, Ciriolo MR, Garaci E, Palamara AT (2011): Redox regulation of the influenza hemagglutinin maturation process: A new cell-mediated strategy for anti-influenza therapy. *Antioxidants and Redox Signaling* 15, 593–606.
- Sheu TG, Deyde VM, Garten RJ, Klimov AI, Gubareva LV (2010): Detection of antiviral resistance and genetic lineage markers in influenza B virus neuraminidase using pyrosequencing. *Antiviral Research* 85, 354–360.
- Shie JJ, Fang JM, Lai PT, Wen WH, Wang SY, Cheng YSE, Tsai KC, Yang AS, Wong CH (2011): A practical synthesis of zanamivir phosphonate congeners with potent anti-influenza activity. *Journal of the American Chemical Society* 133, 17959–17965.
- Shiraishi K, Mitamura K, Sakai-Tagawa Y, Goto H, Sugaya N, Kawaoka Y (2003): High frequency of resistant viruses harboring different mutations in amantadine-treated children with influenza. *Journal of Infectious Diseases* 188, 57–61.
- Sidwell RW, Bailey KW, Wong MH, Barnard DL, Smee DF (2005): In vitro and in vivo influenza virus-inhibitory effects of viramidine. *Antiviral Research* 68, 10–17.
- Sidwell RW, Smee DF (2000): In vitro and in vivo assay systems for study of influenza virus inhibitors. *Antiviral Research* 48, 1–16.
- Sigal GB, Mammen M, Dahmann G, Whitesides GM (1996): Polyacrylamides bearing pendant alpha-sialoside groups strongly inhibit agglutination of erythrocytes by influenza virus: The strong inhibition reflects enhanced binding through cooperative polyvalent interactions. *Journal of the American Chemical Society* 118, 3789–3800.
- Skehel JJ, Wiley DC (2000): Receptor binding and membrane fusion in virus entry: The influenza hemagglutinin. *Annual Review of Biochemistry* 69, 531–569.
- Smee DF, Huffman JH, Morrison AC, Barnard DL, Sidwell RW (2001): Cyclopentane neuraminidase inhibitors with potent in vitro anti-influenza virus activities. *Antimicrobial Agents and Chemotherapy* 45, 743–748.
- Smee DF, Hurst BL, Wong MH, Bailey KW, Tarbet EB, Morrey JD, Furuta Y (2010): Effects of the Combination of Favipiravir (T-705) and Oseltamivir on Influenza A Virus Infections in Mice. *Antimicrobial Agents and Chemotherapy* 54, 126–133.
- Stamatiou G, Kolocouris A, Kolocouris N, Fytas G, Foscolos GB, Neyts J, De Clercq E (2001): Novel 3-(2-adamantyl)pyrrolidines with potent activity against influenza A virus – identification of aminoadamantane derivatives bearing two pharmacophoric amine groups. *Bioorganic and Medicinal Chemistry Letters* 11, 2137–2142.
- Staschke KA, Hatch SD, Tang JC, Hornback WJ, Munroe JE, Colacino JM, Muesing MA (1998): Inhibition of influenza virus hemagglutinin-mediated membrane fusion by a compound related to podocarpic acid. *Virology* 248, 264–274.
- Stewart CR, Karpala AJ, Lowther S, Lowenthal JW, Bean AG (2011): Immunostimulatory motifs enhance antiviral siRNAs targeting highly pathogenic avian influenza H5N1. *Plos One* 6.
- Stimac A, Segota S, Sikiric MD, Ribic R, Frkanec L, Svetlicic V, Tomic S, Vranesic B, Frkanec R (2012): Surface modified liposomes by mannosylated conjugates anchored via the adamantyl moiety in the lipid bilayer. *Biochimica et Biophysica Acta – Biomembranes* 1818, 2252–2259.
- Stoner TD, Krauss S, Turner JCM, Seiler P, Negovetich NJ, Stallknecht DE, Frase S, Govorkova EA, Webster RG (2012): Susceptibility of avian influenza viruses of the N6 subtype to the neuraminidase inhibitor oseltamivir. *Antiviral Research* 93, 322–329.
- Sui HY, Zhao GY, Huang JD, Jin DY, Yuen KY, Zheng BJ (2009): Small interfering RNA targeting M2 gene induces effective and long term inhibition of influenza A virus replication. *Plos One* 4.

- Suzuki T, Takahashi T, Guo CT, Hidari KIPJ, Miyamoto D, Goto H, Kawaoka Y, Suzuki Y (2005): Sialidase activity of influenza A virus in an endocytic pathway enhances viral replication. *Journal of Virology* 79, 11705–11715.
- Sweet C, Hayden FG, Jakeman KJ, Grambas S, Hay AJ (1991): Virulence of rimantadine-resistant human influenza-A (H3N2) viruses in ferrets. *Journal of Infectious Diseases* 164, 969–972.
- Tado M, Abe T, Hatta T, Ishikawa M, Nakada S, Yokota T, Takaku H (2001): Inhibitory effect of modified 5'-capped short RNA fragments on influenza virus RNA polymerase gene expression. *Antiviral Chemistry and Chemotherapy* 12, 353–358.
- Tarbet EB, Maekawa M, Furuta Y, Babu YS, Morrey JD, Smee DF (2012): Combinations of favipiravir and peramivir for the treatment of pandemic influenza A/California/04/2009 (H1N1) virus infections in mice. *Antiviral Research* 94, 103–110.
- Tian L, Wang ZY, Wu H, Wang S, Wang Y, Wang YY, Xu JW, Wang LY, Qi FC, Fang ML, Yu DH, Fang XX (2011): Evaluation of the anti-neuraminidase activity of the traditional Chinese medicines and determination of the anti-influenza A virus effects of the neuraminidase inhibitory TCMs in vitro and in vivo. *Journal of Ethnopharmacology* 137, 534–542.
- Tisdale M (2000): Monitoring of viral susceptibility: new challenges with the development of influenza NA inhibitors. *Reviews in Medical Virology* 10, 45–55.
- Tisdale M, Ellis M, Klumpp K, Court S, Ford M (1995): Inhibition of influenza-virus transcription by 2'-deoxy-2'-fluoroguanosine. *Antimicrobial Agents and Chemotherapy* 39, 2454–2458.
- Tomassini JE, Davies ME, Hastings JC, Lingham R, Mojena M, Raghoobar SL, Singh SB, Tkacz JS, Goetz MA (1996): A novel antiviral agent which inhibits the endonuclease of influenza viruses. *Antimicrobial Agents and Chemotherapy* 40, 1189–1193.
- Tran L, Choi SB, Al-Najjar BO, Yusuf M, Wahab HA, Le L (2011): Discovery of potential M2 channel inhibitors based on the amantadine scaffold via virtual screening and pharmacophore modeling. *Molecules* 16, 10227–10255.
- Ushirogawa H, Ohuchi M (2011): Novel antiviral activity of neuraminidase inhibitors against an avian influenza A virus. *Virology Journal* 8, 411.
- Vass M, Hruska K, Franek M (2008): Nitrofurantoin antibiotics: a review on the application, prohibition and residual analysis. *Veterinarni Medicina* 53, 469–500.
- Vergara-Jaque A, Poblete H, Lee EH, Schulten K, Gonzalez-Nilo F, Chipot C (2012): Molecular basis of drug resistance in A/H1N1 virus. *Journal of Chemical Information and Modeling* 52, 2650–2656.
- Wang XY, Li M, Zheng HY, Muster T, Palese P, Beg AA, Garcia-Sastre A (2000): Influenza A virus NS1 protein prevents activation of NF-kappa B and induction of alpha/beta interferon. *Journal of Virology* 74, 11566–11573.
- Wang W, Zhang P, Yu GL, Li CX, Hao C, Qi X, Zhang LJ, Guan HS (2012): Preparation and anti-influenza A virus activity of kappa-carrageenan oligosaccharide and its sulphated derivatives. *Food Chemistry* 133, 880–888.
- Watson KG, Cameron R, Fenton RJ, Gower D, Hamilton S, Jin B, Krippner GY, Luttick A, McConnell D, MacDonald SJE, Mason AM, Nguyen V, Tucker SP, Wu WY (2004): Highly potent and long-acting trimeric and tetrameric inhibitors of influenza virus neuraminidase. *Bioorganic and Medicinal Chemistry Letters* 14, 1589–1592.
- Wei GW, Meng WX, Guo HJ, Pan WQ, Liu JS, Peng T, Chen L, Chen CY (2011): Potent neutralization of influenza A virus by a single-domain antibody blocking M2 ion channel protein. *Plos One* 6.
- Widjaja I, de Vries E, Tscherne DM, Garcia-Sastre A, Rottier PJM, de Haan CAM (2010): Inhibition of the ubiquitin-proteasome system affects influenza A virus infection at a postfusion step. *Journal of Virology* 84, 9625–9631.
- Wong DDY, Choy KT, Chan RWY, Sia SF, Chiu HP, Cheung PPH, Chan MCW, Peiris JSM, Yen HL (2012): Comparable fitness and transmissibility between oseltamivir-resistant pandemic 2009 and seasonal H1N1 influenza viruses with the H275Y neuraminidase mutation. *Journal of Virology* 86, 10558–10570.
- Wrarmert J, Smith K, Miller J, Langley WA, Kokko K, Larsen C, Zheng NY, Mays I, Garman L, Helms C, James J, Air GM, Capra JD, Ahmed R, Wilson PC (2008): Rapid cloning of high-affinity human monoclonal antibodies against influenza virus. *Nature* 453, 667–671.
- Wu Y, Li JQ, Kim YJ, Wu J, Wang Q, Hao Y (2011): In vivo and in vitro antiviral effects of berberine on influenza virus. *Chinese Journal of Integrative Medicine* 17, 444–452.
- Wu QF, Wang W, Dai XY, Wang ZY, Shen ZH, Ying HZ, Yu CH (2012): Chemical compositions and anti-influenza activities of essential oils from *Mosla dianthera*. *Journal of Ethnopharmacology* 139, 668–671.
- Yamada K, Koyama H, Hagiwara K, Ueda A, Sasaki Y, Kanesashi S, Ueno R, Nakamura HK, Kuwata K, Shimizu K, Suzuki M, Aida Y (2012): Identification of a novel compound with antiviral activity against influenza A virus depending on PA subunit of viral RNA polymerase. *Microbes and Infection* 14, 740–747.
- Yanagita H, Yamamoto N, Fuji H, Liu XL, Ogata M, Yokota M, Takaku H, Hasegawa H, Odagiri T, Tashiro M, Hoshino T (2012): Mechanism of drug resistance

- of hemagglutinin of influenza virus and potent scaffolds inhibiting its function. *Acs Chemical Biology* 7, 552–562.
- Yen HL, Hoffmann E, Taylor G, Scholtissek C, Monto AS, Webster RG, Govorkova EA (2006): Importance of neuraminidase active-site residues to the neuraminidase inhibitor resistance of influenza viruses. *Journal of Virology* 80, 8787–8795.
- Yoshimoto J, Kakui M, Iwasaki H, Fujiwara T, Sugimoto H, Hattori N (1999): Identification of a novel HA conformational change inhibitor of human influenza virus. *Archives of Virology* 144, 865–878.
- Yoshimoto J, Yagi S, Ono J, Sugita K, Hattori N, Fujioka T, Fujiwara T, Sugimoto H, Hashimoto N (2000): Development of anti-influenza drugs: II. Improvement of oral and intranasal absorption and the anti-influenza activity of stachyflin derivatives. *Journal of Pharmacy and Pharmacology* 52, 1247–1255.
- Zaraket H, Saito R, Suzuki Y, Suzuki Y, Caperig-Dapat I, Dapat C, Shabana II, Baranovich T, Suzuki H (2010): Genomic events contributing to the high prevalence of amantadine-resistant influenza A/H3N2. *Antiviral Therapy* 15, 307–319.
- Zarubaev VV, Golod EL, Anfimov PM, Shtro AA, Saraev VV, Gavrilov AS, Logvinov AV, Kiselev OI (2010): Synthesis and anti-viral activity of azolo-adamantanes against influenza A virus. *Bioorganic and Medicinal Chemistry* 18, 839–848.
- Zheng BJ, Chan KW, Lin YP, Zhao GY, Chan C, Zhang HJ, Chen HL, Wong SSY, Lau SKP, Woo PCY, Chan KH, Jin DY, Yuen KY (2008): Delayed antiviral plus immunomodulator treatment still reduces mortality in mice infected by high inoculum of influenza A/H5N1 virus. *Proceedings of the National Academy of Sciences of the United States of America* 105, 8091–8096.
- Zhirnov OP, Klenk ND, Wright PF (2011): Aprotinin and similar protease inhibitors as drugs against influenza. *Antiviral Research* 92, 27–36.
- Zhou HB, Jin ML, Yu ZJ, Xu XJ, Peng YP, Wu HY, Liu JL, Liu H, Cao SB, Chen HC (2007): Effective small interfering RNAs targeting matrix and nucleocapsid protein gene inhibit influenza A virus replication in cells and mice. *Antiviral Research* 76, 186–193.
- Zhu ZB, Li RM, Xiao GK, Chen ZP, Yang J, Zhu QH, Liu SW (2012): Design, synthesis and structure-activity relationship of novel inhibitors against H5N1 hemagglutinin-mediated membrane fusion. *European Journal of Medicinal Chemistry* 57, 211–216.
- Zoidis G, Fytas C, Papanastasiou L, Foscolos GB, Fytas G, Padalko E, De Clercq E, Naesens L, Neyts J, Koloouris N (2006): Heterocyclic rimantadine analogues with antiviral activity. *Bioorganic and Medicinal Chemistry* 14, 3341–3348.
- Zu M, Yang F, Zhou WL, Liu AL, Du GH, Zheng LS (2012): In vitro anti-influenza virus and anti-inflammatory activities of the aflavin derivatives. *Antiviral Research* 94, 217–224.

Received: 2013–03–25

Accepted after corrections: 2013–04–05

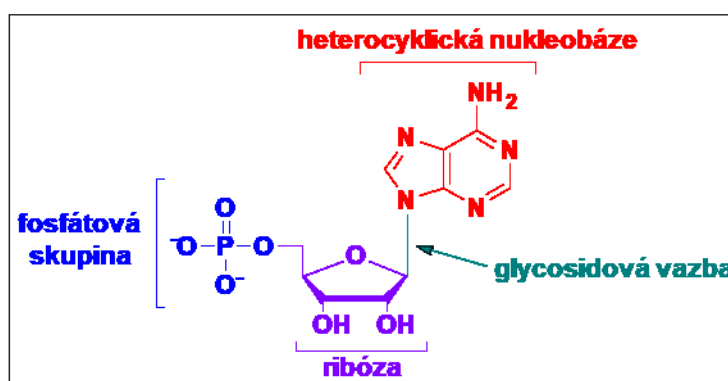
Corresponding Author:

Mgr. Ludek Eyer, Ph.D., Veterinary Research Institute, Hudcova 70, 621 00 Brno, Czech Republic
Tel. +420 533 331 911, E-mail: eyer@vri.cz

4. NUKLEOSIDOVÉ ANALOGY JAKO TERAPEUTIKA ZÁVAŽNÝCH VIROVÝCH INFEKČÍ

Nukleosidové analogy jsou nejvýznamnější a zároveň nejpočetnější skupinou látek s antivirovou aktivitou, které jsou používány pro léčbu závažných virových onemocnění. V současné době je legislativně schváleno přibližně 30 přípravků na bázi nukleosidových analogů pro terapii infekcí vyvolaných herpetickými viry (např. acyklovir a ganciklovir) (De Clercq and Holý, 2005) virem HIV (např. tenofovir) (Benhamou et al., 2003; Ray et al., 2016), virem žloutenky typu B (např. lamivudin/entecavir) (Huang et al., 2016; Lam et al., 2017) a virem žloutenky typu C (např. sofosbuvir) (Stedman, 2014). Přirozeně se vyskytující nukleosidy a nukleotidy hrají důležitou roli v buněčném metabolismu, především při syntéze, methylaci a reparaci nukleových kyselin (DNA a RNA). Jsou hojně zapojeny také do buněčných signálních drah a jsou důležitými aktéry v energetickém metabolismu buňky. Nukleosidy jsou klíčovými molekulami také při replikaci a transkripci virové genomové nukleové kyseliny (NK). Nukleosidové analogy, coby chemicky modifikované nukleosidy, napodobují svojí strukturou molekuly přirozených nukleosidů a mohou tak účinně narušovat nebo zcela inhibovat biochemické a molekulárně-biologické procesy využívané virem pro svoji replikaci v hostitelské buňce (Ariav et al., 2021).

Molekula nukleosidu je složena ze sacharidového (pentózového) kruhu (β -D-ribóza v případě ribonukleotidů nebo 2'-deoxy- β -D-ribóza v případě 2'-deoxyribonukleotidů), který je N-glykosidovou vazbou spojen s heterocyklickou nukleobází, tvořenou adeninem, guaninem, cytosinem nebo tyminem (u DNA) nebo uracilem (u RNA). Na rozdíl od nukleosidů jsou molekuly nukleotidů dále tvořeny jednou, dvěma nebo třemi fosfátovými skupinami připojenými prostřednictvím fosfodiesterové vazby k pentózového kruhu, konkrétně do pozice 5'C. Fosforylace nukleosidů a nukleotidů je třítupňový proces, který je v buňce realizován nukleotidkinázou, nukleosidkinázou a následně nukleosiddifosfátkinázou, což vede k biologické aktivaci nukleosidů, které jsou pak specificky rozpoznávány cílovými buněčnými nebo virovými enzymy. Vhodnými chemickými modifikacemi rozličných atomů a funkčních skupin na molekule nukleosidu bylo doposud vytvořeno mnoho účinných nukleosidových antivirotik, které se vyznačují silnou virus-supresivní aktivitou a minimálními nežádoucími cytotoxickými účinky (Seley-Radtke and Yates, 2018). Struktura molekuly nukleotidu/nukleosidu je schematicky znázorněna na obr. 1.



Obr. 1. Obecná struktura molekuly nukleotidu/nukleosidu

Antivirový účinek nukleosidových analogů může být několikerého druhu. Většina nukleosidových analogů působí jako přímé inhibitory syntézy virové NK. Jako takové kompetují s přirozenými nukleosidy o aktivní místo virových polymeráz a začleňují se do prodlužujících se (nascentních) řetězců virové genomové DNA/RNA, přičemž působí předčasnou terminaci syntézy virové NK. Obligátní terminátory syntézy NK postrádají 3'-hydroxyl, což vede k přerušení tvorby 5'-3' fosfodiesterových vazeb s následujícím nukleosid-monofosfátem a tedy k okamžitému ukončení syntézy virové NK. Naproti tomu neobligátní terminátory se vyznačují přítomností 3'-hydroxylu, který je ovšem stericky stíněn nebo je jeho reaktivita snížena v důsledku přítomnosti elektron-akceptorních skupin v jeho okolí. To ve výsledku vede k postupné terminaci replikujícího se řetězce virové NK (De Clercq and Neyts, 2009). K dalším mechanismům účinku nukleosidových analogů patří inhibice virové methyltransferázy, zodpovědné za metylaci virové RNA a blokáce procesu připojování m7G čepičky (proces označovaný jako „capping“) (Chen et al., 2013; Vernekar et al., 2015). Některé nukleosidové analogy inhibují klíčové enzymy metabolismu nukleosidů/nukleotidů, což vede k vyčerpání (depleci) zásob nukleosidů/nukleotidů v buňce (Leyssen et al., 2005). Jiné nukleosidové analogy působí jako tzv. letální mutageny, které vedou k akumulaci velkého množství bodových mutací ve virovém genomu, což má za následek silné narušení integrity virové genetické informace, tzv. „error catastrophe“ (Crotti et al., 2001; Graci et al., 2002). Je zřejmé, že struktura a mechanismus účinku nukleosidových antivirových léčiv je podobná nukleosidovým léčivům s antikancerogenní aktivitou. Vývoj nukleosidových antivirových léčiv šel proto vždy ruku v ruce s vývojem antitumorových a antileukemických léčiv (Miura and Izuta, 2004).

Antivirovika na bázi nukleosidových analogů se vyznačují některými charakteristickými vlastnostmi, které je zvýhodňují proti jiným druhům antivirových léčiv. Předně mohou selektivně interagovat s virovými polymerázami nebo methyltransferázami, což výrazným způsobem snižuje jejich toxicitu. Dále bylo pozorováno, že rezistence na nukleosidová antivirovika se vytváří s větší obtížností v porovnání s ostatními (nukleosidovými) antivirovými léčivy a rezistentní virové mutanty mají zpravidla výrazně oslabenou replikační kapacitu (vyšší genotypová a fenotypová rezistenční bariéra) (Delang et al., 2011). Na druhé straně mohou chemické modifikace vedoucí ke vzniku nukleosidových analogů narušit jejich schopnost interagovat se specifickými nukleosidovými transportéry i s nukleosidkinázami, což v mnoha případech snižuje nebo zcela eliminuje jejich biologickou aktivitu. Tento problém je možno vyřešit syntézou monofosfátových nebo fosforamidátových profarmak, která se po odštěpení protektivních skupin pomocí buněčných esteráz mění v biologicky aktivní látky (Lam et al., 2010; Clarck et al., 2005).

Následující text podává krátký komentář k jednotlivým autorským publikacím, které jsou prezentovány v tomto habilitačním spisu. Studie pojednávají o antivirových vlastnostech nukleosidových analogů, které byly na našem pracovišti popsány jako účinné inhibitory vybraných virových patogenů z čeledi *Flaviviridae* (z klíšťaty přenášených flavivirů to jsou především VKE, virus vrtivky a virus horečky kyassanurského lesa; z komáry přenášených flavivirů pak virus Zika a virus horečky Západního Nilu), *Coronaviridae* (SARS-CoV-2) nebo *Herpesviridae* (HSV-1 a virus Aujeszkyho choroby). Některé inhibitory byly také testovány proti zástupcům čeledi *Phenuiviridae* (virus horečky údolí Rift) a *Rhabdoviridae* (virus vztekliny). Práce se zabývají detailní charakteristikou antivirového efektu nukleosidů na různých buněčných kulturách i v experimentálním zvířeti, studiem mechanismu účinku prostřednictvím specializovaných metod využívajících rekombinantní virové polymerázy a

v neposlední řadě studiem rezistence na nukleosidová antivirotika s detailní charakterizací genotypových a fenotypových vlastností rezistentních virových mutant.

Studie „*Nucleoside inhibitors of tick-borne encephalitis virus*“ (Eyer et al., 2015) je vůbec první prací popisující inhibiční účinek nukleosidových analogů na replikaci VKE v hostitelské buňce. V této práci byly charakterizovány látky 2'-C-methyladenosin, 7-deaza-2'-C-methyladenosin, 2'-C-methylcytidin, ribavirin, 6-azauridin a profarmakum mericitabin. Pro charakterizaci antivirové aktivity vybraných nukleosidů byly zvoleny dva kmeny VKE, Hypr a Neudoerfl, oba zástupci evropského subtypu VKE. Kmen Hypr byl izolován v 50. letech z mozku dětského pacienta s klíšťovou encefalitidou na území České republiky a vykazuje na rozdíl od kmene Neudoerfl obecně vyšší virulenci a schopnost vyvolat onemocnění. Aktivita látek byla testována na buněčné linii PS (buňky prasečího ledvinového epitelu) a na neuroblastomové linii (UKF-NB-4). Byly tedy zvoleny buněčné linie jak neuronového, tak extraneurálního původu, což je důležité pro studium neurotropních virů přenášených vektory, schopných množit se v rozličných buněčných typech. V rámci této studie byly také zavedeny a optimalizovány zásadní in vitro metody a funkční testy, které byly v následujících pracích rutinně využívány a dále rozvíjeny pro testování nových látek i charakterizaci jejich mechanismu účinku. Vzhledem k tomu, že nukleosidové analogy nebyly proti VKE nikdy před tím testovány, předmětem zájmu této studie byly známé látky, u kterých byl již dříve prokázán antivirový efekt proti viru žloutenky typu C, dobře charakterizovaného zástupce čeledi *Flaviviridae* (Eldrup et al., 2004). Z testovaného souboru látek byla antivirová aktivita proti VKE prokázána u 2'-C-methyladenosinu, 7-deaza-2'-C-methyladenosinu a 2'-C-methylcytidinu, pohybovala se v mikromolárních hodnotách a byla demonstrována pomocí několika na sobě nezávislých in vitro metod, jako jsou titr-redukční test, test redukce cytopatického efektu a imunofluorescenční barvení. S výjimkou 2'-C-methylcytidinu, který vykazoval mírnou cytotoxicitu při 50 μ M, byly ostatní testované látky buněčnou kulturou dobře tolerovány. Tato práce poskytla základ pro navazující studie zabývající se detailně strukturními vlastnostmi inhibitorů VKE a dalších vektorem přenášených flavivirů a analýzou jejich mechanismu účinku.

Zjištění, že 2'-C-methyladenosin, 7-deaza-2'-C-methyladenosin a 2'-C-methylcytidin vykazují výrazný antivirový efekt proti VKE vedlo k rozsáhlejší studii, která si kladla za cíl nalézt obecné strukturní rysy v molekule nukleosidu zodpovídající za antivirový efekt potlačující replikaci VKE v hostitelské buňce. Touto otázkou se detailně zabývá práce „*Structure-activity relationships of nucleoside analogues for inhibition of tick-borne encephalitis virus*“ (Eyer et al., 2016), ve které byl testován soubor 29 nukleosidů modifikovaných v různých pozicích ribózového kruhu nebo heterocyklické nukleobáze. Pozornost byla zaměřena zejména na nukleosidy s methylovou skupinou v pozici 2'C, 2'O, 3'C nebo 3'O, dále na 2'-C-fluoro-2'-C-methylované nukleosidy, 3'-deoxyribonukleosidy, nukleosidy azidované v pozici 4'C, nukleosidy modifikované na heterocyklické nukleobázi a některé neplanociny. Studie jednoznačně prokázala, že nukleosidy methylované v pozici 2'C (zejména 7-deaza-2'-C-methyladenosin) nebo azidované v pozici 4'C (zejména 4'-azidoaracytidin) vykazují výraznou inhibiční aktivitu proti VKE a zanedbatelnou toxicitu. Je zajímavé, že u 4'-azidovaných nukleosidů byl pozorován antivirový efekt závislý na typu buněčné line; tyto látky nejsou aktivní v neuroblastech UKF-NB-4, a to pravděpodobně proto, že tato specializovaná buněčná linie nedisponuje specifickými transportními systémy nebo kinázami pro přenos a aktivaci (fosforylaci) nukleosidů. Methylová skupina zavedená do pozice 2'O nebo 3'C, stejně jako 3'-deoxy modifikace vedly ke ztrátě aktivity, což ukazuje na nezbytnost přítomnosti 2'a 3'-

hydroxylů v molekule nukleosidu pro správnou interakci s aktivním místem virové RNA-dependentní RNA polymerázy (RdRp). Modifikace v oblasti heterocyklické nukleobáze vedly k prudkému nárůstu cytotoxicity, pravděpodobně v důsledku snížení selektivity vůči hostitelským replikačním enzymům. V této práci byl též detailně studován buněčný transport nukleosidových analogů a účinnost fosforylace v cílových buněčných liniích. Mikromolární antivirová aktivita 2'-C-methylovaných a 4'-azidovaných nukleosidových analogů byla později pozorována i u dalších zástupců čeledi *Flaviviridae*, konkrétně pro virus Zika a virus horečky Západního Nilu, a to s využitím buněčných linií PS nebo Vero. Výsledky jsou popsány v navazujících pracích „**Nucleoside inhibitors of zika virus**“ (Eyer et al., 2016) a „**Viral RNA-dependent RNA polymerase inhibitor 7-deaza-2'-C-methyladenosine prevents death in a mouse model of West Nile virus infection**“ (Eyer et al., 2018), rovněž prezentovaných v tomto habilitačním spisu.

7-Deaza-2'-C-methyladenosin byl v předchozích studiích identifikován jako nukleosidový inhibitor VKE s nejsilnějším antivirovým účinkem z celé rodiny 2'-C-methylovaných nukleosidů. Proto byla antivirová aktivita této látky analyzována také in vivo s využitím myšního infekčního modelu. Studie popsaná v práci „**Escape of tick-borne flavivirus from 2'-C-methylated nucleoside antivirals is mediated by a single conservative mutation in NS5 that has a dramatic effect on viral fitness**“ (Eyer et al., 2017) prokazuje, že myši infikované letální dávkou VKE, kterým byl aplikován nukleosid intraperitoneálně (25 mg/kg, dvakrát denně po dobu >10 dní) vykazovaly výrazné snížení mortality (60%) a zmírnění klinických projevů infekce oproti myším, kterým nebyl nukleosid podán (100% mortalita). Taktéž došlo k významné redukci titru viru v orgánech infikovaných myší ošetřených nukleosidem. Antivirový efekt byl pozorován také u speciálních geneticky upravených myší, označovaných IFN $\beta^{+/Δ\beta}$ -luc, které mají jednu z alel pro interferon β nahrazenou genem pro luciferázu. Infekcí indukovaná interferonová odpověď vede u těchto zvířat k produkci luciferázy a po injekci luciferinu lze v místech, kde probíhá infekce, detekovat zřetelný luminiscenční signál (měřeno pomocí zařízení pro „in vivo imaging“). Ještě výraznější antivirový efekt in vivo byl pozorován u myší infikovaných letální dávkou viru horečky západního Nilu. Zvířata vykazovala po intraperitoneální aplikaci nukleosidu (25 mg/kg, dvakrát denně) mortalitu 0%. Látka byla účinná dokonce při aplikaci 3 dny po infekci. Avšak, byla-li aplikovaná 8. den po infekci (doba, kdy dochází k rozvoji klinických symptomů neuroinfekce), antivirová aktivita již nebyla pozorována (100% mortalita). To svědčí o tom, že po průniku viru přes hematoencefalickou bariéru již látka není schopna blokovat replikaci viru v centrálním nervovém systému.

Tatáž práce se dále zabývá studiem rezistence VKE na nukleosidová antivirotika 2'-C-methylované řady. Pasážováním na PS buňkách při vzrůstající koncentraci 7-deaza-2'-C-methyladenosinu byla selektována rezistentní mutanta VKE. Celogenomovým sekvenováním bylo zjištěno, že mutantní varianta nese v aktivním místě virové RdRp mutaci S603T, která zodpovídá za vysoký stupeň rezistence viru na 2'-C-methylované nukleosidy (prokázáno pomocí rekombinantního virového infekčního klonu) a je identická s mutací S828T u HCV (Flint et al., 2014) a S600T u viru Dengue a S604T u viru Zika (Xu et al., 2017). Je velmi zajímavé, že rezistentní mutanty vykazovaly oproti viru standardního typu („wild-type“, WT) sníženou schopnost replikovat se v buněčné kultuře (pomalý růst, dosažení nižšího titru), odlišnou morfologii plaků (malé, matné a nevýrazné plaky) i silně antenuovaný fenotyp v myším infekčním modelu (pouze 40% mortalita oproti 100% u WT). Práce ukazuje, že ačkoli dojde při

replikaci viru v přítomnosti nukleosidového analogu ke vzniku rezistence, rezistentní varianty viru mají výrazně oslabený fenotyp. Toto zjištění představuje důležitou informaci při vývoji nových léčiv proti infekcím vyvolaným VKE a jinými flaviviry.

Dalším velice zajímavým nukleosidovým analogem je galidesivir, označovaný také jako BCX4430. Tento nukleosid byl původně vyvinut jako velmi účinný inhibitor zástupců čeledi *Filoviridae* a později bylo prokázáno, že vykazuje širokospektrální antivirový účinek proti řadě obalených RNA virů z čeledi *Phenuiviridae*, *Arenaviridae*, *Picornaviridae*, *Orthomyxoviridae*, *Coronaviridae* a *Flaviviridae* (Warren et al., 2014). Před několika lety byla látka zařazena do klinických testů pro léčbu infekcí virem Ebola a virem žluté zimnice (Taylor et al., 2016; Julander et al., 2021). Galidesivir je typický C-nukleosid (N-glykosidová vazba je nahrazena C-glykosidovou vazbou). Navíc je u této látky atom kyslíku v pentózovém kruhu nahrazen dusíkem. Hlavním mechanismem účinku tohoto nukleosidu je předčasná a postupná terminace syntézy virové RNA; nukleosid je tedy typický neobligátní terminátor syntézy virové NK (Warren et al., 2014). V naší studii „**Antiviral activity of the adenosine analogue BCX4430 against West Nile virus and tick-borne flaviviruses**“ (Eyer et al., 2017) jsme poprvé popsali a podrobně charakterizovali antivirový účinek galidesiviru na souboru klíšťaty přenášených flavivirů (VKE, virus horečky kyassanurského lesa a virus vrtivky). Z komary přenášených virů vykazoval galidesivir mikromolární antivirový efekt proti viru horečky Západního Nilu (kmen Eg-101, izolován v 50. letech z lidského séra v Egyptě a kmen 10-104, izolován z komára *Culex modestus* v České Republice v r. 2013) (Melnick et al., 1951; Rudolf et al., 2013). Antivirová aktivita látky byla studována s využitím dvou imortalizovaných buněčných linií, vhodných pro kultivaci flavivirů, PS a Vero (ledvinové epitelové buňky kočkodana) a byla též ověřena na lidských neuroblastech SK-N-SH.

Základní popis antivirové aktivity galidesiviru byl následně rozšířen v navazující studii „**An E460D substitution in the NS5 protein of tick-borne encephalitis virus confers resistance to the inhibitor galidesivir (BCX4430) and also attenuates the virus for mice**“ (Eyer et al., 2019), ve které byl jeho mechanismus účinku detailně prostudován s využitím galidesivir-rezistentních mutant VKE. Rezistentní mutanta byla získána pasážováním na PS buňkách při zvyšující se koncentraci galidesiviru. Bylo zjištěno, že v aktivním místě virové RdRp se u rezistentních mutant vyskytuje charakteristická mutace E450D. Význam této mutace pro navození rezistence na galidesivir byla potvrzena pomocí reverzně-genetického systému, který je založen na tzv. infekčních subgenomových amplikonech (ISA) a který byl zaveden a optimalizován také v této práci. Podobně jako u mutant rezistentních na 2'-C-methylované nukleosidy také u galidesivir-rezistentních mutant bylo prokázáno snížené replikační fitness v buněčné kultuře. To však bylo pozorováno jen na samotném začátku infekce (do prvních 36 hodin po infekci). V dalších časových intervalech byly již titry mutantního viru porovnatelné s titry WT. Rovněž morfologie plaků nebyla výrazně pozměněna proti WT, což svědčí pouze o částečné redukci replikačního fitness mutantního viru. Avšak v myším infekčním modelu vykazovaly tyto mutanty vysoký stupeň atenuace; myši infikované mutantním VKE neprojevovaly žádné příznaky neuroinfekce a všechny infikované myši přežily experimentální infekci (0% mortalita proti 100% u kontrolních myší). Studie opět ukázala, že v rámci aktivního místa virové RdRp existuje klíčová oblast pro přísně specifickou interakci s molekulou galidesiviru. Dále je z výsledků zřejmé, že rezistence k nukleosidovému analogu je uskutečněna za cenu snížení replikačního fitness viru, což se projeví zejména při replikaci a šíření viru v tkáních savčího hostitele, podobně jako v případě rezistence na 2'-C-methylované nukleosidy.

Zatímco výše popsané nukleosidy jsou klasické neobligátní terminátory syntézy virové NK, existují i deriváty nukleosidů, které vykazují naprosto odlišný mechanismus účinku. Takovými jsou konjugáty nukleosidů s 2-deoxysacharidy v pozici 5'C, které představují účinné inhibitory N-glykosylačních procesů, plnicích důležitou roli v maturaci strukturních virových proteinů. Práce **“Antiviral Activity of Uridine Derivatives of 2-Deoxy Sugars against Tick-Borne Encephalitis Virus”** (Krol et al., 2019) podrobně studuje tento proces u VKE (opět s využitím kmenů Hypr a Neudoerfl) pomocí série glykosylovaných derivátů uridinu. Některé z připravených analogů vykazují výrazný (mikromolární) antivirový účinek proti VKE. Výsledky ukazují, že tyto nukleosidové deriváty mohou ovlivňovat aktivitu glykosylovaných membránových proteinů E a prM. Jedná se tedy o zajímavý příklad nukleosidů s mechanismem účinku zaměřeným na pozdní fázi virové replikace s cílem ovlivnit správnou funkci klíčových proteinů lokalizovaných na povrchu virové částice.

V medicíně nacházejí často uplatnění také fluor-substituované nukleosidy, a to zejména v boji s nádorovými onemocněními (např. gemcitabin [2'-dideoxy-2',2'-difluorocytidin] a floxuridin [2'-deoxy-5-fluorouridin]), nebo jako antivirová léčiva (např. sofosbuvir, proframakum odvozené z 2'-fluoro-2'-methyluridinu). Fluorované nukleosidy jsou nositeli zvláštních a zajímavých fyzikálně-chemických vlastností, které se uplatňují také při jejich intrakcích s biologickými systémy. Studie **“Broad-Spectrum Antiviral Activity of 3'-Deoxy-3'-Fluoroadenosine against Emerging Flaviviruses”** (Eyer et al., 2021) se zaměřuje na analýzu antivirové aktivity série fluor-substituovaných nukleosidů (modifikovaných na ribózovém kruhu nebo na heterocyklické nukleobázi) proti medicínsky významným zástupcům čeledi *Flaviviridae*, tj. VKE (kmeny Hypr a Neudoerfl), virus Zika (africký kmen MR-766 a brazilský kmen Paraiba_02) a virus horečky Západního Nilu (kmeny Eg-101 a 10-104). Je zajímavé, že z celé testované série (celkem 28 derivátů) vykazoval antivirovou aktivitu pouze jediný derivát, a to 3'-deoxy-3'-fluoroadenosin. Ostatní nukleosidové analogy byly buď zcela neaktivní nebo vysoce cytotoxické. 3'-Deoxy-3'-fluoroadenosin vykazoval mikromolární antivirový účinek potlačující replikaci výše uvedených flavivirů jak v imortalizované kultuře PS buněk, tak v primárních lidských mozkových kortikálních astrocytech (HBCA). Primární buňky byly pro tuto studii vybrány záměrně jako klinicky relevantnější model oproti imortalizovaným buněčným liniím, které v důsledku nestability genomu často vykazují netypické fyziologické vlastnosti. Látka však vykazovala výrazný cytostatický účinek, byla-li na oba buněčné typy aplikována ve vyšších koncentracích (>25 μM), což lze vysvětlit nízkou selektivitou vůči virovým, resp. savčím polymerázám. Tato látka vykazuje rovněž poměrně širokospektrální antivirový efekt proti mnohým RNA a DNA virům (Van Aerschot et al., 1989; Smeets et al., 1992). Toto extrémně široké rozmezí biologické aktivity taktéž svědčí o nízké selektivitě nukleosidu. 3'-Deoxy-3'-fluoroadenosin vykazoval antivirovou aktivitu také v myším infekčním modelu; v případě myší infikovaných VKE významně prodloužil dobu přežití a u myší infikovaných virem horečky Západního Nilu dokonce snížil mortalitu na 30% (ze 100% u kontrolních zvířat). Tato práce je vůbec první studií popisující antivirový efekt fluor-modifikovaného nukleosidu proti VKE a jedna z mála, která popisuje inhibiční účinek těchto látek na ostatní vektorem přenášené flaviviry.

V úzké spolupráci s Ústavem organické chemie a biochemie bylo provedeno několik studií týkajících se zcela nových nukleosidových struktur syntetizovaných na tomto pracovišti. Jako příklad je uvedena práce **“Antiviral Activity of 7-Substituted 7-Deazapurine**

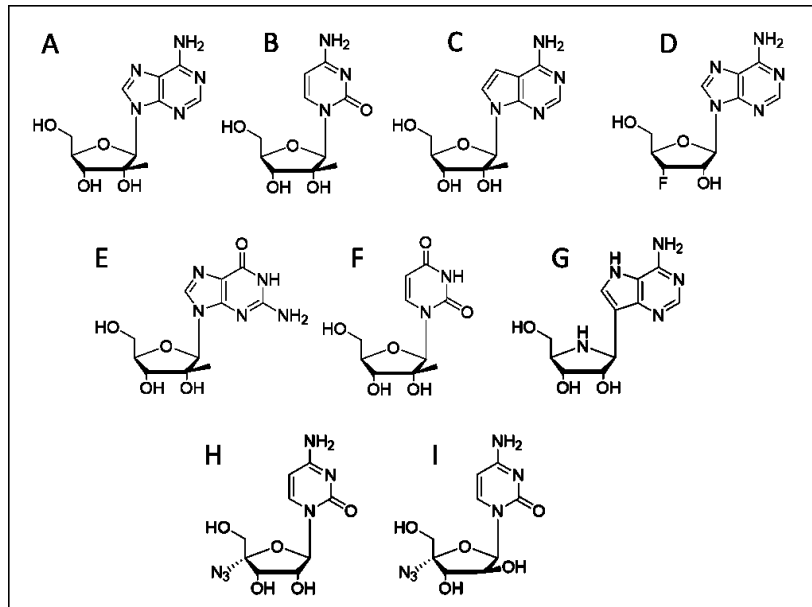
Ribonucleosides, Monophosphate Prodrugs, and Triphosphates against Emerging RNA Viruses (Milisavljevic et al., 2021), která se zabývá syntézou, ověřením antivirové aktivity a objasněním mechanismu účinku derivátů 7-deazaadenosinu substituovaných různými funkčními skupinami (alkyl, alkenyl, alkynyl, aryl, nebo hetaryl) v pozici 7, jejich 5'-O-trifosfátů a také dvou monofosfátových profarmak (fosforamidátových a S-acylthioetanol esterových forem). Byla studována jejich schopnost inhibovat replikaci medicínsky významných flavivirů (VKE, viru Dengue, viru Zika a viru horečky západního Nilu) a také SARS-CoV-2 in vitro (tato práce vznikla již v době koronavirové pandemie). Pomocí metodologických přístupů využívajících rekombinantní flavivirové a koronavirové RdRp bylo prokázáno, že trifosfátové formy testovaných nukleosidů inhibují virové polymerázy a zastavují syntézu replikující se virové RNA. Ethynyl-substituované deriváty nebo nukleosidy modifikované v pozici 7 malou hetarylovou skupinou byly výrazně toxické, zatímco nukleosidy s větší heterocyklickou substitucí vykazovaly antivirovou aktivitu, avšak byly méně toxické. Je překvapivé, že monofosfátová profarmaka se antivirovou aktivitou příliš nelišila od příslušných parentálních nukleosidů, ačkoli bylo prokázáno, že jsou účinně transportovány do buněk i efektivně fosforylovány.

Velmi cenným nástrojem při studiu inhibitorů virové replikace jsou virové reportérové systémy. Práce ***Development and characterization of recombinant tick-borne encephalitis virus expressing mCherry reporter protein: A new tool for high-throughput screening of antiviral compounds, and neutralizing antibody assays*** (Haviernik et al., 2021) se zabývá konstrukcí virového reportéru odvozeného od VKE (kmen Hypr) a jeho využití pro in vitro testování antivirových i pro studium virus-neutralizačního efektu protilátek a protilátkových antisér. Systém je založen na rekombinantním VKE, který nese ve svém genomu gen pro fluorescenční protein (mCherry, ex/em: 580/610 nm) lokalizovaný na 5' konci genu pro virový C protein. Rekombinantní virus se získá po transfekci permissivních buněk ekvimolární směsí tří ISA fragmentů, které svojí sekvencí pokrývají celý genom VKE (součástí prvního fragmentu je silný cytomegalovirový promotor a gen pro mCherry). Tyto fragmenty v buňce rekombinují a dávají vzniknout jediné lineární molekule DNA, která je následně přepsána do mRNA a přeložena do virových proteinů, které následně skládají kompletní infekční virové částice. Reportérový protein mCherry není součástí vzniklých rekombinantních virionů, protože je při translaci z nascentního polyptidového řetězce oddělen (přítomnost tzv. "ribosome-skipping" sekvencí), hromadí se v infikovaných buňkách a je zdrojem intenzivního fluorescenčního signálu. Vyvinutý reportérový systém je dostatečně stabilní (reportérový gen zůstává součástí virového genomu po více než pět pasáží) a byl úspěšně využit k ověření antivirové aktivity některých 2'-C-methylovaných a 4'-azidovaných nukleosidových analogů.

Poslední prací prezentovanou v této části habilitačního spisu je studie ***Antiviral activities of 2,6-diaminopurine-based acyclic nucleoside phosphonates against herpesviruses: In vitro study results with pseudorabies virus (PrV, SuHV-1)*** (Zouharová et al., 2016). Narozdíl od předchozích prací se nezabývá inhibitory flavivirů nebo koronavirů, nýbrž je zaměřena na významného zástupce čeledi *Herpesviridae*, virus Aujeszkyho choroby (pseudorabies virus, PrV). Práce popisuje antivirovou aktivitu série syntetických analogů acyklických nukleosidových fosfonátů na bázi diaminopurinů. Jako nejúčinnější se jevil analog s cyklopropylovou skupinou na 6-amino pozici purinového kruhu. Látka má hydrofobní charakter, což je vhodné pro zvýšenou biologickou dostupnost. Vzhledem k jeho podobnosti s acyklovirem se předpokládá, že nukleosid specificky cílí na virovou DNA-polymerázu a inhibuje

virovou replikaci jako klasický obligátní terminátor syntézy virové DNA. Naproti tomu analogy s funkčními skupinami zavedenými do polohy 2'C se ukázaly jako neúčinné proti infekci PrV, a to i v případě jejich příznivého hydrofobního charakteru.

Struktury vybraných nukleosidů, které byly na našem pracovišti indentifikovány jako významné inhibitory vektorem přenášených flavivirů, zejména VKE, jsou uvedeny na obr. 2.



Obr. 2. Struktury nuleosidových analogů identifikovaných jako mikromolární inhibitory vektorem přenášených flavivirů. (A) 2'-C-methyladenosin, (B) 2'-C-methylcytidin, (C) 7-deaza-2'-C-methyladenosin, (D) 3'-fluoro-3'-deoxyadenosin, (E) 2'-C-methylguanosin, (F) 2'-C-methyluridin, (G) galidesivir, (H) 4'-azidocytidin, (I) 4'-azidoaracytidin.

PŘÍLOHA 2

1. **Eyer L**, Valdés JJ, Gil VA, Nencka R, Hřebabecký H, Šála M, Salát J, Černý J, Palus M, De Clercq E, Růžek D. Nucleoside inhibitors of tick-borne encephalitis virus. *Antimicrob Agents Chemother*. 2015 Sep;59(9):5483-93.
2. **Eyer L**, Šmídková M, Nencka R, Neča J, Kastl T, Palus M, De Clercq E, Růžek D. Structure-activity relationships of nucleoside analogues for inhibition of tick-borne encephalitis virus. *Antiviral Res*. 2016 Sep;133:119-29.
3. **Eyer L**, Nencka R, Huvarová I, Palus M, Joao Alves M, Gould EA, De Clercq E, Růžek D. Nucleoside Inhibitors of Zika Virus. *J Infect Dis*. 2016 Sep 1;214(5):707-11.
4. **Eyer L**, Fojtíková M, Nencka R, Rudolf I, Hubálek Z, Ruzek D. Viral RNA-Dependent RNA Polymerase Inhibitor 7-Deaza-2'-C-Methyladenosine Prevents Death in a Mouse Model of West Nile Virus Infection. *Antimicrob Agents Chemother*. 2019 Feb 26;63(3):e02093-18.
5. **Eyer L**, Kondo H, Zouharova D, Hirano M, Valdés JJ, Muto M, Kastl T, Kobayashi S, Haviernik J, Igarashi M, Kariwa H, Vaculovicova M, Cerny J, Kizek R, Kröger A, Lienenklaus S, Dejmek M, Nencka R, Palus M, Salat J, De Clercq E, Yoshii K, Ruzek D. Escape of Tick-Borne Flavivirus from 2'-C-Methylated Nucleoside Antivirals Is Mediated by a Single Conservative Mutation in NS5 That Has a Dramatic Effect on Viral Fitness. *J Virol*. 2017 Oct 13;91(21):e01028-17.
6. **Eyer L**, Zouharová D, Širmarová J, Fojtíková M, Štefánik M, Haviernik J, Nencka R, de Clercq E, Růžek D. Antiviral activity of the adenosine analogue BCX4430 against West Nile virus and tick-borne flaviviruses. *Antiviral Res*. 2017 Jun;142:63-67.
7. **Eyer L**, Nougairède A, Uhlířová M, Driouich JS, Zouharová D, Valdés JJ, Haviernik J, Gould EA, De Clercq E, de Lamballerie X, Ruzek D. An E460D Substitution in the NS5 Protein of Tick-Borne Encephalitis Virus Confers Resistance to the Inhibitor Galidesivir (BCX4430) and Also Attenuates the Virus for Mice. *J Virol*. 2019 Jul 30;93(16):e00367-19.
8. Krol E, Wandzik I, Brzuska G, **Eyer L**, Růžek D, Szewczyk B. Antiviral Activity of Uridine Derivatives of 2-Deoxy Sugars against Tick-Borne Encephalitis Virus. *Molecules*. 2019 Mar 21;24(6):1129.
9. **Eyer L**, Svoboda P, Balvan J, Vičar T, Raudenská M, Štefánik M, Haviernik J, Huvarová I, Straková P, Rudolf I, Hubálek Z, Seley-Radtke K, de Clercq E, Růžek D. Broad-Spectrum Antiviral Activity of 3'-Deoxy-3'-Fluoroadenosine against Emerging Flaviviruses. *Antimicrob Agents Chemother*. 2021 Jan 20;65(2):e01522-20.
10. Milisavljevic N, Konkolová E, Kozák J, Hodek J, Veselovská L, Sýkorová V, Čížek K, Pohl R, **Eyer L**, Svoboda P, Růžek D, Weber J, Nencka R, Bouřa E, Hocek M. Antiviral Activity of 7-Substituted 7-Deazapurine Ribonucleosides, Monophosphate Prodrugs,

and Triphosphates against Emerging RNA Viruses. *ACS Infect Dis.* 2021 Feb 12;7(2):471-478.

11. Haviernik J, **Eyer L**, Yoshii K, Kobayashi S, Cerny J, Nougairède A, Driouich JS, Volf J, Palus M, de Lamballerie X, Gould EA, Ruzek D. Development and characterization of recombinant tick-borne encephalitis virus expressing mCherry reporter protein: A new tool for high-throughput screening of antiviral compounds, and neutralizing antibody assays. *Antiviral Res.* 2021 Jan;185:104968.
12. Zouharova D, Lipenska I, Fojtikova M, Kulich P, Neca J, Slany M, Kovarcik K, Turanek-Knotigova P, Hubatka F, Celechovska H, Masek J, Koudelka S, Prochazka L, **Eyer L**, Plockova J, Bartheldyova E, Miller AD, Ruzek D, Raska M, Janeba Z, Turanek J. Antiviral activities of 2,6-diaminopurine-based acyclic nucleoside phosphonates against herpesviruses: In vitro study results with pseudorabies virus (PrV, SuHV-1). *Vet Microbiol.* 2016 Feb 29;184:84-93.

Nucleoside Inhibitors of Tick-Borne Encephalitis Virus

Luděk Eyer,^a James J. Valdés,^b Víctor A. Gil,^c Radim Nencka,^d Hubert Hřebabecký,^d Michal Šála,^d Jiří Salát,^a Jiří Černý,^{a,b,e} Martin Palus,^{a,b,e} Erik De Clercq,^f Daniel Růžek^{a,b,e}

Department of Virology, Veterinary Research Institute, Brno, Czech Republic^a; Institute of Parasitology, Biology Centre of the Czech Academy of Sciences, České Budějovice, Czech Republic^b; Joint BSC-CRG-IRB Research Program in Computational Biology, Barcelona Supercomputing Center, Barcelona, Spain^c; Institute of Organic Chemistry and Biochemistry, The Czech Academy of Sciences, Prague, Czech Republic^d; Faculty of Science, University of South Bohemia, České Budějovice, Czech Republic^e; Rega Institute for Medical Research, Leuven, Belgium^f

Tick-borne encephalitis virus (TBEV) is a leading cause of human neuroinfections in Europe and Northeast Asia. There are no antiviral therapies for treating TBEV infection. A series of nucleoside analogues was tested for the ability to inhibit the replication of TBEV in porcine kidney cells and human neuroblastoma cells. The interactions of three nucleoside analogues with viral polymerase were simulated using advanced computational methods. The nucleoside analogues 7-deaza-2'-C-methyladenosine (7-deaza-2'-CMA), 2'-C-methyladenosine (2'-CMA), and 2'-C-methylcytidine (2'-CMC) inhibited TBEV replication. These compounds showed dose-dependent inhibition of TBEV-induced cytopathic effects, TBEV replication (50% effective concentrations [EC₅₀] of 5.1 ± 0.4 μM for 7-deaza-2'-CMA, 7.1 ± 1.2 μM for 2'-CMA, and 14.2 ± 1.9 μM for 2'-CMC) and viral antigen production. Notably, 2'-CMC was relatively cytotoxic to porcine kidney cells (50% cytotoxic concentration [CC₅₀] of ~50 μM). The anti-TBEV effect of 2'-CMA in cell culture diminished gradually after day 3 posttreatment. 7-Deaza-2'-CMA showed no detectable cellular toxicity (CC₅₀ > 50 μM), and the antiviral effect in culture was stable for >6 days posttreatment. Computational molecular analyses revealed that compared to the other two compounds, 7-deaza-2'-CMA formed a large cluster near the active site of the TBEV polymerase. High antiviral activity and low cytotoxicity suggest that 7-deaza-2'-CMA is a promising candidate for further investigation as a potential therapeutic agent in treating TBEV infection.

Tick-borne encephalitis virus (TBEV) belongs to the *Flaviviridae* family, which includes other human- and animal-pathogenic viruses of global importance, such as West Nile virus (WNV), dengue virus (DENV), Japanese encephalitis virus (JEV), yellow fever virus (YFV), and hepatitis C virus (HCV) (1). TBEV virions are approximately 50 nm in diameter and are composed of a spherical nucleocapsid surrounded by a host-derived lipid bilayer. The TBEV genome is a single-stranded, plus-sense RNA about 11 kb in length that encodes a single polyprotein; this polyprotein is co- and posttranslationally processed into 3 structural and 7 nonstructural proteins (2).

In Europe and Northeast Asia, tick-borne encephalitis (TBE) represents one of the most important and serious neuroviral infections. More than 13,000 clinical cases of TBE, including numerous deaths, are reported annually worldwide (3, 4). The considerable increase in TBE incidence in countries where it is endemic and the emergence of the disease in several Western and Northern European countries have made TBE an increasing public health risk. In Europe, the most affected areas are southern Germany, Switzerland, Austria, the Czech Republic, Slovakia, Hungary, Slovenia, the Baltic states, Poland, parts of Scandinavia, and European Russia (5). The disease is usually biphasic: the first stage is febrile with flu-like symptoms, while the second phase manifests most often as meningitis, encephalitis, meningoencephalitis, meningoencephalomyelitis, and radiculitis. There are long-lasting or permanent neuropsychiatric sequelae in 10 to 20% of the infected patients (6). Although human vaccines against TBEV are currently available, the vaccination coverage remains quite low in several of the countries where TBEV is endemic (7). No specific antiviral therapy has been developed for TBE, and patient treatment is limited to supportive care (8). There is thus an urgent need for an effective approach to treatment that is based on specific inhibitors of TBEV replication.

Chemically modified nucleosides, also called nucleoside analogues or nucleoside inhibitors, represent the largest class of antiviral drugs. These compounds generally act via DNA or RNA chain termination with the potential exception of ribavirin, for which the mechanism may depend upon the virus and experimental system (9). Nucleoside analogues have been widely used as inhibitors of numerous medically important viruses, including HIV, herpesvirus, and hepatitis B virus (10, 11). Regarding flaviviruses, nucleoside analogues have been demonstrated to be efficacious in HCV replicon assays (12–16) and also against DENV (17–21), WNV (22), and YFV (23). Some of them were described as broad-spectrum inhibitors of various RNA viruses (24–27). 2'-Modified nucleoside analogues exhibit a high antiflavivirus activity and good pharmacokinetic properties (9). For TBEV inhibition, however, these compounds have not been tested thoroughly, if they have been tested at all. The high degree of homology between the polymerases of TBEV and other flaviviruses (28) suggests, however, that an investigation of nucleoside analogues as inhibitors of TBEV would be worthwhile.

Received 4 April 2015 Returned for modification 28 April 2015

Accepted 18 June 2015

Accepted manuscript posted online 29 June 2015

Citation Eyer L, Valdés JJ, Gil VA, Nencka R, Hřebabecký H, Šála M, Salát J, Černý J, Palus M, De Clercq E, Růžek D. 2015. Nucleoside inhibitors of tick-borne encephalitis virus. *Antimicrob Agents Chemother* 59:5483–5493. doi:10.1128/AAC.00807-15.

Address correspondence to Daniel Růžek, ruzekd@paru.cas.cz.

Supplemental material for this article may be found at <http://dx.doi.org/10.1128/AAC.00807-15>.

Copyright © 2015, American Society for Microbiology. All Rights Reserved.

doi:10.1128/AAC.00807-15

In the present study, a series of nucleoside analogues were tested for the ability to inhibit TBEV replication in cell culture. Particular attention was paid to chemically modified nucleosides that have reported antiviral activity against other flaviviruses, especially HCV (14) or hemorrhagic fever-associated flaviviruses (i.e., Alkhurma hemorrhagic fever virus, Omsk hemorrhagic fever virus, and Kyasanur Forest disease virus) (29). Compounds with favorable inhibitory profiles in the virus titer reduction assays were further assayed for the ability to inhibit virus-induced cytopathic effects and to suppress viral antigen expression in infected cell cultures. The lead compounds were subsequently evaluated for dose-response inhibition of TBEV replication and for potential cytotoxic effects on host cells. Based on these screens, we identified three compounds with strong anti-TBEV activity. The favorable characteristics of one of these compounds, 7-deaza-2'-C-methyladenosine (7-deaza-2'-CMA), indicate that it merits further investigation as a therapeutic agent for treating TBEV infections.

MATERIALS AND METHODS

Cell cultures, virus strains, and antiviral compounds. Porcine kidney stable (PS) cells were cultured at 37°C in Leibovitz (L-15) medium supplemented with 3% precolostral calf serum and a 1% mixture of penicillin and glutamine (Sigma-Aldrich, Prague, Czech Republic) (30). Human neuroblastoma UKF-NB-4 cells were cultured at 37°C in 5% CO₂ in Iscove's modified Dulbecco's medium (IMDM) supplemented with 10% fetal bovine serum and a 1% mixture of penicillin and streptomycin (Sigma-Aldrich) (31). All experiments were performed with TBEV strains Hypr and Neudoerfl, which are representatives of the West European TBEV subtype. Ribavirin and 2'-C-methyladenosine (2'-CMA) were synthesized at the Institute of Organic Chemistry and Biochemistry (Prague, Czech Republic). 7-deaza-2'-C-methyladenosine (7-deaza-2'-CMA), 2'-C-methylcytidine (2'-CMC), and 6-azauridine were purchased from Carbosynth (Compton, United Kingdom). Mericitabine was purchased from ChemScene (Monmouth Junction, NJ). The test compounds were solubilized in 100% (vol/vol) dimethyl sulfoxide (DMSO) to yield 10 mM stock solutions.

Viral titer reduction assay. PS or UKF-NB-4 cells were seeded in 96-well plates (approximately 2×10^4 cells per well) and incubated for 24 h to form a confluent monolayer. Following incubation, the medium was aspirated from the wells and replaced with 200 μ l of fresh medium containing a 50 μ M concentration of the test compound (three wells per compound). The cells were immediately infected with the Hypr or Neudoerfl TBEV strain at a multiplicity of infection (MOI) of 0.1. As a negative control, DMSO was added to virus- and mock-infected cells at a final concentration of 0.5% (vol/vol). After 72 h of incubation, the medium was collected and immediately frozen at -80°C. Viral titers were determined by plaque assay.

Plaque assay. Virus titers were assayed using PS cell monolayers as described previously (32). Briefly, 10-fold dilutions of TBEV were prepared in 24-well tissue culture plates, and PS cells were added in suspension (0.6×10^5 to 1.5×10^5 cells per well). After a 4-h incubation, the suspension was overlaid with 1.5% (wt/vol) carboxymethylcellulose in L-15 medium. Following a 5-day incubation at 37°C, the infected plates were washed with phosphate-buffered saline (PBS) and the cell monolayers were stained with naphthalene black. The virus titer was expressed as PFU per milliliter.

CPE inhibition assay and CPE quantification. The PS cells were seeded in 96-well plates, the test compounds were added, and the cells were infected with TBEV as described for the viral titer reduction assay. Culture medium was collected 3 to 4 days postinfection (p.i.) to yield a 40 to 50% cytopathic effect (CPE) in virus control wells. The CPE was monitored visually using an Olympus BX-5 microscope equipped with an Olympus DP-70 charge-coupled-device (CCD) camera. To quantify the

CPE, both cell death and viability were determined using commercially available colorimetric *in vitro* assays. Cell death was evaluated using the CytoTox 96 nonradioactive cytotoxicity assay (Promega, WI) by following the manufacturer's instructions. This assay is based on quantitative measurement of lactate dehydrogenase, a stable cytosolic enzyme that is released upon cell lysis. Cell death was estimated as the percentage of colorimetric absorbance at 490 nm by the compound-treated cells relative to the absorbance by chemically lysed cells. Cell viability was evaluated by determining formazan exclusion in confluent cell cultures in a colorimetric assay utilizing Dojindo's highly water-soluble tetrazolium salt (Cell Counting Kit-8; Dojindo Molecular Technologies, MD). Cell viability was expressed as the percentage of absorbance at 450 nm by compound-treated cells relative to the absorbance by DMSO-treated cells.

Immunofluorescence staining. PS cells were cultured on slides treated with the test compound (0 to 50 μ M) and infected with the TBEV Hypr strain at an MOI of 0.1. At day 4 postinfection, the cells were subjected to cold acetone-methanol (1:1) fixation for 10 min, rinsed in saline, and blocked with 10% fetal bovine serum. Cells were labeled with a mouse monoclonal antibody that recognizes the flavivirus group surface antigen (1:250; Sigma-Aldrich, Prague, Czech Republic) by incubation for 1 h at 37°C. After a washing with saline-Tween 20 (0.05% [vol/vol]), the cells were labeled with an anti-mouse goat secondary antibody conjugated with fluorescein isothiocyanate (FITC) (1:500) by incubation for 1 h at 37°C. The cells were counterstained with 4',6-diamidino-2-phenylindole (DAPI) (1 μ g ml⁻¹; Sigma-Aldrich) for 30 min at 37°C and mounted in 2.5% 1,4-diazabicyclo[2.2.2]octane (DABCO; Sigma-Aldrich). The images were acquired with an Olympus IX71 epifluorescence microscope equipped with a Hammamatsu OrcaR2 camera and controlled using Xcelence software. The images were processed using Fiji software (33).

Cytotoxicity assays. PS cell monolayers in 96-well plates were treated with test compounds at a concentration range of 0 to 50 μ M (2-fold dilutions, three wells per concentration). At 4 days p.i., the potential cytotoxicity of test compounds was determined in terms of cell viability and death using Cell Counting Kit-8 (Dojindo Molecular Technologies) and the CytoTox 96 nonradioactive cytotoxicity assay (Promega, WI), respectively, as described for CPE quantification. The concentration of compound that reduced cell viability by 50% was considered the 50% cytotoxic concentration (CC₅₀).

Dose-response studies with 2'-CMA, 7-deaza-2'-CMA, and 2'-CMC. PS cell monolayers that were cultured for 24 h in 96-well plates were treated with 200 μ l of medium containing the test compounds (2'-CMA, 7-deaza-2'-CMA, and 2'-CMC) at concentrations from 0 to 50 μ M (2-fold dilution, three wells per concentration) and infected with the TBEV Hypr strain at an MOI of 0.1. The medium was collected from the wells at 1-day intervals (postinfection days 1 to 6), and the viral titers were determined by plaque assays. The obtained virus titers were utilized to construct TBEV growth curves and dose-response curves for selected nucleoside inhibitors. The dose-response curves on postinfection days 3 and 4 were used to estimate the most widely used measures of drug potency: the 50% effective concentration (EC₅₀; the concentration of compound required to inhibit the viral titer by 50% compared to the control value), the selectivity index (SI = CC₅₀/EC₅₀), and the slope value (Hill coefficient). The EC₅₀s were calculated as follows: a dose-response inhibition curve was fitted to a four parameter logistic curve using Prism 5.04 software (GraphPad, Inc., CA) according to the equation $Y = \text{Bottom} + (\text{Top} - \text{Bottom}) / [1 + 10^{\text{Hill coefficient}(\log \text{EC}_{50} - X)}]$. In this equation, X is the logarithm of the concentration, Y is the logarithm of the titer, bottom and top correspond to the asymptotes of the sigmoidal curve, Hill coefficient corresponds to the slope at the inflection point of the curve, and log EC₅₀ is the calculated midpoint of the curve. The EC₅₀ was calculated as $10^{\log \text{EC}_{50}}$. The standard errors of the EC₅₀s were estimated by the delta method.

Computer-aided protein modeling and preparation, and protein-ligand exploration and clustering. The crystal structures of viral polymerases from HCV (PDB codes 1nb4 and 1nb6), WNV (PDB code 2hfz),

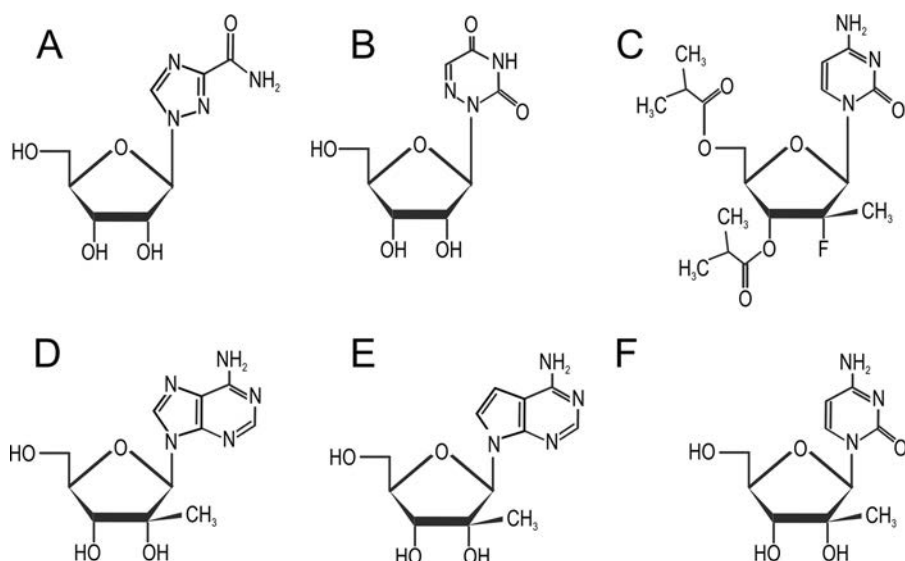


FIG 1 The structures of the nucleoside analogues tested in this study. (A) Ribavirin; (B) 6-azauridine; (C) mericitabine; (D) 2'-CMA; (E) 7-deaza-2'-CMA; (F) 2'-CMC.

and JEV (PDB code 4k6m) were used for computer simulations that would complement the experimental results from this study. The TBEV structure was modeled using Modeler (34). The models were evaluated using the protein model-qualifying servers ModFOLD, QMEAN, and RESPX (35–37). Based on a consensus, the best-ranked TBEV model was then selected for subsequent *in silico* experiments. Since X-ray crystallography methods do not resolve hydrogen atoms, Schrödinger's Maestro Protein Preparation Wizard was used for each viral polymerase structure to assign hydrogen atoms and to optimize the assigned hydrogen-bond network (38). The respective ligands for each protein structure were removed prior to preparation. After protein preparation, an energy minimization (using the default conditions in Schrödinger's Maestro package) (39) was performed for each crystal structure, including the modeled TBEV polymerase structure, to alter the initial conformation and to remove any steric clashes prior to simulations. In addition, the HCV-UTP bound structure (PDB code 1nb6) has two Mn^{2+} ions as co-factors, with several water molecules surrounding the nucleoside. These were also added to all structures and remained constrained for all subsequent simulations.

We used the Protein Energy Landscape Explorer (PELE) algorithm to perform protein-ligand simulations of the three nucleoside triphosphate analogues identified in this study and the aforementioned viral polymerases. For the simulations, we used the triphosphate form of the nucleoside analogues (2'-CMA-TP, 2'-CMC-TP, and 7-deaza-2'-CMA-TP) since they are phosphorylated *in vivo*. A detailed explanation of the PELE algorithm can be found in references (40 and 41), and its many uses can be seen at <https://pele.bsc.es/>. Briefly, PELE performs three steps. First, localized ligand perturbations and protein perturbations are performed using an anisotropic network model (ANM) (42) to move the alpha-carbon backbone toward a new position after minimization. Second, PELE optimizes amino acid side chains in proximity of the ligand using steric filters and a rotamer library (43). Finally, PELE uses a truncated Newton minimizer and a surface generalized implicit solvent for minimization, achieving a local minimum after the initial perturbation (44). These steps are repeated for a desired number of iterations and are performed in parallel using several computer-processing units (CPUs). The output is a series of trajectories that represent conformational changes of the side chains and ligand exploration. A Monte Carlo Metropolis criterion is implemented in the PELE algorithm that accepts or rejects these trajectories based on their calculated energies: if they are equal to or less than (accepts) or greater

than (rejects) the initial calculated energy (45). To calculate the energy, the PELE algorithm uses a standard force field that describes the potential energy of a molecular system, known as optimized potentials for liquid simulations (OPLS-2005) (46). The only parameters that were altered from the unconstrained ligand migration ready-made script provided by the PELE server were the ANM type, which was set to 4, and the addition of ANM mode 6 for favorable protein perturbations. The number of iterations was increased to 2,000 for increased sampling.

Cluster analysis was performed for the TBEV PELE simulations using pyProCT (47), a Python cluster analysis tool specifically adapted for biomolecules. Regular cluster analysis methods require a deep understanding of the data set and the algorithm. In addition, these methods are sensitive to small changes in its parameters. Instead of forcing users to perform a blind analysis, pyProCT implements a hypothesis-driven protocol. First, the user employs domain knowledge to characterize the desired result in terms of measurable clustering attributes (e.g., maximum and minimum number of clusters, size, noise, cluster separation, etc.) Second, the software searches the clustering space to obtain the clusters that best fit the hypothesis. The same script was used for each nucleoside triphosphate analogue in the PELE protein-ligand exploration simulations of the TBEV-modeled polymerase. The script instructs pyProCT to calculate the distances of each nucleoside using (i) an iterative superposition of the protein backbone and (ii) the calculated distances between the heavy atoms and the geometrical center of the ligand. The K-medoids, DBSCAN, spectral clustering, hierarchical (single-linkage), and GROMOS clustering algorithms were used, with up to 50 parameterizations for each one. The allowed clusterings had to have 3 to 20 clusters with a minimum of 300 elements. No more than 20% of the elements could be tagged as noise. The evaluation function that chose the best clustering was a combination of the silhouette index and a naive cohesion measure. This choice of evaluation functions favors results in which the clusters are well separated with a special emphasis on their compactness. Finally, the "atomic_distances" postprocessing option was used in order to obtain a human-readable file with the per-element distances between serine 331 (Ser331) of the TBEV modeled polymerase and the ligand as well as the per-cluster statistics.

RESULTS

Inhibition of TBEV growth, TBEV-induced CPE, and viral antigen expression. Six nucleoside analogues with chemical modifi-

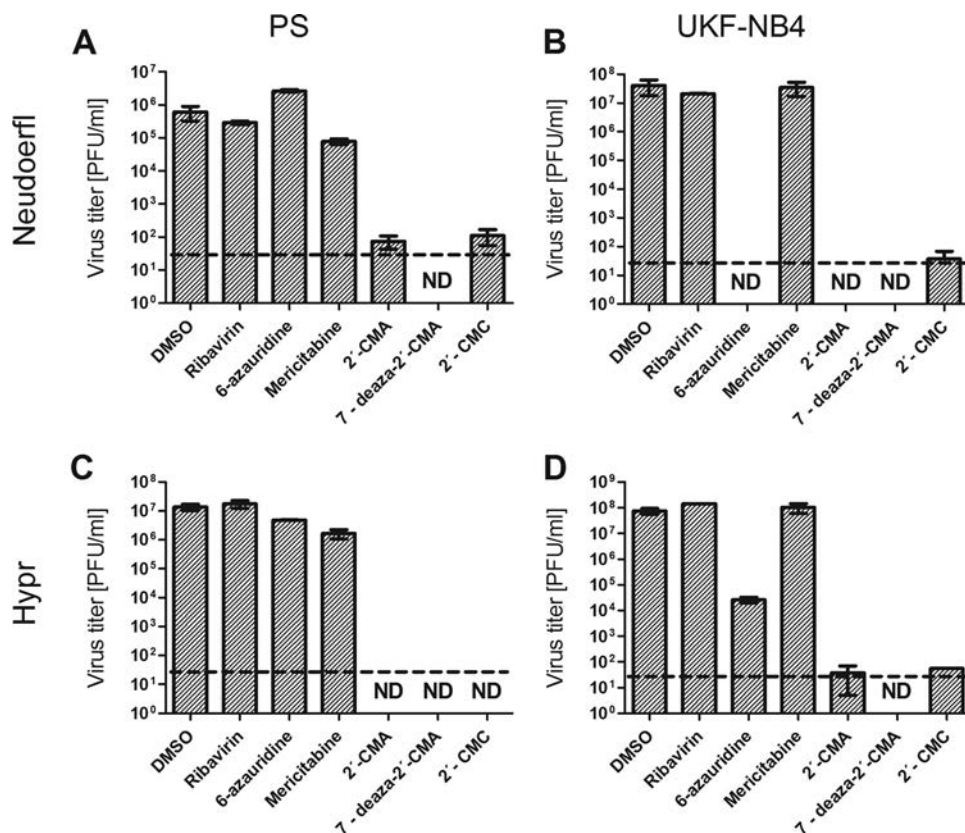


FIG 2 Reduction of TBEV titers by the indicated nucleoside analogues. PS or UKF-NB-4 cells were infected with TBEV (Hypr or Neudoerfl strain) at a multiplicity of infection of 0.1 and treated with nucleoside analogues at 50 μ M. The TBEV titers were determined by the plaque assay 3 days postinfection. DMSO-treated cells were used as a negative control. Bars show the mean values from three biological replicate wells, and the error bars indicate the standard errors of the means ($n = 3$). ND, not detected (below the detection limit). Horizontal dashed lines indicate the minimum detectable threshold of $1.44 \log_{10}$ PFU ml^{-1} .

cations of the ribose or purine/pyrimidine moiety (Fig. 1) were tested for the ability to inhibit the growth of the Hypr and Neudoerfl TBEV strains *in vitro* in PS cells and human neuroblastoma cells. The compounds were tested at a concentration of 50 μ M, and the inhibition of TBEV growth was investigated in the culture supernatants 3 days p.i. using a plaque assay.

The Hypr and Neudoerfl TBEV strains (MOI of 0.1) reached mean peak titers of 10^7 and 10^6 PFU/ml, respectively, in PS cells at 3 days p.i. In human neuroblastoma cells, both TBEV strains reached a viral titer of approximately 10^8 PFU/ml at 3 days p.i. Three of the nucleoside analogues tested, 7-deaza-2'-CMA, 2'-CMA, and 2'-CMC, inhibited the growth of both TBEV strains in PS cells and in human neuroblastoma cells. In PS cells, treatment with 50 μ M each compound reduced virus titers 10^4 - to 10^7 -fold compared to that in a mock-treated culture (Fig. 2A and B). Even greater viral titer reduction (10^6 - to 10^8 -fold) was observed in TBEV-infected human neuroblastoma cells (Fig. 2C and D).

Ribavirin and mericitabine showed weak or no anti-TBEV effects in PS cells and human neuroblastoma cells. 6-Azauridine showed no antiviral effect in PS cells; however, this compound significantly reduced the viral titer (10^3 -fold for Hypr and 10^6 -fold for Neudoerfl) in human neuroblastoma cells (Fig. 2B and D).

To verify the primary screening results, we next investigated the compounds using the CPE inhibition assay. Inhibition of TBEV-induced CPE in PS cells in the presence of the test com-

pounds was monitored using light microscopy 3 to 4 days p.i. The TBEV Hypr strain had a strong CPE on the target PS cells on day 3 p.i. in the absence of nucleoside inhibitors (Fig. 3A). A strong CPE was also observed in PS cell cultures treated with ribavirin (Fig. 3A), mericitabine, and 6-azauridine (see Fig. S1B and C in the supplemental material), indicating that these compounds had no protective effects on the survival and growth of PS cells exposed to TBEV. 6-Azauridine was highly cytotoxic, causing cell death and morphological changes in PS cells. Both adenosine derivatives, i.e., 7-deaza-2'-CMA and 2'-CMA, completely inhibited the CPE at concentrations of 50 μ M and had no adverse morphological effects on growing cells. However, a relatively strong CPE was observed in 2'-CMC-treated PS cell monolayers (Fig. 3A).

The CPE of 7-deaza-2'-CMA, 2'-CMA, and 2'-CMC on TBEV-infected PS cells was evaluated quantitatively in terms of cell viability and death using two independent colorimetric *in vitro* assays. Mock-treated TBEV-infected PS cells showed a high rate of cell death, i.e., 46% dead cells, at day 4 p.i. (Fig. 3B; see Fig. S2 in the supplemental material). TBEV-infected PS cells treated with either 7-deaza-2'-CMA or 2'-CMA showed a low rate of cell death (11 to 15%) and high viability (95 to 105%). The measured values were close to the cell death and viability values determined for mock-treated uninfected PS cells (11% and 100%, respectively) that were used as negative controls (Fig. 3B; see also Fig. S2 in the supplemental material). The results strongly indicate that

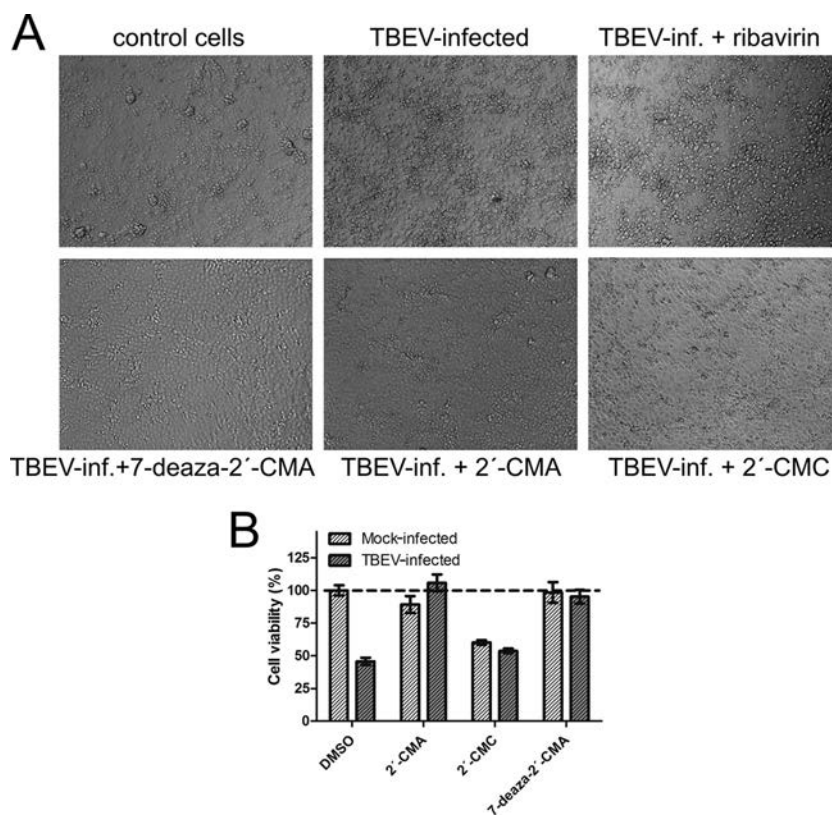


FIG 3 Inhibition of the TBEV-induced cytopathic effect by the indicated nucleoside analogues. PS cells were infected with TBEV strain Hypr at a multiplicity of infection of 0.1 and were left untreated (DMSO) or treated with 50 μ M ribavirin, 7-deaza-2'-CMA, 2'-CMA, or 2'-CMC. Inhibition of the CPE was monitored on day 3 or 4 postinfection (A). (B) Quantification of the CPE in TBEV-infected and mock-infected cells treated with 50 μ M 2'-CMA, 2'-CMC, or 7-deaza-2'-CMA. The CPE was expressed as the percentage of cell viability at day 4 postinfection. The horizontal dashed line indicates cell viability and cell death in DMSO-treated uninfected cells (control). The bars indicate the means, and error bars indicate SEMs ($n = 3$).

7-deaza-2'-CMA and 2'-CMA at concentrations of 50 μ M completely protected PS cells from TBEV, allowing them to survive in the presence of TBEV with no apparent cytotoxicity. For 2'-CMC, development of the CPE was marked by increased cell death (26 to 28%) and decreased cell viability (54 to 60%) (Fig. 3B; see also Fig. S2).

The antiviral effect of 7-deaza-2'-CMA, 2'-CMA and 2'-CMC was further confirmed by immunofluorescence staining, which was used to assess the expression of the TBEV surface E antigen in PS cells as an index of viral infectivity and replication *in vitro*. The TBEV surface E antigen was strongly expressed in TBEV-infected mock-treated cells (Fig. 4), and no virus antigen was detected in mock-infected PS cells (data not shown). Immunofluorescence staining revealed that 7-deaza-2'-CMA, 2'-CMA, and 2'-CMC at concentrations of 50 μ M completely inhibited the expression of the TBEV surface E antigen in virus-infected PS cells (Fig. 4). These results correlated with the strong suppression of TBEV growth in the 7-deaza-2'-CMA-, 2'-CMA-, and 2'-CMC-treated cell cultures (Fig. 2A and C).

Cytotoxicities of TBEV inhibitors. The cytotoxicities of 7-deaza-2'-CMA, 2'-CMA, and 2'-CMC were evaluated in PS cells using a cell viability assay (Fig. 5) and subsequently confirmed by a cell death assay (see Fig. S3 in the supplemental material). No cellular toxicity was seen in cultures of PS cells treated with 7-deaza-2'-CMA at concentrations ranging from 0 to 50 μ M ($CC_{50} > 50$ μ M) 4 days posttreatment (Fig. 5C and Table 1; see

also Fig. S3C). A cell viability assay showed similar results with 2'-CMA ($CC_{50} > 50$ μ M). However, 50 μ M 2'-CMA moderately increased cell death, by $\sim 22\%$, at 4 days after drug administration (Fig. 5A and Table 1; see also Fig. S3A) compared to the rate for mock-treated cells ($\sim 15\%$). For both adenosine derivatives, the concentration of 50 μ M had no detectable effect on cell proliferation. 2'-CMC showed a dose-dependent cytotoxic effect on PS cell cultures 4 days posttreatment. Based on a cell viability assay, the CC_{50} of 2'-CMC was determined to be ~ 50 μ M (Fig. 5B and Table 1; see also Fig. S3B).

Dose-response antiviral activities of the TBEV inhibitors.

The compounds that showed TBEV inhibitory effects in the initial experiments, i.e., 7-deaza-2'-CMA, 2'-CMA, and 2'-CMC, were further evaluated to determine their dose-dependent antiviral activities. PS cells were infected with the Hypr strain (MOI of 0.1) and immediately treated with each compound at a concentration range of 0 to 50 μ M. The culture supernatants were then subjected to the plaque assay. TBEV titers in the culture supernatants were assayed daily on days 1 to 6 p.i. The dose-response curves on postinfection days 3 and 4 were used to estimate the EC_{50} , SI, and slope value.

All three compounds reduced the viral titer in a dose-dependent manner (Fig. 6; see also Fig. S4 in the supplemental material). The shape of the dose-response curves for 7-deaza-2'-CMA changed over time from a flat curve on day 1 p.i. to typical sigmoidal curves with relatively steep slopes on days 2 to 6 p.i. (Fig. 6A).

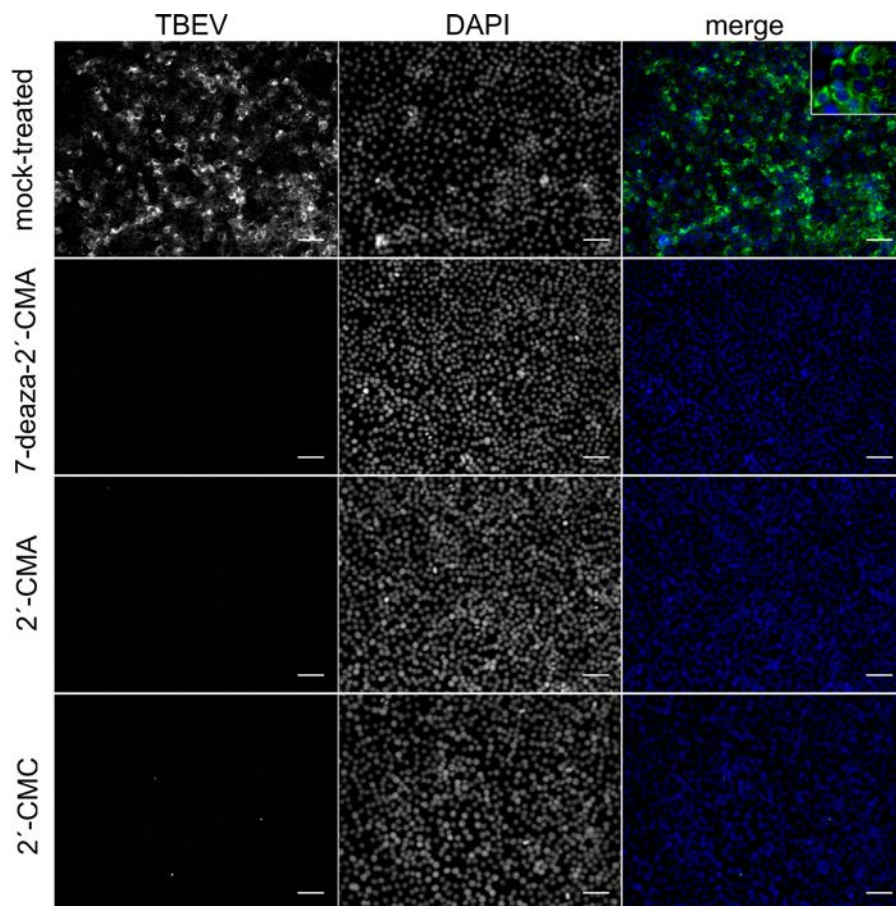


FIG 4 Inhibition of TBEV viral antigen expression by the indicated nucleoside inhibitors. PS cells were infected with TBEV and treated with 0.5% DMSO or with 50 μM 7-deaza-2'-CMA, 2'-CMA, or 2'-CMC. PS cells were fixed on slides at day 4 postinfection and stained with flavivirus-specific antibody labeled with FITC (green) and then counterstained with DAPI (blue). Scale bars, 50 μm .

7-Deaza-2'-CMA reduced the viral titer, showing an EC_{50} of $5.1 \pm 0.4 \mu\text{M}$ and a selectivity index (SI) of >9.8 (Table 1). 7-Deaza-2'-CMA was ineffective in terms of reducing the viral titer at concentrations of 0.1 and 0.5 μM , and the TBEV growth curves were indistinguishable from the TBEV growth curve for mock-treated cells (see Fig. S4A). At a concentration of 3.1 μM , the TBEV inhibitory effect of 7-deaza-2'-CMA became more evident, resulting in $\sim 10^2$ -fold reduction in the titer relative to that in mock-treated cells. Marked inhibitory effects on TBEV replication were observed at concentrations of 7-deaza-2'-CMA at or above 6.2 μM . When the compound was added at concentrations of 12.5, 25, and 50 μM , there was a significant and steady reduction in viral titer (a 10^6 - to 10^7 -fold reduction). At these concentrations, 7-deaza-2'-CMA reduced the mean TBEV titers to below the limit of detection ($1.44 \log_{10}$ PFU ml^{-1}) between p.i. days 4 and 6.

A cytidine derivative, 2'-CMC, also showed marked dose-dependent inhibition of TBEV titers. The shape and particularly the slope of the 2'-CMC dose-response curve were similar to those of 7-deaza-2'-CMA (Fig. 6B). However, 2'-CMC was approximately 3-fold less potent in terms of inhibiting TBEV than was 7-deaza-2'-CMA (EC_{50} of $14.2 \pm 1.9 \mu\text{M}$) (Table 1). The relatively low SI value of ~ 3.5 was due to the considerable cytotoxicity of the compound for PS cells, as described above. At 0.1, 0.5, and 3.1 μM , 2'-CMC inhibited virus replication weakly or not at all. The in-

hibitory effects of 2'-CMC became more evident at concentrations of 6.2 to 12.5 μM , with virus titer reduction of about 10^2 at 6 days p.i. 2'-CMC completely suppressed TBEV replication at concentrations of 25 and 50 μM ; there was a 10^4 - to 10^6 -fold reduction in viral titer during the experimental period (see Fig. S4B in the supplemental material).

2'-CMA showed a significant dose-dependent antiviral effect only at day 3 p.i. (Fig. 6C). The 2'-CMA dose-response curve was characterized by an EC_{50} of $7.1 \pm 1.2 \mu\text{M}$ (SI of about 7) and by a relatively low Hill coefficient (0.7 for 2'-CMA versus 2.7 for 7-deaza-2'-CMA and 2.2 for 2'-CMC [Table 1]). At day 3 p.i., 2'-CMA strongly reduced TBEV titers at concentrations of 20 and 50 μM , resulting in $>10^5$ -fold viral titer inhibition relative to that in mock-treated TBEV-infected cells. Although the initial decrease in viral titers was very strong, the inhibitory effects of 2'-CMA diminished gradually after day 3 p.i., regardless of concentration. The decrease in the antiviral effect of 2'-CMA over time allowed the virus titers in 50 μM 2'-CMA-treated cells to rebound to 1.7×10^6 PFU/ml at day 6 p.i. (see Fig. S4C).

Exploration of NS5B with nucleoside analogues using PELE. Selection and characterization of drug-resistant HCV replicons revealed that serine 282 (Ser282) determines the efficacy of the inhibitory nucleoside 2'-CMA (13). Figure S5 in the supplemental material illustrates the proof of principle for our PELE-based ex-

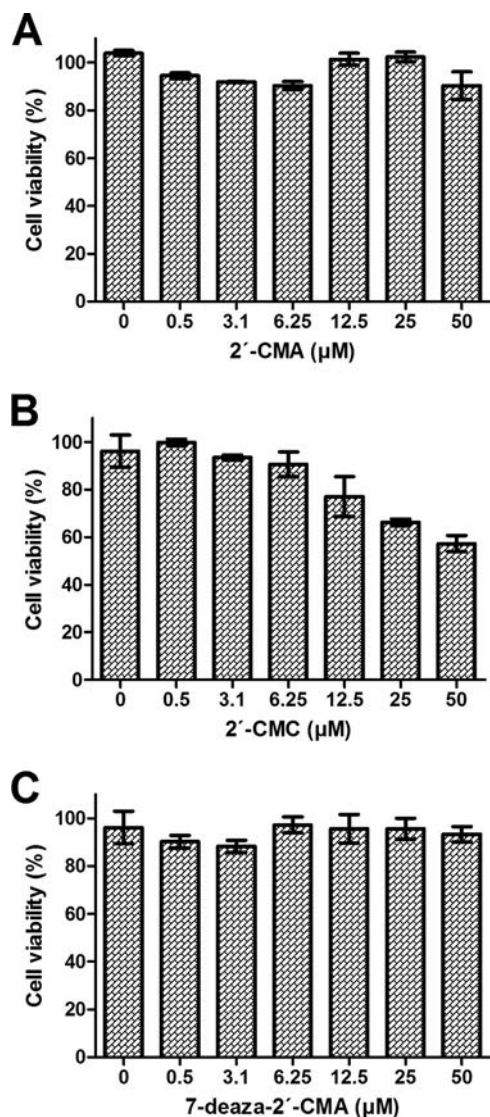


FIG 5 Cytotoxicity of the indicated nucleoside inhibitors. Cytotoxicity was determined by incubating PS cells with the indicated concentrations of 2'-CMA (A), 2'-CMC (B), or 7-deaza-2'-CMA (C) and is expressed in terms of cell viability and cell death at day 4 postinfection. The bars indicate the mean values from three replicate wells, and the error bars indicate the SEMs.

ploration of nucleoside triphosphate analogues with viral polymerases. In the bound crystal structure of HCV (PDB code 1nb6), the distance between the alpha carbon of Ser282 and the geometric center of the heavy atoms of UTP is 9.3 Å as measured using the Maestro package (39). Figure S5 shows that for the most part, UTP explores ~20 to 70 Å away from the Ser282 in both the bound and unbound (or apoenzyme) crystal structures of the HCV polymerase. In both cases, however, there was UTP exploration <20 Å away from the Ser282 (encircled in Fig. S5), and this separate cluster approaches the native position of the bound HCV-UTP complex (*y* axes in Fig. S5; i.e., the geometric center position of all heavy atoms of UTP in PDB code 1nb6).

To further validate the results of the nucleoside triphosphate analogue exploration, we simulated the experimental results reported by Migliaccio et al. (13), who investigated the inhibitory

effect of 2'-CMA using HCV and other phylogenetically related viruses *in vitro*. Figure S6A in the supplemental material shows the exploration of 2'-CMA-triphosphate (2'-CMA-TP) in proximity to the homologous serine residue of the viral polymerases of the HCV (PDB code 1nb6), WNV (PDB code 2hfz), and JEV (PDB code 4k6m) crystal structures. This analysis showed that 2'-CMA-TP spent the majority of the exploration away from the homologous serine residue. Further investigation of whether 2'-CMA is an effective inhibitor of JEV is needed since no such experiments have been reported. Figure S6B shows that the three effective nucleoside triphosphate analogues used in the current study, i.e., 2'-CMA-TP, 2'-CMC-TP, and 7-deaza-2'-CMA-TP, also explored in proximity to the Ser331 of the modeled tertiary structure of TBEV NS5B (the residue homologous to HCV Ser282).

The results from the clustering analysis are summarized in Table S1 in the supplemental material. Visual inspection of all three nucleoside triphosphate analogue clusters for the TBEV polymerase showed two types of clusters. The first type was generated by a partition of the space sampled in the exploration of each nucleoside. Since this zone was densely populated, it was difficult to find a good balance between cluster compactness and separation (which would penalize the silhouette index). The second type of cluster had better-defined boundaries since these clusters formed "natural" aggregates that were created as the nucleoside explored the protein surface in proximity to Ser331 of the TBEV polymerase. From this second group or second type of cluster, we selected those that were <18 Å from the alpha carbon of Ser331 (green areas in Fig. 7A). The logic behind this cutoff criterion is depicted graphically in Fig. S5 in the supplemental material, i.e., the encircled cluster. During the exploration of the HCV polymerase, UTP approaches the binding site (*y* axes in Fig. S5; 2 to 12 Å from its native position) as it "cuts off" from the majority of the modeling for exploration (18 to 20 Å from Ser282; *x* axes in Fig. S5).

All three simulations showed a large cluster (colored the same shade of green in Fig. 7B) with more than half of its elements in proximity to Ser 331 (especially for 7-deaza-2'-CMA-TP). For 2'-CMA-TP and 2'-CMC-TP, there were elements of other clusters (colored different shades of green in Fig. 7B) that also seemed to be in proximity to Ser331 of the TBEV polymerase. Assuming that phylogenetically related viral polymerases have similar binding sites, we used the central position of UTP bound to HCV (PDB code 1nb6) to geometrically determine the pathway toward the predicted binding site of TBEV. The scatter plots in Fig. 7C show that the majority of modeling for the exploration is away from Ser331 (i.e., the first type of cluster; >20 Å). Each scatter plot, however, has a linear correlation (r^2) of >0.9, approaching the predicted binding site of the TBEV polymerase, which is clearly shown by the large single cluster of 7-deaza-2'-CMA-TP (Fig. 7).

TABLE 1 Characteristics of selected TBEV-inhibiting nucleosides

Compound	EC ₅₀ , μM ^a	Hill coefficient ^a	CC ₅₀ , μM ^a (viability assay)	SI (CC ₅₀ /EC ₅₀)
7-deaza-2'-CMA	5.1 ± 0.4	2.7 ± 0.5	>50	>9.8
2'-CMA	7.1 ± 1.2	0.7 ± 0.1	>50	>7.0
2'-CMC	14.2 ± 1.9	2.2 ± 0.5	~50	~3.5

^a Determined from three independent experiments.

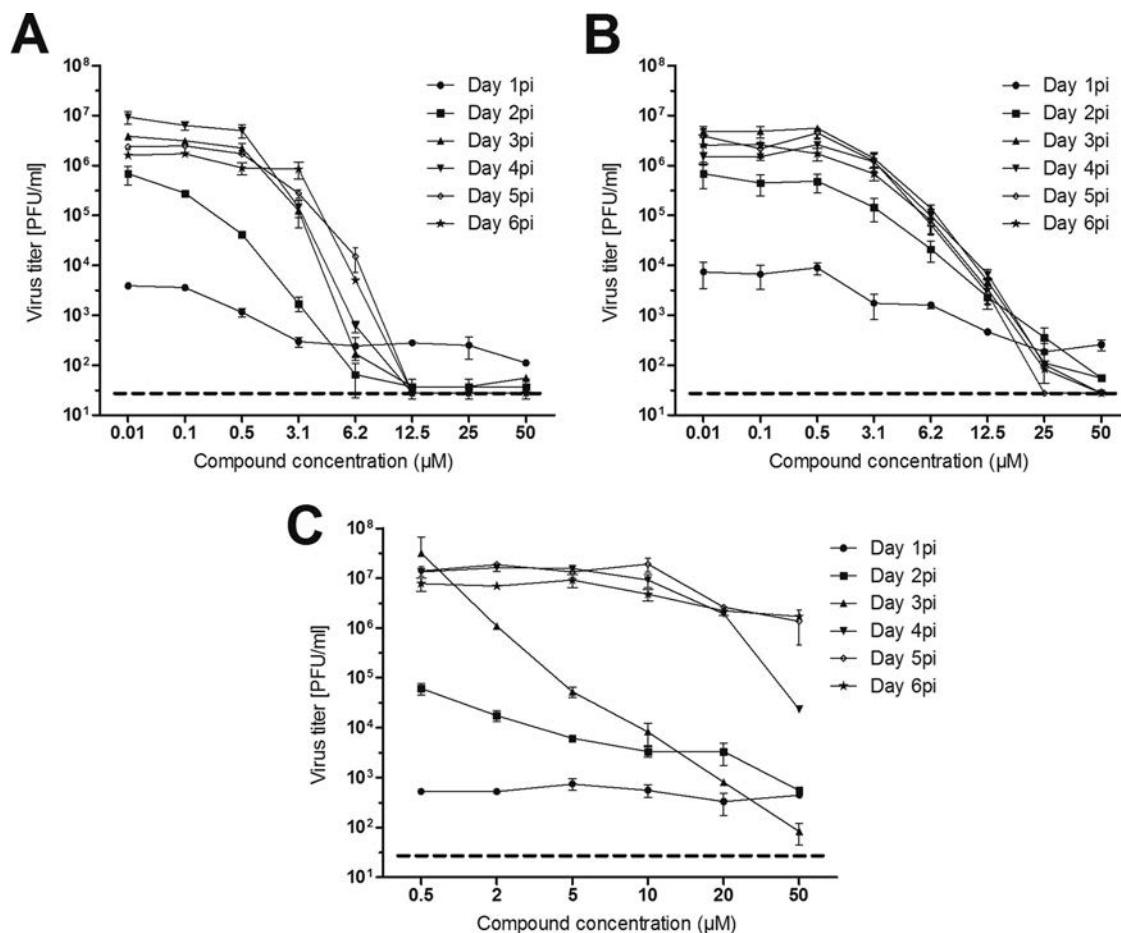


FIG 6 Dose-dependent effect of the indicated TBEV inhibitors on virus titers. PS cells were infected with TBEV at a multiplicity of infection of 0.1 and treated with 7-deaza-2'-CMA (A), 2'-CMC (B), or 2'-CMA (C) at the indicated concentrations. TBEV titers were monitored at days 1 to 6 postinfection. The mean titers from three biological replicates are shown, and error bars indicate SEMs ($n = 3$). The horizontal dashed line indicates the minimum detectable threshold of $1.44 \log_{10}$ PFU ml^{-1} .

DISCUSSION

TBE is a substantial public health problem in some parts of Europe and Asia. At present, there is no specific treatment for TBE other than supportive care. Few studies have tested potential TBEV inhibitors (48), and there is an urgent need for safe, efficient drugs for treating patients with TBE. In this study, a series of nucleoside analogues that were previously reported to inhibit members of the *Flaviviridae* family were tested for the ability to suppress TBEV replication. We could not determine the structure-activity relationship for all of the compounds in this study, although this will be the subject of a future investigation.

The anti-TBEV activity of the compounds was determined in PS cells and in human neuroblastoma cells. PS cells are widely used for TBEV isolation and for multiplication and plaque assays (30). Human neuroblastoma cells are highly sensitive to TBEV infection and represent a valuable model for neuropathogenesis studies of TBEV as well as for studies of several other neurotropic viruses (31). The initial screening was performed using two TBEV strains, Neudoerfl and Hypr, which represent two virulence models. Neudoerfl, the European prototype TBEV strain, exhibits medium virulence, while the Hypr strain is highly virulent (49). Although ribavirin, 6-azauridine, and mericitabine

have been described as potent inhibitors of several flaviviruses (29, 41, 50), these compounds did not reproducibly inhibit TBEV *in vitro* at concentrations of 50 μM . 6-Azauridine has been reported in the literature to be relatively well tolerated by several host cell lines as well as being well tolerated *in vivo* (29). However, in our experiments, this compound had a strong cytotoxic effect on both PS cells (see Fig. S1C in the supplemental material) and human neuroblastoma cells (data not shown), resulting in significantly reduced viral titers in 6-azauridine-treated human neuroblasts (Fig. 2B and D).

Three 2'-C-methyl-substituted nucleosides, 2'-CMC, 2'-CMA, and 7-deaza-2'-CMA, strongly inhibited the *in vitro* growth of TBEV in both cell lines and were selected as lead candidate compounds for further testing. 2'-CMC was recently tested for its ability to inhibit replication of yellow fever virus (23), Alkhurma hemorrhagic fever virus, Kyasanur Forest disease virus, and Omsk hemorrhagic fever virus (29). Moreover, the 3'-valyl ester of 2'-CMC, valopicitabine, showed viral load reductions in patients infected with genotype 1 HCV in clinical trials, although it was subsequently discontinued for the treatment of hepatitis C (55, 56). Our results indicate that 2'-CMC had strong antiviral activity against both the Hypr and Neudoerfl TBEV strains; however, this

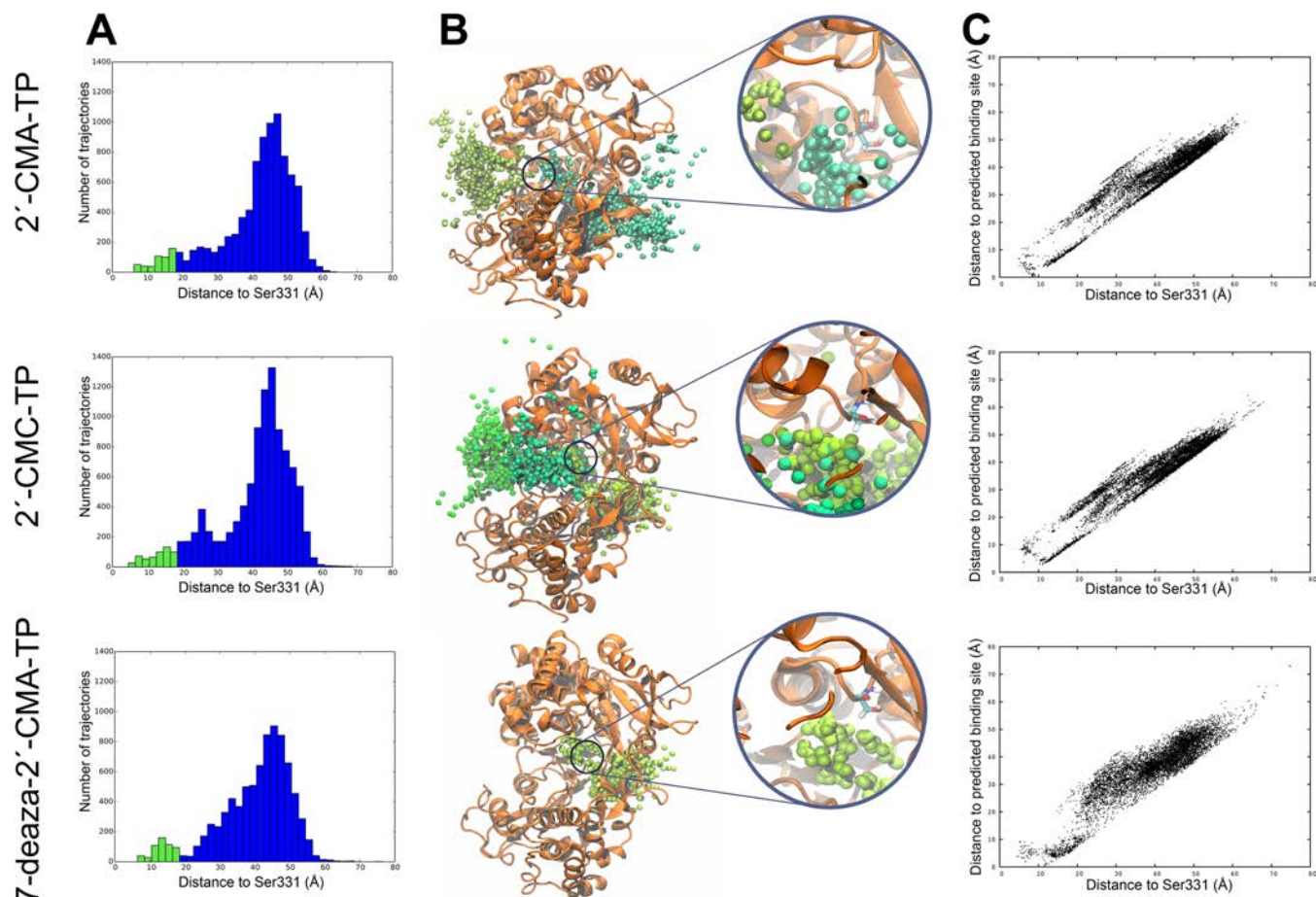


FIG 7 Cluster analyses of nucleoside triphosphate analogue exploration of the TBEV polymerase. (A) The distance for each of the studied nucleoside triphosphate analogues (2'-CMA-TP, 2'-CMC-TP, and 7-deaza-2'-CMA-TP) are shown in the histograms. The 0- to 18-Å range, which denotes the proximity toward Ser331 (*x* axes), is colored light green. (B) Tertiary representations of the selected clusters for each system. Each nucleoside is represented by its C-7 atom. (C) Scatter plots depict the approach of each nucleoside toward the predicted binding site of TBEV.

compound was cytotoxic for PS cells (CC_{50} of about 50 μ M). The substitution of cytosine for adenine in 2'-CMA, a compound that has recently been used for experimental therapy of HCV and DENV infections (18, 51), significantly reduced the cytotoxicity for both cell lines and increased the anti-TBEV inhibitory effect of the compound. However, viral replication gradually rebounded after 3 days in the treated cultures (Fig. 6C). The observed decrease in antiviral activity of 2'-CMA and the rebound in viral titer were probably related to the rapid deamination of 2'-CMA by cellular adenosine deaminase to the inactive inosine derivative (52). Such an intracellular deamination is described as an undesirable effect in the inhibitory activity of 2'-CMA against HCV replication, resulting in poor bioavailability and rapid clearance of 2'-CMA in plasma (14). 2'-CMA could be also inactivated by cellular phosphorylases, which are enzymes that catalyze phosphorylase of the purine glycosidic bond (12). Alternatively, the evolution of 2'-CMA-resistant TBEV mutants could explain the observed viral titer rebound (53).

The incorporation of the 7-deaza moiety into the 2'-CMA molecule eliminated cytotoxicity in both PS cells and human neuroblastoma cells. The potency of 7-deaza-2'-CMA to inhibit TBEV replication was comparable to that of 2'-CMA and was

approximately 3-fold higher than that of 2'-CMC. The inhibitory effect of 7-deaza-2'-CMA was stable over the 6-day experimental period, and there was no rebound in viral titer during this period. The 7-deaza-purine substitution is described as an important modification of the nucleobase that strongly affects the biological properties of the nucleoside analogue. The 7-deaza modification alters the glycosyl torsion angle, which may change the glycosyl bond length. This could lead to a rearrangement in the general electronic character of the purine base and, in particular, to disruption of the alignment of the 3'-hydroxyl function for nucleophilic attack on the alpha phosphorus of the next incoming NTP. The 7-deaza modification may, therefore, result in enhanced potency of the nucleoside analogue in terms of terminating viral RNA synthesis (9, 14). Due to the antiviral activity and low cytotoxicity of 7-deaza-2'-CMA, this nucleoside derivative has been widely tested to determine whether it inhibits the RNA replication of other medically important flaviviruses. For example, 7-deaza-2'-CMA inhibits HCV replication with an EC_{50} of 0.3 μ M with no apparent cytotoxicity and shows promising pharmacokinetic properties in several animal species, including primates (14, 54). Similar antiviral properties have been demonstrated for the 7-deaza-substituted derivative of 2'-C-acetylene-adenosine

sine, which was recently reported to suppress DENV replication in the transient-replicon assay and in a mouse model (18).

To understand the efficacies of 2'-CMA, 2'-CMC, and 7-deaza-2'-CMA for inhibiting TBEV, we simulated the exploration of the TBEV polymerase by the triphosphate form of each nucleoside analogue (Fig. 7). The computational simulations showed that these inhibitors sampled toward the binding site of the TBEV polymerase. There are a couple of other clusters that aggregate toward the TBEV binding site for 2'-CMA-TP and 2'-CMC-TP. Based on our experimental results, we infer that the pathway is represented by the single cluster of 7-deaza-2'-CMA-TP in Fig. 7, but a more robust analysis must be performed to confirm this hypothesis. Takhampunya et al. (41) developed a method for calculating the ligand/drug binding free energy during its exploration toward the active site of a protein. Their results showed strong correlations with experimental data. We are currently using such methods to determine the viral polymerase binding pathways of 2'-CMA, 2'-CMC, and 7-deaza-2'-CMA and their binding free energies.

In conclusion, we identified three compounds with activity against TBEV *in vitro*. These compounds will be tested further in a mouse model of TBEV infection. These compounds, even if they are not clinically effective, may be useful research tools or starting points for drug development efforts against TBEV. Because of its high antiviral activity and low cytotoxicity, 7-deaza-2'-CMA is an attractive candidate for further investigation as a potential therapeutic agent not only for TBE treatment but also for treating other flaviviral neuroinfections.

ACKNOWLEDGMENTS

We are greatly indebted to Jan Kopecký and Libor Grubhoffer for general support of our work, to Ivana Huvarová for excellent technical assistance, to Vladimír Babák for statistical data processing, and to Jiří Volf for preparation of the immunofluorescence images.

This study was supported by Czech Science Foundation projects P502/11/2116 and GA14-29256S and by project LO1218 from the Ministry of Education, Youth and Sports of the Czech Republic under the NPU I program and by AdmireVet project no. CZ.1.05/2.1.00/01.0006-ED 0006/01/01. We acknowledge a grant for the development of research organization (RVO: 61388963). J.J.V. was supported by project CZ.1.07/2.3.00/30.0032, which is cofinanced by the European Social Fund and the state budget of the Czech Republic. V.A.G. was sponsored by the European project PELE (ERC-2009-Adg 25027).

The funders played no role in study design, data collection and analysis, the decision to publish, or the preparation of the manuscript.

REFERENCES

- Baier A. 2011. Flaviviral infections and potential targets for antiviral therapy, p 89–104. In Ruzek D (ed), *Flavivirus encephalitis*. InTech, Rijeka, Croatia.
- Chambers TJ, Hahn CS, Galler R, Rice CM. 1990. Flavivirus genome organization, expression, and replication. *Annu Rev Microbiol* 44:649–688. <http://dx.doi.org/10.1146/annurev.mi.44.100190.003245>.
- Dumpis U, Crook D, Oksi J. 1999. Tick-borne encephalitis. *Clin Infect Dis* 28:882–890. <http://dx.doi.org/10.1086/515195>.
- Heinz FX, Mandl CW. 1993. The molecular biology of tick-borne encephalitis virus. *APMIS* 101:735–745. <http://dx.doi.org/10.1111/j.1699-0463.1993.tb00174.x>.
- Heinz FX, Stiasny K, Holzmann H, Grgic-Vitek M, Kriz B, Essl A, Kundl M. 2013. Vaccination and tick-borne encephalitis, Central Europe. *Emerg Infect Dis* 19:69–76. <http://dx.doi.org/10.3201/eid1901.120458>.
- Ruzek D, Dobler G, Mantke OD. 2010. Tick-borne encephalitis: pathogenesis and clinical implications. *Travel Med Infect Dis* 8:223–232. <http://dx.doi.org/10.1016/j.tmaid.2010.06.004>.
- Zavadská D, Anca I, Andre F, Bakir M, Chlibek R, Cizman M, Ivaskeviciene I, Mangarov A, Meszner Z, Pokorn M, Prymula R, Richter D, Salman N, Simurka P, Tamm E, Tesovic G, Urbancikova I, Usonis V. 2013. Recommendations for tick-borne encephalitis vaccination from the Central European Vaccination Awareness Group (CEVAG). *Hum Vaccin Immunother* 9:362–374. <http://dx.doi.org/10.4161/hv.22766>.
- Puig-Basagoiti F, Tilgner M, Forshey BM, Philpott SM, Espina NG, Wentworth DE, Goebel SJ, Masters PS, Falgout B, Ren P, Ferguson DM, Shi PY. 2006. Triaryl pyrazoline compound inhibits flavivirus RNA replication. *Antimicrob Agents Chemother* 50:1320–1329. <http://dx.doi.org/10.1128/AAC.50.4.1320-1329.2006>.
- De Clercq E, Neyts J. 2009. Antiviral agents acting as DNA or RNA chain terminators. *Handb Exp Pharmacol* 189:53–84. http://dx.doi.org/10.1007/978-3-540-79086-0_3.
- De Clercq E. 2004. Antivirals and antiviral strategies. *Nat Rev Microbiol* 2:704–720. <http://dx.doi.org/10.1038/nrmicro975>.
- De Clercq E. 2011. A 40-year journey in search of selective antiviral chemotherapy. *Annu Rev Pharmacol Toxicol* 51:1–24. <http://dx.doi.org/10.1146/annurev-pharmtox-010510-100228>.
- Eldrup AB, Allerson CR, Bennett CF, Bera S, Bhat B, Bhat N, Bosserman MR, Brooks J, Burlein C, Carroll SS, Cook PD, Getty KL, MacCoss M, McMasters DR, Olsen DB, Prakash TP, Prhac M, Song QL, Tomassini JE, Xia J. 2004. Structure-activity relationship of purine ribonucleosides for inhibition of hepatitis C virus RNA-dependent RNA polymerase. *J Med Chem* 47:2283–2295. <http://dx.doi.org/10.1021/jm030424e>.
- Migliaccio G, Tomassini JE, Carroll SS, Tomei L, Altamura S, Bhat B, Bartholomew L, Bosserman MR, Ceccacci A, Colwell LF, Cortese R, De Francesco R, Eldrup AB, Getty KL, Hou XS, LaFemina RL, Ludmerer SW, MacCoss M, McMasters DR, Stahlhut MW, Olsen DB, Hazuda DJ, Flores OA. 2003. Characterization of resistance to non-obligate chain-terminating ribonucleoside analogs that inhibit hepatitis C virus replication *in vitro*. *J Biol Chem* 278:49164–49170. <http://dx.doi.org/10.1074/jbc.M305041200>.
- Olsen DB, Eldrup AB, Bartholomew L, Bhat B, Bosserman MR, Ceccacci A, Colwell LF, Fay JF, Flores OA, Getty KL, Grobler JA, LaFemina RL, Markel EJ, Migliaccio G, Prhac M, Stahlhut MW, Tomassini JE, MacCoss M, Hazuda DJ, Carroll SS. 2004. A 7-deaza-adenosine analog is a potent and selective inhibitor of hepatitis C virus replication with excellent pharmacokinetic properties. *Antimicrob Agents Chemother* 48:3944–3953. <http://dx.doi.org/10.1128/AAC.48.10.3944-3953.2004>.
- Klumpp K, Leveque V, Le Pogam S, Ma H, Jiang WR, Kang HS, Granycome C, Singer M, Laxton C, Hang JQ, Sarma K, Smith DB, Heindl D, Hobbs CJ, Merrett JH, Symons J, Cammack N, Martin JA, Devos R, Najera I. 2006. The novel nucleoside analog R1479 (4'-azidocytidine) is a potent inhibitor of NS5B-dependent RNA synthesis and hepatitis C virus replication in cell culture. *J Biol Chem* 281:3793–3799. <http://dx.doi.org/10.1074/jbc.M510195200>.
- Klumpp K, Kalayanov G, Ma H, Le Pogam S, Leveque V, Jiang WR, Inocencio N, De Witte A, Rajyaguru S, Tai E, Chanda S, Irwin MR, Sund C, Winqist A, Maltseva T, Eriksson S, Usova E, Smith M, Alker A, Najera I, Cammack N, Martin JA, Johansson NG, Smith DB. 2008. 2'-Deoxy-4'-azido nucleoside analogs are highly potent inhibitors of hepatitis C virus replication despite the lack of 2'-alpha-hydroxyl groups. *J Biol Chem* 283:2167–2175. <http://dx.doi.org/10.1074/jbc.M708929200>.
- Yin Z, Chen YL, Schul W, Wang QY, Gu F, Duraiswamy J, Kondreddi RR, Niyomrattanakit P, Lakshminarayana SB, Goh A, Xu HY, Liu W, Liu B, Lim JY, Ng CY, Qing M, Lim CC, Yip A, Wang G, Chan WL, Tan HP, Lin K, Zhang B, Zou G, Bernard KA, Garrett C, Beltz K, Dong M, Weaver M, He H, Pichota A, Dartois V, Keller Thomas H, Shi PY. 2009. An adenosine nucleoside inhibitor of dengue virus. *Proc Natl Acad Sci U S A* 106:20435–20439. <http://dx.doi.org/10.1073/pnas.0907010106>.
- Chen YL, Yin Z, Duraiswamy J, Schul W, Lim CC, Liu B, Xu HY, Qing M, Yip A, Wang G, Chan WL, Tan HP, Lo M, Liung S, Kondreddi RR, Rao R, Gu H, He H, Keller TH, Shi PY. 2010. Inhibition of dengue virus RNA synthesis by an adenosine nucleoside. *Antimicrob Agents Chemother* 54:2932–2939. <http://dx.doi.org/10.1128/AAC.00140-10>.
- Chen YL, Yin Z, Lakshminarayana SB, Qing M, Schul W, Duraiswamy J, Kondreddi RR, Goh A, Xu HY, Yip A, Liu B, Weaver M, Dartois V, Keller TH, Shi PY. 2010. Inhibition of dengue virus by an ester prodrug of an adenosine analog. *Antimicrob Agents Chemother* 54:3255–3261. <http://dx.doi.org/10.1128/AAC.00397-10>.
- Latour DR, Jekle A, Javanbakht H, Henningsen R, Gee P, Lee I, Tran P, Ren S, Kutach AK, Harris SF, Wang SM, Lok SJ, Shaw D, Li J, Heilek

- G, Klumpp K, Swinney DC, Deval J. 2010. Biochemical characterization of the inhibition of the dengue virus RNA polymerase by beta-D-2'-ethynyl-7-deaza-adenosine triphosphate. *Antiviral Res* 87:213–222. <http://dx.doi.org/10.1016/j.antiviral.2010.05.003>.
21. Lee JC, Tseng CK, Wu YH, Kaushik-Basu N, Lin CK, Chen WC, Wu HN. 2015. Characterization of the activity of 2'-C-methylcytidine against dengue virus replication. *Antiviral Res* 116:1–9. <http://dx.doi.org/10.1016/j.antiviral.2015.01.002>.
 22. Chen H, Liu L, Jones SA, Banavali N, Kass J, Li Z, Zhang J, Kramer LD, Ghosh AK, Li H. 2013. Selective inhibition of the West Nile virus methyltransferase by nucleoside analogs. *Antiviral Res* 97:232–239. <http://dx.doi.org/10.1016/j.antiviral.2012.12.012>.
 23. Julander JG, Jha AK, Choi JA, Jung KH, Smees DF, Morrey JD, Chu CK. 2010. Efficacy of 2'-C-methylcytidine against yellow fever virus in cell culture and in a hamster model. *Antiviral Res* 86:261–267. <http://dx.doi.org/10.1016/j.antiviral.2010.03.004>.
 24. Smees DF, Morris JLB, Barnard DL, Vanaerschot A. 1992. Selective inhibition of arthropod-borne and arenaviruses in vitro by 3'-fluoro-3'-deoxyadenosine. *Antiviral Res* 18:151–162. [http://dx.doi.org/10.1016/0166-3542\(92\)90035-4](http://dx.doi.org/10.1016/0166-3542(92)90035-4).
 25. Smees DF, Alaghamandan HA, Ramasamy K, Revankar GR. 1995. Broad-spectrum activity of 8-chloro-7-deazaguanosine against RNA virus infections in mice and rats. *Antiviral Res* 26:203–209. [http://dx.doi.org/10.1016/0166-3542\(94\)00084-L](http://dx.doi.org/10.1016/0166-3542(94)00084-L).
 26. Ojwang JO, Ali S, Smees DF, Morrey JD, Shimasaki CD, Sidwell RW. 2005. Broad-spectrum inhibitor of viruses in the Flaviviridae family. *Antiviral Res* 68:49–55. <http://dx.doi.org/10.1016/j.antiviral.2005.06.002>.
 27. Chatelain G, Debing Y, De Burghgraeve T, Zmurko J, Saudi M, Rozenki J, Neyts J, Van Aerschot A. 2013. In search of flavivirus inhibitors: evaluation of different tritylated nucleoside analogues. *Eur J Med Chem* 65:249–255. <http://dx.doi.org/10.1016/j.ejmech.2013.04.034>.
 28. Koonin EV, Dolja VV. 1993. Evolution and taxonomy of positive-strand RNA viruses—implications of comparative analysis of amino acid sequences. *Crit Rev Biochem Mol Biol* 28:375–430. <http://dx.doi.org/10.3109/10409239309078440>.
 29. Flint M, McMullan LK, Dodd KA, Bird BH, Khristova ML, Nichol ST, Spiropoulou CF. 2014. Inhibitors of the tick-borne, hemorrhagic fever-associated flaviviruses. *Antimicrob Agents Chemother* 58:3206–3216. <http://dx.doi.org/10.1128/AAC.02393-14>.
 30. Kozuch O, Mayer V. 1975. Pig kidney epithelial (ps) cells—perfect tool for study of flavi-viruses and some other arboviruses. *Acta Virol* 19:498.
 31. Růžek D, Vancova M, Tesarova M, Ahantarig A, Kopecky J, Grubhoffer L. 2009. Morphological changes in human neural cells following tick-borne encephalitis virus infection. *J Gen Virol* 90:1649–1658. <http://dx.doi.org/10.1099/vir.0.010058-0>.
 32. De Madrid AT, Porterfield JS. 1969. A simple micro-culture method for study of group B arboviruses. *Bull World Health Organ* 40:113–121.
 33. Schindelin J, Arganda-Carreras I, Frise E, Kaynig V, Longair M, Pietzsch T, Preibisch S, Rueden C, Saalfeld S, Schmid B, Tinevez JY, White DJ, Hartenstein V, Eliceiri K, Tomancak P, Cardona A. 2012. Fiji: an open-source platform for biological-image analysis. *Nat Methods* 9:676–682. <http://dx.doi.org/10.1038/nmeth.2019>.
 34. Sali A, Blundell TL. 1993. Comparative protein modeling by satisfaction of spatial restraints. *J Mol Biol* 234:779–815. <http://dx.doi.org/10.1006/jmbi.1993.1626>.
 35. McGuffin LJ, Buenavista MT, Roche DB. 2013. The ModFOLD4 server for the quality assessment of 3D protein models. *Nucleic Acids Res* 41:W368–W372. <http://dx.doi.org/10.1093/nar/gkt294>.
 36. Benkert P, Kuenzli M, Schwede T. 2009. QMEAN server for protein model quality estimation. *Nucleic Acids Res* 37:W510–W514. <http://dx.doi.org/10.1093/nar/gkp322>.
 37. Berjanskii M, Zhou J, Liang Y, Lin G, Wishart DS. 2012. Resolution-by-proxy: a simple measure for assessing and comparing the overall quality of NMR protein structures. *J Biomol NMR* 53:167–180. <http://dx.doi.org/10.1007/s10858-012-9637-2>.
 38. Li X, Jacobson MP, Zhu K, Zhao S, Friesner RA. 2007. Assignment of polar states for protein amino acid residues using an interaction cluster decomposition algorithm and its application to high resolution protein structure modeling. *Proteins* 66:824–837.
 39. Schrödinger LLC. 2010. Maestro version 9.1. Schrödinger LLC, New York, NY.
 40. Madadkar-Sobhani A, Guallar V. 2013. PELE web server: atomistic study of biomolecular systems at your fingertips. *Nucleic Acids Res* 41:W322–W328. <http://dx.doi.org/10.1093/nar/gkt454>.
 41. Takhampunya R, Ubol S, Houg HS, Cameron CE, Padmanabhan R. 2006. Inhibition of dengue virus replication by mycophenolic acid and ribavirin. *J Gen Virol* 87:1947–1952. <http://dx.doi.org/10.1099/vir.0.81655-0>.
 42. Atilgan AR, Durell SR, Jernigan RL, Demirel MC, Keskin O, Bahar I. 2001. Anisotropy of fluctuation dynamics of proteins with an elastic network model. *Biophys J* 80:505–515. [http://dx.doi.org/10.1016/S0006-3495\(01\)76033-X](http://dx.doi.org/10.1016/S0006-3495(01)76033-X).
 43. Jacobson MP, Friesner RA, Xiang ZX, Honig B. 2002. On the role of the crystal environment in determining protein side-chain conformations. *J Mol Biol* 320:597–608. [http://dx.doi.org/10.1016/S0022-2836\(02\)00470-9](http://dx.doi.org/10.1016/S0022-2836(02)00470-9).
 44. Still WC, Tempczyk A, Hawley RC, Hendrickson T. 1990. Semianalytical treatment of solvation for molecular mechanics and dynamics. *J Am Chem Soc* 112:6127–6129. <http://dx.doi.org/10.1021/ja00172a038>.
 45. Borrelli KW, Vitalis A, Alcantara R, Guallar V. 2005. PELE: protein energy landscape exploration. A novel Monte Carlo based technique. *J Chem Theory Comput* 1:1304–1311.
 46. Jorgensen WL, Tiradorives J. 1988. The Opls potential functions for proteins—energy minimizations for crystals of cyclic peptides and crambin. *J Am Chem Soc* 110:1657–1666. <http://dx.doi.org/10.1021/ja00214a001>.
 47. Gil VA, Guallar V. 2014. pyProCT: automated cluster analysis for structural bioinformatics. *J Chem Theory Comput* 10:3236–3243. <http://dx.doi.org/10.1021/ct500306s>.
 48. Osolodkin DI, Kozlovskaya LI, Dueva EV, Dotsenko VV, Rogova YV, Frolov KA, Krivokolysko SG, Romanova EG, Morozov AS, Karganova GG, Palyulin VA, Pentkovski VM, Zefirov NS. 2013. Inhibitors of tick-borne flavivirus reproduction from structure-based virtual screening. *ACS Med Chem Lett* 4:869–874. <http://dx.doi.org/10.1021/ml400226s>.
 49. Wallner G, Mandl CW, Ecker M, Holzmann H, Stiasny K, Kunz C, Heinz FX. 1996. Characterisation and complete genome sequences of high- and low-virulence variants of tick-borne encephalitis virus. *J Gen Virol* 77:1035–1042. <http://dx.doi.org/10.1099/0022-1317-77-5-1035>.
 50. Crance JM, Scaramozzino N, Jouan A, Garin D. 2003. Interferon, ribavirin, 6-azauridine and glycyrrhizin: antiviral compounds active against pathogenic flaviviruses. *Antiviral Res* 58:73–79. [http://dx.doi.org/10.1016/S0166-3542\(02\)00185-7](http://dx.doi.org/10.1016/S0166-3542(02)00185-7).
 51. Carroll SS, Tomassini JE, Bosserman M, Getty K, Stahlhut MW, Eldrup AB, Bhat B, Hall D, Simcoe AL, LaFemina R, Rutkowski CA, Wolanski B, Yang ZC, Migliaccio G, De Francesco R, Kuo LC, MacCoss M, Olsen DB. 2003. Inhibition of hepatitis C virus RNA replication by 2'-modified nucleoside analogs. *J Biol Chem* 278:11979–11984. <http://dx.doi.org/10.1074/jbc.M210914200>.
 52. Cristali G, Costanzi S, Lambertucci C, Lupidi G, Vittori S, Volpini R, Camaioni E. 2001. Adenosine deaminase: functional implications and different classes of inhibitors. *Med Res Rev* 21:105–128. [http://dx.doi.org/10.1002/1098-1128\(200103\)21:2<105::AID-MED1002>3.0.CO;2-U](http://dx.doi.org/10.1002/1098-1128(200103)21:2<105::AID-MED1002>3.0.CO;2-U).
 53. Kinney RM, Huang CYH, Rose BC, Kroeger AD, Dreher TW, Iversen PL, Stein DA. 2005. Inhibition of dengue virus serotypes 1 to 4 in Vero cell cultures with morpholino oligomers. *J Virol* 79:5116–5128. <http://dx.doi.org/10.1128/JVI.79.8.5116-5128.2005>.
 54. Carroll SS, Ludmerer S, Handt L, Koepflinger K, Zhang NR, Graham D, Davies ME, MacCoss M, Hazuda D, Olsen DB. 2009. Robust antiviral efficacy upon administration of a nucleoside analog to hepatitis C virus-infected chimpanzees. *Antimicrob Agents Chemother* 53:926–934. <http://dx.doi.org/10.1128/AAC.01032-08>.
 55. Carroll SS, Koepflinger K, Vavrek M, Zhang NR, Handt L, MacCoss M, Olsen DB, Reddy KR, Sun ZL, van Poelje PD, Fujitaki JM, Boyer SH, Linemeyer DL, Hecker SJ, Erion MD. 2011. Antiviral efficacy upon administration of a HepDirect prodrug of 2'-c-methylcytidine to hepatitis C virus-infected chimpanzees. *Antimicrob Agents Chemother* 55:3854–3860. <http://dx.doi.org/10.1128/AAC.01152-10>.
 56. Sofia MJ, Chang W, Furman PA, Mosley RT, Ross BS. 2012. Nucleoside, nucleotide, and non-nucleoside inhibitors of hepatitis C virus NS5B RNA-dependent RNA polymerase. *J Med Chem* 55:2481–2531. <http://dx.doi.org/10.1021/jm201384j>.



Structure-activity relationships of nucleoside analogues for inhibition of tick-borne encephalitis virus



Luděk Eyer^a, Markéta Šmídková^b, Radim Nencka^b, Jiří Neča^a, Tomáš Kastl^a,
Martin Palus^{a, d}, Erik De Clercq^c, Daniel Růžek^{a, d, *}

^a Department of Virology, Veterinary Research Institute, Hudcova 70, CZ-62100 Brno, Czech Republic

^b Institute of Organic Chemistry and Biochemistry, The Czech Academy of Sciences, Fleming Sq. 2, CZ-16610 Prague, Czech Republic

^c Rega Institute for Medical Research, KU Leuven, Minderbroedersstraat 10, B-3000 Leuven, Belgium

^d Institute of Parasitology, Biology Centre of the Czech Academy of Sciences, and Faculty of Science, University of South Bohemia, Branišovská 31, CZ-37005 České Budějovice, Czech Republic

ARTICLE INFO

Article history:

Received 10 February 2016

Received in revised form

5 July 2016

Accepted 24 July 2016

Available online 28 July 2016

Keywords:

Structure-activity relationship

Tick-borne encephalitis

Nucleoside inhibitor

Antiviral activity

Cytotoxicity

ABSTRACT

Tick-borne encephalitis (TBE) represents one of the most serious arboviral neuro-infections in Europe and northern Asia. As no specific antiviral therapy is available at present, there is an urgent need for efficient drugs to treat patients with TBE virus (TBEV) infection. Using two standardised *in vitro* assay systems, we evaluated a series of 29 nucleoside derivatives for their ability to inhibit TBEV replication in cell lines of neuronal as well as extraneural origin. The series of tested compounds included 2'-C- or 2'-O-methyl substituted nucleosides, 2'-C-fluoro-2'-C-methyl substituted nucleosides, 3'-O-methyl substituted nucleosides, 3'-deoxynucleosides, derivatives with 4'-C-azido substitution, heterobase modified nucleosides and neplanocins. Our data demonstrate a relatively stringent structure-activity relationship for modifications at the 2', 3', and 4' nucleoside positions. Whereas nucleoside derivatives with the methylation at the C2' position or azido modification at the C4' position exerted a strong TBEV inhibition activity (EC₅₀ from 0.3 to 11.1 μM) and low cytotoxicity *in vitro*, substitutions of the O2' and O3' positions led to a complete loss of anti-TBEV activity (EC₅₀ > 50 μM). Moreover, some structural modifications of the heterobase moiety resulted in a high increase of cytotoxicity *in vitro*. High antiviral activity and low cytotoxicity of C2' methylated or C4' azido substituted pharmacophores suggest that such compounds might represent promising candidates for further development of potential therapeutic agents in treating TBEV infection.

© 2016 Elsevier B.V. All rights reserved.

1. Introduction

Tick-borne encephalitis virus (TBEV), a causative agent of tick-borne encephalitis (TBE), is a member of the *Flaviviridae* family, which includes many medically important viruses, such as hepatitis C virus (HCV), West Nile virus, Zika virus, dengue virus, Japanese encephalitis virus, yellow fever virus, and several haemorrhagic fever-associated flaviviruses (Baier, 2011). TBE represents one of the most serious arboviral neuro-infections in Europe and northern Asia with thousands of TBEV-infected people and many reported deaths annually (Dumpis et al., 1999; Heinz and Mandl, 1993). The

characteristic clinical symptoms of acute TBE range from a mild meningitis to severe meningoencephalitis/myelitis with the risk of temporary or permanent neurologic sequelae after TBE infection (Ruzek et al., 2010). Although safe and efficient vaccines against TBEV are available, the number of TBE patients in the endemic regions of Europe continuously increases (Heinz et al., 2013; Zavadská et al., 2013). As no specific antiviral therapy is available at present, there is an urgent need for efficient drugs to treat patients with TBEV infection (Puig-Basagoiti et al., 2006).

Inhibitors of viral polymerases are the largest class of approved antiviral drugs, of which the largest number is represented by nucleoside analogue inhibitors (De Clercq, 2011). Mode of action of nucleoside inhibitors is based on the premature termination of viral RNA synthesis (De Clercq and Neyts, 2009). Following intracellular phosphorylation, the 5'-triphosphate metabolites are competitively incorporated into the viral RNA nascent chains, which

* Corresponding author. Veterinary Research Institute, Hudcova 70, CZ-62100 Brno, Czech Republic.

E-mail address: ruzekd@paru.cas.cz (D. Růžek).

prevents further extension of the incorporated analogue by addition of the next nucleoside triphosphate resulting in formation of incomplete (non-functional) viral RNA chains. In general, the antiviral activity of nucleoside inhibitors is predominantly determined by steric interference (hydrogen bonding capability) between the nucleoside triphosphate and the viral polymerase active site. Moreover, the effect of the absence, conformational constraints, or steric/electronic hindrance of the nucleoside 3'-hydroxyl function on formation of a phosphodiester linkage with the incoming nucleoside triphosphate could also play an important role in the efficient termination of viral RNA synthesis (De Clercq, 2004; De Clercq and Neyts, 2009). Cellular uptake and intracellular metabolism (such as deamination, phosphorolysis or phosphorylation) can also considerably influence the antiviral activity of a nucleoside analogue (Eldrup et al., 2004; Tomassini et al., 2005; Ma et al., 2007).

Previously, we identified three 2'-C-methylated nucleoside analogues (i.e., 2'-C-methyladenosine, 2'-C-methylcytidine and 7-deaza-2'-C-methyladenosine) as effective inhibitors of TBEV replication *in vitro* (Eyer et al., 2015). In connection with these results, we report here a structure-activity relationship study based on the antiviral/cytotoxicity profile of 29 nucleoside derivatives, each differing in chemical substituents on the ribose ring and in the type and chemical modifications of the heterobase. We focused our attention on the evaluation of 2', 3', and 4'-modified nucleosides, for which antiviral activity was previously reported for other viruses, especially HCV (Eldrup et al., 2004; Klumpp et al., 2008; Sofia et al., 2012), Zika (Eyer et al., 2016), dengue (Lee et al., 2015), yellow fever (Julander et al., 2010), and haemorrhagic fever-associated flaviviruses (Flint et al., 2014). The tested compounds were characterized using standardised *in vitro* assay systems in terms of inhibition of TBEV replication, inhibition of virus-induced cytopathic effect (CPE) formation, suppression of viral antigen expression in TBEV-infected cell cultures, and evaluation of viability on compound-treated host cells. Based on these screens, we identified the 2'-C-methyl or 4'-C-azido substituents as important for a selective TBEV inhibition and a low cytotoxicity *in vitro*.

2. Material and methods

2.1. Cell cultures, virus strains and antiviral compounds

Porcine kidney stable (PS) cells, a cell line widely used for TBEV isolation, multiplication, and for conducting plaque assays (Kozuch and Mayer, 1975), were cultured at 37 °C in Leibovitz (L-15) medium supplemented with 3% precolostral calf serum and a 1% mixture of penicillin and glutamine (Sigma-Aldrich, Prague, Czech Republic). Human neuroblastoma UKF-NB-4 cells, a valuable model for neuropathogenesis studies of TBEV (Ruzek et al., 2009), were cultured at 37 °C in 5% CO₂ in Iscove's modified Dulbecco's medium (IMDM) with 10% foetal bovine serum and a 1% mixture of antibiotics (Sigma-Aldrich, Prague, Czech Republic). Hypr and Neudoerfl TBEV strains, typical representatives of the West European TBEV subtype, were used for evaluation of the antiviral activity of the test compounds. Nucleoside analogues were purchased as follows: 2'-C-methyl, 2'-O-methyl, and 3'-O-methyl substituted nucleosides, 3'-deoxynucleosides, sofosbuvir, and 6-azauridine from Carbo-synth (Compton, UK), 4'-azidocytidine, balapiravir and RO-9187 from Medchemexpress (Stockholm, Sweden), neplanocin A from Cayman Chemical Company (Ann Arbor, Michigan), 3-deazaneplanocin A from Selleckchem (Munich, Germany), mercitabine from ChemScene (Monmouth Junction, NJ), PSI-6206 from ApexBio (Boston, MA), tubercidin, toyocamycin, sangivamycin, ribavirin and 2'-deoxynucleosides from Sigma-Aldrich (Prague, Czech Republic). Nucleotide triphosphate standards for HPLC

analysis were purchased from TriLink Biotechnologies (San Diego, CA). The test compounds were solubilised in 100% DMSO to yield 10 mM stock solutions.

2.2. *In vitro* antiviral assays

A viral titre inhibition assay was performed to measure the antiviral efficacy of nucleoside analogues in cell culture. PS or UKF-NB-4 cells were seeded in 96-well plates (approximately 2×10^4 cells per well) and incubated for 24 h to form a confluent monolayer. Following incubation, the medium was aspirated from the wells and replaced with 200 µl of fresh medium containing 50 µM of the test compound (three wells per compound), which was inoculated with the Hypr or Neudoerfl TBEV strain at a multiplicity of infection (MOI) of 0.1. As a negative control, DMSO was added to virus- and mock-infected cells at a final concentration of 0.5% (v/v). Culture medium was collected 3 days postinfection (p.i.) to yield a 40–50% CPE in virus control wells. The CPE was monitored visually using the Olympus BX-5 microscope equipped with an Olympus DP-70 CCD camera. Viral titres were determined by plaque assays and expressed as PFU ml⁻¹ (De Madrid and Porterfield, 1969). For dose-response studies, PS cell monolayers were cultured with 200 µl of medium containing the test compounds over the concentration range of 0–50 µM and TBEV (Hypr strain) at an MOI of 0.1. The medium was collected from the wells at 2-day intervals (post-infection days 1, 3 and 5), the viral titres were determined by plaque assays and used to construct TBEV dose-response curves. The dose-response curves on post-infection days 3 were used to estimate the 50% effective concentration (EC₅₀).

2.3. Immunofluorescence staining

To measure the compound-induced inhibition of viral surface antigen expression, a cell-based flavivirus immunostaining assay was performed as previously described (Eyer et al., 2015). Briefly, PS cells were seeded on slides, infected with the TBEV Hypr strain at an MOI of 0.1, treated with the test compound (50 µM) and cultured for 4 days at 37 °C. After a cold acetone-methanol (1:1) fixation and blocking with 10% foetal bovine serum, the cells were incubated with a mouse monoclonal antibody recognising the flavivirus group surface antigen (1:250, Sigma-Aldrich, Prague, Czech Republic) and subsequently labelled with an anti-mouse goat secondary antibody conjugated with FITC (1:500) by incubation for 1 h at 37 °C. The cells were counterstained with DAPI (1 µg ml⁻¹) to visualise the cell nuclei. Finally, the cells were mounted in 2.5% DABCO (Sigma-Aldrich, Czech Republic) and the fluorescence signal was recorded with an Olympus IX71 epifluorescence microscope.

2.4. Cytotoxicity assays

PS cells were grown in 96-well plates overnight to form a confluent monolayer and subsequently treated with test compounds over the concentration range of 0–50 µM. At day 3 p.i., the medium was collected and the potential cytotoxicity of test compounds was determined in terms of cell viability using the Cell Counting Kit-8 (Dojindo Molecular Technologies, Munich, Germany) according to the manufacturer's instructions. The concentration of compound that reduced cell viability by 50% was considered the 50% cytotoxic concentration (CC₅₀).

2.5. Quantification of 2'-C-methylated nucleosides in compound-treated cells

The UKF-NB4 cells were plated at a density of 2×10^5 cells/ml in 6-well plates for 48 h and subsequently exposed to tested

compounds at concentration of 10 or 50 μM . After 0, 2, 4, and 8-h intervals, the cells were rinsed with PBS, harvested by scraping and centrifuged at 2800 rpm for 2 min. The pellet was resuspended in 500 μl methanol and sonicated for 1 min. The obtained suspension (50 μl) was used for protein quantification (BCA method – Pierce BCA Protein Assay Kit, Thermo Scientific, San Jose, CA). After centrifugation, the supernatant was used for quantitative determination of 2'-C-methylated nucleosides using liquid chromatography-tandem mass spectrometry (LC-MS/MS) (Zouharova et al., 2016). An Agilent 1200 chromatographic system (Agilent Technologies, Germany), consisted of binary pump, vacuum degasser, autosampler, and thermostatted column compartment, was used. Separation of modified nucleosides was carried out using a Zorbax Eclipse Plus C18, 2.1 \times 150 mm, 3.5 μm particle size

column (Agilent, USA) under isocratic conditions. Mobile phase contained methanol according to the analyzed nucleoside and 0.1% of formic acid in water. The flow rate of the mobile phase was 0.25 ml/min, the column temperature was set at 40 $^{\circ}\text{C}$. A triple quadrupole mass spectrometer Agilent 6410 Triple Quad LC/MS (Agilent Technologies, USA) with an electrospray interface (ESI) was used for detection of nucleosides in cells. The mass spectrometer was operated in the positive mode and selected ion monitoring (SIM) was used for quantification.

2.6. Crude cellular extract preparation

PS and UKF-NB4 cells (5×10^6) were washed with PBS, resuspended in 2 ml of 50 mM Tris-HCl buffer (pH 7.4) containing 1 mM

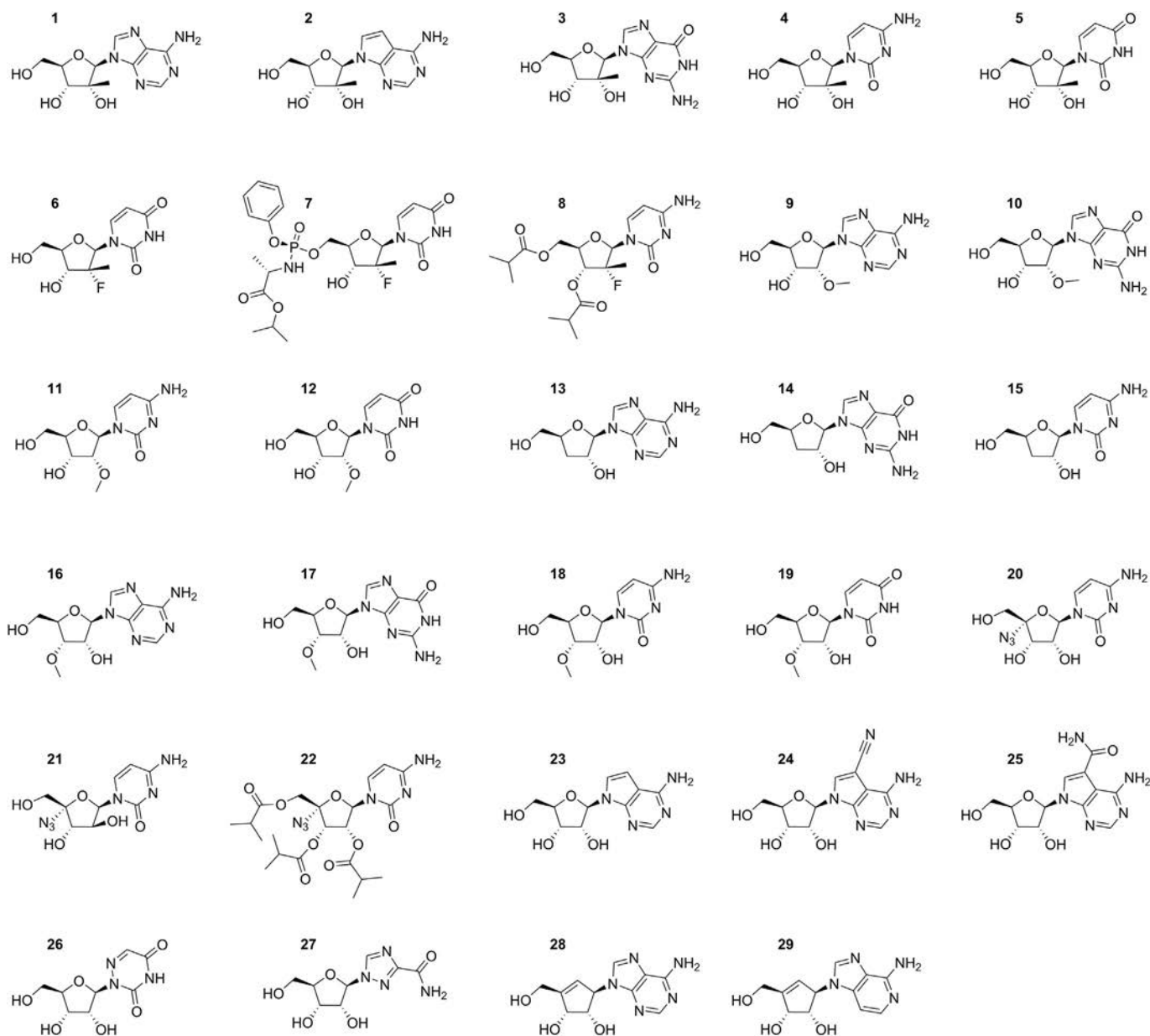


Fig. 1. The structures of the nucleoside analogues tested in this study. (1) 2'-C-methyladenosine, (2) 7-deaza-2'-C-methyladenosine, (3) 2'-C-methylguanosine, (4) 2'-C-methylcytosidine, (5) 2'-C-methyluridine, (6) PSI-6206, (7) sofosbuvir, (8) mericitabine, (9) 2'-O-methyladenosine, (10) 2'-O-methylguanosine, (11) 2'-O-methylcytosidine, (12) 2'-O-methyluridine, (13) 3'-deoxyadenosine, (14) 3'-deoxyguanosine, (15) 3'-deoxycytidine, (16) 3'-O-methyladenosine, (17) 3'-O-methylguanosine, (18) 3'-O-methylcytosidine, (19) 3'-O-methyluridine, (20) 4'-azidocytidine, (21) RO-9187, (22) balapiravir, (23) 7-deazaadenosine (tubercidin), (24) 7-deaza-7-cyanoadenosine (toyocamycin), (25) 7-deaza-7-carbamoyladenine (sangivamycin), (26) 6-azauridine, (27) ribavirin, (28) neplanocin A, (29) 3-deazaneplanocin A.

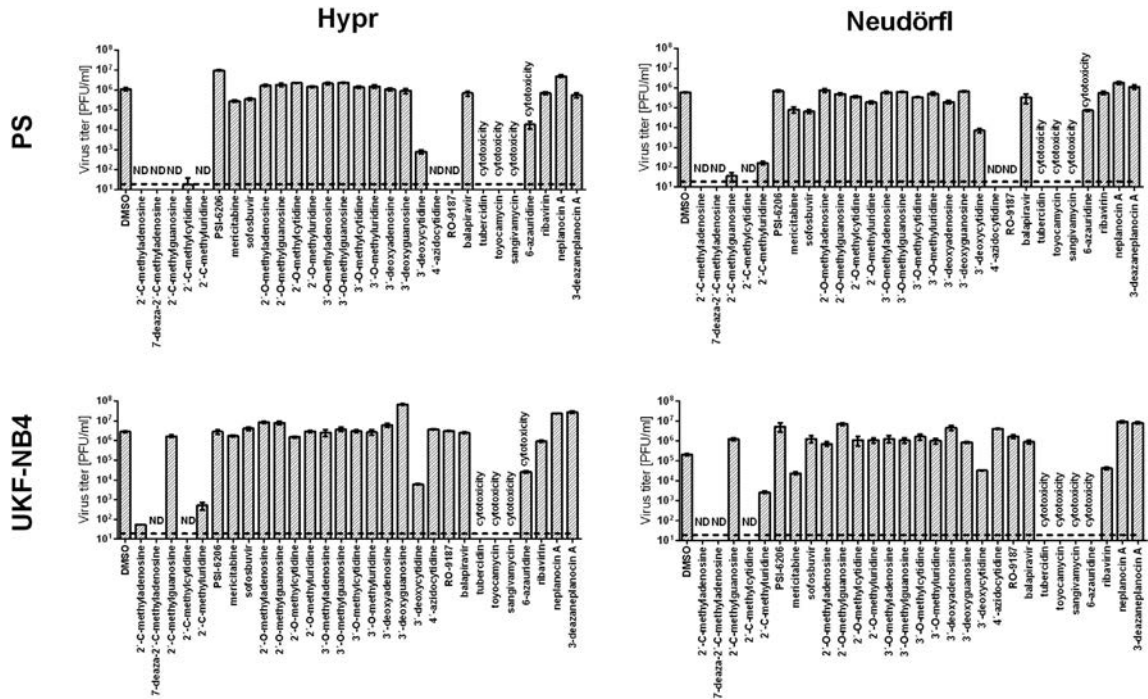


Fig. 2. Reduction of TBEV titres by the indicated nucleoside analogues. PS or UKF-NB-4 cells were infected with TBEV (Hypr or Neudörfli strain) at a multiplicity of infection (MOI) of 0.1 and then treated with 50 μ M nucleoside analogues. The TBEV titres were determined by the plaque assay 3 days p.i. Viral titres are expressed as PFU mL⁻¹. Bars show the mean values from three biological replicate wells, and the error bars indicate the standard errors of the means (n = 3). ND, not detected (below the detection limit). The horizontal dashed line indicates the minimum detectable threshold of 1.44 log₁₀ PFU mL⁻¹.

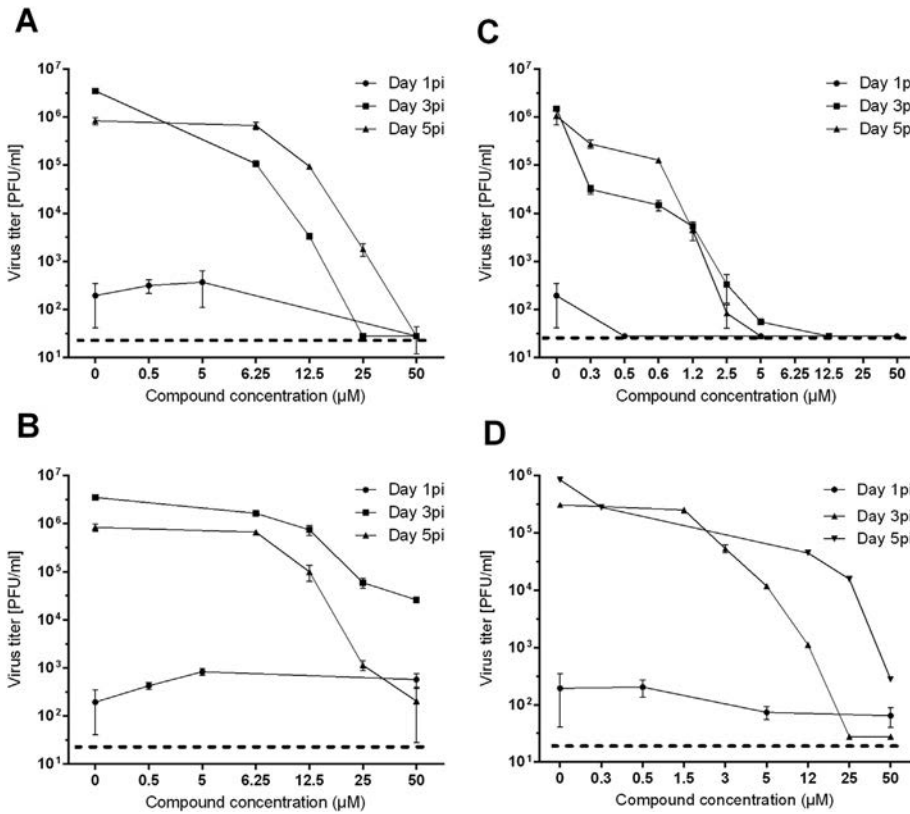


Fig. 3. Dose-dependent effects of the indicated TBEV inhibitors on virus titres. PS cells were infected with TBEV at a multiplicity of infection (MOI) of 0.1 and treated with 2'-C-methylguanosine (A), 2'-C-methyluridine (B), RO-9187 (C) and (D) 4'-azidocytidine at the indicated concentrations. TBEV titres were monitored at days 1, 3, and 5 p.i. The mean titres from three biological replicates are shown, and error bars indicate standard errors of the mean (n = 3). The horizontal dashed line indicates the minimum detectable threshold of 1.44 log₁₀ PFU mL⁻¹.

dithiothreitol, 5 mM MgCl₂, and protease inhibitor and phosphatase inhibitor cocktail (Sigma Aldrich, Prague, Czech Republic) and homogenized using sonication. After that, the homogenate was centrifuged at 30,000g for 30 min. Aliquots (100 µl) were stored at –80 °C until use.

2.7. Metabolism of compounds in crude extract

The tested compounds (2'-C-methylguanosine, 2'-O-methylcytidine, 4'-azidocytidine and RO-9187) at concentration of 100 µM were added to 100 µl of crude extract and incubated at 37 °C for 0, 0.5, 2, 4, and 8 h. The samples were deproteinized by methanol precipitation (400 µl of methanol to 100 µl of sample), centrifuged at 14,000g for 10 min and subsequently used for HPLC analysis.

2.8. HPLC analysis

The samples (50 µl) were injected onto the Supelcosil LC-18-T HPLC column (150 mm × 3 mm I. D., 3 µm). Mobile phase A corresponded to 50 mM KH₂PO₄ (pH 3.1) with 10 mM tetrabutylammonium hydrogensulphate, mobile phase B to 50 mM KH₂PO₄ (pH 3.1) with 10 mM tetrabutylammonium hydrogen sulphate and 30% acetonitrile (v/v) in HPLC-grade water and mobile phase C to 50 mM KH₂PO₄ (pH 3.1) with 10 mM tetrabutylammonium hydrogen sulphate. The gradient started with 100% mobile phase A going isocratically in 5 min, followed by steep change from C to B in 6 min, ongoing nonlinearly to 75% B in 30 min and then going

linearly to 100% mobile phase A in 35 min. The flow rate was 0.75 ml/min. The absorption spectra of the eluate were recorded by a PDA detector. The concentrations of intact compounds and their phosphates in crude extract were calculated from the peak areas by using calibration curves made up from their standards, which are characterized in terms of retention times (Rt) and absorption maxima in [Supplementary Table 1](#).

3. Results

3.1. Modifications of the ribose 2'-position

We described previously that 2'-C-methyladenosine, 2'-C-methylcytidine, and 7-deaza-2'-C-methyladenosine are effective inhibitors of TBEV replication *in vitro* (Eyer et al., 2015). In order to further investigate the structure-activity relationships for the ribose 2'-modifications, we tested a large group of 2'-C- or 2'-O-substituted nucleosides (Fig. 1, structures 1–12) for their anti-TBEV activity and cytotoxicity using standardised *in vitro* assays.

As expected, 2'-C-methylguanosine and 2'-C-methyluridine displayed an inhibitory effect on TBEV replication in PS cells (Fig. 2). Both derivatives reduced the viral titre in a dose-dependent manner (EC₅₀ of 1.4 µM (2'-C-methylguanosine) and 11.1 µM (2'-C-methyluridine)) and the antiviral effect appeared to be stable throughout the five-day experimental period (Fig. 3A,B, Table 1). Surprisingly, 2'-C-methylguanosine failed to inhibit TBEV when applied to human neuroblastoma cells (Fig. 2). 2'-C-

Table 1
TBEV-inhibition and cytotoxicity characteristics of the studied nucleoside analogues.

Structure number ^a	Compound	EC ₅₀ ^{b,c} (µM)	App.EC ₅₀ ^{b,d} (µM)	CC ₅₀ ^b (µM)	SI ^e
(1)	2'-C-methyladenosine	1.4 ± 0.01	7.1 ± 1.2 ^g	>50.0 ^g	>37.03
(2)	7-deaza-2'-C-methyladenosine	1.1 ± 0.03	5.1 ± 0.4 ^g	>50.0 ^g	>46.7
(3)	2'-C-methylguanosine	1.4 ± 0.01	13.5 ± 0.8	>50.0	>35.7
(4)	2'-C-methylcytidine	1.8 ± 0.4	14.2 ± 0.4 ^g	~50.0 ^g	~28.4
(5)	2'-C-methyluridine	11.1 ± 0.4	25.1 ± 7.2	>50.0	>4.5
(6)	PSI-6206	>50.0	>50.0	>50.0	1.0
(7)	sofosbuvir	>50.0	>50.0	>50.0	1.0
(8)	mericitabine	>50.0	>50.0 ^g	>50.0 ^g	1.0
(9)	2'-O-methyladenosine	>50.0	>50.0	>50.0	1.0
(10)	2'-O-methylguanosine	>50.0	>50.0	>50.0 ⁱ	1.0
(11)	2'-O-methylcytidine	>50.0	>50.0	>50.0	1.0
(12)	2'-O-methyluridine	>50.0	>50.0	>50.0	1.0
(13)	3'-deoxyadenosine	>50.0	>50.0	>50.0	1.0
(14)	3'-deoxyguanosine	>50.0	>50.0	>50.0	1.0
(15)	3'-deoxycytidine ^h	41.2 ± 0.01	79.4 ± 2.3	80.2 ± 0.01	1.9
(16)	3'-O-methyladenosine	>50.0	>50.0	>50.0	1.0
(17)	3'-O-methylguanosine	>50.0	>50.0	>50.0	1.0
(18)	3'-O-methylcytidine	>50.0	>50.0	>50.0	1.0
(19)	3'-O-methyluridine	>50.0	>50.0	>50.0	1.0
(20)	4'-azidocytidine	2.7 ± 0.1	9.3 ± 0.3	>50.0	>18.6
(21)	RO-9187	0.3 ± 0.01	1.5 ± 0.2	>50.0 ⁱ	>192.3
(22)	balapiravir	>50.0	>50.0	>50.0	1.0
(23)	7-deazaadenosine (tubercidin)	ND ^f	ND ^f	2.1 ± 0.2	–
(24)	7-deaza-7-cyanoadenosine (toyocamycin)	ND ^f	ND ^f	0.1 ± 0.01	–
(25)	7-deaza-7-carbamoyladenosine (sangivamycin)	ND ^f	ND ^f	0.8 ± 0.1	–
(26)	6-azauridine	ND ^f	ND ^f	7.0 ± 0.5	–
(27)	ribavirin	> 50.0	> 50.0	> 50.0	1.0
(28)	neplanocin A	> 50.0	> 50.0	> 50.0 ⁱ	1.0
(29)	3-deazaneplanocin A	> 50.0	> 50.0	> 50.0	1.0

^a See Fig. 1.

^b Determined from three independent experiments.

^c Calculated as a 50% reduction of viral titers using the Reed-Muench method.

^d Calculated as a point of inflection from dose-response curves using log-transformed viral titers.

^e SI = CC₅₀/EC₅₀.

^f ND, not determined. As TBEV replication is dependent on cell proliferation, the EC₅₀ values of cytotoxic compounds cannot be assessed.

^g Values reported previously by Eyer et al., 2015.

^h Dose-response experiment for 3'-deoxycytidine including the cytotoxicity assay was performed in the concentration range from 0 to 400 µM.

ⁱ Treatment the cell culture with 2'-O-methylguanosine, RO-9187, and neplanocin A at concentration of 50 µM led to a reduction in the cell viability to 84.4, 86.9 and 83.6%, respectively.

Methylguanosine and 2'-C-methyluridine inhibited the expression of the TBEV surface E antigen in PS cells (Fig. 4B, C) and showed no cytotoxic effects at the highest tested concentration of 50 μ M with no detectable effect on cell proliferation (Fig. 5A).

Replacement of the 2'-C-methyl group by the 2'- α -fluoro-2'- β -methyl moiety led to a loss in antiviral activity, as observed in PSI-6206, sofosbuvir and mericitabine ($EC_{50} > 50 \mu$ M). Similarly, 2'-O-methyl substituted nucleosides caused no or negligible activity against both TBEV strains (Fig. 2). A moderate decline of cell viability (to 84.4%) was seen in PS cell cultures treated with 50 μ M of 2'-O-methylguanosine (Fig. 5A).

3.2. Modifications of the ribose 3'-position

Of all 3'-deoxynucleosides tested (Fig. 1, structures 13–15), only 3'-deoxycytidine showed a moderate inhibitory activity (EC_{50} of 41.2 μ M) (Fig. 2). The anti-TBEV activity of 3'-deoxycytidine was accompanied by a slight cytotoxic effect on PS cell monolayers

(Fig. 5A, Table 1). In contrast, 3'-deoxyadenosine and 3'-deoxyguanosine exhibited no detectable inhibitory effect on TBEV replication ($EC_{50} > 50 \mu$ M) (Fig. 2) and were well tolerated by the cultured PS cells (Fig. 5A). Methylation of the 3'-hydroxyl group to generate the corresponding 3'-O-methyl modified structures (Fig. 1, structures 16–19) also resulted in a complete loss in antiviral activity, regardless of the purine/pyrimidine heterobase identity (Fig. 2). 3'-O-Methyl modified derivatives exerted no cytotoxic effects and caused no morphological changes in the PS cell cultures (Fig. 5A).

3.3. Modifications of the ribose 4'-position

4'-Azidocytidine and its arabino-counterpart 2'- α -deoxy-2'- β -hydroxy-4'-azidocytidine, termed RO-9187 (Fig. 1, structures 20 and 21), exhibited a dose-dependent anti-TBEV effect in PS cell cultures (EC_{50} of 2.7 and 0.3 μ M, respectively) (Fig. 3C,D; Table 1). These compounds, however, failed to inhibit TBEV when applied on

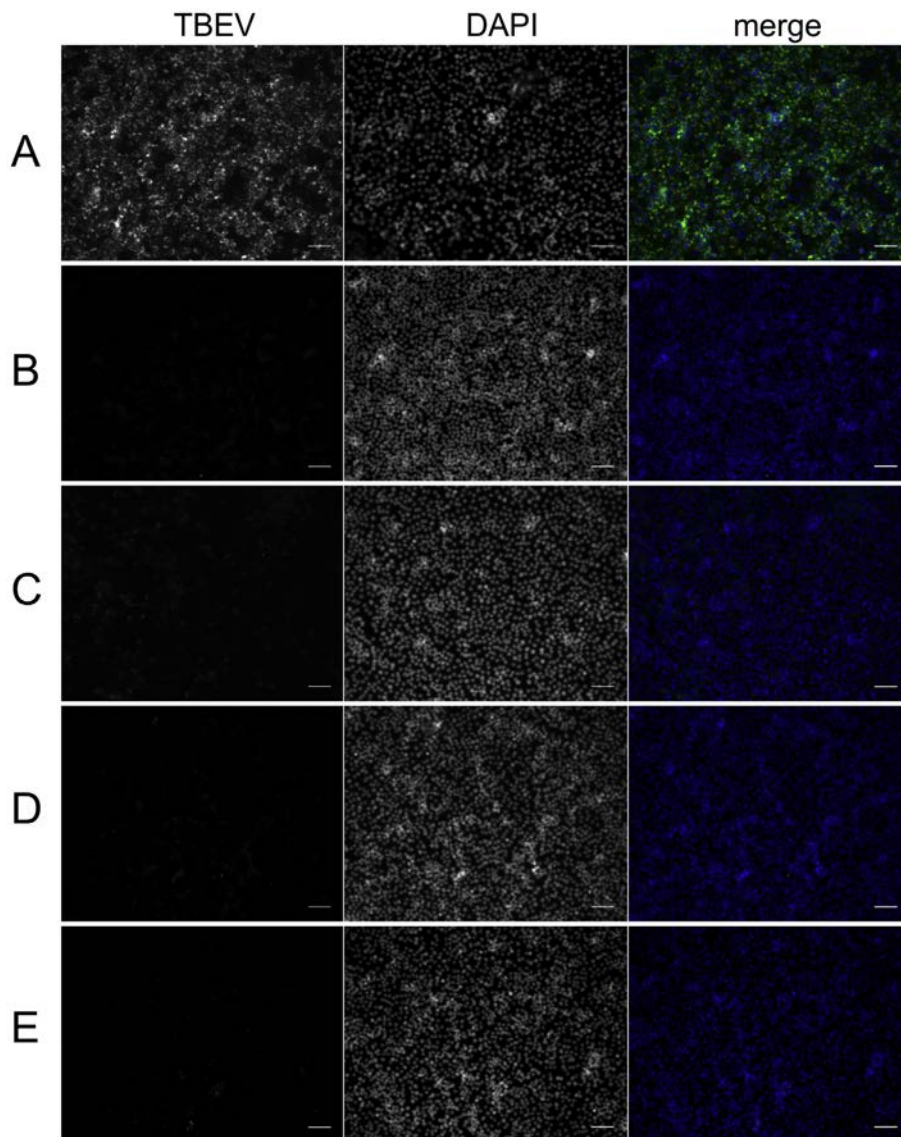


Fig. 4. Inhibition of TBEV viral antigen expression by nucleoside inhibitors. PS cells were infected with TBEV and treated with 0.5% DMSO (A) or with 50 μ M 2'-C-methylguanosine (B), 2'-C-methyluridine (C), RO-9187 (D), and 4'-azidocytidine (E). PS cells were fixed on slides at day 3 postinfection and stained with flavivirus-specific antibody labelled with FITC (green) and counterstained with DAPI (blue). Scale bars, 50 μ m. (For interpretation of the references to colour in this figure legend, the reader is referred to the web version of this article.)

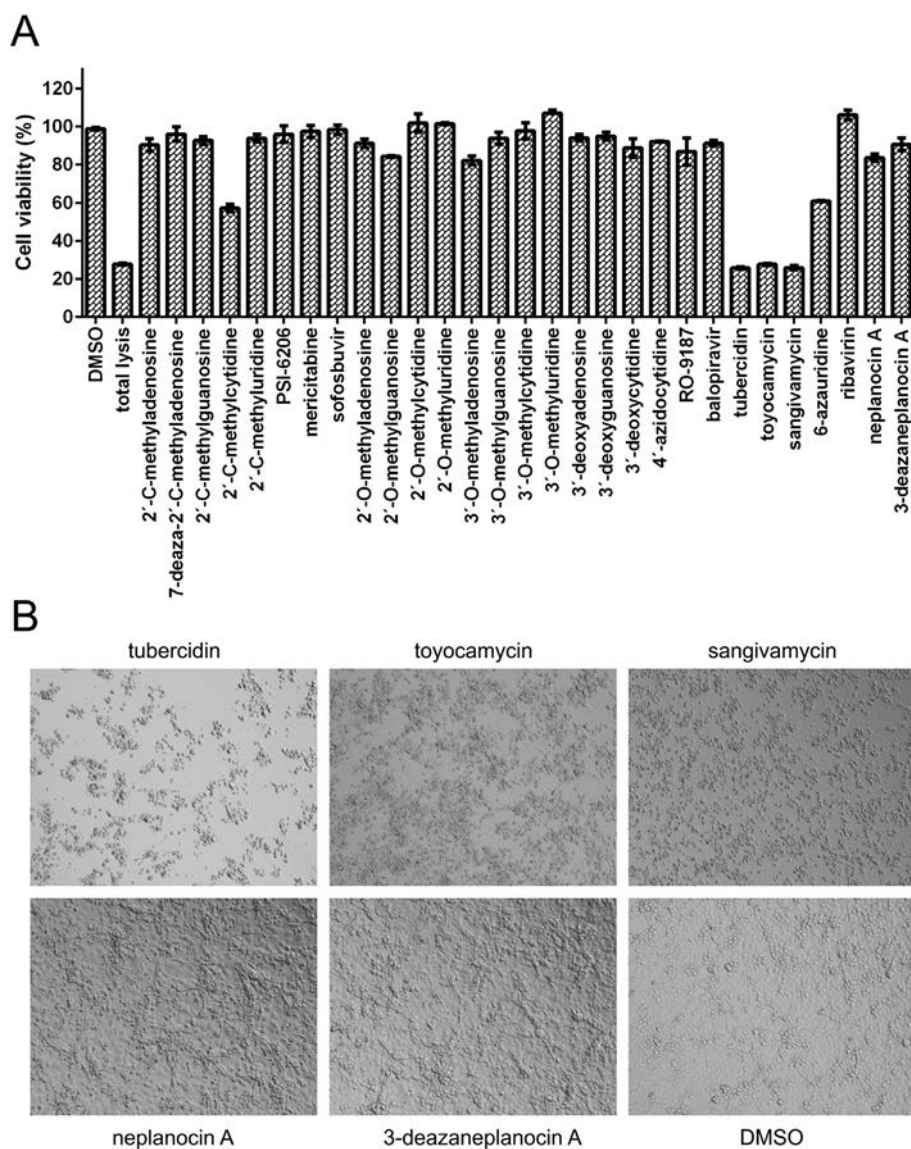


Fig. 5. Cytotoxicity of nucleoside inhibitors. Cytotoxicity was determined by treatment PS cells with the 50 μM of indicated nucleoside analogues and was expressed in terms of cell viability at day 3 postinfection. The bars indicate the mean values from three replicate wells, and the error bars indicate the standard errors of the mean (A). Cytotoxic effects and morphological changes of PS cells induced by the indicated nucleoside analogues (50 μM) at day 3 after treatment (B).

human neuroblastoma cells (Fig. 2). 4'-Azidocytidine and RO-9187 at the concentration of 50 μM showed a significant inhibition of the viral protein E expression in TBEV-infected compound-treated PS cells (Fig. 4D,E). On the other hand, balapiravir (Fig. 1, structure 22), an ester prodrug of 4'-azidocytidine, was found to be completely inactive in inhibiting TBEV *in vitro*. Whereas 4'-azidocytidine and balapiravir exerted no cytotoxic effects on the PS cell cultures, RO-9187 (at 50 μM) showed a slight decrease of the cell viability (to 86.9%) (Fig. 5A).

3.4. Modification of the purine/pyrimidine heterobase

The combination of the 7-deaza modification of adenosine and the 2'-C-methyl-ribose substitution has created a strong TBEV inhibitor, 7-deaza-2'-C-methyladenosine (EC_{50} of 1.1 μM), showing no cytotoxic effect on either PS or UKF-NB4 cells (Table 1). Based on these results, we further tested several heterobase-modified nucleosides in which hydrogen bond donors or acceptors were either

omitted or added, mainly at the heterobase 7-position (Fig. 1, structures 23–27). 7-Deazaadenosine (tubercidin) displayed a strong cytotoxicity on PS cell monolayers (CC_{50} of 2.1 μM) (Fig. 5, Table 1). As TBEV replication is dependent on cell proliferation, the antiviral effect of tubercidin and other cytotoxic compounds could not be assessed (Fig. 2). Similarly, 7-deaza-7-cyano- and 7-deaza-7-carbamoyl substituted derivatives of tubercidin (i.e., toyocamycin and sangivamycin) exerted demonstrable toxicity when dosed at a concentration of 50 μM (CC_{50} values of 0.1 and 0.8 μM , respectively) (Table 1). Ribavirin and 6-azauridine had no protective effects on the survival and growth of PS cells exposed to TBEV (Fig. 2).

3.5. Other nucleoside modifications

Neplanocin A and 3-deazaneplanocin A (Fig. 1, structures 28 and 29), in which the ribofuranose ring is replaced by the cyclopentenyl moiety, exhibited no antiviral activity *in vitro* using both Hypr and Neudoerfl strains and in both the PS and UKF-NB4 cell lines

($EC_{50} > 50 \mu\text{M}$) (Fig. 2). Moreover, neplanocin A exerted a detectable cytotoxic effect on compound-treated PS cells; Treatment the cell culture with compound concentration of $50 \mu\text{M}$ led to a reduction in the cell viability to 83.6%. Morphological changes observed on neplanocin-treated cultures (Fig. 5B) have been probably attributed to an alteration in cellular transmethylation mediated through an effect on S-adenosylhomocysteine hydrolase (Borchardt et al., 1984).

3.6. The kinetics of 2'-C-methylated nucleoside uptake

The kinetics of 2'-C-methylguanosine and 2'-C-methyluridine uptake were studied in UKF-NB4 cells using a rapid and sensitive LC-MS/MS based approach. The highest intracellular amounts of individual compounds were detected at the 2nd h after treatment (Fig. 6). Between posttreatment hours 4 and 8, the intracellular amount of 2'-C-methylated compounds markedly decreased as compared to the 2nd h of the experiment. This phenomenon was probably related to the activation of intracellular phosphorylation pathways and to the intensive conversion of intact nucleoside molecules to their corresponding triphosphate forms (Eldrup et al., 2004). A relatively high amount of intracellular 2'-C-methyluridine was detected in cell cultures treated with $50 \mu\text{M}$ of the compound at 4–8 h after treatment (Fig. 6D). This result is in agreement with a lower anti-TBEV activity of 2'-C-methyluridine (EC_{50} of $11.1 \mu\text{M}$) and could be explained by a reduced intracellular phosphorylation efficiency of the compound.

3.7. Intracellular metabolism of selected nucleosides in PS and UKF-NB4 cells

In order to explain the biological activity of the tested nucleoside analogues in terms of metabolic activation, we performed analysis of metabolic conversion of selected nucleosides to their active triphosphate forms using two distinct cell lines. Cellular

extracts from PS or UKF-NB4 cells were incubated with 2'-C-methylguanosine, 2'-O-methylcytidine, 4'-azidocytidine or RO-9187 ($100 \mu\text{M}$) for 0, 0.5, 2, 4, and 8 h and subsequently analyzed by HPLC.

In PS cells, nucleoside conversion to the corresponding triphosphates was observed in 2'-C-methylguanosine (at 4 and 8 h after treatment) and RO-9187 (at hour 8) (Supplementary Table 2). Triphosphate conversion of 4'-azidocytidine was not observed within 8 h interval. As expected, 2'-O-methylcytidine (showing no anti-TBEV effect) exerted no intracellular conversion to triphosphates in PS cells. No deamination/demethylation of the compounds was observed during the incubation for 8 h in PS cellular extract.

In UKF-NB4 cells, no detachable phosphorylation products were identified in all nucleosides tested (Supplementary Table 2). Our results indicate, that the depletion of 2'-O-methylcytidine, 4'-azidocytidine and RO-9187 in time could be a result of their extensive deamination. As absorption maxima of metabolic products of both azido-derivatives (236.7 nm) were distinct from that of uridine (262.5 nm), it can be expected that no cleavage of azido-group (and no conversion to uridine) occurs in UKF-NB4 cellular extracts. The absorption maximum of 2'-O-methylcytidine metabolic product (262.5 nm) indicates also possible demethylation processes resulting in the extensive conversion of the compound to uridine after the incubation (data not shown).

A detailed study of metabolic activation of TBEV inhibitors in both PS and UKF-NB4 cells goes beyond the scope of this report and will be a subject of a future article.

4. Discussion

Based on the high degree of homology between the TBEV and HCV genomes and similarities at the protein levels (Koonin and Dolja, 1993), we can expect that the mode of TBEV inhibition mediated by 2', 3' and 4'-modified nucleosides is similar to that of

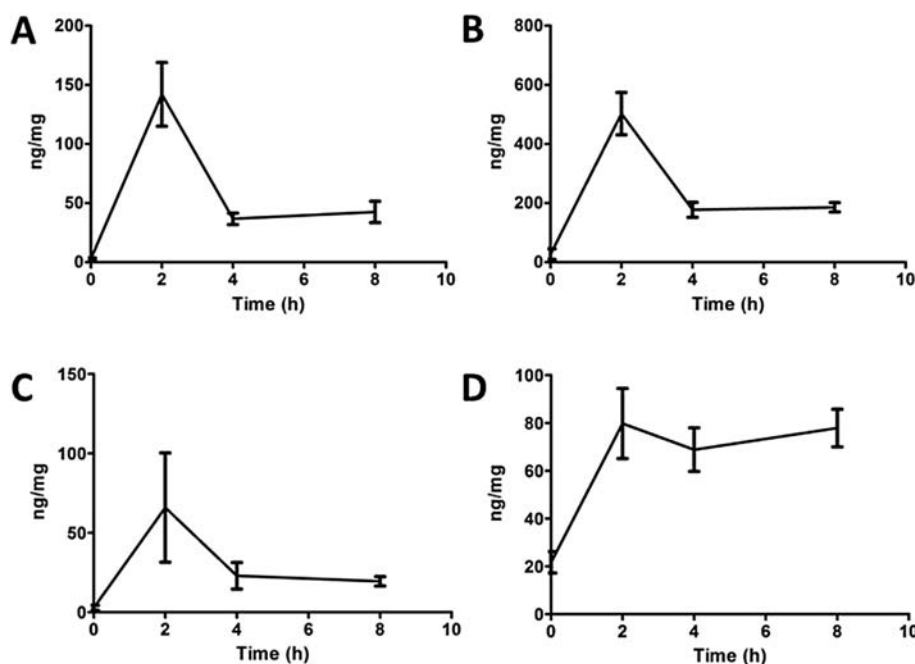


Fig. 6. The kinetics of 2'-C-methylated nucleoside uptake. The UKF-NB4 cells were grown for 48 h and subsequently exposed to 2'-C-methylguanosine at concentration of $10 \mu\text{M}$ (A) or $50 \mu\text{M}$ (B) or 2'-C-methyluridine at concentration of $10 \mu\text{M}$ (C) or $50 \mu\text{M}$ (D). After 0, 2, 4, and 8-h intervals the cells were harvested by scraping and used for quantitative determination of 2'-C-methylated nucleosides by LC-MS/MS. The intracellular amounts of the individual compounds are expressed in ng of compound per mg of cellular proteins. The mean values from three replicate wells are indicated, and the error bars indicate the standard errors of the mean.

HCV, for which the nucleoside activities and interactions with viral polymerase were studied in detail using *in vitro* (Carroll et al., 2003; Klumpp et al., 2006, 2008; Migliaccio et al., 2003; Olsen et al., 2004) and *in vivo* systems (Carroll et al. 2009, 2011). The interactions of three 2'-C-methylated nucleosides with the TBEV-polymerase active site were simulated using advanced computational methods (Eyer et al., 2015).

Evaluation of various modifications at the nucleoside 2'-position revealed, that the introduction of the 2'-C-methyl substituent to the nucleoside β -face resulted in a strong inhibition of TBEV replication *in vitro*. Based on the EC₅₀ values for individual 2'-C-methylated nucleosides tested (ranging from 1.1 to 11.1 μ M), it is obvious that their antiviral activities were slightly affected by the identity of the heterobase. Similarly, the heterobase type can influence the metabolic stability of the 2'-C-methylated nucleoside. Whereas 2'-C-methyladenosine was metabolized rapidly, which was manifested by a gradual disappearance of the compound's antiviral effect (Cristalli et al., 2001; Eyer et al., 2015), the other tested 2'-C-methylated derivatives were characterized by an increased metabolic stability *in vitro*. The cytotoxicity of the 2'-C-methylated nucleosides was observed to be none or negligible, except for 2'-C-methylcytidine (CC₅₀ of 50 μ M) (Eyer et al., 2015). In contrast, tubercidin, toyocamycin and sangivamycin, devoid of the 2'-C-methyl group, were observed to be highly cytotoxic for PS cells at submicromolar concentrations. The cytotoxicity of tubercidin was ascribed to its incorporation into cellular nucleic acids by cellular enzymes, whereas 2'-C-methyl substituted nucleosides were described as poor substrates for human DNA polymerases (Olsen et al., 2004). Taken together, the 2'-C-methyl substituent appeared to be an important structural element for a highly selective TBEV inhibition and a reduced cytotoxicity *in vitro*. It is likely that the 2'-C-methyl substituent does not adversely affect the binding of a nucleoside to the viral polymerase active site; this binding is probably made possible by the presence of some additional steric space in the vicinity of the 2'-carbon, allowing the polymerase active site to accommodate the 2'-C-methyl substituent. After incorporation, such a substituent is probably responsible for efficient termination of viral RNA chain elongation (Carroll et al., 2003).

Interestingly, no or negligible anti-TBEV activity was observed for 2'- α -fluoro-2'- β -methyl or 2'-O-methyl substituted nucleosides. We can speculate that the introduction of the fluoro moiety into the C2' position or the methyl moiety into the O2' position eliminates the 2'- α -hydroxy hydrogen bond donor/acceptor, which results in the complete abrogation of the nucleoside inhibitory activity. The ability of flaviviral polymerases to discriminate against nucleoside triphosphates modified at the 2'-position on the ribose α -face is probably related to the need of the polymerase to avoid the incorporation of 2'- α -deoxynucleoside monophosphates into the viral nascent RNA chain (Eldrup et al., 2004). In case of the NS5B polymerase of HCV, such discrimination against 2'- α -deoxynucleosides was described to be mediated by several conserved amino acid residues (most probably by Asp-225) in the polymerase active site, which are crucial for hydrogen bond formation with the 2'- α -hydroxy group (Bressanelli et al. 2002). Ineffectiveness of 2'- α -deoxynucleosides for TBEV inhibition was also demonstrated in our *in vitro* antiviral assays (data not shown). No anti-TBEV activity of 2'-O-methylcytidine could be also ascribed to its inefficient intracellular conversion to corresponding triphosphate and, moreover, to an extensive deamination/demethylation resulting in a conversion to uridine.

2'- α -Deoxy-2'- β -hydroxy-4'-azidocytidine (RO-9187, an arabino stereoisomer of 4'-azidocytidine) is a compound structurally related to 2'-deoxyribonucleosides, particularly due to the absence of the 2'- α -hydroxy substituent on the ribose ring. Moreover, RO-

9187, similarly to 2'-deoxyribonucleosides and other arabinonucleosides, was described to occupy preferentially the 2'-endo conformation, which is typical for the B-form DNA (Klumpp et al., 2008). This makes RO-9187 significantly different from nucleosides possessing the 2'- α -hydroxy substituent (e.g., natural ribonucleoside substrates or 2'-C-methyl substituted nucleosides), which are characterized by the 3'-endo conformation, typical for the A-form RNA (Eldrup et al., 2004; Klumpp et al., 2008). In sharp contrast to 2'-deoxyribonucleosides, which showed no activity against TBEV in PS cell cultures, RO-9187 was demonstrated to be the strongest TBEV inhibitor of the entire test series (EC₅₀ of 0.3 μ M). Based on this finding, we can assume that some additional hydrogen bonding interactions of the polymerase active site with both the 2'- β -hydroxy substituent and the 4'-azido substituent could compensate for the loss of 2'- α -hydroxy interaction, resulting

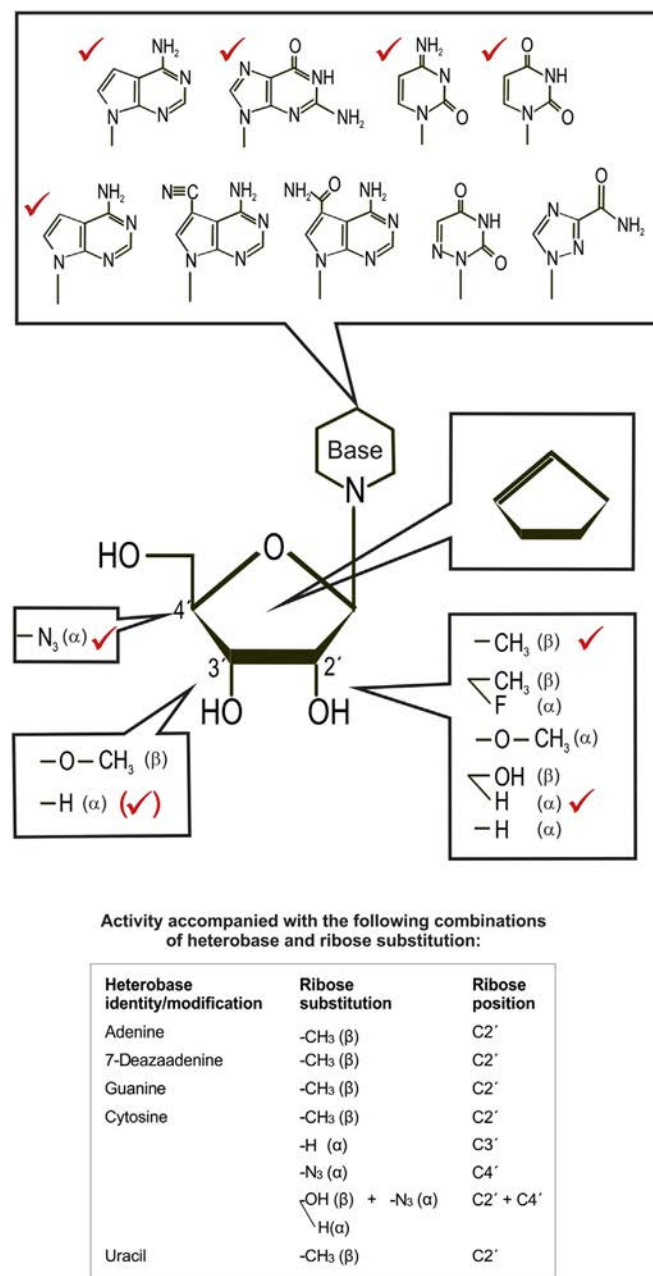


Fig. 7. Structure-activity relationships for substitutions at the 2', 3', and 4' nucleoside positions and for purine/pyrimidine heterobase identity/modifications.

in the strong and selective anti-TBEV activity of RO-9187 (Klumpp et al., 2008). Anti-TBEV activity of RO-9187 was strongly cell line-dependent and was observed only in TBEV-infected PS cell cultures. The same phenomenon was demonstrated also in 4'-azido-cytidine and, surprisingly, in 2'-C-methylguanosine, suggesting possible metabolic differences between PS and human neuroblastoma cell lines. In PS cells, phosphorylation processes were detected and no deamination/demethylation was observed. This is in a sharp contrast with UKF-NB4 cells, where no conversion to triphosphate forms was observed, and extensive deamination or demethylation of the compounds was indicated in this cell line.

3'-Deoxyadenosine, 3'-deoxyguanosine and all tested 3'-O-methylated nucleosides caused no significant inhibition of TBEV replication *in vitro*. Thus, the observed inactivity of 3'-modified nucleosides might be interpreted as the requirement of the TBEV NS5 polymerase active site for a 3'-hydroxyl group to form the appropriate hydrogen bonding interaction with the nucleoside triphosphate molecule. However, 3'-deoxycytidine exerted a moderate anti-TBEV effect (EC₅₀ of 75.9 μM) despite the lack of the 3'-hydroxyl moiety, which indicated that TBEV NS5 polymerase is probably able to bind 3'-deoxynucleoside triphosphates and that the observed inactivity of 3'-modified nucleosides could instead be related to inefficient cellular uptake and metabolism to convert the nucleoside molecule into the corresponding triphosphate form (Eldrup et al., 2004).

In conclusion, our data demonstrate a relatively stringent structure-activity relationship for modifications at the 2', 3', and 4' nucleoside positions (Fig. 7). Of all structural modifications tested, only the methylation of the C2' nucleoside position or the azido modification of the C4' position resulted in an inhibition of TBEV replication and a low cytotoxicity *in vitro*. Other structural modifications, such as introduction of 2'-α-fluoro-2'-β-methyl moiety into the C2' position or various substitutions of the O2' and O3' positions, led to a complete loss of anti-TBEV activity. On the other hand, some structure-activity relationship flexibility was found for change of the purine/pyrimidine heterobase identity; replacement of adenine to guanine, cytosine or uracil appeared to have only a limited effect on the antiviral activity and cytotoxicity of the nucleoside analogue. However, structural modifications of the hydrogen-bonding capacity of the heterobase were strongly accompanied by either an inefficacy against TBEV or a highly increased cytotoxicity. Finally, we identified, that some nucleosides exhibit cell-type dependent anti-TBEV effect, which can be explained by metabolic differences in diverse cell populations. Our results indicate that C2' methylated and C4' azido substituted pharmacophores, even if they are not clinically effective, may represent useful research tools or starting points for antiviral drug development efforts against TBEV infection.

Acknowledgements

The authors are greatly indebted to Dr. Ivana Huvarová for excellent technical assistance and to Dr. Vladimír Babák for computational data processing. This study was supported by Czech Science Foundation project GA14-29256S and 16-20054S, Ministry of Health of the Czech Republic (grant No. 16–34238A), and by project LO1218 with financial support from the Ministry of Education, Youth and Sports of the Czech Republic under the NPU I program. We acknowledge a grant for the development of research organization (RVO: 61388963).

Appendix A. Supplementary data

Supplementary data related to this article can be found at <http://dx.doi.org/10.1016/j.antiviral.2016.07.018>.

References

- Baier, A., 2011. Flaviviral infections and potential targets for antiviral therapy. In: Ruzek, D. (Ed.), *Flavivirus Encephalitis*. InTech, Rijeka, Croatia.
- Borchardt, R.T., Keller, B.T., Patelthombre, U., 1984. Neplanocin-a – a potent inhibitor of S-Adenosylhomocysteine hydrolase and of vaccinia virus multiplication in mouse L929 cells. *J. Biol. Chem.* 259, 4353–4358.
- Bressanelli, S., Tomei, L., Rey, F.A., De Francesco, R., 2002. Structural analysis of the hepatitis C virus RNA polymerase in complex with Ribonucleotides. *J. Virol.* 76, 3482–3492. <http://dx.doi.org/10.1128/JVI.76.7.3482-3492.2002>.
- Carroll, S.S., Koeplinger, K., Vavrek, M., Zhang, N.R., Handt, L., MacCoss, M., Olsen, D.B., Reddy, K.R., Sun, Z.L., van Poelje, P.D., Fujitaki, J.M., Boyer, S.H., Linemeyer, D.L., Hecker, S.J., Erion, M.D., 2011. Antiviral efficacy upon administration of a HepDirect prodrug of 2'-C-Methylcytidine to hepatitis C virus-infected chimpanzees. *Antimicrob. Agents Chemother.* 55, 3854–3860. <http://dx.doi.org/10.1128/AAC.01152-10>.
- Carroll, S.S., Tomassini, J.E., Bosserman, M., Getty, K., Stahlhut, M.W., Eldrup, A.B., Bhat, B., Hall, D., Simcoe, A.L., LaFemina, R., Rutkowski, C.A., Wolanski, B., Yang, Z.C., Migliaccio, G., De Francesco, R., Kuo, L.C., MacCoss, M., Olsen, D.B., 2003. Inhibition of hepatitis C virus RNA replication by 2'-modified nucleoside analogs. *J. Biol. Chem.* 278, 11979–11984. <http://dx.doi.org/10.1074/jbc.M210914200>.
- Carroll, S.S., Ludmerer, S., Handt, L., Koeplinger, K., Zhang, R.N., Graham, D., Davies, M.E., MacCoss, M., Hazuda, D., Olsen, B.D., 2009. Robust antiviral efficacy upon administration of a nucleoside analog to hepatitis C virus-infected chimpanzees. *Antimicrob. Agents Chemother.* 53, 926–934. <http://dx.doi.org/10.1128/AAC.01032-08>.
- Cristalli, G., Costanzi, S., Lambertucci, C., Lupidi, G., Vittori, S., Volpini, R., Camaioni, E., 2001. Adenosine deaminase: functional implications and different classes of inhibitors. *Med. Res. Rev.* 21, 105–128. DOI: 10.1002/1098-1128(200103)21:2<105::AID-MED1002>3.0.CO;2-U.
- De Clercq, E., 2004. Antivirals and antiviral strategies. *Nat. Rev. Microbiol.* 2, 704–720. <http://dx.doi.org/10.1038/nrmicro975>.
- De Clercq, E., 2011. A 40-year journey in search of selective antiviral chemotherapy. *Annu. Rev. Pharmacol. Toxicol.* 51, 1–24. <http://dx.doi.org/10.1146/annurev-pharmtox-010510-100228>.
- De Clercq, E., Neyts, J., 2009. Antiviral agents acting as DNA or RNA chain terminators. In: *Handbook of Experimental Pharmacology*, 189, pp. 53–84. http://dx.doi.org/10.1007/978-3-540-79086-0_3.
- De Madrid, A.T., Porterfield, J.S., 1969. A simple micro-culture method for study of group B arboviruses. *Bull. World Health Organ.* 40, 113–121.
- Dumpis, U., Crook, D., Oksi, J., 1999. Tick-borne encephalitis. *Clin. Infect. Dis.* 28, 882–890. <http://dx.doi.org/10.1086/515195>.
- Eldrup, A.B., Allerson, C.R., Bennett, C.F., Bera, S., Bhat, B., Bhat, N., Bosserman, M.R., Brooks, J., Burlein, C., Carroll, S.S., Cook, P.D., Getty, K.L., MacCoss, M., McMasters, D.R., Olsen, D.B., Prakash, T.P., Prhavc, M., Song, Q.L., Tomassini, J.E., Xia, J., 2004. Structure-activity relationship of purine ribonucleosides for inhibition of hepatitis C virus RNA-dependent RNA polymerase. *J. Med. Chem.* 47, 2283–2295. <http://dx.doi.org/10.1021/jm030424e>.
- Eyer, L., Valdes, J.J., Gil, V.A., Nencka, R., Hrebabecky, H., Sala, M., Salat, J., Cerny, J., Palus, M., De Clercq, E., Ruzek, D., 2015. Nucleoside inhibitors of tick-borne encephalitis virus. *Antimicrob. Agents Chemother.* 59, 5483–5493. <http://dx.doi.org/10.1128/AAC.00807-15>.
- Eyer, L., Nencka, R., Huvarová, I., Palus, M., Joao Alves, M., Gould, E.A., De Clercq, E., Ruzek, D., 2016. Nucleoside inhibitors of Zika virus. *J. Infect. Dis.* <http://dx.doi.org/10.1093/infdis/jiw226> [Epub ahead of print].
- Flint, M., McMullan, L.K., Dodd, K.A., Bird, B.H., Khristova, M.L., Nichol, S.T., Spiropoulou, C.F., 2014. Inhibitors of the tick-borne, hemorrhagic fever-associated flaviviruses. *Antimicrob. Agents Chemother.* 58, 3206–3216. <http://dx.doi.org/10.1128/AAC.02393-14>.
- Heinz, F.X., Mandl, C.W., 1993. The molecular-biology of tick-borne encephalitis-virus. *Apmis* 101, 735–745. <http://dx.doi.org/10.1111/j.1699-0463.1993.tb00174.x>.
- Heinz, F.X., Stiasny, K., Holzmann, H., Grgic-Vitek, M., Kriz, B., Essl, A., Kundi, M., 2013. Vaccination and tick-borne encephalitis, central Europe. *Emerg. Infect. Dis.* 19, 69–76. <http://dx.doi.org/10.3201/eid1901.120458>.
- Julander, J.G., Jha, A.K., Choi, J.A., Jung, K.H., Smeed, D.F., Morrey, J.D., Chu, C.K., 2010. Efficacy of 2'-C-methylcytidine against yellow fever virus in cell culture and in a hamster model. *Antivir. Res.* 86, 261–267. <http://dx.doi.org/10.1016/j.antiviral.2010.03.004>.
- Klumpp, K., Leveque, V., Le Pogam, S., Ma, H., Jiang, W.R., Kang, H.S., Grancyome, C., Singer, M., Laxton, C., Hang, J.Q., Sarma, K., Smith, D.B., Heindl, D., Hobbs, C.J., Merrett, J.H., Symons, J., Cammack, N., Martin, J.A., Devos, R., Najera, I., 2006. The novel nucleoside analog R1479 (4'-azido-cytidine) is a potent inhibitor of NS5B-dependent RNA synthesis and hepatitis C virus replication in cell culture. *J. Biol. Chem.* 281, 3793–3799. <http://dx.doi.org/10.1074/jbc.M510195200>.
- Klumpp, K., Kalayanov, G., Ma, H., Le Pogam, S., Leveque, V., Jiang, W.R., Inocencio, N., De Witte, A., Rajyaguru, S., Tai, E., Chanda, S., Irwin, M.R., Sund, C., Winquist, A., Maltseva, T., Eriksson, S., Usova, E., Smith, M., Alker, A., Najera, I., Cammack, N., Martin, J.A., Johansson, N.G., Smith, D.B., 2008. 2'-deoxy-4'-azido nucleoside analogs are highly potent inhibitors of hepatitis C virus replication despite the lack of 2'-alpha-hydroxyl groups. *J. Biol. Chem.* 283, 2167–2175. <http://dx.doi.org/10.1074/jbc.M708929200>.
- Koonin, E.V., Dolja, V.V., 1993. Evolution and taxonomy of positive-strand rna

- viruses – implications of comparative-analysis of amino-acid-sequences. *Crit. Rev. Biochem. Mol. Biol.* 28, 375–430. <http://dx.doi.org/10.3109/10409239309078440>.
- Kozuch, O., Mayer, V., 1975. Pig kidney epithelial (ps) cells – perfect tool for study of flavi-viruses and some other arboviruses. *Acta Virol.* 19, 498.
- Lee, J.C., Tseng, C.K., Wu, Y.H., Kaushik-Basu, N., Lin, C.K., Chen, W.C., Wu, H.N., 2015. Characterization of the activity of 2'-C-methylcytidine against dengue virus replication. *Antivir. Res.* 116, 1–9. <http://dx.doi.org/10.1016/j.antiviral.2015.01.002>.
- Ma, H., Jiang, W.R., Robledo, N., Leveque, V., Ali, S., Lara-Jaime, T., Masjedizadeh, M., Smith, D.B., Cammack, N., Klumpp, K., Symons, J., 2007. Characterization of the metabolic activation of hepatitis C virus nucleoside inhibitor beta-D-2'-Deoxy-2'-fluoro-2'-C-methylcytidine (PSI-6130) and identification of a novel active 5'-triphosphate species. *J. Biol. Chem.* 282, 29812–29820. <http://dx.doi.org/10.1074/jbc.M705274200>.
- Migliaccio, G., Tomassini, J.E., Carroll, S.S., Tomei, L., Altamura, S., Bhat, B., Bartholomew, L., Bosserman, M.R., Ceccacci, A., Colwell, L.F., Cortese, R., De Francesco, R., Eldrup, A.B., Getty, K.L., Hou, X.S., LaFemina, R.L., Ludmerer, S.W., MacCoss, M., McMasters, D.R., Stahlhut, M.W., Olsen, D.B., Hazuda, D.J., Flores, O.A., 2003. Characterization of resistance to non-obligate chain-terminating ribonucleoside analogs that inhibit hepatitis C virus replication in vitro. *J. Biol. Chem.* 278, 49164–49170. <http://dx.doi.org/10.1074/jbc.M305041200>.
- Olsen, D.B., Eldrup, A.B., Bartholomew, L., Bhat, B., Bosserman, M.R., Ceccacci, A., Colwell, L.F., Fay, J.F., Flores, O.A., Getty, K.L., Grobler, J.A., LaFemina, R.L., Markel, E.J., Migliaccio, G., Prhvac, M., Stahlhut, M.W., Tomassini, J.E., MacCoss, M., Hazuda, D.J., Carroll, S.S., 2004. A 7-deaza-adenosine analog is a potent and selective inhibitor of hepatitis C virus replication with excellent pharmacokinetic properties. *Antimicrob. Agents Chemother.* 48, 3944–3953. <http://dx.doi.org/10.1128/AAC.48.10.3944-3953.2004>.
- Puig-Basagoiti, F., Tilgner, M., Forshey, B.M., Philpott, S.M., Espina, N.G., Wentworth, D.E., Goebel, S.J., Masters, P.S., Falgout, B., Ren, P., Ferguson, D.M., Shi, P.Y., 2006. Triaryl pyrazoline compound inhibits flavivirus RNA replication. *Antimicrob. Agents Chemother.* 50, 1320–1329. <http://dx.doi.org/10.1128/AAC.50.4.1320-1329.2006>.
- Ruzek, D., Dobler, G., Donoso Mantke, O., 2010. Tick-borne encephalitis: pathogenesis and clinical implications. *Travel Med. Infect. Dis.* 8, 223–232. <http://dx.doi.org/10.1016/j.tmaid.2010.06.004>.
- Ruzek, D., Vancova, M., Tesarova, M., Ahantari, A., Kopecky, J., Grubhoffer, L., 2009. Morphological changes in human neural cells following tick-borne encephalitis virus infection. *J. General Virol.* 90, 1649–1658. <http://dx.doi.org/10.1099/vir.0.010058-0>.
- Sofia, M.J., Chang, W., Furman, P.A., Mosley, R.T., Ross, B.S., 2012. Nucleoside, nucleotide, and non-nucleoside inhibitors of hepatitis C virus NS5B RNA-dependent RNA-polymerase. *J. Med. Chem.* 55, 2481–2531. <http://dx.doi.org/10.1021/jm201384j>.
- Tomassini, J.E., Getty, K., Stahlhut, M.W., Shim, S., Bhat, B., Eldrup, A.B., Prakash, T.P., Carroll, S.S., Flores, O., MacCoss, M., McMasters, D.R., Migliaccio, G., Olsen, D.B., 2005. Inhibitory effect of 2'-substituted nucleosides on hepatitis C virus replication correlates with metabolic properties in replicon cells. *Antimicrob. Agents Chemother.* 49, 2050–2058. <http://dx.doi.org/10.1128/AAC.49.5.2050-2058.2005>.
- Zavadská, D., Anca, I., Andre, F., Bakir, M., Chlibek, R., Cizman, M., Ivaskeviciene, I., Mangarov, A., Meszner, Z., Pokorn, M., Prymula, R., Richter, D., Salman, N., Simurka, P., Tamm, E., Tesovic, G., Urbancikova, I., Usonis, V., 2013. Recommendations for tick-borne encephalitis vaccination from the central european vaccination awareness group (CEVAG). *Hum. Vaccines Immunother.* 9, 362–374. <http://dx.doi.org/10.4161/hv.22766>.
- Zouharova, D., Lipenska, I., Fojtikova, M., Kulich, P., Neca, J., Slany, M., Kovarcik, K., Turanek-Knotigova, P., Hubatka, F., Celechovska, H., Masek, J., Koudelka, S., Prochazka, L., Eyer, L., Plockova, J., Bartheldyova, E., Miller, A.D., Ruzek, D., Raska, M., Janeba, Z., Turanek, J., 2016. Antiviral activities of 2,6-diaminopurine-based acyclic nucleoside phosphonates against herpesviruses: *In vitro* study results with pseudorabies virus (PrV, SuHV-1). *Veterinary Microbiol.* 184, 84–93. <http://dx.doi.org/10.1016/j.vetmic.2016.01.010>.

Nucleoside Inhibitors of Zika Virus

Luděk Eyer,¹ Radim Nencka,² Ivana Huvarová,¹ Martin Palus,^{1,3,4} Maria Joao Alves,⁵ Ernest A. Gould,⁶ Erik De Clercq,⁷ and Daniel Růžek^{1,3,4}

¹Department of Virology, Veterinary Research Institute, Brno, ²Institute of Organic Chemistry and Biochemistry, Czech Academy of Sciences, Prague, ³Institute of Parasitology, Biology Center of the Czech Academy of Sciences, and ⁴Faculty of Science, University of South Bohemia, České Budějovice, Czech Republic; ⁵National Institute of Health Dr Ricardo Jorge–CEVDI/INSA, Águas de Moura, Portugal; ⁶Aix Marseille Université, IRD French Institute of Research for Development, EHESP French School of Public Health, EPV UMR_D 190 Emergence des Pathologies Virales, France; and ⁷Rega Institute for Medical Research, KU Leuven, Belgium

There is growing evidence that Zika virus (ZIKV) can cause devastating infant brain defects and other neurological disorders in humans. However, no specific antiviral therapy is available at present. We tested a series of 2'-C- or 2'-O-methyl-substituted nucleosides, 2'-C-fluoro-2'-C-methyl-substituted nucleosides, 3'-O-methyl-substituted nucleosides, 3'-deoxynucleosides, derivatives with 4'-C-azido substitution, heterobase-modified nucleosides, and neplanocins for their ability to inhibit ZIKV replication in cell culture. Antiviral activity was identified when 2'-C-methylated nucleosides were tested, suggesting that these compounds might represent promising lead candidates for further development of specific antivirals against ZIKV.

Keywords. Zika virus; flavivirus; nucleoside analogue; antiviral; therapy.

On 1 February 2016, the World Health Organization declared a public health emergency of international concern regarding neurological disorders associated with the rapid emergence of Zika virus (ZIKV) in Oceania and the Americas [1]. Previously, ZIKV was a relatively neglected mosquito-borne arbovirus in the genus *Flavivirus*, family *Flaviviridae*. ZIKV infections have been known in Africa and Asia since the 1940s. During the last years, the virus caused several outbreaks of infection across Oceania [2]. In May 2015, a ZIKV outbreak was first reported in Brazil, and within months most countries in Latin America and the Caribbean had reported local transmission of the virus [1, 3]. Until recently, ZIKV was associated with benign infection in humans, with common symptoms that include fever, rash, joint pain, and conjunctivitis. The illness was usually mild, with symptoms lasting for several days. However, there is growing evidence in Oceania and the Americas that ZIKV can cause devastating brain birth defects, most prominently

microcephaly [4], and neurological disorders in adults, including Guillain-Barré syndrome, meningoencephalitis [5], and myelitis [6]. At present, neither vaccination nor specific antiviral therapies are available to prevent or treat ZIKV infections, making a search for effective viral inhibitors an international research priority.

Nucleoside analogues are an important class of antiviral agents now commonly used as therapeutics for human viral infections, including AIDS and hepatitis B virus, cytomegalovirus, and herpes simplex virus infections [7]. These agents are generally safe and well tolerated since they target viral but not cellular polymerases and cause premature termination of viral nucleic acid synthesis [7]. In the present study, we evaluated 2'-C- and 2'-O-methyl-substituted nucleosides, 2'-C-fluoro-2'-C-methyl-substituted nucleosides, 3'-O-methyl-substituted nucleosides, 3'-deoxynucleosides, derivatives with a 4'-C-azido substitution, heterobase-modified nucleosides, and neplanocins for their ability to inhibit ZIKV replication in cell culture, with the objective of identifying promising lead candidates for further development of specific antivirals against ZIKV.

METHODS

Vero cells (ATCC CCL-81, African Green Monkey, adult kidney, epithelial) were used for determining ZIKV multiplication, for antiviral assays, and for conducting plaque assays. The cells were cultured at 37°C in 5% CO₂ in Dulbecco's modified Eagle's medium supplemented with 10% fetal bovine serum and a 1% mixture of antibiotics (Sigma-Aldrich, Prague, Czech Republic).

ZIKV strain MR766 (prototype strain, isolated from blood from experimental forest sentinel rhesus monkey, Uganda, 1947; GenBank accession no. AY632535) from the collection of the National Institute of Health Dr Ricardo Jorge–CEVDI/INSA (Águas de Moura, Portugal) and from the European Virus Archive was used for evaluation of the antiviral activity of the test compounds. The virus was passaged >100 times in suckling mice and/or in Vero cells prior to this study.

The following nucleoside analogues were purchased: 2'-C-methyl-, 2'-O-methyl-, and 3'-O-methyl-substituted nucleosides, 3'-deoxynucleosides, sofosbuvir, and 6-azauridine from Carbosynth (Compton, United Kingdom); 4'-azidocytidine, balapiravir, and RO-9187 from Medchemexpress (Stockholm, Sweden); neplanocin A from Cayman Chemical (Ann Arbor, Michigan); 3-deazaneplanocin A from Selleckchem (Munich, Germany); mericitabine from ChemScene (Monmouth Junction, New Jersey); PSI-6206 from ApexBio (Boston, Massachusetts); and tubercidin, toyocamycin, sangivamycin, ribavirin, and 2'-deoxynucleosides from Sigma-Aldrich (Prague, Czech Republic); rigid amphipathic. The test compounds were solubilized

Received 7 April 2016; accepted 24 May 2016; published online 27 May 2016.

Correspondence: D. Růžek, Veterinary Research Institute, Hudcova 70, Brno CZ-62100, Czech Republic (ruzekd@paru.cas.cz).

The Journal of Infectious Diseases® 2016;214:707–11

© The Author 2016. Published by Oxford University Press for the Infectious Diseases Society of America. All rights reserved. For permissions, e-mail journals.permissions@oup.com. DOI: 10.1093/infdis/jiw226

in 100% dimethyl sulfoxide (DMSO) to yield 10 mM stock solutions.

A viral infectivity inhibition assay was performed to measure the antiviral efficacy of nucleoside analogues in cell culture. Vero cells were seeded in 96-well plates (approximately 2×10^4 cells/well) and incubated without the presence of the drug for 24 hours, to form a confluent monolayer. Following incubation, the medium was aspirated from the wells and replaced with 200 μ L of fresh medium containing 50 μ M of the test compound (3 wells/compound), which was inoculated with ZIKV at a multiplicity of infection (MOI) of 0.1 plaque-forming units (PFU) at the same time as the test compound were added. As a negative control, DMSO was added to virus- and mock-infected cells at a final concentration of 0.5% (v/v). Culture medium was monitored for 5 days after infection to yield a 70%–90% cytopathic effect (CPE) in virus control wells, using the Olympus BX-5 microscope equipped with an Olympus DP-70 CCD camera. To quantify the CPE, culture media were collected at the end of the experiment (ie, day 5 after infection), and cell death was determined using the CytoTox 96 Non-Radioactive Cytotoxicity Assay (Promega; Madison, Wisconsin) according to the manufacturer's instructions as described previously [8]. Viral titers were determined by plaque assay and expressed as PFU/milliliter [9]. For dose-response studies, Vero cell monolayers were cultured with 200 μ L of medium containing the test compounds over the concentration range of 0–100 μ M and ZIKV at a MOI of 0.1. Drug addition and virus infection was done at the same time. The medium was collected from the wells at 2 and 3 days after infection, and the viral titers were determined by plaque assay and used to construct ZIKV dose-response curves. The dose-response curves on day 2 after infection were used to estimate the 50% effective concentration (EC_{50}). To measure the compound-induced inhibition of viral surface antigen expression, a cell-based flavivirus immunostaining assay was performed as previously described [8]. For determination of nucleoside analogue cytotoxicity, a colorimetric assay using Dojindo's highly water-soluble tetrazolium salt (Cell Counting Kit-8, Dojindo Molecular Technologies; Rockville, Maryland) and the CytoTox 96 Non-Radioactive Cytotoxicity Assay (Promega; Madison, Wisconsin) were used. The concentration of compound that reduced cell viability by 50% was considered as the 50% cytotoxic concentration (CC_{50}).

RESULTS

A series of 29 nucleoside analogues (Supplementary Figure 1) was tested at a concentration of 50 μ M for their ability to inhibit CPE mediated by ZIKV infection on Vero cells. Inhibition of ZIKV-induced CPE was monitored by light microscopy from days 1 to 5 after infection and quantified at the end of the experiment, using the colorimetric cell death in an in vitro assay. Five of the nucleoside analogues, 7-deaza-2'-C-methyladenosine (7-deaza-2'-CMA), 2'-C-methyladenosine (2'-CMA), 2'-

C-methylcytidine (2'-CMC), 2'-C-methylguanosine (2'-CMG), and 2'-C-methyluridine (2'-CMU), were found to inhibit ZIKV-mediated CPE in cell culture at a concentration of 50 μ M and to reduce significantly the cell death ratio in the test wells when compared with mock-treated ZIKV-infected cells ($P < .05$, by a 2-tailed Student *t* test). All other compounds had no or little effect on ZIKV-induced CPE and cell death. Tubercidin, toyocamycin, and sangivamycin were found to be cytotoxic, causing cell death in all cells at micromolar concentrations. On the basis of these preliminary results, nucleosides with a methyl moiety at the 2'-C position of the ribose ring (7-deaza-2'-CMA, 2'-CMA, 2'-CMC, 2'-CMG, and 2'-CMU) were selected for further testing.

2'-C-methylated derivatives reduced the viral titer in a dose-dependent manner (mean EC_{50} [\pm SD]) of 5.26 ± 0.12 μ M for 2'-CMA, 8.92 ± 3.32 μ M for 7-deaza-2'-CMA, 22.25 ± 0.03 μ M for 2'-CMG, 10.51 ± 0.02 μ M for 2'-CMC, and 45.45 ± 0.64 μ M for 2'-CMU; Figure 1A and Table 1). Dose-response curves for the 2'-C-methylated nucleosides were characterized by a typical sigmoidal shape with relatively steep slopes both on days 2 and 3 after infection (Supplementary Figure 2). Interestingly, 2'-CMU exhibited a relatively weak anti-ZIKV effect, treatment with 100 μ M of the compound reduced virus titers 10^2 -fold as compared to a mock-treated culture. The anti-ZIKV activity of 2'-C-methylated nucleosides was further confirmed by a cell-based flavivirus immunostaining assay. 2'-C-methylated nucleosides exhibited a dose-dependent inhibition of the expression of ZIKV surface E antigen in Vero cells at day 2 after infection (Figure 1C). A strong inhibition of ZIKV antigen expression was observed in 2'-CMA, 7-deaza-2'-CMA, and 2'-CMC as compared to 2'-CMG and 2'-CMU, for which relatively high EC_{50} values were calculated.

The cytotoxicity of 2'-C-methylated nucleosides was assessed in Vero cells. Except for 2'-CMC, which exerted a weak cytotoxic effect on Vero cells (treatment of the cell culture at a compound concentration of 100 μ M led to a reduction in cell viability to 69.3%), all 2'-C-methylated nucleosides tested showed no cytotoxic effects at the highest tested concentration of 100 μ M with no detectable effect on cell proliferation (Table 1 and Figure 1B).

DISCUSSION

ZIKV, a previously neglected mosquito-borne virus, is prompting worldwide concern because of its alarming connection to a neurological birth disorder. In most cases, ZIKV causes a benign disease, but in some patients the infection can manifest as myelitis or meningoencephalitis, or it can trigger Guillain-Barré syndrome, a severe neurological disorder characterized by progressive muscle weakness that can result in respiratory failure [1, 3–6]. No effective therapy for ZIKV infection is available at present; therefore, research on possible antiviral compounds active against ZIKV has become an international priority. Because human cells lack RNA-dependent RNA polymerase (RdRp), this

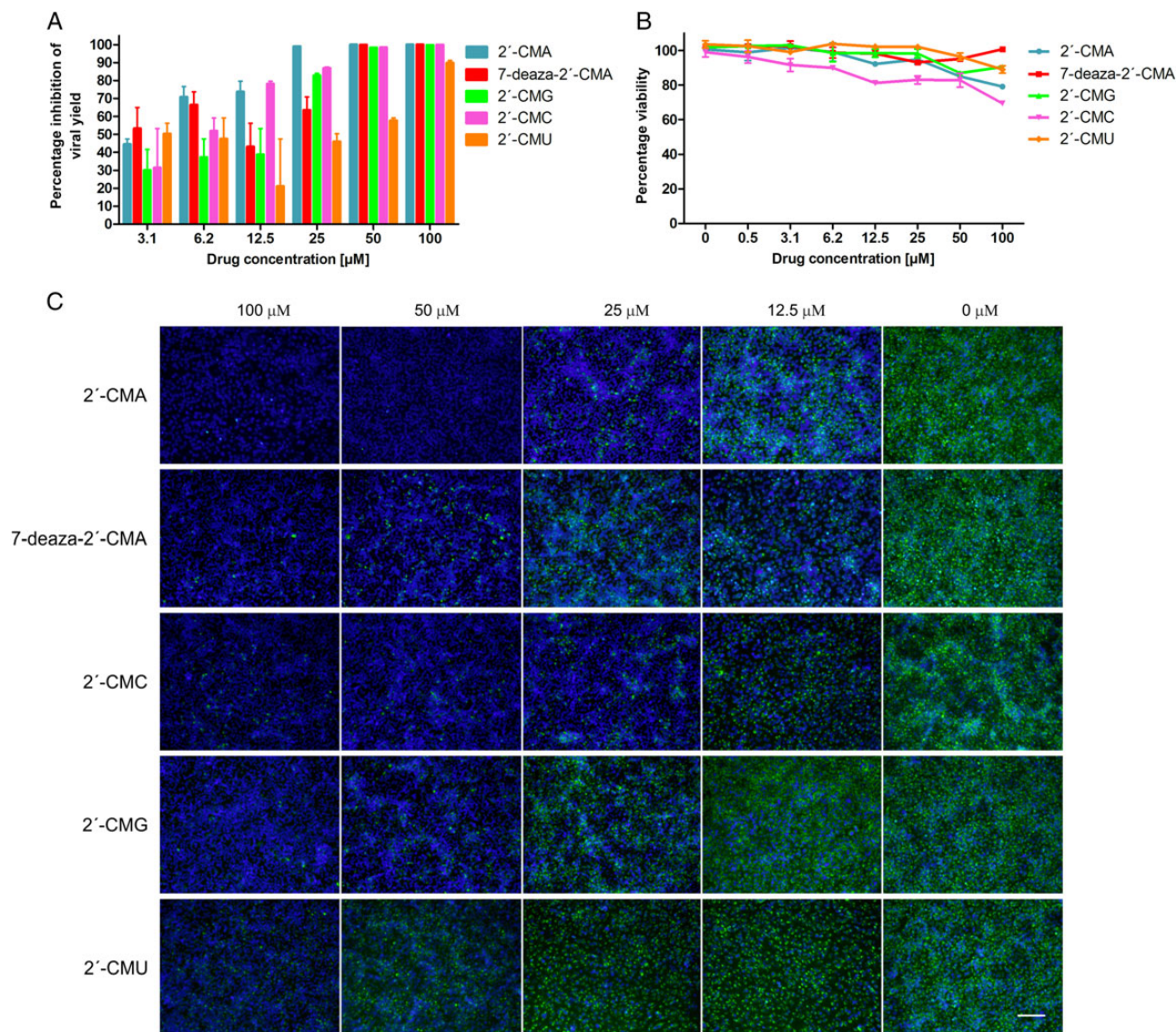


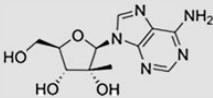
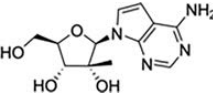
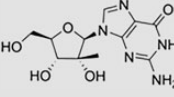
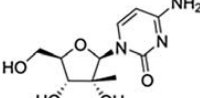
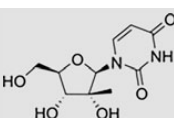
Figure 1. A, Dose-dependent inhibition of Zika virus (ZIKV) replication by 2'-C-methylated nucleosides in Vero cells. Vero cells were treated with different concentrations of 2'-C-methylated nucleosides and at the same time infected with ZIKV. Culture supernatants were collected at 48 hours after infection and analyzed for ZIKV infectivity by plaque assay. B, Viability of Vero cells treated by 2'-C-methylated nucleosides at a range of concentrations of 0–100 μM. Vero cells were exposed to the tested compounds for 72 hours. Viability was measured by a colorimetric assay, using Dojindo's highly water-soluble tetrazolium salt test (triplicate setting) and confirmed by optical microscopy. C, Inhibition of ZIKV antigen expression by nucleoside inhibitors. ZIKV-infected Vero cells were fixed on slides at 48 hours after infection and stained with flavivirus-specific antibody labeled with FITC (green) and counterstained with DAPI (blue). Scale bar, 50 μm.

class of enzymes appears to be one of the most promising targets for antivirals against flaviviruses that use RdRp for replication. Nucleoside analogs can target viral RdRp to terminate viral RNA replication after incorporation into the viral nascent RNA chain [10–12]. Here, we analyzed a library of nucleoside analogues for their *in vitro* activity against ZIKV.

Evaluation of various modifications at the nucleoside 2'-position revealed that the introduction of the 2'-C-methyl substituent to the nucleoside β-face resulted in inhibition of ZIKV replication *in vitro*. Different EC₅₀ values for individual 2'-C-methylated nucleosides (ranging from 5.26 to 45.45 μM)

indicate that their antiviral activities were substantially affected also by the identity of the heterocyclic base moiety. Introduction of guanine or especially uridine into the nucleoside molecule considerably reduced the anti-ZIKV activity *in vitro*. The cytotoxicity of the 2'-C-methylated nucleosides was observed to be either zero or negligible, except for 2'-CMC. The cytotoxicity of the studied compounds was assessed also in human neuroblastoma cells UKF-NB-4 (data not shown) and in porcine kidney cells (PS) [8] with results comparable to those for Vero cells. This is in a sharp contrast with high (submicromolar) cytotoxicity of tubercidin, toyocamycin, and sangivamycin, chemically

Table 1. ZIKV Inhibition and Cytotoxicity Characteristics of Selected Nucleoside Analogues

Compound	Structure	EC ₅₀ , μM, Mean ± SD ^{a,b}	Apparent EC ₅₀ , μM, Mean ± SD ^{a,c}	CC ₅₀ , μM ^a	SI ^d
2'-C-methyladenosine		5.26 ± 0.12	26.41 ± 1.14	>100 ^f	>19.01
7-deaza-2'-C-methyladenosine		8.92 ± 3.32	42.87 ± 1.88	>100	>11.21
2'-C-methylguanosine		22.25 ± 0.03	71.23 ± 4.11	>100	>4.49
2'-C-methylcytidine		10.51 ± 0.02	61.93 ± 3.76	>100 ^g	>9.51
2'-C-methyluridine		45.45 ± 0.64	>100 ^e	>100	>2.20

Abbreviations: CC₅₀, 50% cytotoxic concentration; EC₅₀, 50% effective concentration; SD, standard deviation; ZIKV, Zika virus.

^a Determined from 3 independent experiments.

^b Calculated as a 50% reduction of virus titers, using the Reed-Muench method.

^c Calculated as a point of inflection from dose-response curves, using log-transformed viral titers.

^d The selectivity index (SI) is calculated as CC₅₀/EC₅₀.

^e Treatment with 100 μM of 2'-CMU reduced virus titers 10²-fold compared to a mock-treated culture.

^f Treatment of cell culture with 2'-CMA at a concentration of 100 μM led to a reduction in cell viability to 79.1%.

^g Treatment of cell culture with 2'-CMC at concentration of 100 μM led to a reduction in cell viability to 69.3%.

related structures devoid of the 2'-C-methyl group. Taken together, the 2'-C-methyl substituent appeared to be an important structural element for highly selective ZIKV inhibition and reduced cytotoxicity. We can speculate that the 2'-C-methyl substituent does not prevent binding to the ZIKV RdRp active site and allows the viral RNA chain termination. During the peer review of this manuscript, another group published further evidence that 7-deaza-2'-CMA exhibits anti-ZIKV activity [13].

Interestingly, no or negligible anti-ZIKV activity was observed for 2'-α-fluoro-2'-β-methyl- or 2'-O-methyl-substituted nucleosides, as well as for 3'-O-modified nucleosides. The introduction of the fluoro- moiety into the C2' position or the methyl moiety into the O2' or O3' position probably eliminates the 2'-α-hydroxy or 3'-α-hydroxy hydrogen bond donor/acceptor, which could result in complete abrogation of the nucleoside inhibitory activity. The observed inactivity could be also explained by inefficient cellular uptake and metabolism to convert the nucleoside molecule to the corresponding triphosphate form [14]. A detailed study of the compound uptake and metabolic conversion goes beyond the scope of this brief report and will be a subject of a future report. Neither nucleosides with 4'-azido modification nor nucleosides with chemically modified hetero-base moiety exerted anti-ZIKV activity.

In conclusion, we have demonstrated that 2'-C-methylated nucleosides exerted activity against ZIKV under in vitro conditions. These compounds provide a basis for structure-based optimization and rational design of effective prodrugs, which will be further tested in rodent models for therapy of ZIKV infection.

Supplementary Data

Supplementary materials are available at <http://jid.oxfordjournals.org>. Consisting of data provided by the author to benefit the reader, the posted materials are not copyedited and are the sole responsibility of the author, so questions or comments should be addressed to the author.

Notes

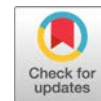
Financial support. This work was supported by the Czech Science Foundation (grantGA14-29256S); the Ministry of Education, Youth, and Sports of the Czech Republic, under the NPU I program (grant IO1218); the National Subvention for the Development of Research Organizations (grant RVO:61388963); the European Virus Archive Goes Global project, which has received funding from the European Union's Horizon 2020 research and innovation program (grant 653316).

Potential conflicts of interest. All authors: No reported conflicts. All authors have submitted the ICMJE Form for Disclosure of Potential Conflicts of Interest. Conflicts that the editors consider relevant to the content of the manuscript have been disclosed.

References

1. Lazear HM, Stringer EM, de Silva AM. The emerging Zika virus epidemic in the Americas: research priorities. *JAMA* 2016; 315:1945-6.

2. Roth A, Mercier A, Lepers C, et al. Concurrent outbreaks of dengue, chikungunya and Zika virus infections - an unprecedented epidemic wave of mosquito-borne viruses in the Pacific 2012–2014. *Euro Surveill* **2014**; 19.
3. Broutet N, Krauer F, Riesen M, et al. Zika virus as a cause of neurologic disorders. *N Engl J Med* **2016**; 374:1506–9.
4. Mlakar J, Korva M, Tul N, et al. Zika virus associated with microcephaly. *N Engl J Med* **2016**; 374:951–8.
5. Carteaux G, Maquart M, Bedet A, et al. Zika virus associated with meningoencephalitis. *N Engl J Med* **2016**; 374:1595–6.
6. Mécharles S, Herrmann C, Poullain P, et al. Acute myelitis due to Zika virus infection. *Lancet* **2016**; 387:1481.
7. De Clercq E, Neyts J. Antiviral agents acting as DNA or RNA chain terminators. *Handb Exp Pharmacol* **2009**; 189:53–84.
8. Eyer L, Valdés JJ, Gil VA, et al. Nucleoside inhibitors of tick-borne encephalitis virus. *Antimicrob Agents Chemother* **2015**; 59:5483–93.
9. De Madrid AT, Porterfield JS. A simple micro-culture method for the study of group B arboviruses. *Bull World Health Organ* **1969**; 40:113–21.
10. Sampath A, Padmanabhan R. Molecular targets for flavivirus drug discovery. *Antiviral Res* **2009**; 81:6–15.
11. Botting C, Kuhn RJ. Novel approaches to flavivirus drug discovery. *Expert Opin Drug Discov* **2012**; 7:417–28.
12. Kok WM. New developments in flavivirus drug discovery. *Expert Opin Drug Discov* **2016**; 11:433–45.
13. Zmurko J, Marques RE, Schols D, et al. The viral polymerase inhibitor 7-deaza-2'-C-methyladenosine is a potent inhibitor of in vitro Zika virus replication and delays disease progression in a robust mouse infection model. *PLoS Negl Trop Dis* **2016**; 10:e0004695.
14. Eldrup AB, Allerson CR, Bennett CF, et al. Structure-activity relationship of purine ribonucleosides for inhibition of hepatitis C virus RNA-dependent RNA polymerase. *J Med Chem* **2004**; 47:2283–95.



Viral RNA-Dependent RNA Polymerase Inhibitor 7-Deaza-2'-C-Methyladenosine Prevents Death in a Mouse Model of West Nile Virus Infection

Luděk Eyer,^{a,b} Martina Fojtíková,^a Radim Nencka,^c Ivo Rudolf,^{d,e} Zdeněk Hubálek,^{d,e}  Daniel Ruzek^{a,b}

^aDepartment of Virology, Veterinary Research Institute, Brno, Czech Republic

^bInstitute of Parasitology, Biology Centre of the Czech Academy of Sciences, Ceske Budejovice, Czech Republic

^cInstitute of Organic Chemistry and Biochemistry, The Czech Academy of Sciences, Prague, Czech Republic

^dThe Czech Academy of Sciences, Institute of Vertebrate Biology, Brno, Czech Republic

^eMasaryk University, Department of Experimental Biology, Brno, Czech Republic

ABSTRACT West Nile virus (WNV) is a medically important emerging arbovirus causing serious neuroinfections in humans and against which no approved antiviral therapy is currently available. In this study, we demonstrate that 2'-C-methyl- or 4'-azido-modified nucleosides are highly effective inhibitors of WNV replication, showing nanomolar or low micromolar anti-WNV activity and negligible cytotoxicity in cell culture. One representative of C2'-methylated nucleosides, 7-deaza-2'-C-methyladenosine, significantly protected WNV-infected mice from disease progression and mortality. Twice daily treatment at 25 mg/kg starting at the time of infection resulted in 100% survival of the mice. This compound was highly effective, even if the treatment was initiated 3 days postinfection, at the time of a peak of viremia, which resulted in a 90% survival rate. However, the antiviral effect of 7-deaza-2'-C-methyladenosine was absent or negligible when the treatment was started 8 days postinfection (i.e., at the time of extensive brain infection). The 4'-azido moiety appears to be another important determinant for highly efficient inhibition of WNV replication *in vitro*. However, the strong anti-WNV effect of 4'-azidocytidine and 4'-azido-aracytidine was cell type dependent and observed predominantly in porcine kidney stable (PS) cells. The effect was much less pronounced in Vero cells. Our results indicate that 2'-C-methylated or 4'-azidated nucleosides merit further investigation as potential therapeutic agents for treating WNV infections as well as infections caused by other medically important flaviviruses.

KEYWORDS West Nile virus, antiviral agents, flavivirus, nucleoside analogs

West Nile virus (WNV) is an emerging representative of the genus *Flavivirus* belonging to the family *Flaviviridae*. This family also includes other medically important human pathogens, such as dengue virus (DENV), Japanese encephalitis virus (JEV), yellow fever virus (YFV), Zika virus (ZIKV), and tick-borne encephalitis virus (TBEV) (1). WNV has been serologically classified into the JEV antigenic complex and divided into eight genotypic lineages; from a medical point of view, the strains pathogenic for humans are designated as lineages 1 and 2 (2). WNV virions (50 nm diameter) are enveloped with a host cell-derived lipid bilayer containing single-stranded, plus-sense genomic RNA 11 kb in length. The WNV genome encodes a single polyprotein processed into three structural (capsid, premembrane or membrane, and envelope) and seven nonstructural (NS1, NS2A, NS2B, NS3, NS4A, NS4B, and NS5) proteins (3–6). NS5 shows RNA-dependent RNA polymerase (RdRp) activity and has been reported to be an important target for antiviral development (4).

Citation Eyer L, Fojtíková M, Nencka R, Rudolf I, Hubálek Z, Ruzek D. 2019. Viral RNA-dependent RNA polymerase inhibitor 7-deaza-2'-C-methyladenosine prevents death in a mouse model of West Nile virus infection. *Antimicrob Agents Chemother* 63:e02093-18. <https://doi.org/10.1128/AAC.02093-18>.

Copyright © 2019 American Society for Microbiology. All Rights Reserved.

Address correspondence to Daniel Ruzek, ruzekd@paru.cas.cz.

L.E. and M.F. contributed equally to this work.

Received 1 October 2018

Returned for modification 6 November 2018

Accepted 4 January 2019

Accepted manuscript posted online 14 January 2019

Published 26 February 2019

WNV circulates in nature within an enzootic transmission cycle between birds as reservoir hosts and bird-feeding mosquitoes, primarily involving *Culex* spp. as principal vectors of WNV (7). WNV was originally isolated in Africa in 1937 (8) and later caused outbreaks in Europe, the Middle East, and parts of Asia and Australia (9). Following its introduction into the United States in 1999, WNV rapidly disseminated across North America and has further spread to Mexico, South America, and the Caribbean (10, 11). In humans, WNV infection often remains subclinical (12, 13), but 20% to 40% of those infected may develop WNV disease, which manifests as a febrile illness that can progress to lethal encephalitis. Symptoms include cognitive dysfunction and acute flaccid paralysis (14–16). Overall, 2,002 cases of WNV disease in humans were reported in the United States in 2017, 67% of which were classified as neuroinvasive disease (e.g., meningitis or encephalitis) and 33% as nonneuroinvasive infection (<https://www.cdc.gov/westnile>). As no vaccines or specific therapies for WNV are currently approved for humans, there is an urgent need for an effective approach to treatment based on specific inhibitors of WNV replication (17).

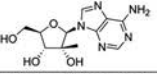
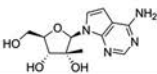
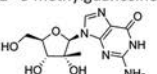
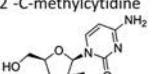
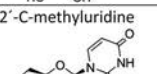
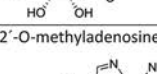
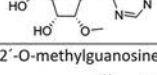
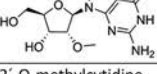
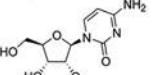
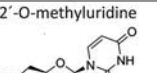
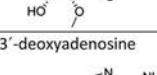
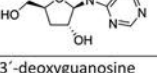
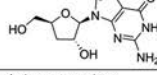
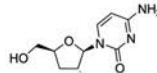
Nucleoside analogs represent an important group of small molecule-based inhibitors that have figured prominently in the search for effective antiviral agents (18). After they enter the cell, nucleoside analogs are phosphorylated by cellular kinases and incorporated into viral nascent RNA chains (19, 20). As the 3' hydroxyl of nucleoside inhibitors is conformationally constrained or sterically/electronically hindered (nonobligate chain terminators) or completely missing (obligate chain terminators), such structures exert a decreased potency to form a phosphodiester linkage with the incoming nucleoside triphosphate during viral RNA replication, resulting in the premature termination of viral nucleic acid synthesis (21). Currently, there are more than 25 approved therapeutic nucleosides used for the treatment of viral infections of high medical importance, such as HIV/AIDS, hepatitis B, hepatitis C, and herpes infections (22–26). Therefore, nucleoside analogs represent promising tools that can be repurposed against mosquito-transmitted flaviviruses, including WNV.

The aim of this study was to assess anti-WNV activity and cytotoxicity in a series of methyl- or azido-substituted nucleosides. We have demonstrated that the 2'-C-methyl or 4'-azido substituents are crucial structural elements for highly efficient WNV inhibition and low cytotoxicity in cell culture. One representative of 2'-methylated nucleosides, 7-deaza-2'-C-methyladenosine (7-deaza-2'-CMA), significantly protected WNV-infected mice from disease progression and mortality, even if the treatment was started 3 days postinfection (p.i.). Thus, 2'-C-methylated or 4'-azidated nucleosides merit further investigation as therapeutic agents for treating WNV infections and, hypothetically, infections caused by other medically important flaviviruses.

RESULTS

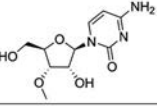
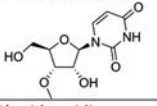
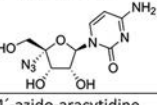
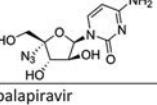
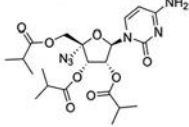
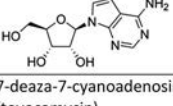
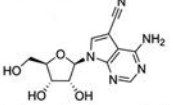
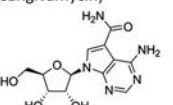
***In vitro* antiviral effect and cytotoxicity of the tested compounds.** Nucleosides with a methyl substituent at the C2' position exhibited nanomolar or low-micromolar dose-dependent anti-WNV activity when tested on either porcine kidney stable (PS) or Vero cell cultures (Table 1, Fig. 1A and B and 2A and B). 7-Deaza-2'-CMA, also denoted as MK-0608, exerted the strongest antiviral effect of all 2'-C-methylated nucleosides tested, characterized by 50% effective concentration (EC_{50}) values of $0.33 \pm 0.08 \mu\text{M}$ and $0.15 \pm 0.05 \mu\text{M}$ for Eg-101 and 13-104, respectively. The anti-WNV effect of 7-deaza-2'-CMA was confirmed also in human neuroblastoma cell line SK-N-SH (Fig. 1D). In this case, treatment with 7-deaza-2'-CMA at a concentration of $50 \mu\text{M}$ resulted in reductions of viral titers of 10^5 -fold (Eg-101) and 10^6 -fold (13-104) compared to that of mock-treated cells. EC_{50} values for 2'-C-methyladenosine, 2'-C-methylguanosine, and 2'-C-methylcytidine in PS cells were slightly higher than those for 7-deaza-2'-CMA, ranging from $0.78 \pm 0.16 \mu\text{M}$ to $0.96 \pm 0.06 \mu\text{M}$ for Eg-101 and from $0.66 \pm 0.15 \mu\text{M}$ to $1.67 \pm 0.50 \mu\text{M}$ for 13-104. Similarly to BCX-4430, which is used as a positive control for *in vitro* antiviral screens, these compounds (at a concentration of $50 \mu\text{M}$) decreased the viral titer 10^5 - to 10^6 -fold compared to that of mock-treated cells, and the *in vitro* antiviral effect was stable up to 5 days p.i. (Fig. 2C). 2'-C-

TABLE 1 WNV inhibition and cytotoxicity characteristics of the studied nucleoside analogues in PS cells

Compound	EC ₅₀ ± SD (μM) ^{a,b}		CC ₅₀ ± SD (μM) ^{a,e}	SI ^c	
	Eg-101	13-101		Eg-101	13-101
2'-C-methyladenosine 	0.86 ± 0.01	0.66 ± 0.15	>50.00	>58.06	>75.20
7-deaza-2'-C-methyladenosine 	0.33 ± 0.08	0.15 ± 0.05	>50.00	>149.63	>333.22
2'-C-methylguanosine 	0.96 ± 0.06	1.67 ± 0.50	>50.00	>52.00	>30.00
2'-C-methylcytidine 	0.78 ± 0.16	0.92 ± 0.12	~50.00	~64.38	~54.42
2'-C-methyluridine 	>50.00	>50.00	>50.00	1.00	1.00
2'-O-methyladenosine 	>50.00	>50.00	>50.00	1.00	1.00
2'-O-methylguanosine 	>50.00	>50.00	>50.00	1.00	1.00
2'-O-methylcytidine 	>50.00	>50.00	>50.00	1.00	1.00
2'-O-methyluridine 	>50.00	>50.00	>50.00	1.00	1.00
3'-deoxyadenosine 	>50.00	>50.00	>50.00	1.00	1.00
3'-deoxyguanosine 	>50.00	>50.00	>50.00	1.00	1.00
3'-deoxycytidine 	>50.00	>50.00	>50.00	1.00	1.00
3'-O-methyladenosine 	>50.00	>50.00	>50.00	1.00	1.00
3'-O-methylguanosine 	>50.00	>50.00	>50.00	1.00	1.00

(Continued on next page)

TABLE 1 (Continued)

3'-O-methylcytidine 	>50.00	>50.00	>50.00	1.00	1.00
3'-O-methyluridine 	>50.00	>50.00	>50.00	1.00	1.00
4'-azidocytidine 	0.50 ± 0.07	0.39 ± 0.28	>50.00	>99.11	>129.60
4'-azido-aracytidine 	0.25 ± 0.07	0.05 ± 0.01	>50.00	>197.94	>962.19
balapiravir 	>50.00	>50.00	>50.00	1.00	1.00
7-deazaadenosine (tubercidin) 	ND ^d	ND ^d	2.10 ± 0.20	-	-
7-deaza-7-cyanoadenosine (toyocamycin) 	ND ^d	ND ^d	0.10 ± 0.01	-	-
7-deaza-7-carbamoyladenosine (sangivamycin) 	ND ^d	ND ^d	0.80 ± 0.10	-	-

^aDetermined from three independent experiments.

^bExpressed as a 50% reduction of viral titers and calculated as inflection points of sigmoidal inhibitory curves, which were obtained by a nonlinear fit of transformed inhibitor concentrations versus normalized response using GraphPad Prism 7.04 (GraphPad Software, Inc., USA).

^cSI = CC₅₀/EC₅₀.

^dND, not determined.

^eValues reported previously by Eyer et al. (27).

Methyluridine was almost inactive against both WNV strains (EC₅₀ > 50 μM) when tested on porcine kidney stable (PS) cell monolayers and exhibited only weak inhibitory activity in Vero cells (Fig. 1A and B). 2'-C-Methyl-modified nucleosides exerted low cytotoxicity in both PS and Vero cells (50% cytotoxic concentration [CC₅₀] > 50 μM) (Table 1, Fig. 1C), except 2'-C-methylcytidin had a CC₅₀ value of ~50 μM in PS cells 3 days posttreatment, as we reported previously (27). 7-Deaza-2'-CMA exerted no cytotoxicity also for human neuroblastoma cells (tested up to 50 μM) (data not shown).

2'-O-Methyl- or 3'-O-methyl-substituted nucleosides demonstrated no inhibitory effects on WNV replication. Similarly, 3'-deoxy nucleosides were completely inactive against WNV (Fig. 1A and B). These compounds did not cause any morphological changes and did not result in decreased PS/Vero cell viability (CC₅₀ > 50 μM) at concentrations up to 50 μM after 3 days posttreatment (Table 1). Interestingly, 7-deazaadenosine (tubercidin) and its 7-cyano- and 7-carbamoyl-substituted deriva-

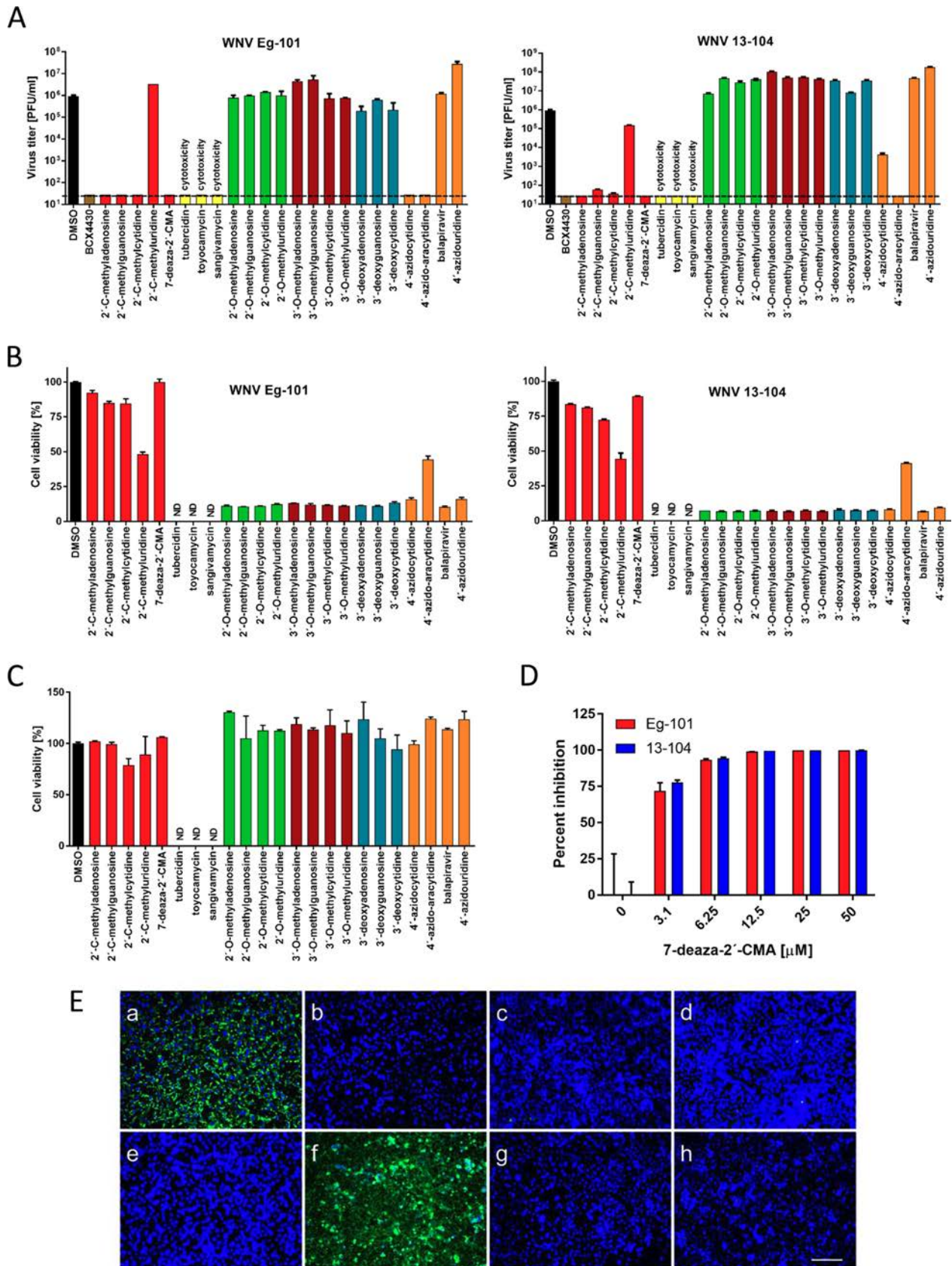


FIG 1 (A) Reduction of West Nile virus (WNV) titers by the indicated nucleoside analogs. PS cells were infected with WNV Eg-101 or 13-104 strain at a multiplicity of infection (MOI) of 0.1 and then treated with 50 μ M nucleoside analogs. WNV titers were determined by plaque assay 3 days (Continued on next page)

tives (toyocamycin and sangivamycin, respectively) were highly cytotoxic at 50 μM ; therefore, their anti-WNV profiles were excluded from further testing (Table 1, Fig. 1A to C).

We evaluated four representatives of 4'-azido-modified nucleoside scaffolds for their potential anti-WNV and cytotoxic effects: 4'-azidocytidine (denoted R-1479), balapiravir (an ester prodrug of 4'-azidocytidine), 4'-azido-aracytidine (a stereoisomeric counterpart of 4'-azidocytidine, denoted RO-9187), and 4'-azidouridine. 4'-Azidocytidine completely inhibited *in vitro* replication of the Eg-101 strain at a concentration of 50 μM (EC_{50} value, $0.50 \pm 0.07 \mu\text{M}$) in PS cells. In the case of the 13-104 strain, the inhibitory effect of 4'-azidocytidine was only partial, manifesting as a 10^3 -fold decrease in viral titer at 50 μM compared to that of mock-infected PS cells. Remarkably strong anti-WNV activity was observed for 4'-azido-aracytidine, with EC_{50} values of $0.25 \pm 0.07 \mu\text{M}$ for Eg-101 and $0.05 \pm 0.01 \mu\text{M}$ for 13-104 (Fig. 1A). The high antiviral potencies of both 4'-azidocytidine and 4'-azido-aracytidine have been demonstrated only in PS cells; in Vero cells, the effect was significantly less pronounced (Fig. 1B). The anti-WNV effects of 4'-azidouridine and balapiravir were completely abrogated ($\text{EC}_{50} > 50 \mu\text{M}$) (Fig. 1A and B). Though treating the PS cell culture with 50 μM 4'-azido-aracytidine slightly reduced the cell viability (86.9%) (27), the cytotoxicity of the other 4'-azido-substituted nucleosides tested in this study was absent or negligible (Table 1, Fig. 1C).

The antiviral effects of WNV inhibitors identified by viral titer/cytopathic effect (CPE) inhibition assays were confirmed by immunofluorescence staining, which was used to assess the expression of WNV surface E antigen in PS cells as an index of viral infectivity and replication *in vitro*. Though the surface E protein was highly expressed in WNV-infected mock-treated cells (Fig. 1E), no viral antigen was detected in mock-infected cells (data not shown). Immunofluorescence staining revealed that 50 μM 7-deaza-2'-CMA, 2'-C-methyladenosine, 2'-C-methylguanosine, 2'-C-methylcytidine, or 4'-azido-aracytidine considerably suppressed the expression of WNV surface E antigen, from both the Eg-101 and 13-104 strain, in virus-infected PS cells. As expected, WNV surface antigen was expressed extensively in cells treated with 2'-C-methyluridine (Fig. 1E). Slight E protein expression was also observed in cells infected with 13-104 strain treated with 4'-azidocytidine (data not shown). The results correlate with the observed inhibition of WNV replication in compound-treated cell cultures.

Antiviral efficacy of 7-deaza-2'-CMA in a mouse model of lethal WNV infection.

Based on the results showing 7-deaza-2'-CMA strongly inhibited WNV replication *in vitro*, we used this nucleoside to demonstrate its anti-WNV effect in a mouse model of WNV infection (Fig. 3A). WNV strain Eg-101 exhibits low pathogenicity in adult mice (28); therefore, WNV strain 13-104 was used in the *in vivo* experiments. BALB/c mice infected subcutaneously with a lethal dose of strain 13-104 (10^3 PFU/mouse) exhibited characteristic clinical signs of infection, such as ruffled fur, hunched posture, tremor, and paralysis of the limbs, within days 7 to 12 days p.i., with the majority of mice requiring euthanasia (Fig. 3B and C). The infection was accompanied by a rapid loss of body weight starting 7 days p.i., with a loss of more than 20% by 12 days p.i. (Fig. 3D). The mortality rate was 95% to 100% with a mean survival time of 10.5 ± 1.9 days (Fig. 2B). Viable virus was detected in the brains of WNV-infected mice 10 days p.i., which was characterized by a mean viral titer of 3.87×10^4 PFU/ml (Fig. 3E).

FIG 1 Legend (Continued)

postinfection. Viral titers are expressed as PFU/ml. The horizontal dashed line indicates the minimum detectable threshold of $1.44 \log_{10}$ PFU/ml. (B) Inhibition of WNV-induced CPE by the indicated nucleoside analogs in Vero cells expressed as a percentage of cell viability 3 days postinfection. ND, not detected (below the detection limit). (C) The cytotoxicity of nucleoside inhibitors was determined by treatment of Vero cells with 50 μM of the indicated nucleoside analogs and was expressed in terms of cell viability 3 days postinfection. ND, not detected (below the detection limit). (D) Anti-WNV effect of 7-deaza-2'-CMA in human neuroblastoma cells (SK-N-SH) within the concentration range from 0 to 50 μM . Bars indicate the mean values from two independent experiments performed in three replicate wells, and the error bars indicate the standard errors of the means. (E) Inhibition of WNV viral antigen expression by nucleoside inhibitors. PS cells were infected with WNV and treated with 0.5% DMSO (a) or 50 μM 2'-C-methyladenosine (b), 7-deaza-2'-CMA (c), 2'-C-methylguanosine (d), 2'-C-methylcytidine (e), 2'-C-methyluridine (f), 4'-azidocytidine (g), or 4'-azido-aracytidine (h). PS cells were fixed with cold methanol-acetone 3 days postinfection and stained with a flavivirus-specific antibody labeled with FITC (green) and counterstained with DAPI (blue). Scale bars, 50 μm .

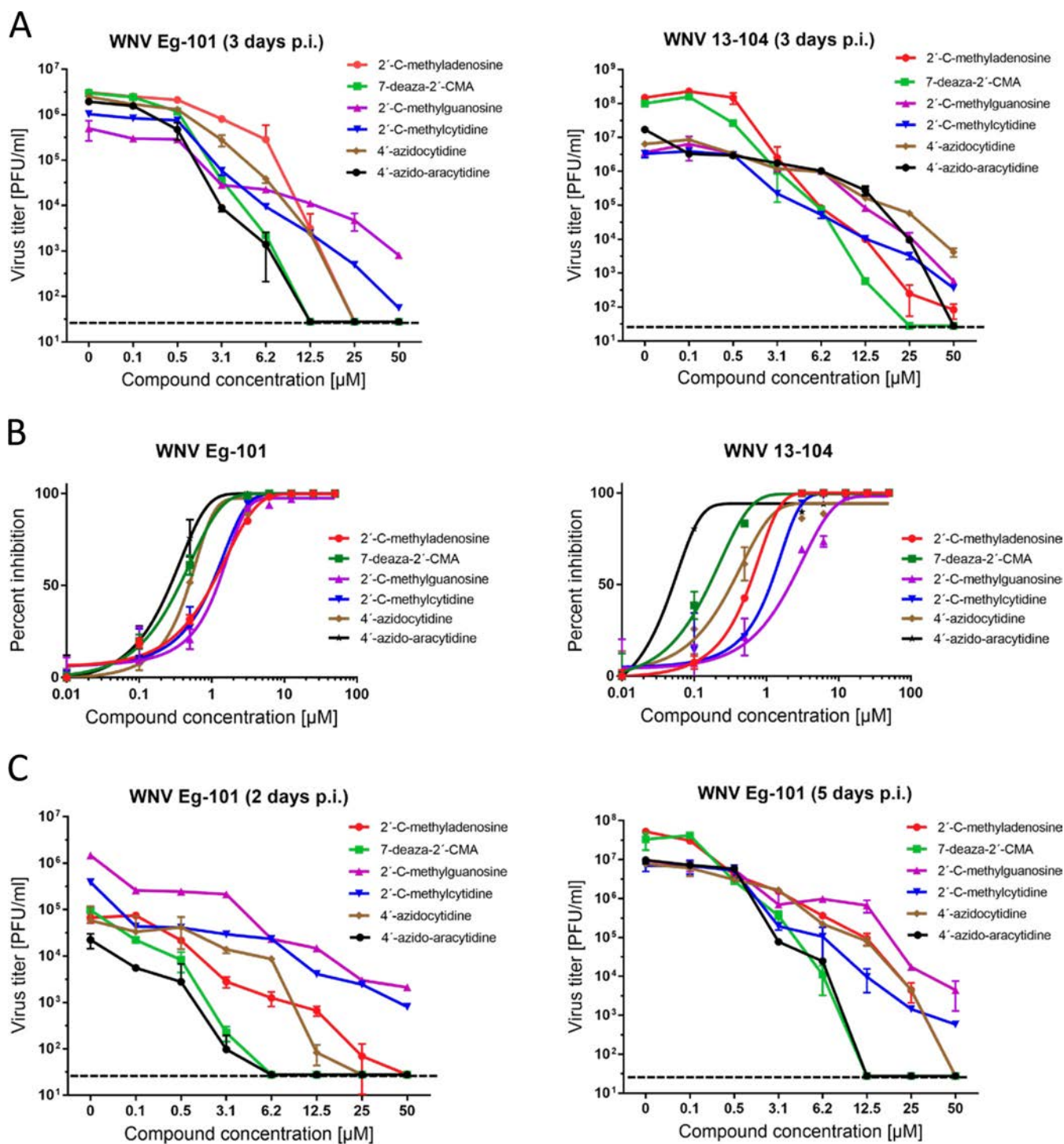


FIG 2 (A) Dose-dependent effects of the indicated West Nile virus (WNV) inhibitors on Eg-101 or 13-104 titer. PS cells were infected with WNV at a multiplicity of infection (MOI) of 0.1 and treated with the appropriate inhibitor at the indicated concentrations 3 days postinfection. The mean titers from two independent experiments performed in three biological replicates are shown, and error bars indicate standard errors of the mean. The horizontal dashed line indicates the minimum detectable threshold of $1.44 \log_{10}$ PFU/ml. (B) Sigmoidal inhibition curves for WNV strains Eg-101 and 13-104 in the presence of a serial dilution of indicated nucleoside analogs. (C) Dose-dependent effects of the indicated WNV inhibitors on Eg-101 titer at 2 and 5 days postinfection in PS cells.

Treatment with 25 mg/kg of 7-deaza-2'-CMA twice a day, initiated at the time of virus inoculation and ceased 19 days p.i., resulted in a 100% survival rate ($P < 0.0001$) among WNV-infected mice (Fig. 3B). Nine of ten animals exhibited no clinical signs during the entire 28-day monitoring period; in one mouse, we observed slightly bristled

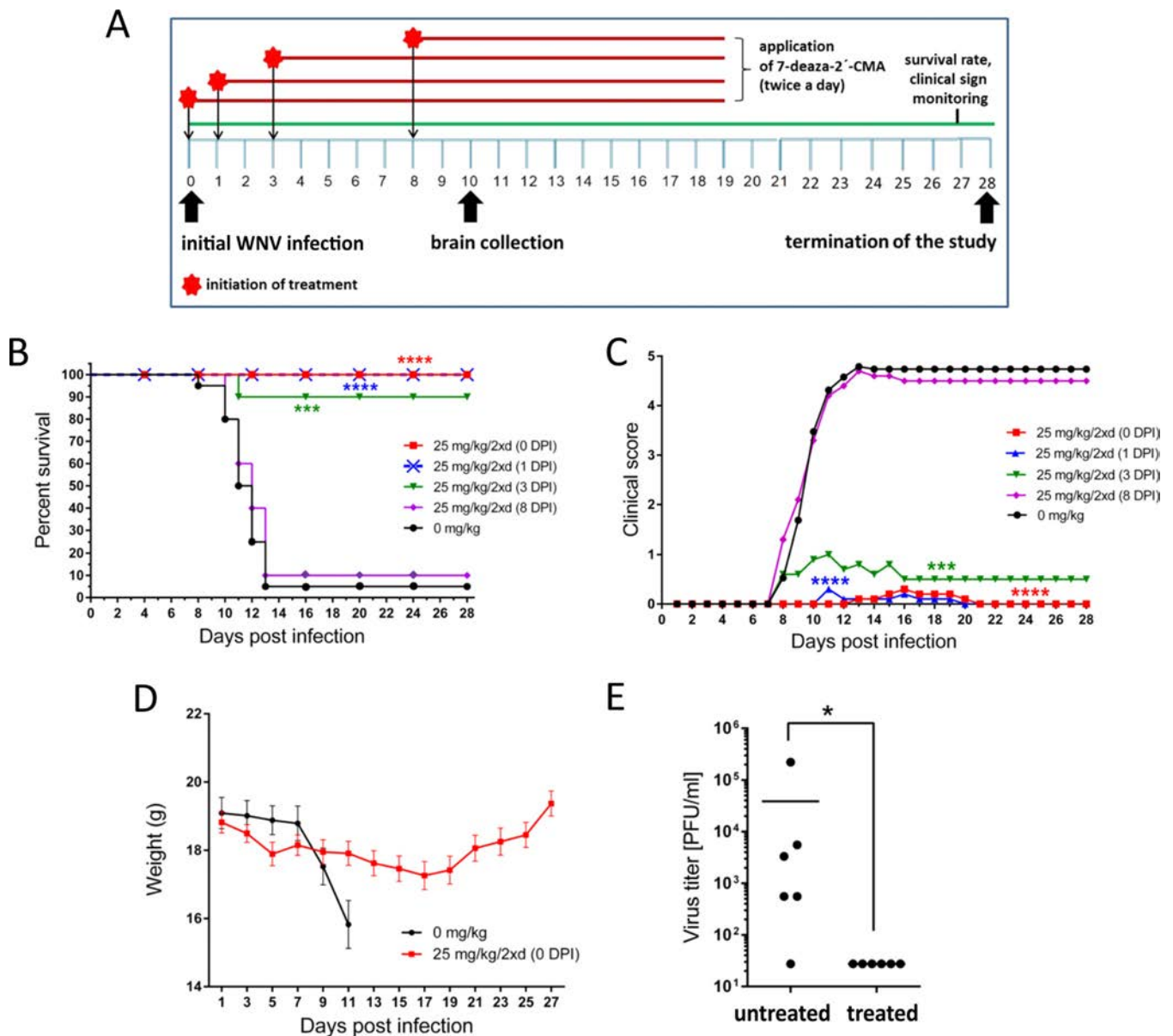


FIG 3 7-Deaza-2'-CMA is effective at treating lethal West Nile virus (WNV) infection in a mouse model. (A) The design of the *in vivo* antiviral experiment. (B) Groups of adult BALB/c mice were infected with a lethal dose of WNV (strain 13-104) and treated twice daily with intraperitoneal 25 mg/kg 7-deaza-2'-CMA or saline (mock treatment) at the indicated times after WNV infection. Survival rates were monitored daily for 28 days. (C) Disease signs were scored as follows: 0, no signs; 1, ruffled fur; 2, slowing of activity or hunched posture; 3, asthenia or mild paralysis; 4, lethargy, tremor, or complete paralysis of the limbs; 5, death. (D) Changes in body weight within a 28-day experimental period. Points indicate the mean body weight values of ten mice, and the error bars indicate the standard errors of the means. (E) Groups of adult BALB/c mice were infected with a lethal dose of WNV and treated with 7-deaza-2'-CMA or saline. On day 10 postinfection, which corresponds to advanced brain infection, the brains of mice were collected and homogenized and the viral titers determined by plaque assay. *, $P < 0.05$; ***, $P < 0.001$; ****, $P < 0.0001$.

fur and slowing activity between 13 and 20 days p.i. (Fig. 3C). WNV-infected 7-deaza-2'-CMA-treated mice had a slight loss of body weight (8.2%) by 17 days p.i.; the weight began to increase again after 18 days p.i. (Fig. 3D). No viable virus was demonstrated in the brains of WNV-infected compound-treated mice 10 days p.i. (Fig. 3E). No apparent toxicity or other side effects were observed in mice treated with 7-deaza-2'-CMA (25 mg/kg, twice a day) throughout the treatment period.

A second study was performed to determine the therapeutic effect of treatment initiated at various times after WNV infection. A delayed start of treatment (25 mg/kg, twice daily), at 1 day p.i., resulted in a 100% survival rate ($P < 0.0001$) (Fig. 3B). Nine of ten animals exhibited no significant signs of disease; in one animal, slightly ruffled fur

was observed between 11 and 20 days p.i. (Fig. 3C). Similarly, treatment started 3 days p.i., at the time of peak of viremia, significantly protected the infected animals from disease development and mortality (90% survival rate, $P < 0.001$) and substantially eliminated the appearance of signs of clinical infection (Fig. 3B and C). However, treatment initiated 8 days p.i. (i.e., when the first signs of disease appeared) was inefficient; in this group of animals, characteristic clinical signs of disease were observed within 7 to 12 days p.i. The infection was 90% lethal with a mean survival time of 11.5 ± 1.29 days (Fig. 3B and C).

DISCUSSION

WNV is a medically important emerging arbovirus able to cause serious neuroinfections in humans, against which no approved antiviral therapy is currently available. Therefore, there is an urgent medical need to develop innovative and effective small-molecule-based antivirals to treat patients with WNV infection (14). Here, we evaluated the antiviral activity and cytotoxicity of 2'-C-methyl-, 2'-O-methyl-, 3'-O-methyl-, 3'-deoxy-, and 4'-azido-modified nucleosides. These compounds were originally developed for the treatment of chronic hepatitis C (29–35), and some were later repurposed to suppress viral infections caused by tick- and mosquito-borne flaviviruses (27, 32, 33, 36–41).

Our *in vitro* antiviral screens revealed that a methyl substituent at the C2' nucleoside position is an important structural determinant to suppress the replication of WNV in cell culture. Nucleosides methylated at the C2' position have also been reported to strongly inhibit TBEV (27, 36, 38), DENV (42, 43), ZIKV (37, 41, 44, 45), Alkhurma hemorrhagic fever virus, Kyasanur Forest disease virus, Omsk hemorrhagic fever virus, and Powassan virus (39), as well as numerous representatives of the *Picornaviridae* and *Caliciviridae* families (46–48). This indicates that 2'-C-methylated nucleosides are broad-range inhibitors of a large variety of single-stranded plus-sense RNA viruses. We observed that the anti-WNV activity of 2'-C-methylated nucleosides is strongly influenced by the identity of the heterocyclic nucleobase and was demonstrated to decrease in the order as follows: 2'-C-methyladenosine > 2'-C-methylcytidine > 2'-C-methylguanosine > 2'-C-methyluridine. The surprisingly low *in vitro* antiviral activity of 2'-C-methyluridine was also previously reported for TBEV and ZIKV (EC₅₀s of $11.1 \pm 0.4 \mu\text{M}$ and $45.45 \pm 0.64 \mu\text{M}$, respectively) (27, 37). This phenomenon might be ascribed to rapid nucleoside degradation with cellular uridine phosphorylase, a cytoplasmic enzyme playing an important role in uridine catabolism (49, 50).

In contrast, 7-deaza-2'-CMA, in which a C2'-methylated riboside is bound to a 7-deaza-modified adenine, exhibited significantly increased anti-WNV efficacy and low cytotoxicity in cell lines of both neuronal (SK-N-SH) and extraneural (PS and Vero) origins. This nucleoside has been reported to have greater metabolic stability, better bioavailability, and a longer half-life in beagle dogs and rhesus monkeys than its parent compound, 2'-C-methyladenosine (33). Moreover, 7-deaza modification introduced into anti-DENV nucleoside 2'-C-ethynyladenosine resulted in a dramatic decrease in compound cytotoxicity, as demonstrated for NIDT008 in multiple cell-based systems and *in vivo* (51). Interestingly, elimination of the C2' methyl from 7-deaza-2'-CMA led to extremely high *in vitro* cytotoxicity of 7-deazaadenosine (tubercidin) and its derivatives sangivamycin and toyocamycin. Our anti-TBEV screens revealed that further modification of 7-deaza-2'-CMA at position 6 (e.g., 6-hydroxyamino or 6-hydrazinyl), position 7 (e.g., 7-nitro, 7-phenyl, 7-fluoro, 7-cyano, 7-ethynyl, or 7-trifluoromethyl), or positions 6 and 7 (e.g., 6-dimethylamino-7-iodo, 6-cyclopropylamino-7-iodo, or 6-morpholino-7-iodo) led to a complete loss of antiviral activity (unpublished results). We can conclude that 7-deaza modification of adenosine combined with a 2'-C-methyl substituent results in higher antiviral activity, decreased toxicity, and improved pharmacokinetic profile (33); however, 7-deaza modification itself is responsible for a conspicuous increase in cytotoxicity. On the other hand, the lack of antiviral activity of O2'- or O3'-methylated or 3'-deoxy-modified nucleosides might be explained by the absence of 2'- and 3'-hydroxyls positioned in the α -face of the nucleoside scaffold, which are

considered to be crucial for specific hydrogen-bonding interactions of the nucleoside molecule with the flaviviral polymerase active site during RNA replication (27, 29). Moreover, 2'-*O*-methylcytidine has been observed to be inefficiently phosphorylated by intracellular kinases and/or extensively deaminated/demethylated in various cell cultures (27).

The 4'-azido moiety appears to be another important determinant of highly efficient inhibition of WNV replication *in vitro*, as exemplified by two cytidine derivatives: 4'-azidocytidine and 4'-azido-aracytidine. The high anti-WNV activity of both compounds has been observed to be strongly cell type dependent and might be ascribed to differences in compound uptake or the metabolic processing of both nucleosides by individual cell lines (52). Cell-type-dependent antiviral activity of 4'-azido-modified nucleosides was also previously reported for TBEV; the compounds were active in PS cells but their activity was completely abrogated in human neuroblasts (27). The cell-type-dependent antiviral effect can sometimes affect the results of antiviral screens; therefore, multiple clinically relevant cell lines are needed for antiviral testing (52). Similarly to 2'-*C*-methyluridine, 4'-azidouridine exhibits no anti-WNV activity, probably because of low metabolic stability and rapid degradation by cellular uridine phosphorylases (49, 50).

Based on our finding that 7-deaza-2'-CMA is a strong inhibitor of WNV replication in cell culture, we evaluated the antiviral effect of this compound in a lethal mouse model of WNV infection. A dose of 25 mg/kg 7-deaza-2'-CMA administered intraperitoneally twice a day starting the day of WNV infection resulted in a 100% survival rate. The treated animals exhibited no clinical signs of neuroinfection, and no viral titer was determined in mouse brains. The same treatment regimen with 7-deaza-2'-CMA (25 mg/kg, twice daily, starting at the time of infection) was used to treat TBEV-infected BALB/c mice, which had slightly lower survival rates (60%) and worse clinical scores than WNV-infected animals (36).

The treatment initiated at the time of infection does not correlate with potential human drug use, as the therapy usually begins during the neurological phase of the disease. Therefore, we tested the therapeutic effect of treatment initiated at various times after WNV infection. Mice infected with WNV have peak viremia between 48 and 72 h p.i. The virus then crosses the blood-brain barrier (BBB) and establishes brain infection (53, 54). Therefore, treatment was started in mice before viremia (1 day p.i.), during peak viremia (3 days p.i.), and at the time of established brain infection (8 days p.i.). A delayed start of treatment (25 mg/kg, twice daily), 1 day p.i., resulted in the survival of all infected mice. Even the treatment initiated 3 days p.i. (at the time of a peak of viremia) showed a high antiviral efficacy, protecting 90% of mice from disease development and mortality. However, animals treated after 8 days p.i. (i.e., at the time of extensive brain infection) had only a slightly higher survival rate and negligibly prolonged mean survival time compared to that of mock-treated mice. The results suggest that treatment with 7-deaza-2'-CMA is highly effective, even when started 1 or 3 days p.i. (i.e., before the virus infects the brain). We do not have any data if 7-deaza-2'-CMA crosses the intact BBB, but disruption of the BBB is one of the hallmarks of flavivirus encephalitis (53), which facilitates drug delivery into the brain. However, the fact that the therapy initiated on day 8 p.i. had no or little effect in terms of protection against the lethal disease is not surprising due to the extensive brain infection and inflammation already present at this time point.

Strong *in vivo* antiviral activity of 7-deaza-2'-CMA has also been demonstrated in other medically important flaviviruses. This compound substantially improves disease outcome, increases survival, and reduces signs of neuroinfection and viral titers in the brains of BALB/c mice infected with TBEV (36). 7-Deaza-2'-CMA also reduces viremia in AG129 mice infected with the African strain of ZIKV (45) and is a potent inhibitor of DENV in a mouse model of dengue viremia (55). Although 7-deaza-2'-CMA has failed in human clinical tests for chronic hepatitis C treatment, probably due to mitochondrial toxicity (56), this compound might still be suitable and safe for short-term therapy of acute flaviviral diseases, including WNV infections (57), and represents one of the most

promising candidates for the treatment of flaviviral infections to date. Alternatively, 7-deaza-2'-CMA can represent a reference compound/comparator in future studies (45).

In conclusion, our results demonstrate that nucleosides with a C2' methyl substituent are potent inhibitors of WNV replication *in vitro*. The leading structure of this group, 7-deaza-2'-CMA, exerted significant anti-WNV activity in a mouse model of WNV infection. This compound protected WNV-infected mice from disease signs/death, even if the treatment was initiated 3 days p.i. Some other substituents were introduced into the C2' nucleoside position previously, particularly 2'-C-ethynyl in anti-DENV nucleoside NITD008 (51,57,58) or 2'-fluoro-2'-C-methyl in the case of sofosbuvir, which inhibits ZIKV *in vitro* and in rodent models of ZIKV infection (59). A variety of promising modifications at C2' indicate that this nucleoside position provides a large chemical space for possible changes/substitutions to develop efficient nucleoside inhibitors of flaviviral replication. Another important structural modification for efficient WNV inhibition is 4'-azido substitution of cytidine-based nucleosides. Although these compounds have been tested only *in vitro*, 4-azido-aracytidine had a nanomolar anti-WNV effect and a good cytotoxicity profile. This molecule will be tested *in vivo* in our future studies. Our data strongly suggest that nucleoside analogs represent a rich source of promising inhibitors for the further design and development of innovative and effective drugs active against important human pathogens, including flaviviruses.

MATERIALS AND METHODS

Ethics statement. This study was carried out in strict accordance with Czech law and guidelines for the use of experimental animals and protection of animals against cruelty (Animal Welfare Act 246/1992 Coll.). All procedures were reviewed by the local ethics committee and approved by the Ministry of Agriculture of the Czech Republic (permit no. 22006/2016-MZE-17214).

Cell cultures, virus strains, and antiviral compounds. PS cells (60), a cell line widely used for the isolation and multiplication of arthropod-borne flaviviruses, were cultured at 37°C in L-15 (Leibovitz) medium containing 1 mM L-glutamine, 4% fetal bovine serum, and 1% penicillin and streptomycin (Sigma-Aldrich, Prague, Czech Republic). Epithelial kidney (Vero) cells from *Cercopithecus aethiops* were cultured in minimum essential medium (MEM) containing 10% fetal bovine serum, 5% L-glutamine, and 1% penicillin and streptomycin (Sigma-Aldrich, Prague, Czech Republic) at 37°C in a 5% CO₂ atmosphere. Human neuroblastoma cells (SK-N-SH) were cultured at 37°C in 5% CO₂ in Iscove's modified Dulbecco's medium (IMDM) with 10% fetal bovine serum and a 1% mixture of antibiotics. Two distinct low-passaged WNV strains were used to evaluate the anti-WNV activity of the tested compounds. Eg-101, a member of genomic lineage 1, was originally isolated from human serum in Egypt in 1951 (61). WNV strain 13-104, a representative of genomic lineage 2, was isolated from the *Culex modestus* mosquito in the Czech Republic in 2013 (62).

2'-C-Methyl-, 2'-O-methyl-, and 3'-O-methyl-substituted nucleoside analogs and 3'-deoxynucleosides were purchased from Carbosynth (Compton, UK). 4'-Azido-modified nucleosides and BCX-4430 were obtained from MedchemExpress (Stockholm, Sweden). Tubercidin, toyocamycin, and sangivamycin were purchased from Sigma-Aldrich (Prague, Czech Republic). 7-Deaza-2'-CMA was synthesized at the Institute of Organic Chemistry and Biochemistry in Prague. Nucleoside analogs were diluted in 100% dimethyl sulfoxide (DMSO) to 10 mM stock solutions.

Antiviral assays. To perform the viral titer reduction assay, PS cells were seeded in 96-well plates (approximately 3×10^4 cells per well) and incubated for 24 h at 37°C to form a confluent monolayer. The medium was then aspirated from the wells and replaced with 200 μ l of fresh medium containing 50 μ M of the test compounds and the appropriate virus strain at a multiplicity of infection (MOI) of 0.1. Virus-infected cells treated with BCX-4430 (63) and DMSO (mock-treated cells) were used as positive and negative controls, respectively. The culture medium was collected 3 days p.i. and viral titers (expressed as PFU/ml) were determined from the collected culture medium by plaque assays (38, 64).

As the antiviral effect of many compounds is cell type dependent, we further tested the anti-WNV activity of nucleoside analogs in Vero cells in cytopathic effect (CPE) inhibition assays. Vero cells were seeded in 96-well plates, incubated to form a confluent monolayer, and treated with virus and tested compounds as described for the viral titer inhibition assay. The cells were examined microscopically for virus-induced CPE. Three days postinfection, the supernatant medium was aspirated from the cells, and the cell culture was stained with naphthalene black. The rate of CPE was expressed in terms of cell viability as the absorbance at 540 nm by compound-treated cells relative to the absorbance by DMSO-treated cells.

The dose-dependent antiviral activities of selected WNV inhibitors were assessed as follows. PS cells were seeded in 96-well plates (approximately 3×10^4 cells per well) and incubated at 37°C to form a confluent monolayer. After a 24-h incubation, the medium was aspirated from the wells and replaced with a fresh medium containing the tested compounds over the concentration range of 0 to 50 μ M and appropriate WNV strain (MOI 0.1). The culture medium was collected continuously 2, 3, and 5 days p.i. The viral titers (expressed as PFU/ml) were determined from the collected supernatant media by a plaque

titration assay and used to construct dose-dependent and inhibition curves. The viral titers obtained 3 days p.i. were used for calculation of the 50% effective concentrations (EC_{50} ; the concentration of compounds required to inhibit the viral titer by 50% compared to the control value). The dose-dependent study was carried out also with human neuroblastoma cells (SK-N-SH) at the concentration range from 0 to 50 μ M.

Immunofluorescence staining. The results obtained from antiviral assays were confirmed by a cell-based flavivirus immunostaining assay, a method based on determining the compound-induced inhibition of viral surface antigen (E protein) expression (38). Briefly, PS cells seeded on 96-well plates were treated with the test compound (50 μ M) and infected with WNV strains Eg-101 or 13-104 at an MOI of 0.1. After a 3-day incubation at 37°C, the cell monolayers were fixed with cold acetone-methanol (1:1), blocked with 10% fetal bovine serum, and incubated with a mouse monoclonal antibody that specifically recognizes the flavivirus group surface antigen (1:250; Sigma-Aldrich, Prague, Czech Republic). After extensive washing, the cells were labeled with an anti-mouse goat secondary antibody conjugated with fluorescein isothiocyanate (FITC; 1:500) and counterstained with DAPI (4',6-diamidino-2-phenylindole; 1 μ g/ml) to visualize the cell nuclei. The fluorescence signal was recorded with an Olympus IX71 epifluorescence microscope.

Cytotoxicity assay. PS, Vero, or SK-N-SH cells grown in 96-well plates for 24 h to form a confluent monolayer were treated with test compounds over the concentration range of 0 to 50 μ M. Three days posttreatment, the cell culture medium was collected, and the potential cytotoxicity of test nucleosides was determined in terms of cell viability using a Cell Counting kit-8 (Dojindo Molecular Technologies, Munich, Germany) according to the manufacturer's instructions. The compound concentration that reduced cell viability by 50% was considered the 50% cytotoxic concentration (CC_{50}).

Mouse infections. To evaluate the anti-WNV effect of 7-deaza-2'-CMA *in vivo*, five groups of 6-week-old female BALB/c mice (purchased from AnLab, Prague, Czech Republic) were subcutaneously injected with WNV strain 13-104 (1,000 PFU/mouse) and treated intraperitoneally with 200 μ l of 7-deaza-2'-CMA (25 mg/kg twice a day at 8-h intervals) as follows: group 1 ($n = 10$), treatment initiated immediately after infection (0 days p.i.); group 2 ($n = 10$), treatment initiated 1 day p.i.; group 3 ($n = 10$), treatment initiated 3 days p.i.; group 4 ($n = 10$), treatment initiated 8 days p.i. (when the first clinical signs appeared); and group 5 ($n = 10$), control animals, treated with vehicle only. 7-Deaza-2'-CMA was freshly solubilized in sterile saline buffer before each injection and administered to the animals for 19 (group 1), 18 (group 2), 16 (group 3), and 11 (group 4) days. The clinical scores, body weights, and survival rates of WNV-infected mice were monitored daily over 28 days. Illness signs were evaluated as follows: 0 for no symptoms; 1 for ruffled fur; 2 for slowing of activity or hunched posture; 3 for asthenia or mild paralysis; 4 for lethargic, tremor, or complete paralysis of the limbs; 5 for death. All mice exhibiting disease consistent with clinical score 4 were terminated humanely (cervical dislocation) immediately upon detection.

For determination of the WNV titer in mouse brains, a group of 6-week-old BALB/c mice were infected subcutaneously with 1,000 PFU of WNV and immediately treated with 7-deaza-2'-CMA twice daily at a concentration of 25 mg/kg. Ten days postinfection, when the clinical symptoms of WNV disease were clearly observable in mice treated with vehicle only, the animals were sacrificed and the brains were collected, weighed, homogenized using Precellys 24 (Bertin Technologies), and prepared as 20% (wt/vol) suspensions in saline. Each homogenate was centrifuged at 5,000 \times g, and the supernatant medium was used to determine virus titer by plaque assay.

Statistical analysis. Data are expressed as means \pm standard deviation (SDs), and the significance of differences between groups was evaluated by the Mann-Whitney *U* test or analysis of variance (ANOVA). Survival rates were analyzed using the log rank Mantel-Cox test. All tests were performed using GraphPad Prism 7.04 (GraphPad Software, Inc., USA). A *P* value of <0.05 was considered significant.

ACKNOWLEDGMENT

This study was supported by a grant from the Czech Science Foundation (grant 16-20054S). The funder had no role in the study design, data collection and analysis, decision to publish, or preparation of the manuscript.

REFERENCES

- Baier A. 2011. Flaviviral infections and potential targets for antiviral therapy, p 89–104. In Ruzek D (ed), *Flavivirus encephalitis*. InTech, Rijeka, Croatia.
- Beasley DWC, Davis CT, Whiteman M, Granwehr B, Kinney RM, Barrett ADT. 2004. Molecular determinants of virulence of West Nile virus in North America. *Arch Virol* 18:35–41.
- Chambers TJ, Hahn CS, Galler R, Rice CM. 1990. Flavivirus genome organization, expression, and replication. *Annu Rev Microbiol* 44: 649–688. <https://doi.org/10.1146/annurev.mi.44.100190.003245>.
- Khromykh AA, Sedlak PL, Guyatt KJ, Hall RA, Westaway EG. 1999. Efficient *trans*-complementation of the flavivirus Kunjin NS5 protein but not of the NS1 protein requires its coexpression with other components of the viral replicase. *J Virol* 73:10272–10280.
- Lin RJ, Chang BL, Yu HP, Liao CL, Lin YL. 2006. Blocking of interferon-induced Jak-Stat signaling by Japanese encephalitis virus NS5 through a protein tyrosine phosphatase-mediated mechanism. *J Virol* 80: 5908–5918. <https://doi.org/10.1128/JVI.02714-05>.
- Liu WJ, Wang XJ, Mokhonov VV, Shi PY, Randall R, Khromykh AA. 2005. Inhibition of interferon signaling by the New York 99 strain and Kunjin subtype of West Nile virus involves blockage of STAT1 and STAT2 activation by nonstructural proteins. *J Virol* 79:1934–1942. <https://doi.org/10.1128/JVI.79.3.1934-1942.2005>.
- Hubalek Z. 2000. European experience with the West Nile virus ecology and epidemiology: could it be relevant for the new world? *Viral Immunol* 13:415–426.
- Smithburn K, Hughes T, Burke A, Paul J. 1940. A neurotropic virus isolated from the blood of a native of Uganda. *Am J Trop Med Hyg* 20:471–492. <https://doi.org/10.4269/ajtmh.1940.s1-20.471>.

9. Dauphin G, Zientara S, Zeller H, Murgue B. 2004. West Nile: worldwide current situation in animals and humans. *Comp Immunol Microbiol Infect Dis* 27:343–355. <https://doi.org/10.1016/j.cimid.2004.03.009>.
10. Deardorff E, Estrada-Franco J, Brault AC, Navarro-Lopez R, Campomanes-Cortes A, Paz-Ramirez P, Solis-Hernandez M, Ramey WN, Davis CT, Beasley DW, Tesh RB, Barrett AD, Weaver SC. 2006. Introductions of West Nile virus strains to Mexico. *Emerg Infect Dis* 12:314–318. <https://doi.org/10.3201/eid1202.050871>.
11. Komar N, Clark GG. 2006. West Nile virus activity in Latin America and the Caribbean. *Rev Panam Salud Publica* 19:112–117.
12. Mostashari F, Bunning ML, Kitsutani PT, Singer DA, Nash D, Cooper MJ, Katz N, Liljebjelke KA, Biggerstaff BJ, Fine AD, Layton MC, Mullin SM, Johnson AJ, Martin DA, Hayes EB, Campbell GL. 2001. Epidemic West Nile encephalitis, New York, 1999: results of a household-based seroepidemiological survey. *Lancet* 358:261–264. [https://doi.org/10.1016/S0140-6736\(01\)05480-0](https://doi.org/10.1016/S0140-6736(01)05480-0).
13. Tsai TF, Popovici F, Cernescu C, Campbell GL, Nedelcu NI. 1998. West Nile encephalitis epidemic in southeastern Romania. *Lancet* 352:767–771.
14. Lim SM, Koraka P, Osterhaus ADME, Martina BEE. 2011. West Nile virus: immunity and pathogenesis. *Viruses* 3:811–828. <https://doi.org/10.3390/v3060811>.
15. Chowdhury MY, Lang R, Nassar F, Ben-David D, Giladi M, Rubinshtein E, Itzhaki A, Mishal J, Siegman-Igra Y, Kitzes R, Pick N, Landau Z, Wolf D, Bin H, Mendelson E, Pitlik SD, Weinberger M. 2001. Clinical characteristics of the West Nile fever outbreak, Israel, 2000. *Emerg Infect Dis* 7:675–678. <https://doi.org/10.3201/eid0704.010414>.
16. Nash D, Mostashari F, Fine A, Miller J, O'Leary D, Murray K, Huang A, Rosenberg A, Greenberg A, Sherman M, Wong S, Layton M, Campbell GL, Roehrig JT, Gubler DJ, Shieh WJ, Zaki S, Smith P. 2001. The outbreak of West Nile virus infection in the New York City area in 1999. *N Engl J Med* 344:1807–1814. <https://doi.org/10.1056/NEJM200106143442401>.
17. Samuel MA, Diamond MS. 2006. Pathogenesis of West Nile virus infection: a balance between virulence, innate and adaptive immunity, and viral evasion. *J Virol* 80:9349–9360. <https://doi.org/10.1128/JVI.01122-06>.
18. De Clercq E. 2011. A 40-year journey in search of selective antiviral chemotherapy. *Annu Rev Pharmacol Toxicol* 51:1–24. <https://doi.org/10.1146/annurev-pharmtox-010510-100228>.
19. De Clercq E. 2004. Antivirals and antiviral strategies. *Nat Rev Microbiol* 2:704–720. <https://doi.org/10.1038/nrmicro975>.
20. De Clercq E. 2008. Emerging antiviral drugs. *Expert Opin Emerg Drugs* 13:393–416. <https://doi.org/10.1517/14728214.13.3.393>.
21. De Clercq E, Neyts J. 2009. Antiviral agents acting as DNA or RNA chain terminators. *Handb Exp Pharmacol* 189:53–84. https://doi.org/10.1007/978-3-540-79086-0_3.
22. Benhamou Y, Tubiana R, Thibault V. 2003. Tenofovir disoproxil fumarate in patients with HIV and lamivudine-resistant hepatitis B virus. *N Engl J Med* 348:177–178. <https://doi.org/10.1056/NEJM200301093480218>.
23. De Clercq E, Holý A. 2005. Acyclic nucleoside phosphonates: A key class of antiviral drugs. *Nat Rev Drug Discov* 4:928–940. <https://doi.org/10.1038/nrd1877>.
24. Huang YS, Chang SY, Sheng WH, Sun HY, Lee KY, Chuang YC, Su YC, Liu WC, Hung CC, Chang SC. 2016. Virological response to tenofovir disoproxil fumarate in HIV-positive patients with lamivudine-resistant hepatitis B virus coinfection in an area hyperendemic for hepatitis B virus infection. *PLoS One* 11:e0169228. <https://doi.org/10.1371/journal.pone.0169228>.
25. Ray AS, Fordyce MW, Hitchcock MJM. 2016. Tenofovir alafenamide: a novel prodrug of tenofovir for the treatment of human immunodeficiency virus. *Antiviral Res* 125:63–70. <https://doi.org/10.1016/j.antiviral.2015.11.009>.
26. Stedman C. 2014. Sofosbuvir, a NS5B polymerase inhibitor in the treatment of hepatitis C: a review of its clinical potential. *Therap Adv Gastroenterol* 7:131–140. <https://doi.org/10.1177/1756283X13515825>.
27. Eyer L, Šmidková M, Nencka R, Neča J, Kastl T, Palus M, De Clercq E, Růžek D. 2016. Structure-activity relationships of nucleoside analogues for inhibition of tick-borne encephalitis virus. *Antiviral Res* 133:119–129. <https://doi.org/10.1016/j.antiviral.2016.07.018>.
28. Kumar M, O'Connell M, Namekar M, Nerurkar VR. 2014. Infection with non-lethal West Nile virus Eg101 strain induces immunity that protects mice against the lethal West Nile virus NY99 strain. *Viruses* 6:2328–2339. <https://doi.org/10.3390/v6062328>.
29. Eldrup AB, Allerson CR, Bennett CF, Bera S, Bhat B, Bhat N, Bosserman MR, Brooks J, Burlein C, Carroll SS, Cook PD, Getty KL, MacCoss M, McMasters DR, Olsen DB, Prakash TP, Prhacv M, Song QL, Tomassini JE, Xia J. 2004. Structure-activity relationship of purine ribonucleosides for inhibition of hepatitis C virus RNA-dependent RNA polymerase. *J Med Chem* 47:2283–2295. <https://doi.org/10.1021/jm030424e>.
30. Klumpp K, Leveque V, Le PS, Ma H, Jiang WR, Kang HS, Granycome C, Singer M, Laxton C, Hang JQ, Sarma K, Smith DB, Heindl D, Hobbs CJ, Merrett JH, Symons J, Cammack N, Martin JA, Devos R, Najera I. 2006. The novel nucleoside analog R1479 (4'-azidoctidine) is a potent inhibitor of NS5B-dependent RNA synthesis and hepatitis C virus replication in cell culture. *J Biol Chem* 281:3793–3799. <https://doi.org/10.1074/jbc.M510195200>.
31. Klumpp K, Kalayanov G, Ma H, Le Pogam S, Leveque V, Jiang WR, Inocencio N, De Witte A, Rajyaguru S, Tai E, Chanda S, Irwin MR, Sund C, Winqvist A, Maltseva T, Eriksson S, Usova E, Smith M, Alker A, Najera I, Cammack N, Martin JA, Johansson NG, Smith DB. 2008. 2'-Deoxy-4'-azido nucleoside analogs are highly potent inhibitors of hepatitis C virus replication despite the lack of 2'-alpha-hydroxyl groups. *J Biol Chem* 283:2167–2175. <https://doi.org/10.1074/jbc.M708929200>.
32. Migliaccio G, Tomassini JE, Carroll SS, Tomei L, Altamura S, Bhat B, Bartholomew L, Bosserman MR, Ceccacci A, Colwell LF, Cortese R, De Francesco R, Eldrup AB, Getty KL, Hou XS, LaFemina RL, Ludmerer SW, MacCoss M, McMasters DR, Stahlhut MW, Olsen DB, Hazuda DJ, Flores OA. 2003. Characterization of resistance to non-obligate chain-terminating ribonucleoside analogs that inhibit hepatitis C virus replication *in vitro*. *J Biol Chem* 278:49164–49170. <https://doi.org/10.1074/jbc.M305041200>.
33. Olsen DB, Eldrup AB, Bartholomew L, Bhat B, Bosserman MR, Ceccacci A, Colwell LF, Fay JF, Flores OA, Getty KL, Grobler JA, LaFemina RL, Markel EJ, Migliaccio G, Prhacv M, Stahlhut MW, Tomassini JE, MacCoss M, Hazuda DJ, Carroll SS. 2004. A 7-deaza-adenosine analog is a potent and selective inhibitor of hepatitis C virus replication with excellent pharmacokinetic properties. *Antimicrob Agents Chemother* 48:3944–3953. <https://doi.org/10.1128/AAC.48.10.3944-3953.2004>.
34. Smith DB, Kalayanov G, Sund C, Winqvist A, Pinho P, Maltseva T, Morison V, Leveque V, Rajyaguru S, Le Pogam S, Najera I, Benkestock K, Zhou XX, Maag H, Cammack N, Martin JA, Swallow S, Johansson NG, Klumpp K, Smith M. 2009. The design, synthesis, and antiviral activity of 4'-azidoctidine analogues against hepatitis C virus replication: the discovery of 4'-azidoarabincytidine. *J Med Chem* 52:219–223. <https://doi.org/10.1021/jm800981y>.
35. Sofía MJ, Chang W, Furman PA, Mosley RT, Ross BS. 2012. Nucleoside, nucleotide, and non-nucleoside inhibitors of hepatitis C virus NS5B RNA-dependent RNA-polymerase. *J Med Chem* 55:2481–2531. <https://doi.org/10.1021/jm201384j>.
36. Eyer L, Kondo H, Zouharova D, Hirano M, Valdés JJ, Muto M, Kastl T, Kobayashi S, Haviernik J, Igarashi M, Kariwa H, Vaculovicova M, Cerny J, Kizek R, Kröger A, Lienenklaus S, Dejmeck M, Nencka R, Palus M, Salat J, De Clercq E, Yoshii K, Ruzek D. 2017. Escape of tick-borne flavivirus from 2'-C-methylated nucleoside antivirals is mediated by a single conservative mutation in NS5 that has a dramatic effect on viral fitness. *J Virol* 91:e01028-17. <https://doi.org/10.1128/JVI.01028-17>.
37. Eyer L, Nencka R, Huvarová I, Palus M, Joao Alves M, Gould EA, De Clercq E, Růžek D. 2016. Nucleoside inhibitors of Zika virus. *J Infect Dis* 214:707–711. <https://doi.org/10.1093/infdis/jiw226>.
38. Eyer L, Valdés JJ, Gil VA, Nencka R, Hřebabecý H, Šála M, Salát J, Černý J, Palus M, De Clercq E, Růžek D. 2015. Nucleoside inhibitors of tick-borne encephalitis virus. *Antimicrob Agents Chemother* 59:5483–5493. <https://doi.org/10.1128/AAC.00807-15>.
39. Flint M, McMullan LK, Dodd KA, Bird BH, Khristova ML, Nichol ST, Spiropoulou CF. 2014. Inhibitors of the tick-borne, hemorrhagic fever-associated flaviviruses. *Antimicrob Agents Chemother* 58:3206–3216. <https://doi.org/10.1128/AAC.02393-14>.
40. Julander JG, Jha AK, Choi JA, Jung KH, Smeed DF, Morrey JD, Chu CK. 2010. Efficacy of 2'-C-methylcytidine against yellow fever virus in cell culture and in a hamster model. *Antiviral Res* 86:261–267. <https://doi.org/10.1016/j.antiviral.2010.03.004>.
41. Lanko K, Eggermont K, Patel A, Kaptein S, Delang L, Verfaillie CM, Neyts J. 2017. Replication of the Zika virus in different iPSC-derived neuronal cells and implications to assess efficacy of antivirals. *Antiviral Res* 145:82–86. <https://doi.org/10.1016/j.antiviral.2017.07.010>.
42. Lee JC, Tseng CK, Wu YH, Kaushik-Basu N, Lin CK, Chen WC, Wu HN. 2015. Characterization of the activity of 2'-C-methylcytidine against dengue virus replication. *Antiviral Res* 116:1–9. <https://doi.org/10.1016/j.antiviral.2015.01.002>.

43. Mateo R, Nagamine CM, Kirkegaard K. 2015. Suppression of drug resistance in dengue virus. *mBio* 6:e01960-15. <https://doi.org/10.1128/mBio.01960-15>.
44. Hercik K, Brynda J, Nencka R, Boura E. 2017. Structural basis of Zika virus methyltransferase inhibition by sinefungin. *Arch Virol* 162:2091–2096. <https://doi.org/10.1007/s00705-017-3345-x>.
45. Zmurko J, Marques RE, Schols D, Verbeken E, Kaptein SJF, Neyts J. 2016. The viral polymerase inhibitor 7-deaza-2'-C-methyladenosine is a potent inhibitor of *in vitro* Zika virus replication and delays disease progression in a robust mouse infection model. *PLoS Negl Trop Dis* 10:e0004695. <https://doi.org/10.1371/journal.pntd.0004695>.
46. Lefebvre DJ, De Vleeschauwer AR, Goris N, Kollanur D, Billiet A, Muraio L, Neyts J, De Clercq K. 2014. Proof of concept for the inhibition of foot-and-mouth disease virus replication by the anti-viral drug 2'-C-methylcytidine in severe combined immunodeficient mice. *Transbound Emerg Dis* 61:E89–E91. <https://doi.org/10.1111/tbed.12069>.
47. Rocha-Pereira J, Jochmans D, Dallmeier K, Leyssen P, Cunha R, Costa I, Nascimento MS, Neyts J. 2012. Inhibition of norovirus replication by the nucleoside analogue 2'-C-methylcytidine. *Biochem Biophys Res Commun* 427:796–800. <https://doi.org/10.1016/j.bbrc.2012.10.003>.
48. Rocha-Pereira J, Jochmans D, Debing Y, Verbeken E, Nascimento MSJ, Neyts J. 2013. The viral polymerase inhibitor 2'-C-methylcytidine inhibits Norwalk virus replication and protects against norovirus-induced diarrhea and mortality in a mouse model. *J Virol* 87:11798–11805. <https://doi.org/10.1128/JVI.02064-13>.
49. Balestri F, Barsotti C, Lutzenberger L, Camici M, Ipata PL. 2007. Key role of uridine kinase and uridine phosphorylase in the homeostatic regulation of purine and pyrimidine salvage in brain. *Neurochem Int* 51: 517–523. <https://doi.org/10.1016/j.neuint.2007.06.007>.
50. Lashkov AA, Shchekotikhin AA, Shtil AA, Sotnichenko SE, Mikhailov AM. 2016. Modified 5-fluorouracil: uridine phosphorylase inhibitor. *Crystallogr Rep* 61:826–829. <https://doi.org/10.1134/S1063774516050138>.
51. Yin Z, Chen YL, Schul W, Wang QY, Gu F, Duraiswamy J, Kondreddi RR, Niyomrattanakit P, Lakshminarayana SB, Goh A, Xu HY, Liu W, Liu B, Lim JY, Ng CY, Qing M, Lim CC, Yip A, Wang G, Chan WL, Tan HP, Lin K, Zhang B, Zou G, Bernard KA, Garrett C, Beltz K, Dong M, Weaver M, He H, Pichota A, Dartois V, Keller TH, Shi PY. 2009. An adenosine nucleoside inhibitor of dengue virus. *Proc Natl Acad Sci U S A* 106:20435–20439. <https://doi.org/10.1073/pnas.0907010106>.
52. Eyer L, Nencka R, de Clercq E, Seley-Radtke K, Růžek D. 2018. Nucleoside analogs as a rich source of antiviral agents active against arthropod-borne flaviviruses. *Antivir Chem Chemother* 26:2040206618761299. <https://doi.org/10.1177/2040206618761299>.
53. Roe K, Kumar M, Lum S, Orillo B, Nerurkar VR, Verma S. 2012. West Nile virus-induced disruption of the blood-brain barrier in mice is characterized by the degradation of the junctional complex proteins and increase in multiple matrix metalloproteinases. *J Gen Virol* 93:1193–1203. <https://doi.org/10.1099/vir.0.040899-0>.
54. Styer LM, Lim PY, Louie KL, Albright RG, Kramer LD, Bernard KA. 2011. Mosquito saliva causes enhancement of West Nile virus infection in mice. *J Virol* 85:1517–1527. <https://doi.org/10.1128/JVI.01112-10>.
55. Schul W, Chen YL, Yin Z, Keller T, Shi PY. 2010. An adenosine nucleoside inhibitor of dengue virus. *Antiviral Res* 86:A24–A25. <https://doi.org/10.1016/j.antiviral.2010.02.347>.
56. Arnold JJ, Sharma SD, Feng JY, Ray AS, Smidansky ED, Kireeva ML, Cho A, Perry J, Vela JE, Park Y, Xu Y, Tian Y, Babusis D, Barauskus O, Peterson BR, Gnat A, Kashlev M, Zhong W, Cameron CE. 2012. Sensitivity of mitochondrial transcription and resistance of RNA polymerase II dependent nuclear transcription to antiviral ribonucleosides. *PLoS Pathog* 8:e1003030. <https://doi.org/10.1371/journal.ppat.1003030>.
57. Chen YL, Yin Z, Lakshminarayana SB, Qing M, Schul W, Duraiswamy J, Kondreddi RR, Goh A, Xu HY, Yip A, Liu B, Weaver M, Dartois V, Keller TH, Shi PY. 2010. Inhibition of dengue virus by an ester prodrug of an adenosine analog. *Antimicrob Agents Chemother* 54:3255–3261. <https://doi.org/10.1128/AAC.00397-10>.
58. Chen YL, Yin Z, Duraiswamy J, Schul W, Lim CC, Liu B, Xu HY, Qing M, Yip A, Wang G, Chan WL, Tan HP, Lo M, Liung S, Kondreddi RR, Rao R, Gu H, He H, Keller TH, Shi PY. 2010. Inhibition of dengue virus RNA synthesis by an adenosine nucleoside. *Antimicrob Agents Chemother* 54: 2932–2939. <https://doi.org/10.1128/AAC.00140-10>.
59. Ferreira AC, Zaverucha-do-Valle C, Reis PA, Barbosa-Lima G, Vieira YR, Mattos M, Silva PP, Sacramento C, de Castro Faria Neto HC, Campanati L, Tanuri A, Brüning K, Bozza FA, Bozza PT, Souza TML. 2017. Sofosbuvir protects Zika virus-infected mice from mortality, preventing short- and long-term sequelae. *Sci Rep* 7:9409. <https://doi.org/10.1038/s41598-017-09797-8>.
60. Kozuch O, Mayer V. 1975. Pig kidney epithelial (PS) cells: a perfect tool for study of flaviviruses and some other arboviruses. *Acta Virol* 19:498.
61. Melnick JL, Paul JR, Riordan JT, Barnett VH, Goldblum N, Zabin E. 1951. Isolation from human sera in Egypt of a virus apparently identical to West Nile virus. *Proc Soc Exp Biol Med* 77:661–665.
62. Rudolf I, Bakonyi T, Sebesta O, Mendel J, Peško J, Betášová L, Blažejová H, Venclíková K, Straková P, Nowotny N, Hubálek Z. 2014. West Nile virus lineage 2 isolated from *Culex modestus* mosquitoes in the Czech Republic, 2013: expansion of the European WNV endemic area to the North? *Euro Surveill* 19:2–5. <https://www.eurosurveillance.org/content/10.2807/1560-7917.ES2014.19.31.20867>.
63. Eyer L, Zouharová D, Širmarová J, Fojtíková M, Štefánik M, Haviernik J, Nencka R, de Clercq E, Růžek D. 2017. Antiviral activity of the adenosine analogue BCX4430 against West Nile virus and tick-borne flaviviruses. *Antiviral Res* 142:63–67. <https://doi.org/10.1016/j.antiviral.2017.03.012>.
64. De Madrid AT, Porterfield JS. 1969. A simple micro-culture method for study of group B arboviruses. *Bull World Health Organ* 40:113–121.



Escape of Tick-Borne Flavivirus from 2'-C-Methylated Nucleoside Antivirals Is Mediated by a Single Conservative Mutation in NS5 That Has a Dramatic Effect on Viral Fitness

Ludek Eyer,^{a,b} Hirofumi Kondo,^c Darina Zouharova,^a Minato Hirano,^c James J. Valdés,^{a,b} Memi Muto,^c Tomas Kastl,^a Shintaro Kobayashi,^c Jan Haviernik,^a Manabu Igarashi,^d Hiroaki Kariwa,^c Marketa Vaculovicova,^{e,f} Jiri Cerny,^{a,b} Rene Kizek,^g Andrea Kröger,^h Stefan Lienenklaus,ⁱ Milan Dejmk, ^j Radim Nencka,^j Martin Palus,^{a,b} Jiri Salat,^a Erik De Clercq,^k Kentaro Yoshii,^c Daniel Ruzek^{a,b}

Department of Virology, Veterinary Research Institute, Brno, Czech Republic^a; Institute of Parasitology, Biology Centre of the Czech Academy of Sciences, Ceske Budejovice, Czech Republic^b; Laboratory of Public Health, Graduate School of Veterinary Medicine, Hokkaido University, Sapporo, Japan^c; Research Center for Zoonosis Control, Hokkaido University, Sapporo, Japan^d; Department of Chemistry and Biochemistry, Mendel University in Brno, Brno, Czech Republic^e; Central European Institute of Technology, Brno University of Technology, Brno, Czech Republic^f; Central Laboratories, Faculty of Pharmacy, University of Veterinary and Pharmaceutical Sciences, Brno, Czech Republic^g; Institute for Medical Microbiology, Otto von Guericke University Magdeburg, Magdeburg, Germany^h; Institute for Laboratory Animal Science, Hannover Medical School, Hannover, Germanyⁱ; Institute of Organic Chemistry and Biochemistry, Czech Academy of Sciences, Prague, Czech Republic^j; Rega Institute for Medical Research, KU Leuven, Leuven, Belgium^k

ABSTRACT Tick-borne encephalitis virus (TBEV) causes a severe and potentially fatal neuroinfection in humans. Despite its high medical relevance, no specific antiviral therapy is currently available. Here we demonstrate that treatment with a nucleoside analog, 7-deaza-2'-C-methyladenosine (7-deaza-2'-CMA), substantially improved disease outcomes, increased survival, and reduced signs of neuroinfection and viral titers in the brains of mice infected with a lethal dose of TBEV. To investigate the mechanism of action of 7-deaza-2'-CMA, two drug-resistant TBEV clones were generated and characterized. The two clones shared a signature amino acid substitution, S603T, in the viral NS5 RNA-dependent RNA polymerase (RdRp) domain. This mutation conferred resistance to various 2'-C-methylated nucleoside derivatives, but no cross-resistance was seen with other nucleoside analogs, such as 4'-C-azidocytidine and 2'-deoxy-2'-beta-hydroxy-4'-azidocytidine (RO-9187). All-atom molecular dynamics simulations revealed that the S603T RdRp mutant repels a water molecule that coordinates the position of a metal ion cofactor as 2'-C-methylated nucleoside analogs approach the active site. To investigate its phenotype, the S603T mutation was introduced into a recombinant TBEV strain (Oshima-IC) generated from an infectious cDNA clone and into a TBEV replicon that expresses a reporter luciferase gene (Oshima-REP-luc2A). The mutants were replication impaired, showing reduced growth and a small plaque size in mammalian cell culture and reduced levels of neuroinvasiveness and neurovirulence in rodent models. These results indicate that TBEV resistance to 2'-C-methylated nucleoside inhibitors is conferred by a single conservative mutation that causes a subtle atomic effect within the active site of the viral NS5 RdRp and is associated with strong attenuation of the virus.

IMPORTANCE This study found that the nucleoside analog 7-deaza-2'-C-methyladenosine (7-deaza-2'-CMA) has high antiviral activity against tick-borne encephalitis virus (TBEV), a pathogen that causes severe human neuroinfections in large areas of

Received 19 June 2017 Accepted 1 August 2017

Accepted manuscript posted online 16 August 2017

Citation Eyer L, Kondo H, Zouharova D, Hirano M, Valdés JJ, Muto M, Kastl T, Kobayashi S, Haviernik J, Igarashi M, Kariwa H, Vaculovicova M, Cerny J, Kizek R, Kröger A, Lienenklaus S, Dejmk M, Nencka R, Palus M, Salat J, De Clercq E, Yoshii K, Ruzek D. 2017. Escape of tick-borne flavivirus from 2'-C-methylated nucleoside antivirals is mediated by a single conservative mutation in NS5 that has a dramatic effect on viral fitness. *J Virol* 91:e01028-17. <https://doi.org/10.1128/JVI.01028-17>.

Editor Terence S. Dermody, University of Pittsburgh School of Medicine

Copyright © 2017 American Society for Microbiology. All Rights Reserved.

Address correspondence to Daniel Ruzek, ruzekd@paru.cas.cz.

K.Y. and D.R. are co-senior authors of this article.

Europe and Asia and for which there is currently no specific therapy. Treating mice infected with a lethal dose of TBEV with 7-deaza-2'-CMA resulted in significantly higher survival rates and reduced the severity of neurological signs of the disease. Thus, this compound shows promise for further development as an anti-TBEV drug. It is important to generate drug-resistant mutants to understand how the drug works and to develop guidelines for patient treatment. We generated TBEV mutants that were resistant not only to 7-deaza-2'-CMA but also to a broad range of other 2'-C-methylated antiviral medications. Our findings suggest that combination therapy may be used to improve treatment and reduce the emergence of drug-resistant viruses during nucleoside analog therapy for TBEV infection.

KEYWORDS antiviral agents, antiviral therapy, escape mutant, tick-borne encephalitis virus, tick-borne pathogens

Nucleoside and nucleotide analogs represent an important class of therapeutic antiviral agents that are commonly used to treat many life-threatening viral diseases (1, 2). In particular, nucleoside/tide derivatives are a backbone of treatment for HIV/AIDS and for chronic hepatitis B virus (HBV) infection (3), with the nucleotide derivative sofosbuvir acting to revolutionize the treatment of chronic hepatitis C virus (HCV) infection (4, 5). The constant struggle to develop novel nucleoside/tide analogs as potential antiviral agents against HCV has yielded numerous interesting derivatives (6) that are potential treatments for diseases caused by other members of the *Flaviviridae* family. Indeed, 2'-methyl nucleoside derivatives act as polymerase reaction terminators (7, 8) and are active against HCV; they also have a profound antiviral effect against several medically important flaviviruses. For instance, 7-deaza-2'-C-methyladenosine (7-deaza-2'-CMA; also known as MK-608) (Fig. 1A), a 2'-methyl nucleoside analog originally developed as an inhibitor of HCV by Merck Research Laboratories (9), has strong antiviral effects against mosquito-borne members of the genus *Flavivirus*, such as dengue virus (DENV) (10) and Zika virus (11, 12). We recently found that 7-deaza-2'-CMA has inhibitory activity *in vitro* against tick-borne encephalitis virus (TBEV), the most medically important tick-borne flavivirus (13, 14).

TBEV is the causative agent of tick-borne encephalitis (TBE), a potentially deadly neuroinfection that is prevalent in large areas of Europe and northern Asia. Despite available effective TBEV vaccines, the number of TBE cases continues to increase in Europe, and the risk areas continue to expand (15, 16). The severities of TBE clinical manifestations range from a mild flu-like infection to meningitis, encephalitis, and meningoencephalitis/radiculitis, with a 10% to 20% risk of long-lasting or permanent neuropsychiatric sequelae (17). Fatality rates range from <2% in Europe to up to 20% in Russia (17). No specific antiviral therapy is currently available; thus, there is an urgent need for efficient drugs to treat patients with TBE (17). Currently, 2'-methyl nucleoside derivatives, and 7-deaza-2'-CMA in particular, represent the lead candidates for further development of antivirals and their prodrug forms as effective therapeutics for this disease (13, 14).

Unfortunately, antiviral therapy based on chemical inhibitors of viral replication is often accompanied by the rapid emergence of drug-resistant "escape" mutants, substantially complicating therapy. Experience with the treatment of HIV, HBV, and HCV shows that resistance can develop rapidly with literally all of the direct-acting antiviral agents (18, 19). In the case of RNA viruses, including flaviviruses, the development of drug resistance is mainly related to the high mutation rates caused by the low fidelity of viral RNA-dependent RNA polymerases (RdRps), which introduce 10^{-4} to 10^{-6} error per nucleotide. This, together with a high viral replication rate, can generate highly variable viral populations that are termed quasispecies. Viral quasispecies represent dynamic mutant networks in which individual sequences are continuously diversified and regenerated by mutations, allowing the population to adapt quickly to changes in the environment, such as the presence of an antiviral drug (20, 21). Drug-resistant variants can rapidly become the dominant part of the viral population and lead to

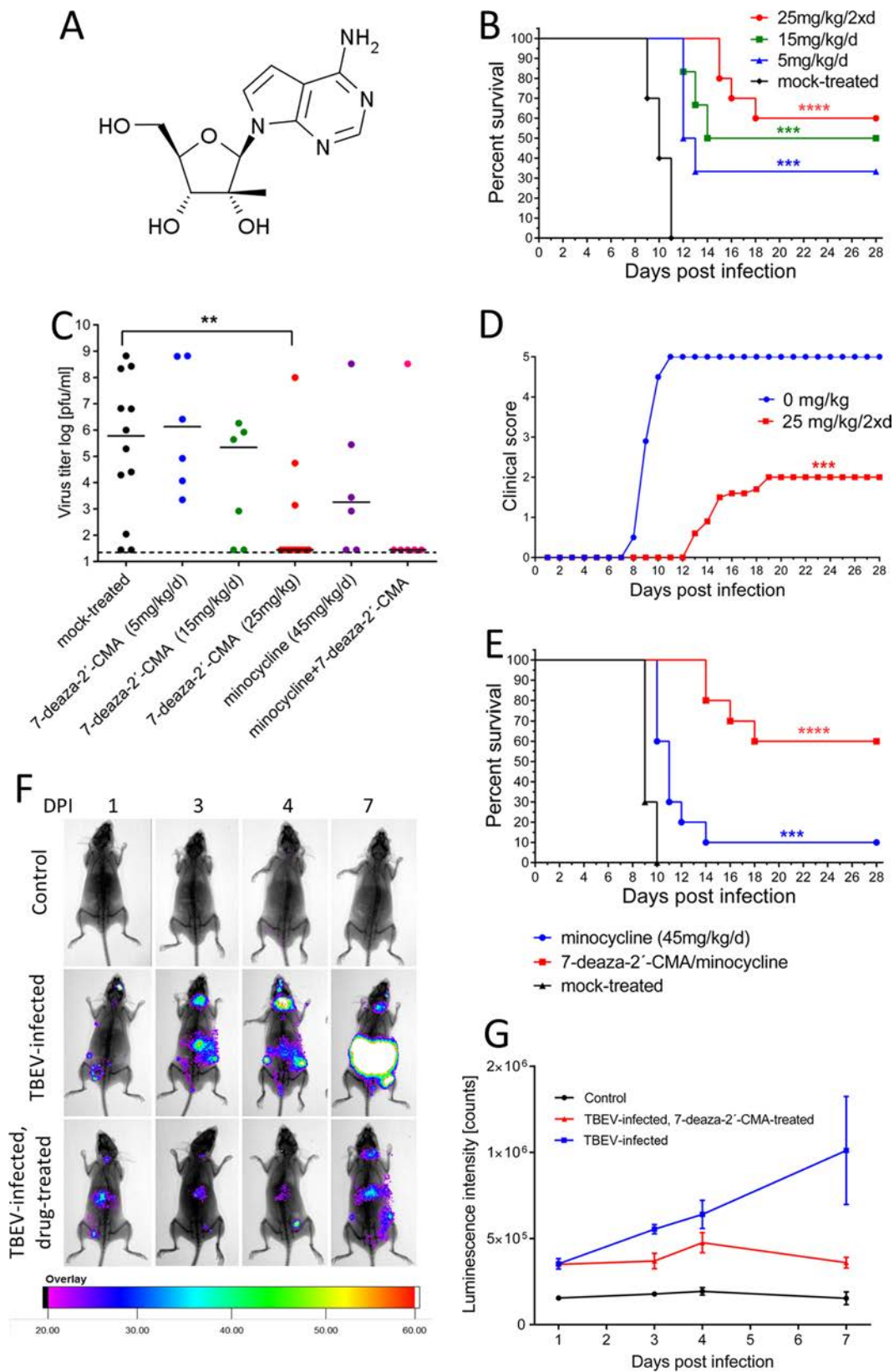


FIG 1 7-Deaza-2'-CMA is effective at treating lethal TBEV infection in a mouse model. (A) Structure of 7-deaza-2'-CMA. (B) Groups of adult BALB/c mice were infected with a lethal dose of TBEV and treated intraperitoneally with the indicated doses of 7-deaza-2'-CMA or mock treated with PBS. Survival was monitored daily for 28 days. (C) Groups of adult BALB/c mice were infected with a lethal dose of TBEV and treated with the indicated dose of 7-deaza-2'-CMA, minocycline, a combination of (Continued on next page)

therapy failure. However, drug-resistant variants often also have a lower replicative capacity or “fitness” than wild-type viruses (22). If the therapy is stopped, the more virulent wild-type virus can again become dominant (22). Thus, it is crucial to identify specific mutations in all antiviral agents that lead to drug resistance, to characterize the replicative capacity of the resistant virus, and to evaluate the risk of potential therapeutic failure.

Here we evaluated the therapeutic effects of 7-deaza-2'-CMA in a lethal mouse model of TBE. We found that 7-deaza-2'-CMA treatment significantly reduced the development of signs of neuroinfection, reduced viral titers in the brain, and increased survival after the infection. We also generated a 7-deaza-2'-CMA-resistant TBEV variant by serial passage of the virus with increasing concentrations of the drug *in vitro*. The fitness of the drug-resistant virus was characterized both *in vitro* and *in vivo* in a mouse model. Whole-genome sequencing was used to identify a specific mutation associated with drug resistance and the phenotype change, and the effect of the identified mutation was confirmed by reverse genetics. The results revealed that a single conservative amino acid substitution in the sequence of the TBEV RNA-dependent RNA polymerase conferred resistance to a broad spectrum of 2'-methylated nucleoside inhibitors and strongly reduced viral replication fitness and viral neuroinvasiveness. In the absence of 7-deaza-2'-CMA, there was a rapid reversion to the wild-type genotype and phenotype *in vitro* but not *in vivo*. Taken together, these results have important implications for the development of drugs based on 2'-methylated nucleoside analogs as therapy for infections caused by flaviviruses.

RESULTS

7-Deaza-2'-CMA is effective at treating lethal TBEV infection in a mouse model.

The antiviral effects of 7-deaza-2'-CMA (Fig. 1A) were examined *in vivo* by use of a mouse model of lethal TBEV infection. Characteristic clinical signs of infection, such as ruffled fur, slowing of activity, asthenia, lethargy, tremor, and mild or complete paralysis of the limbs, typically appeared in TBEV-infected untreated adult BALB/c mice on days 8 to 11 postinfection (p.i.). Subcutaneous infection with 10^3 PFU was 100% lethal, with a mean survival time of 10 ± 1.4 days p.i. (Fig. 1B).

Treatment of TBEV-infected mice with 5 and 15 mg/kg of body weight of 7-deaza-2'-CMA once a day (initiated at the time of virus inoculation and ceased on day 17 p.i.) resulted in survival rates of 35% and 50% ($P < 0.001$) (Fig. 1B), respectively, and was associated with mean survival times of 12.5 ± 0.7 and 13 ± 1.4 days p.i., respectively. Treatment of TBEV-infected mice with 25 mg/kg of 7-deaza-2'-CMA that was initiated at the time of infection, administered twice daily, and ceased on day 17 p.i. resulted in a significantly higher survival rate (60%) ($P < 0.0001$) (Fig. 1B) and significantly reduced the development of clinical signs of neuroinfection ($P < 0.001$) (Fig. 1D). The mean survival time of infected and drug-treated mice was approximately 6.5 days longer than that of infected and mock-treated control mice. No apparent toxicity or other side effects were seen in mice treated with the highest dose of 7-deaza-2'-CMA, i.e., 25 mg/kg twice a day, during the entire 28-day monitoring period. Viral titers were significantly reduced in the brains of treated TBEV-infected mice compared to those in the brains of mock-treated TBEV-infected mice ($P < 0.01$) (Fig. 1C).

Mortality following TBEV infection is the result of both direct virus-mediated damage and immunopathology, so we tested whether treatment with a combination of

FIG 1 Legend (Continued)

7-deaza-2'-CMA and minocycline, or PBS. On day 8 p.i., the brains of the mice were collected and homogenized, and the viral titers were determined using a plaque assay. (D) Illness signs were scored as follows: 0, no symptoms; 1, ruffled fur; 2, slowing of activity or hunched posture; 3, asthenia or mild paralysis; 4, lethargy, tremor, or complete paralysis of the limbs; and 5, death. (E) Groups of adult BALB/c mice were infected with a lethal dose of TBEV and treated intraperitoneally with minocycline, with a combination of minocycline and 7-deaza-2'-CMA, or with PBS. Survival was monitored daily for 28 days. (F and G) IFN $\beta^{+/\Delta\beta}$ -luc mice were infected with a lethal dose of TBEV and treated with 7-deaza-2'-CMA or mock treated with PBS. The bioluminescence signal indicating the IFN- β response to virus infection was scanned using a live-animal imaging device (F) and quantified (G). *, $P < 0.05$; **, $P < 0.01$; ***, $P < 0.001$; ****, $P < 0.0001$.

7-deaza-2'-CMA plus minocycline, a drug with immunomodulatory properties, would increase the survival of TBEV-infected mice. TBEV-infected mice were treated with 7-deaza-2'-CMA two times a day (25 mg/kg/dose) and/or with minocycline (45 mg/kg/day). Treatment with minocycline alone resulted in a significantly higher survival rate ($P < 0.001$) (Fig. 1E) and prolonged the mean survival time of the infected mice (11.8 ± 1.7 days). However, the survival rates and mean survival times after infection were comparable for mice treated with the drug combination and mice treated only with 7-deaza-2'-CMA, so the combination therapy showed no additive effects.

To monitor the antiviral effects of therapy with 7-deaza-2'-CMA in mice before the development of the first clinical signs of neuroinfection, we developed a bioluminescence mouse model of TBEV infection based on $\text{IFN}\beta^{+/A}\beta\text{-luc}$ mice (23). This model allowed us to continuously monitor the development of TBEV infection and the effectiveness of antiviral therapy early in infection (Fig. 1F) by visualizing the host's response to the virus. Monitoring reporter activity in uninfected control mice revealed a background-level luminescence signal that was stable over the 7-day experimental period. In TBEV-infected mice, 2 to 3 times higher levels of luminescence signal were detected as early as day 1 p.i. A further increase in the luminescence signal was observed in the brain, lymph nodes, and peritoneal cavity (probably in the spleen and liver) on day 3 p.i. On day 4 p.i., the bioluminescence signal levels were approximately 5 times higher than those of uninfected controls. On day 7 p.i., when the mice showed the first clinical signs of infection, the signal was 7 times higher in the untreated TBEV-infected mice than in the uninfected controls (Fig. 1F).

Treatment of TBEV-infected $\text{IFN}\beta^{+/A}\beta\text{-luc}$ mice with 7-deaza-2'-CMA (25 mg/kg two times a day) significantly reduced the bioluminescence signals at all investigated intervals. A low bioluminescence signal was detected primarily in the peritoneal cavity and/or lymph nodes; the signals in the brain had low values that were close to the background level (Fig. 1F and G).

TBEV resistance to 7-deaza-2'-CMA is associated with a single mutation in the NS5 gene. The generation of drug-resistant mutants is important for understanding how a drug works at the molecular level and can be helpful clinically in terms of guiding treatment. To select viruses that were resistant to 7-deaza-2'-CMA, TBEV was serially passaged in porcine kidney stable (PS) cells in the presence of increasing concentrations of 7-deaza-2'-CMA (Fig. 2A). Two drug-resistant clones were independently obtained after 12 passages with a maximal concentration of 50 μM 7-deaza-2'-CMA. Whole-genome sequence analysis (Sanger method) of the passaged viruses revealed a single mutation, at amino acid position 603 in the NS5 protein, that changed a serine residue to a threonine (Fig. 2B). This corresponded to a $\text{TCT} \rightarrow \text{ACT}$ nucleotide substitution in the NS5 gene. The same substitution was detected in both drug-resistant clones but not in the wild-type virus passaged in the absence of the drug. Sequencing of viruses after each passage revealed that the virus acquired the S603T mutation at passage 4 and that the mutation was retained until the end of the experiment (Fig. 2C). The S603T mutation mapped to the active site of the RNA-dependent RNA polymerase domain of the NS5 protein (Fig. 2D).

The S603T TBEV mutant is resistant to a broad spectrum of 2'-C-methylated nucleoside inhibitors. To test whether the S603T mutation affects the sensitivity of TBEV to other nucleoside inhibitors, we tested a broad spectrum of nucleoside inhibitors to determine their inhibitory effects on TBEV-infected PS cells *in vitro*. A series of 2'-C-methyl-substituted nucleosides, 4'-C-azidocytidine, and RO-9187 were tested for inhibitory activity against both the S603T TBEV mutant and wild-type TBEV. The sensitivity of the S603T TBEV mutant to 7-deaza-2'-CMA (50% effective concentration [EC_{50}] of $>50 \mu\text{M}$) was 46-fold lower than that of the wild-type virus ($\text{EC}_{50} = 1.07 \pm 0.03 \mu\text{M}$) (Table 1). The S603T TBEV mutant showed high levels of cross-resistance to other 2'-C-methyl-modified nucleosides, such as 2'-C-methyladenosine, 2'-C-methylguanosine, 2'-C-methylcytidine, and 2'-C-methyluridine; their inhibitory effects were reduced dramatically (8- to 30-fold) in the S603T TBEV mutant compared to those against the wild-type virus (Fig. 2E). The inhibitory effects of 4'-C-azidocytidine

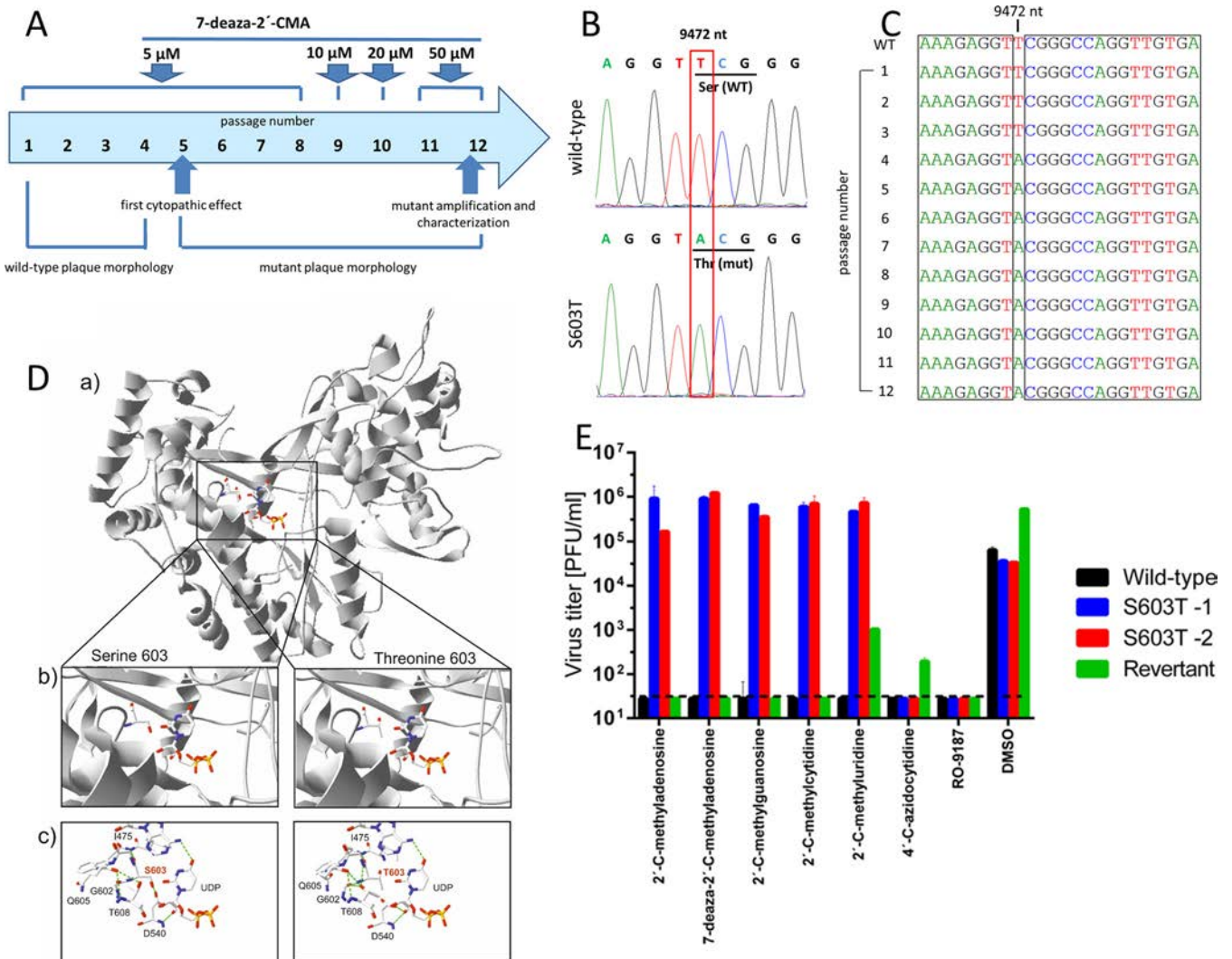


FIG 2 TBEV resistance to 7-deaza-2'-CMA is associated with a single mutation in the NS5 gene. (A) Diagram showing the selection process for the generation of a TBEV strain resistant to 7-deaza-2'-CMA. TBEV was serially passaged in porcine kidney stable (PS) cells in the presence of increasing concentrations of 7-deaza-2'-CMA. (B and C) Whole-genome sequence analysis of the passaged virus revealed a single mutation, at amino acid position 603 in the NS5 protein, that changed a serine residue to a threonine. (D) The S603T mutation was mapped to the active site of the RNA-dependent RNA polymerase domain of the NS5 protein. Structural differences between the wild-type (S603) and mutated (T603) TBEV NS5 polymerases were examined. (a) Models of the wild-type and mutated TBEV NS5 polymerases were created by homology modeling using the structures of the West Nile virus (WNV) (PDB entry 2HFZ), dengue virus (DENV) (PDB entries 2J7U, 4V0Q, and 4V0R), and Japanese encephalitis virus (JEV) (PDB entry 4K6M) polymerases in MODELLER. (b) Closer view of the polymerase active sites. (c) Differences in the active site structures, showing changes in the hydrogen bond network. (E) The sensitivity or resistance of wild-type TBEV, the S603T TBEV mutant, and the revertant to a broad spectrum of diverse nucleoside inhibitors was evaluated in TBEV-infected PS cells *in vitro*. The S603T TBEV mutant showed high levels of resistance to a broad spectrum of 2'-C-methylated nucleoside inhibitors.

and its stereochemical counterpart, RO-9187, were not affected in the S603T TBEV mutant, indicating an absence of cross-resistance between 4'-C-azido-modified and 2'-C-methylated nucleosides (Fig. 2E).

TBEV NS5 S603T escape mechanism from 7-deaza-2'-CMA as determined using all-atom molecular dynamics simulation. All-atom stochastic software (24, 25) was used to determine how the NS5 polymerase from the S603T TBEV mutant helps the virus to escape 2'-C-methylated nucleoside triphosphates (NTPs). The starting position for each NTP (namely, ATP, 2'-C-methyladenosine, 2'-C-methylcytidine, and 7-deaza-2'-CMA) was ~18 Å from the polymerase active site of the wild type and the S603T TBEV mutant via the NTP tunnel. Measurements were obtained for the root mean square deviation (RMSD) from the initial wild-type position for the following response variables: NTP, Mn²⁺ ion cofactor, and water molecule. A few water molecules were

TABLE 1 Sensitivities of wild-type and S603T mutant TBEV strains to 2'-C-methylated and 4'-C-azido-modified nucleosides

Compound	EC ₅₀ (μM) ^a (fold increase compared to wild-type value)	
	Wild type	S603T mutant
7-Deaza-2'-C-methyladenosine	1.07 ± 0.03	>50 (>46.7)
2'-C-Methyladenosine	1.69 ± 0.19	>50 (>29.5)
2'-C-Methylguanosine	1.98 ± 0.12	>50 (>25.3)
2'-C-Methylcytidine	2.24 ± 0.27	>50 (>22.3)
2'-C-Methyluridine	5.79 ± 0.15	>50 (>8.6)
4'-C-Azidocytidine	5.45 ± 0.03	5.36 ± 0.21 (0.98)
RO-9187	0.99 ± 0.00	1.13 ± 0.21 (1.14)

^aDetermined from three independent experiments. EC₅₀s were calculated as concentrations giving a 50% reduction of the viral titer by using the Reed-Muench method.

selected based on the following 2 criteria (since over 20 water molecules were included in the simulations): (i) the water molecule must be in close proximity to the NTP and substrate binding residues, i.e., the catalytic, priming, and interrogating residues (26); and (ii) the water molecule must have an RMSD of >0.5 Å from its initial position for all NTPs and strains.

Two-way analysis of variance (ANOVA) was performed (Table 2). The explanatory variables (NTP and strain) were both significant (*P* < 0.05) for each response variable,

TABLE 2 Descriptive statistics for two-way ANOVA with RMSD data

Molecule and source of variation	df	Sum of squares	Mean square	F value	P value	η ^{2a}
NTP N1						
NTP	3	4,033.08	1,344.36	203.54	<0.0001	0.211
Strain	1	382.39	382.39	57.89	<0.0001	0.020
NTP × strain	3	1,112.68	370.89	56.15	<0.0001	0.058
Error	2,064	13,632.73	6.61			
Water molecule 1						
NTP	3	18.11	6.04	92.33	<0.0001	0.062
Strain	1	113.28	113.28	1,732.35	<0.0001	0.390 ^b
NTP × strain	3	23.96	7.99	122.15	<0.0001	0.083
Error	2,064	134.97				
Water molecule 2						
NTP	3	197.36	65.79	40.17	<0.0001	0.039
Strain	1	1,512.26	1,512.26	923.40	<0.0001	0.296 ^b
NTP × strain	3	13.45	4.49	2.74	0.04	0.003
Error	2,064	3,380.22	1.64			
Water molecule 3						
NTP	3	349.81	116.60	67.72	<0.0001	0.070
Strain	1	397.69	397.69	230.97	<0.0001	0.080
NTP × strain	3	679.31	226.44	131.51	<0.0001	0.136
Error	2,064	3,553.90	1.72			
Mn²⁺ ion A						
NTP	3	385.21	128.40	171.78	<0.0001	0.062
Strain	1	4,006.99	4,006.99	5,360.78	<0.0001	0.649 ^b
NTP × strain	3	240.55	80.18	107.27	<0.0001	0.038
Error	2,064	1,542.76	0.75			
Mn²⁺ ion B						
NTP	3	133.12	44.37	74.31	<0.0001	0.062
Strain	1	128.06	128.06	214.44	<0.0001	0.060
NTP × strain	3	643.12	214.37	358.99	<0.0001	0.301
Error	2,064	1,232.52	0.60			

^aCohen's effect size guideline is as follows: small = 0.01, medium = 0.06, and large = 0.14.

^bLarge effect size (for strain) between wild-type and S603T mutant TBEV NS5 polymerases.

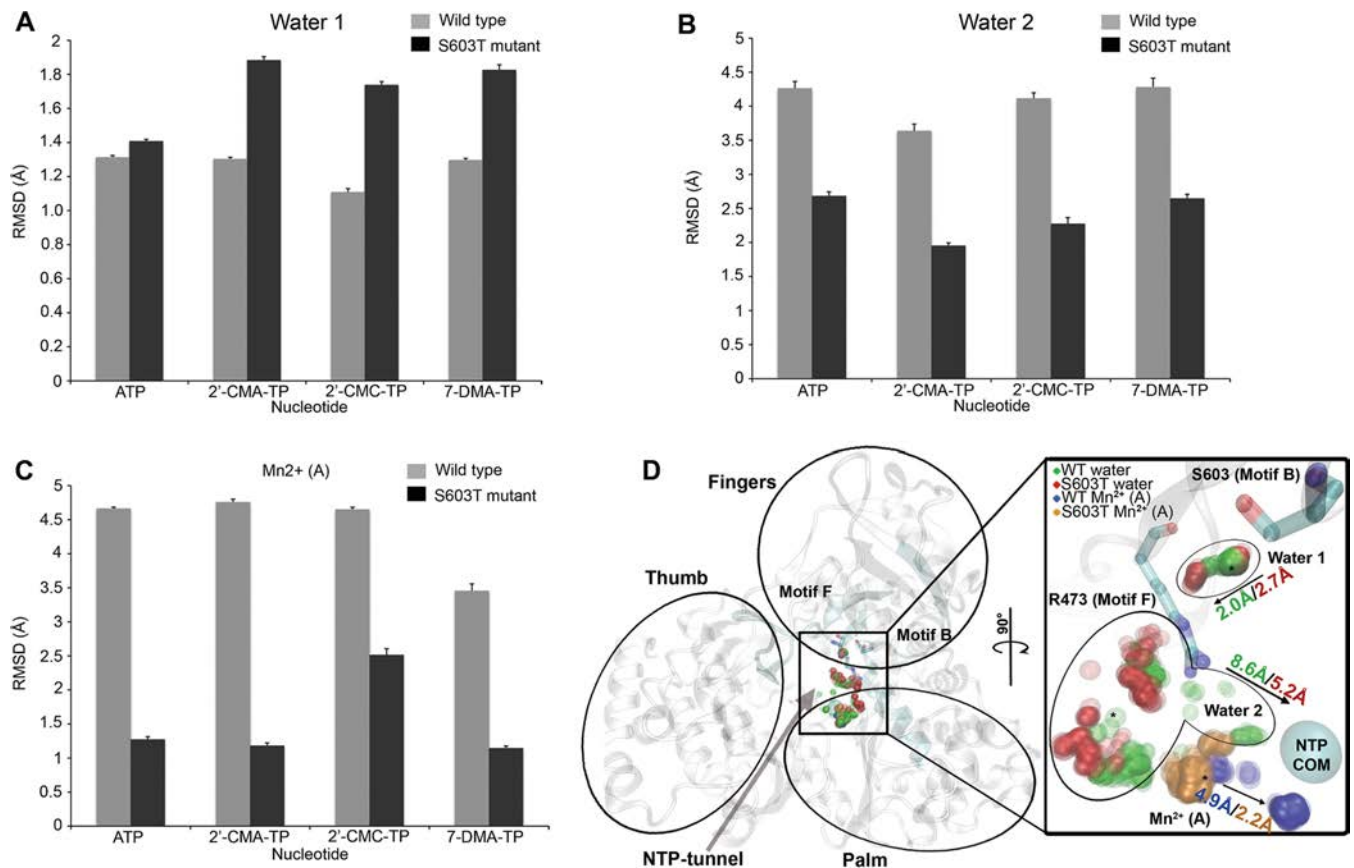


FIG 3 TBEV NS5 S603T mutant mechanism of escape from 7-deaza-2'-CMA as determined by all-atom molecular dynamics simulation. The bar charts show mean RMSD values with standard errors (y axes) for each NTP (x axes). Values for the two water molecules (A and B) and the Mn^{2+} ion (C) with large effect sizes (Table 2) are shown for the wild type (gray bars) and the S603T TBEV polymerase mutant (black bars). (D) TBEV polymerase structure, with the thumb, finger, and palm domains labeled. The B and F motifs are highlighted (cyan) and labeled to show the orientation of the NTP tunnel (arrow). The inset shows the active site turned 90° , which shows the positioning patterns of the two water molecules and the Mn^{2+} ion; dense clusters are shown in darker colors. The interrogating R473 residue of motif F, the S603 residue of motif B, and the active site center of mass (COM) are shown. The arrows indicate the direction of migration, with the largest RMSD shown for the wild type (WT) and the TBEV S603T mutant. The legend in the top left corner of the inset indicates the meaning of the colors for wild-type TBEV and the S603T TBEV mutant for the two water molecules and the Mn^{2+} ion. 2'-CMA, 2'-C-methyladenosine; 2'-CMC, 2'-C-methylcytidine; 7-DMA, 7-deaza-2'-C-methyladenosine; TP, triphosphate.

so the magnitude of the effect size was calculated as eta squared (η^2) and was guided by Cohen's rule of thumb (27) (Table 2). Although small to large effect sizes were noted for the explanatory variable NTP and for the interaction between NTP and strain, we restricted our interpretation to response variables with large effect sizes caused by the strains. Figure 3A shows that one water molecule was farther from its initial position in the S603T TBEV mutant strain than in wild-type TBEV. In contrast, the second water molecule (Fig. 3B) showed a higher deviation in the wild-type virus than in the mutant strain.

Two metal ions are bound within the RdRp catalytic site, with one ion (A) chelating with 3 catalytic aspartic residues and the other (B) chelating with 2 aspartic residues (26). Flavivirus RdRps are structurally homologous to other *Flaviviridae* RdRps (28), and their all-atom mechanism of escape from antiviral drugs is similar to that of the drug-resistant RdRp mutant of hepatitis C virus (29). The concerted positioning of the 2 water molecules and the Mn^{2+} A ion during the 7-deaza-2'-CMA exploration of TBEV polymerase in both strains is shown in Fig. 3D. The first water molecule is between the S603 residue and the conserved arginine, which is both an interrogating and a priming residue (26). The additional hydrophobic methyl group of threonine repels the water toward the arginine, leading to the higher deviation in the S603T TBEV mutant (Fig. 3A). The second water molecule is in proximity to the opening of the NTP tunnel and near

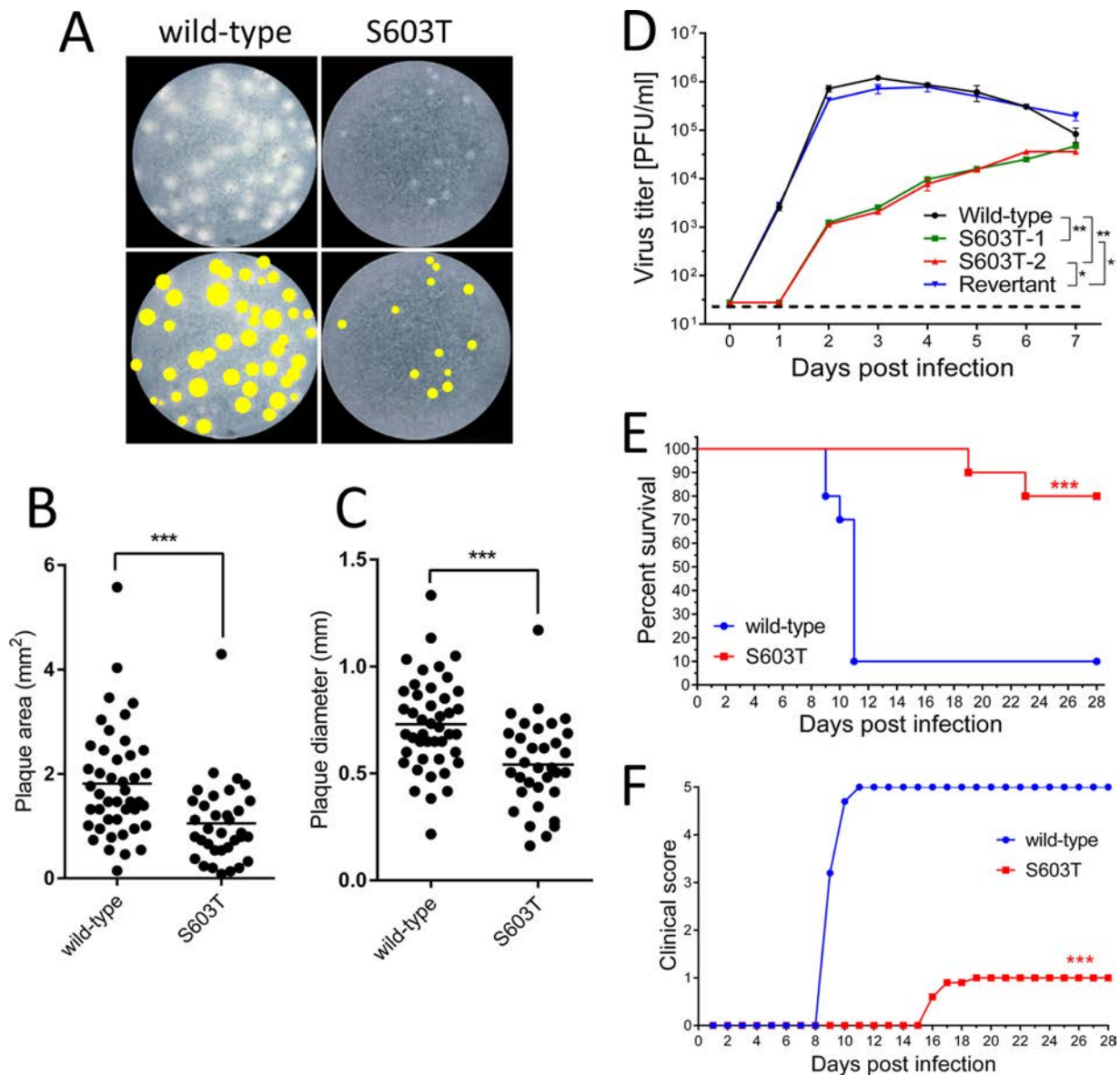


FIG 4 The S603T TBEV mutant has an attenuated phenotype. (A) (Top) The plaque morphology of the S603T TBEV mutant was assayed in a culture of porcine kidney stable (PS) cells and compared to that of the wild-type virus. (Bottom) Images of the plaques were scanned, and the plaque areas (B) and plaque diameters (C) of the wild-type virus and the S603T TBEV mutant were compared. (D) The growth kinetics of the S603T TBEV mutant was compared with the growth kinetics of the wild type and a genetic revertant to assess the replication efficacy of the mutant in PS cells. The neuroinvasiveness of the S603T TBEV mutant was studied in BALB/c mice and was compared to that of the wild-type virus. Adult BALB/c mice were infected subcutaneously with 10^3 PFU of either virus, and survival (E) and the clinical scores for neuroinfection symptoms (F) were monitored for 28 days. *, $P < 0.05$; **, $P < 0.01$; ***, $P < 0.001$.

the Mn^{2+} A ion. The positioning of the hydrophobic methyl group of threonine in the mutant prevents the second water molecule from migrating toward the positioning of the Mn^{2+} A ion, allowing it to maintain a lower RMSD than that for the wild type (Fig. 3B). The second wild-type TBEV water molecule forms large clusters at the Mn^{2+} A ion position, which may cause greater ion displacement than that in the S603T TBEV mutant (Fig. 3C).

The growth fitness of the S603T TBEV mutant is attenuated in cell culture. To characterize the phenotype of the drug-resistant mutant, the plaque morphology and growth properties of the S603T TBEV mutant were assayed in PS cell cultures and compared to those of the wild-type virus (Fig. 4A). Wild-type virus produced plaques that ranged from 269 to 1,333 μm in diameter (mean, $730 \pm 216 \mu m$) and from 0.148

to 5.578 mm² in area (mean, 1.814 ± 1.052 mm²); the plaques were mostly large, clear, round, and regular in shape (Fig. 4A to C). During passage of the virus with increasing concentrations of 7-deaza-2'-CMA, the wild-type-sized plaques gradually disappeared and were increasingly replaced by small and turbid plaques that ranged from 160 to 1,170 μm in diameter (mean, 540 ± 207 μm) and from 0.08 to 4.3 mm² in area (mean, 1.051 ± 0.207 mm²) (Fig. 4A to C). The small-plaque phenotype became the dominant phenotype in the viral population starting at passage 5, and this was maintained during all subsequent passages.

The growth kinetics of the S603T TBEV mutant were compared to those of the wild-type virus to assess the replication efficacy of the mutant in PS cells. The wild-type virus reached a peak titer of 7.2 × 10⁵ PFU/ml on day 2 p.i. Starting on day 4 p.i., the titer declined slightly and was 8.3 × 10⁴ PFU/ml on day 7 p.i. (Fig. 4D). In contrast, the replication capacity of the drug-resistant virus (from the final stock after the 50 μM selection) was significantly lower than that of the wild type. The titers of the S603T TBEV mutant were approximately 10³-fold lower for up to 3 days p.i. On days 4 to 6 p.i., the titers of the S603T TBEV mutant were 10- to 100-fold lower than the wild-type titers; on day 7 p.i., the difference in titers between the mutant and wild-type viruses was less pronounced, and both had titers of about 10⁴ PFU/ml (Fig. 4D).

The neuroinvasiveness of the S603T TBEV mutant is highly attenuated in mice.

The neuroinvasiveness of the S603T TBEV mutant was studied and compared to that of the wild-type virus in BALB/c mice. Adult BALB/c mice (*n* = 10 per group) were infected subcutaneously with 10³ PFU of either virus, and clinical signs of neuroinfection and survival were monitored for 28 days. Mice infected with the wild-type virus showed severe clinical signs of infection (ruffled fur, hunched posture, and hind leg paralysis), with 90% mortality and a mean survival time of 10 ± 1 days (Fig. 4E). Mice infected with the S603T TBEV mutant showed significantly lower mortality (20%) (*P* < 0.001) and a significantly longer mean survival time (21 ± 2.8 days) (*P* < 0.001) than those of mice infected with the wild-type virus (Fig. 4E). There were also considerable differences in the onset of disease signs and clinical scoring outcomes (*P* < 0.0001) (Fig. 4F).

Brains were collected from mice that did not survive infection with the S603T TBEV mutant, viral RNA was isolated and amplified by PCR, and the NS5 gene was sequenced to exclude possible reversion of the S603T mutation to the wild-type genotype during replication in the mouse. We found that TBEV carrying the S603T mutation was present in all of the mouse brains we investigated, indicating that no reverse mutation occurred spontaneously during the infection (Table 3). However, a few additional mutations that led to amino acid substitutions were detected in the NS5 gene of the drug-resistant mutant following propagation in mice (Table 3).

Rapid reversion of the S603T mutant to the wild-type genotype *in vitro* in the absence of 7-deaza-2'-CMA. The stability of the S603T mutant genotype was investigated during serial passages in PS cells in the absence of 7-deaza-2'-CMA. After 5 passages, the S603T mutant genotype reverted to wild type. This correlated with a reemergence of the wild-type phenotype (i.e., large plaques and gross cytopathic effects in PS cell cultures and growth kinetics in PS cells that were comparable to those of the wild-type virus) (Fig. 4D). Moreover, the revertant was sensitive to all 2'-C-methylated nucleosides tested (Fig. 2E). The sensitivity of the virus to 4'-C-azidocytidine and RO-9187 was not affected during virus passaging (Fig. 2E).

Site-directed mutagenesis confirms the role of the S603T mutation in drug resistance and virus attenuation. To examine the direct effects of the S603T mutation on TBEV characteristics, the mutation was introduced into a recombinant TBEV strain (Oshima-IC) generated from an infectious cDNA clone and a TBEV replicon that expresses a reporter luciferase gene (Oshima-REP-luc2A) (30, 31). In the absence of 7-deaza-2'-CMA, the introduced S603T mutation rapidly reverted to the parental sequence (Ser) in the recovered recombinant virus from cells transfected with the Oshima-IC S603T mRNA. The S603T mutant virus was recovered only in the presence of 7-deaza-2'-CMA, and the virus titer was <2 × 10³ PFU/ml, while the titer was >10⁶ PFU/ml in cells transfected with Oshima-IC wild-type mRNA. The focus size of the cells

TABLE 3 Mutations in NS5 of the Hypr virus in the brains of S603T mutant-infected mice

Mouse no.	Presence of mutation ^a										
	nt 7967 (NS5 aa 101) G → A (Arg → Lys)	nt 8967 (NS5 aa 434) C → T (Arg → His)	nt 9022 (NS5 aa 453) T → C (Tyr → His)	nt 9131 (NS5 aa 498) C → T (Ala → Val)	nt 9409 (NS5 aa 582) G → A (Ala → Thr)	nt 9410 (NS5 aa 582) C → T (Ala → Val)	nt 9472 (NS5 aa 603) T → A (Ser → Thr)	nt 9524 (NS5 aa 620) A → T (Gln → Leu)			
1	+	-	-	-	+	-	+	-	-	-	-
2	+	+	+	-	-	+	+	-	-	-	-
3	-	-	-	-	-	-	+	+	+	+	+
4	-	-	-	+	+	-	+	-	-	-	-

^aNucleotide numbering is based on the nucleotide sequence of the TBEV Hypr strain (GenBank accession no. U39292.1).

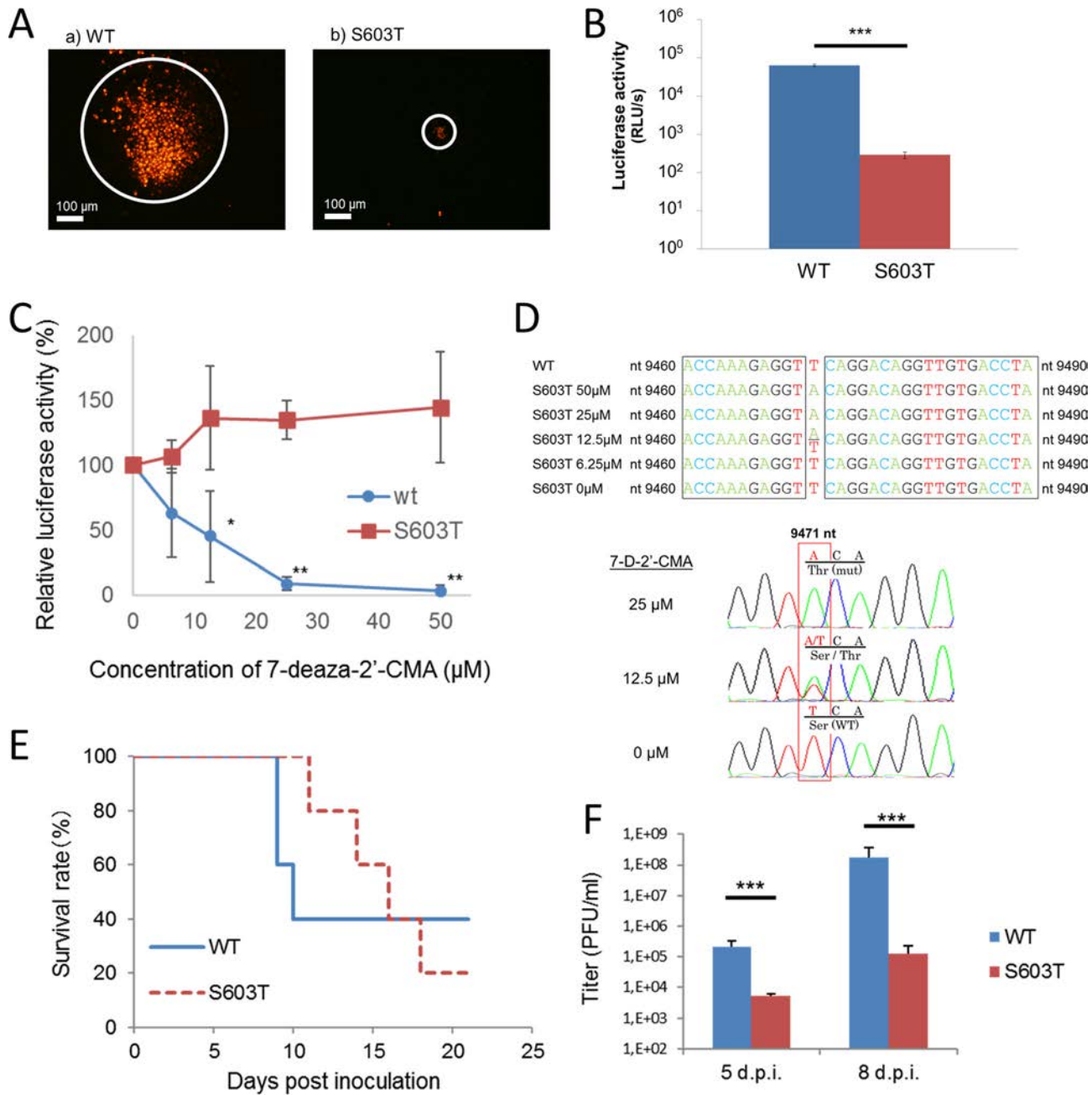


FIG 5 Site-directed mutagenesis confirms the role of the S603T mutation in drug resistance and virus attenuation. (A) Focus formation in baby hamster kidney fibroblasts (BHK cells) infected with Oshima-IC. BHK cells were infected with the Oshima-IC wild-type (a) or S603T mutant (b) virus and stained with anti-TBEV E-specific antibodies at 36 or 72 h postinfection, respectively. (B) Luciferase activity in cells transfected with TBEV replicon RNA. BHK cells were transfected with Oshima-REP-luc2A wild-type or S603T mRNA, and the luciferase activity was examined at 72 h posttransfection. Luciferase activity is expressed in raw light units (RLU). (C) Effect of 7-deaza-2'-CMA on the replication of the TBEV replicon. BHK cells were transfected with Oshima-REP-luc2A wild-type or S603T mRNA, and the luciferase activity was examined at 72 h posttransfection. The luciferase activity in the absence of 7-deaza-2'-CMA (0 μM) was considered the 100% value. *, $P < 0.05$; **, $P < 0.01$ (relative to the value at 0 μM). (D) Stability of the S603T mutation. BHK cells were transfected with Oshima-IC S603T mRNA and incubated for 5 days in the presence of 0 to 50 μM 7-deaza-2'-CMA. Viral RNA was harvested from the cells, and the mutation site was sequenced. (E) Survival curve for mice following intracerebral infection with Oshima-IC. C57BL/6J mice were infected intracerebrally with 50 PFU of the Oshima-IC wild-type or S603T mutant virus and monitored for 21 days. (F) At the indicated number of days after infection, the virus titers in brains were determined using plaque assays. Error bars indicate standard deviations ($n = 6$). ***, $P < 0.001$.

infected with the S603T mutant virus was noticeably smaller than that of cells infected with wild-type virus (Fig. 5A).

The luciferase activity in cells transfected with Oshima-REP-luc2A was significantly reduced by the S603T mutation, indicating that the mutation affected the genomic

TABLE 4 Mutations in NS5 of the virus in the brains of S603T mutant-infected mice

Mouse no.	Presence of mutation ^a			Time of brain collection
	nt 9471 (NS5 aa 603)	nt 9523 (NS5 aa 620)	nt 9660 (NS5 aa 666)	
	A → T (Thr → Ser)	A → T (Gln → Leu)	T → A (Cys → Ser)	
1	–	+	+	Time of death
2	–	+	+	Time of death
3	+	+	+	Time of death
4	–	+	+	Time of death
5	–	–	+	5 days p.i.
6	–	+	–	
7	–	+	+	
8	–	+	+	8 days p.i.
9	–	+	+	
10	–	+	+	

^aNucleotide numbering is based on the nucleotide sequence of the TBEV Oshima strain (GenBank accession no. AB753012.1).

replication of NS5 (Fig. 5B). While the luciferase activity of the wild-type replicon was reduced by 7-deaza-2'-CMA, in a dose-dependent manner, 7-deaza-2'-CMA did not affect the activity of the S603T replicon (Fig. 5C). This indicated that the S603T mutation was responsible for the resistance of the S603T TBEV mutant to 7-deaza-2'-CMA.

Mice were infected intracerebrally with the Oshima-IC wild-type or S603T TBEV strain. The two groups of mice had similar morbidity and mortality rates (Fig. 5E), but the survival time of mice infected with the S603T TBEV mutant was longer (14.75 days) than that of mice infected with wild-type TBEV (9.33 days) ($P < 0.05$). The virus titers in the brain were significantly lower for the mice infected with the S603T mutant than for those infected with the wild-type virus (Fig. 5F). Virus isolates recovered from the brain were subjected to NS5 sequence analysis, and most had the S603T mutation; notably, two additional amino acid substitutions were detected as well (Table 4).

The stability of the S603T mutation was investigated in baby hamster kidney (BHK) cells transfected with Oshima-IC S603T mRNA. After incubation for 5 days in the presence of 7-deaza-2'-CMA, we observed that 7-deaza-2'-CMA at 25 μ M and 50 μ M acted to retain the S603T mutation, while mixed wild-type and mutated genotypes were detected when the concentration of 7-deaza-2'-CMA was 12.5 μ M or lower. In the absence of 7-deaza-2'-CMA, the wild-type genotype dominated (Fig. 5D). This result confirmed that the mechanism underlying the generation of the drug-resistant TBEV mutant and the reversion to the wild-type genotype was due primarily to selection for a particular mutation, not only to a growth advantage of a particular viral clone that was present in the quasispecies.

DISCUSSION

TBEV NS5 is a candidate target for nucleoside analog inhibitors (2). We previously found that 2'-C-methylated nucleoside derivatives, and 7-deaza-2'-CMA in particular, have high antiviral activity against TBEV *in vitro* (13, 14). In the present study, we demonstrated the antiviral effect of 7-deaza-2'-CMA in a lethal rodent model of TBE. A dose of 25 mg/kg 7-deaza-2'-CMA administered twice a day starting on the day of infection showed the highest antiviral efficacy. This dose significantly increased mouse survival, decreased the viral titers in mouse brains, and reduced the clinical signs of neuroinfection in the infected animals (Fig. 1). The treatment started at the time of infection, which does not correlate with potential human drug use, since therapy is usually initiated during the neurological phase of the disease. This scenario is difficult to replicate because TBEV-infected mice usually die within 1 to 2 days after the initial onset of neurological signs of the infection. A transgenic IFN $\beta^{+/\Delta\beta}$ -luc mouse model was used to monitor the development of the infection in the mice by revealing the host beta interferon (IFN- β) response before the appearance of the first clinical signs of infection. Previous work showed that there is a good correlation between the bioluminescence signal and virus replication in these mice (32), allowing nondestructive and

continuous monitoring of viral invasion and the level of virus replication in mouse organs. Indeed, this model is an excellent way to monitor the effectiveness of antiviral therapy in mice that exhibit no signs of disease. Using this model, we confirmed that the treatment of TBEV-infected mice with 7-deaza-2'-CMA reduced virus spread in the body and the level of virus replication in multiple mouse organs and tissues (Fig. 1F and G).

Since TBE is an immunopathological disease that involves both virus damage and pathological immune reactions (33, 34), we tried combination therapy with both 7-deaza-2'-CMA and minocycline, a broad immunomodulatory compound that has anti-inflammatory, antiapoptotic, and neuroprotective properties (35). Minocycline is an antibiotic that is a tetracycline derivative, and it was reported previously that tetracycline could reduce the manifestations of the inflammatory response during TBE (36). Minocycline is effective in animal models of Japanese encephalitis (35, 37, 38) and is under clinical trials in humans with an acute form of viral encephalitis (39). The present study found that minocycline treatment of TBEV-infected mice slightly increased their survival and prolonged their mean survival time, but no additive effects were seen with combination therapy (Fig. 1E). Similar to our study, other studies have found that 7-deaza-2'-CMA is a potent inhibitor of virus replication and disease progression in mice infected with Zika virus (12) and that it reduces viremia in a dengue viremia mouse model (40). In human clinical trials for chronically HCV-infected patients, treatment with 7-deaza-2'-CMA failed due to adverse effects in patients after long-term treatment—possibly by mitochondrial toxicity (41). However, 7-deaza-2'-CMA remains a highly promising lead candidate for the treatment of acute infections caused not only by flaviviruses but also by other important emerging viruses (2, 11–14, 28, 42).

Low replicative fidelity and the high mutation rates of RNA viruses lead to viral resistance to antiviral drugs. Thus, for any antiviral agent, it is crucial to identify specific mutations that are responsible for drug resistance, to characterize the replicative capacity of the resistant virus, and to evaluate the risk of potential therapeutic failure. Here we selected 7-deaza-2'-CMA-resistant TBEV by serial passage of the virus with increasing 7-deaza-2'-CMA concentrations. Whole-genome sequencing revealed a single amino acid substitution, S603T, in the genome of the drug-resistant mutant compared to the genome of a wild-type virus. The mutation was located in the RdRp active site of viral NS5. Interestingly, serine and threonine are considered conservative amino acids, and the substitution caused only subtle changes in the structure of the NS5 RdRp active site (Fig. 2D). The signature high-level resistance mutation S603T conferred resistance not only to 7-deaza-2'-CMA but also to other 2'-C-methylated nucleoside derivatives. There was no cross-resistance of the S603T TBEV mutant to 4'-C-azidocytidine or RO-9187, suggesting that the mechanisms of resistance to 2'-C-methylated and 4'-C-azido compounds might be different (Fig. 2E). We speculate that the absence of the 2'- β -methyl moiety in 4'-C-modified nucleosides may allow these compounds to bind to NS5 and that their conformations are not hindered by the increased steric bulk of the S603T substitution in the NS5 active site (43, 44). Taken together, these results show that the S603T mutation-conferred resistance is directed toward the 2'- β -methyl-ribose moiety and does not involve other substitutions of the ribose ring or the heterobase identity/modifications (45).

Resistance to 2'-C-methylated nucleosides has been studied previously in other members of the *Flaviviridae* family. In HCV, the NS5B S282T amino acid change, which corresponds to an S603T substitution in motif B of TBEV RdRp, was first selected in the presence of 2'-C-methyladenosine (45). Recently, the S603T mutation, which is associated with additional amino acid substitutions in the NS5 active site (mainly the C666S and M644V mutations), was also reported for the 2'-C-methylcytidine-resistant Alkhurma hemorrhagic fever virus (46). The S604T substitution in motif B of the Zika virus recombinant NS5 polymerase corresponds to the S603T substitution in TBEV, and the S604T substitution confers resistance to the nucleoside inhibitor sofosbuvir triphosphate but not to the pyridoxine-derived nonnucleoside small-molecule inhibitor

DMB213 (47). In contrast, two substitutions in the methyltransferase domain of NS5 of dengue virus type 2, A60T and Y201H, confer resistance to 7-deaza-2'-CMA (48).

The all-atom escape from 2'-C-methylated nucleosides by *Flaviviridae* serine mutant polymerases uses a concerted mechanism within the active site that involves substrate binding residues, metal ions, and water molecules. The 2'-C-methylated nucleoside analogs use water molecules as camouflage during active site exploration. The hydrophobic methyl group in the serine-to-threonine mutant repels the water molecules surrounding the analogs, reducing its interrogation by the conserved arginine in motif F (29). This conserved arginine is essential for NTP incorporation (49). During the initial exploration of 7-deaza-2'-CMA, the S603T TBEV mutant polymerase maintains the position of a water molecule near the NTP tunnel opening and the Mn²⁺ A ion. This may explain the reduced replication of the S603T TBEV mutant, since water molecules are used to coordinate the NTP phosphate groups with the metal ions in wild-type polymerases (50) (Fig. 3).

In the Zika virus recombinant NS5 polymerase, the S604T substitution reduces enzyme activity compared to that of the wild-type polymerase (47). However, to the best of our knowledge, no studies have investigated the biological properties of flaviviruses that are resistant to 2'-C-methylated nucleoside analogs. Here we showed that the drug-resistant TBEV strain produced small turbid plaques and showed reduced growth fitness *in vitro* (Fig. 4A to D). This was confirmed by use of a drug-resistant virus that was selected by cell culture passages under the pressure of 7-deaza-2'-CMA as well as by use of an infectious cDNA TBEV clone and replicon with the introduced S603T substitution (Fig. 5A and B). During passaging of the virus under pressure of 7-deaza-2'-CMA, the slowly replicating S603T TBEV mutant probably had a selective advantage in terms of outcompeting other variants with a higher replication rate (20). Reduced replication fitness might limit the spread of the resistant virus in cell cultures and may closely correlate with the altered plaque morphology seen with the mutant clone (51–53). This would explain why rapidly replicating wild-type viruses formed large plaques, whereas the S603T TBEV mutant resulted in small plaques.

The lower replication capacity of the TBEV mutant may explain its rapid reversion to a drug-sensitive phenotype when 7-deaza-2'-CMA is no longer present. Under nonselective conditions, the replication capacity of the S603T TBEV mutant is probably not sufficient to give the mutant a replicative advantage over fitter variants in the viral quasispecies, resulting in elimination of the S603T TBEV mutant from the infected cell culture. This process might be considerably accelerated by spontaneous reverse mutations that contribute to a rapid increase in the wild-type genotypes in the progeny of a viral population when the selective agent is absent (54).

The resistance of the S603T TBEV mutant to 2'-C-methylated nucleoside analogs was associated with strong virus attenuation in mice. We found that the S603T mutation significantly reduced viral neuroinvasiveness after subcutaneous inoculation as well as neurovirulence after intracerebral administration (Fig. 4E and F and 5E and F). After subcutaneous inoculation, TBEV isolates from the brains of dead or sacrificed moribund mice were subjected to sequence analysis and found to contain the S603T mutation. With one exception, the same thing was observed in the brains of mice inoculated intracerebrally. A couple of additional mutations in the NS5 gene were identified in viruses recovered from mice infected with the S603T TBEV mutant, but it is unknown whether these substitutions represent compensatory mutations or random mutations. The Q620L mutation was detected in almost all virus clones that were recovered from mouse brains after intracerebral inoculation with Oshima-IC S603T and from the brain of one mouse following subcutaneous inoculation with the Hypr S603T TBEV mutant (Tables 3 and 4). The effects of these mutations on the biological properties of the virus and on antiviral resistance merit further study in the future.

In conclusion, we found that 7-deaza-2'-CMA is a strong TBEV inhibitor *in vivo*, significantly increases the survival of TBEV-infected mice, and reduces virus titers and the clinical signs of neuroinfection in brains. A single conservative mutation, S603T, in the NS5 RdRp caused only subtle changes in the structure of the polymerase active site

but was associated with cross-resistance to various 2'-C-methylated nucleoside analogs and with strong reductions in viral fitness both *in vitro* and in a mouse model. The S603T TBEV mutant was not coresistant to 4'-C-azidocytidine or RO-9187, suggesting that combination therapy might improve treatment and reduce the emergence of drug-resistant viruses during therapy with 2'-C-methylated nucleoside analogs.

MATERIALS AND METHODS

Ethics statement. This study was carried out in strict accordance with Czech and Japanese laws and guidelines for the use of experimental animals and the protection of animals against cruelty. The animal care and use protocols adhered to the fundamental guidelines for proper conduct of animal experiments and related activities in academic research institutions by the Ministry of Education, Culture, Sports, Science and Technology (notice 71, 1 June 2006), the standards relating to the care and management of laboratory animals and relief of pain of the Ministry of the Environment (notice 84, 30 August 2013), and the Act on Welfare and Management of Animals (revised 5 September 2012) in Japan and to Animal Welfare Act 246/1992 Coll. in the Czech Republic. All procedures were reviewed by local ethics committees and approved by the president of Hokkaido University after review by the Animal Care and Use Committee of Hokkaido University and by the Ministry of Agriculture of the Czech Republic (permit no. MZe 1650).

Virus, cells, and antiviral compounds. The well-characterized, low-passage-number TBEV strain Hypr, a member of the European TBEV subtype, was passaged 6 times in the brains of suckling mice and used in this study (the virus was obtained from the virus collection of the National Institute of Public Health, Prague, Czech Republic). This strain was originally isolated from the blood of a 10-year-old child who died because of TBE in 1953 (55).

PS cells (56) used for plaque assay, viral subculture, and construction of virus growth curves (see below) were obtained from the National Cell Culture Collection, National Institute of Public Health, Prague, Czech Republic. The cells were cultured at 37°C in Leibovitz (L-15) medium supplemented with 3% newborn calf serum plus a 1% mixture of penicillin and glutamine (Sigma-Aldrich). BHK cells (obtained from the American Type Culture Collection [ATCC]) were used for transfection of the Oshima-IC and Oshima-REP-luc2A plasmids and for infection with the Oshima-IC virus.

The following antiviral compounds were purchased: 2'-C-methyl-substituted nucleosides from Carbo-synth (Compton, United Kingdom) and 4'-azidocytidine and 2'-deoxy-2'-beta-hydroxy-4'-azidocytidine (RO-9187) from Medchemexpress (Stockholm, Sweden). For *in vitro* studies, the test compounds were solubilized in 100% dimethyl sulfoxide (DMSO) to yield 10 mM stock solutions.

Plaque assay. Virus titers were evaluated by plaque assay as described previously (13, 14, 57). Briefly, 10-fold dilutions of TBEV in L-15 medium were prepared in 24-well tissue culture plates, and PS cells were added in suspension (0.6×10^5 to 1.5×10^5 cells per well). Following incubation for 4 h, the infected PS cell suspension was overlaid with 1.5% (wt/vol) carboxymethyl cellulose in L-15 medium. After a 5-day cultivation at 37°C, the infected plates were washed extensively with phosphate-buffered saline (PBS), and the cell monolayers were stained with naphthalene black. Plaque numbers were counted, and the virus titer was expressed as the number of PFU per milliliter.

Images of the plaques were scanned on a BioVendor C-series array reader specially modified for plaque assays. Imaging was done sequentially well by well, with illumination from the bottom of the sample and with a full high-definition (HD) camera system. Every image was then processed by BioVendor Analytics software, which automatically counts plaques based on specialized image processing algorithms developed for this task.

Selection of drug-resistant viruses. PS cells were seeded into 96-well plates (approximately 2×10^4 cells per well) and incubated for 24 h to form a confluent monolayer. Following incubation, the medium was aspirated from the wells and replaced with 200 μ l of fresh medium containing 5 μ M 7-deaza-2'-CMA. Simultaneously, the cells were infected with the Hypr TBEV strain at a multiplicity of infection (MOI) of 0.1. The formation of cytopathic effect (CPE) was monitored visually using an Olympus BX-5 microscope, yielding a 40 to 50% CPE in virus-infected cultures. The culture medium was then harvested and used for infection of fresh cell monolayers. A 5 μ M concentration of 7-deaza-2'-CMA was used during the initial 8 passages. The subsequent 4 passages were performed with a gradual increase in drug concentration to 50 μ M (Fig. 2A). In parallel, a control TBEV isolate was not passaged with 7-deaza-2'-CMA but in the presence of 0.5% (vol/vol) DMSO and was used as a mock-selected wild-type virus. After passage 12, the drug-resistant and control TBEV strains were harvested and subjected to an additional subculture to make a virus stock for further testing (titer of about 10^6 PFU/ml for the wild type and 10^4 to 10^5 PFU/ml for the drug-resistant TBEV strain). The *in vitro* selection of drug-resistant TBEV strains was performed in duplicate, resulting in two independent mutant clones, denoted S603T-1 and S603T-2.

In order to reinduce the wild-type virus (revertant) from the S603T TBEV mutant population, the S603T TBEV mutant was repeatedly passaged on PS cells in the absence of 7-deaza-2'-CMA. The sensitivity of the obtained viral progeny to 7-deaza-2'-CMA was determined after each passage by cultivation of the virus in the presence of 7-deaza-2'-CMA (50 μ M). After passage 7, the obtained revertant was subjected to one more passage to prepare a virus stock for further testing (virus titer of about 10^6 PFU/ml). Obtained viruses were subjected to full-length sequence analysis (both mutants as well as the parental virus were sequenced), virulence characterization, and assessment of sensitivity to different classes of antivirals.

Antiviral assays. A viral titer inhibition assay was used to measure the antiviral efficacy of the nucleoside analogs in cell culture and was performed as described previously (13). Briefly, PS cells were seeded in 96-well plates at approximately 2×10^4 cells/well and incubated for 24 h to form a confluent monolayer. The growth medium was then aspirated from the wells and replaced with 200 μ l of fresh medium containing 50 μ M test compound (3 wells per compound) and simultaneously infected with TBEV at an MOI of 0.1. For the mock-treated controls, DMSO was added to virus-infected and mock-infected cells, to a final concentration of 0.5% (vol/vol). The infected cell monolayers were monitored by use of a microscope to yield 70% to 90% CPE. Viral titers were determined by plaque assays and expressed as numbers of PFU per milliliter.

To evaluate the growth kinetics of the drug-resistant TBEV mutant, PS cell monolayers cultured for 24 h in 96-well plates were treated with 200 μ l of medium containing 50 μ M 7-deaza-2'-CMA and infected with TBEV at an MOI of 0.1. For the wild-type and revertant TBEV strains, medium containing 0.5% (vol/vol) DMSO was used. The medium was collected from the wells daily (days 1 to 7 p.i.; three wells at each time point), and the viral titers were determined by plaque assay. The virus titer values were used to construct TBEV growth curves.

For the dose-response studies with 2'-C-methylated and 4'-C-azido-modified nucleoside analogs, PS cell monolayers were cultured with 200 μ l of medium containing individual test compounds at concentrations ranging from 0 to 50 μ M and were simultaneously infected with TBEV at an MOI of 0.1. The medium was collected from the wells on day 3 or 4 p.i. (wild type) or day 6 or 7 p.i. (mutant), and the viral titers were determined by plaque assay and used to construct TBEV dose-response curves and to estimate the 50% effective concentration (EC_{50}).

RNA isolation, PCR, and whole-genome sequencing. RNA was isolated from growth medium or brain tissue homogenate by use of a QIAmp viral RNA minikit (Qiagen). Reverse transcription was performed using a ProtoScript First Strand cDNA kit (New England Biolabs) according to the manufacturer's instructions for the synthesis of first-strand cDNA, which was subsequently used for PCR amplification using 1 μ l of the antisense primer (0.5 μ M). To cover the entire TBEV genome, 35 overlapping DNA fragments were amplified by PCR as described previously (58), using PPP master mix (Top-Bio, Czech Republic), 1 μ l of each primer (stock concentration, 0.01 mM; primer sequences are available upon request), and 1 μ l of template. The cycling conditions were as follows: (i) denaturation (5 min at 95°C) and (ii) 30 cycles of 95°C for 30 s, 57°C for 30 s, and 72°C for 1 min 30 s. The PCR products were visualized in a 1.7% agarose gel in Tris-acetate-EDTA buffer. DNA was purified using a High Pure PCR product purification kit (Roche) according to the manufacturer's recommendations. The PCR products were subsequently directly sequenced (Sanger method) by a commercial service (SEQme, Czech Republic). Both the nucleotide sequence and the deduced amino acid sequence were analyzed using BioEdit Sequence Alignment Editor, version 7.2.0.

Viruses from cDNA clones and replicons. The TBEV Oshima-IC and Oshima-REP-luc2A replicons were prepared from an infectious cDNA clone (28) and a replicon expressing a firefly luciferase gene (29), using the Oshima 5-10 strain (accession no. [AB062003](#)), which was isolated in Hokkaido, Japan, in 1995 (59). Standard PCR mutagenesis techniques were used to construct Oshima-IC and Oshima-REP-luc2A S603T, in which a T-to-A mutation at nucleotide position 9471 was introduced.

RNAs were transcribed from the Oshima-IC and Oshima-REP-luc2A plasmids by use of an mMESSAGE mMACHINE SP6 kit (Thermo Fisher Scientific, Inc., Waltham, MA, USA) and then transfected into BHK cells by use of TransIT-mRNA (Mirus Bio, Madison, WI, USA) as described previously (60).

For the focus assay, monolayers of BHK cells were infected with the Oshima-IC virus, overlaid with medium containing 2% fetal calf serum (FCS) and 1.5% carboxymethyl cellulose, and incubated for the indicated time. After incubation, cells were fixed with 4% (wt/vol) paraformaldehyde and permeabilized with 0.2% (vol/vol) Triton X-100. After blocking with 2% (wt/vol) bovine serum albumin (BSA), the cells were incubated with polyclonal mouse ascites fluid against TBEV. After extensive washing, the cells were incubated with Alexa 488-conjugated anti-mouse IgG antibodies (Thermo Fisher Scientific, Inc.). The cells were observed using a BZ-9000 fluorescence microscope (Keyence, Osaka, Japan).

To prepare cell extracts for the luciferase assays, BHK cells were washed with PBS, lysed using cell culture reporter lysis buffer (Promega, Madison, WI, USA), and incubated at room temperature for 10 min. Luciferase assays were carried out using a luciferase assay system (Promega) according to the manufacturer's instructions.

Infection of mice with TBEV. To evaluate the anti-TBEV effects of 7-deaza-2'-CMA *in vivo*, four groups of 6-week-old female BALB/c mice were injected subcutaneously with TBEV (1,000 PFU/mouse) and immediately treated intraperitoneally with 200 μ l of 7-deaza-2'-CMA, as follows: group 1 mice ($n = 10$) were nontreated control animals, group 2 mice ($n = 6$) were treated with 5 mg/kg once a day, group 3 mice ($n = 6$) were treated with 15 mg/kg once a day, and group 4 mice ($n = 10$) were treated with 25 mg/kg twice a day at 8-h intervals. 7-Deaza-2'-CMA was freshly solubilized in sterile saline buffer before each injection and was administered to the animals for 17 days p.i. The clinical scores and survival rates of the TBEV-infected mice were monitored daily for 28 days. Illness signs were scored as follows: 0, no symptoms; 1, ruffled fur; 2, slowing of activity or hunched posture; 3, asthenia or mild paralysis; 4, lethargy, tremor, or complete paralysis of the limbs; and 5, death.

In order to assess *in vivo* the antiviral efficacy of minocycline, 3 groups ($n = 10$ /group) of 6-week-old female BALB/c mice were infected subcutaneously with TBEV (1,000 PFU/mouse) and immediately treated as follows: group 1 mice were nontreated control animals, group 2 mice were treated with 45 mg/kg minocycline, and group 3 mice were treated with a combination of 45 mg/kg minocycline and 25 mg/kg 7-deaza-2'-CMA (33). Whereas minocycline was injected into the mice once daily for 8 days,

7-deaza-2'-CMA was administered twice daily at 8-h intervals over the 17-day period. The clinical scores and survival rates were monitored daily.

To determine the TBEV titers in mouse brains, groups of 6-week-old BALB/c ($n = 6$ or 12 mice per group) mice were infected subcutaneously with 1,000 PFU of TBEV and treated intraperitoneally with 7-deaza-2'-CMA once daily at concentrations ranging from 0 to 15 mg/kg or twice daily with 25 mg/kg of 7-deaza-2'-CMA. On day 8 p.i., the brains were collected, weighed, and homogenized using Precellys 24 (Bertin Technologies), and 20% (wt/vol) suspensions were prepared in L-15 medium containing 3% newborn calf serum. Each homogenate was clarified by centrifugation at $5,000 \times g$, and the supernatant medium was used for plaque assays.

The anti-TBEV activity of 7-deaza-2'-CMA was further evaluated using *in vivo* bioluminescence imaging of IFN $\beta^{+/Δ}$ β-luc mice (23). The IFN $\beta^{+/Δ}$ β-luc mice were obtained by crossing the mouse strain IFN $\beta^{Δ}$ β-luc/Δβ-luc (*ifnb1^{tm2.2li}*) with albino (Tyrc2J) C57BL/6 mice. Six-week-old IFN $\beta^{+/Δ}$ β-luc mice were divided into 3 groups ($n = 3$ /group) and treated as follows: group 1 mice were mock-infected nontreated control animals, group 2 mice were injected subcutaneously with 1,000 PFU/ml TBEV, and group 3 mice were infected subcutaneously with 1,000 PFU/ml TBEV and injected intraperitoneally with 25 mg/kg of 7-deaza-2'-CMA twice a day for the 8-day experimental period. *In vivo* imaging was performed on days 1, 3, 4, and 7 p.i. Animals were anesthetized by intramuscular administration of a mixture of 10% ketamine (Narkamon) and 2% xylazine (Rometa). Following anesthesia, mice were injected intraperitoneally with 150 mg/kg of D-luciferin (Promega) in PBS. Bioluminescence imaging was carried out using an In-Vivo Xtreme imager (Bruker). The exposure time was 60 s, and 4×4 binning was used to obtain the optimal signal intensity.

To evaluate the virulence of the Hypr S603T mutant in a mouse model of TBEV infection, 2 groups ($n = 10$ /group) of 6-week-old BALB/c female mice were challenged subcutaneously with wild-type virus or with the S603T TBEV mutant (1,000 PFU/mouse). Symptoms of illness, clinical scores, and survival rates of TBEV-infected mice were monitored daily during the 28-day experimental period.

To assess the virulence of the Oshima S603T TBEV mutants by using cDNA clones and replicons, 5-week-old female C57BL/6J mice (Charles River Laboratories Japan, Inc., Yokohama, Japan) were anesthetized and inoculated intracerebrally with ~ 50 PFU of the Oshima-IC virus. The mice were weighed daily and checked for clinical signs of illness for 21 days. Morbidity was defined as $>10\%$ weight loss. To analyze viral titers and gene expression levels, 3 mice were sacrificed on days 5 and 8 p.i., and brain samples were collected following perfusion with cold PBS and stored at -80°C .

Stochastic molecular simulations. A homology-generated model of the TBEV NS5 polymerase was used for simulations as reported previously (13) and was optimized using Schrödinger's Maestro Protein Preparation Wizard tool (61). The S603T TBEV mutant was generated using Schrödinger's Maestro software. Stochastic molecular simulations were performed using the Metropolis Monte Carlo-based Protein Energy Landscape Exploration (PELE) server (24; <https://pele.bsc.es/>). The PELE software applications are explained elsewhere (24, 25). PELE software implements the optimized potentials for liquid simulations (OPLS-2005) (62) and was previously shown to be suitable for metals (63); however, metals are treated as ions and the bonds as ionic rather than covalent. For the simulations, the bonds between the metal ions (Mn^{2+}) and the associated residues from the polymerase were bridged and converted to zero-order bonds.

Modifications to the ready-made PELE script are available upon request. A total of 24 CPUs were used for each simulation. The top 3 CPUs that explored the region close to the TBEV NS5 active site were combined, resulting in ~ 250 frames per simulation. Since our data set represents a large sample size, the central limit theorem (CLT) validates normal-based methods (64, 65). The data were collected using Visual Molecular Dynamics (VMD) software (66). Two-way ANOVA was used to test the differences in the categorical explanatory variables nucleotide triphosphate (or NTP) and strain (wild type or S603T TBEV mutant) for each response variable. The VMD software generated the structural representations.

Statistical analyses. Data are expressed as means \pm standard deviations (SD), and the significance of differences between groups was evaluated using the Mann-Whitney U test or ANOVA. Survival rates were analyzed using the log rank Mantel-Cox test. All tests were performed using GraphPad Prism 5.04 (GraphPad Software, Inc., USA). *P* values of <0.05 were considered statistically significant.

ACKNOWLEDGMENTS

We thank Jan Karasek from BioVendor Instruments, Czech Republic, for help with the scanning and analysis of plaques by use of a prototype instrument and software analytics. We thank Ivana Huvarova for providing excellent technical assistance.

This study was supported by a grant from the Ministry of Health of the Czech Republic (grant 16-34238A); by Project FIT (Pharmacology, Immunotherapy, nanoToxicology), which was funded by the European Regional Development Fund (to D.R.); by grants-in-aid for scientific research (grants 26660220 and 16K15032) from the Ministry of Education, Culture, Sports, Science and Technology of Japan; and by a grant provided by the Ichiro Kanehara Foundation (to K.Y.).

The funders had no role in study design, data collection and analysis, the decision to publish, or preparation of the manuscript.

REFERENCES

- De Clercq E, Li G. 2016. Approved antiviral drugs over the past 50 years. *Clin Microbiol Rev* 29:695–747. <https://doi.org/10.1128/CMR.00102-15>.
- Boldescu V, Behnam MAM, Vasilakis N, Klein CD. 2017. Broad-spectrum agents for flaviviral infections: dengue, Zika and beyond. *Nat Rev Drug Discov* 16:565–586. <https://doi.org/10.1038/nrd.2017.33>.
- Cihlar T, Ray AS. 2010. Nucleoside and nucleotide HIV reverse transcriptase inhibitors: 25 years after zidovudine. *Antiviral Res* 85:39–58. <https://doi.org/10.1016/j.antiviral.2009.09.014>.
- Lawitz E, Mangia A, Wyles D, Rodriguez-Torres M, Hassanein T, Gordon SC, Schultz M, Davis MN, Kayali Z, Reddy KR, Jacobson IM, Kowdley KV, Nyberg L, Subramanian GM, Hyland RH, Arterburn S, Jiang D, McNally J, Brainard D, Symonds WT, McHutchison JG, Sheikh AM, Younossi Z, Gane EJ. 2013. Sofosbuvir for previously untreated chronic hepatitis C infection. *N Engl J Med* 368:1878–1887. <https://doi.org/10.1056/NEJMoa1214853>.
- Schinazi R, Halfon P, Marcellin P, Asselah T. 2014. HCV direct-acting antiviral agents: the best interferon-free combinations. *Liver Int* 34(Suppl 1):S69–S78. <https://doi.org/10.1111/liv.12423>.
- Sofia MJ, Chang W, Furman PA, Mosley RT, Ross BS. 2012. Nucleoside, nucleotide, and non-nucleoside inhibitors of hepatitis C virus NS5B RNA-dependent RNA-polymerase. *J Med Chem* 55:2481–2531. <https://doi.org/10.1021/jm201384j>.
- Hercík K, Kozak J, Šála M, Dejmeck M, Hřebabecký H, Zborníková E, Smola M, Ruzek D, Nencka R, Boura E. 2017. Adenosine triphosphate analogs can efficiently inhibit the Zika virus RNA-dependent RNA polymerase. *Antiviral Res* 137:131–133. <https://doi.org/10.1016/j.antiviral.2016.11.020>.
- Potisopon S, Ferron F, Fattorini V, Selisko B, Canard B. 2017. Substrate selectivity of dengue and Zika virus NS5 polymerase towards 2'-modified nucleotide analogues. *Antiviral Res* 140:25–36. <https://doi.org/10.1016/j.antiviral.2016.12.021>.
- Olsen DB, Eldrup AB, Bartholomew L, Bhat B, Bosserman MR, Ceccacci A, Colwell LF, Fay JF, Flores OA, Getty KL, Grobler JA, LaFemina RL, Markel EJ, Migliaccio G, Prhac M, Stahlhut MW, Tomassini JE, MacCoss M, Hazuda DJ, Carroll SS. 2004. A 7-deaza-adenosine analog is a potent and selective inhibitor of hepatitis C virus replication with excellent pharmacokinetic properties. *Antimicrob Agents Chemother* 48:3944–3953. <https://doi.org/10.1128/AAC.48.10.3944-3953.2004>.
- Chen YL, Yokokawa F, Shi PY. 2015. The search for nucleoside/nucleotide analog inhibitors of dengue virus. *Antiviral Res* 122:12–19. <https://doi.org/10.1016/j.antiviral.2015.07.010>.
- Eyer L, Nencka R, Huvarová I, Palus M, Joao Alves M, Gould EA, De Clercq E, Růžek D. 2016. Nucleoside inhibitors of Zika virus. *J Infect Dis* 214:707–711. <https://doi.org/10.1093/infdis/jiw226>.
- Zmurko J, Marques RE, Schols D, Verbeke E, Kaptein SJ, Neyts J. 2016. The viral polymerase inhibitor 7-deaza-2'-C-methyladenosine is a potent inhibitor of in vitro Zika virus replication and delays disease progression in a robust mouse infection model. *PLoS Negl Trop Dis* 10:e0004695. <https://doi.org/10.1371/journal.pntd.0004695>.
- Eyer L, Valdés JJ, Gil VA, Nencka R, Hřebabecký H, Šála M, Salát J, Černý J, Palus M, De Clercq E, Růžek D. 2015. Nucleoside inhibitors of tick-borne encephalitis virus. *Antimicrob Agents Chemother* 59:5483–5493. <https://doi.org/10.1128/AAC.00807-15>.
- Eyer L, Šmidková M, Nencka R, Neča J, Kastl T, Palus M, De Clercq E, Růžek D. 2016. Structure-activity relationships of nucleoside analogues for inhibition of tick-borne encephalitis virus. *Antiviral Res* 133:119–129. <https://doi.org/10.1016/j.antiviral.2016.07.018>.
- Dumpis U, Crook D, Oksi J. 1999. Tick-borne encephalitis. *Clin Infect Dis* 28:882–890. <https://doi.org/10.1086/515195>.
- Heinz FX, Mandl CW. 1993. The molecular biology of tick-borne encephalitis virus. Review article. *APMIS* 101:735–745. <https://doi.org/10.1111/j.1699-0463.1993.tb00174.x>.
- Růžek D, Dobler G, Donoso Mantke O. 2010. Tick-borne encephalitis: pathogenesis and clinical implications. *Travel Med Infect Dis* 8:223–232. <https://doi.org/10.1016/j.tmaid.2010.06.004>.
- Poveda E, Wyles DL, Mena A, Pedreira JD, Castro-Iglesias A, Cachay E. 2014. Update on hepatitis C virus resistance to direct-acting antiviral agents. *Antiviral Res* 108:181–191. <https://doi.org/10.1016/j.antiviral.2014.05.015>.
- Menéndez-Arias L, Álvarez M, Pacheco B. 2014. Nucleoside/nucleotide analog inhibitors of hepatitis B virus polymerase: mechanism of action and resistance. *Curr Opin Virol* 8:1–9. <https://doi.org/10.1016/j.coviro.2014.04.005>.
- Lauring AS, Andino R. 2010. Quasispecies theory and the behavior of RNA viruses. *PLoS Pathog* 6:e1001005. <https://doi.org/10.1371/journal.ppat.1001005>.
- Lauring AS, Frydman J, Andino R. 2013. The role of mutational robustness in RNA virus evolution. *Nat Rev Microbiol* 11:327–336. <https://doi.org/10.1038/nrmicro3003>.
- Berger KL, Scherer J, Ranga M, Sha N, Stern JO, Quinson AM, Kukulj G. 2015. Baseline polymorphisms and emergence of drug resistance in the NS3/4A protease of hepatitis C virus genotype 1 following treatment with faldaprevir and pegylated interferon alpha 2a/ribavirin in phase 2 and phase 3 studies. *Antimicrob Agents Chemother* 59:6017–6025. <https://doi.org/10.1128/AAC.00932-15>.
- Lienenklaus S, Cornitescu M, Zietara N, Łyszkiewicz M, Gekara N, Jabłńska J, Edenhofer F, Rajewsky K, Bruder D, Hafner M, Staeheli P, Weiss S. 2009. Novel reporter mouse reveals constitutive and inflammatory expression of IFN-beta in vivo. *J Immunol* 183:3229–3236. <https://doi.org/10.4049/jimmunol.0804277>.
- Madadkar-Sobhani A, Guallar V. 2013. PELE web server: atomistic study of biomolecular systems at your fingertips. *Nucleic Acids Res* 41(Web Server issue):W322–W328. <https://doi.org/10.1093/nar/gkt454>.
- Borelli KW, Vitalis A, Alcantara R, Guallar V. 2005. PELE: protein energy landscape exploration. A novel Monte Carlo based technique. *J Chem Theory Comput* 1:1304–1311. <https://doi.org/10.1021/ct0501811>.
- Bressanelli S, Tomei L, Rey FA, De Francesco R. 2002. Structural analysis of the hepatitis C virus RNA polymerase in complex with ribonucleotides. *J Virol* 76:3482–3492. <https://doi.org/10.1128/JVI.76.7.3482-3492.2002>.
- Cohen J. 1988. *Statistical power analysis for the behavioral sciences*. Erlbaum, Hillsdale, NJ.
- Valdés JJ, Gil VA, Butterill PT, Růžek D. 2016. An all-atom, active site exploration of antiviral inhibitors that target Flaviviridae polymerases. *J Gen Virol* 97:2552–2565. <https://doi.org/10.1099/jgv.0.000569>.
- Valdés JJ, Butterill PT, Růžek D. 2017. Flaviviridae viruses use a common molecular mechanism to escape nucleoside analogue inhibitors. *Biochem Biophys Res Commun* 2017:50006–291X(17)30535-1. <https://doi.org/10.1016/j.bbrc.2017.03.068>.
- Hayasaka D, Gritsun TS, Yoshii K, Ueki T, Goto A, Mizutani T, Kariwa H, Iwasaki T, Gould EA, Takashima I. 2004. Amino acid changes responsible for attenuation of virus neurovirulence in an infectious cDNA clone of the Oshima strain of tick-borne encephalitis virus. *J Gen Virol* 85:1007–1018. <https://doi.org/10.1099/vir.0.19668-0>.
- Yoshii K, Ikawa A, Chiba Y, Omori Y, Maeda J, Murata R, Kariwa H, Takashima I. 2009. Establishment of a neutralization test involving reporter gene-expressing virus-like particles of tick-borne encephalitis virus. *J Virol Methods* 161:173–176. <https://doi.org/10.1016/j.jviromet.2009.05.016>.
- Weber E, Finsterbusch K, Lindquist R, Nair S, Lienenklaus S, Gekara NO, Janik D, Weiss S, Kalinke U, Överby AK, Kröger A. 2014. Type I interferon protects mice from fatal neurotropic infection with Langat virus by systemic and local antiviral responses. *J Virol* 88:12202–12212. <https://doi.org/10.1128/JVI.01215-14>.
- Růžek D, Salát J, Palus M, Gritsun TS, Gould EA, Dyková I, Skallová A, Jelinek J, Kopecký J, Grubhoffer L. 2009. CD8⁺ T-cells mediate immunopathology in tick-borne encephalitis. *Virology* 384:1–6. <https://doi.org/10.1016/j.virol.2008.11.023>.
- Palus M, Vojtišková J, Salát J, Kopecký J, Grubhoffer L, Lipoldová M, Demant P, Růžek D. 2013. Mice with different susceptibility to tick-borne encephalitis virus infection show selective neutralizing antibody response and inflammatory reaction in the central nervous system. *J Neuroinflammation* 10:77. <https://doi.org/10.1186/1742-2094-10-77>.
- Mishra MK, Basu A. 2008. Minocycline neuroprotects, reduces microglial activation, inhibits caspase 3 induction, and viral replication following Japanese encephalitis. *J Neurochem* 105:1582–1595. <https://doi.org/10.1111/j.1471-4159.2008.05238.x>.
- Atrasheskaya AV, Fredeking TM, Ignatyev GM. 2003. Changes in immune parameters and their correction in human cases of tick-borne encephalitis. *Clin Exp Immunol* 131:148–154. <https://doi.org/10.1046/j.1365-2249.2003.02050.x>.
- Mishra MK, Dutta K, Saheb SK, Basu A. 2009. Understanding the molecular mechanism of blood-brain barrier damage in an experi-

- mental model of Japanese encephalitis: correlation with minocycline administration as a therapeutic agent. *Neurochem Int* 55:717–723. <https://doi.org/10.1016/j.neuint.2009.07.006>.
38. Dutta K, Mishra MK, Nazmi A, Kumawat KL, Basu A. 2010. Minocycline differentially modulates macrophage mediated peripheral immune response following Japanese encephalitis virus infection. *Immunobiology* 215:884–893. <https://doi.org/10.1016/j.imbio.2009.12.003>.
 39. Kumar R, Basu A, Sinha S, Das M, Tripathi P, Jain A, Kumar C, Atam V, Khan S, Singh AS. 2016. Role of oral minocycline in acute encephalitis syndrome in India—a randomized controlled trial. *BMC Infect Dis* 16:67. <https://doi.org/10.1186/s12879-016-1385-6>.
 40. Schul W, Liu W, Xu HY, Flamand M, Vasudevan SG. 2007. A dengue fever viremia model in mice shows reduction in viral replication and suppression of the inflammatory response after treatment with antiviral drugs. *J Infect Dis* 195:665–674. <https://doi.org/10.1086/511310>.
 41. Arnold JJ, Sharma SD, Feng JY, Ray AS, Smidansky ED, Kireeva ML, Cho A, Perry J, Vela JE, Park Y, Xu Y, Tian Y, Babusis D, Barauskus O, Peterson BR, Gnatt A, Kashlev M, Zhong W, Cameron CE. 2012. Sensitivity of mitochondrial transcription and resistance of RNA polymerase II dependent nuclear transcription to antiviral ribonucleosides. *PLoS Pathog* 8:e1003030. <https://doi.org/10.1371/journal.ppat.1003030>.
 42. Wu R, Smidansky ED, Oh HS, Takhampunya R, Padmanabhan R, Cameron CE, Peterson BR. 2010. Synthesis of a 6-methyl-7-deaza analogue of adenosine that potently inhibits replication of polio and dengue viruses. *J Med Chem* 53:7958–7966. <https://doi.org/10.1021/jm100593s>.
 43. Klumpp K, Kalayanov G, Ma H, Le Pogam S, Leveque V, Jiang WR, Innocent N, De Witte A, Rajyaguru S, Tai E, Chanda S, Irwin MR, Sund C, Winquist A, Maltseva T, Eriksson S, Usova E, Smith M, Alker A, Najera I, Cammack N, Martin JA, Johansson NG, Smith DB. 2008. 2'-Deoxy-4'-azido nucleoside analogs are highly potent inhibitors of hepatitis C virus replication despite the lack of 2'-alpha-hydroxyl groups. *J Biol Chem* 283:2167–2175. <https://doi.org/10.1074/jbc.M708929200>.
 44. Klumpp K, Lévêque V, Le Pogam S, Ma H, Jiang WR, Kang H, Granycome C, Singer M, Laxton C, Hang JQ, Sarma K, Smith DB, Heindl D, Hobbs CJ, Merrett JH, Symons J, Cammack N, Martin JA, Devos R, Najera I. 2006. The novel nucleoside analog R1479 (4'-azidocytidine) is a potent inhibitor of NS5B-dependent RNA synthesis and hepatitis C virus replication in cell culture. *J Biol Chem* 281:3793–3799. <https://doi.org/10.1074/jbc.M510195200>.
 45. Migliaccio G, Tomassini JE, Carroll SS, Tomei L, Altamura S, Bhat B, Bartholomew L, Bosserman MR, Ceccacci A, Colwell LF, Cortese R, De Francesco R, Eldrup AB, Getty KL, Hou XS, LaFemina RL, Ludmerer SW, MacCoss M, McMasters DR, Stahlhut MW, Olsen DB, Hazuda DJ, Flores OA. 2003. Characterization of resistance to non-obligate chain-terminating ribonucleoside analogs that inhibit hepatitis C virus replication in vitro. *J Biol Chem* 278:49164–49170. <https://doi.org/10.1074/jbc.M305041200>.
 46. Flint M, McMullan LK, Dodd KA, Bird BH, Khristova ML, Nichol ST, Spiropoulou CF. 2014. Inhibitors of the tick-borne, hemorrhagic fever-associated flaviviruses. *Antimicrob Agents Chemother* 58:3206–3216. <https://doi.org/10.1128/AAC.02393-14>.
 47. Xu HT, Hassounah SA, Colby-Germinario SP, Oliveira M, Fogarty C, Quan Y, Han Y, Golubkov O, Ibanescu I, Brenner B, Stranix BR, Wainberg MA. 2017. Purification of Zika virus RNA-dependent RNA polymerase and its use to identify small-molecule Zika inhibitors. *J Antimicrob Chemother* 72:727–734. <https://doi.org/10.1093/jac/dkw514>.
 48. Mateo R, Nagamine CM, Kirkegaard K. 2015. Suppression of drug resistance in dengue virus. *mBio* 6:e01960-15. <https://doi.org/10.1128/mBio.01960-15>.
 49. Curti E, Jaeger J. 2013. Residues Arg283, Arg285, and Ile287 in the nucleotide binding pocket of bovine viral diarrhoea virus NS5B RNA polymerase affect catalysis and fidelity. *J Virol* 87:199–207. <https://doi.org/10.1128/JVI.06968-11>.
 50. Steitz TA, Steitz JA. 1993. A general two-metal-ion mechanism for catalytic RNA. *Proc Natl Acad Sci U S A* 90:6498–6502. <https://doi.org/10.1073/pnas.90.14.6498>.
 51. Dobson BM, Procter DJ, Hollett NA, Flesch IE, Newsome TP, Tschärke DC. 2014. Vaccinia virus F5 is required for normal plaque morphology in multiple cell lines but not replication in culture or virulence in mice. *Virology* 456–457:145–156. <https://doi.org/10.1016/j.virol.2014.03.020>.
 52. Mateu CG, Recalde MP, Artuso MC, Hermida G, Linero FN, Scolaro LA, Damonte EB, Pujol CA, Carlucci MJ. 2011. Emergence of herpes simplex virus-1 syncytial variants with altered virulence for mice after selection with a natural carrageenan. *Sex Transm Dis* 38:555–561.
 53. Rubio MP, López-Bueno A, Almendral JM. 2005. Virulent variants emerging in mice infected with the apathogenic prototype strain of the parvovirus minute virus of mice exhibit a capsid with low avidity for a primary receptor. *J Virol* 79:11280–11290. <https://doi.org/10.1128/JVI.79.17.11280-11290.2005>.
 54. McCown MF, Rajyaguru S, Le Pogam S, Ali S, Jiang WR, Kang H, Symons J, Cammack N, Najera I. 2008. The hepatitis C virus replicon presents a higher barrier to resistance to nucleoside analogs than to nonnucleoside polymerase or protease inhibitors. *Antimicrob Agents Chemother* 52:1604–1612. <https://doi.org/10.1128/AAC.01317-07>.
 55. Pospisil L, Jandasek L, Pesek J. 1954. Isolation of new strains of meningoencephalitis virus in the Brno region during the summer of 1953. *Lek List* 9:3–5.
 56. Kozuch O, Mayer V. 1975. Pig kidney epithelial (PS) cells: a perfect tool for the study of flaviviruses and some other arboviruses. *Acta Virol* 19:498.
 57. De Madrid AT, Porterfield JS. 1969. A simple micro-culture method for the study of group B arboviruses. *Bull World Health Organ* 40:113–121.
 58. Růžek D, Gritsun TS, Forrester NL, Gould EA, Kopecký J, Golovchenko M, Rudenko N, Grubhoffer L. 2008. Mutations in the NS2B and NS3 genes affect mouse neuroinvasiveness of a Western European field strain of tick-borne encephalitis virus. *Virology* 374:249–255. <https://doi.org/10.1016/j.virol.2008.01.010>.
 59. Takashima I, Morita K, Chiba M, Hayasaka D, Sato T, Takezawa C, Igarashi A, Kariwa H, Yoshimatsu K, Arikawa J, Hashimoto N. 1997. A case of tick-borne encephalitis in Japan and isolation of the virus. *J Clin Microbiol* 35:1943–1947.
 60. Yoshii K, Igarashi M, Ito K, Kariwa H, Holbrook MR, Takashima I. 2011. Construction of an infectious cDNA clone for Omsk hemorrhagic fever virus, and characterization of mutations in NS2A and NS5. *Virus Res* 155:61–68. <https://doi.org/10.1016/j.virusres.2010.08.023>.
 61. Schrödinger LLC. 2016. Release, 2016-3. Maestro. Schrödinger LLC, New York, NY.
 62. Jorgensen WL, Tirado-Rives J. 1988. The OPLS [optimized potentials for liquid simulations] potential functions for proteins, energy minimizations for crystals of cyclic peptides and crambin. *J Am Chem Soc* 110:1657–1666. <https://doi.org/10.1021/ja00214a001>.
 63. Giannotti MI, Cabeza de Vaca I, Artés JM, Sanz F, Guallar V, Gorostiza P. 2015. Direct measurement of the nanomechanical stability of a redox protein active site and its dependence upon metal binding. *J Phys Chem B* 119:12050–12058. <https://doi.org/10.1021/acs.jpcc.5b06382>.
 64. Läärä E. 2009. Statistics: reasoning on uncertainty, and the insignificance of testing null. *Ann Zool Fennici* 46:138–157.
 65. Zuur AF, Ieno EN, Elphick CS. 2010. A protocol for data exploration to avoid common statistical problems. *Methods Ecol Evol* 1:3–14. <https://doi.org/10.1111/j.2041-210X.2009.00001.x>.
 66. Humphrey W, Dalke A, Schulten K. 1996. VMD: visual molecular dynamics. *J Mol Graph* 14:33–38. [https://doi.org/10.1016/0263-7855\(96\)00018-5](https://doi.org/10.1016/0263-7855(96)00018-5).



Antiviral activity of the adenosine analogue BCX4430 against West Nile virus and tick-borne flaviviruses



Luděk Eyer^{a, b}, Darina Zouharová^a, Jana Širmarová^a, Martina Fojtíková^a,
Michal Štefánik^a, Jan Havierník^a, Radim Nencka^c, Erik de Clercq^d, Daniel Růžek^{a, b, *}

^a Department of Virology, Veterinary Research Institute, Hudcova 70, CZ-62100, Brno, Czech Republic

^b Institute of Parasitology, Biology Centre of the Czech Academy of Sciences, Branišovská 31, CZ-37005, České Budějovice, Czech Republic

^c Institute of Organic Chemistry and Biochemistry, Czech Academy of Sciences, Flemingovo nám. 2, CZ-16610, Prague 6, Czech Republic

^d Rega Institute for Medical Research, KU Leuven, Minderbroedersstraat 10, B-3000, Leuven, Belgium

ARTICLE INFO

Article history:

Received 13 January 2017

Received in revised form

10 March 2017

Accepted 18 March 2017

Available online 21 March 2017

Keywords:

BCX4430

Flavivirus

Adenosine analogue

Nucleoside inhibitor

Antiviral activity

Cytotoxicity

ABSTRACT

There are currently no approved antiviral therapies against medically important human flaviviruses. The imino-C-nucleoside BCX4430 shows broad-spectrum antiviral activity against a wide range of RNA viruses. Here, we demonstrate that BCX4430 inhibits tick-borne species of the genus *Flavivirus*; however, the antiviral effect varies against individual species. Micro-molar BCX4430 levels inhibited tick-borne encephalitis virus (TBEV); while, approximately 3–8-fold higher concentrations were needed to inhibit louping ill virus and Kyasanur Forest disease virus. Moreover, the compound strongly inhibited *in vitro* replication of West Nile virus, a typical mosquito-transmitted flavivirus. Two chemical forms of the compound, i.e. BCX4430 and BCX4430 hydrochloride, were compared and both exerted similar inhibitory profiles in our *in vitro* antiviral assay systems and no or negligible cytotoxicity in porcine kidney stable and Vero cells. The obtained data indicate that, in addition to mosquito-borne flaviviruses, the compound has strong antiviral activity against members of the TBEV serocomplex.

© 2017 Elsevier B.V. All rights reserved.

The genus *Flavivirus* belonging to the *Flaviviridae* family includes more than 70 single-stranded plus-sense RNA viral species. Flaviviruses of human medical importance are typically tick- or mosquito-transmitted viruses such as West Nile virus (WNV), dengue virus (DENV), Japanese encephalitis virus (JEV), yellow fever virus (YFV), tick-borne encephalitis virus (TBEV), Kyasanur Forest disease virus (KFDV), Omsk hemorrhagic fever virus (OHFV), louping ill virus (LIV) (Baier, 2011), and Zika virus (ZIKV) (Lazear et al., 2016). Flaviviral infections are associated with a wide spectrum of distinct clinical manifestations, ranging from relatively mild fever and arthralgia to severe viscerotropic symptoms (YFV and DENV), hemorrhagic fevers (KFDV and OHFV), encephalitis/myelitis (JEV, WNV, TBEV, in sporadic cases also LIV), and

neuropathic or teratogenic manifestations (ZIKV). More than 200 million clinical cases of flaviviral infections, including numerous deaths, are reported annually worldwide (Deval et al., 2014). As there is presently no specific antiviral therapy to treat patients with flaviviral infections, searching for effective small-molecule inhibitors that are active against these viruses is a high research priority.

The broad-range adenosine analogue, BCX4430, has a chemical substitution of nitrogen for oxygen on the ribose ring and carbon for nitrogen at position 7 of the heterobase moiety (Taylor et al., 2016) and is a typical representative of imino-C-nucleosides (De Clercq, 2016). A structural change from a furanose in adenosine to an azasugar in BCX4430 is responsible for alteration of the electrostatic interaction of the sugar ring with RNA-dependent RNA polymerase, resulting in non-obligate chain termination of viral RNA synthesis (Taylor et al., 2016). Previously, BCX4430 was reported to exert *in vitro* antiviral activity against a broad spectrum of RNA viruses from the *Filoviridae*, *Bunyaviridae*, *Arenaviridae*, *Picornaviridae*, *Orthomyxoviridae*, *Paramyxoviridae*, and *Coronaviridae* families (Warren et al., 2014). The *in vitro* antiviral potency of BCX4430 has been determined for YFV, JEV, and DENV2 of the *Flaviviridae* family (Warren et al., 2014) and recently also for representatives of African and Asian lineages of ZIKV (Julander et al.,

Abbreviations: CC₅₀, 50% cytotoxic concentration; DENV, dengue virus; EC₅₀, 50% effective concentration; JEV, Japanese encephalitis virus; KFDV, Kyasanur Forest disease virus; LIV, louping ill virus; MOI, multiplicity of infection; OHFV, Omsk hemorrhagic fever virus; p.i., post-infection; PS, porcine kidney stable; TBEV, tick-borne encephalitis virus; WNV, West Nile virus; YFV, yellow fever virus; and ZIKV, Zika virus.

* Corresponding author. Veterinary Research Institute, Hudcova 70, CZ-62100, Brno, Czech Republic.

E-mail address: ruzekd@paru.cas.cz (D. Růžek).

<http://dx.doi.org/10.1016/j.antiviral.2017.03.012>

0166-3542/© 2017 Elsevier B.V. All rights reserved.

2017). The *in vivo* efficacy of BCX4430 was demonstrated in lethal rodent and non-human primate models of filovirus infection (Warren et al., 2014), as well as in rodent models of Rift Valley fever virus (Warren et al., 2014), YFV (Julander et al., 2014), and ZIKV infections (Julander et al., 2017). Recently, this compound entered phase 1 of the first in-human clinical studies focused on intramuscular administration of BCX4430 in healthy volunteers and it showed promising pharmacokinetics properties and good tolerability (Taylor et al., 2016).

In this comparative study, the *in vitro* antiviral activities of BCX4430 and its hydrochloride form were evaluated for the activity against tick-borne flaviviruses in a number of standardized *in vitro* assay systems. Moreover, WNV was included in our antiviral screens as a representative of mosquito-transmitted flaviviruses with an unknown sensitivity to BCX4430. The selection of viruses for testing was also based on their different clinical manifestations (encephalitic viruses – WNV, LIV and TBEV; hemorrhagic fever associated virus – KFDV).

Porcine kidney stable (PS) cells (Kozuch and Mayer, 1975) were used for antiviral screens, virus multiplication, and virus plaque assays. The cells were cultured at 37 °C in Leibovitz (L-15) medium supplemented with 3% precolostral calf serum and a 1% mixture of penicillin and glutamine (Sigma-Aldrich, Prague, Czech Republic). The following viral strains were tested: WNV (strain Eg101), TBEV (strain Hypr), LIV (strain LI/31), and KFDV (strain W-377). BCX4430 and BCX4430 hydrochloride were purchased from MedchemExpress (Stockholm, Sweden). The test compounds were solubilized in 100% DMSO to yield 10 mM stock solutions. A viral titer inhibition assay was performed to determine the flavivirus sensitivity to BCX4430 in cell culture. The PS cells were seeded in 96-well plates (approximately 2×10^4 cells per well), and incubated for 24 h to form a confluent monolayer. The medium was then aspirated from the wells and replaced with 200 μ l of fresh medium containing 0–50 μ M (for TBEV and WNV) or 0–100 μ M (for LIV and KFDV) of the test compound, which was simultaneously inoculated with the appropriate virus strain at a multiplicity of infection (MOI) of 0.1. Virus-infected cells treated with DMSO (mock-treated cells) were used as controls. Culture medium was collected 1, 3, and 5 days post infection (p.i.) to yield a 40–50% cytopathic effect in virus control wells. Viral titers were determined by plaque assays and expressed as PFU/mL (De Madrid and Porterfielg, 1969). The obtained titer values were used for construction of dose-response and inhibition curves and for estimation of the 50% effective concentration (EC_{50}). To measure the compound-induced inhibition of viral surface antigen expression, a cell-based flavivirus immunostaining assay was performed, as previously described (Eyer et al., 2015). Potential compound cytotoxicity was determined in terms of cell viability using the Cell Counting Kit-8 (Dojindo Molecular Technologies, Munich, Germany), according to the manufacturer's instructions. The concentration of compound that reduced cell viability by 50% was considered the 50% cytotoxic concentration (CC_{50}). In addition to PS cells, the compound cytotoxicity was also evaluated in Vero cells (ATCC CCL-81, African Green Monkey, adult kidney, epithelial), which are widely used for the evaluation of numerous viruses for their sensitivity to antiviral compounds.

We primarily evaluated the antiviral efficacy of BCX4430 against medically important members of the TBEV serocomplex, i.e. TBEV, LIV, and KFDV. In case of TBEV, we observed complete inhibition of viral replication at 25 μ M for BCX4430 and 50 μ M for BCX4430 hydrochloride at day 3 p.i., which corresponded to a TBEV titer reduction of about 10^5 -fold compared with mock-treated cells (Fig. 1A). The TBEV yields from the BCX4430-treated cells were substantially reduced at 1, 3, and 5 days p.i. compared with mock-treated cells, indicating that the inhibitory effect was stable over the 5-day experimental period (Fig. 1B). The TBEV inhibition curves

show the EC_{50} values were 1.48 and 1.67 μ M for BCX4430 and its hydrochloride counterpart, respectively, with favorable selectivity indexes (SI) exceeding 50 (Fig. 1C, Table 1). Immunofluorescence staining revealed that 50 μ M BCX4430 completely inhibited the expression of the surface E antigen in TBEV-infected PS cells (Fig. 2A). The observed inhibitory properties of BCX4430 for TBEV are comparable with recently published values for 2'-C-methylated nucleosides (Eyer et al., 2015), 4'-C-azido modified nucleosides (Eyer et al., 2016a,b), and 2'-C-ethynyl substituted adenosine analogue NITD008 (Lo et al., 2016). This suggests these nucleosides have similar modes of interaction with TBEV polymerase, as well as similar metabolic conversion/transformation pathways within the host cell line. Our experiments were done using a highly virulent TBEV strain (Hypr). However, TBEV strains circulating in the field are biologically highly heterogeneous. Several molecular determinants of virulence, including variation of the 3' non-coding region of the viral genome (Asghar et al., 2014, 2016; Sakai et al., 2014), were described. In our future studies, we plan to investigate the antiviral activity of the tested compounds against a panel of TBEV strains differing in virulence.

Although LIV and KDFV, along with TBEV, are tick-borne flaviviruses, they differ considerably from TBEV in their sensitivity to BCX4430. In LIV and KDFV-infected PS cells, the highest tested concentration of 100 μ M resulted in a virus titer reduction of about 10^3 – 10^5 at day 3 p.i.; however, this compound concentration did not lead to complete inhibition of virus replication in cell culture (Fig. 1A). The incomplete suppression of viral growth was reflected by the EC_{50} values, which were approximately 3–8 fold higher than those for TBEV (Fig. 1C, Table 1). Similar antiviral activity has been previously reported for numerous nucleoside analogues, such as 2'-C-methylcytidine, 6-azauridine, 6-azauridine triacetate, and NITD008, which have been identified as potent KFDV and OHFV inhibitors (Flint et al., 2014; Lo et al., 2016).

Our results demonstrate for the first time that BCX4430 strongly inhibits *in vitro* replication of WNV, a typical mosquito-transmitted flavivirus. We observed complete inhibition of viral replication at BCX4430 concentrations of 25–50 μ M until the fifth day p.i., indicating strong and stable anti-WNV activity (Fig. 1A and B). These results correlated with the dose-dependent suppression of WNV surface E protein in the compound-treated cell cultures (Fig. 2A). The EC_{50} values for WNV were 2.33 and 1.89 μ M for BCX4430 and BCX4430 hydrochloride, respectively (Fig. 1C, Table 1). These values were similar or lower than those of other recently reported nucleoside inhibitors of WNV polymerase or NTPase/helicase (Borowski et al., 2002; Hosmane et al., 2003). The WNV (strain Eg101) seemed to be considerably more susceptible to BCX4430 compared with the mosquito-borne flaviviruses YFV, JEV, and DENV2 with reported EC_{50} values of 14.1, 43.6, and 32.8 μ M, respectively (Warren et al., 2014). Recently, Julander et al. (2017) described the *in vitro* antiviral efficacy of BCX4430 dihydrochloride against both African and Asian lineages of ZIKV with EC_{50} values of 8.7–11.7 μ g/mL.

Cytotoxicity data demonstrated there was a moderate decline of PS cell viability (10–20%) at BCX4430 concentrations of 50, 75, and 100 μ M. For Vero cells, no cytotoxicity was observed at the highest tested concentration of 100 μ M with no detectable effect on cell proliferation. For both cell lines, the CC_{50} values of BCX4430 and its hydrochloride form were estimated to be > 100 μ M (Fig. 2B, Table 1).

In conclusion, we demonstrated that BCX4430 exerts a broad-range antiviral activity against mosquito-borne flaviviruses as well as members of the TBEV serocomplex. The TBEV was inhibited at low micro-molar concentrations of BCX4430, but 3–8-fold higher concentrations were necessary to inhibit LIV and KFDV. The sensitivity of WNV to BCX4430 was similar to that of TBEV. The

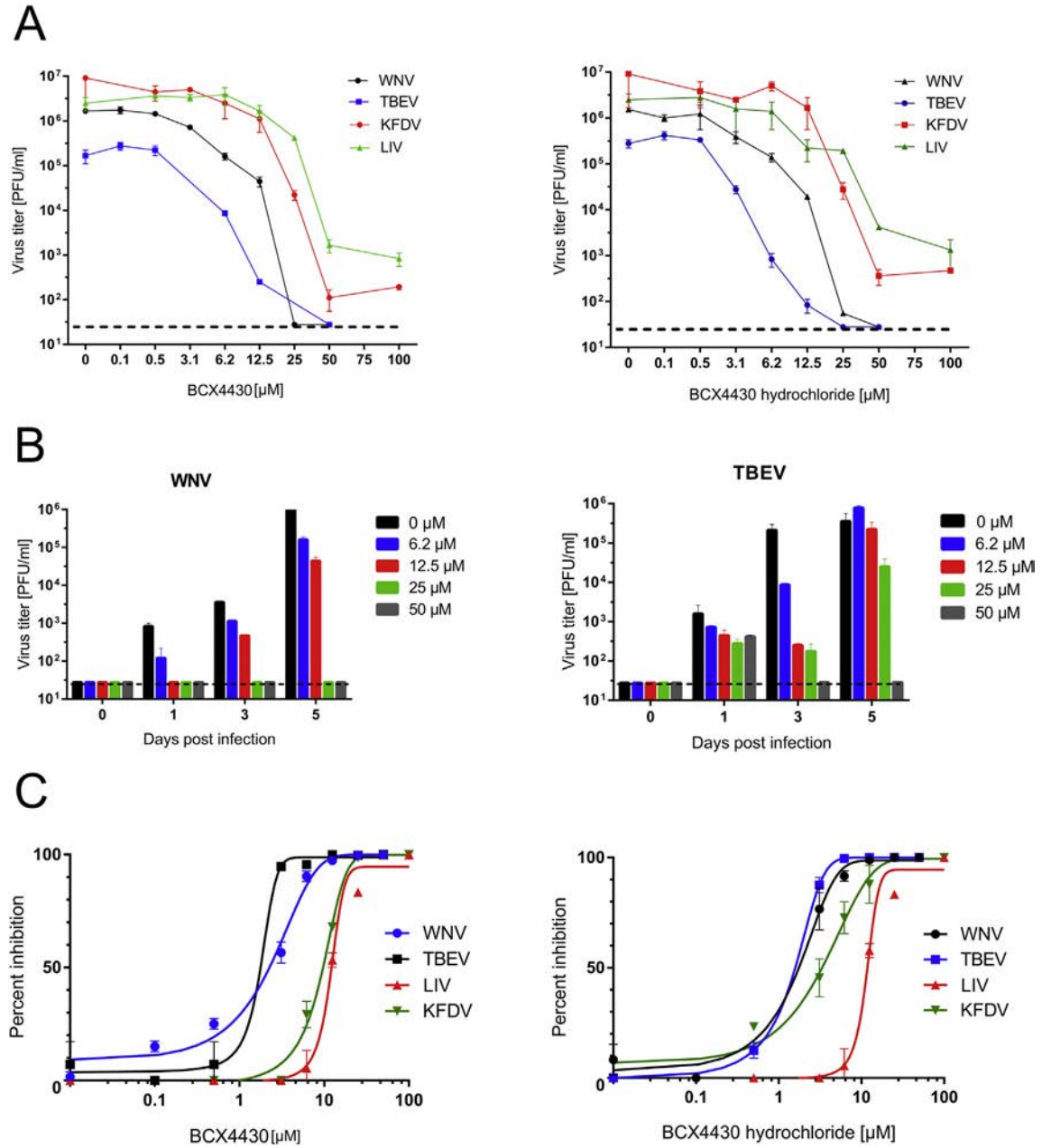


Fig. 1. (A) Dose-dependent effect of BCX4430 and its hydrochloride form on virus titers at day 3 p.i. The PS cells were treated with different compound concentrations and at the same time infected with the indicated virus. Culture supernatants were collected and the viral titers were determined by plaque assay. (B) Reduction of TBEV and WNV titers by BCX4430 at the indicated concentrations over the 5-day experimental period. (C) Inhibition curves of the indicated flaviviruses in the presence of a serial dilution of BCX4430 and its hydrochloride form at day 3 p.i.

Table 1
Virus inhibition and cytotoxicity characteristics of BCX4430 and BCX4430 hydrochloride.

Virus	EC ₅₀ ± SD [μM] ^{a,b}		CC ₅₀ ± SD [μM] ^d		SI ^c	
	BCX4430	BCX4430 hydrochloride	BCX4430	BCX4430 hydrochloride	BCX4430	BCX4430 hydrochloride
TBEV	1.48 ± 0.10	1.67 ± 0.05	>100	>100	67.57	59.88
WNV	2.33 ± 0.33	1.89 ± 0.22	>100	>100	42.92	52.91
LIV	12.33 ± 0.13	12.13 ± 0.11	>100	>100	8.11	8.24
KFDV	11.37 ± 0.14	5.56 ± 0.30	>100	>100	8.80	17.99

^a Determined from 3 independent experiments.

^b Calculated as a 50% reduction of virus titers, using the Reed-Muench method.

^c The selectivity index (SI) calculated as CC₅₀/EC₅₀.

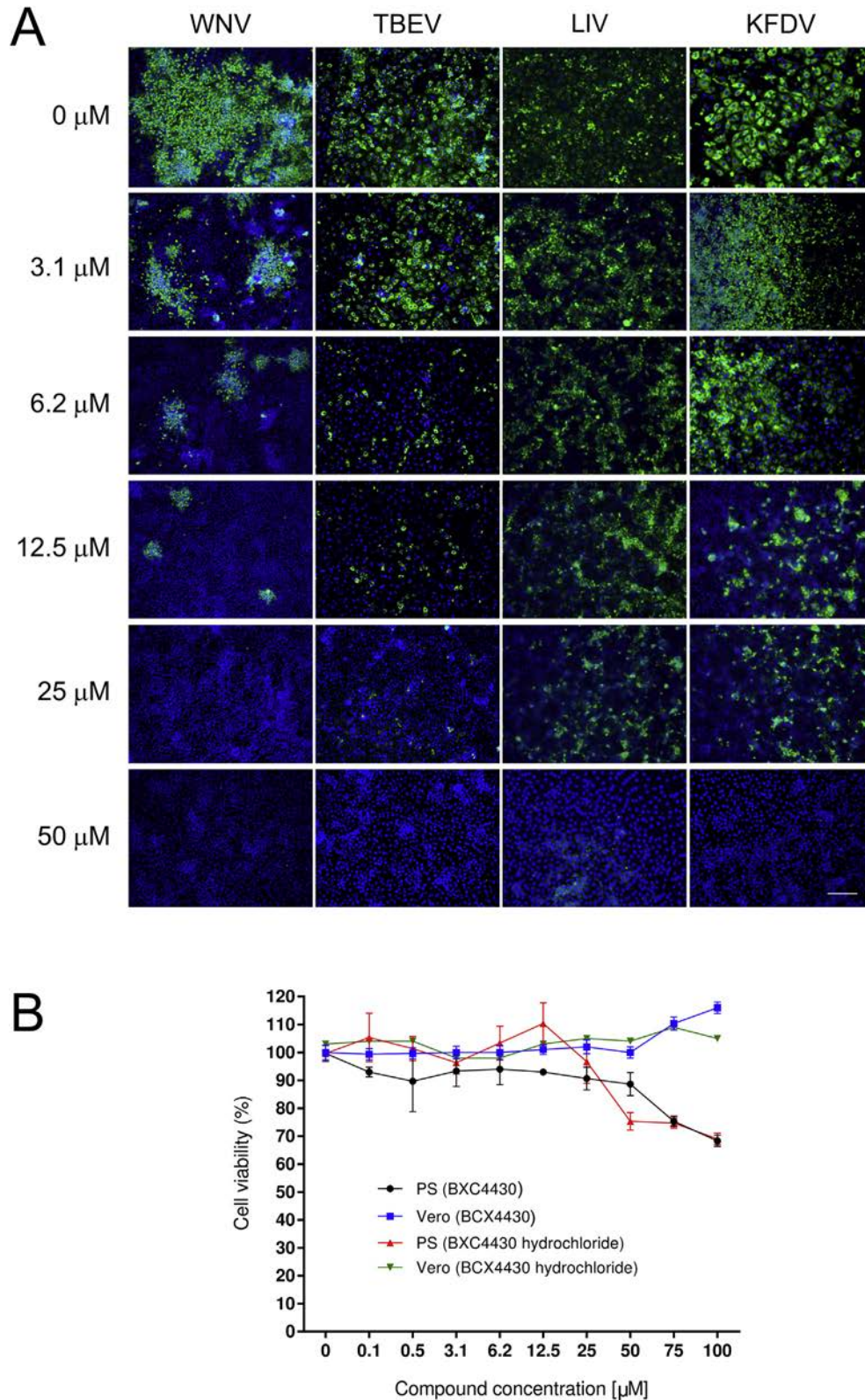


Fig. 2. (A) Inhibition of flaviviral surface E antigen expression by BCX4430. Virus infected PS cells were fixed on slides at 3 days p.i. and stained with flavivirus-specific antibody labeled with FITC (green) and counterstained with DAPI (blue). Scale bar, 50 μm . (B) Cytotoxicity of BCX4430 on PS and Vero cells, within the compound concentration range 0–100 μM , at day 3 p.i. (For interpretation of the references to colour in this figure legend, the reader is referred to the web version of this article.)

observed differences in drug sensitivity in the flaviviruses studied could be related to molecular distinctions in their RNA-dependent RNA polymerases, as well as in cellular uptake and intracellular

metabolism (such as deamination, phosphorolysis, or phosphorylation), which can also considerably influence the antiviral activity of a nucleoside analogue (Eldrup et al., 2004). Interestingly, both

chemical forms of BCX4430 exerted similar inhibitory and cytotoxicity profiles in the applied *in vitro* antiviral assay systems. Our results, together with the findings from previous *in vitro* and *in vivo* studies (Julander et al., 2014, 2017; Warren et al., 2014), indicate that BCX4430 may represent a pan-flavivirus nucleoside inhibitor suitable for further clinical testing as a therapeutic agent in flaviviral infections.

Acknowledgements

The authors are greatly indebted to Dr. Ivana Huvarová for excellent technical assistance. This study was supported by the Czech Science Foundation project GA16-20054S; Czech Agency for Medical Research, Ministry of Health of the Czech Republic (grant No. 16-34238A); and by project LO1218, with financial support from the Ministry of Education, Youth, and Sports of the Czech Republic under the NPU I program. We also acknowledge a grant for the development of research organizations (RVO: 61388963).

References

- Asghar, N., Lee, Y.P., Nilsson, E., Lindqvist, R., Melik, W., Kröger, A., Överby, A.K., Johansson, M., 2016. The role of the poly(A) tract in the replication and virulence of tick-borne encephalitis virus. *Sci. Rep.* 6, 39265. <http://dx.doi.org/10.1038/srep39265>.
- Asghar, N., Lindblom, P., Melik, W., Lindqvist, R., Haglund, M., Forsberg, P., Överby, A.K., Andreassen, Å., Lindgren, P.E., Johansson, M., 2014. Tick-borne encephalitis virus sequenced directly from questing and blood-feeding ticks reveals quasispecies variance. *PLoS One* 9 (7), e103264. <http://dx.doi.org/10.1371/journal.pone.0103264>.
- Baier, A., 2011. Flaviviral infections and potential targets for antiviral therapy. In: Ruzek, D. (Ed.), *Flavivirus Encephalitis*. InTech, Rijeka, Croatia.
- Borowski, P., Lang, M., Haag, A., Schmitz, H., Choe, J., Chen, H.M., Hosmane, R.S., 2002. Characterization of imidazo[4,5-d]pyridazine nucleosides as modulators of unwinding reaction mediated by West Nile virus nucleoside triphosphatase/helicase: evidence for activity on the level of substrate and/or enzyme. *Antimicrob. Agents Chemother.* 46, 1231–1239. <http://dx.doi.org/10.1002/art.40038>.
- De Clercq, E., 2016. C-nucleosides to be revisited. *J. Med. Chem.* 59, 2301–2311. <http://dx.doi.org/10.1021/acs.jmedchem.5b01157>.
- De Madrid, A.T., Porterfield, J.S., 1969. A simple micro-culture method for study of group B arboviruses. *Bull. World Health Org.* 40, 113–121.
- Deval, J., Symons, J.A., Beigelman, L., 2014. Inhibition of viral RNA polymerases by nucleoside and nucleotide analogs: therapeutic applications against positive-strand RNA viruses beyond hepatitis C virus. *Curr. Opin. Virol.* 9, 1–7. <http://dx.doi.org/10.1016/j.coviro.2014.08.004>.
- Eldrup, A.B., Allerson, C.R., Bennett, C.F., Bera, S., Bhat, B., Bhat, N., Bosserman, M.R., Brooks, J., Burlein, C., Carroll, S.S., Cook, P.D., Getty, K.L., MacCoss, M., McMasters, D.R., Olsen, D.B., Prakash, T.P., Prhac, M., Song, Q.L., Tomassini, J.E., Xia, J., 2004. Structure-activity relationship of purine ribonucleosides for inhibition of hepatitis C virus RNA-dependent RNA polymerase. *J. Med. Chem.* 47, 2283–2295. <http://dx.doi.org/10.1021/jm030424e>.
- Eyer, L., Nencka, R., Huvarov, I., Palus, M., Joao Alves, M., Gould, E.A., De Clercq, E., Ruzek, D., 2016a. Nucleoside inhibitors of Zika virus. *J. Infect. Dis.* 214, 707–711. <http://dx.doi.org/10.1093/infdis/jiw226>.
- Eyer, L., Smidkova, M., Nencka, R., Neca, J., Kastl, T., Palus, M., De Clercq, E., Ruzek, D., 2016b. Structure-activity relationships of nucleoside analogues for inhibition of tick-borne encephalitis virus. *Antivir. Res.* 133, 119–129. <http://dx.doi.org/10.1016/j.antiviral.2016.07.018>.
- Eyer, L., Valdes, J.J., Gil, V.A., Nencka, R., Hrebabecky, H., Sala, M., Salat, J., Cerny, J., Palus, M., De Clercq, E., Ruzek, D., 2015. Nucleoside inhibitors of tick-borne encephalitis virus. *Antimicrob. Agents Chemother.* 59, 5483–5493. <http://dx.doi.org/10.1128/AAC.00807-15>.
- Flint, M., McMullan, L.K., Dodd, K.A., Bird, B.H., Khristova, M.L., Nichol, S.T., Spiropoulou, C.F., 2014. Inhibitors of the tick-borne, hemorrhagic fever-associated flaviviruses. *Antimicrob. Agents Chemother.* 58, 3206–3216. <http://dx.doi.org/10.1128/AAC.02393-14>.
- Hosmane, R.S., Zhang, N., Chen, H.M., Koch, V., Schmitz, H., Liao, C.L., Fattom, A.I., Naso, R.B., Borowski, P., 2003. Potent inhibition of NTPases/helicases of the West Nile Virus (WNV) and other flaviviridae by ring-expanded ("fat") nucleoside and nucleotide analogues. *Antivir. Res.* 57, A87. <http://dx.doi.org/10.1021/jm030277k>.
- Julander, J.G., Bantia, S., Taubenheim, B.R., Minning, D.M., Kotian, P., Morrey, J.D., Smee, D.F., Sheridan, W.P., Babu, Y.S., 2014. BCX4430, a novel nucleoside analog, effectively treats yellow fever in a hamster model. *Antimicrob. Agents Chemother.* 58, 6607–6614. <http://dx.doi.org/10.1128/AAC.03368-14>.
- Julander, J.G., Siddharthan, V., Evans, J., Taylor, R., Tolbert, K., Apuli, C., Stewart, J., Collins, P., Gebre, M., Neilson, S., Van Wettere, A., Lee, Y.M., Sheridan, W.P., Morrey, J.D., Babu, Y.S., 2017. Efficacy of the broad-spectrum antiviral compound BCX4430 against Zika virus in cell culture and in a mouse model. *Antivir. Res.* 137, 14–22. <http://dx.doi.org/10.1016/j.antiviral.2016.11.003>.
- Kozuch, O., Mayer, V., 1975. Pig kidney epithelial (ps) cells: a perfect tool for study of flavi-viruses and some other arboviruses. *Acta Virol.* 19, 498.
- Lazear, H.M., Stringer, E.M., de Silva, A.M., 2016. The emerging Zika virus epidemic in the Americas research priorities. *JAMA* 315, 1945–1946. <http://dx.doi.org/10.1001/jama.2016.2899>.
- Lo, M.K., Shi, P.Y., Chen, Y.L., Flint, M., Spiropoulou, C.F., 2016. In vitro antiviral activity of adenosine analog NITD008 against tick borne flaviviruses. *Antivir. Res.* 130, 46–49. <http://dx.doi.org/10.1016/j.antiviral.2016.03.013>.
- Sakai, M., Yoshii, K., Sunden, Y., Yokozawa, K., Hirano, M., Kariwa, H., 2014. Variable region of the 3' UTR is a critical virulence factor in the Far-Eastern subtype of tick-borne encephalitis virus in a mouse model. *J. Gen. Virol.* 95 (Pt 4), 823–835. <http://dx.doi.org/10.1099/vir.0.060046-0>.
- Taylor, R., Kotian, P., Warren, T., Panchal, R., Bavari, S., Julander, J., Dobo, S., Rose, A., El-Kattan, Y., Taubenheim, B., Babu, Y., Sheridan, W.P., 2016. BCX4430-A broad-spectrum antiviral adenosine nucleoside analog under development for the treatment of Ebola virus disease. *J. Infect. Public. Health* 9, 220–226. <http://dx.doi.org/10.1016/j.jiph.2016.04.002>.
- Warren, T.K., Wells, J., Panchal, R.G., Stuthman, K.S., Garza, N.L., Van Tongeren, S.A., Dong, L., Retterer, C.J., Eaton, B.P., Pegoraro, G., Honnold, S., Bantia, S., Kotian, P., Chen, X.L., Taubenheim, B.R., Welch, L.S., Minning, D.M., Babu, Y.S., Sheridan, W.P., Bavari, S., 2014. Protection against filovirus diseases by a novel broad-spectrum nucleoside analogue BCX4430. *Nature* 508, 402–405. <http://dx.doi.org/10.1038/nature13027>.



An E460D Substitution in the NS5 Protein of Tick-Borne Encephalitis Virus Confers Resistance to the Inhibitor Galidesivir (BCX4430) and Also Attenuates the Virus for Mice

Ludek Eyer,^{a,b} Antoine Nougairède,^c Marie Uhlířová,^a  Jean-Sélim Driouich,^c Darina Zouharová,^a James J. Valdés,^{a,b} Jan Haviernik,^a Ernest A. Gould,^c Erik De Clercq,^d Xavier de Lamballerie,^c  Daniel Ruzek^{a,b}

^aDepartment of Virology, Veterinary Research Institute, Brno, Czech Republic

^bInstitute of Parasitology, Biology Centre of the Czech Academy of Sciences, Ceske Budejovice, Czech Republic

^cUnité des Virus Émergents (Aix-Marseille Univ-IRD 190-Inserm 1207-IHU Méditerranée Infection), Marseille, France

^dKU Leuven, Rega Institute of Medical Research, Leuven, Belgium

ABSTRACT The adenosine analogue galidesivir (BCX4430), a broad-spectrum RNA virus inhibitor, has entered a phase 1 clinical safety and pharmacokinetics study in healthy subjects and is under clinical development for treatment of Ebola and yellow fever virus infections. Moreover, galidesivir also inhibits the reproduction of tick-borne encephalitis virus (TBEV) and numerous other medically important flaviviruses. Until now, studies of this antiviral agent have not yielded resistant viruses. Here, we demonstrate that an E460D substitution in the active site of TBEV RNA-dependent RNA polymerase (RdRp) confers resistance to galidesivir in cell culture. Galidesivir-resistant TBEV exhibited no cross-resistance to structurally different antiviral nucleoside analogues, such as 7-deaza-2'-C-methyladenosine, 2'-C-methyladenosine, and 4'-azido-aracytidine. Although the E460D substitution led to only a subtle decrease in viral fitness in cell culture, galidesivir-resistant TBEV was highly attenuated *in vivo*, with a 100% survival rate and no clinical signs observed in infected mice. Furthermore, no virus was detected in the sera, spleen, or brain of mice inoculated with the galidesivir-resistant TBEV. Our results contribute to understanding the molecular basis of galidesivir antiviral activity, flavivirus resistance to nucleoside inhibitors, and the potential contribution of viral RdRp to flavivirus neurovirulence.

IMPORTANCE Tick-borne encephalitis virus (TBEV) is a pathogen that causes severe human neuroinfections in Europe and Asia and for which there is currently no specific therapy. We have previously found that galidesivir (BCX4430), a broad-spectrum RNA virus inhibitor, which is under clinical development for treatment of Ebola and yellow fever virus infections, has a strong antiviral effect against TBEV. For any antiviral drug, it is important to generate drug-resistant mutants to understand how the drug works. Here, we produced TBEV mutants resistant to galidesivir and found that the resistance is caused by a single amino acid substitution in an active site of the viral RNA-dependent RNA polymerase, an enzyme which is crucial for replication of the viral RNA genome. Although this substitution led only to a subtle decrease in viral fitness in cell culture, galidesivir-resistant TBEV was highly attenuated in a mouse model. Our results contribute to understanding the molecular basis of galidesivir antiviral activity.

KEYWORDS BCX4430, galidesivir, attenuation, drug resistance, mutation, tick-borne encephalitis virus

Flaviviruses (family *Flaviviridae*, genus *Flavivirus*) cause widespread human morbidity and mortality throughout the world. These viruses are typically transmitted to humans by mosquito or tick vectors. Tick-borne encephalitis virus (TBEV) is a typical

Citation Eyer L, Nougairède A, Uhlířová M, Driouich J-S, Zouharová D, Valdés JJ, Haviernik J, Gould EA, De Clercq E, de Lamballerie X, Ruzek D. 2019. An E460D substitution in the NS5 protein of tick-borne encephalitis virus confers resistance to the inhibitor galidesivir (BCX4430) and also attenuates the virus for mice. *J Virol* 93:e00367-19. <https://doi.org/10.1128/JVI.00367-19>.

Editor Julie K. Pfeiffer, University of Texas Southwestern Medical Center

Copyright © 2019 American Society for Microbiology. All Rights Reserved.

Address correspondence to Daniel Ruzek, ruzekd@paru.cas.cz.

Received 1 March 2019

Accepted 24 May 2019

Accepted manuscript posted online 29 May 2019

Published 30 July 2019

flavivirus transmitted by *Ixodes* spp. ticks. TBEV is a causative agent of tick-borne encephalitis (TBE), a severe and potentially lethal neuroinfection in humans (1). The disease is prevalent in the sylvatic areas of Europe and Asia, with more than 13,000 cases of TBE being reported annually (2, 3). The clinical presentation of TBE ranges from mild fever to severe encephalitis or encephalomyelitis. In many cases, survivors of TBE suffer long-term or even permanent debilitating sequelae (4). As for other flaviviral infections, there is no specific treatment for TBE other than supportive therapy. Thus, the search for antiviral agents for specific chemotherapy of TBE and related viruses is urgent.

Among the different strategies aimed at inhibiting virus or cell components involved in TBEV replication, the viral nonstructural NS5 protein, an RNA-dependent RNA polymerase (RdRp), has become an attractive target for specific and effective inhibition of viral replication, with limited measurable effect on the host cells (5). Several molecules, mainly nucleoside analogues, were found to be potent inhibitors of the TBEV NS5 polymerase activity (6–9). The mechanism of action of these nucleoside analogues is based on their initial metabolization to the active triphosphate (nucleotide) form by cellular kinases and subsequent incorporation into the nascent genome by the RdRp, leading to premature chain termination (5). Galidesivir (also known as BCX4430 or Immucillin-A, Fig. 1A) is an adenosine analogue with two structural modifications: (i) it is a C-nucleoside characterized by a C-glycosidic bond instead of the usual N-glycosidic bond, and (ii) the furanose oxygen has been replaced by an imino group (10). Galidesivir is known to have a broad-spectrum antiviral effect against more than 20 different medically important RNA viruses across nine different virus families (flaviviruses, togaviruses, bunyaviruses, arenaviruses, paramyxoviruses, coronaviruses, filoviruses, orthomyxoviruses, and picornaviruses) (10–15). Low micromolar levels of galidesivir were previously shown to inhibit TBEV with no or negligible cytopathic effect (CPE) on the host cells (7). A phase 1 clinical safety and pharmacokinetics study in healthy subjects has been completed, and at present, galidesivir is under clinical development as an antiviral drug for treatment of Ebola virus infection (14), as well as for the treatment of yellow fever (<https://clinicaltrials.gov/ct2/show/NCT03891420>). Its broad-spectrum antiviral activity makes this drug a promising candidate for development of therapy not only for Ebola or yellow fever viruses infection but also other important diseases caused by various RNA viruses, including TBEV.

Although galidesivir has been studied intensively and is known to inhibit a wide range of RNA viruses, there are no published reports of resistance to this compound. Experience with the treatment of other RNA virus infections shows that resistance can develop rapidly with any of the direct-acting antiviral agents (16–18). Due to the low fidelity of viral RdRps in general, the mutation frequency is estimated to be 10^{-4} to 10^{-6} errors per nucleotide (19). The high mutation frequency and high replication rate of viral RNA copies enable the viruses quickly to adapt to changes in the environment, including the introduction of antiviral drugs. Identification of mutations conferring antiviral resistance provides information not only about the risk of generation of drug-resistant mutants but also helps to elucidate molecular mechanisms of the antiviral action. This is an integral and essential part of development and testing of any new antiviral drug (17).

In the present study, we identified and described a specific amino acid substitution in the TBEV NS5 polymerase that confers resistance to galidesivir. This substitution had only a limited effect on viral reproduction *in vitro* but had a cost on viral fitness when tested *in vivo* using mice. Our findings are important for understanding the mechanism of action of galidesivir and for the use of this molecule as an antiviral drug against TBEV and other emerging RNA viruses. In addition, we highlight the discovery of a potential contribution of viral RdRp to flavivirus neurovirulence.

(This article was submitted to an online preprint archive [20].)

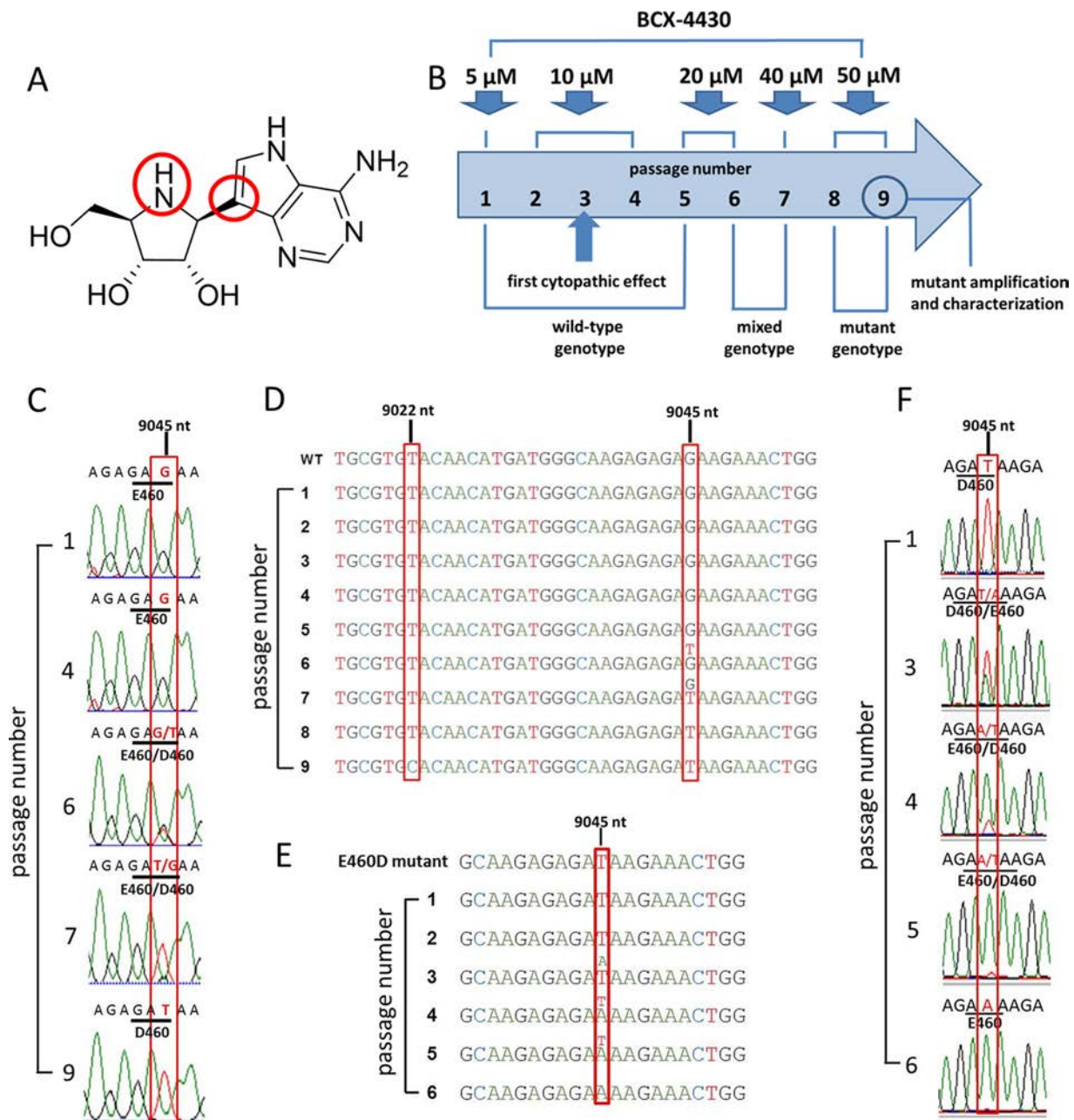


FIG 1 TBEV resistance to galidesivir is associated with a single mutation in the NS5 gene. (A) The structure of the nucleoside analogue galidesivir. (B) Scheme of the selection process for generation of TBEV resistance to galidesivir. TBEV was serially passaged in PS cells in the presence of increasing galidesivir concentrations. (C) Whole-genome sequence analysis of the passaged viruses revealed a mutation at the amino acid position 460 in the NS5 protein, changing the glutamic acid residue to aspartic acid. (D) In the E460D/Y453H mutant, both amino acid changes E460D (nucleotide position G9045T) and Y453H (nucleotide position T9022C) were detected in the NS5 protein after 5 and 8 passages in the presence of galidesivir, respectively. (E) Rapid reinduction of the wild-type genotype in PS cells after serial passage of TBEV in PS cells in the absence of galidesivir. (F) During serial passage of the *in vitro*-selected E460D mutant virus in PS cells in the absence of galidesivir, the amino acid codon GAT (in the mutant) was changed to the codon GAA (in the revertant).

RESULTS

TBEV resistant to galidesivir has two amino acid substitutions in the NS5 protein. Studies of drug-resistant virus mutants are crucial for understanding molecular interactions of antiviral drugs with target viral proteins, as well as for development of efficient and specific antiviral therapies. In order to select TBEV resistant to galidesivir, the virus was serially passaged in porcine kidney stable (PS) cell monolayers in the presence of increasing concentrations of galidesivir up to 50 μ M (Fig. 1B); this process

resulted in selection of two independent drug-resistant TBEV mutant strains. Whole-genome sequencing of the passaged viruses revealed that both selected TBEV mutants carried a single amino acid change E460D, which corresponds to the nucleotide substitution G9045T in the NS5 gene (Fig. 1C and D). Sequencing of viruses after each passage showed that this mutation was acquired after 5 passages. In passages 6 and 7, mixed mutated and wild-type genotypes were detected; from passage 8 onward, the mutated genotype dominated until the end of the experiment (passage 9) (Fig. 1D). Interestingly, in one of the selected TBEV mutants, an additional amino acid change Y453H was detected; this mutation, which was acquired after eight passages, corresponds to the nucleotide substitution T9022C in the NS5 gene (Fig. 1D). Mutations E460D and Y453H were not present in the wild-type virus passaged in the absence of the selection agents. Both mutations mapped to the active site of the RdRp domain of the NS5 protein. The *in vitro*-selected TBEV mutants (denoted as E460D and E460D/Y453H) were further evaluated for their sensitivity/resistance to galidesivir at concentrations ranging from 0 to 50 μM and compared to the mock-selected wild-type virus (Fig. 2A). Whereas *in vitro* replication of wild-type was completely inhibited by galidesivir at a concentration of 12.5 μM (50% effective concentration [EC_{50}] of $0.95 \pm 0.04 \mu\text{M}$), both mutants were approximately 7-fold less sensitive to the compound, showing EC_{50} values of 6.66 ± 0.04 and $7.20 \pm 0.09 \mu\text{M}$, respectively, for E460D and E460D/Y453H (Fig. 2A, Table 1).

Site-directed mutagenesis confirms that E460D determines TBEV drug resistance. In order to demonstrate the direct effect of the amino acid substitutions E460D and Y453H on TBEV phenotype, the appropriate mutations were introduced into recombinant TBEV strains generated by the rapid reverse-genetics approach based on the use of subgenomic overlapping DNA fragments (21, 22). The entire TBEV strain Hypr genome flanked at the 5' and 3' untranslated regions by the pCMV and HDR/SV40pA was *de novo* synthesized in three double-stranded DNA fragments of approximately 4.4, 4.5, and 3.1 kb in length, overlapping by 80 to 120 pb. The substitutions E460D (G9045T) and Y453H (T9022C) were introduced into the NS5 gene located on fragment III using mutagenic PCR primers (Table 2). After transfection of the subgenomic fragments into permissive BHK-21 cells, the following recombinant TBEV strains were successfully rescued: E460D-Rec (E460D substitution in the NS5 gene), Y453H-Rec (Y453H substitution in the NS5 gene), and recombinant wild type (no introduced mutations). The presence of the E460D and Y453H substitutions in the viral genomes was confirmed by whole-genome sequencing of all recombinant viruses. Despite repeated attempts, the E460D/Y453H-Rec mutant (both mutations E460D and Y453H in the NS5 gene) was not rescued from the transfected BHK-21 cell culture. E460D-Rec was found to be 7.9-fold less sensitive to galidesivir than the engineered wild type, showing an EC_{50} value of $6.32 \pm 1.01 \mu\text{M}$ (Table 1). On the other hand, Y453H-Rec was highly sensitive to galidesivir; the replication of this mutant strain was completely inhibited at 12.5 μM , showing an EC_{50} value of $0.81 \pm 0.01 \mu\text{M}$ (Table 1). Thus, the results indicate that the E460D (not Y453H) substitution is solely responsible for the drug-resistant phenotype of TBEV (Fig. 2A).

The E460D mutation decreases TBEV replication fitness in cell culture during the first 36 h postinfection. To characterize the phenotypic properties of the drug-resistant mutant *in vitro*, the growth kinetics (Fig. 2B) and plaque morphology (Fig. 2C) of the recombinant TBEV mutant E460D-Rec were assayed in cultures of PS cells and compared to the wild-type virus. The wild-type virus amplified in the absence of galidesivir (Fig. 2B, red line) showed a short lag period within the interval from 0 to 12 h postinfection (p.i.). Starting 24 h p.i., the wild-type TBEV exerted an exponential increase in virus infectivity, reaching a peak titer of 3×10^6 PFU/ml within 72 h p.i. and gradually declining thereafter. In contrast, the presence of galidesivir (25 μM) completely inhibited replication of the wild-type virus (Fig. 2B, violet line).

In comparison to the wild-type virus, the E460D-Rec mutant cultured in the absence of galidesivir (Fig. 2B, blue line) showed a prolonged lag-period within the interval from 0 to 36 h p.i. However, subsequently, the infectivity of the mutant virus increased

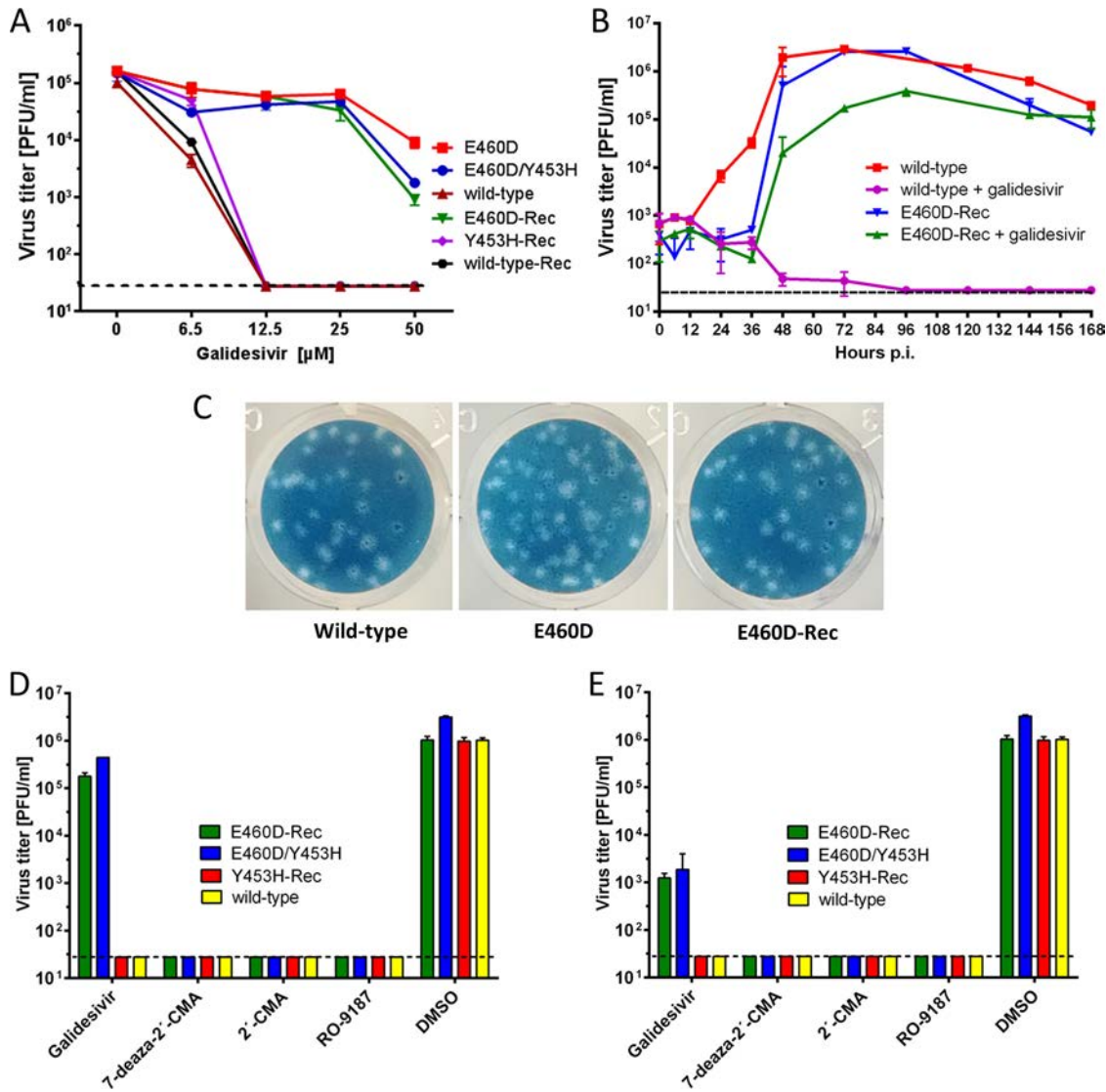


FIG 2 Phenotypic properties of TBEV mutant resistant to galidesivir *in vitro*. (A) Dose-response curves for TBEV mutants E460D, E460D/E453H, E460D-Rec, Y453H-Rec, and corresponding wild types grown in PS cells in the presence of galidesivir at the indicated compound concentrations. Only TBEVs bearing the E460D mutation (i.e., E460D, E460D/E453H, and E460D-Rec) were resistant to galidesivir, indicating that this mutation is responsible for the resistance phenotype. (B) Growth kinetics of the E460D-Rec mutant and wild-type TBEV in the presence (25 μM) or absence (0 μM) of galidesivir within the 7-day experimental period to assess the replication efficacy of the mutant TBEV in PS cells. (C) Plaque morphology of the E460D and E460D-Rec mutants was assessed in PS cell monolayers and compared to the wild-type virus. (D and E) The sensitivity/resistance profiles of the E460D/Y453H, E460D-Rec, and Y453H-Rec to diverse nucleoside inhibitors (concentrations of 25 μM [D] and 50 μM [E]) were evaluated in PS cells and compared to the corresponding wild-type TBEV. The mean titers from two independent experiments, each performed in triplicate, are shown, and error bars indicate the standard errors of the mean. The horizontal dashed line indicates the minimum detectable threshold of 1.44 \log_{10} PFU/ml.

exponentially, reaching a peak of 2.6×10^6 PFU/ml at 72 h p.i. After that, the titer gradually declined to 5.5×10^4 PFU/ml. The considerably longer lag period of the E460D-Rec mutant could be explained by a slightly decreased replication capacity (attenuation) of the mutant when amplified in PS cell culture. The decrease in replication capacity of E460D-Rec was manifested particularly in the first few hours after cell culture infection and was no longer detectable in the later stages of the infection.

The E460D-Rec mutant cultured in the presence of galidesivir (25 μM) (Fig. 2B, green line) also exerted an extended lag period within the interval from 0 to 36 h p.i.; there was even a moderate decrease in viral titers after 36 h p.i. Beginning at 48 h p.i., the mutant showed an exponential infectivity and reached a peak titer of 3.9×10^5 PFU/ml

TABLE 1 Inhibitory properties of galidesivir for the obtained TBEVs

Method used to generate wild-type/mutated virus	Virus	EC ₅₀ (μM) ^a
<i>In vitro</i> selection (passaging in PS cells)	E460D	6.66 ± 0.04 (7.01)
	E460D/Y453H	7.20 ± 0.09 (7.57)
	Wild type	0.95 ± 0.04
Reverse genetics	E460D-Rec	6.32 ± 1.01 (7.90)
	Y453H-Rec	0.81 ± 0.01 (1.01)
	E460D/Y453H-Rec	Not rescued
	Wild-type-Rec	0.80 ± 0.01

^aDetermined from three independent experiments. Values are expressed as a 50% reduction in viral titer and were calculated according to the Reed-Muench method. PS cells were infected with the virus (MOI of 0.1) and cultivated at galidesivir concentrations ranging from 0 to 50 μM for 3 days. The fold increase compared to the wild-type value is indicated in parentheses.

at day 96 h p.i. The results clearly indicate that the resistance of TBEV to galidesivir is only partial; the growth of the mutant strain in the presence of galidesivir was partially inhibited compared to the wild type (Fig. 2B, red line) or the E460D-Rec mutant grown in the absence of galidesivir (Fig. 2B, blue line).

The plaque morphology of the drug-resistant TBEV mutant was similar to that of wild-type virus; both viruses produced large and clear plaques which were round and regular in shape and did not change in shape and size during all the consecutive passages (Fig. 2C). The similarity in plaque morphology of drug-resistant and wild-type TBEVs is in agreement with similar growth kinetics of both viruses and supports our assumption that the mutation E460D affects the viral replication in PS cell culture only to a limited extent.

The E460D TBEV mutant is sensitive to 7-deaza-2'-C-methyladenosine, 2'-C-methyladenosine and 4'-azido-aracytidine. To test whether or not E460D and Y453H substitutions affect sensitivity of TBEV to structurally different nucleoside inhibitors, we evaluated selected nucleoside analogues with previously reported anti-TBEV activity (6) for their capacity to inhibit the *in vitro* replication of galidesivir-resistant TBEV. Inhibitory effects of 7-deaza-2'-C-methyladenosine, 2'-C-methyladenosine, and 4'-azido-aracytidine (RO-9187) at concentrations of 25 and 50 μM were not affected in the E460D/Y453H mutant, which was obtained by serial subculture in PS cells in the presence of galidesivir (Fig. 2D and E). The same drug sensitivity profile, characterized by complete inhibition of virus replication, was determined for two recombinant TBEVs generated by reverse genetics: E460D-Rec and Y453H-Rec. Wild-type virus was used as a positive control in this *in vitro* antiviral study (Fig. 2D and E). The EC₅₀ values of 7-deaza-2'-C-methyladenosine, 2'-C-methyladenosine, and 4'-azido-aracytidine for the galidesivir-resistant mutant were analogous to those for the wild-type virus (not shown) and corresponded to the values reported previously (6).

Mouse neuroinvasiveness of the E460D TBEV mutant is highly attenuated. The degree of neuroinvasiveness of the E460D TBEV mutant was assessed in BALB/c mice and was compared to that of the wild-type virus. Adult BALB/c mice were infected subcutaneously (s.c.) with 10³ PFU of either virus and survival rates, and clinical signs of neuroinfection were monitored for 28 days. Wild-type virus produced fatal infections in all mice, with mean survival times of 11 ± 2.2 days; infected mice showed severe signs of disease, such as ruffled fur, hunched posture, tremor, and hind leg paralysis (Fig. 3A and C). In contrast, all mice infected with the drug-resistant TBEV mutant E460D (obtained by serial *in vitro* subculture in the presence of galidesivir) survived ($P < 0.0001$), displaying no clinical signs of TBEV infection through the entire 28-day experimental period (Fig. 3A and C). The same survival data (100% survival rate, $P < 0.0001$) and clinical scores (no signs of neuroinfection) were obtained when recombinant TBEV mutant (E460D-Rec) was used for mouse infection using the same infectious dose and administration route (Fig. 3B and D).

Mouse serum, spleen, and brain samples were harvested for titration at various time points after s.c. inoculation of the galidesivir-resistant and wild-type TBEV. At early

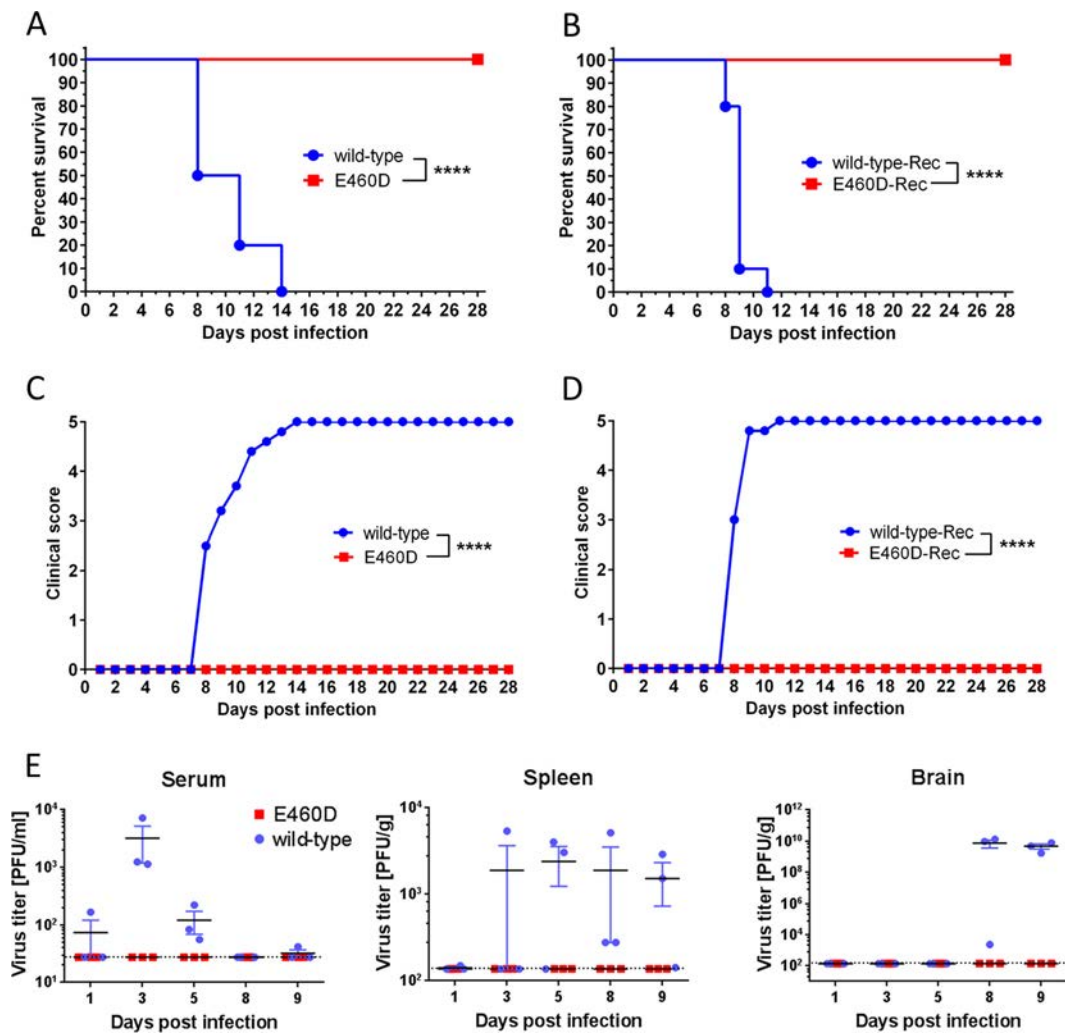


FIG 3 Phenotypic properties of the TBEV mutant resistant to galidesivir in mice. The extent of neuroinvasiveness of the E460D and E460D-Rec TBEV mutants was investigated in BALB/c mice and compared to that of the wild-type virus. Adult BALB/c mice were infected s.c. with 10^3 PFU of either virus, and survival (A and B) and clinical scores of the neuroinfection (C and D) were monitored for 28 days. ****, $P < 0.0001$. (E) Viral titers in blood sera, brains, and spleens of wild-type or E460D-infected BALB/c mice (infectious dose of 10^3 PFU) were determined by plaque assay at days 1, 3, 5, 8, and 9 p.i. The titers for three mice per interval are shown, and bars indicate means \pm the standard errors of the mean. The dotted lines indicate detection limits.

stages of the infection (day 1 p.i.), the wild-type virus showed a slight viremia in one of the three animals tested (10^2 PFU/ml). The wild-type virus caused a peak viremia on day 3 p.i. (approximately 2×10^3 PFU/ml); the viral titers in sera gradually decreased to the detection limit of plaque assay by day 9 p.i. No wild-type virus was detected in brains collected on days 1, 3, and 5 p.i.; however, the virus was detected in brains on days 8 and 9 p.i. at high titers reaching up to 10^{10} PFU/g. In spleens, the wild-type TBEV was first detected on day 3 p.i. and was present at a constant level (viral titers around 2×10^3 PFU/g) until the end of the experiment (Fig. 3E). In contrast, the E460D TBEV mutant was not detected neither in any serum, spleen, or brain samples collected during the whole experimental period (Fig. 3E).

Rapid reinduction of wild-type genotype in the absence of galidesivir. In general, mutant genotypes rapidly revert to the wild type in the absence of the selection agents. Indeed, after three passages in PS cells in the absence of galidesivir, a pool comprising mutated and wild-type genotypes was detected. Moreover, from passage 5 onward the wild-type genotype dominated in the infected PS cell culture (Fig. 1E). Interestingly, the codon GAT encoding an aspartic acid in the E460D mutant had changed to the codon

GAA in the revertant, not to GAG as seen in mock-selected wild-type virus; both codons, GAA (in the revertant) and GAG (in the wild type), are synonymous and encode a glutamic acid residue (Fig. 1F). In contrast, after six passages in the presence of galidesivir at concentrations up to 25 μM , the E460D substitution was retained, even at low concentrations of galidesivir (6.25 μM), and did not result in reversion to the wild-type genotype (data not shown).

DISCUSSION

Galidesivir is an adenosine analogue originally developed for filovirus infection treatment (Ebola and Marburg) with high antiviral potency against a broad spectrum of RNA viruses (10, 14), including TBEV (7) and other medically important arthropod-borne flaviviruses (10, 12, 13). Currently, this compound entered first-in-human clinical studies that focused on intramuscular administration in healthy volunteers showing promising pharmacokinetics properties and good tolerability (14). This makes galidesivir a promising candidate drug to treat patients with TBE or with other flaviviral infections. However, antiviral therapy based on small molecule inhibitors of viral replication can be accompanied by rapid evolution of drug resistance, which can abolish the progress of infection treatment and finally lead to the failure of the therapy (23). Therefore, for each new antiviral agent, the risks of resistance are important to assess in terms of (i) identification of key mutations conferring virus drug resistance and (ii) phenotype characterization of drug-resistant mutants.

Serial *in vitro* passaging of TBEV in the presence of increasing concentrations of galidesivir (up to 50 μM) resulted in generation of two drug-resistant TBEV mutants which were \sim 7-fold less sensitive to galidesivir than the mock-selected wild-type virus. The first TBEV mutant was characterized by a single amino acid change E460D; the other one carried two amino acid changes, E460D and Y453H. Both mutations mapped to the active site of the viral RdRp. The location of the resistance-associated mutations within the viral RdRp active site is essential to understand the mechanism of action of galidesivir; this compound prevents the binding of subsequent nucleotides to the RdRp active site, being considered a nonobligate chain terminator of viral RNA synthesis (10, 24). Single amino acid changes within the RdRp were previously identified in flaviviruses resistant to structurally different nucleoside analogues, as exemplified by the mutations S600T, S603T, S604T, and S282T conferring a high-level resistance to the 2'-C-methylated nucleosides in dengue virus, TBEV, Zika virus, and hepatitis C virus, respectively (8, 25–28). In Alkhurma haemorrhagic fever virus, the mutation S603T was associated with additional amino acid substitutions located in the NS5 RdRp active site, particularly with C666S and M644V (29).

Using a previously described reverse-genetics system (21, 22), we have demonstrated that the E460D mutation alone is crucial for resistance of TBEV to galidesivir; the recombinant E460D-Rec mutant was \sim 7-fold less sensitive to galidesivir compared to the wild type. On the other hand, the growth kinetics of the Y453H-Rec mutant was almost indistinguishable from that of wild-type virus; it is likely that Y453H can represent a compensation mutation or was acquired randomly. Because of the unique structural features of galidesivir (a C-glycosidic bond and a furanose oxygen on the ribose ring replaced by nitrogen) (11), no cross-resistance was seen to structurally different nucleoside analogues, such as 7-deaza-2'-C-methyladenosine, 2'-C-methyladenosine, and 4'-azidoaracytidine.

The E460D TBEV mutant showed similar growth kinetics to the wild-type virus when cultured *in vitro* on PS cell monolayers. Although a decreased replication capacity of the E460D mutant was observed in the first few hours after cell culture infection (0 to 36 h p.i.), both viruses reached a peak titer of about 10^5 to 10^6 PFU/ml at days 2 to 4 after infection. Similarly, the plaque morphology of the E460D mutant and wild-type virus were almost identical to each other; large, clear, and round plaques reflected the rapid and aggressive spread of both mutant and wild-type viruses in PS cell cultures. Thus, the E460D TBEV mutant differs from the recently isolated S603T TBEV mutant resistant to 2'-C-methylated nucleosides; the S603T mutant exerted significantly decreased

replication capacity in PS cells and a completely different plaque morphology (small, turbid plaques) compared to the wild-type virus (8). Our results demonstrate that antiviral resistance developed against two structurally different nucleoside analogues with the same mechanism of action can result in different effects on viral replication capacity in cell culture. Interestingly, in some drug-resistant virus mutants the cell type-dependent replication fitness was observed, as seen in chikungunya virus resistant to T-705 showing the attenuated phenotype in mosquito cell culture, whereas the replication fitness in Vero cells was similar to that of the wild type (30).

Although the introduction of the E460D mutation affects amplification of the virus in PS cell culture (i.e., *in vitro*) only slightly (within the interval 0 to 36 h p.i.), the E460D substitution resulted in a total loss of neuroinvasiveness for mice, *in vivo*; the E460D-infected animals all survived and displayed no clinical signs of neuroinfection during the 28-day experimental period. In contrast, infection with wild-type virus resulted in fatal infections for all animals. No virus was detected in the sera, spleens, or brains of mice inoculated with the E460D TBEV. In contrast, wild-type TBEV replicated efficiently in the inoculated mice, causing viremia and infection in the spleen and brain. The replication of the E460D mutant seems to be slower compared to the wild-type (as indicated by the comparison of the growth curves of these two viruses in cell culture) and, it is therefore likely that the virus is rapidly eliminated by the innate immunity soon after the inoculation. Attenuation of *in vivo* replication have previously been reported for drug-resistant RNA or DNA viral mutants, e.g., for TBEV resistance to 2'-C-methylated nucleosides (8), chikungunya virus resistance to T-705 (30), ribavirin resistance to porcine reproductive and respiratory syndrome virus (31), vaccinia virus resistance to acyclic nucleoside phosphonates (32), and pleconaril resistance to coxsackievirus (33).

The mutant genotype rapidly reverted to wild type when the virus was cultured in PS cell monolayers in the absence of selection agents. However, reversion was not observed when the virus was cultured in the presence of galidesivir in concentrations ranging from 6.25 to 25 μ M. Thus, under the selection pressure of galidesivir the mutation provides a replicative advantage over wild-type variants in the virus quasi-species population resulting in predominance of the mutant in the infected cell culture, despite the fact that the replication characteristics of both variants in cell culture are similar. The rapid reversion to glutamic acid in the absence of drug also suggests there is strong preference of an acidic residue at this position, which is consistent with the high conservation of E460 among flaviviral NS5 polymerases (among different TBEV strains, as well as among other representatives of the *Flaviviridae* family).

We conclude that the resistance of TBEV to the nucleoside analogue galidesivir is conferred by the single amino acid substitution E460D in the NS5 protein. Although this subtle mutation in the active site of the viral RdRp occurs after a few *in vitro* passages of TBEV in the presence of galidesivir, the E460D TBEV mutant displays a dramatically attenuated phenotype in mice showing high survival rates and a reduction in the clinical signs of neuroinfection. The E460D substitution did not confer cross-resistance to unrelated antiviral nucleoside analogues, such as 7-deaza-2'-C-methyladenosine, 2'-C-methyladenosine, and 4'-azido-aracytidine. This suggests that a combination treatment based on two or more inhibitors could be a possible strategy in order to minimize the risk of the emergence of viral drug resistance after therapeutic treatment with galidesivir.

MATERIALS AND METHODS

Ethics statement. This study was carried out in strict accordance with the Czech national law and guidelines on the use of experimental animals and protection of animals against cruelty (Animal Welfare Act no. 246/1992 Coll.). The protocol was approved by the Committee on the Ethics of Animal Experiments of the Institute of Parasitology and of the Departmental Expert Committee for the Approval of Projects of Experiments on Animals of the Academy of Sciences of the Czech Republic (permit 29/2016).

Virus, cells, and antiviral compounds. A well-characterized, low-passage-number TBEV strain Hypr (34), a member of the European TBEV subtype, was used in this study. Before use, the virus was subcultured intracerebrally six times in suckling mice. Porcine kidney stable (PS) cells (35) were used for viral subculture, selection of drug-resistant viruses, viral growth kinetics studies, and plaque assays. The

cells were cultured at 37°C in Leibovitz (L-15) medium supplemented with 3% newborn calf serum and a 1% mixture of penicillin and glutamine (Sigma-Aldrich, Prague, Czech Republic). BHK-21 cells (obtained from the American Type Culture Collection [ATCC]), used for transfection of Hypr-derived subgenomic fragments, were cultured at 37°C with 5% CO₂ in minimal essential medium (MEM) containing 7% bovine serum, 1% penicillin/streptomycin, and glutamine. Galidesivir (BCX4430) and 4'-azido-aracytidine (RO-9187) were purchased from MedChemExpress (Stockholm, Sweden); 2'-C-methyladenosine and 7-deaza-2'-C-methyladenosine were obtained from Carbosynth (Compton, UK). For *in vitro* studies, the test compounds were solubilized in 100% DMSO to yield 10 mM stock solutions.

Selection of drug-resistant viruses. The *in vitro* selection of drug-resistant TBEV clones was performed as described previously (8). Briefly, PS cells seeded in 96-well plates (2×10^4 cells per well) and incubated to form a confluent monolayer were infected with TBEV at a multiplicity of infection (MOI) of 0.1 and cultivated in the presence of 5 μ M galidesivir. After 3 to 5 days, the culture medium was harvested and used for infection of fresh cell monolayers. Individual passages were performed with gradually increasing concentrations of galidesivir as follows: passage 1 at 5 μ M, passages 2 to 4 at 10 μ M, passages 5 and 6 at 20 μ M, passage 7 at 40 μ M, and passages 8 and 9 at 50 μ M (Fig. 1B). In parallel, control TBEV was also passaged in the absence of galidesivir (with 0.5% [vol/vol] dimethyl sulfoxide [DMSO]) as a mock-selected wild-type virus. After passage 9, the drug-resistant and control TBEVs were subjected to an additional subculture to prepare virus stocks for further testing (average titers were between 10^5 and 10^6 PFU/ml). The *in vitro* selection protocol was carried out in duplicate, resulting in two independent TBEV mutants, denoted as E460D and E490D/Y453H. In order to recover the revertant wild-type virus from the E460D population, the E460D virus pool was repeatedly subcultured in PS cells in the absence of galidesivir; after six serial subcultures, the obtained revertant was amplified in PS cells to prepare a virus stock for further testing. Each of these viruses was subjected to full-length sequence analysis, sensitivity/resistance assessment to galidesivir and other nucleoside analogues, and virulence characterization in mice.

RNA isolation, PCR, and whole-genome sequencing. RNA was isolated from growth media by using a QIAmp viral RNA minikit (Qiagen). Reverse transcription was performed by using a ProtoScript first-strand cDNA kit (New England Biolabs) according to the manufacturer's instructions for the synthesis of first-strand cDNA, which was subsequently used for PCR amplification. To cover the whole genome of TBEV, 35 overlapping DNA fragments were produced by PCR as described previously (36). DNA was purified by using a High Pure PCR product purification kit (Roche, Prague, Czech Republic) according to the recommendations of the manufacturer. The PCR products were directly sequenced by commercial service (SEQme, Czech Republic) using the Sanger sequencing method. Both nucleotide and deduced amino acid sequences were analyzed by using the BioEdit sequence alignment editor, version 7.2.0.

Reverse-genetics system for TBEV hypr. The reverse-genetics system used in this study was based on the generation of infectious subgenomic overlapping DNA fragments that encompass the entire viral genome, as previously described (21, 22). Three *de novo*-synthesized DNA fragments cloned into a pUC57 vector were used in this study (GenScript, Piscataway, NJ): fragment I (nucleotide positions 1 to 3662), fragment II (nucleotide positions 3545 to 8043), and fragment III (nucleotide positions 7961 to 11100). The first and last fragments were flanked, respectively, at the 5' and 3' ends with the human cytomegalovirus promoter (pCMV) and the hepatitis delta ribozyme, followed by the simian virus 40 polyadenylation signal (HDR/SV40pA) (Fig. 4).

Fragments I and II were generated using the SuPreMe method (22). Briefly, plasmids that contained the DNA fragments I and II were digested by using *AgeI*/*FseI* and *SmaI*/*DraI* restriction enzymes, respectively (New England BioLabs, Ipswich, MA) (Fig. 4). Fragment III was used as the template to generate by PCR two overlapping amplicons according to the original ISA method (21). Unmodified primers were used to generate two unmodified amplicons (i.e., production of wild-type virus). Mutated primers located on the targeted region were used to generate two mutated amplicons (i.e., production of mutated viruses, denoted as E460D-Rec, Y453H-Rec, and E460D/Y453H-Rec) (Table 2, Fig. 4).

The PCR was performed using a Platinum SuperFI PCR master mix (Thermo Fisher Scientific, Prague, Czech Republic). The mixture (final volume, 50 μ l) contained 45 μ l of SuperMix and 2 μ l of DNA template (fragment III) at 1 ng/ μ l. Assays were performed on a Biometra TProfessional standard gradient thermocycler and the following conditions: 94°C for 2 min, followed by 40 cycles of 94°C for 15 s, 60°C for 30 s, and 68°C for 5 min and a final elongation step of 68°C for 10 min. The size of the PCR products was verified by gel electrophoresis and purified using an Amicon Ultra 0.5-ml kit (Millipore, Prague, Czech Republic).

An equimolar mixture of these four DNA fragments was used for cell transfection. A DNA-lipid complex was prepared as follows: 12 μ l of Lipofectamine 3000 (Thermo Fisher Scientific, Prague, Czech Republic) was diluted in 250 μ l of Opti-MEM medium (Life Technologies) and then mixed with a master solution of DNA that contained 3 μ g of DNA and 6 μ l of P3000 reagent diluted in 250 μ l of Opti-MEM medium. After a 45-min incubation at room temperature, BHK-21 cells were transfected as described previously (37) and incubated for 5 to 7 days. Cell supernatant media were then harvested and serially passaged twice in fresh BHK-21 culture.

Growth kinetics, dose-response studies, and viral inhibition assays. To evaluate growth kinetics of drug-resistant TBEV mutants, PS cell monolayers incubated for 24 h in 96-well plates were treated with 200 μ l of medium containing galidesivir at concentrations of 25 μ M (compound-treated cells) or 0.5% (vol/vol) DMSO (mock-treated cells) and simultaneously infected with TBEV; an MOI of 0.1 was used for all TBEV mutant/wild-type samples tested. The medium was collected from the wells daily at days 1 to 7 p.i. (three wells per interval). Viral titers (expressed as PFU/ml) were determined by plaque assay as described previously (9, 38) and used to construct TBEV growth curves.

TABLE 2 Unmodified and mutated primers used to generate two overlapping amplicons of fragment III (fragment IIIa and IIIb), i.e., to produce recombinant wild-type and mutated viruses

Primer type	Fragment III position	Forward or reverse	Generation of wild-type/mutated virus	Primer sequence ^a
Primers to amplify fragment IIIa	14–36	Forward	Wild-type-Rec	ATACACCATTGGTGAAGAGGGC
	975–1034	Reverse		CTTTCTCTCTTCATCCACGAGGTGCCAGAATGCAGG
	1070–1097	Reverse	E460D-Rec	ATCCTCTACAGCCTCTCTTGC
	1059–1090	Reverse	Y453H-Rec	CAGTTTCTT A TCTCTCTTCCCATCATG
Primers to amplify fragment IIIb	1048–1096	Reverse	E460D/Y453H-Rec	TCTCTCTTCCCATCATGTTGT G CACGCA
	1009–1072	Forward	Wild-type-Rec	AGTTTCTT A TCTCTCTTCCCATCATGTTGT G CACGCA
	1079–1100	Forward	E460D-Rec	TGGCGCGCATC
	1049–1074	Forward	Y453H-Rec	ACCTCGTGGATGAAGAGAGAGAAAGGCACCTCATGGG
Primers to amplify fragment IIIb	1059–1107	Forward	E460D/Y453H-Rec	GAGATGCGCGCACTGCGTGTAC
	3050–3071	Reverse	Wild-type-Rec	CAAGAGAGATAAGAAACTGGGA
			E460D-Rec	ATGCGCGCACTGCGTGCACAACATGA
			E460D/Y453H-Rec	TGGCGCGCAACATGATGGGCAAGAGAGATAAGAAAC
				CTCAGGGTCAATGCCAGCGCTT

^aThe T9022C and G9045T mutations and their complementary counterparts are indicated in boldface.

For dose-response studies, 200- μ l portions of fresh medium containing galidesivir at concentrations ranging from 0 to 50 μ M were added to PS cell monolayers, infected with TBEV at an MOI of 0.1, and incubated for 3 to 4 days p.i. The medium was then collected from the wells, and the viral titers were determined by plaque assay. The obtained viral titer values were used for the construction of TBEV dose-response/inhibition curves and to estimate the EC_{50} of the drug.

To measure the sensitivity/resistance of the obtained TBEV mutants to galidesivir and several structurally unrelated nucleoside analogues in cell culture by viral titer inhibition assay, confluent PS cell monolayers cultured for 24 h at 37°C in 96-well plates were treated with galidesivir, 7-deaza-2'-C-

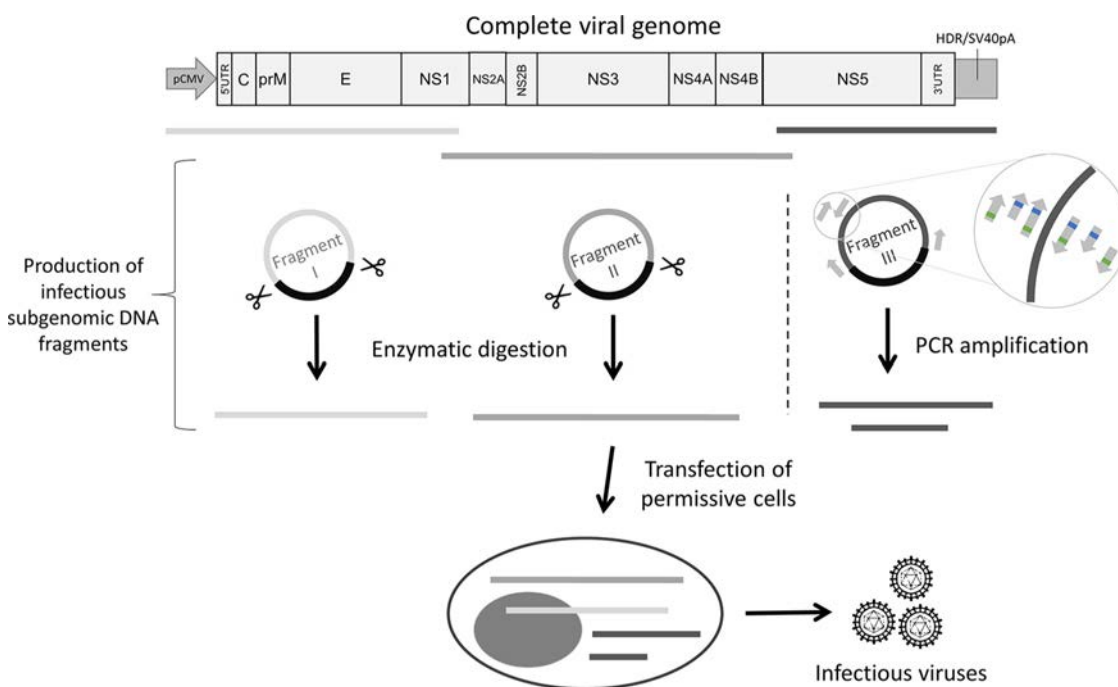


FIG 4 General overview of the reverse-genetics method presented in the present study. The reverse-genetics method used here was based on the generation of infectious subgenomic overlapping DNA fragments that encompass the entire viral genome. Three *de novo*-synthesized DNA fragments cloned into a pUC57 vector were used. The first and last fragments were flanked, respectively, at the 5' and 3' ends with the human cytomegalovirus promoter (pCMV) and the hepatitis delta ribozyme, followed by the simian virus 40 polyadenylation signal (HDR/SV40pA). Fragments I and II were generated by using the SuPreMe method: plasmids were digested using restriction enzymes. Fragment III was used as the template to generate by PCR two overlapping amplicons according to the original ISA method. Unmodified primers were used to generate two unmodified amplicons (i.e., the production of wild-type virus). Mutated primers located on the targeted region were used to generate two mutated amplicons (green and blue squares represent, respectively, mutations G9045T and T9022C). An equimolar mix of these four DNA fragments was used to transfect BHK-21 cells.

methyladenosine, 2'-C-methyladenosine, or 4'-azido-aracytidine (RO-9187) at concentrations of 25 or 50 μ M and simultaneously infected with TBEV at an MOI of 0.1 (three wells per compound). As a mock-treated control, DMSO was added to virus- and mock-infected cells at a final concentration of 0.5% (vol/vol). The formation of a cytopathic effect (CPE) was monitored visually using an Olympus BX-5 microscope to yield a 70 to 90% CPE in virus-infected cultures, and viral titers were determined by plaque assays from cell culture supernatants.

Mouse infections. To evaluate the virulence of the Hypr E460D mutant in mice, four groups of 6-week-old BALB/c female mice (purchased from AnLab, Prague, Czech Republic) were infected s.c. with TBEV (1,000 PFU/mouse, which represents a lethal dose causing 90 to 100% mortality of BALB/c mice, if the TBEV Hypr strain is used for the infection [8]) as follows: group 1 ($n = 10$), infected with *in vitro* mock-selected wild type; group 2 ($n = 10$), infected with *in vitro*-selected mutant (E460D); group 3 ($n = 10$), infected with recombinant wild-type TBEV; and group 4 ($n = 10$), infected with recombinant mutant (E460D-Rec). The survival rates of TBEV-infected mice were monitored daily over the 28-day experimental period. At the same time, monitoring symptoms of illness and evaluation of clinical scores were performed in infected animals. Signs of sickness were scored as follows: 0, no symptoms; 1, ruffled fur; 2, slowing of activity or hunched posture; 3, asthenia or mild paralysis; 4, lethargy, tremor, or complete paralysis of the limbs; and 5, death. All mice exhibiting disease consistent with clinical score 4 were terminated humanely (cervical dislocation) immediately upon detection.

In order to investigate the spread of the virus in the infected animals, two groups of 6-week-old BALB/c female mice were inoculated subcutaneously with TBEV (1,000 PFU/mouse) as follows: group 1 ($n = 15$), infected with *in vitro* mock-selected wild type, and group 2 ($n = 15$), infected with *in vitro*-selected mutant (E460D). Three mice of each group were terminated on day 1, 3, 5, 8, and 9 p.i., and the sera, brains, and spleens of the infected animals were collected. The organs were weighed, homogenized using Precellys 24 (Bertin Technologies), and prepared as 20% (wt/vol) suspension in L-15 medium containing 3% newborn calf serum. The homogenates were clarified by centrifugation at $5,000 \times g$, and the supernatant medium was used for plaque assay.

Statistical analyses. Data are expressed as means \pm the standard deviations, and the significance of differences between groups was evaluated using the Mann-Whitney U test or analysis of variance. Survival rates were analyzed by using the log-rank Mantel-Cox test. All tests were performed using GraphPad Prism 5.04 (GraphPad Software, Inc., San Diego, CA). *P* values of <0.05 were considered statistically significant.

ACKNOWLEDGMENTS

This study was supported by a grant from the Ministry of Education, Youth, and Sports of the Czech Republic (grant LTAUSA18016) (to L.E.), by a grant from the Ministry of Health of the Czech Republic (grant 16-34238A), and by Project FIT (Pharmacology, Immunotherapy, Nanotoxicology; CZ.02.1.01/0.0/0.0/15_003/0000495) from the Ministry of Education, Youth, and Sports of the Czech Republic and the Ministry of Agriculture of the Czech Republic (RO0518) (both to D.R.).

REFERENCES

- Ruzek D, Avšič Županc T, Borde J, Chrdle A, Eyer L, Karganova G, Kholodilov I, Knap N, Kozlovskaya L, Matveev A, Miller AD, Osolodkin DI, Överby AK, Tikunova N, Tkachev S, Zajkowska J. 2019. Tick-borne encephalitis in Europe and Russia: review of pathogenesis, clinical features, therapy, and vaccines. *Antiviral Res* 164:23–51. <https://doi.org/10.1016/j.antiviral.2019.01.014>.
- Dumpis U, Crook D, Oksi J. 1999. Tick-borne encephalitis. *Clin Infect Dis* 28:882–890. <https://doi.org/10.1086/515195>.
- Heinz FX, Mandl CW. 1993. The molecular-biology of tick-borne encephalitis virus. *APMIS* 101:735–745. <https://doi.org/10.1111/j.1699-0463.1993.tb00174.x>.
- Ruzek D, Dobler G, Mantke OD. 2010. Tick-borne encephalitis: pathogenesis and clinical implications. *Travel Med Infect Dis* 8:223–232. <https://doi.org/10.1016/j.tmaid.2010.06.004>.
- Eyer L, Nencka R, de Clercq E, Seley-Radtke K, Růžek D. 2018. Nucleoside analogs as a rich source of antiviral agents active against arthropod-borne flaviviruses. *Antivir Chem Chemother* 26:1–28.
- Eyer L, Šmídková M, Nencka R, Neča J, Kastl T, Palus M, De Clercq E, Růžek D. 2016. Structure-activity relationships of nucleoside analogues for inhibition of tick-borne encephalitis virus. *Antiviral Res* 133:119–129. <https://doi.org/10.1016/j.antiviral.2016.07.018>.
- Eyer L, Zouharová D, Šímarová J, Fojtíková M, Štefánik M, Haviernik J, Nencka R, de Clercq E, Růžek D. 2017. Antiviral activity of the adenosine analogue BCX4430 against West Nile virus and tick-borne flaviviruses. *Antiviral Res* 142:63–67. <https://doi.org/10.1016/j.antiviral.2017.03.012>.
- Eyer L, Kondo H, Zouharová D, Hirano M, Valdes JJ, Muto M, Kastl T, Kobayashi S, Haviernik J, Igarashi M, Kariwa H, Vaculovicova M, Cerny J, Kizek R, Kroger A, Lienenklaus S, Dejmeck M, Nencka R, Palus M, Salat J, De Clercq E, Yoshii K, Ruzek D. 2017. Escape of tick-borne flavivirus from 2'-C-methylated nucleoside antivirals is mediated by a single conservative mutation in NS5 That has a dramatic effect on viral fitness. *J Virol* 91:1–20.
- Eyer L, Valdés JJ, Gil VA, Nencka R, Hřebabeký H, Šála M, Salát J, Černý J, Palus M, De Clercq E, Růžek D. 2015. Nucleoside inhibitors of tick-borne encephalitis virus. *Antimicrob Agents Chemother* 59:5483–5493. <https://doi.org/10.1128/AAC.00807-15>.
- Warren TK, Wells J, Panchal RG, Stuthman KS, Garza NL, Van Tongeren SA, Dong L, Retterer CJ, Eaton BP, Pegoraro G, Honnold S, Bantia S, Kotian P, Chen X, Taubenheim BR, Welch LS, Minning DM, Babu YS, Sheridan WP, Bavari S. 2014. Protection against flavivirus diseases by a novel broad-spectrum nucleoside analogue BCX4430. *Nature* 508:402–405. <https://doi.org/10.1038/nature13027>.
- De Clercq E. 2016. C-nucleosides to be revisited. *J Med Chem* 59:2301–2311. <https://doi.org/10.1021/acs.jmedchem.5b01157>.
- Julander JG, Siddharthan V, Evans J, Taylor R, Tolbert K, Apuli C, Stewart J, Collins P, Gebre M, Neilson S, Van Wettere A, Lee YM, Sheridan WP, Morrey JD, Babu YS. 2017. Efficacy of the broad-spectrum antiviral compound BCX4430 against Zika virus in cell culture and in a mouse model. *Antiviral Res* 137:14–22. <https://doi.org/10.1016/j.antiviral.2016.11.003>.
- Julander JG, Bantia S, Taubenheim BR, Minning DM, Kotian P, Morrey JD, Smee DF, Sheridan WP, Babu YS. 2014. BCX4430, a novel nucleoside analog, effectively treats Yellow Fever in a hamster model. *Antimicrob Agents Chemother* 58:6607–6614. <https://doi.org/10.1128/AAC.03368-14>.

14. Taylor R, Kotian P, Warren T, Panchal R, Bavari S, Julander J, Dobo S, Rose A, El-Kattan Y, Taubenheim B, Babu Y, Sheridan WP. 2016. BCX4430: a broad-spectrum antiviral adenosine nucleoside analog under development for the treatment of Ebola virus disease. *J Infect Public Health* 9:220–226. <https://doi.org/10.1016/j.jiph.2016.04.002>.
15. Westover JB, Mathis A, Taylor R, Wandersee L, Bailey KW, Sefing EJ, Hickerson BT, Jung KH, Sheridan WP, Gowen BB. 2018. Galidesivir limits Rift Valley fever virus infection and disease in Syrian golden hamsters. *Antiviral Res* 156:38–45. <https://doi.org/10.1016/j.antiviral.2018.05.013>.
16. Bagaglio S, Uberti-Foppa C, Morsica G. 2017. Resistance mechanisms in hepatitis C virus: implications for direct-acting antiviral use. *Drugs* 77:1043–1055. <https://doi.org/10.1007/s40265-017-0753-x>.
17. Irwin KK, Renzette N, Kowalik TF, Jensen JD. 2016. Antiviral drug resistance as an adaptive process. *Virus Evol* 2:1–10.
18. Poveda E, Wyles DL, Mena A, Pedreira JD, Castro-Iglesias A, Cachay E. 2014. Update on hepatitis C virus resistance to direct-acting antiviral agents. *Antiviral Res* 108:181–191. <https://doi.org/10.1016/j.antiviral.2014.05.015>.
19. Lauring AS, Frydman J, Andino R. 2013. The role of mutational robustness in RNA virus evolution. *Nat Rev Microbiol* 11:327–336. <https://doi.org/10.1038/nrmicro3003>.
20. Eyer L, Nougairède A, Uhlířová M, Driouich J-S, Zouharová D, Valdés JJ, Haviernik J, Gould EA, De Clercq E, de Lamballerie X, Ruzek D. 2019. An E460D substitution in the NS5 protein of tick-borne encephalitis virus confers resistance to the inhibitor galidesivir (BCX4430) and also attenuates the virus for mice. *bioRxiv* <https://doi.org/10.1101/563544>.
21. Aubry F, Nougairède A, de Fabritus L, Querat G, Gould EA, De Lamballerie X. 2014. Single-stranded positive-sense RNA viruses generated in days using infectious subgenomic amplicons. *J Gen Virol* 95:2462–2467. <https://doi.org/10.1099/vir.0.068023-0>.
22. Driouich J-S, Ali SM, Amroun A, Aubry F, de Lamballerie X, Nougairède A. 2018. SuPreMe: a rapid reverse genetics method to generate clonal populations of recombinant RNA viruses. *Emerg Microbes Infect* 7:1–11. <https://doi.org/10.1038/s41426-018-0040-2>.
23. Pawlowsky JM. 2011. Treatment failure and resistance with direct-acting antiviral drugs against hepatitis C virus. *Hepatology* 53:1742–1751. <https://doi.org/10.1002/hep.24262>.
24. De Clercq E, Neyts J. 2009. Antiviral agents acting as DNA or RNA chain terminators. *Handb Exp Pharmacol* 189:53–84. https://doi.org/10.1007/978-3-540-79086-0_3.
25. Hercik K, Brynda J, Nencka R, Boura E. 2017. Structural basis of Zika virus methyltransferase inhibition by sinefungin. *Arch Virol* 162:2091–2096. <https://doi.org/10.1007/s00705-017-3345-x>.
26. Hercik K, Kozak J, Sala M, Dejmek M, Hrebabecky H, Zbornikova E, Smola M, Ruzek D, Nencka R, Boura E. 2017. Adenosine triphosphate analogs can efficiently inhibit the Zika virus RNA-dependent RNA polymerase. *Antiviral Res* 137:131–133. <https://doi.org/10.1016/j.antiviral.2016.11.020>.
27. Migliaccio G, Tomassini JE, Carroll SS, Tomei L, Altamura S, Bhat B, Bartholomew L, Bosserman MR, Ceccacci A, Colwell LF, Cortese R, De Francesco R, Eldrup AB, Getty KL, Hou XS, LaFemina RL, Ludmerer SW, MacCoss M, McMasters DR, Stahlhut MW, Olsen DB, Hazuda DJ, Flores OA. 2003. Characterization of resistance to non-obligate chain-terminating ribonucleoside analogs that inhibit hepatitis C virus replication *in vitro*. *J Biol Chem* 278:49164–49170. <https://doi.org/10.1074/jbc.M305041200>.
28. Xu HT, Hassounah SA, Colby-Germinario SP, Oliveira M, Fogarty C, Quan YD, Han YS, Golubkov O, Ibanescu I, Brenner B, Stranix BR, Wainberg MA. 2017. Purification of Zika virus RNA-dependent RNA polymerase and its use to identify small-molecule Zika inhibitors. *J Antimicrob Chemother* 72:727–734.
29. Flint M, McMullan LK, Dodd KA, Bird BH, Khristova ML, Nichol ST, Spiropoulou CF. 2014. Inhibitors of the tick-borne, hemorrhagic fever-associated flaviviruses. *Antimicrob Agents Chemother* 58:3206–3216. <https://doi.org/10.1128/AAC.02393-14>.
30. Delang L, Yen PS, Vallet T, Vazeille M, Vignuzzi M, Failloux AB. 2018. Differential transmission of antiviral drug-resistant chikungunya viruses by *Aedes* mosquitoes. *mSphere* 3:e00230-18.
31. Khatun A, Shabir N, Seo BJ, Kim BS, Yoon KJ, Kim WI. 2016. The attenuation phenotype of a ribavirin-resistant porcine reproductive and respiratory syndrome virus is maintained during sequential passages in pigs. *J Virol* 90:4454–4468. <https://doi.org/10.1128/JVI.02836-15>.
32. Gammon DB, Snoeck R, Fiten P, Krecmerova M, Holy A, De Clercq E, Opendakker G, Evans DH, Andrei G. 2008. Mechanism of antiviral drug resistance of vaccinia virus: identification of residues in the viral DNA polymerase conferring differential resistance to antipoxvirus drugs. *J Virol* 82:12520–12534. <https://doi.org/10.1128/JVI.01528-08>.
33. Groarke JM, Pevear DC. 1999. Attenuated virulence of pleconaril-resistant coxsackievirus B3 variants. *J Infect Dis* 179:1538–1541. <https://doi.org/10.1086/314758>.
34. Pospisil L, Jandasek L, Pesek J. 1954. Isolation of new strains of meningoencephalitis virus in the Brno region during the summer of 1953. *Lek List* 9:3–5.
35. Kozuch O, Mayer V. 1975. Pig kidney epithelial (Ps) cells: perfect tool for study of flaviviruses and some other arboviruses. *Acta Virol* 19:498.
36. Ruzek D, Gritsun TS, Forrester NL, Gould EA, Kopecky J, Golovchenko M, Rudenko N, Grubhoffer L. 2008. Mutations in the NS2B and NS3 genes affect mouse neuroinvasiveness of a Western European field strain of tick-borne encephalitis virus. *Virology* 374:249–255. <https://doi.org/10.1016/j.virol.2008.01.010>.
37. Aubry F, Nougairède A, de Fabritus L, Piorkowski G, Gould EA, De Lamballerie X. 2015. ISA-Lation of single-stranded positive-sense RNA viruses from non-infectious clinical/animal samples. *PLoS One* 10:1–10.
38. De Madrid AT, Porterfield JS. 1969. A simple micro-culture method for the study of group B arboviruses. *Bull World Health Organ* 40:113–121.

Article

Antiviral Activity of Uridine Derivatives of 2-Deoxy Sugars against Tick-Borne Encephalitis Virus

Ewelina Krol ^{1,*}, Ilona Wandzik ^{2,3}, Gabriela Brzuska ¹, Luděk Eyer ^{4,5}, Daniel Růžek ^{4,5}
and Boguslaw Szewczyk ¹

¹ Department of Recombinant Vaccines, Intercollegiate Faculty of Biotechnology, University of Gdansk and Medical University of Gdansk, Abrahamowa 58, 80-307 Gdansk, Poland; gabriela.brzuska@phdstud.ug.edu.pl (G.B.); szewczyk@biotech.ug.gda.pl (B.S.)

² Department of Organic Chemistry, Bioorganic Chemistry and Biotechnology, Faculty of Chemistry, Silesian University of Technology, Krzywoustego 4, 44-100 Gliwice, Poland; Ilona.Wandzik@polsl.pl

³ Biotechnology Center, Silesian University of Technology, Krzywoustego 8, 44-100 Gliwice, Poland

⁴ Department of Virology, Veterinary Research Institute, Hudcova 70, CZ-62100 Brno, Czech Republic; eyer@vri.cz (L.E.); ruzekd@paru.cas.cz (D.R.)

⁵ Institute of Parasitology, Biology Centre of the Czech Academy of Sciences, Branisovska 31, CZ-37005 Ceske Budejovice, Czech Republic

* Correspondence: ewelina@biotech.ug.gda.pl; Tel.: +48-58-523-63-83

Academic Editor: Hidenori Tanaka

Received: 20 February 2019; Accepted: 18 March 2019; Published: 21 March 2019



Abstract: Tick-borne encephalitis virus (TBEV) is a causative agent of tick-borne encephalitis (TBE), one of the most important human infections involving the central nervous system. Although effective vaccines are available on the market, they are recommended only in endemic areas. Despite many attempts, there are still no specific antiviral therapies for TBEV treatment. Previously, we synthesized a series of uridine derivatives of 2-deoxy sugars and proved that some compounds show antiviral activity against viruses from the Flaviviridae and Orthomyxoviridae families targeting the late steps of the *N*-glycosylation process, affecting the maturation of viral proteins. In this study, we evaluated a series of uridine derivatives of 2-deoxy sugars for their antiviral properties against two strains of the tick-borne encephalitis virus; the highly virulent TBEV strain Hypr and the less virulent strain Neudoerfl. Four compounds (**2**, **4**, **10**, and **11**) showed significant anti-TBEV activity with IC₅₀ values ranging from 1.4 to 10.2 μM and low cytotoxicity. The obtained results indicate that glycosylation inhibitors, which may interact with glycosylated membrane TBEV E and prM proteins, might be promising candidates for future antiviral therapies against TBEV.

Keywords: tick-borne encephalitis; antivirals; glycosylation inhibition; uridine; 2-deoxy sugars

1. Introduction

Serious viral infectious diseases transmitted by invertebrate vectors have always been a major public health problem in all parts of the world. One of the diseases of growing importance which belongs to this group is tick-borne encephalitis (TBE). TBE is a seasonal disorder of the central nervous system which may lead to serious medical complications in humans, including meningitis, meningoencephalitis, or even death [1]. The causative agent of the zoonosis-tick-borne encephalitis virus (TBEV) is transmitted, as the name implies, by ticks. TBEV is a member of the *Flavivirus* genus in the Flaviviridae family which includes, among others, hepatitis C virus (HCV), West Nile virus, Zika virus, dengue virus, Japanese encephalitis virus, and yellow fever virus.

TBEV is a small, single-stranded, positive-polarity RNA virus with an enveloped virion approximately 50 nm in diameter [2]. Three subtypes of TBEV, including European (TBEV-Eu),

Siberian (TBEV-Sib), and Far Eastern (TBEV-FE), are known [3], but a new subtype derived from TBEV-Sib, Baikalian (TBEV-Bkl), has also been described [4]. Recently, another subtype, Himalayan (Him-TBEV), was identified in wild rodents [5]. The principal reservoir and vector of TBEV are the hard ticks: *Ixodes ricinus*—a vector of TBEV-Eu and *Ixodes persulcatus*—a vector of TBEV-FE and TBEV-Sib. The course of infection with a particular subtype shows significant clinical differences with different case fatality rates in humans. The most likely route for humans to become infected with TBEV is a tick bite. However, TBEV can also be transmitted through the consumption of unpasteurized milk and milk products from infected animals such as goats, sheep, and cows [6].

The incidence of TBE has markedly increased during the past 20 years, which makes TBE, after Lyme disease, the second most serious disease transmitted by ticks [7]. TBEV is mainly endemic in Europe, Russia, and Asia [8,9]; however, the virus extends its range outside endemic areas. Recently, a new TBE endemic outbreak has been identified in Finnish Lapland, a place where TBEV has never been found before [10]. This suggests the expansion of the range of distribution of ticks and with them this threatening viral pathogen. Although vaccines against TBE based on inactivated viruses are available, the vaccination is not mandatory but only recommended for residents and tourists traveling to endemic areas. Vaccines are rarely used as a prevention tool, which results in more than 12,000 human cases reported annually [11,12]. Despite numerous strategies of research, currently there is no licensed therapeutic available for the treatment of TBEV infections [13]. Patients diagnosed with TBE infection are usually treated to alleviate the symptoms, e.g., to reduce the inflammation and intracranial pressure by anti-inflammatory drugs. Therefore, the development of new effective antiviral compounds is highly demanded.

The TBEV envelope contains two viral proteins which play a major role in viral entry into the target cells: glycoprotein E and the small membrane protein prM/M. Protein E contains the major antigenic epitopes that induce the formation of protective antibodies during immune response. Both TBEV proteins possess at least one conserved *N*-glycosylation site [14]. The removal of glycans of viral proteins usually impairs their proper folding and stability. For TBEV, it has been proven that the loss of glycosylation of protein E affects the conformation of the protein, consequently reducing the infectivity of secreted virions [15]. It has been reported that the virus composed of glycoprotein E lacking the *N*-glycan chains was not infectious in a mouse model, confirming that glycosylation inhibition may be a new target for anti-TBEV compounds.

The composition of glycan chains in viral glycoproteins can be modulated by glycosyltransferases (GTs) during the maturation step and thus may affect viral survival. Active compounds interacting with GTs could potentially contain covalently bound carbohydrate units. Previously, several uridine derivatives of various lipophilicity containing 2-deoxy sugar moieties were synthesized and some of them were tested for inhibitory activity against GTs [16–19]. Some of the compounds were reported to exert *in vitro* antiviral activity against viruses belonging to the Flaviviridae family (classical swine fever virus (CSFV) and HCV) as well as against the influenza virus from the Orthomyxoviridae family [16,20–22]. The *in vitro* efficacy of compounds against these viruses was related to the impaired maturation of viral proteins targeting the late step of *N*-glycosylation (cis- or very early medial-Golgi), confirming their wide spectrum of activity. Viruses belonging to the same family group exhibit a high degree of homology in terms of genomic organization, protein function, and replication strategy. As TBEV, together with HCV and CSFV, belongs to the Flaviviridae family, it can be therefore assumed that compounds having antiviral activity against HCV and CSFV may also have significant activity against TBEV.

In the present study, the antiviral activity of uridine derivatives of 2-deoxy sugars was evaluated against TBEV. We showed that four compounds strongly inhibit the propagation of TBEV, exhibiting similar inhibitory profiles and low cytotoxicity to the host cells.

2. Results

2.1. Anti-TBEV Activity of Uridine Derivatives of 2-Deoxy Sugars

Previously, we synthesized uridine derivatives of 2-deoxy sugars (Figure 1) and reported that a few compounds from that series exert in vitro antiviral activity against CSFV [20], HCV [21], and the influenza virus [16,22]. In this comparative study, the synthesized compounds were evaluated for antiviral activity against another emerging virus—TBEV. To investigate the anti-TBEV activity, initially, the cytotoxicity of compounds in A549 cells was examined using the MTS assay to select nontoxic doses for further experiments. All tested compounds showed almost no cytotoxic effect at a concentration of 50 μ M and the viability of A549 cells ranged from 95 to 100% for all tested compounds. The calculated cytotoxic concentration (CC_{50}) values for compounds 1–11 (shown in Figure 1) required to reduce cell viability by 50% were 74, 141, 97, 119, 79, 196, 223, 225, 238, 121, and 141 μ M, respectively.

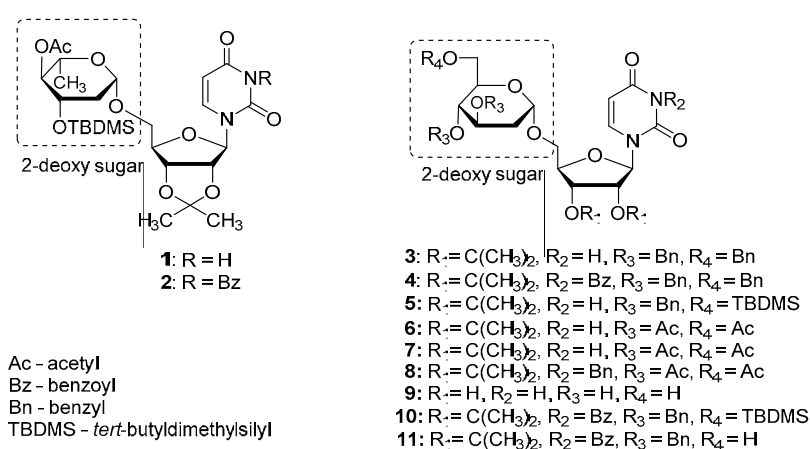


Figure 1. The structures of uridine derivatives of 2-deoxy sugars used in the study: 1–11.

The preliminary screening of the 11 synthesized compounds was performed using Hypr and Neudoerfl TBEV strains in a cytopathic effect (CPE) inhibition assay and plaque reduction assay. All compounds were examined in the CPE inhibition assay, using the colorimetric assay to quantify the impact of synthesized compounds on cell death after infection. The TBEV Hypr strain (multiplicity of infection (MOI) of 0.1) without inhibitory treatment caused a severe CPE, including cell detachment and death detected 96 h post-infection (p.i.) in A549-infected cells. A protective effect of some compounds on cell survival indicates their potential antiviral activity. A high rate of A549 cell death (about 49%) was observed in Hypr-infected DMSO-treated cells (positive control) (Figure 2). The cells treated with uridine derivatives of 2-deoxy sugars (compounds 2, 4, 10, and 11) at 50 μ M showed a low rate of cell death. Compounds 2 and 4 were the most active and completely inhibited the TBEV-induced CPE, protecting almost 99% of the A549 cells from cell death. Compounds 10 and 11 also decreased cell death and the calculated viability values after inhibitory treatment were 90 and 81%, respectively. The remaining tested compounds were not active, which was exhibited by a lack of inhibition of cell death after inhibitory treatment in comparison to the mock-treated Hypr-infected A549 cells.

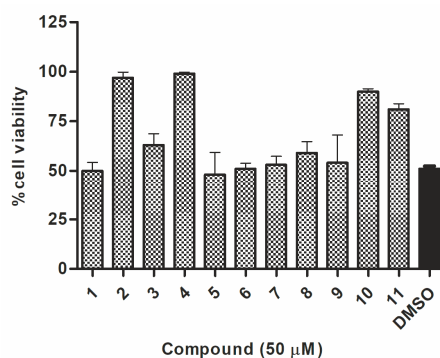


Figure 2. The effect of compounds 1–11 on the tick-borne encephalitis virus (TBEV)-induced cytopathic effect in A549 cells. A549 cells were infected with TBEV Hypr strain at a multiplicity of infection (MOI) of 0.1 and treated with 50 μ M of compounds or DMSO (positive control). Cell death was measured and expressed as the percentage of cell viability 96 h post-infection (p.i.). Error bars indicate standard deviations from three experiments.

Additionally, in the plaque reduction assay, the compounds were tested at a concentration of 50 μ M for their ability to inhibit the propagation of TBEV at a low multiplicity of infection (MOI) of 0.001 to visualize single plaques using the immunoperoxidase monolayer assay (IPMA). Neudoerfl-infected A549 cells treated with DMSO were used as positive controls. The TBEV Neudoerfl strain is not a highly cytopathic virus, so after 48 h the areas of infected cells could be detected by the immunostaining of protein E. The results showed that compounds 2, 4, 10, and 11 caused nearly a complete inhibition of TBEV infection in comparison to the positive controls (TBEV-infected cells treated with DMSO), which was manifested by the reduction of size and number of infected plaques after 48 h of inhibitory treatment (Figure 3). Compounds 1, 3, and 5–9 showed minor or no antiviral effect (data not shown).

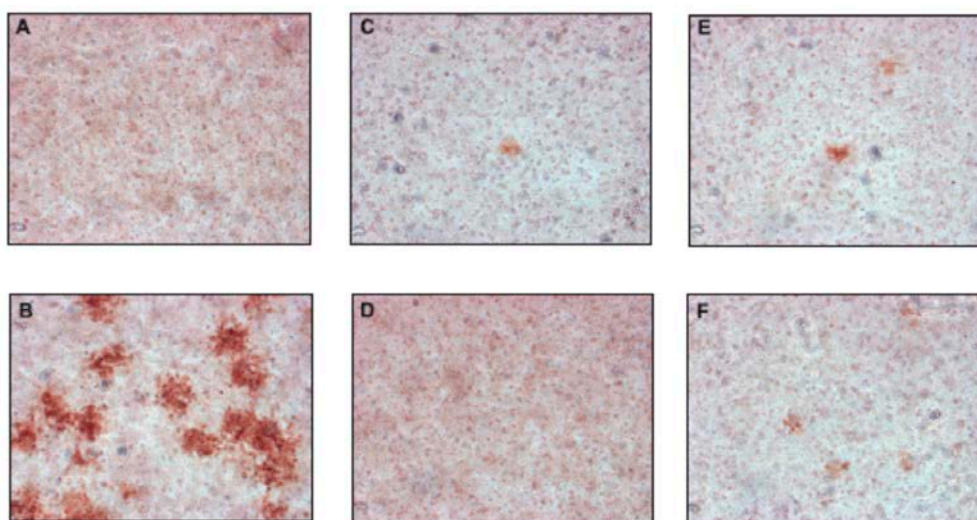


Figure 3. The effect of selected uridine derivatives of 2-deoxy sugars on TBEV propagation in A549 cells. A549 cells were infected with the TBEV Neudoerfl strain at an MOI of 0.001 (B–F) or mock infected (A). After virus removal at 2 h p.i., the cells were washed and overlaid with carboxymethylcellulose in Dulbecco’s Modified Eagle’s Medium with DMSO (B) or 50 μ M of compounds 2 (C), 4 (D), 10 (E), and 11 (F). At 48 h p.i., cells were fixed and infected foci were visualized by immunostaining with the monoclonal anti-Flavivirus group antigen antibody (4G2).

To verify these preliminary results, the influence of compounds at a dose of 50 μ M on TBEV growth was tested. Hypr and Neudoerfl TBEV titers from DMSO- and inhibitory-treated cells, infected at an MOI of 0.1, were determined in the culture supernatants at 72 h p.i. using a plaque assay. The obtained

results confirmed that four of uridine derivatives—compounds **2**, **4**, **10**, and **11**—displayed an inhibitory effect on TBEV growth in A549 cells, which was in agreement with previous results (Figure 4). Nearly complete inhibition of viral growth was observed. Hypr and Neudoerfl strains without inhibitory treatment achieved titers of approximately 1×10^7 plaque-forming unit/ml (PFU/ml) in A549 cells. All four active uridine derivatives significantly reduced viral titers compared to positive controls, indicating their antiviral activity. After treatment with compounds **2**, **4**, **10**, and **11**, the titers were reduced 1×10^7 – 1×10^5 -fold compared to positive controls. Other compounds—**1**, **3**, and **5–9**—did not affect viral growth as no significant reduction in titers of both TBEV strains was observed. All these results strongly correlate with the results obtained in previous experiments (Figures 2 and 3).

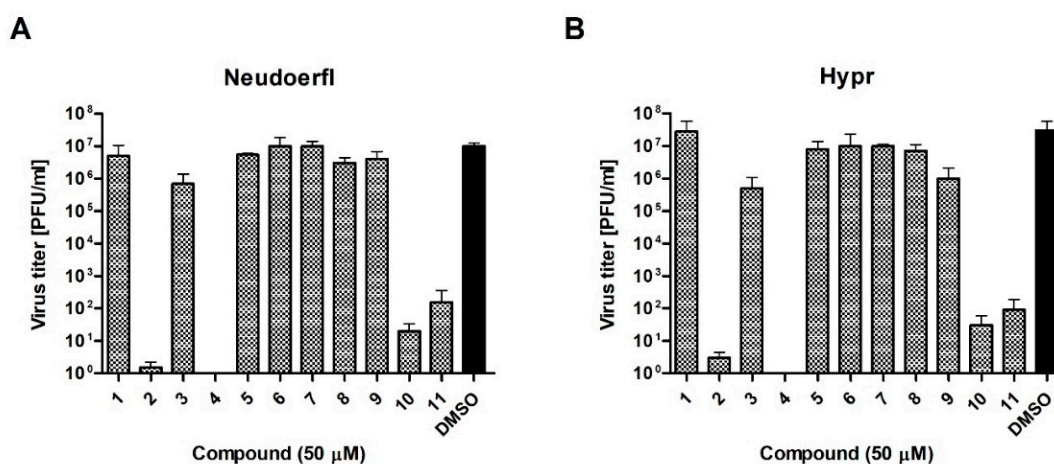


Figure 4. The effect of synthesized compounds on Neudoerfl and Hypr TBEV titers in A549 cells. A549 cells were infected with TBEV Neudoerfl (A) or Hypr (B) strain at an MOI of 0.1 and treated with 50 μM of compounds. At 72 h p.i., the supernatants were collected and viral titers were determined by the plaque assay. Error bars indicate standard deviations from three experiments.

2.2. Dose-Response of Anti-TBEV Activity of Uridine Derivatives of 2-Deoxy Sugars

The four compounds with the highest antiviral activity in the preliminary screening at 50 μM were further evaluated in dose-response assays. A549 cells infected with Neudoerfl TBEV strain (MOI = 0.001) were incubated for 2 days with an overlay medium containing increasing concentrations (0–50 μM) of compounds **2**, **4**, **10**, and **11**. The plaque reduction assay, which measures the extent of viral infection (visualization of the foci), was performed as described above. For all tested compounds, the dose-dependent reduction in average size and number of positive infected foci was observed in the plaque-reduction assay. As shown in Figure 5, compound **4** was the most active, exhibiting the lowest dose needed for the complete inhibition of plaque formation. After treatment with 50 and 25 μM of compound **4**, no plaques were detected. Additionally, the immunostaining of protein E revealed that compound **4**, at the lowest dose tested of 6.25 μM, significantly reduced the number of plaques by 90% in comparison to the TBEV-infected cells treated with DMSO. Moreover, no plaques were detected after treatment with 50 μM of compound **2**; 25 μM of this compound significantly reduced the number of plaques by 98%. Compounds **10** and **11** were slightly less active; 50 and 25 μM of these compounds reduced the number of plaques by around 82–96%.

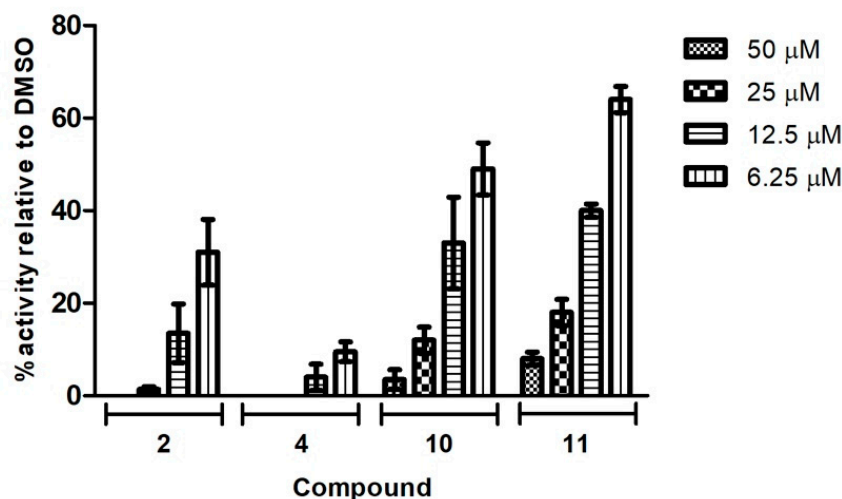


Figure 5. The effect of compounds on TBEV propagation in A549 cells. A549 cells were infected with the TBEV Neudoerfl strain at an MOI of 0.001. After virus removal at 2 h p.i., the cells were washed and overlaid with carboxymethylcellulose in D-MEM medium with DMSO or increasing doses of compounds. At 48 h p.i., cells were fixed and infected foci were visualized by immunostaining with the monoclonal anti-Flavivirus group antigen antibody (4G2). Plaques were counted and presented as a percentage in comparison to the number in DMSO-treated cells expressed as 100%. Error bars indicate standard deviations from three experiments.

The culture supernatants collected on days 1, 2, and 3 p.i. from the Neudoerfl-infected A549 cells treated with compounds **2**, **4**, **10**, and **11** at concentrations ranging from 0 to 50 μM were subjected to the plaque assay to determine the TBEV titers. The highest titer (1×10^7 PFU/ml) for positive control—the titer for TBEV collected from non-treated cells—was observed 3 days post infection. Therefore, the dose-response curves obtained from day 3 p.i. were used to calculate the half-maximum inhibitory concentration (IC_{50}) value for each tested compound. All tested uridine derivatives of 2-deoxy sugars significantly reduced viral titers in a dose-dependent manner, indicating high anti-TBEV activity (Figure 6). The TBEV yields after inhibitory treatment were reduced each day post-infection, indicating their stable activity. Compound **4** was the most active because the decrease in viral titer observed 3 days p.i. was the highest. When compound **4** was added to the cells at concentrations of 50 and 25 μM , no virus was detected. At the lowest concentration of 6.25 μM , a 10^4 -fold reduction of the viral titer was observed in comparison to the TBEV-infected mock-treated cells. The calculated IC_{50} value for this compound was 1.4 μM . For compound **2**, treatment with a dose of 50 μM also reduced the TBEV titer to undetectable levels, confirming its activity. Other doses caused around 10^2 – 10^1 -fold titer reduction. Compounds **10** and **11** at all tested doses caused 1×10^4 – 1×10^1 -fold reduction in viral titers. The IC_{50} values for compounds **2**, **10**, and **11** were 5.3, 6.5, and 10.2 μM , respectively. The calculated selectivity indices (SIs) defined as the $\text{CC}_{50}/\text{IC}_{50}$ ratio for compounds **2**, **4**, **10**, and **11** were 26.6, 85, 18.6, and 13.8, respectively.

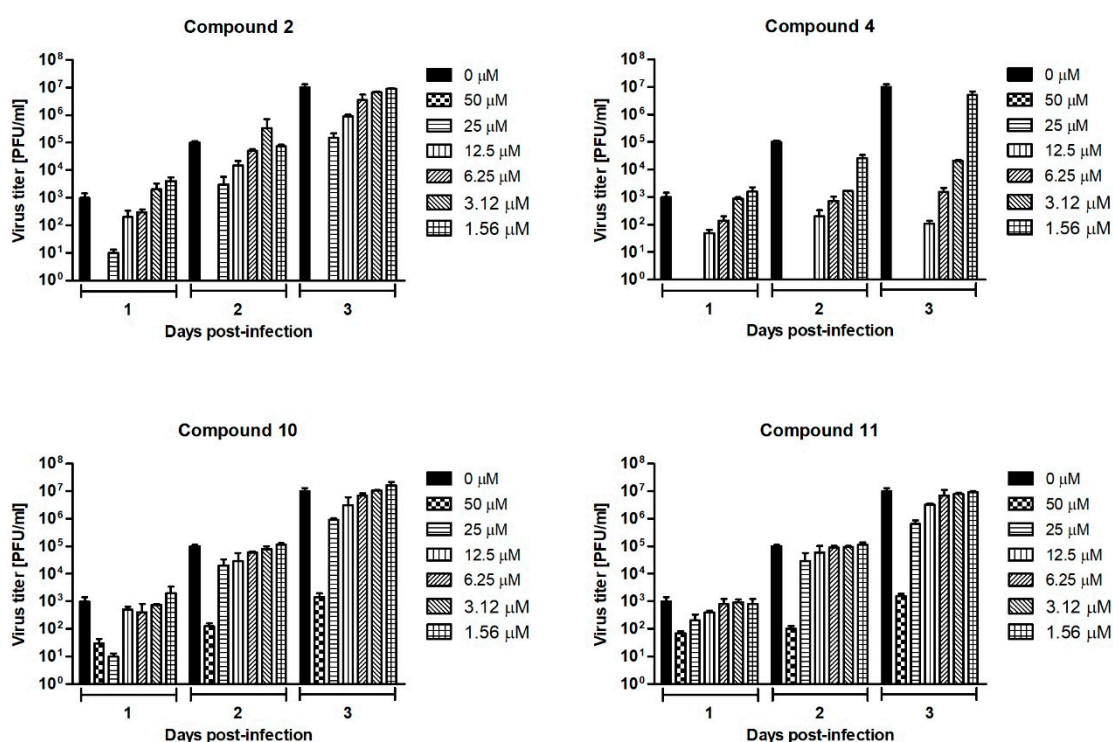


Figure 6. Dose-dependent effect of compounds 2, 4, 10, and 11 on TBEV titers over a 3-day experiment. A549 cells were infected with TBEV Neudoerfl strain at an MOI of 0.1 and treated with different concentrations of compounds. Culture supernatants were collected at days 1, 2, and 3 post-infection and TBEV titers were determined by the plaque assay. Error bars indicate standard deviations from three experiments.

2.3. The Effect of Uridine Derivatives of 2-Deoxy Sugars on Protein Synthesis

We previously proved that synthesized uridine derivatives of 2-deoxy sugars belong to *N*-glycosylation inhibitors [20]. The antiviral activity of studied compounds is based on the inhibition of the synthesis of viral proteins, which has a direct impact on virus propagation as has been shown for hepatitis C virus, classical swine fever virus, and influenza A virus. The antiviral effect was further confirmed by Western blot analysis, where the effect of compounds on TBEV glycoprotein synthesis was determined. For all tested compounds, a dose-dependent reduction in the yield of E and prM proteins in cells infected with the Neudoerfl TBEV strain was observed. The representative results for the most active compound, 4, are shown in Figure 7. Compound 4 at a very low concentration (6.25 μM) completely inhibited the synthesis of both proteins, as they were not detected in the Western blot analysis. Both the non-glycosylated or under-glycosylated forms of both proteins were not detected in the experiment. This was probably due to the rapid degradation of incorrectly matured proteins, as was observed for other viruses in previous experiments.

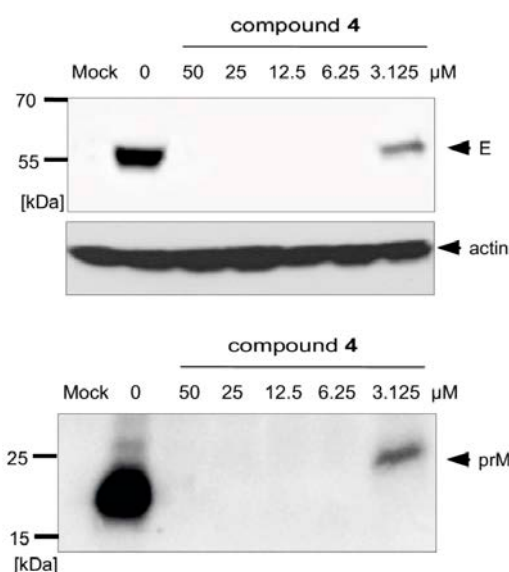


Figure 7. Effect of compound 4 on glycoprotein E and prM protein synthesis. A549 cells were infected with the TBEV Neudoerfl strain at an MOI of 0.1 and treated with different concentrations of the compound. At 48 h p.i., cells were lysed and proteins were separated by SDS-PAGE (gradient 10–20% polyacrylamide) under non-reducing conditions. Western blot analysis was performed using the monoclonal anti-Flavivirus group antigen antibody (4G2) for the detection of glycoprotein E, rabbit monospecific polyclonal serum for pr fragment detection, and anti-actin monoclonal antibody.

3. Discussion

Tick-borne encephalitis virus is as an important tick-borne pathogen which causes thousands of infections annually. A large percentage of infections are asymptomatic or have non-specific symptoms, thus many cases of infection are not reported by primary care physicians. This suggests that the scale of the problem is much greater. Inactivated virus-based vaccines which provide safe and reliable protection are available; however, they are offered only to at-risk travelers. Numerous studies have been carried out to develop new antiviral compounds against TBE virus. Although some compounds showed significant antiviral activity in *in vitro* studies, none of them were approved for use in humans.

Due to the urgent need for new effective anti-TBEV compounds, we evaluated the activity of previously reported compounds belonging to uridine derivatives of 2-deoxy sugars. In our previous studies, we reported that four compounds from these series exhibited antiviral activity against some members of the Flaviviridae family. These compounds were found to impair the maturation of viral proteins by interacting with glycosyltransferases active during the late steps (cis- or very early medial-Golgi) of the *N*-glycosylation process. Based on the high degree of homology between all members of the Flaviviridae family, e.g., CSFV, HCV, and TBEV, we expected that the activity of the selected compounds against TBEV would be similar to that of CSFV and HCV [20]. Additionally, we proved that uridine derivatives of 2-deoxy sugars possess antiviral activity against other viruses from outside the Flaviviridae family, e.g., the influenza virus belonging to the Orthomyxoviridae family, which indicates their broad spectrum of activity against many viruses [16,22].

The envelope glycoproteins, the most exposed structural elements of virions, play a vital role in the viral life cycle. They participate in the assembly of infectious particles and play a role in viral entry since they enable interaction with specific cell surface receptors and induce fusion between the viral envelope and the host cell membrane. Therefore, glycoproteins are assumed to be important factors of virulence and pathogenicity. TBEV possesses two viral membrane proteins, glycoprotein E and protein prM/M. Protein E mediates entry into the host cells and induces the generation of immune responses [23]. The major role of the prM/M membrane protein is a chaperone-like activity during the maturation of protein E [24]. Both TBEV envelope proteins are *N*-glycosylated. Glycoprotein E

possesses one or two glycosylation sites depending on the viral strain and protein prM/M contains one conserved *N*-glycosylation site. The significance of the glycosylation process of viral proteins for viral growth, secretion, and pathogenicity of different types of viruses was confirmed in many studies. The important role of *N*-glycans attached to viral glycoproteins for TBEV infectivity has also been previously reported. Initially, it was shown that the inhibition of *N*-glycosylation reduced the secretion of progeny viruses from infected cells [25]. Moreover, targeting the *N*-glycosylation of protein E resulted in a significant decrease in the secretion of TBEV-like particles [24]. It has also been proven that *N*-glycosylation inhibition affects the folding and stability of protein E. The changes in the conformational structure of protein E affected by *N*-glycosylation inhibition results in reduced TBEV infectivity, which was confirmed in *in vivo* mouse studies [15]. These findings suggest that targeting the glycosylation process can be used to attenuate TBEV infection, which may be the basis for an innovative antiviral approach.

In the current study, the antiviral activities of 11 uridine derivatives of 2-deoxy sugars were determined using two TBEV strains. The antiviral screening was performed with Neudoerfl and Hypr TBEV strains, which differ in virulence level. Initially, using the CPE inhibition assay as well as the plaque reduction assay in A549 cells, we tested the anti-TBEV activity of all compounds at 50 μ M. Our results suggested that four out of the 11 compounds were active against TBEV, significantly inhibiting the viral infection, while compound **4** was the most active (Figures 2 and 3). The results were further confirmed in other experiments where the activity of potential glycosylation inhibitors on viral growth was tested. We showed that, as in the previous experiments, only compounds **2**, **4**, **10**, and **11** strongly inhibited the growth of both TBEV strains, thus significantly reducing viral titers (Figure 4). Structural analysis of the studied compounds indicated that the presence of a benzoyl group at the uracil nitrogen had a positive impact on the antiviral activity, as was evidenced by the most active compounds **2**, **4**, **10**, and **11** containing a benzoyl group at the uracil nitrogen.

Further, dose-dependent experiments were performed with the four selected compounds. The antiviral properties of the compounds at various concentrations were demonstrated in the plaque reduction assay as well as in the plaque assay to determine viral titers where the impact of different amounts of compounds was tested. All tested compounds caused a dose-dependent inhibition of TBEV production observed as the decrease of the average size and number of positive infected foci (Figure 5) and viral titer (Figure 6). TBEV was inhibited by these compounds at low micromolar concentrations. Compound **4** showed the highest antiviral activity, displaying an IC_{50} value of 1.4 μ M. The IC_{50} values of the active compounds **2**, **10**, and **11** were 5.3, 6.5, and 10.2, respectively. The significant reduction in viral titer after inhibitory treatment was in agreement with previously published data, where a reduction in the virus yield of infectious recombinant virus expressing protein E lacking the *N*-glycans was observed [15].

As mentioned before, the inhibition of *N*-glycosylation also affects the folding and stability of the TBEV protein E. Therefore, the influence of selected uridine derivatives of 2-deoxy sugars on protein synthesis was examined. We demonstrated that compound **4** caused a dose-dependent decrease in the synthesis of proteins E and prM (Figure 7), which could be the main reason for the reduction of TBEV production in other experiments. Less glycosylated or non-glycosylated forms of proteins E and prM were not detected by Western blot, indicating the very quick degradation of incorrectly matured proteins. The same results were observed for proteins of other viruses, e.g., HCV, CSFV, and influenza virus, in our previous studies [16,20–22].

In conclusion, we demonstrated that compounds **2**, **4**, **10**, and **11** exert significant antiviral activity against TBEV. The observed results, together with our previous findings, confirm that the selected compounds possess a broad-range antiviral activity targeting the *N*-glycosylation process, and may constitute a novel class of inhibitors with a mechanism of action different from the currently tested antiviral drugs. These compounds may be the starting point for the synthesis of other antiviral compounds with some modifications to potentially improve their activity.

4. Materials and Methods

4.1. Antiviral Compounds, Cells, and Viruses

The compounds were synthesized as previously described [16–18]. The stock solutions of tested compounds were dissolved in dimethyl sulfoxide (DMSO) and stored at $-20\text{ }^{\circ}\text{C}$ until use.

A549 cells (adenocarcinomic human alveolar basal epithelial cells) (ATCC[®] CCL-185[™]) were cultured in Dulbecco's Modified Eagle's Medium (D-MEM) (Sigma-Aldrich, Saint Louis, MO, USA) supplemented with 8% heat-inactivated fetal bovine serum (FBS), 2 mM L-glutamine, 0.2% bovine serum albumin, 25 mM HEPES buffer, 100 U/ml penicillin, and 100 $\mu\text{g}/\text{ml}$ streptomycin at $37\text{ }^{\circ}\text{C}$ under 5% CO_2 .

The Neudoerfl TBEV strain, kindly provided by Dr. Karin Stiasny (Center for Virology, Medical University of Vienna, Vienna, Austria), and the Hypr TBEV strain were used in this study. Both viruses were grown in A549 cells for 3–4 days until the cytopathic effect was visible. Virus titers were determined by the plaque assay.

4.2. Cell Viability Assay

A549 cell viability was measured by the CellTiter 96 AQueous non-radioactive cell proliferation assay (MTS) (Promega, Madison, WI, USA) according to the manufacturer's instructions. The half-maximal cytotoxic concentration (CC_{50}) values of compounds that reduce cell viability by 50% was calculated using the GraphPad Prism software (version 5.01, GraphPad Software, San Diego, CA, USA) from the dose-response curves.

4.3. CPE Inhibition Assay

A549 cells seeded in 96-well plates together with various doses of tested compounds or DMSO (positive control) were infected with the Hypr TBEV strain at an MOI of 0.1. After 96 h p.i., CPE (cell death) was determined using the colorimetric CytoTox 96[®] Non-Radioactive Cytotoxicity Assay (Promega, Madison, WI, USA) according to the manufacturer's instructions. This assay measures lactate dehydrogenase (LDH), a stable cytosolic enzyme that is released upon cell lysis. The absorbance at 450 nm was read using a plate reader.

4.4. Plaque Reduction Assay

Confluent monolayers of A549 cells in 12-well plates were inoculated with TBEV for 2 h at $37\text{ }^{\circ}\text{C}$. After the removal of the virus, the cells were washed and overlaid with carboxymethylcellulose in D-MEM medium with DMSO or different concentrations of compounds. Two days post-infection, cells were washed with phosphate-buffered saline (PBS), fixed with methanol, and infected foci were visualized by immunostaining with the monoclonal anti-Flavivirus group antigen antibody (4G2) (Absolute Antibody, Oxford, UK; diluted 1:1500 in PBS, 1% Tween 20, 5% FBS), followed with anti-mouse horseradish peroxidase (HRP)-conjugated secondary antibody (diluted 1:2000 in PBS containing 1% Tween 20 and 5% FBS). Plaques were detected using a Vector Nova Red kit (Vector Laboratories Ltd., Peterborough, UK) and counted.

4.5. Plaque Assay

Monolayers of A549 cells cultured in 24-well culture plates were inoculated with 10-fold dilutions of TBEV strains for 4 h at $37\text{ }^{\circ}\text{C}$. After the removal of the virus, the cells were overlaid with carboxymethylcellulose in D-MEM medium. After 5 days the medium was washed away and after a few washes with PBS, the cells were stained with naphthalene black to visualize the plaques. The virus titers were expressed as PFU per milliliter.

4.6. Dose-Response of Anti-TBEV Activity of Uridine Derivatives of 2-Deoxy Sugars

A549 cells were infected with the TBEV Neudoerfl strain (MOI = 0.1) and treated with tested compounds at a concentration range from 0 to 50 μ M. Culture supernatants were collected on days 1, 2, and 3 post-infection and used for the determination of viral titers using the plaque assay. The dose-response curves prepared from data obtained at day 3 post-infection were used to calculate the half-maximum inhibitory concentration (IC₅₀) values for each compound, indicating the concentration required to reduce the viral titer by 50% compared to the control, using GraphPad Prism software.

4.7. Western Blot Analysis

Overnight, A549 cells in 12-well plates were infected with the Neudoerfl TBEV strain at an MOI of 0.1. After 2 h, the medium was collected and fresh medium with different concentrations of compounds or DMSO was added for 48 h. Cells were lysed at 4 °C for 1 h with TNET buffer (20 mM Tris-HCl (pH 7.4), 150 mM NaCl, 1 mM EDTA, 1% Triton X-100). Proteins were separated by SDS-PAGE under non-reducing conditions, transferred to PVDF membranes, and detected with a specific monoclonal anti-Flavivirus group antigen antibody (4G2) (1:1500 dilution), rabbit monospecific polyclonal serum raised against prM protein (1:1500 dilution), or anti-actin antibody (1:1000 dilution) as primary antibodies. Anti-rabbit or anti-mouse peroxidase (HRP)-conjugated secondary antibodies (diluted 1:2000) were used as secondary antibodies. Antigen-antibody complexes were detected using a Super Signal West Pico Substrate system (Pierce, Dallas, TX, USA) using Chemidoc XRS[®] (BioRad, Hercules, CA, USA) and analyzed.

Author Contributions: E.K. conceived, designed, and performed all the in vitro antiviral experiments. E.K. also analyzed and interpreted the data, wrote the manuscript, conceived the study, acquired the funding, and supervised the research. I.W. designed and synthesized the chemical compounds used in the paper. G.B. helped in some experiments. L.E. and D.R. contributed new reagents and analytic tools. B.S. revised the manuscript. All authors read and approved the final version of the manuscript.

Funding: This research was funded by the National Science Centre, Poland, grant number UMO-2015/19/D/NZ6/01717.

Acknowledgments: We thank Karin Stiasny from the Center for Virology, Medical University of Vienna, Vienna, Austria for the TBEV Neudoerfl strain.

Conflicts of Interest: The authors declare no conflict of interest.

References

1. Dumpis, U.; Crook, D.; Oksi, J. Tick-borne encephalitis. *Clin. Infect. Dis.* **1999**, *28*, 882–890. [[CrossRef](#)] [[PubMed](#)]
2. Füzik, T.; Formanová, P.; Růžek, D.; Yoshii, K.; Niedrig, M.; Plevka, P. Structure of tick-borne encephalitis virus and its neutralization by a monoclonal antibody. *Nat. Commun.* **2018**, *9*, 436. [[CrossRef](#)] [[PubMed](#)]
3. Lindquist, L.; Vapalahti, O. Tick-borne encephalitis. *Lancet* **2008**, *371*, 1861–1871. [[CrossRef](#)]
4. Kovalev, S.Y.; Mukhacheva, T.A. Reconsidering the classification of tick-borne encephalitis virus within the Siberian subtype gives new insights into its evolutionary history. *Infect. Genet. Evol.* **2017**, *55*, 159–165. [[CrossRef](#)] [[PubMed](#)]
5. Dai, X.; Shang, G.; Lu, S.; Yang, J.; Xu, J. A new subtype of eastern tick-borne encephalitis virus discovered in Qinghai-Tibet Plateau, China. *Emerg. Microb. Infect.* **2018**, *7*, 74. [[CrossRef](#)] [[PubMed](#)]
6. Růžek, D.; Dobler, G.; Donoso Mantke, O. Tick-borne encephalitis: Pathogenesis and clinical implications. *Travel. Med. Infect. Dis.* **2010**, *8*, 223–232. [[CrossRef](#)]
7. Mantke, O.D.; Escadafal, C.; Niedrig, M.; Pfeffer, M. Tick-borne encephalitis in Europe, 2007 to 2009. *Euro. Surveill.* **2011**, *16*, 19976.
8. Süss, J. Tick-borne encephalitis 2010: Epidemiology, risk areas, and virus strains in Europe and Asia—an overview. *Ticks Tick Borne Dis.* **2011**, *2*, 2–15. [[CrossRef](#)]
9. Steffen, R. Epidemiology of tick-borne encephalitis (TBE) in international travellers to Western/Central Europe and conclusions on vaccination recommendations. *J. Travel Med.* **2016**, *23*, 1–10.

10. Jääskeläinen, A.E.; Tonteri, E.; Sironen, T.; Pakarinen, L.; Vaheri, A.; Vapalahti, O. European Subtype Tick-borne Encephalitis Virus in Ixodes persulcatus Ticks. *Emerg. Infect. Dis.* **2011**, *17*, 323–325. [[CrossRef](#)]
11. Mansfield, K.L.; Johnson, N.; Phipps, L.P.; Stephenson, J.R.; Fooks, A.R.; Solomon, T. Tick-borne encephalitis virus—A review of an emerging zoonosis. *J. Gen. Virol.* **2009**, *90*, 1781–1794. [[CrossRef](#)]
12. Ruzek, D.; Županc, T.A.; Borde, J.; Chrdle, A.; Eyer, L.; Karganova, G.; Kholodilov, I.; Knap, N.; Kozlovskaya, L.; Matveev, A.; et al. Tick-borne encephalitis in Europe and Russia: Review of pathogenesis, clinical features, therapy, and vaccines. *Antivir. Res.* **2019**, *164*, 23–51. [[CrossRef](#)]
13. Taba, P.; Schmutzhard, E.; Forsberg, P.; Lutsar, I.; Ljøstad, U.; Mygland, Å.; Levchenko, I.; Strle, F.; Steiner, I. EAN consensus review on prevention, diagnosis and management of tick-borne encephalitis. *Eur. J. Neurol.* **2017**, *24*, 1214–e61. [[CrossRef](#)]
14. Rey, F.A.; Heinz, F.X.; Mandl, C.; Kunz, C.; Harrison, S.C. The envelope glycoprotein from tick-borne encephalitis virus at 2 Å resolution. *Nature* **1995**, *375*, 291–298. [[CrossRef](#)]
15. Yoshii, K.; Yanagihara, N.; Ishizuka, M.; Sakai, M.; Kariwa, H. N-linked glycan in tick-borne encephalitis virus envelope protein affects viral secretion in mammalian cells, but not in tick cells. *J. Gen. Virol.* **2013**, *94*, 2249–2258. [[CrossRef](#)]
16. Krol, E.; Wandzik, I.; Krejmer-Rabalska, M.; Szewczyk, B. Biological Evaluation of Uridine Derivatives of 2-Deoxy Sugars as Potential Antiviral Compounds against Influenza A Virus. *Int. J. Mol. Sci.* **2017**, *18*, 1700. [[CrossRef](#)]
17. Wandzik, I.; Bieg, T.; Czaplicka, M. Synthesis of 2-deoxy-hexopyranosyl derivatives of uridine as donor substrate analogues for glycosyltransferases. *Bioorgan. Chem.* **2009**, *37*, 211–216. [[CrossRef](#)]
18. Wandzik, I.; Bieg, T.; Kadela, M. Simultaneous removal of benzyl and benzyloxycarbonyl protective groups in 5'-O-(2-deoxy-alpha-D-glucopyranosyl)uridine by catalytic transfer hydrogenolysis. *Nucleosides Nucleotides Nucleic Acids* **2008**, *27*, 1250–1256. [[CrossRef](#)]
19. Paszkowska, J.; Kania, B.; Wandzik, I. Evaluation of the Lipophilicity of Selected Uridine Derivatives by Use of Rp-Tlc, Shake-Flask, and Computational Methods. *J. Liq. Chromatogr. Relat. Technol.* **2012**, *35*, 1202–1212. [[CrossRef](#)]
20. Krol, E.; Wandzik, I.; Szeja, W.; Gryniewicz, G.; Szewczyk, B. In vitro antiviral activity of some uridine derivatives of 2-deoxy sugars against classical swine fever virus. *Antivir. Res.* **2010**, *86*, 154–162. [[CrossRef](#)]
21. Krol, E.; Wandzik, I.; Pastuch-Gawolek, G.; Szewczyk, B. Anti-Hepatitis C Virus Activity of Uridine Derivatives of 2-Deoxy Sugars. *Molecules* **2018**, *23*, 1547. [[CrossRef](#)] [[PubMed](#)]
22. Krol, E.; Wandzik, I.; Gromadzka, B.; Nidzworski, D.; Rychlowska, M.; Matlacz, M.; Tyborowska, J.; Szewczyk, B. Anti-influenza A virus activity of uridine derivatives of 2-deoxy sugars. *Antivir. Res.* **2013**, *100*, 90–97. [[CrossRef](#)] [[PubMed](#)]
23. Heinz, F.X.; Allison, S.L. Structures and mechanisms in flavivirus fusion. *Adv. Virus Res.* **2000**, *55*, 231–269. [[PubMed](#)]
24. Lorenz, I.C.; Allison, S.L.; Heinz, F.X.; Helenius, A. Folding and dimerization of tick-borne encephalitis virus envelope proteins prM and E in the endoplasmic reticulum. *J. Virol.* **2002**, *76*, 5480–5491. [[CrossRef](#)] [[PubMed](#)]
25. Goto, A.; Yoshii, K.; Obara, M.; Ueki, T.; Mizutani, T.; Kariwa, H.; Takashima, I. Role of the N-linked glycans of the prM and E envelope proteins in tick-borne encephalitis virus particle secretion. *Vaccine* **2005**, *23*, 3043–3052. [[CrossRef](#)]

Sample Availability: Samples of the compounds 1–11 are available from the authors.



© 2019 by the authors. Licensee MDPI, Basel, Switzerland. This article is an open access article distributed under the terms and conditions of the Creative Commons Attribution (CC BY) license (<http://creativecommons.org/licenses/by/4.0/>).



Broad-Spectrum Antiviral Activity of 3'-Deoxy-3'-Fluoroadenosine against Emerging Flaviviruses

Luděk Eyer,^{a,b} Pavel Svoboda,^{a,c} Jan Balvan,^{d,e} Tomáš Vičar,^{d,f} Matina Raudenská,^{e,g} Michal Štefánek,^{a,e} Jan Havierník,^{a,i} Ivana Huvarová,^a Petra Straková,^a Ivo Rudolf,^{h,i} Zdeněk Hubálek,^h Katherine Seley-Radtke,^j Erik de Clercq,^k Daniel Růžek^{a,b}

^aDepartment of Virology, Veterinary Research Institute, Brno, Czech Republic

^bInstitute of Parasitology, Biology Centre of the Czech Academy of Sciences, Ceske Budejovice, Czech Republic

^cDepartment of Pharmacology and Pharmacy, Faculty of Veterinary Medicine, University of Veterinary and Pharmaceutical Sciences Brno, Brno, Czech Republic

^dDepartment of Pathological Physiology, Faculty of Medicine, Masaryk University, Brno, Czech Republic

^eDepartment of Chemistry and Biochemistry, Mendel University in Brno, Brno, Czech Republic

^fDepartment of Biomedical Engineering, Faculty of Electrical Engineering and Communication, Brno University of Technology, Brno, Czech Republic

^gDepartment of Physiology, Faculty of Medicine, Masaryk University, Brno, Czech Republic

^hInstitute of Vertebrate Biology, Czech Academy of Sciences, Brno, Czech Republic

ⁱDepartment of Experimental Biology, Masaryk University, Brno, Czech Republic

^jDepartment of Chemistry and Biochemistry, University of Maryland, Baltimore County, Baltimore, Maryland, USA

^kRega Institute for Medical Research, KU Leuven, Leuven, Belgium

Luděk Eyer and Pavel Svoboda contributed equally to this work. Author order was determined both alphabetically and in order of decreasing seniority.

ABSTRACT Emerging flaviviruses are causative agents of severe and life-threatening diseases, against which no approved therapies are available. Among the nucleoside analogues, which represent a promising group of potentially therapeutic compounds, fluorine-substituted nucleosides are characterized by unique structural and functional properties. Despite having first been synthesized almost 5 decades ago, they still offer new therapeutic opportunities as inhibitors of essential viral or cellular enzymes active in nucleic acid replication/transcription or nucleoside/nucleotide metabolism. Here, we report evaluation of the ant flaviviral activity of 28 nucleoside analogues, each modified with a fluoro substituent at different positions of the ribose ring and/or heterocyclic nucleobase. Our antiviral screening revealed that 3'-deoxy-3'-fluoroadenosine exerted a low-micromolar antiviral effect against tick-borne encephalitis virus (TBEV), Zika virus, and West Nile virus (WNV) (EC_{50} values from $1.1 \pm 0.1 \mu\text{M}$ to $4.7 \pm 1.5 \mu\text{M}$), which was manifested in host cell lines of neural and extraneural origin. The compound did not display any measurable cytotoxicity up to concentrations of $25 \mu\text{M}$ but had an observable cytostatic effect, resulting in suppression of cell proliferation at concentrations of $>12.5 \mu\text{M}$. Novel approaches based on quantitative phase imaging using holographic microscopy were developed for advanced characterization of antiviral and cytotoxic profiles of 3'-deoxy-3'-fluoroadenosine *in vitro*. In addition to its antiviral activity in cell cultures, 3'-deoxy-3'-fluoroadenosine was active *in vivo* in mouse models of TBEV and WNV infection. Our results demonstrate that fluoro-modified nucleosides represent a group of bioactive molecules with excellent potential to serve as prospective broad-spectrum antivirals in antiviral research and drug development.

KEYWORDS nucleoside analogue, 3'-deoxy-3'-fluoroadenosine, flavivirus, tick-borne encephalitis virus, antiviral activity, cytotoxicity, mouse model

Emerging flaviviruses (genus *Flavivirus*, family *Flaviviridae*) are transmitted by blood-sucking arthropods, such as ticks or mosquitoes, and are causative agents of serious

Citation Eyer L, Svoboda P, Balvan J, Vičar T, Raudenská M, Štefánek M, Havierník J, Huvarová I, Straková P, Rudolf I, Hubálek Z, Seley-Radtke K, de Clercq E, Růžek D. 2021. Broad-spectrum antiviral activity of 3'-deoxy-3'-fluoroadenosine against emerging flaviviruses. *Antimicrob Agents Chemother* 65:e01522-20. <https://doi.org/10.1128/AAC.01522-20>.

Copyright © 2021 American Society for Microbiology. All Rights Reserved.

Address correspondence to Luděk Eyer, eyer@vri.cz.

Received 17 July 2020

Returned for modification 10 August 2020

Accepted 14 November 2020

Accepted manuscript posted online 23 November 2020

Published 20 January 2021

human diseases such as dengue fever, yellow fever, West Nile fever, Japanese encephalitis, and tick-borne encephalitis (1). More than 400 million clinical cases of flavivirus-induced infections are reported annually worldwide, which are in many cases fatal (2). No approved therapy is currently available against infections caused by medically important flaviviruses. Development of new and effective antiviral drugs and therapeutic strategies for infections caused by emerging flaviviruses and other viruses responsible for life-threatening diseases is extremely important. It is particularly crucial in the current era of increased global travel, as well as emerging issues with increasing numbers of zoonotic infections due to the loss of animal habitats, and the growing spread of viral vectors as a result of climate change.

Nucleoside/nucleotide analogues can alter essential biochemical processes by sufficiently mimicking the structure of natural nucleosides/nucleotides for cellular or viral enzyme recognition. This capability makes these compounds attractive candidates for treating various diseases, including those resulting from viral (3, 4), bacterial (5), fungal (6), or parasitic infections (7, 8), or various types of cancers (9, 10). As antivirals, nucleoside analogues operate via numerous modes of action, among which suppression of viral nucleic acid synthesis is considered particularly important due to their highly specific interactions with viral polymerases that subsequently result in premature DNA/RNA chain termination (11). Other modes of action for antiviral nucleosides include: (i) blocking the viral methyltransferases responsible for viral RNA methylation and capping (12, 13); (ii) suppression of *de novo* nucleotide biosynthesis and depletion of the cellular nucleotide pool (14); (iii) accumulation of mutations in viral genomes, leading to error catastrophe (15, 16); and (iv) immunomodulation that promotes the Th1 lymphocyte-based antiviral response (17).

Nucleoside analogues modified with a fluoro substituent at different positions of a sugar ring and/or heterocyclic (purine/pyrimidine) nucleobase were initially synthesized in the 1970s. Soon after, researchers noted unique properties that the fluorine imparts to the nucleoside scaffold (18, 19). In drug design, fluorine is often used as an isosteric replacement because of its similar size to hydrogen, as well as its similar electronegativity to the hydroxyl moiety in ribo/deoxyribonucleosides (20). Because of the exquisite electronegativity of fluorine, this substituent significantly influences the conformational properties of the nucleoside sugar ring by "locking" it into a specific conformation, e.g., in C2'-endo/C3'-exo, C2'-exo/C3'-endo or other variations of the envelope/half-chair pentose conformations. This effect can substantially influence the recognition of a nucleoside analogue by DNA/RNA polymerases, reverse transcriptases, and nucleoside/nucleotide kinases. These differences occur because each enzyme prefers a different nucleoside/nucleotide conformation, with the ultimate result being efficient enzyme inhibition and cessation of viral replication (21–23). Furthermore, fluorine increases the stability of neighboring bonds (e.g., *N*-glycosidic or phosphoester bonds), which renders fluoro-modified nucleosides resistant to unwanted catabolic degradation by nucleoside phosphorylases, esterases, and other intracellular hydrolases (21, 24). Finally, fluorine, when incorporated into a pyrimidine or purine base, considerably alters the steric and electronic properties of the base, as well as the hydrogen bonding interactions between the enzyme active site and nucleoside analogue (25–27). Based on these unique properties, use of fluorine substituents is widely agreed to be an advantageous drug modification, and numerous fluorine-substituted nucleoside-based drugs have been developed. Many of these candidates have shown potent anticancer activity (e.g., gemcitabine [2'-dideoxy-2',2'-difluorocytidine] [28] or floxuridine [2'-deoxy-5-fluorouridine] [29]), while others have been approved to treat serious and life-threatening viral infections, e.g., sofosbuvir, a McGuigan ProTide of 2'-fluoro-2'-methyluridine for treatment of chronic hepatitis C (HCV) infections (30).

Here, we have evaluated the antflaviviral activity of a series of 28 nucleoside analogues modified with a fluoro substituent at different positions of the ribose ring (predominantly at C2' and C3') and/or at the C2 or C5 position of the heterocyclic nucleobase. We also tested several fluoro-modified arabino nucleosides. Our antiviral

screening revealed that the vast majority of the investigated compounds showed no antiflaviviral effect or were substantially cytotoxic at the tested concentrations. Among the compounds we tested, however, 3'-deoxy-3'-fluoroadenosine exerted a high antiflaviviral potency *in vitro*, showing low-micromolar antiviral effects against tick-borne encephalitis virus (TBEV), Zika virus (ZIKV), and West Nile virus (WNV). 3'-Deoxy-3'-fluoroadenosine displayed observable cytostatic effects at high concentrations, but was well tolerated in the tested cell lines at compound levels of $<12.5 \mu\text{M}$. In addition, a quantitative phase imaging (QPI) approach based on high-resolution holographic microscopy was developed and optimized for advanced characterization/description of antiviral efficacy and cytotoxicity of 3'-deoxy-3'-fluoroadenosine in cell culture. Finally, we also demonstrated an antiviral effect of 3'-deoxy-3'-fluoroadenosine in mouse models of TBEV and WNV infection. To the best of our knowledge, this study is one of the few to describe an antiviral effect of a fluoro-substituted nucleoside against emerging flaviviruses. It also is the first to demonstrate antiviral activity of fluorinated nucleosides against TBEV, a virus responsible for serious neuroinfections in Europe and Northeast Asia. Moreover, our work demonstrates that fluoro-modified nucleoside scaffolds represent an interesting group of bioactive molecules characterized by unique structural properties with potential for use in antiviral research, drug development, and structure optimization as prospective broad-spectrum antivirals.

RESULTS

Initial antiviral screening of fluoro-substituted nucleosides. A series of 28 fluoro-modified nucleoside analogues was initially evaluated for potency in inhibiting TBEV-induced cytopathic effect (CPE) in porcine kidney stable (PS) cells. PS cells are an immortalized cell line widely used for isolation and multiplication of TBEV and other flaviviruses (31). Our attention was predominantly focused on nucleosides with a fluoro-substituent located at the C2', C3', C2, or C5 positions. For some nucleosides, we evaluated both of the ribo- and arabino-stereoisomers. For several of the compounds, a C2'-fluoro-substituent was combined with other halogen or alkyl moieties at the C2, C5, or N2 positions, resulting in di-substituted compounds (Fig. 1).

In this initial screening, all compounds were tested against TBEV (strain Hypr) at a single concentration of $25 \mu\text{M}$ using a 24-h pretreatment assay. We observed that TBEV-infected PS cell monolayers treated with 3'-deoxy-3'-fluoroadenosine, 3'-deoxy-3'-fluoroguanosine, or 3'-deoxy-3'-flouridine had higher cell viability (70.0, 36.1, and 35.8%, respectively) compared to virus-infected cells treated with other compounds tested ($<30\%$), as well as to virus-infected mock-treated cells (14.6%) (Fig. 2A).

To analyze the anti-TBEV activity of the 3'-deoxy-3'-fluoro-substituted nucleosides in more detail, we tested the antiviral potency of these compounds at concentrations of 0, 6.25, 12.5, and $25 \mu\text{M}$. Viral titers were determined from the collected media using the plaque assay after 72 h of cultivation. Although 3'-deoxy-3'-fluoroguanosine and 3'-deoxy-3'-flouridine did not reduce viral titers in TBEV-infected cells, 3'-deoxy-3'-fluoroadenosine showed remarkable inhibitory activity (Fig. 2B to D). For this nucleoside, compound concentrations of $6.25 \mu\text{M}$ reduced the virus titer by more than 2 orders of magnitude, whereas concentrations of 12.5 and $25 \mu\text{M}$ resulted in total abrogation of viral replication *in vitro* (Fig. 2B). Based on the observed antiviral activity of 3'-deoxy-3'-fluoroadenosine, we selected this nucleoside for further antiviral/cytotoxicity studies.

Dose-dependent antiflavivirus activity of 3'-deoxy-3'-fluoroadenosine. We next evaluated the antiviral activity of 3'-deoxy-3'-fluoroadenosine using three representative flaviviruses, i.e., TBEV (strains Hypr and Neudoerfl), ZIKV (strains MR-766 and Paraiba_01), and WNV (strains Eg-101 and 13-104). For antiviral assays, two cell lines were preferentially used: PS cells and human brain cortical astrocytes (HBCA) cells, the latter of which are primary cells of neural origin that are considered to be a clinically relevant model for *in vitro* antiflaviviral studies.

To assess the antiviral effect of 3'-deoxy-3'-fluoroadenosine against TBEV, we initially tested three treatment regimens differing by the time of drug addition to virus-

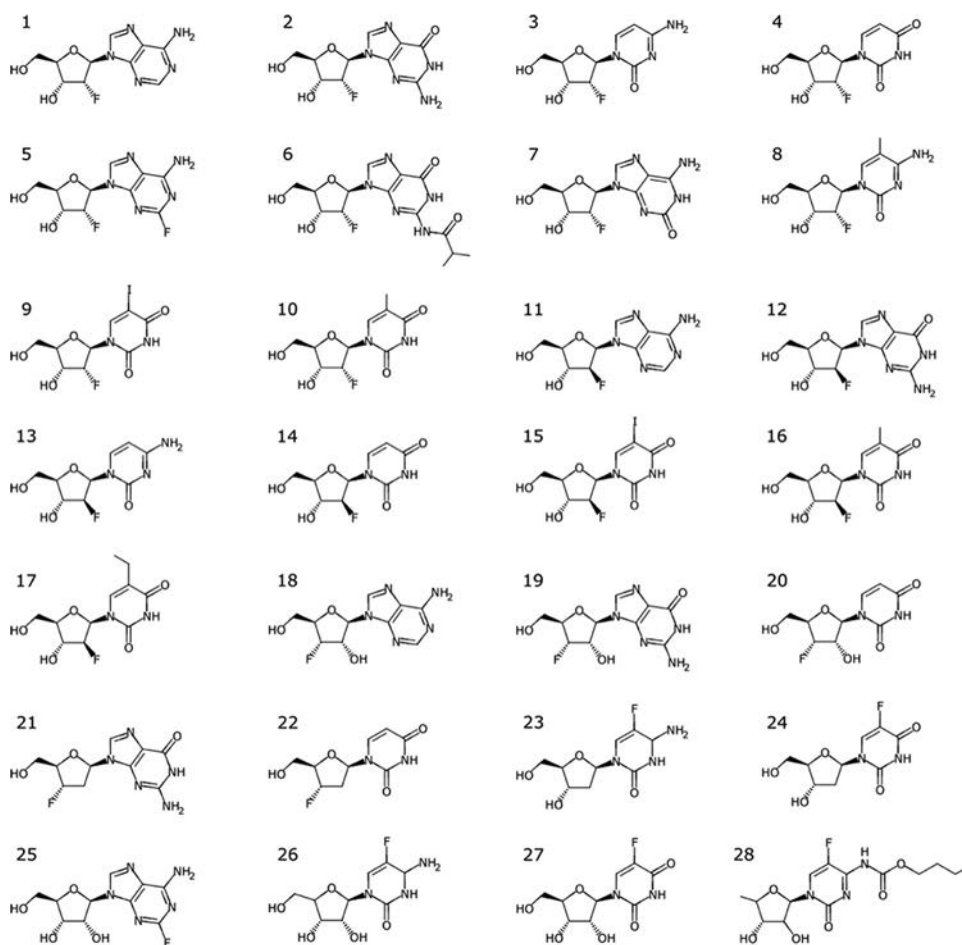


FIG 1 Structures of fluorinated nucleosides used in this study. (1) 2'-Deoxy-2'-fluoroadenosine; (2) 2'-deoxy-2'-fluoroguanosine; (3) 2'-deoxy-2'-fluorocytidine; (4) 2'-deoxy-2'-fluorouridine; (5) 2'-deoxy-2'-fluoro-2-fluoroadenosine; (6) 2'-deoxy-2'-fluoro-N2-isobutylguanosine; (7) 2'-deoxy-2'-fluoroisoguanosine; (8) 2'-deoxy-2'-fluoro-5-methylcytidine; (9) 2'-deoxy-2'-fluoro-5-iodouridine; (10) 2'-deoxy-2'-fluoro-5-methyluridine; (11) 2'-deoxy-2'-fluoroarabinoadenosine; (12) 2'-deoxy-2'-fluoroarabinothymine; (13) 2'-deoxy-2'-fluoroarabinothymine; (14) 2'-deoxy-2'-fluoroarabinothymine; (15) 2'-deoxy-2'-fluoro-5-iodoarabinothymine; (16) 2'-deoxy-2'-fluoro-5-methylarabinothymine; (17) 2'-deoxy-2'-fluoro-5-ethylarabinothymine; (18) 3'-deoxy-3'-fluoroarabinothymine; (19) 3'-deoxy-3'-fluoroarabinothymine; (20) 3'-deoxy-3'-fluoroarabinothymine; (21) 2',3'-dideoxy-3'-fluoroarabinothymine; (22) 2',3'-dideoxy-3'-fluoroarabinothymine; (23) 2'-deoxy-5-fluorocytidine; (24) 2'-deoxy-5-fluorouridine (floxuridine); (25) 2-fluoroarabinothymine; (26) 5-fluorocytidine; (27) 5-fluorouridine; and (28) capecitabine.

infected cells (see Materials and Methods) as follows: (i) a 24-h pretreatment; (ii) a simultaneous treatment; and (iii) a 2-h posttreatment. Notably, 3'-deoxy-3'-fluoroarabinothymine showed a strong anti-TBEV effect in all tested treatment regimens. Although all of the dose-response curves were similar in shape and slope, the compound-induced inhibitory activity was most pronounced using the pretreatment assay, as was obvious from the 100% inhibition of viral replication at compound concentrations higher than 10 μM (Fig. 2E and F). Based on these results, we decided to use a 24-h pretreatment for all other analyses of the nucleoside's antiviral activity.

Anti-TBEV potency in PS cells reached low-micromolar concentrations, with 50% effective concentration (EC_{50}) values of $2.2 \pm 0.6 \mu\text{M}$ and $1.6 \pm 0.3 \mu\text{M}$ for Hypr and Neudoerfl strains, respectively. The antiviral activity of 3'-deoxy-3'-fluoroarabinothymine was slightly lower in HBCA cells, providing EC_{50} values of $3.1 \pm 1.1 \mu\text{M}$ for Hypr and $4.5 \pm 1.5 \mu\text{M}$ for Neudoerfl (Fig. 3E and F; Table 1). For both cell lines, the anti-TBEV effect of 3'-deoxy-3'-fluoroarabinothymine was stable over time, and the inhibition of virus replication was clearly apparent at 48 and 72 h postinfection (p.i.). (Fig. 3A to D).

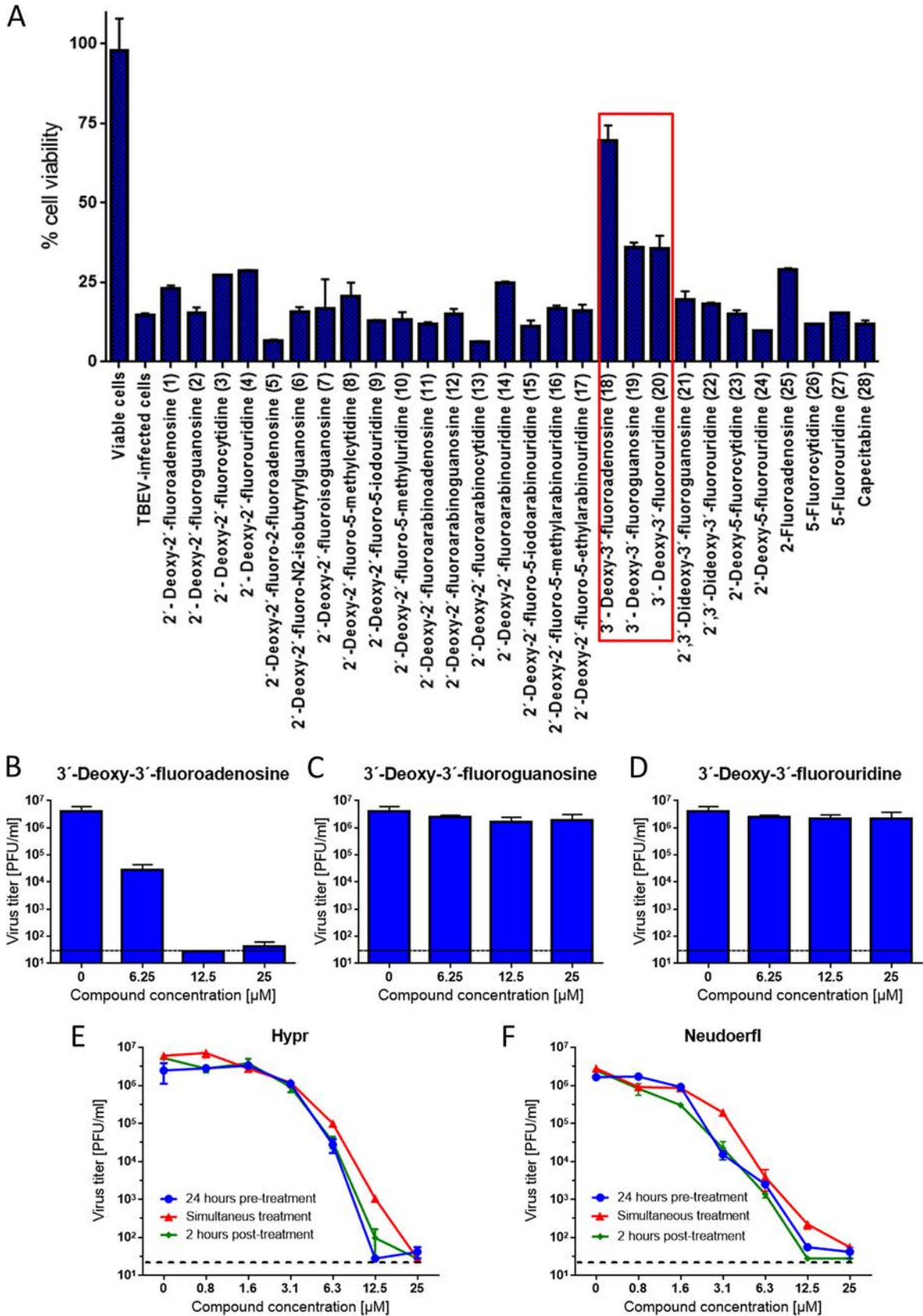


FIG 2 Inhibition of TBEV-induced CPE formation by the indicated fluoro-substituted nucleosides. (A) PS cells were pretreated with the compounds (25 μM) for 24 h and subsequently infected with TBEV (strain Hypr) at an MOI of 0.1. The infected cells were then (Continued on next page)

TABLE 1 Antiviral and cytotoxicity characteristics of 39-deoxy-3-adenosine

Virus	Strain	EC ₅₀ (mM) ^{a,b}		CC ₅₀ (mM) ^a		SI ^c	
		PS	HBCA	PS	HBCA	PS	HBCA
TBEV	Hypr	2.2 ± 0.6	3.1 ± 1.1			> 11.4	> 8.1
	Neudoerfl	1.6 ± 0.3	4.5 ± 1.5			> 15.6	> 5.6
ZIKV	MR-766	1.1 ± 0.1	4.7 ± 1.3	> 25	> 25	> 22.7	> 5.3
	Paraiba_01	1.6 ± 0.2	4.5 ± 1.4			> 15.6	> 5.6
WNV	Eg-101	3.7 ± 1.2	4.3 ± 0.3			> 6.8	> 5.8
	13-104	4.7 ± 1.5	4.3 ± 0.6			> 5.3	> 5.8

^aDetermined from three independent experiments. EC₅₀, 50% effective concentration; CC₅₀, 50% cytotoxic concentration.

^bExpressed as a 50% reduction in viral titers and calculated as inflection points of sigmoidal inhibitory curves, which were obtained by a nonlinear fit of transformed inhibitor concentrations versus normalized response using GraphPad Prism 7.04 (GraphPad Software, Inc., USA).

^cSI (selectivity index) = CC₅₀/EC₅₀.

Sensitivity of both ZIKV strains to 39-deoxy-39-fluoroadenosine appeared to be comparable to that for TBEV. In PS cells, the anti-ZIKV effect was characterized by EC₅₀ values of 1.1 ± 0.1 μM and 1.6 ± 0.2 μM for MR-766 and Paraiba_01, respectively (Fig. 3E; Table 1). After 72 h p.i., complete inhibition of virus replication was achieved at concentrations of 25 μM (for MR-766) and 12.5 μM and 25 μM (for Paraiba_01) (Fig. 3B). The efficacy of 39-deoxy-39-fluoroadenosine in suppressing ZIKV replication in HBCA was 3- to 4-fold lower than in PS cells, but it still reached low-micromolar values for both ZIKV strains (EC₅₀ values of 4.7 ± 1.3 μM and 4.5 ± 1.4 μM) (Fig. 3D and F; Table 1). In addition to ZIKV, 39-deoxy-39-fluoroadenosine significantly inhibited *in vitro* replication of both tested WNV strains. Compared with TBEV and ZIKV, the anti-WNV effect was characterized by slightly higher EC₅₀ values: 3.7 ± 1.2 μM (for Eg-101) and 4.7 ± 1.5 μM (for 13-104) in PS cells, and 4.3 ± 0.3 μM (for Eg-101) and 4.3 ± 0.6 μM (for 13-104) for HBCA cells (Fig. 3C, D, and F; Table 1).

Dose-dependent antiviral effects of 39-deoxy-39-fluoroadenosine identified in viral titer inhibition assays were confirmed by immunofluorescent staining, which was used to assess the expression of flaviviral surface E antigen in PS cells as a parameter of viral infectivity and replication *in vitro*. Although the surface E protein was highly expressed in virus-infected mock-treated cells (Fig. 4A), we observed a gradually decreasing fluorescence signal in cell monolayers treated with ascending compound concentrations monitored at 72 h p.i. A nucleoside concentration of 25 μM was strong enough to completely inhibit protein E expression of all tested flaviviruses in PS cell culture (Fig. 4A).

We then proceeded to study the antiviral activity of 39-deoxy-39-fluoroadenosine using a monitoring system based on QPI with high-resolution holographic microscopy to measure multiple parameters describing the physiological state of the monitored cells. These parameters included the following: (i) covered area (μm²) and (ii) cell dry mass (pg) (both used to characterize cell growth and proliferation activity); (iii) cell speed (μm/min) (describing cell movement intensity); (iv) circularity (characterizing

FIG 2 Legend (Continued)

incubated with the compounds for 72 h. Following incubation, PS monolayers were stained by naphthalene black and absorbance was measured at 540 nm. 39-Deoxy-39-fluoro-modified nucleosides that were further analyzed for their antiviral activity/toxicity are framed in red. Compound numbers correspond to those in Fig. 1. (B to D) TBEV titer reduction with 39-deoxy-39-fluoroadenosine (B), 39-deoxy-39-fluoroguanosine (C), and 39-deoxy-39-fluorouridine (D) at the indicated concentrations. The treatment regimen for B to D was the same as that for A; after 72 h of incubation, virus titers were determined using a plaque assay. (E) Antiviral activity of 39-deoxy-39-fluoroadenosine against TBEV strain Hypr when the compound was added to PS cells at 24 h prior to infection (blue), simultaneously with infection (red), or 2 h after infection (green). The growth media were collected after 72 h of cultivation and analyzed using the plaque assay. (F) Antiviral activity of 39-deoxy-39-fluoroadenosine against TBEV strain Neudoerfl in PS cells at a 24 h pretreatment (blue), simultaneous treatment (red) or 2 h posttreatment (green). The growth media were analyzed using the plaque assay after 72 h of incubation. The mean titers or % cell viabilities from three biological replicates are shown, and error bars indicate standard errors of the mean (*n* = 3). The horizontal dashed line indicates the minimum detectable threshold of 1.44 log₁₀ PFU/ml.

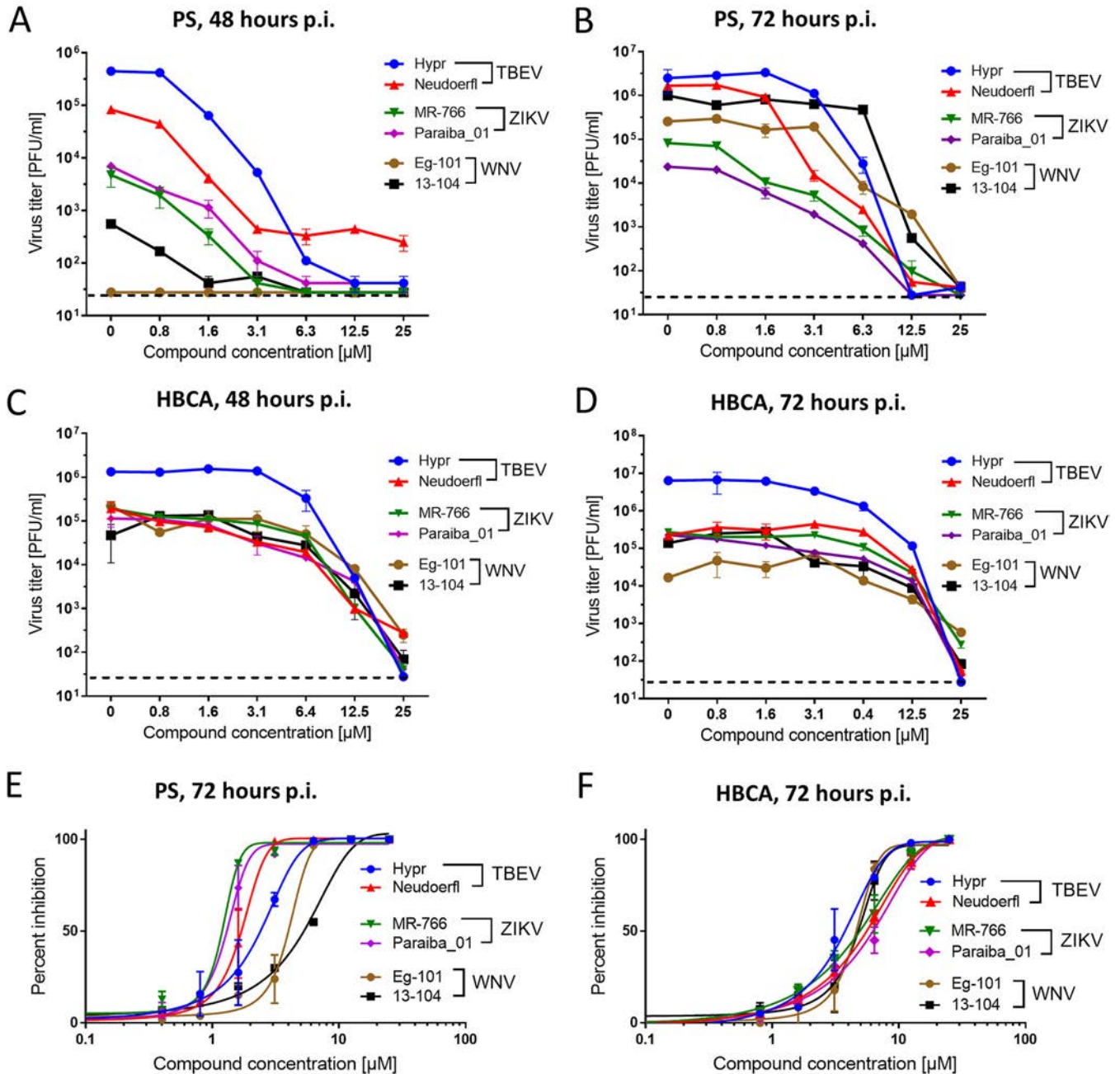


FIG 3 Dose-dependent anti-flaviviral activity of 3'-deoxy-3'-fluoroadenosine and cytotoxicity studies. (A and B) Growth curves for TBEV, ZIKV, and WNV in PS cells treated with 3'-deoxy-3'-fluoroadenosine at the indicated concentrations. PS cells were pretreated with the compounds at the indicated concentrations for 24 h and subsequently infected with the indicated flaviviruses at an MOI of 0.1. The infected cells were then incubated with the compound for 48 h p.i. or 72 h p.i. and viral titers were determined using the plaque assay. Data used for construction of dose-response curves for Hypr and Neudoerfl TBEV at 72 h p.i. (B) were reused from Fig. 2E and F, as those were two identical experiments. (C and D) Growth curves for TBEV, ZIKV, and WNV in HBCA cells treated with 3'-deoxy-3'-fluoroadenosine at the indicated concentrations. The treatment regimen was the same as in A and B, with the viral titers determined after 48 or 72 h p.i. (E and F) Inhibition curves of 3'-deoxy-3'-fluoroadenosine for the indicated flaviviruses cultivated with the compound in PS cells (E) or HBCA cells (F) for 72 h p.i. The mean titers from three biological replicates are shown, and error bars indicate standard errors of the mean ($n=3$). The horizontal dashed line indicates the minimum detectable threshold of 1.44 log₁₀ PFU/ml.

morphological changes of the cells and the rate of round cells); (v) density (pg/μm²); and (vi) cell dynamic score (to determine cell death).

QPI revealed that control cells displayed typical signs of normal physiological growth, proliferation, and movement, a low degree of morphological circularity (normal-shaped cells prevailed), and low mass density related to a low degree of apoptosis. In contrast, heat-killed cells exhibited sharp and fast alterations in cellular parameters

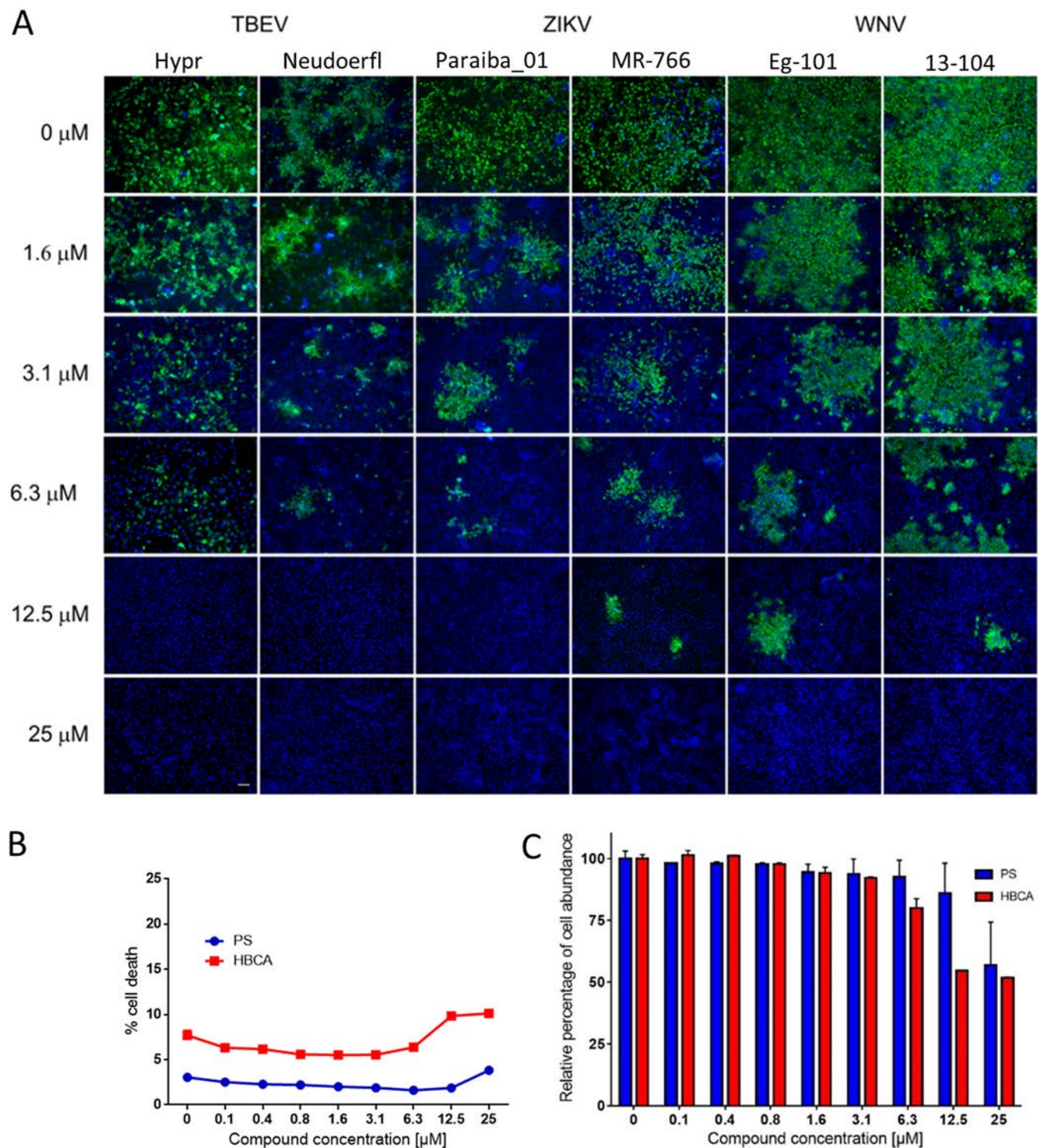


FIG 4 Inhibition of flavivirus surface E antigen expression by 3'-deoxy-3'-fluoroadenosine and cytotoxicity studies. (A) PS cells were pretreated with the compound for 24 h and subsequently infected with the indicated flaviviruses at an MOI of 0.1. PS cells were fixed on slides at 72 h postinfection, stained with flavivirus-specific antibody labeled with FITC (green), and counterstained with DAPI (blue). Scale bar, 50 μm . (B and C) Cytotoxicity of 3'-deoxy-3'-fluoroadenosine expressed as a percentage of cell death (B) and relative percentage of cell abundance (C). The mean percentage of cell death or mean relative percentage of cell abundance from three biological replicates is shown, and error bars indicate standard errors of the mean ($n = 3$).

and low cell dynamic scores typical of lytic cell death (Fig. 5 and 6; Fig. S1 in the supplemental material). TBEV-infected cell monolayers were characterized by low values for the covered area, gradually decreasing cell dry mass, and slowing cell speed. Moreover, TBEV-infected cells exhibited an increased cell circularity and higher mass

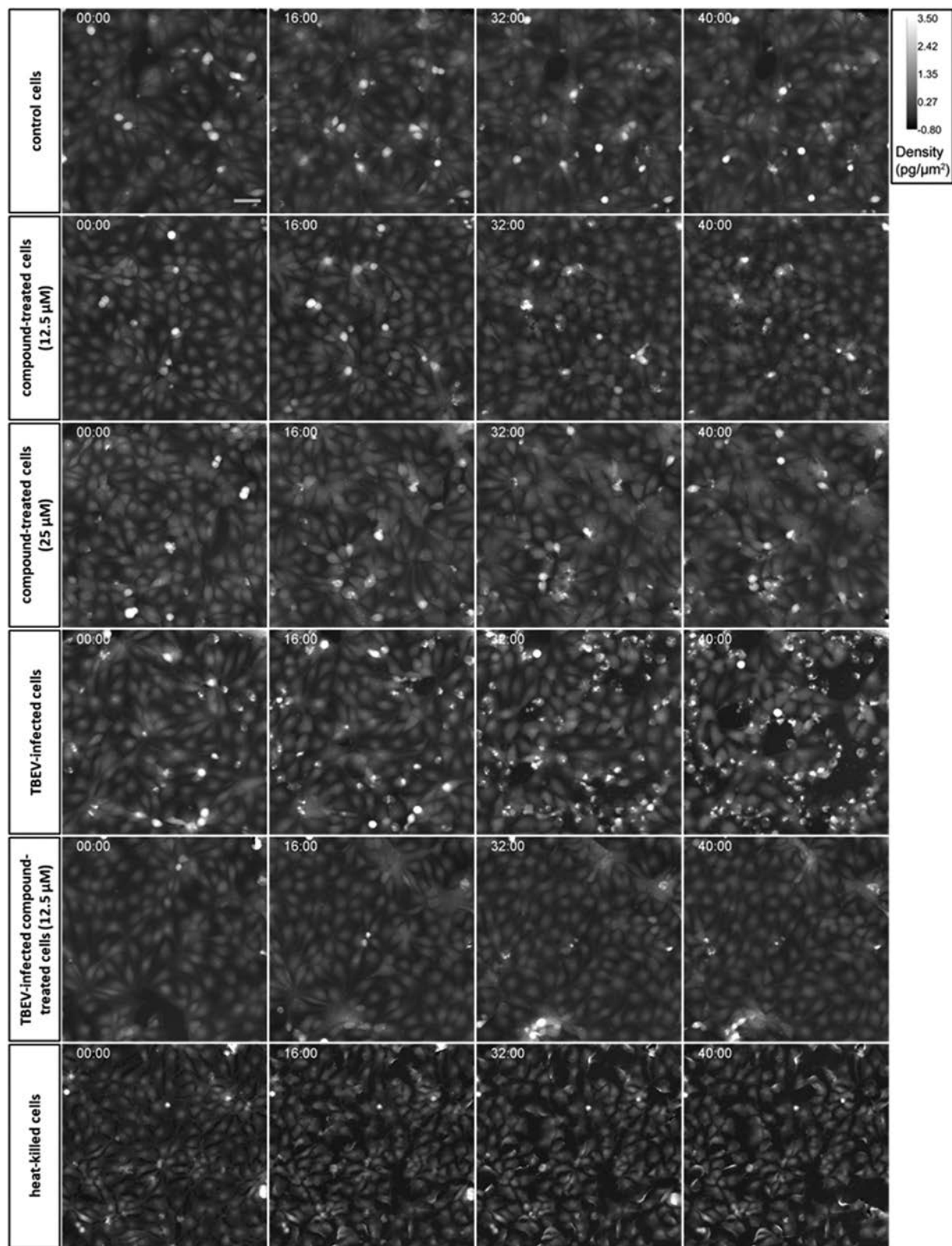


FIG 5 Real-time QPI signals for PS cells at different time points. PS cells in flow chambers were treated with the compound and inoculated with TBEV (strain Hypr) as described in the Materials and Methods. Control cells, compound-treated cells ($12.5 \mu\text{M}$, and $25 \mu\text{M}$), and TBEV-infected compound-treated cells ($12.5 \mu\text{M}$) maintained normal growth in a confluent monolayer with no morphological signs of ongoing cell death. TBEV-infected cells underwent apoptotic cell death with the presence of blebbing and apoptotic bodies (at 16 h, 32 h, and 40 h). Heat-killed cells underwent a lytic form of cell death without the presence of blebbing cells and apoptotic bodies. Scale bar = $30 \mu\text{m}$.

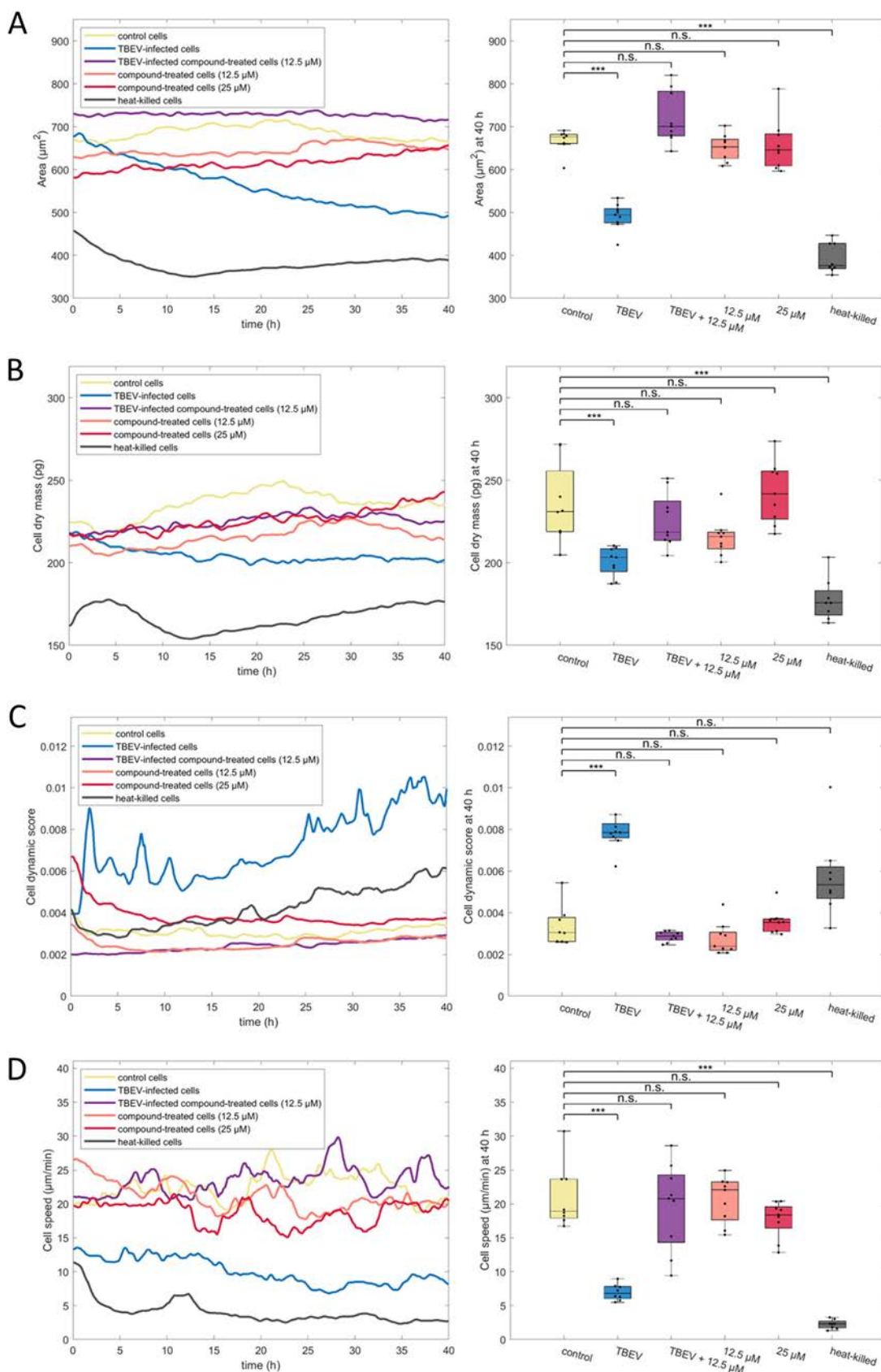


FIG 6 Real-time QPI parameters for PS cells for advanced characterization/description of antiviral efficacy and cytotoxicity of 3'-deoxy-3'-fluoroadenosine in cell culture. (A) Real-time QPI-measured area of the cell population (left) and the endpoint area values of the cell population after 40 h of treatment. (Continued on next page)

density, related to a virus-induced CPE formation/apoptosis, as also demonstrated by the cell dynamic score, an average intensity change in cell pixels typical for membrane blebbing, and intensive changes in CPE-associated cell mass distribution. Finally, TBEV-infected cells treated with 3'-deoxy-3'-fluoroadenosine (12.5 μ M) showed parameter values similar to those of control cells, highlighting the ability of 3'-deoxy-3'-fluoroadenosine to inhibit viral replication and suppress CPE formation and apoptosis (Fig. 5 and 6; Fig. S1).

Cytotoxicity of 3'-deoxy-3'-fluoroadenosine. We investigated the potential cytotoxicity of 3'-deoxy-3'-fluoroadenosine for PS and HBCA cells in terms of (i) cell death and (ii) relative percentage of cell abundance (a parameter corresponding with the total abundance of lactate dehydrogenase in the cell population, which can be used as an index of total cell count), using the CytoTox 96 non-radioactive cytotoxicity assay (Promega, WI, USA). Measurement of the released amount of lactate dehydrogenase in compound-treated cells revealed no substantial toxicity of 3'-deoxy-3'-fluoroadenosine for PS cells up to 25 μ M (cell death values were $3.8 \pm 0.1\%$ for compound-treated cells [25 μ M] and $3.0 \pm 0.3\%$ for mock-treated cells) (Fig. 4B). For HBCA, the compound was only slightly cytotoxic at a concentration of 25 μ M (cell death value of $10.1 \pm 0.2\%$) compared with mock-treated cells (cell death value of $7.7 \pm 0.8\%$) (Fig. 4B).

Treatment with 3'-deoxy-3'-fluoroadenosine resulted in substantial differences in relative percentage of cell abundance, however, in compound-treated PS/HBCA cells compared to mock-treated monolayers, where a relative percentage of cell abundance in PS monolayers treated with the compound at 25 μ M was only $56.9 \pm 17.3\%$ compared to control cells. Of note, this parameter was not substantially affected when the cell monolayers were treated with compound concentrations of 12.5 μ M or less (Fig. 4C). This effect was even higher in HBCA cells and reached $80.0 \pm 3.8\%$, $54.7 \pm 0.1\%$, and $51.8 \pm 0.3\%$ for concentrations of 6.3, 12.5, and 25 μ M, respectively (Fig. 4C). The observed differences in relative percentage of cell abundance indicated that the compound concentrations of 25 μ M (for PS) and 12.5 μ M and 25 μ M (for HBCA) considerably suppressed cell proliferation (Fig. 4C) but did not result in extensive cell death or cell monolayer damage (Fig. 4B). Based on these results, it can be concluded that 3'-deoxy-3'-fluoroadenosine exerted an observable cytostatic effect at the above-mentioned concentrations for both cell lines tested.

QPI of cells treated with 12.5 μ M or 25 μ M 3'-deoxy-3'-fluoroadenosine yielded dose-response curves that were similar in shape and slope to those for control cells. They were, however, somewhat flatter, indicating slower progress in area coverage and growth of cell dry mass and almost the same degree of mass density within the whole monitoring period. This result can be explained as a consequence of the compound's cytostatic effect, which confirmed the findings obtained previously in colorimetric cell-based assays. We found no signs of apoptosis or other types of cell death in compound-treated PS cells (Fig. 5 and 6; Fig. S1).

Antiviral efficacy of 3'-deoxy-3'-fluoroadenosine in a mouse model of lethal flavivirus infection. Based on the observation that 3'-deoxy-3'-fluoroadenosine strongly inhibited replication of emerging flaviviruses *in vitro*, we then proceeded to investigate its anti-WNV and anti-TBEV effects in mouse infection models (Fig. 7A). BALB/c mice injected subcutaneously with a lethal dose of WNV strain Eg-101 (10^3 PFU/mouse) exhibited characteristic clinical signs of infection, such as ruffled fur,

FIG 6 Legend (Continued)

A significant drop in cell-covered area was noticeable after TBEV and heat treatment. This effect of TBEV was reversed after 3'-deoxy-3'-fluoroadenosine treatment. (B) Real-time QPI-measured cell dry mass (left) and the endpoint cell dry mass values after 40 h of treatment (right). A significant drop in cell dry mass was noticeable after TBEV and heat treatment. This effect of TBEV was reversed after 3'-deoxy-3'-fluoroadenosine treatment. (C) Real-time QPI-measured cell dynamic score (left) and the endpoint cell dynamic score values after 40 h of treatment (right). High cell dynamic score indicating apoptosis was observable after TBEV treatment. This effect of TBEV was reversed after 3'-deoxy-3'-fluoroadenosine treatment. (D) Real-time QPI-measured cell speed (left) and the endpoint cell-speed values of cells after 40 h of treatment (right). n.s., not significant, $P > 0.05$; *, $P < 0.05$; ***, $P < 0.001$. Boxes: main box edges are 25th and 75th percentiles, central line indicates the median, and whiskers indicate the lowest and highest values of the 1.5 interquartile range. Each dot in the boxplot represents the average value for one field of view.

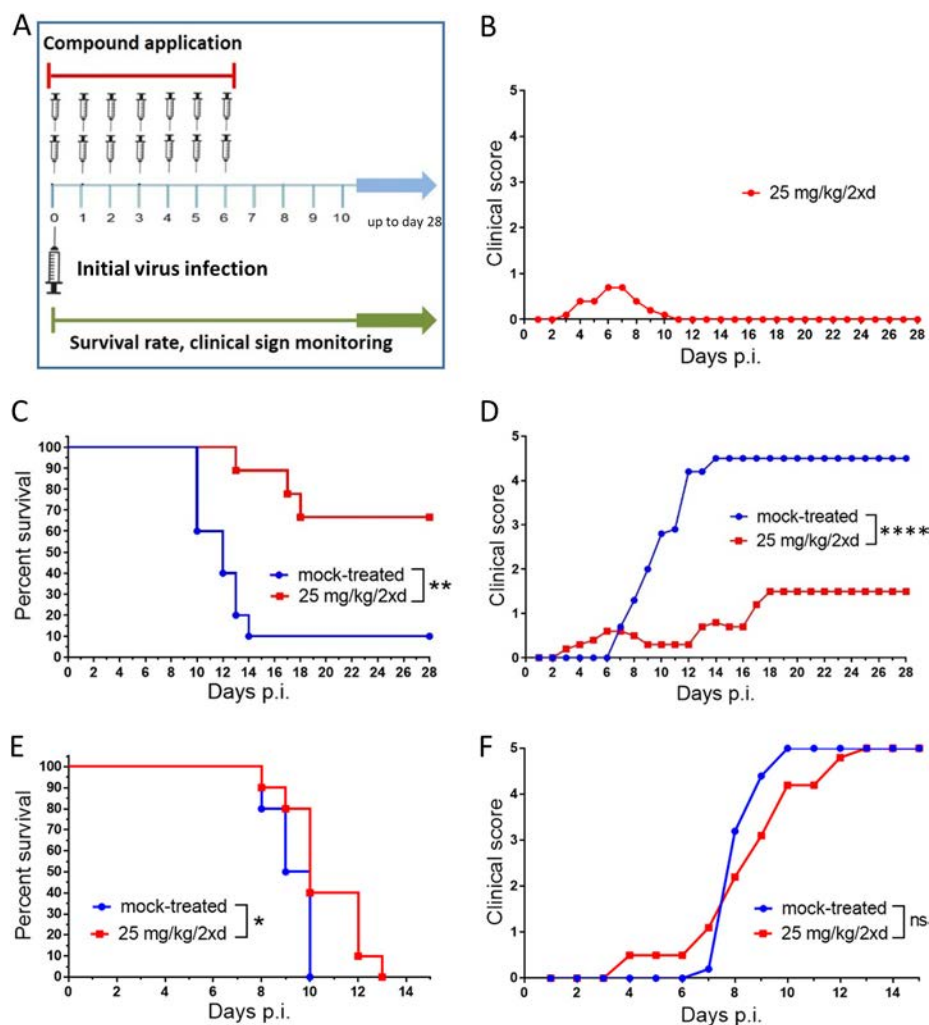


FIG 7 Antiviral efficacy of 3'-deoxy-3'-fluoroadenosine in mouse models of WNV and TBEV infection. (A) The design of the *in vivo* antiviral experiment. (B) Toxicity evaluation of 3'-deoxy-3'-fluoroadenosine in mice. The compound (25 mg/kg) was administered twice daily to adult BALB/c mice for 6 days. (C) Groups of adult BALB/c mice were infected with a lethal dose of WNV (strain Eg-101) and treated twice daily with intraperitoneal 25 mg/kg 3'-deoxy-3'-fluoroadenosine or phosphate-buffered saline (mock treatment) at the indicated times after WNV infection. Survival rates were monitored daily. (D) Clinical signs of WNV infection were scored daily as follows: 0, no signs; 1, ruffled fur; 2, slowing of activity or hunched posture; 3, asthenia or mild paralysis; 4, lethargy, tremor, or complete paralysis of the limbs; and 5, death. (E) Groups of adult BALB/c mice were infected with a lethal dose of TBEV (strain Hypr) and treated twice daily with intraperitoneal 25 mg/kg 3'-deoxy-3'-fluoroadenosine or phosphate-buffered saline (mock treatment) at the indicated times after TBEV infection. Survival rates were monitored daily. (F) Clinical signs of TBEV infection were scored daily as described in D. ns, not significant, $P > 0.05$; *, $P < 0.05$; **, $P < 0.01$; ****, $P < 0.0001$.

hunched posture, tremor, and paralysis of the limbs, within 7 to 13 days p.i., with most mice requiring euthanasia. The mortality rate was 90%, with a mean survival time of 12 ± 1.6 days p.i. Similarly, mice injected with TBEV strain Hypr (10^3 PFU/mouse, a subcutaneous route) showed typical signs of infection within days 8 to 10 days p.i. The mortality rate was ultimately 100%, with a mean survival time of 9.0 ± 1.0 days (Fig. 7C and D).

In order to evaluate toxicity of the compound *in vivo*, 3'-deoxy-3'-fluoroadenosine (a dose of 25 mg/kg/2×day) was administered to BALB/c mice intraperitoneally for 6 days and clinical scores of the treated animals were monitored daily. In seven mice, the treatment was associated with moderate side effects starting at day 3 after treatment initiation (manifested by slightly ruffled hair or hunched posture), which led to a gradual increase in the average clinical score up to 0.7 within days 6 to 7. After we

stopped the compound administration (at day 6), the observed side effects gradually disappeared (Fig. 7B). As expected, moderate side effects were observed in both WNV- or TBEV-infected compound-treated mice starting on day 3 or 4 p.i. (Fig. 7D and F). The increase of clinical score was probably related with the cytostatic activity of the compound, as demonstrated by *in vitro* (cell-based) assays.

In WNV-infected BALB/c mice, 3'-deoxy-3'-fluoroadenosine (25 mg/kg/2×day) administered intraperitoneally (the administration was initiated from the time of virus inoculation and ceased at day 6 p.i.) significantly protected the animals from disease development and mortality (70% survival rate, $P < 0.01$). In 70% of WNV-infected compound-treated mice, no signs of clinical infection were observed up to the end of the experiment (day 28 p.i.). In 30% of mice, the compound substantially prolonged the time of mouse survival (14.5 ± 2.4 days) compared with controls (Fig. 7C and D).

Treatment with 25 mg/kg/2×day of 3'-deoxy-3'-fluoroadenosine initiated at the time of TBEV inoculation and ceasing at day 6 p.i. resulted in a slight but statistically significant survival prolongation among TBEV-infected compound-treated mice ($P < 0.05$). Although all treated mice eventually died, they showed slightly slowed development of clinical signs of neuroinfection within days 8 to 13 p.i. and had an increased mean survival time of 10.5 ± 1.9 days compared with control animals (Fig. 7E and F).

DISCUSSION

Fluoro-substituted nucleosides show unique chemical, biochemical, and biological properties and are widely used as treatment for numerous viral, bacterial, fungal, and protozoal infections, in addition to many cancers (18, 19). So far, however, only a few of these compounds have been tested against flaviviruses to assess their antiviral *in vitro* and *in vivo* effects (32–34). In this study, we evaluated the antiviral activity of a series of 28 fluoro-modified nucleosides against TBEV in the PS cell line. To our surprise, we found little to no inhibition of virus-induced CPE formation by almost all of the tested compounds, and some of them proved to be highly cytotoxic. No antiviral activity or high toxicity was observed in particular with nucleosides modified with a fluoro-substituent at C2', C2, or C5. Inactivity of 2'-fluoro-modified nucleosides against TBEV could be explained by elimination of the 2'-hydroxy hydrogen bond donor, which results in a dramatic decrease in hydrogen-bonding capacity with the polymerase or the incoming nucleoside triphosphate and the inability of such nucleosides to trigger inhibition of viral RNA synthesis (35).

Changes in stereochemistry at the C2' position from the ribo-configuration to the arabino-orientation also can lead to compound inactivity, as illustrated with a series of 2'-deoxy-2'-fluoroarabinonucleosides tested in this study. Similarly, the addition of a fluoro-substituent to the C2/C5 positions of a purine/pyrimidine yielded compounds with no anti-TBEV efficacy, likely due to electronic or steric hindrance with the viral NS5 RdRp active site (35). Alternatively, inactivity of these nucleoside analogues may be the result of inefficient compound uptake mediated by specific nucleoside transporters, low conversion efficacy into active (phosphorylated) forms by cellular kinases, or a high degradation rate caused by nucleoside/nucleotide catabolic enzymes (4). As a result, those mechanisms could be interesting targets for further investigation.

As might be expected, nucleosides lacking the 3'-hydroxyl group could be potent inhibitors of flaviviral NS5 RdRp-mediated RNA synthesis, acting as obligate RNA chain terminators (11). Indeed, 3'-deoxy-3'-fluoroguanosine 5'-triphosphate was previously described as interacting directly with NS5B RdRp of HCV, resulting in suppression of viral RNA synthesis by disruption of further extension of the replicating viral RNA (35). The potency to inhibit HCV NS5B polymerase activity was also observed in 3'-deoxy-3'-fluoroadenosine 5'-triphosphate; however, the inhibitory activity was considerably lower than its guanosine counterpart (35). Our *in vitro* antiviral assays revealed that two 3'-deoxy-3'-fluoro-substituted nucleosides, 3'-deoxy-3'-fluoroguanosine and 3'-deoxy-3'-fluorouridine, did not suppress multiplication of TBEV in PS cells. In contrast,

3'-deoxy-3'-fluoroadenosine, a nucleoside first synthesized in the late 1980s at the Rega Institute for Medical Research in Belgium (36, 37), showed potent, low-micromolar antiviral inhibition of *in vitro* TBEV replication. Moreover, this compound suppressed replication of two other medically important flaviviruses, WNV and ZIKV, in PS cells, as well as in primary HBCA cells. The antiviral effect was stable over time, with inhibition of viral replication observed at 48 and 72 h p.i., and the compound was highly active even if added to PS cells at 2 h after infection. The ability of 3'-deoxy-3'-fluoroadenosine to inhibit multiple arthropod-borne flaviviruses demonstrates potent, broad-spectrum antiviral activity across the genus *Flavivirus*. Broad-spectrum inhibitory effects for 3'-deoxy-3'-fluoroadenosine have also been described in earlier papers for numerous RNA viruses of the *Picornaviridae*, *Togaviridae*, *Reoviridae*, and *Arenaviridae* families (36, 38).

Notably, we did not observe any measurable *in vitro* cytotoxicity of 3'-deoxy-3'-fluoroadenosine in PS and HBCA cells within compound concentrations used for antiviral activity evaluation (0 to 25 μ M). This result is in agreement with earlier studies showing a minimum cytotoxic concentration of 40 μ M for primary rabbit kidney cells, Vero cells, and HeLa cells (36, 37). However, 3'-deoxy-3'-fluoroadenosine did have observable cytostatic effects at 25 μ M in PS cells and at 12.5 μ M and 25 μ M in HBCA cells. Cytostatic properties of 3'-deoxy-3'-fluoroadenosine were previously described for murine leukemia cells (L1210), human B-lymphoblast (Raji) cells, human T-lymphocyte (H9) cells, and human T4-lymphocytes (MT-4), acting at concentrations ranging from 1.6 to 23 μ M (37, 39).

It could be speculated that the cytostatic activity is related to low selectivity of 3'-deoxy-3'-fluoroadenosine 5'-triphosphate for viral RdRps over other types of polymerases. The extremely broad range of viruses sensitive to this nucleoside, including vaccinia virus among DNA viruses, supports this hypothesis (36). In accordance with this claim, 3'-deoxy-3'-fluoroadenosine has also been described as terminating RNA synthesis catalyzed by DNA-dependent RNA polymerase from *E. coli* (40). In addition, 3'-deoxy-3'-fluoroadenosine inhibited incorporation of ³H-labeled uridine into cellular RNA, resulted in abrogation of cellular RNA synthesis in actively growing Vero cells (38). Alternatively, the broad range of antiviral activity of 3'-deoxy-3'-fluoroadenosine and the reported suppression of cellular RNA synthesis could also be explained as a result of compound-mediated inhibition of purine/pyrimidine biosynthesis and nucleotide depletion, as was recently described for a broad-spectrum antiviral and anticancer drug gemcitabine (2'-dideoxy-2',2'-difluorocytidine) (41). In order to explain a broad spectrum antiviral efficacy of 3'-deoxy-3'-fluoroadenosine, this compound was also tested for its potential inhibition of S-adenosylhomocysteine (SAH) hydrolase. However, no inhibitory activity to SAH hydrolase was demonstrated, unless it was used at a rather high concentration (36).

Based on our observation that 3'-deoxy-3'-fluoroadenosine showed a strong antiviral potency in cell culture (*in vitro*), we evaluated its activity *in vivo* using mouse models of WNV and TBEV infection. Treatment of WNV-infected mice with 25 mg/kg of 3'-deoxy-3'-fluoroadenosine twice a day resulted in a significant decrease of mortality and in a substantial elimination of clinical signs of neuroinfection. In TBEV-infected mice, the antiviral effect of 3'-deoxy-3'-fluoroadenosine (25 mg/kg/2 \times day) was not as strong; however, the compound administration resulted in significantly longer survival time and slower progress of development of clinical signs compared with control animals. A lower efficacy of 3'-deoxy-3'-fluoroadenosine against TBEV (strain Hypr) *in vivo* could be explained by a rapid/aggressive course of TBEV infection in mice, where the average survival time of TBEV-infected mice was shorter than that of WNV-infected mice (9.0 \pm 1.0 days versus 12 \pm 1.6 days, respectively). 3'-Deoxy-3'-fluoroadenosine was previously demonstrated to show high efficacy in suppressing the formation of tail lesions in vaccinia virus-infected rodents. The compound, administered intravenously for 5 days at concentrations of 50 and 100 mg/kg/day, reduced the number of pox tail

lesions by 25% and 80%, respectively. A dose of 200 mg/kg/day was reported to be lethal for mice (36).

Previous studies have shown that nucleosides with antiviral activity against arthropod-borne flaviviruses contain one of the following sugar ring modifications: (i) a methyl substitution at C2⁹ (42), (ii) an ethynyl substitution at C2⁹ (43, 44), or (iii) an azido substitution at C4⁹ (45). An observable (but weaker) antiflaviviral effect also has been reported for nucleosides with (iv) a cyano substitution at C1⁹ (46). These chemical modifications are used in combination with appropriate heterocyclic bases or their modified counterparts (e.g., with 7-deazaadenine) and/or with modifications of *N*-glycosidic bond (e.g., switching to a *C*-glycosidic bond) (4). Herein we have described the first results showing that a fluoro-substitution at the C3⁹ position of adenosine represents another useful nucleoside modification that exhibited low-micromolar inhibitory activity against emerging flavivirus replication. While the increased cytostatic activity of 3⁹-deoxy-3⁹-fluoroadenosine *in vitro* limits its potential use for further clinical applications; however, additional chemical modifications could improve this compound's cytotoxic/cytostatic profile. This is exemplified by 2⁹-deoxy-2⁹-fluorinated nucleosides, in which the addition of C2⁹ methyl and C5⁹ phosphoramidate groups led to increased nucleoside selectivity toward viral RdRp, manifested as high inhibitory potency and low toxicity. These characteristics have been demonstrated for the anti-HCV drug sofosbuvir (47, 48), illustrating the considerable potential of fluoro-substituted nucleoside analogues as prospective starting points in developing effective antivirals for treating flavivirus-associated diseases.

MATERIALS AND METHODS

Ethics statement. This study was carried out in strict accordance with Czech law and guidelines for the use of experimental animals and protection of animals against cruelty (Animal Welfare Act 246/1992 Coll.). All procedures were reviewed by the local ethics committee and approved by the Ministry of Agriculture of the Czech Republic (permit no. 13522/2019-MZE-18134).

Cell cultures, virus strains, and antiviral compounds. PS cells (31) were cultured at 37°C in Leibovitz (L-15) medium. HBCA (ScienCell, Carlsbad, CA) cells were cultivated in Astrocyte medium (Thermo Fisher Scientific). The media were supplemented with 3% (L-15) and 6% (Astrocyte medium) newborn calf serum and 100 U/ml penicillin, 100 µg/ml streptomycin, and 1% glutamine (Sigma-Aldrich, Prague, Czech Republic).

The following emerging flaviviruses were tested: TBEV (strains Hypr and Neudoerfl, both members of the West European TBEV subtype, provided by the Collection of Arboviruses, Institute of Parasitology, Biology Center of the Czech Academy of Sciences, Ceske Budejovice, Czech Republic <http://www.arboviruscollection.cz/index.php?lang=en>), ZIKV (African strain MR-766 and Brazilian strain Paraiba_01, kindly provided by Carla Torres Braconi and Paolo M. de A. Zanotto, University of Sao Paulo), and WNV (Eg-101, a member of genomic lineage 1, originally isolated from human serum in Egypt, and 13–104, a representative of genomic lineage 2, isolated from the *Culex modestus* mosquito in the Czech Republic).

Nucleoside analogues were purchased from Carbosynth (Compton, UK) (2⁹-deoxy-2⁹-fluoroadenosine, 2⁹-deoxy-2⁹-fluoroguanosine, 2⁹-deoxy-2⁹-fluorocytidine, 2⁹-deoxy-2⁹-fluorouridine, 2⁹-deoxy-2⁹-fluoro-2-fluoroadenosine, 2⁹-deoxy-2⁹-fluoro-*N*2-isobutyrylguanosine, 2⁹-deoxy-2⁹-fluoroisoguanosine, 2⁹-deoxy-2⁹-fluoro-5-methylcytidine, 2⁹-deoxy-2⁹-fluoro-5-iodouridine, 2⁹-deoxy-2⁹-fluoro-5-methyluridine, 2⁹-deoxy-2⁹-fluoroarabinoadenosine, 2⁹-deoxy-2⁹-fluoroarabinoguanosine, 2⁹-deoxy-2⁹-fluoroarabincytidine, 2⁹-deoxy-2⁹-fluoroarabinouridine, 2⁹-deoxy-2⁹-fluoro-5-iodoarabinouridine, 2⁹-deoxy-2⁹-fluoro-5-methylarabinouridine, 2⁹-deoxy-2⁹-fluoro-5-ethylarabinouridine, 3⁹-deoxy-3⁹-fluoroadenosine, 3⁹-deoxy-3⁹-fluoroguanosine, 3⁹-deoxy-3⁹-fluorouridine, 2⁹,3⁹-dideoxy-3⁹-fluoroguanosine, and 2⁹,3⁹-dideoxy-3⁹-fluorouridine) and from Sigma-Aldrich (Prague, Czech Republic) (2-fluoroadenosine, 5-fluorocytidine, 2⁹-deoxy-5-fluorocytidine, capecitabine, 5-fluorouridine, and 2⁹-deoxy-5-fluorouridine [floxuridine]). Test compounds were solubilized in 100% dimethyl sulfoxide (DMSO) to yield 10 mM stock solutions.

Initial antiviral screening with CPE reduction assay. The 28 fluoro-substituted nucleosides were first screened at a single concentration of 25 µM for their ability to inhibit cytopathic effects (CPE) mediated by TBEV infection (strain Hypr) in PS cells. The cells were seeded in 96-well plates (approximately 2 × 10⁴ cells per well) and incubated for 24 h to form a confluent monolayer. Following incubation, the medium was aspirated from the wells and replaced with 200 µl of fresh medium containing 25 µM of the test compound (three wells per compound) and incubated for an additional 24 h (i.e., 24-h pretreatment). DMSO was added to virus-infected cells as a negative control at a final concentration of 0.5% (vol/vol). After 24 h, the medium was aspirated again and replaced with 200 µl of compound-containing medium (25 µM) inoculated with TBEV at a multiplicity of infection (MOI) of 0.1. The CPE was monitored visually using the Olympus BX-5 microscope equipped with an Olympus DP-70 CCD camera. At 72 h p.i.,

cell monolayers were stained by naphthalene black. The rate of CPE was expressed in terms of cell viability as the absorbance at 540 nm by compound-treated cells relative to the absorbance by DMSO-treated cells, as described previously (49). To analyze the anti-TBEV activity of 3'-deoxy-3'-fluoroadenosine, 3'-deoxy-3'-fluoroguanosine, and 3'-deoxy-3'-fluorouridine in more detail, we treated PS cell monolayers with these compounds at concentrations of 0, 6.25, 12.5, and 25 μM and incubated for 24 h. Then, the growth medium was aspirated and replaced with fresh medium containing the same concentrations of the tested compounds and TBEV inoculum (strain Hypr, MOI of 0.1). Viral titers were estimated from the collected media using the plaque assay after a 72-h cultivation.

Optimization of the compound treatment regimen. PS cells were seeded in 96-well plates (approximately 2×10^4 cells per well) and incubated for 24 h to form a confluent monolayer. For testing the optimal compound treatment regimen, we performed three independent experiments, differing in the time of drug addition to infected PS cells. (i) For a pretreatment assay, 200 μl of medium with 3'-deoxy-3'-fluoroadenosine at a concentration range of 0 to 25 μM (2-fold dilutions, three wells per concentration) was added to PS cell monolayers at 24 h prior to infection. After a 24-h incubation, medium was aspirated and replaced with 200 μl of fresh compound-containing medium in the same concentration range and inoculated with TBEV (Hypr or Neudoerfl) at an MOI of 0.1. Cells were then incubated for an additional 72 h. (ii) For a simultaneous treatment, medium containing 3'-deoxy-3'-fluoroadenosine at a concentration range of 0 to 25 μM inoculated with TBEV (MOI of 0.1) was added to cells and incubated for 72 h. (iii) For the posttreatment assay, PS cells were first infected with TBEV (MOI of 0.1), and after 2 h (the time needed for virus adsorption and internalization), medium containing 3'-deoxy-3'-fluoroadenosine at a concentration range of 0 to 25 μM was added to the infected cells and incubated for 72 h. Following incubation, the viral titers were determined from the collected supernatant media by a plaque assay and used to construct dose-response curves.

Dose-response studies using the viral titer reduction assay. To study the dose-response effect of 3'-deoxy-3'-fluoroadenosine, we used a viral titer reduction assay. PS or HBCA cell monolayers were pretreated with medium containing 3'-deoxy-3'-fluoroadenosine at a concentration range of 0 to 25 μM (2-fold dilutions, three wells per compound) for 24 h. The medium was aspirated, replaced with 200 μl of fresh medium containing the compound at the same concentration range, inoculated with TBEV (strains Hypr and Neudoerfl), ZIKV (strains MR-766 and Paraiba_1), or WNV (strains Eg-101 and 13-104) at an MOI of 0.1, and incubated for an additional 48 or 72 h. Viral titers were determined from the collected supernatant media by a plaque assay and used to construct dose-response and inhibition curves. The data used for TBEV strains Hypr and Neudoerfl (24 h pretreatment) in Fig. 2E and F were reused in Fig. 3B, as those were two identical experiments. The viral titers obtained at 72 h p.i. were used for calculation of the 50% effective concentrations (EC_{50} ; the concentration of compound required to inhibit the viral titer by 50% compared to the control value). The individual points of the inhibition curves were calculated by transformation of virus titer values to percent inhibition according to equation 1,

$$\text{Percent inhibition} = 100 - (A/B \times 100) \quad (1)$$

where A is the virus titer for the individual compound concentrations tested (0.8 to 25 μM) (PFU/ml) and B is the virus titer for a compound concentration of 0 μM (PFU/ml).

Plaque assays. Plaque assays were performed in PS cells (to determine TBEV titers) or Vero cells (for ZIKV and WNV titers) as described previously (42, 50). Briefly, 10-fold dilutions of TBEV, WNV, or ZIKV were prepared in 24-well tissue culture plates, and PS (for TBEV) or Vero (for WNV and ZIKV) cells were added to each well (0.6 to 1.5×10^5 cells per well). After a 4-h incubation, the suspension was overlaid with 1.5% (wt/vol) carboxymethylcellulose in L-15 (for PS) or Dulbecco's modified Eagle's medium (DMEM) (for Vero). Following a 5-day incubation at 37°C, the infected plates were washed with phosphate-buffered saline, and the cell monolayers were stained with naphthalene black. The virus titer was expressed as PFU/ml.

Immunofluorescence staining. To measure the compound-induced inhibition of viral surface antigen expression, a cell-based flavivirus immunostaining assay was performed as previously described (42). Briefly, PS cells were seeded onto 96-well microtitration plates and treated with the test compound at a concentration range of 0 to 25 μM (2-fold dilutions, three wells per concentration) for 24 h. After a 24-h pretreatment, the cell monolayers were infected with the appropriate flaviviruses at an MOI of 0.1 and cultured for 3 days at 37°C. After cold acetone-methanol (1:1) fixation and blocking with 10% fetal bovine serum, we incubated the cells with a mouse monoclonal antibody targeting the flavivirus group surface antigen (protein E) (1:250; antibody clone D1-4G2-4-15; Sigma-Aldrich, Prague, Czech Republic) and subsequently labeled it with an anti-mouse goat secondary antibody conjugated with fluorescein isothiocyanate (FITC; 1:500) by incubation for 1 h at 37°C. The cells were counterstained with 4',6-diamidino-2-phenylindole (DAPI; 1 $\mu\text{g/ml}$) for visualization of the cell nuclei and the fluorescence signal was recorded with an Olympus IX71 epifluorescence microscope.

Cytotoxicity assays. PS or HBCA cell monolayers in 96-well plates were treated with 3'-deoxy-3'-fluoroadenosine at a concentration range of 0 to 25 μM (2-fold dilutions, three wells per concentration) and cultured for 96 h (a 24-h pretreatment followed by a 72-h incubation, i.e., the same time duration as for antiviral assays). The cytotoxic/cytostatic activity of 3'-deoxy-3'-fluoroadenosine was determined in terms of (i) cell death or (ii) relative percentage of cell abundance using the CytoTox 96 non-radioactive cytotoxicity assay (Promega, Fitchburg, WI, USA) following the manufacturer's instructions. This assay is based on quantitative measurement of lactate dehydrogenase, a stable cytosolic enzyme that is released upon cell lysis. Cell death was estimated as the percentage of colorimetric absorbance at 490 nm by the compound-treated cells relative to the absorbance by totally lysed

(chemically killed) cells. We assessed relative percentage of cell abundance as the percentage of colorimetric absorbance at 490 nm by lysed compound-treated cells relative to the absorbance by lysed mock-treated cells.

Quantitative phase imaging. Quantitative phase imaging (QPI) was performed using a multimodal holographic microscope, Q-PHASE (TELIGHT a.s., Brno, Czech Republic). PS cells were seeded in flow chambers μ -Slide I Luer Family (Ibidi, Martinsried, Germany) (approximately 2×10^4 cells per chamber) and cultivated for 24 h to form a confluent monolayer. We performed the following independent experiments based on: (i) mock-infected and mock-treated cells as a negative control (growth medium was aspirated from the chamber and replaced with fresh medium); (ii) TBEV-infected and mock-treated cells (growth medium was aspirated from the chamber and replaced with fresh medium containing TBEV [Hypr] of MOI = 0.1); (iii) TBEV-infected cells treated with 3'-deoxy-3'-fluoroadenosine at a concentration of 12.5 μ M (growth medium was aspirated from the chamber and replaced with fresh medium containing TBEV [Hypr, MOI = 0.1] and 12.5 μ M of the compound; virus and compound were added to the cells in the same time); (iv) mock-infected and compound-treated cells (12.5 μ M) (growth medium was aspirated and replaced with fresh medium containing 12.5 μ M of the compound); (v) mock-infected and compound-treated cells (25 μ M) (growth medium was aspirated and replaced with fresh medium with 25 μ M of the compound); and (vi) heat-killed cells used as a model of lytic cell death (a positive control). Cells were cultivated in the chambers for 40 h postinfection and the QPI parameters, such as covered area, cell dry mass, cell speed, circularity, density, and cell dynamic score were continuously monitored. To maintain ideal cultivation conditions (37°C, 60% humidified air) during time-lapse experiments, cells were placed in a gas chamber (H201-Mad City Labs [MCL]-Z100/500 piezo Z-stages; Okolab, Ottaviano NA, Italy). To image enough cells in one field of view, we chose the Nikon Plan 10 \times /0.30. For each treatment, nine fields of view were observed with a frame rate of 3 min/frame for 40 h.

Holograms were captured using a CCD camera (XIMEA MR4021 MC-VELETA). Complete QPI reconstruction and image processing were performed with Q-PHASE control software. Cell dry mass values were derived according to references 51 and 52 from the phase (equation 2), where m is cell dry mass density (in pg/ μ m²), φ is detected phase (in rad), λ is wavelength in μ m (0.65 μ m in Q-PHASE), and α is specific refraction increment ($\sim 0.18 \mu$ m³/pg). All values in the formula except the φ are constant. The value of φ (phase) is measured directly by the microscope.

$$m = \frac{\varphi\lambda}{2\pi\alpha} \quad (2)$$

Integrated phase shift through a cell is proportional to its dry mass, which enables studying changes in cell mass distribution (52).

Image analysis was performed with customized MATLAB software developed by our laboratory. The analysis process consists of segmentation, the interconnection of matching cells in adjacent time frames, and extraction of the analyzed dynamical and morphological cell features. The details of the cell segmentation algorithm that we used are described in reference 53. Cell death detection and the distinction between apoptotic and lytic cell death using QPI have been described in detail (54).

Mouse infections. We evaluated the anti-TBEV effect of 3'-deoxy-3'-fluoroadenosine using five groups of 6-week-old female BALB/c mice (purchased from AnLab, Prague, Czech Republic) as follows: group 1 ($n = 10$) intraperitoneally injected with 3'-deoxy-3'-fluoroadenosine at 25 mg/kg/2 \times day to evaluate the compound toxicity; group 2 ($n = 10$) was subcutaneously injected with TBEV strain Hypr (10^3 PFU/mouse) and treated intraperitoneally with 200 μ l of 3'-deoxy-3'-fluoroadenosine at 25 mg/kg/2 \times day (treatment started simultaneously with infection); group 3 ($n = 10$) was subcutaneously injected with TBEV strain Hypr (10^3 PFU/mouse) and treated with vehicle (control animals); group 4 ($n = 10$) was subcutaneously injected with WNV strain Eg-101 (10^3 PFU/mouse) and treated intraperitoneally with 200 μ l of 3'-deoxy-3'-fluoroadenosine at 25 mg/kg/2 \times day (treatment started simultaneously with infection); and group 5 ($n = 10$) was subcutaneously injected with WNV strain Eg-101 (10^3 PFU/mouse) and treated with vehicle (control animals). 3'-Deoxy-3'-fluoroadenosine was freshly solubilized in sterile saline buffer before each injection and administered to the animals twice daily for 6 days. The clinical scores and survival rates of virus-infected mice were monitored daily throughout the experiment for 28 days. Illness signs were evaluated as follows: 0 for no symptoms; 1 for ruffled fur; 2 for slowing of activity or hunched posture; 3 for asthenia or mild paralysis; 4 for lethargy, tremor, or complete paralysis of the limbs; and 5 for death. All mice exhibiting disease consistent with a clinical score of 4 were terminated humanely (cervical dislocation) immediately upon detection.

Statistical analysis. Data are expressed as mean \pm standard deviation (SD) and the significance of differences between groups was evaluated using the one sample Wilcoxon test (to compare clinical scores of treated mice with control animals) or ANOVA followed by Tukey-Kramer posttest (to compare multiple QPI parameters in compound-treated/TBEV-infected cells with controls). Survival rates were analyzed using the logrank Mantel-Cox test. All tests were performed with GraphPad Prism 7.04 (GraphPad Software, Inc., San Diego, CA, USA). $P < 0.05$ was considered significant.

SUPPLEMENTAL MATERIAL

Supplemental material is available online only.

SUPPLEMENTAL FILE 1, PDF file, 0.4 MB.

ACKNOWLEDGMENTS

This study was supported by a grant from the Ministry of Education, Youth, and Sports of the Czech Republic (grant LTAUSA18016) (to L.E.).

REFERENCES

- Baier A. 2011. Flaviviral infections and potential targets for antiviral therapy, p 89–104. In Ruzek D (ed), *Flavivirus encephalitis*. InTech, Rijeka, Croatia.
- Pierson TC, Diamond MS. 2020. The continued threat of emerging flaviviruses. *Nat Microbiol* 5:796–812. <https://doi.org/10.1038/s41564-020-0714-0>.
- De Clercq E. 2011. A 40-year journey in search of selective antiviral chemotherapy. *Annu Rev Pharmacol Toxicol* 51:1–24. <https://doi.org/10.1146/annurev-pharmtox-010510-100228>.
- Eyer L, Nencka R, de Clercq E, Seley-Radtke K, Růžek D. 2018. Nucleoside analogs as a rich source of antiviral agents active against arthropod-borne flaviviruses. *Antivir Chem Chemother* 26:2040206618761299. <https://doi.org/10.1177/2040206618761299>.
- Niu G, Tan H. 2015. Nucleoside antibiotics: biosynthesis, regulation, and biotechnology. *Trends Microbiol* 23:110–119. <https://doi.org/10.1016/j.tim.2014.10.007>.
- Andriole VT. 1999. Current and future antifungal therapy: new targets for antifungal agents. *J Antimicrob Chemother* 44:151–162. <https://doi.org/10.1093/jac/44.2.151>.
- Wataya Y, Hiraoka O, Sonobe Y, Yoshioka A, Matsuda A, Miyasaka T, Saneyoshi M, Ueda T. 1984. Anti-parasite activity of nucleoside analogues in *Leishmania tropica* promastigotes. *Nucleic Acids Symp Ser (Oxf)* 15:69–71.
- Wataya Y, Satake H, Hiraoka O, Aji T, Morishige K, Kimura JY, Ishii A, Matsuda A, Ueda T, Fukukawa K. 1986. Anti-parasite activity of nucleoside analogues: the metabolism of carbocyclic inosine in promastigotes of *Leishmania tropica* and *Leishmania donovani* and its activity against amastigotes of *Leishmania donovani* in vitro. *Nucleic Acids Symp Ser (Oxf)* 17:149–151.
- Guinan M, Benckendorff C, Smith M, Miller GJ. 2020. Recent advances in the chemical synthesis and evaluation of anticancer nucleoside analogues. *Molecules* 25:2050. <https://doi.org/10.3390/molecules25092050>.
- Miura S, Izuta S. 2004. DNA polymerases as targets of anticancer nucleosides. *Curr Drug Targets* 5:191–195. <https://doi.org/10.2174/1389450043490578>.
- De Clercq E, Neyts J. 2009. Antiviral agents acting as DNA or RNA chain terminators. *Handb Exp Pharmacol* 189:53–84. https://doi.org/10.1007/978-3-540-79086-0_3.
- Chen H, Liu L, Jones SA, Banavali N, Kass J, Li Z, Zhang J, Kramer LD, Ghosh AK, Li H. 2013. Selective inhibition of the West Nile virus methyltransferase by nucleoside analogs. *Antiviral Res* 97:232–239. <https://doi.org/10.1016/j.antiviral.2012.12.012>.
- Vernekar SK, Qiu L, Zhang J, Kankanala J, Li H, Geraghty RJ, Wang Z. 2015. 5'-Silylated 3'-1,2,3-triazolyl thymidine analogues as inhibitors of West Nile virus and Dengue virus. *J Med Chem* 58:4016–4028. <https://doi.org/10.1021/acs.jmedchem.5b00327>.
- Leyssen P, Balzarini J, De Clercq E, Neyts J. 2005. The predominant mechanism by which ribavirin exerts its antiviral activity in vitro against flaviviruses and paramyxoviruses is mediated by inhibition of inosine monophosphate dehydrogenase. *J Virol* 79:1943–1947. <https://doi.org/10.1128/JVI.79.3.1943-1947.2005>.
- Crotty S, Cameron CE, Andino R. 2001. RNA virus error catastrophe: direct molecular test by using ribavirin. *Proc Natl Acad Sci U S A* 98:6895–6900. <https://doi.org/10.1073/pnas.111085598>.
- Graci JD, Cameron CE. 2002. Quasispecies, error catastrophe, and the antiviral activity of ribavirin. *Virology* 298:175–180. <https://doi.org/10.1006/viro.2002.1487>.
- Weiland O, Milich DR, Söllberg M, Hultgren C. 1998. The antiviral compound ribavirin modulates the T helper (Th)1/Th2 subset balance in hepatitis B and C virus-specific immune responses. *J Gen Virol* 79:2381–2391. <https://doi.org/10.1099/0022-1317-79-10-2381>.
- Seley-Radtke KL, Yates MK. 2018. The evolution of nucleoside analogue antivirals: a review for chemists and non-chemists. 2018. Part I: early structural modifications to the nucleoside scaffold. *Antiviral Res* 154:66–86. <https://doi.org/10.1016/j.antiviral.2018.04.004>.
- Yates MK, Seley-Radtke KL. 2019. The evolution of antiviral nucleoside analogues: a review for chemists and non-chemists. Part II: complex modifications to the nucleoside scaffold. *Antiviral Res* 162:5–21. <https://doi.org/10.1016/j.antiviral.2018.11.016>.
- Liu P, Sharon A, Chu CK. 2008. Fluorinated nucleosides: synthesis and biological implication. *J Fluor Chem* 129:743–766. <https://doi.org/10.1016/j.jfluchem.2008.06.007>.
- Wojtowicz-Rajchel H. 2012. Synthesis and applications of fluorinated nucleoside analogues. *J Fluor Chem* 143:11–48. <https://doi.org/10.1016/j.jfluchem.2012.06.026>.
- Saenger W. 1984. Defining terms for the nucleic acids, p 9–28. In Cantor CR (ed), *Principles of nucleic acid structure*, Springer-Verlag Inc., New York.
- Ikeda H, Fernandez R, Wilk A, Barchi JJ, Jr, Huang X, Marquez VE. 1998. The effect of two antipodal fluorine-induced sugar puckers on the conformation and stability of the Dickerson-Drew dodecamer duplex [d(CGCGAATTCGCG)]₂. *Nucleic Acids Res* 26:2237–2244. <https://doi.org/10.1093/nar/26.9.2237>.
- Park BK, Kitteringham NR, O'Neill PM. 2001. Metabolism of fluorine-containing drugs. *Annu Rev Pharmacol Toxicol* 41:443–470. <https://doi.org/10.1146/annurev.pharmtox.41.1.443>.
- De Clercq E. 2010. Historical perspectives in the development of antiviral agents against poxviruses. *Viruses* 2:1322–1339. <https://doi.org/10.3390/v2061322>.
- Whitley RJ. 1996. The past as prelude to the future: history, status, and future of antiviral drugs. *Ann Pharmacother* 30:967–971. <https://doi.org/10.1177/106002809603000911>.
- Kaufman HE, Heidelberger C. 1964. Therapeutic antiviral action of 5-trifluoromethyl-2'-deoxyuridine in herpes simplex keratitis. *Science* 145:585–586. <https://doi.org/10.1126/science.145.3632.585>.
- Hertel LW, Boder GB, Kroin JS, Rinzel SM, Poore GA, Todd GC, Grindey GB. 1990. Evaluation of the antitumor activity of gemcitabine (2',2'-difluoro-2'-deoxycytidine). *Cancer Res* 50:4417–4422.
- Jin C, Zhang H, Zou J, Liu Y, Zhang L, Li F, Wang R, Xuan W, Ye M, Tan W. 2018. Floxuridine homomeric oligonucleotides “hitchhike” with albumin in situ for cancer chemotherapy. *Angew Chem Int Ed Engl* 57:8994–8997. <https://doi.org/10.1002/anie.201804156>.
- Sofia MJ, Bao D, Chang W, Du J, Nagarathnam D, Rachakonda S, Reddy PG, Ross BS, Wang P, Zhang HR, Bansal S, Espiritu C, Keilman M, Lam AM, Steuer HM, Niu C, Otto MJ, Furman PA. 2010. Discovery of a β -D-2'-deoxy-2'- α -fluoro-2'- β -C-methyluridine nucleotide prodrug (PSI-7977) for the treatment of hepatitis C virus. *J Med Chem* 53:7202–7218. <https://doi.org/10.1021/jm100863x>.
- Kozuch O, Mayer V. 1975. Pig kidney epithelial (PS) cells: a perfect tool for study of flaviviruses and some other arboviruses. *Acta Virologica* 19:498.
- Mumtaz N, Jimmerson LC, Bushman LR, Kiser JJ, Aron G, Reusken CBEM, Koopmans MPG, van Kampen JJA. 2017. Cell-line dependent antiviral activity of sofosbuvir against Zika virus. *Antiviral Res* 146:161–163. <https://doi.org/10.1016/j.antiviral.2017.09.004>.
- Bullard-Feibelman KM, Govero J, Zhu Z, Salazar V, Veselinovic M, Diamond MS, Geiss BJ. 2017. The FDA-approved drug sofosbuvir inhibits Zika virus infection. *Antiviral Res* 137:134–140. <https://doi.org/10.1016/j.antiviral.2016.11.023>.
- Ferreira AC, Zaverucha-do-Valle C, Reis PA, Barbosa-Lima G, Vieira YR, Mattos M, Silva PP, Sacramento C, de Castro Faria Neto HC, Campanati L, Tanuri A, Brüning K, Bozza FA, Bozza PT, Souza TML. 2017. Sofosbuvir protects Zika virus-infected mice from mortality, preventing short- and long-term sequelae. *Sci Rep* 7:9409. <https://doi.org/10.1038/s41598-017-09797-8>.
- Eldrup AB, Allerson CR, Bennett CF, Bera S, Bhat B, Bhat N, Bosserman MR, Brooks J, Burllein C, Carroll SS, Cook PD, Getty KL, MacCoss M, McMasters DR, Olsen DB, Prakash TP, Prhavic M, Song QL, Tomassini JE, Xia J. 2004. Structure-activity relationship of purine ribonucleosides for inhibition of hepatitis C virus RNA-dependent RNA polymerase. *J Med Chem* 47:2283–2295. <https://doi.org/10.1021/jm030424e>.
- Van Aerschot A, Herdewijn P, Janssen G, Cools M, De Clercq E. 1989. Synthesis and antiviral activity evaluation of 3'-fluoro-3'-deoxyribonucleosides:

- broad-spectrum antiviral activity of 3'-fluoro-3'-deoxyadenosine. *Antiviral Res* 12:133–150. [https://doi.org/10.1016/0166-3542\(89\)90047-8](https://doi.org/10.1016/0166-3542(89)90047-8).
37. Van Aerschot A, Balzarini J, De Clercq E, Herdewijn P. 1989. Synthesis of 3'-fluoro-3'-deoxyribonucleosides: anti-HIV-1 and cytostatic properties. *Nucleosides, Nucleotides & Nucleic Acids* 8:1123–1124. <https://doi.org/10.1080/07328318908054305>.
 38. Smee DF, Morris JL, Barnard DL, Van Aerschot A. 1992. Selective inhibition of arthropod-borne and arenaviruses in vitro by 3'-fluoro-3'-deoxyadenosine. *Antiviral Res* 18:151–162. [https://doi.org/10.1016/0166-3542\(92\)90035-4](https://doi.org/10.1016/0166-3542(92)90035-4).
 39. Mikhailopulo IA, Poopeiko NE, Prikota TI, Sivets GG, Kvasyuk EI, Balzarini J, De Clercq E. 1991. Synthesis and antiviral and cytostatic properties of 3'-deoxy-3'-fluoro- and 2'-azido-3'-fluoro-2',3'-dideoxy-D-ribofuranosides of natural heterocyclic bases. *J Med Chem* 34:2195–2202. <https://doi.org/10.1021/jm00111a040>.
 40. Mikhailopulo IA, Pricota TI, Poopeiko NE, Sivets GG, Kvasyuk EI, Sviryaeva TV, Savochkina LP, Beabealashvili RS. 1989. 3'-Fluoro-3'-deoxyribonucleoside 5'-triphosphates: synthesis and use as terminators of RNA biosynthesis. *FEBS Lett* 250:139–141. [https://doi.org/10.1016/0014-5793\(89\)80706-9](https://doi.org/10.1016/0014-5793(89)80706-9).
 41. Lee K, Kim D-E, Jang K-S, Kim S-J, Cho S, Kim C. 2017. Gemcitabine, a broad-spectrum antiviral drug, suppresses enterovirus infections through innate immunity induced by the inhibition of pyrimidine biosynthesis and nucleotide depletion. *Oncotarget* 8:115315–115325. <https://doi.org/10.18632/oncotarget.23258>.
 42. Eyer L, Valdés JJ, Gil VA, Nencka R, Hřebabecký H, Šála M, Salát J, Černý J, Palus M, De Clercq E, Růžek D. 2015. Nucleoside inhibitors of tick-borne encephalitis virus. *Antimicrob Agents Chemother* 59:5483–5493. <https://doi.org/10.1128/AAC.00807-15>.
 43. Chen YL, Yin Z, Duraiswamy J, Schul W, Lim CC, Liu B, Xu HY, Qing M, Yip A, Wang G, Chan WL, Tan HP, Lo M, Liung S, Kondreddi RR, Rao R, Gu H, He H, Keller TH, Shi PY. 2010. Inhibition of dengue virus RNA synthesis by an adenosine nucleoside. *Antimicrob Agents Chemother* 54:2932–2939. <https://doi.org/10.1128/AAC.00140-10>.
 44. Lo MK, Shi PY, Chen YL, Flint M, Spiropoulou CF. 2016. In vitro antiviral activity of adenosine analog NITD008 against tick borne flaviviruses. *Antiviral Res* 130:46–49. <https://doi.org/10.1016/j.antiviral.2016.03.013>.
 45. Eyer L, Šmídková M, Nencka R, Neča J, Kastl T, Palus M, De Clercq E, Růžek D. 2016. Structure-activity relationships of nucleoside analogues for inhibition of tick-borne encephalitis virus. *Antiviral Res* 133:119–129. <https://doi.org/10.1016/j.antiviral.2016.07.018>.
 46. Lo MK, Jordan R, Arvey A, Sudhamsu J, Shrivastava-Ranjan P, Hotard AL, Flint M, McMullan LK, Siegel D, Clarke MO, Mackman RL, Hui HC, Perron M, Ray AS, Cihlar T, Nichol ST, Spiropoulou CF. 2017. GS-5734 and its parent nucleoside analog inhibit Filo-, Pneumo-, and Paramyxoviruses. *Sci Rep* 7:43395. <https://doi.org/10.1038/srep43395>.
 47. Lam AM, Murakami E, Espiritu C, Steuer HM, Niu C, Keilman M, Bao H, Zennou V, Bourne N, Julander JG, Morrey JD, Smee DF, Frick DN, Heck JA, Wang P, Nagarathnam D, Ross BS, Sofia MJ, Otto MJ, Furman PA. 2010. PSI-7851, a pronucleotide of beta-D-2'-deoxy-2'-fluoro-2'-C-methyluridine monophosphate, is a potent and pan-genotype inhibitor of hepatitis C virus replication. *Antimicrob Agents Chemother* 54:3187–3196. <https://doi.org/10.1128/AAC.00399-10>.
 48. Clark JL, Hollecker L, Mason JC, Stuyver LJ, Tharnish PM, Lostia S, McBrayer TR, Schinazi RF, Watanabe KA, Otto MJ, Furman PA, Stec WJ, Patterson SE, Pankiewicz KW. 2005. Design, synthesis, and antiviral activity of 2'-deoxy-2'-fluoro-2'-C-methylcytidine, a potent inhibitor of hepatitis C virus replication. *J Med Chem* 48:5504–5508. <https://doi.org/10.1021/jm0502788>.
 49. Eyer L, Fojtiková M, Nencka R, Rudolf I, Hubálek Z, Ruzek D. 2019. Viral RNA-dependent RNA polymerase inhibitor 7-deaza-2'-C-methyladenosine prevents death in a mouse model of West Nile virus infection. *Antimicrob Agents Chemother* 63:e02093-18. <https://doi.org/10.1128/AAC.02093-18>.
 50. De Madrid AT, Porterfield JS. 1969. A simple micro-culture method for study of group B arboviruses. *Bull World Health Organ* 40:113–121.
 51. Prescher JA, Bertozzi CR. 2005. Chemistry in living systems. *Nat Chem Biol* 1:13–21. <https://doi.org/10.1038/nchembio0605-13>.
 52. Park Y, Depeursinge C, Popescu G. 2018. Quantitative phase imaging in biomedicine. *Nature Photon* 12:578–589. <https://doi.org/10.1038/s41566-018-0253-x>.
 53. Feith M, Vičar T, Gumulec J, Raudenská M, Gjörloff Wingren A, Masařík M, Balvan J. 2020. Quantitative phase dynamics of cancer cell populations affected by blue light. *Appl Sci* 10:2597. <https://doi.org/10.3390/app10072597>.
 54. Vicar T, Raudenska M, Gumulec J, Balvan J. 2020. The quantitative-phase dynamics of apoptosis and lytic cell death. *Sci Rep* 10:1566. <https://doi.org/10.1038/s41598-020-58474-w>.

Antiviral Activity of 7-Substituted 7-Deazapurine Ribonucleosides, Monophosphate Prodrugs, and Triphosphates against Emerging RNA Viruses

Nemanja Milisavljevic, Eva Konkolová, Jaroslav Kozák, Jan Hodek, Lucia Veselovská, Veronika Sýkorová, Karel Cížek, Radek Pohl, Luděk Eyer, Pavel Svoboda, Daniel Růžek, Jan Weber, Radim Nencka, Evžen Bouřa, and Michal Hocek*



Cite This: *ACS Infect. Dis.* 2021, 7, 471–478



Read Online

ACCESS |



Metrics & More



Article Recommendations

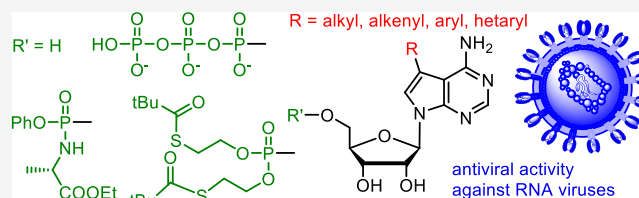


Supporting Information

ABSTRACT: A series of 7-deazaadenine ribonucleosides bearing alkyl, alkenyl, alkynyl, aryl, or hetaryl groups at position 7 as well as their 5'-O-triphosphates and two types of monophosphate prodrugs (phosphoramidates and S-acylthioethanol esters) were prepared and tested for antiviral activity against selected RNA viruses (Dengue, Zika, tick-borne encephalitis, West Nile, and SARS-CoV-2). The modified triphosphates inhibited the viral RNA-dependent RNA polymerases at micromolar concentrations

through the incorporation of the modified nucleotide and stopping a further extension of the RNA chain. 7-Deazaadenosine nucleosides bearing ethynyl or small hetaryl groups at position 7 showed (sub)micromolar antiviral activities but significant cytotoxicity, whereas the nucleosides bearing bulkier heterocycles were still active but less toxic. Unexpectedly, the monophosphate prodrugs were similarly or less active than the corresponding nucleosides in the *in vitro* antiviral assays, although the bis(S-acylthioethanol) prodrug **14h** was transported to the Huh7 cells and efficiently released the nucleoside monophosphate.

KEYWORDS: 7-deazapurine ribonucleosides, monophosphate prodrugs, triphosphates, RNA viruses, antiviral activity



RNA viruses are the causative agents of many life-threatening human diseases. The *Flaviviridae* family includes mostly arthropod-borne viruses, e.g., Yellow fever virus (YFV),¹ Dengue virus (DENV),^{2,3} West-Nile virus (WNV),⁴ Zika virus (ZIKV),⁵ tick-borne encephalitis virus (TBEV),⁶ or Japanese encephalitis virus (JEV).⁷ *Coronaviridae*⁸ is another family of viruses highly relevant to human diseases⁹ and includes the severe-acute respiratory syndrome coronavirus (SARS-CoV),¹⁰ Middle-east respiratory syndrome coronavirus (MERS-CoV),¹⁰ and the new severe acute respiratory syndrome coronavirus 2 (SARS-CoV-2).¹¹ The global pandemics recently caused by the SARS-CoV-2 virus showed that we need broad spectrum antivirals against RNA viruses for the treatment of new emerging viruses in the future. RNA-dependent RNA polymerases are one of the few viral enzymes that can serve as targets for specific therapy through small molecules, mostly nucleoside or nucleotide analogues.^{12,13} The nucleoside analogues need activation by cellular nucleos(t)ide kinases to the corresponding 5'-triphosphates (NTPs), which are the active species inhibiting the polymerases. There are several clinical drugs targeting these enzymes, i.e., sofosbuvir used for treatment of hepatitis C virus (HCV) infection¹⁴ or remdesivir recently approved for the treatment of infections caused by SARS-CoV-2^{15,16} or Ebola virus (EBOV).^{17,18} In order to achieve selectivity toward

the viral RNA polymerases, some sugar modifications are introduced at position 1', 2', or 4'. However, since the sugar-modified nucleosides are often bad substrates for nucleoside kinases, different types of lipophilic 5'-monophosphate prodrugs^{19,20} are typically used in order to penetrate through the cell membrane and release the corresponding nucleoside 5'-monophosphate in the cell to circumvent the difficult first phosphorylation step.

Within our systematic study of the biological activity of ribonucleosides derived from 7-deazapurines²¹ and their hetero-fused analogues, we identified^{22,23} some 7-deazaadenosine derivatives bearing small heterocycles at position 7 (**1e,f**) to possess potent and selective cytotoxic activity and act through intracellular activation to NTPs and incorporation to DNA causing DNA damage and apoptosis.²⁴ The same compounds also showed significant anti-HCV activity, which might have been the result of the cytotoxicity. Also, other laboratories have reported^{25,26} some anti-RNA viral activities

Received: November 25, 2020

Published: January 4, 2021

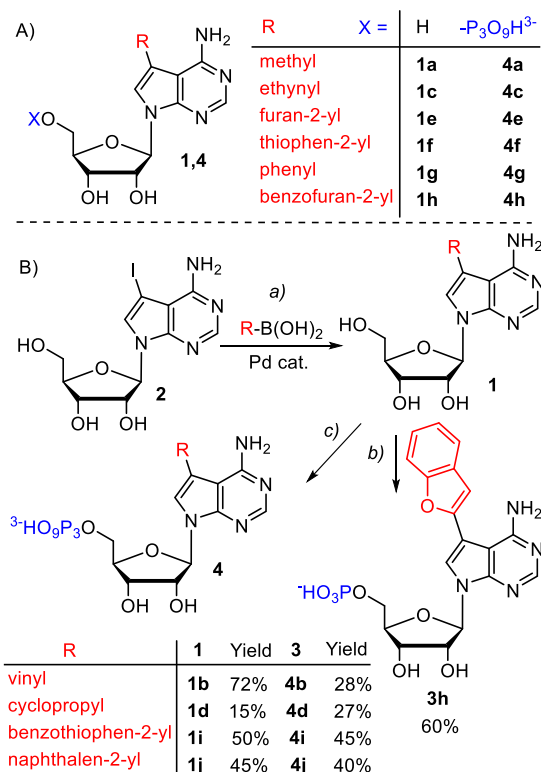


of related 7-substituted deazapurine nucleosides. On the other hand, 7-deazaadenosine derivatives bearing bulkier aromatic groups (**1h,j**) were noncytotoxic but still inhibited mycobacterial adenosine kinase.²⁷ The possibility of tuning of cytotoxicity by the bulkiness of the (het)aryl substituent at position 7 suggested that it might also influence the selectivity toward viral versus cellular RNA polymerases. Therefore, we decided to systematically study the activities of 7-substituted 7-deazaadenosine NTPs against viral RNA polymerases and the activity of the corresponding nucleosides and 5'-monophosphate prodrugs against selected RNA viruses.

RESULTS AND DISCUSSION

Chemistry. Some of the nucleosides (**1**) and nucleoside triphosphates (NTPs; **4**) used in this study were reported previously (Scheme 1 A).^{22,28} The nucleosides were prepared

Scheme 1. (A) Structures of Previously Reported Nucleosides and Nucleoside Triphosphates; (B) Synthesis of New Derivatives^a



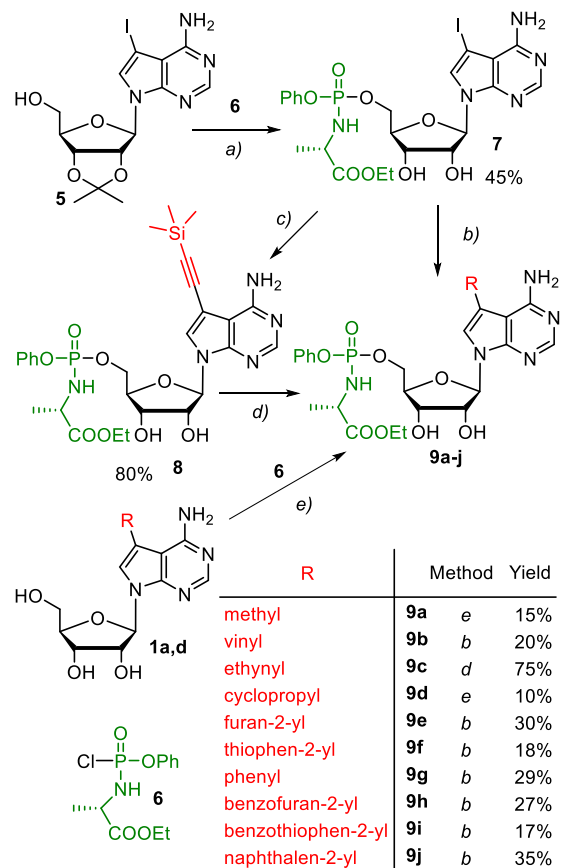
^aReagents and conditions: (a) R-B(OH)₂, Pd(OAc)₂, TPPTS, H₂O/ACN (2:1), Na₂CO₃, 100 °C, 2 h; (b) POCl₃, PO(OMe)₃, 0 °C, 2 h, TEAB; (c) POCl₃, PO(OMe)₃, 0 °C, 1–4 h; (NH₄BF₄)₂P₂O₇, Bu₃N, ACN, 0 °C, 1 h.

through functionalization of 7-iodotubercidin **2**, while the triphosphates were prepared either via Suzuki-Miyaura coupling of iodinated NTPs or by phosphorylation of already modified nucleosides. New nucleosides were prepared via Suzuki coupling of 7-iodotubercidin **2** with corresponding alkyl-, alkenyl-, or arylboronic acids using Pd(OAc)₂, TPPTS ligand, and Na₂CO₃ as a base in water/acetonitrile.²² The yield of the cross-coupling reaction of **2** with cyclopropylboronic acid was very low, yet we were still able to prepare a sufficient amount of the desired nucleoside **1d**. Monophosphate **3h** and

triphosphates **4b–j** were prepared by phosphorylation²⁹ of the corresponding modified nucleosides using POCl₃ in PO(OMe)₃, followed by the reaction with pyrophosphate and triethylammonium bicarbonate (TEAB) for triphosphates or by the addition of TEAB alone for monophosphate **3h** to give the desired products in acceptable yields (Scheme 1 B).

The synthesis of modified phosphoramidate prodrugs (ProTides)^{20,30,31} was mostly based on the introduction of the alkenyl- or aryl groups at position 7 of iodinated nucleoside phosphoramidate **7** through the Suzuki-Miyaura cross-coupling reactions (Scheme 2), in analogy to our previous paper.³² The

Scheme 2^a



^aReagents and conditions: (a) (1) tBuMgCl, phosphochloridate **6**, THF, 0 °C, 45 min, (2) H₂O quenching, and (3) TFA, r.t., 1 h; (b) R-B(OH)₂, Pd(OAc)₂, TPPTS, Na₂CO₃, 100 °C, 1 h; (c) TMS-acetylene, Pd(PPh₃)₂Cl₂, CuI, Et₃N, DMF, r.t., 16 h; (d) KF, MeOH, r.t., 1 h; (e) NMI, phosphochloridate **6**, THF, r.t., 16 h.

iodinated intermediate **7** was prepared in good yields by 5'-O-phosphorylation of 2',3'-isopropylidene protected nucleoside **5** with alanine ethylester phosphochloridate **6** in the presence of tBuMgCl followed by acidic deprotection. The Suzuki-Miyaura cross-coupling reactions of ProTide intermediate **7** with vinyl- or arylboronic acids gave the desired 7-vinyl (**9b**) or 7-aryl derivatives (**9e–j**) in moderate yields caused by partial hydrolysis of the phosphoramidates during the reaction and isolation. Ethynyl derivative **9c** was prepared via Sonogashira coupling of **7** with TMS-acetylene followed by subsequent desilylation of the protected intermediate **8** with KF in MeOH. The direct cross-coupling attachment of methyl and cyclopropyl groups into the position 7 of 7-deazaadenine would

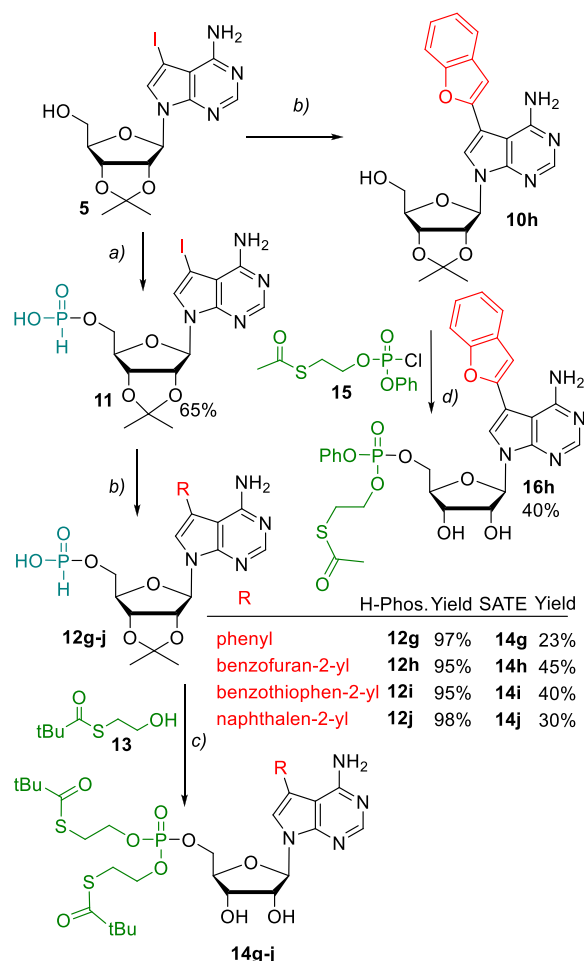
require conditions that are not compatible with the phosphoramidate group. Hence, we decided to prepare phosphoramidates **9a** and **9d** by phosphorylation of the modified nucleosides **1a** and **1d**. To minimize the number of synthetic steps, we applied a procedure for 5'-O-phosphorylation of the free nucleoside with phosphochloridate **6** in the presence of *N*-methylimidazole (NMI). We obtained the desired products **9a** and **9d** in low yields, but we were able to recover most of the starting nucleosides **1a** and **1d**.

In order to have an alternative type of monophosphate prodrug, which would be easier to hydrolyze in different types of cells to release NMPs, we decided to prepare *S*-acylthioethanol (SATE)^{33–37} esters of 5'-monophosphates from at least several examples of 7-aryl-substituted 7-deazaadenosines. We have chosen the bis(*t*BuSATE) prodrugs, which showed good chemical stability and promising antiviral activities in other types of nucleosides.^{34–37} They were prepared from the corresponding functionalized H-phosphonates (Scheme 3). The starting H-phosphonate precursor **11**

was prepared by reacting 2',3'-*O*-isopropylidene nucleoside **5** with diphenyl phosphite.^{38,39} The Suzuki-Miyaura cross-coupling reactions of **11** with arylboronic acids gave the 7-(het)aryl-7-deazaadenosine-5'-*O*-H-phosphonate intermediates **12g–j** in excellent yields. The H-phosphonates **12g–j** were then activated with pivaloyl chloride (PivCl) and reacted with *S*-pivaloyl-2-thioethanol **13**,³³ oxidized by iodine, and then deprotected by TFA to provide final bis(*t*BuSATE) derivatives **14g–j** in moderate yields. We also prepared one example of a mixed mono-SATE⁴⁰ phenyl ester **16h**, which was synthesized by 5'-*O*-phosphorylation of the protected nucleoside **10h** with phosphochloridate **15** and subsequent acidic deprotection.

Biological Profiling. Inhibition of Viral RNA Polymerases by Modified NTPs 4a–4j. At first, we investigated the inhibition effect of 7-substituted 7-deazaadenosine 5'-*O*-triphosphates on RNA-dependent RNA polymerases from RNA viruses. Using a recently published procedure,⁴¹ we tested the inhibition of three different flaviviral RNA polymerases from ZIKV, JEV, and WNV. Table 1 shows that

Scheme 3. Preparation of SATE Prodrugs from H-Phosphonates^a



^aReagents and conditions: (a) diphenyl phosphite, pyridine, r.t., 1.5 h, 2 M TEAB, 30 min, r.t.; (b) R–B(OH)₂, Pd(OAc)₂, TPPTS, Cs₂CO₃, 100 °C, 1 h; (c) (1) PivCl, pyridine, 5 min, r.t., (2) *S*-pivaloyl-2-thioethanol, pyridine, r.t., 5 min, (3) I₂/H₂O/pyridine, r.t. 15 min, and (4) TFA/DCM 1:1, r.t., 30 min; (d) *t*BuMgCl, phosphochloridate **15**, THF, 0 °C, 45 min, TFA/DCM 1:1, r.t., 30 min.

Table 1. In Vitro Inhibition (IC₅₀) of Different Viral RNA Polymerases with Modified NTPs 4a–j

compound	ZIKV (IC ₅₀ [μM])	JEV (IC ₅₀ [μM])	WNV (IC ₅₀ [μM])
4a	3.2 (±0.3)	3.2 (±0.26)	2.30 (±0.38)
4b	23 (±3)	25 (±8)	4.0 (±1.5)
4c	2.10 (±0.17)	2.7 (±0.55)	1.40 (±0.24)
4d	4.60 (±0.51)	11 (±4)	3.0 (±1.32)
4e	1.20 (±0.07)	1.7 (±0.23)	0.7 (±0.10)
4f	1.40 (±0.10)	2.6 (±0.43)	1.60 (±0.36)
4g	3.10 (±0.31)	6.0 (±1.14)	4.0 (±0.99)
4h	0.50 (±0.04)	0.5 (±0.06)	0.3 (±0.05)
4i	3.30 (±0.30)	7.0 (±1.31)	1.5 (±0.37)
4j	4.5 (±0.27)	8.0 (±2.63)	4.0 (±1.45)
RemTP	1.36 (±0.03)	2.14 (±0.07)	1.66 (±0.06)

most of the NTPs exerted inhibition at single digit micromolar concentrations. The most active was the 7-benzofuryl NTP **4h**, which showed submicromolar inhibition of all three enzymes, which is better than previously reported activities of remdesivir triphosphate (**RemTP**).⁴¹ A significant effect was also observed in 7-furyl and 7-thienyl derivatives **4e** and **4f**. Figure 1 shows the gel electrophoresis noncompetitive RNA polymerase assay based on the detection of the extension of RNA primer, which was used to study the mechanism of action. As we expected, all the tested flaviviral polymerases were able to incorporate the most active derivative **4h** into the newly synthesized RNA chain, but in contrast to **RemTP**, the extension of the primer stopped after the incorporation of the modified nucleotide.

In Vitro Antiviral Activity of Nucleosides and Prodrugs. The *in vitro* antiviral activities of all nucleosides and prodrugs against selected RNA viruses were determined using an immunofluorescence assay (DENV, ZIKV) in Huh7 cells,⁴² or the virus was quantified by a virus titer reduction assay followed by a plaque assay (TBEV, WNV).⁴³ Due to the lower infection of SARS-CoV-2 in Huh7 cells, only the initial screening was performed using the immunofluorescence assay and the RNA reduction assay was performed to determine anti-SARS-CoV-2 activity.⁴⁴ We used ribavirin,⁴³ 7-deaza-2'-methyladenosine,⁴⁵ or remdesivir¹⁸ as standards, and the results are summarized in Table 2. The nucleosides bearing

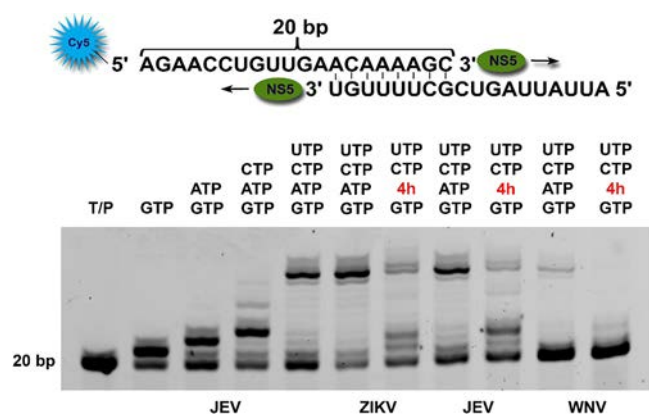


Figure 1. Gel electrophoresis based polymerase assay: the incorporation of nucleotide derived from NTP **4h** was monitored for each flaviviral RdRp (substrate: GTP, **4h**, CTP, UTP) and compared with the extension of RNA primer with a mix of natural NTPs (substrate: GTP, ATP, CTP, UTP). (Left) The template/primer (T/P) 20 bp band corresponds to the unreacted primer, followed by control reactions performed with JEV polymerase in the presence of the indicated NTPs, followed by a comparison of the reaction with ATP/**4h** using the indicated flaviviral polymerases.

small substituents (**1a,b,d**) were mostly inactive, whereas 7-ethynyladenosine **1c** exerted a micromolar antiviral effect but also cytotoxicity. Nucleosides bearing smaller hetaryl groups (**1e,f**) were also active but cytotoxic, which is in accord with our previous works on their cytotoxic effects in diverse leukemia and cancer cell lines. 7-Phenyl-7-deazaadenosine **1g** was completely inactive, whereas nucleosides bearing bulkier (het)aryl groups (**1h–j**) exerted micromolar antiviral activities and slightly reduced cytotoxicity. The phosphoramidite prodrugs **9a–j** were mostly comparably or less active than the parent nucleosides and followed the same trend in substituent effects and cytotoxicity. The bis(SATE) prodrugs **14g–j** and mono(SATE) **16h** were prepared only from the bulkier 7-(hetaryl)-7-deazaadenosines where we expected lower cytotoxicity due to the bulky substituents.²⁷ However, the antiviral activities of these prodrugs were similar or lower compared to the parent nucleosides, and the cytotoxicity was not reduced. The most potent was the effect of nucleosides and prodrugs against the ZIKV and DENV viruses, whereas only a few compounds showed a considerable effect against TBEV or WNV. Interestingly, we found three compounds, **1c**, **1e**, and **9c**, that exerted submicromolar activity against the SARS-CoV-2 virus, but in all these cases, we observed micromolar cytotoxicity.

Table 2. Antiviral Activities (EC_{50}) and Cytotoxicity (CC_{50}) of Nucleosides and Prodrugs against RNA Viruses in Huh7 Determined by an Immunofluorescence Assay

compound	DENV (EC_{50} [μ M])	ZIKV (EC_{50} [μ M])	TBEV (EC_{50} [μ M])	WNV (EC_{50} [μ M])	SARS-CoV-2 (spike) (EC_{50} [μ M]) ^c	Huh7 (CC_{50} [μ M])
1a	>50	>50	>50	>50	n.a. ^b	>50
1b	31 (\pm 3.8)	>50	>50	>50	n.a. ^b	>50
1c	5.4 (\pm 1.8)	0.99 (\pm 0.57)	1.3 (\pm 0.11)	n.a.	0.58 (\pm 0.27)	3.6 (\pm 0.4)
1d	>50	22 (\pm 7)	>50	>50	n.a. ^b	>50
1e	34 (\pm 19)	0.39 (\pm 0.2)	>5	n.a.	0.1 (\pm 0.03)	11 (\pm 2.5)
1f	8.0 (\pm 2.2)	0.21 (\pm 0.15)	>50	>50	n.a. ^b	29 (\pm 9)
1g	>50	>50	>50	>50	n.a. ^b	>50
1h	13 (\pm 2)	2.2 (\pm 0.8)	>5	>5	1.5 (\pm 0.28)	15 ^a
1i	2.8 (\pm 0.6)	4.3 (\pm 1.3)	>5	3.1 (\pm 0.91)	7.6 (\pm 3.4)	9.6 (\pm 0.7)
1j	1.8 (\pm 0.31)	3.3 (\pm 1.3)	>5	>5	14 (\pm 4.2)	17 (\pm 0.8)
9a	>50	26 (\pm 15)	>50	>50	n.a. ^b	>50
9b	42 (\pm 18)	>50	>50	>50	>50	>50
9c	1.2 (\pm 0.2)	2.3 (\pm 0.7)	1.4 (\pm 0.57)	n.a.	0.79 (\pm 0.28)	5.0 (\pm 0.6)
9d	>50	>50	>50	>50	n.a. ^b	>50
9e	3.3 (\pm 0.6)	0.37 (\pm 0.14)	>50	>50	n.a. ^b	30 (\pm 2.8)
9f	21 (\pm 8)	0.56 (\pm 0.43)	>50	>50	n.a. ^b	>50
9g	\sim 50 ^a	4.1 (\pm 2.8)	>50	>50	>50	>50
9h	>50	>50	>50	4.4 (\pm 1.2)	>50	>50
9i	4.3 (\pm 1)	2.7 (\pm 0.6)	>5	>5	19 (\pm 7)	13 (\pm 1)
9j	6.4 (\pm 1.9)	12 (\pm 5.5)	18 (\pm 3.4)	6.2 (\pm 0.63)	\sim 35 ^a	21 (\pm 1.8)
14g	>50	8.5 (\pm 3.9)	>5	>5	8.0 ^a	11 (\pm 0.8)
14h	\sim 40 ^a	6.1 (\pm 2.1)	22 (\pm 1.4)	19.5 (\pm 8.2)	2.8 (\pm 1.4)	38 (\pm 4)
14i	>50	4.3 (\pm 1)	>5	>5	16 ^a	8.7 (\pm 1.2)
14j	>50	5.6 (\pm 2.4)	>5	>5	18 ^a	17 (\pm 1.8)
16h	>50	8.3 (\pm 2.5)	>50	>50	19 ^a	>50
ribavirin	62 (\pm 11)	6.1 (\pm 1.4)				>50
7-deaza-2'-Me-adenosine			3.7 (\pm 0.34)	1.4 (\pm 0.63)		>50
remdesivir					0.021 (\pm 0.007)	>50

^aThe 95% confidence intervals of EC_{50} were too wide to determine the SD. ^bThe compounds were inactive in the preliminary immunofluorescence assay and hence not tested further in the immunofluorescence assay using serial dilutions of the compounds. ^cThe activity against SARS-CoV-2 was determined by the RNA reduction assay.

Metabolism of Selected Compounds in Huh7 Cells. To investigate the intracellular formation of NMPs from nucleosides and prodrugs, we studied the uptake and metabolism of three selected compounds (**1h**, **9h**, and **14h**) in Huh7 cells (Table 3). As a reference substance, we chose recently

Table 3. Amounts of the Rest of the Treating Compounds (1h, 9h, 14h) and Corresponding Monophosphate (3h) in Huh7 (pM/5 × 10⁵ cells) in Different Dosing Concentrations and after Different Times

dosing (μM)	time (h)	1h	3h	9h	3h	14h	3h
10	24	2.8	1.0	6	0.47	100	460
	48	2.6	0.8	3	0.22	11	240
	72	2.3	0.7	1	0.1	1.1	80
25	24	5.9	2.2	16.7	1.1	<i>a</i>	<i>a</i>
	48	4.5	1.7	8.8	0.4	<i>a</i>	<i>a</i>
	72	10	1.6	3.9	0.2	<i>a</i>	<i>a</i>

^aMeasurement not possible; toxic concentration for the cells.

reported⁴⁶ 4-methyl-9-(β-D-ribofuranosyl)-9H-pyrido-[4',3':4,5]pyrrolo[2,3-d]pyrimidine whose mechanism of action was already confirmed and involves the activation by phosphorylation to form NTP and its incorporation to DNA and partially also to RNA. The corresponding synthetic ribonucleoside monophosphate **3h** was used as the analytical standard. The cellular uptake and intracellular phosphorylation was tested using the Huh7 cell line (hepatocellular carcinoma) at two different concentrations of treated compounds (10 and 25 μmol/L) after 24, 48, or 72 h of treatment *in vitro*, according to the previously reported procedure.⁴⁶ The uptake of nucleoside **1h** was rather poor, and the formation of NMP was also very low. The uptake of ProTide **9h** was 2–3 times more efficient, but the level of NMP **3h** was even lower than in case of nucleoside **1h**. On the other hand, the cellular uptake of bis(SATE) prodrug **14h** was ca. 2 orders of magnitude higher, and most of the prodrug released NMP **3h**, reaching a level of up to 460 pM/5 × 10⁵ cells after 24 h of treatment with 10 μmol/L of prodrug **14h**. This amount of **3h** was comparable with the amount of NMP formed from previously⁴⁶ reported tricyclic nucleoside after the same time. The higher dose (25 μmol/L) of prodrug **14h** was already toxic for the cells, and hence, the level of NMP could not be determined. Apparently, the bis(SATE) prodrug is the best form to deliver the compound into the Huh7 cells and be activated into a monophosphate, yet the bis(SATE) prodrugs were not more active in the *in vitro* antiviral activity assays compared to the free nucleosides (see above). On the other hand, in cells treated with prodrugs **9h** or **14h**, the concentrations of nucleoside **1h** were negligible (at least 100 times lower than the concentration of NMP **3h**), which indicates that a dephosphorylation of the NMP **3h** by phosphatases is not the reason for poor activity of the prodrugs. The results suggest that the transport and phosphorylation or release of the monophosphate are not the limiting factors in the MOA of these nucleosides or prodrugs, whereas the further phosphorylations of NMPs to triphosphates might be the critical steps.

CONCLUSIONS

We have prepared and tested a series of 7-substituted 7-deazaadenine ribonucleosides (**1a–j**) and their 5'-O-triphosphates (**4a–j**) as well as monophosphate prodrugs phosphoramidates (**9a–j**), bis-SATE (**14h–j**), and mono-SATE (**16h**).

The aim was to investigate whether we can achieve an antiviral effect and selectivity against viral RNA polymerases through base modifications at position 7. We found that all the 7-modified NTPs **4a–j** were micromolar inhibitors of the viral RNA-dependent RNA polymerases. The most active was the bulky 7-benzofuryl derivative **4h**, which inhibited the viral polymerases through the incorporation and stopping of the further extension of the RNA chain. This compound was promising because the previous studies²⁷ showed that the nucleoside containing this bulky modification (**1h**) was noncytotoxic because it was not a substrate of adenosine kinases and hence did not get efficiently phosphorylated in the cell. The nucleosides and prodrugs were tested for *in vitro* antiviral activities against several RNA viruses, and we found several nucleosides and prodrugs showing micromolar or submicromolar activities against ZIKV, WNV, DENV, TBEV, or SARS-CoV-2 viruses and low toxicity to Huh7 cells. In most cases, the monophosphate prodrugs (ProTides or bis(SATE)) were comparably or less active in these assays than the corresponding nucleosides. This finding was quite surprising since it is known from many previous studies^{12–20,30,31} that the monophosphate prodrugs of antiviral nucleosides are typically much more efficient in the transport and release of the NMPs, which are then further phosphorylated to active NTPs that act as polymerase inhibitors. To have a deeper insight into this problem, we also tested the transport through cellular membrane and intracellular phosphorylation (of **1h**) of the release of NMP **3h** from prodrugs **9h** and **14h**, which showed that the best form of the compound for the transport and release of NMP was the bis-SATE prodrug **14h**. However, this result is contrary to the *in vitro* antiviral activity of compound **14h**, which was only comparable or somewhat lower than the activity of the corresponding nucleoside **1h**. We can only speculate that this might be due to other alternative mechanisms of action of nucleoside **1h**, which may not involve the activation through phosphorylation. This study clearly shows that the current monophosphate prodrug approaches^{14–20,30,31} may fail to improve the activity of antiviral nucleosides in some specific cases.

METHODS

Only representative general synthetic procedures are given below. For the full experimental details and characterization of all compounds, see the Supporting Information.

General Procedure A: Suzuki Cross-Coupling Reactions with 7-Iodotubercidin. A water/AN mixture (2:1, 15 mL) was added through a septum to an argon purged vial containing **2** (200 mg, 0.51 mmol), boronic acid (1 mmol) and Na₂CO₃ (270 mg, 2.55 mmol), followed by the addition of the degassed solution of Pd(OAc)₂ (5 mg, 0.02 mmol) and TPPTS ligand (72 mg, 0.12 mmol) in water/AN (2:1, 10 mL). After the argon/vacuum exchange, the reaction mixture was left stirring at 100 °C for 2 h. The mixture was cooled to room temperature, coevaporated with silica gel, and purified by high performance reverse phase flash chromatography (0 → 100% MeOH in water).

General Procedure B: Phosphorylation of Modified Nucleosides. Modified nucleoside (1 equiv) was dried at 60 °C overnight under vacuum. It was then suspended in PO(OMe)₃ and stirred at room temperature for 15 min, followed by cooling to 0 °C and the addition of POCl₃ (1.2 equiv). The reaction mixture was left stirring at 0 °C (1–4 h), and then, an ice cold solution of (NH₄)₂H₂P₂O₇ (5 equiv)

and tributyl amine (5 equiv) in anhydrous AN (5 mL) was added. The reaction mixture was stirred at 0 °C for another hour. Then, an aqueous solution of TEAB (2 M, 2 mL, 4 mmol) was added, and the mixture was evaporated under reduced pressure. The residue was coevaporated several times with water. The product was purified by chromatography on a DEAE Sephadex column (0 → 1.2 M aq. TEAB) and then by HPLC (C-18 column, 0.1 M TEAB in water to 0.1 M TEAB in 50% aq. MeOH); it was coevaporated several times with water and, where possible, converted to the sodium salt form (Dowex 50 in Na⁺ cycle).

General Procedure C: Preparation of ProTides from Modified Nucleosides. Modified nucleoside (1 equiv) was dried at 100 °C and dissolved in freshly distilled THF (3 mL). Anhydrous NMI (5 equiv) was added dropwise, and the solution was left stirring at room temperature for 30 min. Phosphochloridate **6** (5 equiv) was then added dropwise to give a white suspension that was left stirring at room temperature for 16 h to give a clear solution again. Volatiles are removed *in vacuo*, and the final product is purified by HPLC (C-18 column, 0 → 100% AN in water) and lyophilized from tBuOH.

General Procedure D: Suzuki-Miyaura Coupling of the ProTides. A water/AN mixture (2:1, 15 mL) was added through a septum to an argon purged vial containing **7** (0.12 mmol), boronic acid (0.23 mmol) and Na₂CO₃ (37 mg, 0.35 mmol), followed by the addition of the degassed solution of Pd(OAc)₂ (1.5 mg, 5 μmol) and TPPTS ligand (15 mg, 29 μmol) in water/AN (2:1, 3 mL). After the argon/vacuum exchange, the reaction mixture was left stirring at 100 °C for 1 h. The mixture was cooled to room temperature; volatiles were removed *in vacuo*, and the residue was coevaporated several times with MeOH, purified by HPLC (C-18 column, 0 → 100% AN in water), and lyophilized from tBuOH.

General Procedure E: Suzuki-Miyaura Coupling on H-Phosphonates. A water/AN mixture (3:1, 12 mL) was added through a septum to an argon purged vial containing **10** (80 mg, 0.13 mmol), boronic acid (0.4 mmol) and Cs₂CO₃ (200 mg, 0.61 mmol), followed by the addition of the degassed solution of Pd(OAc)₂ (1.8 mg, 8 μmol) and TPPTS ligand (22 mg, 40 μmol) in water/AN (3:1, 3 mL). After the argon/vacuum exchange, the reaction mixture was left stirring at 100 °C for 1 h. The mixture was cooled to room temperature; volatiles were removed *in vacuo*, and the residue was coevaporated several times with MeOH and purified by HPLC (C-18 column, 0 → 100% AN in 0.1 M TEAB). Fractions were collected; solvents were removed *in vacuo*, and the residue was evaporated several times with MeOH and then with MeOH and cyclohexane to yield the final compound as a white solid.

General Procedure F: Synthesis of SATE Prodrugs from H-Phosphonates. H-Phosphonates **10a–d** (90 μmol) were coevaporated with dry pyridine (2 × 5 mL) followed by dissolution in 4 mL of the same solvent. Pivaloyl chloride (270 μmol) was added, and reaction mixture was stirred for 5 min at room temperature. Then, S-pivaloyl-2-thioethanol (0.9 mmol), which was previously coevaporated two times with 5 mL of dry pyridine, was dissolved in the same solvent (1 mL); the mixture was then added to the reaction, which was left stirring for 10 more minutes. Then, water (100 μL) and iodine (25 mg, 100 μmol) were added, and the reaction was stirred for an additional 15 min. The solvent was removed *in vacuo*, and the residue was coevaporated with toluene two times and extracted

with DCM and saturated Na₂S₂O₃. The crude mixture was then dissolved in 2 mL of TFA/DCM (1:1) and stirred for half an hour at room temperature. The solvents were removed *in vacuo*, and the residue was coevaporated several times with MeOH and lyophilized from tBuOH to provide the white lyophilizate.

■ ASSOCIATED CONTENT

Supporting Information

The Supporting Information is available free of charge at <https://pubs.acs.org/doi/10.1021/acsinfecdis.0c00829>.

Complete experimental part with synthesis and characterization of all new compounds and methods for biological profiling and enzymatic assays (PDF)

Copies of NMR spectra (PDF)

■ AUTHOR INFORMATION

Corresponding Author

Michal Hocek – Institute of Organic Chemistry and Biochemistry, Czech Academy of Sciences, CZ-16000 Prague 6, Czech Republic; Department of Organic Chemistry, Faculty of Science, Charles University in Prague, CZ-12843 Prague 2, Czech Republic; orcid.org/0000-0002-1113-2047; Email: hocek@uochb.cas.cz

Authors

Nemanja Milisavljevic – Institute of Organic Chemistry and Biochemistry, Czech Academy of Sciences, CZ-16000 Prague 6, Czech Republic; Department of Organic Chemistry, Faculty of Science, Charles University in Prague, CZ-12843 Prague 2, Czech Republic

Eva Konkolová – Institute of Organic Chemistry and Biochemistry, Czech Academy of Sciences, CZ-16000 Prague 6, Czech Republic

Jaroslav Kozák – Institute of Organic Chemistry and Biochemistry, Czech Academy of Sciences, CZ-16000 Prague 6, Czech Republic

Jan Hodek – Institute of Organic Chemistry and Biochemistry, Czech Academy of Sciences, CZ-16000 Prague 6, Czech Republic

Lucia Veselovská – Institute of Organic Chemistry and Biochemistry, Czech Academy of Sciences, CZ-16000 Prague 6, Czech Republic

Veronika Sýkorová – Institute of Organic Chemistry and Biochemistry, Czech Academy of Sciences, CZ-16000 Prague 6, Czech Republic

Karel Čížek – Institute of Organic Chemistry and Biochemistry, Czech Academy of Sciences, CZ-16000 Prague 6, Czech Republic

Radek Pohl – Institute of Organic Chemistry and Biochemistry, Czech Academy of Sciences, CZ-16000 Prague 6, Czech Republic

Luděk Eyer – Department of Virology, Veterinary Research Institute, CZ-62100 Brno, Czech Republic; Institute of Parasitology, Biology Centre of the Czech Academy of Sciences, CZ-37005 České Budějovice, Czech Republic

Pavel Svoboda – Department of Virology, Veterinary Research Institute, CZ-62100 Brno, Czech Republic; Department of Pharmacology and Pharmacy, Faculty of Veterinary Medicine, University of Veterinary and Pharmaceutical Sciences Brno, CZ-61242 Brno, Czech Republic

Daniel Růžek – Department of Virology, Veterinary Research Institute, CZ-62100 Brno, Czech Republic; Institute of Parasitology, Biology Centre of the Czech Academy of Sciences, CZ-37005 České Budějovice, Czech Republic; orcid.org/0000-0003-4655-2380

Jan Weber – Institute of Organic Chemistry and Biochemistry, Czech Academy of Sciences, CZ-16000 Prague 6, Czech Republic

Radim Nencka – Institute of Organic Chemistry and Biochemistry, Czech Academy of Sciences, CZ-16000 Prague 6, Czech Republic; orcid.org/0000-0001-6167-0380

Evžen Bouřa – Institute of Organic Chemistry and Biochemistry, Czech Academy of Sciences, CZ-16000 Prague 6, Czech Republic; orcid.org/0000-0002-9652-4065

Complete contact information is available at:

<https://pubs.acs.org/10.1021/acsnfecdis.0c00829>

Notes

The authors declare no competing financial interest.

ACKNOWLEDGMENTS

This work was supported by the Academy of Sciences of the Czech Republic (RVO 61388963 and the Praemium Academiae award to M.H.), the Czech Science Foundation (19-08124S to M.H.), Ministry of Health of the Czech Republic (NU20-05-00472 to R.N., E.B., and D.R.), Ministry of Education, Youth, and Sports of the Czech Republic (LTAUSA18016 to L.E. and R.N.), the European Regional Development Fund OP RDE (No. CZ.02.1.01/0.0/0.0/16_019/0000729 to N.M., L.V., and V.S.), and Gilead Sciences, Inc. This work was also supported by the European Virus Archive goes Global (EVAg) project from the Horizon 2020 research and innovation programme under grant agreement No. 653316.

REFERENCES

- (1) Monath, T. P., and Vasconcelos, P. F. C. (2015) Yellow fever. *J. Clin. Virol.* 64, 160–173.
- (2) Guzman, M. G., Halstead, S. B., Artsob, H., Buchy, P., Farrar, J., Gubler, D. J., Hunsperger, E., Kroeger, A., Margolis, H. S., Martínez, E., Nathan, M. B., Pelegrino, J. L., Simmons, C., Yoksan, S., and Peeling, R. W. (2010) Dengue: a continuing global threat. *Nat. Rev. Microbiol.* 8, S7–16.
- (3) Bhatt, S., Gething, P. W., Brady, O. J., Messina, J. P., Farlow, A. W., Moyes, C. L., Drake, J. M., Brownstein, J. S., Hoen, A. G., Sankoh, O., Myers, M. F., George, D. B., Jaenisch, T., Wint, G. R. W., Simmons, C. P., Scott, T. W., Farrar, J. J., and Hay, S. I. (2013) The global distribution and burden of dengue. *Nature* 496, 504–507.
- (4) Suthar, M. S., Diamond, M. S., and Gale, M. (2013) West Nile virus infection and immunity. *Nat. Rev. Microbiol.* 11, 115–128.
- (5) Musso, D., and Gubler, D. J. (2016) Zika Virus. *Clin. Microbiol. Rev.* 29, 487–524.
- (6) Dumpis, U., Crook, D., and Oksi, J. (1999) Tick-Borne Encephalitis. *Clin. Infect. Dis.* 28, 882–890.
- (7) Unni, S. K., Růžek, D., Chhatbar, C., Mishra, R., Johri, M. K., and Singh, S. K. (2011) Japanese encephalitis virus: from genome to infectome. *Microbes Infect.* 13, 312–321.
- (8) Chen, Y., Liu, Q., and Guo, D. (2020) Emerging coronaviruses: Genome structure, replication, and pathogenesis. *J. Med. Virol.* 92, 418–423.
- (9) Zumla, A., Chan, J. F. W., Azhar, E. I., Hui, D. S. C., and Yuen, K.-Y. (2016) Coronaviruses - drug discovery and therapeutic options. *Nat. Rev. Drug Discovery* 15, 327–347.

(10) de Wit, E., van Doremalen, N., Falzarano, D., and Munster, V. J. (2016) SARS and MERS: recent insights into emerging coronaviruses. *Nat. Rev. Microbiol.* 14, 523–534.

(11) Wu, F., Zhao, S., Yu, B., Chen, Y.-M., Wang, W., Song, Z.-G., Hu, Y., Tao, Z.-W., Tian, J.-H., Pei, Y.-Y., Yuan, M.-L., Zhang, Y.-L., Dai, F.-H., Liu, Y., Wang, Q.-M., Zheng, J.-J., Xu, L., Holmes, E. C., and Zhang, Y.-Z. (2020) A new coronavirus associated with human respiratory disease in China. *Nature* 579, 265–269.

(12) De Clercq, E., and Li, G. (2016) Approved Antiviral Drugs over the Past 50 Years. *Clin. Microbiol. Rev.* 29, 695–747.

(13) Jordheim, L. P., Durantel, D., Zoulim, F., and Dumontet, C. (2013) Advances in the development of nucleoside and nucleotide analogues for cancer and viral diseases. *Nat. Rev. Drug Discovery* 12, 447–464.

(14) Sofia, M. J., Bao, D., Chang, W., Du, J., Nagarathnam, D., Rachakonda, S., Reddy, P. G., Ross, B. S., Wang, P., Zhang, H.-R., Bansal, S., Espiritu, C., Keilman, M., Lam, A. M., Steuer, H. M. M., Niu, C., Otto, M. J., and Furman, P. A. (2010) Discovery of a β -D-2'-deoxy-2'- α -fluoro-2'- β -C-methyluridine nucleotide prodrug (PSI-7977) for the treatment of hepatitis C virus. *J. Med. Chem.* 53, 7202–7218.

(15) Liang, C., Tian, L., Liu, Y., Hui, N., Qiao, G., Li, H., Shi, Z., Tang, Y., Zhang, D., Xie, X., and Zhao, X. (2020) A promising antiviral candidate drug for the COVID-19 pandemic: A mini-review of remdesivir. *Eur. J. Med. Chem.* 201, 112527.

(16) Eastman, R. T., Roth, J. S., Brimacombe, K. R., Simeonov, A., Shen, M., Patnaik, S., and Hall, M. D. (2020) Remdesivir: A Review of Its Discovery and Development Leading to Emergency Use Authorization for Treatment of COVID-19. *ACS Cent. Sci.* 6, 672–683.

(17) Warren, T. K., Jordan, R., Lo, M. K., Ray, A. S., Mackman, R. L., Soloveva, V., Siegel, D., Perron, M., Bannister, R., Hui, H. C., Larson, N., Strickley, R., Wells, J., Stuthman, K. S., Van Tongeren, S. A., Garza, N. L., Donnelly, G., Shurtleff, A. C., Retterer, C. J., Gharaibeh, D., Zamani, R., Kenny, T., Eaton, B. P., Grimes, E., Welch, L. S., Gomba, L., Wilhelmsen, C. L., Nichols, D. K., Nuss, J. E., Nagle, E. R., Kugelman, J. R., Palacios, G., Doerffler, E., Neville, S., Carra, E., Clarke, M. O., Zhang, L., Lew, W., Ross, B., Wang, Q., Chun, K., Wolfe, L., Babusis, D., Park, Y., Stray, K. M., Trancheva, I., Feng, J. Y., Barauskas, O., Xu, Y., Wong, P., Braun, M. R., Flint, M., McMullan, L. K., Chen, S.-S., Fearn, R., Swaminathan, S., Mayers, D. L., Spiropoulou, C. F., Lee, W. A., Nichol, S. T., Cihlar, T., and Bavari, S. (2016) Therapeutic efficacy of the small molecule GS-5734 against Ebola virus in rhesus monkeys. *Nature* 531, 381–385.

(18) Siegel, D., Hui, H. C., Doerffler, E., Clarke, M. O., Chun, K., Zhang, L., Neville, S., Carra, E., Lew, W., Ross, B., Wang, Q., Wolfe, L., Jordan, R., Soloveva, V., Knox, J., Perry, J., Perron, M., Stray, K. M., Barauskas, O., Feng, J. Y., Xu, Y., Lee, G., Rheingold, A. L., Ray, A. S., Bannister, R., Strickley, R., Swaminathan, S., Lee, W. A., Bavari, S., Cihlar, T., Lo, M. K., Warren, T. K., and Mackman, R. L. (2017) Discovery and Synthesis of a Phosphoramidate Prodrug of a Pyrrolo[2,1-f][triazin-4-amino] Adenine C-Nucleoside (GS-5734) for the Treatment of Ebola and Emerging Viruses. *J. Med. Chem.* 60, 1648–1661.

(19) Pradere, U., Garnier-Amblard, E. C., Coats, S. J., Amblard, F., and Schinazi, R. F. (2014) Synthesis of nucleoside phosphate and phosphonate prodrugs. *Chem. Rev.* 114, 9154–9218.

(20) Mehellou, Y., Rattan, H. S., and Balzarini, J. (2018) The prodrug technology: from the concept to the clinic. *J. Med. Chem.* 61, 2211–2226.

(21) Perlíková, P., and Hocek, M. (2017) Pyrrolo[2,3-d]pyrimidine (7-deazapurine) as a privileged scaffold in design of antitumor and antiviral nucleosides. *Med. Res. Rev.* 37, 1429–1460.

(22) Bourderioux, A., Naus, P., Perlíková, P., Pohl, R., Pichová, I., Votruba, I., Dzubák, P., Konečný, P., Hajdúch, M., Stray, K. M., Wang, T., Ray, A. S., Feng, J. Y., Birkus, G., Cihlar, T., and Hocek, M. (2011) Synthesis and significant cytostatic activity of 7-hetaryl-7-deazaadenosines. *J. Med. Chem.* 54, 5498–5507.

- (23) Nauš, P., Caletková, O., Konečný, P., Džubák, P., Bogdanová, K., Kolář, M., Vrbková, J., Slavětinská, L., Tloušťová, E., Perlíková, P., Hajdúch, M., and Hocek, M. (2014) Synthesis, cytostatic, antimicrobial, and anti-HCV activity of 6-substituted 7-(het)aryl-7-deazapurine ribonucleosides. *J. Med. Chem.* 57, 1097–1110.
- (24) Perlíková, P., Rylová, G., Nauš, P., Elbert, T., Tloušťová, E., Bourderioux, A., Slavětinská, L. P., Motyka, K., Doležal, D., Znojek, P., Nová, A., Harvanová, M., Džubák, P., Šiller, M., Hlaváč, J., Hajdúch, M., and Hocek, M. (2016) 7-(2-Thienyl)-7-Deazaadenosine (AB61), a New Potent Nucleoside Cytostatic with a Complex Mode of Action. *Mol. Cancer Ther.* 15, 922–937.
- (25) Di Francesco, M. E., Avolio, S., Pompei, M., Pesci, S., Monteagudo, E., Pucci, V., Giuliano, C., Fiore, F., Rowley, M., and Summa, V. (2012) Synthesis and antiviral properties of novel 7-heterocyclic substituted 7-deaza-adenine nucleoside inhibitors of Hepatitis C NSSB polymerase. *Bioorg. Med. Chem.* 20, 4801–4811.
- (26) Lin, C., Yu, J., Hussain, M., Zhou, Y., Duan, A., Pan, W., Yuan, J., and Zhang, J. (2018) Design, synthesis, and biological evaluation of novel 7-deazapurine nucleoside derivatives as potential anti-dengue virus agents. *Antiviral Res.* 149, 95–105.
- (27) Snašel, J., Nauš, P., Dostál, J., Hnízda, A., Fanfrlík, J., Brynda, J., Bourderioux, A., Dušek, M., Dvořáková, H., Stolaříková, J., Zábanská, H., Pohl, R., Konečný, P., Džubák, P., Votruba, I., Hajdúch, M., Rezáčová, P., Veverka, V., Hocek, M., and Pichová, I. (2014) Structural basis for inhibition of mycobacterial and human adenosine kinase by 7-substituted 7-(Het)aryl-7-deazaadenine ribonucleosides. *J. Med. Chem.* 57, 8268–8279.
- (28) Milisavljevič, N., Perlíková, P., Pohl, R., and Hocek, M. (2018) Enzymatic synthesis of base-modified RNA by T7 RNA polymerase. A systematic study and comparison of 5-substituted pyrimidine and 7-substituted 7-deazapurine nucleoside triphosphates as substrates. *Org. Biomol. Chem.* 16, 5800–5807.
- (29) Kovács, T., and Ötvös, L. (1988) Simple synthesis of 5-vinyl- and 5-ethynyl-2'-deoxyuridine-5'-triphosphates. *Tetrahedron Lett.* 29, 4525–4528.
- (30) Thornton, P. J., Kadri, H., Miccoli, A., and Mehellou, Y. (2016) Nucleoside phosphate and phosphonate prodrug clinical candidates. *J. Med. Chem.* 59, 10400–10410.
- (31) Alanazi, A. S., James, E., and Mehellou, Y. (2019) The prodrug technology: where next? *ACS Med. Chem. Lett.* 10, 2–5.
- (32) Nauš, P., Caletková, O., Perlíková, P., PoštováSlavětinská, L., Tloušťová, E., Hodek, J., Weber, J., Džubák, P., Hajdúch, M., and Hocek, M. (2015) Synthesis and biological profiling of 6- or 7-(het)aryl-7-deazapurine 4'-C-methylribonucleosides. *Bioorg. Med. Chem.* 23, 7422–7438.
- (33) Périgaud, C., Gosselin, G., Lefebvre, I., Girardet, J.-L., Benzaria, S., Barber, I., and Imbach, J.-L. (1993) Rational design for cytosolic delivery of nucleoside monophosphates: "SATE" and "DTE" as enzyme-labile transient phosphate protecting groups. *Bioorg. Med. Chem. Lett.* 3, 2521–2526.
- (34) Périgaud, C., Gosselin, G., Girardet, J., Korba, B., and Imbach, J. (1999) The S-acyl-2-thioethyl pronucleotide approach applied to acyclovir. Part I. Synthesis and in vitro anti-hepatitis B virus activity of bis(S-acyl-2-thioethyl)phosphotriester derivatives of acyclovir. *Antiviral Res.* 40, 167–178.
- (35) Hantz, O., Périgaud, C., Borel, C., Jamard, C., Zoulim, F., Trepo, C., Imbach, J., and Gosselin, G. (1999) The SATE pronucleotide approach applied to acyclovir. Part II. Effects of bis(SATE)phosphotriester derivatives of acyclovir on duck hepatitis B virus replication in vitro and in vivo. *Antiviral Res.* 40, 179–187.
- (36) Valette, G., Pompon, A., Girardet, J. L., Cappellacci, L., Franchetti, P., Grifantini, M., La Colla, P., Loi, A. G., Périgaud, C., Gosselin, G., and Imbach, J. L. (1996) Decomposition pathways and in vitro HIV inhibitory effects of isodda pronucleotides: toward a rational approach for intracellular delivery of nucleoside 5'-monophosphates. *J. Med. Chem.* 39, 1981–1990.
- (37) Lefebvre, I., Périgaud, C., Pompon, A., Aubertin, A. M., Girardet, J. L., Kim, A., Gosselin, G., and Imbach, J. L. (1995) Mononucleoside phosphotriester derivatives with S-acyl-2-thioethyl bioreversible phosphate-protecting groups: intracellular delivery of 3'-azido-2',3'-dideoxythymidine 5'-monophosphate. *J. Med. Chem.* 38, 3941–3950.
- (38) Sun, Q., Edathil, J. P., Wu, R., Smidansky, E. D., Cameron, C. E., and Peterson, B. R. (2008) One-pot synthesis of nucleoside 5'-triphosphates from nucleoside 5'-H-phosphonates. *Org. Lett.* 10, 1703–1706.
- (39) Sobkowski, M., Wenska, M., Kraszewski, A., and Stawiński, J. (2000) Studies on reactions of nucleoside H-phosphonates with bifunctional reagents. Part VI. Reaction with diols. *Nucleosides, Nucleotides Nucleic Acids* 19, 1487–1503.
- (40) Gouy, M.-H., Jordheim, L. P., Lefebvre, I., Cros, E., Dumontet, C., Peyrottes, S., and Périgaud, C. (2009) Special feature of mixed phosphotriester derivatives of cytarabine. *Bioorg. Med. Chem.* 17, 6340–6347.
- (41) Konkolova, E., Dejmek, M., Hřebabeký, H., Šála, M., Böserle, J., Nencka, R., and Boura, E. (2020) Remdesivir triphosphate can efficiently inhibit the RNA-dependent RNA polymerase from various flaviviruses. *Antiviral Res.* 182, 104899.
- (42) Tichý, M., Pohl, R., Tloušťová, E., Weber, J., Bahador, G., Lee, Y.-J., and Hocek, M. (2013) Synthesis and biological activity of benzo-fused 7-deazaadenosine analogues. 5- and 6-substituted 4-amino- or 4-alkylpyrimido[4,5-b]indole ribonucleosides. *Bioorg. Med. Chem.* 21, 5362–5372.
- (43) Eyer, L., Valdés, J. J., Gil, V. A., Nencka, R., Hřebabeký, H., Šála, M., Salát, J., Černý, J., Palus, M., De Clercq, E., and Růžek, D. (2015) Nucleoside inhibitors of tick-borne encephalitis virus. *Antimicrob. Agents Chemother.* 59, 5483–5493.
- (44) Wang, M., Cao, R., Zhang, L., Yang, X., Liu, J., Xu, M., Shi, Z., Hu, Z., Zhong, W., and Xiao, G. (2020) Remdesivir and chloroquine effectively inhibit the recently emerged novel coronavirus (2019-nCoV) in vitro. *Cell Res.* 30, 269–271.
- (45) Eyer, L., Fojtíková, M., Nencka, R., Rudolf, I., Hubálek, Z., and Růžek, D. (2019) Viral RNA-dependent RNA polymerase inhibitor 7-deaza-2'-C-methyladenosine prevents death in a mouse model of West Nile virus infection. *Antimicrob. Agents Chemother.* 63, No. e02093-18.
- (46) Veselovská, L., Kudlová, N., Gurská, S., Lišková, B., Medvedíková, M., Hodek, O., Tloušťová, E., Milisavljevic, N., Tichý, M., Perlíková, P., Mertlíková-Kaiserová, H., Trylčová, J., Pohl, R., Klepetářová, B., Džubák, P., Hajdúch, M., and Hocek, M. (2020) Synthesis and Cytotoxic and Antiviral Activity Profiling of All-Four Isomeric Series of Pyrido-Fused 7-Deazapurine Ribonucleosides. *Chem. - Eur. J.* 26, 13002–13015.



Research paper

Development and characterization of recombinant tick-borne encephalitis virus expressing mCherry reporter protein: A new tool for high-throughput screening of antiviral compounds, and neutralizing antibody assays

Jan Haviernik^{a,b}, Ludek Eyer^{a,c}, Kentaro Yoshii^{d,e}, Shintaro Kobayashi^e, Jiri Cerny^f, Antoine Nougairède^g, Jean-Sélim Driouch^g, Jiri Volf^a, Martin Palus^{a,c}, Xavier de Lamballerie^g, Ernest A. Gould^g, Daniel Ruzek^{a,c,*}

^a Veterinary Research Institute, Hudcova 70, CZ-62100, Brno, Czech Republic

^b Department of Experimental Biology, Faculty of Science, Masaryk University, Kamenice 5, 625 00 Brno, Czech Republic

^c Institute of Parasitology, Biology Centre of the Czech Academy of Sciences, Branisovska 31, 37005, Ceske Budejovice, Czech Republic

^d National Research Center for the Control and Prevention of Infectious Diseases, Nagasaki University, 1-12-4 Sakamoto, Nagasaki City 852-8523, Japan

^e Laboratory of Public Health, Faculty of Veterinary Medicine, Hokkaido University, Sapporo, 060-0818, Japan

^f Faculty of Tropical AgriSciences, Czech University of Life Sciences in Prague, Prague 165 00, Czech Republic

^g Unité des Virus Émergents (Aix-Marseille Univ-IRD 190-Inserm 1207-IHU Méditerranée Infection), Marseille, France



ARTICLE INFO

Keywords:

Tick-borne encephalitis virus
Reporter virus
Neutralization test
Antivirals

ABSTRACT

The flavivirus, tick-borne encephalitis virus (TBEV) is transmitted by *Ixodes* spp. ticks and may cause severe and potentially lethal neurological tick-borne encephalitis (TBE) in humans. Studying TBEV requires the use of secondary methodologies to detect the virus in infected cells. To overcome this problem, we rationally designed and constructed a recombinant reporter TBEV that stably expressed the mCherry reporter protein. The resulting TBEV reporter virus (named mCherry-TBEV) and wild-type parental TBEV exhibited similar growth kinetics in cultured cells; however, the mCherry-TBEV virus produced smaller plaques. The magnitude of mCherry expression correlated well with progeny virus production but remained stable over <4 passages in cell culture. Using well-characterized antiviral compounds known to inhibit TBEV, 2'-C-methyladenosine and 2'-deoxy-2'-β-hydroxy-4'-azidocytidine (RO-9187), we demonstrated that mCherry-TBEV is suitable for high-throughput screening of antiviral drugs. Serum samples from a TBEV-vaccinated human and a TBEV-infected dog were used to evaluate the mCherry-based neutralization test. Collectively, recombinant mCherry-TBEV reporter virus described here provides a powerful tool to facilitate the identification of potential antiviral agents, and to measure levels of neutralizing antibodies in human and animal sera.

1. Introduction

Tick-borne encephalitis virus (TBEV) is the most important member of the tick-borne encephalitis serogroup within the family *Flaviviridae*, genus *Flavivirus* (Simmonds et al., 2017). Flaviviruses are small enveloped spherical viruses (about 50 nm in diameter). They possess a single-stranded positive-sense RNA genome of about 11 kb in length (Simmonds et al., 2017). TBEV is the aetiological agent of human neurological disease known as tick-borne encephalitis (TBE). It is prevalent in large regions of Europe and Asia – from Western Europe to Japan (Ruzek et al., 2019; Taba et al., 2017). It is estimated that 10,

000–13,000 cases of TBE occur annually. Clinical manifestations of TBE range from asymptomatic or mild febrile illness to severe and potentially fatal encephalitis or encephalomyelitis. Mortality in Europe is estimated to be less than 1%, but about 25% of patients who recover from acute TBE suffer from postencephalitic syndrome characterized by long-lasting or even permanent sequelae; hence, the burden on public health services is significant (Ruzek et al., 2019; Bogovic and Strle, 2015; Taba et al., 2017).

Humans typically may acquire TBE when infected ticks take a bloodmeal from them. Thus, the ticks are not only transmission vectors but also serve, together with small mammals, as reservoirs of the virus in

* Corresponding author. Veterinary Research Institute, Hudcova 70, CZ-62100, Brno, Czech Republic.

E-mail address: ruzekd@paru.cas.cz (D. Ruzek).

<https://doi.org/10.1016/j.antiviral.2020.104968>

Received 1 September 2020; Received in revised form 26 October 2020; Accepted 29 October 2020

Available online 4 November 2020

0166-3542/© 2020 Elsevier B.V. All rights reserved.

natural foci (Diaz et al., 2013). Tick saliva containing the virus is injected into the skin of the host, via the salivary gland, whilst the infected tick feeds on the host (Hermance and Thangamani, 2018). *Ixodes ricinus* ticks are the predominant vector of TBEV in Europe, while in Asia the virus is transmitted mainly by *Ixodes persulcatus* (Ruzek et al., 2019).

Less frequently, the virus can be also acquired when humans consume unpasteurized milk or dairy products from infected sheep, goats, or cows, resulting in biphasic milk fever (Gresikova et al., 1959; Ruzek et al., 2019; Salat and Ruzek, 2020). Also, rare cases of TBEV transmission have been recorded following solid organ transplantation (Lipowski et al., 2017). TBE is preventable with vaccines, which are based on inactivated whole-virus particles, are well tolerated, and generally confer high levels of protection (Riccardi et al., 2019). However, in several endemic countries, vaccination coverage still remains low. There are no approved antiviral drugs to treat TBE, although several candidate antivirals effective against TBEV have been identified (Ruzek et al., 2019; Eyer et al., 2018).

Studying TBEV, including screening of antiviral compounds and testing for the presence of neutralizing antibodies, requires the use of laborious secondary approaches to detect the presence of the virus in infected cells and/or in animal models of infection. One of several possible approaches to overcome these limitations is to develop a recombinant TBEV that expresses a traceable reporter protein that enables direct monitoring, visualization, and quantification of virus replication (Li et al., 2016). Several reporter-tagged *Flaviviridae* viruses have been generated (Moser et al., 1998; Pierson et al., 2006; Koutsoudakis et al., 2006; Tamura et al., 2018; Tamura et al., 2019; Li et al., 2017; Yun et al., 2020; Eyre et al., 2017; Zou et al., 2011; Schoggins et al., 2012; Suphatrakul et al., 2018); however, the accommodation of foreign genes into the small flavivirus genome is often difficult to achieve and the recombinant viruses carrying large reporter genes are usually genetically unstable (Tamura et al., 2019). Herein, we have generated a recombinant replication-competent TBEV expressing the mCherry (a bright red monomeric fluorescent protein, which is highly photostable and resistant to photobleaching) reporter gene to track, with ease, the *in vitro* infection. Notably, we observed a good correlation between the expressions of mCherry and virus replication. The mCherry expression remained relatively stable during a few passages in cell culture. Thus, the mCherry-TBEV provides a unique opportunity to use this tool for high-throughput screening of antiviral compounds, and the detection of neutralizing antibody in cell culture systems.

2. Material and Methods

2.1. Ethics statement

The use of human serum samples was approved by the Ethics Committee of the Hospital in Ceske Budejovice (approval No. 103/19) and the Biology Center of the Czech Academy of Sciences (approval No. 1/2018). The use of animal serum samples was approved by the Ministry of Agriculture of the Czech Republic (Approval No. 14102/2015-MZE-17214).

2.2. Virus, cells and antiviral compounds

Low-passage TBEV strain Hypr, a highly pathogenic member of the European TBEV subtype, was used in this study. The virus was provided by the Collection of Arboviruses, Institute of Parasitology, Biology Centre of the Czech Academy of Sciences, Ceske Budejovice, Czech Republic (<http://www.arboviruscollection.cz/index.php?lang=en>). Porcine kidney stable (PS) cells (obtained from the National Cell Culture Collection, National Institute of Public Health, Prague, Czech Republic) were used for immunofluorescence staining assay, viral titer reduction, and plaque assays. The cells were cultured at 37 °C in Leibovitz (L-15) medium supplemented with 3% newborn calf serum and 100 U/mL

Penicillin, 100 µg/mL Streptomycin (Sigma-Aldrich, Prague, Czech Republic) and 1% L-glutamine. Baby hamster kidney cells, BHK-21 [C-13] (ATCC® CCL-10™), used for transfection of mCherry-TBEV subgenomic fragments, viral growth kinetics studies, mCherry-TBEV passages, and live cell imaging, were cultured at 37 °C with 5% CO₂ in minimal essential medium (MEM) containing 10% bovine serum, 100 U/mL Penicillin, 100 µg/mL Streptomycin (Sigma-Aldrich), and 1% L-glutamine.

Antiviral compounds 2'-C-methyladenosine was obtained from Carbosynth (Compton, UK) and 2'-deoxy-2'-β-hydroxy-4'-azidocytidine (RO-9187) was purchased from MedChemExpress (Monmouth Junction, NJ). For *in vitro* studies, the test compounds were solubilized in 100% DMSO to yield 10 mM stock solutions.

2.3. Plaque assay

Virus titers were assayed using PS cell monolayers and a modified protocol by De Madrid and Porterfield (1969), as described previously (Eyer et al., 2015). Briefly, 10-fold dilutions of WT and mCherry modified TBEV were prepared in 24-well tissue culture plates, and 1 × 10⁵ PS cells per well were added. After a 4 h incubation at 37 °C, the suspension was overlaid with 1.5% (w/vol) carboxymethylcellulose in L-15 medium. Following a 5-day incubation at 37 °C, the infected plates were washed with phosphate-buffered saline (PBS) and the cell monolayers were stained with naphthalene black. The virus titer was expressed as plaque forming units (pfu) per milliliter.

Images of the plaques were scanned on a BioVendor C-series array reader specially modified for plaque assays. Imaging was done sequentially well by well, with illumination from the bottom of the sample and with a full high-definition (HD) camera system. Every image was then processed by BioVendor Analytics software, which automatically counts plaques based on specialized image processing algorithms developed for this task, as described previously (Eyer et al., 2017).

2.4. Immunofluorescence staining

PS cells were plated on 96-well tissue culture plates and infected with the passage 1, 3 and 5 of mCherry-TBEV at an MOI of 0.1. At day 2 post-infection, the cells were fixed with 4% p-formaldehyde for 15 min at room temperature, gently washed 3x in PBS, and permeabilized with 1% Triton X-100 in PBS, and blocked with 10% fetal bovine serum. Cells were labeled with a mouse monoclonal antibody that recognizes the flavivirus group surface antigen (1:250; MAB10216; Sigma-Aldrich) by incubation for 1 h at 37 °C. After washing with saline-Tween 20 (0.05% [vol/vol]), the cells were labeled with an anti-mouse goat secondary antibody conjugated with fluorescein isothiocyanate (FITC) (1:500) by incubation for 1 h at 37 °C. The cells were counterstained with 4',6-diamidino-2-phenylindole (DAPI) (1 µg/ml; Sigma-Aldrich) for 30 min at 37 °C to visualize the cell nuclei. The images were acquired with an Olympus IX81 epifluorescence microscope equipped with a Hamamatsu OrcaR2 camera and controlled using Xcellence software. The images were processed by ImageJ/Fiji software (Schindelin et al., 2012; Rueden et al., 2017).

2.5. RNA isolation and RT-PCR

RNA was isolated from medium of mCherry-TBEV-infected cell cultures by use of a QIAmp viral RNA minikit (Qiagen) by following the protocol recommended by the manufacturer. The QIAGEN® OneStep RT-PCR Kit (Qiagen) was used for RT-PCR amplification. The reaction mixture (final volume 25 µl) contained 5 µl of QIAGEN OneStep RT-PCR Buffer, 1 µl of dNTP mix, 5 µl of 5x Q-Solution, 1 µl of QIAGEN OneStep RT-PCR Enzyme Mix, 9 µl of RNase-free water, 1 µl of each primer (stock concentration, 0.01 mM; Supplementary Table 1), and 2 µl of template. The cycling conditions were as follows: Reverse transcription (30 min at 50 °C), Initial PCR activation (15 min at 95 °C), 3-step cycling: 30 cycles

of 94 °C for 30 s, 55 °C for 30 s, and 72 °C for 1 min, followed by Final extension (10 min at 72 °C). The PCR products were visualized in a 1.7% Agarose gel in Tris-acetate-EDTA buffer.

2.6. Reverse genetics system for mCherry-TBEV

The reverse genetics system used in this study was based on the generation of infectious subgenomic overlapping DNA fragments that encompass the entire viral genome as previously described (Aubry et al., 2014; Driouich et al., 2018; Eyer et al., 2019). Three *de novo* synthesized DNA fragments cloned into a pUC57 or a PC11 vector were used in this study (GenScript, Piscataway, NJ, USA): fragment I (nucleotide position 1 to 3662), fragment II (nucleotide position 3545 to 8043), and fragment III (nucleotide position 7961 to 11100). The first and last fragments were flanked respectively in 5' and 3' with the human cytomegalovirus promoter (pCMV) and the hepatitis delta ribozyme followed by the simian virus 40 polyadenylation signal (HDR/SV40pA). The mCherry gene was located within fragment I downstream of the full-length 5'UTR and the first 72 nucleotides of the C gene, which are necessary for flavivirus replication. The mCherry coding sequence was flanked by the P2A and T2A ribosome skipping sequences at its 5' and 3' ends (Suphatrakul et al., 2018), respectively, and followed by the sequence coding the full-length C protein (also including the first 72 nucleotides inserted before the mCherry sequence).

Fragments I, II and III were used as templates to generate the overlapping amplicons following the original ISA method (Aubry et al., 2014). The PCR was performed using the PrimeStar MAX DNA polymerase (Takara). The mixture (final volume, 50 µl) contained 25 µl of PrimeSTAR MAX premix, 1 µl of DNA template (fragment I, II or III) at 1 ng/µl and 1 µl of each primer. Assays were performed on a Bio-Rad T100™ Thermal Cycler with the following conditions: 30–35 cycles of 98 °C for 10 s, 55 °C for 5 s, 72 °C for 5 s/kb. Size of the PCR products was verified by gel electrophoresis and purified using an Amicon Ultra 0.5 ml kit (Millipore).

An equimolar mixture of the three DNA fragments was used for cell transfection. DNA-lipid complex was prepared as follows: 2 µl of XtremeGENE™ HP DNA Transfection Reagent (Roche) was diluted in 200 µl Opti-MEM medium (Life Technologies) and then mixed with 2.1 µg of DNA from the equimolar mixture. After 15-min incubation at room temperature, the mixture was added to BHK-21 cells and incubated for 3–5 days. Cell supernatant media were then harvested and virus titer was determined by plaque assay.

2.7. Growth kinetics

To evaluate comparatively the growth kinetics of mCherry-TBEV and wild-type TBEV, confluent BHK-21 cell monolayers in 96-well plates were infected with an MOI of 0.1 and 1 of the respective viruses. Cell culture medium was collected from the wells every 6 h up to 48 h and after that point every 12 h up to 96 h post-infection (three wells per interval) and analyzed by plaque assay to construct growth curves.

To measure the mCherry activity, the cells were lysed using Reporter Lysis 5x Buffer (Promega) following the protocol recommended by the manufacturer, and fluorescence intensity measurement was performed using Hybrid Multimode Microplate Reader Synergy H1 (BioTek) with the following parameters: Plate type (96 WELL PLATE), Fluorescence (Endpoint) excitation 580/emission 610, Optics (Top) and Gain (100), Light Source (Xenon Flash), Lamp Energy (High), Read Speed (Normal), Delay (100 msec), and Read Heights (7 mm). Each interval was measured in triplicate.

2.8. Live cell imaging

BHK-21 cells were cultured on Thermo Scientific™ Nunc™ Lab-Tek™ Chamber slide (Thermo Scientific™) and infected with the mCherry-TBEV Hypr at an MOI of 0.1. The cell nuclei were visualized by

using Hoechst 33342 dye (Invitrogen™) by following the protocol recommended by the manufacturer. The images were acquired with an Olympus IX81 epifluorescence microscope equipped with incubator for live cell imaging. During the experiment, the cells were cultured in 37 °C under 5% CO₂ atmosphere directly on the microscope stage. Olympus 10x UPLFLN lenses and Hammamatsu OrcaR2 camera controlled by Olympus Xcellence software was used for image acquisition.

Hoechst 33342 was detected with DAPI filter set (Olympus U-MWU2, excitation 330–385/emission 420) with 15 ms exposure time, mCherry was detected with TxRed filter set (Olympus u-MWIY2, excitation: 545–580/emission: 610 F) with 60 ms of exposure time. The images were taken every 15 min since the moment of infection for a period of 72 h. The images were processed by ImageJ/Fiji software (Schindelin et al., 2012; Rueden et al., 2017).

2.9. mCherry-TBEV passages

For passage zero (P0), BHK-21 cells grown in 24-well plate, were transfected with the three genomic fragments of mCherry-TBEV, as described above. After 3 days, the cell culture media were harvested, and virus titers were determined by plaque assay. In passage 1 (P1), BHK-21 cells were infected with mCherry-TBEV rescued from P0 at an MOI 0.01. After 2 days, the cell culture media were harvested, and virus titers were determined by plaque assay. The virus at an MOI 0.1 was transferred to fresh BHK-21 cells and serially passaged under the same conditions until passage 4 (P4). Each passage was performed in triplicate. The mCherry-TBEV-infected BHK-21 cells at passage 0, 2, and 4 were also stained for viral envelope protein expression by immunofluorescence microscopy as described previously, and the immunofluorescence signal was compared to mCherry expression.

2.10. mCherry-TBEV based antiviral assay

PS cells were seeded in 96-well plates (approximately 2×10^4 cells per well) and incubated for 24 h to form a confluent monolayer. Following incubation, the medium was aspirated from the wells and replaced with 200 µl of fresh medium containing the 2'-C-methyladenosine at concentrations of 0, 1.5, 3.125, 4, 5, 6.25, 10, 12.5, 25, and 50 µM, and RO-9187 at concentrations of 0, 0.1, 0.19, 0.39, 0.78, 1.5, 3.125, 5, 6.25, 10, 12.5, 25, and 50 µM. DMSO was added to control cells as a negative control at a final concentration of 0.5% (v/v). Simultaneously, the cells were infected with mCherry-TBEV at an MOI of 1. After 72 h of incubation, the mCherry activity was measured by Multimode Microplate Reader Synergy H1 (BioTek) with the following parameters: Plate type (96 WELL PLATE), Fluorescence (Area Scan), Matrix Size (5 × 5) excitation 580/emission 610, Optics (Bottom) and Gain (150), Light Source (Xenon Flash), Lamp Energy (High), Read Speed (Normal), Delay (100 msec), and Read Heights (7 mm). The mCherry signal was also analyzed by fluorescence microscopy. Cell nuclei were stained with Hoechst 33342 dye (Invitrogen™). The images were acquired with an Olympus IX81 epifluorescence microscope equipped with a Hammamatsu OrcaR2 camera and controlled using Xcellence software. Cell culture media were collected and analyzed by plaque assay, as described above. All experiments were performed in triplicate.

2.11. Neutralization assay

Serum samples from a TBEV-vaccinated human, and an experimentally TBEV-infected dog (adult beagle, infected subcutaneously with 10^6 pfu of TBEV, were collected on day 28 post-infection) and used for the mCherry-TBEV-based neutralization assays. Serum samples from serologically negative control human and dog were used as controls. The sera were inactivated by incubation at 56 °C for 30 min. Two-fold serial dilutions from 1:10 to 1:10,240 of the sera were incubated with 3×10^4 pfu of mCherry-TBEV for 90 min at 37 °C in a 96-well plate. After

incubation, a suspension of PS cells (3×10^4 cells per well) was added to each well. After 48 h of incubation at 37 °C, the mCherry activity was measured as described for antiviral assays. All experiments were performed in triplicate.

2.12. Statistical analyses

Data are expressed as means \pm standard deviations (SD), and the significance of differences between groups was evaluated using the Mann-Whitney *U* test. All tests were performed using GraphPad Prism 7 (GraphPad Software, Inc., La Jolla, CA, USA), version 7.04. Differences with $p < 0.05$ were considered to be statistically significant.

3. Results

3.1. Rescue of recombinant mCherry-TBEV

To generate TBEV expressing mCherry, we used a previously established reverse genetics system for the rescue of recombinant TBEV, based on the use of infectious subgenomic overlapping DNA fragments that encompass the entire viral genome (Aubry et al., 2014; Eyer et al., 2019). Three *de novo* synthesized genomic fragments were cloned into pUC57 or pC11 plasmids; fragment I contained a gene for mCherry (Fig. 1A). The recombinant virus was produced as described in Materials and Methods. Three days post-transfection, cell culture supernatants were harvested, and the rescued virus was sequenced by Sanger sequencing and characterized phenotypically. The mean titer of the rescued virus was $5.0 \times 10^5 \pm 2.2 \times 10^5$ pfu/mL. The transfected cells

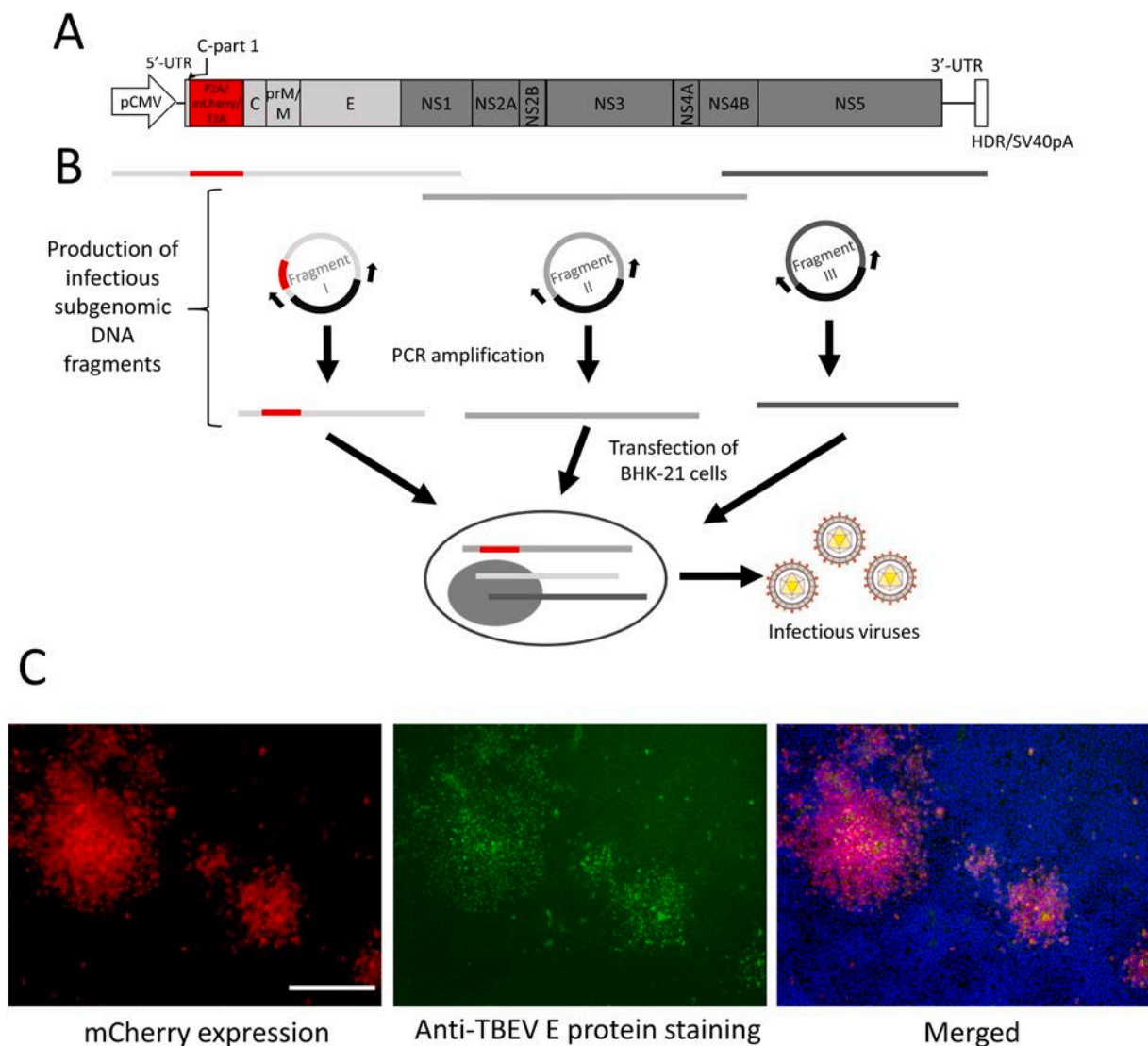


Fig. 1. Construction of mCherry-TBEV. Schematic representation of mCherry-encoding TBEV genome structure. The mCherry gene was inserted downstream of the full-length 5'UTR and the first 72 nucleotides of the C gene, which are necessary for flavivirus replication. The mCherry coding sequence was flanked by the P2A and T2A ribosome skipping sequences at its 5' and 3' ends, respectively, and followed by the sequence coding the full-length C protein (A). General overview of the reverse-genetics method used in the present study to generate mCherry-encoding TBEV. Three *de novo* synthesized DNA fragments cloned into a pUC57 or a PC11 vector were used in this study. The first and last fragments were flanked respectively in 5' and 3' with the human cytomegalovirus promoter (pCMV) and the hepatitis delta ribozyme followed by the simian virus 40 polyadenylation signal (HDR/SV40pA). The mCherry gene was located within fragment I. Fragments I, II and III were used as templates to generate the overlapping amplicons by PCR and an equimolar mixture of the three DNA fragments was used for cell transfection of BHK-21 cells, and infectious mCherry-TBEV was harvested 3–5 days post-transfection (B). The transfected BHK-21 cell cultures were examined for mCherry (red fluorescence) and viral envelope protein (green fluorescence) expression. Cells were labeled with a mouse monoclonal antibody that recognizes the flavivirus group surface antigen and an anti-mouse goat secondary antibody conjugated with fluorescein isothiocyanate (FITC). Scale bar, 200 μ m (C).

were examined for expression of viral envelope protein by immunofluorescence staining. Using this approach, expression of viral envelope protein in the transfected cells was demonstrated and it was found that the numbers of immunofluorescence positive and mCherry expressing cells were similar (Fig. 1C).

3.2. Growth kinetics and plaque morphology of wild-type TBEV and mCherry-TBEV in cultured cells

Following the recovery procedure, growth kinetics of wild-type TBEV and mCherry-TBEV was investigated in BHK-21 cells using MOIs of 0.1 and 1. Both wild-type TBEV and mCherry-TBEV exhibited similar growth kinetics in BHK-21 cells at both MOIs, with maximum increase between 18 and 60 h p.i. or 12–36 h corresponding with peak titers of 1×10^8 or 1×10^9 in case of MOI 0.1 and 1, respectively (Fig. 2A). The mCherry-TBEV growth kinetics correlated with the mCherry fluorescence signal measured in cell culture lysates (Fig. 2B) and visualized by live cell imaging (Fig. 2C). As shown in Fig. 2B, the mCherry signal increased in proportion to virus titer in culture, with maximal increase between 24 and 60 h p.i. and 18–36 h p.i. for MOI 0.1 and 1, respectively (Fig. 2B). These data validate that the presence of mCherry gene did not significantly affect the virus reproduction properties in mammalian cell cultures, and the mCherry reporter expression accurately reflects the replication of mCherry-TBEV in the infected cells (Fig. 2A–C).

The morphology of plaques produced by wild-type and mCherry-TBEV in PS cells was compared. The size of plaques produced by mCherry-TBEV was smaller than those produced by wild-type TBEV (Fig. 2D). Wild-type TBEV produced plaques ranging from 747 to 1334 μm in diameter (mean, $924 \pm 276 \mu\text{m}$) and from 0.151 to 1.396 mm^2 in area (mean, $0.728 \pm 0.388 \text{mm}^2$); mCherry-TBEV produced plaques that ranged from 131 to 705 μm in diameter (mean, $415 \pm 154 \mu\text{m}$) and from 0.013 to 0.710 mm^2 in area (mean, $0.203 \pm 0.187 \text{mm}^2$) ($p < 0.0001$). Both viruses produced plaques that were clear, round, and regular in shape (Fig. 2D).

3.3. Stability of mCherry during serial passages of mCherry-TBEV

To test the stability of the recovered mCherry-TBEV, we passaged the virus in BHK-21 cells for four rounds. In each passage, BHK-21 cells were infected with mCherry-TBEV at an MOI of 0.1. We examined mCherry expression in passage 0, 2, and 4, and the mCherry expression was compared with expression of viral envelope protein detected by immunofluorescence staining (Fig. 3). While mCherry-positive cells were detected in each passage, the percentage of mCherry-positive cells was decreasing (Fig. 3E). We also investigated plaque morphology of mCherry-TBEV in each passage. While plaques at passage 0 and 1 were small (plaque diameter was $438 \pm 95 \mu\text{m}$ and $478 \pm 214 \mu\text{m}$, respectively), starting from passage 2 the mean plaque diameter was significantly larger (625 ± 201 , 607 ± 195 , and $656 \pm 193 \mu\text{m}$ at passage 2, 3, and 4, respectively). The same trend was observed also when plaque area was calculated; starting from passage 2, the plaque area was significantly larger (mean, $0.169 \pm 0.088 \text{mm}^2$ (P0); $0.337 \pm 0.197 \text{mm}^2$ (P2); $0.366 \pm 0.198 \text{mm}^2$ (P4)). However, the plaque diameter and area values at passage 4 were still significantly lower compared to a wild-type TBEV ($924 \pm 276 \mu\text{m}$ in diameter and $0.728 \pm 0.388 \text{mm}^2$ in area) (Fig. 3C and D).

For further investigation of mCherry-TBEV stability, viral RNA from infected cells at each passage was isolated and used for RT-PCR to amplify partial sequence of the C gene containing the mCherry gene, and wild-type variant of the C gene. Results from RT-PCR revealed that the frequency of the mCherry variant was decreasing with each passage, but still detectable on passage 4. On the other hand, the frequency of a revertant with wild-type C gene; i.e., containing an mCherry deletion in the C gene, was increasing with each passage (Fig. 3B).

3.4. Evaluation of the antiviral activity of two compounds using mCherry-TBEV

We utilized the mCherry-TBEV to assay the *in vitro* anti-TBEV activity of two different nucleoside analogues known to have TBEV inhibitory properties; i.e., 2'-C-methyladenosine and RO-9187 (Eyer et al., 2015, 2016). PS cells were treated with different non-toxic concentrations of the drugs and simultaneously infected with mCherry-TBEV. Culture supernatants were harvested to examine viral titres and cell monolayers were subjected to fluorescence signal measurement as described in Material and Methods. Consistent with prior studies (Eyer et al., 2015, 2016), we observed that both antivirals exhibited a dose-dependent inhibition of the virus production in the presence of increasing concentration of the drug. Moreover, the decrease in virus production was correlated with reducing reporter activity to background levels at the highest doses (Fig. 4). These results confirm the feasibility of using mCherry-TBEV to develop high-throughput drug screening assays based on the monitoring of production of a fluorescent signal and without the need for secondary methodologies to detect the virus in the infected cells.

3.5. Neutralization assay based on mCherry-TBEV

We used human and animal TBE-ELISA-positive serum to evaluate whether mCherry-TBEV could be used to measure antibody neutralizing activity. The human serum was collected from a TBEV-vaccinated individual. The animal serum originated from a TBEV-infected dog. TBEV antibody negative human and canine sera were used as negative controls. Based on the mCherry activity measured on a microplate fluorescence reader, 50% neutralizing (inhibitory) concentration (IC_{50}) was calculated to correspond to dilution 1:389 for the human antibody (95% confidence: 1:230–1:649), and 1:804 (95% confidence 1:537–1:1217) for the canine serum (Fig. 5). When evaluated using a fluorescence microscope, the highest neutralization (endpoint) activity was observed up to dilution 1:80 in case of human serum, and 1:160 in case of the canine serum. TBEV antibody negative serum samples exhibited no mCherry-TBEV neutralizing activity in this assay, as measured either using a microplate fluorescence reader or observed by fluorescence microscopy (Fig. 5). The results indicate that the mCherry-TBEV can be useful to assess the neutralizing activity of TBEV-specific antibodies in human and animal sera. Either a microplate fluorescence reader or fluorescence microscopy can be used to determine the virus neutralization antibody titers using this assay; however, the measurement of mCherry activity using the microplate reader is more sensitive and can be used as a quantitative test to measure antibody-mediated TBEV neutralization.

4. Discussion

In this study, we developed an infectious, replication competent TBEV that encodes the mCherry reporter gene. Several attempts to generate reporter flaviviruses, such as dengue virus, Japanese encephalitis virus, West Nile virus or Zika virus, were reported (Tamura et al., 2018; Pierson et al., 2006; Yun et al., 2020; Li et al., 2017; Eyre et al., 2017; Zou et al., 2011; Schoggins et al., 2012; Suphatrakul et al., 2018). Various fluorescent (GFP, eGFP, mCherry, mAmetrine, miRFP703, LSSmKate2, mCardinal, mNeptune2, etc.) and bioluminescent (NanoLuc luciferase, HiBiT luciferase, Renilla and firefly luciferase, etc.) proteins were used as reporter genes in these viruses (Tamura et al., 2018; Pierson et al., 2006; Yun et al., 2020; Li et al., 2017; Eyer et al., 2017; Zou et al., 2011; Schoggins et al., 2012; Suphatrakul et al., 2018). A primary consideration in the design of viruses involving reporter genes is their different properties, based on the purpose of the study (Nogales et al., 2019). The mCherry reporter used in this study is a bright red monomeric fluorescent protein derived from DsRed of *Discosoma* sp. (Shaner et al., 2004). The mCherry is considered to be the best

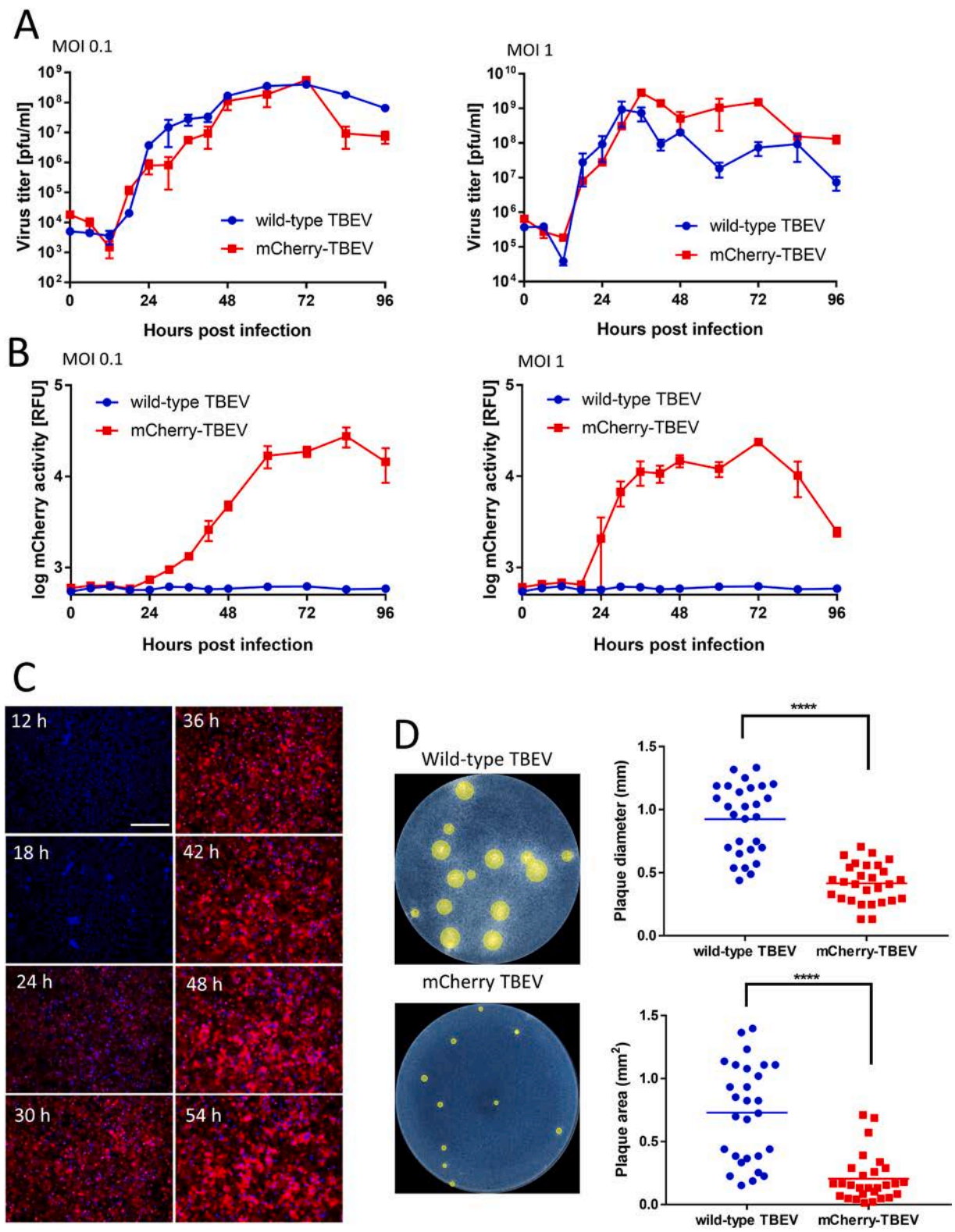


Fig. 2. Characterization of mCherry-TBEV. Growth kinetics of wild-type TBEV and mCherry-TBEV were investigated in BHK-21 cells using MOIs of 0.1 and 1. Cell culture medium was collected from the wells at indicated time points and used for plaque assay to construct growth curves (A). To measure the mCherry activity, the cells were lysed and fluorescence was measured as described in Materials and Methods and expressed in relative fluorescence units [RFU] (B). The mCherry expression in the infected BHK-21 cells was also visualized by live-cell imaging. Scale bar, 200 μ m (C). The plaque morphology of the mCherry-TBEV was assayed in a culture of porcine kidney stable (PS) cells and compared to that of the wild-type virus. Images of the plaques were scanned on a BioVendor C-series array reader, and the plaque diameters and plaque areas of the wild-type virus and the mCherry-TBEV were compared. ****, $P < 0.0001$ (D).

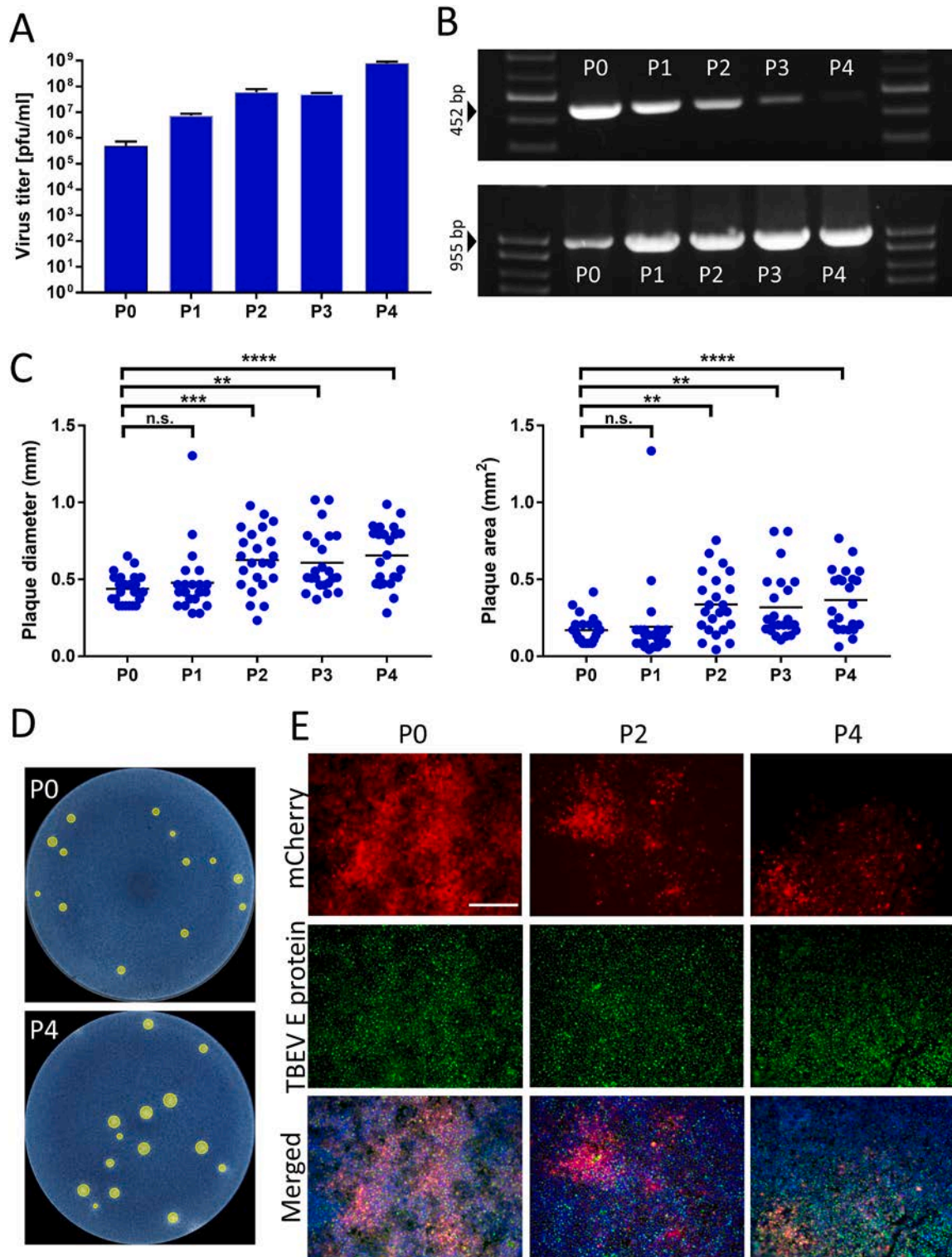


Fig. 3. Genetic stability of mCherry-TBEV in BHK-21 cells. To test the stability of the recovered mCherry-TBEV, we passaged the virus in BHK-21 cells for four rounds. In each passage, BHK-21 cells were infected with mCherry-TBEV at an MOI of 0.1. Viral titer in cell culture passage after each passage was investigated using plaque assay (A). Viral RNA from infected cells at each passage was isolated and used for RT-PCR to amplify partial sequence of C gene containing mCherry gene (upper panel), and wild-type variant of the C gene (lower panel) (B). The plaque morphology of the virus after each passage was assayed in a culture of porcine kidney stable (PS). Images of the plaques were scanned on a BioVendor C-series array reader, and the plaque diameters and plaque areas were measured. n.s., not significant; **, $P < 0.01$; ***, $P < 0.001$; ****, $P < 0.0001$ (C). Representative pictures of plaques after P0 and P4 are shown (D). After P0, P2, and P4, the infected BHK-21 cells were fixed, viral envelope protein expression (green) was detected by immunofluorescence assay using a mouse monoclonal antibody that recognizes the flavivirus group surface antigen and an anti-mouse goat secondary antibody conjugated with fluorescein isothiocyanate (FITC), and compared to mCherry expression (red). Scale bar, 200 μm (E).

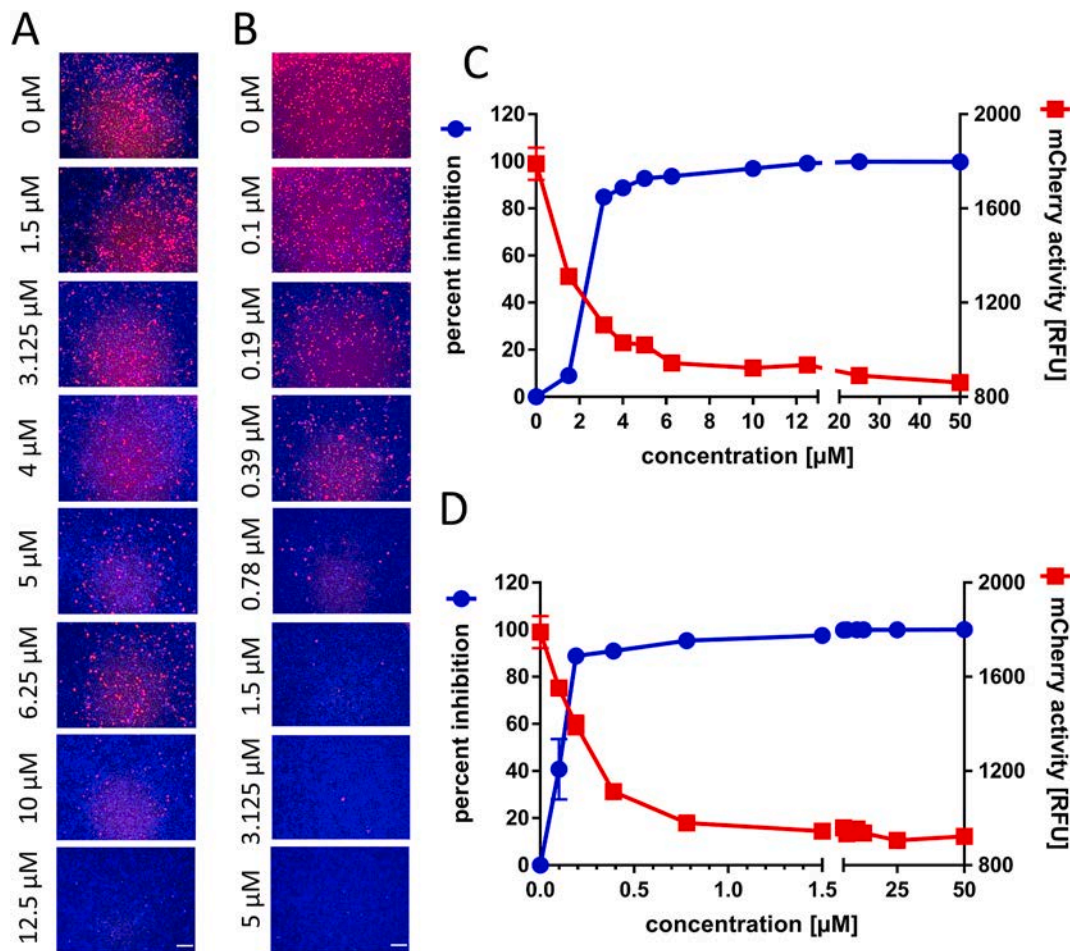


Fig. 4. Antiviral drug evaluation based on mCherry-TBEV. PS cells were treated with different concentrations of the 2'-C-methyladenosine, or RO-9187, and simultaneously infected with mCherry-TBEV at an MOI of 1. DMSO was added to virus-infected cells as a negative control at a final concentration of 0.5% (v/v). After 72 h of incubation, cell nuclei were stained with Hoechst 33342 dye (blue), and the mCherry expression was visualized by fluorescence microscopy (A, 2'-C-methyladenosine; B, RO-9187). mCherry activity was measured by an automated reader (expressed in relative fluorescence units [RFU]), and cell culture media were collected and analyzed by plaque assay (C, 2'-C-methyladenosine; D, RO-9187). Scale bars, 250 μm.

general-purpose red fluorescence protein that is highly photostable and resistant to photobleaching, and suitable for long-term imaging (Shaner et al., 2005).

Full-length infectious clones of viruses, especially of flaviviruses, are often difficult to work with because many of the flaviviral cDNA clones are toxic for the bacterial cells (Gritsun and Gould, 1995; Tamura et al., 2018). To overcome these limitations, the reverse genetics system based on the generation of three infectious subgenomic overlapping DNA fragments that encompass the entire viral genome was used in this study (Aubry et al., 2014; Driouich et al., 2018). The mCherry gene was inserted immediately after the flavivirus promoter including the complete 5'UTR and the first 72 nucleotides (24 codons) of the C gene within the first genomic fragment. A similar position of the reporter gene insertion has been used to generate Japanese encephalitis and dengue reporter viruses (Zou et al., 2011; Schoggins et al., 2012; Li et al., 2017; Suphatrakul et al., 2018). The reporter gene was flanked on both sides with Ribosome-skipping 2 A sequences, which has been found to be necessary for the reporter gene stability of the dengue virus genome (Suphatrakul et al., 2018). This simple reverse genetics method facilitated the rescue of infectious TBEV from genomic DNA material without requiring cloning, propagation of cDNA into bacteria or *in vitro* RNA transcription (Aubry et al., 2014), and in contrast to traditional methodologies, the modified virus was prepared in days, which is another significant advantage of this straightforward approach (Aubry et al., 2014).

Insertion of reporter genes into flavivirus genomes often leads to attenuation of viral replication, demonstrated by slower growth rates and smaller plaques than those of the wild-type virus (Yun et al., 2020; Ávila-Pérez et al., 2018; Li et al., 2017; Zou et al., 2011). In agreement with these observations, the size of plaques produced by mCherry-TBEV was smaller than those produced by wild-type TBEV. However, both wild-type TBEV and mCherry-TBEV exhibited similar growth kinetics in BHK-21 cells. The magnitude of the mCherry activity produced by mCherry-TBEV correlated directly with increasing TBEV titer in the cell culture.

The insertion of the reporter gene into the viral genome creates a selective pressure for the reporter-expressing virus to delete the inserted gene or its part that is not necessary for viral replication (Yun et al., 2020). To investigate the genetic stability of the mCherry gene in the TBEV genome, the virus was serially passaged in cell culture. Passaging of the mCherry-TBEV led to formation of plaques that were growing in size and becoming increasingly heterogeneous over time. RT-PCR revealed that frequency of the mCherry gene-containing variant was decreasing, while the frequency of the revertant with wild-type TBEV genotype was increasing with each passage. Generally, the mCherry-TBEV remained relatively stable over <4 passages in cell culture. The instability of the reporter gene is unsurprising and is consistent with previous studies on another reporter flavivirus systems (Schoggins et al., 2012; Yun et al., 2020; Li et al., 2017).

Reporter-expressing viruses provide a powerful tool to investigate

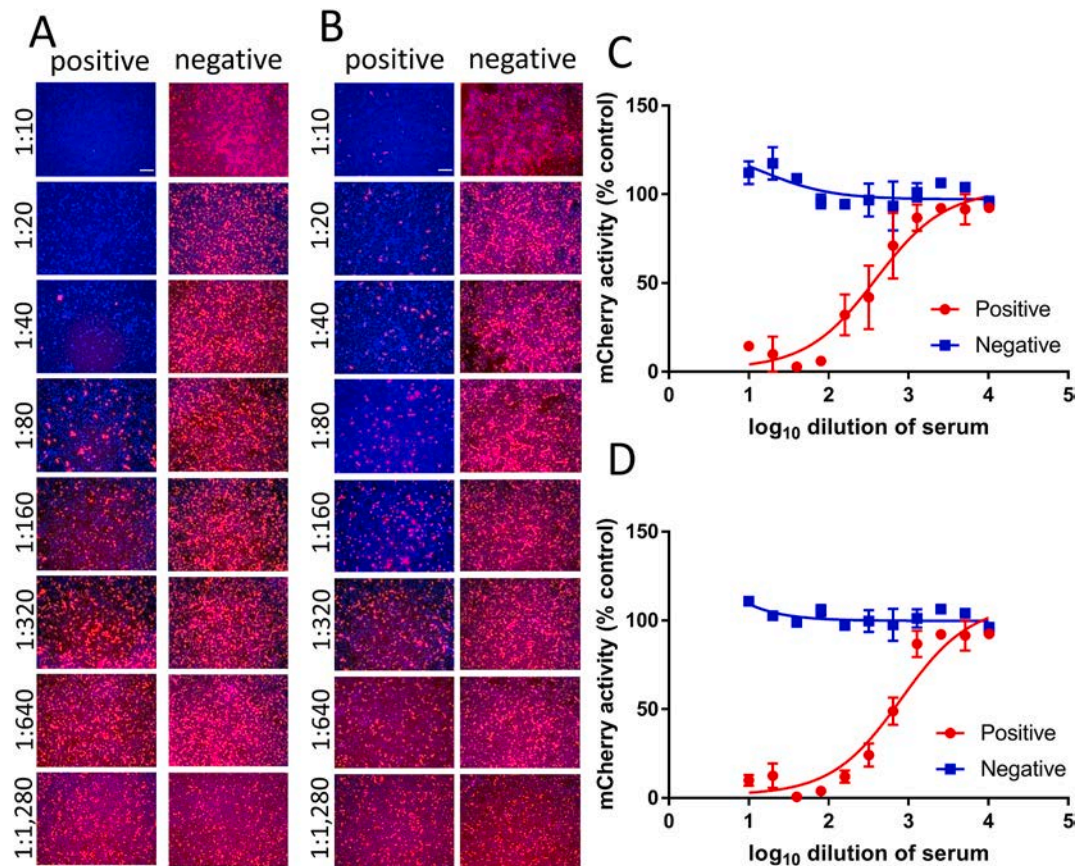


Fig. 5. Neutralization assay based on mCherry-TBEV. mCherry-TBEV was incubated with serial dilutions of serum samples from TBEV-vaccinated (positive) and serologically negative humans, and experimentally TBEV-infected (positive) and control (negative) dogs for 90 min at 37 °C in a 96-well plate. After incubation, a suspension of PS cells (3×10^4 cells per well) was added to each well. After 48 h of incubation at 37 °C, the mCherry expression was visualized using fluorescence microscopy (A, human samples; B, canine samples), and mCherry activity was measured using an automated reader and are expressed as percentage of mCherry activity of the negative control (no antibody) (C, human samples; D, canine samples). Scale bars, 250 μ m.

several aspects of virus biology *in vitro*, such as quantitative measurement of viral replication, and tracking of infected individual cells (Yun et al., 2020; Pierson et al., 2006). However, this approach also facilitates establishment of methods for rapid and high-throughput screening of candidate antiviral agents and neutralizing antibody assays, without the need to use secondary methodologies to detect the virus in the infected cells (Yun et al., 2020; Pierson et al., 2006; Lo et al., 2004; Cai et al., 2018). Having optimized the mCherry-TBEV reporter assay, we tested this system against two known TBEV inhibitors, 2'-C-methyladenosine (2'-CMA) and 2'-deoxy-2'- β -hydroxy-4'-azidocytidine (RO-9187) (Eyer et al., 2015, Eyer et al., 2017). Consistent with previous reports based on cytopathic effect (CPE)- and plaque-based assays (Eyer et al., 2015, Eyer et al., 2017), both 2'-CMA and RO-9187 showed a dose-dependent inhibition of mCherry-TBEV, reducing mCherry activity to background levels at the highest drug concentrations. The mCherry activity also correlated with the level of virus replication as demonstrated by plaque assay. Thus, our results demonstrate that the measurement of mCherry activity reflects inhibition of TBEV replication and represents a viable alternative to classical methodologies used for anti-TBEV drug discovery.

In addition to small molecule inhibition, the mCherry-TBEV system was found to be useful for detecting TBEV-neutralizing antibodies in human and animal sera and represents an alternative to a standard plaque-reduction neutralization test (PRNT). PRNT is the most specific diagnostic test and it is required to confirm the diagnosis of TBE infection (Yoshii et al., 2009). However, formation of plaques depends on the cell type and culture conditions, and needs to be determined individually by the investigator (Yoshii et al., 2009). A surrogate screening

system based on a reporter-gene expressing virus-like particles (VLPs) of TBEV was successfully established and validated previously (Yoshii et al., 2009). The mCherry-TBEV system represents another approach that enables rapid quantification of virus neutralization, which can be performed on a large scale. Compared to the reporter-expressing VLPs, use of mCherry-TBEV retains all complexities of the viable TBEV particles. On the other hand, the use of mCherry-TBEV is limited in ordinary diagnostic or hospital laboratories, as it needs to be performed under appropriate biosafety conditions. Therefore, it is more suitable for research labs with high-level biocontainment facilities required to handle viable TBEV.

The use of mCherry as a readout of TBEV replication can be performed with a fluorescence microscope or microplate fluorescence reader. This is the primary advantage of the mCherry-TBEV system over classical CPE, plaque- or antigen-based assays, or luciferase-based reporter viruses, leading to significant reduction in assay turn-around time and reduction of the use of reagents (Lo et al., 2014; Li et al., 2016). In summary, mCherry-TBEV provides a powerful quantitative tool to facilitate the identification of potential antiviral agents and to measure levels of neutralizing antibodies in human and animal sera.

Acknowledgements

We thank Jan Karasek from BioVendor Instruments, Czech Republic, for help with the scanning and analysis of plaques by use of a prototype instrument and software analytics.

This study was supported by a grant from the Czech Science Foundation (grant No. 20-14325 S) (to D.R.). DR, LE, KY and SK were

supported by the project Mobility Plus JSPS-18-08 funded by the Czech Academy of Sciences and Japanese Society for Promotion of Science.

Appendix A. Supplementary data

Supplementary data to this article can be found online at <https://doi.org/10.1016/j.antiviral.2020.104968>.

References

- Aubry, F., Nougairède, A., de Fabritius, L., Querat, G., Gould, E.A., de Lamballerie, X., 2014. Single-stranded positive-sense RNA viruses generated in days using infectious subgenomic amplicons. *J. Gen. Virol.* 95 (Pt 11), 2462–2467. <https://doi.org/10.1099/vir.0.068023-0>.
- Ávila-Pérez, G., Nogales, A., Martín, V., Almazán, F., Martínez-Sobrido, L., 2018. Reverse genetic approaches for the generation of recombinant Zika virus. *Viruses* 10 (11), 597. <https://doi.org/10.3390/v10110597>.
- Bogovic, P., Strle, F., 2015. Tick-borne encephalitis: a review of epidemiology, clinical characteristics, and management. *World J Clin Cases* 3 (5), 430–441. <https://doi.org/10.12998/wjcc.v3.i5.430>.
- Cai, Y., Iwasaki, M., Beitzel, B.F., Yú, S., Postnikova, E.N., Cubitt, B., DeWald, L.E., Radoshitzky, S.R., Bollinger, L., Jahrling, P.B., Palacios, G.F., de la Torre, J.C., Kuhn, J.H., 2018. Recombinant lassa virus expressing green fluorescent protein as a tool for high-throughput drug screens and neutralizing antibody assays. *Viruses* 10 (11), 655. <https://doi.org/10.3390/v10110655>.
- De Madrid, A.T., Porterfield, J.S., 1969. A simple micro-culture method for the study of group B arboviruses. *Bull. World Health Organ.* 40 (1), 113–121.
- Eyer, L., Kondo, H., Zouharova, D., Hirano, M., Valdés, J.J., Muto, M., Kastl, T., Kobayashi, S., Haviernik, J., Igarashi, M., Kariwa, H., Vaculovicova, M., Cerny, J., Kizek, R., Kröger, A., Lienenklaus, S., Dejmek, M., Nencka, R., Palus, M., Salat, J., De Clercq, E., Yoshii, K., Ruzek, D., 2017. Escape of tick-borne flavivirus from 2'-C-methylated nucleoside antivirals is mediated by a single conservative mutation in NS5 that has a dramatic effect on viral fitness. *J. Virol.* 91 (21), 17–e01028. <https://doi.org/10.1128/JVI.01028-17>.
- Eyer, L., Nencka, R., de Clercq, E., Seley-Radtke, K., Růžek, D., 2018. Nucleoside analogs as a rich source of antiviral agents active against arthropod-borne flaviviruses. *Antivir. Chem. Chemother.* 26 <https://doi.org/10.1177/2040206618761299>, 2040206618761299.
- Eyer, L., Šmídková, M., Nencka, R., Neča, J., Kastl, T., Palus, M., De Clercq, E., Růžek, D., 2016. Structure-activity relationships of nucleoside analogues for inhibition of tick-borne encephalitis virus. *Antivir. Res.* 133, 119–129. <https://doi.org/10.1016/j.antiviral.2016.07.018>.
- Diaz, L.A., Flores, F.S., Quaglia, A., Contigiani, M.S., 2013. Intertwined arbovirus transmission activity: reassessing the transmission cycle paradigm. *Front. Physiol.* 3, 493. <https://doi.org/10.3389/fphys.2012.00493>.
- Driouch, J.S., Ali, S.M., Amroun, A., Aubry, F., de Lamballerie, X., Nougairède, A., 2018. SuPREme: a rapid reverse genetics method to generate clonal populations of recombinant RNA viruses. *Emerg. Microb. Infect.* 7 (1), 40. <https://doi.org/10.1038/s41426-018-0040-2>.
- Eyer, L., Valdés, J.J., Gil, V.A., Nencka, R., Hřebabecký, H., Šála, M., Salát, J., Černý, J., Palus, M., De Clercq, E., Růžek, D., 2015. Nucleoside inhibitors of tick-borne encephalitis virus. *Antimicrob. Agents Chemother.* 59 (9), 5483–5493. <https://doi.org/10.1128/AAC.00807-15>.
- Eyre, N.S., Aloia, A.L., Joyce, M.A., Chulanetra, M., Tyrrell, D.L., Beard, M.R., 2017. Sensitive luminescent reporter viruses reveal appreciable release of hepatitis C virus NS5A protein into the extracellular environment. *Virology* 507, 20–31. <https://doi.org/10.1016/j.virol.2017.04.003>.
- Gresikova, M., Rehacek, J., 1959. [Isolation of the tick encephalitis virus from the blood and milk of domestic animals (sheep and cow) after infection by ticks of the family Ixodes ricinus L.]. *Arch. Gesamte Virusforsch.* 9, 360–364.
- Gritsun, T.S., Gould, E.A., 1995. Infectious transcripts of tick-borne encephalitis virus, generated in days by RT-PCR. *Virology* 214 (2), 611–618. <https://doi.org/10.1006/viro.1995.0072>.
- Hernance, M.E., Thangamani, S., 2018. Tick-Virus-Host interactions at the cutaneous interface: the nidus of flavivirus transmission. *Viruses* 10 (7), 362. <https://doi.org/10.3390/v10070362>.
- Koutsoudakis, G., Kaul, A., Steinmann, E., Kallis, S., Lohmann, V., Pietschmann, T., Bartenschlager, R., 2006. Characterization of the early steps of hepatitis C virus infection by using luciferase reporter viruses. *J. Virol.* 80 (11), 5308–5320. <https://doi.org/10.1128/JVI.02460-05>.
- Li, X.F., Li, X.D., Deng, C.L., Dong, H.L., Zhang, Q.Y., Ye, Q., Ye, H.Q., Huang, X.Y., Deng, Y.Q., Zhang, B., Qin, C.F., 2017. Visualization of a neurotropic flavivirus infection in mouse reveals unique viscerotropism controlled by host type I interferon signaling. *Theranostics* 7 (4), 912–925. <https://doi.org/10.7150/thno.16615>.
- Li, Y., Li, L.F., Yu, S., Wang, X., Zhang, L., Yu, J., Xie, L., Li, W., Ali, R., Qiu, H.J., 2016. Applications of replicating-competent reporter-expressing viruses in diagnostic and molecular virology. *Viruses* 8 (5), 127. <https://doi.org/10.3390/v8050127>.
- Lipowski, D., Popiel, M., Perlejewski, K., Nakamura, S., Bukowska-Osko, I., Rzakiewicz, E., Dzieciatkowski, T., Milecka, A., Wenski, W., Ciszek, M., Debska-Slizien, A., Ignacak, E., Cortes, K.C., Pawelczyk, A., Horban, A., Radkowski, M., Laskus, T., 2017. A cluster of fatal tick-borne encephalitis virus infection in organ transplant setting. *J. Infect. Dis.* 215 (6), 896–901. <https://doi.org/10.1093/infdis/jix040>.
- Lo, M.K., Nichol, S.T., Spiropoulou, C.F., 2014. Evaluation of luciferase and GFP-expressing Nipah viruses for rapid quantitative antiviral screening. *Antivir. Res.* 106, 53–60. <https://doi.org/10.1016/j.antiviral.2014.03.011>.
- Moser, C., Tratschin, J.D., Hofmann, M.A., 1998. A recombinant classical swine fever virus stably expresses a marker gene. *J. Virol.* 72 (6), 5318–5322.
- Nogales, A., Ávila-Pérez, G., Rangel-Moreno, J., Chiem, K., DeDiego, M.L., Martínez-Sobrido, L., 2019. A novel fluorescent and bioluminescent bioreporter influenza A virus to evaluate viral infections. *J. Virol.* 93 (10), 19–e00032. <https://doi.org/10.1128/JVI.00032-19>. PMID: 30867298; PMCID: PMC6498038.
- Pierson, T.C., Sánchez, M.D., Puffer, B.A., Ahmed, A.A., Geiss, B.J., Valentine, L.E., Altamura, L.A., Diamond, M.S., Doms, R.W., 2006. A rapid and quantitative assay for measuring antibody-mediated neutralization of West Nile virus infection. *Virology* 346 (1), 53–65. <https://doi.org/10.1016/j.virol.2005.10.030>.
- Riccardi, N., Antonello, R.M., Luzzati, R., Zajkowska, J., Di Bella, S., Giacobbe, D.R., 2019. Tick-borne encephalitis in Europe: a brief update on epidemiology, diagnosis, prevention, and treatment. *Eur. J. Intern. Med.* 62, 1–6. <https://doi.org/10.1016/j.ejim.2019.01.004>.
- Rueden, C.T., Schindelin, J., Hiner, M.C., DeZonia, B.E., Walter, A.E., Arena, E.T., Elceiri, K.W., 2017. ImageJ2: ImageJ for the next generation of scientific image data. *BMC Bioinf.* 18 (1), 529. <https://doi.org/10.1186/s12859-017-1934-z>.
- Ruzek, D., Avšič Županc, T., Borde, J., Chrdle, A., Eyer, L., Karganova, G., Kholodilov, I., Knap, N., Kozlovskaya, L., Matveev, A., Miller, A.D., Osolodkin, D.I., Överby, A.K., Tikunova, N., Tkachev, S., Zajkowska, J., 2019. Tick-borne encephalitis in Europe and Russia: review of pathogenesis, clinical features, therapy, and vaccines. *Antivir. Res.* 164, 23–51. <https://doi.org/10.1016/j.antiviral.2019.01.014>.
- Salat, J., Ruzek, D., 2020. Tick-borne encephalitis in domestic animals. *Acta Virol.* 64 (2), 226–232. <https://doi.org/10.4149/av.2020.212>.
- Schindelin, J., Arganda-Carreras, I., Frise, E., Kaynig, V., Longair, M., Pietzsch, T., Preibisch, S., Rueden, C., Saalfeld, S., Schmid, B., Tinevez, J.Y., White, D.J., Hartenstein, V., Eliceiri, K., Tomancak, P., Cardona, A., 2012. Fiji: an open-source platform for biological-image analysis. *Nat. Methods* 9 (7), 676–682. <https://doi.org/10.1038/nmeth.2019>.
- Schoggins, J.W., Dorner, M., Feulner, M., Imanaka, N., Murphy, M.Y., Ploss, A., Rice, C.M., 2012. Dengue reporter viruses reveal viral dynamics in interferon receptor-deficient mice and sensitivity to interferon effectors in vitro. *Proc. Natl. Acad. Sci. U. S. A.* 109 (36), 14610–14615. <https://doi.org/10.1073/pnas.1212379109>.
- Shaner, N.C., Campbell, R.E., Steinbach, P.A., Giepmans, B.N., Palmer, A.E., Tsien, R.Y., 2004. Improved monomeric red, orange and yellow fluorescent proteins derived from *Drosophila* sp. red fluorescent protein. *Nat. Biotechnol.* 22 (12), 1567–1572. <https://doi.org/10.1038/nbt1037>. Epub. 2004.Nov.21. PMID: 15558047.
- Shaner, N.C., Steinbach, P.A., Tsien, R.Y., 2005. A guide to choosing fluorescent proteins. *Nat. Methods* 2 (12), 905–909. <https://doi.org/10.1038/nmeth819>. PMID: 16299475.
- Simmonds, P., Becher, P., Bukh, J., Gould, E.A., Meyers, G., Monath, T., Muerhoff, S., Pletnev, A., Rico-Hesse, R., Smith, D.B., Stapleton, J.T., 2017. Ictv report consortium. ICTV virus taxonomy profile: Flaviviridae. *J. Gen. Virol.* 98 (1), 2–3. <https://doi.org/10.1099/jgv.0.000672>.
- Suphatrakul, A., Duangchinda, T., Jupatanakul, N., Prasittisa, K., Onnong, S., Pengon, J., Siridechadilok, B., 2018. Multi-color fluorescent reporter dengue viruses with improved stability for analysis of a multi-virus infection. *PLoS One* 13 (3), e0194399. <https://doi.org/10.1371/journal.pone.0194399>.
- Taba, P., Schmutzhard, E., Forsberg, P., Lutsar, I., Ljøstød, U., Å, Mygland, Levchenko, I., Strle, F., Steiner, I., 2017. EAN consensus review on prevention, diagnosis and management of tick-borne encephalitis. *Eur. J. Neurol.* 24 (10), e61–1214. <https://doi.org/10.1111/ene.13356>.
- Tamura, T., Fukuhara, T., Uchida, T., Ono, C., Mori, H., Sato, A., Fauzyah, Y., Okamoto, T., Kurosu, T., Setoh, Y.X., Imamura, M., Tautz, N., Sakoda, Y., Khromykh, A.A., Chayama, K., Matsuura, Y., 2018. Characterization of recombinant Flaviviridae viruses possessing a small reporter tag. *J. Virol.* 92 (2), 17–e01582. <https://doi.org/10.1128/JVI.01582-17>.
- Tamura, T., Igarashi, M., Enkhbold, B., Suzuki, T., Okamoto, M., Ono, C., Mori, H., Izumi, T., Sato, A., Fauzyah, Y., Okamoto, T., Sakoda, Y., Fukuhara, T., Matsuura, Y., 2019. Vivo dynamics of reporter Flaviviridae viruses. *J. Virol.* 93 (22), 19–e01191. <https://doi.org/10.1128/JVI.01191-19>.
- Yoshii, K., Ikawa, A., Chiba, Y., Omori, Y., Maeda, J., Murata, R., Kariwa, H., Takashima, I., 2009. Establishment of a neutralization test involving reporter gene-expressing virus-like particles of tick-borne encephalitis virus. *J. Virol Methods* 161 (1), 173–176. <https://doi.org/10.1016/j.jviromet.2009.05.016>.
- Yun, S.I., Song, B.H., Woolley, M.E., Frank, J.C., Julander, J.G., Lee, Y.M., 2020. Development, characterization, and application of two reporter-expressing recombinant Zika viruses. *Viruses* 12 (5), 572. <https://doi.org/10.3390/v12050572>.
- Zou, G., Xu, H.Y., Qing, M., Wang, Q.Y., Shi, P.Y., 2011. Development and characterization of a stable luciferase dengue virus for high-throughput screening. *Antivir. Res.* 91 (1), 11–19. <https://doi.org/10.1016/j.antiviral.2011.05.001>.



Antiviral activities of 2,6-diaminopurine-based acyclic nucleoside phosphonates against herpesviruses: *In vitro* study results with pseudorabies virus (PrV, SuHV-1)



Darina Zouharova^{a,1}, Ivana Lipenska^{a,1}, Martina Fojtikova^{a,1}, Pavel Kulich^a, Jiri Neca^a, Michal Slany^a, Kamil Kovarcik^a, Pavlina Turanek-Knotigova^a, Frantisek Hubatka^a, Hana Celechovska^a, Josef Masek^a, Stepan Koudelka^{a,b}, Lubomir Prochazka^a, Ludek Eyer^a, Jana Plockova^a, Eliska Bartheldyova^a, Andrew D. Miller^c, Daniel Ruzek^{a,d}, Milan Raska^{a,e}, Zlatko Janeba^f, Jaroslav Turanek^{a,*}

^a Veterinary Research Institute, Department of Pharmacology and Immunotherapy, Brno, Czech Republic

^b International Clinical Research Center, St. Anne's University Hospital, Brno, Czech Republic

^c King's College London, Institute of Pharmaceutical Science, London, United Kingdom, and GlobalAcorn Ltd., London, United Kingdom

^d Institute of Parasitology, Biology Centre of the Czech Academy of Sciences, and Faculty of Science, University of South Bohemia, Ceske Budejovice, Czech Republic

^e Palacky University of Olomouc, Faculty of Medicine, Department of Immunology, Czech Republic

^f Institute of Organic Chemistry and Biochemistry, The Czech Academy of Sciences, Prague, Czech Republic

ARTICLE INFO

Article history:

Received 1 December 2015

Received in revised form 13 January 2016

Accepted 14 January 2016

Keywords:

Pseudorabies

Acyclic nucleoside phosphonates

DNA viruses

Cidofovir

Antiviral drugs

DNA polymerase

ABSTRACT

Pseudorabies virus (PrV), a causative agent of Aujeszky's disease, is deadly to most mammals with the exception of higher primates and men. This disease causes serious economic losses among farm animals, especially pigs, yet many European countries are today claimed to be Aujeszky's disease free because of the discovery of an efficient vaccination for pigs. In reality, the virus is still present in wild boar. Current vaccines are neither suitable for dogs nor are there anti-PrV drugs approved for veterinary use. Therefore, the disease still represents a high threat, particularly for expensive hunting dogs that can come into close contact with infected boars. Here we report on the anti-PrV activities of a series of synthetic diaminopurine-based acyclic nucleoside phosphonate (DAP-ANP) analogues. Initially, all synthetic DAP-ANPs under investigation are shown to exhibit minimal cytotoxicity by MTT and XTT tests (1–100 μ M range). Thereafter *in vitro* infection models are established using PrV virus SuHV-1, optimized on PK-15 and RK-13 cell lines. Out of the six DAP-ANP analogues tested, analogue VI functionalized with a cyclopropyl group on the 6-amino position of the purine ring proves the most effective antiviral DAP-ANP analogue against PrV infection, aided by sufficient hydrophobic character to enhance bioavailability to its cellular target viral DNA-polymerase. Four other DAP-ANP analogues with functional groups introduced to the C2' position are shown ineffective against PrV infection, even with favourable hydrophobic properties. Cidofovir[®], a drug approved against various herpesvirus infections, is found to exert only low activity against PrV in these same *in vitro* models.

© 2016 Elsevier B.V. All rights reserved.

1. Introduction

Pseudorabies, also known as “Aujeszky's disease”, is an acute, frequently fatal disease caused by PrV, also known as suid

herpesvirus 1 (SuHV-1), which belongs to the genus *Varicellovirus*, in the Alphaherpesvirinae subfamily of the family *Herpesviridae* (Pomeranz et al., 2005). Among the most known viruses in the *Varicellovirus* genus are varicellazoster virus (VZV), bovine herpesvirus 1 (BHV-1) and equine herpesvirus 1 (EHV-1) (McGeoch and Cook, 1994). PrV is a pathogen spread mostly among swine and is lethal for almost all mammals except for higher primates and humans. Only wild pigs are able to survive infection and they serve as a natural reservoir of PrV. Dogs, especially hunting dogs, can be infected with this virus by close

* Corresponding author at: Department of Pharmacology and Immunotherapy, Veterinary Research Institute Hudcova 70 621 00 Brno, Czech Republic.

E-mail address: turanek@vri.cz (J. Turanek).

¹ These authors contributed equally to this work.

contact with the blood or saliva of shot and wounded wild boar. Consumption of contaminated raw pork or offal is another source of fatal infection in farm and companion dogs (Zhang et al., 2015; Cay and Letellier, 2009). Much has been discovered so far about PrV neurovirulence, neuropathogenesis, the properties of viral proteins involved in those processes, and genome sequences. PrV has also been used as a model herpesvirus to study virus biology and may be used for tracing neural pathways (Pomeranz et al., 2005). While in swine, PrV is transferred to various organs by viremic and lymphatic pathways (Wittmann et al., 1980), there is no evidence of viral replication in the tissues of experimentally infected dogs, except for in tissues of the nervous system. Therefore, the non-neural tissue damage in infected dogs is primarily induced indirectly by PrV. Histological findings in the central nervous systems (CNS) of PrV-infected dogs were found to be restricted to the brainstem (Zhang et al., 2015). Secondary findings of cardiac lesions were made in both the naturally and experimentally PrV-infected dogs (Olson and Miller, 1986). At present only vaccines for swine are available for the prophylaxis of Aujeszky's disease in pig farms. Inactivated vaccines are not effective in dogs and attenuated vaccines are lethal for dogs as well as for farm animals like lambs and sheep (Kong et al., 2013; Van Alstine et al., 1984). Some attempts to develop recombinant protein (rPrV) and DNA vaccines for swine were described in literature. Many of the rPrV vaccine candidates that have been reported in literature albeit they have not been further pursued so are not yet commercially available (Krishnan, 2000; Dong et al., 2014; Kim et al., 2008; Van Rooij et al., 2010). Despite the significant progress made, the efficacy of potentially safe DNA vaccines requires considerable improvement owing to the high mortality rate from the disease in vaccinated animals (Woodland, 2004; Yoon et al., 2006; Fischer et al., 2003).

In the case of chemotherapy, there are no currently approved veterinary drugs against Aujeszky's disease, and there are only limited reports concerning inhibition studies focused on inhibition of PrV proliferation by various preparations. Some natural compounds have been found to be effective *in vitro* against various herpesviruses, but failed against PrV (De Almeida et al., 1998). *In vitro* inhibition of PrV replication was demonstrated for combination of Acyclovir and Ribavirin (Pancheva, 1991). The antiviral effects of lithium chloride and natural compound diammonium glycyrrhizinate were demonstrated *in vitro* on VERO cells (Sui et al., 2010). Several nucleotide based drugs like bromovinyl deoxyuridine, acyclovir and 2'-nor-2'-deoxyguanosine have been studied as *in vitro* inhibitors and in mice models *in vivo*. Mice survival was most prolonged post administration of 2'-nor-2'-deoxyguanosine (Field, 1985).

Recently, a new largescale method for synthesis of antiretroviral agent 9-[2-(*R*)-(phosphonomethoxy) propyl]-2,6-diaminopurine, (*R*)-PMPDAP, was developed (Krecmerova et al., 2013) and used for synthesis of analogues of diaminopurine-based acyclic

nucleoside phosphonate (DAP-ANP) (Holy et al., 1999; Jansa et al., 2012). We tested these compound *in vitro* various herpesviruses, especially strains resistant against established antiviral drugs, including PrV which is of importance in veterinary medicine. Two of these DAP-ANP analogues were found to be highly active against PrV in model *in vitro* cell culture studies, while Cidofovir[®], a marketed drug active against many viruses including herpes, adeno, polyoma, papilloma, poxviruses and retroviruses (De Clercq, 1998; De Clercq, 2002), only exerted low anti PrV activity. This is the first study focused on the antiviral effects of DAP-ANP analogues against PrV.

2. Materials and methods

2.1. Syntheses and structure of nucleotide analogues

A series of 6 DAP-ANP analogues (Table 1 and Fig. 1) differing in their hydrophobicity and substitution in the side chain were synthesized according to previously reported methods (Krecmerova et al., 2013; Holy et al., 1999; Jansa et al., 2012; Holy et al., 2001; Jansa et al., 2011). Cidofovir[®] (active compound (*S*)-HPMPC); (*S*)-1-[3-hydroxy-2-(phosphonylmethoxypropyl)]cytosine as well as its inactive (*R*)-isomer were kindly gifted by prof. Antonín Holý.

2.2. Chromatographic analyses HPLC–MS/MS and hydrophobicity of tested compounds expressed as capacity factor

Sample analyses were performed by using high performance liquid chromatography in tandem with mass spectrometry. An Agilent 1200 chromatographic system (Agilent Technologies, Germany), consisting of binary pump, vacuum degasser, auto sampler, UV detector and thermostat column compartment, was used. Separation of modified nucleotides was carried out using Zorbax Eclipse Plus, 2.1 × 150 mm, 3.5 μm particle size column (Agilent Technologies, USA) under isocratic conditions. Mobile phase contained 0.8% of methanol and 0.1% of formic acid in water. The flow rate of the mobile phase was 0.25 ml/min, the column temperature was set at 40 °C. UV detector was used for determination of nucleotides capacity factors. A triple quadrupole mass spectrometer Agilent 6410 Triple Quad LC/MS (Agilent Technologies, USA) with an electrospray interface (ESI) was used for quantification of tested compounds in cells. The mass spectrometer was operated in the positive ion mode. Multiple reaction monitoring (MRM) with the mass transitions *m/z* 329.1–191.2, 216.9, 247.0 and 281.2 was used. Relative hydrophobicity of tested compounds was expressed as capacity factor *k'* to compare their potential to penetrate cell membranes.

2.3. In vitro testing—tissue culture

MDCK, MDBK, PK-15, RK-13, VERO cell lines were tested to select appropriate cell line for *in vitro* assays. Cell line PK-15 and RK-13 were selected as the best model with respect to virus multiplication and sensitivity for XTT/MTT cytotoxicity tests. The data obtained on these cell lines gave long term coherent results. The cultures were grown in Dulbecco's minimal essential medium (DMEM/High Glucose, HyClone, Thermo Scientific) supplemented with antibiotics, fungizone and 10% foetal bovine serum (FBS). The cells were cultured at 37 °C in a humidified atmosphere containing 5% CO₂ (HERAcell 150i CO2 incubator, Thermo Scientific, Germany).

2.4. In vitro testing—virus strain

SuHV-1CAPM V-166 isolate was obtained from the Collection of Pathogenic Microorganisms (Veterinary Research Institute, Brno) and was used throughout these experiments. This isolate was

Table 1
Molecular formulae and weight of chosen antivirals.

Compound	Molecular formula	Molecular weight (Da)
I	C ₈ H ₁₃ N ₆ O ₄ P	288
II	C ₉ H ₁₂ N ₆ O ₅ PNa ₂	362
III	C ₁₀ H ₁₆ N ₆ O ₅ P	318
IV	C ₁₀ H ₁₄ N ₅ O ₄ P	302
V	C ₇ H ₁₀ N ₄ O ₅ PF ₃	365
VI	C ₁₁ H ₁₇ N ₆ O ₄ P	328
CIDOFOVIR	C ₈ H ₁₄ N ₃ O ₆ P	279

Note: I: 9-[2-(phosphonomethoxy) ethyl]-2,6-diaminopurine; II: (*S*)-9-[2-hydroxy-3-(phosphonomethoxy) propyl]-2,6-diaminopurine; III: (*R*)-9-[3-hydroxy-2-(phosphonomethoxy) propyl]-2,6-diaminopurine; IV: (*R*)-9-[2-(phosphonomethoxy) propyl]-2,6-diaminopurine; V: (*R,S*)-9-[3,3,3-trifluoro-2-(phosphonomethoxy) propyl]-2,6-diaminopurine; VI: N 6-cyclopropyl-9-[2-(phosphonomethoxy) ethyl]-2,6-diaminopurine.

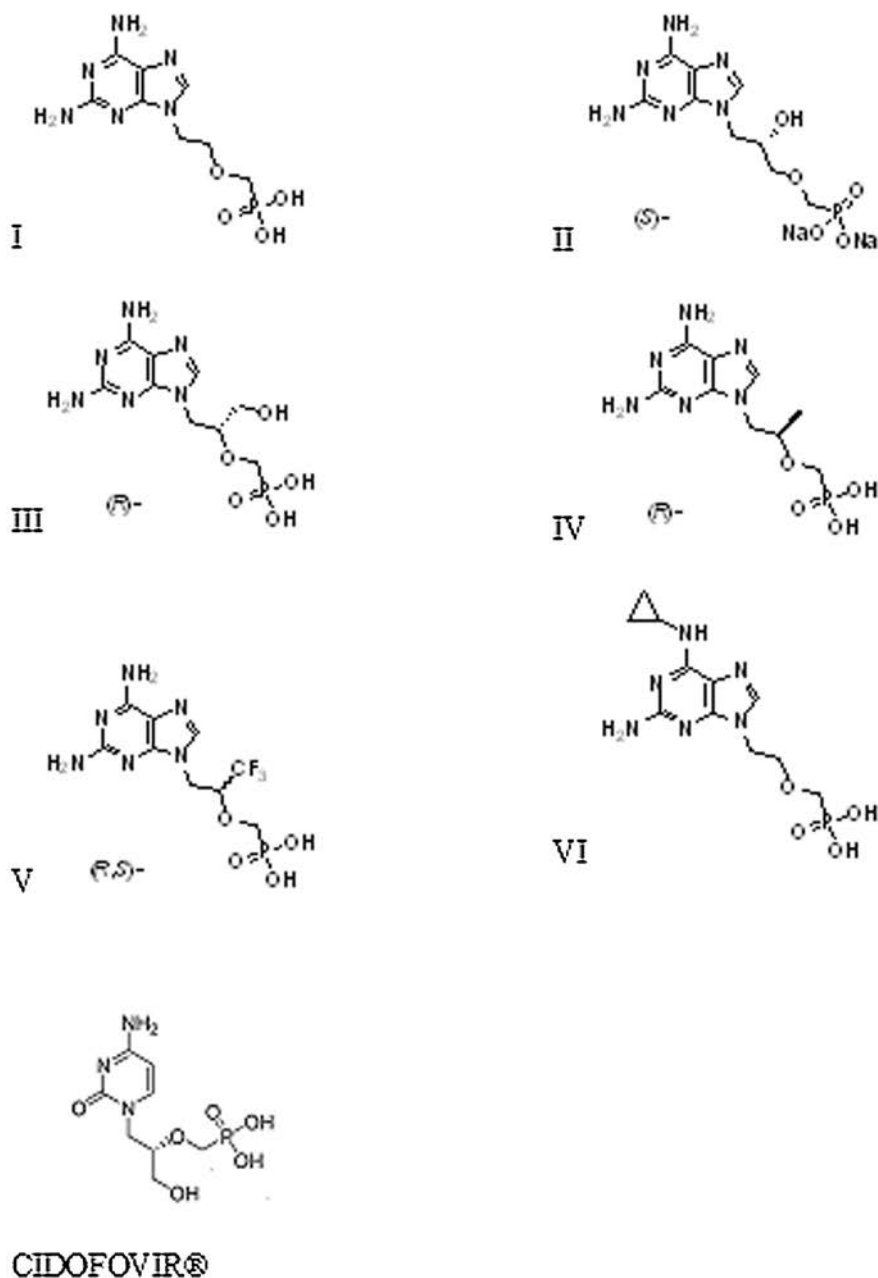


Fig. 1. Structural formulae of tested DAP-ANP analogues.

found to be the most aggressive *in vitro* against tested cell lines. Virus working stock was prepared by infecting a monolayer of cells at low multiplicity of infection and stored at -70°C in aliquots until used. Working solution of virus was prepared at the titre of 10^{-5} PFU.

2.5. In vitro cytotoxicity

MTT (Sigma–Aldrich) or XTT Cell Viability Kit (Cell Signalling Technology) test were used to determine cell viability. The test was performed according to manual provided by the producer. All kinds of cell cultures were plated at a density of 1.5×10^5 cells/ml (100 μl per well) in 96-well plates for 24 h and subsequently exposed to tested compounds. Antivirotics were tested at the concentration range of 0.78–100 μM , exposure times were 24 h. The volume of 20 μl of MTT (2.5 g/l) was added to each well and

plates were incubated for 3 h at 37°C , then 100 μl 10% SDS was added and incubated 24 h at room temperature. In case of XTT (solubilisation step based on SDS was omitted), 50 μl was added to each well and plates were incubated for 24 h at 37°C . The absorbance of the formazan solution at MTT was measured at 540 nm and at XTT at 450 nm using ELx800 Absorbance Microplate Reader (BioTek Instruments Ltd., USA) and analysed through Gen5 Data Analysis Software (BioTek Instruments Ltd.). Cytotoxicity data were confirmed by direct observation by optical microscopy (Eclipse TS200, Nikon, China) (Li et al., 2008, 2009).

2.6. Assaying of antiviral activity—XTT test

Cell cultures were plated at density of 1.5×10^5 cells/ml (100 μl of cells in each well) in 96-well plates for 24 h and subsequently exposed to tested compounds. Virus SuHV-1CAPM V-166 isolate

was added (titre 10^{-5} PFU) into each well 4 h later. After 6 days of incubation with virus the cell viability was determined by XTT test.

2.7. Inhibition of replication of viral DNA assayed by quantitative PCR

DNA isolation was done using DNeasy Blood & Tissue Kit (QIAGEN) following the producer's protocol. DNA isolation was based on a manufacturer protocol (DNeasy Blood & Tissue, QIAGEN) slightly modified to include mechanical homogenization with zirconia/silica beads (0.2 mm) in a MagNA Lyser instrument (Roche, Mannheim, Germany) at 6400 rpm for 60 s (Slana et al., 2010). The isolated DNA was used as a template for the duplex qPCR assay. The detection of Pseudorabies virus was achieved via primers and probes specific for *gB* gene (Accession KF711983). Primers (gB718F 5'-ACAAGTTCAAGGCCACATCTAC-3'; gB812R 5'-GTCYGTGAAGCGGTTCTGAT-3') were adopted from Ma et al. (2008) while probe was newly designed (gBprobe1 5'-FAM-ACGTCATCGTCACGACCGTGTGGTC-Cy5-3'). Previously published internal amplification control (IAC) was introduced to eliminate false negative samples (Slana et al., 2008). A typical optimized reaction mixture (total volume 20 μ l) contained 1 \times 480 Probe master qPCR Kit (Roche), 10 pmol of the primer set, 2 pmol of the *gB* probe, 3.5 pmol of the IAC probe, 0.2 U of Uracil DNA Glycosylase (Roche), 5 \times 10² copies of IAC diluted in TE buffer and 5 μ l of DNA template. Each run consisted of the following steps: initial denaturation at 95 °C for 7 min and 47 cycles at 95 °C for 5 s, 56 °C for 30 s and 72 °C for 10 s. The instrument LightCycler 480, (Roche, Switzerland) was used for qPCR analyses of viral DNA. Inhibition curves were calculated by the software PRISM version 5.0 (GraphPad, USA).

2.8. Quantification of tested drugs in cells in vitro—cell preparation

Cell cultures of PK-15 line were plated at density of 2×10^5 cells/ml (3 ml of cells in each well) in 6-well plates for 24 h and subsequently exposed to tested compounds (10 μ M concentration of compounds). After certain intervals of time (0 h; 1 h; 1.5 h; 2 h; 4 h; 8 h; 24 h) the cells were rinsed with PBS (phosphate buffered saline) and harvested by scraping and centrifuged (2800 rpm, 2 min) and the supernatant was discarded.

2.9. Penetration of drugs into cells and assay of intracellular concentration

Cells (samples in triplicates) were resuspended in 500 μ l methanol and sonicated for 1 min (SonoPlus 200, Bandelin, Germany). 50 μ l of the mixture was taken for the protein quantification (BCA method—Pierce BCA Protein Assay Kit, Thermo SCIENTIFIC), which is correlated to the amount of cells. The rest of the mixture was centrifuged, the supernatant was used for quantification of tested drugs by HPLC-MS/MS as described above.

2.10. Transmission electron microscopy—ultrathin section method

3% Glutaraldehyde-fixed PK-15 cells untreated or treated by 10 μ l and 50 μ l within ATV exposed to PrV were centrifuged at 800 rpm. The pellets were rinsed in Milonig buffer, post-fixed in 1% OsO₄ solution in Milonig buffer, dehydrated in 50, 70, 90, 100% acetone, embedded in Epon-Durcupan mixture (Epon 812 Serva; Durcupan, ACM Fluka) and polymerized at 60 °C for 72 h. Ultrathin sections (the thickness of 60 nm) were cut with glass knives on UC 7 ultramicrotome (UC 7, Leica, Austria). The sections were contrasted by 2% aqueous uranyl acetate and 1% aqueous lead citrate. The sections were examined under a Philips EM 208 S Morgagni transmission electron microscope (FEI, Czech Republic).

3. Results

3.1. Chromatographic separation and hydrophobicity of tested compound

The hydrophobicity of tested DAP-ANP analogues was measured to get a better insight into the ability of various analogues to penetrate through the cell membrane. Hydrophobicity of each compound was estimated by HPLC and expressed in terms of a capacity factor *k'* as defined below (see Table 2). This method is sensitive and relatively simple to allow comparison of various structural modifications in various positions with respect to their contribution to the overall hydrophobicity of the molecule. The expected hydrophobicity of tested compounds based on their structural formulae is in a good agreement with the capacity factor *k'* calculated from chromatographic data (Fig. 2 and Table 2). Tested DAP-ANP analogues possessed a range of hydrophobicities as measured by their corresponding capacity factors (Table 2). Analogues I, II and III possessed very similar hydrophobicities. Therefore, addition of 2'-hydroxyl (II) or 2'-hydroxymethyl (III) functionalities did not change hydrophobicities very much compared with parent analogue I. On the other hand, 2'-methyl (IV) and especially 2'-trifluoromethyl (V) functionalizations had more profound effects on analogue hydrophobicities. The most hydrophobic analogue VI was modified by cyclopropylation of the 6-amino group of the purine ring. An overlay of chromatograms for individual compounds is presented (Fig. 2).

3.2. Characterisation of in vitro cytotoxic effect of DAP-ANP analogues

All tested DAP-ANP analogues, including Cidofovir[®] as a positive control, were found not cytotoxic against PK-15 and RK-13 cell lines within the concentration range 1–100 μ M and 24 h exposition time. Both XTT and MTT tests gave the same results which were in a good accordance with direct observation by optical microscopy (*data not shown*). Representative data on viability of PK-15 cells treated by compound I or VI is presented at Fig. 3. These analogues demonstrated significant antiviral activity on both cell lines although differing in their hydrophobicities.

3.3. Antiviral effect of the tested compounds

The XTT test was used for prescreening antiviral activities of the DAP-ANP analogues with Cidofovir[®] as positive control. Analogues II, III and IV were not able to protect cells against viral infection resulting in visible cytopathic effects and decreases in local cell viabilities. As expected, optical isomer (R)-HPMPC was inactive in both cell lines, while Cidofovir[®] was inactive in PK-15 cell line and weakly active at 100 μ M concentration in RK-13 cell line (*data not shown*). Analogues I and VI were able to inhibit significant cytopathic effect caused by PrV infection. Therefore, these two

Table 2
Hydrophobicities of DAP-ANP analogues expressed as capacity factors.

Compound	Capacity factor <i>k'</i>	STD
I	0.747	0.006
II	0.695	0.012
III	0.724	0.008
IV	2.114	0.017
V	7.698	0.030
VI	9.040	0.035

Mobile phase: 0.8% of methanol and 0.1% of formic acid in water. The flow rate: 0.25 ml/min. The column temperature was set at 40 °C. UV detector was used for determination for capacity factors of nucleotides; capacity factor *k'* is expressed as $k' = R_t/R_0$ where is R_t retention time, and R_0 is dead volume (R_t for non retained standard).

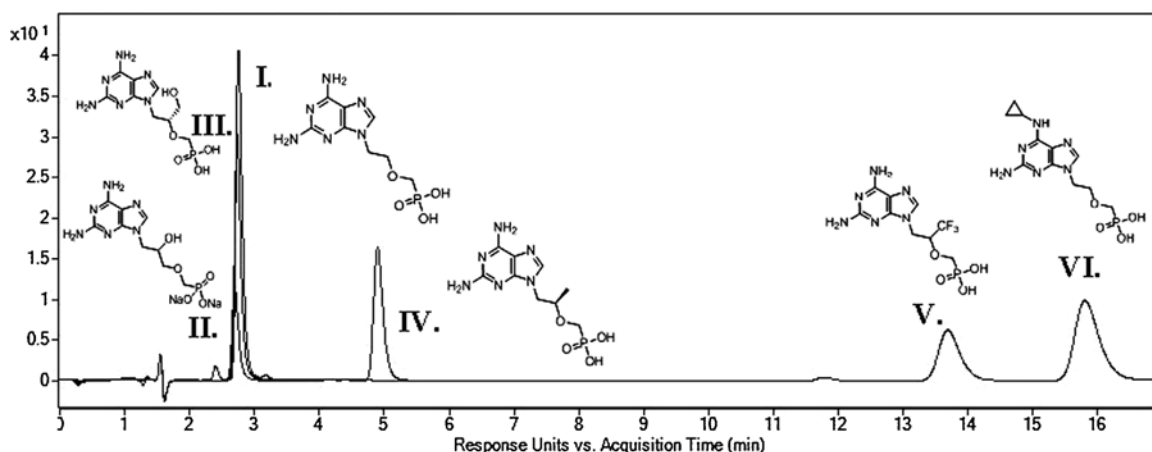


Fig. 2. HPLC separation of individual analogues (chromatographic conditions are described in Section 2). Analogues I, II and III were eluted in similar R_t , therefore the chromatogram was prepared as overlay of individual separations for analogues I, II, III, and chromatogram of the mixture of analogues IV, V and VI.

compounds were advanced to more detailed viral replication assays making use of qPCR. Indeed, viral DNA replication was inhibited by both analogues I a VI in dose dependent manner as demonstrated by qPCR analyses (Fig. 4). Indeed only compounds I and VI were able to inhibit viral DNA replication in a concentration dependent manner (Fig. 4) leading to essentially total inhibition of viral DNA replication at higher concentrations of both, reducing the level of residual viral DNA by approx. six orders of magnitude to detection limit. IC_{50} were estimated to be in submicromolar range and their selectivity index was estimated to be higher then 100 for compound I and higher then 1000 for compound VI ($SI \geq 100/IC_{50}$). In comparison, *S* optical isomer of HPMPIC reduced the level of viral DNA in RK-13 cells by only two orders of magnitude at a concentration of 100 μ M (data not shown).

The antiviral effects of analogues I and VI were confirmed by optical microscopy, which demonstrated preservation of cell monolayers and significant reductions in cytopathic effects induced by PrV. Infected control cells lost monolayer organisation, and were observed dead or in final stages of apoptosis characterised by disintegration of nucleus and release of cytoplasm. Cells treated with analogues I or VI remained adherent, nuclei were of normal appearance with 1–4 nucleoli and cells exhibited well organised structures. Some cellular debris originating from dead cells was observable on cell monolayers, which is an event common during long term cultivation. Micrographs (Fig. 5) clearly demonstrate the antiviral effects of analogue VI (10 μ M) on the PK-15 cell line.

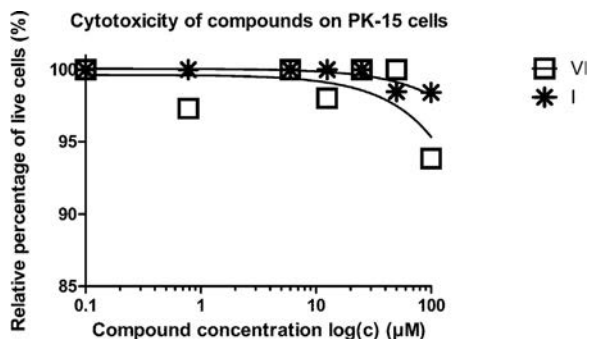


Fig. 3. Viability of PK-15 cells treated by DAP-ANP analogues I and VI. PK-15 cells were exposed for 24 h to DAP-ANP analogues I or VI within the concentration range of 0.8–100 μ M. Viability was assayed by XTT test (triplicate setting) and confirmed by optical microscopy. Owing to logarithmic scale of concentration, point at 0.1 μ M represents untreated controls without added drugs.

3.4. Demonstration of antiviral effects at subcellular levels by electron microscopy

Electron microscopy was used to confirm viral replication and cessation of viral replication in tissue culture. Typical signs of massive production of viruses were found in the nuclei of control infected cells. Typical clusters of crystalline arrayed capsids are seen in nuclei (Fig. 6C). Virus particles are shed into medium or directly transmitted to neighbouring cells by exocytosis–endocytosis mechanism (Fig. 6B). Morphological changes in cell structures are also typical for virus induced apoptosis. Finally detachment of cells, condensation of chromatin, disappearance of nucleoli, destruction of nuclei and of nuclear membranes are well recognisable (Fig. 6B, C, E). By contrast, cells treated with either analogue I or VI were protected against massive viral infection damage and virus induced apoptosis (Fig. 6F). In a small portion of cells the process of viral replication was induced, but most viral particles produced appeared defective and probably without encapsulated DNA (Fig. 6G, H). These electron microscopy data confirmed results obtained by XTT viability tests (Fig. 3), qPCR (Fig. 4) and optical microscopy (Fig. 5).

3.5. Penetration of drug into cells as assayed by HPLC-MS/MS

The concentration of tested DAP-ANP analogues in cells was assayed by HPLC-MS/MS. Cellular penetration of drugs into cells typically obeys simple saturation kinetic and is a rapid process. A representative curve for hydrophobic analogue VI is presented (Fig. 7B) showing how analogues VI reached approx 90% saturation in 2 h.

Hydrophobic analogue V as well VI was also found to penetrate cells rapidly in comparison to the more hydrophilic analogues I, II, III, IV and positive control (*S*)-HPMPIC (Fig. 7A). Curiously, although both DAP-ANP analogues I and VI were the most potent antiviral agents, yet analogue I accumulated much less readily into target cells than VI given that I is much more hydrophilic in character than VI. Therefore, increasing hydrophilicity did not appear to correlate directly with increasing antiviral efficacy.

4. Discussion

Viral DNA-polymerase is an established molecular target for antiviral drugs directed against herpesviruses. The effectiveness of antiviral drugs such as ganciclovir and acyclovir that act at the viral DNA-polymerase is well documented in literature against

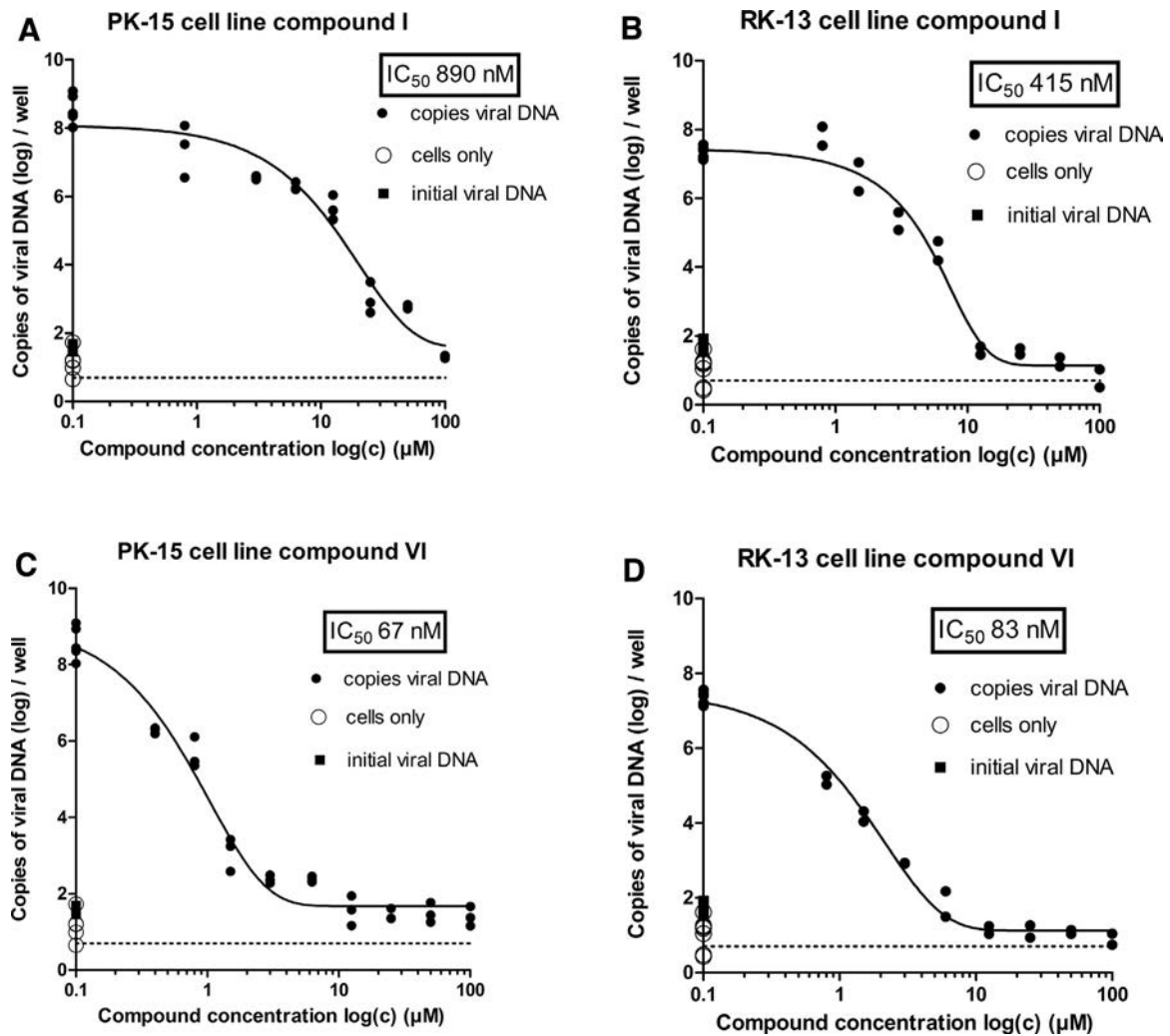


Fig. 4. qPCR assay of inhibitory effect of compound I (Fig. 4A, B) a VI (Fig. 4C, D) on replication of viral DNA. Dashed lines represent detection limit of the qPCR method for PrV DNA. Assays were run in triplicates (PK-15 cells) or duplicates (RK-13 cells). Full squares represent values of viral DNA (the number of copies per reaction) added to cell culture to initiate infection. Theoretically, these values represent maximal possible level of residual viral DNA assayed by qPCR if replication is totally inhibited. Open circles represent negative control (cells without added virus). Full circles represent copies of viral DNA in infected cells.

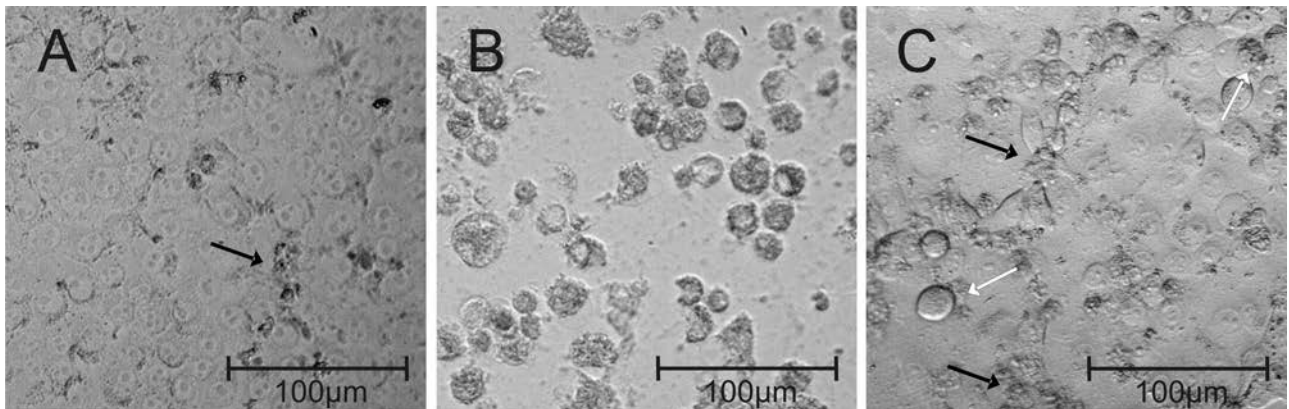


Fig. 5. Cytopathic effect induced by PrV in PK-15 cells and protective effect of analogue VI at 10 μM concentration. (A) control PK-15 cells exhibit intact and well-organised monolayer. Nuclei with 1–4 nucleoli are recognisable, black arrow marks debris upon cell monolayer; (B) destruction of cell monolayer induced by PrV. The most of the cells are shriveled as the sign of the final stage of necrosis; (C) cells treated by 10 μM concentration of compound VI. Necrotic morphology is observed in some cells, but the cell monolayer is preserved; black arrows mark locations of cell debris, white arrows pick out necrotic cells. Micrographs were taken at day 6 after inoculation of tissue culture by virus.

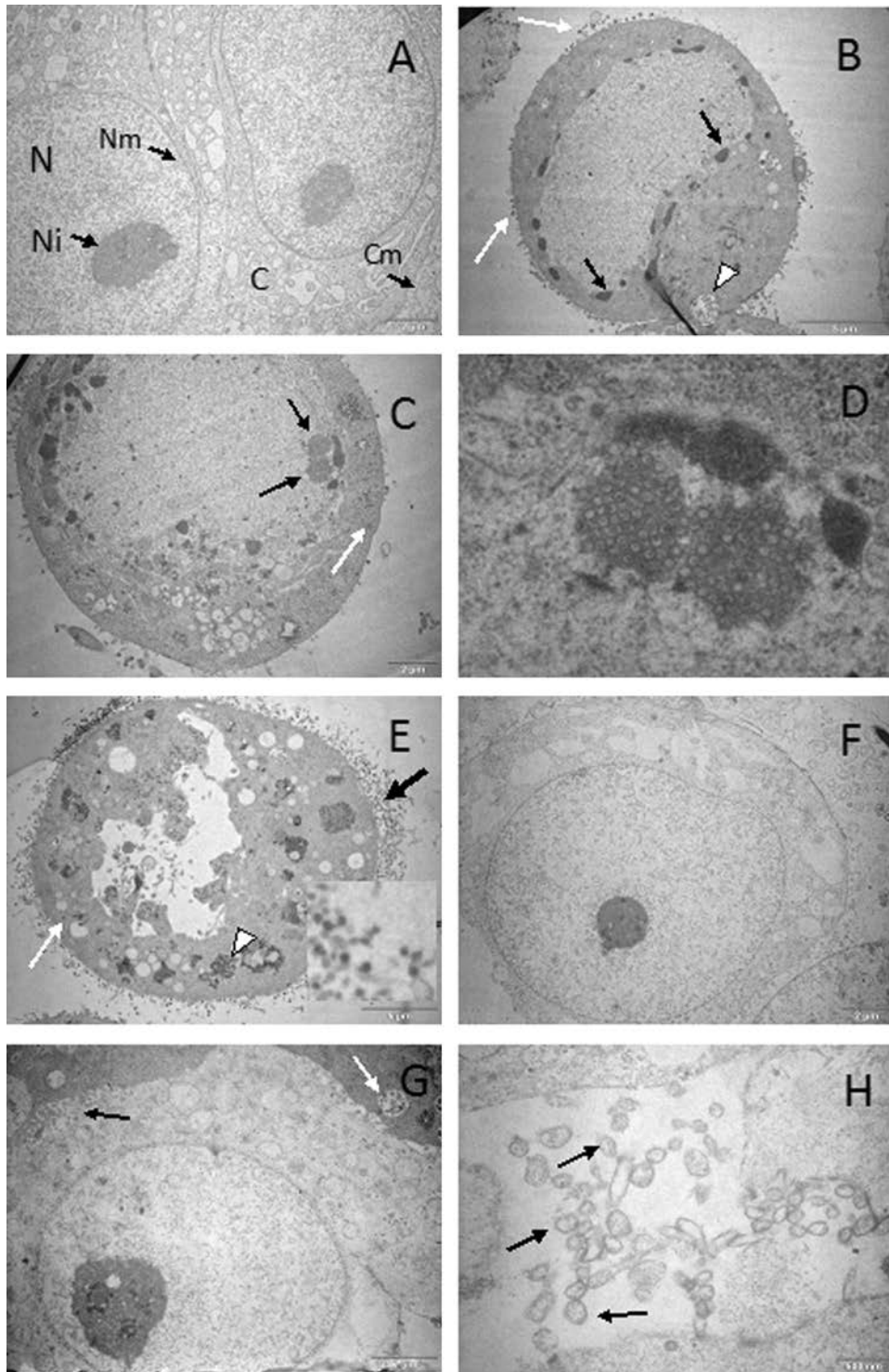


Fig. 6. Inhibition of viral replication in PK-15 cells demonstrated by electron microscopy. (A) Control untreated and uninfected PK-15 cells. (N—nucleus; Ni—nucleoli; Nm—nuclear membrane; C—cytoplasm; Cm—cytoplasm membrane). (B) PK-15 cells infected by PrV. Chromatin is condensed close to the rest of the nuclear membrane (black arrow), nucleoli have disappeared, the cell has lost adherence, complete viral particles are shed into medium (white arrows), note the vacuoli with viral particles which are directly transported into a neighbour cell (white arrow head). (C) PK-15 cells infected by PrV. Two clusters of crystalline arrayed capsids (capsids of A type) are seen in the nucleus (black arrows). (D) Detail from (C). Two clusters of crystalline arrayed capsids (black arrows) are positioned close to the rest of condensed nuclear DNA (black arrowhead). In some capsids the process of incorporation of viral DNA starts (note black dot inside the capsid). (E) Massive shedding of viral particles from PK-15 cells. Cell has lost adherence, the nucleus is completely destroyed and vacuoli are filled with matured viral particles (white arrowhead). Some immature and mature viral particles are presented in cytoplasm (white arrow) and matured viral particles are released from the cell into the medium in large numbers (thick black arrows). Insert shows matured viral particles shed into medium. (F) PK-15 cells treated with compound VI (10 μ M) and infected with PrV. The observed cell is in a monolayer surrounded by other cells. No pathological changes are observable in nucleus or in cytoplasm. Viral particles are not observed in most cells. (G) PK-15 cells treated with compound VI (10 μ M) and infected with PrV. Small portion of cells become infected and produce viral particles. The production is not massive and infection does not cause pathological changes in the nuclei and cytoplasm of most of cells. Only a small number of apoptotic cells are observed and the monolayer is kept intact. The viral particles produced are in large portion defective in DNA content. Viral particles are seen in vacuoli (white arrow) and released into intercellular spaces (black arrows). (H) Detail of viral particles produced by PK-15 cell treated with analogue VI (10 μ M). Most of the particles are defective and do not contain viral DNA (black arrows).

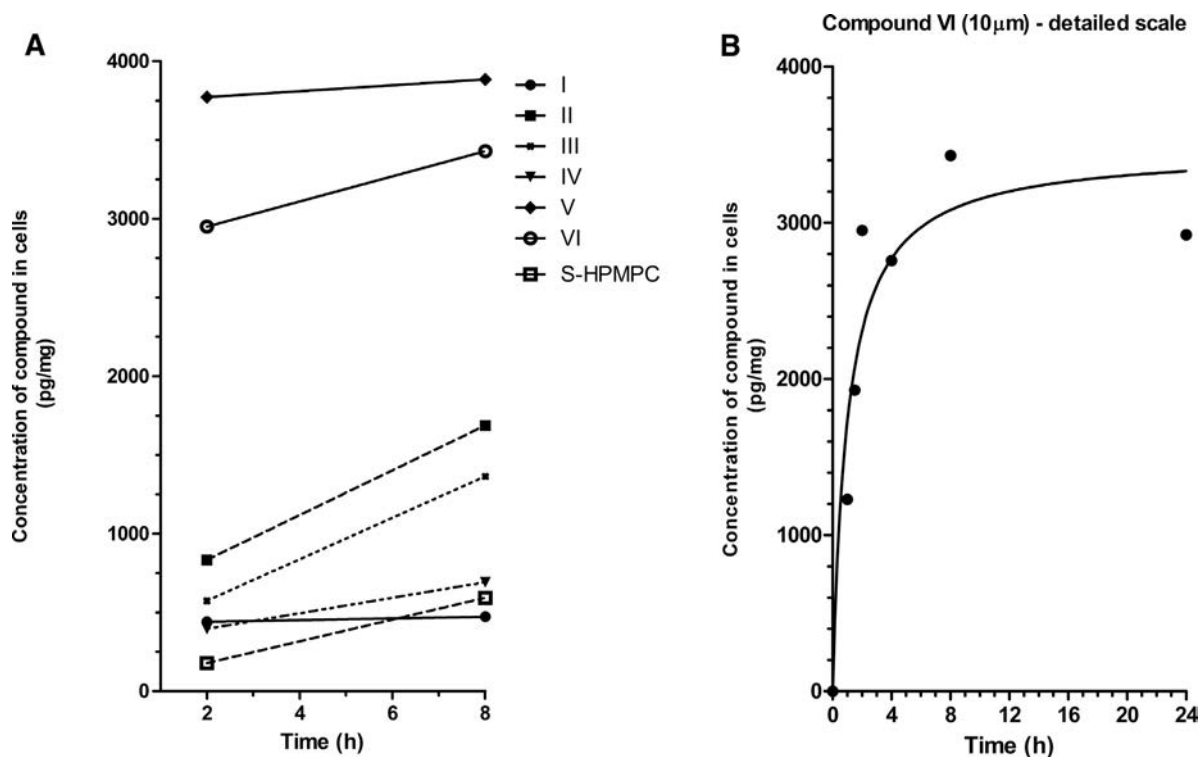


Fig. 7. Penetration of drug into cells as assayed by HPLC-MS/MS. (A) Intracellular concentration of tested DAP-ANP analogues in PK-15 cells at time 2 and 8 h of incubation. PK-15 cells were incubated in triplicates for 2 and 8 h with tested compounds (10 μ M). Obtained samples were analysed by HPLC-MS/MS (details are described in Section 2). (B) Penetration of analogue VI into PK-15 cells. PK-15 cells were incubated in triplicate for various times with analogue VI (10 μ M). Obtained samples were analysed by HPLC-MS/MS (details are described in Section 2).

herpesvirus infections in both human and animals (Garré et al., 2007; De Clercq et al., 2006). Overall we have tested about 30 acyclic nucleoside phosphonate (ANP) analogues looking for active molecules grouped according to their nucleobase structure into various structural families. Here we report on the screening of six bespoke diaminopurine-based acyclic nucleoside phosphonate (DAP-ANP) analogues. Of these, two analogues I and VI (Fig. 1) were found active against PrV infection and were studied in more detail.

In *in vitro* infection assays, penetration of drugs through cell membranes is a primary obstacle to reaching cellular targets. In our previous paper we have shown that entrapment of Cidofovir into cationic liposomes can significantly improve antiviral effects *in vitro* against BHV-1 (Korvasova et al., 2012). The primary reason for this was that nanocarriers like liposomes can facilitate drug delivery to cells by promoting improved internalization into cells by endocytosis. Alternatively, ANPs have been rendered more bioavailable to their cellular targets by preparation of prodrugs increasing their hydrophobic character through esterification of their phosphonate moieties. Indeed, hydrophobicity is a crucial factor that correlates with cell penetration in the absence of transmembrane transport mechanisms. For this reason, increasing drug hydrophobicity can be an important way to improve drug bioavailability to cellular targets *in vitro* and even *in vivo*.

Here we observe that the two analogues V and VI are rendered more hydrophobic than parent DAP-ANP analogue I by introduction of C2'-CF₃- and N⁶-cyclopropyl moieties respectively. Yet the most active DAP-ANP analogues were actually found to be parent analogue I and N-cyclopropyl analogue VI (compare Table 2, Figs. 2, 4 and 7A). Having said this, apparent cellular IC₅₀ values estimated from PrV cellular infection models (Fig. 4) clearly demonstrate that analogue VI is 10-fold more effective than parent I. On the other hand, analogue VI appears to be 10-fold more bioavailable to target in cells than parent I (Fig. 7A). It cannot be determined for now

whether higher hydrophobicity or lower inhibitory constant K_i (or both) are responsible for higher antiviral activity of compound VI in comparison to compound I. Therefore we would suggest that both analogue I and VI are in fact likely to have equivalent levels of efficacy once at target. Accordingly, the importance of ensuring optimal drug bioavailability to target is clear in order to optimise drug performance. All cell lines tested in preliminary experiments (MDCK, MDBK, PK-15, RK-13, VERO) were susceptible towards PrV viral strain SuHV-1CAPM V-166 and cytopathic effects were observed after virus inoculation in all cases. On the other hand, all tested DAP-ANP analogues did not exhibit cytotoxicity towards any of these cell lines. Therefore, it can be assumed, that analogues I and VI are selective inhibitors of viral DNA polymerase, but not eukaryotic host cell DNA polymerase.

Viral infections of cell lines PK-15 and RK-13 were studied in detail in each case since both represent standard model tissue culture models for *in vitro* PrV infection. The course of viral infection documented by electron microscopy (Fig. 6B–E) is in accordance with data published by others in PrV-infected cell cultures (Klupp et al., 2001; Klupp et al., 2005; Robbins et al., 1986) or pig's tissues (Aleman et al., 2003). Contrary to some publications (Aleman et al., 2003), production of L-particles appeared low. The multiplication of PrV in cell lines was documented by electron microscopy and qPCR, including the presence of crystal-like arrays of capsids in nuclei, viral particles plus agglomerates of tegument protein in cellular cytoplasm, and shedding of complete viral particles into extracellular medium followed by apoptosis of the infected cells. In non-treated cells the numbers of copies of viral DNA reached the value of 10⁶–10⁷ (6 days after cultivation) (Fig. 4). Administration of analogues I and VI was seen to reduce the number of copies of viral DNA to basal levels comparable to DNA levels in viral inoculum added to cell culture. Inhibition of viral DNA replication was also accompanied by a reduction in numbers

of viral particles in cells and culture medium. Proteins of late phase of virus replication cycle were not found present. Furthermore, nuclear capsid and aggregates of tegument proteins—typical products of late phase of viral replication – were not observable in cells treated by the active compounds either. All these facts implicate the inhibition of viral DNA polymerase resulting in suppressed replication of viral DNA, as expected for ANP analogues related to the well established inhibitors of viral DNA polymerase such as Cidofovir[®]. Intriguingly, when Cidofovir[®] was evaluated in the assays described here, mild antiviral activity was seen (viral DNA replication was reduced by 1–2 order of magnitude at 100 μ M concentration) against both bovine herpesvirus BHV-1 (Korvasova et al., 2012) and PrV (*data not shown*), whereas analogues I and VI (as well as II, III, IV and V) were not active *in vitro* against BHV-1 in MDBK cells. Such selectivity is of interest for future studies on structural relationship between herpesvirus DNA-polymerases and different classes of ANP inhibitors.

Although antiviral chemotherapy has become a standard practice in treatment of herpesvirus infection in humans, the veterinary use of antiviral drugs is rare. Treatment of feline herpesvirus-1 infections could be mentioned as an example (Williams et al., 2005). Nucleotide based drugs like bromovinyl deoxyuridine, acyclovir and 2'-nor-2'-deoxyguanosine were tested for their anti-PrV effect *in vitro* and *in vivo* using lab mice. Substantial prolongation of mouse survival has been demonstrated with 2'-nor-2'-deoxyguanosine (Field, 1985). Correspondingly, while there has been intensive research running in the field of PrV vaccine development, only limited attention has been focused on antiviral drug therapy. Currently most published studies are focused on *in vitro* experiments. These include the use of the herb *Houttuynia cordata* belonging to traditional Chinese herb medicine that was tested *in vitro* (Ren et al., 2011) as well as Glycyrrhizin, the most important bioactive compound of liquorice root (*Glycyrrhiza radix*), that was used in combination with lithium chloride (Sui et al., 2010). Direct antiviral effects have yet to be demonstrated in *in vivo* model experiments. In our case, now that antiviral effects have been demonstrated *in vitro*, with minimal cytotoxicities, and lead analogues I and VI are now ready for studies with the mouse model of Aujeszky's disease, followed by early stage "clinical" studies with dogs infected by PrV. Anti-viral drug therapy of Aujeszky's disease in dogs is a real challenge because of the short time between the first symptoms of infection and death (1–3 days) and the tendency of PrV to replicate inside of neurons (Kramer and Enquist, 2013; Zhang et al., 2015). Accordingly, anti-viral drugs should be administered as soon as first symptoms of disease are observed although this will lead to little improvement unless the drugs are properly bioavailable to the sites of PrV replication in the nuclei of neurons as well. Another important aspect of future potential treatment should also be the preservation of neuro-motoric function of treated dogs and suppression of viral reactivation. These aspects are of importance in general too in the treatment of other herpesviruses infections.

5. Conclusion

Two 2,6-diaminopurine-based acyclic nucleoside phosphonates (DAP-ANPs) were selected as promising structures for further development into potential drugs with antiviral activity against PrV. *In vitro* data demonstrated considerable antiviral activity by both analogues I and VI although the greater bioavailability of VI to target appeared to promote a 10-fold drop in apparent cellular IC₅₀ compared with I. Further modification of the purine 6-amino functional group is of interest to prepare future ANPs that might be more effective even than analogue VI. On the other hand, the sorts of functionalizations of the acyclic bridge moiety from purine to phosphonate that gave rise to inactive

analogues, II, III, IV and V did not appear to promote antiviral activities at all so can be disregarded going forward. *In vivo* studies with analogue I and VI will now be progressed in order to demonstrate antiviral activity and safety in the standard murine model of PrV infection.

Conflicts of interest

None.

Acknowledgements

By this paper we would like to revere the memory of prof. Antonín Holý, deceased in 2012, who pioneered the field of antiviral drugs at the Institute of Organic Chemistry and Biochemistry, Prague and whose world-wide scientific influence was appreciated.

Project CENATOX, Grant Agency of Czech Republic, GAP503/12/G147 (Jaroslav Turánek); the Ministry of Education, Youth and Sports CZ.1.07/2.3.00/20.0164 (Jaroslav Turánek, Milan Raška), MZE0002716202 Czech Ministry of Agriculture; postdoc position of Štěpán Koudelka was supported by the European Social Fund and the State Budget of the Czech Republic—Project FNUSA-ICRC, Support for Neurological Research and Development Teams through Postdoc Position Formations CZ.1.07/2.3.00/30.0043.

Luděk Eyer, Michal Slaný, Kamil Kovařík and Daniel Růžek were supported by a project LO1218, with financial support from the MEYS of the Czech Republic under the NPU I program.

The team headed by Jaroslav Turánek, Daniel Růžek, Milan Raška and Andrew D. Miller are obligated to the Ministry of Education, Youth and Sports for supporting the project "FIT" (Pharmacology, Immunotherapy, nanoToxicology).

References

- Aleman, N., Quiroga, M.I., Lopez-Pena, M., Vazquez, S., Guerrero, F.H., Nieto, J.M., 2003. L-Particle production during primary replication of pseudorabies virus in the nasal mucosa of swine. *J. Virol.* 77, 5657–5667.
- Cay, A.B., Letellier, C., 2009. Isolation of Aujeszky's disease virus from two hunting dogs in Belgium after hunting wild boars. *Vlaams Diergeneeskundig Tijdschrift* 78, 194–195.
- De Almeida, A.P., Miranda, M.M.F.S., Simoni, I.C., Wigg, M.D., Lagrota, M.H.C., Costa, S.S., 1998. Flavonol monoglycosides isolated from the antiviral fractions of *Persea americana* (Lauraceae) leaf infusion. *Phytother. Res.* 12, 562–567.
- De Clercq, E., 1998. Antiviral agents that are active against CMV: potential of cidofovir for the treatment of CMV and other virus infections. *Monogr. Virol. Basel. Karger* 21, 193–214.
- De Clercq, E., 2002. Cidofovir in the treatment of poxvirus infections. *Antiviral Res.* 55, 1–13.
- De Clercq, E., Brancale, A., Hodge, A.V., Field, H.J., 2006. Antiviral Chemistry & Chemotherapy's current antiviral agents FactFile 2006 (1st edition). *Antivir. Chem. Chemother.* 17, 113–166.
- Dong, B., Zarlenga, D.S., Ren, X., 2014. An overview of live attenuated recombinant pseudorabies viruses for use as novel vaccines. *J. Immunol. Res.* 824630.
- Field, H.J., 1985. Chemotherapy of Aujeszky's disease (pseudorabies) in the mouse by means of nucleoside analogues: bromovinyldeoxyuridine acyclovir, and dihydropropoxymethylguanine. *Antiviral Res.* 5, 157–168.
- Fischer, L., Barzu, S., Andreoni, C., Buisson, N., Brun, A., Audonnet, J.C., 2003. DNA vaccination of neonate piglets in the face of maternal immunity induces humoral memory and protection against a virulent Pseudorabies virus challenge. *Vaccine* 21, 1732–1741.
- Garré, B., Van der Meulen, K., Nugent, J., Neyts, J., Croubels, S., De Backer, P., Nauwynck, H., 2007. In vitro susceptibility of six isolates of equine herpesvirus 1 to acyclovir ganciclovir, cidofovir, adefovir, PMEDAP and foscarnet. *Vet. Microbiol.* 122, 43–51.
- Holy, A., Guenter, J., Dvorakova, H., Masojidkova, M., Andrei, G., Snoeck, R., Balzarini, J., De Clercq, E., 1999. Structure–antiviral activity relationship in the series of pyrimidine and purine N-[2-(2-phosphonomethoxy)ethyl] nucleotide analogues 1. Derivatives Substituted at the carbon atoms of the base. *J. Med. Chem.* 42, 2064–2086.
- Holy, A., Votruba, I., Tloustova, E., Masojidkova, M., 2001. Synthesis and cytostatic activity of N-[2-(2-phosphonomethoxy)alkyl] derivatives of N⁶-substituted adenines 2,6-diaminopurines and related compounds. *Collect. Czech Chem. Commun.* 66, 1545–1592.

- Jansa, P., Kolman, V., Kostinova, A., Dracinsky, M., Mertlikova-Kaiserova, H., Janeba, Z., 2011. Efficient synthesis and biological properties of the 2'-trifluoromethyl analogues of acyclic nucleosides and acyclic nucleoside phosphonates. *Collect. Czech Chem. Commun.* 76, 1187–1198.
- Jansa, P., Baszczynski, O., Prochazkova, E., Dracinsky, M., Janeba, Z., 2012. Microwave-assisted hydrolysis of phosphonate diesters: an efficient protocol for the preparation of phosphonic acids. *Green Chem.* 14, 2282–2288.
- Kim, S.J., Kim, H.K., Han, Y.W., Aleyas, A.G., George, J.A., Yoon, H.A., Yoo, D.J., Kim, K., Eo, S.K., 2008. Multiple alternating immunizations with dna vaccine and replication incompetent adenovirus expressing gB of pseudorabies virus protect animals against lethal virus challenge. *J. Microbiol. Biotechnol.* 18, 1326–1334.
- Klupp, B.G., Granzow, H., Karger, A., Mettenleiter, T.C., 2005. Identification, subviral localization, and functional characterization of the pseudorabies virus UL17 protein. *J. Virol.* 79, 13442–13453.
- Klupp, B.G., Granzow, H., Mundt, E., Mettenleiter, T.C., 2001. Pseudorabies virus UL37 gene product is involved in secondary envelopment. *J. Virol.* 75, 8927–8936.
- Kong, H., Zhang, K., Liu, Y., Shang, Y., Wu, B., Liu, X., 2013. Attenuated live vaccine (Bartha-K16) caused pseudorabies (Aujeszky's disease) in sheep. *Vet. Res. Commun.* 37, 329–332.
- Korvasova, Z., Drasar, L., Masek, J., Turanek Knotigova, P., Kulich, P., Matiasovic, J., Kovarcik, K., Bartheldyova, E., Koudelka, S., Skrabalova, M., Miller, A.D., Holy, A., Ledvina, M., Turanek, J., 2012. Antiviral effect of HPMPC (Cidofovir[®]), entrapped in cationic liposomes: In vitro study on MDBK cell and BHV-1 virus. *J. Control Release* 160, 330–338.
- Kramer, T., Enquist, L.W., 2013. Directional spread of alphaherpesviruses in the nervous system. *Viruses* 5, 678–707.
- Krecmerova, M., Jansa, P., Dracinsky, M., Sazelova, P., Kasicka, V., Neyts, J., Auwerx, J., Kiss, E., Goris, N., Stepan, G., Janeba, Z., 2013. 9-[2-(*R*)-(phosphonomethoxy)propyl]-2,6-diaminopurine (*R*)-PMPDAP and its prodrugs: optimized preparation, including identification of by-products formed, and antiviral evaluation in vitro. *Bioorg. Med. Chem.* 21, 1199–1208.
- Krishnan, B.R., 2000. Current status of DNA vaccines in veterinary medicine. *Adv. Drug Deliv. Rev.* 43, 3–11.
- Li, X., Turanek, J., Knoetigova, P., Kudlackova, H., Masek, J., Pennington, D.B., Rankin, S.E., Knuton, B.L., Lehmler, H.J., 2008. Synthesis and biocompatibility evaluation of fluorinated: single-tailed glucopyranoside surfactants. *New J. Chem.* 32, 2169–2179.
- Li, X., Turanek, J., Knoetigova, P., Kudlackova, H., Masek, J., Pennington, D.B., Rankin, S.E., Knuton, B.L., Lehmler, H.J., 2009. Hydrophobic tail length: degree of fluorination and headgroup stereochemistry are determinants of the biocompatibility of (fluorinated) carbohydrate surfactants. *Colloids Surf. B Biointerfaces* 73, 65–74.
- Ma, W., Kelly, M., Lager, K.M., Richt, J.A., Stoffregen, W.A., Zhou, F., Yoon, K.J., 2008. Development of real-time polymerase chain reaction assays for rapid detection and differentiation of wild-type pseudorabies and gene-deleted vaccine viruses. *J. Vet. Diagn. Invest.* 20, 440–447.
- McGeoch, D.J., Cook, S., 1994. Molecular phylogeny of the alphaherpesvirinae subfamily and a proposed evolutionary timescale. *J. Mol. Biol.* 22, 9–22.
- Olson, G.R., Miller, L.D., 1986. Studies on the pathogenesis of heart lesions in dogs infected with pseudorabies virus. *Can. J. Vet. Res.* 50, 245–250.
- Pancheva, S.N., 1991. Potentiating effect of ribavirin on the anti-herpes activity of acyclovir. *Antiviral Res.* 16, 151–161.
- Pomeranz, L.E., Reynolds, A.E., Hengartner, C.J., 2005. Molecular biology of pseudorabies virus: impact on neurovirology and veterinary medicine. *Microbiol. Mol. Biol. Rev.* 69, 462–500.
- Ren, X., Sui, X., Yin, J., 2011. The effect of Houttuynia cordata injection on pseudorabies herpesvirus (PrV) infection in vitro. *Pharm. Biol.* 49, 161–166.
- Robbins, A.K., Whealy, M.E., Watson, R.J., Enquist, L.W., 1986. Pseudorabies virus gene encoding glycoprotein gIII is not essential for growth in tissue culture. *J. Virol.* 59, 635–645.
- Slana, I., Kaevska, M., Kralik, P., Horvathova, A., Pavlik, I., 2010. Distribution of Mycobacterium avium subsp avium and M: a. hominissuis in artificially infected pigs studied by culture and IS901 and IS1245 quantitative real time PCR. *Vet. Microbiol.* 144, 437–443.
- Slana, I., Kralik, P., Kralova, A., Pavlik, I., 2008. On-farm spread of Mycobacterium avium subsp: paratuberculosis in raw milk studied by IS900 and F57 competitive real time quantitative PCR and culture examination. *Intl. J. Food Microbiol.* 128, 250–257.
- Sui, X., Yin, J., Ren, X., 2010. Antiviral effect of diammonium glycyrrhizinate and lithium chloride on cell infection by pseudorabies herpesvirus. *Antiviral Res.* 85, 346–353.
- Van Alstine, W., Anderson, T., Reed, D., Wheeler, J., 1984. Vaccine induced pseudorabies in lambs. *J. Am. Vet. Med. Assoc.* 185, 409–410.
- Van Rooij, E.M., Rijsewijk, F.A., Moonen-Leusen, H.W., Bianchi, A.T., Rziha, H.J., 2010. Comparison of different prime-boost regimes with DNA and recombinant Orf virus based vaccines expressing glycoprotein D of pseudorabies virus in pigs. *Vaccine* 28, 1808–1813.
- Williams, D.L., Robinson, J.C., Lay, E., Field, H., 2005. Efficacy of topical aciclovir for the treatment of feline herpetic keratitis: results of a prospective clinical trial and data from in vitro investigations. *Vet. Rec.* 157, 254–257.
- Wittmann, G., Jakubik, J., Ahl, R., 1980. Multiplication and distribution of Aujeszky's disease (pseudorabies) virus in vaccinated and non-vaccinated pigs after intranasal infection. *Arch. Virol.* 66, 227–240.
- Woodland, D.L., 2004. Jump-starting the immune system: prime-boosting comes of age. *Trends Immunol.* 25, 98–104.
- Yoon, H.A., Aleyas, A.G., George, J.A., Park, S.O., Han, Y.W., Kang, S.H., Cho, J.G., Eo, S.K., 2006. Differential segregation of protective immunity by encoded antigen in DNA vaccine against pseudorabies virus. *Immunol. Cell Biol.* 84, 502–511.
- Zhang, L., Zhong, C., Wang, J., Lu, Z., Liu, L., Yang, W., Lyu, Y., 2015. Pathogenesis of natural and experimental pseudorabies virus infections in dogs. *Virol. J.* 12, 44.

5. ANTIVIROTIKA STRUKTURNĚ ODLIŠNÁ OD NUKLEOSIDŮ

Kromě nukleosidových analogů byla popsána řada inhibitorů, chemicky odlišných od nukleosidů, které interagují s různými virovými proteiny, např. s reverzními transkriptázami, proteázami, neuramidinázami, nebo povrchovými proteiny zodpovědnými za adsorpci viru na buněčný receptor a následnou fúzi. Další typy inhibitorů mohou rozpoznávat různé buněčné struktury a blokovat některé buněčné biochemické dráhy, které virus využívá pro svoji replikaci (např. blokace autofagie). V současnosti se řada takových léčiv používá při terapii infekcí vyvolaných HIV, virem žloutenek, herpetickými virem nebo virem chřipky, často v kombinaci s nukleosidovými antiviroty. Jako příklad takových léčiv uvedme legislativně schválené inhibitory reverzní transkriptázy HIV nevirapin, delavirdin nebo andefavirenz (Usach et al., 2013). K dalším patří inhibitory NS3/4A proteázy viru žloutenky typu C (např. simeprevir, asunaprevir, paritaprevir a mnohé další) (Banerjee and Reddy, 2016), nebo inhibitory neuramidinázy viru chřipky (např. adamantan a jeho deriváty) (Eyer and Hruška, 2013). Následující text se blíže zabývá takovými antiviroty, které uplatňují svůj antivirový účinek v různých fázích virového životního cyklu a které byly popsány v pracích, jež jsou prezentovány v tomto habilitačním spisu.

5.1. INHIBITORY FÚZE VIRIONU S HOSTITELSKOU BUŇKOU

Fúze obalených virů s hostitelskou buňkou je jedním s klíčových kroků, které se uplatňují při iniciaci virové infekce. Některé obalené viry vstupují do buňky prostřednictvím fúze virové membrány (obalu) s plazmatickou membránou hostitelské buňky (např. zástupci čeledi *Herpesviridae* nebo *Poxviridae*). Jiné viry, např. flaviviry nebo koronaviry, využívají pro vstup do buňky receptorem zprostředkovanou endocytózu. V takovém případě dochází k fúzi virového obalu s membránou endozomu.

V tomto habilitačním spisu je prezentována práce „**Arbidol (Umifenovir): A broad-spectrum antiviral drug that inhibits medically important arthropod-borne flaviviruses**“ (Haviernik et al., 2018), která popisuje antivirový účinek arbidolu, látky, která byla legislativně schválena v Rusku a Číně pro léčbu chřipky a která je širokospektrálním antivirotem proti četným RNA a DNA virům. Z hlediska mechanismu účinku dochází k interkalaci arbidolu do lipidové membrány viru a k interakci s virovými fúzními proteiny (Blaising et al., 2014). U viru chřipky bylo prokázáno, že arbidol interaguje s molekulami hemagglutininu a blokuje pH-indukovanou přeměnu hemagglutininu do aktivní fúzogenní formy (Villalain et al., 2010). V naší laboratoři jsme popsali antivirový účinek arbidolu proti některým klíšťatům a komárům přenášeným flavivirům, konkrétně VKE, viru horečky západního Nilu a viru Zika ve Vero buňkách, na kterých arbidol vykazoval příznivý cytotoxický profil. Inhibiční efekt arbidolu byl silně závislý na typu buněčné kultury, např. v buňkách PS, neuroblastech nebo buňkách lidského hepatokarcinomu (Huh-7) nebyl efekt patrný a pro mnohé testované buněčné linie i primární buňky byla látka značně toxická. Později, v souvislosti s koronavirovou pandemií byla aktivita arbidolu prokázána i proti SARS-CoV-2 (Alavi Darazam et al., 2021).

5.2. INHIBITORY ACIDIFIKACE BUNĚČNÝCH ENDOZOMŮ

Viry, které využívají pro svůj vstup do hostitelské buňky receptorem zprostředkovanou endocytózu, vyžadují pro správnou funkci svých fúzogenních proteinů snížené pH uvnitř

endozomů. Toho je dosaženo pomocí vakuolárních (H⁺)ATPáz (V-ATPáz), což jsou proteinové komplexy tvořené z několika podjednotek, lokalizované v membráně endozomu, které jsou zodpovědné za přenos protonů do vnitřního prostoru (lumenu) endozomu. Energie potřebná pro přenos protonů proti koncentračnímu gradientu je získávána štěpením molekul ATP, proto má proteinový komplex charakter ATPázy (Jefferies et al., 2008). V současnosti bylo popsáno několik inhibitorů buněčných V-ATPáz, řada z nich má výrazné antikancerogenní, antibakteriální, antiparazitární a antivirové účinky. Mezi klasické inhibitory V-ATPáz patří bafilomycin A1, avšak recentně byly objeveny desítky dalších, jako např. konkanamycin, archazolid, apikulareny, lobatamidy, oximidiny, 3-bromopyruvát a mnoho dalších (Pérez-Sayás et al., 2009).

Přírodní látka diphyllin, patřící do rodiny rostlinných arylnaftalidových lignanů původně izolovaných z rostlin používaných v tradiční čínské medicíně (např. *Cleistanthus collinus*, *Justicia gendarussa* nebo *Haplophyllum bucharicum*) (Jullian-Pawlicki et al., 2015; Cui et al., 2020; Lv et al., 2021), byl popsán jako silný inhibitor SARS-CoV-2 ve studii „**Antiviral activity of vacuolar ATPase blocker diphyllin against SARS-CoV-2**“ (Štefánik et al., 2021), kde byl jeho inhibiční účinek analyzován na buněčné linii Vero a CaCo-2 (buňky kolorektálního adenokarcinomu běžně používané pro kultivaci SARS-CoV-2) a porovnán s jeho glykosylovaným protějškem cleistanthinem B a několika strukturně podobnými deriváty helioxanthiny. Později byla publikována další práce „**Diphyllin Shows a Broad-Spectrum Antiviral Activity Against Multiple Medically Important Enveloped RNA and DNA Viruses**“ (Štefánik et al., 2022), která demonstruje neobyčejně široký antivirový efekt diphyllinu na souboru obalených RNA a DNA virů z čeledi *Flaviviridae*, *Phenuiviridae*, *Rhabdoviridae* a *Herpesviridae* s využitím početných buněčných linií a primárních buněk. Mechanismus účinku byl hlouběji studován s využitím metody pro vizualizaci acidifikovaných endozomů pomocí akrydinové oranže a byl porovnán s aktivitou bafilomycinu A1, známého a dobře charakterizovaného inhibitoru V-ATPáz (Hu et al., 2017). Je zajímavé, že diphyllin působí výraznou inhibicí také u zástupců čeledi *Herpesviridae*, které nepoužívají pro svůj vstup do buňky endozomy a nejsou tedy závislé na jejich acidifikaci pomocí endozomálních V-ATPáz. Je zřejmé, že antivirový efekt diphyllinu je pravděpodobně založený i na jiných molekulárních mechanismech a tento jev bude detailně prozkoumán v navazujících studiích.

5.3. NENUKLEOSIDOVÉ INHIBITORY VIROVÝCH POLYMERÁZ

Virové polymerázy lze účinně inhibovat také řadou nenukleosidových antivirotik, které mají různorodou chemickou strukturu a vážou se do rozličných míst na molekule polymerázy. Mohou kompetovat o aktivní místo polymerázy a bránit vstupu nukleosid-trifosfátů, nezbytných pro syntézu virové NK, do aktivního místa. Dále mohou vystupovat jako alosterické inhibitory, interagovat s distálními regiony na molekule polymerázy a ovlivňovat tak konformaci aktivního místa enzymu nepřímo (“z dálky”) (Sarisky, 2004). Vznik mutant rezistentních na nenukleosidové inhibitory virových polymeráz je zpravidla rychlejší a snadnější než v případě nukleosidových antivirotik (nižší genotypová rezistenční bariéra) (Delang et al., 2011). I přes to nacházejí tyto inhibitory uplatnění léčbě virových infekcí, zejména v kombinaci s nukleosidovými analogy nebo jinými dostupnými inhibitory.

Jedním z příkladů takových inhibitorů je látka PR673, helikální dikation („helquat“), popsaná v práci „**A Helquat-like Compound as a Potent Inhibitor of Flaviviral and Coronaviral**“

Polymerases“ (Konkolová et al., 2022). Práce byla realizována v úzké spolupráci s Ústavem organické chemie a biochemie AV ČR. Ligand PR673 účinně inhiboval enzymovou aktivitu rekombinantních flavivirových a koronavirových polymeráz a působil jako supresor replikace VKE i SARS-CoV-2 v buněčné kultuře PS a Vero. Přesný mechanismus interakce ligandu s virovou polymerázou zůstává nejasný. I když látka zastavuje syntézu virové RNA, neinkorporuje se do replikující se virové NK a nebrání navázání následujícího nukleosid-monofosfátu do nacentního řetězce. Nelze také vyloučit, že se přímo váže na virovou RNA a tím znemožňuje její interakci s virovou polymerázou.

Další studie opět realizovaná ve spolupráci s Ústavem organické chemie a biochemie AV ČR „**Non-Nucleotide RNA-Dependent RNA Polymerase Inhibitor That Blocks SARS-CoV-2 Replication“** (Dejmek et al., 2021) popisuje syntézu a mechanismus antivirového účinku inhibitoru HeE1-2Tyr a příbuzných derivátů proti významným zástupcům čeledi *Coronaviridae*, a sice SARS-CoV-2 a kočičímu koronaviru FIPV (původce infekční peritonitidy koček). Tato látka a podobné pyridobenzothiazolové deriváty byly původně popsány jako nenukleosidové inhibitory flavivirové RdRp (Tarantino et al., 2016; Cannalire et al., 2019). V této práci je detailně popsán antivirový účinek těchto látek s využitím rekombinantních koronavirových polymeráz. Látky inhibují také replikaci obou koronavirů v buněčných kulturách Vero, CaCo-2 (buňky kolorektálního adenokarcinomu běžně používané pro kultivaci SARS-CoV-2) a CRFK (imortalizovaná linie odvozená z buněk kůry kočičích ledvin vhodné pro FIPV). HeE1-2Tyr a příbuzné deriváty pravděpodobně působí jako kompetitivní inhibitory interagující s částí aktivního místa virové RdRp, označované jako „RNA template tunnel“. Spolu s PR673 popsanou výše představují tyto látky jedny z mála dosud popsaných nenukleosidových inhibitorů koronavirové polymerázy s potenciálním využitím pro kombinační terapii závažných koronavirových infekcí u člověka i u zvířat.

5.4. LIGANDY STABILIZUJÍCÍ GUANINOVÉ KVADRUPEXY

Guaninové kvadruplexy (G4) jsou nekanonické sekundární struktury NK (DNA nebo RNA), které se vyskytují v genomech eukaryot, prokaryot i virů a plní důležité regulační funkce. Jsou tvořeny čtveřicemi (tetradami) guaninových zbytků, které se vzájemně stabilizují prostřednictvím nekovalentních π - π (patrových) interakcí mezi aromatickými cykly guaninů a vodíkových vazeb Hoogsteenova typu. Za fyziologických podmínek koordinují monovalentní kation kovu. Podle orientace fosfodiesterových vazeb rozlišujeme několik topologických typů G4, jmenovitě paralelní, antiparalelní a hybridní G4. U virů bylo zjištěno, že G4 hrají důležitou roli při replikaci, transkripci a translaci genomové NK a dále jsou důležité při integraci virových genomů do genomů hostitelských buněk a při navození latentní fáze infekce. Existují nízkomolekulární látky, tzv. ligandy vázající se na G4, které stabilizují G4 struktury, což vede k inhibici replikace viru v buňce (Ruggiero et al., 2018).

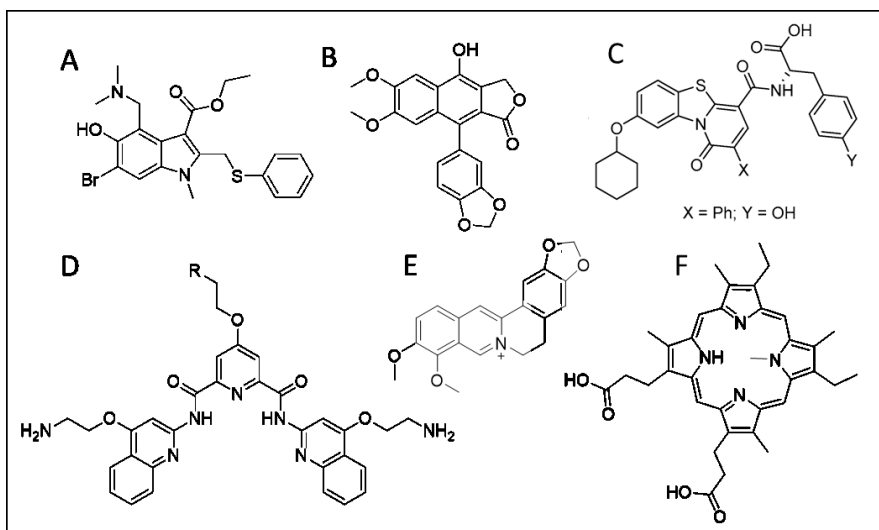
Práce **“Guanine quadruplexes in the RNA genome of the tick-borne encephalitis virus: Their role as a new antiviral target and in virus biology“** (Holoubek et al., 2022) se zabývá identifikací G4 v genomu VKE, jejich biofyzikální charakterizací pomocí spektroskopických metod (např. pomocí cirkulárního dichroismu) a studiem jejich interakcí s G4-vázajícími ligandy. Tyto ligandy, např. pyridostatin, karboxy pyridostatin, přírodní alkaloid berberin, bischinolinový derivát PhenDC3 a některé látky z rodiny porfyrinů (TMPyP4 a N-methylmesoporphyrin IX) vykazovaly překvapivý inhibiční účinek na replikaci viru v buněčné

kultuře. Pomocí testů využívajících rekombinantní flavivirovou polymerázu bylo prokázáno, že ligandy zastavují syntézu templátové RNA, odvozené od genomové RNA viru, obsahující ve svojí sekvenci G4 motif. Význam G4 pro replikaci VKE byl dále studován prostřednictvím virových mutant, které nesly stabilizovaný nebo naopak destabilizovaný G4 lokalizovaný na rozhraní genů NS4B a NS5. Mutanty se stabilizovaným G4 vykazovaly sníženou replikační fitness oproti WT, zatímco mutanty s destabilizovanou strukturou G4 podléhaly rychlé reverzi a navozovaly standardní genotyp. Antivirový účinek G4-vázajících ligandů byl výrazně zesílen právě u virových variant, které disponovaly stabilizovaným G4 motivem. Práce představuje G4 struktury jako zcela nové cíle pro antivirovou terapii a G4-vázající ligandy jako kandidátní látky pro vývoj nových inhibitorů virové replikace.

5.5. OSTATNÍ STUDOVANÉ INHIBITORY VIROVÝCH PATOGENŮ

Ve studii „*FDA-Approved Drugs Efavirenz, Tipranavir, and Dasabuvir Inhibit Replication of Multiple Flaviviruses in Vero Cells*“ (Štefánik et al., 2020) bylo identifikováno několik dalších nenukleosidových antivirotek aktivních proti komáry a klíšťaty přenášeným flavivirům. Studie je založena na in silico screeningu knihovny FDA-schválených látek a jejich interakci s vybranými strukturálními a nestrukturálními proteiny viru Zika (jmenovitě s NS5 methyltransferázou, NS3 helikázou, proteázou a NS5 RdRp). Tento virtuální screening identifikoval 12 kandidátních látek, z nichž efavirenz, tipranavir a dasabuvir vykazovaly inhibiční aktivitu také v buněčných systémech a nebyly výrazně cytotoxické pro buňky PS, Vero, neuroblasty UKF-NB-4 a primární lidské mozkové kortikální astrocyty. Přesný mechanismus účinku i cílové struktury pro tyto látky v rámci flavivirového infekčního systému zbývá experimentálně určit. To platí zejména pro efavirenz a tipranavir, které jsou popsány jako inhibitory HIV, ale (první je inhibitorem reverzní transkriptázy (Ren et al., 2000), druhý blokuje virovou proteázu (Wong-Sam et al., 2018)), nicméně jejich význam pro inhibici flavivirů je dosud nejasný. Dasabuvir je nenukleosidový inhibitor NS5B polymerázy viru žloutenky typu C (Kati et al., 2015) a vzhledem k podobnosti tohoto viru s flaviviry přenášenými klíšťaty/komáry lze očekávat, že bude mít i u nich podobný mechanismus účinku.

Struktury vybraných inhibitorů chemicky odlišných od nukleosidů, popsanych v této práci, jsou znázorněny na obr. 3.



Obr. 3. Struktury vybraných nenukleosidových inhibitorů flavivirů a koronaviřů, studovaných v této práci. (A) Arbidol, (B) diphyllin, (C) HeE1-2Tyr, (D) pyridostatin, (E) berberin, (F) N-methylmesoporphyrin IX.

PŘÍLOHA 3

1. Haviernik J, Štefánik M, Fojtíková M, Kali S, Tordo N, Rudolf I, Hubálek Z, **Eyer L**, Ruzek D. Arbidol (Umifenovir): A Broad-Spectrum Antiviral Drug That Inhibits Medically Important Arthropod-Borne Flaviviruses. *Viruses*. 2018 Apr 10;10(4):184.
2. Stefanik M, Strakova P, Haviernik J, Miller AD, Ruzek D, **Eyer L**. Antiviral Activity of Vacuolar ATPase Blocker Diphyllin against SARS-CoV-2. *Microorganisms*. 2021 Feb 25;9(3):471.
3. Štefánik M, Bhosale DS, Haviernik J, Straková P, Fojtíková M, Dufková L, Huvarová I, Salát J, Bartáček J, Svoboda J, Sedlák M, Růžek D, Miller AD, **Eyer L**. Diphyllin Shows a Broad-Spectrum Antiviral Activity against Multiple Medically Important Enveloped RNA and DNA Viruses. *Viruses*. 2022 Feb 9;14(2):354.
4. Konkolova E, Krejčová K, **Eyer L**, Hodek J, Zgarbová M, Fořtová A, Jirasek M, Teplý F, Reyes-Gutierrez PE, Růžek D, Weber J, Boura E. A Helquat-like Compound as a Potent Inhibitor of Flaviviral and Coronaviral Polymerases. *Molecules*. 2022 Mar 15;27(6):1894.
5. Dejmek M, Konkol'ová E, **Eyer L**, Straková P, Svoboda P, Šála M, Krejčová K, Růžek D, Boura E, Nencka R. Non-Nucleotide RNA-Dependent RNA Polymerase Inhibitor That Blocks SARS-CoV-2 Replication. *Viruses*. 2021 Aug 11;13(8):1585.
6. Holoubek J, Bednářová K, Haviernik J, Huvarová I, Dvořáková Z, Černý J, Outlák M, Salát J, Konkol'ová E, Boura E, Růžek D, Vorlíčková M, **Eyer L**, Renčiuk D. Guanine quadruplexes in the RNA genome of the tick-borne encephalitis virus: their role as a new antiviral target and in virus biology. *Nucleic Acids Res*. 2022 May 6;50(8):4574-4600.
7. Stefanik M, Valdes JJ, Ezebuo FC, Haviernik J, Uzochukwu IC, Fojtikova M, Salat J, **Eyer L**, Ruzek D. FDA-Approved Drugs Efavirenz, Tipranavir, and Dasabuvir Inhibit Replication of Multiple Flaviviruses in Vero Cells. *Microorganisms*. 2020 Apr 20;8(4):599.

Communication

Arbidol (Umifenovir): A Broad-Spectrum Antiviral Drug That Inhibits Medically Important Arthropod-Borne Flaviviruses

Jan Haviernik ^{1,†}, Michal Štefánik ^{1,†}, Martina Fojtíková ¹, Sabrina Kali ², Noël Tordo ^{2,3}, Ivo Rudolf ⁴, Zdeněk Hubálek ⁴, Luděk Eyer ^{1,5,‡} and Daniel Ruzek ^{1,5,*} 

¹ Department of Virology, Veterinary Research Institute, Hudcova 70, CZ-62100 Brno, Czech Republic; haviernik@vri.cz (J.H.); stefanik@vri.cz (M.Š.); fojtikova@vri.cz (M.F.); eyer@vri.cz (L.E.)

² Unit Antiviral Strategies, Institut Pasteur, 25 Dr. Roux, 75724 Paris CEDEX 15, France; sabrina.kali@pasteur.fr (S.K.); ntordo@pasteur.fr (N.T.)

³ Institut Pasteur de Guinée, route de Donka, Conakry, Guinea

⁴ Institute of Vertebrate Biology, Czech Academy of Sciences, Kvetna 8, CZ-60365 Brno, Czech Republic; rudolf@ivb.cz (I.R.); zhubalek@brno.cas.cz (Z.H.)

⁵ Institute of Parasitology, Biology Centre of the Czech Academy of Sciences, Branisovska 31, CZ-37005 Ceske Budejovice, Czech Republic

* Correspondence: ruzekd@paru.cas.cz

† These authors contributed equally to this work.

‡ L.E. and D.R. are co-senior authors of this article.

Received: 20 February 2018; Accepted: 5 April 2018; Published: 10 April 2018



Abstract: Arthropod-borne flaviviruses are human pathogens of global medical importance, against which no effective small molecule-based antiviral therapy has currently been reported. Arbidol (umifenovir) is a broad-spectrum antiviral compound approved in Russia and China for prophylaxis and treatment of influenza. This compound shows activities against numerous DNA and RNA viruses. The mode of action is based predominantly on impairment of critical steps in virus-cell interactions. Here we demonstrate that arbidol possesses micromolar-level anti-viral effects (EC_{50} values ranging from 10.57 ± 0.74 to $19.16 \pm 0.29 \mu\text{M}$) in Vero cells infected with Zika virus, West Nile virus, and tick-borne encephalitis virus, three medically important representatives of the arthropod-borne flaviviruses. Interestingly, no antiviral effects of arbidol are observed in virus infected porcine stable kidney cells (PS), human neuroblastoma cells (UKF-NB-4), and human hepatoma cells (Huh-7 cells) indicating that the antiviral effect of arbidol is strongly cell-type dependent. Arbidol shows increasing cytotoxicity when tested in various cell lines, in the order: Huh-7 < HBCA < PS < UKF-NB-4 < Vero with CC_{50} values ranging from 18.69 ± 0.1 to $89.72 \pm 0.19 \mu\text{M}$. Antiviral activities and acceptable cytotoxicity profiles suggest that arbidol could be a promising candidate for further investigation as a potential therapeutic agent in selective treatment of flaviviral infections.

Keywords: flavivirus; arbidol; umifenovir; antiviral activity; cytotoxicity; cell-type dependent antiviral effect

1. Introduction

Arthropod-borne flaviviruses (genus *Flavivirus*, family *Flaviviridae*) include human pathogens of global medical importance such as dengue virus (DENV), Yellow fever virus (YFV), West Nile virus (WNV), Japanese encephalitis virus (JEV), Zika virus (ZIKV), Kyasanur Forest disease virus (KFDV), Omsk hemorrhagic fever virus (OHFV) and tick-borne encephalitis virus (TBEV). These viruses are

causative of many serious diseases with a broad spectrum of clinical symptoms ranging from near asymptomatic or mild flu-like infections through neurological diseases (WNV, TBEV) to viscerotropic (DENV), hemorrhagic (KFDV, OHFV) or even teratogenic manifestations (ZIKV) [1,2]. Up to 200 million new cases of infection caused by arthropod-borne flaviviruses are reported annually [1]. These viruses can be widespread, as exemplified by the epidemiological outbreaks of WNV infection across North America, Mexico, South America, and the Caribbean during 1999–2002 [3,4], or ZIKV infection in Oceania and Latin America during 2014–2016 [5]. At present, there is no effective antiviral therapy directed against these viruses, and therefore, search for small molecule-based inhibitors represents an unmet medical need.

Arbidol, also known as umifenovir, is a broad-spectrum antiviral compound developed at the Russian Research Chemical and Pharmaceutical Institute about 25 years ago [6] and licensed in Russia and China for the prophylaxis and treatment of human influenza A and B infections, plus post-influenza complications [7]. Subsequently, arbidol was shown to be active against numerous DNA/RNA and enveloped/non-enveloped viruses [8]. The predominant mode of action of arbidol is based on its intercalation into membrane lipids leading to the inhibition of membrane fusion between virus particles and plasma membranes, and between virus particles and the membranes of endosomes [9]. In influenza virus, arbidol was observed to interact with virus hemagglutinin (HA), causing an increase in HA stability thereby preventing the pH-induced transition of HA into its a functional fusogenic state [10]. In the case of hepatitis C virus (HCV) arbidol interacts with HCV envelope protein to cause various degrees of inhibition to critical membrane fusion events [11,12]. Alternatively, arbidol may also be immunomodulatory, and as such be capable of interferon induction and/or macrophage activation [13]. Due to such broad-spectrum antiviral activities, arbidol represents a promising candidate for treatment of viral infections in humans.

Accordingly, we describe here using standardized in vitro assay systems the cytotoxicities and antiviral activities of arbidol against three representative flaviviruses; ZIKV and WNV as emerging mosquito-borne pathogens, and TBEV as an important tick-borne pathogen. Since antiviral compounds are extensively inactivated/metabolized in the intracellular environment [14,15], different cell lines were utilized to assess simultaneously both the antiviral and corresponding cytotoxic effects of arbidol.

2. Material and Methods

Arbidol (ethyl-6-bromo-4-[(dimethylamino)methyl]-5-hydroxy-1-methyl-2-[(phenylthio)methyl]-indole-3-carboxylate hydrochloride monohydrate) (Figure 1A) was obtained from Sigma-Aldrich (St. Louis, MO, USA), solubilized in 100% DMSO to yield 10 mM stock solution. The following viral strains/isolates were used in this study: ZIKV (MR766, a representative of the African ZIKV lineage; Paraiba_01, a member of the Asian ZIKV lineage), WNV (strains Eg101 and 13-104), and TBEV (strain Hypr, a typical representative of the West European TBEV subtype). As ZIKV, WNV and TBEV are neurotropic viruses, cell lines of both neuronal as well as extraneural origin were selected for antiviral screens, virus multiplication and plaque assays. Porcine kidney stable (PS) cells [16] were cultured in Leibovitz (L-15) medium, human brain cortical astrocytes (HBCA) (ScienCell, Carlsbad, CA, USA) were cultivated in Astrocyte medium (Thermo Fisher Scientific, Waltham, MA, USA), human neuroblastoma UKF-NB-4 cells [17] were cultured in Iscove's modified Dulbecco's medium (IMDM), Vero cells (ATCC CCL-81, African Green Monkey, adult kidney, epithelial) and human hepatocellular carcinoma cells (Huh-7) were grown in Dulbecco's modified Eagle's medium (DMEM). The media were supplemented with 3% (L-15), 6% (Astrocyte medium), or 10% (IMDM and DMEM) newborn calf serum and a 1% mixture of antibiotics and antimycotics and 1% glutamine (Sigma-Aldrich, Prague, Czech Republic).

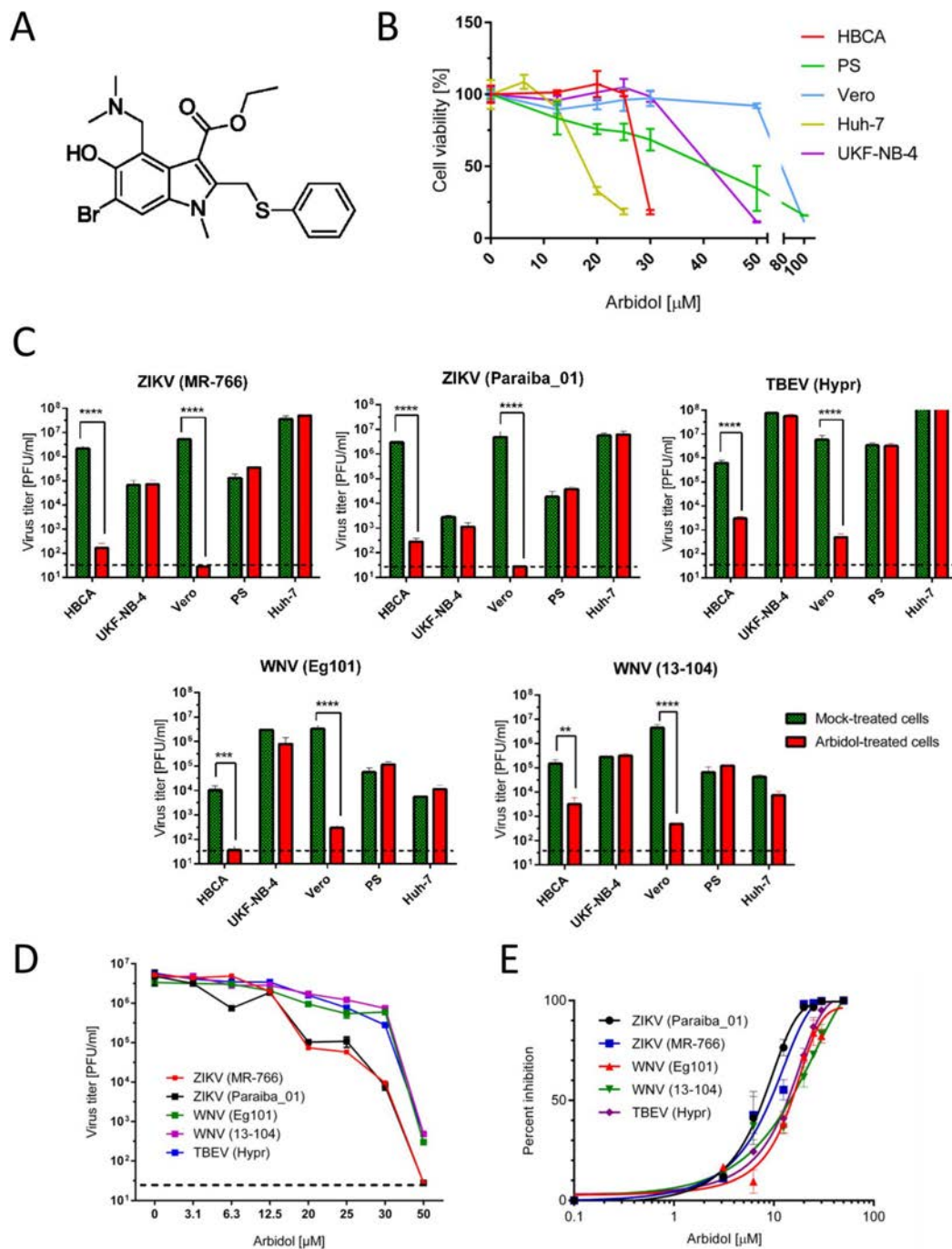


Figure 1. (A) Structure of arbidol. (B) Cytotoxicities of arbidol with Huh-7, PS, UKF-NB-4, HUCA, and Vero cells within the compound concentration ranges 0–100 μ M, 48 h post infection. (C) Antiviral effects of arbidol against ZIKV, WNV and TBEV infection in different cell lines. Given differential arbidol cytotoxicities with respect to different cell lines, indicated cell lines were treated with different maximum concentrations of arbidol (12.5 μ M for Huh-7, 25 μ M for HUCA and PS, 30 μ M for UKF-NB-4, and 50 μ M for Vero) 24 h prior to virus infection. Culture supernatants were then collected 48 h post infection and individual viral titers were determined by plaque assay. (D) Dose-dependent effects of arbidol on virus titers 48 h post infection in Vero cells. The horizontal dashed line indicates the minimum detectable threshold of 1.44 \log_{10} PFU/mL. (E) Inhibition of indicated flaviviruses in the presence of a serial dilution of arbidol. Data from two (C) or three (B–E) independent experiments done in triplicates. ** $p < 0.01$; *** $p < 0.001$; **** $p < 0.0001$.

The compound cytotoxicity was determined in terms of cell viability using the Cell Counting Kit-8 (Dojindo Molecular Technologies, Munich, Germany) according to the manufacturer's instructions and expressed as the 50% cytotoxic concentration (CC_{50}), which represents the concentration of compound that reduced cell viability by 50%. A viral titer reduction assay was performed to determine the flavivirus sensitivity to arbidol in cell culture. Host cells were seeded in 96-well plates (approximately 2×10^4 cells per well) and incubated for 24 h at 37 °C to form a confluent monolayer. The medium was then aspirated from the wells and replaced with 200 μ L of fresh medium containing 0–12.5 μ M (for Huh-7), 0–25 μ M (for HBCA and PS), 0–30 μ M (for UKF-NB-4), or 0–50 μ M (for Vero) of arbidol and incubated for 24 h (the concentration ranges were based on different cytotoxicity effects of arbidol for individual cell lines, as described below). The medium was then removed from wells and replaced with fresh medium containing arbidol and appropriate virus strain at a multiplicity of infection (MOI) of 0.1. After 2 h incubation, the medium was replaced with fresh medium containing arbidol and incubated for 48 h at 37 °C. Then, the supernatant medium was collected and viral titers were determined by plaque assays, expressed as PFU/mL [18] and used for construction of dose-response and inhibition curves and for estimation the 50% effective concentration (EC_{50}). For construction of growth curves, Vero cells were infected as described above and treated with arbidol at a concentration of 50 μ M. Supernatant media were collected every six hours until 48 h p.i. Viral titers in supernatants were determined using plaque assay. In all experiments, DMSO was added to virus-infected cells as a negative control at a concentration corresponding to a dilution of the initial arbidol-DMSO stock. A cell-based flavivirus immunostaining assay was performed to measure the arbidol-induced inhibition of viral surface antigen (E protein) expression, as previously described [19].

Differences in viral titer between groups were evaluated by unpaired parametric two-tailed *t*-test using GraphPad Prism 7 (GraphPad Software, Inc., La Jolla, CA, USA), version 7.04. Differences with $p < 0.05$ were considered to be statistically significant.

3. Results and Discussion

We initially determined arbidol cytotoxicity profiles for Huh-7, Vero, PS, UKF-NB-4, and HBCA cells. As is apparent (Figure 1B), arbidol was differentially cytotoxic. Lowest cytotoxicities were observed with Vero cells ($CC_{50} = 89.72 \pm 0.19 \mu$ M). This level of cytotoxicity was about 5 times lower than observed with Huh-7 cells ($CC_{50} = 18.69 \pm 0.1 \mu$ M) that were the most susceptible cells studied. Experiments with other cell types, namely PS, UKF-NB-4, and HBCA gave rise to CC_{50} values ranging from 24.78 ± 0.01 to $46.99 \pm 0.1 \mu$ M (Table 1). The variable cytotoxic effects of arbidol may be related to its broad-spectrum activity impairing crucial cellular metabolic pathways or critical steps in virus-cell interactions [11,20]. This contrasts with other antiviral drugs that preferentially target viral proteins, such as nucleoside inhibitors of viral polymerases, for which the CC_{50} values usually do not exceed typically 100 μ M [21].

Table 1. Cytotoxicity of arbidol for various cell lines of neurone or extraneural origin.

Cell Line	CC_{50} (μ M) ^a
Human brain cortical astrocytes (HBCA)	24.78 ± 0.01
Human neuroblastoma UKF-NB-4 cells	46.99 ± 0.10
Vero cells	89.72 ± 0.19
Human hepatocarcinoma cells (Huh-7)	18.69 ± 0.10
Porcine kidney stable cells (PS)	46.81 ± 1.65

^a Determined from three independent experiments performed in triplicate. Calculated as a 50% reduction in cell viability using the Reed-Muench method.

The antiviral effects of arbidol against two ZIKV strains (MR766 and Paraiba_01) were evident in both Vero and HBCA cells 48 h after infection. Whereas in HBCA the highest arbidol concentration tested (25 μ M) caused a reduction in ZIKV titer of about 10^4 -fold compared to the situation in

mock-treated cells, in Vero cells viral replication was inhibited completely at 50 μM . ZIKV replication was not inhibited in UKF-NB-4, PS, and Huh-7 cells, suggesting that the antiviral effects of arbidol are strongly cell type-dependent (Figure 1C). This phenomenon has been described previously with many other antiviral compounds and is thought to arise from differences in the expression levels of intracellular enzymes/proteins involved in metabolism and transport [21]. These differences apparently ensure that the same inhibitor should exhibit different EC_{50} values according to the cell line employed [22,23]. For example, sofosbuvir was found to be differentially active against ZIKV infection depending on the cultivated cells used, owing to differences in intracellular processing [24].

Based on these results, we further evaluated the inhibitory potential of arbidol against viral infections in Vero cells in particular. For instance, the EC_{50} values for ZIKV infections in Vero cells were found to be 12.09 ± 0.77 and 10.57 ± 0.74 μM respectively for MR766 and Paraiba_01 strains (Figure 1D,E, Table 2). The antiviral effects of arbidol were further confirmed by immunofluorescence staining. Using this method, a dose-dependent inhibition of ZIKV surface E antigen expression was observed in Vero cells (Figure 2). The observed anti-ZIKV properties are comparable with those of previously reported small-molecules, such as nucleoside analogues, that are known to exert anti-ZIKV inhibitions in the micromolar range (0.2 to 22 μM) according to the cell-based assay systems used [25–28].

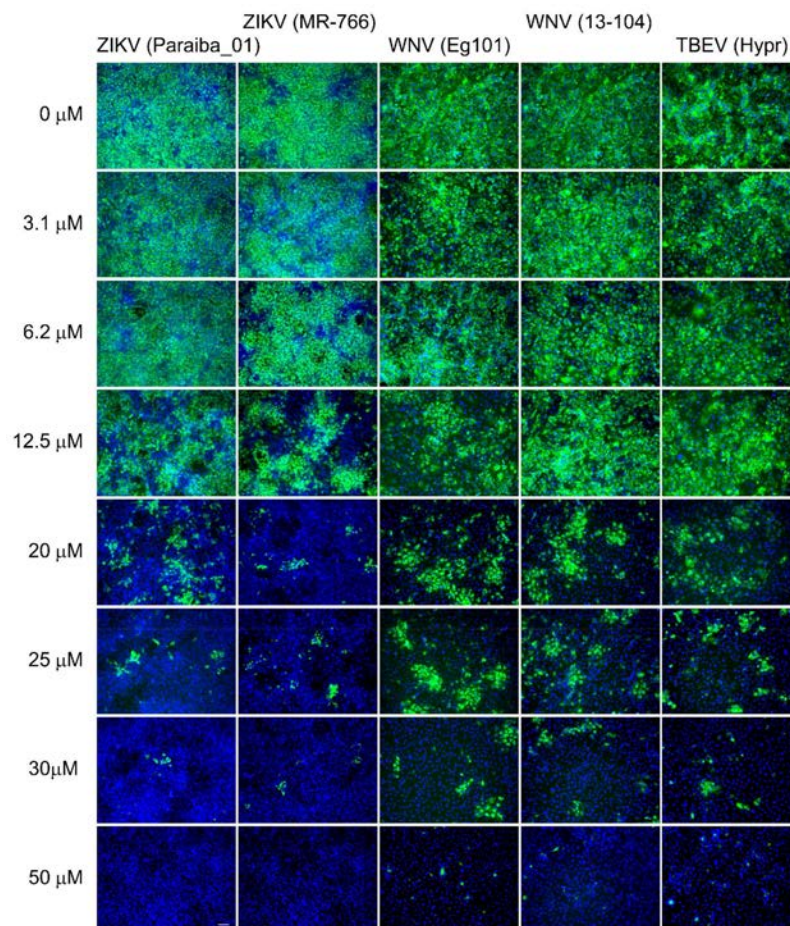


Figure 2. Inhibition of flaviviral surface E antigen expression by arbidol. Vero cells infected with virus were fixed on slides 48 h after infection and stained with flavivirus-specific antibody labeled with FITC (green) and counterstained with DAPI (blue). Scale bar, 50 μm .

Table 2. Anti-flaviviral activity and cytotoxicity characteristics of arbidol in Vero cells.

Virus	Strain	EC ₅₀ (μM) ^{a,b}	CC ₅₀ (μM) ^{a,c}	SI (CC ₅₀ /EC ₅₀)
ZIKV	MR-766	12.09 ± 0.77		7.42
	Paraiba_01	10.57 ± 0.74		8.49
WNV	Eg101	18.78 ± 0.21	89.72 ± 0.19	4.78
	13-104	19.16 ± 0.29		4.68
TBEV	Hypr	18.67 ± 0.15		4.81

^a Determined from three independent experiments performed in triplicate. ^b Calculated as a 50% reduction in viral titers using the Reed-Muench method. ^c CC₅₀ value determined for Vero cells. SI, selectivity index.

Arbidol also showed significant *in vitro* antiviral efficacies when tested against two strains of WNV (Eg101 and 13-104). As with ZIKV, the anti-WNV effects of arbidol were most obvious when incubated at 25 and 50 μM with WNV-infected HBCA and Vero cells for 48 h. By contrast, there were little or no antiviral effects observed in UKF-NB-4, PS, and Huh-7 virus infected cells (Figure 1C). EC₅₀ values in Vero cells were found to be 18.78 ± 0.21 and 19.16 ± 0.29 μM for Eg101 and 13-104, respectively, values that were slightly higher (about two-times) in comparison to values found with ZIKV (Figure 1D,E, Table 2). This observed arbidol-mediated decrease in WNV titer was strongly correlated with dose-dependent inhibition of viral surface E antigen expression in the compound-treated Vero cell culture (Figure 2).

Finally, TBEV (strain Hypr) infections in HBCA and Vero cells (Figure 1C), also proved susceptible to arbidol-mediated inhibition in dose-dependent manners, as shown by EC₅₀ values of 18.67 ± 0.15 μM (Figure 1D,E, Table 2). However, when arbidol was introduced at the highest appropriate concentrations (25 μM for HBCA and 50 μM for Vero cells) inhibition of TBEV replication remained incomplete in cell culture, although the viral titer was reduced by 10³-fold compared with non-treated cells (Figures 1C and 2).

In Vero cells, arbidol administration was found to inhibit viral replication in all cases. In fact, a rapid reduction of viral titer was observed within the first 6 h p.i.; then the titer remained low (or even below detection limit) until the end of the experiment. In untreated cells, there was a peak in virus production between 12 and 30 h p.i. reaching a maximum of 10^{6.5} to 10⁸ PFU/mL (Supplementary Figure S1).

Our data agree with numerous reports of *in vitro* arbidol-mediated inhibition of other viruses of medical interest. Arbidol inhibits replication of various subtypes of human influenza A and B viruses with EC₅₀ values ranging from 3 to 9 μg/mL [29]. Arbidol is also known to inhibit Chikungunya virus replication in Vero cells or in primary human fibroblasts with EC₅₀ values < 10 μg/mL [30], plus inhibit Crimean-Congo hemorrhagic fever virus replication with an EC₅₀ value of 2.8 μg/mL [31]. Furthermore, treatment of human hepatocellular carcinoma cells Huh 7.5.1 with 15 μM of arbidol for 24 h to 48 h, led to inhibition of HCV replication by up to 10³-fold [11]. Overall, arbidol exhibits a broad range antiviral effects against respiratory syncytial virus, hepatitis B virus, adenovirus, parainfluenza virus, avian coronavirus, coxsackie B3 virus, and hantaan virus indicating broad-spectrum antiviral activities [11,32,33]. Besides *in vitro* studies, arbidol also exerts substantial antiviral effects in various animal models of infection and has been used with effect in clinical trials for the prevention and treatment of influenza [33].

4. Conclusions

In conclusion, we have demonstrated that arbidol has substantial antiviral activities against ZIKV, WNV and TBEV *in vitro* with EC₅₀ values ranging from 10.57 ± 0.74 to 19.16 ± 0.29 μM. The observed antiviral effects were strongly cell-type dependent being substantial only in HBCA and Vero cells. Arguably, such cell line variability results from differences in arbidol up-take or metabolic processing by the different individual cell lines concerned. Arbidol-mediated cytotoxicities are also cell line dependent, with Huh-7 cells being the most susceptible and Vero cells the least. Our data broaden the possibility for future *in vivo* testing of arbidol in animal models of flavivirus infection.

Supplementary Materials: The following are available online at <http://www.mdpi.com/1999-4915/10/4/184/s1>, Figure S1: Growth curves of West Nile virus (WNV), Zika virus (ZIKV), and tick-borne encephalitis virus (TBEV) in Vero cells treated or mock-treated with arbidol.

Acknowledgments: We thank Carla Torres Braconi and Paolo M. de A. Zanotto (University of Sao Paolo) for providing us with the ZIKV strain Paraiba_01, and the European Virus Archive Goes Global project (which has received funding from the European Union's Horizon 2020 research and innovation program (Grant 653316)) for providing us with ZIKV strain MR766. We also thank Andrew D. Miller (Veterinary Research Institute, Brno, Czech Republic) for language correction of the manuscript.

Author Contributions: Daniel Ruzek, Luděk Eyer, Noël Tordo and Sabrina Kali designed and conceived this study. Jan Haviernik, Michal Štefánik and Martina Fojtková performed the experiments. Ivo Rudolf and Zdeněk Hubálek contributed new reagents/analytic tools. Luděk Eyer, Daniel Ruzek and Noël Tordo wrote the manuscript. All authors read and approved the manuscript.

Conflicts of Interest: The authors declare that they have no competing interests.

Funding: This work was supported by the Czech Science Foundation (Grant 16-20054S); the Ministry of Education, Youth, and Sports of the Czech Republic, under the NPU I program (Grant LO1218); by Project "FIT" (Pharmacology, Immunotherapy, nanoToxicology), which was funded by the European Regional Development Fund.

References

- Baier, A. Flaviviral infections and potential targets for antiviral therapy. In *Flavivirus Encephalitis*, 1st ed.; Ruzek, D., Ed.; InTech: Rijeka, Croatia, 2011; pp. 89–104, ISBN 978-953-307-669-0.
- Lazear, H.M.; Stringer, E.M.; de Silva, A.M. The Emerging Zika Virus Epidemic in the Americas Research Priorities. *JAMA* **2016**, *315*, 1945–1946. [[CrossRef](#)] [[PubMed](#)]
- Hayes, E.B.; Sejvar, J.; Zaki, S.R.; Lanciotti, R.S.; Bode, A.V.; Campbell, G.L. Virology, pathology, and clinical manifestations of West Nile virus disease. *Emerg. Infect. Dis.* **2005**, *11*, 1174–1179. [[CrossRef](#)] [[PubMed](#)]
- Samuel, M.A.; Diamond, M.S. Pathogenesis of West Nile virus infection: A balance between virulence, innate and adaptive immunity, and viral evasion. *J. Virol.* **2006**, *80*, 9349–9360. [[CrossRef](#)] [[PubMed](#)]
- Malone, R.W.; Homan, J.; Callahan, M.V.; Glasspool-Malone, J.; Damodaran, L.; Schneider Ade, B.; Zimler, R.; Talton, J.; Cobb, R.R.; Ruzic, I.; et al. Zika Virus: Medical Countermeasure Development Challenges. *PLoS Negl. Trop. Dis.* **2016**, *10*, e0004530. [[CrossRef](#)] [[PubMed](#)]
- Panischeva, E.K.; Mikerova, N.I.; Nikolayeva, I.S.; Fomina, A.N.; Cherkasova, A.A.; Golovanova, E.A.; Krylova, L.Y. Synthesis and Antiviral Activity of 5-Hydroxyindole Derivatives. *Pharm. Chem.* **1988**, *22*, 1455–1458.
- Boriskin, Y.S.; Leneva, I.A.; Pecheur, E.I.; Polyak, S.J. Arbidol: A broad-spectrum antiviral compound that blocks viral fusion. *Curr. Med. Chem.* **2008**, *15*, 997–1005. [[CrossRef](#)] [[PubMed](#)]
- Pecheur, E.I.; Borisevich, V.; Halfmann, P.; Morrey, J.D.; Smee, D.F.; Prichard, M.; Mire, C.E.; Kawaoka, Y.; Geisbert, T.W.; Polyak, S.J. The Synthetic Antiviral Drug Arbidol Inhibits Globally Prevalent Pathogenic Viruses. *J. Virol.* **2016**, *90*, 3086–3092. [[CrossRef](#)] [[PubMed](#)]
- Villalain, J. Membranotropic Effects of Arbidol, a Broad Anti-Viral Molecule, on Phospholipid Model Membranes. *J. Phys. Chem. B* **2010**, *114*, 8544–8554. [[CrossRef](#)] [[PubMed](#)]
- Leneva, I.A.; Russell, R.J.; Boriskin, Y.S.; Hay, A.J. Characteristics of arbidol-resistant mutants of influenza virus: Implications for the mechanism of anti-influenza action of arbidol. *Antivir. Res.* **2009**, *81*, 132–140. [[CrossRef](#)] [[PubMed](#)]
- Boriskin, Y.S.; Pecheur, E.I.; Polyak, S.J. Arbidol: A broad-spectrum antiviral that inhibits acute and chronic HCV infection. *Virol. J.* **2006**, *3*, 56. [[CrossRef](#)] [[PubMed](#)]
- Pecheur, E.I.; Lavillette, D.; Alcaras, F.; Molle, J.; Boriskin, Y.S.; Roberts, M.; Cosset, F.L.; Polyak, S.J. Biochemical mechanism of hepatitis C virus inhibition by the broad-spectrum antiviral arbidol. *Biochemistry* **2007**, *46*, 6050–6059. [[CrossRef](#)] [[PubMed](#)]
- Liu, Q.; Xiong, H.R.; Lu, L.; Liu, Y.Y.; Luo, F.; Hou, W.; Yang, Z.Q. Antiviral and anti-inflammatory activity of arbidol hydrochloride in influenza A (H1N1) virus infection. *Acta Pharmacol. Sin.* **2013**, *34*, 1075–1083. [[CrossRef](#)] [[PubMed](#)]
- Lane, A.N.; Fan, T.W.M. Regulation of mammalian nucleotide metabolism and biosynthesis. *Nucleic Acids Res.* **2015**, *43*, 2466–2485. [[CrossRef](#)] [[PubMed](#)]
- Peterson, L.W.; McKenna, C.E. Prodrug approaches to improving the oral absorption of antiviral nucleotide analogues. *Expert Opin. Drug Deliv.* **2009**, *6*, 405–420. [[CrossRef](#)] [[PubMed](#)]

16. Kozuch, O.; Mayer, V. Pig Kidney Epithelial (Ps) Cells—Perfect Tool for Study of Flaviviruses and Some Other Arboviruses. *Acta Virol.* **1975**, *19*, 498. [[PubMed](#)]
17. Ruzek, D.; Vancova, M.; Tesarova, M.; Ahantarig, A.; Kopecky, J.; Grubhoffer, L. Morphological changes in human neural cells following tick-borne encephalitis virus infection. *J. Gen. Virol.* **2009**, *90*, 1649–1658. [[CrossRef](#)] [[PubMed](#)]
18. DeMadrid, A.T.; Porterfield, J.S. A Simple Micro-Culture Method for Study of Group B Arboviruses. *Bull. World Health Organ.* **1969**, *40*, 113–121.
19. Eyer, L.; Valdés, J.J.; Gil, V.A.; Nencka, R.; Hřebabeký, H.; Šála, M.; Salát, J.; Černý, J.; Palus, M.; de Clercq, E.; Růžek, D. Nucleoside Inhibitors of Tick-Borne Encephalitis Virus. *Antimicrob. Agents Chemother.* **2015**, *59*, 5483–5493. [[CrossRef](#)] [[PubMed](#)]
20. Chapel, C.; Zitzmann, N.; Zoulim, F.; Durantel, D. Virus morphogenesis and viral entry as alternative targets for novel hepatitis C antivirals. *Future Virol.* **2006**, *1*, 197–209. [[CrossRef](#)]
21. Eyer, L.; Nencka, R.; de Clercq, E.; Seley-Radtke, K.; Ruzek, D. Nucleoside analogs as a rich source of antiviral agents active against arthropod-borne Flaviviruses. *Antivir. Chem. Chemother.* **2018**. [[CrossRef](#)] [[PubMed](#)]
22. Becher, F.; Landman, R.; Mboup, S.; Kane, C.N.; Canestri, A.; Liegeois, F.; Vray, M.; Prevot, M.H.; Leleu, G.; Benech, H. Monitoring of didanosine and stavudine intracellular triphosphorylated anabolite concentrations in HIV-infected patients. *AIDS* **2004**, *18*, 181–187. [[CrossRef](#)] [[PubMed](#)]
23. Gao, W.Y.; Shirasaka, T.; Johns, D.G.; Broder, S.; Mitsuya, H. Differential Phosphorylation of Azidothymidine, Dideoxycytidine, and Dideoxyinosine in Resting and Activated Peripheral-Blood Mononuclear-Cells. *J. Clin. Investig.* **1993**, *91*, 2326–2333. [[CrossRef](#)] [[PubMed](#)]
24. Mumtaz, N.; Jimmerson, L.C.; Bushman, L.R.; Kiser, J.J.; Aron, G.; Reusken, C.B.E.M.; Koopmans, M.P.G.; van Kampen, J.J.A. Cell-line dependent antiviral activity of sofosbuvir against Zika virus. *Antivir. Res.* **2017**, *146*, 161–163. [[CrossRef](#)] [[PubMed](#)]
25. Deng, Y.Q.; Zhang, N.N.; Li, C.F.; Tian, M.; Hao, J.N.; Xie, X.P.; Shi, P.Y.; Qin, C.F. Adenosine Analog NITD008 Is a Potent Inhibitor of Zika Virus. *Open Forum Infect. Dis.* **2016**, *3*, ofw175. [[CrossRef](#)] [[PubMed](#)]
26. Eyer, L.; Nencka, R.; Huvarová, I.; Palus, M.; Joao Alves, M.; Gould, E.A.; de Clercq, E.; Růžek, D. Nucleoside Inhibitors of Zika Virus. *J. Infect. Dis.* **2016**, *214*, 707–711. [[CrossRef](#)] [[PubMed](#)]
27. Julander, J.G.; Siddharthan, V.; Evans, J.; Taylor, R.; Tolbert, K.; Apuli, C.; Stewart, J.; Collins, P.; Gebre, M.; Neilson, S.; et al. Efficacy of the broad-spectrum antiviral compound BCX4430 against Zika virus in cell culture and in a mouse model. *Antivir. Res.* **2017**, *137*, 14–22. [[CrossRef](#)] [[PubMed](#)]
28. Sacramento, C.Q.; de Melo, G.R.; de Freitas, C.S.; Rocha, N.; Hoelz, L.V.; Miranda, M.; Fintelman-Rodrigues, N.; Marttorelli, A.; Ferreira, A.C.; Barbosa-Lima, G.; et al. The clinically approved antiviral drug sofosbuvir inhibits Zika virus replication. *Sci. Rep.* **2017**, *7*, 40920. [[CrossRef](#)] [[PubMed](#)]
29. Leneva, I.A.; Fedyakina, I.T.; Guskova, T.A.; Glushkov, R.G. Sensitivity of various influenza virus strains to arbidol. Influence of arbidol combination with different antiviral drugs on reproduction of influenza virus A. *Terapevticheskii arkhiv* **2005**, *77*, 84–88. [[PubMed](#)]
30. Delogu, I.; Pastorino, B.; Baronti, C.; Nougairede, A.; Bonnet, E.; De Lamballerie, X. In vitro antiviral activity of arbidol against Chikungunya virus and characteristics of a selected resistant mutant. *Antivir. Res.* **2011**, *90*, 99–107. [[CrossRef](#)] [[PubMed](#)]
31. Oestereich, L.; Rieger, T.; Neumann, M.; Bernreuther, C.; Lehmann, M.; Krasemann, S.; Wurr, S.; Emmerich, P.; de Lamballerie, X.; Ölschläger, S.; Günther, S. Evaluation of Antiviral Efficacy of Ribavirin, Arbidol, and T-705 (Favipiravir) in a Mouse Model for Crimean-Congo Hemorrhagic Fever. *PLoS Negl. Trop. Dis.* **2014**, *8*, e2804. [[CrossRef](#)] [[PubMed](#)]
32. Deng, H.Y.; Luo, F.; Shi, L.Q.; Zhong, Q.; Liu, Y.J.; Yang, Z.Q. Efficacy of arbidol on lethal hantaan virus infections in suckling mice and in vitro. *Acta Pharmacol. Sin.* **2009**, *30*, 1015–1024. [[CrossRef](#)] [[PubMed](#)]
33. Shi, L.; Xiong, H.; He, J.; Deng, H.; Li, Q.; Zhong, Q.; Hou, W.; Cheng, L.; Xiao, H.; Yang, Z. Antiviral activity of arbidol against influenza A virus, respiratory syncytial virus, rhinovirus, coxsackie virus and adenovirus in vitro and in vivo. *Arch. Virol.* **2007**, *152*, 1447–1455. [[CrossRef](#)] [[PubMed](#)]





Article

Antiviral Activity of Vacuolar ATPase Blocker Diphyllin against SARS-CoV-2

Michal Stefanik^{1,2}, Petra Strakova¹, Jan Haviernik¹, Andrew D. Miller^{1,2,3} , Daniel Ruzek^{1,4}
and Ludek Eyer^{1,4,*}

¹ Department of Virology, Veterinary Research Institute, CZ-62100 Brno, Czech Republic; stefanik@vri.cz (M.S.); strakova.petra@vri.cz (P.S.); haviernik@vri.cz (J.H.); miller@vri.cz (A.D.M.); ruzekd@paru.cas.cz (D.R.)

² Department of Chemistry and Biochemistry, Mendel University in Brno, CZ-61300 Brno, Czech Republic

³ KP Therapeutics (Europe) s.r.o., CZ-61200 Brno, Czech Republic

⁴ Institute of Parasitology, Biology Centre of the Czech Academy of Sciences, CZ-37005 Ceske Budejovice, Czech Republic

* Correspondence: eyer@vri.cz

Abstract: Severe Acute Respiratory Syndrome Coronavirus 2 (SARS-CoV-2) is a causative agent of the pandemic coronavirus disease 2019 (COVID-19), which has resulted in over two million deaths worldwide to date. Diphyllin and diphyllinosides are known as natural blockers of cellular vacuolar ATPases, and so can act as inhibitors of the pH-dependent fusion of viral envelopes with host cell endosomal membranes. Such pH-dependent fusion is a critical early step during the SARS-CoV-2 replication cycle. Accordingly, the anti-SARS-CoV-2 profiles and cytotoxicities of diphyllin, diphyllinoside cleistanthin B, and two structurally related compounds, helioxanthin 8-1 and helioxanthin 5-4-2, are evaluated here using in vitro cell-based assay systems. Neither helioxanthin exhibits any obvious anti-SARS-CoV-2 effects in vitro. By contrast diphyllin and cleistanthin B do exhibit anti-SARS-CoV-2 effects in Vero cells, with respective 50% effective concentrations (EC₅₀) values of 1.92 and 6.51 μM. Diphyllin displays anti-SARS-CoV-2 effect also in colorectal adenocarcinoma (CaCo-2) cells. Moreover, when diphyllin is added at various times post infection, a significant decrease in viral titer is observed in SARS-CoV-2-infected Vero cells, even at high viral multiplicities of infection. Importantly, neither diphyllin nor cleistanthin B are found cytotoxic to Vero cells in concentrations up to 100 μM. However, the cytotoxic effect of diphyllin is more pronounced in Vero E6 and CaCo-2 cells. Overall, our data demonstrate that diphyllin and diphyllin analogues might be perfected as anti-SARS-CoV-2 agents in future preclinical studies, most especially if nanomedicine approaches may be invoked to optimize functional drug delivery to virus infected cells.

Keywords: Severe Acute Respiratory Syndrome Coronavirus 2 (SARS-CoV-2); vacuolar ATPase blocker; diphyllin; cleistanthin B; helioxanthin; antiviral activity; cytotoxicity



Citation: Stefanik, M.; Strakova, P.; Haviernik, J.; Miller, A.D.; Ruzek, D.; Eyer, L. Antiviral Activity of Vacuolar ATPase Blocker Diphyllin against SARS-CoV-2. *Microorganisms* **2021**, *9*, 471. <https://doi.org/10.3390/microorganisms9030471>

Academic Editor:
Javier Sanchez-Cespedes

Received: 11 February 2021
Accepted: 22 February 2021
Published: 25 February 2021

Publisher's Note: MDPI stays neutral with regard to jurisdictional claims in published maps and institutional affiliations.



Copyright: © 2021 by the authors. Licensee MDPI, Basel, Switzerland. This article is an open access article distributed under the terms and conditions of the Creative Commons Attribution (CC BY) license (<https://creativecommons.org/licenses/by/4.0/>).

1. Introduction

Severe Acute Respiratory Syndrome Coronavirus 2 (SARS-CoV-2), formerly known as 2019 novel coronavirus (2019-nCoV), is a causative agent of coronavirus disease 2019 (COVID-19). SARS-CoV-2 was firstly identified from the respiratory tract of pneumonia patients in Wuhan, China, in late December 2019, after which the virus spread to numerous other countries around the world over the next few months [1]. As a result, on March 11, 2020, the World Health Organization (WHO) announced COVID-19 to be a new pandemic disease [1]. As of 1 February 2021, there have been more than 101 million confirmed cases of COVID-19 globally, including over two million deaths (<https://covid19.who.int/>, accessed on 1 February 2021). SARS-CoV-2 is an airborne virus, which is typically transmitted from person to person via respiratory droplets, although transmission through contaminated surfaces is also highly likely. The clinical course of COVID-19 can be complex. In most cases, the infection is asymptomatic or relatively mild, accompanied by fever, cough, shortness

of breath, and muscle ache [2]. In some cases, however, particularly in elderly patients and those with cardiac and respiratory disorders, SARS-CoV-2 infection may progress to serious and life-threatening acute respiratory distress syndrome (ARDS) or pneumonia [3,4] resulting in sepsis, multiple organ dysfunction, and death [2]. Around 3–29% patients may need admission to intensive care units [5]. Although, several types of vaccination strategies are currently available, new highly anti-COVID-19 drugs are needed urgently to combat the disease. Numerous anti-COVID-19 clinical trials are ongoing seeking to repurpose known drugs against SARS-CoV-2 infections, including trials with remdesivir, favipiravir, or hydroxychloroquin [1]. However, the primary unmet medical need is for the development of genuine, small molecule anti-SARS-CoV-2 drugs that are novel and very specific in mechanism of action.

An essential step in the infection cycle of enveloped viruses is a frequently pH-dependent fusion of viral envelopes with host cell endosomal membranes. Cell entry of enveloped viruses takes place by endocytosis. During endocytosis, a vacuolar ATPase (V-ATPase) acts as a proton pump to increase the proton concentration and so cause the acidification of inner endosome compartments [6]. Therefore, inhibitors of V-ATPase have the potential to act as de facto inhibitors, as well of the pH-dependent fusion of viral envelopes with host cell endosomal membranes. Given this, the V-ATPase represents an attractive novel and specific new antiviral drug target, and small molecule inhibitors represent a promising group of potential novel and specific new antiviral agents [7]. For this reason, we chose to investigate diphyllin and its analogues. Diphyllin and the diphyllinosides are natural compounds of the arynaphtalide lignan family, extracted from the plants *Cleistanthus collinus*, *Justicia gendarussa*, *Haplophyllum bucharicum*, plus some others, which are widely used in traditional Chinese medicine [8]. Furthermore, these natural compounds are known V-ATPase inhibitors with the ability to suppress acidification in human osteoclasts [9], to decrease V-ATPase activity and infectivity in gastric adenocarcinoma cells [10], and to inhibit the replication cycles of many fungal [11], bacterial [12], and viral pathogens. Of particular relevance here, diphyllin and the diphyllinosides have already been demonstrated to exhibit some inhibitory effects in vitro and in vivo against several enveloped viruses, such as influenza virus [13], HIV-1 [14], Zika virus (ZIKV) [6], feline infectious peritonitis virus (FIPV) [7], and vesicular stomatitis virus (VSV) [15]. Apart from diphyllin and diphyllinosides, numerous other structurally related compounds have been identified with interesting biological properties [15], as exemplified by helioxanthins, whose molecular mechanisms of action are still poorly understood [16]. Here we evaluate diphyllin for its ability to inhibit replication of SARS-CoV-2 in vitro and compare its antiviral and cytotoxic properties with those of diphyllinoside cleistanthin B (diphyllin-4- β -D-glucopyranoside), helioxanthin 8-1, and helioxanthin 5-4-2, whose antiviral activities have been reported previously [17–19] (Figure 1).

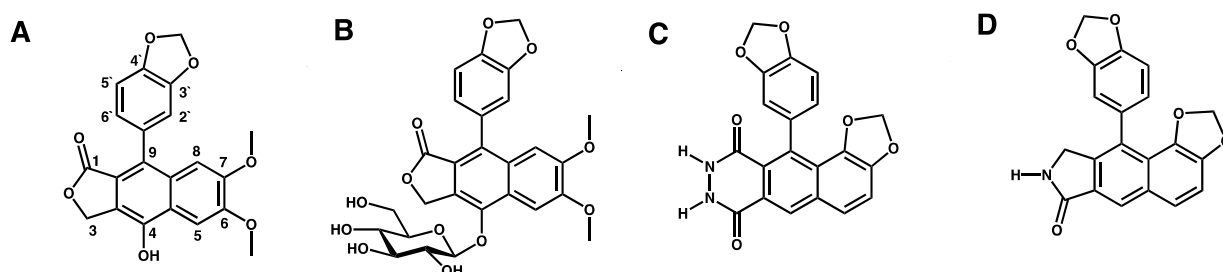


Figure 1. Structures of the studied compounds. (A) Diphyllin, (B) cleistanthin B, (C) helioxanthin 8-1, and (D) helioxanthin 5-4-2.

2. Materials and Methods

2.1. Compounds, Virus, and Cell Lines

Diphyllin was synthesized by Apigenex (Prague, Czech Republic), cleistanthin B was obtained from WuXi AppTec (Tianjin, China), helioxanthin 8-1 and helioxanthin 5-4-2 were

purchased from MedChemExpress (Stockholm, Sweden). All compounds were solubilized in dimethyl sulfoxide (DMSO) as 10 mM stock solutions. SARS-CoV-2 (strain SARS-CoV-2/human/Czech Republic/951/2020 was isolated from a clinical sample at the National Institute of Health, Prague, Czech Republic), and kindly provided by Dr. Jan Weber, Institute of Organic Chemistry and Biochemistry, Prague, Czech Republic. This was passaged five times through Vero E6 cells (ATCC CRL-1586) for multiplication before use. Vero cells (ATCC CCL-81, African Green Monkey, adult kidney, epithelial cells) were used for antiviral, cytotoxicity, and immunostaining assay studies. Otherwise, Vero E6 cells (ATCC CRL-1586) were used again for plaque assays. Both Vero cell lines were grown in Dulbecco's modified Eagle's medium (DMEM) supplemented with 10% newborn calf serum, 100 U/mL penicillin, 100 µg/mL streptomycin, and 1% glutamine (Sigma–Aldrich, Prague, Czech Republic). Colorectal adenocarcinoma cells (CaCo-2, ATCC HTB-37) were used for further characterization of the antiviral and cytotoxicity effects of diphyllin, and were grown in DMEM medium, containing, 20% newborn calf serum with 100 U/mL penicillin, 100 µg/mL streptomycin, and 1% glutamin (Sigma–Aldrich, Prague, Czech Republic).

2.2. Cytotoxicity Assay

To determine the cytotoxicity of diphyllin, Vero cells (ATCC CCL-81), Vero E6 cells (ATCC CRL-1586), and CaCo-2 cells (ATCC HTB-37) were seeded in 96-well microtitration plates (2×10^4 cells/well) and incubated for 24 h. After incubation, diphyllin was added to the cells, in a concentration range from 0 to 100 µM, and the treated cells were further cultivated for 48 h at 37 °C. The cytotoxicities of cleistanthin B, helioxanthin 8-1 and helioxanthin 5-4-2 were tested in a similar way but only in Vero cells (ATCC CCL-81). All cytotoxicities were measured in terms of cell viability as determined with Cell Counting Kit-8 (Dojindo Molecular Technologies, Munich, Germany), used according to manufacturer's instructions. The respective concentrations of each compound under investigation were determined that reduced cell viability by 50% (CC₅₀ values).

2.3. Antiviral Assays

The antiviral efficacies of diphyllin, cleistanthin B, helioxanthin 8-1, and helioxanthin 5-4-2 were initially tested at a single concentration of 50 µM/well with Vero cells (ATCC CCL-81) using a viral titer reduction assay. Since Vero cells were observed to be the most resistant to diphyllin cytotoxicity, we chose this cell line to perform crucial antiviral cell-based assays. Growth medium was aspirated from Vero confluent monolayers cultivated in 96-well microtiter plates for 24 h and subsequently replaced with fresh medium (200 µL) containing the compounds under investigation and SARS-CoV-2 at a multiplicity of infection (MOI) of 0.1. Drug dosing and virus infection were performed simultaneously. Vero cells treated with either DMSO 0.5% (*v/v*) or remdesivir (50 µM) were used as controls. Drug-treated virus-infected cells were then cultured for 48 h at 37 °C. Viral titers were determined from collected supernatant media by a plaque assay.

In order to study the dose-response effects of diphyllin and cleistanthin B, the same experimental procedure was performed, as described above, with slight modifications. Growth medium was aspirated from Vero cell monolayers, replaced with fresh medium (200 µL) containing the compounds under evaluation in the concentration range 0 to 50 µM and SARS-CoV-2 at an MOI of 0.1, then cells were cultivated for 48 h at 37 °C. Viral titers were determined from the collected supernatant media and used to construct dose-dependent curves from which 50% effective concentrations (EC₅₀ values) were calculated. The anti- SARS-CoV-2 effect of diphyllin was studied also in CaCo-2 cells (ATCC HTB-37). Owing to the higher sensitivity of CaCo-2 cells to diphyllin cytotoxicity, only lower concentrations were tested (i.e., 1.5, and 3.0 µM).

For testing whether or not diphyllin retained its antiviral activity even when added at various time intervals after infection, we performed four independent post-treatment assays, each differing in the time of drug addition to infected Vero cells (ATCC CCL-81). The cells were seeded in 96-well plates (2×10^4 cells/well) and incubated for 24 h to

form a confluent monolayer. The cell monolayers were then infected with SARS-CoV-2 (MOI of 0.1). Medium containing diphyllin (at either 12.5, 25, or 50 μM) was added to infected cells 2, 4, 6, and 24 h post infection (h.p.i). Cells were then further incubated up to 48 h. Following incubation, the viral titers were determined from the collected supernatant media by plaque assay and the viral surface antigen expression visualized using an immunostaining assay.

The dependence of diphyllin antiviral efficacy on viral MOI was tested as follows. Vero cells (ATCC CCL-81) were seeded in 96-well plates (2×10^4 cells per well) and incubated for 24 h to form a confluent monolayer. The obtained Vero cell monolayers were subsequently treated with a fresh medium containing diphyllin, at concentrations of 25 and 50 μM , and infected with SARS-CoV-2 at three different MOIs of 0.1, 1, and 10. The infected cells were then further incubated for 48 h. Thereafter, viral titers were determined from collected supernatants by plaque assay.

2.4. Plaque Assay

Plaque assays were performed in Vero E6 cells (ATCC CRL-1586), using a modified protocol originally developed by De Madrid and Porterfield [20]. In Vero E6 cells, SARS-CoV-2 forms large, circular plaques, which are regular in shape and size, and, therefore, this cell line is particularly suitable for plaque assays and subsequent viral titer quantification. Briefly, 10-fold dilutions of virus were prepared in 24-well tissue culture plates, and the cells were added to each well ($0.6\text{--}1.5 \times 10^5$ cells/well). After 4 h incubation, the suspension was overlaid with 1.5% (*w/v*) carboxymethylcellulose in DMEM. Following a 5-day incubation at 37 °C, the infected plates were washed with phosphate-buffered saline, and the cell monolayers were stained with naphthalene black. The virus titer was expressed as plaque forming units (PFU)/mL.

2.5. Immunofluorescence Staining

To measure the compound-induced inhibition of viral surface antigen expression, a cell-based immunostaining assay was performed as previously described [21], with minor modifications. Briefly, Vero cells (ATCC CCL-81) were seeded onto 96-well microtitration plates and 24 h later the confluent monolayers were infected with SARS-CoV-2 at MOI of 0.1. Then, diphyllin or cleistanthin B were added at different concentrations to cell monolayers that were then cultured for 48 h at 37 °C. After cold acetone–methanol (1:1, *v/v*) fixation and blocking with 10% fetal bovine serum, cells were incubated with a rabbit (2019-nCoV) spike S1 antibody (1:50; Sino Biological, Duesseldorfer, Germany) and subsequently incubated for 1 h at 37 °C with anti-rabbit goat secondary antibodies conjugated with fluorescein isothiocyanate (FITC; 1:250; Sigma–Aldrich, Prague, Czech Republic). Cells were counterstained with 4',6-diamidino-2-phenylindole (DAPI) (1 $\mu\text{g}/\text{mL}$) for the visualization of cell nuclei and fluorescence signals were recorded with an Olympus IX71 epifluorescence microscope.

2.6. Statistics Analysis

Data were expressed as mean \pm standard deviation (SD), and the significance between groups was evaluated by the unpaired parametric two-tailed t-test using GraphPad Prism 7.04 (GraphPad Software, Inc., San Diego, CA, USA). $P < 0.05$ was considered significant. EC_{50} and CC_{50} values were calculated as inflection points in sigmoidal inhibitory and cell viability curves, which were obtained by a nonlinear fit of transformed inhibitor concentrations versus normalized response using GraphPad Prism 7.04.

3. Results and Discussion

Diphyllin, diphyllinoside cleistanthin B, and two structurally related helioxanthins (Figure 1) were evaluated for their *in vitro* cytotoxic profiles, and their anti-SARS-CoV-2 activities. Diphyllin cytotoxicity was assessed in Vero, Vero E6, and CaCo-2 cells over the concentration range 0 to 100 μM at 48 h post treatment. In Vero cells, diphyllin was found

well tolerated, showing a CC_{50} value of $>100 \mu\text{M}$ (Figure 2A and Table 1). Diphyllin cytotoxicity in the Vero E6 cell line was greater such that cell viability declined to approx. 75% with $50 \mu\text{M}$ diphyllin although a CC_{50} value of $>100 \mu\text{M}$ was still determined (Figure 2A). Diphyllin exhibited its highest cytotoxicity in CaCo-2 cells ($CC_{50} 54.6 \pm 4.8 \mu\text{M}$) (Figure 2A). The cytotoxicities of cleistanthin B, helioxanthin 8-1, and helioxanthin 5-4-2 were determined only in Vero cells. Whereas cleistanthin B showed a decent cytotoxicity profile over the tested concentration range, helioxanthin 8-1 caused a decline of cell viability to $70.6 \pm 2.4\%$ at $100 \mu\text{M}$. Treatment with helioxanthin 5-4-2 resulted in a larger decrease in cell viability to $60 \pm 5.8\%$ at $100 \mu\text{M}$ (Figure 2B).

Table 1. Antiviral and cytotoxicity characteristics of diphyllin and cleistanthin B in Vero cells.

Compound	EC_{50} (μM) ^{1,2}	CI ³	CC_{50} (μM) ¹	SI ⁴
diphyllin	1.92	1.52 to 2.43	>100	>52.08
cleistanthin B	6.51	4.71 to 8.98	>100	>15.36
helioxanthin 8-1	>50	N. D.	>100	N. D.
helioxanthin 5-4-2	>50	N. D.	>100	N. D.

¹ Determined from three independent experiments. ² Defined as the critical concentration at which a 50% reduction in viral titers is observed as calculated by the inflection point of sigmoidal dose-response curves, generated using GraphPad Prism 7.04 (GraphPad Software, Inc., USA) by nonlinear fitting of transformed inhibitor concentrations versus normalized response. ³ confidence interval (CI) calculated using GraphPad Prism 7.04 (GraphPad Software, Inc., USA). ⁴ selectivity index (SI) = CC_{50}/EC_{50} . N. D.; not determined.

Interestingly, Vero cells do appear to be more resistant to the cytotoxic effects of diphyllin and other diphyllin-related compounds compared to other cell types, as reported by other authors. Chen et al. [13] measured diphyllin cytotoxicity in Mardin–Darby canine kidney (MDCK) and A549 cells resulting in CC_{50} values of 3.48 and 24.01 μM , respectively. Similarly, diphyllin was shown to be cytotoxic for fcwf-4 cells ($CC_{50} 5.99 \mu\text{M}$). Notably, diphyllin-poly(ethylene glycol)-block-poly(lactide-co-glycolide) (PLGA) nanoparticles were much less cytotoxic (CC_{50} of 77.3 μM) in comparison to free diphyllin [7]. On the other hand, Asano et al. [15] reported that minimum cytotoxic concentrations of diphyllin, diphyllin apioside, diphyllin apioside-acetate, and justicidins A, C, and D (Figure 1 and Figure S1) were 63 $\mu\text{g}/\text{mL}$ in RL-33 cells. Approximately 2–4-fold lower toxicities were observed using justicidinioside A, B, and C (Figure S1) with minimum cytotoxic concentrations of 125 and 250 $\mu\text{g}/\text{mL}$ identified in RL-33 cells. The cytotoxicity of helioxanthin 8-1 was studied in dstet5 cells and CC_{50} values were determined from 18 μM to 45 μM [19]. The CC_{50} values of helioxanthin 5-4-2 in HepG2 cells reached single-digit micromolar values [18].

In evaluating the antiviral potency of diphyllin, cleistanthin B, helioxanthin 8-1, and helioxanthin 5-4-2, Vero cells infected with SARS-CoV-2 (MOI of 0.1) were treated with a single concentration of each compound under investigation ($50 \mu\text{M}$), then cells were cultivated for 48 h.p.i. Under these conditions, diphyllin completely inhibited virus replication, resulting in a viral titer decrease of 10^6 -fold compared with the situation with virus-infected mock-treated cells. This effect was comparable with the antiviral effect of remdesivir used as a positive control (Figure 2C). The antiviral effect of cleistanthin B was somewhat lower than that of diphyllin resulting in a decrease in viral titer of 10^3 -fold. Interestingly, helioxanthin 8-1 and helioxanthin 5-4-2 appeared to be inactive against SARS-CoV-2 at the tested concentration and were therefore excluded from further antiviral analyses (Figure 2C). This was somewhat surprising to us given that the tested helioxanthin analogues have been described elsewhere to exhibit broad-range antiviral activities [16,18,19].

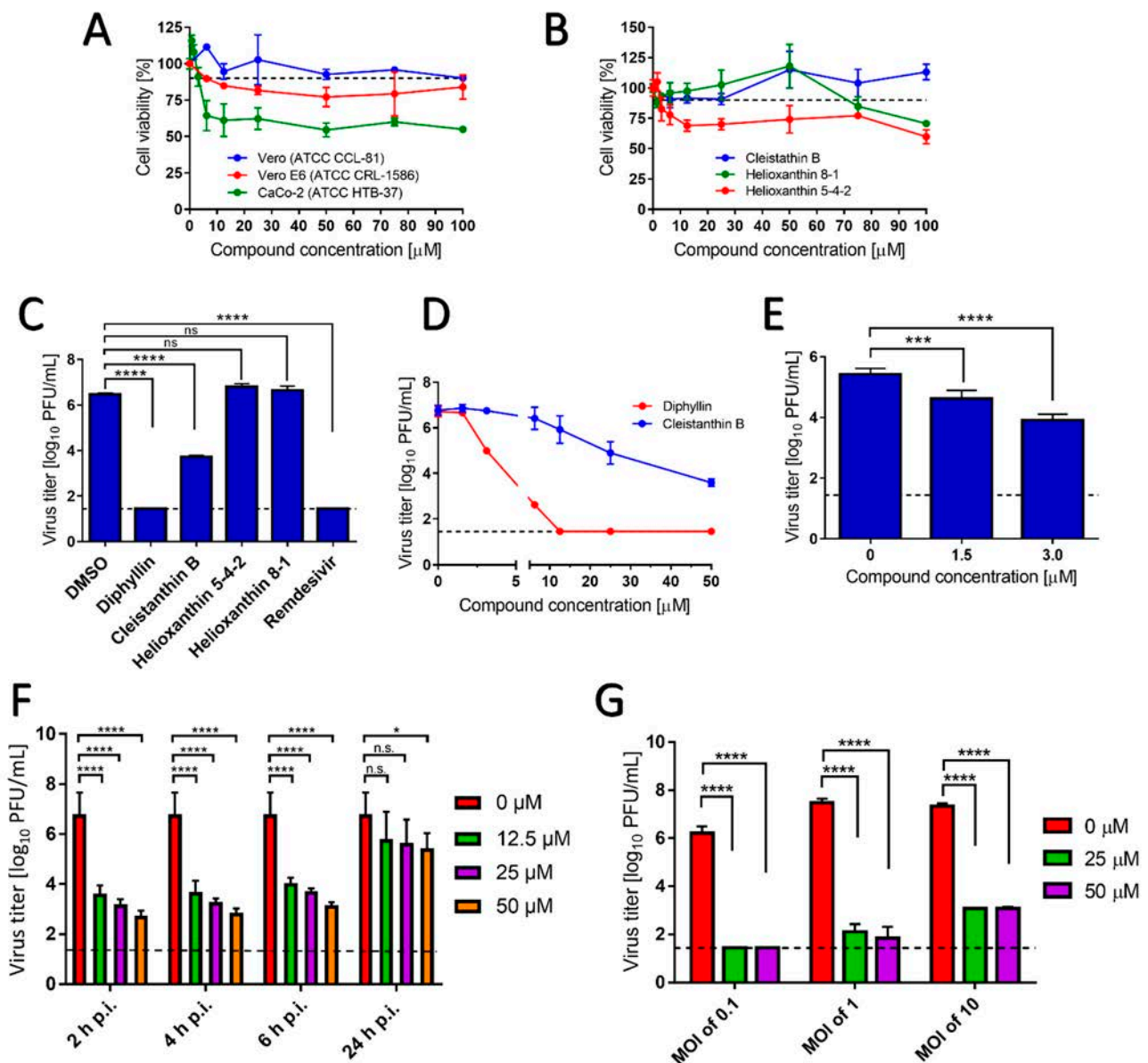


Figure 2. (A) Cytotoxicities of diphyllin in Vero, Vero E6, and CaCo-2 cells are shown and expressed as percentage of cell viability. The cells were treated with diphyllin at the indicated concentrations and incubated for 48 h. (B) Cytotoxicities of cleistanthin B, helioxanthin 8-1, and helioxanthin 5-4-2 in Vero cells are shown. The cells were treated with the compounds at the indicated concentrations and incubated for 48 h. (C) Anti-SARS-CoV-2 activities of diphyllin, cleistanthin B, helioxanthin 8-1, and helioxanthin 5-4-2 are shown as measured in Vero cells infected with SARS-CoV-2 (multiplicity of infection (MOI) of 0.1) and simultaneously treated with each compound under investigation (50 μM). Infected cells were incubated separately with each compound under investigation for 48 h post infection (h.p.i.) and viral titers were determined using the plaque assay. Remdesivir was used as a positive control. (D) Growth curves are shown of SARS-CoV-2 in Vero cells treated with diphyllin and cleistanthin B (at the indicated concentrations). Vero cells were infected with the virus (MOI of 0.1) and simultaneously treated with the compounds under investigation, then incubated for 48 h.p.i. Viral titers were quantified using the plaque assay. (E) Anti-SARS-CoV-2 activities are shown in CaCo-2 cells using diphyllin at the indicated concentrations. (F) Anti-SARS-CoV-2 activities are shown in SARS-CoV-2-infected Vero cells that were treated with diphyllin 2, 4, 6, and 24 h.p.i. (at the indicated concentrations) then incubated up to 48 h. (G) Anti-SARS-CoV-2 activities are shown in SARS-CoV-2-infected Vero cells (MOIs of 0.1, 1, and 10) that were treated with diphyllin (at the indicated concentrations) and then incubated for 48 h.p.i. Viral titers were determined by a plaque assay. The mean titers from three biological replicates are shown, and error bars indicate standard errors of the mean. The horizontal dashed line indicates the minimum detectable threshold of 1.44 \log_{10} plaque forming units (PFU)/mL. n.s., not significant; *, $p < 0.05$; ***, $p < 0.001$; ****, $p < 0.0001$.

The dose-dependent anti-SARS-CoV-2 effects of diphyllin and cleistanthin B (0 to 50 μM) were quantified in Vero cells by plaque assay 48 h.p.i. Using this assay, diphyllin was observed to reduce viral titers with an EC_{50} value of 1.92 μM (Figure 2D, Table 1). Diphyllin notably mediated complete inhibition of viral replication at $\geq 12.5 \mu\text{M}$. In comparison, cleistanthin B was observed to reduce viral titers with an EC_{50} value of 6.51 μM indicating that this compound is 3.4-fold less potent than diphyllin (Figure 2D, Table 1). In addition, cleistanthin B was only able to reduce viral titer by 10^3 -fold at the highest tested concentration of 50 μM 48 h.p.i. (Figure 2D). These dose-dependent antiviral effects of diphyllin and cleistanthin B were further confirmed by immunofluorescence staining used to monitor the level of coronavirus spike S1 antigen expression in Vero cells as a measure of both viral infectivity and successful viral replication in vitro (Figure 3A). Although S1 protein was highly expressed in virus-infected mock-treated cells, S1 protein fluorescence was observed to decrease towards virtually undetectable in Vero cell monolayers 48 h.p.i. when infected cells were treated with ascending concentrations of diphyllin (12.5, 25, and 50 μM). In virus-infected cells treated with cleistanthin B, the decrease in S1 antigen expression was less obvious compared with diphyllin (Figure 3A), in agreement with results from virus titer reduction assays (Figure 2D).

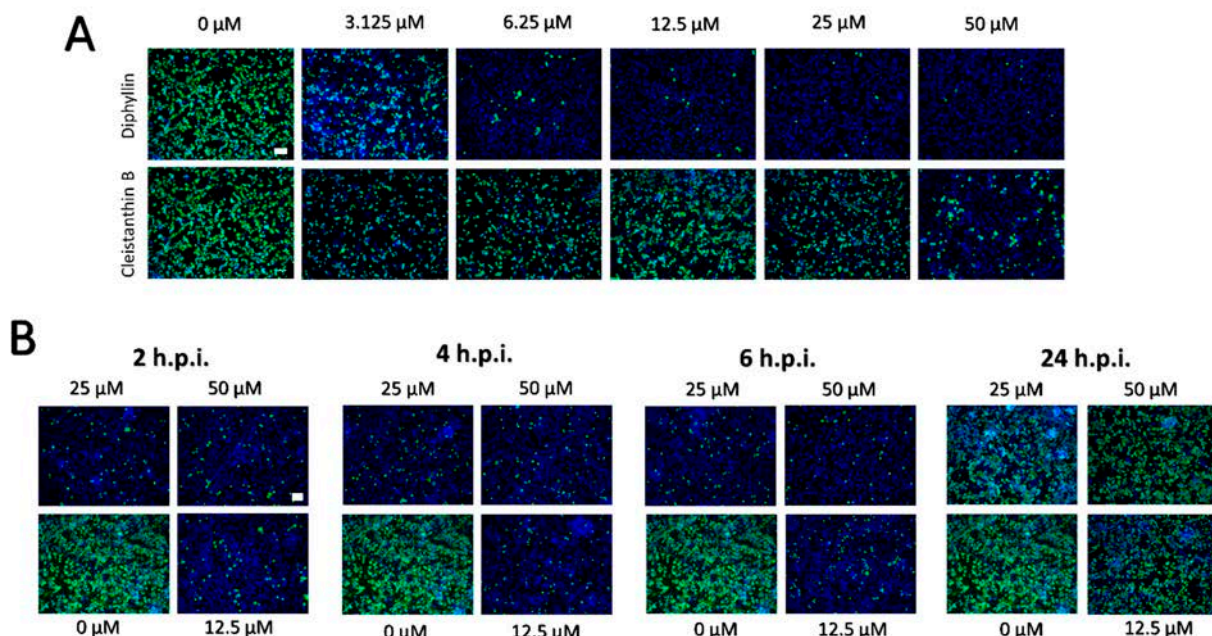


Figure 3. (A) Inhibition of SARS-CoV-2 viral antigen expression by diphyllin and cleistanthin B. Compound-treated and virus-infected Vero cells cultivated for 48 h.p.i. were fixed on slides, then stained with a SARS-CoV-2 specific antibody labeled with FITC (green), and counterstained with DAPI (blue). (B) Immunofluorescence staining of Vero cell cultures infected with SARS-CoV-2 and treated with diphyllin at 2, 4, 6, and 24 h.p.i. The immunofluorescent staining procedure was identical as in (A). Scale bars; 50 μM .

Owing to the superior antiviral activity of diphyllin, further anti-SARS-CoV-2 studies were performed only with this compound. Initially, the anti-SARS-CoV-2 effect of diphyllin was assessed in CaCo-2 cells, which represents another highly susceptible cell line frequently used for SARS-CoV-2 multiplication, virus pathogenesis studies, and antiviral assays. Given that this cell line appeared considerably more sensitive to diphyllin cytotoxicity than Vero cells, antiviral studies were only performed using lower diphyllin concentrations (1.5 and 3.0 μM) resulting in only a moderate but nonetheless statistically significant decrease in viral titer (approximately 1 and 2 orders of magnitude, respectively) compared the situation with control cells (Figure 2E). Following this, time-of-addition assays were performed in which diphyllin was administered in ascending concentrations (12.5, 25, and 50 μM) between 2, 4, 6, and 24 h.p.i. Even up to 6 h.p.i., viral titers were

decreased up to 4 orders of magnitude. Moreover, a statistically significant decline in viral titers was even observed in virus-infected Vero cells, even when diphyllin was added at a concentration of 50 μM 24 h.p.i. (Figure 2F). The anti-SARS-CoV-2 time-of-addition effects of diphyllin were further confirmed by means of viral antigen immunostaining (Figure 3B). Finally, the anti-SARS-CoV-2 effect of diphyllin (at 25 and 50 μM) was further tested using viral MOIs of 1 and 10, instead of the MOI of 0.1 used previously here (see above). Although, the antiviral activity of diphyllin at high MOIs was weaker than with a MOI of 0.1, nevertheless the compound reduced viral titers more than 10^6 -fold (MOI of 1) and 10^5 -fold (MOI of 10) 48 h.p.i (Figure 2G). These data clearly demonstrate the strong antiviral potency of diphyllin given that diphyllin is able to suppress SARS-CoV-2 replication even in a single-cycle infection model at high MOI.

Our data here strongly interlock to support the view that diphyllin is a potent agent against anti-SARS-CoV2. Elsewhere, diphyllin has been described to inhibit endosomal acidification in fcwf-4 cells, resulting in nanomolar suppression of the replication of FIPV, another member of the *Coronaviridae* family [7]. Diphyllin has also been shown to be potent in vitro against influenza virus in MDCK cells [13] and against HIV-1 in human peripheral blood mononuclear cells (PBMC) [17]. Furthermore, a combination treatment of diphyllin with oseltamivir and amantadine has been shown to have more anti-influenza efficacy in cell cultures than diphyllin itself [13]. In comparison, diphyllin derivatives, justicidin A and B, differing from diphyllin by a C4-methoxy group or C4-hydrogen (in place of the C4-hydroxy group) (Figure 1 and Figure S1), have been shown, respectively, to exhibit anti-VSV effects when tested in RL-33 cells. Although, justicidins C and D with a C3-carbonyl lactone ring (instead of the C1-carbonyl lactone ring in diphyllin) (Figure 1 and Figure S1) were found to be approximately 100-fold less active [15].

Turning to diphyllinosides, these diphyllin derivatives differ from diphyllin in the conjugation of pentofuranose or hexopyranose rings of different types or positions and have also been found to possess potent antiviral activities [6,14,15,17]. For instance, diphyllin apioside and diphyllin apioside-acetate, with pentofuranose rings attached to C4 (Figure S1), have been found equivalent in anti-VSV assays compared with free diphyllin [15]. In contrast, justicidiniosides A–C, characterized by a β -glucopyranose (Glc) on C6' of the 1,3-benzodioxole moiety (Figure S1), have been found 100–1000-fold less potent than diphyllin although with better cytotoxicity profiles [15]. Otherwise, patentiflorin A (Figure S1) has been shown to block ZIKV replication in both human and monkey cell lines and exhibits broad-spectrum antiviral activities in vitro across the *Flaviviridae* family, even preventing mortality in a rodent in vivo model of ZIKV infection [6]. This same patentiflorin A also displayed nanomolar activity against four clinical HIV-1 isolates, using a standardized human PBMC assay, which was 20–30 times more potent than either free diphyllin or cleistanthin B [17]. Finally, justiprocin B (Figure S1) was also found to exhibit broad spectrum nanomolar inhibition of HIV strains in PBMC, including of those strains resistant to reverse transcriptase inhibitors zidovudine and nevirapine [14]. Nevertheless, what appears to be the case for these diphyllinosides is that the active component is diphyllin while the sugar moieties act to modulate (decrease or increase) the antiviral potency [6,15].

4. Conclusions

The presented study demonstrates that both diphyllin and cleistanthin B possess low-micromolar anti-SARS-CoV-2 activities in Vero cells with negligible cytotoxicities in both cases. The anti-SARS-CoV-2 effect of diphyllin was approximately 4-fold stronger than that of cleistanthin B and caused a statistically significant suppression of viral replication, even if applied at various times post-infection and at high MOIs. Diphyllin also showed an antiviral effect in CaCo-2 cells. Our results indicate, that diphyllin itself, and to a lesser extent cleistanthin B, are potentially interesting natural compounds with strong antiviral potency against SARS-CoV-2. However, both compounds suffer from poor solubility and

correspondingly poor in vivo bioavailability. These problems will need to be addressed if either or both compounds are to be developed for clinical use.

Supplementary Materials: The following are available online at <https://www.mdpi.com/2076-2607/9/3/471/s1>, Figure S1: Structures of diphyllin analogues and diphyllinosides.

Author Contributions: M.S., A.D.M., D.R., and L.E. conceptualized the study. M.S., P.S., and J.H., performed the experiments. M.S., A.D.M., D.R., and L.E. wrote the manuscript. All authors commented, revised, and approved the final version of the paper.

Funding: This study was supported by the Ministry of Education, Youth and Sports of the Czech Republic: project “FIT” (Pharmacology, Immunotherapy, nanoToxicology) CZ.02.1.01/0.0/0.0/15 003/0000495 (to D.R. and A.D.M.) and grant LTAUSA18016 (to L.E).

Institutional Review Board Statement: Not applicable.

Informed Consent Statement: Not applicable.

Data Availability Statement: The datasets generated and analyzed during the current study are available from the corresponding author on reasonable request.

Acknowledgments: We are greatly indebted to Ivana Huvarová for excellent technical assistance.

Conflicts of Interest: The authors declare no conflict of interest. The funders had no role in the design of the study; in the collection, analyses, or interpretation of data; in the writing of the manuscript, or in the decision to publish the results.







References

1. Tu, Y.F.; Chien, C.S.; Yarmishyn, A.A.; Lin, Y.Y.; Luo, Y.H.; Lin, Y.T.; Lai, W.Y.; Yang, D.M.; Chou, S.J.; Yang, Y.P.; et al. A Review of SARS-CoV-2 and the Ongoing Clinical Trials. *Int. J. Mol. Sci.* **2020**, *21*, 2657. [\[CrossRef\]](#)
2. Huang, C.; Wang, Y.; Li, X.; Ren, L.; Zhao, J.; Hu, Y.; Zhang, L.; Fan, G.; Xu, J.; Gu, X.; et al. Clinical features of patients infected with 2019 novel coronavirus in Wuhan, China. *Lancet* **2020**, *395*, 497–506. [\[CrossRef\]](#)
3. Guan, W.J.; Ni, Z.Y.; Hu, Y.; Liang, W.H.; Ou, C.Q.; He, J.X.; Liu, L.; Shan, H.; Lei, C.L.; Hui, D.S.C.; et al. China Medical Treatment Expert Group for Covid-19. Clinical Characteristics of Coronavirus Disease 2019 in China. *N. Engl. J. Med.* **2020**, *382*, 1708–1720. [\[CrossRef\]](#) [\[PubMed\]](#)
4. Paraskevis, D.; Kostaki, E.G.; Magiorkinis, G.; Panayiotakopoulos, G.; Sourvinos, G.; Tsiodras, S. Full-genome evolutionary analysis of the novel corona virus (2019-nCoV) rejects the hypothesis of emergence as a result of a recent recombination event. *Infect. Genet. Evol.* **2020**, *79*, 104212. [\[CrossRef\]](#) [\[PubMed\]](#)
5. Wang, D.; Hu, B.; Hu, C.; Zhu, F.; Liu, X.; Zhang, J.; Wang, B.; Xiang, H.; Cheng, Z.; Xiong, Y.; et al. Clinical Characteristics of 138 Hospitalized Patients With 2019 Novel Coronavirus-Infected Pneumonia in Wuhan, China. *JAMA* **2020**, *323*, 1061–1069. [\[CrossRef\]](#)
6. Martinez-Lopez, A.; Persaud, M.; Chavez, M.P.; Zhang, H.; Rong, L.; Liu, S.; Wang, T.T.; Sarafianos, S.G.; Diaz-Griffero, F. Glycosylated diphyllin as a broad-spectrum antiviral agent against Zika virus. *EBioMedicine* **2019**, *47*, 269–283. [\[CrossRef\]](#) [\[PubMed\]](#)
7. Hu, C.J.; Chang, W.S.; Fang, Z.S.; Chen, Y.T.; Wang, W.L.; Tsai, H.H.; Chueh, L.L.; Takano, T.; Hohdatsu, T.; Chen, H.W. Nanoparticulate vacuolar ATPase blocker exhibits potent host-targeted antiviral activity against feline coronavirus. *Sci. Rep.* **2017**, *7*, 13043. [\[CrossRef\]](#)
8. Cui, Q.; Du, R.; Liu, M.; Rong, L. Lignans and Their Derivatives from Plants as Antivirals. *Molecules* **2020**, *25*, 183. [\[CrossRef\]](#)
9. Sørensen, M.G.; Henriksen, K.; Neutzsky-Wulff, A.V.; Dziegiel, M.H.; Karsdal, M.A. Diphyllin, a novel and naturally potent V-ATPase inhibitor, abrogates acidification of the osteoclastic resorption lacunae and bone resorption. *J. Bone Miner. Res.* **2007**, *22*, 1640–1648. [\[CrossRef\]](#)
10. Shen, W.; Zou, X.; Chen, M.; Liu, P.; Shen, Y.; Huang, S.; Guo, H.; Zhang, L. Effects of diphyllin as a novel V-ATPase inhibitor on gastric adenocarcinoma. *Eur. J. Pharmacol.* **2011**, *667*, 330–338. [\[CrossRef\]](#)
11. Rocha, M.P.; Campana, P.R.V.; Scoaris, D.O.; Almeida, V.L.; Lopes, J.C.D.; Shaw, J.M.H.; Silva, C.G. Combined In Vitro Studies and in Silico Target Fishing for the Evaluation of the Biological Activities of Diphyllia cymosa and Podophyllum hexandrum. *Molecules* **2018**, *23*, 3303. [\[CrossRef\]](#)
12. Di Giorgio, C.; Delmas, F.; Akhmedjanova, V.; Ollivier, E.; Bessonova, I.; Riad, E.; Timon-David, P. In vitro antileishmanial activity of diphyllin isolated from Haplophyllum bucharicum. *Planta Med.* **2005**, *71*, 366–369. [\[CrossRef\]](#)
13. Chen, H.W.; Cheng, J.X.; Liu, M.T.; King, K.; Peng, J.Y.; Zhang, X.Q.; Wang, C.H.; Shrestha, S.; Schooley, R.T.; Liu, Y.T. Inhibitory and combinatorial effect of diphyllin, a v-ATPase blocker, on influenza viruses. *Antivir. Res.* **2013**, *99*, 371–382. [\[CrossRef\]](#)
14. Zhang, H.J.; Rumschlag-Booms, E.; Guan, Y.F.; Liu, K.L.; Wang, D.Y.; Li, W.F.; Nguyen, V.H.; Cuong, N.M.; Soejarto, D.D.; Fong, H.H.S.; et al. Anti-HIV diphyllin glycosides from Justicia gendarussa. *Phytochemistry* **2017**, *136*, 94–100. [\[CrossRef\]](#) [\[PubMed\]](#)

15. Asano, J.; Chiba, K.; Tada, M.; Yoshii, T. Antiviral activity of lignans and their glycosides from *Justicia procumbens*. *Phytochemistry* **1996**, *42*, 713–717. [[CrossRef](#)]
16. Yeo, H.; Li, Y.; Fu, L.; Zhu, J.L.; Gullen, E.A.; Dutschman, G.E.; Lee, Y.; Chung, R.; Huang, E.S.; Austin, D.J.; et al. Synthesis and antiviral activity of helioxanthin analogues. *J. Med. Chem.* **2005**, *48*, 534–546. [[CrossRef](#)] [[PubMed](#)]
17. Zhang, H.J.; Rumschlag-Booms, E.; Guan, Y.F.; Wang, D.Y.; Liu, K.L.; Li, W.F.; Nguyen, V.H.; Cuong, N.M.; Soejarto, D.D.; Fong, H.H.S.; et al. Potent Inhibitor of Drug-Resistant HIV-1 Strains Identified from the Medicinal Plant *Justicia gendarussa*. *J. Nat. Prod.* **2017**, *80*, 1798–1807. [[CrossRef](#)]
18. Li, Y.; Fu, L.; Yeo, H.; Zhu, J.L.; Chou, C.K.; Kou, Y.H.; Yeh, S.F.; Gullen, E.; Austin, D.; Cheng, Y.C. Inhibition of hepatitis B virus gene expression and replication by helioxanthin and its derivative. *Antivir. Chem. Chemother.* **2005**, *16*, 193–201. [[CrossRef](#)]
19. Ying, C.; Tan, S.; Cheng, Y.C. Helioxanthin analogue 8-1 inhibits duck hepatitis B virus replication in cell culture. *Antivir. Chem. Chemother.* **2010**, *21*, 97–103. [[CrossRef](#)]
20. De Madrid, A.T.; Porterfield, J.S. A simple micro-culture method for the study of group B arboviruses. *Bull. World Health Organ.* **1969**, *40*, 113–121.
21. Eyer, L.; Valdés, J.J.; Gil, V.A.; Nencka, R.; Hřebabecký, H.; Šála, M.; Salát, J.; Černý, J.; Palus, M.; De Clercq, E.; et al. Nucleoside inhibitors of tick-borne encephalitis virus. *Antimicrob. Agents Chemother.* **2015**, *59*, 5483–5493. [[CrossRef](#)] [[PubMed](#)]

Article

Diphyllin Shows a Broad-Spectrum Antiviral Activity against Multiple Medically Important Enveloped RNA and DNA Viruses

Michal Štefánik^{1,2} , Dattatry Shivajirao Bhosale^{1,3}, Jan Haviernik^{1,4}, Petra Straková^{1,4}, Martina Fojtíková¹, Lucie Dufková¹, Ivana Huvarová¹, Jiří Salát^{1,4}, Jan Bartáček³ , Jan Svoboda³ , Miloš Sedlák³ , Daniel Růžek^{1,4,5} , Andrew D. Miller^{1,2,6,*}  and Luděk Eyer^{1,4,*}

- ¹ Laboratory of Emerging Viral Diseases, Veterinary Research Institute, Hudcova 296/70, CZ-621 00 Brno, Czech Republic; stefanik@vri.cz (M.Š.); bhosale@vri.cz (D.S.B.); haviernik@vri.cz (J.H.); strakova.petra@vri.cz (P.S.); fojtikova@vri.cz (M.F.); dufkova@vri.cz (L.D.); huvarova@vri.cz (I.H.); salat@vri.cz (J.S.); ruzekd@paru.cas.cz (D.R.)
- ² Department of Chemistry and Biochemistry, Mendel University in Brno, Zemědělská 1665/1, CZ-613 00 Brno, Czech Republic
- ³ Faculty of Chemical Technology, Institute of Organic Chemistry and Technology, University of Pardubice, Studentská 573, CZ-532 10 Pardubice, Czech Republic; jan.bartacek@upce.cz (J.B.); jan.svoboda@upce.cz (J.S.); milos.sedlak@upce.cz (M.S.)
- ⁴ Biology Centre of the Czech Academy of Sciences, Institute of Parasitology, Branišovská 1160/31, CZ-370 05 Ceske Budejovice, Czech Republic
- ⁵ Department of Experimental Biology, Faculty of Science, Masaryk University, Kamenice 735/5, CZ-625 00 Brno, Czech Republic
- ⁶ KP Therapeutics (Europe) s.r.o., Purkyňova 649/127, CZ-612 00 Brno, Czech Republic
- * Correspondence: miller@vri.cz (A.D.M.); eyer@vri.cz (L.E.)



Citation: Štefánik, M.; Bhosale, D.S.; Haviernik, J.; Straková, P.; Fojtíková, M.; Dufková, L.; Huvarová, I.; Salát, J.; Bartáček, J.; Svoboda, J.; et al. Diphyllin Shows a Broad-Spectrum Antiviral Activity against Multiple Medically Important Enveloped RNA and DNA Viruses. *Viruses* **2022**, *14*, 354. <https://doi.org/10.3390/v14020354>

Academic Editor: Graciela Andrei

Received: 28 December 2021

Accepted: 4 February 2022

Published: 9 February 2022

Publisher's Note: MDPI stays neutral with regard to jurisdictional claims in published maps and institutional affiliations.



Copyright: © 2022 by the authors. Licensee MDPI, Basel, Switzerland. This article is an open access article distributed under the terms and conditions of the Creative Commons Attribution (CC BY) license (<https://creativecommons.org/licenses/by/4.0/>).

Abstract: Diphyllin is a natural arylnaphtalide lignan extracted from tropical plants of particular importance in traditional Chinese medicine. This compound has been described as a potent inhibitor of vacuolar (H⁺)ATPases and hence of the endosomal acidification process that is required by numerous enveloped viruses to trigger their respective viral infection cascades after entering host cells by receptor-mediated endocytosis. Accordingly, we report here a revised, updated, and improved synthesis of diphyllin, and demonstrate its antiviral activities against a panel of enveloped viruses from *Flaviviridae*, *Phenuiviridae*, *Rhabdoviridae*, and *Herpesviridae* families. Diphyllin is not cytotoxic for Vero and BHK-21 cells up to 100 μM and exerts a sub-micromolar or low-micromolar antiviral activity against tick-borne encephalitis virus, West Nile virus, Zika virus, Rift Valley fever virus, rabies virus, and herpes-simplex virus type 1. Our study shows that diphyllin is a broad-spectrum host cell-targeting antiviral agent that blocks the replication of multiple phylogenetically unrelated enveloped RNA and DNA viruses. In support of this, we also demonstrate that diphyllin is more than just a vacuolar (H⁺)ATPase inhibitor but may employ other antiviral mechanisms of action to inhibit the replication cycles of those viruses that do not enter host cells by endocytosis followed by low pH-dependent membrane fusion.

Keywords: enveloped virus; diphyllin; cleistanthin B; vacuolar ATPase inhibitor; antiviral activity; cytotoxicity

1. Introduction

Diphyllin **1** and diphyllin glycosides (diphyllinosides) are natural compounds of the arylnaphtalide lignan family [1,2]. These compounds were initially extracted from the plants *Cleistanthus collinus*, *Justicia gendarussa*, *Haplophyllum bucharicum*, and some others, widely used in traditional Chinese medicine [2–5]. Diphyllin **1** was originally reported to decrease potently vacuolar (H⁺)ATPase (or V-ATPase) activities in human osteoclasts [6], gastric adenocarcinoma cells [7], and in human hepatoma cells [8], plus neutralize the

pH of lysosomes at nanomolar concentrations [9]. Hence, strong anticancer [10,11] and anti-inflammatory [5,12] properties have been described. Subsequently, diphyllin 1 and its derivatives have been characterized as direct inhibitors of V-ATPases [13].

These V-ATPases are large multisubunit protein complexes located in endosomal membranes, responsible for pumping protons into endosomal compartments while consuming ATP [14]. In cells, endosome acidification is essential for the proper functioning of the endocytic pathway, the gradual maturation of endosomes into lysosomes, vesicle trafficking, protein sorting, and the degradation of some vesicle-borne molecules [15]. Critically, endosome acidification is also known to be essential for the cell entry of some viruses, including enveloped RNA viruses, that make use of the endosome acidification process to mediate fusion of viral envelopes with endosomal membranes following the entry of virus particles into host cells via receptor-mediated endocytosis [16]. Accordingly, the inhibition of V-ATPase-mediated endosome acidification should act to inhibit these viral replication cycles. Hence, V-ATPase inhibitors could represent genuine next-generation small-molecule antiviral agents intended to abrogate viral infection processes [17]. In line with this, diphyllin 1 and diphyllinosides were found previously to exert substantial antimicrobial effects [2,18] and were found able to inhibit the replication of many fungal [19], bacterial [20], and protozoal pathogens [21]. Critically, diphyllin 1 and its glycosides were also found to inhibit the replication cycle of some enveloped RNA viruses [13,17,22–25].

Building on our previous work focused on the evaluation of the antiviral activities of diphyllin 1 against Severe Acute Respiratory Syndrome Coronavirus 2 (SARS-CoV-2) [26], we now demonstrate diphyllin 1 activity against the tick- and mosquito-borne flaviviruses, such as tick-borne encephalitis virus (TBEV), West Nile virus (WNV), and Zika virus (ZIKV). Other medically important enveloped viruses from the *Phenuiviridae* family (Rift Valley fever virus, RVFV), from the *Rhabdoviridae* family (rabies virus, RABV), and even from the *Herpesviridae* family (herpes simplex virus type 1, HSV-1), were also found susceptible to diphyllin 1 treatment. The antiviral activities and cytotoxicities of diphyllin 1 were also compared with these characteristics of a selected diphyllinoside as previously, for the sake of completeness [26]. Our results demonstrate that diphyllin 1 is a genuine, broad-spectrum antiviral agent able to abrogate infection by multiple enveloped RNA and DNA viruses. We also demonstrate that diphyllin is more than just a vacuolar (H⁺)ATPase inhibitor but may employ other antiviral mechanisms of action to inhibit the replication cycles of those viruses that do not enter host cells by endocytosis and acid pH-dependent membrane fusion. Finally, an important aspect of these studies was the creation of a revised, updated, and improved synthesis of diphyllin 1. The primary reason for this synthesis was the cost-effective provision of diphyllin 1 in sufficient quantities for the multiple in vitro antiviral experiments described here. Other potential benefits will be outlined later.

2. Materials and Methods

2.1. General Methods

Unless otherwise stated, reagents and solvents were purchased from commercial sources (Sigma Aldrich, St Louis, MO, USA; Acros Organics, Carlsbad, CA, USA; Merck Chemicals, Darmstadt, Germany; TCI Europe, Zwijndrecht, Belgium). Commercial grade reagents were used without further purification. Reactions were monitored by thin-layer chromatography plates coated with 0.2 mm silica gel 60 F254 (Merck Chemicals, Darmstadt, Germany). TLC plates were visualized by UV irradiation (254 nm). All melting points were determined on a Melting Point B-540 apparatus (Büchi, Flawil, Switzerland) and are uncorrected. IR spectra were recorded on a Nicolet 6700FT-IR spectrometer (Thermo Fisher Scientific, Waltham, MA, USA) over the range of 400–4000 cm⁻¹ using the ATR technique. NMR spectra were measured in CDCl₃, DMSO-d₆ solution at ambient temperature on a Bruker Avance™ III 400 spectrometer at frequencies ¹H (400 MHz) and ¹³C (100.26 MHz) or a Bruker Ascend™ 500 spectrometer at frequencies ¹H (500.13 MHz), ¹³C (125.76 MHz) (Bruker, Billerica, MA, USA). The chemical shift, δ , was measured relative to CDCl₃ 7.27 p.p.m. or DMSO-d₆ 2.5 p.p.m. using tetramethylsilane (TMS) as an internal

standard. Coupling constants (J) were all reported in (Hz). Elemental analysis (C, H, N) was performed on an automatic microanalysis Flash 2000 Organic elemental analyzer (Thermo Fisher Scientific, Waltham, MA, USA). Mass spectrometry with high resolution was determined using the “dried droplet” method with a MALDI mass spectrometer LTQ Orbitrap XL (Thermo Fisher Scientific, Waltham, MA, USA) equipped with a nitrogen laser (337 nm, 60 Hz). Spectra were measured in the positive ion mode and in regular mass extent at a resolution of 100,000 at m/z 400. The matrix used was 2,5-dihydrobenzoic acid (DBH).

2.2. Synthesis of benzo[d][1,3]dioxole-5-carbaldehyde **2**

To a solution of 3,4-dihydroxybenzaldehyde (13.8 g, 99 mmol) in cooled acetonitrile (CH_3CN) (200 mL), were added potassium carbonate (K_2CO_3) (40 g, 289 mmol) and dibromomethane (10.4 mL, 119 mmol). The reaction mixture was then stirred at 90 °C for 24 h. After completion (monitored by TLC), the reaction mixture was cooled to room temperature and filtered. The filtrate was concentrated then extracted with ethyl acetate and water. Thereafter, the organic layer was dried over anhydrous sodium sulfate, concentrated, and the residue purified by column chromatography eluting with ethyl acetate:*n*-hexane (1:1, *v/v*) to yield compound **2** (14 g, 94%) as a brown solid. Mp 40–42 °C. IR(ATR): 3081, 3063, 2998, 2985, 2918, 2851, 2793, 2752, 2722, 1669, 1599, 1487, 1446, 1253, 1035, 927, 864, and 811 cm^{-1} . ^1H NMR (CDCl_3 , 500.13 MHz): δ 9.80 (1H, s, $-\text{CHO}$), 7.41 (1H, dd, $J = 1.5$ Hz, $J = 8.0$ Hz, Ar- $\underline{\text{H}}$), 7.33 (1H, d, $J = 1.5$ Hz, Ar- $\underline{\text{H}}$), 6.99 (1H, d, $J = 8.0$ Hz, Ar- $\underline{\text{H}}$), and 6.07 (2H, s, $-\text{O}-\text{CH}_2-\text{O}-$). ^{13}C NMR (CDCl_3 , 125.67 MHz): δ 190.4, 153.2, 148.8, 131.9, 128.8, 108.4, 107.0, and 102.2. CHN analysis: Calculated for $\text{C}_8\text{H}_6\text{O}_3$ (150.13): C, 64.00; H, 4.03. Found: C, 64.07 \pm 0.01; H, 4.10 \pm 0.02. HRMS: m/z calculated for $\text{C}_8\text{H}_6\text{O}_3$: 151.03897 $[\text{M}+\text{H}]^+$; found: 151.03925 $[\text{M}+\text{H}]^+$.

2.3. Synthesis of 2-(2-bromo-4,5-dimethoxyphenyl)-[1,3]dithiane **3**

To a round bottom flask containing dry benzene (300 mL) were added 2-bromo-4,5-dimethoxybenzaldehyde (12.3 g, 50.2 mmol), 1,3-propanedithiol (5.04 mL, 50.2 mmol), and *p*-toluenesulfonic acid (*p*-TsOH) (0.48 g, 2.79 mmol). The flask was then connected to a Dean-Stark trap and the reaction mixture heated under reflux for 10 h. After completion (monitored by TLC), the reaction mixture was cooled to room temperature, solvent was removed under reduced pressure, and the residue was partitioned between diethyl ether (100 mL), 1M NaOH (100 mL), water (200 mL), and brine (200 mL). The organic layer was subsequently dried over anhydrous sodium sulfate, concentrated, and the residue was purified by column chromatography eluting with ethyl acetate:*n*-hexane (1:3, *v/v*) to yield compound **3** (16.7 g, 100%) as a white solid. Mp 125–126 °C. IR (ATR): 3068, 2996, 2965, 2899, 1598, 1505, 1484, 1461, 1449, 1379, 1259, 1250, 1028, 968, 906, 906, 808, 779, 760, and 578 cm^{-1} . ^1H NMR (CDCl_3 , 400 MHz): δ . 7.15 (1H, s, Ar- $\underline{\text{H}}$), 6.97 (1H, s, Ar- $\underline{\text{H}}$), 5.52 (1H, s, $-\text{CH}_2-\text{S}-\text{CH}-\text{Ar}$), 3.89 (3H, s, $-\text{OCH}_3$), 3.84 (3H, s, $-\text{OCH}_3$), 3.12 (2H, brd, $J = 12.4$ Hz, $-\text{S}-\text{CH}_2-\text{CH}_2-\text{CH}_2-\text{S}-$), 2.90 (2H, brdt $J = 14.8, 2.8$ Hz, $-\text{S}-\text{CH}_2-\text{CH}_2-\text{CH}_2-\text{S}-$), 2.17 (1H, m, $-\text{S}-\text{CH}_2-\text{CHH}-\text{CH}_2-\text{S}-$), and 1.93 (1H, m, $-\text{S}-\text{CH}_2-\text{CHH}-\text{CH}_2-\text{S}-$). ^{13}C NMR (CDCl_3 , 100.26 MHz): δ 149.4, 149.0, 130.2, 115.3, 113.0, 111.1, 56.29, 56.28, 49.3, 32.4, and 25.1. CHN analysis: Calculated for $\text{C}_{12}\text{H}_{15}\text{BrO}_2\text{S}_2$ (335.28): C, 42.99; H, 4.51; S, 19.13. Found: C, 43.37 \pm 0.28; H, 4.45 \pm 0.02; S, 18.63 \pm 0.14. HRMS: m/z calculated for $\text{C}_{12}\text{H}_{15}\text{BrO}_2\text{S}_2$: 334.97696 $[\text{M}+\text{H}]^+$; found: 334.97817 $[\text{M}+\text{H}]^+$.

2.4. Synthesis of benzo[1,3]dioxol-5-yl-(2-[1,3]dithian-2-yl-4,5-dimethoxyphenyl)-methanol **4**

Dithiane **3** (14 g, 41.7 mmol) was dissolved in dry tetrahydrofuran (THF) (200 mL), then *n*-butyl lithium (*n*-BuLi) (39 mL, 1.6 mL solution in *n*-hexane, 62.6 mmol) was added at -78 °C under a N_2 atmosphere, after which the reaction mixture was stirred for 1 h. A solution of piperonal **2** (6.89 g, 45.9 mmol) in dry THF (30 mL) was further added at -78 °C, then the reaction mixture was stirred for 2 h, before warming to room temperature over 3 h. After completion (monitored by TLC), the reaction mixture was quenched with a saturated solution of ammonium chloride (90 mL), then extracted with ethyl acetate and

water. Thereafter the organic layer was further extracted with brine solution (150 mL), dried over anhydrous sodium sulfate, and evaporated under reduced pressure, giving a crude product residue that was purified by flash chromatography eluting with ethyl acetate:*n*-hexane (1:3, *v/v*) to yield compound **4** (15 g, 89%) as a white solid. Mp 75–76 °C. IR (ATR): 3491, 3076, 2996, 2933, 2894, 2848, 2776, 1606, 1509, 1486, 1446, 1440, 1235, 1167, 1082, 1034, 925, 894, 821, 755, 667 cm⁻¹. ¹H NMR (CDCl₃, 400 MHz): δ. 7.12 (1H, s, Ar-H), 6.88 (1H, d, *J* = 1.6 Hz, Ar-H), 6.85 (1H, brd, *J* = 8.0, 1.2 Hz, Ar-H), 6.82 (1H, s, Ar-H), 6.78 (1H, d, *J* = 8 Hz, Ar-H), 6.14 (1H, s, -Ar-CH-OH-Ar), 5.94 (2H, s, -O-CH₂-O-), 5.39 (1H, s, -CH₂-S-CH-Ar), 3.90 (3H, s, -OCH₃), 3.79 (3H, s, -OCH₃), 2.97 (2H, brtd, *J* = 9.6, 6 Hz, -S-CH₂-CH₂-CH₂-S-), 2.85 (2H, brtd, *J* = 14.4, 3.6 Hz, -S-CH₂-CH₂-CH₂-S-), 2.58 (1H, s, -Ar-CH-OH-Ar), 2.13 (1H, m, -S-CH₂-CHH-CH₂-S-), 1.89 (1H, m, -S-CH₂-CHH-CH₂-S-). ¹³C NMR (CDCl₃, 100.26 MHz): δ 148.96, 148.93, 147.8, 146.9, 137.2, 133.4, 129.0, 120.0, 111.5, 110.6, 108.1, 107.4, 101.1, 72.1, 56.6, 56.0, 48.0, 32.67, 32.60, 25.1. CHN analysis: Calculated for C₂₀H₂₂O₅S₂ (406.52): C, 59.09; H, 5.45; S, 15.78. Found: C, 58.79 ± 0.15; H, 5.32 ± 0.01; S, 15.63 ± 0.08. HRMS: *m/z* calculated for C₂₀H₂₂O₅S₂: 407.09814 [M+H]⁺; 429.08009 [M+Na]⁺; found: 407.09865 [M+H]⁺; 429.08237 [M+Na]⁺.

2.5. Synthesis of benzo[1,3]dioxol-5-yl-(2-[1,3]dithian-2-yl-4,5-dimethoxyphenyl)-methanone **5**

Dimethoxyphenyl alcohol **4** (13 g, 32 mmol) was dissolved in dichloromethane (CH₂Cl₂) (200 mL), then activated manganese dioxide (MnO₂) (48 g, 552 mmol) added. Thereafter the reaction mixture was stirred at room temperature under a N₂ atmosphere for 16 h. After completion (monitored by TLC), the reaction mixture was filtered through a plug of Celite and washed with dichloromethane (400 mL). Thereafter, the filtrate was evaporated under reduced pressure to dryness giving compound **5** (12 g, 93%) as a white solid. Mp 150–152 °C. IR (ATR): 3065, 3004, 2918, 2901, 2848, 2828, 1656, 1600, 1513, 1483, 1464, 1436, 1237, 1178, 1033, 955, 892, 827, 765, and 582 cm⁻¹. ¹H NMR (CDCl₃, 400 MHz): δ 7.35 (1H, d, *J* = 0.4 Hz, Ar-H), 7.31 (1H, dd, *J* = 8.0, 2.0 Hz, Ar-H), 7.26 (1H, s, Ar-H), 6.79 (1H, d, *J* = 8.0 Hz, Ar-H), 6.75 (1H, s, Ar-H), 6.02 (2H, s, -O-CH₂-O-), 5.39 (1H, s, -CH₂-S-CH-Ar), 3.94 (3H, s, -OCH₃), 3.77 (3H, s, -OCH₃), 2.89 (2H, brtd, *J* = 12.4, 2.4 Hz, -S-CH₂-CH₂-CH₂-S-), 2.77 (2H, brtd, *J* = 14.4, 3.6 Hz, -S-CH₂-CH₂-CH₂-S-), 2.05 (1H, m, -S-CH₂-CHH-CH₂-S-), and 1.84 (1H, m, -S-CH₂-CHH-CH₂-S-). ¹³C NMR (CDCl₃, 100.26 MHz): δ 195.0, 152.1, 151.1, 148.1, 147.1, 132.7, 131.6, 129.8, 127.6, 112.1, 111.9, 109.6, 107.8, 102.0, 56.29, 56.22, 47.6, 32.3, and 25.1. CHN analysis: Calculated for C₂₀H₂₀O₅S₂ (404.50): C, 59.39; H, 4.98; S, 15.85. Found: C, 60.01 ± 0.10; H, 4.99 ± 0.02; S, 15.67 ± 0.05. HRMS: *m/z* calculated for C₂₀H₂₀O₅S₂: 405.08249 [M+H]⁺; 427.06444 [M+Na]⁺; found: 405.08321 [M+H]⁺; 427.06552 [M+Na]⁺.

2.6. Synthesis of 9-benzo[1,3]dioxol-5-yl-9-hydroxy-4-([1,3]dithian-2-yl)-6,7-dimethoxy-3a,4,4,9a-tetrahydro-3H-naphtho[2,3-*c*]furan-1-one **6**

Benzophenone intermediate **5** (12 g, 29.7 mmol) was dissolved in dry THF (200 mL), lithium hexamethyldisilazide (LiHMDS) (1.0 M in THF, 39 mL) added at -65 °C under a N₂ atmosphere, and then the reaction mixture was stirred at -65 °C for 4 h to generate a deep purple anion. Following this, a solution of 2(5H)-furanone (3.2 g, 38.6 mmol, in dry THF) was then added drop by drop over 15 min. Thereafter, the reaction mixture was stirred at -65 °C under a N₂ atmosphere for another 48 h. After completion (monitored by TLC), the reaction mixture was warmed to room temperature for 1 h and quenched with H₂O (5 mL), before the organic solvent was evaporated under reduced pressure. The resulting crude product residue was then purified by column chromatography eluting with ethyl acetate:*n*-hexane (4:1, *v/v*) to yield compound **6** (3.7 g, 26%) as a white solid. Mp 205–207 °C. IR (ATR): 3503, 3087, 2973, 2935, 2904, 2847, 2825, 1766, 1741, 1608, 1514, 1502, 1481, 1464, 1454, 1435, 1372, 1361, 1301, 1263, 1235, 1173, 1081, 1062, 1018, 973, 948, 893, 818, 785, 729, and 636 cm⁻¹. ¹H NMR (DMSO-*d*₆, 500.13 MHz): δ 7.43 (1H, s, Ar-H), 6.86 (1H, d, *J* = 8.0 Hz, Ar-H), 6.80 (1H, d, *J* = 1.5 Hz, Ar-H), 6.74 (1H, dd, *J* = 7.0, 2.0 Hz, Ar-H), 6.40 (1H, s, Ar-H), 6.08 (1H, s, -Ar-C-OH-CH-), 6.00 (2H, s, -O-CH₂-O-), 4.30 (1H, m, -C-CH-CH₂-O-), 4.06 (2H, m, -C-CH-CH₂-O-), 3.77 (3H, s, -OCH₃), 3.51 (3H,

s, $-\text{OCH}_3$), 3.43 (1H, brtd, $J = 13.7, 2.5$ Hz, $-\text{S-CH}_2\text{-CH}_2\text{-CHH-S-}$), 3.27 (1H, brt, $J = 13.5$ Hz, $-\text{S-CH}_2\text{-CH}_2\text{-CHH-S-}$), 3.08 (1H, brd, $J = 6.0$ Hz, $-\text{Ar-C-OH-CH-CO}$), 2.87 (1H, brd, $J = 15.0$ Hz, $-\text{S-CH}_2\text{-CH}_2\text{-CHH-S-}$), 2.71 (1H, brd, $J = 14.5$ Hz, $-\text{S-CH}_2\text{-CH}_2\text{-CHH-S-}$), 2.17 (1H, brd, $J = 14.5$ Hz, $-\text{S-CH}_2\text{-CH}_2\text{-CHH-S-}$), and 1.77 (1H, brq, $J = 13.0$ Hz, $-\text{S-CH}_2\text{-CH}_2\text{-CHH-S-}$). ^{13}C NMR (DMSO- d_6 , 125.76 MHz): δ 174.2, 148.7, 148.5, 146.7, 145.7, 143.6, 133.8, 126.4, 119.3, 112.5, 109.4, 107.5, 106.7, 101.0, 69.9, 68.3, 55.5, 55.3, 51.0, 49.0, 41.0, 28.1, 26.2, and 23.7. CHN analysis: Calculated for $\text{C}_{24}\text{H}_{24}\text{O}_7\text{S}_2$ (488.57): C, 59.00; H, 4.95; S, 13.13. Found: C, 58.68 ± 0.18 ; H, 5.23 ± 0.02 ; S, 12.82 ± 0.07 . HRMS: m/z calculated for $\text{C}_{24}\text{H}_{24}\text{O}_7\text{S}_2$: 511.08557 $[\text{M}+\text{Na}]^+$; 527.05950 $[\text{M}+\text{K}]^+$; found: 511.08816 $[\text{M}+\text{Na}]^+$; 527.06223 $[\text{M}+\text{K}]^+$.

2.7. Synthesis of 9-benzol[1,3]dioxol-5-yl-9-hydroxy-6,7-dimethoxy-3,3a,9,9a-tetrahydronaphtho[2,3-c]furan-1,4-dione 7

A solution of lactone **6** (3.5 g, 7.1 mmol) in aqueous acetonitrile (85%, *v/v*, 50 mL) with mercuric oxide (HgO) (1.6 g, 7.8 mmol) and mercury chloride (HgCl₂) (4.2 g, 15.7 mmol) was heated under reflux for 5 h. After completion (monitored by TLC), the reaction mixture was cooled to room temperature, filtered through a Celite bed, and the filtrate evaporated under reduced pressure. The resulting crude product residue was then dissolved in chloroform (150 mL), and extracted with a saturated solution of ammonium carbonate. Thereafter the organic layer was extracted with brine solution (150 mL), dried over anhydrous sodium sulfate and evaporated under reduce pressure. The resulting crude product residue was purified by flash chromatography eluting with ethyl acetate:*n*-hexane (2:3, *v/v*) to yield compound **7** (1.257 g, 44.2%) as a white solid. Mp 103–104 °C. IR (ATR): 3451, 2966, 2919, 2850, 2640, 1747, 1735, 1665, 1593, 1505, 1484, 1460, 1436, 1364, 1320, 1278, 1239, 1212, 1145, 1129, 1096, 1080, 1031, 1010, 987, 904, 820, 794, 765, 723 cm^{-1} . ^1H NMR (CDCl₃, 400 MHz): δ 7.48 (1H, s, Ar-H), 7.25 (1H, s, Ar-H), 6.86 (1H, d, $J = 2.0$ Hz, Ar-H), 6.65 (1H, d, $J = 8.0$ Hz, Ar-H), 6.41 (1H, dd, $J = 8.4, 2.5$ Hz, Ar-H), 5.94 (2H, s, $-\text{O-CH}_2\text{-O-}$), 5.74 (1H, s, $-\text{Ar-C-OH-CH-}$), 4.73 (1H, d, $J = 9.6$ Hz, $-\text{CO-CH-CHH-O-}$), 4.30 (1H, dd, $J = 9.2, 5.6$ Hz, $-\text{CO-CH-CHH-O-}$), 3.96 (3H, s, $-\text{OCH}_3$), 3.94 (3H, s, $-\text{OCH}_3$), 3.44 (1H, d, $J = 7.2$ Hz, $-\text{Ar-C(OH)-CH-CO-O-}$), and 3.09 (1H, dd, $J = 5.6, 4.8$ Hz, $-\text{CO-CH-CH}_2\text{-O-}$). ^{13}C NMR (CDCl₃, 100.26 MHz): δ 193.0, 176.9, 155.9, 149.7, 148.2, 147.6, 141.2, 138.5, 125.5, 120.1, 108.8, 108.1, 107.9, 107.0, 101.5, 72.5, 70.8, 56.5, 56.2, 50.4, and 46.1. CHN analysis: Calculated for $\text{C}_{21}\text{H}_{18}\text{O}_8$ (398.36): C, 63.32; H, 4.55. Found: C, 63.21 ± 0.03 ; H, 4.69 ± 0.01 . HRMS: m/z calculated for $\text{C}_{21}\text{H}_{18}\text{O}_8$: 421.08939 $[\text{M}+\text{Na}]^+$; 437.06333 $[\text{M}+\text{K}]^+$; found: 421.09018 $[\text{M}+\text{Na}]^+$; 437.06448 $[\text{M}+\text{K}]^+$.

2.8. Synthesis of 9-(3',4'-methylenedioxyphenyl)-4-hydroxy-6,7-dimethoxynaphtho[2,3-c]furan-1(3H)-one (Diphyllin) 1

Benzofuranone **7** (1.084 g, 2.7 mmol) and *p*-TsOH (0.362 g, 1.9 mmol) were heated under reflux in benzene (80 mL) for 15 h. After completion (monitored by TLC), the reaction mixture was cooled to room temperature and the solvent removed under reduced pressure. The crude product residue was then purified by flash chromatography eluting with ethyl acetate:*n*-hexane (1:1, *v/v*) to yield compound **1** (0.730 g, 70%) as a yellow solid that was recrystallized. Mp 275–277 °C. IR (ATR): 3197, 3006, 2955, 2923, 2853, 2648, 1703, 1613, 1594, 1507, 1492, 1455, 1433, 1358, 1332, 1227, 1211, 1192, 1169, 1125, 1084, 1035, 1007, 930, 948, 915, 860, 768, 730, and 719 cm^{-1} . ^1H NMR (DMSO- d_6 , 400 MHz): δ 10.4 (1H, s, Ar-OH), 7.61 (1H, s, Ar-H), 7.01 (1H, d, $J = 8.0$ Hz, Ar-H), 6.95 (1H, s, Ar-H), 6.86 (1H, d, $J = 1.6$ Hz, Ar-H), 6.75 (1H, dd, $J = 10.0, 5.6$ Hz, Ar-H), 6.11 (2H, s, $-\text{O-CH}_2\text{-O-}$), 5.35 (2H, s, $-\text{O-CH}_2\text{-Ar}$), 3.94 (3H, s, $-\text{OCH}_3$), 3.65 (3H, s, $-\text{OCH}_3$). ^{13}C NMR (DMSO- d_6 , 100.26 MHz): δ 169.6, 150.4, 149.6, 146.8, 146.6, 144.8, 129.5, 129.4, 128.8, 123.7, 123.2, 121.6, 118.6, 111.0, 107.8, 105.4, 101.0, 100.7, 66.6, 55.5, and 55.1. CHN analysis: Calculated for $\text{C}_{21}\text{H}_{16}\text{O}_7$ (380.35): C, 66.31; H, 4.24. Found: C, 66.45 ± 0.10 ; H, 4.56 ± 0.02 . HRMS: m/z calculated for $\text{C}_{21}\text{H}_{16}\text{O}_7$: 381.09688 $[\text{M}+\text{H}]^+$; 403.07882 $[\text{M}+\text{Na}]^+$; 419.05276 $[\text{M}+\text{K}]^+$; found: 381.09809 $[\text{M}+\text{H}]^+$; 403.08028 $[\text{M}+\text{Na}]^+$; 419.05421 $[\text{M}+\text{K}]^+$. Previously reported data $[\text{M}-\text{H}]^+$ 379.0825 [24].

2.9. Viruses, Cells, and Compounds

Our antiviral studies were performed using typical representatives of the following virus families: (i) *Flaviviridae* (TBEV, strain Hypr, a representative of the European TBEV subtype, provided by the Collection of Arboviruses, Institute of Parasitology, Biology Centre of the Czech Academy of Sciences, Ceské Budějovice, Czech Republic (<http://www.arboviruscollection.cz/index.php?lang=en>, accessed on 10 January 2022); ZIKV, the Brazilian strain Paraiba_01; kindly provided by Prof. Paolo M. de A. Zanotto, University of São Paulo, Brasil; WNV, strain Eg-101, provided by the Collection of Arboviruses, Institute of Parasitology, Biology Centre of the Czech Academy of Sciences, Ceske Budejovice, Czech Republic); (ii) *Phenuiviridae* (RFVE, strain H13/96, kindly provided by Karel Bilek, National Institute of Nuclear, Chemical and Biological Protection, Czech Republic); (iii) *Rhabdoviridae* (RABV, strain CVS-11, kindly provided by Prof. Anthony R. Fooks, Animal and Plant Health Agency, UK); and (iv) *Herpesviridae* (HSV-1, strain MacIntyre, kindly provided by Prof. Andreas Sauerbrei, German Reference Laboratory of HSV und VZV, Germany).

Vero cells (ATCC CCL-81, African Green Monkey, adult kidney, epithelial), baby hamster kidney cells (BHK-21, ATTC CCL-10), and human hepatocarcinoma cells (Huh-7) were grown in Dulbecco's modified Eagle's medium (DMEM); porcine kidney stable (PS) [27] were cultured in Leibovitz (L-15) medium; human brain cortical astrocytes (HBCA, ScienCell, Carlsbad, CA, USA) were cultivated in Astrocyte medium; human neuroblastoma UKF-NB-4 cells [28] were cultured in Iscove's modified Dulbecco's medium (IMDM). The media were supplemented with 3% (L-15), 6% (Astrocyte medium), or 10% (IMDM and DMEM) newborn calf serum plus 100 U/mL penicillin, 100 µg/mL streptomycin, and 1% glutamine (Sigma-Aldrich, Prague, Czech Republic). Vero, HBCA, UKV-NB-4, Huh-7, and BHK-21 cells were cultured at 37 °C under 5% CO₂, whereas PS cells were cultivated at 37 °C under a normal atmosphere (without CO₂ supplementation).

For all antiviral/cytotoxicity assays, we used in-house synthesized diphyllin **1** (Scheme 1, Figure 1A), whose biological activities were compared with the commercially synthesized compound purchased from Apigenex (Prague, Czech Republic) (Figure S1). To compare the biological activities of both compounds, we performed a viral titer reduction assay; virus and compound were added simultaneously to Vero cells and cultivated for 48 h at 37 °C under 5% CO₂ (see Section 2.11. simultaneous treatment). The diphyllinoside known as diphyllin-4-β-D-glucopyranoside (cleistanthin B) **8** was obtained from WuXi AppTec (Tianjin, China). All compounds were solubilized in dimethyl sulfoxide (DMSO) as 10 mM stock solutions.

2.10. Cytotoxicity Assays

To determine the cytotoxicities of diphyllin **1** and diphyllinoside cleistanthin B **8**, we used multiple cells/cell lines of neural and extraneural origin. Vero, PS, UKF-NB-4, Huh-7, or HBCA cells were seeded in 96-well microtitration plates (2×10^4 cells/well), and incubated for 24 h at 37 °C. After incubation, diphyllin **1** or cleistanthin B **8** were added to the cells (0 to 100 µM) then treated cells were further cultivated for 48 h at 37 °C. Cytotoxicity of diphyllin **1** for BHK-21 cells was measured after 72 h cultivation. In order to evaluate Vero cell cytotoxicities from exposure to diphyllin **1**, the cells were seeded in 96-well microtitration plates (2×10^4 cells/well), incubated for 24 h at 37 °C under 5% CO₂, and then diphyllin **1** or cleistanthin B **8** (0 to 100 µM) was added. The treated cells were further cultivated for 48, 72, and 144 h at 37 °C under 5% CO₂. Cytotoxicity of bafilomycin A1 (0 to 200 µM) was assayed in Vero cells after a 48-h incubation at 37 °C under 5% CO₂. The cytotoxicity measured in terms of cell viability was determined with Cell Counting Kit-8 (Dojindo Molecular Technologies, Munich, Germany), according to the manufacturer's instructions. The respective concentrations of each compound under investigation that reduced cell viability by 50% (CC₅₀ values) were determined.

2.11. Antiviral Assays

Viral titre reduction assays were performed to determine the sensitivity of the tested viruses to diphyllin 1 in cell culture. Vero cells were used for the evaluation of the antiviral efficacy of diphyllin 1 against TBEV, WNV, ZIKV, RVFV, and HSV-1. Host cells were seeded in 96-well plates (approximately 2×10^4 cells per well) and incubated for 24 h at 37 °C under 5% CO₂ to form a confluent monolayer.

For each virus, two independent experiments were performed in triplicate in each case. In each independent experiment, infected Vero cells were treated with drug at three different times, as follows: (i) 2 h pre-treatment assays—media (200 µL) with diphyllin 1 (0 to 25 µM) (2-fold dilution, three wells per concentration) were added to cell monolayers 2 h prior to infection. After 2 h incubation at 37 °C under 5% CO₂, media were aspirated and replaced with fresh compound-containing media (200 µL) in the same concentration range, then inoculated with the appropriate virus at an MOI of 0.1. Cells were further incubated for 48 h at 37 °C under 5% CO₂; (ii) simultaneous treatment assays—media containing diphyllin 1 (0 to 25 µM) were inoculated with the appropriate virus (MOI of 0.1) and added to cells that were then incubated for 48 h at 37 °C under 5% CO₂; (iii) 2 h post-treatment assays—Vero cells were first infected with the appropriate virus (MOI of 0.1), and 2 h after infection (the time needed for virus adsorption and internalization), media containing diphyllin 1 (0 to 25 µM) were added to infected cells that were then incubated for 48 h at 37 °C under 5% CO₂.

Following incubation, media were collected and viral titers were determined by plaque assay (see below) to construct dose-dependent inhibition curves. Since the greatest inhibitory effects were observed in 2 h pre-treatment assays, then titer values determined from these assays were also used to estimate 50% effective concentration (EC₅₀) values. The antiviral activity of cleistanthin B 8 was determined only for TBEV in Vero cells, using the same protocol as described above. Media were collected 48 h after infection, and TBEV titers were estimated using plaque assays once again.

For anti-RABV assays, a suspension of BHK-21 cells (5×10^4 cells per a well) was incubated with diphyllin 1 (0 to 25 µM) and with RABV ($10^{6.58}$ TCID₅₀/mL) at 37 °C under 5% CO₂ for 40 min, mixing every 10 min. Following incubation, the RABV-infected cells were seeded on 96 well plates and cultivated for 72 h at 37 °C under 5% CO₂ (a longer incubation time was used compared with other viruses tested since RABV does not typically generate sufficiently high titers when incubated for 48 h). Thereafter, media samples were collected, and the RABV RNA was quantified using quantitative real-time PCR (RT-qPCR). Two independent experiments were performed in triplicate (as above).

Antiviral assays with bafilomycin A1 were performed with Vero cells seeded in 96-well plates (2×10^4 cells per well) and incubated for 24 h at 37 °C under 5% CO₂ to form a confluent monolayer. Media containing bafilomycin A1 (0 to 100 nM) were simultaneously infected with ZIKV (strain Paraiba_01) or HSV-1 (strain MacIntyre) (MOI of 0.1) and added to cells that were then incubated for 48 h at 37 °C under 5% CO₂. Viral titers were determined by plaque assays.

2.12. Plaque Assay

To quantify the viral titres for ZIKV, WNV, RVFV, and HSV-1, plaque assays were performed using Vero cells. For TBEV viral titer determination, we performed PS cell-based plaque assays. In both cases, a modified protocol was used as originally developed by De Madrid and Porterfield [29]. Briefly, 10-fold dilutions of the virus were prepared in 24-well tissue culture plates, and the cells were added to each well ($0.6\text{--}1.5 \times 10^5$ cells/well). After 4 h incubation, the suspension was overlaid with 3% (*w/v*) carboxymethylcellulose in DMEM (for Vero cells) or L15 (for PS cells). Following day 5 of incubation at 37 °C and 5% CO₂ (DMEM) or in a normal atmosphere (L15), the infected plates were washed with phosphate-buffered saline, and the cell monolayers were stained with naphthalene black. The virus titer was expressed as plaque-forming units (PFU)/mL.

2.13. Quantitative Reverse Transcription PCR (RT-qPCR)

RABV RNA was isolated from growth media supernatants using the QIAmpViral RNA mini kit (Qiagen, Germantown, MD, USA) following the manufacturer's instructions. RT-qPCR measurements were performed on the LightCycler 480 II in a 96-well plate block (Roche, Basel, Switzerland) using the Advanced kit for Tick-borne encephalitis (Genesig, Germantown, MD, USA) and Lyophilised OneStep qRT-PCR (Oasig) according to manufacturer's instructions. RABV RNA copy numbers/mL was calculated from calibration curves based on standards provided by the manufacturer (Genesig, Germantown, MD, USA).

2.14. Immunofluorescence Staining

In order to measure the compound-induced inhibition of viral antigen expression, a cell-based immunostaining assay for TBEV, WNV, ZIKV, RVFV, RABV, and HSV-1 was performed. Vero cells were used for the cultivation of TBEV, WNV, ZIKV, RVFV, and HSV-1 and BHK-1 cells for RABV cultivation.

Vero cells were seeded onto 96-well microtitration plates, cultivated for 24 h, and then treated with diphyltin 1 (0 to 25 μ M) (2-fold dilution, three wells per concentration) for 2 h. Thereafter, cell monolayers were infected with the appropriate virus (MOI of 0.1) and cultured for 48 h at 37 °C under 5% CO₂. After incubation, the cells were fixed with cold acetone:methanol (1:1, *v/v*) and blocked with 10% fetal bovine serum. For flavivirus immunostaining (i.e., TBEV, WNV, and ZIKV), cells were incubated with a mouse monoclonal antibody targeting the flavivirus group surface antigen (protein E) (1:250; antibody clone D1-4G2-4-15; Sigma-Aldrich, Prague, Czech Republic). Anti-Herpes Simplex Virus Type 1/2 antibody (1:250; antibody clone M4091313) and Anti-Nucleoprotein antibody (1:250; AA 1-245, UniProt: P21700) were obtained from Antibodies-online GmbH (Aachen, Germany) and were used for the immunostaining of HSV-1 and RVFV, respectively. Subsequently, cells were labeled with an anti-mouse goat secondary antibody conjugated with fluorescein isothiocyanate (FITC; 1:500; Sigma-Aldrich, Prague, Czech Republic) following 1 h incubation at 37 °C. Cells were then counterstained with 4',6-diamidino-2-phenylindole (DAPI; 1 μ g/mL; Sigma-Aldrich, Prague, Czech Republic) to visualize cell nuclei. Fluorescence signals were recorded using an Olympus IX71 epifluorescence microscope (Olympus Corporation, Tokyo, Japan).

For the immunostaining of RABV-infected cells, a suspension of BHK-21 cells (5×10^4 cells per well) was incubated with diphyltin 1 (0 to 25 μ M) (2-fold dilution, three wells per concentration) and RABV ($10^{6.58}$ TCID₅₀/mL) at 37 °C for 40 min, mixing every 10 min. Following incubation, the RABV-infected cells were seeded on a 96 well plate and cultivated for 72 h. After fixation with cold acetone–methanol (1:1, *v/v*) and blocking with 10% fetal bovine serum, the cells were incubated with an Anti-Rabies-Specific monoclonal antibody (1:250; Art.No. PA1202; Enzo Life Science, NY, USA) labeled with FITC (green). As above, cell nuclei were counterstained with DAPI (1 μ g/mL), and fluorescence signals were recorded, also as described above.

2.15. Analysis of Endosomal Acidification Effects

Vero cells (1×10^6 cells/well) were cultured in a 6-well microtiter plate for 24 h. Then, the growth medium was aspirated and replaced with a fresh medium containing diphyltin 1 (100 μ M) or bafilomycin A1 (100 nM) at 37 °C for 20 min. Bafilomycin A1 was used as a positive control, and DMSO 1% (*v/v*) was applied as a negative control. Acridine orange dye (1 μ g/mL; Sigma-Aldrich) was added to each well and incubated at 37 °C for 10 min. Fluorescence signals were recorded using an Olympus IX71 epifluorescence microscope (Olympus Corporation, Tokyo, Japan). The red and green fluorescence signals were acquired using Texas Red and FITC excitation filters, respectively.

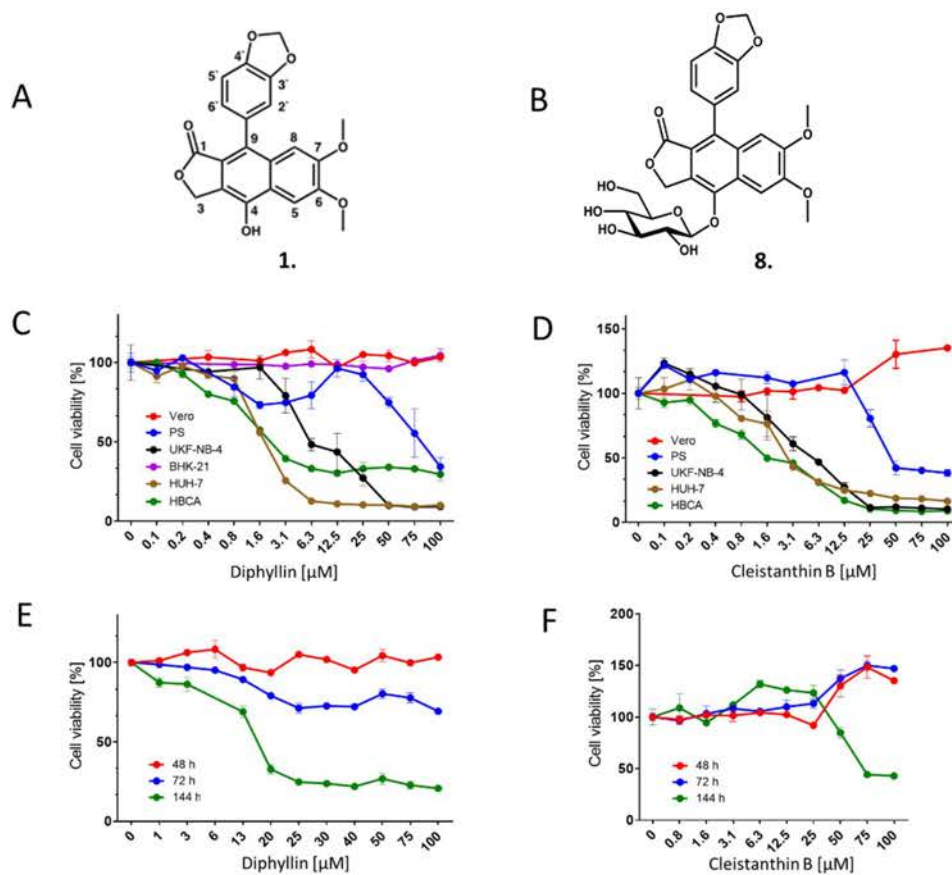
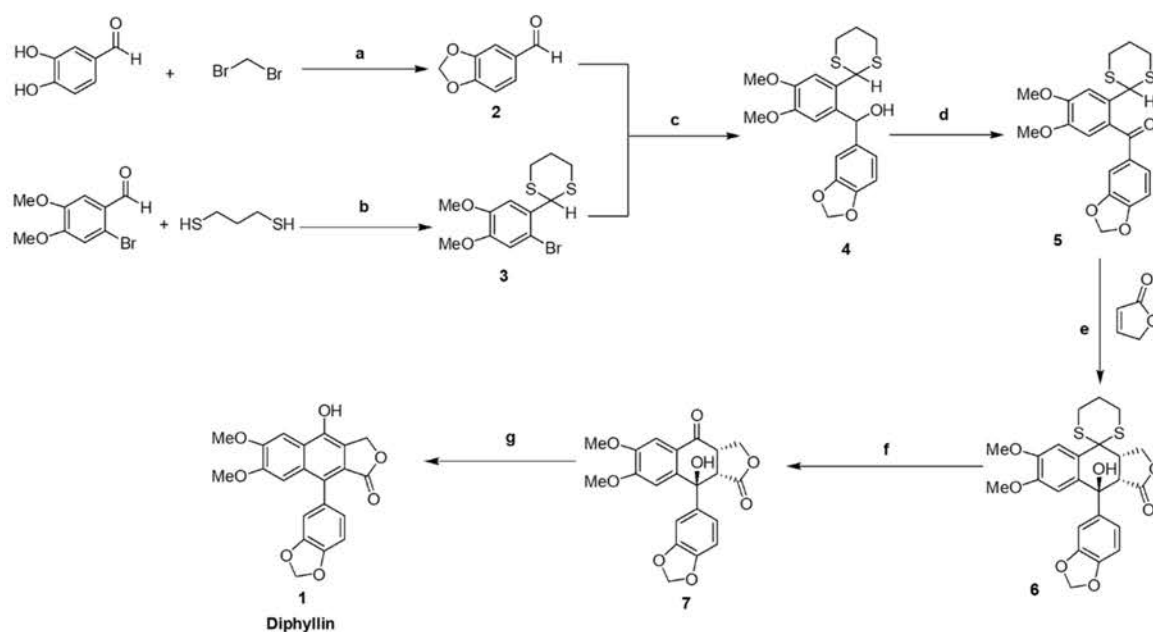


Figure 1. Cytotoxicity of diphyllin 1 and cleistanthin B 8. (A) Structure of diphyllin 1; atom numbering is included. (B) Structure of cleistanthin B 8. (C) Cytotoxicities of diphyllin 1 for Vero, PS, UKF-NB-4,

BHK-21, Huh-7, and HBCA were expressed as a percentage of cell viability at the indicated drug concentration. The cells were seeded in 96-well plates for 24 h, then treated with diphyllin **1** and incubated for 48 h. Diphyllin **1**-treated BHK-21 cells were incubated for 72 h. Cell viabilities were measured by Cell Counting Kit-8. (D) Cytotoxicities of cleistanthin **B 8** were expressed as percentage cell viability at the indicated drug concentration. The experimental procedure was the same as in (C). (E) Time-dependent cytotoxic effects of diphyllin **1** on Vero cells. Vero cells were seeded in 96-well plates for 24 h, then treated with diphyllin **1** at the indicated concentrations. Cell viabilities were determined after 48, 72, and 144 h of incubation. (F) Time-dependent cytotoxic effects of cleistanthin **B 8** on Vero cells, as determined after 48, 72, and 144 h of incubation.

2.16. Mechanistic Analysis of Diphyllin-Mediated Antiviral Effects

Vero cells were seeded in 6-well plates and incubated for 24 h at 37 °C under 5% CO₂ until confluent. Thereafter, a virus inoculum (10⁶ PFU/mL, ZIKV strain Paraiba_01 or HSV-1 strain MacIntyre) and diphyllin **1** (100 µM) or bafilomycin A1 (100 nM) were added to the cells and incubated for 3 h. Following incubation, Vero cells were washed with culture medium to remove the compounds, and the non-adsorbed virus and fresh medium with 4% (*w/v*) carboxymethylcellulose were added to the cells. After further incubation for 72 (with HSV-1) or 120 h (with ZIKV), Vero cell monolayers were stained with naphthalene black, and the number of plaques was counted. Control cells were not washed, and the compounds and virus were retained in cell culture until the end of the experiment. Following a 3 h incubation, 4% (*w/v*) carboxymethylcellulose was added to the cells, and the cells were incubated for 72 or 120 h, as described above. Then, the monolayers were stained with naphthalene black, and the number of plaques was counted.

3. Results

3.1. Synthesis of Diphyllin **1**

Our revised, updated, and improved synthesis of diphyllin **1** was devised with reference to previous literature [24,30,31] and is illustrated (Scheme 1). Although diphyllin **1** is a known compound, the published synthetic routes proved difficult to implement in our hands, and key intermediates were incompletely characterized throughout. Here we have resolved these difficulties and omissions to describe a robust, scalable, fully characterized synthesis. Exceptionally, our synthetic route began with the formation of benzo-[d]-[1,3]dioxole-5-carbaldehyde **2** from 3,4-dihydroxybenzaldehyde. In parallel, 2-(2-bromo-4,5-dimethoxyphenyl)-[1,3]dithiane **3** was prepared by combination of 2-bromo-4,5-dimethoxybenzaldehyde with 1,3-propanedithiol. Both **2** and **3** were coupled efficiently to give alcohol **4** following initial transmetallation of **3** with *n*-butyl lithium. Oxidation of **4** with MnO₂ gave rise to benzophenone intermediate **5** as a crystalline compound. Thereafter, the formation of key intermediate **6**, through intermolecular Michael-addition of 2(5H)-furanone to **5** with subsequent ring closure, proved the most challenging step. Reagents previously described in the literature for this purpose [24], such as lithium diisopropylamine (LDA), resulted in multiple product formation. In the event, key intermediate **6** was only prepared successfully through judicious use of the reagent LiHMDS in dry THF at −65 °C for 48 h. The use of this reagent also enabled the recovery of unreacted starting materials by column chromatography for reuse in subsequent repeat reactions. Thereafter, dithiane deprotection of key intermediate **6** was then carried out in the standard way, and the resulting compound **7** was aromatized with *p*-toluenesulfonic acid to give diphyllin **1** (Scheme 1). This was obtained in excellent purity but found to be rather light-sensitive and subject to surface coloration with detrimental effects on antivirus activities. Therefore, once prepared, diphyllin **1** samples were customarily stored in the dark in the fridge (2–8 °C), until further required. The elemental analysis of diphyllin **1**, C₂₁H₁₆O₇ (380.35) was calculated as C, 66.31; H, 4.24, and found to be C, 66.45 ± 0.10; H, 4.56 ± 0.02. These compare to values of C, 66.73 ± 0.07; H, 4.35 ± 0.01 measured from a small control sample of diphyllin **1** provided commercially (Apigenex, Prague, Czech Republic).

A functional comparison between our synthetic diphyllin **1** and the commercial product was carried out using an anti-TBEV antiviral assay. Both compounds (0–25 μM), when cultured in TBEV-infected Vero cells, resulted in sigmoidal growth curves of similar shapes and slopes with EC_{50} values of 1.04 μM and 1.24 μM for the in house and commercially synthesized compounds, respectively. This indicates that the biological activities of both compounds were essentially identical (Figure S1).

3.2. Cytotoxicity of Diphyllin **1** and Cleistanthin B **8**

The cytotoxicities of diphyllin **1** and diphyllinoside cleistanthin B **8** were determined with respect to five different immortalized cell lines (i.e., Vero, PS, BHK-21, UKF-NB-4, and Huh-7 cells) and primary HBCA cells. These cells were used since they are often used for in vitro cultivation and for antiviral assays with numerous medically important viruses. The UKF-NB-4 and HBCA cells are of neural origin and so are highly suitable for in vitro multiplication and antiviral studies involving neurotropic viruses. Diphyllin **1** and cleistanthin B **8** were found to be substantially cytotoxic to UKF-NB-4, Huh-7, and HBCA cells 48 h post-administration, in a dose-dependent manner (Figure 1C,D).

The CC_{50} values for UKF-NB-4, Huh-7, and HBCA cells were calculated to be 11.13, 1.89, and 3.39 μM , respectively (for diphyllin **1**), and 6.17, 3.96, and 2.08 μM , respectively (for cleistanthin B **8**) (Table 1). Diphyllin **1** and cleistanthin B **8** were found to be slightly cytotoxic for PS cells (CC_{50} values of 92.44 and 78.86 μM , respectively) (Figure 1C,D, Table 1). Only Vero cells and BHK-21 cells proved essentially robust to diphyllin **1** and cleistanthin B **8** administration up to a concentration threshold of 100 μM . The prolonged incubation of Vero cells with diphyllin **1** and cleistanthin B **8** up to 72 h did not have substantial cytotoxic effects. However, the 144 h incubation of diphyllin **1** with Vero cells did result in a significant decrease in Vero cell viability (CC_{50} of 18.19 μM). Interestingly, cleistanthin B **8** was less cytotoxic, when incubated for 144 h with Vero cells (CC_{50} of 80.73 μM) (Figure 1E,F; Table 1). Based on the observed cytotoxicity profiles of the cell lines studies, Vero cells were used for all antiviral assays with TBEV, WNV, ZIKV, RVFV, and HSV-1, whereas BHK-1 cells were used for anti-RABV assays.

Table 1. Cytotoxicities of diphyllin **1** and cleistanthin B **8** for multiple cell types after a 48 h incubation.

Cell Type	Diphyllin 1		Cleistanthin B 8	
	CC_{50} (μM) ^{1,2}	95% CI (μM)	CC_{50} (μM) ^{1,2}	95% CI (μM)
Vero (48 h)	>100	-	>100	-
Vero (72 h)	>100	-	>100	-
Vero (144 h)	18.19	15.1 to 21.65	80.73	66.54 to 104.2
PS (48 h)	92.44	62.9 to 140.5	78.86	48.17 to 129.40
UKF-NB-4 (48 h)	11.13	7.21 to 17.35	6.17	4.53 to 8.43
Huh-7 (48 h)	1.89	1.53 to 2.32	3.96	3.01 to 5.243
HBCA (48 h)	3.39	2.07 to 5.71	2.08	1.77 to 2.45
BHK-21 (72 h)	>100	-	-	-

¹ Determined from three biological replicates of two independent experiments. ² Expressed as a 50% reduction in cell viability and calculated from the inflection points of sigmoidal percentage cell viability curves, which were obtained by a nonlinear fit of transformed inhibitor concentrations versus normalized response using GraphPad Prism 7.04 (GraphPad Software, Inc., USA).

3.3. Antiviral Activity of Diphyllin **1** and Cleistanthin B **8** against Tick- and Mosquito-Borne Flaviviruses

The antiviral activities of diphyllin **1** and cleistanthin B **8** were first evaluated against a representative of the tick-transmitted arboviruses, namely TBEV (Hypr strain). For the anti-TBEV assays, we used three different treatment regimens, differing in the time of drug addition to cell monolayers (2 h pre-treatment, simultaneous treatment, and 2 h post-treatment, see above). Diphyllin **1** showed strong antiviral activities against TBEV in all three treatment regimens (Figure 2A). However, antiviral activities were most pronounced when diphyllin **1** was administered 2 h prior to infection (2 h pre-treatment, EC_{50} of

0.85 μM). The differences in viral titer decrease between individual treatment regimens were obvious mostly at high compound concentrations and did not have substantial effects on the EC_{50} values. Using the 2 h pre-treatment, diphyllin 1 was able to almost completely eliminate TBEV replication in Vero cell culture at concentrations between 12.5 and 25 μM (Figure 2A,H, Table 2). By contrast, although the peak anti-TBEV activity of cleistanthin B 8 was observed in pre-treatment assays, the level of activity was almost 6.3-fold lower than observed with diphyllin 1 (Figure 2B, Table 2). Owing to this low antiviral activity compared to diphyllin 1 and only a comparable cytotoxicity profile, cleistanthin B 8 was excluded from further antiviral analyses.

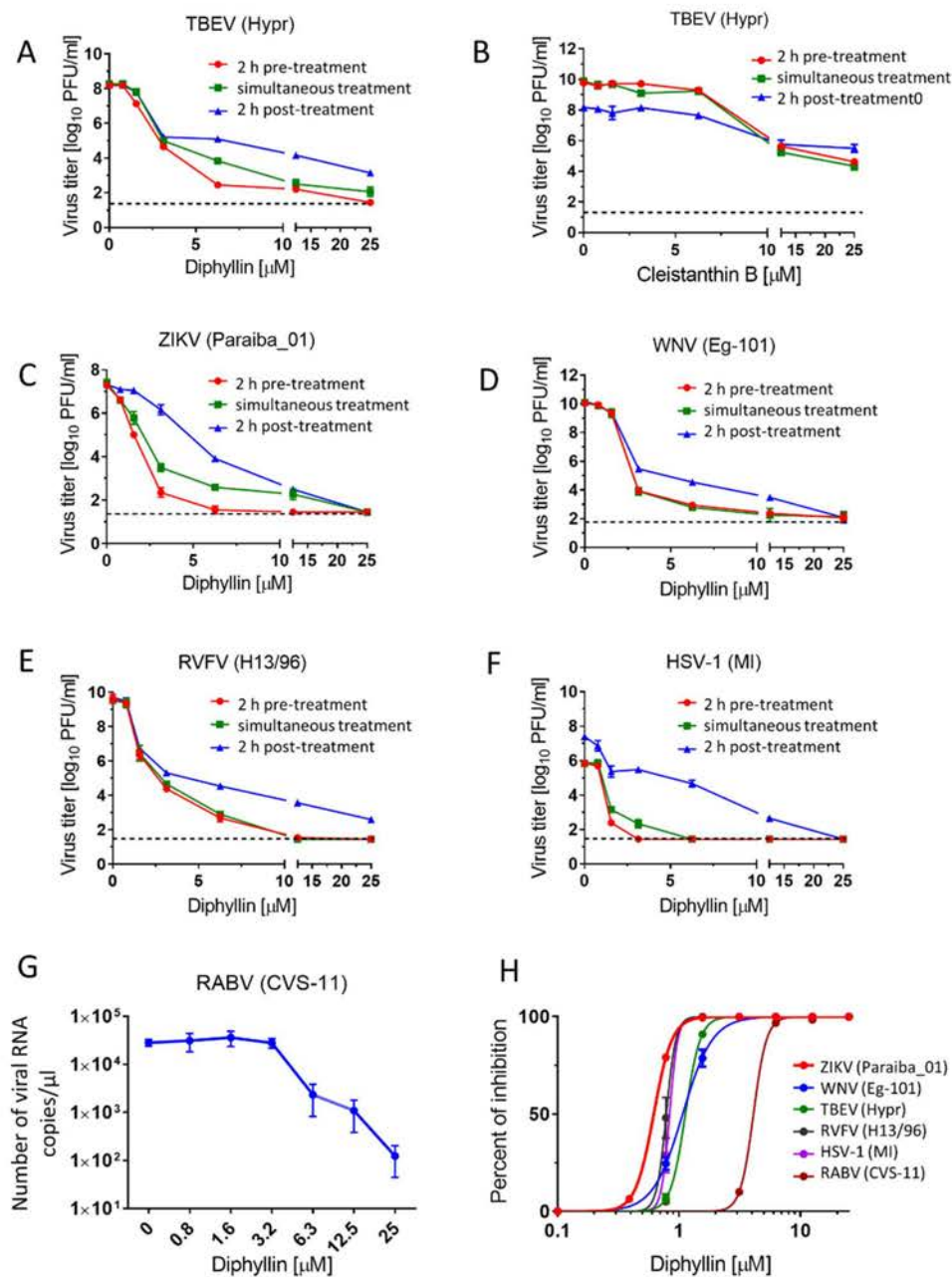


Figure 2. Antiviral activities of diphyllin 1 and cleistanthin B 8. (A,C–F) Anti-antiviral activities of diphyllin 1. Vero cell monolayers were treated with diphyllin 1 (0 to 25 μM) either 2 h prior to TBEV

(A), ZIKV (C), WNV (D), RVFV (E), and HSV-1 (F) infection (at a MOI of 0.1) (2 h pre-treatment), simultaneously with virus infection (simultaneous treatment), or 2 h after infection (2 h post-treatment). The infected cells were then incubated for 48 h, after which cell media were collected, and viral titers were determined using a plaque assay and expressed as PFU/mL. (B) Anti-TBEV activity of cleistanthin B 8 (0 to 25 μ M). The experimental procedure was the same as in (A). (G) Anti-RABV activity of diphyllin 1. A suspension of BHK-21 cells was incubated with diphyllin 1 (0 to 25 μ M) and with RABV ($10^{6.58}$ TCID₅₀/mL) at 37 °C for 40 mins. Following incubation, the RABV-infected cells were seeded on 96 well plates and cultivated for 72 h then, media were collected, and the RABV RNA was quantified by RT-qPCR. (H) Inhibition curves for diphyllin 1 were constructed from the viral titer values (2 h pre-treatment) in order to estimate EC₅₀ values for the indicated viruses. The mean titers from three biological replicates of two independent experiments are shown, and error bars indicate standard errors of the mean ($n = 3$). The horizontal dashed line indicates the minimum detectable threshold of 1.44 log₁₀ PFU/mL. MI, MacIntyre.

Table 2. Antiviral and cytotoxicity properties of diphyllin 1 or cleistanthin B 8 in Vero (after a 48 h incubation) or BHK-21 cells (after a 72 h incubation).

Virus/Strain	Cell Type	Compound	EC ₅₀ (μ M) ^{1,2}	95% CI (μ M)	CC ₅₀ (μ M) ^{1,2}	SI (CC ₅₀ /EC ₅₀)
TBEV/Hypr	Vero	Diphyllin 1	0.85	0.47 to 1.42	>100	>117.64
TBEV/Hypr	Vero	Cleistanthin B 8	5.53	4.26 to 7.19	>100	>18.08
WNV/Eg-101	Vero	Diphyllin 1	0.78	0.52 to 1.15	>100	>128.20
ZIKV/Paraiba_01	Vero	Diphyllin 1	0.54	0.33 to 0.87	>100	>185.19
RVFV/H13/96	Vero	Diphyllin 1	0.46	0.29 to 0.70	>100	>217.39
RABV/CVS-11	BHK-21	Diphyllin 1	6.33	2.86 to 14.90	>100	>15.80
HSV-1/MacIntyre	Vero	Diphyllin 1	0.59	0.35 to 0.96	>100	>169.49

¹ Determined from three biological replicates of two independent experiments. ² Expressed as a 50% reduction in virus titer or cell viability as calculated at inflection points of sigmoidal virus titer or percentage cell viability curves, which were obtained by a nonlinear fit of transformed inhibitor concentrations versus normalized response using GraphPad Prism 7.04 (GraphPad Software, Inc., USA).

Thereafter, diphyllin 1 was evaluated against another medically important emerging flavivirus, namely WNV (strain Eg-101), a representative of the mosquito-borne flaviviruses. ZIKV (strain Paraiba_01, from Brasil), another key member of the *Flaviviridae* family, which is transmitted by mosquitoes, was also studied here but as a positive control, given that ZIKV was recently found susceptible to a diphyllin analog, diphyllinoside patentiflorin A [13]. As with TBEV, Vero cells were treated with diphyllin 1 2 h prior to infection (2 h pre-treatment), simultaneously with infection (simultaneous treatment), and 2 h after infection (2 h post-treatment) (Figure 2C,D). We observed the highest antiviral activities when diphyllin 1 was administered 2 h pre-treatment (EC₅₀ values of 0.78 and 0.54 μ M for WNV and ZIKV, respectively). Furthermore, using 2 h pre-treatment, diphyllin 1 was able to completely suppress WNV and ZIKV replication in Vero cell culture at concentrations between 12.5 and 25 μ M (Figure 2C,D, Table 2).

3.4. Antiviral Activity of Diphyllin 1 against RVFV, RABV, and HSV-1

Out of curiosity, the antiviral activities of diphyllin 1 were further tested against one representative each of enveloped RNA viruses from the *Phenuiviridae* family (RVFV, strain H13/96) and the *Rhabdoviridae* family (RABV, strain CVS-11), plus one representative of the enveloped DNA viruses from the *Herpesviridae* family (HSV-1, strain MacIntyre). The sensitivity of RVFV and HSV-1 to diphyllin 1 was evaluated with Vero cell infection, whereas anti-RABV assays were performed with BHK-21 cells. Both cell lines were robust to diphyllin 1 administration up to a concentration threshold of 25 μ M (see above). In these cases, diphyllin 1 also showed strong antiviral activities against RVFV, although once again, antiviral activities were most pronounced when diphyllin 1 was administered 2 h prior to infection (2 h pre-treatment, EC₅₀ of 0.46 μ M) with complete suppression of viral replication between 12.5 and 25 μ M. Very similar results were observed in HSV-1

(2 h pre-treatment, EC₅₀ of 0.59 μ M) with complete viral suppression starting at 2.5 μ M (Figure 2E,F,H, Table 2). The ability of diphyllin 1 to inhibit RABV replication in cell culture was studied by quantification of viral genome RNA in cell culture media using RT-qPCR 72 h post-infection. Diphyllin 1 was shown to be a strong inhibitor of RABV RNA synthesis (EC₅₀ of 6.33 μ M), resulting in a 10² drop in RABV RNA copies/ μ L compared with RABV-infected control BHK-21 cells (Figure 2G,H; Table 2). Higher EC₅₀ values compared to other viruses are largely due to different methodologies for determining viral titer in anti-RABV assays (RT-qPCR instead of plaque assay, different conditions during infection, etc.).

3.5. Inhibition of Expression of Virus Antigens with Diphyllin 1

Diphyllin 1 dose-dependent antiviral effects were confirmed by immunofluorescent staining, which detects expression of viral antigens of TBEV, WNV, ZIKV, RVFV, and HSV-1 in Vero cells in vitro as a marker of viral infectivity and replication. Compared with control cells, a clear decrease in fluorescence signal was observed with increasing diphyllin 1 concentrations, monitored 48 h post-infection. In line with the viral titer data shown above (Figure 2A,C–H, Table 2), viral surface antigen expression in Vero cell culture was eliminated at administered diphyllin 1 concentrations between 12.5 and 25 μ M (Figure 3). The effect of diphyllin 1 administration on the expression of RABV surface antigens was the least pronounced of all viruses tested, although the obvious decrease in fluorescence signal intensity was still observed at diphyllin 1 concentrations between 12.5 and 25 μ M (Figure 3), in keeping with diphyllin 1 mediated reductions in RABV RNA copies/ μ L.

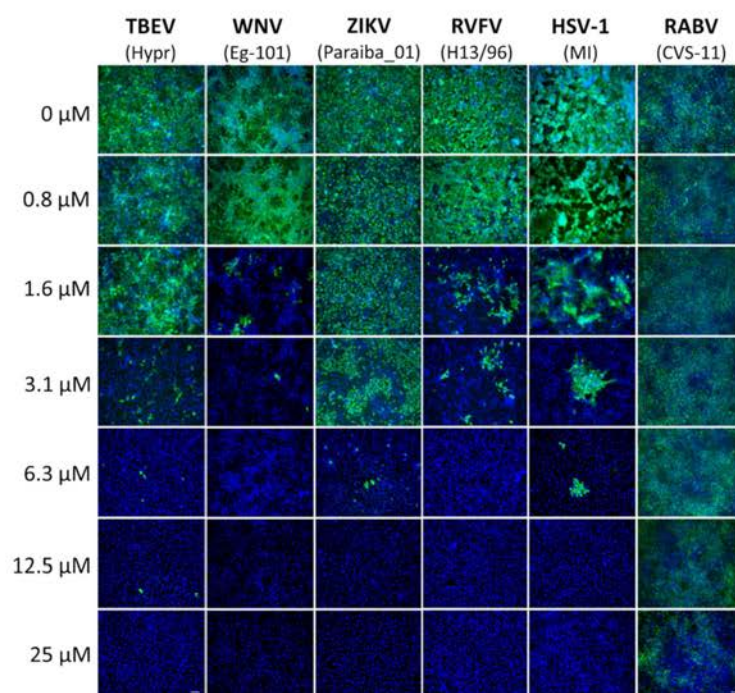


Figure 3. Inhibition of viral surface antigen expression by diphyllin 1. For immunostaining of TBEV-, WNV-, ZIKV-, RVFV-, and HSV-1-infected cells, Vero cell monolayers were treated with diphyllin 1 (at the indicated concentrations) and infected with the appropriate virus (MOI of 0.1). Cells were fixed on slides 48 h after infection, stained with viral antigen-specific antibody (primary antibody), and an anti-mouse goat antibody conjugated with FITC (green) (secondary antibody), plus counterstained with DAPI (blue). For immunostaining of RABV-infected cells, a suspension of BHK-21 cells was infected with RABV ($10^{6.58}$ TCID₅₀/mL) at 37 °C for 40 min and incubated with diphyllin 1 (0 to 25 μ M), mixing every 10 min. Following incubation, the RABV-infected cells were seeded on 96-well plates and cultivated for 72 h. After fixation and blocking, the cells were incubated with an antirabies-specific antibody labeled with FITC (green), and the cell nuclei were counterstained with DAPI (blue). MI, MacIntyre. Scale bars, 50 μ m.

3.6. Mechanism of Action of Diphyllin 1

Diphyllin 1, as a known V-ATPase inhibitor, should act as a blocker of endosomal acidification in Vero cells. This was verified by comparing the effect on cells of diphyllin 1 (at 100 μ M), bafilomycin A1 (at 100 nM) (a well-documented endosome acidification blocker that also inhibits V-ATPases [13,17]), and DMSO (1%, *v/v*, used as negative control), all in the presence of acridine orange dye. After cell uptake, this dye enters endosome compartments, and those that are at neutral pH appear green under the fluorescence microscope, while those that have become mildly acidic appear red owing to dye protonation. According to our data, control cells treated with DMSO exhibited an extensive red fluorescent signal indicative of a high number of acidic endosomes (Figure 4A). By contrast, in cells treated with diphyllin 1 (100 μ M), red fluorescence intensities appear much reduced, indicative of a much lower number of acidic endosomes and an increased number of neutral endosomes. This situation is all the more obvious in cells treated with bafilomycin A1 (100 nM). Taken together, these data confirm that diphyllin 1 is able to inhibit endosomal acidification in Vero cells, consistent with its known role as a V-ATPase inhibitor, although bafilomycin A1 is considerably more potent in this regard. Please note that cell nuclei were clearly visible in acridine orange-stained Vero cells too, since acridine orange is a strong nucleic acid binder that emits green fluorescence when bound to dsDNA (Figure 4A).

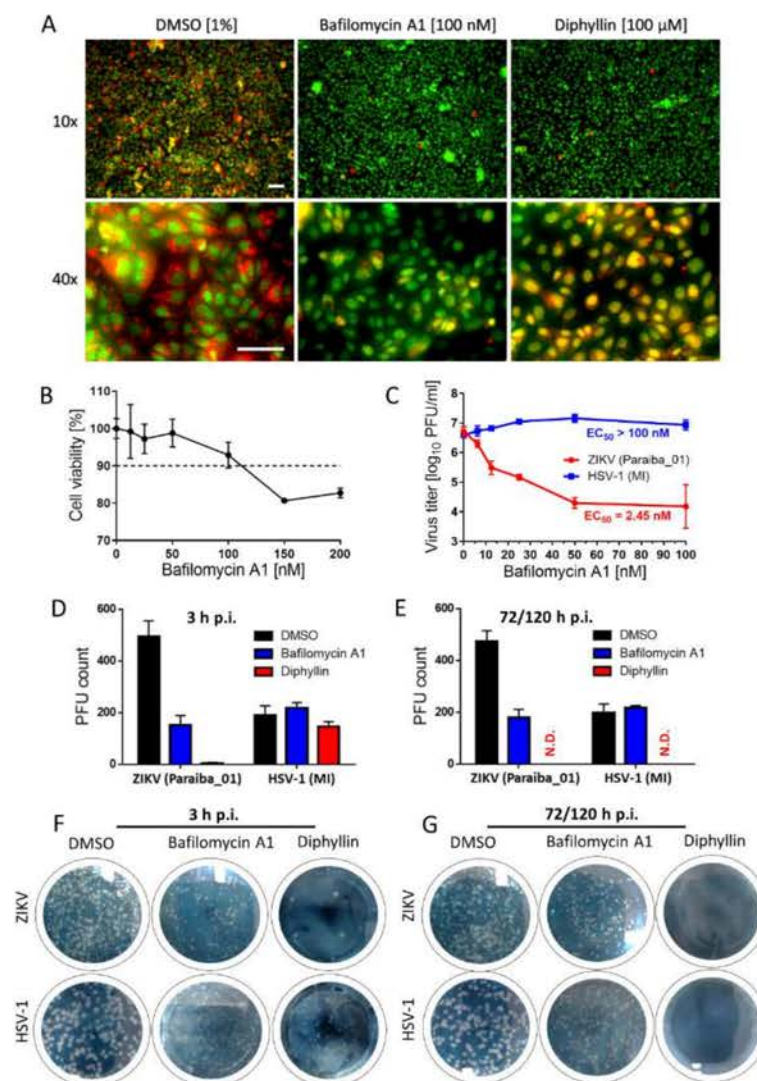


Figure 4. Diphyllin 1 mechanism of action assessment and comparison of biological activity of diphyllin 1 with that of bafilomycin A1. (A) Analysis of endosomal acidification with acridine orange

labeling. Vero cells cultured in 96-well microtiter plates were treated with diphyllin 1, bafilomycin A1, or DMSO (1%, *v/v*) (controls) at the indicated concentrations at 37 °C for 20 min and then incubated with acridine orange dye (1 µg/mL). Scale bars, 50 µm. (B) Cytotoxicity of bafilomycin A1 for Vero cells in the indicated concentration range. The cells were seeded in 96-well plates for 24 h, then treated with bafilomycin A1 and incubated for 48 h. (C) Anti-ZIKV and anti-HSV-1 activities of bafilomycin A1 in Vero cells. Vero cell monolayers were treated with bafilomycin A1 and simultaneously inoculated with ZIKV or HSV-1 (MOI of 0.1). The infected cells were then incubated for 48 h, after which cell media were collected, and viral titers were determined using a plaque assay. (D) Anti-ZIKV and anti-HSV-1 activities of diphyllin 1 (100 µM) and bafilomycin A1 (100 nM) in Vero cells measured after 3 h p.i. DMSO-treated cells were used as controls. Vero cell monolayers inoculated with the indicated viruses and diphyllin 1 (100 µM), bafilomycin A1 (100 nM), or DMSO (1%, *v/v*) were added to the cells for 3 h at 37 °C. After extensive washing, fresh medium with 4% (*w/v*) carboxymethylcellulose was added to the cell monolayers. After 72 h (for HSV-1) or 120 h (for ZIKV), the cells were stained with naphthalene black, and the number of plaques was determined. (E) Control cells were inoculated with the appropriate viruses and incubated with the compounds for 72 or 120 h for HSV-1 and ZIKV, respectively. Then, the cells were stained with naphthalene black, and the number of plaques was determined. (F,G) ZIKV and HSV-1-infected Vero cell monolayers in 6-well plates treated with the indicated compounds. The experimental conditions were described above, see (D,E). The horizontal dashed line represents 90% threshold for compound cytotoxicity assessment. MI: MacIntyre; N.D.: not detected.

Following the above, cytotoxicity studies were performed with bafilomycin A1 to establish that concentrations of ≥ 150 nM reduced Vero cell viabilities to approximately 80% compared with control cells (Figure 4B). Therefore subsequent functional bafilomycin A1-based studies were performed with a concentration maximum of 100 nM only, even though concentrations in the 100–200 nM were widely used during previous bafilomycin A1-based studies [13,22]. In functional studies, bafilomycin A1 was shown to affect a dose-dependent reduction in ZIKV (strain Paraiba_01) virus titers 48 h post-infection of Vero cells with virus and the addition of bafilomycin A1 (Figure 4C). The EC₅₀ value was found to be 2.44 nM, suggesting that bafilomycin A1 is 10³-fold more potent inhibitor of the ZIKV replication cycle than diphyllin 1. By contrast, bafilomycin A1 had no effect on the corresponding HSV-1 (strain MacIntyre) virus titers (Figure 4C) up to 100 nM.

Additional anti-ZIKV and anti-HSV-1 studies were then performed with Vero cells subject to simultaneous treatment with virus and bafilomycin A1 (100 nM) or diphyllin 1 (100 µM) for 3 h after which plaque numbers were counted at 72 h p.i. (with HSV-1) and 120 h p.i. (with ZIKV). We used a longer incubation period (120 h) for the ZIKV-based experiment, as such incubation time was needed for the formation of clear, well observable plaques. Control (virus-infected, mock-treated) cells were incubated with the compounds for the whole experimental period, i.e., for 72/120 h p.i. These data at 3 h p.i. (virus-infected, drug-treated cells, Figure 4D,F) and 72/120 h p.i. (control cells, Figure 4E,G) reveal that ZIKV was susceptible to inhibition by both drugs at 3 h p.i. and 120 h p.i. In contrast, HSV-1 was not susceptible to bafilomycin A1 treatment at 3 h p.i. or 72 h p.i. Moreover, HSV-1 was not susceptible to diphyllin 1 treatment at 3 h p.i., but was highly susceptible to diphyllin 1 at 72 h p.i. These data were not only consistent with the anti-ZIKV and anti-HSV-1 properties of diphyllin 1 measured previously (EC₅₀ values were 0.54 and 0.59 µM, respectively—see Table 2) but also suggested that the anti-HSV-1 mechanisms of action of diphyllin 1 target later stages of the HSV-1 replication cycle (i.e., replication/assembly phases) rather than the early stages (i.e., cell entry/fusion phases).

4. Discussion

Since diphyllin 1 is very often found in plants in the form of glycosides, initial efforts were made to cross-compare biological activities of diphyllin 1 with the glycoside analogue cleistanthin B 8. Prior to full antiviral studies, the cytotoxicity profiles of diphyllin 1 and cleistanthin B 8 were studied in a range of cell lines. Vero and BHK-1 cells were resistant to the administration of both compounds. However, both compounds were cytotoxic for PS,

UKF-NB-5, and Huh-7 cell lines, and also for primary human astrocytes HBCA (Figure 1, Table 1). Indeed, diphyllin 1 has been found cytotoxic to many other cell lines besides such as Mardin-Darby canine kidney cells (MDCK, CC_{50} of 3.48 μ M) [22], human lung carcinoma cells (A549, CC_{50} of 24.01 μ M) [22], feline macrophage-like cells (fcwf-4, CC_{50} of 5.99 μ M) [17], and rabbit lung cells (RL-33 CC_{50} , of 63 μ g/mL) [25]. Given the anticancer capabilities of diphyllin 1 and analogs [7,8,32–36], such activities against multiple immortalized cell lines should not perhaps be so surprising. Accordingly, diphyllin is similar to other V-ATPase blockers, which were recently described to have significant anticancer potencies indicative of general anticancer drugs. These include, plecomacrolide antibiotics, classical V-ATPase inhibitors such as concanamycin and bafilomycin A1, benzolactone enamides (apicularens, lobatamides, oximidines, and cruentaren), archazolid, indolyis, and late-generation V-ATPase inhibitors, such as FR202126, 3-bromopyruvate, or tributyltin chloride [37]. Importantly, the antiviral effects of diphyllin 1 are observed at considerably lower (non-cytotoxic) concentrations.

Here we demonstrate that diphyllin 1 acts as a sub-micromolar or low-micromolar inhibitor of multiple enveloped RNA viruses from the *Flaviviridae*, *Phenuiviridae*, and *Rhabdoviridae* families (Figure 2, Table 2), while cleistanthin B 8 displayed significantly lower antiviral effects compared with those for diphyllin 1 and was not therefore studied further here. In comparison, a diphyllin 1 and the diphyllin analog patentiflorin A have been shown previously to block ZIKV replication in vitro and prevented mortality in a rodent in vivo model of ZIKV infection as alluded to above [13]. In contrast with our study, the ZIKV infectivity in diphyllin 1-treated cells was evaluated using immunofluorescence staining-based method demonstrating the anti-ZIKV effect of diphyllin 1 even in nanomolar concentrations [13]. Furthermore, analogs patentiflorin A and justiprocurin B, were found to display nanomolar activity against four clinical HIV-1 isolates in human peripheral blood mononuclear cells (PBMC) cells [23,24] as well broad spectrum nanomolar inhibition of HIV-1 strains resistant to several reverse transcriptase inhibitors [24]. In addition, diphyllin 1 itself has been shown to inhibit the replication of feline infectious peritonitis virus (FIPV), a member of the *Coronaviridae* family, in fcwf-4 cells. Furthermore, diphyllin 1 has also been shown to be potent in vitro against influenza virus in MDCK cells [22]. Some other diphyllin derivatives (e.g., justicidin A and B, and some others) have also been found active against vesicular stomatitis virus (VSV) when tested in RL-33 cells [25]. Therefore, taken together with our data here, there can be no doubt that diphyllin 1 is a potentially useful broad antiviral agent through its broad cellular cytotoxicity profile suggests that this antiviral agent would be best targeted to sites of viral infection by means of drug delivery nanoparticles and other nanomedicine approaches [17].

In mechanistic terms, the success of diphyllin 1 as a broad antiviral agent, as demonstrated here using complementary in vitro virus infection models, might seem somewhat paradoxical. Given that diphyllin 1 is a known V-ATPase inhibitor and hence inhibitor of endosome acidification, then this mechanism of action should account for the inhibition of the replication cycle of viruses that enter host cells by endocytosis followed by acid pH-induced membrane fusion [13,17,22]. This is certainly true of *Flaviviridae*, *Bunyaviridae*, and *Rhabdoviridae* families. All these viruses enter host cells through endocytosis and require low pH-induced fusion of viral envelope with endosome membrane to continue their replication cycles [16]. Consistent with this argument, our data here indicate clearly that the mechanism of action of diphyllin 1 against ZIKV, a member of the *Flaviviridae* family, takes place during the early phases of the virus replication cycle on a time scale consistent with a mechanism of action involving V-ATPase inhibition and the direct modulation of endosome acidification to abrogate the virus replication cycle, all in keeping with the known mechanism of ZIKV host cell entry by endocytosis [13].

On the other hand, diphyllin 1 also exhibits sub-micromolar antiviral potency against HSV-1, a virus that enters cells by plasma membrane interactions and cell surface fusion (not via endocytosis) at neutral pH (with no need for V-ATPase activity) [16]. Hence, our observed diphyllin-mediated anti-HSV-1 effects cannot be based on the inhibition of HSV-1

early cell entry but rather on the suppression of other, later stages of the HSV-1 replication cycle. Accordingly, diphyllin 1, in marked contrast to bespoke V-ATPase inhibitors such as bafilomycin A1, must be able to employ additional, alternative antiviral mechanisms of action to abrogate viral replication cycles at different stages as appropriate. Indeed, besides being a V-ATPase inhibitor, diphyllin 1 and diphyllinosides have also been shown to target topoisomerase II α [38], to induce apoptosis and protective autophagy through reactive oxygen species production [8], block voltage-gated K⁺ channels in mouse neuroblastoma cells [39], stimulate interferon- γ production [40], reduce nitric oxide levels [41], and modulate TNF- α , and IL-12 production in mouse macrophages [12]. Hence, we speculate that any or even some of these alternative capabilities might be used to suppress viral infection cycles that do not begin with endocytosis followed by acid pH-induced fusion of viral and endosomal membranes.

Besides diphyllin 1 and bafilomycin A1, broad-spectrum antiviral activity was previously demonstrated also for other V-ATPase blockers, such as saliphenylhalamide (SaliPhe), tenatoprazole, esomeprazole, and ammonium chloride, to name a few. The expected molecular target for SaliPhe is a binding site of the proton translocation domain of cellular V-ATPase; this compound can effectively inhibit several wild types of influenza viruses [42]. A similar mode of action was also considered for ammonium chloride, which showed inhibitory activity against human rhinoviruses [43]. In addition, ammonium chloride blocked infection of human papillomavirus (PV) type 16 by preventing the transport of PV viral particles from early endosomes to caveosomes [44]. Multiple modes of antiviral action were also described for tenatoprazole and esomeprazole. In addition to proton pump blocking, these compounds were observed to inhibit the budding of some enveloped viruses (e.g., HIV-1, Ebola virus, or Dengue virus) by blocking the interaction of Tsg101 protein, a member of the host endosomal sorting complex required for transport (ESCRT), with ubiquitin. Inhibition of Tsg101-ESCRT interaction blocks delivery of ESCRT to budding viral sites, causing the suppression of the virus particle release by membrane scission [45]. It is clear from these examples that different compounds, originally established as classical proton pump inhibitors, can interact with different cellular targets, resulting in a strong effect on the viral replication process. This phenomenon probably also applies to diphyllin 1.

Finally, we note that in our efforts to uncover the range and extent of the antiviral activities of diphyllin 1, as described here, we also outlined a revised, updated, and improved synthesis of diphyllin 1 to support these *in vitro* studies. The further benefits of this synthesis are two-fold: (1) it will enable the cost-effective provision of much larger quantities of this compound for future *in vivo* follow-up experiments using animal models of virus infections; and (2) it will make possible the preparation of new *in house* diphyllin analogs suitable for future structure-activity correlation experiments. In particular, the synthesis will make possible the relatively facile preparation of new diphyllin analogs through functional group substitutions of at C-3, C-4, C-2', C-3', C-4', C-5', and C-6' (see Figure 1A). We expect to report the results of such structure-activity correlation experiments in due course, building on the results of the studies described here.

5. Conclusions

We have prepared diphyllin 1 *de novo*, and this was shown to be a strong inhibitor of multiple viruses of the *Flaviviridae*, *Phenuiviridae*, *Rhabdoviridae*, and *Herpesviridae* families using Vero and BHK-21 viral infection cell models. These data convincingly suggest that diphyllin 1 is a broad-spectrum host-targeting antiviral agent blocking replication of multiple medically important enveloped RNA and DNA viruses. The next stage will be the implementation of *in vivo* model studies making use of drug delivery nanoparticles and other nanomedicine approaches to optimize antiviral effects while minimizing undesirable off-target cytotoxicities.

Supplementary Materials: The following are available online at <https://www.mdpi.com/article/10.3390/v14020354/s1>, Figure S1: Functional comparison between our synthetic diphyllin **1** and the commercial product

Author Contributions: Conceptualization, M.Š., A.D.M., M.S., D.R. and L.E.; methodology, M.Š., D.S.B., J.H., P.S., M.F., L.D., I.H., J.S. (Jiří Salát), J.B. and J.S. (Jan Svoboda); validation, M.Š. and D.S.B.; formal analysis, M.Š., D.S.B., J.H., P.S., M.F., L.D., I.H., J.S. (Jiří Salát), J.B. and J.S. (Jan Svoboda); investigation, M.Š., A.D.M., D.R. and L.E.; resources, M.S., A.D.M., D.R. and L.E.; data curation, A.D.M., D.R. and L.E.; writing—original draft preparation, M.Š. and D.S.B.; writing—review and editing, A.D.M., D.R. and L.E.; visualization, A.D.M., D.R. and L.E.; supervision, A.D.M., M.S., D.R. and L.E.; project administration, A.D.M., D.R. and L.E.; funding acquisition, A.D.M., D.R. and L.E. All authors have read and agreed to the published version of the manuscript.

Funding: This study was supported by the Ministry of Education, Youth and Sports (MŠMT) of the Czech Republic with the award of OPVVV Project FIT (CZ.02.1.01/0.0/0.0/15_003/0000495) that is financially supported by the European Fund for Regional Development (to D.R. and A.D.M.) and of grant LTAUSA18016 (to L.E).

Institutional Review Board Statement: Not applicable.

Informed Consent Statement: Not applicable.

Data Availability Statement: The datasets generated and analyzed during the current study are available from the corresponding author on reasonable request.

Conflicts of Interest: A.D.M. is a shareholder in KP Therapeutics (Europe) s.r.o. The remaining authors otherwise declare no conflicts of interest. The funders had no role in the design of the study; in the collection, analyses, or interpretation of data; in the writing of the manuscript, or in the decision to publish the results.

References






- Jullian-Pawlicki, N.; Lequart-Pillon, M.; Huynh-Cong, L.; Lesur, D.; Cailleu, D.; Mesnard, F.; Laberche, J.C.; Gontier, E.; Boitel-Conti, M. Arylnaphthalene and aryltetralin-type lignans in hairy root cultures of *Linum perenne*, and the stereochemistry of 6-methoxypodophyllotoxin and one diastereoisomer by HPLC-MS and NMR spectroscopy. *Phytochem. Anal.* **2015**, *26*, 310–319. [[CrossRef](#)]
- Cui, Q.; Du, R.; Liu, M.; Rong, L. Lignans and Their Derivatives from Plants as Antivirals. *Molecules* **2020**, *25*, 183. [[CrossRef](#)]
- Lv, J.-P.; Yang, S.; Dong, J.-X.; Jin, H. New cyclopeptide alkaloids from the whole plant of *Justicia procumbens* L. *Nat. Prod. Res.* **2021**, *35*, 4032–4040. [[CrossRef](#)] [[PubMed](#)]
- Ramesh, C.; Ravindranath, N.; Ram, T.S.; Das, B. Arylnaphthalide Lignans from *Cleistanthus collinus*. *Chem. Pharm. Bull.* **2003**, *51*, 1299–1300. [[CrossRef](#)] [[PubMed](#)]
- Prieto, J.M.; Recio, M.C.; Giner, R.M.; Máñez, S.; Massmanian, A.; Waterman, P.G.; Ríos, J.L. Topical Anti-Inflammatory Lignans from *Haplophyllum hispanicum*. *Zeitschrift Naturforschung C* **1996**, *51*, 618–622. [[CrossRef](#)] [[PubMed](#)]
- Sørensen, M.G.; Henriksen, K.; Neutzsky-Wulff, A.V.; Dziegiel, M.H.; Karsdal, M.A. Diphyllin, a Novel and Naturally Potent V-ATPase Inhibitor, Abrogates Acidification of the Osteoclastic Resorption Lacunae and Bone Resorption. *J. Bone Miner. Res.* **2007**, *22*, 1640–1648. [[CrossRef](#)]
- Shen, W.; Zou, X.; Chen, M.; Liu, P.; Shen, Y.; Huang, S.; Guo, H.; Zhang, L. Effects of diphyllin as a novel V-ATPase inhibitor on gastric adenocarcinoma. *Eur. J. Pharmacol.* **2011**, *667*, 330–338. [[CrossRef](#)]
- Lu, Y.; Zhang, R.; Liu, S.; Zhao, Y.; Gao, J.; Zhu, L. ZT-25, a new vacuolar H⁺-ATPase inhibitor, induces apoptosis and protective autophagy through ROS generation in HepG2 cells. *Eur. J. Pharmacol.* **2016**, *771*, 130–138. [[CrossRef](#)]
- Zhang, Z.; Ma, J.; Zhu, L.; Zhao, Y. Synthesis and identification of cytotoxic diphyllin glycosides as vacuolar H⁺-ATPase inhibitors. *Eur. J. Med. Chem.* **2014**, *82*, 466–471. [[CrossRef](#)]
- Henkin, J.M.; Ren, Y.; Soejarto, D.D.; Kinghorn, A.D. The Search for Anticancer Agents from Tropical Plants. *Prog. Chem. Org. Nat. Prod. Prog. Chem. Org. Nat. Prod.* **2018**, *107*, 1–94.
- Zhao, Y.; Ni, C.; Zhang, Y.; Zhu, L. Synthesis and Bioevaluation of Diphyllin Glycosides as Novel Anticancer Agents. *Arch. Pharma.* **2012**, *345*, 622–628. [[CrossRef](#)] [[PubMed](#)]
- Rao, Y.K.; Fang, S.-H.; Tzeng, Y.-M. Anti-inflammatory activities of constituents isolated from *Phyllanthus polyphyllus*. *J. Ethnopharmacol.* **2006**, *103*, 181–186. [[CrossRef](#)] [[PubMed](#)]
- Martinez-Lopez, A.; Persaud, M.; Chavez, M.P.; Zhang, H.; Rong, L.; Liu, S.; Wang, T.T.; Sarafianos, S.G.; Diaz-Griffero, F. Glycosylated diphyllin as a broad-spectrum antiviral agent against Zika virus. *EBioMedicine* **2019**, *47*, 269–283. [[CrossRef](#)] [[PubMed](#)]

14. Jefferies, K.C.; Cipriano, D.J.; Forgac, M. Function, structure and regulation of the vacuolar (H⁺)-ATPases. *Arch. Biochem. Biophys.* **2008**, *476*, 33–42. [[CrossRef](#)] [[PubMed](#)]
15. Hu, Y.-B.; Dammer, E.B.; Ren, R.-J.; Wang, G. The endosomal-lysosomal system: From acidification and cargo sorting to neurodegeneration. *Transl. Neurodegener.* **2015**, *4*, 18. [[CrossRef](#)] [[PubMed](#)]
16. White, J.M.; Whittaker, G.R. Fusion of Enveloped Viruses in Endosomes. *Traffic* **2016**, *17*, 593–614. [[CrossRef](#)]
17. Hu, C.-M.J.; Chang, W.-S.; Fang, Z.-S.; Chen, Y.-T.; Wang, W.-L.; Tsai, H.-H.; Chueh, L.-L.; Takano, T.; Hohdatsu, T.; Chen, H.-W. Nanoparticulate vacuolar ATPase blocker exhibits potent host-targeted antiviral activity against feline coronavirus. *Sci. Rep.* **2017**, *7*, 13043. [[CrossRef](#)] [[PubMed](#)]
18. MacRae, W.; Hudson, J.; Towers, G. The Antiviral Action of Lignans. *Planta Med.* **1989**, *55*, 531–535. [[CrossRef](#)] [[PubMed](#)]
19. Rocha, M.; Campana, P.; Scoaris, D.; Almeida, V.; Lopes, J.; Shaw, J.; Silva, C. Combined In Vitro Studies and in Silico Target Fishing for the Evaluation of the Biological Activities of *Diphyllia cymosa* and *Podophyllum hexandrum*. *Molecules* **2018**, *23*, 3303. [[CrossRef](#)]
20. Thamburaj, S.; Ramaraj, E.; Sethupathy, S.; Kamalanathan, C.; Raji, A.; Rajasekharan, S.K. Antibacterial and antibiofilm activities of diphyllin against fish pathogens. *Microb. Pathog.* **2020**, *145*, 104232. [[CrossRef](#)]
21. Giorgio, C.D.; Delmas, F.; Akhmedjanova, V.; Ollivier, E.; Bessonova, I.; Riad, E.; Timon-David, P. In Vitro Antileishmanial Activity of Diphyllin Isolated from *Haplophyllum bucharicum*. *Planta Med.* **2005**, *71*, 366–369. [[CrossRef](#)]
22. Chen, H.-W.; Cheng, J.X.; Liu, M.-T.; King, K.; Peng, J.-Y.; Zhang, X.-Q.; Wang, C.-H.; Shresta, S.; Schooley, R.T.; Liu, Y.-T. Inhibitory and combinatorial effect of diphyllin, a v-ATPase blocker, on influenza viruses. *Antivir. Res.* **2013**, *99*, 371–382. [[CrossRef](#)] [[PubMed](#)]
23. Zhang, H.-J.; Rumschlag-Booms, E.; Guan, Y.-F.; Liu, K.-L.; Wang, D.-Y.; Li, W.-F.; Nguyen, V.H.; Cuong, N.M.; Soejarto, D.D.; Fong, H.H.; et al. Anti-HIV diphyllin glycosides from *Justicia gendarussa*. *Phytochemistry* **2017**, *136*, 94–100. [[CrossRef](#)]
24. Zhang, H.-J.; Rumschlag-Booms, E.; Guan, Y.-F.; Wang, D.-Y.; Liu, K.-L.; Li, W.-F.; Nguyen, V.H.; Cuong, N.M.; Soejarto, D.D.; Fong, H.H.S.; et al. Potent Inhibitor of Drug-Resistant HIV-1 Strains Identified from the Medicinal Plant *Justicia gendarussa*. *J. Nat. Prod.* **2017**, *80*, 1798–1807. [[CrossRef](#)] [[PubMed](#)]
25. Asano, J.; Chiba, K.; Tada, M.; Yoshii, T. Antiviral activity of lignans and their glycosides from *Justicia procumbens*. *Phytochemistry* **1996**, *42*, 713–717. [[CrossRef](#)]
26. Stefanik, M.; Strakova, P.; Haviernik, J.; Miller, A.D.; Ruzek, D.; Eyer, L. Antiviral Activity of Vacuolar ATPase Blocker Diphyllin against SARS-CoV-2. *Microorganisms* **2021**, *9*, 471. [[CrossRef](#)] [[PubMed](#)]
27. Kozuch, O.; Mayer, P. Pig Kidney Epithelial (Ps) Cells—Perfect Tool for Study of Flavi-Viruses and Some Other Arboviruses. *Acta Virol.* **1975**, *19*, 498.
28. Růžek, D.; Vancová, M.; Tesařová, M.; Ahantarig, A.; Kopecký, J.; Grubhoffer, L. Morphological changes in human neural cells following tick-borne encephalitis virus infection. *J. Gen. Virol.* **2009**, *90*, 1649–1658. [[CrossRef](#)]
29. De Madrid, A.T.; Porterfield, J.S. A simple micro-culture method for the study of group B arboviruses. *Bull. World Health Organ.* **1969**, *40*, 113–121.
30. Wang, F.; Wang, X.; Zhang, M.-X.; Yang, Y.-H.; Zhu, H.-L. Synthesis, biological evaluation and molecular modeling of 1H-benzo[d]imidazole derivatives as novel anti-tubulin polymerization agents. *RSC Adv.* **2015**, *5*, 74425–74437. [[CrossRef](#)]
31. Kamal, A.; Daneshlab, M.; Atchison, K.; Micetich, R.G. Synthesis of ring-a-opened isopropodophyllins as potential DNA topoisomerase II inhibitors. *Bioorganic Med. Chem. Lett.* **1994**, *4*, 1513–1518. [[CrossRef](#)]
32. Chen, H.; Liu, P.; Zhang, T.; Gao, Y.; Zhang, Y.; Shen, X.; Li, X.; Shen, W. Effects of diphyllin as a novel V-ATPase inhibitor on TE-1 and ECA-109 cells. *Oncol. Rep.* **2018**, *39*, 921–928. [[CrossRef](#)] [[PubMed](#)]
33. Al-Qathama, A.; Gibbons, S.; Prieto, J.M. Differential modulation Of BAX/BCL-2 ratio and onset of caspase-3/7 Activation induced by derivatives of JUSTICIDIN B in human melanoma CELLS A375. *Oncotarget* **2017**, *8*, 95999–96012. [[CrossRef](#)] [[PubMed](#)]
34. Pan, S.; Cai, H.; Gu, L.; Cao, S. Cleistanthin A inhibits the invasion and metastasis of human melanoma cells by inhibiting the expression of matrix metalloproteinase-2 and -9. *Oncol. Lett.* **2017**, *14*, 6217–6223. [[CrossRef](#)] [[PubMed](#)]
35. Liu, S.; Wang, L.; Ding, W.; Wang, D.; Wang, X.; Luo, Q.; Lu, Y.; Zhu, L. Cleistanthin A inhibits the invasion of MDA-MB-231 human breast cancer cells: Involvement of the β -catenin pathway. *Pharmacol. Rep.* **2019**, *72*, 188–198. [[CrossRef](#)]
36. Jiang, R.-W.; Zhou, J.-R.; Hon, P.-M.; Li, S.-L.; Zhou, Y.; Li, L.-L.; Ye, W.-C.; Xu, H.-X.; Shaw, P.-C.; But, P.P.-H. Lignans from *Dysosma versipellis* with Inhibitory Effects on Prostate Cancer Cell Lines. *J. Nat. Prod.* **2007**, *70*, 283–286. [[CrossRef](#)]
37. Pérez-Sayáns, M.; Somoza-Martín, J.M.; Barros-Angueira, F.; Rey, J.M.; García-García, A. V-ATPase inhibitors and implication in cancer treatment. *Cancer Treat Rev.* **2009**, *35*, 707–713. [[CrossRef](#)]
38. Gui, M.; Shi, D.-K.; Huang, M.; Zhao, Y.; Sun, Q.-M.; Zhang, J.; Chen, Q.; Feng, J.-M.; Liu, C.-H.; Li, M.; et al. D11, a novel glycosylated diphyllin derivative, exhibits potent anticancer activity by targeting topoisomerase II α . *Investig. New Drugs* **2010**, *29*, 800–810. [[CrossRef](#)]
39. Leung, Y.-M.; Tsou, Y.-H.; Kuo, C.-S.; Lin, S.-Y.; Wu, P.-Y.; Hour, M.-J.; Kuo, Y.-H. Arylnaphthalene lignans from *Taiwania cryptomerioides* as novel blockers of voltage-gated K channels. *Phytomedicine* **2010**, *18*, 46–51. [[CrossRef](#)]
40. Yi, L.; Chen, L.; Guo, X.; Lu, T.; Wang, H.; Ji, X.; Zhang, J.; Ren, Y.; Pan, P.; Douglas Kinghorn, A.D.; et al. A Synthetic Disaccharide Derivative of Diphyllin, TAARD, Activates Human Natural Killer Cells to Secrete Interferon-Gamma via Toll-Like Receptor-Mediated NF- κ B and STAT3 Signaling Pathways. *Front. Immunol.* **2018**, *9*, 1509. [[CrossRef](#)]

41. Day, S.-H.; Lin, Y.-C.; Tsai, M.-L.; Tsao, L.-T.; Ko, H.-H.; Chung, M.-I.; Lee, J.-C.; Wang, J.-P.; Won, S.-J.; Lin, C.-N. Potent Cytotoxic Lignans from *Justicia procumbens* and Their Effects on Nitric Oxide and Tumor Necrosis Factor- α Production in Mouse Macrophages. *J. Nat. Prod.* **2002**, *65*, 379–381. [[CrossRef](#)]
42. Müller, K.-H.; Kainov, D.E.; El Bakkouri, K.; Saelens, X.; De Brabander, J.K.; Kittel, C.; Samm, E.; Muller, C.P. The proton translocation domain of cellular vacuolar ATPase provides a target for the treatment of influenza A virus infections. *Br. J. Pharmacol.* **2011**, *164*, 344–357. [[CrossRef](#)] [[PubMed](#)]
43. Pfanzagl, B.; Andergassen, D.; Edlmayr, J.; Niespodziana, K.; Valenta, R.; Dieter Blaas, D. Entry of human rhinovirus 89 via ICAM-1 into HeLa epithelial cells is inhibited by actin skeleton disruption and by bafilomycin. *Arch. Virol.* **2014**, *159*, 125–140. [[CrossRef](#)] [[PubMed](#)]
44. Dabydeen, S.A.; Meneses, P.I. The role of NH₄Cl and cysteine proteases in Human Papillomavirus type 16 infection. *Virol. J.* **2009**, *20*, 109. [[CrossRef](#)] [[PubMed](#)]
45. Watanabe, S.M.; Ehrlich, L.S.; Strickland, M.; Li, X.; Soloveva, V.; Goff, A.J.; Stauff, C.B.; Bhaduri-McIntosh, S.; Tjandra, N.; Carter, C. Selective Targeting of Virus Replication by Proton Pump Inhibitors. *Sci. Rep.* **2020**, *10*, 4003.

Article

A Helquat-like Compound as a Potent Inhibitor of Flaviviral and Coronaviral Polymerases

Eva Konkolova ^{1,†} , Kateřina Krejčová ^{1,†}, Luděk Eyer ^{2,†}, Jan Hodek ¹, Michala Zgarbová ¹ , Andrea Fořtová ², Michael Jirasek ¹, Filip Těpy ¹, Paul E. Reyes-Gutierrez ¹, Daniel Růžek ^{2,3,4} , Jan Weber ¹  and Evzen Boura ^{1,*} 

¹ Institute of Organic Chemistry and Biochemistry, Academy of Sciences of the Czech Republic, v.v.i., Flemingovo nám. 2, 16610 Prague, Czech Republic; eva.konkolova@uochb.cas.cz (E.K.); krejcov@uochb.cas.cz (K.K.); jan.hodek@uochb.cas.cz (J.H.); michala.zgarbova@uochb.cas.cz (M.Z.); michal.jirasek@uochb.cas.cz (M.J.); filip.teply@uochb.cas.cz (F.T.); reyes.gutierrez@uochb.cas.cz (P.E.R.-G.); jan.weber@uochb.cas.cz (J.W.)

² Laboratory of Emerging Viral Diseases, Veterinary Research Institute, Hudcova 296/70, 62100 Brno, Czech Republic; eyer@vri.cz (L.E.); andrea.fortova@vri.cz (A.F.); ruzekd@paru.cas.cz (D.R.)

³ Institute of Parasitology, Biology Centre of the Czech Academy of Sciences, Branišovská 1160/31, 37005 Ceske Budejovice, Czech Republic

⁴ Department of Experimental Biology, Faculty of Science, Masaryk University, 62500 Brno, Czech Republic

* Correspondence: boura@uochb.cas.cz

† These authors contributed equally to this work.

Abstract: Positive-sense single-stranded RNA (+RNA) viruses have proven to be important pathogens that are able to threaten and deeply damage modern societies, as illustrated by the ongoing COVID-19 pandemic. Therefore, compounds active against most or many +RNA viruses are urgently needed. Here, we present PR673, a helquat-like compound that is able to inhibit the replication of SARS-CoV-2 and tick-borne encephalitis virus in cell culture. Using in vitro polymerase assays, we demonstrate that PR673 inhibits RNA synthesis by viral RNA-dependent RNA polymerases (RdRps). Our results illustrate that the development of broad-spectrum non-nucleoside inhibitors of RdRps is feasible.

Keywords: helquat-like compound; RNA-dependent RNA-polymerase; SARS-CoV-2; Flaviviruses; antiviral agents



Citation: Konkolova, E.; Krejčová, K.; Eyer, L.; Hodek, J.; Zgarbová, M.; Fořtová, A.; Jirasek, M.; Těpy, F.; Reyes-Gutierrez, P.E.; Růžek, D.; et al.

A Helquat-like Compound as a Potent Inhibitor of Flaviviral and Coronaviral Polymerases. *Molecules* **2022**, *27*, 1894. <https://doi.org/10.3390/molecules27061894>

Academic Editors: Francesc Xavier Ruiz and Joy Y. Feng

Received: 21 February 2022

Accepted: 9 March 2022

Published: 15 March 2022

Publisher's Note: MDPI stays neutral with regard to jurisdictional claims in published maps and institutional affiliations.



Copyright: © 2022 by the authors. Licensee MDPI, Basel, Switzerland. This article is an open access article distributed under the terms and conditions of the Creative Commons Attribution (CC BY) license (<https://creativecommons.org/licenses/by/4.0/>).

1. Introduction

Flaviviruses (family *Flaviviridae*) and coronaviruses (family *Coronaviridae*) both belong among single-stranded positive-sense RNA (+RNA) viruses. Members of these viral families include important human pathogens, such as the yellow fever virus (YFV), Zika virus (ZIKV), tick-borne encephalitis virus (TBEV), West Nile virus (WNV), Middle East respiratory syndrome coronavirus (MERS-CoV), severe acute respiratory syndrome coronavirus (SARS-CoV), OC43 coronavirus (OC43-CoV) and the severe acute respiratory syndrome coronavirus 2 (SARS-CoV-2) [1–4]. Unfortunately, both families have proved that they hold pandemic potential, as demonstrated recently by the ZIKV, MERS-CoV and SARS-CoV outbreaks [5–8]. Nonetheless, the ZIKV, MERS-CoV and SARS-CoV viruses were contained. It was the SARS-CoV-2 that revealed the full potential of +RNA viruses to cause harm to humans. According to the WHO (<https://covid19.who.int/>, accessed on 20 February 2022), the COVID-19 pandemic has already claimed 6 million lives worldwide at the beginning of March 2022.

Small molecule-based antiviral treatments are urgently needed. The first FDA-approved small molecule to be used against COVID-19 was remdesivir [9], and recently orally available drugs molnupiravir and Paxlovid were approved in several countries as well. Molnupiravir targets the RNA-dependent RNA polymerase (RdRp), a key enzyme in the replication of RNA viruses [10]. The primary target of Paxlovid is the SARS-CoV-2 main protease, which is involved in the processing of the coronaviral polyprotein [11]. Importantly, new

SARS-CoV-2 variants, such as omicron, that partially escape vaccine-induced immunity are sensitive to these compounds [12]. In addition, other coronaviral enzymes, including exonuclease, endonuclease, helicase and methyltransferase, have recently been biochemically and structurally described [13–17], and their inhibitors have been reported [18–21]; however, none of these compounds have been developed enough to enter clinical trials. Furthermore, often, the simultaneous administration of several compounds is necessary to efficiently combat a virus and to prevent the development of escape mutants, as illustrated by the highly efficient highly active antiretroviral therapy (HAART) against the HIV virus [22].

Here, we present compound PR673 bearing a rather unusual helquat-like chemical structure (Figure 1A) that was discovered while screening against the SARS-CoV-2 virus, but is actually more active against flaviviruses. We use in vitro polymerase assays to show that this compound interferes with RNA syntheses performed by the viral RdRps.

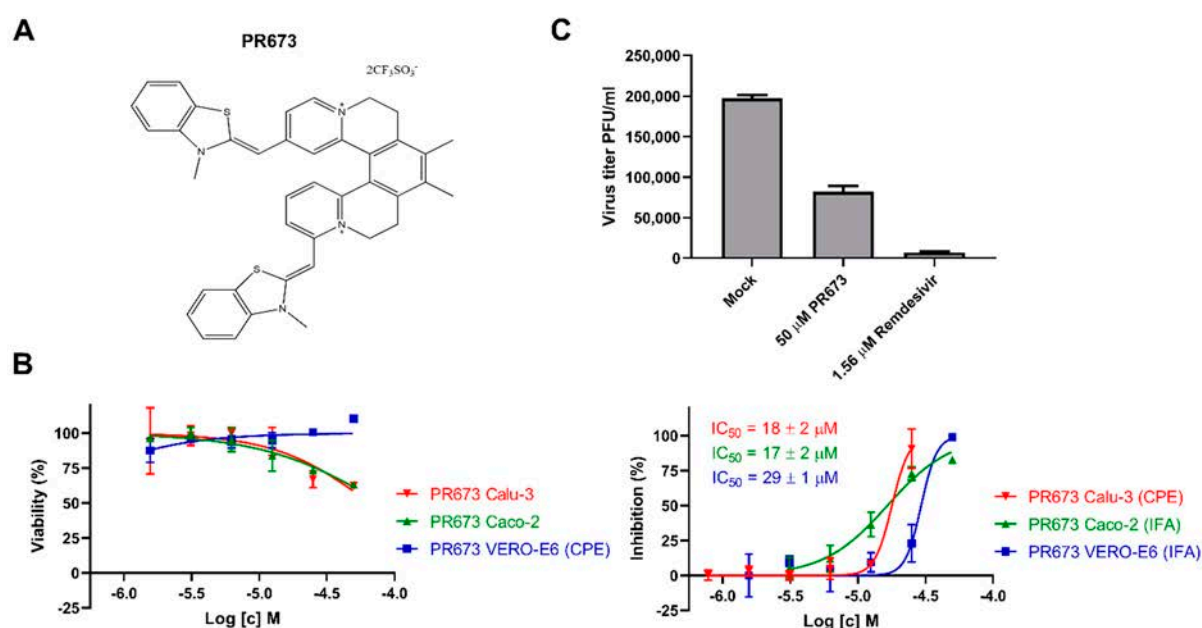


Figure 1. Inhibitory activity of PR673 against SARS-CoV-2. (A) The chemical structure of PR673. (B) Left panels: dependence of viability of VERO-E6, Calu-3 and Caco-2 cells on PR673 concentration; right panels: dependence of inhibition of SARS-CoV-2 in VERO-E6, Calu-3 and Caco-2 cells on PR673 concentration. (C) Comparison of PR673 and remdesivir in SARS-CoV-2 yield reduction assay. The VERO-E6 cells were incubated with PR673, remdesivir and a mock followed by SARS-CoV-2 infection at MOI 0.04 for 3 days, and the virus yield was determined by plaque assay in VERO-E6 cells.

2. Results

2.1. Identification of PR673

We screened the IOCB library [23] using a phenotypic assay against SARS-CoV-2. Briefly, the IOCB-library compounds were screened at a 64 μM concentration in triplicates in VERO-E6 cells against SARS-CoV-2, and the inhibition of the virus-induced cytopathic effect (CPE) was monitored. We identified an interesting helquat-like compound (PR673) (Figure 1A) that inhibited the replication of the virus in VERO-E6 cells. This activity was further verified in VERO-E6 and Caco-2 cells using SARS-CoV-2 nucleoprotein expression detected by the immunofluorescence assay (IFA) (Figure 1B, Supplementary Figure S1), which we could also confirm using the protection of cells from the virus-induced cytopathic effect (CPE) in Calu-3 cells (Figure 1B). PR673 inhibited SARS-CoV-2 with an EC_{50} value of 29 μM in VERO-E6 cells (Figure 1B) and yielded a 58% reduction in viral plaques at 50 μM (Figure 1C), while exhibiting no cell toxicity in Vero E6 cells (Figure 1B). The compound effectively inhibited virus-induced CPE in Calu-3 cells and virus replication in Caco-2 cells, with EC_{50} values of 18 μM and 17 μM , respectively. We observed mild cytotoxicity at the highest used concentration for Caco-2 and Calu-3 cell lines, but the CC_{50} of PR673 for both

cell lines was above 50 μM (Figure 1B). Nonetheless, it must be noted that PR673 was much less active than the COVID-19 drug remdesivir (Figure 1C).

2.2. PR673 Inhibits the Coronavirus RdRp

We next aimed to discover the molecular target of this compound. Based on the chemical structure, we speculated that the RdRp is the target of PR673. The SARS-CoV-2 RdRp is a heterotrimeric protein complex composed of nsp7, nsp8 and nsp12. We prepared this RdRp recombinantly, as reported before [21], and measured the inhibitory activity of PR673. Indeed, it targeted the SARS-CoV-2 RdRp: the synthesis of RNA was totally blocked at a PR673 concentration above 12.5 μM (Figure 2, SARS-CoV-2 panel).

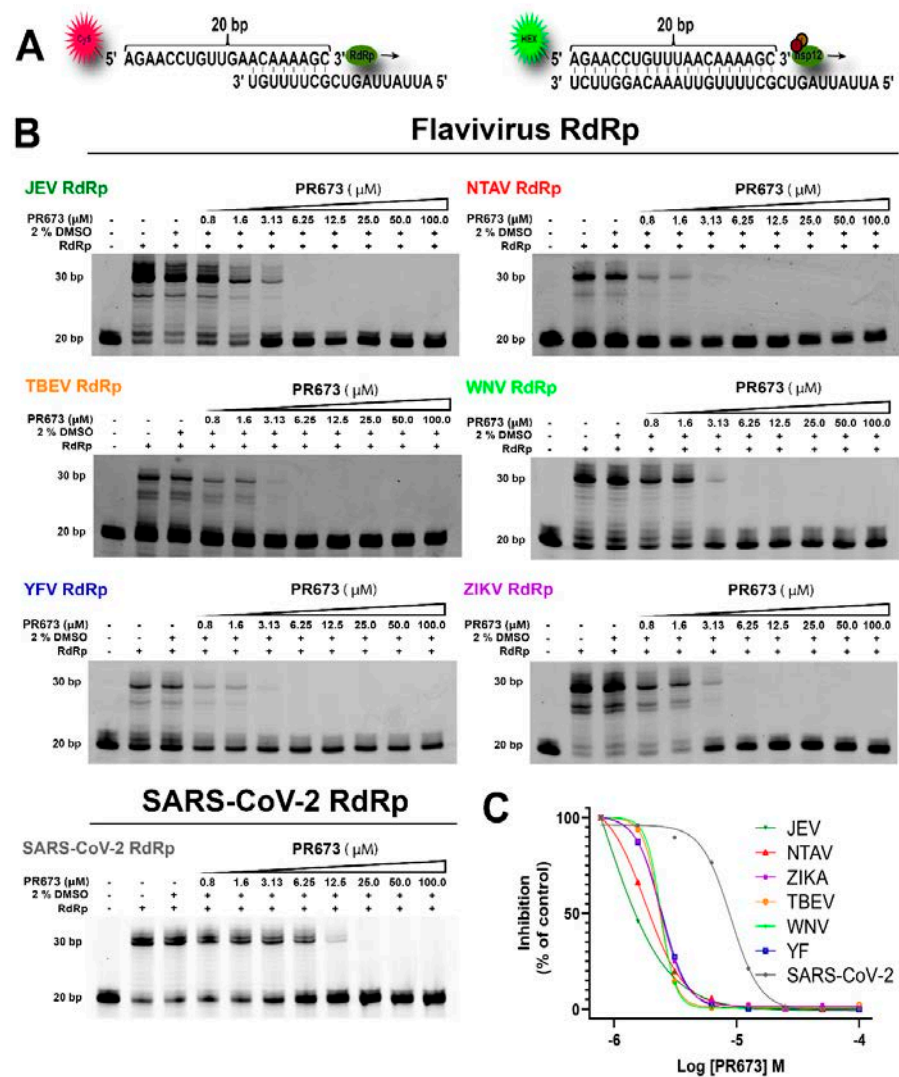


Figure 2. Analysis of PR673 inhibitory activity against various RdRps using a primer extension assay. (A) The RNA primer and RNA templates used in this assay. The RNA primer contains a fluorescent label at the 5' end (Cy5 or Hex for flaviviral RdRp, or SARS-CoV-2 RdRp, respectively). The arrow indicates the direction of primer extension. (B) Serial dilutions of PR673 (in μM), as indicated on the top of the gel, and a constant concentration of the polymerase (20 nM) and template/primer (10 nM) were used in the assay. The reactions were initiated by adding 10 μM NTPs. The reactions continued at 33 $^{\circ}\text{C}$ for 1 h; then, the reactions were stopped by the addition of stop buffer, and the products were separated on denaturing polyacrylamide gels. (C) The percentages of inhibition (against control) in panel B were plotted against the logarithm of concentrations of PR673; the results were fitted to sigmoidal dose–response curves.

2.3. PR673 Inhibitory Activity against Flaviviral RdRps

Further, we sought to decipher whether PR673 inhibited other viral RdRps. We chose several members of the *Flaviviridae* family, namely the Japanese encephalitis virus (JEV), Ntaya virus (NTAV), tick-borne encephalitis virus (TBEV), yellow fever virus (YFV) and Zika virus (ZIKV), and we prepared their polymerases recombinantly. In each case, we observed a strong inhibition of RNA synthesis in low micromolar concentrations of PR673 (Figures 2 and 3).

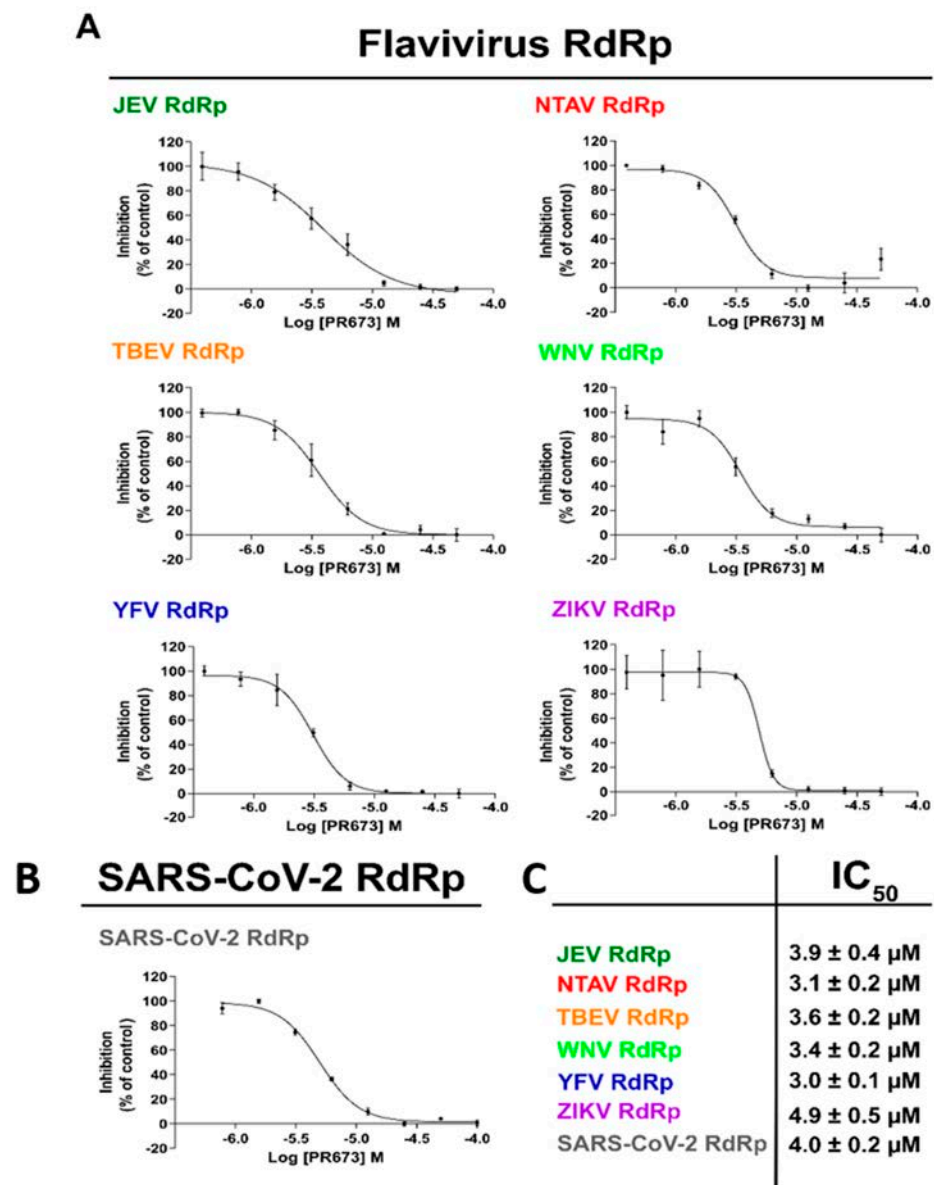


Figure 3. Measurement of the IC₅₀ values of PR673. The IC₅₀ values were established for each tested polymerase with PR673 using radioactively labeled elongation products. (A) The RNA hairpin used in this assay. The arrow indicates the direction of primer extension. (B) The percentages of inhibition (against control) were plotted against the logarithm of concentrations of PR673, and the results were fitted to sigmoidal dose–response curves. Error bars represent the standard error of three independent measurements. (C) The table of IC₅₀ values. The IC₅₀ values were extrapolated from LogIC₅₀ according to the GraphPad algorithm.

We then established IC₅₀ values for each of the aforementioned RdRp enzymes using a radioactive assay because it is more sensitive and accurate than alternative methods. The reaction mixture contained the viral RdRp, the hairpin-containing RNA as the template

and radioactively labeled ATP ($[\alpha\text{-}^{32}\text{P}]\text{-ATP}$). Our results showed that PR673 inhibits all of the tested polymerases, with IC_{50} values ranging from $3.0 \pm 0.1 \mu\text{M}$ to $4.9 \pm 0.5 \mu\text{M}$ (Figure 4). The yellow fever virus RdRp was inhibited the most and the Zika RdRp the least; however, the observed differences were rather low.

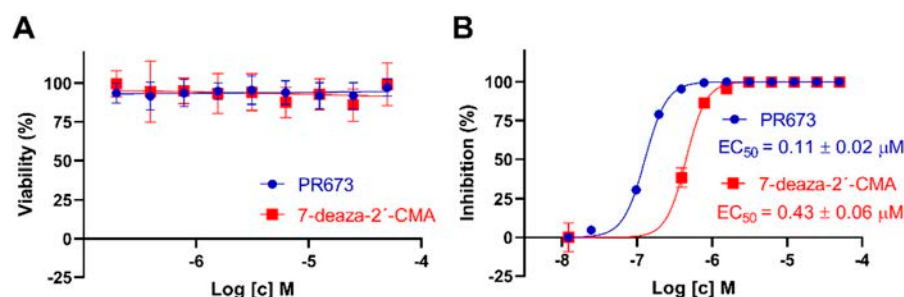


Figure 4. Cytotoxicity and anti-TBEV activity of PR673 in PS cells. **(A)** Cytotoxicity of PR673 for PS cells expressed as percentage of cell viability at the indicated drug concentrations. The cells were seeded in 96-well plates for 24 h, then treated with the compounds and incubated for 48 h. Cell viabilities were measured by Cell Counting Kit-8. **(B)** Anti-TBEV activity of PR673 in PS cells. The cell monolayers were treated with the compounds (0 to 50 μM) and infected simultaneously with TBEV (Hypr) at MOI of 0.1. The infected cells were then incubated for 48 h, after which, cell media were collected and viral titers determined using a plaque assay. The obtained titers were used to construct dose-dependent inhibition curves (as indicated) and to calculate EC_{50} values. 7-deaza-2'-CMA (in the same concentration range) was used as a positive control.

2.4. PR673 Inhibits Replication of the TBEV in Cell Culture

Since we observed a strong inhibition of all tested flaviviral RdRps *in vitro*, we decided to test whether PR673 could inhibit a flavivirus in cell culture. We used the TBEV (strain Hypr) for which we have well established assays [24,25]. We first tested the cytotoxicity of PR673 in porcine kidney stable cells (PS cells) that are widely used for TBEV multiplication, anti-TBEV assays and TBEV-based plaque assays [26]. We also used 7-deaza-2'-C-methyladenosine (7-deaza-2'-CMA) as a positive control because this compound is a well-established inhibitor of the TBEV RdRp [25]. The cytotoxicity was evaluated in a concentration range of 0 to 50 μM ; both compounds appeared as non-cytotoxic for PS cells up to 50 μM when incubated with the cells for 48 h. Similarly to 7-deaza-2'-CMA, the CC_{50} values of PR673 were estimated to be $>50 \mu\text{M}$ (Figure 4A).

Next, we tested the anti-TBEV activity of PR673 in PS cells and compared its anti-TBEV activity with that of 7-deaza-2'-CMA. PR673 exerted a dose-dependent anti-TBEV effect, with an EC_{50} value of 0.11 μM . The complete inhibition of TBEV replication was observed at a compound concentration of 0.4 μM . The anti-TBEV activity of PR673 was almost four-fold higher in comparison to 7-deaza-2'-CMA (Figure 4B).

3. Discussion

More small molecules active against SARS-CoV-2 are needed. Two compounds targeting the RdRp (remdesivir and molnupiravir) and the 3C-like protease inhibitor nirmatrelvir (sold under the name Paxlovid) are already available as human medicines. In addition, inhibitors of other coronaviral enzymes, such as the helicase [27,28], endo- and exonuclease [29,30] or the methyltransferases [18,19,31], have been actively developed. However, the goal is to develop compounds that would be active against multiple viruses or even multiple viral families. These so-called broad-spectrum antivirals could be a powerful weapon to combat future pandemics. One such example is remdesivir. It was originally discovered by Gilead when screening for compounds active against the respiratory syncytial virus, and was later both developed to combat the Ebola outbreak in 2014 and repurposed against SARS-CoV-2 [32–34]. Recently, we showed that it can also effectively inhibit flaviviral RdRps [35]. Remdesivir is a nucleotide analog that is metabolized into remdesivir triphosphate; upon incorporation into RNA, it acts as a delayed chain terminator. In fact,

nucleoside analogs can be divided into three classes: (i) mutagenic nucleosides, such as ribavirin, that are able to cause mutational catastrophe [36]; (ii) obligate chain terminators that usually lack the ribosyl C3'-hydroxyl group [37]; and (iii) delayed chain terminators, such as remdesivir [38]. Our experiments with PR673 demonstrate that it acts as a pseudo-obligate chain terminator. It can clearly stop the synthesis of RNA *in vitro* by recombinant RdRps (Figure 2), which explains its effect on the replication of SARS-CoV-2 and TBEV (Figures 1 and 4). However, obligate chain terminators are incorporated into RNA, and their chemical nature prevents the incorporation of another nucleoside [39], which is clearly not the case for PR673. It could possibly compete for one of the RNA binding sites that are present and relatively conserved at viral RdRps, such as the entry site or the exit tunnel [40–42]. We cannot rule out the possibility that PR673 is an allosteric inhibitor; however, this is not probable because it is active on relatively distant RdRps, where an allosteric site is unlikely to be conserved. In any case, PR673 illustrates that the development of non-nucleoside antivirals active against a broad spectrum of viruses is feasible.

4. Material and Methods

4.1. Anti-SARS-CoV-2 Activity Determination Using Immunofluorescence Assay

Anti-SARS-CoV-2 activity was tested in VERO-E6 (ATCC CRL-1586) and Caco-2 cells (ATCC HTB-37) using immunofluorescence assay. VERO-E6 cells were seeded one day before experiment in DMEM medium with 10% FBS, 100 U of penicillin/mL and 100 µg of streptomycin/mL (all Merck KGaA, Darmstadt, Germany) in 96-well plate. Day after, two-fold serial dilution of compound was added to the cells in triplicate in complete DMEM medium with 2% FBS. After one hour, cells were infected with SARS-CoV-2 (hCoV-19/Czech Republic/NRL_6632_2/2020, multiplicity of infection MOI = 0.02) and incubated for 3 days in 5% CO₂ at 37 °C. After incubation, medium was removed, cells were fixed using 4% paraformaldehyde (PFA), washed 3× with PBS, permeabilized with 0.2% Triton-X100 for 5 min at room temperature and incubated for 2 h with anti-SARS-CoV-2 antibody (mouse monoclonal anti-nucleoprotein IgG, Institute of Molecular Genetics, Czech Republic). Subsequently, cells were washed 3× with PBS and incubated for 1.5 h with 1:250 dilution of Cy3-labeled donkey anti-mouse IgG (Jackson ImmunoResearch, Cambridgeshire) at RT, and fluorescent foci were visualized using a fluorescence microscope (Olympus IX 81, Hamburg, Germany). Cellular DNA was labeled with DAPI (4',6-diamidino-2-phenylindole) (Merck KGaA, Darmstadt, Germany) nucleic acid stain. Cells were incubated with DAPI (0.1 µg/mL) for 10 min and subsequently washed with 1× PBS. Immunofluorescence assay in Caco-2 cells was performed similarly as above, with following changes. The MOI of SARS-CoV-2 was 0.002, permeabilization was performed with methanol at −20 °C for ten minutes and, as a secondary antibody, the 1:200 dilution of FITC-labelled goat anti-mouse IgG (Jackson ImmunoResearch) was used. The fluorescent images of both cell lines were analyzed by ImageJ (NIH) and the compound concentration required to reduce fluorescence by 50% (EC₅₀) was calculated using nonlinear regression analysis with GraphPad Prism software.

4.2. Anti-SARS-CoV-2 Activity Determination Using Cytopathic Effect-Based Assay

For CPE-based assay, two-fold serial dilutions of compounds were added in triplicate in a 96-well plate with Calu-3 cells (ATCC HTB-55) seeded day before in DMEM medium with 10% FBS, 100 U of penicillin/mL and 100 µg of streptomycin/mL. After 1 h incubation, SARS-CoV-2 was added at MOI 0.04. Following a three-day incubation at 37 °C in 5% CO₂ the cell viability was evaluated by XTT cell viability assay. Four hours after addition of XTT solution, the absorbance was measured using EnVision plate reader (PerkinElmer) and the compound concentrations required to reduce viral cytopathic effect by 50% (EC₅₀) were calculated using nonlinear regression analysis using GraphPad Prism software.

4.3. Cytotoxicity Determination in SARS-CoV-2 Assays

Cytotoxicity was evaluated by incubating the same two-fold serial dilutions of compound as in antiviral assays with VERO-E6, Caco-2 and Calu-3 cells. After three days' incubation at 37 °C in 5% CO₂, the cell viability was determined by addition of 50:1 mixture of XTT labeling reagent (1 mg/mL) and PMS electron-coupling reagent (0.383 mg/mL) (both Merck KGaA, Darmstadt, Germany), and the compound concentrations resulting in 50% reduction in viability (CC₅₀) were calculated as above in the antiviral activity determination using CPE-based assay.

4.4. SARS-CoV-2 Yield Reduction Assay

The VERO-E6 cells were incubated with and without a tested compound (at different concentrations) for 1 h, followed by SARS-CoV-2 infection at MOI 0.04 for 3 days at 37 °C in 5% CO₂. Virus yield was determined by a plaque assay in a 24-well plate. Briefly, 100 µL of the supernatant was added to VERO-E6 cell monolayer, incubated for 4 h at 37 °C in 5% CO₂ and overlaid with 3% carboxymethyl cellulose. After a 5-day incubation, the cells were fixed and stained with Naphthalene black and the plaques were counted.

4.5. Anti-TBEV Studies

TBEV strain Hypr, a representative of the European TBEV subtype, was provided by the Collection of Arboviruses, Institute of Parasitology, Biology Centre of the Czech Academy of Sciences, Ceske Budejovice, Czech Republic (<http://www.arboviruscollection.cz/index.php?lang=en>, accessed on 20 February 2022). Porcine kidney stable (PS) cells [26] were cultured in Leibovitz (L-15) medium and supplemented with 3% newborn calf serum, 100 U/mL penicillin, 100 µg/mL streptomycin and 1% glutamine (Sigma-Aldrich KGaA, Darmstadt, Germany). PS cells were cultivated at 37 °C under a normal atmosphere (without CO₂ supplementation).

To determine the cytotoxicity of PR673, PS cells were seeded in 96-well microtitration plates (2×10^4 cells per well) and incubated for 24 h at 37 °C. After incubation, PR673 was added to the cells (0 to 50 µM). 7-deaza-2'-CMA (Carbosynth, Compton, UK) in the same concentration range was used as a positive control. Then, the treated cells were cultivated for 48 h at 37 °C. The cytotoxicity measured in terms of cell viability was determined with Cell Counting Kit-8 (Dojindo Molecular Technologies) according to manufacturer's instructions. The respective concentrations of each compound that reduced cell viability by 50% (CC₅₀ values) were determined. The experiment was performed in triplicate.

TBEV titer reduction assays were performed to determine anti-TBEV activity of PR673 in the PS cell culture. The cells were seeded in 96-well plates (2×10^4 cells per well) and incubated for 24 h at 37 °C to form a confluent monolayer. Subsequently, the cells were infected with TBEV (multiplication of infection of 0.1), simultaneously treated with PR673 at concentrations of 0 to 50 µM and incubated for 48 h at 37 °C. Following incubation, media were collected and viral titers determined by plaque assay [25] to construct dose-dependent inhibition curves and to estimate 50% effective concentration (EC₅₀) values. Similarly to the cytotoxicity assays, the experiment was performed in triplicate and the 7-deaza-2'-CMA was used as a positive control.

4.6. Protein Expression and Purification

NS5 proteins and SARS-CoV-2 nsp12, nsp8 and nsp7 were expressed with appropriate purification and folding tags, as detailed in Supplementary Table S1 and as described before [21,35,39]. Briefly, all of the proteins were expressed in bacterial cells, except for the full length nsp12 protein, which was expressed in insect cells. Other genes were expressed in *E. coli* (BL-21 CodonPlus (DE3)-RIL). Transformed cells were grown to an optimal OD₆₀₀ in LB medium at 37 °C; then, the protein expression was induced by addition of IPTG to 0.4 mM and the cells were grown at 18 °C for 16 h. The recombinant proteins were purified using Ni²⁺ affinity chromatography followed by tag cleavage (when appropriate), and further purified using size exclusion chromatography.






References

1. Moureau, G.; Cook, S.; Lemey, P.; Nougairede, A.; Forrester, N.L.; Khasnatinov, M.; Charrel, R.N.; Firth, A.E.; Gould, E.A.; de Lamballerie, X. New Insights into Flavivirus Evolution, Taxonomy and Biogeographic History, Extended by Analysis of Canonical and Alternative Coding Sequences. *PLoS ONE* **2015**, *10*, e0117849.
2. Simmonds, P.; Becher, P.; Bukh, J.; Gould, E.A.; Meyers, G.; Monath, T.; Muerhoff, S.; Pletnev, A.; Rico-Hesse, R.; Smith, D.B.; et al. ICTV Virus Taxonomy Profile: Flaviviridae. *J. Gen. Virol.* **2017**, *98*, 2–3. [[CrossRef](#)] [[PubMed](#)]
3. Abdelaziz, O.S.; Waffa, Z. Neuropathogenic human coronaviruses: A review. *Rev. Med. Virol.* **2020**, *30*, e2118. [[CrossRef](#)] [[PubMed](#)]
4. Shchelkanov, M.Y.; Popova, A.Y.; Dedkov, V.G.; Akimkin, V.G.; Maleev, V.V. History of Investigation and Current Classification of Coronaviruses (Nidovirales: Coronaviridae). *Russ. J. Infect. Immun.* **2020**, *10*, 221–246. [[CrossRef](#)]
5. Pierson, T.C.; Diamond, M.S. The continued threat of emerging flaviviruses. *Nat. Microbiol.* **2020**, *5*, 796–812. [[CrossRef](#)] [[PubMed](#)]
6. Graham, R.L.; Donaldson, E.F.; Baric, R.S. A decade after SARS: Strategies for controlling emerging coronaviruses. *Nat. Rev. Microbiol.* **2013**, *11*, 836–848. [[CrossRef](#)] [[PubMed](#)]
7. de Wit, E.; van Doremalen, N.; Falzarano, D.; Munster, V.J. SARS and MERS: Recent insights into emerging coronaviruses. *Nat. Rev. Microbiol.* **2016**, *14*, 523–534. [[CrossRef](#)] [[PubMed](#)]
8. Paixao, E.S.; Barreto, F.; Teixeira Mda, G.; Costa Mda, C.; Rodrigues, L.C. History, Epidemiology, and Clinical Manifestations of Zika: A Systematic Review. *Am. J. Public Health* **2016**, *106*, 606–612. [[CrossRef](#)]
9. Rubin, D.; Chan-Tack, K.; Farley, J.; Sherwat, A. FDA Approval of Remdesivir—A Step in the Right Direction. *N. Engl. J. Med.* **2020**, *383*, 2598–2600. [[CrossRef](#)]
10. Fischer, W.; Eron, J.J.; Holman, W.; Cohen, M.S.; Fang, L.; Szewczyk, L.J.; Sheahan, T.P.; Baric, R.; Mollan, K.R.; Wolfe, C.R.; et al. Molnupiravir, an Oral Antiviral Treatment for COVID-19. *medRxiv* **2021**. [[CrossRef](#)]
11. Owen, D.R.; Allerton, C.M.N.; Anderson, A.S.; Aschenbrenner, L.; Avery, M.; Berritt, S.; Boras, B.; Cardin, R.D.; Carlo, A.; Coffman, K.J.; et al. An oral SARS-CoV-2 M(pro) inhibitor clinical candidate for the treatment of COVID-19. *Science* **2021**, *374*, 1586–1593. [[CrossRef](#)] [[PubMed](#)]
12. Li, P.F.; Wang, Y.N.; Lavrijsen, M.; Lamers, M.M.; de Vries, A.C.; Rottier, R.J.; Bruno, M.J.; Peppelenbosch, M.P.; Haagmans, B.L.; Pan, Q.W. SARS-CoV-2 Omicron variant is highly sensitive to molnupiravir, nirmatrelvir, and the combination. *Cell Res.* **2022**, *32*, 322–324. [[CrossRef](#)] [[PubMed](#)]
13. Frazier, M.N.; Dillard, L.B.; Krahn, J.M.; Perera, L.; Williams, J.G.; Wilson, I.M.; Stewart, Z.D.; Pillon, M.C.; Deterding, L.J.; Borgnia, M.J.; et al. Characterization of SARS2 Nsp15 nuclease activity reveals it's mad about U. *Nucleic Acids Res.* **2021**, *49*, 10136–10149. [[CrossRef](#)] [[PubMed](#)]
14. Newman, J.A.; Douangamath, A.; Yadzani, S.; Yosaatmadja, Y.; Aimon, A.; Brandao-Neto, J.; Dunnett, L.; Gorrie-stone, T.; Skyner, R.; Fearon, D.; et al. Structure, mechanism and crystallographic fragment screening of the SARS-CoV-2 NSP13 helicase. *Nat. Commun.* **2021**, *12*, 4848. [[CrossRef](#)] [[PubMed](#)]
15. Cihlova, B.; Huskova, A.; Boserle, J.; Nencka, R.; Boura, E.; Silhan, J. High-Throughput Fluorescent Assay for Inhibitor Screening of Proteases from RNA Viruses. *Molecules* **2021**, *26*, 3792. [[CrossRef](#)] [[PubMed](#)]
16. Nencka, R.; Silhan, J.; Klima, M.; Otava, T.; Kocek, H.; Krafcikova, P.; Boura, E. Coronaviral RNA-methyltransferases: Function, structure and inhibition. *Nucleic Acids Res.* **2022**, *50*, 635–650. [[CrossRef](#)] [[PubMed](#)]
17. Konkolova, E.; Klima, M.; Nencka, R.; Boura, E. Structural analysis of the putative SARS-CoV-2 primase complex. *J. Struct. Biol.* **2020**, *211*, 107548. [[CrossRef](#)] [[PubMed](#)]
18. Otava, T.; Sala, M.; Li, F.; Fanfrlik, J.; Devkota, K.; Perveen, S.; Chau, I.; Pakarian, P.; Hobza, P.; Vedadi, M.; et al. The Structure-Based Design of SARS-CoV-2 nsp14 Methyltransferase Ligands Yields Nanomolar Inhibitors. *ACS Infect. Dis.* **2021**, *7*, 2214–2220. [[CrossRef](#)]
19. Devkota, K.; Schapira, M.; Perveen, S.; Khalili Yazdi, A.; Li, F.; Chau, I.; Ghiabi, P.; Hajian, T.; Loppnau, P.; Bolotokova, A.; et al. Probing the SAM Binding Site of SARS-CoV-2 Nsp14 In Vitro Using SAM Competitive Inhibitors Guides Developing Selective Bisubstrate Inhibitors. *SLAS Discov.* **2021**, *26*, 1200–1211. [[CrossRef](#)]
20. Perveen, S.; Khalili Yazdi, A.; Devkota, K.; Li, F.; Ghiabi, P.; Hajian, T.; Loppnau, P.; Bolotokova, A.; Vedadi, M. A High-Throughput RNA Displacement Assay for Screening SARS-CoV-2 nsp10-nsp16 Complex toward Developing Therapeutics for COVID-19. *SLAS Discov.* **2021**, *26*, 620–627. [[CrossRef](#)] [[PubMed](#)]
21. Dejmek, M.; Konkolova, E.; Eyer, L.; Strakova, P.; Svoboda, P.; Sala, M.; Krejcová, K.; Ruzek, D.; Boura, E.; Nencka, R. Non-Nucleotide RNA-Dependent RNA Polymerase Inhibitor That Blocks SARS-CoV-2 Replication. *Viruses* **2021**, *13*, 1585. [[CrossRef](#)] [[PubMed](#)]
22. Eggleton, J.S.; Nagalli, S. *Highly Active Antiretroviral Therapy (HAART)*; StatPearls: Treasure Island, FL, USA, 2022.
23. Tykvar, J.; Navratil, V.; Kugler, M.; Sacha, P.; Schimer, J.; Hlavackova, A.; Tenora, L.; Zemanova, J.; Dejmek, M.; Kral, V.; et al. Identification of Novel Carbonic Anhydrase IX Inhibitors Using High-Throughput Screening of Pooled Compound Libraries by DNA-Linked Inhibitor Antibody Assay (DIANA). *SLAS Discov.* **2020**, *25*, 1026–1037. [[CrossRef](#)] [[PubMed](#)]
24. Eyer, L.; Smidkova, M.; Nencka, R.; Neca, J.; Kastl, T.; Palus, M.; De Clercq, E.; Ruzek, D. Structure-activity relationships of nucleoside analogues for inhibition of tick-borne encephalitis virus. *Antivir. Res.* **2016**, *133*, 119–129. [[CrossRef](#)] [[PubMed](#)]
25. Eyer, L.; Valdes, J.J.; Gil, V.A.; Nencka, R.; Hrebabecky, H.; Sala, M.; Salat, J.; Cerny, J.; Palus, M.; De Clercq, E.; et al. Nucleoside inhibitors of tick-borne encephalitis virus. *Antimicrob. Agents Chemother.* **2015**, *59*, 5483–5493. [[CrossRef](#)] [[PubMed](#)]

26. Kozuch, O.; Mayer, V. Pig kidney epithelial (PS) cells: A perfect tool for the study of flaviviruses and some other arboviruses. *Acta Virol.* **1975**, *19*, 498.
27. Zeng, J.; Weissmann, F.; Bertolin, A.P.; Posse, V.; Canal, B.; Ulferts, R.; Wu, M.; Harvey, R.; Hussain, S.; Milligan, J.C.; et al. Identifying SARS-CoV-2 antiviral compounds by screening for small molecule inhibitors of nsp13 helicase. *Biochem. J.* **2021**, *478*, 2405–2423. [[CrossRef](#)] [[PubMed](#)]
28. Perez-Lemus, G.R.; Menendez, C.A.; Alvarado, W.; Bylehn, F.; de Pablo, J.J. Toward wide-spectrum antivirals against coronaviruses: Molecular characterization of SARS-CoV-2 NSP13 helicase inhibitors. *Sci. Adv.* **2022**, *8*, eabj4526. [[CrossRef](#)] [[PubMed](#)]
29. Rona, G.; Zeke, A.; Miwatani-Minter, B.; de Vries, M.; Kaur, R.; Schinlever, A.; Garcia, S.F.; Goldberg, H.V.; Wang, H.; Hinds, T.R.; et al. The NSP14/NSP10 RNA repair complex as a Pan-coronavirus therapeutic target. *Cell Death Differ.* **2022**, *29*, 285–292. [[CrossRef](#)]
30. Canal, B.; Fujisawa, R.; McClure, A.W.; Deegan, T.D.; Wu, M.; Ulferts, R.; Weissmann, F.; Drury, L.S.; Bertolin, A.P.; Zeng, J.K.; et al. Identifying SARS-CoV-2 antiviral compounds by screening for small molecule inhibitors of nsp15 endoribonuclease. *Biochem. J.* **2021**, *478*, 2465–2479. [[CrossRef](#)]
31. Khalili Yazdi, A.; Li, F.; Devkota, K.; Perveen, S.; Ghiabi, P.; Hajian, T.; Bolotokova, A.; Vedadi, M. A High-Throughput Radioactivity-Based Assay for Screening SARS-CoV-2 nsp10-nsp16 Complex. *SLAS Discov.* **2021**, *26*, 757–765. [[CrossRef](#)]
32. Warren, T.K.; Jordan, R.; Lo, M.K.; Ray, A.S.; Mackman, R.L.; Soloveva, V.; Siegel, D.; Perron, M.; Bannister, R.; Hui, H.C.; et al. Therapeutic efficacy of the small molecule GS-5734 against Ebola virus in rhesus monkeys. *Nature* **2016**, *531*, 381–385. [[CrossRef](#)] [[PubMed](#)]
33. Gordon, C.J.; Tchesnokov, E.P.; Feng, J.Y.; Porter, D.P.; Gotte, M. The antiviral compound remdesivir potently inhibits RNA-dependent RNA polymerase from Middle East respiratory syndrome coronavirus. *J. Biol. Chem.* **2020**, *295*, 4773–4779. [[CrossRef](#)] [[PubMed](#)]
34. Gordon, C.J.; Tchesnokov, E.P.; Woolner, E.; Perry, J.K.; Feng, J.Y.; Porter, D.P.; Gotte, M. Remdesivir is a direct-acting antiviral that inhibits RNA-dependent RNA polymerase from severe acute respiratory syndrome coronavirus 2 with high potency. *J. Biol. Chem.* **2020**, *295*, 6785–6797. [[CrossRef](#)] [[PubMed](#)]
35. Konkolova, E.; Dejmek, M.; Hrebabecky, H.; Sala, M.; Boserle, J.; Nencka, R.; Boura, E. Remdesivir triphosphate can efficiently inhibit the RNA-dependent RNA polymerase from various flaviviruses. *Antivir. Res.* **2020**, *182*, 104899. [[CrossRef](#)] [[PubMed](#)]
36. Anderson, J.P.; Daifuku, R.; Loeb, L.A. Viral error catastrophe by mutagenic nucleosides. *Annu. Rev. Microbiol.* **2004**, *58*, 183–205. [[CrossRef](#)] [[PubMed](#)]
37. Seley-Radtke, K.L.; Yates, M.K. The evolution of nucleoside analogue antivirals: A review for chemists and non-chemists. Part 1: Early structural modifications to the nucleoside scaffold. *Antivir. Res.* **2018**, *154*, 66–86. [[CrossRef](#)] [[PubMed](#)]
38. Eastman, R.T.; Roth, J.S.; Brimacombe, K.R.; Simeonov, A.; Shen, M.; Patnaik, S.; Hall, M.D. Remdesivir: A Review of Its Discovery and Development Leading to Emergency Use Authorization for Treatment of COVID-19. *ACS Central Sci.* **2020**, *6*, 672–683. [[CrossRef](#)]
39. De Clercq, E.; Neyts, J. Antiviral agents acting as DNA or RNA chain terminators. In *The Handbook of Experimental Pharmacology*; Springer: Berlin/Heidelberg, Germany, 2009; pp. 53–84.
40. Menendez-Arias, L.; Andino, R. Viral polymerases. *Virus Res.* **2017**, *234*, 1–3. [[CrossRef](#)]
41. Dubankova, A.; Boura, E. Structure of the yellow fever NS5 protein reveals conserved drug targets shared among flaviviruses. *Antivir. Res.* **2019**, *169*, 104536. [[CrossRef](#)]
42. Dubankova, A.; Humpolickova, J.; Klima, M.; Boura, E. Negative charge and membrane-tethered viral 3B cooperate to recruit viral RNA dependent RNA polymerase 3D (pol). *Sci. Rep.* **2017**, *7*, 17309. [[CrossRef](#)]

Brief Report

Non-Nucleotide RNA-Dependent RNA Polymerase Inhibitor That Blocks SARS-CoV-2 Replication

Milan Dejmeck^{1,†}, Eva Konkolová^{1,†} , Luděk Eyer^{2,3}, Petra Straková^{2,3} , Pavel Svoboda^{2,3,4} , Michal Šála¹, Kateřina Krejčová¹, Daniel Růžek^{2,3,*} , Evzen Boura^{1,*}  and Radim Nencka^{1,*}

- ¹ Institute of Organic Chemistry and Biochemistry, Czech Academy of Sciences, Flemingovo náměstí 542/2, 160 00 Praha, Czech Republic; dejmek@uochb.cas.cz (M.D.); eva.konkolova@uochb.cas.cz (E.K.); sala@uochb.cas.cz (M.Š.); katerina.krejцова@uochb.cas.cz (K.K.)
- ² Veterinary Research Institute, Emerging Viral Diseases, Hudcova 296/70, 621 00 Brno, Czech Republic; eyer@vri.cz (L.E.); strakova.p@centrum.cz (P.S.); svoboda@vri.cz (P.S.)
- ³ Institute of Parasitology, Biology Centre of the Czech Academy of Sciences, Branišovská 1160/31, 370 05 České Budějovice, Czech Republic
- ⁴ Department of Pharmacology and Pharmacy, Faculty of Veterinary Medicine, University of Veterinary Sciences Brno, Palackého tř. 1946/1, 612 42 Brno, Czech Republic
- * Correspondence: ruzeckd@paru.cas.cz (D.R.); boura@uochb.cas.cz (E.B.); nencka@uochb.cas.cz (R.N.)
- † These authors contributed equally.

Abstract: SARS-CoV-2 has caused an extensive pandemic of COVID-19 all around the world. Key viral enzymes are suitable molecular targets for the development of new antivirals against SARS-CoV-2 which could represent potential treatments of the corresponding disease. With respect to its essential role in the replication of viral RNA, RNA-dependent RNA polymerase (RdRp) is one of the prime targets. HeE1-2Tyr and related derivatives were originally discovered as inhibitors of the RdRp of flaviviruses. Here, we present that these pyridobenzothiazole derivatives also significantly inhibit SARS-CoV-2 RdRp, as demonstrated using both polymerase- and cell-based antiviral assays.

Keywords: non-nucleotide inhibitor; RNA-dependent RNA polymerase; SAR-CoV-2; COVID-19; antiviral agents



Citation: Dejmeck, M.; Konkolová, E.; Eyer, L.; Straková, P.; Svoboda, P.; Šála, M.; Krejčová, K.; Růžek, D.; Boura, E.; Nencka, R. Non-Nucleotide RNA-Dependent RNA Polymerase Inhibitor That Blocks SARS-CoV-2 Replication. *Viruses* **2021**, *13*, 1585. <https://doi.org/10.3390/v13081585>

Academic Editor: Tomas Ruml

Received: 4 July 2021

Accepted: 9 August 2021

Published: 11 August 2021

Publisher's Note: MDPI stays neutral with regard to jurisdictional claims in published maps and institutional affiliations.



Copyright: © 2021 by the authors. Licensee MDPI, Basel, Switzerland. This article is an open access article distributed under the terms and conditions of the Creative Commons Attribution (CC BY) license (<https://creativecommons.org/licenses/by/4.0/>).

1. Introduction

Coronaviruses are positive-sense RNA viruses that cause numerous important human and animal diseases. These viruses are classified into four genera including *Alphacoronavirus* and *Deltacoronavirus* [1]. While infectivity of gammacoronaviruses and deltacoronaviruses is limited to animals, mostly birds [2], alphacoronaviruses and betacoronaviruses comprise numerous mammalian and human pathogens [3,4]. Important alphacoronaviruses are Human coronaviruses (HCoV) 229E and NL63, as well as Feline coronavirus (FIPV) and Porcine epidemic diarrhea virus (PEDV). Betacoronaviruses include the rest of human coronaviruses (HCoV-OC43, HCoV-HKU1, Severe acute respiratory syndrome coronavirus (SARS-CoV and SARS-CoV-2), Middle East respiratory syndrome coronavirus (MERS-CoV)) and a number of other animal pathogens. While coronaviruses that have persisted in the human population for a long time (HCoV-229E, HCoV-NL63, HCoV-OC43, and HCoV-HKU1) cause milder upper respiratory illnesses, SARS-CoV, SARS-CoV-2, and MERS-CoV are highly pathogenic viruses causing severe lower respiratory illness that can progress to life-threatening pneumonia with significant mortality rates [5,6].

SARS-CoV-2 is responsible for the largest pandemic of acute viral disease that our world has faced since the Spanish flu [7]. Although the mortality of this disease is not as high as in that of SARS-CoV or MERS-CoV infections, the disease caused by this virus (COVID-19) has significantly changed the world in which we live [8]. In particular, mortality in older age groups is alarming [9], and although we already have vaccines [10] as well as several drugs based on both monoclonal antibodies and small molecules, the

effectiveness of these treatments is limited by several factors, including the high mutation rate of this virus [11]. Therefore, it is essential that pharmaceutical research focuses on the widest possible range of molecular targets and that we seek to find substances that we can use in combination with already known drugs to reduce the risk of the development of resistance. One of the main molecular targets in viruses is their polymerase, which is responsible for the replication of their genetic information. The example of HIV has shown that a combination of nucleoside and non-nucleoside reverse transcriptase inhibitors can lead to a very effective therapy for this serious disease [12]. Therapies for diseases caused by other viral pathogens, such as hepatitis B and C viruses (HBV and HCV), also rely largely on polymerase inhibitors [13,14]. Therefore, it is not surprising that the main approach for the development of new antivirals against SARS-CoV-2, as well as other coronaviruses, is based on targeting the RNA-dependent RNA polymerase (RdRp) as a central replication enzyme of the virus [15]. RdRp is part of the large coronaviral replication complex that also includes RNA methyltransferases, helicase, nsp9, and probably the N protein [16]. The coronaviral RdRp is a highly conserved heterotrimeric protein complex that is composed of two accessory but essential proteins (nsp7 and nsp8) and the catalytic subunit nsp12 [17]. While the first nucleoside-based RdRp inhibitor has already been approved by the relevant authorities around the world [18], information on potent non-nucleoside inhibitors of this key enzyme is rather scarce. Recently, suramin was reported as a potent non-nucleoside inhibitor of SARS-CoV-2 RdRp, and its mode of action was supported by a cryo-EM structure [19]. Also, several natural products including corilagin [20] and lycorine [21] exert inhibition potency against SARS-CoV-2 RdRp. Although efforts have been made to identify new non-nucleoside inhibitors of this enzyme by *in silico* methods since the beginning of the pandemic, the results of these studies are unfortunately rarely supported by experimental data [22].

HeE1-2Tyr (compound **16**) was initially identified by Tarantino et al. as a potent inhibitor of RdRp from Dengue virus (DENV), West Nile virus, and Yellow fever virus, all members of genus *Flavivirus* [23–26]. This compound was crystallized in complex with the RdRp from DENV 3. It was shown that the drug binds on the thumb side of the RNA-binding site, with significant movement of the priming loop. The authors also suggested that there is another possible binding site of the compound that is hidden by the priming loop. This hypothesis has been supported by point mutation experiments [23].

Here, we report on the identification of HeE1-2Tyr (**16**) and its derivatives as potential inhibitors of SARS-CoV-2 RdRp. The drugs exert activity not only against SARS-CoV-2 but also against FIPV. Our study started with the screening of our small collection of various nucleoside triphosphate and non-nucleoside inhibitors of polymerases from different viruses against SARS-CoV-2 RdRp and, in parallel, a screening of our complementary nucleoside, nucleotide prodrug, and non-nucleoside derivative library against SARS-CoV-2 in cell-based assays. To our surprise, we identified HeE1-2Tyr (**16**), which we prepared as a standard for our studies on flavivirus RdRps, as an effective inhibitor of SARS-CoV-2 RdRp that also exerted significant activity against the virus in cell cultures.

2. Material and Methods

2.1. Protein Expression and Purification

SARS-CoV-2 nsp7 (GeneBank: YP_009725303), nsp8 (GeneBank: YP_009725304,) and nsp12 (GeneBank: YP_009725307) genes were commercially synthesized as codon-optimized for *E. coli* (Invitrogen). The gene for nsp7 was cloned into a modified pRSF-Duet vector containing an N-terminal 6×His tag, followed by a GB1 solubility tag, a 10×Asp spacer sequence, and a tobacco etch virus (TEV) protease cleavage site in cloning site 1. The nsp8 gene was subsequently cloned into cloning site 2 without any tag. The gene for nsp12 was cloned into the pAceBac vector with cleavable 6×His on the C-terminus. The nsp7/nsp8 protein complex was expressed and purified as described previously for truncated nsp7/nsp8 in *E. coli* [27]. The SARS-CoV-2 nsp12 plasmid was used to prepare recombinant baculovirus Sf9 insect cells that were infected at $1-2 \times 10^6$ cell/mL with the

tertiary recombinant baculovirus. After 68 h, the cells were collected by centrifugation, resuspended in lysis buffer (50 mM HEPES 7.4, 300 mM NaCl, 20 mM imidazole, 3 mM MgCl₂, 10% (v/v) glycerol, and 3 mM β-mercaptoethanol) and sonicated (Q700 Sonicator, QSonica). The lysate was subsequently cleared by centrifugation, and the supernatant was incubated with Ni-NTA agarose (Thermo Scientific) and washed with lysis buffer; finally, the protein was eluted with lysis buffer supplemented with 300 mM imidazole. Nsp12 protein was further purified by size-exclusion chromatography using Superdex 200 16/600 (GE Healthcare) in size-exclusion buffer (20 mM HEPES 7.4, 300 mM NaCl, 1 mM MgCl₂, 10% (v/v) glycerol, and 3 mM β-mercaptoethanol). Fractions containing the pure nsp12 protein were concentrated to 5 mg/mL, flash-frozen, and stored at −80 °C until needed.

2.2. Fluorescence-Based Primer Extension Polymerase Assay

The polymerase activity was determined in a primer extension reaction using a fluorescently labeled primer (HEX-5'-AGAACCUGUUGAACAAAAGC-3') and an RNA template (5'-AUUAUUAGCUGCUUUUGUUCAACAGGUUCU-3'). The polymerase activity assay was performed in a total volume of 10 μL containing the reaction buffer (10 mM Tris pH 8.0, 2 mM MgCl₂, 10 mM KCl, 1 mM β-mercaptoethanol), 10 μM NTPs, 0.5 μM T/P complex, 1 μM nsp12 polymerase, and 3 μM nsp7/nsp8 complex. The reactions were incubated for 1 h with various concentrations of the inhibitors tested at 30 °C and stopped by adding 20 μL of the stop buffer (80% formamide, 50 mM EDTA). The samples were denatured at 95 °C for 10 min, and primer extension products were separated on a 20% denaturing polyacrylamide gel (8 M urea, 1× TBE, 20% acrylamide (19:1)) and scanned on a Typhoon 5 Biomolecular Imager (GE Healthcare).

2.3. Radioactivity-Based Primer Extension Polymerase Assay

The assay was performed as above, except that the reaction mixture contained 0.5 μM T/P complex (P-5'-AGAACCUGUUGAACAAAAGC-3', T-5'-U25-GCUUUUGUUCAACAGGUUCU-3') and 0.01 μCi/μL [α -³²P]-ATP. After incubation, 5 μL of the reaction mixtures was spotted on an anion-exchange cellulose filter paper (Whatman™ Grade DE81 DEAE cellulose paper; GE Healthcare) in triplicates. The Whatman filter was then dried, subsequently washed with 0.125 mM Na₂HPO₄, water, and ethanol, and dried again. The dry filter paper was then analyzed using phosphorimaging, the plate was scanned on Amersham Typhoon 5 Biomolecular Imager (GE Healthcare), products were quantified with Image Studio Lite (LI-COR), and the data were processed using GraphPad version 6 (GraphPad Prism version 6, GraphPad Software, San Diego, CA, USA).

2.4. Viruses and Cell Lines

Two representatives of the *Coronaviridae* family, i.e., SARS-CoV-2 (strain SARS-CoV-2/human/Czech Republic/951/2020 isolated from a clinical sample at the National Institute of Health, Prague, Czech Republic, and kindly provided by Dr. Jan Weber, Institute of Organic Chemistry and Biochemistry, Prague, Czech Republic) and feline infectious peritonitis virus (FIPV, ATCC VR990, a pathogen of domestic cats and other felines), were used for our antiviral cell-based studies. The experiments with the live coronaviruses were performed in our BSL3 facility.

Vero cells (ATCC CCL-81, African Green Monkey, adult kidney, epithelial) and Vero E6 cells (ATCC CRL-1586) were cultured in Dulbecco's modified Eagle's medium (DMEM) supplemented with 10% newborn calf serum, 100 U/mL penicillin, 100 μg/mL streptomycin, and 1% glutamine (Sigma-Aldrich, Prague, Czech Republic) at 37 °C and 5% CO₂. Colorectal adenocarcinoma cells (CaCo-2, ATCC HTB-37) were grown in DMEM medium, containing, 20% newborn calf serum with 100 U/mL penicillin, 100 μg/mL streptomycin, and 1% L-glutamine (Sigma-Aldrich, Prague, Czech Republic) at 37 °C and 5% CO₂. *Felis catus* kidney cortex cells (CRFK, ATCC CCL-94) were grown in DMEM supplemented with 10% newborn calf serum, 100 U/mL penicillin, 100 μg/mL streptomycin, and 1% glutamine (Sigma-Aldrich, Prague, Czech Republic) at 37 °C and 5% CO₂. Vero (ATCC

CCL-81), CaCo-2 (ATCC HTB-37), and CRFK (ATCC CCL-94) cells were used for antiviral and cytotoxicity assays, and Vero E6 cells (ATCC CRL-1586) were used to perform plaque assays.

2.5. Cytotoxicity Studies

Vero (ATCC CCL-81), CaCo-2 (ATCC HTB-37), and CRFK (ATCC CCL-94) cells were seeded into each well of 96-well microtiter plates (approx. 2×10^4 cells per a well) and were incubated for 24 h at 37 °C and 5% CO₂. Cell monolayers in 96-well plates were treated with the compounds remdesivir, HeE1-2Tyr (**16**), **17**, or **18** at the concentration of 50 µM or with 1% DMSO (*w/w*) (for the initial screening; Vero and CRFK cell lines) or with the compounds remdesivir, HeE1-2Tyr (**16**) and **17** in concentration ranges from 0 to 50 µM (for dose–response studies; 2-fold dilutions, three wells per concentration; Vero, CaCo-2, and CRFK cell lines) and cultured for 48 h. The cytotoxic activity of the compounds was determined in terms of cell viability using a Cell Counting Kit-8 (Dojindo Molecular Technologies, Munich, Germany) following the manufacturer’s instructions. The assay is based on the quantitative reduction of WST-8 tetrazolium salt to yellow formazan by cellular dehydrogenases. Cell viability was estimated as the percentage of colorimetric absorbance at 450 nm of the compound-treated cells relative to the absorbance of mock-treated cells. The concentration of compound that reduced cell viability by 50% was considered the 50% cytotoxic concentration (CC₅₀).

2.6. Antiviral Efficacy of the Studied Compounds in Cell-Based Assays

To study the antiviral effects of compounds HeE1-2Tyr (**16**), **17**, and **18**, we used a viral titer reduction assay. Vero (ATCC CCL-81), CaCo-2 (ATCC HTB-37), and CRFK (ATCC CCL-94) cells were seeded into each well of 96-well microtiter plates (approx. 2×10^4 cells per a well) and incubated for 24 h at 37 °C and 5% CO₂. Then, the medium was aspirated, replaced with 200 µL of fresh medium containing compounds HeE1-2Tyr (**16**), **17**, or **18** at the concentration of 50 µM (for the initial screening) or with compounds HeE1-2Tyr (**16**) or **17** in the concentration range of 0 to 50 µM (for dose–response antiviral studies; 2-fold dilution, three wells per compound). The treated cells were simultaneously inoculated with SARS-CoV-2 (for Vero and CaCo-2 cells) or FIPV (for CRFK cells) at an MOI of 0.1 and incubated for an additional 48 h. Virus-infected cells treated with remdesivir (at the same concentrations) or DMSO (1% *w/w*) were used as positive and negative controls, respectively. Viral titers were determined from the collected supernatant media by a plaque assay and used to construct dose–response curves (dependence of the viral titers [PFU/mL] on the compound concentration [µM]) and inhibition curves (dependence of the inhibition percentage on the compound concentration [µM]) and for calculation of the 50% effective concentrations (EC₅₀; the concentration of compound required to inhibit the viral titer by 50% compared to the control value).

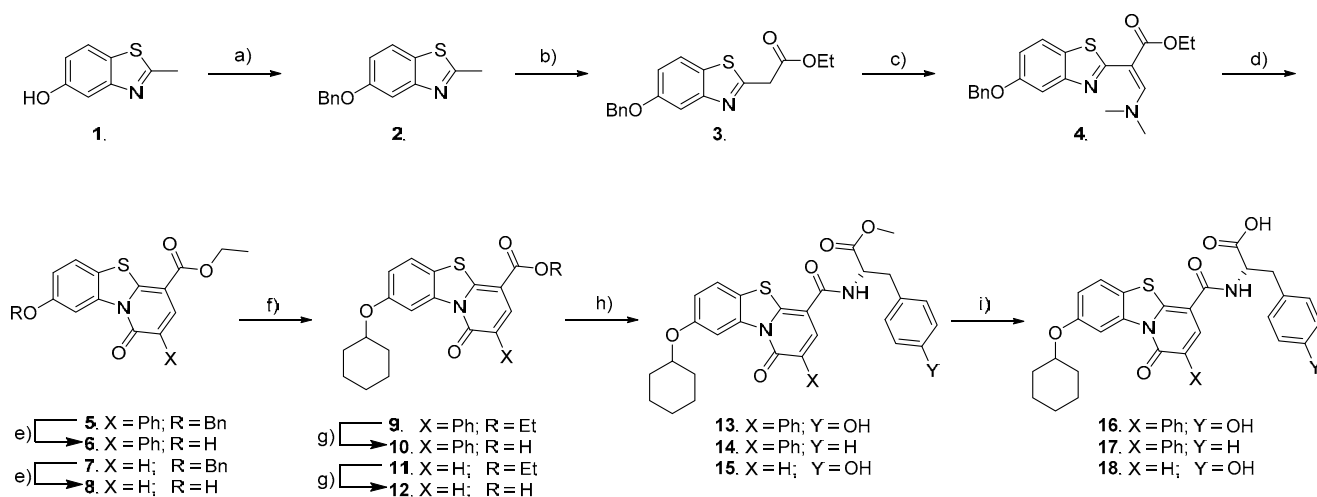
2.7. Plaque Assay

Plaque assays were performed using Vero E6 cells (ATCC CRL-1586) as described previously [28,29]. Briefly, 10-fold dilutions of SARS-CoV-2 or FIPV were prepared in 24-well tissue culture plates, and the cells were added to each well ($0.6\text{--}1.5 \times 10^5$ cells per well). After a 4 h incubation at 37 °C and 5% CO₂, the suspension was overlaid with 1.5% (*w/v*) carboxymethylcellulose in a two-fold concentrated DMEM medium. Following a 5-day incubation at 37 °C and 5% CO₂, the infected plates were washed with phosphate-buffered saline, and the cell monolayers were stained with naphthalene black. The virus titer was expressed as plaque-forming units (PFU)/mL.

3. Results and Discussion

Although the synthesis of HeE1-2Tyr (**16**) and its derivatives has been well documented by work of Tarantino et al., we devised a modified approach in order to have easier access to a broader range of substituents in the 8-OH position of the benzothiazolo

pyridinone (Scheme 1). To achieve this goal, we decided to protect the 5-OH group of the benzothiazole throughout the stages of central core construction. This way, the alkyl substituent could be introduced by the Mitsunobu reaction just prior to the introduction of the amino acid residue. After initial experiments with a TBDMS, which proved difficult to install and not very stable, we decided to use benzyl for this purpose. The 2-methyl group was then converted to an ethyl acetate by a reaction of an appropriate salt with ethyl carbonate. By using LiHMDS we achieved a very good yield in a short reaction time compared to methods using sodium hydride. A dimethylaminomethylene group was then introduced by the Vilsmeier–Haack reaction, and the pyridinone ring was subsequently closed by heating compound **4** with a neat acyl anhydride—acetic or phenylacetic. The benzyl group was comfortably cleaved using methansulfonic acid, providing compounds suitable for the Mitsunobu reaction, which afforded products **9** and **11**, respectively. Workup of compounds **5–8** proved to be very easy, as these compounds are very poorly soluble, and reaction conversions are high. The rest of the synthesis was performed in a similar way as reported by Tarantino et al. An ethyl ester function was saponified, and *L*-Tyrosine and *L*-Phenylalanine methylesters, respectively, were connected to the free carboxylic acid by EDC-HOBt peptide coupling. This set of conditions proved to provide the best yields in the short optimization we performed. This procedure gave HeE1-2Tyr (**16**), as well two novel analogues **17** and **18**, in excellent yields. Detailed descriptions of the synthesis is provided in the Supplementary File.



a) BnOH, PPh₃, DIAD, dioxane, RT, 48 h, 96 %; b) LiHMDS, (EtO)₂CO, THF, -78°C to RT, 30 min, 82 %; c) POCl₃, DMF, 90°C, 30 min, 81 %; d) Respective anhydride, 100°C, 5 h, 99 % for **5**, 94 % for **7**; e) CH₃SO₃H, DCM, RT, 3 h, 76 % for **6**, 82 % for **8**; f) Cyclohexanol, PPh₃, DIAD, dioxane, RT, 48 h, 89 % for **9**, 87 % for **11**; g) NaOH, MeOH-H₂O, reflux, 3 h, 84 % for **10**, 94 % for **12**; h) TyrOMe.HCl or PheOMe.HCl, EDC, HOBt, TEA, DCM, DMF, RT, 12h, 92 % for **13**, 91 % for **14**, 92 % for **15**; i) LiOH, THF-H₂O, 30 min, 88 % for **16**; 90 % for **17**, 88 % for **18**.

Scheme 1. Synthetic pathway to HeE1-2Tyr (**16**) and its derivatives.

Our *in vitro* RdRp assay confirmed the inhibitory effect of compounds HeE1-2Tyr (**16**), **17**, and **18** against SARS-CoV-2 polymerase. The compounds were initially tested at one concentration (100 μ M), which confirmed that compounds HeE1-2Tyr (**16**), **17**, and **18** inhibit SARS-CoV-2 RdRp. Subsequently, the RdRp assay was used to determine the IC₅₀ values. Surprisingly, compound HeE1-2Tyr (**16**) was found to be the best inhibitor, with IC₅₀ of 27.6 \pm 2.1 μ M, while the inhibition effect of compound **18** was rather weak (IC₅₀ = 85.5 \pm 2.0 μ M, Figure 1).

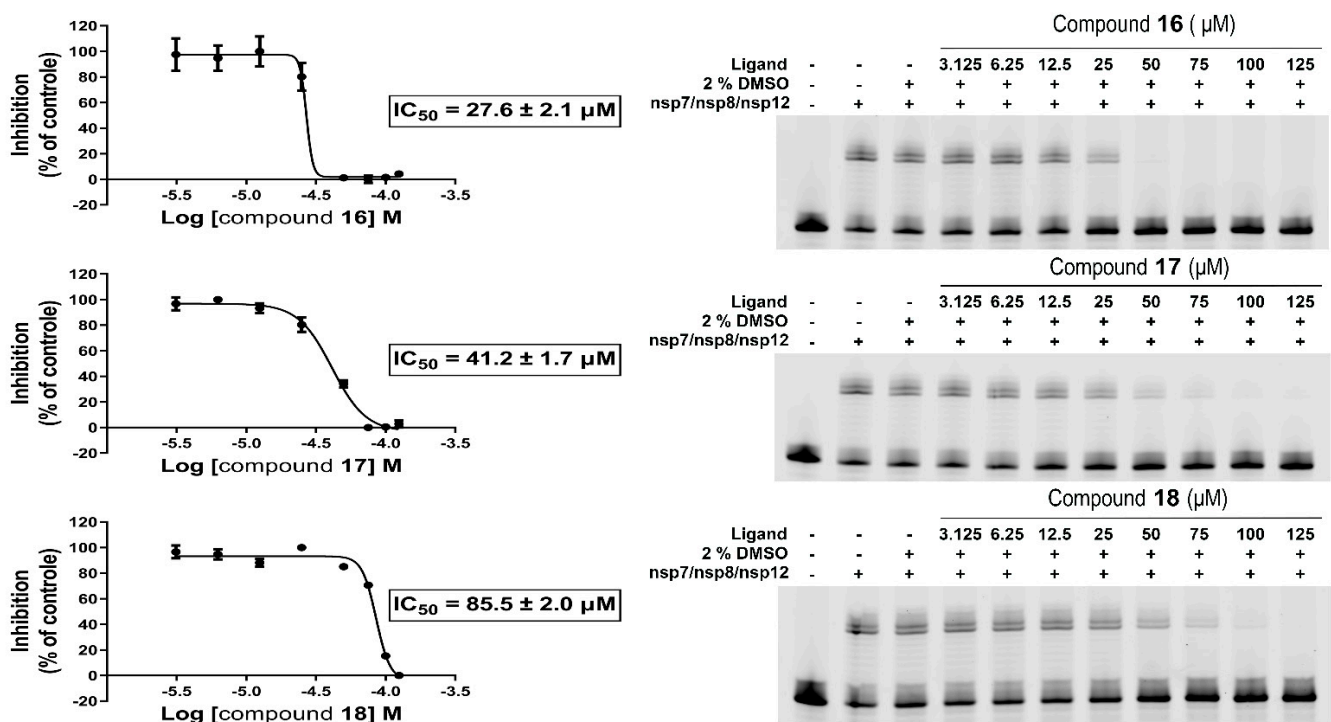


Figure 1. Inhibitions of SARS-CoV-2 RdRp by compounds 16, 17, and 18. (left) IC_{50} values were established for each tested compound using a radioactive primer extension assay. Error bars represent the standard error of the mean ($n = 3$). (right) A fluorescence-based primer extension assay. Formation of the 40-nt product decreases with increasing concentration of the compound.

Based on our findings that the compounds showed inhibitory activities in SARS-CoV-2 RdRp assays, we next evaluated cytotoxicity and antiviral activity of HeE1-2Tyr (16), 17, and 18 in cell-based systems. The compounds were initially tested at one single concentration of 50 μM against SARS-CoV-2 and FIPV in Vero and CRFK cells, respectively. This initial screening revealed that all compounds at 50 μM were not cytotoxic for both cell lines (Figure 2A). Moreover, compounds HeE1-2Tyr (16) and 17 were found to completely inhibit the replication of both coronaviruses (Figure 2B). Surprisingly, compound 18 was found to be inactive against SARS-CoV-2 and FIPV in both cell-based systems tested ($\text{EC}_{50} > 50 \mu\text{M}$) (Figure 2B). The inactivity could be explained by its poor cellular uptake or extensive degradation by cellular catabolic enzymes. Therefore, compound 18 was excluded from further testing.

The cytotoxicity of compounds HeE1-2Tyr (16) and 17 was studied in detail using Vero, CaCo-2, and CRFK cells in a concentration range from 0 to 50 μM . Both compounds showed good cytotoxicity profiles for the studied cell lines and were characterized by CC_{50} values $> 50 \mu\text{M}$ (Figure 2C–E; Tables 1–3). Interestingly, compound 17 caused a moderate increase in cell viability in Vero and CaCo-2 cells (to approx. 125% of untreated cells) but was slightly cytotoxic for CRFK cells (cell viability of approx. 60%) at the highest concentration tested (50 μM) (Figure 2C–E). The observed changes in the viability of cells treated by compound 17, however, did not affect the CC_{50} values, which were calculated to be $> 50 \mu\text{M}$ for all the cell lines tested.

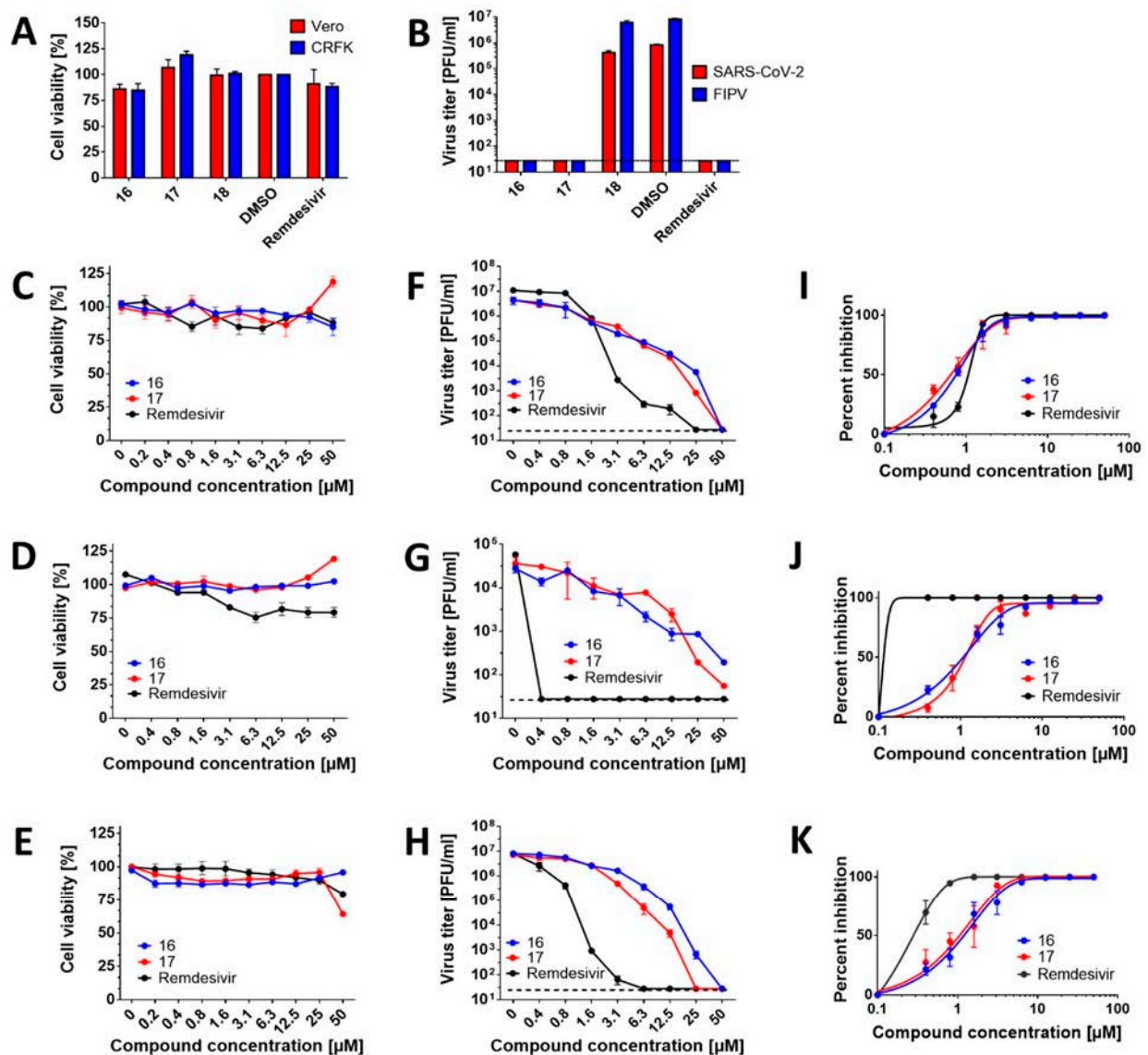


Figure 2. Antiviral efficacy and cytotoxicity of the studied RdRp inhibitors in cell-based assays. **(A)** Cytotoxicity of the indicated compounds in Vero and CRFK cells. The cell monolayers were treated with the compounds (50 μ M) and incubated for 48 h. The cell-mediated conversion of tetrazolium salt WST-8 to formazan was monitored by absorbance measurement (450 nm). Cytotoxicity was expressed in terms of cell viability percentage. **(B)** Anti-SARS-CoV-2 and anti-FIPV efficacies of the indicated compounds in Vero and CRFK cells, respectively. The cell monolayers were treated with the compounds (50 μ M), infected with the respective virus at a MOI of 0.1, and incubated for 48 h. The supernatant media were collected, and viral titers were determined by plaque assays. **(C–E)** Dose-dependent cytotoxic effects of the compounds in Vero (C), CaCo-2 (D), and CRFK (E) cells. The cell monolayers were treated with the compounds in the concentration range from 0 to 50 μ M and incubated for 48 h. Cytotoxicity was determined, as described for (A). **(F,G)** Dose-dependent anti-SARS-CoV-2 activity of the compounds in Vero (F) and CaCo-2 (G) cells. The cell monolayers were treated with the compounds in the concentration range 0–50 μ M and simultaneously infected with SARS-CoV-2 at a MOI of 0.1. The infected cells were incubated with the compounds for 48 h p.i., and viral titers were determined using the plaque assay. **(H)** Dose-dependent anti-FIPV activity of the compounds in CRFK cells. The protocol was the same as described for (F,G). **(I–K)** Inhibitory curves for the indicated compounds in Vero (I), CaCo-2 (J), and CRFK (K) cells. The mean titers from three biological replicates are shown, and error bars indicate standard errors of the mean ($n = 3$). The horizontal dashed line indicates the minimum detectable threshold of $1.44 \log_{10}$ PFU/mL.

Table 1. Anti-SARS-CoV-2 activity and cytotoxicity of the tested compounds in Vero cells.

Compound	EC ₅₀ (μM) (95% CI) ^{a,b}	CC ₅₀ (μM) ^a	SI ^c
16	0.6535 (0.4376–0.9760)	>50	>76.5
17	0.5273 (0.4423–0.6286)	>50	>94.8
18	>50	>50	>1
Remdesivir	0.9012 (0.7997–1.016)	>50	>55.5

[^a] Determined from three independent experiments. [^b] Expressed as a 50% reduction in viral titers and calculated as inflection points of sigmoidal inhibitory curves which were obtained by a nonlinear fit of transformed inhibitor concentrations versus normalized response using GraphPad Prism 7.04 (GraphPad Software, Inc., USA). [^c] CC₅₀/EC₅₀.

Table 2. Anti-SARS-CoV-2 activity and cytotoxicity of the tested compounds in CaCo-2 cells.

Compound	EC ₅₀ (μM) (95% CI) ^{a,b}	CC ₅₀ (μM) ^a	SI ^c
16	0.9493 (0.5131–1.756)	>50	>52.7
17	0.9959 (0.5427–1.827)	>50	>50.2
18	>25	>50	>2
Remdesivir	<0.3	>50	>216.9

For [^{a–c}] see Table 1.

Table 3. Anti-FIPV activity and cytotoxicity of the tested compounds in CRFK cells.

Compound	EC ₅₀ (μM) (95% CI) ^{a,b}	CC ₅₀ (μM) ^a	SI ^c
16	1.062 (0.8188–1.377)	>50	>47.1
17	0.9989 (0.8274–1.206)	>50	>50.1
18	>50	>50	>1
Remdesivir	0.2230 (0.1694–0.2937)	>50	>224.2

For [^{a–c}] see Table 1.

We further evaluated the dose-dependent, anti-coronaviral activities of compounds HeE1-2Tyr (**16**) and **17**. Anti-SARS-CoV-2 potency of both compounds in Vero cells reached sub-micro molar concentrations, with EC₅₀ values of 653.5 nM (for **16**) and 527.3 nM (for **17**). These values were similar or even better than those of remdesivir (EC₅₀ = 901.2 nM) (Figure 2F,I, Table 1). Although the EC₅₀ values for HeE1-2Tyr (**16**) and **17** were slightly lower compared with those for remdesivir, the growth inhibition curve slopes for remdesivir were substantially steeper than those for HeE1-2Tyr (**16**) and **17**, indicating that remdesivir had a superior inhibitory profile over HeE1-2Tyr (**16**) and **17**. In CaCo-2 cells, compounds HeE1-2Tyr (**16**) and **17** showed EC₅₀ values close to 1 μM (949.3 and 995.9 nM, respectively) and had somewhat lower antiviral potencies compared with remdesivir (EC₅₀ < 300 nM) (Figure 2G,J, Table 2). Because of their low cytotoxicity, both compounds were characterized by relatively high selectivity indexes (>70 in Vero cells and >50 in CaCo-2 cells) (Tables 1 and 2). In vitro replication of FIPV, another member of the *Coronaviridae* family used in our antiviral study, was also strongly suppressed with compounds HeE1-2Tyr (**16**) and **17**. The anti-FIPV activity of these compounds was characterized by EC₅₀ values of about 1 μM, was approx. 5-fold lower compared with remdesivir (EC₅₀ = 223 nM), and showed selectivity indexes exceeding 40 (Figure 2H,K, Table 3).

In conclusion, HeE1-2Tyr (**16**) and its derivatives are potent non-nucleoside inhibitors of coronaviral RdRp that probably act as competitive inhibitors interacting via RNA template tunnel in contrast to chain terminator inhibitors such as remdesivir. These compounds represent suitable candidates for the preparation of clinically usable compounds against SAR-CoV-2 and other coronaviruses, as we have shown with an FIPV example. Compounds HeE1-2Tyr (**16**) and **17** showed significant activity against these coronaviruses in cell cultures. We have also unveiled that one of the mechanisms of action of these compounds is the inhibition of RdRp SARS-CoV-2. This key virus enzyme was inhibited by these compounds, with HeE1-2Tyr (**16**) and **17** showing significantly higher activity compared to **18**. This suggests that the phenyl substituent on the pyridinone portion of the

backbone may significantly affect the activity of these derivatives, both in the polymerase assay and in the cell lines. Clearly, further chemical modification and optimization to enhance potency and physicochemical properties will be required for the eventual use of this type of compounds in clinical practice; however, the derivatives of HeE1-2Tyr (**16**) may be one of the rare non-nucleoside inhibitors of coronavirus replication that interfere with RdRp, a key enzyme of these viruses. Although remdesivir is the only RdRp-targeting inhibitor approved by the FDA and EMA for clinical use, some studies suggest that its in vivo effects are suboptimal. Experience with other viral diseases suggests that combinations with other polymerase inhibitors can provide a significant synergistic effect and prevent the evolution of drug-resistant virus mutants; therefore, the introduction of new types of inhibitors may have a significant impact on improving the clinical outcome for patients.

Supplementary Materials: The following are available online at <https://www.mdpi.com/article/10.3390/v13081585/s1>, Supplementary File S1: chemical synthesis of the compounds and NMR spectra.

Author Contributions: M.D. and E.K. contributed equally; conceptualization, M.D., D.R., E.B. and R.N.; synthesis M.D. and M.Š.; methodology, E.K., L.E., P.S. (Petra Straková), P.S. (Pavel Svoboda), K.K.; writing—original draft preparation, M.D., E.K., L.E., D.R., E.B. and R.N.; supervision and funding acquisition, L.E., D.R., E.B. and R.N. All authors have read and agreed to the published version of the manuscript.

Funding: The work was supported by the European Regional Development Fund; OP RDE; Project: “Chemical Biology for Drugging Undruggable Targets (ChemBioDrug)” (No. CZ.02.1.01/0.0/0.0/16_019/0000729), Ministry of Health of the Czech Republic (grant NU20-05-00472), the Czech Academy of Sciences (RVO: 61388963), and Gilead Sciences Inc. This study was also supported by a grant from the Ministry of Education, Youth, and Sports of the Czech Republic (grant LTAUSA18016) (to L.E. and R.N.).

Institutional Review Board Statement: Not applicable.

Informed Consent Statement: Not applicable.

Data Availability Statement: Not applicable.

Conflicts of Interest: The research was partially sponsored by Gilead Sciences Inc., Foster City, CA, USA.

References

1. Cui, J.; Li, F.; Shi, Z.L. Origin and evolution of pathogenic coronaviruses. *Nat. Rev. Microbiol.* **2019**, *17*, 181–192. [[CrossRef](#)]
2. De Wit, J.J.; Cook, J.K.A. Spotlight on avian coronaviruses. *Avian Pathol.* **2020**, *49*, 313–316. [[CrossRef](#)]
3. Monchatre-Leroy, E.; Boue, F.; Boucher, J.M.; Renault, C.; Moutou, F.; Gouilh, M.A.; Umhang, G. Identification of Alpha and Beta Coronavirus in Wildlife Species in France: Bats, Rodents, Rabbits, and Hedgehogs. *Viruses* **2017**, *9*, 364. [[CrossRef](#)]
4. Chen, Y.; Liu, Q.Y.; Guo, D.Y. Emerging coronaviruses: Genome structure, replication, and pathogenesis. *J. Med. Virol.* **2020**, *92*, 418–423. [[CrossRef](#)]
5. De Wit, E.; Van Doremalen, N.; Falzarano, D.; Munster, V.J. SARS and MERS: Recent insights into emerging coronaviruses. *Nat. Rev. Microbiol.* **2016**, *14*, 523–534. [[CrossRef](#)]
6. Zumla, A.; Chan, J.F.W.; Azhar, E.I.; Hui, D.S.C.; Yuen, K.-Y. Coronaviruses—Drug discovery and therapeutic options. *Nat. Rev. Drug Discov.* **2016**, *15*, 327–347. [[CrossRef](#)]
7. Gorbalenya, A.E.; Baker, S.C.; Baric, R.S.; De Groot, R.J.; Drosten, C.; Gulyaeva, A.A.; Haagmans, B.L.; Lauber, C.; Leontovich, A.M.; Neuman, B.W.; et al. The species Severe acute respiratory syndrome-related coronavirus: Classifying 2019-nCoV and naming it SARS-CoV-2. *Nat. Microbiol.* **2020**, *5*, 536–544. [[CrossRef](#)]
8. Lu, L.; Zhong, W.Y.; Bian, Z.W.; Li, Z.M.; Zhang, K.; Liang, B.X.; Zhong, Y.Z.; Hu, M.J.; Lin, L.; Liu, J.; et al. A comparison of mortality-related risk factors of COVID-19, SARS, and MERS: A systematic review and meta-analysis. *J. Infect.* **2020**, *81*, E18–E25. [[CrossRef](#)]
9. Finelli, L.; Gupta, V.; Petigara, T.; Yu, K.; Bauer, K.A.; Puzniak, L.A. Mortality Among US Patients Hospitalized With SARS-CoV-2 Infection in 2020. *JAMA Netw. Open* **2021**, *4*, e216556. [[CrossRef](#)]
10. Tumban, E. Lead SARS-CoV-2 Candidate Vaccines: Expectations from Phase III Trials and Recommendations Post-Vaccine Approval. *Viruses* **2021**, *13*, 54. [[CrossRef](#)]
11. Wu, D.; Koganti, R.; Lambe, U.P.; Yadavalli, T.; Nandi, S.S.; Shukla, D. Vaccines and Therapies in Development for SARS-CoV-2 Infections. *J. Clin. Med.* **2020**, *9*, 1885. [[CrossRef](#)]

12. Pedersen, O.S.; Pedersen, E.B. Non-nucleoside reverse transcriptase inhibitors: The NNRTI boom. *Antivir. Chem. Chemother.* **1999**, *10*, 285–314. [[CrossRef](#)]
13. Dayal, V.; Kumar, A.; Jha, S.K.; Sharan, A.; Kumar, U.; Shahi, S.K. Viral Hepatitis (plus Antiviral Therapy) Combination therapy of lamivudine and adefovir in patients of HBeAg positive chronic hepatitis B. *J. Gastroenterol. Hepatol.* **2013**, *28*, 419.
14. Das, D.; Pandya, M. Recent Advancement of Direct-acting Antiviral Agents (DAAs) in Hepatitis C Therapy. *Mini-Rev. Med. Chem.* **2018**, *18*, 584–596. [[CrossRef](#)]
15. Vicenti, I.; Zazzi, M.; Saladini, F. SARS-CoV-2 RNA-dependent RNA polymerase as a therapeutic target for COVID-19. *Expert Opin. Ther. Pat.* **2021**, *31*, 325–337. [[CrossRef](#)]
16. Perry, J.K.; Appleby, T.C.; Bilello, J.P.; Feng, J.Y.; Schmitz, U.; Campbell, E.A. An atomistic model of the coronavirus replication-transcription complex as a hexamer assembled around nsp15. *bioRxiv* **2021**. [[CrossRef](#)]
17. Hillen, H.S.; Kokic, G.; Farnung, L.; Dienemann, C.; Tegunov, D.; Cramer, P. Structure of replicating SARS-CoV-2 polymerase. *Nature* **2020**, *584*, 154–156. [[CrossRef](#)]
18. Pruijssers, A.J.; George, A.S.; Schafer, A.; Leist, S.R.; Gralinski, L.E.; Dinno, K.H.; Yount, B.L.; Agostini, M.L.; Stevens, L.J.; Chappell, J.D.; et al. Remdesivir Inhibits SARS-CoV-2 in Human Lung Cells and Chimeric SARS-CoV Expressing the SARS-CoV-2 RNA Polymerase in Mice. *Cell Rep.* **2020**, *32*, 107940. [[CrossRef](#)]
19. Yin, W.C.; Luan, X.D.; Li, Z.H.; Zhou, Z.W.; Wang, Q.X.; Gao, M.Q.; Wang, X.X.; Zhou, F.L.; Shi, J.J.; You, E.R.; et al. Structural basis for inhibition of the SARS-CoV-2 RNA polymerase by suramin. *Nat. Struct. Mol. Biol.* **2021**, *28*, 319–325. [[CrossRef](#)]
20. Li, Q.; Yi, D.; Lei, X.; Zhao, J.; Zhang, Y.; Cui, X.; Xiao, X.; Jiao, T.; Dong, X.; Zhao, X.; et al. Corilagin inhibits SARS-CoV-2 replication by targeting viral RNA-dependent RNA polymerase. *Acta Pharm. Sin. B* **2021**, *11*, 1555–1567. [[CrossRef](#)]
21. Jin, Y.H.; Min, J.S.; Jeon, S.; Lee, J.; Kim, S.; Park, T.; Park, D.; Jang, M.S.; Park, C.M.; Song, J.H.; et al. Lycorine, a non-nucleoside RNA dependent RNA polymerase inhibitor, as potential treatment for emerging coronavirus infections. *Phytomedicine* **2021**, *86*, 153440. [[CrossRef](#)]
22. Agrawal, N.; Goyal, A. Potential Candidates against COVID-19 Targeting RNA-Dependent RNA Polymerase: A Comprehensive Review. *Curr. Pharm. Biotechnol.* **2021**. [[CrossRef](#)]
23. Tarantino, D.; Cannalire, R.; Mastrangelo, E.; Croci, R.; Querat, G.; Barreca, M.L.; Bolognesi, M.; Manfroni, G.; Cecchetti, V.; Milani, M. Targeting flavivirus RNA dependent RNA polymerase through a pyridobenzothiazole inhibitor. *Antivir. Res.* **2016**, *134*, 226–235. [[CrossRef](#)]
24. Cannalire, R.; Tarantino, D.; Piorkowski, G.; Carletti, T.; Massari, S.; Felicetti, T.; Barreca, M.L.; Sabatini, S.; Tabarrini, O.; Marcello, A.; et al. Broad spectrum anti-flavivirus pyridobenzothiazolones leading to less infective virions. *Antivir. Res.* **2019**, *167*, 6–12. [[CrossRef](#)]
25. Cannalire, R.; Chan, K.W.K.; Burali, M.S.; Gwee, C.P.; Wang, S.; Astolfi, A.; Massari, S.; Sabatini, S.; Tabarrini, O.; Mastrangelo, E.; et al. Pyridobenzothiazolones Exert Potent Anti-Dengue Activity by Hampering Multiple Functions of NS5 Polymerase. *ACS Med. Chem. Lett.* **2020**, *11*, 773–782. [[CrossRef](#)] [[PubMed](#)]
26. Felicetti, T.; Burali, M.S.; Gwee, C.P.; Chan, K.W.K.; Alonso, S.; Massari, S.; Sabatini, S.; Tabarrini, O.; Barreca, M.L.; Cecchetti, V.; et al. Sustainable, three-component, one-pot procedure to obtain active anti-flavivirus agents. *Eur. J. Med. Chem.* **2021**, *210*, 112992. [[CrossRef](#)]
27. Konkolova, E.; Dejmeck, M.; Hrebabecky, H.; Sala, M.; Boserle, J.; Nencka, R.; Boura, E. Remdesivir triphosphate can efficiently inhibit the RNA-dependent RNA polymerase from various flaviviruses. *Antivir. Res.* **2020**, *182*, 104899. [[CrossRef](#)] [[PubMed](#)]
28. De Madrid, A.T.; Porterfield, J.S. A simple micro-culture method for the study of group B arboviruses. *Bull. World Health Organ.* **1969**, *40*, 113–121. [[PubMed](#)]
29. Eyer, L.; Valdes, J.J.; Gil, V.A.; Nencka, R.; Hrebabecky, H.; Sala, M.; Salat, J.; Cerny, J.; Palus, M.; De Clercq, E.; et al. Nucleoside Inhibitors of Tick-Borne Encephalitis Virus. *Antimicrob. Agents Chemother.* **2015**, *59*, 5483–5493. [[CrossRef](#)]

Guanine quadruplexes in the RNA genome of the tick-borne encephalitis virus: their role as a new antiviral target and in virus biology

Jiří Holoubek^{1,2,3,†}, Klára Bednářová^{4,†}, Jan Havierník^{1,3}, Ivana Huvarová¹, Zuzana Dvořáková⁴, Jiří Černý⁵, Martina Outláš^{6,7}, Jiří Salát^{1,3}, Eva Konkol'ová⁸, Evzen Boura⁸, Daniel Růžek^{1,2,3}, Michaela Vorlíčková⁴, Luděk Eyer^{1,3,*} and Daniel Renčíuk^{4,*}

¹Veterinary Research Institute, Emerging Viral Diseases, Brno CZ-62100, Czech Republic, ²Department of Experimental Biology, Faculty of Science, Masaryk University, CZ-62500 Brno, Czech Republic, ³Institute of Parasitology, Biology Centre of the Czech Academy of Sciences, CZ-37005 Ceske Budejovice, Czech Republic, ⁴Department of Biophysics of Nucleic Acids, Institute of Biophysics of the Czech Academy of Sciences, Brno CZ-61200, Czech Republic, ⁵Faculty of Tropical Agrisciences, Czech University of Life Sciences Prague, CZ-16500 Prague, Czech Republic, ⁶Department of Biophysical Chemistry and Molecular Oncology, Institute of Biophysics of the Czech Academy of Sciences, Brno CZ-61200, Czech Republic, ⁷National Centre for Biomolecular Research, Faculty of Science, Masaryk University, CZ-62500 Brno, Czech Republic and ⁸Institute of Organic Chemistry and Biochemistry of the Czech Academy of Sciences, CZ-16000 Prague, Czech Republic

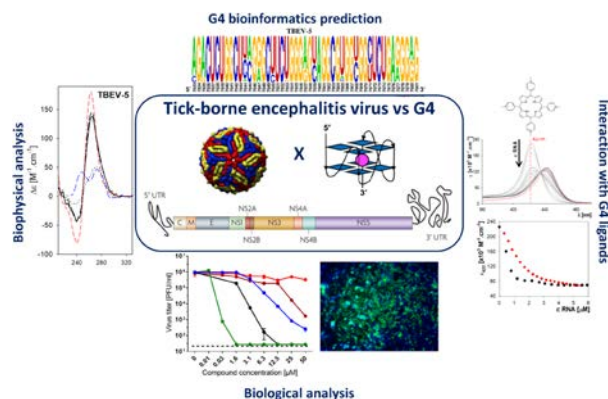
Received July 02, 2021; Revised March 21, 2022; Editorial Decision March 23, 2022; Accepted March 25, 2022

ABSTRACT

We have identified seven putative guanine quadruplexes (G4) in the RNA genome of tick-borne encephalitis virus (TBEV), a flavivirus causing thousands of human infections and numerous deaths every year. The formation of G4s was confirmed by biophysical methods on synthetic oligonucleotides derived from the predicted TBEV sequences. TBEV-5, located at the NS4b/NS5 boundary and conserved among all known flaviviruses, was tested along with its mutated variants for interactions with a panel of known G4 ligands, for the ability to affect RNA synthesis by the flaviviral RNA-dependent RNA polymerase (RdRp) and for effects on TBEV replication fitness in cells. G4-stabilizing TBEV-5 mutations strongly inhibited RdRp RNA synthesis and exhibited substantially reduced replication fitness, different plaque morphology and increased sensitivity to G4-binding ligands in cell-based systems. In contrast, strongly destabilizing TBEV-5 G4 mutations caused rapid reversion to the wild-type genotype. Our results suggest that there is a threshold of stability for G4 sequences in the TBEV genome, with any deviation

resulting in either dramatic changes in viral phenotype or a rapid return to this optimal level of G4 stability. The data indicate that G4s are critical elements for efficient TBEV replication and are suitable targets to tackle TBEV infection.

GRAPHICAL ABSTRACT



INTRODUCTION

Guanine quadruplexes (G4s) are non-canonical four-stranded conformations of nucleic acids. G4s can be formed

*To whom correspondence should be addressed. Tel: +420 541 517 202; Email: renciuk@ibp.cz
Correspondence may also be addressed to Luděk Eyer. Tel: +420 533 331 911; Email: eyer@vri.cz

†The authors wish it to be known that, in their opinion, the first two authors should be regarded as joint First Authors.

within DNA or RNA when two or more G-tetrads stack on top of each other and coordinate monovalent cations, such as physiological K^+ and Na^+ , in the G4 central cavity. Each tetrad is composed of four guanine residues connected through Hoogsteen hydrogen bonds. G4s can fold intramolecularly from a single G-rich strand or intermolecularly through the association of separate strands. The relative orientation of participating guanine tracts defines the parallel, the antiparallel or mixed topology of G4s, which is directly correlated to the conformational state, *anti* or *syn*, of the N-glycosidic bond between the G base and the sugar (1). In the case of RNA, guanosine residues prefer the *anti* conformation of the glycosidic bond which limits the topology of the RNA G4 to parallel types. Potential quadruplex forming sequences (PQS) have been found in the genomes of numerous eucaryotic and procaryotic species (2) and G4 have been shown to act as structural switches of multiple cellular processes (3).

Essential functions for G4 sequences have also been demonstrated in numerous DNA and RNA viruses (4) involving different stages of viral life cycles and the presence of G4 was correlated with the type of infection they cause (5). Regarding DNA viruses, multiple G4 clusters in the herpes simplex virus 1 (HSV-1) genome are required for efficient viral DNA replication (6). Nuclear antigen 1 encoded by the Epstein-Barr virus (EBV) genome binds G4s at the viral replication origin and interacts with the replication complex and with human metaphase chromosomes. This ensures the maintenance of the viral genome throughout mitosis. (7). G4s in the telomeric regions of the human herpesvirus 6 (HHV6) are involved in the mechanism of HHV-6 integration into the telomeres of human chromosomes. This process is considered as one possible mode of virus latency (8). Additional to these DNA viruses, there are several reports of G4s in RNA viruses. The long terminal promoter (LTR) in the HIV-1 genome was demonstrated to form G4 structures that are responsible for promoter activity regulation. In addition, these G4s are also involved in reverse transcription and viral latency establishment (9). G-rich sequences were recently identified in the genomes of two medically important filoviruses, Ebola and Marburg. These sequences are likely involved in filovirus-specific L gene expression (10).

The first evidence of the guanine quadruplex in the *Flaviviridae* family came from studies of the hepatitis C virus (HCV) (11). In the HCV, RNA synthesis was observed to be modulated by G4 formation in the viral negative RNA strand (12). Nucleolin, a host cell protein, recognized another G4 in the HCV genome and this interaction suppressed viral replication and expression (13). HCV RNA quadruplexes were later observed in infected cells using the fluorescent quadruplex-specific thioflavin-T-derivative (14). Fleming *et al.* reported that the RNA genome of the Zika virus (ZIKV) and other members of the genus *Flavivirus* contain conserved RNA quadruplexes (15). Several G4 sequences were discovered in the positive strand of the ZIKV genome: seven of these are conserved within more than 50 flavivirus genomes, indicating an essential role in the flaviviral life cycle. They also suggested that the RNA G4s in the ZIKV genome might serve as a framework for installing epitranscriptomic mark N6-methyladenosine (16).

Recently, several novel conserved potential G4s were identified in the ZIKV RNA genome, which were further analyzed by biophysical and biochemical approaches. Treatment of ZIKV-infected cells with G4-binding ligands resulted in the significant inhibition of infectious ZIKV yield, suppression of viral genome replication and viral protein synthesis (17,18). The potential role of G4s as antiviral targets was recently reviewed (19,20).

In this work, we studied the occurrence and structure of potential G4 sequences in the genome of the tick-borne encephalitis virus (TBEV), the most medically important representative of flaviviruses transmitted by ticks. The TBEV is prevalent over large forested areas of Europe and Asia, causing tick-borne encephalitis (TBE) in humans. TBE is a serious and potentially fatal neural infection with an estimated annual number of disease cases of >13 000 (21). The TBEV comprises three main subtypes: Western/European, Siberian and Far Eastern with the possibility of several minor subtypes also existing (22). The TBEV, as a typical flavivirus, is a small (~50 nm in diameter), enveloped, icosahedral virus (23) that possesses a positive-sense single-stranded RNA genome of ~11 kb in length. The genome encodes one large open reading frame (ORF) which is flanked by a 5' and a 3' untranslated regions (UTR). The 5' end of the genome is capped and the 3' end is not polyadenylated. The ORF encodes a single polyprotein co- and posttranslationally cleaved by viral and cellular proteases into three structural (C, prM, and E) and six nonstructural (NS1, NS2a, NS3, NS4a, NS4b and NS5) proteins (21).

Herein, the TBEV genome was investigated for the presence of G4s using multiple bioinformatics, biophysical, and biological approaches. Initially, the genome was examined using available G4-search algorithms to predict the potential formation of G4s directly from the primary structure of RNA sequence and the conservation among different TBEV strains and within the *Flavivirus* genus was explored. Selected quadruplex-forming sites were characterized as synthetic oligoribonucleotides in terms of structure, thermodynamic stability and formation kinetics, by circular dichroism, UV absorption spectroscopy and native polyacrylamide gel electrophoresis. The interactions of the G4 motifs located in the TBEV genome with small molecule-based G4-ligands were assessed by thiazole orange fluorescence displacement assay, titration assays using changes in absorption of ligands upon binding to RNA and G4-stabilization assay. We also investigated whether the formation of G4 affects *in vitro* RNA synthesis by the flaviviral RNA-dependent RNA polymerase (RdRp). The antiviral and cytotoxic properties of selected G4 ligands were studied in cell-based assay systems to demonstrate G4-mediated mechanisms at biological levels. Finally, site-directed mutagenesis was used to introduce conformation-specific mutations into a conserved G4 motif in the TBEV genome in order to assess the growth kinetics, plaque morphology and sensitivity of the mutated viruses to G4 ligands. Our results bring novel insights into the structure and folding of TBEV genomic RNA, which are crucial to understanding the molecular basis of TBEV pathogenesis. This new information can be essential for new antiviral treatments and the development of novel vaccination strategies.

MATERIALS AND METHODS

Bioinformatics analysis

The TBEV strain Neudoerfl reference genome sequence (NC_001672.1, sequence identical to U27495.1), genomic sequences of other TBEV strains, as well as genomes of all viruses of the *Flavivirus* genus, reported in (15), were downloaded from the Nucleotide database of the NCBI. Genome sequence alignments were performed using the MUSCLE algorithm (24) with the default setting embedded in the UGENE package (25). A rough phylogenetic tree was calculated in UGENE using the PHYLIP Neighbour Joining method (F84 model; Transition/Transversion ratio 2; Bootstrapping OFF; Gamma-distribution rates across sites OFF). Potential G4-forming regions selected for further bioinformatics analysis were extracted as multiFASTA files with gaps trimmed.

G4 prediction for the TBEV genome (NC.001672.1) was performed with QGRS mapper (max G4 length = 30 nt; min G-tract length = 2 nt) (26), pqsfinder (max length = 30 nt, min G-tract = 2 nt, loop min len = 1 nt, max bulges = 0, max mismatches = 0) (27), G4Hunter (window size = 20 nt; threshold = 1.49) (28) and G4RNA screener (window size = 20 nt; step size = 5 nt) (29).

G4Hunter scores of extracted regions from aligned genomes in multi FASTA files of members of the *Flavivirus* genus as well as TBEV strains were calculated using the G4HunterTable utility (30) in R studio. RNA sequence logos of the aligned set of 204 TBEV strains were prepared as frequency plots using the 'weblogo' tool (31).

Oligonucleotides

Synthetic RNA oligonucleotides were purchased from Merck (Haverhill, UK) and were desalted and lyophilized by the provider. For clarity, we did not use the standard r(...) notation as most of the oligonucleotides were RNA. Lyophilized oligonucleotides were dissolved in 1 mM sodium phosphate buffer, pH 7 with 0.3 mM EDTA to a 10 mM nucleoside concentration stock solution. The precise concentration of the oligonucleotides used for each experiment was determined from UV absorption at 260 nm in buffer at 90°C using molar absorption coefficients calculated according to our previous work, e.g. (32) and shown in Table 1. All sequences used in this study and their labels are summarized in Table 1.

G4 ligands

Pyridostatin (PDS) (33), hemin (34), bisquinolinium derivative PhenDC3 (35), thioflavin T (ThT) (36), thiazole orange (TO) (37), crystal violet (CV) (38), acridine derivative BRACO-19 (39), hydroxyantraquinone natural compound aloe-emodin (40) and natural alkaloid berberine (41) were purchased from Sigma-Aldrich (Prague, Czech Republic). N-Methylmesoporphyrin IX (NMM) (42,43) and 5,10,15,20-tetrakis-(N-methyl-4-pyridyl)porphine (TMPyP4) (42,44) were obtained from Santa Cruz Biotechnology (Heidelberg, Germany). Carboxy pyridostatin (cPDS) (45,46), bisquinolinium derivative 360A (47) and polymerase I inhibitor CX5461 (48) were from

MedChemExpress (Stockholm, Sweden). Test compounds were solubilized according to the recommendations of the provider in water or in 100% (v/v) dimethyl sulfoxide (DMSO) to yield stock solutions of desired concentration, usually 10 mM.

Spectroscopy of circular dichroism (CD)

CD measurements were conducted on a Jasco J-815 dichrograph (Jasco Corp., Tokyo, Japan). Presented CD spectra were collected as an average of four measurements between 330 nm and 210 nm with data pitch 0.5 nm at 200 nm min⁻¹ acquisition speed. Spectra were measured in 1 cm-pathlength quartz cells (Hellma GmbH, Müllheim, Germany) at 23°C. CD signals are expressed as the difference in the molar absorption $\Delta\epsilon$ of the left- and right-handed circularly polarized light and the molarity is related to strands. The experimental conditions were changed directly in the cells by adding stock solutions of buffers and the final concentration was corrected for the volume increase. Spectra or values labelled 'after annealing' were observed in the same buffer as the previous ones after heating to 95°C for 5 min and slow linear cooling back to 23°C within 5 h.

Titration experiments using UV absorption

Absorption measurements during titration experiments were conducted in a Specord 250 Plus spectrophotometer (Analytik Jena, Jena, Germany). Whole absorption spectra of RNA with ligand or control were taken from 200 to 700 nm with 1 nm step and 10 nm s⁻¹ acquisition speed at 23°C. Two types of titration experiments were performed: (i) for RNA-to-Ligand experiments, 1000 μ l of ligands were prepared into 1 cm-pathlength quartz cells to a 4 μ M concentration in 1 \times IC buffer (25 mM sodium phosphate buffer, pH 7, 110 mM KCl, 10 mM NaCl). Twenty consecutive additions of 10 μ l of RNA at 40 μ M strand concentration in 1 \times IC buffer were performed, with absorption spectra measurement after each addition. (ii) For the Ligand-to-RNA experiments, 1000 μ l of RNA were prepared into 1 cm-pathlength quartz cells to a 4 μ M strand concentration in 1 \times IC buffer. Then 25 consecutive additions of 10 μ l ligands at 40 μ M strand concentration in 1 \times IC buffer were carried out, along with absorption spectra measurement after each addition. Absorption spectra were recalculated into molar units with known molar absorption coefficients of ligands.

Fluorescence measurements and fluorescence intercalator displacement assay (FID)

FID assay was performed either with TO, as described in Tran *et al.* (49), or with (ThT, where only the probe and excitation and emission wavelengths were modified. RNA oligonucleotides were pre-incubated in 1 \times IC buffer for 1 h at 25°C. Two molar equivalents of TO or ThT in the same buffer were added and the mixture was incubated for 1 h at 25°C. Next, five equivalents of ligand were added to each sample and the mixture was incubated for 30 min at 25°C. The total reaction volume was 80 μ l with 1 μ M RNA, 2 μ M TO or ThT and 5 μ M tested final ligand concentration. Fluorescence was measured in 96-well opaque microplates

Table 1. Labels, primary sequences and molar extinction coefficients of oligonucleotides used for structural studies in the paper

Label	Sequence	ϵ [$M^{-1} \cdot cm^{-1}$] ^a	Position ^b	Protein
TBEV-1	AAGGUAAGGGGGGCGGUC	194 000	154	Core protein C
TBEV-1mut	AAGUAAGAGGAGCGGUC	194 900		
TBEV-1b	AAGGUAAGGGGGGCGGUC	265 300	154	Core protein C
TBEV-2	UUGGAGUGGGGGCGGAUGUUGGUU	250 700	2447	Envelope / NS1
TBEV-2mut	UUGGAGUGAGUGCGGAUGUUGGUU	243 200		
TBEV-3	AUGGUGGGCACGGAAGGAC	201 400	2863	NS1
TBEV-3mut	AUGGUGAGCACGAAAGGAC	199 500		
TBEV-4	UCGGGGAGGGGGAGGCA	182 400	7382	NS4b
TBEV-4mut	UCGAGGAGUGAGAGGCA	179 900		
TBEV-5	CUGGGGUAGGCGUGGUGGUU	215 000	7652	NS4b / NS5
TBEV-5mut	CUGUGUGUAUGCGUGUUGGUU	210 700	—	—
TBEV-6	CUGGGAGUUGGAACGAGGUGUGGUC	280 300	8440	NS5 (RNA pol)
TBEV-6mut	CUGAGAGUUGAACGAGUUGUGGUC	276 000		
TBEV-7	UUGUGGGGGAGGCUAGGAGGCGAA	268 000	10653	3'-UTR
TBEV-7mut	UUGUGUAGCGAAGCUAGGAUGCGAA	256 800		
R-psG4	AAUGGGUGGGUGGGUGGGUAA	230 000		

^a ϵ calculated for strand using nearest-neighbor model.

^bPosition of the first nucleotide in TBEV reference genome NC_001672.1.

(SPL Life Sciences) at 25°C by Synergy H1 hybrid reader (BioTek) with excitation at 492 nm (TO)/430 nm (ThT) and the emission collected at 533 nm (TO)/480 nm (ThT) and gain set to 100. Each condition was tested in triplicate, fluorescence intensity was averaged and SD calculated. The percentage of TO/ThT displacement was derived similarly as in Carvalho *et al.* (50), using the formula: Displacement (%) = $100 - [100 \times (FI - Fb)/(FI_0 - Fb)]$, where FI stands for fluorescence with ligand, FI_0 for fluorescence without ligand and Fb for fluorescence of background.

Fluorescence measurements of ThT upon interaction with RNA oligonucleotides were performed in a similar way as FID with ThT without addition of the tested ligand.

Temperature-dependent absorption measurements and thermal difference spectra

Temperature melting measurements were conducted in a Varian Cary 4000 spectrophotometer (Varian, Mulgrave, Australia). Whole absorption spectra were taken at each temperature step (1°C) from 230 to 400 nm with a 1 nm step and 600 nm min⁻¹ acquisition speed. Four consecutive temperature ramps were run between 23°C and 95°C with 1°C step (alternating denaturation and renaturation processes) and 2 min waiting time at each temperature, giving an average temperature change of 0.25°C min⁻¹. As a blank, a similar cell with only 1× IC buffer was used. Absorbance spectra were recalculated to molar units similarly to CD spectra and molar absorbance at 297 nm was plotted as a function of temperature to give melting and annealing curves. These were dual-baseline corrected with linear baselines fitting pre- and post-melting parts of observed melting curves (51) and melting temperatures (T_m) were calculated as a temperature, where baseline-corrected molar absorbance is equal to 0.5.

Thermal difference spectra (TDS) were calculated as the difference between molar absorption spectra measured at 95°C and at 23°C during the first temperature ramp of the melting experiment in 1× IC buffer.

Viruses and cell cultures

TBEV strains Neudoerfl and Hypr, both members of the West European TBEV subtype, were provided by the Collection of Arboviruses, Institute of Parasitology, Biology Center of the Czech Academy of Sciences, Ceske Budejovice, Czech Republic, <http://www.arboviruscollection.cz/index.php?lang=en>. All work with infectious TBEV was performed in biosafety level 3 facility at the Veterinary Research Institute, Brno, Czech Republic. Porcine stable kidney (PS) cells, an immortalized cell line widely applied for TBEV isolation and multiplication (52) were used as a model cell line for antiviral and cytotoxicity cell-based assays. All experiments based on the transfection of Infectious Subgenomic Amplicons (ISA) or viral RNA (see below) were performed in BHK-21 cells (ATTC CCL-10), because this cell line is highly susceptible to uptake and/or recombine the transfected nucleic acid (53–55). The cells were cultured in Leibovitz (L-15) medium (PS) and Dulbecco's modified Eagle's medium (DMEM) (BHK-21) supplemented with 3% (L15) and 10% (DMEM) newborn calf serum and 100 U/ml penicillin, 100 µg/ml streptomycin and 1% glutamine (Sigma-Aldrich, Prague, Czech Republic). BHK-21 cells were cultivated at 37°C in 5% CO₂, whereas PS cells were cultured at 37°C in a normal atmosphere (without CO₂ supplementation).

Cytotoxicity assay

To determine the cytotoxicity of G4 ligands, PS cells were seeded in 96-well microtitration plates (2×10^4 cells/well) and incubated for 24 h. After incubation, the test ligands were added to the cells in a concentration range from 0 to 50 µM (three wells per compound in two independent experiments) and the treated cells were cultivated for 48 h at 37°C. Cytotoxicity was determined in terms of cell viability using the Cell Counting Kit-8 (Dojindo Molecular Technologies, Munich, Germany) according to the manufacturer's instructions and expressed as 50% cytotoxic concentration (CC₅₀, the amount required to cause a 50% reduction in cell viability).

Virus titer reduction assays

The antiviral efficacy of G4 ligands, which showed a low cytotoxicity for PS cells (PDS, cPDS, NMM, TMPyP4, hemin, 360A, PhenDC3, BRACO-19 and berberine), was initially tested at a single concentration of 50 μ M in PS cells using a viral titer reduction assay. The cells were seeded in 96-well plates (approximately 2×10^4 cells per well) and incubated for 24 h to form a confluent monolayer. Following incubation the medium was aspirated from the wells and replaced with 200 μ l of fresh medium containing 50 μ M of the appropriate G4 ligand (three wells per compound in two independent experiments) and inoculated with TBEV (Neudoerfl or Hypr) at a multiplicity of infection (MOI) of 0.1. DMSO was added to virus-infected cells as a negative control at a final concentration of 0.5% (v/v). Viral titers were estimated from the collected media using a plaque assay after 48-h cultivation. To study the dose-response antiviral effect of the selected G4-binding ligands (PDS, cPDS, NMM, TMPyP4, PhenDC3 and berberine) the same experimental procedure was performed as described above with slight modifications. Growth medium was aspirated from PS cell monolayers, replaced with 200 μ l of fresh medium containing the compounds from 0 to 50 μ M and TBEV (strains Neudoerfl or Hypr) at an MOI of 0.1 and cultivated for 48 or 72 h at 37°C. Viral titers were determined by plaque assays. Viral titer values obtained from the PS-based antiviral assays at experimental interval 48 h.p.i. were used to construct dose-dependent curves and calculate the 50% effective concentrations (EC₅₀).

Plaque assay

Plaque assays were performed in PS cells to determine TBEV titers as described previously (56,57). Briefly, 10-fold dilutions of TBEV were prepared in 24-well tissue culture plates and the cells were added to each well ($0.6\text{--}1.5 \times 10^5$ cells per well). After a 4-h incubation, the suspension was overlaid with 1.5% (w/v) carboxymethylcellulose in L-15 medium. Following a 5-day incubation at 37°C the infected plates were washed with phosphate-buffered saline and the cell monolayers were stained with naphthalene black. The virus titer was expressed as plaque-forming units (PFU)/ml.

Immunofluorescence staining

To measure the G4 ligand-induced inhibition of viral surface antigen expression, a cell-based flavivirus immunostaining assay was performed as previously described (57). Briefly, PS cells were seeded onto 96-well microtitration plates to form a confluent monolayer. After a 24-h incubation, the cells were treated with G4 ligands at concentrations of 0, 10 and 50 μ M then simultaneously infected with TBEV strains Neudoerfl and Hypr at an MOI of 0.1 and cultured for 48 h at 37°C. For NMM, concentrations of 0, 10 and 25 μ M were used. We did not use NMM at 50 μ M due to observable changes in cell morphology and monolayer coherence at this concentration. The experiment was performed in triplicate. After cold acetone-methanol (1:1) fixation and blocking with 10% fetal bovine serum we incubated the cells with a mouse monoclonal antibody targeting the flavivirus

group surface antigen (protein E) (1:250; antibody clone D1-4G2-4-15; Sigma-Aldrich, Prague, Czech Republic) and labelled it with an anti-mouse goat secondary antibody conjugated with fluorescein isothiocyanate (FITC; 1:500) by incubation for 1 h at 37°C. The cells were counterstained with 4',6-diamidino-2-phenylindole (DAPI; 1 μ g/ml) for visualization of the cell nuclei and the fluorescence signal was recorded with an Olympus IX71 epifluorescence microscope. The level of viral antigen expression in the presence of G4 ligands was quantified and expressed as a percentage of infected (viral antigen expressing) cells relative to mock-infected cells.

Quantification of viral RNA synthesis

The effect of G4 ligands (concentrations of 0, 10 and 50 μ M; for NMM we used 25 μ M instead of 50 μ M) on viral genomic RNA replication efficacy was studied using quantitative real-time PCR (RT-qPCR). RNA was isolated from growth media supernatants using the QIAmpViral RNA mini kit (Qiagen, Germantown, MD, USA) following manufacturer's instructions. RT-qPCR measurements were performed on the LightCycler 480 II in a 96-well plate block (Roche, Basel Switzerland) using the Advanced Kit for Tick-borne Encephalitis (Genesig, Germantown, MD, USA) and Lyophilized OneStep qRT-PCR (Oasig) following manufacturer's instructions. TBEV copy numbers/ μ l were calculated from calibration curves based on standards provided by the manufacturer (Genesig, Germantown, MD, USA).

Adhesion assay

The adhesion assay was used to distinguish whether the ligands show an antiviral effect before entering the cell (inhibition of viral adsorption/fusion) or act in the post-entry phase. This assay was performed in PS cells seeded in 6-well plates. Virus inoculum (10⁶ PFU/ml, TBEV strain Hypr) was pre-treated with PDS, cPDS, berberine, PhenDC3 (at 50 μ M), or NMM (at 25 μ M) for 1 h at 37°C then diluted to 100 PFU/ml and used to infect PS cells in 6-well plates for 1 h at 4°C. Following inoculation, the PS cells were washed with PBS three times to remove the non-adsorbed virus and then fresh medium with 1.5% carboxymethylcellulose was added to the cells. After 5 days of incubation at 37°C, the PS cell monolayers were stained with naphthalene black and the plaque count was determined.

Transfection of viral RNA pre-treated with G4 ligands

Viral genome RNA from the TBEV strain Hypr was isolated using a QIAmpViral RNA mini kit (Qiagen, Germantown, MD, USA) following manufacturer's instructions. The isolated RNA (a mixture of viral RNA and carrier RNA from the QIAmpViral RNA mini kit, a total concentration of 50 ng/ μ l) was incubated with selected G4 ligands i.e. PDS and berberine at 0, 10, 50 and 200 μ M or NMM at 0, 10, 25 and 200 μ M for 1 h at 4°C. We also intentionally used an extremely high ligand concentration (200 μ M) to make the effect as pronounced as possible. The other two concentrations (10 and 25/50 μ M) were the same as in the

previous cell-based experiments. The RNA-lipid complex was prepared as follows: 1 μ l of TransIT[®]-mRNA reagent and 1 μ l of mRNA Boost reagent from TransIT[®]-mRNA Transfection Kit (Mirus Bio, Madison, WI, USA) was diluted in 50 μ l Opti-MEM medium (Life Technologies) and then mixed with 0.5 μ l of isolated RNA pre-treated with the corresponding G4 ligands. After a 5-min incubation at room temperature, the mixture was added to BHK-21 cells and incubated for 24 h at 37°C. Cell supernatant media were then harvested and virus titer was determined by plaque assay.

Expression and purification of RNA-dependent RNA polymerase from Japanese encephalitis virus (JEV RdRp)

The gene encoding JEV RdRp (GeneBank: NP_775674.1) was synthesized as codon optimized for *Escherichia coli* and was cloned into pET28b vector (European Virus Archive goes Global, EVA_g) containing N-terminal 6x His followed by TEV cleavage site. The gene was expressed in *E. coli* (BL-21 CodonPlus (DE3)-RIL) and purified using our protocol optimized for viral polymerase (58). Cells were harvested and the pellet was resuspended in a lysis buffer (50 mM Tris-HCl pH 8.0, 20 mM imidazole, 500 mM NaCl, 10% glycerol, 3 mM β -mercaptoethanol) and sonicated (Q700 Sonicator, QSonica). The lysate was removed by centrifugation and the supernatant was incubated with Ni-NTA agarose (Machery-Nagel), washed with lysis buffer and finally the protein was eluted with lysis buffer supplemented with 300 mM imidazole. The 6x His-TEV tag was digested using TEV protease at 4°C overnight. The protein was then further purified by affinity chromatography using a HiTrap Heparin HP column (GE Healthcare), followed by size exclusion chromatography using a Superdex 200 16/600 (GE Life Sciences) in 20 mM Tris pH 8.0, 800 mM NaCl, 10% glycerol, 3 mM β -mercaptoethanol. Fractions containing JEV polymerase were concentrated to 5 mg/ml, flash frozen in liquid nitrogen and stored at -80°C.

Template and primer preparation for polymerase stop assays

DNA single strands (Table S1), containing TBEV-5 and its mutated variants, denoted as *positive*, *negative* and *super-negative* (see below) together with primer binding sites and T7 RNA polymerase promoter, were acquired as synthetic oligonucleotides (Merck). The double stranded form was prepared by two-step PCR (30 cycles, 98°C/10 s denaturation and 45°C/30 s annealing + elongation) using 100 ng of single stranded template, forward (TAATAC-GACTCACTA) and reverse (GCGTGTCTCG) primers and PrimeStar GXL polymerase (Takara Bio Inc). PCR products were purified by QIAquick columns (Qiagen) into 50 μ l of elution buffer. RNA templates (Figure 7A) were prepared from the PCR products above using a HiScribe T7 In Vitro Transcription Kit (New England Biolabs) according to the provider protocol with 8 μ l of the PCR product as a template. RNA was purified using a Monarch RNA Cleanup Kit (New England Biolabs). Primers (DNA d(GCGTGTCTCG) for SuperScript IV and RNA GCGUGUCUCG for JEV RdRp) and DNA template single strands (see above) were labelled by ³²P us-

ing γ -³²P-ATP and T4 polynucleotide kinase (New England Biolabs). Labelled DNA was purified using CentriSpin columns (Princeton Separations) and the specific activity was measured.

Reverse transcription by SuperScript IV

RNA templates (0.5 μ M) were pre-incubated in SuperScript IV buffer (ThermoFisher Scientific) together with ³²P-labelled DNA primer (0.1 μ M), dNTP mix (1 mM each) and 50, 10 or 2 μ M of selected G4 ligands in total volume of 10 μ l for 3 min at 75°C. Samples labelled CTRL were prepared in absence of G4 ligands. Samples were then slowly cooled down to room temperature over 2 h. 0.4 μ l of SuperScript IV reverse transcriptase (ThermoFisher Scientific) was added and the mixture was incubated for 60 min at 37°C. Reaction was stopped by adding 0.5 μ l of 2 M NaOH and by heating for 5 min at 95°C, which also ensured alkaline hydrolysis of template RNA.

Synthesis of complementary strand by JEV RdRp

RNA templates (0.25 μ M) were pre-incubated in JEV RdRp buffer (5 mM Tris, pH 7.4, 10 mM DTT, 0.5% Triton X-100, 1% glycerol) supplemented with 2 mM MnCl₂ and 50 mM KCl, together with ³²P-labelled RNA primer (0.05 μ M), NTP mix (1 mM each) and 50, 10 or 2 μ M of selected G4 ligands in total volume of 20 μ l for 3 min at 75°C. Samples labelled CTRL were prepared in absence of G4 ligands. Samples were then slowly cooled to room temperature over 2 h. 0.5 μ l of 7 μ M JEV RdRp was added and the mixture was incubated for 120 min at 37°C. MnCl₂ was used instead of the natural MgCl₂ cofactor because it substantially increases the activity of the recombinant flaviviral polymerases under the *in vitro* conditions, as reported (59–61).

Denaturing PAGE of polymerase products and products quantification

The generated DNA or RNA was purified by ethanol-acetate precipitation, then dissolved in 2 μ l of loading dye (bromophenol blue and xylene cyanol in formamide), denatured by heating for 5 min at 95°C and 1.5 μ l (around 130 kcpm) was loaded onto a pre-heated 40 cm denaturing polyacrylamide gel (16% acrylamide mixture 29:1 mono:bis, 7 M urea, 1x TBE). Electrophoresis was performed in 1x TBE for 90 min at 45 W. The gel was then exposed to a Phosphor imager screen for 15 h (SuperScript IV) or 2 h (JEV RdRp) and the image was digitalized by a Typhoon FLA 9500 device. Observed lanes were background corrected by subtracting the signal density average from the no-label region and the integrated density of each lane was normalized to the same value. Relative fraction of full products in each lane, corresponding to a manually chosen part, was calculated. Relative ratio (in %) between tested samples and CTRL was calculated.

Site directed mutagenesis of the TBEV-5 region

We used a reverse genetics system derived from TBEV (strain Hypr) to construct recombinant TBEV bearing

conformation-specific mutations in the TBEV-5 sequence located in NS4b/NS5 genes. This reverse genetics system was based on the generation of infectious subgenomic overlapping DNA fragments that encompass the entire viral genome as previously described (53–55). Three de-novo synthesized DNA fragments cloned into a pUC57 or a pC11 (GenScript, Piscataway, NJ, USA) cover the following parts in the TBEV genome: fragment I (nucleotide position 1 to 3662), fragment II (nucleotide position 3545 to 8043), and fragment III (nucleotide position 7961–11 100). The first and last fragments are flanked respectively in 5' and 3' with the human cytomegalovirus promoter (pCMV) and the hepatitis delta ribozyme followed by the simian virus 40 polyadenylation signal (HDR/SV40pA).

Fragments I, II and III were used as templates to generate the overlapping amplicons following the original ISA method (53). Unmodified primers (Table S2) were used to generate three unmodified amplicons (i.e. production of wild-type virus). Mutated primers located on the targeted region (TBEV-5) of fragment II (Table S2) were used to generate two mutated amplicons, i.e. fragment IIa and IIb; these mutated fragments together with unmodified fragments I and III were used to produce three mutated viruses, denoted as the *positive* (T7653G/G7656A/T7659G/T7665G/T7671G), *negative* (G7656A/G7662A/G7677A), and *super-negative* (G7656A/G7662A/G7670C/G7677A) TBEV mutants (Figure 10B). In comparison with wild-type (*WT*), the *positive* G4-specific TBEV mutant was designed to fold a highly stabilized G4 in the TBEV-5 sequence, whereas the *negative* and *super-negative* mutants had a decreased or completely eliminated ability to form G4 in TBEV-5. ISA fragment amplification and BHK-21 transfection were performed, as described previously (55). Cell supernatant media were then harvested and titers of the recombinant viruses were determined by plaque assay. The presence of mutations in the genome of the obtained mutant viruses was verified by sequencing (Sanger method).

Growth kinetics of recombinant G4-specific TBEV mutants

To evaluate the growth kinetics of the obtained G4-specific TBEV mutants, PS cells incubated for 24 h in 96-well plates were infected with the recombinant wild-type virus or with the *positive*, *negative* or *super-negative* TBEV mutants at an MOI of 0.1. The growth kinetics of the *positive* TBEV mutant was further compared with that of the wild-type virus at a 10-fold lower MOI (0.01). The growth medium was collected from the wells daily on days 1 to 7 p.i. (three wells per interval). Viral titers (expressed as PFU/ml) were determined by plaque assay and used to construct TBEV growth curves. Plaque assays were also used to compare the plaque morphology of the mutated TBEV with that of the wild-type virus. After a 168-h cultivation in PS cells, viral RNA was isolated as described above and the presence of conformation-specific mutations in the TBEV-5 region of the individual mutated viruses verified by the Sanger sequencing method.

Sensitivity studies of G4-specific TBEV mutants to G4 ligands

In order to study the sensitivity / resistance of the recombinant viruses mutated in the TBEV-5 region to the selected G4 ligands, 200- μ l portions of fresh medium containing PDS or berberine at concentrations ranging from 0 to 50 μ M were added to PS cell monolayers, infected with TBEV wild-type or with mutated variants (the *positive*, *negative* and *super-negative* TBEV mutants) at an MOI of 0.1, and incubated for 24 and 48 h. The medium was then collected from the wells and the viral titers were determined by plaque assay. The obtained viral titer values were used to construct dose-response curves, to assess the replication capacity of the mutated viruses in the presence of PDS or berberine and to compare the replication fitness of G4-specific TBEV mutants with that of the wild-type virus.

RESULTS AND DISCUSSION

Identification of potential G4 sites in the TBEV genome and its complement

The TBEV genome consists of one molecule of RNA, i.e. a single-strand, with a positive (coding) polarity that directly serves as a template for viral genome transcription and polyprotein translation. For purposes of G4 as a translation regulator or as a structural element in genome organization, only the coding strand needs to be analyzed. However, the negative strand is formed later in the viral life cycle to serve as a template for genome strand amplification; thus, the negative strand-G4 might influence viral RNA replication. Therefore, we analyzed the presence of potential G4 motifs in both positive (coding) and negative (anticoding, complementary) TBEV genome RNA strands to directly obtain sequences with potential G4-mediated function for subsequent biophysical and biological studies and to show their conservation, which is considered a strong indicator of the G4 role. Overall analysis of G4 content in all known viruses and its relationship to virus pathogenicity was already reported (5,62). In contrast to these studies, we employed a combination of several G4-search algorithms, namely QGRS mapper (26), pqsfinder (27), G4 Hunter (28) and G4RNA screener (29), because various search algorithms identify quadruplexes using different conditions such as optimal G4 pattern (QGRS mapper, pqsfinder) or G to C ratio and tract length (G4Hunter, G4RNA screener) (63). Briefly, pattern-based algorithms (i) identify preferentially intramolecular G4, but (ii) cannot penalize cytosines that outcompete guanines in WC-pairs instead of Hoogsteen-hydrogen bonds in guanine tetrads; (iii) GC-based algorithms compensate for cytosines, but (iv) give a high score to oligo-G sequences unable to form intramolecular G4. None of the algorithms will automatically discard G4-prone sequences neighboring C-blocks that might outcompete G-blocks in Watson–Crick base pairs, as evaluated for the TBEV-1b sequence below, with sufficient efficacy and manual check of the hits needed to be performed. The analysis was performed using the genome sequence of the TBEV strain Neudoerfl (NCBI ref seq. NC_001672.1 or U27495.1, sequences are identical), which consists of 11 141 nt with 31.73% guanine and 22.04% cytosine content.

With a 40-nt maximum total length in QGRS mapper and pqsfinder, we did not observe any region within positive or negative RNA able to theoretically form a three or more-tetrad intramolecular quadruplex. Two-tetrad monomolecular RNA quadruplexes were predicted to be stable by theoretical methods (64) and our ongoing research supports their existence. It should be noted that the formation of their DNA counterparts strongly depends on additional stabilizing elements (capping base pairs or triads) resulting from primary sequence (65). However, direct experimental evidence of such RNA quadruplexes still has not been obtained. In the positive strand we observed 47 non-overlapping hits with QGRS mapper at threshold 19; 18 hits with pqsfinder at threshold 26; 18 hits with G4 Hunter at threshold 1.49 and 14 hits with G4 Screener (Figure 1). For hits identified by G4 Screener, we selected sequences with a score above the respective threshold (40 for cGcC, 1.49 for G4Hunter and 0.9 for G4NN) for at least two out of the three incorporated algorithms. The thresholds, dimensionless relative values, were set based on algorithm author recommendations or empirical comparisons with experimental data. In most cases, sequences predicted by G4Hunter or G4RNA Screener were predicted by QGRS mapper but not vice versa. We observed six sequences that were predicted by all four algorithms. Only one of them, TBEV-5, overlaps with some of the G4 sequences identified to be conserved within the genus *Flavivirus*, namely with NS5-A (15). We took all six predicted sequences for subsequent studies together with the TBEV-3 sequence which was predicted only by pattern-based algorithms. The TBEV-1b sequence is a 3'-extended variant of TBEV-1 that includes a native neighboring five-cytosine block. The observed sequences are listed in Table 1.

With the same search algorithms settings and thresholds, applied on the complementary i.e. negative strand, we observed only four non-overlapping hits with QGRS mapper, one hit with pqsfinder that overlaps with a QGRS mapper identified hit, one hit with G4 Hunter that is distinct from QGRS mapper/ pqsfinder hits and one with G4 Screener, overlapping the G4 Hunter hit (Supplementary Figure S1). Thus, even under relatively mild conditions, we did not identify any potential quadruplex-forming site within the sequence complementary to the TBEV reference genome.

Conservation of TBEV-selected G4 sites within the *Flavivirus* genus and among TBEV strains

We then checked the conservation within the *Flavivirus* genus (Figure 2), in terms of propensity to form G4, of regions both identified by us and those previously reported (15). G4 conservation was evaluated using the G4HunterTable utility (30), with extended sequences of interest selection on aligned genomes (see MM section). Sequences identified in (15) were taken as reported in associated SI, leading to lengths between 80 and 130 nucleotides. Sequences identified by us in the TBEV reference genome were extended by 20 nucleotides at each end to give a final length between 60 and 70 nt. We chose this approach, instead of selecting the part of the sequence with the highest

score, to integrate the potential effect of additional neighboring G- and C-tracts. Sequence length is also the reason why the values reported in Figure 2 are lower than the 1.49 score, generally accepted for stable G4. The varying lengths of selected sequences limits the possibility of direct comparison between various sequences and so only one sequence between different species or strains should be compared.

All the potential G4 regions identified previously (15) have a more or less conserved propensity to form G4 among the whole *Flavivirus* genus. Out of the G4 regions identified by us on a reference TBEV genome (NCBI ref seq. NC_001672.1) only the extended variant of TBEV-5 has relatively conserved G4-formation tendency among the whole *Flavivirus* genus (Figure 2). The G4-propensity of regions corresponding to other TBEV regions is significantly conserved only among tick-borne flaviviruses. TBEV-7 is located within the variable region of the 3' UTR, which is not present in all TBEV genomes, and its propensity to form G4 is more or less independent of phylogeny within the *Flavivirus* genus. The region around TBEV-3 shows a G4Hunter score close to zero due to the extension that leads to the incorporation of the C₆ tract at 5' proximity to the G4 site. G4Hunter scores of regions around TBEV-1 are reduced as well, compared to those observed above in a search mode, for a similar reason.

Similar to our approach to members of the *Flavivirus* genus above, we aligned 204 genomes of TBEV strains, prepared a rough phylogenetic tree and followed the propensity to form G4 of regions identified by us by calculating the G4Hunter score (Figure 3B). Sequences of extended TBEV regions, with a frequency of individual nucleotides in the TBEV set at specific positions, represented as RNA sequence logos, are shown in Figure 3A. The significant differences in G4Hunter scores are often the result of single nucleotide substitutions mostly inside contiguous G (negative effect on G4Hunter score) or C (positive effect on G4Hunter score) tracts. A significantly higher G4Hunter score for TBEV-4 in the European TBEV strains, especially compared with the Siberian subtype, is given by the presence of G or A at positions 7386 and 7392 (NCBI ref seq. NC_001672.1), potentially altering the G4 formation probability. Contrastingly, the lower G4Hunter score observed for the region around the TBEV-1 site of European strains is due to C occurring at positions 149 and 173 of the reference genome. The Far East and Siberian strains have in one or both positions U. In this case, the potential effect of particular nucleotides at the respective positions is not directly mediated by altering G4 but by altering the cytosine tract potentially outcompeting the guanines from G4 to a hairpin structure. These two effects of nucleotide variability at specific positions might quantitatively differ in real RNA: G4 is probably more sensitive to a disrupted continuous G4-tract than Watson-Crick base pairs-stabilized hairpin to disruption of continuous C-tract. In the case of the TBEV-5, used for subsequent interaction studies (see below), the dominant part of the variability in G4hunter score among TBEV strains is given by G/A substitutions disrupting two G-tracts, one in the middle of the studied region and one at 3' end (Figure 3A).

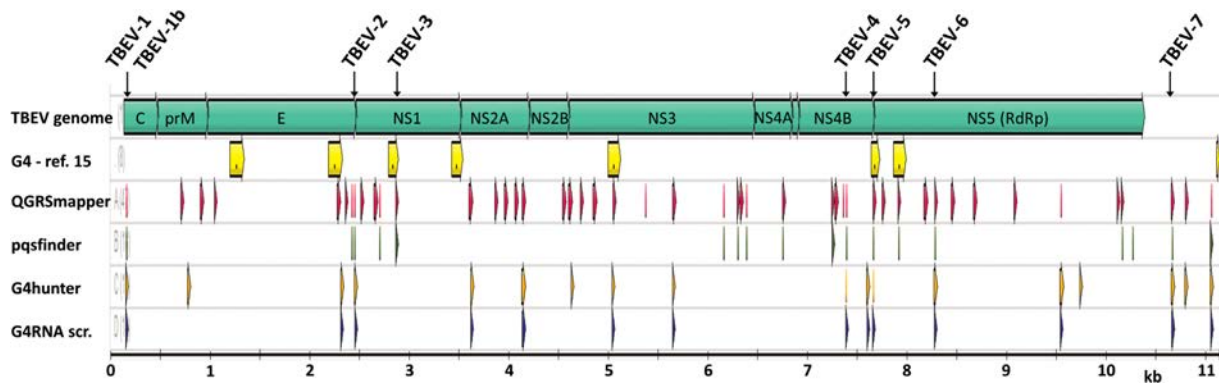


Figure 1. Localization of G4 (black labels with arrows on top) in tick-borne encephalitis virus (TBEV) genome (NC.001672.1) predicted using QGRS mapper (red), pqsfinder (green), G4 Hunter (orange) and G4 RNA Screener (blue). Yellow arrows in the second lane represent conserved G-rich regions reported in (15).

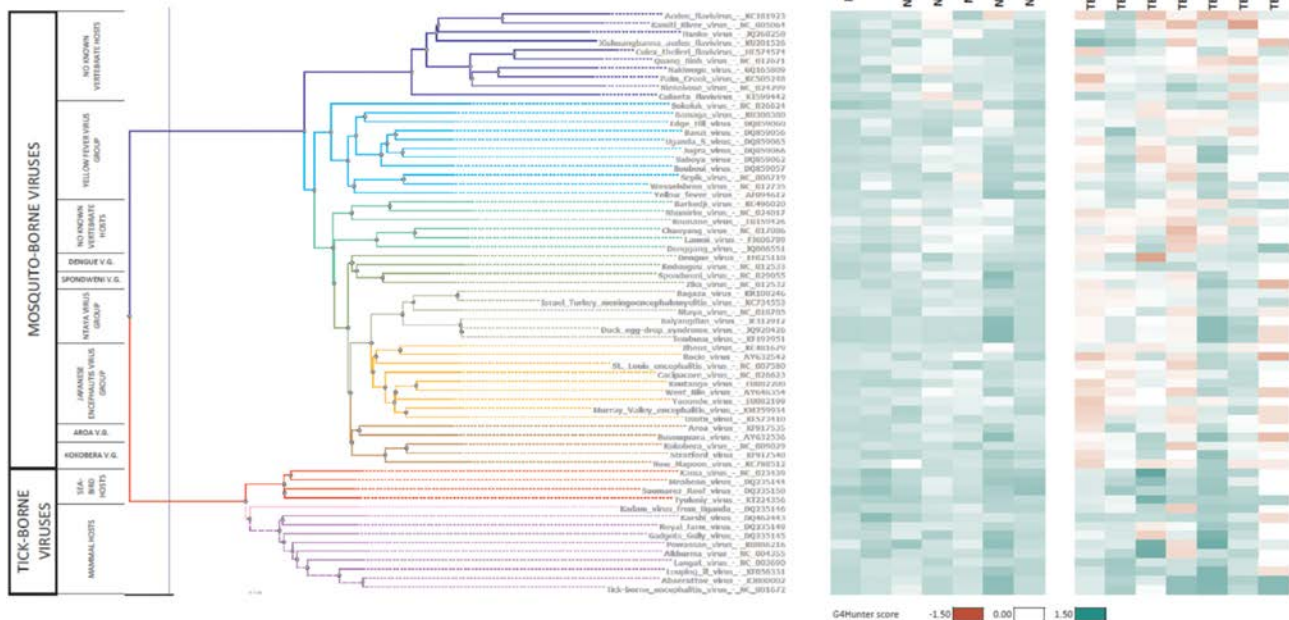


Figure 2. Phylogenetic tree of Flavivirus genus with distinguished main subgroups (left) and heat map representing G4-scores (right), calculated using G4HunterTable, for conserved potential G4 fragments identified by Fleming *et al.* (15) (first set) and by us (second set). Missing values for TBEV-7 correspond to genomes with missing primary sequence of this region in the database. The color coding ranges from red (score -1.5) through white (score 0) to green (score 1.5).

Biophysical properties of selected TBEV G4

Next, we experimentally verified the G4 formation of RNA sequences identified in the previous chapter on synthetic oligonucleotides using CD and UV absorption spectroscopy and native PAGE. As a positive control oligonucleotide that forms regular intramolecular three-tetrad parallel G4, we chose the sequence AAUGGGUGGGUGGGUGGGUAA (R-psG4), giving CD spectrum with a dominant positive peak at 263 nm with molar CD values around $180 \text{ M}^{-1} \text{ cm}^{-1}$ and negative CD peak around 240 nm, indicating parallel G4 (Figure 4). R-psG4, however, does not melt in $1 \times \text{IC}$ buffer below 90°C and the absorbance remains almost constant during temperature increase (Supplementary Figure S2). For each

TBEV oligonucleotide, we also designed a negative control of the same length with several guanines substituted by other bases (Table 1). All seven TBEV sequences (Table 1) produced in $1 \times \text{IC}$ buffer CD spectra with a positive peak around 263 nm (Figure 4A, C). The CD spectra of the TBEV-4 and to some extent also TBEV-7 correspond to the positive control and the spectra of TBEV-1, 2, and 5 have a similar shape but are reduced in the dominant positive peak at 263 nm. All these spectra significantly differ from that observed in low salt conditions (1 mM sodium phosphate buffer, pH 7), where we do not expect formation of any stable secondary structure, especially a guanine quadruplex. The addition of $1 \times \text{IC}$ buffer thus induces some kind of conformational change that corresponds to the formation of a parallel quadruplex. The negative controls of TBEV-1,

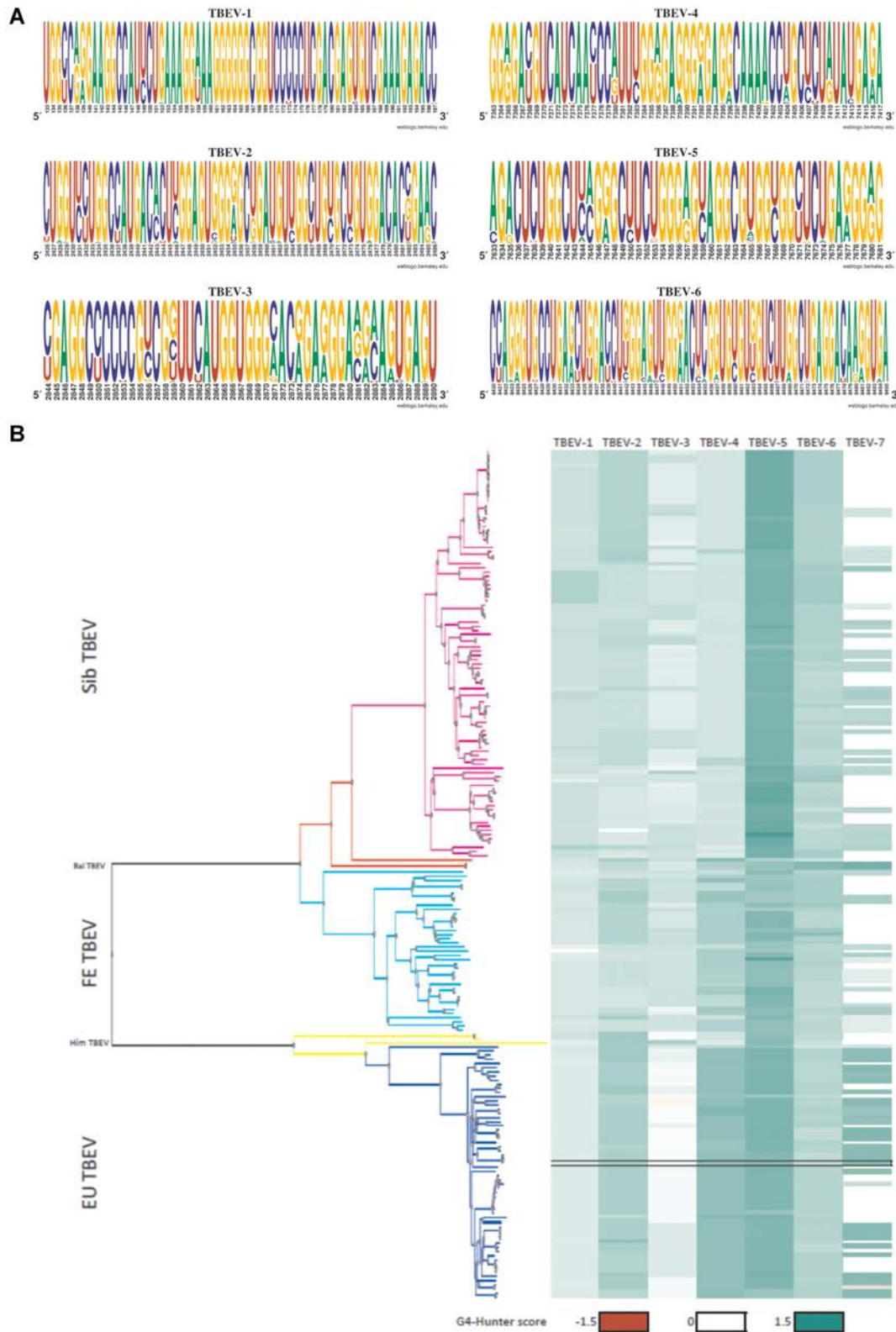


Figure 3. A) RNA sequence logos of the aligned set of 204 TBEV strains were prepared as frequency plots using the ‘weblogo’ tool (31). TBEV-7 sequence-based logo is not shown as only part of the TBEV strains contains this region. B) Phylogenetic tree of TBEV variants with distinguished main subgroups (left) and G4-scores (right), calculated using G4HunterTable, for conserved potential G4 fragments identified in chapter 3.1. Missing values for TBEV-7 correspond to genomes with missing primary sequence of this region in the database. The darker the green, the higher the G4 score. Reference sequence NC_001672.1 is highlighted.

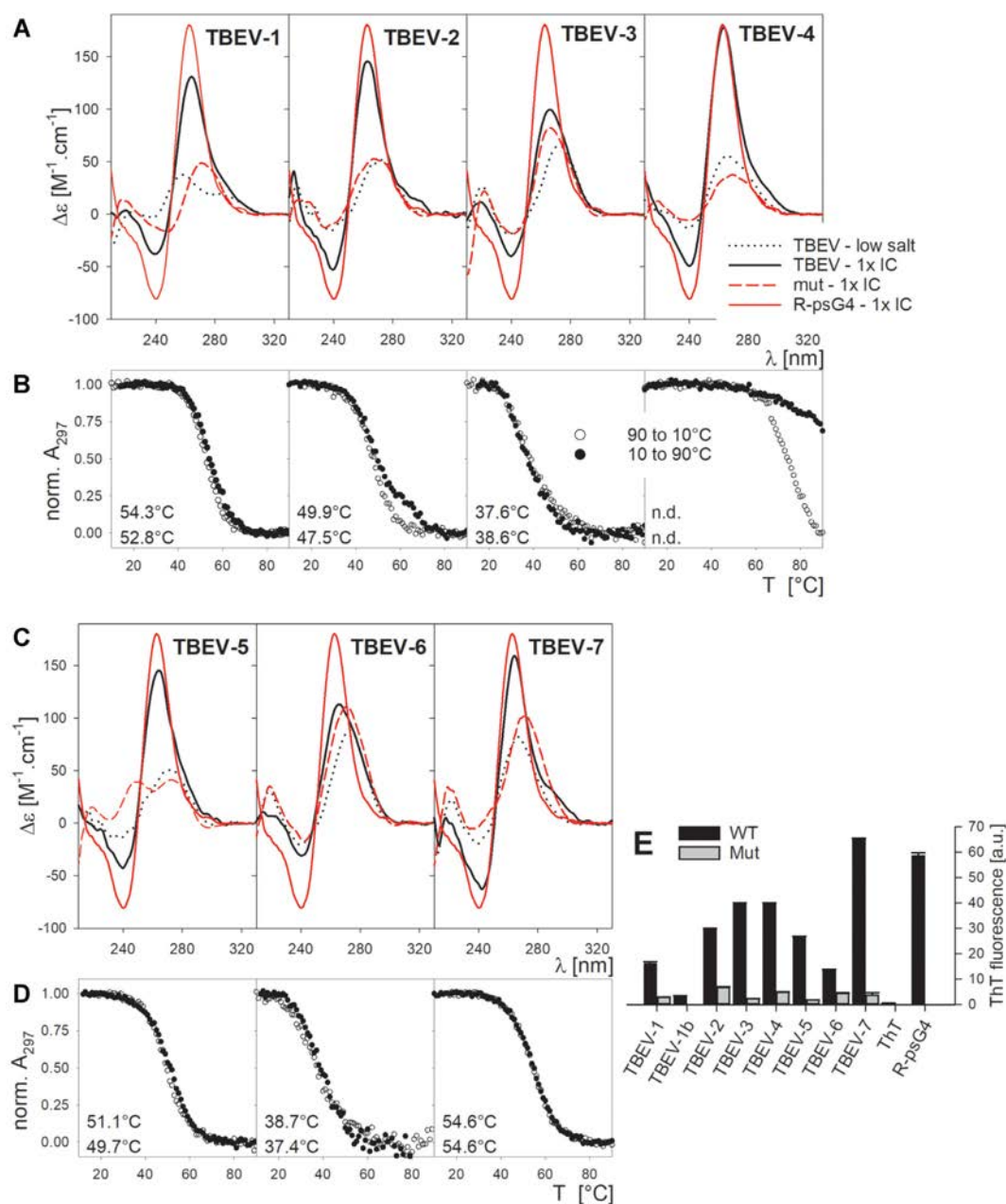


Figure 4. CD spectra (A, C), denaturation/renaturation curves (B, D) and fluorescence upon incubation with thioflavin T (E) of TBEV and control oligonucleotides. (A, C) CD spectra were measured in 1 mM sodium phosphate buffer, pH 7 (dotted black) and in 1x IC buffer (solid black). Red solid CD spectra correspond to reference oligonucleotide R-psG4. Red dashed CD spectra correspond to mutated variants of particular TBEV sequences. (B, D) Renaturation (empty circles) and denaturation (full circles) curves expressed from the absorbance at 297 nm, normalized to 0–1 scale using dual-baseline correction. Observed T_{den}/T_{ren} are shown. n.d. – values could not be determined. E: Fluorescence (in arbitrary units) of thioflavin T (ThT) upon incubation with TBEV oligonucleotides and their mutated variants in 1x IC buffer at room temperature.

2, 4, 5 and 7 provide CD spectra with significantly lowered 263 nm positive peaks with amplitudes close to the ones of wild-type sequences in low salt conditions (Figure 4A, C). CD spectra of TBEV-3 and TBEV-6 in 1x IC buffer have a low positive peak at 263 nm, differing in shape from the positive control, and the spectra are close in shape and amplitudes both to those observed in 1mM sodium phosphate buffer and to the respective negative controls. We suppose that there was only a limited formation of G4 for these oligonucleotides at the conditions we used,

thus the TBEV-3 and TBEV-6 are not suitable sequences for subsequent analyses. G4 formation of all wild-type sequences is supported by the sigmoidal melting profiles observed at 297 nm by absorption spectroscopy, from which melting temperatures were calculated (Figure 4B, D). The melting profile of TBEV-4 is, however, incomplete, due to extreme stability of the TBEV-4 quadruplex and the melting temperature could not be calculated. Such sigmoidal profiles are missing for the negative control oligonucleotides in the same conditions (Supplementary

Figure S3). All sequences with a high positive peak at 263 nm i.e. TBEV-1, 2, 4, 5 and 7, have melting temperatures close to or above 50°C and a significant negative TDS band at 297 nm, typical for some unusual secondary structures of nucleic acids including guanine quadruplexes (Supplementary Figure S4). TBEV-3 and TBEV-6 have melting temperatures much lower and at ambient temperature a significant fraction of unfolded oligonucleotides might exist (Figure 4B, C). Also, their thermal difference spectra show only a small negative peak around 297 nm, compared to other TBEV G4 supporting the reduced G4-formation propensity (Supplementary Figure S4). TBEV-2 and especially TBEV-4 show hysteresis between melting and annealing curves, indicating the presence of intermolecular G4 rather than a slowly forming intramolecular species. Native polyacrylamide gel electrophoresis (Supplementary Figure S5) provides smeared bands for most of the wild-type variants, indicating a mixture of different species in fast dynamic equilibrium. In the case of TBEV-2 and TBEV-4 the fraction of intermolecular species is much more significant, which makes them unsuitable for subsequent analyses. Based on the results of CD and melting experiments we expect that the negative controls do not form any stable secondary structure and thus they migrate as monomolecular species according to their length. The dominant bands of all wild-type oligonucleotides migrate either faster or at the same speed as the respective negative controls, indicating the formation of monomolecular species. For TBEV-6 we observed two electrophoretic bands corresponding to the monomolecular species. We assigned one band to G4 and the other to an unfolded species. All oligonucleotides mentioned above induce ThT fluorescence upon co-incubation, supporting G4 formation and no significant ThT fluorescence was observed upon interaction with any negative control oligonucleotide (Figure 4E). The ThT fluorescence intensity positively correlates with the stability of G4 and with the ability to form a monomolecular structure. As we mentioned in the first chapter of the Results section, the presence of a neighboring cytosine tract close to the potential quadruplex forming site might reduce the G4 formation ability, which might not be reflected by G4-search algorithms. We thus selected a 3' extended variant of TBEV-1 (TBEV-1b) involving a native five-cytosine block close to the G4 (Table 1). TBEV-1b provides a high positive CD peak around 265 nm of similar amplitude as the positive control, but at 210 nm provides a significant negative CD signal that was not observed for any of the above-mentioned wild-type oligonucleotides (Supplementary Figure S6). Such a shape of CD spectrum is usually attributed to the presence of double-helical DNA or RNA A-form (66). TBEV-1b does not provide a sigmoidal melting profile at 297 nm, typical for guanine quadruplexes, but we also did not observe a clear sigmoidal melting profile of TBEV-1b around 260 nm indicating the melting of an A-form structure (Supplementary Figure S6). TBEV-1b does not induce significant ThT fluorescence, which supports the absence of G4 formation. This 3' extended variant of TBEV-1 therefore does not form guanine quadruplexes, however, we cannot confirm our hypothesis that the neighboring cytosine tract might outcompete guanines necessary for G4 formation into an

alternative A-DNA structure. The inability of TBEV-1b to form G4 might thus be the result of a destabilizing effect of the significant 3' sequence extension, irrespective of cytosine content, when compared to TBEV-1.

For subsequent studies, we chose fragment TBEV-5 because (i) TBEV-5 is localized in the part of the genome coding viral NS5 protein with methyltransferase and RNA-dependent-RNA-polymerase activities, both crucial for TBEV RNA genome replication; (ii) TBEV-5 is present and conserved not only among various TBEV strains but also among the members of the *Flavivirus* genus (while TBEV-7 is missing for some strains); (iii) TBEV-5 forms a stable (in contrast to TBEV-3 or TBEV-6) mainly monomolecular (in contrast to TBEV-2 or TBEV-4) quadruplex and (iv) TBEV-5 is not adjacent to any cytosine-rich tract which could potentially disrupt G4 formation (in contrast to TBEV-1).

Interaction of TBEV-5 and its non-G4-forming variant with known G4 ligands

Next, we studied the interaction of TBEV-5 with several reported G4 ligands, namely *N*-methyl mesoporphyrin IX (NMM) (42,43), TMPyP4 (42,44), ThT (36), CV (38), TO (37), CX-5461 (48), 360A (47), PDS (33), cPDS (45,46), PhenDC3 (35), hemin (34), berberine (41), BRACO-19 (39) and aloe-emodin (40). We first used the TO fluorescence displacement assay (37,49), further accompanied by absorption spectroscopy and G4 stabilization assay (Figures 5 and 6). The combination of several assays was used because (i) the ligands might have different modes of interaction with G4, which could influence the results of the FID assay; (ii) for absorption titration, only several ligands give suitable absorption bands that are not affected by RNA presence, i.e. are localized at wavelengths longer than 310 nm and (iii) vice versa, some ligands absorb around 297 nm, which affects the G4 stability determination.

The FID assay was initially performed at 1 μM RNA, with either TBEV-5 or its non-G4 variant TBEV-5mut, 2 μM TO and 5 μM tested ligand. It should be noted that we observed a significant fluorescence of TO in the presence of TBEV-5mut, reaching around 40% of the TO fluorescence in the presence of TBEV-5 (Supplementary Figure S7A). This indicates low selectivity of TO for G4 structure, at least in the case of RNA G4. Moreover, TO probably causes G4 distortions as shown by CD at 5-time excess of TO to RNA (Supplementary Figure S7B). For comparison, we performed an FID assay also with ThT as a probe. ThT is very selective for G4, with only minimal fluorescence in the presence of TBEV-5mut, and neither distort existing G4 of TBEV-5 nor induce G4 formation by TBEV-5mut. For most ligands, the results of the FID assay with TO and ThT are comparable (Figure 5A). For TMPyP4, 360A and PhenDC3, we observed almost 100% displacement of the probe, indicating excellent TBEV-5 binders. BRACO-19 displaces 60–80% of the probe, 50–70% displacement was observed for NMM and 20–40% for CV, CX-5461, PDS, cPDS and hemin. Aloe-emodin did not significantly displace ThT. Generally, ThT is displaced to a greater extent than TO. Interestingly, berberine displaced around 50% of ThT but did not displace TO. The reciprocal experiment showed that TO almost entirely displaces ThT in TBEV-5

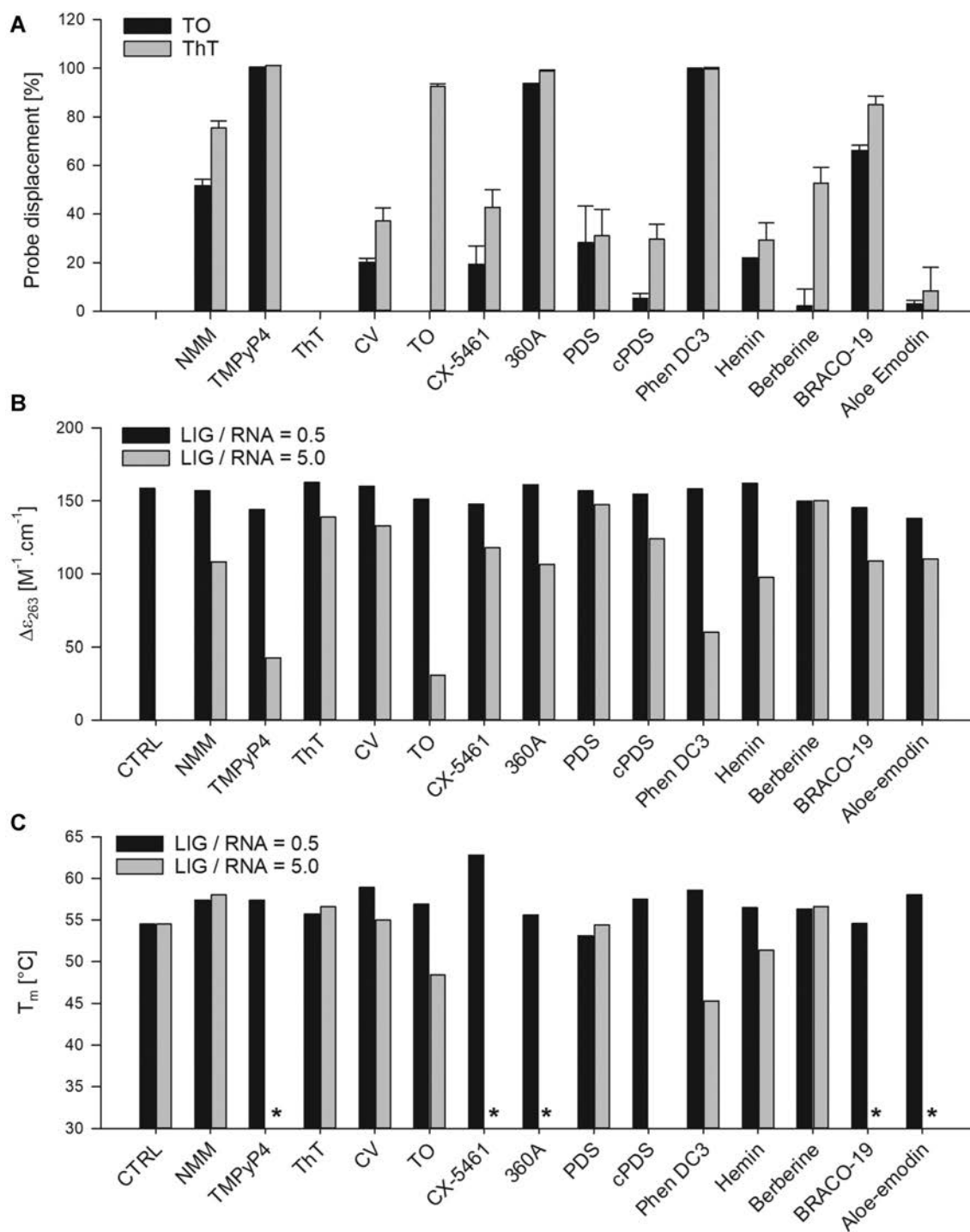


Figure 5. (A) Relative displacement of TO or ThT in FID experiment by various ligands. (B) Molar CD at 263 and (C) melting temperatures of TBEV-5 alone (CTRL) and in the presence of ligands at two different ratios after titration experiments, where TBEV-5 was titrated into a fixed amount of ligand (LIG/RNA = 0.5) or, vice versa, ligands were titrated to a fixed amount of TBEV-5 (LIG/RNA = 5.0). * Corresponds to cases where the experimental data do not allow T_m calculation.

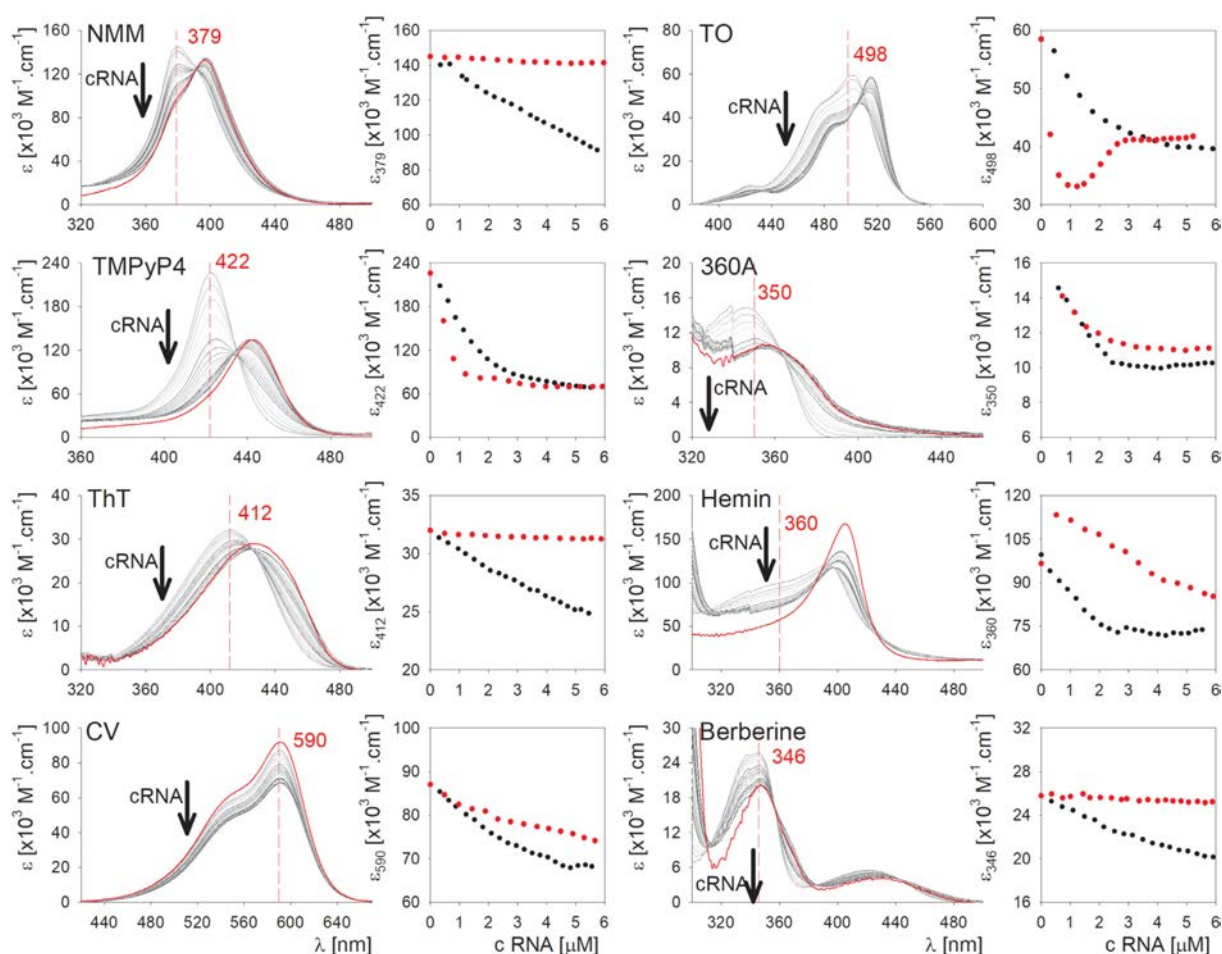


Figure 6. Molar UV absorption spectra of ligand ($4 \mu\text{M}$) with increasing concentration of TBEV-5 RNA in the ligand absorption region, measured at 23°C in $1 \times \text{IC}$ buffer and molar absorptivity of ligand at selected wavelength as a function of concentration of TBEV-5 (black circles) or TBEV-5mut (red circles). Red dashed line in spectra indicates wavelength used for absorbance versus RNA concentration plot. Red spectrum corresponds to the starting spectrum from the reverse experiment, where ligand was titrated into RNA corresponding to 1:5 ligand to RNA ratio.

G4 but ThT does not displace TO at all, indicating TO as a stronger binder than ThT but with limited G4 selectivity (see above). We did not observe any significant fluorescence of TBEV-5 or TBEV-5mut alone or with any of the used ligands in the absence of TO or ThT at respective settings.

In the next step, we followed the absorbance of ligands in the visible light region upon titration with TBEV-5 and TBEV-5mut RNA (Figure 6). In the visible region, where there is no absorbance interference of the RNA, only NMM, TMPyP4, ThT, CV, TO, 360A, Hemin and berberine provide significant absorption bands and so titration data of only these ligands are presented. For CV titration, we did not observe isosbestic points that are associated with the presence of two spectral components belonging to free and bound ligands at different ratios. Moreover, the ligand-RNA interaction-induced changes in absorption of TO and, in the case of TBEV-5mut, hemin are quite complex. TBEV-5 binds all tested ligands at $4 \mu\text{M}$ concentration at the micromolar range (Figure 6) with TMPyP4 reaching 50% TBEV-5 saturation at lowest concentration, thus being the best binder. However, a control experiment with TBEV-5mut, which does not form G4, showed that TMPyP4, TO,

and 360A provide similar titration curves and thus bind non-specifically. We identified NMM, ThT, berberine and hemin as ligands that specifically bind G4, though the concentration necessary for 50% saturation of TBEV-5 G4 is higher than in case of TMPyP4, indicating lower binding affinity. A reverse experiment where the ligand was gradually titrated into a fixed amount of RNA (Supplementary Figure S8) confirmed these results. The absorption spectra of the fully bound ligand (Figure 6) were observed during the reverse experiment at which the ligand to RNA ratio was around 5 to 1. Precise determination of the dissociation constant and binding stoichiometry for all ligands was impossible due to the complex absorbance changes upon titration of some ligands with TBEV-5 or insignificant absorbance changes after titration with mutated variant TBEV-5mut at the selected ranges of concentrations.

After the titration experiments we measured CD spectra of TBEV-5 and TBEV-5mut in the presence of ligands (Supplementary Figures S8 and S9) to see whether the ligands disrupt G4 formed by TBEV-5 or support G4 formation, possibly also in the case of TBEV-5mut. For the RNA-to-Ligand experiment (Figure 6), the final ratio of ligand

to RNA was 1 to 2, whereas for the Ligand-to-RNA experiment (Supplementary Figure S8), the final ratio of ligand to RNA was 5 to 1. For simplicity, we express only CD at 263 nm (Figure 5B). At 5-times ligand excess, all ligands except berberine and, to a lesser extent, ThT, CV, and PDS, decrease CD at 263 nm, indicating G4 structure alterations. The effect is most pronounced for TMPyP4, TO, and PhenDC3. At 1:2 ligand to RNA ratio, only small changes in CD were observed. Ligands do not cause significant changes in the CD of TBEV-5mut that could be attributed to induction of the G4 formation (Supplementary Figure S9).

Finally, we determined the stability of TBEV-5 G4 in the presence of interacting ligands. At 5-times molar excess of ligand, mild stabilization, represented by an increase in T_m up to 3.5°C, was observed only for NMM, ThT and berberine, i.e. ligands previously identified as specific G4 binders (Figure 5C). 360A seems to significantly increase T_m as well but the melting curve is partially distorted and the observed stabilization is not convincing. The other ligands either destabilize TBEV-5 or cause a strong distortion of melting curves, as in the case of BRACO-19, CX-5461, PhenDC3, TO, cPDS, aloe-emodin and TMPyP4. At 1:2 ligand to RNA ratio, all ligands except PDS and BRACO-19 moderately increase melting temperature by no more than 5°C. We did not observe any sigmoidal melting curves expressed from the absorbance at 297 nm for TBEV-5mut in the presence of any of the tested ligands (Supplementary Figure S10). This confirms the CD data and indicates that none of the ligands can induce G4 formation on the altered sequence.

Recently, BRACO-19 and TMPyP4 were shown to specifically interact with RNA G4 derived from the Nipah virus (67) and ZIKV genomes (17). The reported specificity of TMPyP4 towards RNA G4 contrasts with our results (Figure 6).

Activity of flaviviral RNA-dependent RNA polymerase in the presence of G4 ligands and on mutated TBEV-5 templates

The generally expected mechanism of action of the G4 ligands is based on the stabilization of viral genomic G4s, which impedes the progress of viral polymerase and causes viral replication errors. We therefore tested the effect of selected G4 ligands of flaviviral RNA-dependent-RNA-polymerase, in our case derived from the Japanese encephalitis virus, to synthesize the complementary strand. For this study, we limited the repertoire of used ligands, based on the results presented in the previous chapter, to: NMM, which is a selective and good G4 binder; PDS and cPDS, both excellent G4 binders according to the FID assay; berberine, reported antiviral compound with modest G4-binding ability and good selectivity; PhenDC3, a very strong G4 binder and TMPyP4, the most widely used G4 ligand as a reference with excellent G4 affinity, though G4 non-specific. All ligands were tested at 50, 10 and 2 μ M concentrations. Besides the wild-type template (*WT*) containing the TBEV-5 sequence, we prepared for the experiment three mutant variants (Figure 7A). The *positive* mutant has four U to G substitutions and one G to A, resulting in a sequence with a G₃NG₄N₄G₃NG₃ pattern that

is able to form a three-tetrad G4 of substantial thermodynamic stability (68). The *negative* mutant has three G to A substitutions, compared to the wild-type, resulting in a G₂NG₂N₇G₂NG₂ pattern, still theoretically able to fold into a two-tetrad monomolecular G4. The repertoire of codons for glycine, however, does not allow the introduction of more G4-destabilizing mutations. Positive and negative mutants code for synonymous codons as wild-type and therefore do not alter the amino acid sequence of the subsequent translation product. The *super-negative* mutant contains one more G to C substitution, compared to the negative, resulting in further disruption of one G2 block but at the expense of the change of a codon from Gly to Ala. It has to be noted that even though the synonymous codons code for the same amino acid, the usage of these codons, as well as the amount of corresponding tRNAs etc. might differ. This should not affect the *in vitro* polymerase stop assay but might somehow influence subsequent biological assays. As a reference experiment, we performed an analogous polymerase stop assay involving commercial reverse transcriptase (RT) SuperScript IV that was described to stall on RNA G4 in template strands (69). The activity of enzymes is measured as a ratio of full product of the new strand synthesis to the total labelled DNA or RNA and normalized to the control experiment with no ligand.

Using a *wild-type* template we observed around 1% of labelled primer extended by polymerase into a full product RNA (Figure 7B, Supplementary Figure S11 and S12). All tested ligands significantly inhibited RdRp synthesis of RNA in a concentration dependent manner (Figure 7C, Supplementary Figure S11). PhenDC3, PDS, cPDS and TMPyP4 reduce the activity to <10% of the no-ligand control even at 2 μ M ligand concentration. NMM decreases the activity to around 15% at 50 and 10 μ M and 35% at 2 μ M. Berberine has strong inhibitory effect only at 50 μ M concentration but at 10 and 2 μ M >50% of the RdRp activity is retained. In control experiment with reverse transcriptase, we observed with *wild-type* template around 30% of labelled primer converted into a full product DNA (Figure 7D, Supplementary Figure S13 and S14). The reverse transcription experiment confirmed the most pronounced inhibitory activity of PhenDC3 ranging from a reduction to <10% at 50 μ M ligand to 40% at 2 μ M and a modest inhibitory effect of PDS and cPDS between reduction to <10% and 25% at 50 μ M of PDS or cPDS, respectively and 60–70% at 2 μ M ligand (Figure 7E, Supplementary Figure S13). NMM and TMPyP4 inhibits reverse transcriptase only at 50 μ M and berberine does not inhibit RT even at 50 μ M concentration. TMPyP4 at 50 μ M concentration causes the formation of a smear on denaturing PAGE of the RdRp products that prevents correct quantification of the RdRp activity. We did not observe any such smear on the denaturing PAGE of RT products.

Using a *positive* template led to almost complete inhibition of full product synthesis by RdRp, even in the control experiment (Figure 7B), i.e. irrespectively of the presence of any ligand. In the case of reverse transcription on the *positive* template, we observed a reduction of full product ratio from 40% to 15%, i.e. by more than 50%, compared to the *wild-type* template (Figure 7D). Moreover, the RT on the *positive* template is much more sensitive to the

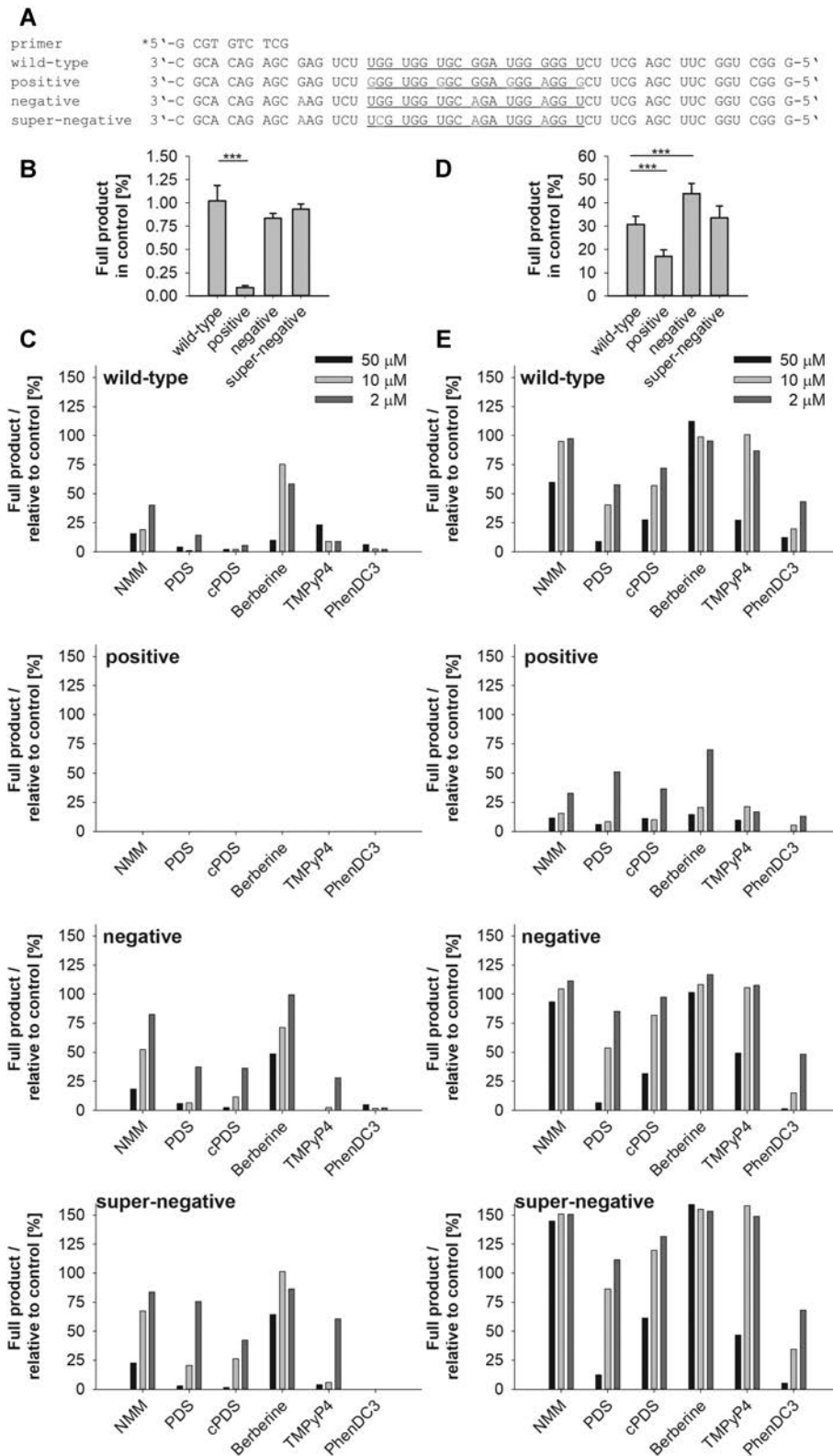


Figure 7. Fraction of full products of the polymerization reaction using four different templates (A), catalyzed by Japanese encephalitis virus RdRp (B and C) or SuperScript IV reverse transcriptase (D and E), in the presence of three concentrations (50, 10 and 2 μ M) of six tested G4 ligands. (A) Primer and templates used for polymerase reactions. Underlining indicates TBEV-5 region. Red letters indicate nucleoside substitutions relative to wild-type. In case of JEV RdRp a RNA variant of primer, with U instead of T, was used. (B and D) Relative ratio of full product within whole control lane in JEV RdRp (B) and SuperScript IV (D) reactions. (C and E) Relative amount of full product in the presence of different concentrations of various G4 ligands normalized to the amount in control sample (no ligands). Data in panels (B) and (D) represent mean \pm SD from three-four independent experiments. *** $P < 0.001$ (unpaired t -test).

presence of ligands. We observed a reduction in full product synthesis to less than 20%, compared to no-ligand control, for all samples except the lowest (2 μM) concentration of NMM, PDS, cPDS and berberine. The results of RdRp on *negative* and *super-negative* templates are quite similar. We did not observe significant change in full product fraction, compared to the *wild-type* template (Figure 7B). Interestingly, PhenDC3 still almost completely inhibits the activity of RdRp on both templates which might indicate inhibitory effects unrelated to the formation of G4 though no significant effect of PhenDC3 on HCV RdRp when using a non-G4 template has been reported (12). Compared to the *wild-type* template, all other ligands have a much lower inhibitory effect on RdRp synthesis at 10 and 2 μM concentration but still almost fully prevent RNA synthesis at 50 μM . The RdRp inhibitory effect is lowest in case of berberine and NMM where the ratio of full product reaches 70–100% of the control. Reference experiments with RT (Figure 7E) confirmed the strong inhibitory effect of PhenDC3 even at 10 μM concentration and PDS at 50 μM . cPDS and TMPyP4 significantly inhibits RT only at 50 μM , but at 10 and 2 μM concentrations no reduction or even increase of full product synthesis was observed. NMM and berberine did not inhibit RT even at 50 μM concentration on *negative* and *super-negative* templates. Interestingly, with RT we observed significant increase in full product fraction with *negative* template but not with the *super-negative* one, when compared to the *wild-type* template (Figure 7D).

Because the TBEV is a typical vector-borne pathogen, we took into account that TBEV replication occurs not only at 37°C in mammal hosts, but also at a considerably lower temperature in tick cells. We tested the RdRp activity also at 28°C and 20°C and we added two RNA templates that were derived from TBEV-3 and TBEV-6 regions (Supplementary Figure S15A); i.e. representing quadruplexes with lower thermodynamic stability, compared to TBEV-5 *wild-type*. First, our RdRp cannot efficiently synthesize RNA at 20°C (Supplementary Figure S12 and S15B). At 28°C the fraction of full product RNA is still reduced, compared to the reaction performed at 37°C, but the relative ratio of full product RNA between reaction with *wild-type*, *positive*, *negative* and *super-negative* template is similar to that at 37°C. Interestingly, the template derived from the TBEV-3 region does not allow efficient synthesis of RNA with RdRp even at 37°C. Control experiment with reverse transcriptase (Supplementary Figure S14 and S15C), however, clearly shows that TBEV-3 template allows synthesis of DNA. We thus hypothesize that the TBEV-3 template, or the nascent product might form and alternative structural motif that can be efficiently overcome by reverse transcriptase but not by flaviviral RdRp. TBEV-6 derived template behaves comparably to the TBEV-5 *wild-type* one.

In conclusion, our results indicate that the activity of flaviviral RdRp is strongly inhibited by the presence of G4 and can be further modulated by small-molecule ligands. The ability of G4 ligands to inhibit RdRp activity does not correlate with the G4 selectivity of the ligands but with their ability to bind RNA, including non-G4-forming variants. This might indicate G4-nonspecific inhibitory effects.

The effect of G4-ligands on TBEV replication

Based on our observation that the studied G4 ligands interacted with G4s derived from the TBEV genome sequence, we next explored their ability to suppress TBEV replication in cell-based systems. To study the biological properties of G4 ligands, we firstly evaluated the influence of the ligands on cell viability to determine their cytotoxicity for PS cells. Cytotoxicities of the G4 ligands were studied after 48-h cultivation in the presence of the compound concentration range of 0–50 μM . Notably, TO and CV displayed the highest cytotoxicity of all compounds tested and were characterized by CC_{50} values <2 μM (Figure 8A, Table 2). Relatively high cytotoxicities were also observed for CX-5461 and ThT, which showed CC_{50} values of <15 μM (Figure 8A, Table 2). These compounds were therefore excluded from further antiviral analyses. The observed cytotoxicities could be ascribed to a low selectivity of G4 ligands toward viral versus cellular G4s; these compounds could bind and (de)stabilize cellular G4s resulting in a significant decrease in cell proliferation and metabolic activity. A low selectivity of G4 ligands results from their molecular structure: most G4 ligands are composed of a large planar aromatic core that stacks on the G tetrad, reducing the probability of discrimination / recognition among different G4s (4). On the other hand, PDS, cPDS, NMM, TMPyP4, hemin, 360A, PhenDC3, BRACO-19, berberine and aloe emodin exerted good cytotoxicity profiles when used for PS cell treatment and their CC_{50} values exceeded the highest tested concentration (>50 μM) (Figure 8A, Table 2). Notably, we determined that PS cells treated with 50 μM of NMM displayed observable changes in cell morphology and in mechanical monolayer cohesion, although the metabolic activity and viability of the cells were not altered. Based on this finding, we used a maximal NMM concentration of 25 μM for all further *in vitro* experiments (apart from 50 μM as it was used for other G4 ligands). The G4 ligands with no/negligible cytotoxicity were selected for subsequent studies of ligand-mediated anti-TBEV activity.

A series of ten G4 ligands previously observed to show low cytotoxicity for PS cells was initially evaluated for their anti-TBEV potency in PS monolayers. In this initial screening, all compounds were tested against two TBEV strains Neudoerfl and Hypr, at a single concentration of 50 μM 48 h.p.i. We observed that hemin, 360A, BRACO-19 and aloe emodin (at 50 μM) showed no virus inhibition effects *in vitro* (Figure 8B). Our results with BRACO-19 contrast with results observed for the ZIKV virus, another member of the *Flavivirus* genus (17) where BRACO-19 was reported to decrease ZIKV virus titers at 100 μM concentration significantly. It is likely that these G4 ligands display poor cellular up-take into PS cells, as reported for numerous compounds having high molecular weights and/or protonated side chains on their molecules (4). Alternatively, they could be rapidly inactivated/degraded by cellular catabolism enzymes. As such, these mechanisms could be attractive targets for further investigation.

In contrast, PDS, cPDS, NMM, TMPyP4, PhenDC3 and berberine suppressed replication of both TBEV strains, which corresponded to a decline of viral titers 10^2 to 10^4 -fold compared with control cells (Figure 8B). The most sub-

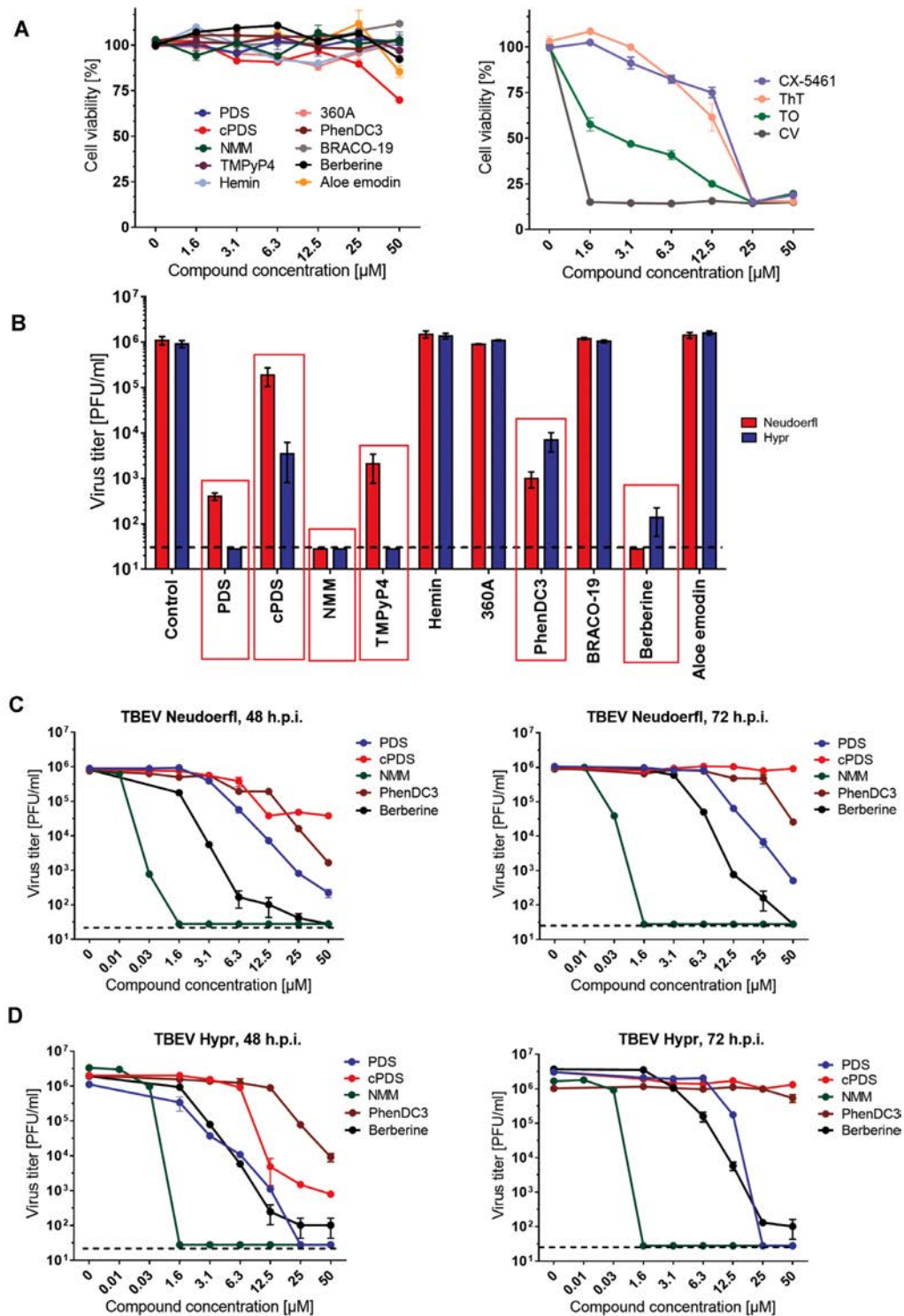


Figure 8. Antiviral activity and cytotoxicity of G4 ligands in cell-based assays. (A) Cytotoxicity of the indicated G4-ligands for porcine kidney stable (PS) cells determined in a concentration range of 0–50 μM and expressed as a percentage of cell viability. PS cells were seeded in 96-well plates for 24 h, then treated with G4 ligands and incubated for 48 h. (B) Inhibition of TBEV replication by the indicated G4-ligands. PS cell monolayers were treated with the indicated G4 ligands (50 μM) and simultaneously infected with TBEV strains Neudoerfl and Hypr at MOI of 0.1. The infected cells were then incubated with the compounds for 48 h. Following incubation, media supernatants were collected and viral titers were determined using a plaque assay and expressed as PFU/ml. Compounds PDS, cPDS, NMM, TMPyP4, berberine and PhenDC3 (marked in red) were selected for further evaluation of their antiviral potencies. (C, D) The dose-dependent anti-TBEV activities of the indicated G4-ligands were determined for TBEV Neudoerfl (C) and Hypr (D) strains. PS cell monolayers were treated with the compounds at concentrations of 0–50 μM and infected with the respective TBEV strain at MOI of 0.1. The infected cells were then incubated with the compounds for 48 h p.i. or 72 h p.i. and viral titers were determined using the plaque assay. The mean titers from three biological replicates of two independent experiments are shown and error bars indicate standard errors of the mean ($n = 3$). The horizontal dashed line indicates the minimum detectable threshold of $1.44 \log_{10}$ PFU/ml.

Table 2. Antiviral and cytotoxicity properties of G4-ligands incubated with virus-infected PS cells for 48 h.p.i.

G4-ligand	Neudoerfl		Hypr		CC ₅₀ [μM] ^{a,c}	95% CI	SI (CC ₅₀ /EC ₅₀)	
	EC ₅₀ [μM] ^{a,b}	95% CI	EC ₅₀ [μM] ^{a,b}	95% CI			Neudoerfl	Hypr
PDS	2.94	2.80 to 3.09	1.29	0.94 to 1.77	>50	-	>17.01	>36.76
cPDS	4.45	3.40 to 5.82	5.52	4.92 to 6.20	>50	-	>11.23	>9.05
NMM	0.01	0.005 to 0.028	0.02	0.021 to 0.023	>50	-	>5000	>2 500
TMPyP4	N.D. ^d	-	N.D. ^d	-	>50	-	-	-
Hemin	>50	-	>50	-	>50	-	>1	>1
360A	>50	-	>50	-	>50	-	>1	>1
PhenDC3	5.77	4.82 to 6.91	5.68	4.74 to 6.81	>50	-	>8.66	>8.08
BRACO-19	>50	-	>50	-	>50	-	>1	>1
Berberin	1.26	1.08 to 1.48	1.57	1.51 to 1.64	>50	-	>39.68	>31.84
Aloe emodin	>50	-	>50	-	>50	-	>1	>1
CX5461	^e	-	^e	-	14.14	12.20 to 16.39	-	-
ThT	^e	-	^e	-	10.56	9.18 to 12.14	-	-
TO	N.D. ^f	-	N.D. ^f	-	1.80	1.43 to 2.28	N.D.	N.D.
CV	N.D. ^f	-	N.D. ^f	-	<1.60	-	N.D.	N.D.

^aDetermined from three independent experiments.

^bExpressed as a 50% reduction in viral titers and calculated as inflection points of sigmoidal inhibitory curves, which were obtained by a nonlinear fit of transformed inhibitor concentrations versus normalized response using GraphPad Prism 7.04 (GraphPad Software, Inc., USA).

^cExpressed as a 50% reduction in cell viability and calculated as inflection points of sigmoidal viability curves, which were obtained by a nonlinear fit of transformed inhibitor concentrations versus normalized response, see ^b.

^dWe were not able to evaluate the anti-TBEV effects of TMPyP4 accurately. Repeated virus cultivations in the presence of TMPyP4 provided extremely variable results that were not consistent enough to calculate the exact EC₅₀ values.

^eNo antiviral effect was observed at the lowest non-cytotoxic concentration of 5 μM.

^fAntiviral activities of TO and CV were not determined, as both compounds were highly cytotoxic (reduction of cell viability by ≥50%) in the tested concentration range (1.6–50 μM).

N.D.; not determined

stantial anti-TBEV effect was observed for NMM (EC₅₀ in nanomolar values; Table 2); this compound completely suppressed TBEV replication at 1.6 μM. Anti-TBEV activities of PDS and berberine were in low micromolar levels with the EC₅₀ values ranging from 1.2 to 2.9 μM for both studied TBEV strains. Anti-TBEV activity for PDS, berberine, and NMM became stable over time and was observable in both experimental intervals, 48 and 72 h.p.i. (Figure 8C and D). Other G4 ligands, cPDS and PhenDC3, showed EC₅₀ values around 5 μM. However, both compounds exerted only partial inhibitory effects on virus replication being manifested by virus titer decrease by 1.5 to 3 orders of magnitude at the highest concentration tested (50 μM). Anti-TBEV effects of cPDS and PhenDC3 gradually disappeared or dropped significantly at 72 h.p.i. Unfortunately, we were not able to evaluate the anti-TBEV effects of TMPyP4 accurately. Repeated virus cultivations in the presence of TMPyP4 provided highly variable results that were not consistent enough to calculate the exact EC₅₀ values (Table 2).

Furthermore, the anti-TBEV effects of G4 ligands identified in viral titer inhibition assays were confirmed by immunofluorescence staining, which was used to evaluate the expression of TBEV surface E antigen in the infected cells (Figure 9A-D). The E protein was highly expressed in virus-infected mock-treated cells; approx. 30% and 60% of virus antigen expressing cells were observed in Neudoerfl- and Hypr-infected cells, respectively (Figure 9A-D). The relatively low percentage of virus antigen expressing cells can be attributed to the fact that the virus antigen expression was monitored at the time interval of 48 h.p.i. In this time interval, the inhibitory effects of G4 ligands were very well observable but this time was not enough for the virus to

spread to all the cells in the monolayer. This was particularly true for the TBEV Neudoerfl strain which is, moreover, characterized by a considerably lower replication capacity compared with the TBEV Hypr strain (70). In contrast, we detected a highly reduced or completely suppressed viral protein E expression in cell monolayers treated with PDS, cPDS, berberine and PhenDC3 at concentrations of 10 and 50 μM, and with NMM at the concentration of 10 and 25 μM at 48 h.p.i. (approx. 5% and 2% of infected cells observed for ligand concentrations 10 and 25/50 μM, respectively, Figure 9A-D).

The inhibitory effect of the G4 ligands on TBEV replication was further demonstrated on a TBEV RNA level using RT-qPCR. All studied compounds (at concentrations of 10 and 50 μM, for NMM at concentrations of 10 and 25 μM) caused a dose-dependent reduction of viral RNA copies in the infected cell culture at 48 h.p.i. The strongest inhibitory effect was demonstrated for NMM (a complete inhibition of RNA synthesis at 25 μM for both TBEV strains) whereas the weakest inhibitory activity was observed in berberine, which, however, reduced numbers of viral RNA copies by about 40% for Hypr and 25% for Neudoerfl (Figure 9E, F). Our results clearly show that the studied G4 ligands have a direct effect on TBEV RNA replication.

We further tested the anti-TBEV activity of PDS, cPDS, berberine, PhenDC3 (at 50 μM) and NMM (at 25 μM) using an adhesion assay to demonstrate in which step of the viral replication cycle the G4 ligand-mediated inhibitory effect is exerted (Supplementary Figure S16). This assay should distinguish the compounds differing in a mechanism of antiviral action which can thus be divided into two groups: 1) compounds affecting the virus adsorption/fusion and 2) compounds acting inside the infected cells and im-

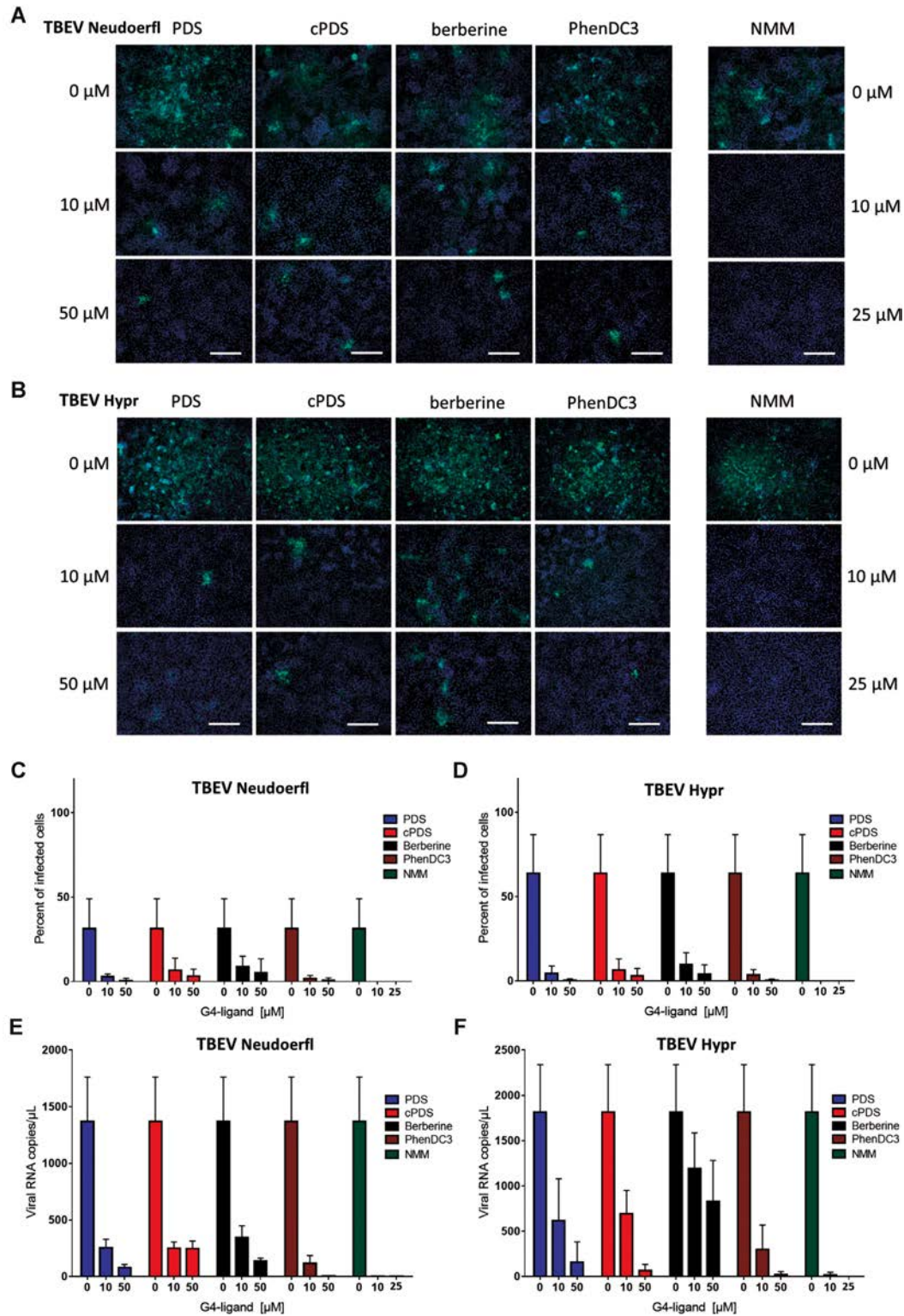


Figure 9. Inhibition of TBEV surface antigen expression and viral RNA synthesis by G4 ligands. (A, B) Fluorescence staining of PS cell culture infected with the TBEV Neudoerfl (A) and Hypr (B) strain at a MOI of 0.1 in the presence of G4 ligands at the indicated concentrations. PS cells were fixed on slides at 48 h post-infection, stained with mouse flavivirus-specific antibody as a primary antibody, and anti-mouse goat secondary antibody conjugated with FITC (green) and counterstained with DAPI (blue). Scale bars, 200 μm. (C, D) The level of TBEV Neudoerfl (C) and Hypr (D) antigen expression in the presence of G4 ligands was quantified and expressed as a percentage of infected (viral antigen expressing) cells relative to mock-infected cells. Mean percentage of infected cells from two independent experiments are shown and error bars indicate the standard errors of the mean ($n = 3$). (E, F) The effect of G4 ligands on TBEV Neudoerfl (E) and Hypr (F) RNA copy numbers was studied using quantitative real-time PCR (RT-qPCR). The mean viral RNA copy numbers/μL are shown and error bars indicate standard errors of the mean (Neudoerfl: $n = 15$ for controls, $n = 3$ for individual ligand-treated samples; Hypr: $n = 30$ for controls, $n = 6$ for individual ligand treated samples).

pairing virus replication/assembly machinery. This assay revealed that the antiviral action of PDS, cPDS, berberine, and PhenDC3 (at 50 μM) takes effect in the post-entry/fusion phase of the viral replication cycle (mechanism 2) (Supplementary Figure S16). The mode of action of PDS was recently studied also by Zou *et al.* (18) showing that PDS is involved in the ZIKV replication period rather than entry which is in agreement with our observations. To confirm these results, we performed the transfection of the isolated viral RNA pre-treated with the selected ligands (i.e. berberine and PDS at 0, 10, 50, and 200 μM). We hypothesized that if the ligand interacts directly with the viral RNA then the transfected viral RNA pre-treated with the ligand has a decreased capacity to be replicated, transcribed or translated to form viable viral particles, being manifested by a decrease in viral titers. Indeed, after transfection of viral RNA pre-treated by berberine or PDS we observed a partial (for berberine at 0–200 μM and for PDS at 10 μM) or a complete (for PDS at 50 and 200 μM) suppression of infectious viral particle formation (Supplementary Figure S17). These results support our previous findings that berberine and PDS showed anti-TBEV activity based on the ligand-viral RNA interaction. This mechanism of action can also be expected for cPDS and PhDC3.

On the other hand, the adhesion assay showed that NMM (at 25 μM) caused virus inhibition prior to the entry/fusion steps of the viral replication cycle (mechanism 1) (Supplementary Figure S16). This is not surprising as porphyrins with negatively charged/polar site chains were previously demonstrated to incorporate into liposomes (71,72) and viral envelopes to act as viral entry/fusion inhibitors (73–76). However, it is interesting that when we transfected the viral RNA pre-treated with NMM at 25 and 200 μM , no viable viral particle formation was observed (Supplementary Figure S17). We can speculate that NMM could have multiple modes of antiviral action; 1) this compound blocks the viral entry/fusion machinery and also 2), when crossing the plasmatic membrane, interacts with viral RNA and suppresses viral genome replication. The latter hypothesis (the antiviral activity of NMM based on ligand-viral RNA interaction and G4 stabilization) was supported by our biophysical results as well as by biochemical methods based on the reverse-transcriptase and/or flaviviral RdRp stalling assays. It should also be noted that porphyrins were previously described to recognize various molecular targets (76) and their biological activities can be associated, in addition to interacting with G4s and viral/liposomal membranes, also with heme metabolism impairment and heme oxygenase inhibition (77–79) and photodynamic inactivation of pathogens via reactive oxygen species generation (80–82).

Other examples of multiple modes of action for G4 ligands were reported for berberine and related benzyloisoquinoline alkaloids, which were described not only to interact with nucleic acids and inhibit nucleic acid synthesis and reverse transcriptase activity (83), but also could regulate signaling pathways based on MEK-ERK, NF- κB and AMPK/mTOR, which are necessary for viral replication (84). The multiple mode of action was recently demonstrated also for PDS. This compound, in addition to the G4 stabilization, interacts with ZIKV NS2B-NS3 protease and

reduces its catalytic activity (18). Taken together, molecular mechanisms of antiviral activities for many G4 ligands appear to be more complex, making it difficult to link and correlate directly the results obtained using biophysical, biochemical, and biological methodological approaches.

Phenotype properties of recombinant TBEV mutated in the TBEV-5 region

To address the question if G4 structures are relevant to virus replication, a site-directed mutagenesis approach (Figure 10A) was used to introduce conformation-specific mutations into the TBEV-5 sequence of recombinant TBEV variants (Figure 10B). The selected mutations reflect those used for an *in vitro* study of flaviviral RdRp in the previous chapter on TBEV-5 sequence (Figure 7A). Thus, after transfection of the subgenomic fragments into permissive BHK-21 cells, the following recombinant TBEV variants (G4-specific TBEV mutants) were successfully rescued: 1) the *positive* TBEV mutant (T7653G/G7656A/T7659G/T7665G/T7671G) forming a highly stabilized quadruplex within the TBEV-5 sequence. 2) The *negative* mutant (G7656A/G7662A/G7677A) with an impaired ability to fold TBEV-5 quadruplex. 3) The *super-negative* mutant (G7656A/G7662A/G7670C/G7677A) with a completely abolished TBEV-5 quadruplex formation. Finally, 4) the recombinant wild-type virus with no introduced mutations in the TBEV-5 sequence (Figure 10B). As mentioned above, all mutations were synonymous and their introduction did not result in amino acid substitution apart from the only exception of the G2A amino acid substitution in the NS5 gene of the *super-negative* mutant. This substitution was, however, necessary for the complete destabilization of the TBEV-5 quadruplex. As G2A represents a substitution for a structurally/functionally similar amino acid and because it is located outside of the methyltransferase or RdRp active sites we are convinced that this change does not significantly affect the NS5 activity.

To characterize the phenotypic properties of the obtained G4-specific TBEV mutants *in vitro*, the growth kinetics and plaque morphology of the recombinant mutated viruses were assayed in PS cells and compared with wild-type (Figure 11). The recombinant wild-type virus amplified in PS cells (MOI of 0.1) showed a short lag period within the interval from 0 to 18 h p.i. Starting 24 h p.i., the wild-type TBEV exerted an exponential increase in virus infectivity reaching a peak titer of 4.2×10^6 PFU/ml within 72 h p.i. and gradually declining thereafter (Figure 11A).

The *positive* mutant cultured in PS cells at MOI of 0.1 showed a substantially decreased replication fitness (Figure 11A), which was manifested by viral titers 1–1.5 orders of magnitude lower than the wild-type within the intervals 24–96 h p.i. After 96 h of cultivation in PS cells, the *positive* TBEV mutant reached a peak titer of 4.6×10^5 PFU/ml. The strongly altered replication fitness of the *positive* TBEV mutant was even more pronounced, when PS cells were infected with this mutated virus at MOI of 0.01 (Figure 11B). Importantly, the decreased replication capacity of the *positive* TBEV mutant resulted also in dramatic changes in plaque morphology; this mutated virus formed

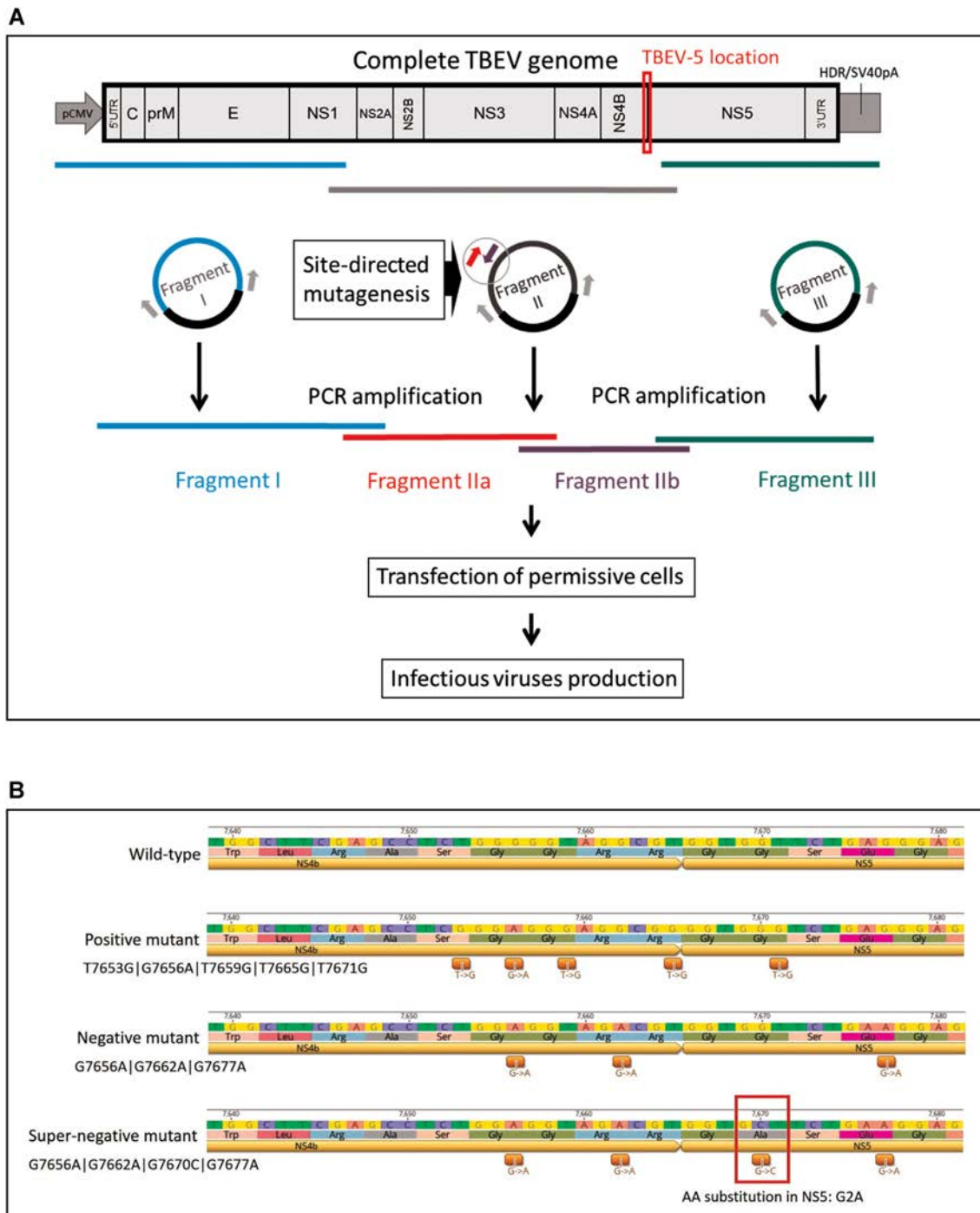


Figure 10. Site-directed mutagenesis to form recombinant TBEV mutated in the TBEV-5 region. **(A)** Schematic representation of the reverse-genetics system used in this study. The reverse-genetics system was based on the generation of infectious subgenomic overlapping DNA fragments that encompass the entire viral genome. Three de novo-synthesized DNA fragments (I, II and III) cloned into a pUC57 or pC11 vectors were used. Fragment I was flanked with the human cytomegalovirus promoter (pCMV) at the 5' end and fragment III with the hepatitis delta ribozyme, followed by the simian virus 40 polyadenylation signal (HDR/SV40pA) at the 3' end. Unmodified primers were used to generate unmodified amplicons I, II, and III (i.e. the production of wild-type virus). Mutated primers located on the targeted TBEV-5 region on fragment II were used to generate two mutated sub-amplicons IIa and IIb (red and violet) (i.e. the production of the positive, negative, and super-negative TBEV mutants). An equimolar mix of these four DNA fragments was used to transfect BHK-21 cells to obtain infectious viral particles. After transfection, the infectious viral particles were rescued and the presence of the desired mutations in the TBEV-5 region was confirmed by sequencing. **(B)** Genotypes of the recombinant TBEV mutated in the TBEV-5 region and the wild-type virus. The introduced mutations are indicated. The scheme was generated using the Geneious Prime® software, version 2021.2.2 (Biomatters, Ltd.; New Zealand).

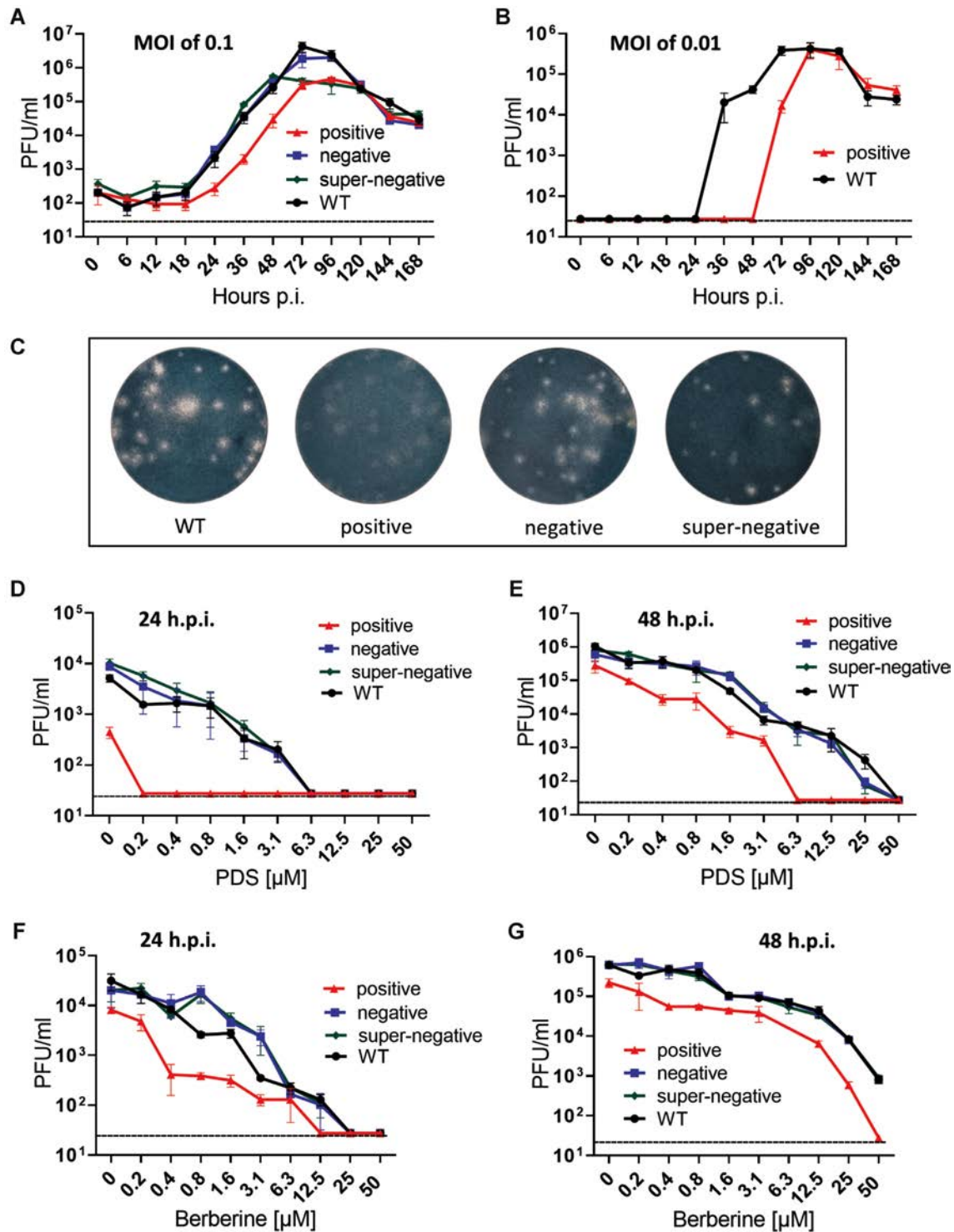


Figure 11. Phenotype properties of the recombinant TBEV mutated in the TBEV-5 sequence. (A) Growth kinetics of the positive, negative, and super-negative mutants, and wild-type TBEV at MOI of 0.1 within the 7-day experimental period to assess the replication efficacy of the mutant TBEV in PS cells. (B) Growth kinetics of the positive TBEV mutant and the wild-type virus at MOI of 0.01 within the 7-day experimental period in PS cells. (C) Plaque morphology of G4-specific TBEV mutants was assessed in PS cell monolayers and compared to the wild-type virus. (D, E) The sensitivity profiles of the positive, negative, and super-negative TBEV mutants to PDS were evaluated in PS cells and compared to the corresponding wild-type TBEV at 24 h p.i. (D) and 48 h p.i. (E). (F, G) The sensitivity profiles of G4-specific TBEV mutants to berberine were evaluated in PS cells and compared to the corresponding wild-type TBEV at 24 h p.i. (F) and 48 h p.i. (G) Experiments were performed in three biological replicates. The mean titers are shown, and error bars indicate the standard errors of the mean. The horizontal dashed line indicates the minimum detectable threshold of 1.44 log₁₀ PFU/ml.

turbid (cloudy) and indistinct plaques, compared with large and clear plaques of the wild-type (Figure 11C). The sequence analysis of the *positive* TBEV mutant revealed the partial reverse of the mutated TBEV-5 sequence to the wild-type genotype, as both mutated and reverted genotypes were identified in RNA samples isolated from the supernatant media after a 168-h cultivation of the *positive* TBEV mutant in PS cells (Supplementary Table S3). The reverted genotype was determined in one from three analyzed RNA samples and, moreover, in this RNA sample the reversals occurred only in the positions T7653G, T7659G, T7665G and T7671G. The mutation at position 7656 was retained. These observations clearly indicate that the high stabilization of the TBEV-5 G4 resulted in a strong impairment of the viral replication, which could be explained by the inhibitory effect of the stabilized G4 on the RdRp-directed RNA replication process, as was also demonstrated using the flaviviral RdRp stalling assays (see above). Thus, the *positive* TBEV mutant population was subject to a selection pressure which led to the gradual elimination of the G4-stabilizing mutations and to the restoration of the wild-type genotype configuration, when the mutated virus was cultivated for 168 h in cell culture.

The growth kinetics of the *negative* mutant was almost indistinguishable from the wild-type virus (Figure 11A). After a lag period (0–18 h p.i.) the *negative* TBEV mutant entered an exponential replication phase and reached a peak titer of 1.8×10^6 PFU/ml at 96 h p.i. At the end of the experiment (at 168 h p.i.), the virus titer dropped to 2.0×10^4 PFU/ml. The plaque morphology of the *negative* mutant was similar to that of the wild-type virus; both recombinant viruses produced large and clear plaques which were round and regular in shape and did not change in shape and size during all cultivation experiments (Figure 11C). Interestingly, the *negative* TBEV mutant maintained the introduced mutations during the whole cultivation experiment (for 168 h); in all analyzed RNA samples only the mutated genotype was detected (Supplementary Table S3). It is evident that destabilization of the TBEV-5 G4 in the *negative* TBEV mutant did not affect the virus replication significantly and, therefore, there was no/negligible selection pressure to eliminate the mutated TBEV-5 sequence and revert to the wild-type genotype. We suppose that the mutagenesis of multiple quadruplex forming sequences located in multiple viral genes could lead to more pronounced changes in viral replication fitness. This will be a subject of our future research.

The replication fitness of the *super-negative* TBEV mutant was also similar to that of wild-type (Figure 11A). The similarity in replication kinetics was most pronounced at the intervals of 0 to 48 h p.i. The *super-negative* TBEV mutant reached the peak titer of 5.6×10^5 PFU/ml at 48 h p.i. In later phases of cultivation in PS cells, the replication of the *super-negative* TBEV mutant gradually declined to 4.3×10^4 PFU/ml. The plaque morphology of the *super-negative* mutant was indistinguishable from plaques formed by the *negative* mutant and wild-type (Figure 11C). Notably, a complete reversion to the wild-type genotype was observed, after the *super-negative* TBEV mutant was cultured in PS cells for 168 h (only mutation G7677A was retained in one of the analyzed samples, Supplementary Table S3). The extensive impairment to fold G4 in TBEV-5 was

probably highly disadvantageous for virus replication in cell culture and therefore, there was a strong selection pressure to completely eliminate the introduced conformation-specific mutations afterwards. The rapid reversion to the wild-type genotype could also explain the similar phenotype properties of the *super-negative* mutant and the wild-type virus.

Finally, we investigated the sensitivity of the G4-specific TBEV mutants to two selected G4 ligands (PDS and berberine, concentration range from 0 to 50 μ M). We examined the dose-dependent effect of both ligands on virus replication at two cultivation periods (24 and 48 h p.i.). The growth curves of the *negative* and *super-negative* TBEV mutants cultivated in the presence of PDS exerted very similar shapes and slopes as that of the wild-type (Figure 11D, E). Replication of the three recombinant viruses were completely inhibited at the compound concentration of 6.3 μ M at 24 h p.i. and 50 μ M at 48 h p.i., demonstrating no substantial differences in sensitivities of the *negative* and *super-negative* TBEV mutants and wild-type to PDS. These results are not surprising given that the replication fitness of the *negative* and *super-negative* mutants are similar with that of the wild-type virus. In a sharp contrast, however, the *positive* mutant exhibited an increased sensitivity to PDS compared to the wild-type virus and to both *negative* and *super-negative* mutants. At 24 h p.i. virus replication was completely suppressed even at the minimal PDS concentration tested (0.2 μ M). The increased sensitivity of the *positive* TBEV mutant was clearly apparent also after a 48-h cultivation; the growth curve of the *positive* mutant had a markedly steep slope and the mutated virus was completely inhibited at the PDS concentration of 6.3 μ M (Figure 11D, E). Similar results, although less pronounced, were obtained also when the mutated viruses and the wild-type TBEV were cultured in the presence of berberine at both cultivation intervals (24 and 48 h p.i.) (Figure 11F, G).

CONCLUSIONS

In this study, we predicted seven potential G4 forming sequences in the RNA genome of TBEV located in the C, NS1, NS4b and NS5 genes and the 3'-UTR. The ability to form stable monomolecular G4 was confirmed by biophysical methods for five of the potential G4 forming sequences. All observed G4s were parallel stranded. With the NS4b/NS5 derived G4 (TBEV-5), the best hit in terms of phylogenetic conservation and G4 properties, we observed strong interactions with selected small molecule-based G4 ligands, which were later demonstrated to show low cytotoxicity and potent antiviral efficacies against TBEV in cell-based systems. PDS, cPDS, NMM, TMPyP4, PhenDC3 and berberine also caused the suppression of viral surface E protein expression and the decrease in viral RNA copy numbers in virus-infected PS cell culture. While PDS and berberine showed detectable antiviral effects only in the late phase of the TBEV life cycle, NMM exerted an inhibitory effect also in the early steps (entry/fusion) of TBEV replication. Thus, it is evident that even well-characterized G4-binding ligands can affect different stages of the viral replication cycle and may recognize multiple viral/host molecular targets, other than G4s alone. The observed antiviral

effect of such compounds could then be the result of partial inhibition processes at different levels of the viral replication cycle. Moreover, the TBEV mutant forming a highly stabilized monomolecular TBEV-5 quadruplex (the *positive* mutant) showed a substantially decreased replication capability, altered plaque morphology and increased susceptibility to selected G4 ligands. From the mechanistic point of view, the alterations in TBEV phenotype mutated in the TBEV-5 region can be explained by the G4-mediated inhibition of viral RNA synthesis, as also demonstrated using the *in vitro* flaviviral RdRp stalling assay. In contrast, the TBEV mutants with destabilized TBEV-5 quadruplexes (the *negative* and *super-negative* mutants) showed no phenotype differences compared with the wild-type virus. The *super-negative* mutant, moreover, exerted a rapid reversal to the wild-type genotype. Our results indicate that there is a stability threshold for G4 sequences located in the RNA genome of TBEV and that mutational shift from this stability threshold to form strongly (de)stabilized G4s is severely penalized, either by viral replication fitness decrease or by rapid reversion back to this optimal level of G4 stability. The findings of our study represent a solid base for new directions in the drugability of tick-borne encephalitis, present G4s in the TBEV RNA genome as prospective targets for novel small molecule-based drugs, which bind G4 structures, alter their stability and disrupt the viral replication cycle.

SUPPLEMENTARY DATA

Supplementary Data are available at NAR Online.

FUNDING

Czech Science Foundation [20-20229S to D.Re., L.E.]; SYMBIT [CZ.02.1.01/0.0/0.0/15_003/0000477] financed from the ERDF; EU Horizon 2020 [653316 (EVAg)]. Funding for open access charge: Czech Science Foundation [20-20229S].

Conflict of interest statement. None declared.

REFERENCES

1. Neidle, S. and Balasubramanian, S. (2006) In: *Quadruplex Nucleic Acids*. Royal Society of Chemistry, London, Cambridge.
2. Huppert, J.L. and Balasubramanian, S. (2005) Prevalence of quadruplexes in the human genome. *Nucleic Acids Res.*, **33**, 2908–2916.
3. Varshney, D., Spiegel, J., Zyner, K., Tannahill, D. and Balasubramanian, S. (2020) The regulation and functions of DNA and RNA G-quadruplexes. *Nat. Rev. Mol. Cell Biol.*, **21**, 459–474.
4. Ruggiero, E. and Richter, S.N. (2018) G-quadruplexes and G-quadruplex ligands: targets and tools in antiviral therapy. *Nucleic Acids Res.*, **46**, 3270–3283.
5. Bohálová, N., Cantara, A., Bartas, M., Kaura, P., Štastný, J., Pečinka, P., Fojta, M., Mergny, J.L. and Brázda, V. (2021) Analyses of viral genomes for G-quadruplex forming sequences reveal their correlation with the type of infection. *Biochimie*, **186**, 13–27.
6. Artusi, S., Nadai, M., Perrone, R., Biasolo, M.A., Palù, G., Flamand, L., Calistri, A. and Richter, S.N. (2015) The herpes simplex-1 genome contains multiple clusters of repeated G-quadruplex: implications for the antiviral activity of a G-quadruplex ligand. *Antiviral Res.*, **118**, 123–131.
7. Murat, P., Zhong, J., Lekieffre, L., Cowieson, N.P., Clancy, J.L., Preiss, T., Balasubramanian, S., Khanna, R. and Tellam, J. (2014) G-quadruplexes regulate epstein-barr virus-encoded nuclear antigen 1 mRNA translation. *Nat. Chem. Biol.*, **10**, 358–364.
8. Gilbert-Girard, S., Gravel, A., Artusi, S., Richter, S.N., Wallaschek, N., Kaufers, B.B. and Flamand, L. (2017) Stabilization of telomere G-Quadruplexes interferes with human herpesvirus 6A chromosomal integration. *J. Virol.*, **91**, e00402–17.
9. Perrone, R., Nadai, M., Poe, J.A., Frasson, I., Palumbo, M., Palù, G., Smithgall, T.E. and Richter, S.N. (2013) Formation of a unique cluster of G-quadruplex structures in the HIV-1 nef coding region: implications for antiviral activity. *PLoS One*, **8**, e73121.
10. Wang, S.-R., Zhang, Q.-Y., Wang, J.-Q., Ge, X.-Y., Song, Y.-Y., Wang, Y.-F., Li, X.-D., Fu, B.-S., Xu, G.-H., Shu, B. *et al.* (2016) Chemical targeting of a G-Quadruplex RNA in the ebola virus l gene. *Cell Chem. Biol.*, **23**, 1113–1122.
11. Wang, S.-R., Min, Y.-Q., Wang, J.-Q., Liu, C.-X., Fu, B.-S., Wu, F., Wu, L.-Y., Qiao, Z.-X., Song, Y.-Y., Xu, G.-H. *et al.* (2016) A highly conserved G-rich consensus sequence in hepatitis c virus core gene represents a new anti-hepatitis c target. *Sci. Adv.*, **2**, e1501535.
12. Jaubert, C., Bedrat, A., Bartolucci, L., Di Primo, C., Ventura, M., Mergny, J.-L., Amrane, S. and Andreola, M.-L. (2018) RNA synthesis is modulated by G-quadruplex formation in hepatitis c virus negative RNA strand. *Sci. Rep.*, **8**, 8120–8120.
13. Bian, W.-X., Xie, Y., Wang, X.-N., Xu, G.-H., Fu, B.-S., Li, S., Long, G., Zhou, X. and Zhang, X.-L. (2019) Binding of cellular nucleolin with the viral core RNA G-quadruplex structure suppresses HCV replication. *Nucleic Acids Res.*, **47**, 56–68.
14. Luo, X., Xue, B., Feng, G., Zhang, J., Lin, B., Zeng, P., Li, H., Yi, H., Zhang, X.-L., Zhu, H. *et al.* (2019) Lighting up the native viral RNA genome with a fluorogenic probe for the live-cell visualization of virus infection. *J. Am. Chem. Soc.*, **141**, 5182–5191.
15. Fleming, A.M., Ding, Y., Alenko, A. and Burrows, C.J. (2016) Zika virus genomic RNA possesses conserved G-Quadruplexes characteristic of the flaviviridae family. *ACS Infect. Dis.*, **2**, 674–681.
16. Fleming, A.M., Nguyen, N.L.B. and Burrows, C.J. (2019) Colocalization of m(6)A and G-Quadruplex-Forming sequences in viral RNA (HIV, zika, hepatitis b, and SV40) suggests topological control of adenosine N(6)-Methylation. *ACS Central Sci.*, **5**, 218–228.
17. Majeed, P., Pattnaik, A., Sahoo, B.R., Shankar, U., Pattnaik, A.K., Kumar, A. and Nayak, D. (2021) Inhibition of zika virus replication by G-quadruplex-binding ligands. *Mol. Ther. Nucleic Acids*, **23**, 691–701.
18. Zou, M., Li, J.Y., Zhang, M.J., Li, J.H., Huang, J.T., You, P.D., Liu, S.W. and Zhou, C.Q. (2021) G-quadruplex binder pyridostatin as an effective multi-target ZIKV inhibitor. *Int. J. Biol. Macromol.*, **190**, 178–188.
19. Abiri, A., Lavigne, M., Rezaei, M., Nikzad, S., Zare, P., Mergny, J.-L. and Rahimi, H.-R. (2021) Unlocking G-Quadruplexes as antiviral targets. *Pharmacol. Rev.*, **73**, 897–923.
20. Ruggiero, E., Zanin, I., Terreri, M. and Richter, S.N. (2021) G-Quadruplex targeting in the fight against viruses: an update. *Int. J. Mol. Sci.*, **22**, 10984.
21. Ruzek, D., Avšič Županc, T., Borde, J., Chrdle, A., Eyer, L., Karganova, G., Kholodilov, I., Knap, N., Kozlovskaya, L., Matveev, A. *et al.* (2019) Tick-borne encephalitis in europe and russia: review of pathogenesis, clinical features, therapy, and vaccines. *Antiviral Res.*, **164**, 23–51.
22. Deviatkin, A.A., Karganova, G.G., Vakulenko, Y.A. and Lukashov, A.N. (2020) TBEV subtyping in terms of genetic distance. *Viruses*, **12**, 1240.
23. Füzik, T., Formanová, P., Růžek, D., Yoshii, K., Niedrig, M. and Plevka, P. (2018) Structure of tick-borne encephalitis virus and its neutralization by a monoclonal antibody. *Nat. Commun.*, **9**, 436–436.
24. Edgar, R.C. (2004) MUSCLE: multiple sequence alignment with high accuracy and high throughput. *Nucleic Acids Res.*, **32**, 1792–1797.
25. Okonechnikov, K., Golosova, O., Fursov, M. and team, t.U. (2012) Unipro UGENE: a unified bioinformatics toolkit. *Bioinformatics*, **28**, 1166–1167.
26. Kikin, O., D'Antonio, L. and Bagga, P.S. (2006) QGRS mapper: a web-based server for predicting G-quadruplexes in nucleotide sequences. *Nucleic Acids Res.*, **34**, W676–W682.
27. Hon, J., Martínek, T., Zendlulka, J. and Lexa, M. (2017) pqsfinder: an exhaustive and imperfection-tolerant search tool for potential quadruplex-forming sequences in R. *Bioinformatics*, **33**, 3373–3379.
28. Bedrat, A., Lacroix, L. and Mergny, J.-L. (2016) Re-evaluation of G-quadruplex propensity with G4Hunter. *Nucleic Acids Res.*, **44**, 1746–1759.

29. Garant, J.-M., Perreault, J.-P. and Scott, M.S. (2017) Motif independent identification of potential RNA G-quadruplexes by G4RNA screener. *Bioinformatics*, **33**, 3532–3537.
30. Lacroix, L. (2019) G4HunterApps. *Bioinformatics*, **35**, 2311–2312.
31. Crooks, G.E., Hon, G., Chandonia, J.M. and Brenner, S.E. (2004) WebLogo: a sequence logo generator. *Genome Res.*, **14**, 1188–1190.
32. Kejnovska, I., Renciuik, D., Palacky, J. and Vorlickova, M. (2019) In: Yang, D. and Lin, C. (eds). *G-Quadruplex Nucleic Acids: Methods and Protocols*. Humana Press Inc, Totowa, Vol. **2035**, pp.25–44.
33. Rodriguez, R., Müller, S., Yeoman, J.A., Trentesaux, C., Riou, J.-F. and Balasubramanian, S. (2008) A novel small molecule that alters shelterin integrity and triggers a DNA-damage response at telomeres. *J. Am. Chem. Soc.*, **130**, 15758–15759.
34. Travascio, P., Bennet, A.J., Wang, D.Y. and Sen, D. (1999) A ribozyme and a catalytic DNA with peroxidase activity: active sites versus cofactor-binding sites. *Chem. Biol.*, **6**, 779–787.
35. Chung, W.J., Heddi, B., Hamon, F., Teulade-Fichou, M.P. and Phan, A.T. (2014) Solution structure of a G-quadruplex bound to the bisquinolinium compound phen-dc(3). *Angew. Chem. Int. Ed. Engl.*, **53**, 999–1002.
36. Mohanty, J., Barooah, N., Dhamodharan, V., Harikrishna, S., Pradeepkumar, P.I. and Bhasikuttan, A.C. (2013) Thioflavin T as an efficient inducer and selective fluorescent sensor for the human telomeric G-quadruplex DNA. *J. Am. Chem. Soc.*, **135**, 367–376.
37. Monchaud, D., Allain, C. and Teulade-Fichou, M.P. (2006) Development of a fluorescent intercalator displacement assay (G4-FID) for establishing quadruplex-DNA affinity and selectivity of putative ligands. *Bioorg. Med. Chem. Lett.*, **16**, 4842–4845.
38. Kong, D.M., Ma, Y.E., Wu, J. and Shen, H.X. (2009) Discrimination of G-quadruplexes from duplex and single-stranded DNAs with fluorescence and energy-transfer fluorescence spectra of crystal violet. *Chemistry*, **15**, 901–909.
39. Gowan, S.M., Harrison, J.R., Patterson, L., Valenti, M., Read, M.A., Neidle, S. and Kelland, L.R. (2002) A G-quadruplex-interactive potent small-molecule inhibitor of telomerase exhibiting in vitro and in vivo antitumor activity. *Mol. Pharmacol.*, **61**, 1154–1162.
40. Wang, S., Yan, W.W., He, M., Wei, D., Long, Z.J. and Tao, Y.M. (2020) Aloe emodin inhibits telomerase activity in breast cancer cells: transcriptional and enzymological mechanism. *Pharmacol. Rep.*, **72**, 1383–1396.
41. Franceschin, M., Rossetti, L., D'Ambrosio, A., Schirripa, S., Bianco, A., Ortaggi, G., Savino, M., Schultes, C. and Neidle, S. (2006) Natural and synthetic G-quadruplex interactive berberine derivatives. *Bioorg. Med. Chem. Lett.*, **16**, 1707–1711.
42. Arthanari, H., Basu, S., Kawano, T.L. and Bolton, P.H. (1998) Fluorescent dyes specific for quadruplex DNA. *Nucleic Acids Res.*, **26**, 3724–3728.
43. Yett, A., Lin, L., Beseiso, D., Miao, J. and Yatsunyk, L. (2019) N-methyl mesoporphyrin IX as a highly selective light-up probe for G-quadruplex DNA. *J. Porphyrins Phthalocyanines*, **23**, 1195–1215.
44. Izbicka, E., Wheelhouse, R.T., Raymond, E., Davidson, K.K., Lawrence, R.A., Sun, D.Y., Windle, B.E., Hurley, L.H. and Von Hoff, D.D. (1999) Effects of cationic porphyrins as G-quadruplex interactive agents in human tumor cells. *Cancer Res.*, **59**, 639–644.
45. Di Antonio, M., Biffi, G., Mariani, A., Raiber, E.A., Rodriguez, R. and Balasubramanian, S. (2012) Selective RNA versus DNA G-quadruplex targeting by in situ click chemistry. *Angew. Chem. Int. Ed. Engl.*, **51**, 11073–11078.
46. Rocca, R., Talarico, C., Moraca, F., Costa, G., Romeo, I., Ortuso, F., Alcaro, S. and Artese, A. (2017) Molecular recognition of a carboxy pyridostatin toward G-quadruplex structures: why does it prefer RNA? *Chem. Biol. Drug Des.*, **90**, 919–925.
47. Granotier, C., Pennarun, G., Riou, L., Hoffschir, F., Gauthier, L.R., De Cian, A., Gomez, D., Mandine, E., Riou, J.F., Mergny, J.L. et al. (2005) Preferential binding of a G-quadruplex ligand to human chromosome ends. *Nucleic Acids Res.*, **33**, 4182–4190.
48. Xu, H., Di Antonio, M., McKinney, S., Mathew, V., Ho, B., O'Neil, N.J., Santos, N.D., Silvester, J., Wei, V., Garcia, J. et al. (2017) CX-5461 is a DNA G-quadruplex stabilizer with selective lethality in BRCA1/2 deficient tumors. *Nat. Commun.*, **8**, 14432–14432.
49. Tran, P.L., Largy, E., Hamon, F., Teulade-Fichou, M.P. and Mergny, J.L. (2011) Fluorescence intercalator displacement assay for screening G4 ligands towards a variety of G-quadruplex structures. *Biochimie*, **93**, 1288–1296.
50. Carvalho, J., Lopes-Nunes, J., Paula Cabral Campello, M., Paulo, A., Milici, J., Meyers, C., Mergny, J.L., Salgado, G.F., Queiroz, J.A. and Cruz, C. (2020) Human papillomavirus G-Rich regions as potential antiviral drug targets. *Nucleic Acid Ther.*, **31**, 68–81.
51. Mergny, J.L. and Lacroix, L. (2003) Analysis of thermal melting curves. *Oligonucleotides*, **13**, 515–537.
52. Kozuch, O. and Mayer, V. (1975) Pig kidney epithelial (PS) cells: a perfect tool for the study of flaviviruses and some other arboviruses. *Acta Virol.*, **19**, 498.
53. Aubry, F., Nougairède, A., de Fabritus, L., Querat, G., Gould, E.A. and de Lamballerie, X. (2014) Single-stranded positive-sense RNA viruses generated in days using infectious subgenomic amplicons. *J. Gen. Virol.*, **95**, 2462–2467.
54. Driouich, J.S., Ali, S.M., Amroun, A., Aubry, F., de Lamballerie, X. and Nougairède, A. (2018) SuPREMe: a rapid reverse genetics method to generate clonal populations of recombinant RNA viruses. *Emerg. Microbes Infect.*, **7**, 40.
55. Eyer, L., Nougairède, A., Uhlřřová, M., Driouich, J.S., Zouharová, D., Valdés, J.J., Haviernik, J., Gould, E.A., De Clercq, E., de Lamballerie, X. et al. (2019) An E460D substitution in the NS5 protein of tick-borne encephalitis virus confers resistance to the inhibitor galidesivir (BCX4430) and also attenuates the virus for mice. *J. Virol.*, **93**, e00367-19.
56. De Madrid, A.T. and Porterfield, J.S. (1969) A simple micro-culture method for the study of group B arboviruses. *Bull. World Health Organ.*, **40**, 113–121.
57. Eyer, L., Valdés, J.J., Gil, V.A., Nencka, R., Hřřebabeký, H., řřála, M., Salát, J., Āerný, J., Palus, M., De Clercq, E. et al. (2015) Nucleoside inhibitors of tick-borne encephalitis virus. *Antimicrob. Agents Chemother.*, **59**, 5483–5493.
58. Konkolova, E., Dejmek, M., Hřřebabeký, H., řřála, M., Břřerle, J., Nencka, R. and Boura, E. (2020) Remdesivir triphosphate can efficiently inhibit the RNA-dependent RNA polymerase from various flaviviruses. *Antiviral Res.*, **182**, 104899.
59. Lu, G., Bluemling, G.R., Collop, P., Hager, M., Kuiper, D., Gurale, B.P., Painter, G.R., De La Rosa, A. and Kolykhalov, A.A. (2017) Analysis of ribonucleotide 5'-Triphosphate analogs as potential inhibitors of zika virus RNA-Dependent RNA polymerase by using nonradioactive polymerase assays. *Antimicrob. Agents Chemother.*, **61**, e01967-16.
60. Niyomrattanakit, P., Abas, S.N., Lim, C.C., Beer, D., Shi, P.Y. and Chen, Y.L. (2011) A fluorescence-based alkaline phosphatase-coupled polymerase assay for identification of inhibitors of dengue virus RNA-dependent RNA polymerase. *J. Biomol. Screen.*, **16**, 201–210.
61. Sáez-Álvarez, Y., Arias, A., Del Águila, C. and Agudo, R. (2019) Development of a fluorescence-based method for the rapid determination of zika virus polymerase activity and the screening of antiviral drugs. *Sci. Rep.*, **9**, 5397.
62. Lavezzo, E., Berselli, M., Frasson, I., Perrone, R., Palù, G., Brazzale, A.R., Richter, S.N. and Toppo, S. (2018) G-quadruplex forming sequences in the genome of all known human viruses: a comprehensive guide. *PLoS Comput. Biol.*, **14**, e1006675.
63. Puig Lombardi, E. and Londoño-Vallejo, A. (2019) A guide to computational methods for G-quadruplex prediction. *Nucleic Acids Res.*, **48**, 1603.
64. Islam, B., Stadlbauer, P., Vorlicřřková, M., Mergny, J.L., Otyepka, M. and řřponer, J. (2020) Stability of two-quartet G-Quadruplexes and their dimers in atomistic simulations. *J. Chem. Theory Comput.*, **16**, 3447–3463.
65. Kejnovská, I., Stadlbauer, P., Trantřřřek, L., RenĀiuik, D., Gajarský, M., KrafĀřřik, D., Palacký, J., Bednřřřřová, K., řřponer, J., Mergny, J.-L. et al. (2021) G-Quadruplex formation by DNA sequences deficient in guanines: two tetrad parallel quadruplexes do not fold intramolecularly. *Chem. Eur. J.*, **27**, 12115–12125.
66. Kypřř, J., Kejnovska, I., Renciuik, D. and Vorlickova, M. (2009) Circular dichroism and conformational polymorphism of DNA. *Nucleic Acids Res.*, **37**, 1713–1725.
67. Majee, P., Kumar Mishra, S., Pandya, N., Shankar, U., Pasadi, S., Muniyappa, K., Nayak, D. and Kumar, A. (2020) Identification and characterization of two conserved G-quadruplex forming motifs in the nipah virus genome and their interaction with G-quadruplex specific ligands. *Sci. Rep.*, **10**, 1477.
68. Zhang, A.Y.Q., Bugaut, A. and Balasubramanian, S. (2011) A sequence-independent analysis of the loop length dependence of

- intramolecular RNA G-quadruplex stability and topology. *Biochemistry*, **50**, 7251–7258.
69. Kwok, C.K., Marsico, G., Sahakyan, A.B., Chambers, V.S. and Balasubramanian, S. (2016) rG4-seq reveals widespread formation of G-quadruplex structures in the human transcriptome. *Nat. Methods*, **13**, 841.
70. Wallner, G., Mandl, C.W., Ecker, M., Holzmann, H., Stiasny, K., Kunz, C. and Heinz, F.X. (1996) Characterization and complete genome sequences of high- and low- virulence variants of tick-borne encephalitis virus. *J. Gen. Virol.*, **77**, 1035–1042.
71. Kepczyński, M. and Ehrenberg, B. (2002) Interaction of dicarboxylic metalloporphyrins with liposomes. The effect of pH on membrane binding revisited. *Photochem. Photobiol.*, **76**, 486–492.
72. Kepczyński, M., Pandian, R.P., Smith, K.M. and Ehrenberg, B. (2002) Do liposome-binding constants of porphyrins correlate with their measured and predicted partitioning between octanol and water? *Photochem. Photobiol.*, **76**, 127–134.
73. Assuncao-Miranda, I., Cruz-Oliveira, C., Neris, R.L.S., Figueiredo, C.M., Pereira, L.P.S., Rodrigues, D., Araujo, D.F.F., Da Poian, A.T. and Bozza, M.T. (2016) Inactivation of dengue and yellow fever viruses by heme, cobalt-protoporphyrin IX and tin-protoporphyrin IX. *J. Appl. Microbiol.*, **120**, 790–804.
74. Cruz-Oliveira, C., Almeida, A.F., Freire, J.M., Caruso, M.B., Morando, M.A., Ferreira, V.N.S., Assuncao-Miranda, I., Gomes, A.M.O., Castanho, M. and Poian, A.T. (2017) Mechanisms of vesicular stomatitis virus inactivation by protoporphyrin IX, zinc-protoporphyrin IX, and mesoporphyrin IX. *Antimicrob. Agents Chemother.*, **61**, 14.
75. Man, D., Slota, R., Broda, M.A., Mele, G. and Li, J. (2011) Metalloporphyrin intercalation in liposome membranes: ESR study. *J. Biol. Inorg. Chem.*, **16**, 173–181.
76. Neris, R.L.S., Figueiredo, C.M., Higa, L.M., Araujo, D.F., Carvalho, C.A.M., Vercoza, B.R.F., Silva, M.O.L., Carneiro, F.A., Tanuri, A., Gomes, A.M.O. et al. (2018) Co-protoporphyrin IX and Sn-protoporphyrin IX inactivate zika, chikungunya and other arboviruses by targeting the viral envelope. *Sci. Rep.*, **8**, 13.
77. Schmidt, W.N., Mathahs, M.M. and Zhu, Z.W. (2012) Herne and HO-1 inhibition of HCV, HBV, and HIV. *Front. Pharmacol.*, **3**, 13.
78. Chung, S.W., Hall, S.R. and Perrella, M.A. (2009) Role of haem oxygenase-1 in microbial host defence. *Cell. Microbiol.*, **11**, 199–207.
79. Wegiel, B., Nemeth, Z., Correa-Costa, M., Bulmer, A.C. and Otterbein, L.E. (2014) Heme oxygenase-1: a metabolic nuke. *Antioxid. Redox. Signal.*, **20**, 1709–1722.
80. Costa, L., Faustino, M.A.F., Neves, M., Cunha, A. and Almeida, A. (2012) Photodynamic inactivation of mammalian viruses and bacteriophages. *Viruses-Basel*, **4**, 1034–1074.
81. Pushpan, S.K., Venkatraman, S., Anand, V.G., Sankar, J., Parmeswaran, D., Ganesan, S. and Chandrashekar, T.K. (2002) Porphyrins in photodynamic therapy - a search for ideal photosensitizers. *Curr. Med. Chem. Anticancer Agents*, **2**, 187–207.
82. Wiehe, A., O'Brien, J.M. and Senge, M.O. (2019) Trends and targets in antiviral phototherapy. *Photochem. Photobiol. Sci.*, **18**, 2565–2612.
83. Maiti, M. and Kumar, G.S. (2010) Polymorphic nucleic acid binding of bioactive isoquinoline alkaloids and their role in cancer. *J. Nucleic Acids*, **2010**, <https://doi.org/10.4061/2010/593408>.
84. Warowicka, A., Nawrot, R. and Gozdzicka-Jozefiak, A. (2020) Antiviral activity of berberine. *Arch. Virol.*, **165**, 1935–1945.



Article

FDA-Approved Drugs Efavirenz, Tipranavir, and Dasabuvir Inhibit Replication of Multiple Flaviviruses in Vero Cells

Michal Stefanik^{1,2}, James J. Valdes^{1,3}, Fortunatus C. Ezebuo⁴ , Jan Haviernik^{1,5}, Ikemefuna C. Uzochukwu⁴ , Martina Fojtikova¹, Jiri Salat¹, Ludek Eyer^{1,3} and Daniel Ruzek^{1,3,*}

¹ Department of Virology, Veterinary Research Institute, Hudcova 70, CZ-62100 Brno, Czech Republic; stefanik@vri.cz (M.S.); valdjj@gmail.com (J.J.V.); haviernik@vri.cz (J.H.); fojtikovamartina@seznam.cz (M.F.); salat@vri.cz (J.S.); eyer@vri.cz (L.E.)

² Department of Chemistry and Biochemistry, Mendel University in Brno, Zemedelska 1, CZ-613 00 Brno, Czech Republic

³ Institute of Parasitology, Biology Centre of the Czech Academy of Sciences, Branisovska 31, CZ-37005 Ceske Budejovice, Czech Republic

⁴ Department of Pharmaceutical and Medicinal Chemistry, Faculty of Pharmaceutical Sciences, Nnamdi Azikiwe University, PMB 5025 Awka 420281, Nigeria; fortunatus.ezebuo@unn.edu.ng (F.C.E.); ic.uzochukwu@unizik.edu.ng (I.C.U.)

⁵ Faculty of Science, Masaryk University, Kamenice 5, CZ-625 00 Brno, Czech Republic

* Correspondence: ruzekd@paru.cas.cz

Received: 10 February 2020; Accepted: 15 April 2020; Published: 20 April 2020



Abstract: Vector-borne flaviviruses (VBFs) affect human health worldwide, but no approved drugs are available specifically to treat VBF-associated infections. Here, we performed in silico screening of a library of U.S. Food and Drug Administration-approved antiviral drugs for their interaction with Zika virus proteins. Twelve hit drugs were identified by the docking experiments and tested in cell-based antiviral assay systems. Efavirenz, tipranavir, and dasabuvir at micromolar concentrations were identified to inhibit all VBFs tested; i.e., two representatives of mosquito-borne flaviviruses (Zika and West Nile viruses) and one representative of flaviviruses transmitted by ticks (tick-borne encephalitis virus). The results warrant further research into these drugs, either individually or in combination, as possible pan-flavivirus inhibitors.

Keywords: FDA; flavivirus; Zika virus; tick-borne encephalitis virus; West Nile virus; antiviral

1. Introduction

The genus *Flavivirus* (family Flaviviridae) comprises more than 50 members, most of which are transmitted by mosquitoes and ticks (vector-borne flaviviruses, VBF) [1]. Despite similarities in genomic organization, replication strategy, and physicochemical properties, flaviviruses can cause a variety of diseases with clinical presentations ranging from mild fever to hemorrhagic fever, encephalitis, Guillain–Barré syndrome, and microcephaly [2]. Important human pathogens include yellow fever virus, dengue virus, West Nile virus (WNV), Zika virus (ZIKV), Japanese encephalitis virus, and tick-borne encephalitis virus (TBEV) [3,4]. No approved effective antiviral therapy directed against these viruses is currently available. To address this urgent medical need, we interrogated a library of U.S. Food and Drug Administration (FDA)-approved antiviral drugs for the ability to block flavivirus replication in vitro. Such approved drugs have well-documented modes of action, safety, and pharmacokinetic and pharmacodynamic profiles. Therefore, identifying them might expedite the regulatory process for their approval in clinical use more rapidly than new compounds [5–9].

In this study, we first performed *in silico* screening of a library of FDA-approved antiviral drugs for their interaction with ZIKV proteins (NS3 helicase and protease, NS5 RNA-dependent RNA polymerase, and methyltransferase). The cytotoxicities and antiviral activities of the identified hit compounds were tested against three representative flaviviruses: ZIKV and WNV as emerging mosquito-borne pathogens, and TBEV as an important tick-borne pathogen. Our results identified three FDA-approved drugs—efavirenz (an antiretroviral drug that targets the HIV-1 reverse transcriptase enzyme), tipranavir (a nonpeptidic protease inhibitor that targets the HIV protease), and dasabuvir (an inhibitor of NS5B polymerase, terminating RNA polymerization and stopping the replication of the genome of hepatitis C virus)—that inhibit flavivirus infection *in vitro*. To the best of our knowledge, none of these three drugs have been previously reported to have anti-VBF activity.

2. Materials and Methods

2.1. *In Silico* Screen of the Library of FDA-Approved Drugs

Bioinformatics mining of the Protein Data Bank (PDB) was done to identify ZIKV proteins whose 3D structures have been deposited. The 3D atomic coordinates of six identified ZIKV protein structures (NS3 helicase (5K8T), protease (5H6V), and NS5 methyltransferase (5MRK, 5KQS, and 5ULP)) and RNA-dependent RNA polymerase (5U04) were obtained from PDB [10] and prepared for molecular docking simulation using UCSF Chimera 1.9 [11] and AutoDockTools 1.5.6 [12,13]. Briefly, all duplicate chains and hetero molecules were deleted, and polar hydrogen atoms were added. Grid box sizes, centers, and exhaustiveness were assigned to the proteins at 1.0 Å, as shown in Table 1. Respective pdbqt files were created for molecular docking simulations studies.

Table 1. Grid box centers and sizes used for molecular docking simulations.

Protein	Center			Size			Exhaustiveness
	x	y	z	x	y	z	
5MRK	18.216	7.699	4.793	13	18	15	8
5K8T	115.969	2.824	64.433	14	19	14	8
5H6V	−8.522	3.178	−14.473	12	10	17	8
5KQS	52.145	10.164	−2.722	15	15	12	8
5ULP	−2.874	−1.66	26.51	15	17	16	8
5U04	25.036	68.817	103.577	12	16	16	8

Key: methyltransferases (5MRK, 5KQS, and 5ULP), NS3 helicase (5K8T), protease (5H6V), NS5 RNA-dependent RNA polymerase (5U04).

A library of 1960 FDA-approved drugs were obtained from Drug Bank [14] as of July 6, 2017. From this library, 73 were identified as FDA-approved antiviral drugs. These antiviral drugs were converted to their respective 3D coordinates with Open Babel 2.3.0 [15] and prepared for molecular docking simulation using AutoDockTools 1.5.6 [12,13]. Briefly, rotatable bonds were determined, all hydrogens were added, Gasteiger charges were computed, and pdbqt files were created for docking simulations studies. The prepared receptors and drugs then were used for the molecular docking simulation.

To validate the molecular docking simulations protocol, the experimental complexes of sinefungin (SFG), 7N-methyl-8-hydroguanosine-5'-diphosphate (M7G), 5'-[[[(3s)-3-amino-3-carboxypropyl] [(4-fluorophenyl)methyl]amino]-5'-deoxyadenosine (KBI), 5'-guanosine-diphosphate-monothiophosphate (GSP), and (s)-2-acetamido-6-amino-n-((s)-5-guanidino-1-oxopentan-2-yl) hexanamide (7HS) with their ZIKV target proteins (NS5 methyltransferase (5MRK, 5KQS, 5ULP), NS3 helicase (5K8T), and protease (5H6V)) from PDB were reproduced *in silico* after ligands were obtained from the ZINC[®] database [16] or extracted from the protein and subjected to geometry optimization. Blind docking was first performed with 5U04 and subsequently validated using M7G. AutoDockVina[®] has a high accuracy in predicting binding free energies by setting the

receptor rigid while appraising flexible ligands with a comparatively low standard error [17,18]. Therefore, receptor conformational flexibilities were neglected by rigid receptor docking. The approved drugs were docked into the receptors using AutoDockVina[®] after the validation of molecular docking protocols. The simulations were performed locally on a Linux platform using a configuration file and script (Supplementary Material S1) containing information on the grid box centers and sizes (Table 1) of prepared receptors and selected drugs.

2.2. Induced Fit Simulations

The ZIKV polymerase, PDB: 5U0B without its methyltransferase domain (residues 1–267), and the ZIKV protease, PDB: 5YOF, were used for molecular docking, as previously indicated, with an increased box size of 25_{xyz}. These ZIKV structures were used since they are at higher resolution with no missing residues. The docked ZIKV enzymes were then prepared and optimized for induced fit simulations using the Schrödinger's Maestro Protein Preparation Wizard [19]. Steric clashes were eliminated via local minimization. Note that the Maestro Protein Preparation Wizard created protonation states during optimization (default) that were used in the induced fit simulations.

The induced fit simulations were performed using the Metropolis Monte Carlo-based Protein Energy Landscape Exploration server (PELE). The PELE server is freely available at pele.bsc.es and has been previously explained [20,21]. Briefly, the PELE software executes three steps: (1) a protein/ligand local perturbation, (2) a residue side chain sampling, and (3) a global minimization. The three steps are repeated for a number of iterations within 24 h. The Metropolis Monte Carlo-based method employed by PELE accepts iterations if the enthalpy of evaporation is equal to or less than its initial value. An iteration is rejected if the enthalpy is greater than its initial value. The change in enthalpy (ΔH) is calculated by the force field known as the optimized potentials for liquid simulations (OPLS-2005) [22]. The inhibitor binding enthalpy (ΔH_L) is calculated according to Equation (1):

$$\Delta H_L = \Delta H_{ab} - (\Delta H_a + \Delta H_b) \quad (1)$$

where ΔH_{ab} is the enthalpy of the entire system, including inhibitors, and ΔH_a and ΔH_b are their separate enthalpy values.

For this study, the PELE ligand refinement ready-made script was used on the re-docked apo-enzymes for initial induced fit simulations. Alterations to the ready-made script were how long the inhibitor explores a region (wait for = 5) and the region explored (spawn within = 2–7 Å). The induced fit simulations were repeated for the narrow active site and binding cavities of the ZIKV polymerase until the inhibitor approximates its coordinates within 4.5 Å. The best pose/iteration of the ZIKV polymerase simulations that approximates the coordinates was chosen for the following two steps. (1) The best pose/iteration was refined using the PELE protein motion ready-made script. (2) Multiple polymerase dockings were conducted using top representatives in an ensemble cluster (UCSF Chimera 1.9 [11]) from the protein motion simulation. For all ZIKV enzymes, pose/iteration that approximates its respective inhibitor coordinates was chosen for several rounds of induced fit simulations until the inhibitors approached < 1 Å. The modifications made on the ligand refinement ready-made script for these subsequent induced fit simulations are in Supplementary Material S2. Finally, the PELE protein motion ready-made script was used to calculate the average ΔH_L and positions of analogous/identical co-crystallized inhibitors and were compared with protein motion simulations of the ZIKV enzymes from the pose/iteration < 1 Å. The first 20 iterations were eliminated since the simulation reached equilibrium at this point.

2.3. Viruses, Cells, and Tested Compounds

The following viral strains were tested: WNV (strains Eg101, a member of genomic lineage 1 isolated from human serum in Egypt; and 13-104, a representative of genomic lineage 2 isolated from the *Culex modestus* mosquito in the Czech Republic), TBEV (strain Hypr, highly pathogenic

representative of the European subtype of TBEV), and ZIKV (MR-766, a representative of the African ZIKV lineage; and Paraiba_01, a member of the Asian ZIKV lineage).

Vero cells (ATCC CCL-81, African Green Monkey, adult kidney, epithelial) were cultured in Dulbecco's Modified Eagle Medium containing 10% fetal bovine serum, 1% L-glutamine, 100 U/mL penicillin, and 100 µg/mL streptomycin (Sigma-Aldrich, Prague, Czech Republic) at 37 °C in a 5% CO₂ atmosphere. PS cells (porcine kidney stable) were cultured at 37 °C in Leibovitz (L-15) medium supplemented with 3% fetal bovine serum, 100 U/mL penicillin, 100 µg/mL streptomycin, and 1% L-glutamine (Sigma-Aldrich, Prague, Czech Republic). Human brain cortical astrocytes (HBCAs; ScienCell, Carlsbad, CA, USA) were cultivated at 37 °C under 5% CO₂ atmosphere in Astrocyte medium (ScienCell, Carlsbad, CA, USA), supplemented with 6% fetal bovine serum, 100 U/mL penicillin, 100 µg/mL streptomycin (Sigma-Aldrich), and 1% astrocyte growth supplement (ScienCell, Carlsbad, CA, USA). Human neuroblastoma UKF-NB-4 cells were cultured at 37 °C and 5% CO₂ atmosphere in Iscove's Modified Dulbecco's Medium, supplemented with 10% fetal bovine serum, 100 U/mL penicillin, 100 µg/mL streptomycin, and 1% L-glutamine (Sigma-Aldrich, Prague, Czech Republic).

Paritaprevir, dolutegravir, raltegravir potassium, elvitegravir, efavirenz, and tauroursodeoxycholate sodium were obtained from Sigma-Aldrich (St. Louis, MO, USA) and delavirdine mesylate, tipranavir, dasabuvir (ABT-333), saquinavir mesylate, maraviroc, and trifluridine were obtained from ChemScene, LLC (Monmouth Junction, NJ, USA). 7-deaza-2'-C-methyladenosine was purchased from Carbosynth (Compton, United Kingdom). Compounds were solubilized in dimethyl sulfoxide (DMSO; 100% *v/v*) to make stock solution with a concentration of 10 mM.

2.4. Cytotoxicity Assay

For detailed cytotoxicity studies, Vero, HBCA, and UKF-NB-4 cells were seeded onto 96-well plates at a density of 10,000 cells per well and incubated for 24 h at 37 °C before being used in the experiment to form a confluent monolayer. After the incubation, tested compounds were added to the cells at concentrations of 0, 3.125, 6.25, 12.5, 25, 50, 75, and 100 µM, and treated under the same regime as during antiviral testing; i.e., pretreatment for 24 h with culture medium containing appropriate drug concentrations, then the medium was exchanged with fresh compound-containing medium. After 48 h post medium exchange, cytotoxicity was measured using the Cell Counting Kit-8 (Dojindo Molecular Technologies, Inc., Munich, Germany) according to the manufacturer's instructions. The 50% cytotoxic concentration (CC₅₀) values, representing the concentration of compound that reduced cell viability by 50%, were calculated using GraphPad Prism (version 7.04, GraphPad Software, San Diego, CA, USA) as a nonlinear regression (inhibitor vs. normalized response, variable slope). All assays were performed in three independent experiments done in triplicate.

2.5. Antiviral Assays

2.5.1. Inhibition of ZIKV-Mediated Cytopathic Effect in a Simultaneous Treatment Assay

Twelve compounds that were found to bind with a high affinity to the selected ZIKV proteins in the *in silico* simulation experiment (paritaprevir, dolutegravir, raltegravir, efavirenz, elvitegravir, tipranavir, saquinavir, dasabuvir, delavirdine, maraviroc, trifluridine, and sodium tauroursodeoxycholate) were first screened for their ability to inhibit the cytopathic effect (CPE) mediated by ZIKV (strain MR-766) infection in Vero cells. In this initial screening, all compounds were tested at a single concentration of 50 µM. DMSO was added to virus-infected cells as a negative control at a concentration corresponding to a dilution of the initial drug–DMSO stock (at a maximal final concentration of 0.5% (*v/v*)). Culture medium containing appropriate drug concentrations and simultaneously inoculated with virus (multiplicity of infection = 0.1) was added to the cell monolayers. After 48 h of incubation at 37 °C, culture media were collected, and CPE was quantified using the Cell Counting Kit-8 (Dojindo Molecular Technologies, Inc., Munich, Germany) and expressed as percentage of cell viability. All assays were performed in three independent experiments done in triplicate.

2.5.2. Anti-ZIKV Activity in a Simultaneous Treatment Assay

Compounds that reduced ZIKV-mediated CPE (>90% viability of the cells in the culture compared to the uninfected cells) were further investigated for their activity to inhibit ZIKV growth in Vero cells. The compounds were tested at a single concentration of 50 μ M. DMSO was added to virus-infected cells as a negative control at a concentration corresponding to a dilution of the initial drug–DMSO stock (at a maximal final concentration of 0.5% (v/v)). Culture medium containing appropriate drug concentrations and simultaneously inoculated with virus (strain MR-766, multiplicity of infection = 0.1) was added to the cell monolayers. After 48 h of incubation at 37 °C, culture media were collected, and subjected to plaque assay as described above. All assays were performed in three independent experiments done in triplicate.

2.5.3. Anti-ZIKV Activity in a Post-Treatment Assay

Dasabuvir, efavirenz, and tipranavir (i.e., drugs that inhibited ZIKV in a simultaneous treatment assay) were further used in a post-treatment antiviral study. The potency of these compounds to inhibit ZIKV 2 h post-infection was assayed in Vero cells. The cells were infected with ZIKV (strain MR-766) at multiplicity of infection = 0.1. After 2 h, the medium containing virus was removed and replaced with a fresh medium containing the tested compounds at concentration of 50 μ M. DMSO was added to virus-infected cells as a negative control at a concentration corresponding to a dilution of the initial drug–DMSO stock (at a maximal final concentration of 0.5% (v/v)). After 48 h of incubation, culture media were harvested and subjected to plaque assay. 7-deaza-2'-C-methyladenosine was used at the same concentration and treatment regime as a reference compound. All assays were performed in three independent experiments done in triplicate.

2.5.4. Anti-VBFs Activity in a Pretreatment Assay, Dose Response Study

Dose response studies of dasabuvir, efavirenz, and tipranavir were done in Vero cells infected with TBEV, WNV, and ZIKV. The antiviral effects of dasabuvir and efavirenz were evaluated at compound concentrations of 0, 12.5, 25, 30, 40, and 50 μ M; tipranavir was tested at 0, 25, 40, 50, 75, and 100 μ M. The cells were pretreated with tested compounds for 24 h. Then the medium was removed, and the cells were infected with the individual viruses at a multiplicity of infection of 0.1 in culture media containing appropriate drug concentration. The compound inhibitory effect was assayed against WNV (strains Eg101 and 13-104), TBEV (strain Hypr), and ZIKV (strains MR-766 and Paraiba_01). DMSO was added to virus-infected cells as a negative control at a concentration corresponding to a dilution of the initial drug–DMSO stock (at a maximal final concentration of 0.5% (v/v)). After 48 h of incubation at 37 °C, culture media were collected, and viral titer was quantified by plaque assay. All assays were performed in three independent experiments done in triplicate.

2.5.5. Anti-ZIKV Activity in Human Neural Cells a Pretreatment Assay

For further characterization of the compound-mediated anti-ZIKV effect, we used UKF-NB-4 and HBCA cells, as target cells of neural origin. The cells were pretreated with serial dilutions of the drugs for 24 h. The highest drug concentration represented the highest non-toxic (>90% viability of the treated cells) concentrations for the particular cell type (for HBCA: 12.5 μ M dasabuvir, 12.5 μ M tipranavir, 3.125 μ M efavirenz; for UKF-NB-4: 6.25 μ M dasabuvir, 50 μ M tipranavir, 12.5 μ M efavirenz). Then the medium was removed, and the cells were infected with Paraiba_01 strain of ZIKV at a multiplicity of infection of 0.1 in culture media containing appropriate drug concentration. DMSO was added to virus-infected cells as a negative control at a concentration corresponding to a dilution of the initial drug–DMSO stock (at a maximal final concentration of 0.5% (v/v)). After 48 h of incubation at 37 °C, culture media were collected, and viral titer was quantified by plaque assay. All assays were performed in three independent experiments done in triplicate.

2.6. Plaque Assay

Plaque assays were performed in Vero cells (for ZIKV and WNV titers) or in the PS cells (to determine TBEV titers) as described previously [23–25]. The obtained viral titer values were recalculated to percentages of viral titer inhibition, applied to constructing the dose-response and inhibition curves, and used to calculate the 50% effective concentration (EC₅₀). We calculated EC₅₀ values using GraphPad Prism as a nonlinear regression (agonist vs. normalized response) from three independent experiments done in triplicate.

2.7. Immunofluorescence Staining of Viral Antigen

The results obtained from antiviral assays were confirmed using a cell-based flavivirus immunostaining assay with a mouse monoclonal antibody that specifically recognizes the flavivirus group surface antigen, as described previously [25]. Briefly, Vero cells seeded onto 96-well plates were treated with the test compound (0, 40, or 50 µM dasabuvir or efavirenz; 0, 75, or 100 µM tipranavir) and infected with the individual viruses at a multiplicity of infection of 0.1. After incubation at 37 °C for 48 h, the cell monolayers were fixed with cold acetone-methanol (1:1), blocked with 10% fetal bovine serum, and incubated with the flavivirus antibody (1:250; Sigma-Aldrich, Prague, Czech Republic). After washing, the cells were labeled with an anti-mouse goat secondary antibody conjugated with fluorescein isothiocyanate (FITC; 1:500) and counterstained with DAPI (4',6-diamidino-2-phenylindole; 1 µg/mL) to allow visualization of the cell nuclei. The fluorescence signal was recorded with an Olympus IX71 epifluorescence microscope and processed by ImageJ software.

3. Results and Discussion

To date, there are no specific antivirals available for clinical use with activity against VBFs—excluding preclinical studies of small molecules with known anti-ZIKV properties [7]. To address this gap, and to identify large molecule drugs, we conducted an *in silico* screen of an FDA-approved library for antiviral drugs using ZIKV protein structures as a VBF-representative model (Table 1). These are the initial steps in our computational and biological workflow (Figure 1). From the *in silico* screening, we identified 12 of the 73 antiviral drugs with favorable docking scores. The 12 FDA-approved antiviral drugs are paritaprevir, dolutegravir, raltegravir, efavirenz, elvitegravir, tipranavir, saquinavir, dasabuvir, delavirdine, maraviroc, trifluridine, and sodium tauroursodeoxycholate. These 12 *in silico* selected antiviral drugs were then tested *in vitro* for an anti-ZIKV effect on Vero cells at a concentration of 50 µM (simultaneous treatment assay). Inhibition of ZIKV-induced CPE was monitored by light microscopy and quantified at 48 h after infection using the *in vitro* assay for quantitative evaluation of the cell viability, as previously described [26]. From the *in vitro* screening, four antivirals (efavirenz, tipranavir, dolutegravir, and dasabuvir) inhibited ZIKV-mediated CPE in cell culture (>90% viability of the infected cells compared to uninfected controls) at a concentration of 50 µM (Figure 2A). However, only three of these (efavirenz, tipranavir, and dasabuvir) reduced ZIKV titer in the culture at this concentration (Figure 2B). The antiviral effect of efavirenz, tipranavir, and dasabuvir was further demonstrated in another experiment, when these drugs were applied to ZIKV-infected Vero cells 2 h post-infection (post-treatment assay; Supplementary Figure S1). The anti-ZIKV effect of tipranavir and dasabuvir was even stronger compared to 7-deaza-2'-C-methyladenosine, which is known to be an effective ZIKV inhibitor with documented activity both *in vitro* [26] as well as *in vivo* [27], and was used as a reference compound in our study (Supplementary Figure S2).

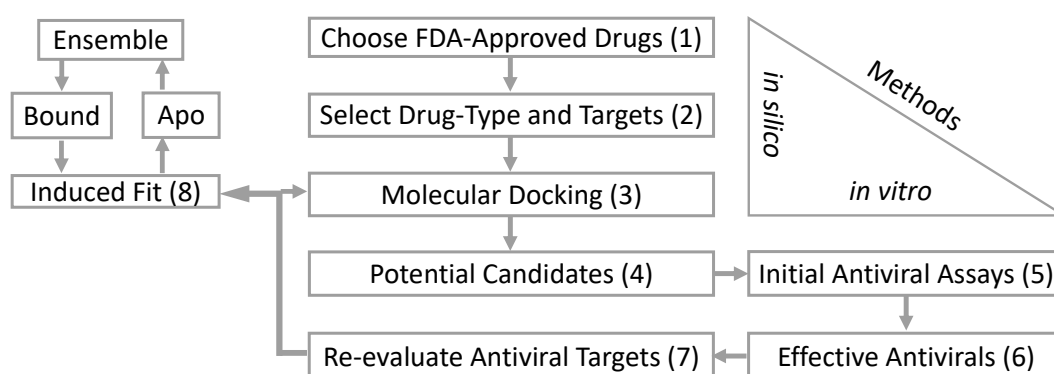


Figure 1. The workflow schematic indicates that a total of 1960 U.S. Food and Drug Administration (FDA)-approved drugs were downloaded from Drug Bank in the year 2017 (1). Excluding FDA-approved small molecule antiviral drugs (<900 daltons), only 73 were >1000 daltons. These 73 antivirals were then screened *in silico* with six Zika virus (ZIKV) proteins (2; Table 1). After the molecular docking screen (3), 12 FDA-approved antiviral drugs resulted in favorable scores (4). An *in vitro* assay of these 12 antivirals (5) resulted in three effective anti-ZIKV FDA-approved drugs (6). The drugs and targets were re-evaluated by searching the Protein Data Bank (PDB) for similar co-crystallized compounds (7). The molecular dockings were repeated using the average coordinates from various inhibitors. Finally, a series of induced fit simulations and dockings (8) were conducted on the favorable re-docked structures. The structures were then compared to similar co-crystallized compounds.

According to the initial molecular docking results, dasabuvir and tipranavir bind to the ZIKV methyltransferase (PDB: 5MRK) and efavirenz binds to ZIKV protease (PDB: 5H6V). These are apparent false positives since the non-nucleoside efavirenz and the non-peptidomimetic tipranavir have co-crystallized structures with HIV polymerase [28] and HIV protease [29], respectively. To date, there are no co-crystallized structures with dasabuvir. As a non-nucleoside inhibitor, however, dasabuvir is known to interact with hepatitis C (HCV) polymerase [30]. Given the dearth of ZIKV structures co-crystallized with non-nucleoside and non-peptidomimetic inhibitors, and the ZIKV structural diversity with HIV enzymes, the three effective ZIKV FDA-approved antivirals were therefore re-evaluated for subsequent molecular docking.

A PDB search resulted in 16 HCV and three Dengue polymerases co-crystallized with non-nucleoside inhibitors. Among the HCV polymerases, the non-nucleoside inhibitor 28V (PubChem ID: 46220530) is similar in composition to dasabuvir. A similar PDB search did not reveal any flavivirus proteases co-crystallized with non-peptidomimetic inhibitors. We therefore used the positions of two macrocyclic HCV protease inhibitors. The PDB accession numbers are in Supplementary Table S1. The average positions of the binding coordinates are shown with the ZIKV structures (Figure 3A,B). The ZIKV polymerase and protease, with respective inhibitors, were prepared for molecular docking as previously indicated. Conformational changes between bound and apo-enzymes at the binding site are necessary for an accurate docking pose. The top docking poses that approximate their respective average binding coordinates (Figure 3A,B) were therefore used for a series of induced fit simulations and molecular dockings—the final step of the workflow (Figure 1).

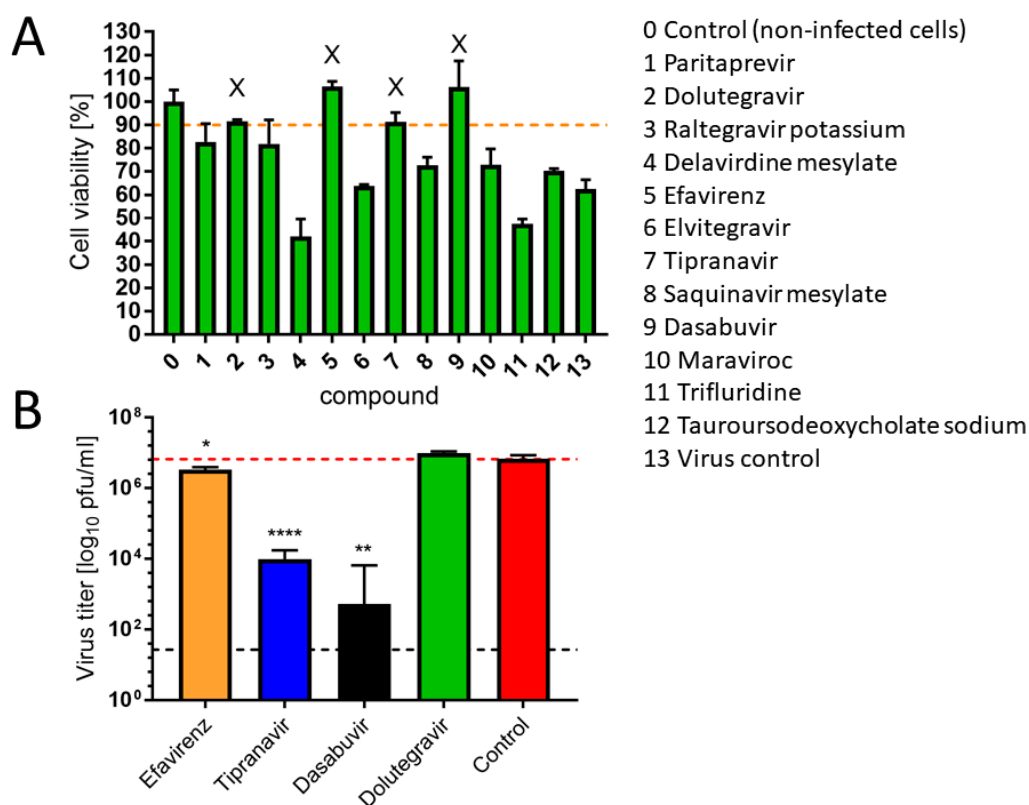


Figure 2. During the initial screening, all compounds identified by the molecular docking were tested at a single concentration of 50 μ M for inhibition of ZIKV-mediated cytopathic effect (CPE) (simultaneous treatment assay). Dimethyl sulfoxide (DMSO) was added to virus-infected cells as a negative control and to control, non-infected cells, at a concentration corresponding to a dilution of the initial drug–DMSO stock. Culture medium containing appropriate drug concentrations and virus inoculum (multiplicity of infection = 0.1) was added to the cell monolayers. After 48 h of incubation at 37 °C, culture media were collected, and CPE was quantified using the Cell Counting Kit-8 and expressed as percentage of cell viability. The horizontal dashed line indicates 90% cell viability compared to uninfected cells (A). Inhibitory effect of the compounds that reduced ZIKV-mediated CPE (>90% viability of the cells in the culture compared to the uninfected cells; marked by X in (A)) on ZIKV growth, as determined by plaque assay. Horizontal dashed line indicates the minimum detectable threshold of 1.44 \log_{10} pfu/mL (black), and the mean virus titer in control (untreated) cells (red). Data were analyzed by Student's *t*-test (GraphPad Prism, version 7.04); *, $p < 0.05$; **, $p < 0.01$; ****, $p < 0.0001$ (B).

None of the PDB non-nucleoside co-crystallized with flavivirus polymerases (Supplementary Table S1) indicate that efavirenz will bind at the HIV polymerase site (Figure 3A). Molecular docking and induced fit simulations also showed that efavirenz binding at the HIV position caused large, unnatural conformational changes at the palm domain (data not shown). We therefore focused on the average polymerase binding site (Figure 3A) for efavirenz simulations. Although both efavirenz and tipranavir approach their respective binding coordinates, the enthalpy values were slightly less favorable than their co-crystallized analogs (Figure 3C). This may be due to the structural-sequence diversity between HIV and flavivirus enzymes, indicating a distinct allosteric binding site for efavirenz and tipranavir, or that these antivirals may not be as effective for ZIKV (compared with HIV).

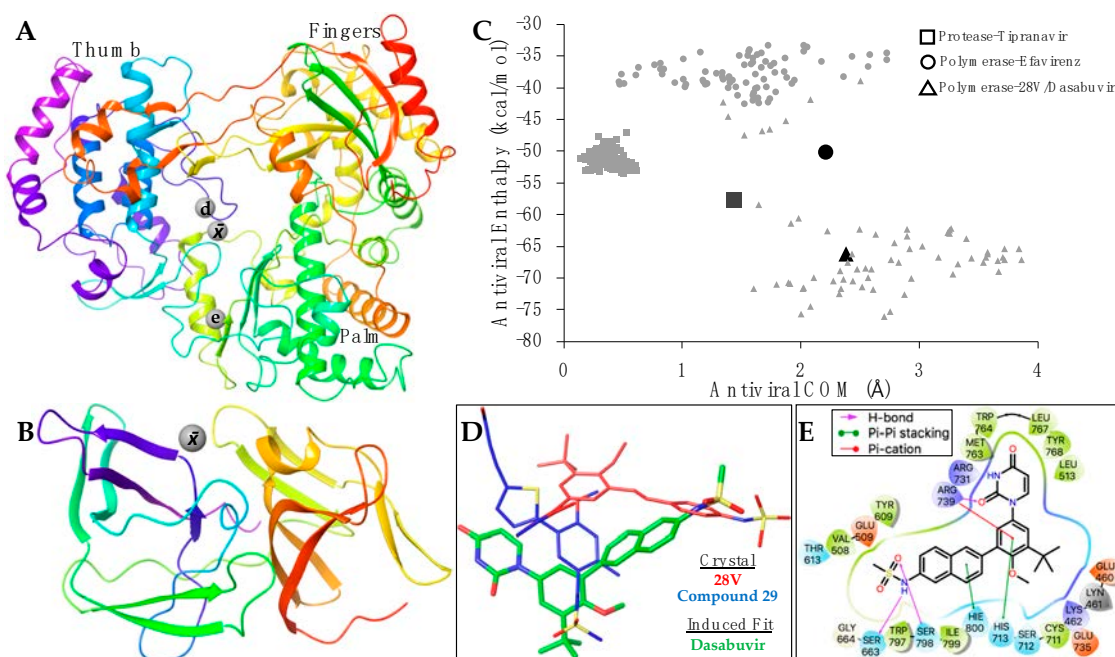


Figure 3. The PDB ZIKV polymerase (A; PDB: 5U0B) and protease (B; PDB: 5YOF) are color-coded from the amine-terminus (red) to the carboxyl-terminus (purple). The total average (\bar{x}), Dengue average (d), and HIV polymerase-efavirenz (e) binding coordinates are labeled and shown as grey spheres. The domains of ZIKV polymerase (A) are also labeled. The protein motion simulation results (C) show the enthalpy (y-axis) and the center of mass (COM) of the antivirals migration within its respective coordinates (x-axis). The darker/larger geometric shapes indicate average results for crystal structures of HIV protease-tipranavir (square; PDB: 6DIF), HIV polymerase-efavirenz (circle; PDB: 1FK9), and HCV polymerase-28V (triangle; PDB: 4MKB). The legend indicates the antiviral and target. The superposition (D) of co-crystallized antiviral structures 28V (red; PDB: 4MKB), compound 29 (blue; PDB: 5HMZ), and the best pose/iteration of ZIKV polymerase-dasabuvir (green). A ligand diagram (E) indicating the interacting ZIKV polymerase residues with dasabuvir and type of interaction (legend).

Of the three antivirals, however, dasabuvir clusters within the average enthalpy and coordinates of the analog 28V co-crystallized with HCV polymerase (Figure 3C). Although dasabuvir approximates the position of 28V, the coordination of dasabuvir resembles that of the non-nucleosides bound to Dengue polymerases (Figure 3A). The Dengue polymerase bound to compound 29 (PDB: 5HMZ) was used as an example (Figure 3D). Aside from the electrostatic interactions between ZIKV polymerase and dasabuvir, there are five residues that form direct contact (Figure 3E). Hydrogen bonds are formed at the methanesulfonamide group of dasabuvir with ZIKV polymerase residues Ser663 and Ser798, and Arg739 forms bonds with the dioxypyrimidine group. Pi-cation interactions are also coordinated by Arg739 along with the pi-pi stacking of His713 at the methoxyphenyl group. Lastly, His800 forms pi-pi stacking with naphthalene group of dasabuvir (Figure 3E).

We then evaluated the cytotoxic profiles and antiviral potency of efavirenz, tipranavir, and dasabuvir in detail using three cell lines: Vero cells, human neuroblastoma cells UKF-NB-4, and primary HBCAs. Both UKF-NB-4 and HBCA are target cells for neurotropic and neuroinvasive VBFs and therefore represent a clinically relevant model for our cytotoxicity/antiviral studies. In Vero cells, we observed no cytotoxicity across a concentration range 0–100 μM in the case of tipranavir ($\text{CC}_{50} > 100 \mu\text{M}$; Table 2). Dasabuvir and efavirenz exerted only moderate cytotoxicity in Vero cells (CC_{50} values of 101.50 and 73.57 μM , respectively). For UKF-NB-4 cells, the highest toxicity was associated with dasabuvir (CC_{50} , 21.28 μM), followed by efavirenz (CC_{50} , 31.85 μM) and tipranavir (CC_{50} , 89.17 μM). Of interest, the three drugs showed the highest cytotoxicity in HBCAs, with CC_{50} values of 25.98 μM for dasabuvir, 34.03 μM for tipranavir, and 16.68 μM for efavirenz (Table 3).

We previously had observed a similar trend of selective toxicity (increasing toxicity as follows: Vero < UKF-NB-4 < HBCA) in our study focused on the toxicity comparison of antiviral drug arbidol in multiple cell types [31]. Our hypothesis is that the selective toxicity can be a result of different levels of drug uptake by distinct cell types and/or different levels of enzymatic conversion of the compounds into toxic metabolites.

Table 2. Virus inhibition and cytotoxicity characteristics of efavirenz, tipranavir, and dasabuvir in Vero cells.

	Virus (Strain)	EC ₅₀ (μM) ^a	95% CI (μM) ^b	CC ₅₀ (μM) ^c	95% CI (μM) ^b	Selectivity Index (SI) (CC ₅₀ /EC ₅₀)
Efavirenz	ZIKV (Paraiba_01)	25.78	23.54–28.03			2.85
	ZIKV (MR-766)	30.41	29.72–31.10			2.41
	TBEV (Hypr)	15.86	14.17–17.54	73.57	64.27–87.43	4.63
	WNV (Eg101)	21.94	19.58–24.30			3.35
	WNV (13-104)	16.32	14.79–17.86			4.50
Tipranavir	ZIKV (Paraiba_01)	29.85	25.59–34.11			4.51
	ZIKV (MR-766)	30.29	27.68–32.90			4.45
	TBEV (Hypr)	35.54	32.98–38.10	134.90	130.50–143.30	3.79
	WNV (Eg101)	32.70	30.61–34.78			4.12
	WNV (13-104)	24.17	21.07–27.27			5.58
Dasabuvir	ZIKV (Paraiba_01)	16.12	14.27–17.97			6.29
	ZIKV (MR-766)	15.50	11.00–19.99			6.54
	TBEV (Hypr)	15.20	8.41–21.99	101.50	95.02–113.50	6.67
	WNV (Eg101)	18.12	17.06–19.18			5.60
	WNV (13-104)	15.65	12.68–18.62			6.48

^a EC₅₀ (50% effective concentration) values were calculated using GraphPad Prism (version 7.04, GraphPad Software, San Diego, CA, USA) as a nonlinear regression (agonist vs. normalized response) from three independent experiments done in triplicate. ^b 95% CI; 95% confidence interval. ^c CC₅₀ values, representing the concentration of compound that reduced cell viability by 50%, were calculated using GraphPad Prism as a nonlinear regression (inhibitor vs. normalized response, variable slope).

Table 3. Cytotoxicity characteristics of efavirenz, tipranavir, and dasabuvir in UKF-NB-4 and HBCA cells.

	Cell Type	CC ₅₀ (μM) ^a	95% CI (μM) ^b
Efavirenz	UKF-NB-4	31.85	29.93–33.79
	HBCA	16.68	12.70–21.68
Dasabuvir	UKF-NB-4	21.28	20.13–22.48
	HBCA	25.98	22.98–29.87
Tipranavir	UKF-NB-4	89.17	86.90–91.46
	HBCA	34.03	30.28–38.17

^a CC₅₀ values, representing the concentration of compound that reduced cell viability by 50%, were calculated using GraphPad Prism (version 7.04, GraphPad Software, San Diego, CA, USA) as a nonlinear regression (inhibitor vs. normalized response, variable slope). ^b 95% CI; 95% confidence interval.

As the antiviral effect of the compounds was most pronounced using the pretreatment assays, we used this treatment regimen for all further antiviral analyses. We evaluated the antiviral effects of efavirenz, tipranavir, and dasabuvir in Vero cells against two representatives of mosquito-borne flaviviruses, ZIKV and WNV, and one representative of tick-borne flavivirus (TBEV) (pretreatment assay). All three inhibitors exhibited micromolar antiviral potency against all VBFs tested and reduced viral titers in a dose-dependent manner (Figure 4; Table 2).

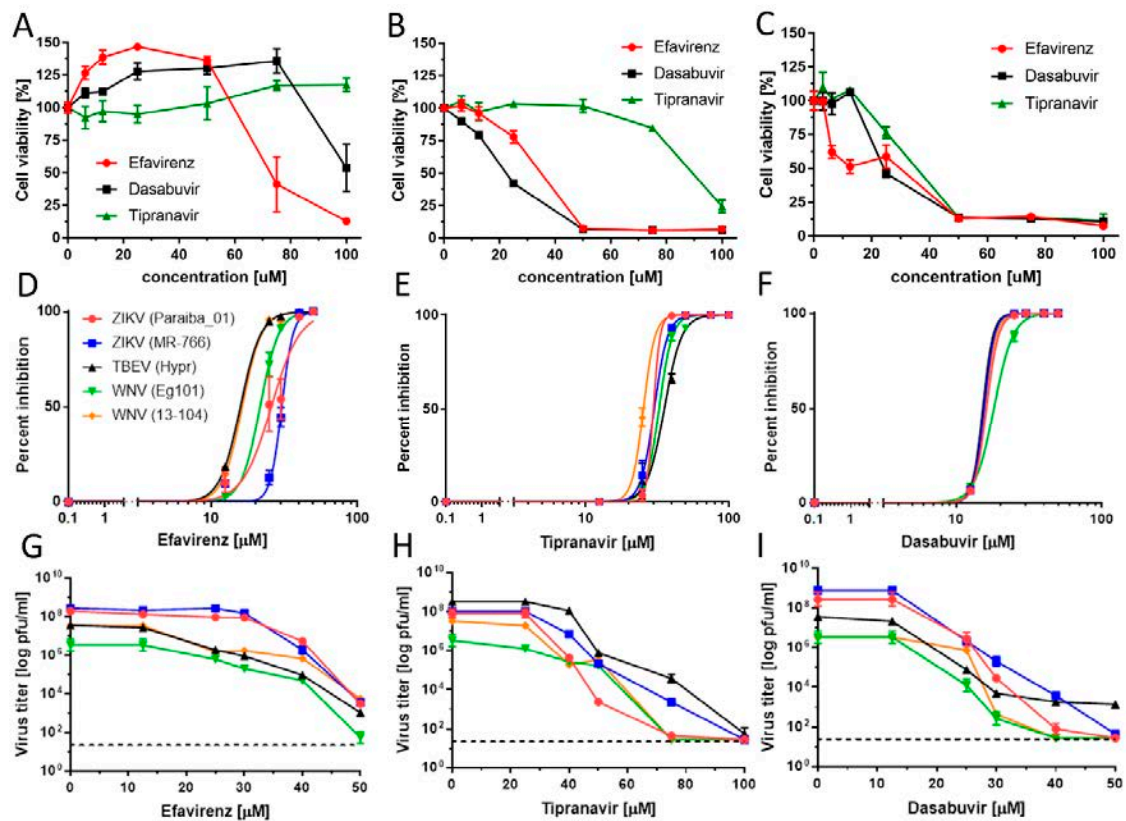


Figure 4. Cytotoxicity of efavirenz, tipranavir, and dasabuvir in Vero (A), UKF-NB-4 (B), and Human brain cortical astrocyte (HBCA) (C) cells, within the compound concentration range 0–100 µM, at 72 h post-treatment. (D–F) Virus titer inhibition curves of the indicated flaviviruses in Vero cells in the presence of serial dilutions of efavirenz (D), tipranavir (E), and dasabuvir (F) in a pretreatment assay. Dose-dependent effect of efavirenz (G), tipranavir (H), and dasabuvir (I) on virus titers in Vero cells in a pretreatment assay (legends as in D).

Efavirenz inhibited all investigated viruses with EC_{50} values ranging from 15.86 to 30.41 µM. The strongest inhibitory effect was seen for TBEV (EC_{50} , 15.86 µM) and WNV (EC_{50} , 16.32 and 21.94 µM for 13-104 and Eg101, respectively). The inhibitory effect of efavirenz against ZIKV was less pronounced, with EC_{50} values of 25.78 and 30.41 µM for Paraiba_01 and MR-766, respectively. Tipranavir inhibited all VBFs tested with similar EC_{50} values, ranging from 24.17 (WNV 13-104) to 35.54 µM (TBEV). Dasabuvir showed the strongest and most robust antiviral effect in Vero cells (EC_{50} values from 15.20 (TBEV) to 18.82 µM (WNV Eg101)) (Figure 4F,I; Table 2). We further confirmed the anti-VBF activity of efavirenz, tipranavir, and dasabuvir in a cell-based flavivirus immunostaining assay, which showed a dose-dependent inhibition of surface E antigen expression by all VBFs tested in Vero cells (Figure 5).

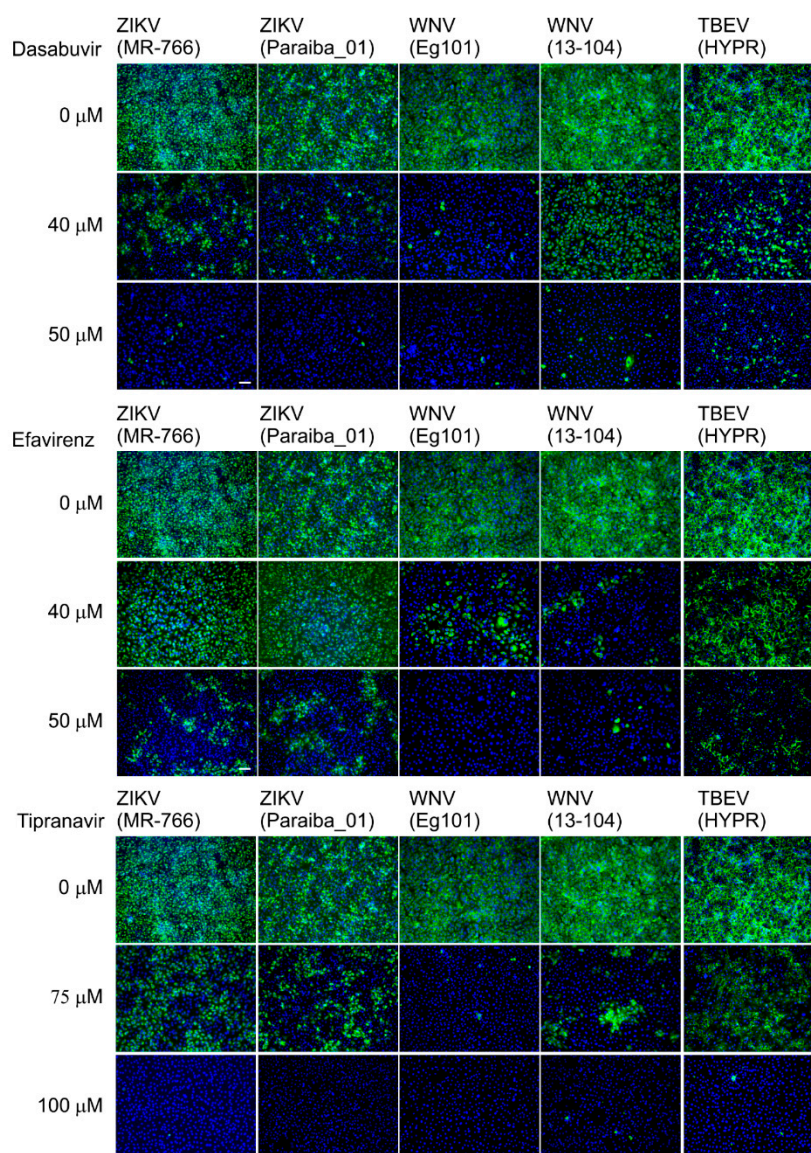


Figure 5. Inhibition of flaviviral surface E antigen expression by efavirenz, tipranavir, and dasabuvir. Virus-infected Vero cells were fixed on slides at 48 h p.i. and stained with flavivirus-specific antibody labeled with fluorescein isothiocyanate (FITC, green) and counterstained with 4',6-diamidino-2-phenylindole (DAPI, blue). Scale bar, 50 μm .

To investigate the antiviral effect of efavirenz, tipranavir, and dasabuvir in target cell types, primary HBCAs and human neuroblastoma cells (UKF-NB-4) were infected with Paraiba_01 strain of ZIKV and treated with serial dilutions of the drugs. At 48 h of incubation, we collected cell culture supernatants and quantified virus titer by plaque assay. In UKF-NB-4 cells, only tipranavir exhibited a significant antiviral effect against ZIKV (approx. 10^3 -fold at concentration 50 μM) (Figure 6C). The antiviral effect of dasabuvir was very low in these cells, resulting in a virus titer reduction of approximately 1 \log_{10} pfu/mL at the highest concentration of the drug in comparison with mock-treated control cells (Figure 6B). No antiviral effect of efavirenz was observed in UKF-NB-4 and HBCA cells at any concentration tested (Figure 6A,D). In ZIKV-infected HBCAs, treatment with dasabuvir significantly suppressed ZIKV replication in cell culture in a dose-dependent manner; treatment with 12.5 μM of dasabuvir completely suppressed ZIKV replication in the cell culture (Figure 6E). Similarly, treatment with tipranavir significantly reduced ZIKV growth in HBCAs in a dose-dependent manner; treatment with 12.5 μM of tipranavir reduced ZIKV replication in the HBCA culture by about 10^3 -fold (Figure 6F).

dose-dependent manner; treatment with 12.5 μM of tipranavir reduced ZIKV replication in the HBCA culture by about 10^3 -fold (Figure 6F).

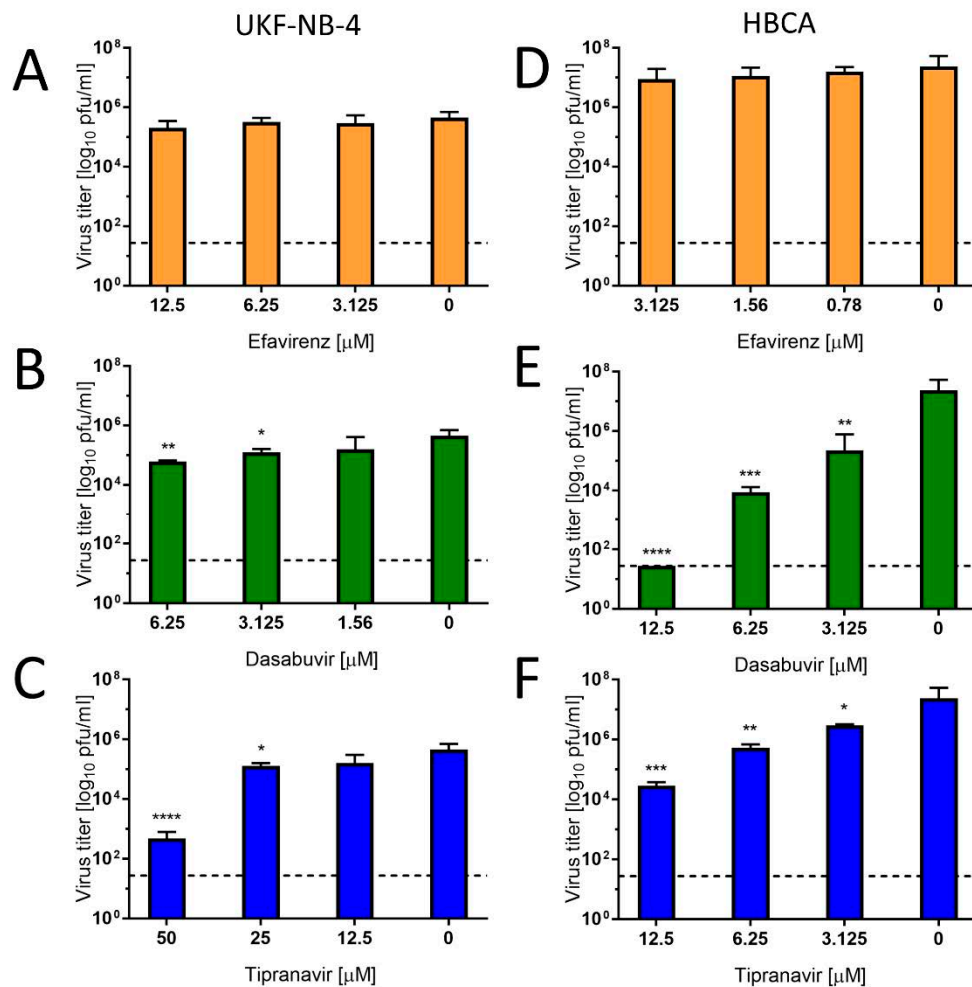


Figure 6. Inhibitory effect of efavirenz, tipranavir, and dasabuvir against ZIKV, strain Paraiba_01 in UKF-NB-4 (A, B, and C) and HBCA (C, D, and E) cells using a pretreatment assay. The cells were treated with serial dilutions of the drugs. The highest drug concentration represented the highest non-toxic concentrations for the particular cell type. Culture supernatants were collected at 48 h p.i., and the viral titers were determined by plaque assay. Horizontal dashed lines indicate the minimum detectable threshold of 1.44 log₁₀ pfu/mL. Data were analyzed using Student's *t*-test (GraphPad Prism, version 7.04); * $p < 0.05$; ** $p < 0.01$; *** $p < 0.001$; **** $p < 0.0001$. Overall, the highest and most robust antiviral effect was observed for tipranavir in human neural cells. Dasabuvir exhibited anti-ZIKV effects in astrocytes and a slight effect in neuroblastoma cells, while efavirenz had no or negligible anti-ZIKV activity in either astrocytes or neuroblastoma cells. This result indicates a cell-type-dependent activity of dasabuvir and efavirenz, which may result from differences in drug uptake or metabolic processing by different cell types. We previously observed similar cell-type-dependent activities in case of anti-VBF activities of arbidol, when the antiviral effect was found to be substantial only in HBCA and Vero cells [31], as well as for several nucleoside analogues, whose antiviral effect was studied in PS and UKF-NB-4 cells [32]. Repurposing of approved drugs could accelerate the development of novel therapeutic strategies, particularly for emerging life-threatening infections for which therapies are lacking [33]. In such cases, Repurposing of approved drugs could accelerate the development of novel therapeutic strategies, particularly for emerging life-threatening infections for which therapies are lacking [33]. In such cases, broad-spectrum antiviral drugs with effectiveness against a wide range of viral species are extremely suitable. Previous studies aimed to discover potential anti-ZIKV therapeutics via a drug-repurposing screen. The results involved different hits from the screens, and no common compounds were identified among the studies [6,7,34]. In the current work, we identified three FDA-approved drugs—tipranavir,

dasabuvir, and efavirenz—that exert antiviral activities against multiple flaviviruses in vitro and that were not identified in the previous anti-ZIKV screening studies.

A sulfonamide-containing dihydropyrene tipranavir is a non-peptidomimetic protease inhibitor currently used in combination with ritonavir to treat HIV-1 infections. It is advantageous particularly in treatment-experienced patients infected with protease inhibitor-resistant HIV-1 strains [35]. Tipranavir exhibits low-nanomolar anti-HIV activity in H9 cells (EC_{90} , 0.1 μ M), and for multidrug-resistant HIV isolates, the EC_{90} values range from 0.31 to 0.86 μ M [35,36]. To the best of our knowledge, the current work is the first study that demonstrates its activity against flaviviruses.

Dasabuvir (previously known as ABT-333) is an inhibitor of the hepatitis C virus (HCV) and approved for use in combination with ombitasvir/paritaprevir/ritonavir for the treatment of chronic HCV infection [37,38]. In the HCV subgenomic replicon system, dasabuvir inhibits genotype 1a and 1b replicons with EC_{50} values of 7.7 and 1.8 nM, respectively [30]. In our in vitro assays, dasabuvir had a micromolar EC_{50} , which was comparable to other small molecule inhibitors that showed effectiveness in laboratory animals infected with VBFs [25–27,39,40]. The antiviral activity of dasabuvir was demonstrated regardless if applied before infection, at the time of infection, or post-infection (Figures 2B and 4, Supplementary Figure S1). The mechanism of action of dasabuvir is based on its interaction with HCV NS5B (an NS5B non-nucleoside polymerase inhibitor), leading to premature termination of synthesis of viral RNA genome [41]. Considering the structural similarities of HCV and VBF RNA-dependent RNA polymerases [42], the mechanism of action of dasabuvir could be analogous.

Efavirenz is a non-nucleoside inhibitor that also targets HIV reverse transcriptase. In combination with other antiretroviral drugs, this agent significantly reduces HIV viral load, attenuating or preventing damage to the immune system and reducing the risk of developing AIDS [34]. The 90–95% inhibitory concentration of efavirenz for wild-type laboratory-adapted HIV strains and clinical isolates ranges from 1.7 to 25 nM when cultivated in lymphoblastoid cell lines, macrophage/monocyte cultures, and peripheral blood mononuclear cells. Efavirenz demonstrates in vitro synergistic activity against HIV-1 in combination with zidovudine, indinavir, or didanosine [43].

In summary, our present study yielded three major findings. First, our results identified three FDA-approved drugs—efavirenz, tipranavir, and dasabuvir—that inhibit replication of multiple flaviviruses in vitro in Vero cells. All three inhibitors exhibited micromolar antiviral potency against all viruses tested and reduced viral titers in a dose-dependent manner. Secondly, the anti-ZIKV effect of these drugs in Vero cells was demonstrated regardless if the compounds were applied before infection, at the time of infection, or even post-infection. Third, the anti-ZIKV effect of dasabuvir and tipranavir was confirmed also in human neural cells, which represent target cell types for the virus. One of possible limitations of our study is the fact that the mechanism of action of the identified compounds remains elusive. Future studies are also needed to investigate the anti-flavivirus effect of the identified compounds in vivo.

4. Conclusions

Efavirenz, tipranavir, and dasabuvir at micromolar concentrations were identified to inhibit two representatives of mosquito-borne flaviviruses (ZIKV and WNV) and one representative of flaviviruses transmitted by ticks (TBEV). All foregoing results do not necessarily indicate that efavirenz, tipranavir, and dasabuvir are suitable candidates for treating humans infected by VBFs. These results, however, do identify novel activities. Further research on these FDA-approved antiviral drugs, either individually or in combination, will consider them as possible pan-flavivirus inhibitors.

Supplementary Materials: The following are available online at <http://www.mdpi.com/2076-2607/8/4/599/s1>, Supplementary Material S1: Configuration file and script containing information on the grid box centers and sizes of prepared receptors and selected drugs. Supplementary Material S2: The modifications made on the ligand refinement ready-made script for the induced fit simulations in PELE. Supplementary Table S1: PDB accession numbers indicated by target-location. Supplementary Figure S1: Inhibitory effect of efavirenz, tipranavir, and dasabuvir on ZIKV growth in Vero cells in a post-treatment assay. Supplementary Figure S2: Inhibitory effect of a reference compound (7-deaza-2'-C-methyladenosine) on ZIKV growth in Vero cells.

Author Contributions: Conceptualization: M.S., J.J.V., F.C.E., L.E., and D.R.; methodology: M.S., J.J.V., F.C.E., J.H., I.C.U., M.F., J.S., L.E., and D.R.; supervision: F.C.E., J.J.V., L.E., and D.R.; draft preparation: M.S., J.J.V., F.C.E., L.E., and D.R.; manuscript revision: all authors. All authors have read and agreed to the published version of the manuscript.

Funding: The authors acknowledge financial support from the Ministry of Health of the Czech Republic (grant No. 16-34238A) and Ministry of Education, Youth and Sports of the Czech Republic (project “FIT” Pharmacology, Immunotherapy, nanoToxicology; grant No. CZ.02.1.01/0.0/0.0/15_003/0000495).

Conflicts of Interest: The authors declare no conflict of interest. The funders had no role in the design of the study; in the collection, analyses, or interpretation of data; in the writing of the manuscript, or in the decision to publish the results.

References

1. Simmonds, P.; Becher, P.; Bukh, J.; Gould, E.A.; Meyers, G.; Monath, T.; Muerhoff, S.; Pletnev, A.; Rico-Hesse, R.; Smith, D.B.; et al. Ictv Report Consortium. ICTV Virus Taxonomy Profile: Flaviviridae. *J. Gen. Virol.* **2017**, *98*, 2–3. [[CrossRef](#)] [[PubMed](#)]
2. Deval, J.; Symons, J.A.; Beigelman, L. Inhibition of viral RNA polymerases by nucleoside and nucleotide analogs: Therapeutic applications against positive-strand RNA viruses beyond hepatitis C virus. *Curr. Opin. Virol.* **2014**, *9*, 1–7. [[CrossRef](#)] [[PubMed](#)]
3. Baier, A. Flaviviral infections and potential targets for antiviral therapy. In *Flavivirus Encephalitis*, 1st ed.; Ruzek, D., Ed.; InTech: Rijeka, Croatia, 2011; pp. 89–104.
4. Lazear, H.M.; Stringer, E.M.; de Silva, A.M. The Emerging Zika Virus Epidemic in the Americas Research Priorities. *JAMA-J. Am. Med. Assoc.* **2016**, *315*, 1945–1946. [[CrossRef](#)] [[PubMed](#)]
5. Han, Y.; Mesplède, T.; Xu, H.; Quan, Y.; Wainberg, M.A. The antimalarial drug amodiaquine possesses anti-ZIKA virus activities. *J. Med. Virol.* **2018**, *90*, 796–802. [[CrossRef](#)] [[PubMed](#)]
6. Adcock, R.S.; Chu, Y.K.; Golden, J.E.; Chung, D.H. Evaluation of anti-Zika virus activities of broad-spectrum antivirals and NIH clinical collection compounds using a cell-based, high-throughput screen assay. *Antivir. Res.* **2017**, *138*, 47–56. [[CrossRef](#)]
7. Barrows, N.J.; Campos, R.K.; Powell, S.T.; Prasanth, K.R.; Schott-Lerner, G.; Soto-Acosta, R.; Galarza-Muñoz, G.; McGrath, E.L.; Urrabaz-Garza, R.; Gao, J.; et al. A Screen of FDA-Approved Drugs for Inhibitors of Zika Virus Infection. *Cell Host. Microbe.* **2016**, *20*, 259–270. [[CrossRef](#)]
8. Madrid, P.B.; Chopra, S.; Manger, I.D.; Gilfillan, L.; Keepers, T.R.; Shurtleff, A.C.; Green, C.E.; Iyer, L.V.; Dilks, H.H.; Davey, R.A.; et al. A systematic screen of FDA-approved drugs for inhibitors of biological threat agents. *PLoS ONE* **2013**, *8*, e60579. [[CrossRef](#)]
9. Pascoalino, B.S.; Courtemanche, G.; Cordeiro, M.T.; Gil, L.H.; Freitas-Junior, L. Zika antiviral chemotherapy: Identification of drugs and promising starting points for drug discovery from an FDA-approved library. *F1000Research* **2016**, *5*, 2523. [[CrossRef](#)]
10. Berman, H.M.; Westbrook, J.; Feng, Z.; Gilliland, G.; Bhat, T.N.; Weissig, H.; Shindyalov, I.N.; Bourne, P.E. The Protein Data Bank. *Nucleic Acids Res.* **2000**, *28*, 235–242. [[CrossRef](#)]
11. Pettersen, E.F.; Goddard, T.D.; Huang, C.C.; Couch, G.S.; Greenblatt, D.M.; Meng, E.C.; Ferrin, T.E. UCSF Chimera—a visualization system for exploratory research and analysis. *J. Comput. Chem.* **2004**, *25*, 1605–1612. [[CrossRef](#)]
12. Sanner, M.F. Python: A programming language for software integration and development. *J. Mol. Graph. Model.* **1999**, *17*, 57–61. [[PubMed](#)]
13. Morris, G.M.; Huey, R.; Lindstrom, W.; Sanner, M.F.; Belew, R.K.; Goodsell, D.S.; Olson, A.J. AutoDock4 and AutoDockTools4: Automated docking with selective receptor flexibility. *J. Comput. Chem.* **2009**, *30*, 2785–2791. [[CrossRef](#)] [[PubMed](#)]
14. Wishart, D.S.; Knox, C.; Guo, A.C.; Cheng, D.; Shrivastava, S.; Tzur, D.; Gautam, B.; Hassanali, M. DrugBank: A knowledgebase for drugs, drug actions and drug targets. *Nucleic Acids Res.* **2008**, *36*, D901–D906. [[CrossRef](#)] [[PubMed](#)]
15. O’Boyle, N.M.; Banck, M.; James, C.A.; Morley, C.; Vandermeersch, T.; Hutchison, G.R. Open Babel: An open chemical toolbox. *J. Cheminform.* **2011**, *3*, 33. [[CrossRef](#)] [[PubMed](#)]
16. Irwin, J.J.; Sterling, T.; Mysinger, M.M.; Bolstad, E.S.; Coleman, R.G. ZINC: A free tool to discover chemistry for biology. *J. Chem. Inf. Model.* **2012**, *52*, 1757–1768. [[CrossRef](#)] [[PubMed](#)]

17. Trott, O.; Olson, A.J. AutoDock Vina: Improving the speed and accuracy of docking with a new scoring function, efficient optimization, and multithreading. *J. Comput. Chem.* **2010**, *31*, 455–461. [[CrossRef](#)]
18. Keshavarz, F.; Alavianmehr, M.M.; Yousefi, R. Molecular interaction of Benzalkonium Ibuprofenate and its discrete ingredients with human serum albumin. *Phys. Chem. Res.* **2013**, *1*, 111–116.
19. Sastry, G.M.; Adzhigirey, M.; Day, T.; Annabhimoju, R.; Sherman, W. Protein and ligand preparation: Parameters, protocols, and influence on virtual screening enrichments. *J. Comput.-Aided Mol. Des.* **2013**, *27*, 221–234. [[CrossRef](#)]
20. Madadkar-Sobhani, A.; Guallar, V. PELE web server: Atomistic study of biomolecular systems at your fingertips. *Nucleic Acids Res.* **2013**, *41*, W322–W328. [[CrossRef](#)]
21. Borrelli, K.W.; Vitalis, A.; Alcantara, R.; Guallar, V. PELE: Protein Energy Landscape Exploration. A Novel Monte Carlo Based Technique. *J. Chem. Theory Comput.* **2005**, *1*, 1304–1311. [[CrossRef](#)]
22. Jorgensen, W.L.; Maxwell, D.S.; Tirado-Rives, J. Development and Testing of the OPLS All-Atom Force Field on Conformational Energetics and Properties of Organic Liquids. *J. Am. Chem. Soc.* **1996**, *118*, 11225–11236. [[CrossRef](#)]
23. De Madrid, A.T.; Porterfield, J.S. A simple micro-culture method for the study of group B arboviruses. *Bull. World Health Organ.* **1969**, *40*, 113–121.
24. Eyer, L.; Valdés, J.J.; Gil, V.A.; Nencka, R.; Hřebabecký, H.; Šála, M.; Salát, J.; Černý, J.; Palus, M.; De Clercq, E.; et al. Nucleoside inhibitors of tick-borne encephalitis virus. *Antimicrob. Agents Chemother.* **2015**, *59*, 5483–5493. [[CrossRef](#)] [[PubMed](#)]
25. Eyer, L.; Fojtíková, M.; Nencka, R.; Rudolf, I.; Hubálek, Z.; Ruzek, D. Viral RNA-Dependent RNA Polymerase Inhibitor 7-Deaza-2'-C-Methyladenosine Prevents Death in a Mouse Model of West Nile Virus Infection. *Antimicrob. Agents Chemother.* **2019**, *63*, e02093-18. [[CrossRef](#)]
26. Eyer, L.; Nencka, R.; Huvarová, I.; Palus, M.; Joao Alves, M.; Gould, E.A.; De Clercq, E.; Růžek, D. Nucleoside Inhibitors of Zika Virus. *J. Infect. Dis.* **2016**, *214*, 707–711. [[CrossRef](#)] [[PubMed](#)]
27. Zmurko, J.; Marques, R.E.; Schols, D.; Verbeken, E.; Kaptein, S.J.; Neyts, J. The Viral Polymerase Inhibitor 7-Deaza-2'-C-Methyladenosine Is a Potent Inhibitor of In Vitro Zika Virus Replication and Delays Disease Progression in a Robust Mouse Infection Model. *PLoS Negl. Trop. Dis.* **2016**, *10*, e0004695. [[CrossRef](#)] [[PubMed](#)]
28. Ren, J.; Milton, J.; Weaver, K.L.; Short, S.A.; Stuart, D.I.; Stammers, D.K. Structural basis for the resilience of efavirenz (DMP-266) to drug resistance mutations in HIV-1 reverse transcriptase. *Structure* **2000**, *8*, 1089–1094. [[CrossRef](#)]
29. Wong-Sam, A.; Wang, Y.F.; Zhang, Y.; Ghosh, A.K.; Harrison, R.W.; Weber, I.T. Drug Resistance Mutation L76V Alters Nonpolar Interactions at the Flap-Core Interface of HIV-1 Protease. *ACS Omega* **2018**, *3*, 12132–12140. [[CrossRef](#)]
30. Kati, W.; Koev, G.; Irvin, M.; Beyer, J.; Liu, Y.; Krishnan, P.; Reisch, T.; Mondal, R.; Wagner, R.; Molla, A.; et al. In vitro activity and resistance profile of dasabuvir, a nonnucleoside hepatitis C virus polymerase inhibitor. *Antimicrob. Agents Chemother.* **2015**, *59*, 1505–1511. [[CrossRef](#)]
31. Haviernik, J.; Štefánik, M.; Fojtíková, M.; Kali, S.; Tordo, N.; Rudolf, I.; Hubálek, Z.; Eyer, L.; Ruzek, D. Arbidol (Umifenovir): A Broad-Spectrum Antiviral Drug That Inhibits Medically Important Arthropod-Borne Flaviviruses. *Viruses* **2018**, *10*, E184. [[CrossRef](#)]
32. Eyer, L.; Smidkova, M.; Nencka, R.; Neča, J.; Kastl, T.; Palus, M.; De Clercq, E.; Růžek, D. Structure-activity relationships of nucleoside analogues for inhibition of tick-borne encephalitis virus. *Antivir. Res.* **2016**, *133*, 119–129. [[CrossRef](#)] [[PubMed](#)]
33. Wang, S.; Liu, Y.; Guo, J.; Wang, P.; Zhang, L.; Xiao, G.; Wang, W. Screening of FDA-Approved Drugs for Inhibitors of Japanese Encephalitis Virus Infection. *J. Virol.* **2017**, *91*, e01055-17. [[CrossRef](#)]
34. Xu, M.; Lee, E.M.; Wen, Z.; Cheng, Y.; Huang, W.K.; Qian, X.; Tcw, J.; Kouznetsova, J.; Ogden, S.C.; Hammack, C.; et al. Identification of small-molecule inhibitors of Zika virus infection and induced neural cell death via a drug repurposing screen. *Nat. Med.* **2016**, *22*, 1101–1107. [[CrossRef](#)] [[PubMed](#)]
35. Schapiro, J.M.; Scherer, J.; Boucher, C.A.; Baxter, J.D.; Tilke, C.; Perno, C.F.; Maggiolo, F.; Santoro, M.M.; Hall, D.B. Improving the prediction of virological response to tipranavir: The development and validation of a tipranavir-weighted mutation score. *Antivir. Ther.* **2010**, *15*, 1011–1019. [[CrossRef](#)] [[PubMed](#)]
36. Luna, B.; Townsend, M.U. Tipranavir: The first nonpeptidic protease inhibitor for the treatment of protease resistance. *Clin Ther.* **2007**, *29*, 2309–2318. [[CrossRef](#)] [[PubMed](#)]

37. King, J.R.; Zha, J.; Khatri, A.; Dutta, S.; Menon, R.M. Clinical Pharmacokinetics of Dasabuvir. *Clin. Pharmacokinet.* **2017**, *56*, 1115–1124. [[CrossRef](#)]
38. Trivella, J.P.; Gutierrez, J.; Martin, P. Dasabuvir: A new direct antiviral agent for the treatment of hepatitis C. *Expert Opin Pharmacother.* **2015**, *16*, 617–624. [[CrossRef](#)]
39. Julander, J.G.; Bantia, S.; Taubenheim, B.R.; Minning, D.M.; Kotian, P.; Morrey, J.D.; Smee, D.F.; Sheridan, W.P.; Babu, Y.S. BCX4430, a novel nucleoside analog, effectively treats yellow fever in a Hamster model. *Antimicrob Agents Chemother.* **2014**, *58*, 6607–6614. [[CrossRef](#)]
40. Eyer, L.; Kondo, H.; Zouharova, D.; Hirano, M.; Valdés, J.J.; Muto, M.; Kastl, T.; Kobayashi, S.; Haviernik, J.; Igarashi, M.; et al. Escape of Tick-Borne Flavivirus from 2'-C-Methylated Nucleoside Antivirals Is Mediated by a Single Conservative Mutation in NS5 That Has a Dramatic Effect on Viral Fitness. *J. Virol.* **2017**, *91*, e01028-17. [[CrossRef](#)]
41. Gentile, I.; Buonomo, A.R.; Borgia, G. Dasabuvir: A Non-Nucleoside Inhibitor of NS5B for the Treatment of Hepatitis C Virus Infection. *Rev. Recent Clin. Trials.* **2014**, *9*, 115–123. [[CrossRef](#)]
42. Černý, J.; Černá Bolfíková, B.; Valdés, J.J.; Grubhoffer, L.; Růžek, D. Evolution of tertiary structure of viral RNA dependent polymerases. *PLoS ONE* **2014**, *9*, e96070. [[CrossRef](#)] [[PubMed](#)]
43. Duarte, H.; Cruz, J.P.; Aniceto, N.; Ribeiro, A.C.; Fernandes, A.; Paixão, P.; Antunes, F.; Morais, J. Population Approach to Efavirenz Therapy. *J. Pharm. Sci.* **2017**, *106*, 3161–3166. [[CrossRef](#)] [[PubMed](#)]



© 2020 by the authors. Licensee MDPI, Basel, Switzerland. This article is an open access article distributed under the terms and conditions of the Creative Commons Attribution (CC BY) license (<http://creativecommons.org/licenses/by/4.0/>).

6. SHRnutí

Prezentované práce nastiňují pohled na strukturu inhibitorů medicínsky významných virů, zejména flavivirů, koronavirů a herpesvirů, a předkládají metodologický koncept pro testování nových antivirových látek i pro studium jejich mechanismu účinku. Práce zabývající se nucleosidovými analogy mapují chemický prostor v rámci molekuly nukleosidu/nukleotidu s cílem nalézt inhibitory s maximálním antivirovým a minimálním cytotoxickým účinkem. Kromě toho jsou prezentované práce zaměřeny na popis antivirového účinku inhibitorů strukturně odlišných od nukleosidů, které ve srovnání s nukleosidovými analogy cílí na odlišné části virového replikačního cyklu. Lze předpokládat, že kombinací uvedených inhibitorů, případně vývojem zcela nových nových struktur s vylepšenými biologickými vlastnostmi bude možné získat ještě silnější (nanomolární) inhibitory virové replikace. Je ovšem třeba zdůraznit, že současná antivirová léčiva používaná v klinické praxi se nejčastěji zaměřují na léčbu chronických virových nálezů, při kterých se virus v organismu množí relativně pomalu a perzistuje v infikovaných buňkách a tkáních po dlouhou dobu. Emergentní virová onemocnění, kterými jsou flavivirové nebo koronavirové infekce, představují klasické příklady akutních virových infekcí, spojených nejen s masivní replikací viru v infikovaných tkáních, ale také s nežádoucí imunologickou odezvou, tzv. cytokinovou bouří. Použití inhibitorů replikace virů v hostitelské buňce pro léčbu takových infekcí bude třeba přesně zacílit na vhodnou fázi virové infekce a kombinovat tento typ inhibitorů s imunomodulačními látkami. Takové studie budou rovněž předmětem našich budoucích prací.

7. POUŽITÁ LITERATURA

- Alavi Darazam I, Shokouhi S, Mardani M, Pourhoseingholi MA, Rabiei MM, Hatami F, Shabani M, Moradi O, Gharehbagh FJ, Irvani SSN, Amirdosara M, Hajiesmaeili M, Rezaei O, Khoshkar A, Lotfollahi L, Gachkar L, Dehbsneh HS, Khalili N, Soleymaninia A, Kusha AH, Shoushtari MT, Torabinavid P. 2021. Umifenovir in hospitalized moderate to severe COVID-19 patients: A randomized clinical trial. *Int Immunopharmacol* 99: 107969.
- Albertini AAV, Baquero E, Ferlin A, Gaudin Y. 2012. Molecular and Cellular Aspects of Rhabdovirus Entry *Viruses* 4: 117–139.
- Appolinario CM, Jackson AC. 2015. Antiviral therapy for human rabies. *Antivir Ther* 20: 1-10.
- Ariav Y, Ch'ng JH, Christofk HR, Ron-Harel N, Erez A. 2021. Targeting nucleotide metabolism as the nexus of viral infections, cancer, and the immune response. *Sci Adv* 7:eabg6165.
- Auksė M, Alvydas L, Göran G, Sirkka V, Åke L, Lars L. 2002. Tickborne Encephalitis in an Area of High Endemicity in Lithuania: Disease Severity and Long-Term Prognosis. *Clin Infect* 35: 650-658.
- Baier A. 2011. Flaviviral infections and potential targets for antiviral therapy. In: Ruzek D (ed) *Flavivirus Encephalitis*. 1st ed. Rijeka: InTech, pp. 89-104.
- Banerjee D, Reddy KR. 2016. Review article: safety and tolerability of direct-acting anti-viral agents in the new era of hepatitis C therapy. *Aliment Pharmacol Ther* 43: 674-696.
- Benhamou Y, Tubiana R and Thibault V. 2003. Tenofovir disoproxil fumarate in patients with HIV and lamivudine-resistant hepatitis B virus. *N Engl J Med* 348: 177–178.
- Blaising J, Polyak S J, Pécheur E-I. 2014. Arbidol as a broad-spectrum antiviral: An update. *Antivir Res* 107: 84-94.
- Bogovič P, Stupica D, Rojko T, Lotrič-Furlan S, Avšič-Županc T, Kastrin A, Lusa L, Strle F. 2018. The long-term outcome of tick-borne encephalitis in Central Europe. *Ticks Tick Borne Dis* 9: 369-378.
- Boshra H, Lorenzo G, Busquets N, Brun A. 2011. Rift Valley Fever: Recent Insights into Pathogenesis and Prevention. *J Virol* 85: 6098–6105.
- Broutet N, Krauer F, Riesen M, Khalakdina A, Almiron M, Aldighieri S, Espinal M, Low N, Dye C. 2016. Zika virus as a cause of neurologic disorders. *N Engl J Med* 374: 1506–1509.
- Cannalire R, Tarantino D, Piorkowski G, Carletti T, Massari S, Felicetti T, Barreca ML, Sabatini S, Tabarrini O, Marcello A, Milani M, Cecchetti V, Mastrangelo E, Manfroni G, Gilles Q. 2019. Broad spectrum anti-flavivirus pyridobenzothiazolones leading to less infective virions. *Antivir Res* 167: 6–12.
- Clark JL, Hollecker L, Mason JC, Stuyver LJ, Tharnish PM, Lostia S, McBrayer TR, Schinazi RF, Watanabe KA, Otto MJ, Furman PA, Stec WJ, Patterson SE, Pankiewicz KW. 2005. Design, synthesis, and antiviral activity of 2'-deoxy-2'-fluoro-2'-C-methylcytidine, a potent inhibitor of hepatitis C virus replication. *J Med Chem* 48 :5504–5508.
- Clé M, Beck C, Salinas S, Lecollinet S, Gutierrez S, Van de Perre P, Baldet T, V Foulongne V, Simonin Y. 2019. Usutu virus: A new threat? *Epidemiol Infect.* 147:e232.
- Crotty S, Cameron CE, Andino R. 2001. RNA virus error catastrophe: direct molecular test by using ribavirin. *Proc Natl Acad Sci U S A* 98: 6895–6900.
- Cui J, Li F, Shi ZL. 2019. Origin and evolution of pathogenic coronaviruses. *Nat Rev Microbiol* 17: 181–192.
- Cui Q, Du R, Liu M, Rong L. 2020. Lignans and Their Derivatives from Plants as Antivirals. *Molecules* 25: 183.

- De Clercq E, Holy A. 2005. Acyclic nucleoside phosphonates: a key class of antiviral drugs. *Nat Rev Drug Discov* 4: 928–940.
- De Clercq E, Neyts J. 2009. Antiviral agents acting as DNA or RNA chain terminators. *Handb Exp Pharmacol* 189: 53–84.
- De Clercq, Guangdi L. 2016. Approved Antiviral Drugs over the Past 50 Years. 29: 695-747. 2014: 659–669.
- De Wit E, Van Doremalen N, Falzarano D, Munster VJ. 2016. SARS and MERS: Recent insights into emerging coronaviruses. *Nat Rev Microbiol* 14: 523–534.
- Delang L, Vliegen I, Froeyen M, Neyts J. 2011. Comparative study of the genetic barriers and pathways towards resistance of selective inhibitors of hepatitis C virus replication. *Antimicrob Agents Chemother*. 55:4103-4113.
- Deval J, Symons JA, Beigelman L. 2014. Inhibition of viral RNA polymerases by nucleoside and nucleotide analogs: therapeutic applications against positive-strand RNA viruses beyond hepatitis C virus. *Curr Opin Virol* 9: 1-7.
- Doherty PC. 2013. *Pandemics*. Oxford University Press.
- Ebel GD. 2010. Update on Powassan virus: emergence of a North American tick-borne flavivirus. *Annu Rev Entomol* 55:95-110.
- Eldrup AB, Allerson CR, Bennett CF, Bera S, Bhat B, Bhat N, Bosserman MR, Brooks J, Burlein C, Carroll SS, Cook PD, Getty KL, MacCoss M, McMasters DR, Olsen DB, Prakash TP, Prhavic M, Song QL, Tomassini JE, Xia J. 2004. Structure-activity relationship of purine ribonucleosides for inhibition of hepatitis C virus RNA-dependent RNA polymerase. *J Med Chem* 47: 2283-2295.
- Eyer L, Hruska K. 2013. Antiviral agents targeting the influenza virus: A review and publication analysis. *Vet Med* 58: 113-185.
- Flint M, McMullan LK, Dodd KA, Bird BH, Khristova ML, Nichol ST, Spiropoulou CF. 2014. Inhibitors of the tick-borne, hemorrhagic fever-associated flaviviruses. *Antimicrob Agents Chemother* 58: 3206-3216.
- Füzik T, Formanová P, Růžek D, Yoshii K, Niedrig M, Plevka P. 2018. Structure of tick-borne encephalitis virus and its neutralization by a monoclonal antibody. *Nat Commun* 9: 436.
- Gardner CL, Ryman KD. 2010. Yellow fever: a reemerging threat. *Clin Lab Med*. 30: 237-260.
- Graci JD, Cameron CE. 2002. Quasispecies, error catastrophe, and the antiviral activity of ribavirin. *Virology* 298: 175–180.
- Gritsun TS, Lashkevich VA, Gould EA. 2003. Tick-borne encephalitis. *Antivir Res* 57: 129-146.
- Gritsun TS, Nuttall PA, Gould EA. 2003. Tick-borne Flaviviruses. *Adv Virus Res* 61: 317-371.
- Haglund M, Günther G. 2003. Tick-borne encephalitis—pathogenesis, clinical course and long-term follow-up. *Vaccine*, 21 (Supplement 1), S11-S18.
- Heinz FX, Mandl CW. 1993. The Molecular-Biology of Tick-Borne Encephalitis-Virus. *APMIS* 101: 735-45.
- Helesic J, Bartoníčka T, Krbková L. 2007. Bat rabies in Europe and the Czech Republic. *Klin Mikrobiol Infekc Lek* 13: 93-98.
- Holbrook MR. 2012. Kyasanur forest disease. *Antiviral Res* 96: 353-62.
- Hu C-MJ, Chang W-S, Fang Z-S, Chen Y-T, Wang W-L, Tsai H-H, Chueh L-L, Takano T, Hohdatsu T, Chen H-W. 2017. Nanoparticulate vacuolar ATPase blocker exhibits potent host-targeted antiviral activity against feline coronavirus. *Sci Rep* 7: 13043.
- Huang C, Wang Y, Li X, Ren L, Zhao J, Hu Y, Zhang L, Fan G, Xu J, Gu X, Cheng Z, Yu T, Xia J, Wei Y, Wu W, Xie X, Yin W, Li H, Liu M, Xiao Y, Gao H, Li Guo, Xie J, Wang G, Jiang R, Gao Z,

- Jin Q, Wang J, Cao B. 2020. Clinical features of patients infected with 2019 novel coronavirus in Wuhan, China. *Lancet* 395, 497–506.
- Huang YS, Chang SY, Sheng WH, et al. Virological response to tenofovir disoproxil fumarate in HIV-positive patients with lamivudine-resistant hepatitis B virus coinfection in an area hyperendemic for hepatitis B virus infection. *PLoS One* 2016; 11: e0169228.
- Hubalek Z. 2000. European experience with the West Nile virus ecology and epidemiology: could it be relevant for the new world? *Viral Immunol* 13: 415–426.
- Chambers TJ, Hahn CS, Galler R, Rice CM. 1990. Flavivirus genome organization, expression, and replication. *Annu Rev Microbiol* 44: 649–688.
- Chen H, Liu L, Jones SA, Banavali N, Kass J, Li Z, Zhang J, Kramer LD, Ghosh AK, Li H. 2013. Selective inhibition of the West Nile virus methyltransferase by nucleoside analogs. *Antiviral Res* 97: 232–239.
- Chen Y, Liu QY, Guo DY. 2020. Emerging coronaviruses: Genome structure, replication, and pathogenesis. *J Med Virol* 92: 418–423.
- Chowers MY, Lang R, Nassar F, Ben-David D, Giladi M, Rubinshtein E, Itzhaki A, Mishal J, Siegman-Igra Y, Kitzes R, Pick N, Landau Z, Wolf D, Bin H, Mendelson E, Pitlik SD, Weinberger M. 2001. Clinical characteristics of the West Nile fever outbreak, Israel, 2000. *Emerg Infect Dis* 7: 675–678.
- Jefferies KC, Cipriano DJ, Forgac M. 2008. Function, structure and regulation of the vacuolar (H⁺)-ATPases. *Arch Biochem Biophys* 476: 33–42.
- Jeffries CL, Mansfield KL, Phipps LP, Wakeley PR, Mearns R. 2014. Schock A, Bell S, Breed AC, Fooks AR, Johnson N. Louping ill virus: an endemic tick-borne disease of Great Britain. *J Gen Virol* 95: 1005–1014.
- Julander JG, Demarest JF, Taylor R, Gowen BB, Walling DM, Mathis A, Babu YS. 2021. An update on the progress of galidesivir (BCX4430), a broad-spectrum antiviral. *Antivir Res*. 195: 105180.
- Jullian-Pawlicki N, Lequart-Pillon M, Huynh-Cong L, Lesur D, Cailleu D, Mesnard F, Laberche JC, Gontier E, Boitel-Conti M. 2015. Arylnaphthalene and aryltetralin-type lignans in hairy root cultures of *Linum perenne*, and the stereochemistry of 6-methoxypodophyllotoxin and one diastereoisomer by HPLC-MS and NMR spectroscopy. *Phytochem Anal* 26: 310–319.
- Kati W, Koev G, Irvin M, Beyer J, Liu Y, Krishnan P, Reisch T, Mondal R, Wagner R, Molla A, Maring, Collins C. 2015. In vitro activity and resistance profile of dasabuvir, a nonnucleoside hepatitis C virus polymerase inhibitor. *Antimicrob Agents Chemother* 59: 1505–1511.
- Kis Z, Tak K, Ibrahim D, Papathanasiou MM, Chachuat B, Shah N, Kontoravdi C. 2022. Pandemic-response adenoviral vector and RNA vaccine manufacturing. *Vaccines* 7 :29.
- Komar N, Clark GG. 2006. West Nile virus activity in Latin America and the Caribbean. *Rev Panam Salud Publica* 19: 112–117.
- Kríz B, Benes C, Daniel M. 2009. Alimentary transmission of tick-borne encephalitis in the Czech Republic (1997–2008). *Epidemiol Mikrobiol Imunol* 58: 98–103
- Kumar S, Verma A, Yadav P, Dubey SK, Azhar EI, Maitra SS, Dwivedi VD. 2022. Molecular pathogenesis of Japanese encephalitis and possible therapeutic strategies. *Arch Virol*. 2: 1–24.
- Lam AM, Murakami E, Espiritu C, Steuer HM, Niu C, Keilman M, Bao H, Zennou V, Bourne N, Julander JG, Morrey JD, Smee DF, Frick DN, Heck JA, Wang P, Nagarathnam D, Ross BS, Sofia MJ, Otto MJ, Furman PA. 2010. PSI-7851, a pronucleotide of beta-D-2'-deoxy-2'-

- fluoro-2'-C-methyluridine monophosphate, is a potent and pan-genotype inhibitor of hepatitis C virus replication. *Antimicrob Agents Chemother* 54: 3187–3196.
- Lam YF, Seto WK, Wong D, Cheung K-S, Fung J, Mak L-Y, Yuen J, Chong C-K, Lai C-L, Yuen M-F. 2017. Seven-year treatment outcome of entecavir in a real-world cohort: effects on clinical parameters, HBsAg and HBcrAg levels. *Clin Trans Gastroenterol* 8: e125.
- Lazear HM, Stringer EM, de Silva AM. 2016. The emerging Zika virus epidemic in the Americas: research priorities. *JAMA* 315: 1945–1946.
- Leyssen P, Balzarini J, De Clercq E, Neyts J. 2005. The predominant mechanism by which ribavirin exerts its antiviral activity in vitro against flaviviruses and paramyxoviruses is mediated by inhibition of inosine monophosphate dehydrogenase. *J Virol* 79:1943–1947.
- Lim SM, Koraka P, Osterhaus ADME, Martina BEE. 2011. West Nile virus: immunity and pathogenesis. *Viruses* 3: 811–828.
- Lindquist L, Vapalahti O. Tick-borne encephalitis. 2008. *The Lancet*, 371: 1861-1871.
- Lv JP, Yang S, Dong JX, Jin H. 2021. New cyclopeptide alkaloids from the whole plant of *Justicia procumbens* L. *Nat Prod Res* 35: 4032–4040.
- Majerus LM, Rode RO, Sabljic ER. 2009. [Post-encephalitic syndrome in patients with tick-borne encephalitis]. *Acta Medica Croatica*, 63: 269-278.
- Malavige GN, Fernando S, Fernando DJ, Seneviratne SL. 2004. Dengue viral infections. *Postgrad Med J* 80: 588-601.
- Mécharles S, Herrmann C, Poullain P, Tran T-H, Deschamps N, Mathon G, Landais A, Breurec S, Lannuzel A. 2016. Acute myelitis due to Zika virus infection. *Lancet*; 387: 1481.
- Melnick JL, Paul JR, Riordan JT, Barnett VH, Goldblum N, Zabin E. 1951. Isolation from human sera in Egypt of a virus apparently identical to West Nile virus. *Proc Soc Exp Biol Med* 77: 661–665.
- Mickiene A., Laiskonis A., Gunther G., Vene S., Lundkvist A., Lindquist L. Tickborne encephalitis in an area of high endemicity in lithuania: disease severity and long-term prognosis. *Clin Infect Dis*. 2002. 35: 650-658.
- Miura S, Izuta S. 2004. DNA polymerases as targets of anticancer nucleosides. *Curr Drug Targets* 5: 191–195.
- Mlakar J, Korva M, Tul N, Popović M, Poljšak-Prijatelj M, Mraz J, Kolenc M, Resman Rus K, Vesnaver Vipotnik T, Fabjan Vodusek V, Vizjak A, Pižem J, Petrovec M, Avšič Županc T. 2016. Zika virus associated with microcephaly. *N Engl J Med* 374 :951–958.
- Monchatre-Leroy E, Boue F, Boucher JM, Renault C, Moutou F, Gouilh MA, Umhang G. 2017. Identification of Alpha and Beta Coronavirus in Wildlife Species in France: Bats, Rodents, Rabbits, and Hedgehogs. *Viruses* 9: 364.
- Monto AS. 2006. Vaccines and Antiviral Drugs in Pandemic Preparedness. *Emerg Infect Dis*. 12: 55–60.
- Mostashari F, Bunning ML, Kitsutani PT, Singer DA, Nash D, Cooper MJ, Katz N, Liljebjelke KA, Biggerstaff BJ, Fine AD, Layton MC, Mullin SM, Johnson AJ, Martin DA, Hayes EB, Campbell GL. 2001. Epidemic West Nile encephalitis, New York, 1999: results of a household-based seroepidemiological survey. *Lancet* 358: 261–264.
- Nihala HCH, Sheeba P, Honey S. 2021. Corona Viruses: A Review on SARS, MERS and COVID-19. *Microbiol Insights*. 14:11786361211002481.
- Paraskevis D, Kostaki EG, Magiorkinis G, Panayiotakopoulos G, Sourvinos G, Tsiodras S. 2020. Full-genome evolutionary analysis of the novel corona virus (2019-nCoV) rejects the

- hypothesis of emergence as a result of a recent recombination event. *Infect Genet Evol* 79: 104212.
- Pérez-Sayáns M, Somoza-Martín JM, Barros-Angueira F, Rey JM, García-García A. 2009. V-ATPase inhibitors and implication in cancer treatment. *Cancer Treat Rev*. 35: 707-713.
- Pierson TC, Diamond MS. 2020. The continued threat of emerging flaviviruses. *Nat Microbiol* 5: 796-812.
- Ray AS, Fordyce MW, Hitchcock MJM. 2016. Tenofovir alafenamide: a novel prodrug of tenofovir for the treatment of human immunodeficiency virus. *Antiviral Res* 125: 63–70.
- Ren J, Milton J, Weaver KL, Short SA, Stuart DI, Stammers, DK. 2000. Structural basis for the resilience of efavirenz (DMP-266) to drug resistance mutations in HIV-1 reverse transcriptase. *Structure* 8: 1089–1094.
- Roth A, Mercier A, Lepers C, Hoy D, Duituturaga S, Benyon E, Guillaumot L, Souares Y. 2014. Concurrent outbreaks of dengue, chikungunya and Zika virus infections - an unprecedented epidemic wave of mosquito-borne viruses in the Pacific 2012–2014. *Euro Surveill* 19: 20929.
- Rudolf I, Bakonyi T, Sebesta O, Mendel J, Peško J, Betášová L, Blažejová H, Venclíková K, Straková P, Nowotny N, Hubálek Z. 2014. West Nile virus lineage 2 isolated from *Culex modestus* mosquitoes in the Czech Republic, 2013: expansion of the European WNV endemic area to the North? *Euro Surveill* 19: 2–5.
- Ruggiero E and Richter SN. 2018. G-quadruplexes and G-quadruplex ligands: targets and tools in antiviral therapy. *Nucleic Acids Res* 46: 3270–3283.
- Ruzek D, Avšič Županc T, Borde J, Chrdle A, Eyer L, Karganova G, Kholodilov I, Knap N, Kozlovskaya L, Matveev A, Miller AD, Osolodkin DI, Överby AK, Tikunova N, Tkachev S, Zajkowska J. 2019. Tick-borne encephalitis in Europe and Russia: Review of pathogenesis, clinical features, therapy, and vaccines. *Antivir Res* 164: 23-51.
- Růžek D, Yakimenko VV, Karan LS, Tkachev SE. 2010. Omsk haemorrhagic fever. *Lancet*. 376: 2104-2113.
- Sarisky RT. 2004. Non-nucleoside inhibitors of the HCV polymerase. *J Antimicrob Chemother*. 54: 14-16.
- Sehrawat S, Kumar D, Rouse BT. 2018. Herpesviruses: Harmonious Pathogens but Relevant Cofactors in Other Diseases? *Front Cell Infect Microbiol*. 8: 177.
- Seley-Radtke KL, Yates MK. 2018. The evolution of nucleoside analogue antivirals: a review for chemists and non-chemists. 2018. Part 1: early structural modifications to the nucleoside scaffold. *Antiviral Res* 154: 66–86.
- Smee DF, Morris JL, Barnard DL, Van Aerschot A. 1992. Selective inhibition of arthropod-borne and arenaviruses in vitro by 3'-fluoro-3'-deoxyadenosine. *Antiviral Res* 18: 151–162.
- Smithburn K, Hughes T, Burke A, Paul J. 1940. A neurotropic virus isolated from the blood of a native of Uganda. *Am J Trop Med Hyg* 20: 471–492.
- Stedman C. 2014. Sofosbuvir, a NS5B polymerase inhibitor in the treatment of hepatitis C: a review of its clinical potential. *Ther Adv Gastroenterol* 7: 131–140.
- Takane Y, Nakajima K, Kikegawa Y. 2022. Urban climate changes during the COVID-19 pandemic: integration of urban-building-energy model with social big data. *Climate and Atmospheric Science* 5: 1-10.
- Tarantino D, Cannalire R, Mastrangelo E, Croci R, Querat G, Barreca ML, Bolognesi M, Manfroni G, Cecchetti V, Milani M. 2016. Targeting flavivirus RNA dependent RNA polymerase through a pyridobenzothiazole inhibitor. *Antivir Res* 134: 226–235.

- Taylor R, Kotian P, Warren T, Panchal R, Bavari S, Julander J, Dobo S, Rose A, El-Kattan Y, Taubenheim B, Babu Y, Sheridan WP. 2016. BCX4430 - A broad-spectrum antiviral adenosine nucleoside analog under development for the treatment of Ebola virus disease. *J Infect Public Health* 9: 220-226.
- Tu YF, Chien CS, Yarmishyn AA, Lin YY, Luo YH, Lin YT, Lai WY, Yang DM, Chou SJ, Yang YP, Wang M-L, Chiou S-H. 2020. A Review of SARS-CoV-2 and the Ongoing Clinical Trials. *Int J Mol Sci* 21: 2657.
- Usach I, Melis V, Peris J-E. 2013. Non-nucleoside reverse transcriptase inhibitors: a review on pharmacokinetics, pharmacodynamics, safety and tolerability. *J Int AIDS Soc* 16: 18567.
- Van Aerschot A, Herdewijn P, Janssen G, Cools M, De Clercq E. 1989. Synthesis and antiviral activity evaluation of 3'-fluoro-3'-deoxyribonucleosides. *Antiviral Res* 12:133–150
- Vernekar SK, Qiu L, Zhang J, Kankanala J, Li H, Geraghty RJ, Wang Z. 2015. 5'-Silylated 3'-1,2,3-triazolyl thymidine analogues as inhibitors of West Nile virus and Dengue virus. *J Med Chem* 58: 4016–4028.
- Villalain J. 2010. Membranotropic Effects of Arbidol, a Broad Anti-Viral Molecule, on Phospholipid Model Membranes. *J Phys Chem* 114: 8544-8554.
- Warren TK, Wells J, Panchal RG, Stuthman KS, Garza NL, Van Tongeren SA, Dong L, Retterer CJ, Eaton BP, Pegoraro G, Honnold S, Bantia S, Kotian P, Chen X, Taubenheim BR, Welch LS, Minning DM, Babu YS, Sheridan WP, Bavari S. 2014. Protection against filovirus diseases by a novel broad-spectrum nucleoside analogue BCX4430. *Nature* 508: 402-405.
- Wong-Sam A, Wang YF, Zhang Y, Ghosh AK, Harrison RW, Weber IT. 2018. Drug Resistance Mutation L76V Alters Nonpolar Interactions at the Flap-Core Interface of HIV-1 Protease. *ACS Omega* 3: 12132–12140.
- Xu H-T, Hassounah SA, Colby-Germinario SP, Oliviera M, Fogarty C, Quan Y, Han Y, Golubkov O, Ibanescu I, Brenner B, Stranix BR, Wainberg MA. 2017. Purification of Zika virus RNA-dependent RNA polymerase and its use to identify smallmolecule Zika inhibitors. *J Antimicrob Chemother* 72: 727–734.
- Yoshii K. 2019. Epidemiology and pathological mechanisms of tick-borne encephalitis. *J Vet Med Sci* 81: 343-347.
- Zilber, LA. 1939. Vesennij – vesenne-letnij – epidemičeskij kleščevoj encefalit. *Arkhiv Biol Nauk* 56: 255-261.
- Zouharova D, Lipenska I, Fojtikova M, Kulich P, Neca J, Slany M, Kovarcik K, Turanek-Knotigova P, Hubatka F, Celechovska H, Masek J, Koudelka S, Prochazka L, Eyer L, Plockova J, Bartheldyova E, Miller AD, Ruzek D, Raska M, Janeba Z, Turanek J. 2016. Antiviral activities of 2,6-diaminopurine-based acyclic nucleoside phosphonates against herpesviruses: In vitro study results with pseudorabies virus (PrV, SuHV-1). *Vet Microbiol*. 184: 84-93.
- Zumla A, Chan JFW, Azhar EI, Hui DSC, Yuen K-Y. 2016. Coronaviruses—Drug discovery and therapeutic options. *Nat Rev Drug Discov* 15: 327–347.